MAG 2025 CLEAN AIR ACT SECTION 179B(b) RETROSPECTIVE DEMONSTRATION OF THE IMPACT OF INTERNATIONAL EMISSIONS ON OZONE CONCENTRATIONS IN THE MARICOPA NONATTAINMENT AREA

APPENDICES

SEPTEMBER 2025

MARICOPA ASSOCIATION of GOVERNMENTS

MAG 2025 CLEAN AIR ACT SECTION 179B(b) RETROSPECTIVE DEMONSTRATION OF THE IMPACT OF INTERNATIONAL EMISSIONS ON OZONE CONCENTRATIONS IN THE MARICOPA NONATTAINMENT AREA

APPENDIX A –
Technical Analyses in Support of the MAG 2025 Clean Air Act §179B(b) Retrospective Demonstration for the Maricopa Ozone Nonattainment Area

SEPTEMBER 2025

MARICOPA ASSOCIATION of GOVERNMENTS

Prepared for:

Maricopa Association of Governments
302 North First Avenue, Suite 200
Phoenix, AZ 85003

Prepared by:

Ramboll Americas Engineering Solutions, Inc.
7250 Redwood Blvd., Suite 105
Novato, California 94945

Eastern Research Group, Inc.
561 Virginia Rd., Building 4 – Suite 300
Concord, Massachusetts 01742

September 2025
1940113557

Technical Analyses in Support of the MAG 2025 Clean Air Act §179B(b) Retrospective Demonstration for the Maricopa Ozone Nonattainment Area

RAMBOLL

Contents

Acronyms and Abbreviations **1**

1.0 Overview **3**
1.1 Introduction 3
1.2 Report Organization 4
1.3 Summary of Results 4

2.0 Conceptual Model **8**
2.1 The Maricopa Airshed 8
2.2 Summary of Ozone Air Quality 8
2.3 Ozone and Precursor Monitoring 10
2.4 Additional Conceptual Elements for the 179B Demonstration 16
2.4.1 Exceedances during the 2021-2023 DV Period 16
2.4.2 Vertically Integrated Wind Roses 20
2.4.3 Transport of International Emissions 22

3.0 Modeling to Quantify International Contribution **25**
3.1 EPA Recommended Ozone Design Value Projection Procedure 25
3.2 Source Apportionment Modeling 26
3.2.1 Model Configuration 27
3.2.2 Model Results 30
3.3 EPA Modeling Confirming Attainment "But For" International Emissions 32
3.4 EPA Modeling Confirming Mexico Contributions in Maricopa 32

4.0 Precursor Emission Trends **34**

5.0 Transport Pattern Analysis **38**
5.1 Air Parcel Trajectory Calculations 38
5.2 2021-2023 Design Values with Potential Mexico Transport Excluded 43

6.0 Conclusions **46**

7.0 References **49**

TABLES

Table 2-1. Ozone monitoring sites in the Maricopa NAA. 11
Table 2-2. Possible wildfire-impacted ozone exceedance dates occurring in 2021-2023 (from Appendix B of the MAG's 2025 Clean Air Act Section 179B(b) Retrospective Demonstration). Shaded bold dates represent the subset of 31 atypical wildfire days recommended for exclusion from modeling due to their importance to design value calculations. 17
Table 2-3. Phoenix and Tucson sounding parameters. 20
Table 3-1. CAMx source apportionment emission sector groups. 27
Table 3-2. Modeled international anthropogenic (IA) contributions to 2021-2023 DVs and resulting DVs with IA contributions removed. 31
Table 3-3. Observed 2018-2020 DV (ppb), scaled modeled contributions (EPA, 2021) from global natural, US anthropogenic, international anthropogenic (IA), and mixed

anthropogenic, and the DV reflecting removal of IA. DVs are truncated to whole numbers to reflect the form of the ozone NAAQS. 32
Table 3-4. EPA (2023) model-projected 2023 ozone DV and key source contributions averaged over the highest 5 sites in the Maricopa NAA where projected DVs range from 70.0 to 70.8 ppb: Arizona (AZ), California (CA), Canada and Mexico (C&M), fires, and boundary conditions (BC). The table also shows those values scaled to the maximum observed 2021-2023 DV of 80 ppb. 33
Table 4-1. NOx emissions and percent change from 2017 to 2023, US and three northern Mexico States combined. 35
Table 4-2. VOC emissions and percent change from 2017 to 2023, US and three northern Mexico States combined. 36
Table 4-3. Mexico point source emissions, 2017 and 2023. 36
Table 4-4. Mexico airport emissions, 2017 and 2023. 36
Table 4-5. Mexico area source emissions, 2017 and 2023. 37
Table 4-6. Mexico nonroad emissions, 2017 and 2023. 37
Table 4-7. Mexico on-road emissions, 2017 and 2023. 37
Table 5-1. Maricopa NAA ozone exceedance days in 2021-2023 analyzed with HYSPLIT back trajectories. 39

FIGURES

Figure 2-1. Topography within and surrounding the Maricopa NAA for the 2015 ozone standard. 9
Figure 2-2. Ozone monitoring stations in the Maricopa NAA. 12
Figure 2-3. Peak 8-hour ozone DVs in the Maricopa NAA from 2000 through 2024 (taken from MAG's full conceptual model). 13
Figure 2-4. 8-hour ozone DVs at monitors in the Maricopa NAA from 2000 through 2024, for (a) all days and (b) excluding all exceedance days possibly impacted by wildfires since 2017 (taken from MAG's full conceptual model). 14
Figure 2-5. Number of 8-hour ozone exceedance days (MDA8 ozone above 70 ppb) in the Maricopa NAA from 2000 through 2024. 15
Figure 2-6. Five-year average number of ozone exceedance days (MDA8 ozone above 70 ppb) in the Maricopa NAA from 2000 to 2024. 15
Figure 2-7. Number of ozone exceedance days in 2021 through 2023 at each of the Maricopa NAA ozone monitors, considering all possible wildfire days (grey) and non-wildfire days (orange). 18
Figure 2-8. Annual 4th high MDA8 ozone in 2021 through 2023 at each of the Maricopa NAA ozone monitors considering contributions from all possible wildfire days (grey) and non-wildfire days (orange). 19
Figure 2-9. Vertically integrated wind roses for Phoenix (upper) and Tucson (lower) during all monitored exceedance days (left) and no wildfire impacted days (right) during the 2021-2023 ozone seasons. 21
Figure 2-10. Schematic conceptual model of pollutant transport from Asia to North America (from HTAP, 2010). Blue text on left refers to Asian continental boundary layer processes, red text along bottom refers to low level transport, and black/white text along top and right refers to high altitude transport. 22
Figure 2-11. Examples of modeled surface background ozone (ppb) from Baker et al. (2015; left) showing July 2011 average US background from the CAMx regional

photochemical model, and from Zhang et al. (2020; right) showing tracked ozone from Asia on May 24, 2017 from the AM4 global model. 23
Figure 2-12. Results from Baker et al. (2015) showing examples of US background ozone contribution (ppb) from the western CAMx boundary and from three sets of vertical model layers; boundary layer (left), mid troposphere (middle), stratosphere (right). 23
Figure 3-1. Map of nested CAMx modeling domains for the MAG ozone modeling platform. 26
Figure 3-2. OSAT source region map for the 36 km North American domain. 28
Figure 3-3. OSAT source region map for the 12 km Arizona domain. 29
Figure 3-4. OSAT source region map for the 4 km Maricopa NAA domain. 30
Figure 3-5. Time series of simulated Asia/intercontinental and Mexico IA contributions to MDA8 ozone during the 2023 ozone season averaged over all Maricopa NAA monitoring sites. 31
Figure 4-1. NOx emission trends from 2017 to 2023 in the Maricopa NAA (left) and the three northern border Mexican States of Baja California, Sonora, and Chihuahua combined (right). 34
Figure 4-2. VOC emissions trends from 2017 to 2023 in the Maricopa NAA (left) and the three northern border Mexican States of Baja California, Sonora, and Chihuahua combined (right). 35
Figure 5-1. Location and coverage of the 5 initiation points at 3 vertical levels for HYSPLIT back trajectories: 3-D view (upper), planar view (lower). The Maricopa NAA is outlined in green. 40
Figure 5-2. Examples of ensemble trajectory plots initiated on 4 specific Maricopa NAA exceedance days in 2021-2023 that represent 4 types of transport patterns: (northerly at top left, easterly/southeasterly at top right, southerly at bottom left, and westerly at bottom right). 42
Figure 5-3. Summary of HYSPLIT-based transport pattern groups for 2021–2023 exceedance days in the Maricopa NAA. 43
Figure 5-4. Summary of HYSPLIT-based transport pattern groups for 2021–2023 exceedance days in the Maricopa NAA by month: all exceedance days (upper), and excluding all possible wildfire-impacted days (lower). 44
Figure 5-5. Recalculated 2021-2023 DVs for different wildfire and potential Mexican transport scenarios for each monitoring site in the Maricopa NAA. 45

APPENDICES

APPENDIX A Methods to Estimate 2017 and 2023 Mexico Emissions
APPENDIX B Example HYSPLIT Control File for May 5, 2021, 19 UTC (12 PM 100 m initiation height, Maricopa NAA northeast corner initiation point)
APPENDIX C Plots of HYSPLIT 3-day Ensemble Trajectories from Each Maricopa NAA Ozone Exceedance Day in 2021–2023

Acronyms and Abbreviations

ADEQ	Arizona Department of Environmental Quality
AGL	Above ground level
AQS	Air Quality System monitoring database
BC	Boundary conditions for the modeling domain
CAA	Clean Air Act
CAMx	Comprehensive Air Quality model with extensions
CB7r1	Carbon Bond version 7 revision 1
CFR	Code of Federal Regulations
CMAQ	Community Multiscale Air Quality model
CO	Carbon monoxide
DV	Design value
DVB	Base ozone design value
DVS	Scenario ozone design value
EPA	Environmental Protection Agency
FIP	Federal Implementation Plan
H4MDA8	Fourth-highest maximum daily 8-hour average
HCHO	Formaldehyde
HNO_3	Nitric acid
HONO	Nitrous acid
hPa	Hectopascals
HTAP	Hemispheric Transport of Air Pollution
IA	International anthropogenic
IC	Initial conditions for the modeling domain
IGRA	Integrated Global Radiosonde Archive
km	Kilometers
MAG	Maricopa Association of Governments
MCAQD	Maricopa County Air Quality Department
MDA8	Maximum daily 8-hour average
MSL	Mean sea level
MST	Mountain Standard Time
N_2O_5	Dinitrogen pentoxide
NAA	Nonattainment Area
NAAQS	National Ambient Air Quality Standard
NO	Nitric oxide
NO_2	Nitrogen dioxide
NO_3	Nitrate radical
NOx	Nitrogen oxides
O_3	Ozone
OSAT	Ozone Source Apportionment Technology
PAMS	Photochemical Assessment Monitoring Stations
PAN	Peroxyacetyl nitrate
PCAQCD	Pinal County Air Quality Control District
PNA	Peroxynitric acid
ppb	Parts per billion by volume

ppm	Parts per million by volume
RCEI	Regional Climate Extremes Index
RNO_3	Organic nitrates
RRF	Relative Response Factor
SIP	State Implementation Plan
SLAMS	State and local air monitoring stations
SMAT-CE	Software for Model Attainment Test - Community Edition
SMOKE	Sparse Matrix Operator Kernel Emissions processing system
SRP-MIC	Salt River Pima-Maricopa Indian Community
UHI	Urban heat island
US	United States
UTC	Universal Time Coordinate
VOC	Volatile organic compounds
WRF	Weather Research and Forecasting model

1.0 Overview

This report provides the primary technical analyses for inclusion in the Maricopa Association of Government's (MAG) 2025 Clean Air Act (CAA) Section 179B(b) Retrospective Demonstration to the US Environmental Protection Agency (EPA). In accordance with CAA §179B(b), the MAG demonstration shows that the Maricopa Ozone Nonattainment Area (NAA) would have attained the 2015 ozone National Ambient Air Quality Standard (NAAQS) by the Moderate attainment date of August 3, 2024, "but for emissions emanating from outside of the United States." This report is designated as Appendix A in the MAG 2025 Clean Air Act Section 179B(b) Retrospective Demonstration.

1.1 Introduction

On October 26, 2015, the EPA revised the primary (health-based) and secondary (welfare-based) ozone (O_3) NAAQS from 0.075 to 0.070 parts per million by volume (ppm) (Federal Register, 2015). The statistical form of the NAAQS is defined as the 3-year average of annual 4th highest daily maximum 8-hour average (MDA8) ozone concentration measured at each monitor. This is referred to as the "design value" (DV). The EPA designates nonattainment areas based on monitored DVs that exceed 0.070 ppm (or 70.9 parts per billion[1], ppb) based on certified, quality-assured air quality measurement data.

The Maricopa NAA in south-central Arizona includes the Phoenix Metropolitan Area and covers much of the urbanized portion of Maricopa County, portions of the Tonto National Monument in Gila County, and a portion of northern Pinal County. The NAA experiences episodically high ozone levels during late spring through early autumn months when MDA8 ozone measurements often exceed 70 ppb.

On June 4, 2018, EPA initially designated the Maricopa NAA as a Marginal area for the 2015 ozone NAAQS, with an attainment date of August 3, 2021 (Federal Register, 2018). On October 7, 2022, EPA reclassified the NAA as a Moderate area due to continued exceedances, with an attainment date of August 3, 2024 (Federal Register, 2022). On October 18, 2023, EPA published a Finding of Failure to Submit a plan revision addressing Moderate Area requirements for the Maricopa NAA by the due date of January 1, 2023 (Federal Register, 2023), which triggered CAA sanctions and Federal Implementation Plan (FIP) requirements. Between December 2024 and April 2025, the Arizona Department of Environmental Quality (ADEQ) submitted four State Implementation Plan (SIP) revisions for the Maricopa NAA. EPA has reviewed all submissions, found them complete under 40 CFR 51 Appendix V, and terminated the sanctions clocks initiated on October 18, 2023.

Despite continuous emission reductions in anthropogenic sources within the Maricopa NAA, exceedances have continued through 2024, and ozone design value concentrations have increased since 2017. The CAA provides some regulatory flexibility for nonattainment areas impacted by foreign contributions if they fail to attain. According to §179B(b) of the Act, a State may develop a technical demonstration showing that the nonattainment area would have attained the ozone standard by a past attainment date "but for" the contribution from international emissions. EPA approval of the MAG CAA Section 179B(b) demonstration will prevent the Maricopa NAA from being reclassified to higher and stricter classifications of Serious and above.

[1] Appendix U to 40 CFR Part 50 (Section 3, paragraph (e)) requires the design value to be reported in ppm with additional digits to the right of the third decimal place truncated.

1.2 Report Organization

This report involves several types of technical analyses that cumulatively build a body of evidence for the transport of ozone and its precursors from international sources to the Maricopa NAA. Each of these analyses are described in the following sections. The primary analysis involves global and regional photochemical modeling that quantifies contributions to 2023 ozone DVs from foreign anthropogenic sources across the northern hemisphere. We present conceptual and photochemical modeling evidence that long range (7-10 day) transport from Asia and intercontinental sources contribute toward high ozone levels in the Maricopa NAA, especially in the late spring and early summer. Photochemical modeling also provides evidence of significant ozone transport from Mexico, particularly in the summer months of July and August. As the Maricopa NAA is located in close proximity with Mexico (approximately 100 miles from the nearest border), additional analyses lend supporting weight of evidence for frequent medium-range (3-day) transport from Mexico within the North American monsoon circulation that contributes to NAA ozone exceedance events.

Specifically, the report incorporates the following analyses:

1. Expand MAG's conceptual model of sources and conditions that lead to exceedances of the 2015 ozone standard within the Maricopa NAA by establishing the importance of international transport and identifying days influenced by increasingly impactful wildfire influences so that international impacts can be accurately quantified.

2. Conduct global/regional photochemical modeling to quantify contributions from international anthropogenic sources to 2023 ozone DVs.

3. Present recent continental-scale modeling conducted by EPA that confirm consistent estimates of international transport specifically to the Maricopa NAA.

4. Compare 2017-2023 emission inventories for the Maricopa NAA and the three northern border states of Mexico that comprise the nearest international sources.

5. Conduct medium-range air parcel trajectory analyses to understand the frequency of international transport from international areas within North America.

Section 1 of this report presents historical context and summarizes the analyses and results supporting the Maricopa NAA §179B(b) demonstration. Section 2 summarizes the conceptual model of factors that cause or contribute to ozone exceedances in the Maricopa NAA (as developed by MAG), trends in monitored ozone and precursor concentrations at Maricopa monitors, and additional synopses developed by Ramboll specifically focused on transport of ozone and precursors from international source areas. Section 3 describes photochemical source apportionment modeling results that quantify and substantiate the evidence for international anthropogenic contributions to Maricopa NAA ozone exceedances. Section 3 also summarizes recent EPA photochemical modeling that confirms consistent levels of international anthropogenic (IA) contributions. Sections 4 and 5 present additional weight of evidence analyses: Section 4 tabulates annual ozone precursor emission trends in the NAA and northern Mexico, while Section 5 presents air parcel trajectories leading up to exceedance days during the 2021-2023 Moderate attainment period. Section 6 summarizes our results and conclusions.

1.3 Summary of Results

The following lines of evidence demonstrate that the Maricopa NAA would have attained the 2015 ozone NAAQS by the Moderate attainment date of August 3, 2024 but for international anthropogenic contributions.

- **Physical setting (Section 2):** The Maricopa NAA extends over 5,288 square miles and contains the Phoenix Metropolitan Area, a highly urbanized and industrial area located along the channel and flood plain of the Salt River within the Sonoran Desert. The area experiences a summer continental climate with hot, dry summers dominated by persistent high-pressure systems spanning much of the Intermountain West. The typical daily pattern of mountain/valley up- and down-slope wind flows within the Phoenix Valley are consistently observed during daytime (westerly valley breeze) and nighttime (easterly mountain breeze), features that exacerbate air mass pooling (stagnation) and local recirculation under strong capping inversions and contribute to degraded air quality. In addition, the urban heat island (UHI) effect, which affects chemical rates and inter-daily circulation patterns, has increased since 2000 due to rapid urbanization.
- **Conceptual model of ozone episodes (Section 2):** During the summer season, ozone levels are influenced by meteorological systems operating at multiple scales including: deep vertical circulations caused by stratospheric intrusion and blocking high-pressure systems; lower-level vertical mixing due to the development of daytime turbulence and dissipation of nocturnal inversion layers; local mountain-valley breezes driven by terrain and topographic features; and long-range transport of upwind pollutants from other states and countries. These features are consistent with locally stagnant conditions associated with a sinking/compressing warm air mass within a deep dome of high pressure centered over the western US, which suppresses vertical mixing depth and cloud formation. High temperatures lead to increased emission rates for biogenic and evaporative processes, along with higher chemical oxidation rates. Since 2000, extreme weather events in the Southwest have increased along with the frequency of wildfire events, which have exacerbated ozone levels. Recent high-resolution satellite data reveal profound, distinct impacts from wildfire smoke on NO_2 and formaldehyde concentrations within Arizona.
- **Conceptual model of international transport (Section 2):** The area's proximity to the southern US border suggests contributions of ozone from Mexico. As a summer phenomenon, ozone episodes coincide with the seasonal western North American Monsoon, which brings humid air northward from Mexico into Arizona during July and August. This establishes a common transport corridor for pollutants emitted in Mexico to reach the Maricopa NAA within a few days. Wind patterns through the boundary layer on exceedance days over both Phoenix and Tucson are predominantly (75%) from the southeast toward Mexico. While this characterizes wind conditions at single points, multi-day air parcel trajectories (Section 5) indicate a similar yet slightly higher frequency of transport paths that extend back to Mexico.

  However, there is another common transport pattern linking Asia (and other areas of the northern hemisphere) to the western US. As documented in the published literature, persistent global circulation patterns establish a direct transport route in the mid to upper troposphere that brings pollutant-laden air to North America within 7 to 10 days. Sinking air within a high-pressure dome over the western US brings transported ozone and precursors toward the surface, while complex topography enhances vertical circulations, and thus the western US experiences the greatest ozone impacts from intercontinental transport. This transport mechanism is especially persistent throughout the spring and summer seasons. Moreover, a recent multi-decadal trend analysis through 2021 indicates that free tropospheric ozone over western North America continues to increase despite a decreasing trend in boundary layer ozone, affirming vertically different sources and mechanisms.
- **Concentration trends (Section 2):** Despite years of success in reducing ozone precursor emissions, namely nitrogen oxides (NOx) and volatile organic compounds (VOC), the region faces significant challenges in meeting the ozone standard. These include elevated ozone levels related to the increasing frequency and quantity of emissions from wildfire events as well as international transport. While the number of

ozone exceedance days above 70 ppb has decreased by 62% over the past 25 years, a noticeable increase has occurred since 2017 with the majority (60%) of exceedance days associated with possible wildfire impacts. However, NAA ozone DVs have remained relatively flat since 2017 when all possible wildfire-impacted days are removed from DV calculations.

- **Source apportionment modeling (Section 3):** Source apportionment modeling is the most direct line of evidence for this demonstration and is the only analysis that explicitly provides an estimate of the IA contributions in the NAA. The Comprehensive Air quality Model with extensions (CAMx) was run with Ozone Source Apportionment Technology (OSAT) using MAG's 2023 modeling database to quantify local, regional, and international contributions to ozone within the NAA. The modeling domain covers southwestern North America with multiple grid resolutions. Boundary conditions (BC) for the domain were developed from an application of the GEOS-Chem global chemistry transport model, which included a breakout of precursors and ozone generated from all non-US international anthropogenic (IA) emissions. OSAT separately tracked natural and anthropogenic emissions from the US and Mexico within the domain, along with other global IA and natural ozone via BCs. Using EPA's SMAT-CE software, OSAT results were used to project what the 2021-2023 DVs would be in the absence of IA contributions in the Maricopa NAA. All IA sources were found to contribute approximately 15 ppb to site-averaged and site-maximum ozone levels, which reduce 2021-2023 DVs well below the 70 ppb ozone standard at all sites. These findings reinforce the significant role of international transport in shaping ozone levels in the Maricopa NAA.

  Modeling results also show that during April through June and September when stronger westerly winds are predominant, IA contributions via BCs dominate while contributions from Mexico and local emissions are much smaller. During July through August, coinciding with southerly monsoonal flow, BC IA decreases dramatically while Mexican contributions increase and comprise the majority of total IA.

- **Confirmatory EPA modeling (Section 3):** In 2021, EPA modeled US and international source attribution to 2018-2020 DVs in areas not attaining the 2015 ozone NAAQS by the 2021 Marginal attainment date. EPA reported contributions from 4 sectors at peak (controlling) monitors in each nonattainment area: global natural, US anthropogenic, IA, and mixed anthropogenic (US and IA). The IA contribution at the peak Phoenix monitor was estimated at 8.5 ppb. Removing the IA sector from the peak 79 ppb DV results in 70.5 ppb; i.e., the Maricopa NAA would have attained the standard in 2020 but for the IA contribution.

  Additionally, in 2023, EPA used source apportionment modeling to estimate state-by-state anthropogenic and other contributions to model-projected 2021-2023 ozone DVs in Moderate nonattainment areas. Emission contributions from each state were separately tracked, along with other contributions such as the portions of Canada and Mexico within the US modeling domain, wild and prescribed fires, and boundary conditions. None of the EPA projected 2021-2023 DVs at sites within the Maricopa NAA exceeded 70 ppb, suggesting modeled attainment. About 3 ppb was attributed to emissions from the northern portion of Mexico included within the domain. This is over 4 times higher than EPA's threshold for linking monitors to contributing upwind states, 50% more contribution than from California, and roughly equivalent to both California and fires combined. Additional IA contributions are associated with EPA's BCs, but EPA did not break out global IA and natural components in their modeled BCs. Arizona's own contribution was 20% of the total 2021-2023 DV.

- **Precursor emissions and trends (Section 4):** Emission inventory trends for the Maricopa NAA show that NOx emissions have declined by 38% from 2017 to 2023, mostly due to reductions in the on-road sector. VOC emissions have decreased by 4% over the same period. Meanwhile, emissions in the three northern Mexican states

bordering the southwest US (Baja California, Sonora, Chihuahua) have increased by 6% for NOx and by 2% for VOC. Furthermore, total and per capita NOx and VOC emissions in those Mexican states are several times larger than in the Maricopa NAA (6 and 11 times larger for 2017 and 2023 total NOx, respectively; 3 and 5 times larger for per capita 2017 and 2023 NOx, respectively; over 5 times larger for both 2017 and 2023 total VOC; and 2.5 times larger for both 2017 and 2023 per capita VOC). The proximity, magnitude, and recent trendline of Mexican emissions relative to the Maricopa NAA provide supporting evidence for the 179B(b) demonstration by indicating a neighboring source of transported IA emissions.

- **Trajectory analyses (Section 5):** Three-day (medium-range) upstream air parcel transport pathways arriving in the Maricopa NAA on all exceedance days during 2021-2023 were analyzed using the HYSPLIT trajectory model. This was done to assess transport over the scale of western North America. Four types of distinct transport patterns were subjectively identified where three of the four (west, south, southeast) involve transport from Mexico. While not the focus of this medium-range analysis, two of the four patterns (west and north) also involve longer-term transport from Canada, Asia, and other areas of the northern hemisphere. In total, medium-range trajectories indicate that 80% of air parcels pass over some portion of Mexico prior to arriving to the Maricopa NAA on exceedance days. Extending the trajectories further back in time (7-10 days) would illustrate the global nature of ozone transport on all exceedance days by passing over source regions across the entire northern hemisphere, including Asia and Europe. That exercise is captured in the global photochemical modeling presented in Section 3. Focusing on medium-range transport allows for an understanding of the frequency of international transport from international areas within North America - in this case revealing the significance of Mexico as a source region for the NAA. Three-day transport patterns and relative frequencies are consistent whether considering all 160 exceedance days or 84 days with no possible wildfire impacts. When excluding wildfires and possible Mexican transport days in the 2021-2023 DV calculations, peak DVs of 80 ppb are reduced to 69 ppb (attaining the NAAQS) and only a single site (Pinnacle Peak) would remain above the standard at 71 ppb. On average (i.e., across all monitors) the reduction in DV from the exclusion of wildfire and Mexican transport days is 8.4 ppb.

Based on these results, we conclude that international anthropogenic emissions contribute to ozone exceedances in the Maricopa NAA, and the area would have attained the 2015 ozone NAAQS by the Moderate attainment date of August 3, 2024, but for that contribution.

2.0 Conceptual Model

The conceptual model summarized here was developed by MAG and characterizes the environmental factors that lead to high ozone events throughout the April-September ozone season in the Maricopa NAA. It includes information regarding the morphology of the region, ozone concentration and precursor emission patterns, local versus regional meteorology/transport, and wildfire influences. The full MAG ozone conceptual model document is provided in Appendix B of MAG's 2025 Clean Air Act Section 179B(b) Retrospective Demonstration. This section also includes additional analyses developed specifically for this demonstration, characterizing the conditions associated with international transport including a well-developed and referenced conceptual model of transport from Asia to North America as summarized in the published literature.

2.1 The Maricopa Airshed

The Phoenix Metropolitan Area is located in south-central Arizona along the channel and flood plain of the Salt River. In 2023 the Phoenix-Mesa-Chandler metro population was 5.1 million, with 1.65 million in Phoenix. The valley is surrounded by flat desert wastelands and by barren, brush, and eastern forest mountains ranging widely in elevation (Figure 2-1). The elevation of downtown Phoenix is about 350 meters above mean sea level (MSL) and surrounding mountain peaks rise as high as 1,400 meters MSL. Since Phoenix is in the Sonoran Desert, the area experiences a continental summer climate with hot, dry summers dominated by persistent high-pressure systems spanning much of the Intermountain West. With normally dry air with clear skies, the valley experiences intense surface heating during daytime, and radiative cooling during nighttime. The typical daily pattern of mountain/valley up- and down-slope wind flows within the Phoenix Valley are consistently observed during daytime (westerly valley breeze) and nighttime (easterly mountain breeze), regardless of air quality. The topographic obstructions to wind flow at the foot of the eastern mountains are a key factor for air mass convergence and increasing ozone concentrations in the eastern suburbs. In addition, the UHI effect, which affects chemical rates and inter-daily circulation patterns, has increased since 2000 due to rapid urbanization. The area's proximity to the southern US border, along with southerly transport during the mid-summer North American monsoon, result in contributions of background ozone from Mexico.

2.2 Summary of Ozone Air Quality

During the summer season, ozone levels are influenced by meteorological systems operating at multiple scales, including deep vertical mixing caused by stratospheric intrusion and blocking high-pressure systems; lower-level vertical mixing due to the development of daytime turbulence and dissipation of nocturnal inversion layers; local mountain-valley breezes driven by terrain and topographic features; and long-range transport of upwind pollutants from other states and countries. Additionally, strong solar radiation and drier air enhance ozone formation. Ozone exceedances are typically linked to the interaction of these large- and small-scale meteorological systems with local emissions. Note that urban heat flux has shown a strong upward trend since 2000, driven by the rapid growth of urbanization.

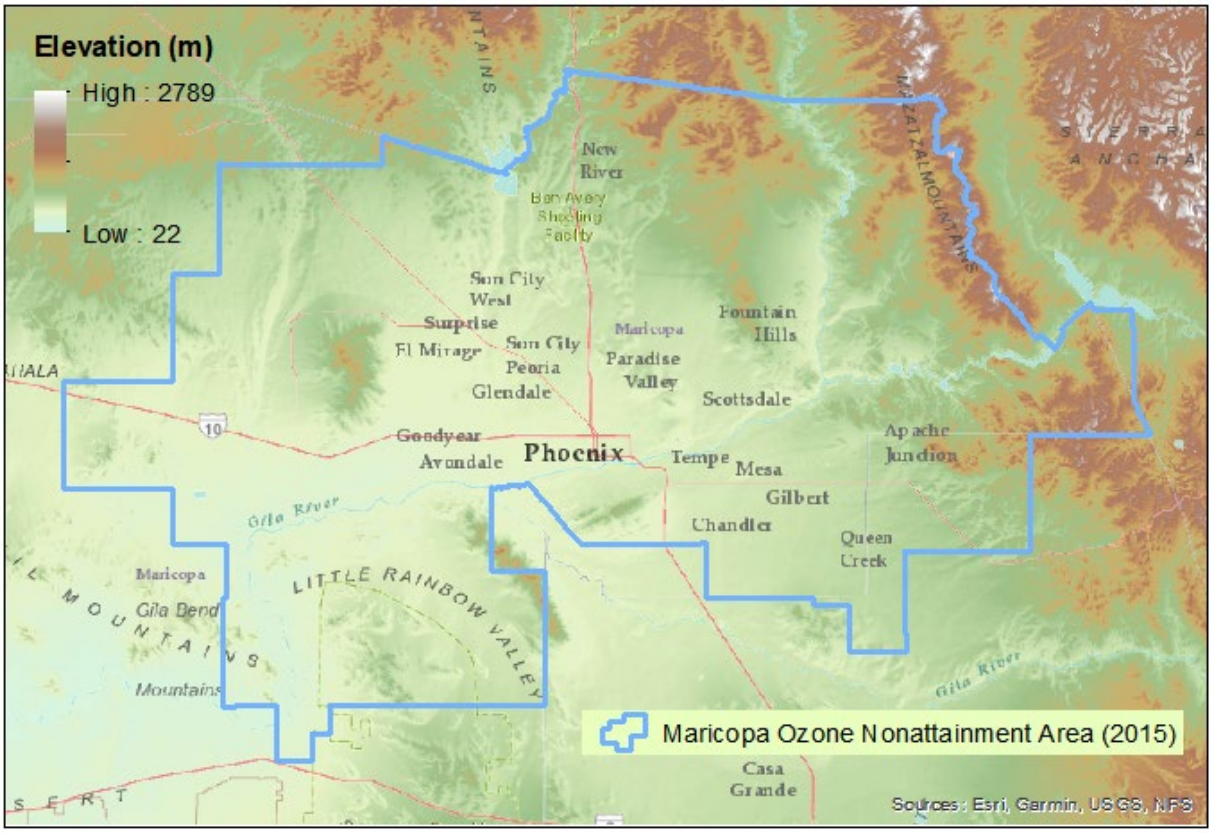

Figure 2-1. Topography within and surrounding the Maricopa NAA for the 2015 ozone standard.

Characteristics of ozone exceedances in the Maricopa NAA:

- Since 2000, extreme weather events in the Southwest, as indicated by the Regional Climate Extremes Index (RCEI), have increased along with the frequency of wildfire events, which are linked to these extreme conditions. The variation in ozone exceedances has mirrored this trend. This suggests that changes in large-scale atmospheric systems are altering regional meteorological conditions, which in turn influence regional ozone levels. These extreme weather patterns, including increased wildfires, exacerbate ozone pollution as smoke and other pollutants contribute to higher concentrations of ozone in the atmosphere.
- The combination and interaction of favorable large- and local-scale systems contribute to extreme ozone concentrations and widespread exceedances across the NAA monitoring sites.
- Monitors with the highest frequency of exceedances are located downwind (east and north) of the urban core.

Key ozone formation factors in the Maricopa NAA:

- Multiple days of intense solar radiation, high temperatures and stagnant conditions, combined with sustained natural and anthropogenic emissions, lead to a photochemical buildup of ozone pollution.
- Daytime temperatures often exceed 100°F, while the UHI effect causes overnight temperatures to remain elevated.

- Sustained valley/mountain breeze circulation pattern traps ozone in basin.
- The inversion layer traps ozone and ozone precursors from the previous day, enhancing ozone concentration due to strong vertical mixing after sunrise.
- Westerly regional and long-range transport patterns bring pollution and wildfire smoke from throughout western North America.
- Frequent long-range transport due to wind shifts during the summer monsoon season brings ozone and ozone precursors from Mexico into the region.
- Stratospheric intrusions contribute to downward transport of ozone-rich air mass from upper levels.
- High-resolution satellite data link summer ozone exceedances to consistently higher NO_2 levels (esp. morning/early afternoon) and reveal profound, distinct impacts of wildfire smoke on NO_2 and formaldehyde (HCHO).

2.3 Ozone and Precursor Monitoring

A network of 26 state and local air monitoring stations (SLAMS) operates within or near the Maricopa NAA (Table 2-1, Figure 2-2). These instruments meet standardized EPA requirements. The operating agencies include the Arizona Department of Environmental Quality (ADEQ), Maricopa County Air Quality Department (MCAQD), Pinal County Air Quality Control District (PCAQCD) and the Salt River Pima-Maricopa Indian Community (SRP-MIC). All sites continuously monitor and report hourly ozone, while a subset also measure the precursors nitrogen dioxide (NO_2), volatile organic compounds (VOC), and/or carbon monoxide (CO). The network also includes a comprehensive list of meteorological measurements, including temperature, humidity, wind speed and direction. One of the locations (JLG Supersite) operates under the Photochemical Assessment Monitoring Stations (PAMS) program and reports measurements of speciated VOC. PAMS sites are required for enhanced monitoring of ozone precursor chemicals in areas with populations over 1,000,000 and with nonattainment designations of Moderate and above. Additional site information is available in MAG's full conceptual model.

Table 2-1. Ozone monitoring sites in the Maricopa NAA.

AQS ID	Site Name	Owning Agency	Elev. (m)	Land Use	Date Established	ID
04-007-0010	Tonto National Monument	ADEQ	786	Desert	1988-04-01	TN
04-013-0019	West Phoenix	MCAQD	333	Residential	1984-01-01	WP
04-013-1003	Mesa	MCAQD	383	Commercial	1976-01-01	ME
04-013-1004	North Phoenix	MCAQD	378	Residential	1968-01-01	NP
04-013-1010	Falcon Field	MCAQD	384	Desert	1989-06-01	FF
04-013-2001	Glendale	MCAQD	350	Residential	1974-01-01	GL
04-013-2005	Pinnacle Peak	MCAQD	733	Residential	1988-02-01	PP
04-013-3002	Central Phoenix	MCAQD	339	Residential	1961-01-01	CP
04-013-3003	South Scottsdale	MCAQD	368	Residential	1973-01-01	SS
04-013-4003	South Phoenix	MCAQD	326	Residential	1999-10-01	SP
04-013-4004	West Chandler	MCAQD	366	Residential	2000-07-01	WC
04-013-4005	Tempe	MCAQD	352	Residential	2000-07-01	TE
04-013-4008	Cave Creek	MCAQD	587	Residential	2001-07-20	CC
04-013-4010	Dysart	MCAQD	359	Commercial	2003-07-01	DY
04-013-4011	Buckeye	MCAQD	258	Agricultural	2004-08-01	BE
04-013-7020	Senior Center	SRP-MIC	377	Residential	2004-05-01	SC
04-013-7021	Red Mountain	SRP-MIC	394	Desert	2002-05-27	RM
04-013-7022	Lehi	SRP-MIC	412	Residential	2003-05-01	LE
04-013-7024	High School	SRP-MIC	366	Residential	2006-03-30	HS
04-013-9508	Humboldt Mountain	MCAQD	1582	Forest	1995-08-01	HM
04-013-9702	Blue Point	MCAQD	436	Desert	1993-01-01	BP
04-013-9704	Fountain Hills	MCAQD	505	Residential	1996-04-01	FH
04-013-9706	Rio Verde*	MCAQD	478	Residential	1997-01-01	RV
04-013-9997	JLG Supersite	ADEQ	346	Residential	1993-07-01	JLG
04-021-3001	Apache Junction	PCAQCD	525	Commercial	1987-01-01	AJ
04-021-8001	Queen Valley	ADEQ	634	Desert	2001-01-01	QV

* Rio Verde has not monitored since 2017 and is included for historical trends.

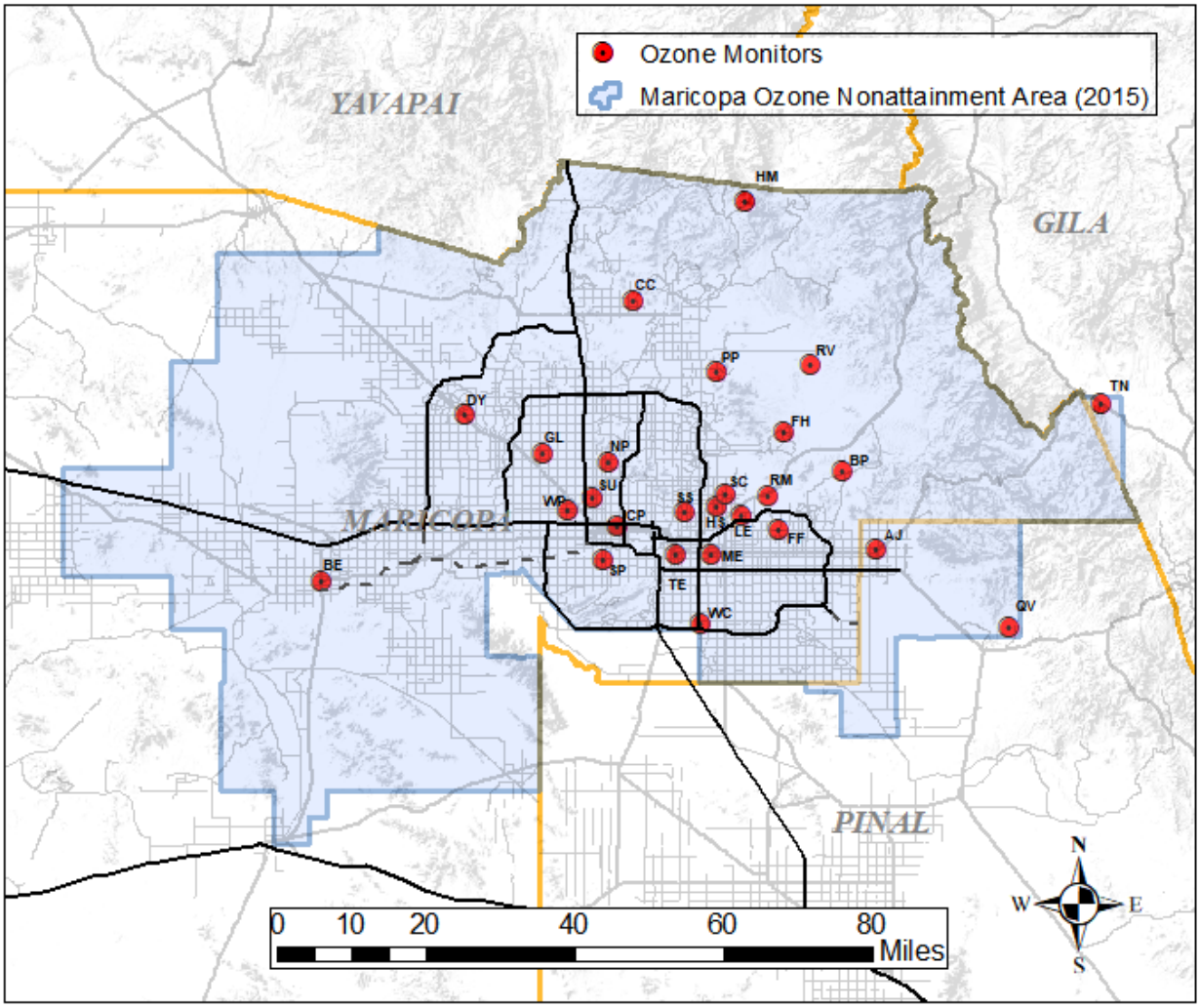

Figure 2-2. Ozone monitoring stations in the Maricopa NAA.

Figure 2-3 presents the annual peak 8-hour ozone DVs in the Maricopa NAA from 2000 through 2024 from MAG's full conceptual model, as well as the regressed DV trendlines. Although the annual peak DV has recently increased since 2017, the 25-year trendline shows a decrease of 0.3 ppb per year. When all possible wildfire-impacted days identified by MAG are excluded from the annual DV calculations since 2017, the associated DV trend from 2017 through 2024 flattens and the 25-year trendline improves to 0.5 ppb per year.

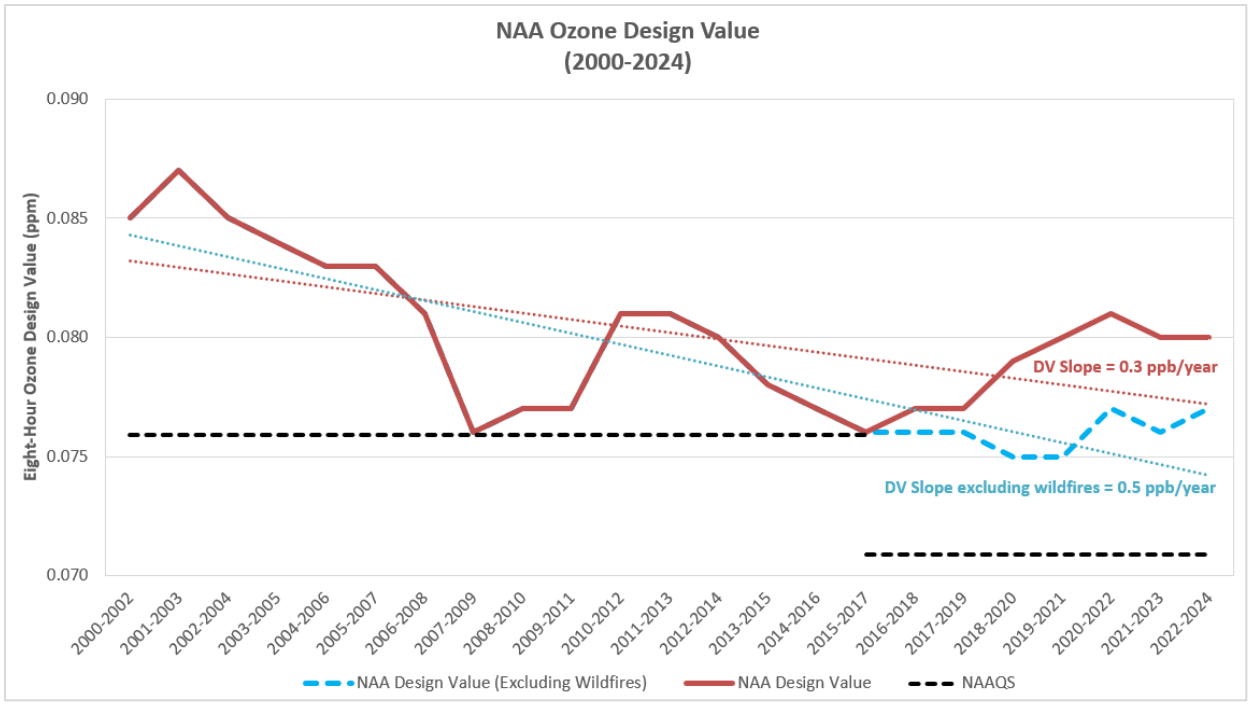

Figure 2-3. Peak 8-hour ozone DVs in the Maricopa NAA from 2000 through 2024 (taken from MAG's full conceptual model).

Figure 2-4 shows the 8-hour ozone design values at each of the 26 ozone monitors in the Maricopa NAA from 2000 to 2024 from MAG's full conceptual model. Since 2000, annual peak DVs have occurred at the following eight sites: North Phoenix (11 times), Pinnacle Peak (7 times), Mesa (5 times), Humboldt Mountain (4 times), JLG Supersite (2 times), Red Mountain (2 times), Glendale (1 time), Lehi (1 time), and Rio Verde (1 time). Excluding all possible wildfire-impacted days from the design value calculation since 2017, annual peak design values have occurred at the following seven sites: North Phoenix (9 times), Mesa (6 times), Humboldt Mountain (4 times), Pinnacle Peak (3 times), Red Mountain (2 times), Falcon Field (2 times), Lehi (2 times), JLG Supersite (1 time), South Scottsdale (1 time), and Rio Verde (1 time). Buckeye has consistently recorded the regional minimum design values. Among the 14 ozone monitors operating for the entire period of 2000-2024, Humboldt Mountain had the largest ozone decrease of 12 ppb and JLG Supersite had an ozone increase of 2 ppb. Excluding all possible wildfire-impacted days since 2017, Humboldt Mountain had the largest ozone decrease of 16 ppb and JLG Supersite had the smallest ozone decrease of 2 ppb.

a)

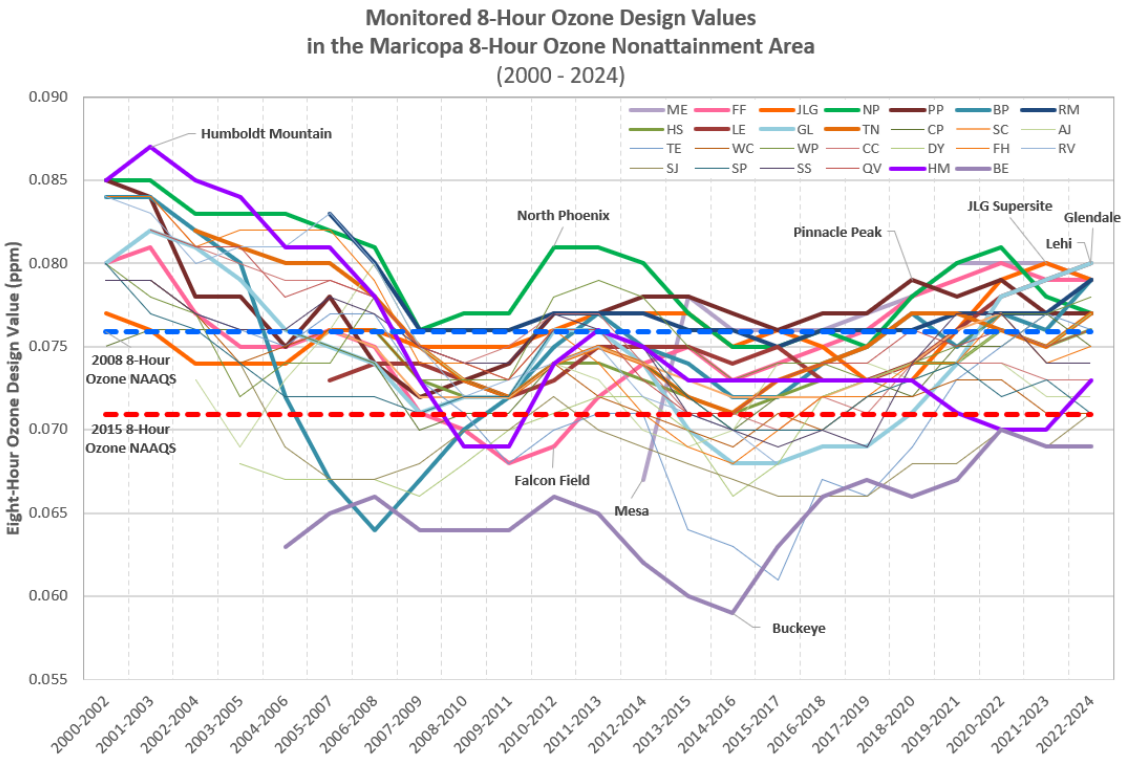

b)

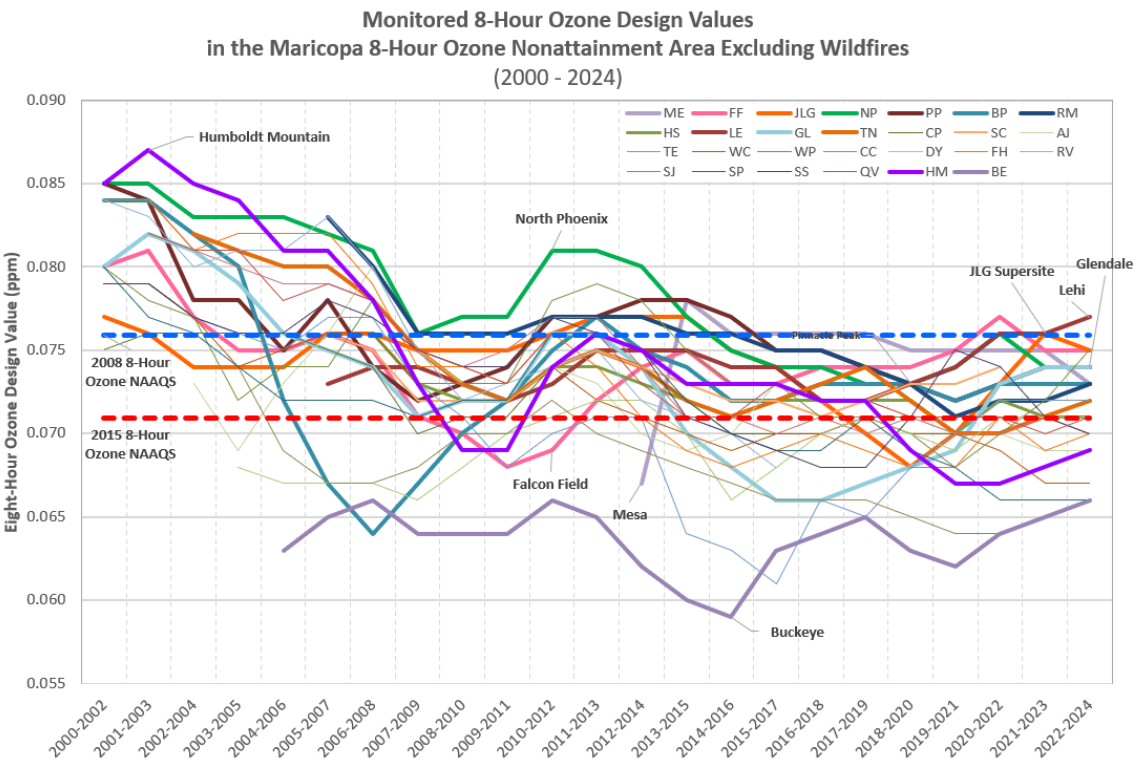

Figure 2-4. 8-hour ozone DVs at monitors in the Maricopa NAA from 2000 through 2024, for (a) all days and (b) excluding all exceedance days possibly impacted by wildfires since 2017 (taken from MAG's full conceptual model).

Due to continuous reductions in anthropogenic emissions from federal and local control measures, and disregarding all possible wildfire impacted exceedance days since 2017 (as determined by MAG), the number of ozone exceedance days (MDA8 ozone above 70 ppb)

recorded by at least one monitoring site in the Maricopa NAA has decreased over the past 25 years (Figure 2-5). However, including all possible wildfire impacted days, the recent trend shows a marked increase since 2017. The number of exceedances was highest in 2000 and lowest in 2009 during the last major recession and again in 2020 during the COVID-19 pandemic. Splitting the record into five averaging periods (5 years each; Figure 2-6) reveals a clear downward trend. Comparing 2000-2004 averages with 2020-2024 averages, the number of exceedances has decreased by 62%.

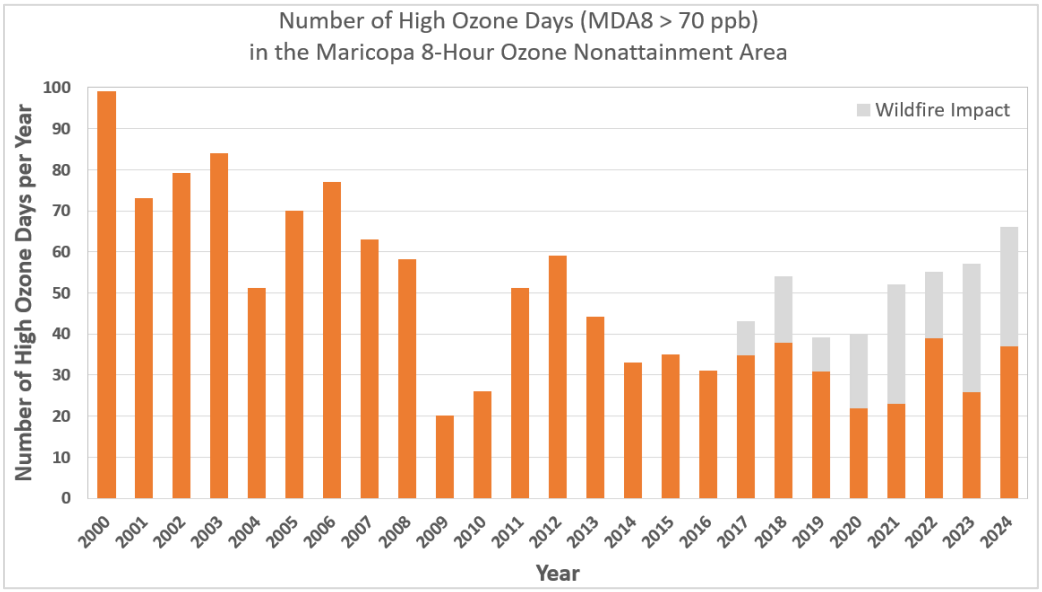

Figure 2-5. Number of 8-hour ozone exceedance days (MDA8 ozone above 70 ppb) in the Maricopa NAA from 2000 through 2024.

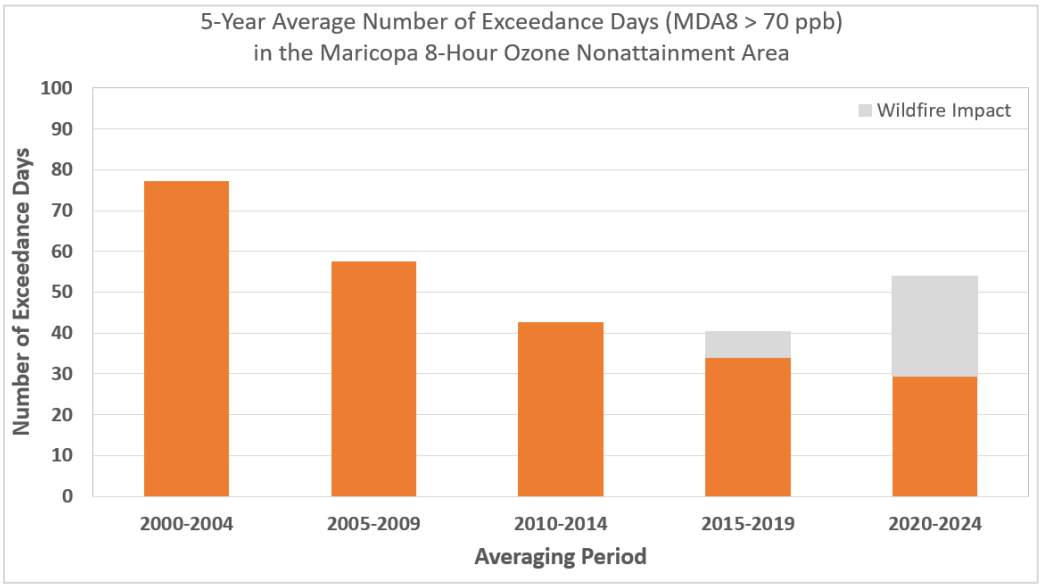

Figure 2-6. Five-year average number of ozone exceedance days (MDA8 ozone above 70 ppb) in the Maricopa NAA from 2000 to 2024.

2.4 Additional Conceptual Elements for the 179B Demonstration

2.4.1 Exceedances during the 2021-2023 DV Period

The three years spanning 2021-2023 comprise the 2023 DV period and thus represent conditions during the latest monitoring period that failed to attain the 2015 ozone NAAQS by the Moderate attainment date of August 3, 2024. This section examines the number of ozone exceedance days and the 4th highest MDA8 ozone concentrations (H4MDA8) in 2021–2023 at all Maricopa NAA monitors, with and without all 76 possible wildfire smoke impacted days as provided by MAG (29 in 2021, 16 in 2022, 31 in 2023). The list of 76 wildfire smoke impacted days (Table 2-2) was developed through a collaborative effort between meteorologists and air quality experts at the ADEQ, MAG, MCAQD, and PCAQCD. The 76 wildfire smoke impacted days shown in Table 2-2 do not necessarily represent every exceedance day when smoke impacts were possible, but rather they represent days when the collaborative group agreed evidence existed (presence of smoke, elevated atypical concentrations, etc.) to indicate wildfire smoke and associated ozone precursor emissions impacted nonattainment area monitors. For photochemical modeling purposes and in accordance with EPA guidance, MAG selected 31 wildfire-impacted exceedance days out of the 76 identified days as those to be considered "atypical events" and therefore excluded from modeling exercises. The 31 days were selected for exclusion as atypical events due to their significant impact on the 2021-2023 design value. Evidence for excluding the 31 selected days is provided in Appendix C of the MAG 2025 Clean Air Act Section 179B(b) Retrospective Demonstration.

Removing all possible wildfire days leads to a set of "typical" exceedance days that represent no possible fire influences, i.e., caused by a normal mix of natural and anthropogenic precursors from local, regional, and international sources. These ozone metrics form the basis from which to analyze international transport impacts on ozone concentrations in the Maricopa NAA.

Figure 2-7 presents the number of ozone exceedance days each year at each of the Maricopa NAA ozone monitors. The total number of measured exceedance days are presented as a stacked bar where exceedance days associated with wildfire smoke (grey) are placed above the number of exceedance days that were not impacted by wildfire smoke (orange). The total number of exceedances is over 30 days per year for some years and monitors. Excluding all possible wildfire smoke days, the typical number of exceedances ranges up to 15 days per year at most sites. Averaging over the three years and all monitors reveals that most exceedance days were associated with possible wildfire impacts. Considering only the highest impacted sites, nearly 60% of exceedances are associated with possible wildfire impacts.

Figure 2-8 presents the H4MDA8 each year at each of the Maricopa NAA ozone monitors. The contributions associated with wildfire smoke (grey) are stacked above the contributions on non-smoke days (orange) to show the total H4MDA8. Excluding all possible wildfire impacted days reduces the number of monitor-years with H4MDA8 exceeding the NAAQS from 68 to 40. The average reduction in H4MDA8 when excluding all possible wildfire days is approximately 5 ppb. Nevertheless, even with all possible wildfire days removed, 2021-2023 DVs at several monitors continue to exceed the 2015 ozone NAAQS by a few ppb. This analysis does not consider international contributions to the H4MDA8 values, which are assessed in the following sections.

Table 2-2. Possible wildfire-impacted ozone exceedance dates occurring in 2021-2023 (from Appendix B of the MAG's 2025 Clean Air Act Section 179B(b) Retrospective Demonstration). Shaded bold dates represent the subset of 31 atypical wildfire days recommended for exclusion from modeling due to their importance to design value calculations.

2021	2022	2023
6/11/2021	4/25/2022	5/14/2023
6/12/2021	4/26/2022	5/15/2023
6/15/2021	4/29/2022	5/16/2023
6/16/2021	4/30/2022	5/21/2023
6/18/2021	**6/15/2022**	6/17/2023
6/28/2021	**6/16/2022**	**6/22/2023**
6/29/2021	6/21/2022	**6/23/2023**
7/1/2021	6/22/2022	**6/24/2023**
7/13/2021	7/13/2022	**6/25/2023**
7/14/2021	7/14/2022	**6/26/2023**
7/17/2021	**7/15/2022**	**6/30/2023**
7/19/2021	**7/16/2022**	7/1/2023
7/20/2021	**7/17/2022**	7/2/2023
7/21/2021	7/18/2022	7/7/2023
7/22/2021	7/22/2022	7/8/2023
7/27/2021	7/23/2022	7/18/2023
7/28/2021		7/19/2023
7/30/2021		7/21/2023
7/31/2021		7/22/2023
8/3/2021		7/23/2023
8/4/2021		**7/24/2023**
8/5/2021		**7/25/2023**
8/6/2021		**7/26/2023**
8/17/2021		**7/27/2023**
8/24/2021		**7/28/2023**
8/25/2021		**7/29/2023**
8/26/2021		**7/31/2023**
8/27/2021		**8/1/2023**
9/5/2021		**8/17/2023**
		8/18/2023
		8/22/2023

Figure 2-7. Number of ozone exceedance days in 2021 through 2023 at each of the Maricopa NAA ozone monitors, considering all possible wildfire days (grey) and non-wildfire days (orange).

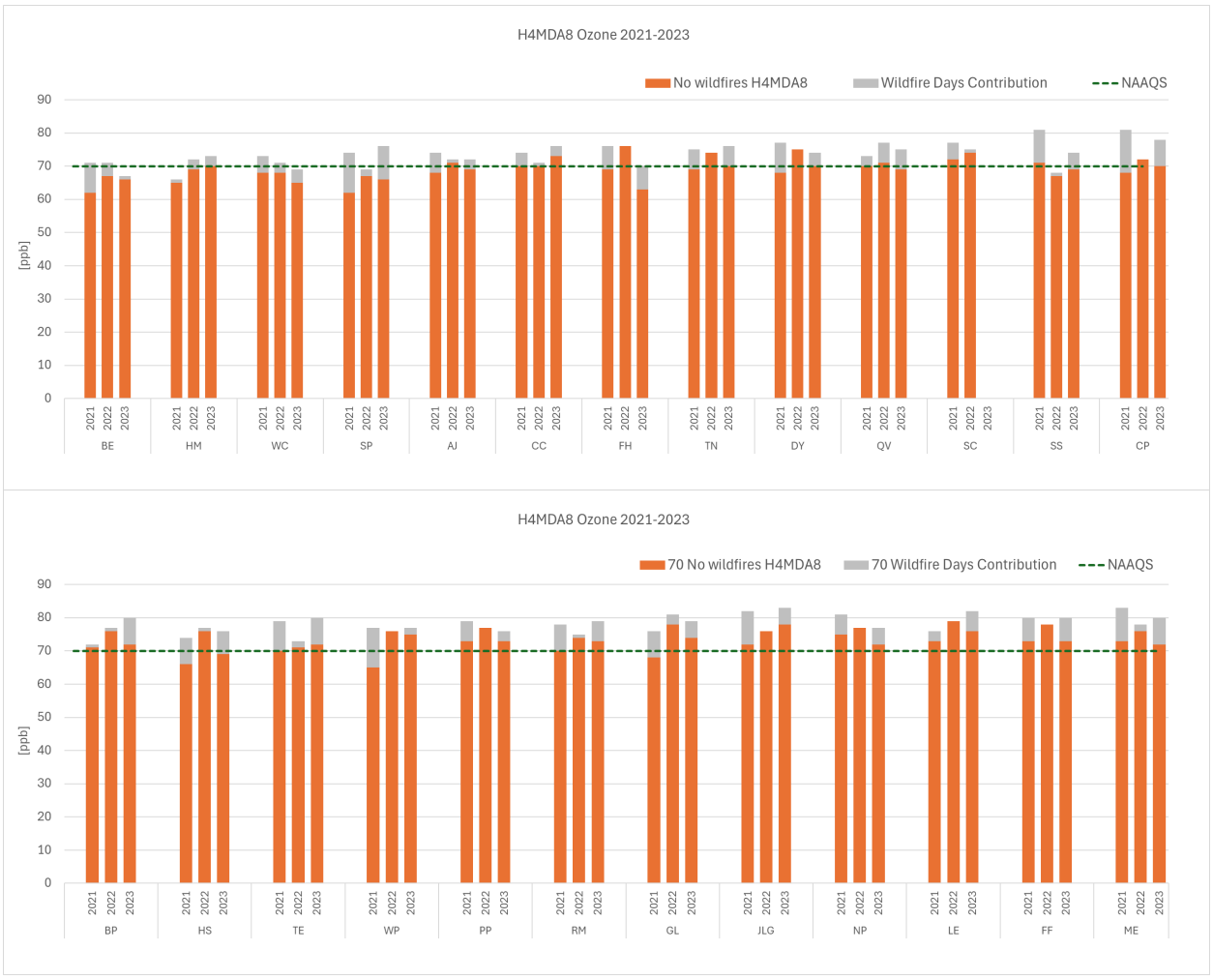

Figure 2-8. Annual 4th high MDA8 ozone in 2021 through 2023 at each of the Maricopa NAA ozone monitors considering contributions from all possible wildfire days (grey) and non-wildfire days (orange).

2.4.2 Vertically Integrated Wind Roses

This section presents an analysis of local vertically-integrated winds based on radiosonde data to assess prevailing flow within the atmospheric depth representative of the typical summer boundary layer over southern Arizona. The analysis is presented in the form of wind rose diagrams, populated with wind data during each of the 2021-2023 exceedance days.

Soundings above Phoenix and Tucson (Table 2-3) were obtained from the Integrated Global Radiosonde Archive version 2 (IGRA v2.2).[2] Tucson was selected since it is an intermediate location between Mexico and Phoenix. Globally, weather balloons are launched twice daily, typically at 00:00 UTC and 12:00 UTC. For Arizona, the sounding launches occur at 5:00 AM and 5:00 PM MST. The 5:00 AM measurements, representing flow into the basin prior to an exceedance day, are more relevant than the 5:00 PM measurements that represent flow out of the basin after most ozone is formed. Therefore, the analysis is based on the 12:00 UTC (5:00 AM MST) measurements only. In addition, we consider winds up through 700 hPa (approximately 3,000 meters or 10,000 feet above sea level) to represent typical boundary layer depths and to limit terrain influences.

Table 2-3. Phoenix and Tucson sounding parameters.

City	Station ID	Latitude (degrees N)	Longitude (degrees W)	Elevation (meters)
Phoenix	USM00074626	33.4500	-111.9500	386.0
Tucson	USM00072274	32.2278	-110.9558	751.4

Figure 2-9 displays vertically-integrated wind rose diagrams for Phoenix (upper) and Tucson (lower) during 2021-2023 exceedance days in Phoenix. Wind roses are remarkably consistent and show a predominantly east-southeast morning wind pattern. The number of available soundings that are included in the wind roses on all exceedance days represent a robust dataset from a statistical standpoint: 112 days and 147 for Phoenix and Tucson, respectively. These numbers reduce to 48 and 76, respectively, when all possible wildfire impacted days are removed. Note that the Phoenix wind rose on non-wildfire impacted exceedance days shows a much stronger frequency for southeast winds than the Tucson data. The figures also report the percentage of days with boundary layer winds that could potentially transport emissions from Mexico to the Maricopa NAA (i.e., West through South through East). Regardless of site or number of days, the percentage of days with potential transport from the direction of Mexico is roughly 75%. This shows that most exceedance days are associated with morning transport from the south. Note that exceedance days with southerly transport may include contributions from international sources beyond Mexico, which are not addressed by this type of analysis and will be quantified by source apportionment modeling in Section 3.

2 https://www.ncei.noaa.gov/data/integrated-global-radiosonde-archive/access/data-y2d/

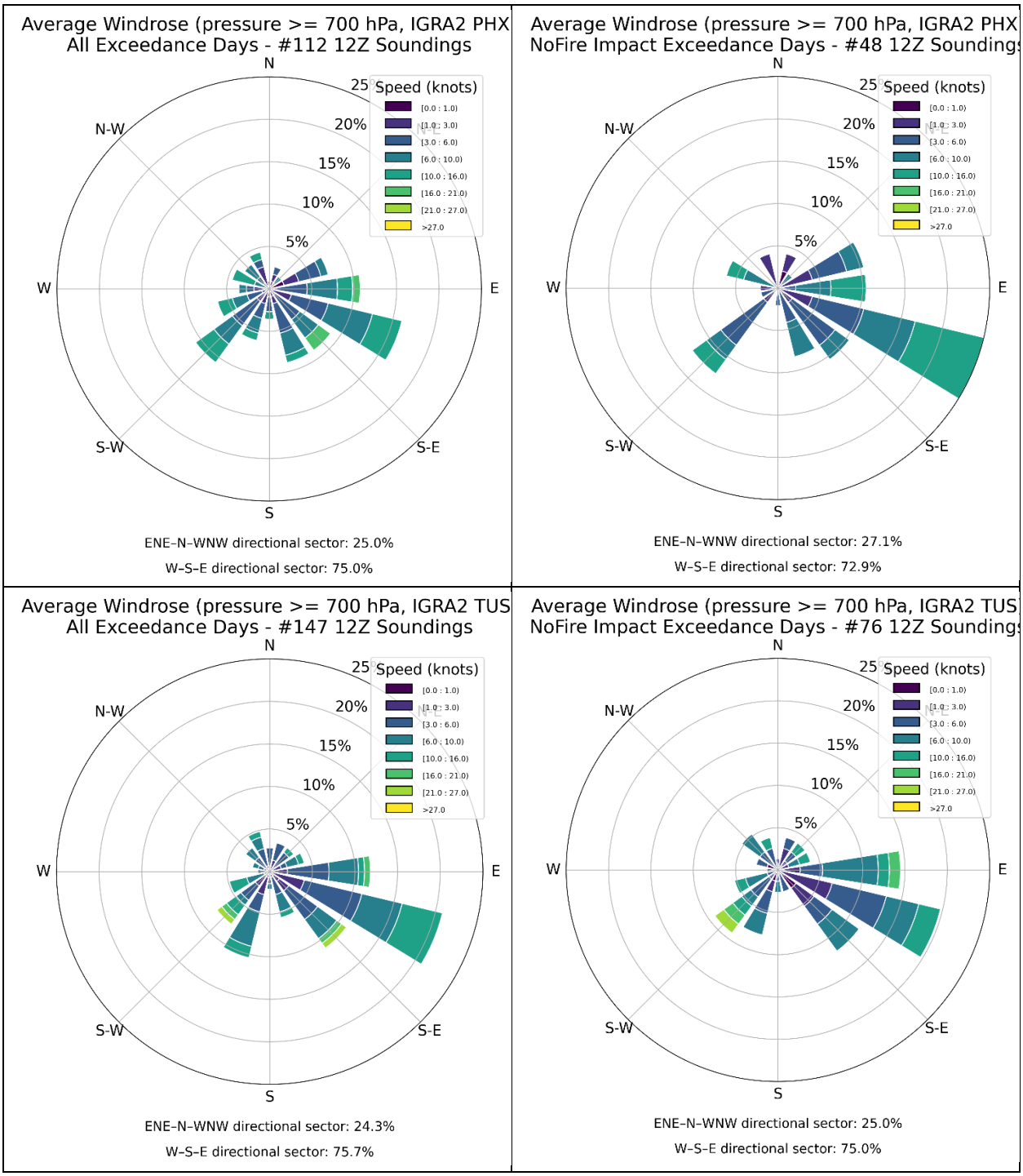

Figure 2-9. Vertically integrated wind roses for Phoenix (upper) and Tucson (lower) during all monitored exceedance days (left) and no wildfire impacted days (right) during the 2021-2023 ozone seasons.

2.4.3 Transport of International Emissions

As a summer phenomenon, ozone episodes in the Maricopa NAA coincide with the seasonal North American monsoonal circulation pattern. This lower-level atmospheric flow pattern brings humid air northward from Mexico into the Sonoran Desert and Great Basin states during July and August. This establishes a common transport corridor for pollutants emitted in Mexico to rapidly reach the Maricopa NAA. However, there is another common transport pattern in the mid to upper atmosphere linking Asia to the western US, which is a more significant source of IA contributions during the late spring through early summer.

As summarized from HTAP (2010), seasonally persistent global circulation patterns establish a direct transport route within the upper troposphere that brings pollutant-laden air from Asia to North America within days to weeks (Figure 2-10). Over eastern Asia, a persistent low-pressure trough lofts air and associated pollutants to the upper troposphere. While rapidly transported across the Pacific, the chemical lifetimes of ozone and peroxyacetyl nitrate (PAN, an ozone precursor) increase because low temperatures minimize destruction (Jiang et al., 2016). Sinking air within the persistent high-pressure dome over the western US brings transported ozone and PAN toward the surface, while complex topography and deep boundary layer mixing enhances vertical transport (Zaveri et al., 1995). Thus, high-altitude locations throughout the western US experience the greatest ozone impacts from intercontinental transport. This transport mechanism is especially persistent throughout the summer season.

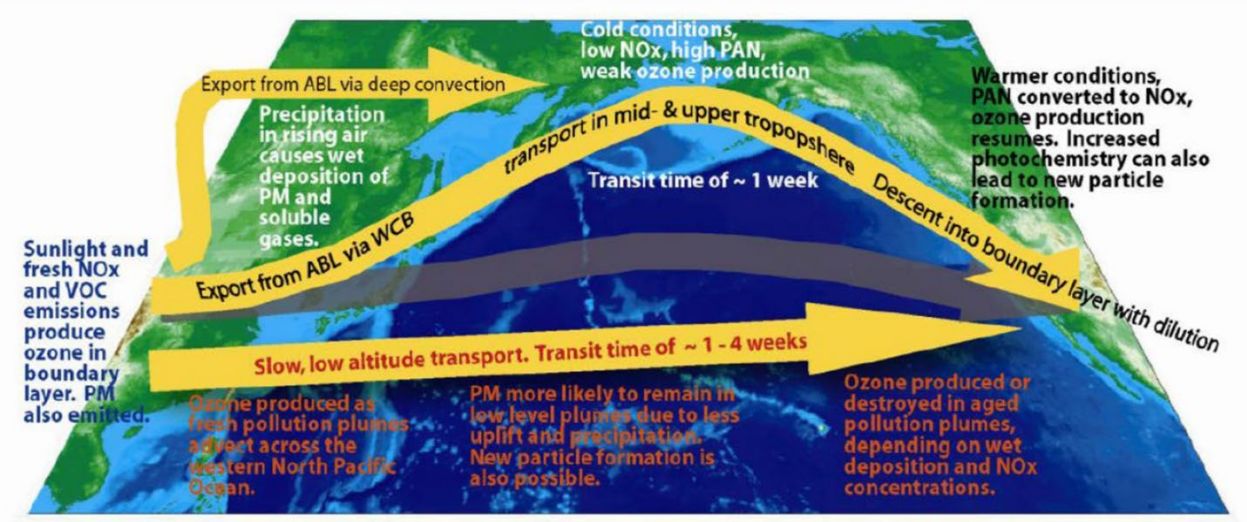

Figure 2-10. Schematic conceptual model of pollutant transport from Asia to North America (from HTAP, 2010). Blue text on left refers to Asian continental boundary layer processes, red text along bottom refers to low level transport, and black/white text along top and right refers to high altitude transport.

Baker et al. (2015) and Zhang et al. (2020) employed different modeling techniques that assessed and confirmed the importance of deep vertical transport of global ozone from the middle and upper troposphere to the western US. Interestingly, both studies referenced above show that summer surface background ozone often peaks over the Intermountain West because of sinking motion from the mid-troposphere (Figures 2-11 and 2-12) and circulations induced by elevated topography. This pattern is also consistent with other literature (Langford et al., 2017; Mathur et al., 2022).

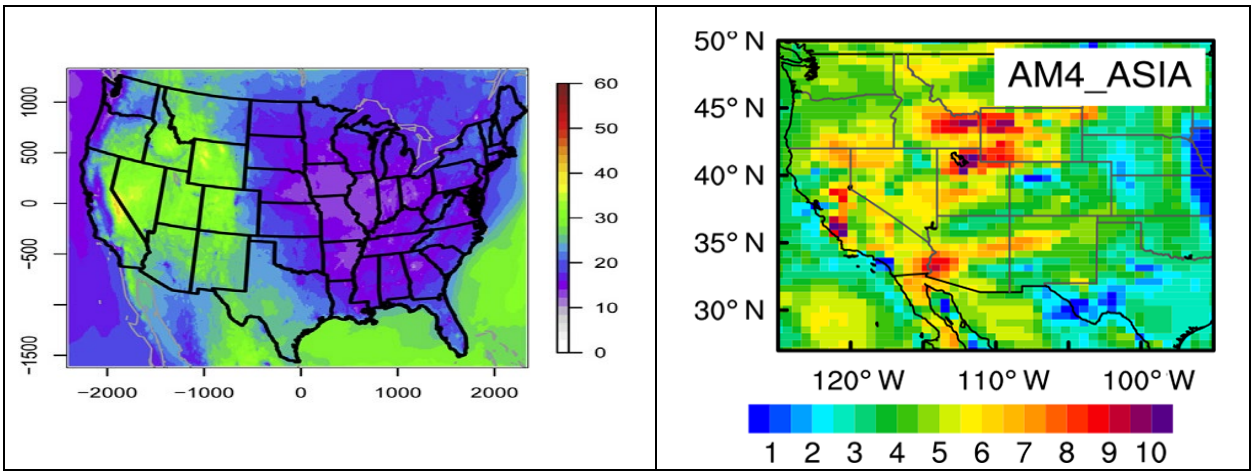

Figure 2-11. Examples of modeled surface background ozone (ppb) from Baker et al. (2015; left) showing July 2011 average US background from the CAMx regional photochemical model, and from Zhang et al. (2020; right) showing tracked ozone from Asia on May 24, 2017 from the AM4 global model.

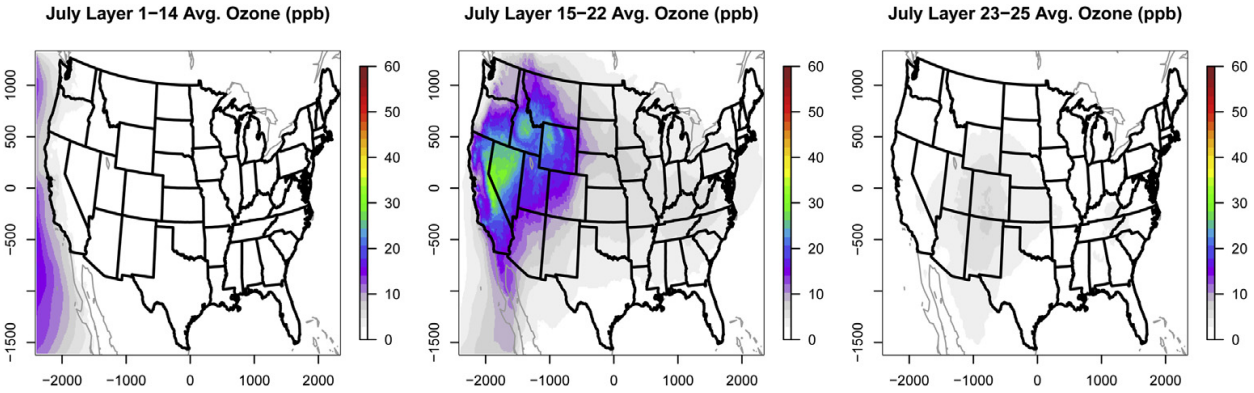

Figure 2-12. Results from Baker et al. (2015) showing examples of US background ozone contribution (ppb) from the western CAMx boundary and from three sets of vertical model layers; boundary layer (left), mid troposphere (middle), stratosphere (right).

There is extensive research linking decadal increases in Asian emissions to intercontinental transport. During the 1990s and 2000s, Asian NOx emissions increased quickly (van der A et al., 2017) along with transported ozone (Verstraeten et al., 2015; Lin et al., 2017). Numerous other studies (Huang, et al., 2017; Nopmongcol et al., 2017) have estimated resulting ozone transport to North America up through 2010. While Jaffe et al. (2018) present a consensus from the literature that Asian transport had peaked around 2010, a recent multi-decadal trend analysis through 2021 (Chang et al., 2023, and references therein) indicates that free tropospheric ozone over western North America continues to increase despite a decreasing trend in boundary layer ozone, affirming vertically different sources and mechanisms.

In summary, there is overwhelming evidence from more than a decade of scientific literature that transport of ozone from Asia has raised background ozone levels in the western US. According to numerous modeling analyses presented in the literature, the atmosphere over the western US represents an area of consistently maximum impact from this phenomenon given climatological presence of summertime high pressure with sinking motions and enhanced vertical circulations induced by complex terrain. Therefore, it is

expected that Asian emissions, along with other sources throughout the northern hemisphere, impact NAA ozone concentrations by raising background ozone and ozone precursors entering western North America.

3.0 Modeling to Quantify International Contribution

MAG employed the Comprehensive Air quality Model with extensions (CAMx; Ramboll, 2024) and the Community Multiscale Air Quality (CMAQ; EPA, 2025a) model to support the Clean Air Act (CAA) §179B(b) retrospective demonstration for the Maricopa NAA. Both models simulate ozone air quality over southwestern North America during the 2023 summer ozone season. MAG uses the CAMx Ozone Source Apportionment Technology (OSAT) to quantify local, regional, and international/global contributions to ozone concentrations within the NAA. A complete description of the development of MAG's modeling datasets is available in Appendix B of MAG's 2025 Clean Air Act Section 179B(b) Retrospective Demonstration.

3.1 EPA Recommended Ozone Design Value Projection Procedure

EPA photochemical modeling guidance details procedures on using modeling results to project responses to monitored ozone DV – referred to as a "modeled attainment test". EPA has developed the Software for Model Attainment Test - Community Edition (SMAT-CE; EPA, 2025b) that codifies the recommended procedures as outlined in Chapter 4 of EPA's modeling guidance (EPA, 2018, pages 99-110). Model output from a reference or "base" case and an emission scenario are used in a relative sense to scale the base ozone DV (DVB) to the scenario ozone DV (DVS) at each monitoring site. Note that usually the emission scenario represents a future year emissions projection, but it can equally represent effects from removing ozone contributions in the same year. The model-derived Relative Response Factor (RRF) is defined individually at each monitoring site as the ratio of average scenario MDA8 ozone concentration ($O3_S$) to the average base MDA8 ozone concentrations ($O3_B$), where the average is over the same set of several modeled high ozone days in the base case. This is expressed mathematically below:

$$DVS = DVB \times RRF$$

$$RRF = \Sigma(O3_S) / \Sigma(O3_B)$$

The site-specific DVB is defined as the three-year average ozone DV centered on the base modeling year. As each year's DV is itself defined as the three-year average of the 4th highest MDA8 ozone concentration each year (H4MDA8), the DVB is thus based on 5 years of H4MDA8 ozone concentrations centered on the base year, such that the central year is weighted by a factor of 3/9, the 2nd and 4th years are each weighted by a factor of 2/9, and the 1st and 5th years are each weighted by a factor of 1/9. This approach accounts for interannual variability affecting DVs in and around the base year. The Maricopa NAA modeled base year is 2023 so the DVB at each site would normally be defined from five years of H4MDA8 ozone spanning 2021 through 2025. As 2025 data are not complete, we assigned DVB to the single 2023 DV period (i.e., H4MDA8 spanning 2021 through 2023). DVS values were determined by removing IA source contributions from total simulated ozone in the numerator of the RRF calculation.

The RRF is determined from maximum MDA8 ozone concentrations near each monitor, averaged over 10 days with the highest base year modeled MDA8 ozone concentrations.

Near the Monitor: This means that the highest modeled base MDA8 ozone is selected from one of a 3x3 array of grid cells centered on the monitor. The scenario MDA8 ozone is selected from the same grid cell of the 3x3 array.

10 Highest Base Year MDA8 Ozone Days: Modeled MDA8 ozone concentrations are averaged over 10 days with the highest base modeled ozone concentrations near the monitor, provided MDA8 ozone on the chosen days are each ≥60 ppb. If there are less than 10 days meeting this criterion, then only the days meeting this criterion are used in the average,

provided there are at least 5 days available for the RRF calculation. If there are less than 5 days meeting this criterion, EPA recommends that RRFs not be calculated for the given site and the regional EPA office should be consulted if the site is an important high DV site.

3.2 Source Apportionment Modeling

The MAG modeling platform consists of a set of three nested grids, with the largest domain covering southwestern North America at 36 km horizontal resolution, an Arizona domain at 12 km resolution, and the finest resolution covering the Maricopa NAA at 4 km resolution (Figure 3-1). All nested domains resolve the atmosphere in 23 layers spanning from the surface up to the tropopause. The modeling period extends over the 2023 summer ozone season. The modeling system includes requisite three-dimensional meteorological fields for all grids developed using the Weather Research and Forecasting (WRF) model, as well as all anthropogenic, biogenic, and fire emission inventories within the domain developed using the Sparse Matrix Operator Kernel Emissions (SMOKE) processing system. Three-dimensional initial/boundary conditions (IC/BC) for the master domain were developed from Ramboll's application of the GEOS-Chem global chemistry model for the 2023 year. The GEOS-Chem runs included: (1) a full representation of ozone, particulate matter, precursors, and products from the entire globe, and (2) a scenario in which all IA emissions were removed. OSAT uses time- and space-resolved BC concentration differences between the two global model scenarios to track the global IA contributions to total simulated ozone at NAA monitors.

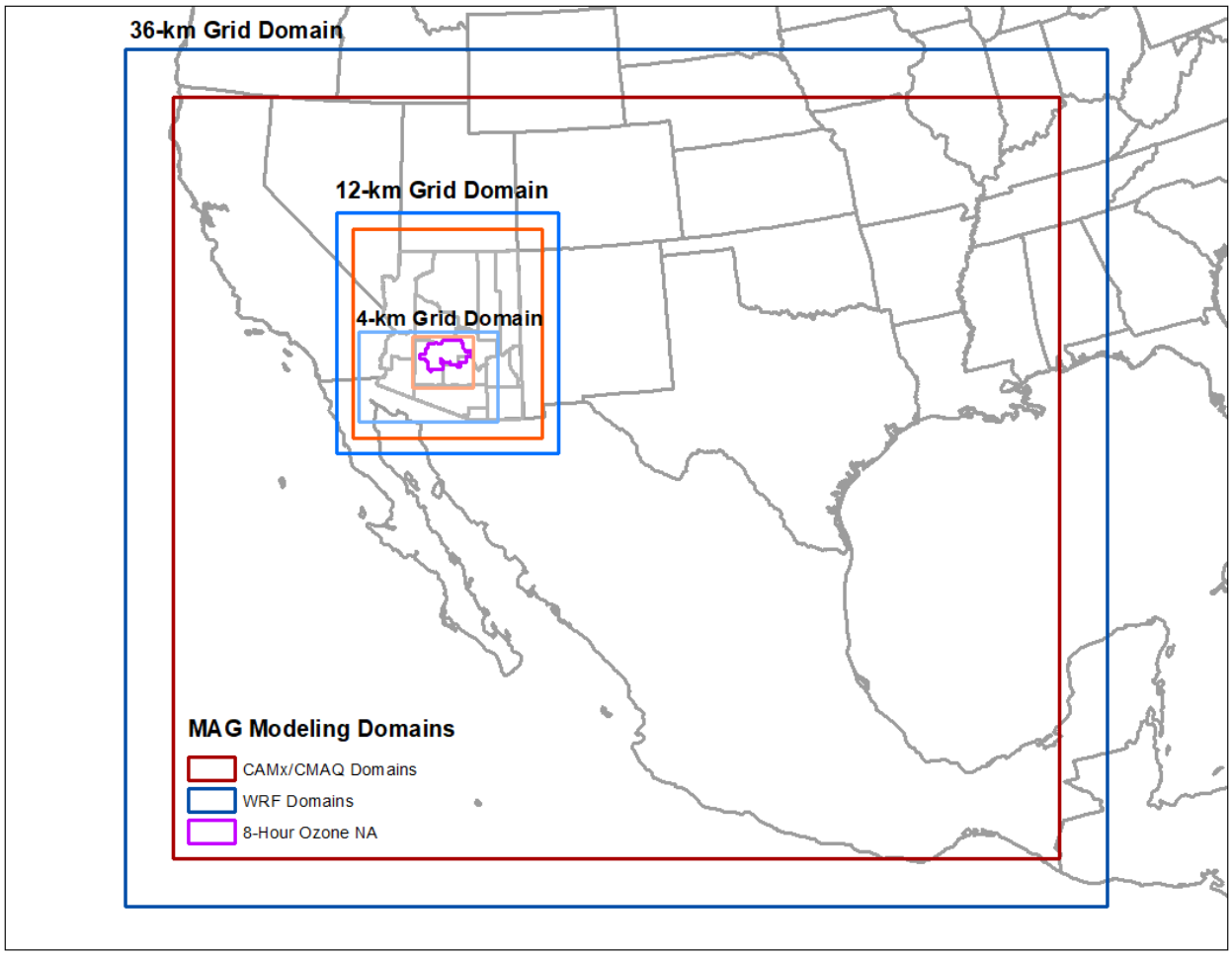

Figure 3-1. Map of nested CAMx modeling domains for the MAG ozone modeling platform.

3.2.1 Model Configuration

CAMx version 7.32 was applied on the 36/12/4 km grid system for the base year 2023 scenario. The Carbon Bond version 7 revision 1 (CB7r1) gas-phase chemical mechanism was selected to be consistent with MAG's modeling.

OSAT uses reactive tracers assigned to each selected source group and region to determine precursor and ozone contributions across the modeling domain. These reactive tracers operate in parallel to the host photochemical grid model, accessing the model's transport, dispersion, chemistry, and deposition algorithms. There are 10 reactive tracers used to track ozone formation for each user-defined source group (i):

VOCi	VOC emissions
NITi	Nitric oxide (NO) and nitrous acid (HONO) emissions
RGNi	Nitrogen dioxide (NO_2), nitrate radical (NO_3), and dinitrogen pentoxide (N_2O_5)
TPNi	Peroxyacetyl nitrate (PAN), analogues of PAN, and peroxynitric acid (PNA)
NTRi	Organic nitrates (RNO_3)
HN3i	Gaseous nitric acid (HNO_3)
O3Ni	Ozone formed under NOx sensitive conditions
O3Vi	Ozone formed under VOC sensitive conditions
OONi	Odd oxygen in NO_2 formed from O3Ni
OOVi	Odd oxygen in NO_2 formed from O3Vi

At each time step and grid cell where ozone is formed, OSAT determines whether the ozone formation is more VOC-sensitive or NOx-sensitive and apportions the ozone formed to source groups based on the relative contribution of the limiting precursor to the total precursor (e.g., to VOC_i/ $\sum VOC_i$ under VOC sensitive conditions). Applying OSAT for 2023 allows us to quantify IA impacts on simulated MDA8 ozone during the Moderate attainment year. Three emission sector groups were tracked by OSAT (Table 3-1). This is sufficient to track the IA contributions along with anthropogenic, natural, and fire sources. OSAT tracked two source apportionment IC and BC groups: one group represents global IA ozone and precursors and the other represents global natural and US emissions. Three geographic regions were defined in OSAT, namely the Maricopa NAA, the rest of the US including 200 km territorial waters, and Mexico. Each region is defined specifically at the resolution of each modeling grid (Figures 3-2 through 3-4). This configuration results in 130 individual tracers ([3 sectors x 3 regions + 4 IC/BC] x 10 ozone-related chemical tracers). The sum of O3N and O3V tracers for anthropogenic Mexico emissions and IC/BC IA represent the total international contribution from international emissions for the purposes of this 179B(b) demonstration.

Table 3-1. CAMx source apportionment emission sector groups.

OSAT Group ID	Group Name	Description
1	Anthropogenic	All anthropogenic emissions within the modeling domain
2	Biogenic + Lightning	All biogenic and lightning emissions within the modeling domain
3	Fires	Wildfire, agricultural, and prescribed fire emissions within the modeling domain
IC/BC 1	International Anthropogenic	Non-US anthropogenic emissions based on zero-out GEOS-Chem simulations
IC/BC 2	Global Natural + US Anthropogenic	Global natural emissions plus US anthropogenic emissions based on zero-out GEOS-Chem simulations

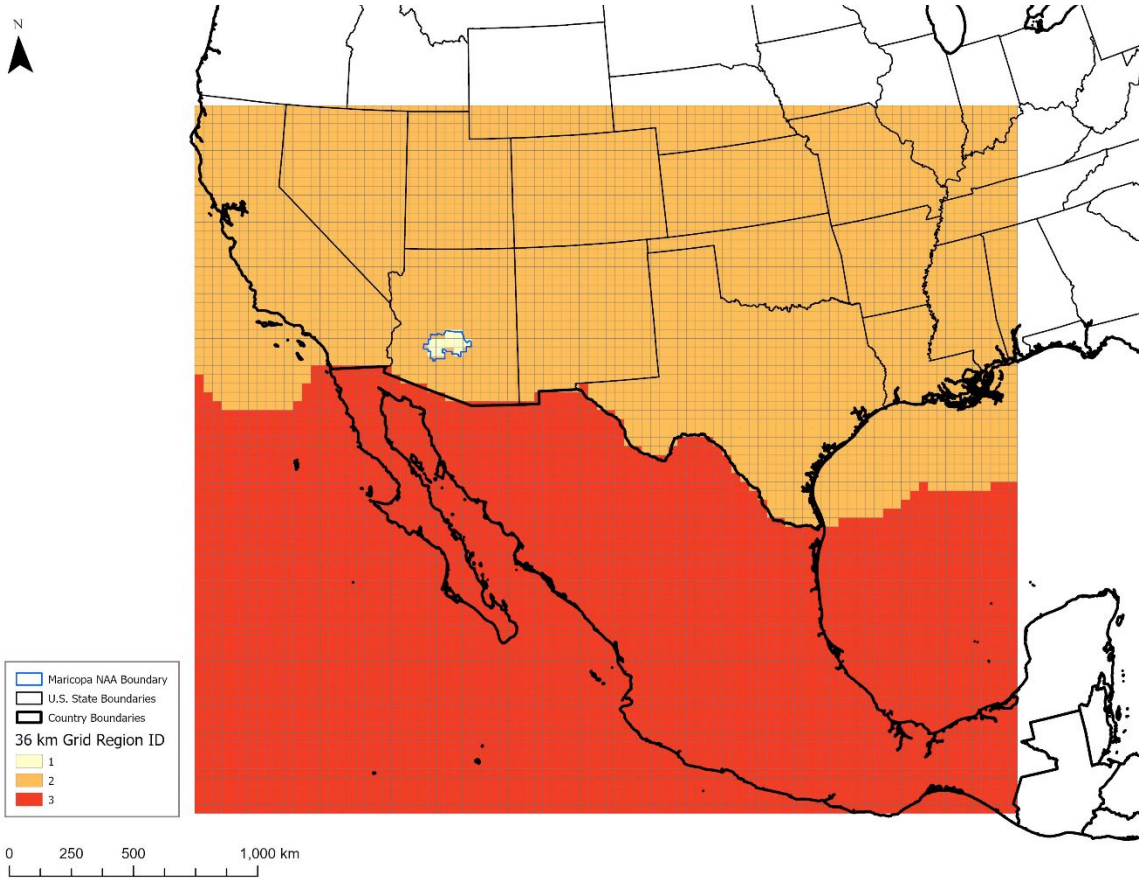

Figure 3-2. OSAT source region map for the 36 km North American domain.

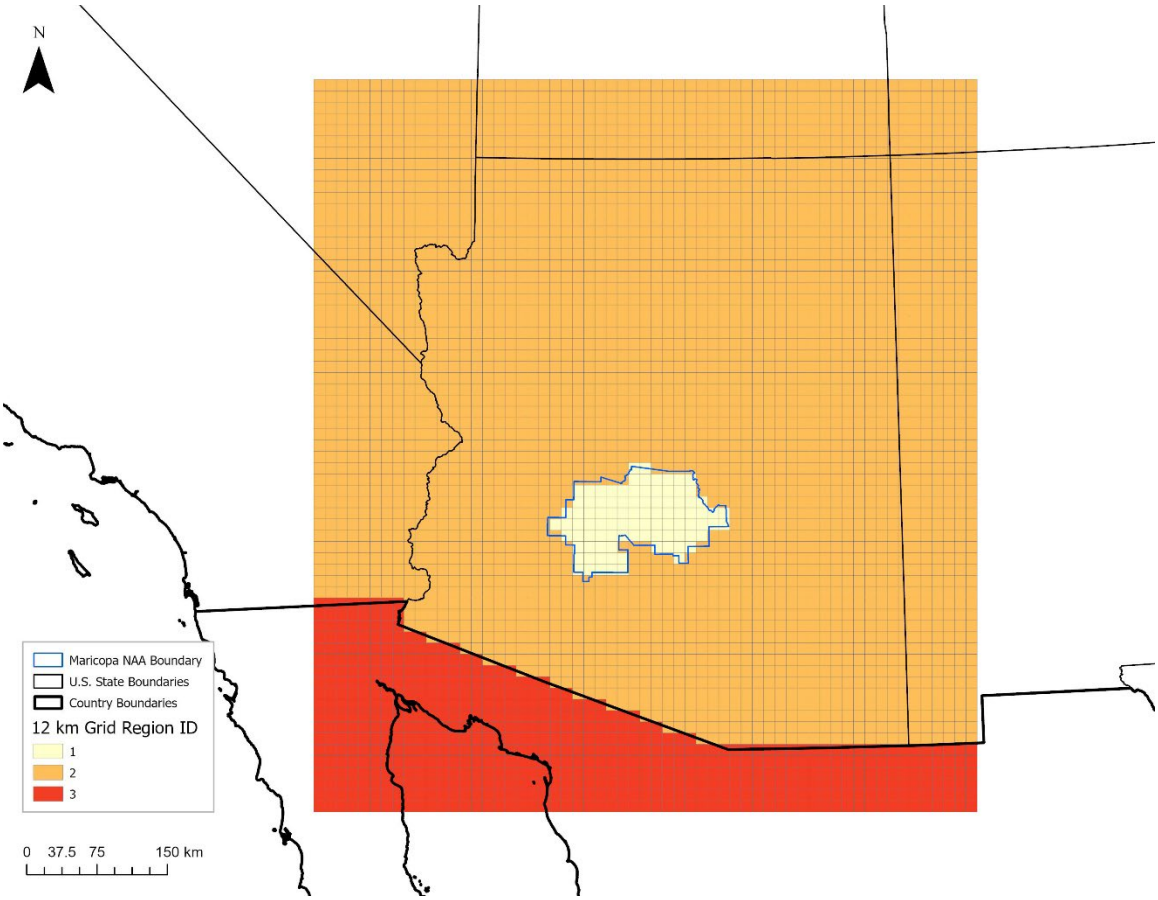

Figure 3-3. OSAT source region map for the 12 km Arizona domain.

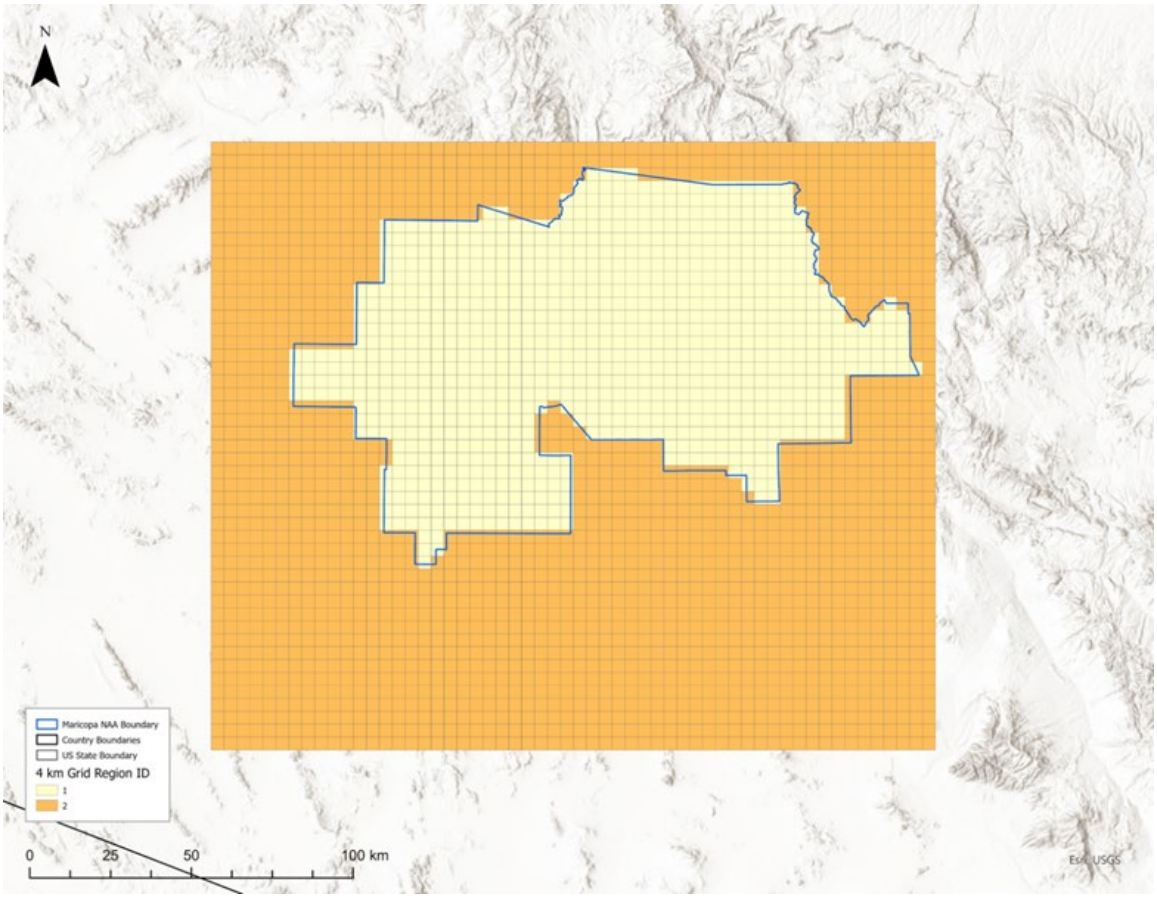

Figure 3-4. OSAT source region map for the 4 km Maricopa NAA domain.

3.2.2 Model Results

The 2023 OSAT results were extracted at the locations of all Maricopa NAA monitoring sites from the 4 km grid output files. Modeled hourly ozone tracer and cumulative ozone concentrations were post-processed to MDA8 ozone each day, that is, the unique 8-hour period defining total MDA8 ozone at each grid cell on each day was used to time-average all ozone tracers.

To quantify IA impacts on 2023 projected DVs, we applied SMAT-CE v2.1 using two monitoring datasets: (1) the official EPA data containing 2021-2023 MDA8 ozone DVs for all official sites operating in the Maricopa NAA; and (2) adjusted 2021-2023 MDA8 ozone DVs from MAG that reflect the removal of 31 atypical wildfire days (as discussed in Section 2.4.1). The SMAT-CE configuration followed the default SMAT approach to use the maximum ozone from a 3x3 set of grid cells surrounding each monitoring site. The top 10 modeled days from these grid arrays were used to define the RRF at each site. The monitor-specific RRF was applied to the two different ozone DVs to project the 2023 ozone DV reflecting the removal of all IA impacts.

Table 3-2 presents results from these calculations. All IA sources contribute approximately 15 ppb to site-averaged and site-maximum ozone levels, which reduce 2021-2023 DVs well below the 70 ppb ozone standard. Site-specific DVs range 49-66 ppb when IA contributions are removed from official 2023 DVs, 48-63 ppb when IA contributions are removed from adjusted 2023 DVs (31 atypical wildfire impact days removed), and 49-62 ppb when IA contributions are removed from adjusted 2023 DVs using adjusted RRF (top 10 modeled

days do not include coincident atypical wildfire impact days). These findings reinforce the significant role of international transport and wildfires in shaping ozone levels in the Maricopa NAA.

Table 3-2. Modeled international anthropogenic (IA) contributions to 2021-2023 DVs and resulting DVs with IA contributions removed.

	DV Source	DV 2023 (ppb)	DV no IA (ppb)	Total IA Contribution (ppb)
Site Average	EPA	75	60	15.3
	MAG	73	58	14.8
	MAG-RRF	73	57	15.6
Site Max	EPA	80	66	14.0
	MAG	77	63	13.4
	MAG-RRF	77	62	15.0

Definitions:

EPA: Official 2023 DV recorded in EPA's Air Quality System (AQS) database. Note that Site Max of 80 ppb occurs at two monitoring sites: Mesa and JLG Supersite.

MAG: Adjusted 2023 DV after 31 atypical wildfire-impacted days are removed. Note that Site Max of 77 ppb occurs at four monitoring sites: North Phoenix, Glendale, Lehi, and JLG Supersite.

MAG-RRF: MAG adjusted DV and adjusted RRF after the top-10 modeled days are defined with coincident atypical wildfire-impacted days removed

Figure 3-5 shows site-averaged "landscape" time series (i.e., stacked area plots) of simulated MDA8 ozone contributions from BC IA and Mexico IA sectors to illustrate the evolution of relative contributions from international source regions over time. During April through June when stronger westerly winds are predominant, IA contributions via BCs (Asia/Intercontinental) dominate while contributions from Mexico are much smaller. This pattern occurs again in September. During July through August, coinciding with southerly monsoonal flow, BC IA decreases dramatically while Mexican contributions increase and comprise most of the total IA.

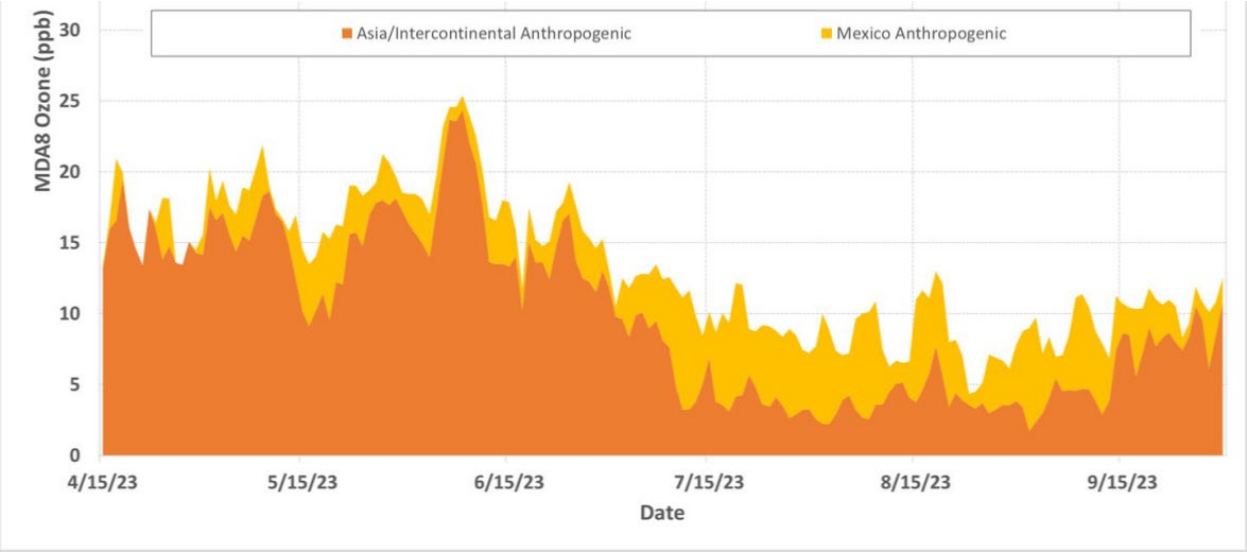

Figure 3-5. Time series of simulated Asia/intercontinental and Mexico IA contributions to MDA8 ozone during the 2023 ozone season averaged over all Maricopa NAA monitoring sites.

3.3 EPA Modeling Confirming Attainment "But For" International Emissions

The EPA (2021) analyzed modeled US and international source attribution information from the EPA's 2020 Ozone Policy Assessment (EPA, 2020a) for areas not attaining the 2015 ozone NAAQS by the August 2021 Marginal attainment date. EPA reported contributions from 4 sectors at peak (controlling) monitors in each nonattainment area: global natural, US anthropogenic, IA, and mixed anthropogenic (US and IA). The latter sector is a product of the modeling method employed. Since attributions were determined using a series of zero-out simulations, non-linear ozone chemical responses from separately removing each anthropogenic sector disallowed a precise accounting of US vs. IA contributions. This complication is alleviated when using models instrumented with in-line source apportionment algorithms, such as the CAMx/OSAT modeling described above.

EPA ran CMAQ for the base year of 2016 on a national grid with 12 km grid spacing and 35 vertical layers. All modeling results were shifted to local standard time and averaged to the MDA8 metric for consistency with observed 2018-2020 DV data. Total ozone and sector concentrations were averaged across the 10 highest modeled days at each grid cell coinciding with the peak monitor in each nonattainment area. Modeled mean sector concentrations were scaled to represent their relative contribution to the 2018-2020 DV in a manner similar to the RRF method applied in the Final Revised Cross-State Air Pollution Rule Update (EPA, 2020b).

Table 3-3 lists the relative contributions by sector applied to the 2018-2020 DV value at the peak DV site in Phoenix. According to EPA's modeling, the IA contribution was estimated at 8.5 ppb, but source apportionment modeling would estimate a larger contribution by accounting for some fraction of the 5.1 ppb mixed anthropogenic component (for a total ozone contribution range of 8.5-13.6 ppb). Removing just the IA sector from the 79 ppb DV results in 70.5 ppb; i.e., the Maricopa NAA would have attained the standard in 2020 but for the IA contribution.

Table 3-3. Observed 2018-2020 DV (ppb), scaled modeled contributions (EPA, 2021) from global natural, US anthropogenic, international anthropogenic (IA), and mixed anthropogenic, and the DV reflecting removal of IA. DVs are truncated to whole numbers to reflect the form of the ozone NAAQS.

Site	2018-2020 DV	Natural	US	IA	Mix	DV without IA
Phoenix, AZ-05	79	27.0	38.3	8.5	5.1	70

3.4 EPA Modeling Confirming Mexico Contributions in Maricopa

EPA (2023) describes source apportionment modeling to support the final disapproval action for "Good Neighbor State Implementation Plans Addressing Interstate Transport Obligations for the 2015 Ozone National Ambient Air Quality Standards."[3] EPA employed nationwide photochemical modeling for the summer of 2016 to project ozone DVs at individual monitoring sites within Moderate nonattainment areas to the 2023 attainment year and to estimate state-by-state anthropogenic and other contributions to 2023 ozone DVs. Modeling was conducted using CAMx on the 2016v3 national modeling platform.

Attainment year ozone contributions were determined by CAMx source apportionment modeling using 2023 projected emission inventories. Emission contributions from each state were separately tracked, along with contributions from tribal lands, offshore marine vessels

[3] https://www.epa.gov/Cross-State-Air-Pollution/final-disapproval-good-neighbor-state-implementation-plans-addressing

and oil/gas development, the portions of Canada and Mexico within the modeling domain, biogenic emissions, wild and prescribed fires, lightning NOx, and BCs. Note that BCs represent the totality of global pollutants entering the US domain, but they were not stratified into natural and anthropogenic components.

Like the process we described above, source apportionment results were used in a relative sense, using an RRF, to apportion the projected 2021-2023 DV at each monitoring location. Total MDA8 ozone and tracked contributions were calculated each day, then averaged over the top 10 modeled total ozone days. The ratio of each averaged contribution to averaged total ozone defined the RRF. This was then multiplied by the 2023 projected DV to yield DV contributions.

Appendix C in EPA (2023) tabulates 2023 projected ozone DVs and associated source contributions at each of 19 Maricopa County monitors that operated over the 5-year period from 2014 to 2018 (centered on 2016). None of the projected 2023 DVs exceed 70 ppb, so modeled projections from the 2016 base year suggest that the Maricopa NAA would attain the ozone NAAQS in 2023. Table 3-4 lists key source contributions averaged over the highest 5 sites where projected 2023 DVs range from 70.0 to 70.8 ppb: Arizona, California (the largest upwind contributing state), Canada and Mexico, fires, and BCs. The table also shows those values further scaled to the actual peak monitored 2021-2023 DV of 80 ppb. Arizona's own contribution is 20% of the total 2023 DV. Assuming that Mexico comprises most, if not all, of the Canada and Mexico sector due to the proximity and flow patterns into the Maricopa NAA, about 3 ppb is attributed to emissions from the northern portion of Mexico included within the EPA's modeling domain. Furthermore, it is over 4 times higher than EPA's threshold for linking states to upwind sources (0.7 ppb), 50% more contribution than from California, and roughly equivalent to both California and fires combined. Additional IA contributions from other countries are associated with boundary conditions, but that is impossible to quantify since the EPA modeling of boundary conditions did not segregate the natural and anthropogenic global sources entering the domain.

Table 3-4. EPA (2023) model-projected 2023 ozone DV and key source contributions averaged over the highest 5 sites in the Maricopa NAA where projected DVs range from 70.0 to 70.8 ppb: Arizona (AZ), California (CA), Canada and Mexico (C&M), fires, and boundary conditions (BC). The table also shows those values scaled to the maximum observed 2021-2023 DV of 80 ppb.

	2023 DV	AZ	CA	C&M	Fires	BC
Projected DV	70	14.4	1.9	2.9	1.7	43.3
Actual DV	80	16.3	2.1	3.3	1.9	49.1

4.0 Precursor Emission Trends

This section compares ozone precursor emission inventories and 2017-2023 trends between the Maricopa NAA and the three Mexican states of Baja California, Sonora, and Chihuahua, which share their northern border with California, Arizona, New Mexico, and Texas, respectively. The proximity and magnitude of Mexican emissions sources relative to the Maricopa NAA, along with their upward trend from 2017 to 2023, provide supporting evidence for the 179B(b) demonstration by indicating a neighboring source of transported IA emissions. From a comparative standpoint, it is not useful to tally precursor emissions from all international anthropogenic emissions outside of North America as they are multiple orders of magnitude larger than total US emissions. While source apportionment results presented in Section 3 indicate that Mexico ozone contributions comprise a smaller fraction of total IA contributions relative to the rest of the northern hemisphere during late spring and early summer, contributions from Mexico versus other foreign sources become roughly equivalent during the monsoonal period of July through August. Therefore, emissions from Mexico contribute a large portion of total IA through much of the Maricopa ozone season.

Eastern Research Group, Inc. (ERG) developed comprehensive anthropogenic air emission inventories of VOC and NOx in the three Mexican states. ERG applied methodologies consistent with EPA's 2022v2 emissions modeling platform and conventions for 2017 and 2023.

As shown in Figure 4-1 and Table 4-1, NOx emissions in the Maricopa NAA declined by 38% from 2017 to 2023, mostly due to the on-road sector being subject to federal regulations on engines and fuels coupled with the vehicle fleet's transition toward cleaner vehicles. The Mexico three-state total NOx increased by 6% over the same period. Per capita emissions for the Maricopa NAA and the combined Mexico three-state area are also presented in Table 4-1; these per capita emissions were developed using 2017 and 2023 population estimates (Poppen, 2025; INEGI, 2024). Total NOx emissions in the three Mexico states are over 6 times larger than in the Maricopa NAA in 2017 and have grown to 11 times larger in 2023. Normalizing for their much larger size, per capita NOx emissions in the three Mexico states are 3 times larger than in the Maricopa NAA in 2017 and have grown to 5 times larger in 2023.

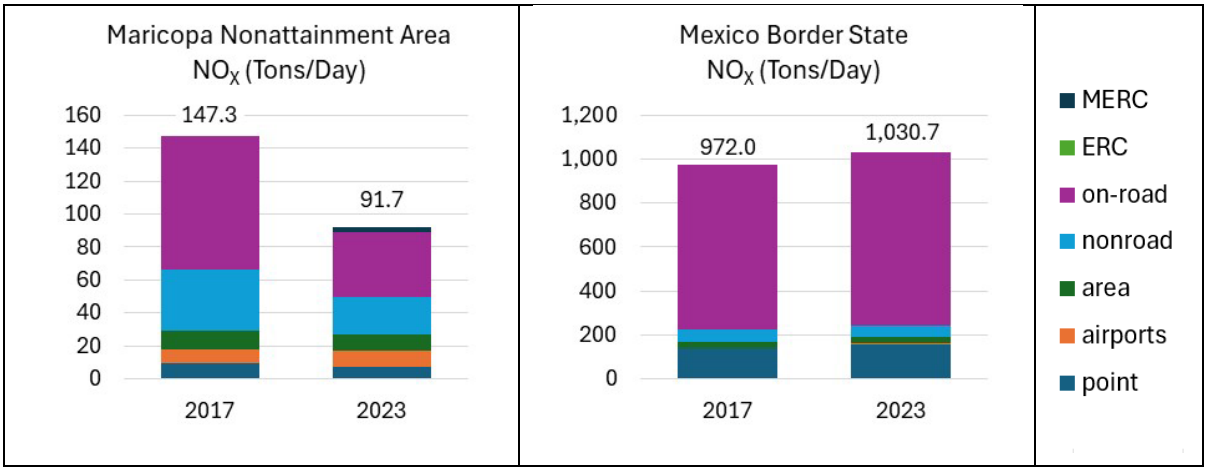

Figure 4-1. NOx emission trends from 2017 to 2023 in the Maricopa NAA (left) and the three northern border Mexican States of Baja California, Sonora, and Chihuahua combined (right).

Table 4-1. NOx emissions and percent change from 2017 to 2023, US and three northern Mexico States combined.

Category	Maricopa Nonattainment Area			Mexico Border States		
	2017 (TPD)	2023 (TPD)	Percent Change	2017 (TPD)	2023 (TPD)	Percent Change
Point	9.35	7.49	-20%	136.77	158.63	16%
Airports	8.43	9.79	16%	3.11	3.33	7%
Area	11.51	9.25	-20%	29.27	29.35	0.3%
Nonroad	37.22	22.80	-39%	53.12	50.81	-4%
On-Road	80.74	39.59	-51%	749.72	788.63	5%
ERC		0.01				
MERC		2.74				
Total	**147.26**	**91.66**	**-38%**	**971.99**	**1,030.75**	**6%**
Per capita (lbs/day)	**0.062**	**0.036**	**-43%**	**0.185**	**0.194**	**5%**

The change in VOC emissions (Figure 4-2) is consistent with the NOx trends, though the magnitude of change is smaller. Table 4-2 shows that total VOC emissions decrease by 4% in the Maricopa NAA and increase by 2% in the three Mexico border states. Area source VOC is the largest sector (Figure 4-2) in both the US and the Mexican States, and it modestly increases in both countries over 2017 to 2023 (Table 4-2). In the Maricopa NAA, total VOC declines in 2023 due to reductions in on-road mobile sources. Total VOC emissions in the three Mexico states are over 5 times larger than in the Maricopa NAA in both 2017 and 2023. Per capita VOC emissions in the three Mexico States are about 2.5 times larger than in the Maricopa NAA in 2017 and 2023.

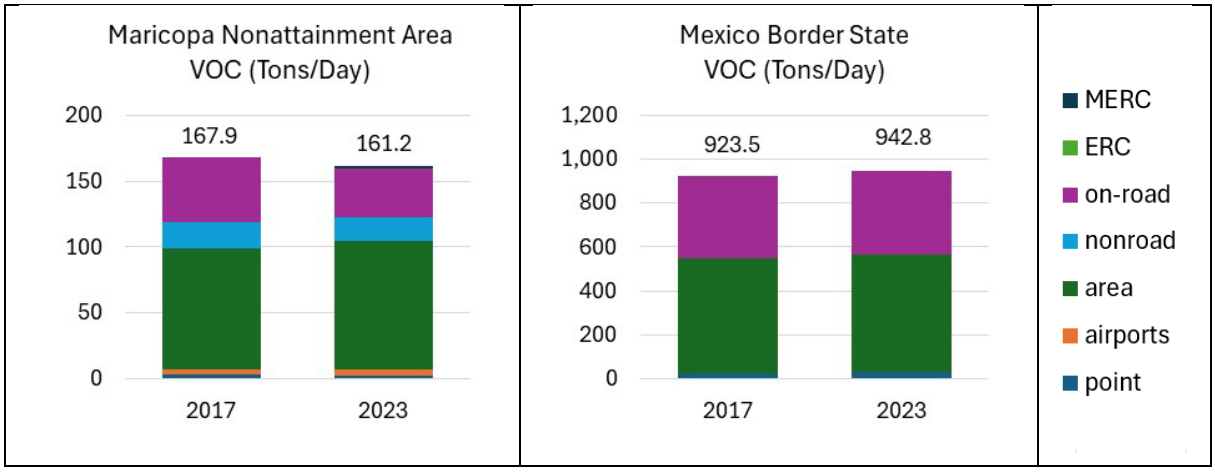

Figure 4-2. VOC emissions trends from 2017 to 2023 in the Maricopa NAA (left) and the three northern border Mexican States of Baja California, Sonora, and Chihuahua combined (right).

Table 4-2. VOC emissions and percent change from 2017 to 2023, US and three northern Mexico States combined.

Category	Maricopa Nonattainment Area			Mexico Border States		
	2017 (TPD)	2023 (TPD)	Percent Change	2017 (TPD)	2023 (TPD)	Percent Change
Point	3.01	1.99	-34%	26.88	31.04	15%
Airports	4.21	4.90	16%	0.66	0.70	6%
Area	91.59	97.32	6%	518.70	531.35	2%
Nonroad	20.23	18.40	-9%	3.29	3.05	-7%
On-Road	48.82	37.16	-24%	374.00	376.69	1%
ERC		0.03				
MERC		1.37				
Total	167.86	161.18	-4%	923.53	942.83	2%
Per capita (lbs/day)	**0.071**	**0.063**	**-11%**	**0.175**	**0.177**	**1%**

Tables 4-3 through 4-7 list Mexico VOC and NOx emissions at the state level for each major sector. Appendix A of this report describes the methodology to develop the stationary and nonroad sectors; these are presented together because they share a common base year from recent work ERG performed for the EPA and the use of new projections from 2017 to 2023 derived from Mexico government agency data sources. Appendix A of this report also describes the on-road sector methodology which relied on the MOVES-Mexico 2023 model applied at the state level for years 2017 and 2023 for both the general on-road inventory and an additional on-road source category representing Mexico and US vehicles idling at border crossings while waiting to enter the US.

Table 4-3. Mexico point source emissions, 2017 and 2023.

State	VOC (Tons/Day)			NO_x (Tons/Day)		
	2017	2023	Percent Change	2017	2023	Percent Change
Baja California	9.11	10.85	19%	28.15	34.85	24%
Chihuahua	9.16	10.67	16%	60.68	70.84	17%
Sonora	8.61	9.51	11%	47.95	52.95	10%
Total	**26.88**	**31.04**	**15%**	**136.77**	**158.63**	**16%**

Table 4-4. Mexico airport emissions, 2017 and 2023.

State	VOC (Tons/Day)			NO_x (Tons/Day)		
	2017	2023	Percent Change	2017	2023	Percent Change
Baja California	0.13	0.14	6%	1.63	1.72	6%
Chihuahua	0.12	0.14	13%	0.66	0.74	13%
Sonora	0.41	0.43	6%	0.82	0.86	6%
Total	**0.66**	**0.70**	**7%**	**3.11**	**3.33**	**7%**

Table 4-5. Mexico area source emissions, 2017 and 2023.

State	VOC (Tons/Day)			NO_x (Tons/Day)		
	2017	2023	Percent Change	2017	2023	Percent Change
Baja California	162.27	165.51	2%	3.53	3.71	5%
Chihuahua	217.96	229.16	5%	20.32	20.09	-1%
Sonora	138.47	136.68	-1%	5.42	5.55	2%
Total	**518.70**	**531.35**	**2%**	**29.27**	**29.35**	**0.3%**

Table 4-6. Mexico nonroad emissions, 2017 and 2023.

State	VOC (Tons/Day)			NO_x (Tons/Day)		
	2017	2023	Percent Change	2017	2023	Percent Change
Baja California	0.47	0.39	-17%	5.62	5.03	-11%
Chihuahua	1.46	1.41	-3%	26.26	24.38	-7%
Sonora	1.36	1.25	-8%	21.21	21.40	1%
Total	**3.29**	**3.05**	**-7%**	**53.12**	**50.81**	**-4%**

Table 4-7. Mexico on-road emissions, 2017 and 2023.

State	VOC (Tons/Day)			NOx (Tons/Day)		
	2017	2023	Percent Change	2017	2023	Percent Change
General On-Road Inventory						
Baja California	139.04	139.41	0%	279.30	293.89	5%
Chihuahua	141.08	142.43	1%	291.40	307.29	5%
Sonora	91.48	92.71	1%	176.57	185.54	5%
Border Crossing Idling Inventory						
Baja California	1.54	1.58	2%	1.55	1.40	-9%
Chihuahua	0.59	0.30	-49%	0.62	0.25	-59%
Sonora	0.27	0.27	-1%	0.28	0.26	-9%
Total	**374.00**	**376.69**	**1%**	**749.72**	**788.63**	**5%**

5.0 Transport Pattern Analysis

5.1 Air Parcel Trajectory Calculations

This section presents the results of a HYSPLIT[4] back trajectory analysis that explores the medium-range (3-day) origins of air parcels that arrived in the Maricopa NAA on ozone exceedance days during 2021–2023. Table 5-1 lists the days for which HYSPLIT was run and differentiates between two sets of days: one listing all exceedance days and the other excluding all 76 possible wildfire-impacted days as determined by MAG. The HYSPLIT model was run for each exceedance day and results from each run were grouped with similar transport pathways. Separate groups were developed for all and no wildfire impacted days. The HYSPLIT analysis demonstrates the potential for transport and establishes a plausible physical linkage, while the quantitative chemical impact of that transport is determined by the photochemical source apportionment modeling as discussed in Section 3.

While helpful in understanding general air pathways upwind of a receptor area over a limited timeframe, the HYSPLIT model includes some inherent limitations (Fleming et al., 2012; Stein et al, 2015). First, HYSPLIT back trajectories estimate the path of a single air parcel and do not account for diffusion or dispersion of air within that parcel. Diffusion is the microscopic phenomenon of random molecular motions and dispersion is a macroscopic phenomenon due to turbulence or atmospheric flow patterns below resolved scales. Both effects tend to mix and spread the constituents of an air parcel over time and space. Second, there are uncertainties due to the reliance on modeled meteorological data with spatial averaging over grid cells and discrete (rather than continuous) modeled time steps.

To mitigate these uncertainties, it is generally preferable to consider an ensemble of back-trajectories released at different locations and times, rather than a single parcel back-trajectory, since the divergence of an ensemble reflects dispersion patterns associated with resolved meteorology. Depending on how the ensemble is structured, different sensitivities are explored, and although the ensemble does not estimate true uncertainties it highlights potential variability and reduces the tendency to interpret a single back-trajectory as an absolute path and to assign source-receptor relationships.

For these reasons, ensemble HYSPLIT back-trajectory runs were performed by defining trajectory initiation (ending) points at the center and corners of a 3-D box covering the Maricopa NAA airshed and centered on Phoenix (33.501874 °N, 112.074461°W). The corners of the box were offset from the Phoenix center point by ±0.25° (~25 km) in the north/south direction and by ±0.50° (~40 km) in the east/west direction. As shown in Figure 5-1 the area of the box (shaded grey) roughly covers the central urbanized area of the Maricopa NAA and is sufficiently large that it contains multiple (~32) meteorological data points in the 12-km meteorological analysis dataset used to drive the HYSPLIT calculations (described below). The initiation heights at each of the five coordinates were set at 100, 500 and 1,000 m above ground (AGL). These elevated heights were selected to be within the most chemically active portion of the atmospheric boundary layer during midday and afternoon hours. Two initiation times per day were specified to coincide with the typical period of rapid ozone formation (12 PM) and deep boundary layer with well-mixed conditions in the afternoon (3 PM). Thirty HYSPLIT trajectories per exceedance day were initiated with this ensemble configuration.

[4] https://www.ready.noaa.gov/HYSPLIT.php

Table 5-1. Maricopa NAA ozone exceedance days in 2021-2023 analyzed with HYSPLIT back trajectories.

All Exceedance Days			All Possible Wildfire-Impacted Days Removed		
2021	**2022**	**2023**	**2021**	**2022**	**2023**
5/5/2021	4/25/2022	4/11/2023	5/5/2021	5/6/2022	4/11/2023
5/6/2021	4/26/2022	4/16/2023	5/6/2021	5/12/2022	4/16/2023
5/12/2021	4/29/2022	4/20/2023	5/12/2021	5/13/2022	4/20/2023
5/13/2021	4/30/2022	5/8/2023	5/13/2021	5/15/2022	5/8/2023
5/24/2021	5/6/2022	5/9/2023	5/24/2021	5/25/2022	5/9/2023
5/26/2021	5/12/2022*	5/11/2023	5/26/2021	5/26/2022	5/11/2023
5/27/2021	5/13/2022	5/12/2023	5/27/2021	6/1/2022	5/12/2023
5/28/2021	5/15/2022	5/14/2023	5/28/2021	6/2/2022	5/17/2023
6/9/2021	5/25/2022	5/15/2023	6/9/2021	6/27/2022	5/20/2023
6/11/2021	5/26/2022	5/16/2023	6/24/2021	6/28/2022	5/22/2023
6/12/2021	6/1/2022	5/17/2023	6/26/2021	6/29/2022	6/1/2023
6/15/2021	6/2/2022	5/20/2023	7/2/2021	6/30/2022	6/4/2023
6/16/2021	6/15/2022	5/21/2023	7/4/2021	7/10/2022	6/8/2023
6/18/2021	6/16/2022	5/22/2023	7/8/2021	8/4/2022	6/9/2023
6/24/2021	6/21/2022	6/1/2023	7/9/2021	8/5/2022	6/13/2023
6/26/2021	6/22/2022	6/4/2023	8/1/2021	8/6/2022	6/14/2023
6/28/2021	6/27/2022	6/8/2023	8/2/2021	8/8/2022	6/15/2023
6/29/2021	6/28/2022	6/9/2023	8/28/2021	8/10/2022	6/29/2023
7/1/2021	6/29/2022	6/13/2023	8/29/2021	8/11/2022	7/3/2023
7/2/2021	6/30/2022	6/14/2023	8/30/2021	8/13/2022	8/15/2023
7/4/2021	7/10/2022	6/15/2023	9/3/2021	8/15/2022	8/16/2023
7/8/2021	7/13/2022	6/17/2023	9/4/2021	8/16/2022	8/24/2023
7/9/2021	7/14/2022	6/22/2023		8/17/2022	8/25/2023
7/13/2021	7/15/2022	6/23/2023		8/18/2022	8/26/2023
7/14/2021	7/16/2022	6/24/2023		8/22/2022	8/28/2023
7/17/2021	7/17/2022	6/25/2023		8/23/2022	8/29/2023
7/19/2021	7/18/2022	6/26/2023		8/24/2022	8/30/2023
7/20/2021	7/22/2022	6/29/2023		8/25/2022	
7/21/2021	7/23/2022	6/30/2023		8/26/2022	
7/22/2021	8/4/2022	7/1/2023		8/30/2022	
7/27/2021	8/5/2022	7/2/2023		8/31/2022	
7/28/2021	8/6/2022	7/3/2023		9/1/2022	
7/30/2021	8/8/2022	7/7/2023		9/2/2022	
7/31/2021	8/10/2022	7/8/2023		9/7/2022	
8/1/2021	8/11/2022	7/18/2023		9/8/2022	
8/2/2021	8/13/2022	7/19/2023			
8/3/2021	8/15/2022	7/21/2023			
8/4/2021	8/16/2022	7/22/2023			
8/5/2021	8/17/2022	7/23/2023			
8/6/2021	8/18/2022	7/24/2023			
8/17/2021	8/22/2022	7/25/2023			
8/24/2021	8/23/2022	7/26/2023			
8/25/2021	8/24/2022	7/27/2023			
8/26/2021	8/25/2022	7/28/2023			
8/27/2021	8/26/2022	7/29/2023			
8/28/2021	8/30/2022	7/31/2023			
8/29/2021	8/31/2022	8/1/2023			
8/30/2021	9/1/2022	8/15/2023			
9/3/2021	9/2/2022	8/16/2023			
9/4/2021	9/7/2022	8/17/2023			
9/5/2021	9/8/2022	8/18/2023			
		8/22/2023			
		8/24/2023			
		8/25/2023			
		8/26/2023			
		8/28/2023			
		8/29/2023			
		8/30/2023			

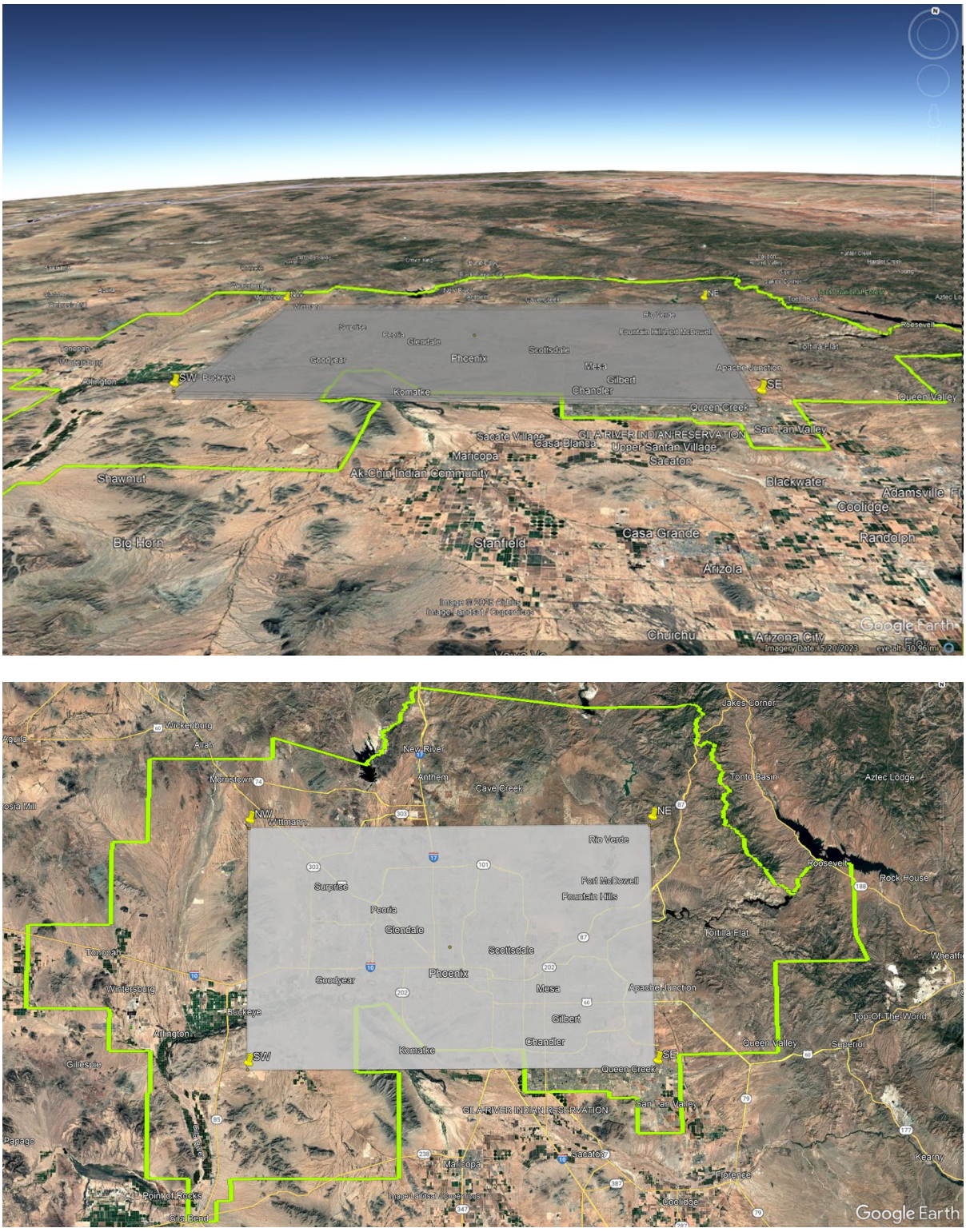

Figure 5-1. Location and coverage of the 5 initiation points at 3 vertical levels for HYSPLIT back trajectories: 3-D view (upper), planar view (lower). The Maricopa NAA is outlined in green.

All HYSPLIT back trajectories were calculated for 72 hours (3 days) to assess medium range transport over the scale of western North America. Extending the trajectories further back in time (7-10 days) would illustrate the global nature of ozone transport on all exceedance days by passing over source regions across the entire northern hemisphere, including Asia and Europe. That exercise is captured in the global photochemical modeling done in Section 3. Focusing on medium-range transport allows for an understanding of the frequency of international transport from international areas within North America. To drive the trajectory calculations, we selected the NAM12 meteorological analyses[5] (a North American 12 km spatial resolution product) as it was the most feasible high resolution dataset to available.[6] A sample HYSPLIT control file is shown in Appendix B of this report. The isentropic vertical velocity option was employed as it best represents three-dimensional synoptic-scale flow and is not subject to discretization and numerical uncertainties related to model-calculated vertical velocities. The vertical velocity option is set in the fifth line of the HYSPLIT control file, and the value of 2 corresponds to the isentropic option.

Figure 5-2 shows selected 3-day ensemble trajectories initiated on four different Maricopa NAA exceedance days to illustrate different transport patterns described below. Each hourly trajectory point is color-coded according to starting altitude and initiation hour. These four days characterize four distinct transport patterns that we have subjectively identified from all 160 exceedance day ensembles (provided in Appendix C of this report). Three of the four patterns include potential transport from Mexico (west, south, southeast). While not the particular focus of this medium-range analysis, two of the four patterns (west and north) also involve longer-term transport from Canada, Asia, and other areas of the northern hemisphere.

The upper left ensemble shows transport primarily from the NNW over the 3 days prior to April 22, 2022, and has generally consistent trajectories for all 30 members in the ensemble. This pattern indicates strong wind with 3-day origins in the northwestern US and no potential for transport from Mexico. However, this pattern suggests transport from Canada and potentially Asia over a longer period. The upper right ensemble shows transport from the east on August 15, 2023, and exhibits strong winds with more variation as air masses originate from both northeast and southeast directions. Most trajectories, however, pass close to Ciudad Juarez and northern Mexico within approximately 1 day, while the meridional (north-south) variations occur farther upwind (i.e., around 3 days back in time) with origins in Texas and Mexico. The lower left ensemble shows more stagnant conditions with slower and more variable winds (i.e., shorter 3-day back-trajectories) on May 13, 2021. This pattern indicates potential for more local and regional buildup with evidence of transport from south of Phoenix, Mexico, and the Gulf of California following a cyclonic flow pattern. The lower right ensemble on April 29, 2022, shows strong transport from the west, which includes southern California and the US-Mexico border, with 3-day origins extending over the eastern Pacific Ocean. Air masses that follow this pattern pass over the Mexican cities of Tijuana and Mexicali prior to arriving in Phoenix. This pattern also suggests potential transport from Asia over a longer period. According to source apportionment modeling, long-range contributions from the west are often highest in the spring and early summer. Intercontinental transport does not always lead to an exceedance, but it does persistently raise ozone levels over the western US.

[5] https://www.ncei.noaa.gov/access/metadata/landing-page/bin/iso?id=gov.noaa.ncdc:C00630

[6] A high resolution HRRR 3 km dataset was considered but found to be impractical due to dataset size.

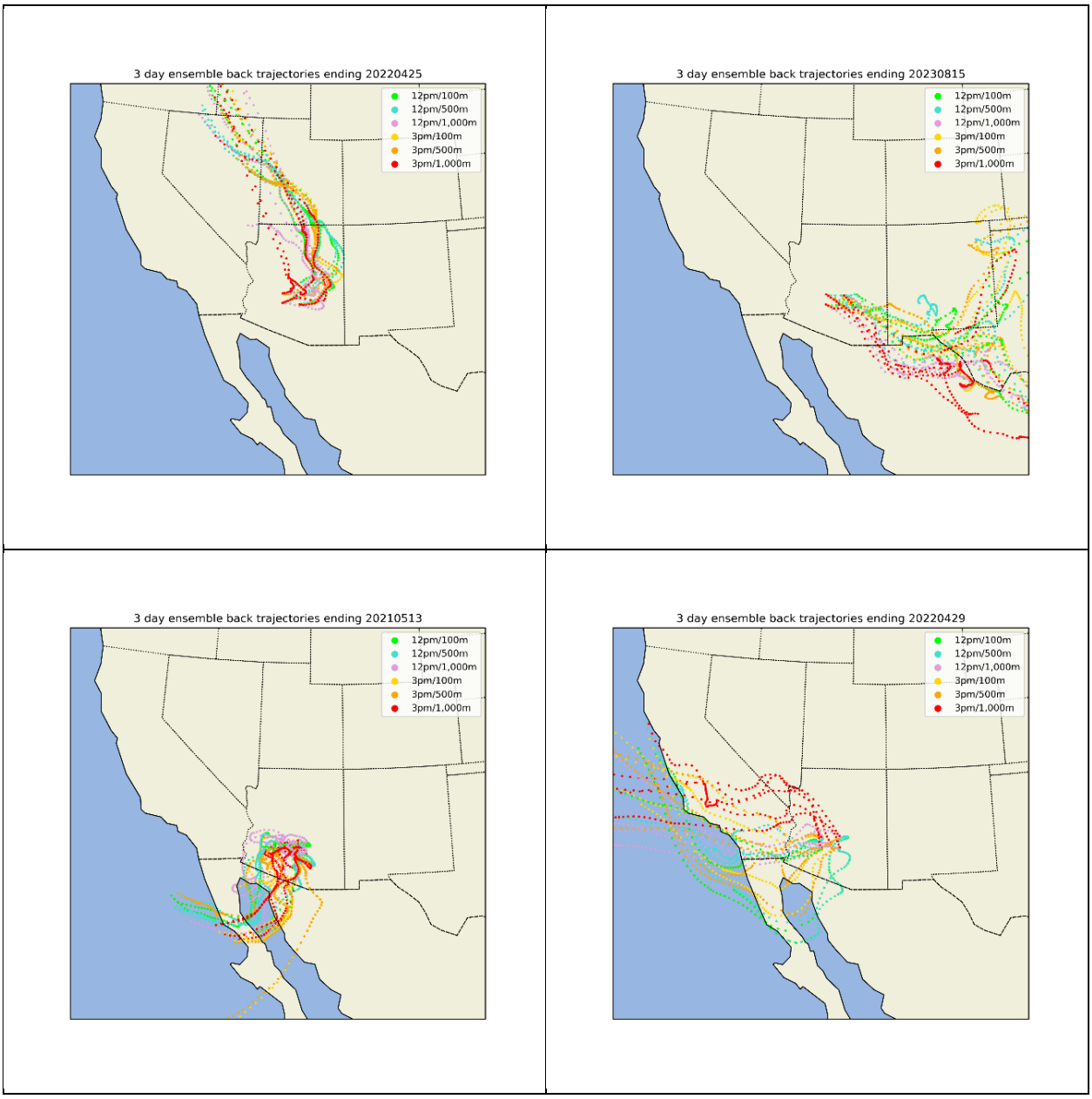

Figure 5-2. Examples of ensemble trajectory plots initiated on 4 specific Maricopa NAA exceedance days in 2021-2023 that represent 4 types of transport patterns: (northerly at top left, easterly/southeasterly at top right, southerly at bottom left, and westerly at bottom right).

Figure 5-3 summarizes the number of exceedance days that fall into each of the four transport patterns described above for two different cases. The left bar displays the distribution based on all 2021-2023 exceedance days while the right bar displays the distribution after excluding all 76 possible wildfire days. For all exceedance days, twenty-six of the 160 ensembles (16%) were consistent with the northerly transport pattern with no indication of transport from Mexico; 44 days (28%) were consistent with the easterly pattern toward the Juarez region; 51 days (32%) were consistent with the southerly pattern into Mexico; and 39 days (24%) were consistent with the westerly pattern into southern California and along the Mexican border. In total, 134 of 160 days (84%) indicate air parcel origins passing over some portion of Mexico. For non-wildfire exceedance days, the largest

reduction in frequency occurs for the days with transport from the south. For this case, 67 of 84 days (80%) indicate air parcel origins passing over some portion of Mexico, which remains consistent with results based on all exceedance days.

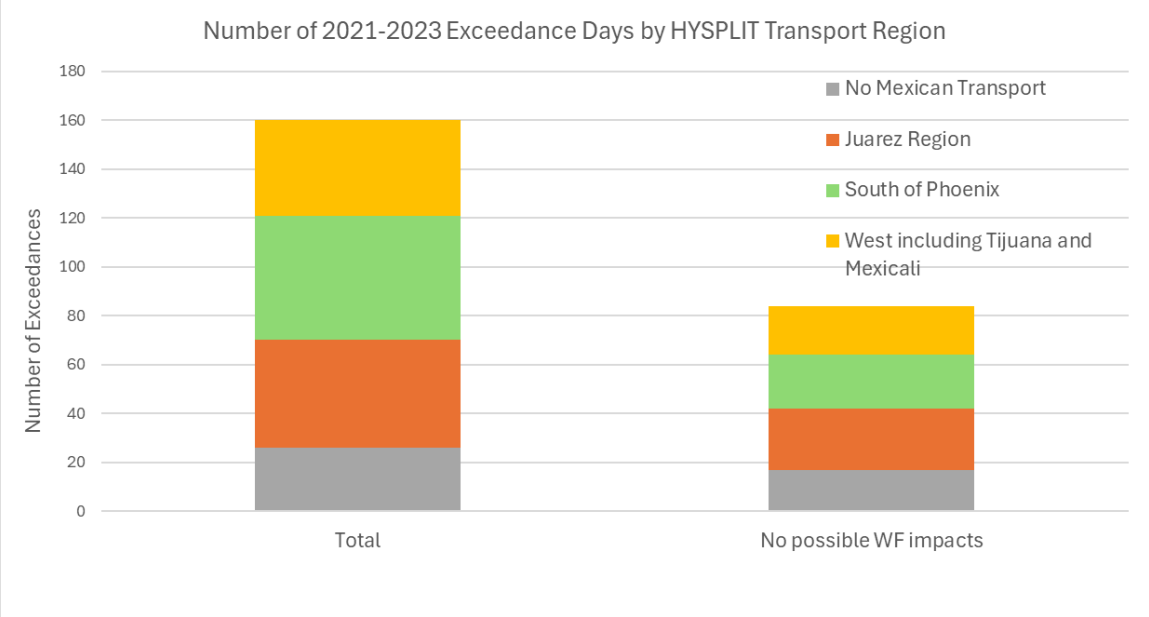

Figure 5-3. Summary of HYSPLIT-based transport pattern groups for 2021–2023 exceedance days in the Maricopa NAA.

Figure 5-4 is a similar plot that differentiates the transport patterns by month to provide additional insight into seasonal variability. The upper plot is for all exceedance days and the lower plot excludes the possible wildfire-impacted days. Note that most of the possible wildfire-impacted days occurred in June and July. After excluding the possible wildfire-impacted days, most days (52%) were associated with transport from the east with air mass origins that may include Ciudad Juarez and northern Mexico. In all months between April and September, most 3-day transport patterns pass over some portions of Mexico.

5.2 2021-2023 Design Values with Potential Mexico Transport Excluded

The Maricopa NAA 2021-2023 DVs were recalculated after excluding days with potential transport from Mexico. The recalculated DVs are presented in Figure 5-5 for each monitor. Four scenarios are considered: (1) actual DVs based on all exceedance days, (2) recalculated DVs based on excluding all possible 2021-2023 wildfire days (Table 5-1); (3) recalculated DVs based on excluding potential Mexican transport days (i.e., as assessed by the HYSPLIT analysis), and (4) recalculated DVs based on excluding all possible wildfire days and potential Mexican transport days. The Senior Center (SC) DV is not included since there were no measurements in 2023 and therefore the 2021-2023 three-year DV could not be calculated. Peak DVs of 80 ppb at Mesa (ME) and the JLG Supersite (JLG) are both reduced to 69 ppb when excluding wildfires and possible Mexican transport days, which would attain the 70 ppb NAAQS. On average (i.e., across all monitors) the reduction in DV due to exclusion of wildfires and Mexican transport is 8.4 ppb. All Maricopa NAA monitors except Pinnacle Peak (PP) would attain the NAAQS in this case. PP would be the controlling monitor (71 ppb) for the NAA in this scenario.

Figure 5-4. Summary of HYSPLIT-based transport pattern groups for 2021–2023 exceedance days in the Maricopa NAA by month: all exceedance days (upper), and excluding all possible wildfire-impacted days (lower).

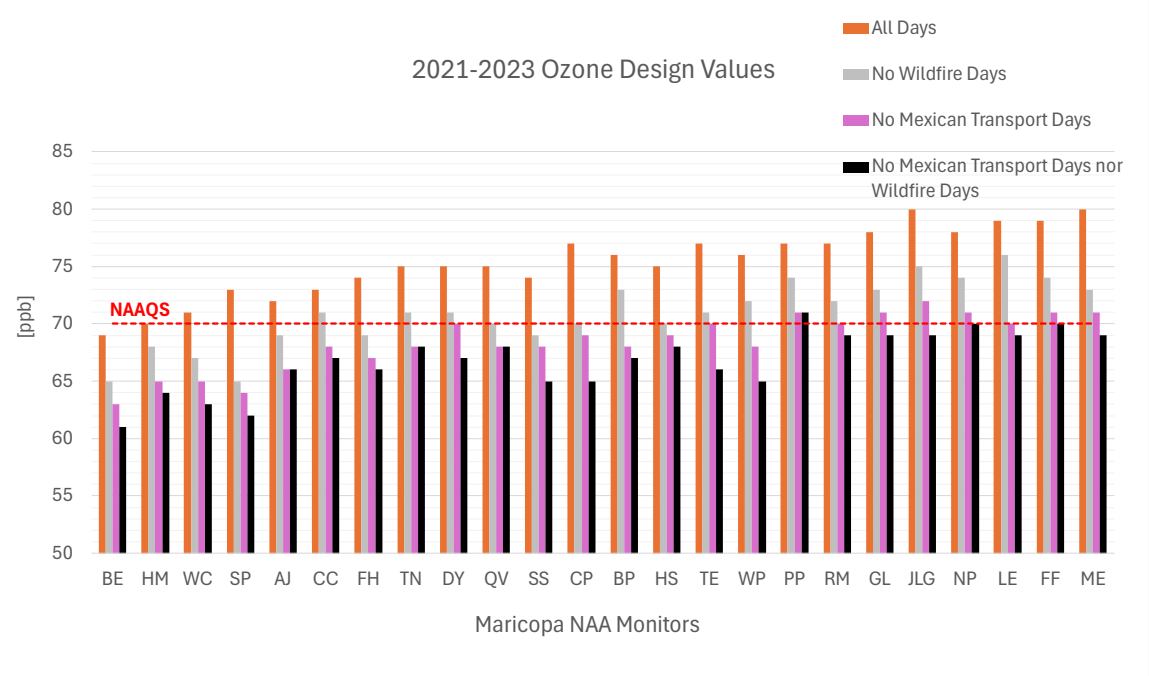

Figure 5-5. Recalculated 2021-2023 DVs for different wildfire and potential Mexican transport scenarios for each monitoring site in the Maricopa NAA.

6.0 Conclusions

The following lines of evidence collectively demonstrate that the Maricopa NAA would have attained the 2015 ozone NAAQS by the Moderate attainment date of August 3, 2024 but for international anthropogenic contributions.

Conceptual model of ozone episodes

- During the summer season, ozone levels in the Maricopa NAA are influenced by meteorological systems operating at multiple scales, all of which are consistent with locally stagnant conditions associated with a sinking/compressing warm air mass within a deep dome of high pressure centered over the western US.

Conceptual model of international transport

- The proximity of the Maricopa NAA to the southern US border suggests contributions of ozone from Mexico. Wind patterns through the boundary layer over both Phoenix and Tucson on NAA exceedance days are predominantly (75%) from the southeast toward Mexico.
- As a summer phenomenon, ozone episodes coincide with the seasonal western North American Monsoon, which brings humid air northward from Mexico into Arizona during July and August. This establishes a common transport corridor for pollutants emitted in Mexico to reach the Maricopa NAA within a few days.
- Another common transport pattern links Asia (and other areas of the northern hemisphere) to the western US. Persistent global circulation patterns establish a direct transport route in the mid to upper troposphere that brings pollutant-laden air to North America within 1 to 2 weeks. Sinking air within a high-pressure dome over the western US brings transported ozone and precursors toward the surface, while complex topography enhances vertical circulations, and thus the western US experiences the greatest ozone impacts from intercontinental transport. This transport mechanism is especially persistent throughout the spring and summer seasons.
- A recent multi-decadal trend analysis through 2021 indicates that free tropospheric ozone over western North America continues to increase despite a decreasing trend in boundary layer ozone, affirming vertically different sources and mechanisms.

Concentration trends

- Despite years of success in reducing precursor emissions, the region faces significant challenges in meeting the ozone standard.
- These include extreme weather events in the Southwest that have significantly elevated background ozone concentrations related to more frequent contributions from wildfire events.
- While the number of ozone exceedance days above 70 ppb has decreased by 62% over the past 25 years, a noticeable increase has occurred since 2017 with the majority (60%) of exceedance days associated with possible wildfire impacts. However, NAA ozone DVs have remained rather flat since 2017 when all possible wildfire-impacted days are removed from DV calculations.

Source apportionment modeling

- Source apportionment modeling is the most direct line of evidence for this demonstration and is the only analysis that explicitly provides an estimate of the global international anthropogenic (IA) contributions in the NAA.
- On the top-10 highest modeled ozone days in the Maricopa NAA, IA emissions were found to contribute approximately 15 ppb to site-averaged and site-maximum ozone

levels, which reduce 2021-2023 DVs well below the 70 ppb ozone standard at all sites. These findings reinforce the significant role of international transport in shaping ozone levels in the Maricopa NAA.

- During April through June and September when stronger westerly winds are predominant, IA contributions via photochemical model boundary conditions (BC) dominate while contributions from Mexico and local emissions are much smaller.
- During July through August, coinciding with southerly monsoonal flow, BC IA decreases while Mexican contributions increase and comprise the majority of total IA.

Confirmatory EPA modeling

- EPA modeling in 2021 reported an IA contribution to 2018-2020 DV at the peak Phoenix monitor of 8.5 ppb. Removing the IA sector from the peak 79 ppb DV results in 70.5 ppb; i.e., the Maricopa NAA would have attained the standard in 2020 but for the IA contribution.
- EPA source apportionment modeling in 2023 attributed about 3 ppb of 2021-2023 ozone DVs in the Maricopa NAA to emissions from the northern portion of Mexico included within the modeling domain. This is over 4 times higher than EPA's threshold for linking monitors to contributing upwind states, 50% more contribution than from California, and roughly equivalent to both California and fires combined. Additional IA contributions are associated with EPA's BCs, but EPA did not break out global IA and natural components in their modeled BCs. Arizona's own contribution was 20% of the total 2021-2023 DV.

Precursor emissions and trends

- Emission inventory trends for the Maricopa NAA show that NOx emissions have declined by 38% from 2017 to 2023. VOC emissions have decreased by 4% over the same period.
- Meanwhile, emissions in the three northern Mexican states bordering the southwest US (Baja California, Sonora, Chihuahua) have increased by 6% for NOx and by 2% for VOC.
- Furthermore, total and per capita NOx and VOC emissions in those Mexican states are several times larger than in the Maricopa NAA.
- The proximity, magnitude, and recent trendline of Mexican emissions relative to the Maricopa NAA provide supporting evidence for the 179B(b) demonstration.

Trajectory analyses

- Three-day upstream air parcel transport pathways on Maricopa NAA exceedance days over 2021-2023 identified four types of distinct transport patterns. Three of the four (west, south, southeast) involve transport from Mexico, while two of the four (west and north) also involve longer-term transport from Canada, Asia, and other areas of the northern hemisphere.
- In total, trajectories indicate that 80% of air parcels pass over some portion of Mexico prior to arriving to the Maricopa NAA on exceedance days.
- Three-day transport patterns and relative frequencies are consistent whether considering all 160 exceedance days or 84 days with no possible wildfire impacts (as determined by MAG).
- When excluding wildfires and possible Mexican transport days in the 2021-2023 DV calculations, peak DVs of 80 ppb are reduced to 69 ppb (attaining the NAAQS) and only a single site (Pinnacle Peak) would remain above the standard at 71 ppb.
- On average (i.e., across all monitors) the reduction in DV from the exclusion of wildfire and Mexican transport days is 8.4 ppb.

Based on these technical analyses we conclude that the Maricopa nonattainment area would have attained the EPA 2015 ozone standard by August 3, 2024, but for the impact of international emissions.

7.0 References

Baker, K.R., C. Emery, P. Dolwick, G. Yarwood, 2015. Photochemical grid model estimates of lateral boundary contributions to ozone and particulate matter across the continental United States. *Atmos. Environ.*, 123, 49-62. http://dx.doi.org/10.1016/j.atmosenv.2015.10.055.

Chang, K.-L., O.R. Cooper, G. Rodriguez, L.T. Iraci, E.L. Yates, M.S. Johnson, et al., 2023. Diverging ozone trends above western North America: Boundary layer decreases versus free tropospheric increases. *J. Geophys. Res.: Atmospheres*, 128, e2022JD038090. https://doi.org/10.1029/2022JD038090.

EPA, 2018. "Modeling Guidance for Demonstrating Attainment of Air Quality Goals for Ozone, PM2.5 and Regional Haze" (EPA 454/R-18-009, November 2018). https://www3.epa.gov/ttn/scram/guidance/guide/O3-PM-RH-Modeling_Guidance-2018.pdf.

EPA, 2020a. Policy Assessment for the Review of the Ozone National Ambient Air Quality Standards (No. EPA-452/R-20-001). https://www.epa.gov/sites/production/files/2020-05/documents/o3-final_pa-05-29-20compressed.pdf.

EPA, 2020b. Air Quality Modeling Technical Support Document for the Final Revised Cross-State Air Pollution Rule Update. https://www.epa.gov/sites/default/files/2021-03/documents/air_quality_modeling_tsd_final_revised_csapr_update.pdf.

EPA, 2021. Modeled U.S. and International Contributions for 2015 Ozone NAAQS Nonattainment Areas. Memorandum from Barron Henderson and Heather Simon (EPA, OAQPS) to the Ozone Determination of Attainment by the Attainment Date Rule Docket (EPA-HQ-OAR-2021-0742). December 10, 2021. https://www.regulations.gov/docket/EPA-HQ-OAR-2021-0742.

EPA, 2023. Air Quality Modeling Technical Support Document, 2015 Ozone NAAQS SIP Disapproval Final Action (January 31, 2023). https://downloads.regulations.gov/EPA-HQ-OAR-2021-0663-0085/content.pdf.

EPA, 2025a. CMAQ Documentation. https://www.epa.gov/cmaq/cmaq-documentation.

EPA, 2025b. Photochemical Modeling Tools: SMAT-CE. https://www.epa.gov/scram/photochemical-modeling-tools.

ERG, 2016. Adaptation of the Vehicle Emission Model MOVES to Mexico. Final Technical Report for the Mexico Low Emissions Development Program (January 31). https://www.epa.gov/sites/default/files/2021-03/documents/usaid-inecc-2016-01-31.pdf (accessed August 2025).

ERG, 2023. Strengthening Mexican Emissions Inventories and Related Capacity to Support the Border 2025 Program Air Objectives and Improve Understanding of Mexico-U.S. Transboundary Air Pollution, Task 3 Final Report. Eastern Research Group, Inc., Sacramento, California (April 14).

ERG, 2024. Continued Strengthening of Mexican Emissions Inventories and Related Capacity to Support the Border 2025 Program Air Objectives and Improve Understanding of Mexico-U.S. Transboundary Air Pollution, Task 3 Final Report. Eastern Research Group, Inc., Sacramento, California (May 14).

Federal Register, 2015. National Ambient Air Quality Standards for Ozone. Environmental Protection Agency, 40 CFR Parts 50, 51, 52, 53, and 58 [EPA-HQ-OAR-2008-0699; FRL-9933-18-OAR]. https://www.federalregister.gov/documents/2015/10/26/2015-26594/national-ambient-air-quality-standards-for-ozone.

Federal Register, 2018. Additional Air Quality Designations for the 2015 Ozone National Ambient Air Quality Standards. Environmental Protection Agency, 40 CFR Part 81 [EPA-HQ-OAR-2017-0548; FRL-9977-72-OAR]. https://www.federalregister.gov/documents/2018/06/04/2018-11838/additional-air-quality-designations-for-the-2015-ozone-national-ambient-air-quality-standards.

Federal Register, 2022. Determinations of Attainment by the Attainment Date, Extensions of the Attainment Date, and Reclassification of Areas Classified as Marginal for the 2015 Ozone National Ambient Air Quality Standards. Environmental Protection Agency, 40 CFR Parts 52 and 81 [EPA-HQ-OAR-2021-0742; FRL-8425-02-OAR]. https://www.federalregister.gov/documents/2022/10/07/2022-20460/determinations-of-attainment-by-the-attainment-date-extensions-of-the-attainment-date-and.

Federal Register, 2023. Findings of Failure To Submit State Implementation Plan Revisions for Reclassified Moderate Nonattainment Areas for the 2015 Ozone National Ambient Air Quality Standards (NAAQS). Environmental Protection Agency, 40 CFR Part 52 [EPA-HQ-OAR-2023-0442; FRL-11287-01-OAR]. https://www.federalregister.gov/documents/2023/10/18/2023-22987/findings-of-failure-to-submit-state-implementation-plan-revisions-for-reclassified-moderate.

Fleming, Z.L., Monks, P.S., Manning, A.J., 2012. Review: untangling the influence of air-mass history in interpreting observed atmospheric composition. *Atmos. Res.*, 104–105, 1-39. https://doi.org/10.1016/j.atmosres.2011.09.009.

HTAP, 2010. Hemispheric Transport of Air Pollution 2010: Part A: Ozone and Particulate Matter Air Pollution Studies, No. 17. Prepared by the Task Force on Hemispheric Transport of Air Pollution, F. Dentener, T. Keating, and H. Akimoto, Eds. https://core.ac.uk/download/pdf/83641741.pdf.

Huang, M., Carmichael, G. R., Pierce, et al., 2017. Impact of intercontinental pollution transport on North American ozone air pollution: an HTAP phase 2 multi-model study. *Atmospheric Chemistry and Physics*, 17(9), 1680-7316. doi:10.5194/acp-17-5721-2017.

INEGI, 2024. Encuesta Nacional de Dinámica Demográfica (National Survey of Demographic Dynamics) for 2018 and 2023 (May 22). https://en.www.inegi.org.mx/programas/enadid/2023/

INEGI, 2025. Gross Domestic Product by State (PIBE), Instituto Nacional de Estadística y Geografía (July 4). https://en.www.inegi.org.mx/programas/pibent/2018/#tabular_data

Jaffe, D.A., O.R. Cooper, A.M. Fiore, B.H. Henderson, G.S. Tonnesen, A.G. Russell, D.K. Henze, A.O. Langford, M. Lin, T. Moore, 2018. Scientific assessment of background ozone over the U.S.: Implications for air quality management. *Elem. Sci. Anth*., 6: 56. DOI: https://doi.org/10.1525/elementa.309.

Jiang, Z., Worden, J.R., Payne, V.H., Zhu, L., Fischer, E., Walker, T. and Jones, D.B., 2016. Ozone export from East Asia: The role of PAN. *Journal of Geophysical Research: Atmospheres*, 121(11), pp.6555-6563.

Langford, A. O., Alvarez, R. J., II, Brioude, J., Fine, R., Gustin, M. S., Lin, M. Y., et al., 2017. Entrainment of stratospheric air and Asian pollution by the convective boundary layer in the southwestern U.S. *Journal of Geophysical Research: Atmospheres*, 122, 1312–1337. https://doi.org/10.1002/2016JD025987.

Lin, M., Horowitz, L. W., Payton, R., Fiore, A. M., & Tonnesen, G., 2017. US surface ozone trends and extremes from 1980 to 2014: quantifying the roles of rising Asian emissions, domestic controls, wildfires, and climate. *Atmospheric Chemistry and Physics*, 17(4), 2943-2970. doi:10.5194/acp-17-2943-2017.

Mathur, R., Kang, D., Napelenok, S. L., Xing, J., Hogrefe, C., Sarwar, G., et al., 2022. How have divergent global emission trends influenced long-range transported ozone to North America? *Journal of Geophysical Research: Atmospheres*, 127, e2022JD036926. https://doi.org/10.1029/2022JD036926.

Nopmongcol, U., Liu, Z., Stoeckenius, T., & Yarwood, G., 2017. Modeling intercontinental transport of ozone in North America with CAMx for the Air Quality Model Evaluation International Initiative (AQMEII) Phase 3. *Atmospheric Chemistry and Physics*, 1680-7324. doi:10.5194/acp-17-9931-2017.

Poppen, 2025. Personal communication between Matthew Poppen (MAG) and Marty Wolf (ERG). Email received July 31.

Ramboll, 2024. User's Guide: Comprehensive Air quality Model with extensions (CAMx), version 7.30. www.camx.com.

SENER, 2024a. Prospectiva de Gas Natural 2023-2037. Secretaría de Energía (SENER) (April 3). http://base.energia.gob.mx/Prospectivas23/PGN_23-37_F.pdf.

SENER, 2024b. Prospectiva de Petróleo Crudo y Petrolíferos 2023-2037. Secretaría de Energía (SENER) (April 3). http://base.energia.gob.mx/Prospectivas23/PPP_23-37.pdf.

SENER, 2024c. Prospectiva de Gas L.P. 2023-2037. Secretaría de Energía (SENER) (April 3). http://base.energia.gob.mx/Prospectivas23/PGLP_23_37_F.pdf.

SENER, 2025. Balance Nacional de Energía 2023. Secretaría de Energía (SENER) (February 10). https://www.gob.mx/cms/uploads/attachment/file/977268/Balance_Nacional_de_Energ_a_2023.FINAL06.02.2025.1.pdf.

Stein, A.F., Draxler, R.R., Rolph, G.D., Stunder, B.J.B., Cohen, M.D., Ngan, F., 2015. NOAA's HYSPLIT Atmospheric Transport and Dispersion Modeling System. *Bulletin of*

the American Meteorological Society, 96(12), 2059–2077. doi:10.1175/BAMS-D-14-00110.1.

US CBP, 2025. Historical Wait Times (at U.S. Border Crossings). Data Retrieval Tool provided by the U.S. Customs and Border Protection. https://bwt.cbp.gov/historical (accessed June 2025).

US DOT, 2025. Border Crossing Entry Data. Query Tool provided by U.S. Department of Transportation, Bureau of Transportation Statistics. https://data.bts.gov/stories/s/Tables-Query-Tool/6rt4-smhh (accessed June 2025).

van der A, R. J., Mijling, B., Ding, J., Koukouli, M., Liu, F., Li, Q., et al., 2017. Cleaning up the air: effectiveness of air quality policy for SO2 and NOx emissions in China. *Atmospheric Chemistry and Physics*, 17(3), 1775-1789. doi:10.5194/acp-17-1775-2017.

Verstraeten, W. W., Neu, J. L., Williams, J. E., Bowman, K. W., Worden, J. R., & Folkert, B. K., 2015. Rapid increases in tropospheric ozone production and export from China. *Nature Geoscience*, 8(9), 690-695. doi:10.1038/ngeo2493.

Zaveri, R. A., Saylor, R. D., Peters, L. K., McNider, R., & Song, A., 1995. A model investigation of summertime diurnal ozone behavior in rural mountainous locations. *Atmospheric Environment*, 29(9), 1043-1065. doi:10.1016/1352-2310(94)00319-G

Zhang, L., M. Lin, A.O. Langford, L.W. Horowitz, C.J. Senff, E. Klovenski, Y. Wang, R.J. Alvarez, I. Petropavlovskikh, P. Cullis, C.W. Sterling, J. Peischl, T.B. Ryerson, S.S. Brown, Z.C.J. Decker, G. Kirgis, S. Conley, 2020. Characterizing sources of high surface ozone events in the southwestern US with intensive field measurements and two global models. *Atmos. Chem. Phys*., 20, 10379–10400. https://doi.org/10.5194/acp-20-10379-2020.

APPENDIX A

Methods to Estimate 2017 and 2023 Mexico Emissions

APPENDIX A Methods to Estimate 2017 and 2023 Mexico Emissions

A.1 Stationary, Airports, and Nonroad Sources

ERG developed Mexican state-level emissions for area, point, and nonroad sources using the 2018 Mexico National Emissions Inventory (Inventario Nacional de Emisiones or INEM), developed by Mexico's Ministry of Environment and Natural Resources (Secretaría de Medio Ambiente y Recursos or SEMARNAT). The three most recent inventories developed and published by SEMARNAT are for base years 2016, 2018, and 2020. Recently, ERG completed a project for the EPA that included a detailed quality assurance (QA) and quality control (QC) review of the 2018 INEM data for the Mexican border states. Based on the review findings and discussions with EPA and SEMARNAT, ERG performed technical updates to improve the data quality of the 2018 INEM for the border states. Examples of these improvements include revising emissions calculations to avoid double-counting, correcting inaccurate emission factors and conversion factors, correcting spreadsheet calculation errors, excluding perchloroethylene from VOC estimates (dry cleaning category), and methodological improvements to certain area source categories.

Because 2018 is adjacent to 2017 and the data have been thoroughly reviewed and updated, ERG used the revised 2018 INEM data as proxy for the 2017 base year in the current project (ERG, 2023; ERG, 2024). As the first step, ERG compiled municipality-level (i.e., county equivalent) VOC and NOx emissions from point, area, and nonroad (including airports) sources for Baja California, Chihuahua, and Sonora from the 2018 INEM. All emissions were then converted from megagrams (or metric tons) to short tons (or US tons).

ERG excluded area source emissions from drycleaning and forest wildfires categories from the 2018 INEM. For the drycleaning category, the 2018 INEM only reported perchloroethylene emissions under VOCs. Perchloroethylene is classified as "VOC-exempt" by EPA, and therefore these emissions were excluded. Because the scope of work for this project only includes anthropogenic (i.e., man-made) emissions, forest wildfire emissions were excluded. Additionally, the 2018 INEM included a partial emissions estimate from border crossings under the nonroad source type. Since the border crossing emissions are estimated separately under on-road sources (Section A.3), they were excluded from the Mexico nonroad source emissions.

A.1.1 Emissions Projections Methodology

ERG developed factors to project the 2018 INEM emissions to 2023. The projection factors were based on Source Category Codes (SCCs) for area and nonroad sources (including airports) and North American Industry Classification System (NAICS) codes for point sources. The general equation used to calculate projection factors is:

$$PF_{S,C} = \frac{Surrogate_{2023,S,C}}{Surrogate_{2018,S,C}}$$

Where:

$PF_{S,C}$ = Projection factor for state S and inventory code C (SCCs for area and nonroad and NAICS for point sources);
$Surrogate_{2018,S,C}$ = 2018 surrogate data for inventory code C and state S; and
$Surrogate_{2023,S,C}$ = 2023 surrogate data for inventory code C and state S.

Mexico specific surrogate data for 2018 and 2023 were used to develop projection factors for area, nonroad, and point sources. Surrogate data were compiled from the following sources:

- Mexico's National Institute of Statistics, Geography and Informatics (Instituto Nacional de Estadística y Geografía or INEGI)
- Mexico's Secretariat of Energy (Secretaría de Energía or SENER)

Emissions were then projected to 2023 using:

$$Emissions_{2023,S,C} = Emissions_{2018,S,C} \times PF_{S,C}$$

Where:

$Emissions_{2023,S,C}$ = 2023 emissions for state S and inventory code C;
$Emissions_{2018,S,C}$ = 2018 emissions for state S and inventory code C; and

The remainder of this section provides information on the specific surrogates used for projections and data sources.

A.1.2 Point Source Projections

State-level totals from the 2018 INEM for point source VOC and NOx emissions are presented in Table 4-3. The 2018 INEM reported emissions data from 968 point source facilities for the three Mexican states of Baja California, Sonora, and Chihuahua. In addition to emissions and location information, the point source data included facility NAICS codes and fuel information.

Mexico's INEGI publishes information from various national economic and demographic surveys (e.g., population census, economic census, and industrial surveys). State-level data on annual gross product output (in millions of 2018 pesos), by industry type (indicated by 2- or 3-digit NAICS codes), are available from INEGI for 2003-2023 (INEGI, 2025). ERG mapped the NAICS codes from the point source inventory to the NAICS codes in the INEGI product output data.

ERG then used the gross product output data to calculate projection factors for all point sources except electricity generating units (EGUs). For EGUs (NAICS 22111 - electric power generation), ERG developed projection factors based on the reported EGU fuel type (natural gas, diesel, or heavy fuel oil). Mexico's SENER provides data on annual fuel consumption by fuel type, sector (residential, commercial, energy, industrial, and transportation) and region (SENER, 2024a; SENER, 2024b). The fuel consumption data are available for the following regions:

- Noroeste (Northwest) – This region includes Baja California and Sonora. ERG used the regional data for both states.
- Noreste (Northeast) – This region includes Chihuahua.
- Centro Occidente (Central West)
- Centro (Central)
- Sur-sureste (South-southeast)

The projection factors based on INEGI and SENER data were then used to project VOC and NOx emissions for all point sources. State-level totals for the 2023 projected point source emissions are presented in Table 4-3.

Table A-1 presents a listing of the point source 3-digit NAICS codes reported for the three states and their projection surrogate assignments and projection factor values. Projection surrogates and factors for EGUs are listed in Table A-2.

Table A-1. Point source (except EGUs) projection surrogates and factors.

NAICS Code	NAICS Description	Projection Surrogate	Projection Factor (Unitless)		
			Baja California	Chihuahua	Sonora
112	Animal Production	GDP112	1.19	1.13	1.17
211	Oil and Gas Extraction	GDP211	1.10	1.04	1.04
212	Mining (except Oil and Gas)	GDP212	1.00	1.14	0.94
311	Food Manufacturing	GDP311	1.17	1.09	1.10
312	Beverage and Tobacco Product Manufacturing	GDP312	0.99	1.05	1.70
313	Textile Mills	GDP313-314	1.19	0.92	0.75
314	Textile Product Mills	GDP313-314	1.19	0.92	0.75
315	Apparel Manufacturing	GDP315-316	1.00	0.69	0.36
316	Leather and Allied Product Manufacturing	GDP315-316	1.00	0.69	0.36
321	Wood Product Manufacturing	GDP321	1.00	0.64	0.96
322	Paper Manufacturing	GDP322-323	1.08	0.91	1.08
323	Printing and Related Support Activities	GDP322-323	1.08	0.91	1.08
324	Petroleum and Coal Products Manufacturing	GDP324-326	1.13	1.14	1.26
325	Chemical Manufacturing	GDP324-326	1.13	1.14	1.26
326	Plastics and Rubber Products Manufacturing	GDP324-326	1.13	1.14	1.26
327	Nonmetallic Mineral Product Manufacturing	GDP327	0.80	1.24	0.94
331	Primary Metal Manufacturing	GDP331-332	1.26	1.28	1.31
332	Fabricated Metal Product Manufacturing	GDP331-332	1.26	1.28	1.31
333	Machinery Manufacturing	GDP333-336	1.21	1.20	1.16
334	Computer and Electronic Product Manufacturing	GDP333-336	1.21	1.20	1.16
335	Electrical Equipment, Appliance, and Component Manufacturing	GDP333-336	1.21	1.20	1.16
336	Transportation Equipment Manufacturing	GDP333-336	1.21	1.20	1.16
339	Miscellaneous Manufacturing	GDP339	1.05	1.35	0.95
486	Pipeline Transportation	GDP48-49	1.12	1.14	1.04
493	Warehousing and Storage	GDP48-49	1.12	1.14	1.04
562	Waste Management and Remediation Services	GDP56	0.29	0.27	0.32

Table A-2. Point Source EGU projection surrogates and factors.

EGU Fuel	Projection Surrogate	Projection Factor (Unitless)			Data Source
		Baja California	Chihuahua	Sonora	
Natural Gas	EGU-NG	1.39	0.97	1.39	SENER, 2024a
Heavy Fuel Oil	EGU-COMBUSTOLEO	0.27	2.85	0.27	SENER, 2024b
Distillate Fuel Oil	EGU-DIESEL	0.15	0.11	0.15	SENER, 2024b

A.1.3 Area Source Projections

State-level totals from the 2018 INEM for area source VOC and NOx emissions are presented in Table 4-5. ERG used Mexico-specific data from SENER and INEGI to project the 2018 emissions to 2023. ERG assigned projection surrogates to area source categories based on the reported SCCs. Depending on the SCC, population data, fuel consumption data by sector, or product output data (in millions of 2018 pesos) were used to develop state-level projection factors. The following data were used for developing projection factors:

- Population – 2018 and 2023 state level population estimates (INEGI, 2024)
- Diesel, natural gas, and LPG – 2018 and 2023 fuel consumption quantities by sector for the Noroeste (Northwest) Region (Baja California and Sonora) and the Noreste (Northeast) Region (Chihuahua) (SENER, 2024a; SENER, 2024b; SENER, 2024c)
- Gasoline – 2018 and 2023 total fuel consumption quantities by State (SENER, 2024b)
- Wood – 2018 and 2023 wood consumption quantities for the residential sector at the national level (SENER, 2025). Residential wood consumption data are not available at the state or regional levels. Projection factors developed from the national residential wood consumption data were used for the three states.
- Gross product output – 2018 and 2023 product output data (in millions of 2018 pesos) by state and industry type (indicated by 2-digit or 3-digit NAICS codes) (INEGI, 2025)
- Unchanged – a constant projection factor of 1.0 was used when a source category was not expected to change. For the area source categories of pesticide application and agricultural field burning, 2018 emissions were held constant for 2023 (i.e., a no growth scenario was used). These area source categories were not expected to vary significantly from year to year, and appropriate activity data could not be reasonably assigned. This assignment was made for pesticides and agricultural burning categories because total agricultural acreage does not significantly change over time.

Table A-3 lists all the area source SCCs in the three states, their respective projection surrogates, and projection factors used to project 2018 emissions to 2023.

Table A-3. Area source projection surrogates and factors.

SCC	SCC Description	Projection Surrogate	Projection Factors (Unitless)			Data Source
			Baja California	Chihuahua	Sonora	
30290005	Agricultural LPG combustion	LPG - Agricultural	1.17	1.00	1.17	SENER, 2024c
2102004000	Industrial diesel combustion	Diesel - Industrial	1.20	0.51	1.20	SENER, 2024b
2102007000	Industrial LPG combustion	LPG - Industrial	0.87	1.04	0.87	SENER, 2024c
2103006000	Commercial natural gas combustion	Natural Gas - Commercial	2.00	0.92	2.00	SENER, 2024a
2103007000	Commercial LPG combustion	LPG - Commercial	0.96	0.95	0.96	SENER, 2024c
2104006000	Residential natural gas combustion	Natural gas - Residential	1.08	0.57	1.08	SENER, 2024a
2104007000	Residential LPG combustion	LPG - Residential	1.05	1.01	1.05	SENER, 2024c
2104008000	Residential wood combustion	Wood - Residential	0.98	0.98	0.98	SENER, 2025
2302002000	Commercial cooking - Charbroiling	Population	1.04	1.01	0.98	INEGI, 2024
2302050000	Bakeries - Bread making	Population	1.04	1.01	0.98	INEGI, 2024
2401001000	Architectural surface coatings	Population	1.04	1.01	0.98	INEGI, 2024
2401005000	Autobody refinishing	Population	1.04	1.01	0.98	INEGI, 2024
2401008000	Traffic markings	Population	1.04	1.01	0.98	INEGI, 2024
2401020000	Industrial surface coatings - Wood furniture	GDP337	1.11	0.82	0.89	INEGI, 2025
2401050000	Industrial surface coatings - Finished metal products	GDP331-332	1.26	1.28	1.31	INEGI, 2025
2401065000	Industrial surface coatings - Electronic and electrical products	GDP333-336	1.21	1.20	1.16	INEGI, 2025
2401070000	Industrial surface coatings - Motor vehicle manufacturing	GDP333-336	1.21	1.20	1.16	INEGI, 2025
2401090000	Industrial surface coatings - Miscellaneous manufacturing	GDP339	1.05	1.35	0.95	INEGI, 2025

SCC	SCC Description	Projection Surrogate	Projection Factors (Unitless)			Data Source
			Baja California	Chihuahua	Sonora	
2415000000	Degreasing	GDP Degreasing[a]	1.08	1.10	1.05	INEGI, 2025
2425010000	Graphic arts - Lithography	Population	1.04	1.01	0.98	INEGI, 2024
2425020000	Graphic arts - Letterpress	Population	1.04	1.01	0.98	INEGI, 2024
2425030000	Graphic arts - Rotogravure	Population	1.04	1.01	0.98	INEGI, 2024
2425040000	Graphic arts - Flexography	Population	1.04	1.01	0.98	INEGI, 2024
2460100000	Consumer solvents - All personal care products	Population	1.04	1.01	0.98	INEGI, 2024
2460200000	Consumer solvents - All household products	Population	1.04	1.01	0.98	INEGI, 2024
2460400000	Consumer solvents - All automotive aftermarket products	Population	1.04	1.01	0.98	INEGI, 2024
2460500000	Consumer solvents - Coatings and related products	Population	1.04	1.01	0.98	INEGI, 2024
2460600000	Consumer solvents - Adhesives and sealants	Population	1.04	1.01	0.98	INEGI, 2024
2460800000	Consumer solvents - All FIFRA related products	Population	1.04	1.01	0.98	INEGI, 2024
2460900000	Consumer solvents - Miscellaneous products	Population	1.04	1.01	0.98	INEGI, 2024
2461020000	Asphalt application	Population	1.04	1.01	0.98	INEGI, 2024
2461850000	Pesticide application	Constant/No Growth	1.00	1.00	1.00	None
2501060050	Gasoline service stations	Gasoline - Total	0.80	1.03	0.87	SENER, 2024b
2505030120	Gasoline tank truck transport	Gasoline - Total	0.80	1.03	0.87	SENER, 2024b
2610030000	Open burning - Household waste	Population	1.04	1.01	0.98	INEGI, 2024
2620000000	Landfills	Population	1.04	1.01	0.98	INEGI, 2024
2630020000	Wastewater treatment (publicly owned treatment works)	Population	1.04	1.01	0.98	INEGI, 2024

SCC	SCC Description	Projection Surrogate	Projection Factors (Unitless)			Data Source
			Baja California	Chihuahua	Sonora	
2801500000	Agricultural field burning	Constant/No Growth	1.00	1.00	1.00	None
2810030000	Structure fires	Population	1.04	1.01	0.98	INEGI, 2024
2850000010	Hospital sterilization operations	Population	1.04	1.01	0.98	INEGI, 2024
2899001999	Brick kilns	GDP23	1.06	1.32	1.13	INEGI, 2025
2909000001	LPG leaks (tanks, piping, regulators, connectors, valves, appliances, and pilot lights)	LPG - Total	0.98	1.11	0.98	SENER, 2024c
2909000002	LPG combustion - unburnt hydrocarbons (slip)	LPG - Total	0.98	1.11	0.98	SENER, 2024c
2909000003	LPG fugitive emissions - Total storage & transport	LPG - Total	0.98	1.11	0.98	SENER, 2024c

[a] Includes gross product output data (millions of 2018 pesos) for NAICS 21-23, 31-33, and 43-93.

A.1.4 Nonroad Source Projections

State-level totals from the 2018 INEM for VOC and NOx emissions from airports and nonroad sources are presented in Tables 4-4 and 4-6, respectively. ERG used Mexico-specific data from SENER and INEGI to project the 2018 emissions to 2023. ERG assigned projection surrogates to airports and nonroad sources based on the reported SCCs. Depending on the SCC, population data, fuel consumption data by sector, or product output data (in millions of 2018 pesos) were used to develop state-level projection factors.

The following data were used for developing projection factors:

- Diesel and jet fuel – 2018 and 2023 fuel consumption quantities for the transportation sector in the Noroeste (Northwest) Region (Baja California and Sonora) and the Noreste (Northeast) Region (Chihuahua) (SENER, 2024b). Diesel fuel consumption in the transportation sector was broken down by motor vehicles, marine, and locomotives. For jet fuel, consumption was only available for the total transportation sector. Transportation sector fuel consumption data for diesel were only available at the Region level.
- Gasoline – 2018 and 2023 total fuel consumption quantities for all sectors, by State (SENER, 2024b). All gasoline was consumed by the transportation sector in Baja California, Chihuahua, and Sonora.

Table A-4 lists all the applicable airports and nonroad SCCs in the three states, their respective projection surrogates, and projection factors used to project 2018 emissions to 2023.

Table A-4. Airports and other nonroad source projection surrogates and factors.

SCC	SCC Description	Projection Surrogate	Projection Factor (Unitless)		
			Baja California	Chihuahua	Sonora
2270002022	Construction Equipment – Diesel	Diesel (motor vehicles)	0.81	1.06	0.81
2270005022	Agricultural Equipment – Diesel	Diesel (motor vehicles)	0.81	1.06	0.81
2270008005	Airports – ground Support Equipment	Jet fuel (transportation)	1.06	1.13	1.06
2275020000	Airports – Commercial Aircrafts	Jet fuel (transportation)	1.06	1.13	1.06
2275070000	Airports – Auxiliary Power Units	Jet fuel (transportation)	1.06	1.13	1.06
2280000000	CMV	Diesel (marine)	0.57	N/A[a]	0.57
2285002006	Locomotives – Diesel, Line Haul	Diesel (locomotives)	1.17	0.84	1.17
2285002010	Locomotives – Diesel, Yard	Diesel (locomotives)	1.17	0.84	1.17
2291001000	Bus Terminals – LDGV[b] and LDGT[b]	Gasoline (total)	0.80	1.03	0.87
2291075000	Bus Terminals - HDDV[b]	Diesel (motor vehicles)	0.81	1.06	0.81

[a] Commercial Marine Vessel (CMV) emissions do not occur in Chihuahua (landlocked state).
[b] LDGV – light duty gasoline vehicles, LDGT – light duty gasoline trucks, and HDDV – heavy duty diesel vehicles.

A.2 Methods to Estimate 2017 and 2023 Mexico Emissions – On-road Sources

On-road sources of emissions include motorcycles, light-duty vehicles (cars and light trucks), buses, and heavy-duty trucks operating on Mexico's roadways. These vehicles emit combustion-related VOC and NOx (among other pollutants) as exhaust through the tailpipe and additional VOC from evaporation of fuel through liquid leaks and vapor escaping from fuel lines and tanks. The analysis for this sector used the most recently updated MOVES-Mexico model available from the Comisión Ambiental de la Megalópolis (CAMe) in Mexico City, MOVES-Mexico 2023, to model the emissions from Mexico-registered vehicles. The model tracks additional vehicle types compared to the US version of MOVES, including source types Taxi, Microbus, and Metrobus, and it excludes source types Refuse Truck and Motor Home (Table A-5).

Table A-5. MOVES-Mexico model source type IDs and names, by three vehicle groups.

Motorcycle and LDVs		Buses		Heavy-Duty Trucks	
11	Motorcycle	41	Intercity Bus	52	Single Unit Short-haul Truck
21	Passenger Car	42	Transit Bus	53	Single Unit Long-haul Truck
22	Taxi	43	School Bus	61	Combination Short-haul Truck
31	Passenger Truck	44	Microbuses Colectivos	62	Combination Long-haul Truck
32	Light Commercial Truck	45	Metrobus		

The MOVES-Mexico model is an adapted version of EPA's MOVES model and was first developed with updates to the vehicle fleet, activity, and emission rates to replace US defaults where possible and to reflect the significant differences in emission standards between Mexico and the US (ERG, 2016). Since that time, the MOVES-Mexico framework has been improved upon as new data became available. The MOVES-Mexico 2023 model is a Mexico-specific MOVES database (named 'movesmexdb20230310') that works directly with the US version of MOVES2014b without any software modification. MOVES-Mexico can estimate on-road emissions for calendar years 1990 and 1999 through 2050 at the national, state, and municipality level. EPA is currently incorporating MOVES-Mexico 2023 based on-road emissions into the 2022v2 emissions modeling platform and has prepared the base year 2022. This work and the 2022v2 platform used same MOVES-Mexico database and inputs, which corrects the projection of vehicle-miles traveled (VMT) from a 2018 base year through 2050 to better reflect the reduced activity of personal vehicles during and after the COVID-19 pandemic. The VMT updates for this work reduce post-2018 VMT from motorcycles and light-duty vehicles in Mexico by adopting the same growth as in the US, which has historical VMT data through year 2023 (Figure A-1), yielding a net increase in VMT of 13% in 2023 compared to 2017. ERG noted a similar pattern in the number of border crossings where personal vehicle crossings decreased in 2020 and had a slow recovery in the subsequent near years. ERG did not adjust the MOVES-Mexico 2023 VMT trend for buses or heavy-duty trucks in this analysis, consistent with the 2022v2 platform. The model shows a 4% decrease in VMT from buses and a 25% increase in VMT from heavy-duty trucks from 2017 to 2023.

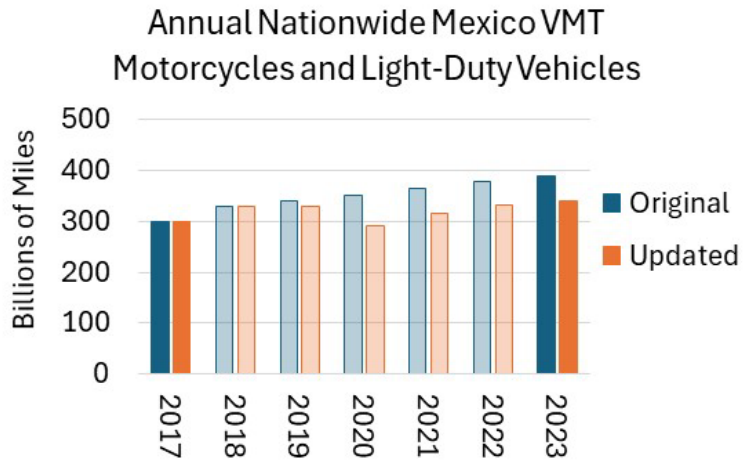

Figure A-1. Updates to original VMT in the MOVES-Mexico 2023 model.

Consistent with the 2022v2 platform, MOVES-Mexico 2023 was applied at the national scale using mostly Mexico default information except for an input database to correct the personal vehicle VMT trend and other inputs related to fuels and methane emissions that ERG developed under contract with EPA. Table A-6 lists the run specification (hereafter "RunSpec") file settings for the general on-road inventory. The general on-road inventory does not include northbound vehicles waiting at the US-Mexico border, because idling activity at the border is not explicitly accounted for in the model. Therefore, ERG performed a separate analysis to include emissions from this known on-road activity.

Table A-6. RunSpec file settings for MOVES-Mexico general on-road inventory.

MOVES-Mexico Navigation Panel	RunSpec Setting
Scale	**Onroad** model; **National** Domain/Scale; **Inventory** Calculation Type
Time Spans	Years **2017, 2023** (separate runs); Months **April** through **September**; Days **Weekend, Weekday**; Hours **00:00 to 23:59**; Time Aggregation Level **Month** (for runs with exhaust emission processes), **Hour** (separate runs with evaporative hydrocarbons; requires hourly)
Geographic Bounds	**State** region; **Baja California, Sonora, Chihuahua** state selections
On-road Vehicle Equipment	**All** Fuels; **All** Source Use Types
Road Type	**All** Road Types
Pollutants and Processes	**All** Emission Processes for NO_X and VOC, plus all MOVES prerequisite pollutants for VOC
Manage Input Data Sets	User input database **movesmex2023_v2updates_rev2**, containing the 2022v2 platform tables FuelFormulation, FuelSupply, HCspeciation, methaneTHCratio, and HPMSVtypeYear (VMT)
General Output	User named output database **mvsmx_mag179b_out**. Unit selection **grams, Joules, miles**. Activity selection **Distance Traveled, Source Hours Operating**
Output Emissions Detail	**Month, State,** and **Source Use Type** output detail

ERG estimated emissions from northbound traffic idling at the US-Mexico border using emission factors derived from the MOVES-Mexico model, paired with average wait times

from US Customs and Border Protection (US CBP, 2025) and the number of vehicle crossings from the US Department of Transportation Bureau of Transportation Statistics (BTS) (US DOT, 2025). Approximately half the vehicles waiting to enter the US are assumed to be US-registered vehicles, which must meet US emission standards and therefore are modeled using EPA's MOVES5 model, the most current version as of August 2025. Table A-7 shows that the MOVES-Mexico and US MOVES5 model settings are nearly identical for the border idling analysis. The RunSpec settings are as consistent as possible with the general on-road inventory in the three Mexican border states, except for low-speed assumptions, and limiting the applicable road types and source types. ERG edited the "AvgSpeedDistribution" table model input by setting 100% of the travel time to occur within the lowest speed bin of 2.5 miles per hour. This speed bin corresponds to model drive cycles with a relatively high amount of idle and start/stop operation.

Table A-7. RunSpec file settings for border idling MOVES runs.

MOVES Navigation Panel	MOVES-Mexico RunSpec Setting	US MOVES5 RunSpec Setting
Scale	Same as Table A-6	Same as Table A-6[a]
Time Spans	Same as Table A-6	Same as Table A-6
Geographic Bounds	Same as Table A-6	**State** region; **California** (separate run)**, Arizona, New Mexico** state selections
On-road Vehicle Equipment	**All** Fuels; Most Source Use Types (excluded Taxi, Transit Bus, School Bus, Microbus, and Metrobus)[b]	**All** Fuels; Most Source Use Types (excluded Transit Bus, School Bus, Refuse Truck, Motor Home)[b]
Road Type	**Urban Unrestricted Access** Road Type	**Urban Unrestricted Access** Road Type
Pollutants and Processes	Same as Table A-6	Same as Table A-6
Manage Input Data Sets	User input database **movesmex2023_v2updates_rev2** already referenced in Table A-6 and **speed_bin1_in**, containing avgSpeedDistribution table with 100% of travel time in the lowest speed bin (2.5 mph average)	User input database **speed_bin1_mvs5_in** and **lev_06_20250106** for the separate runs for California only[c]
General Output	User named output database **bordercrossings_mx_upd_out**	User named output database **bordercrossings_us_upd_out**
Output Emissions Detail	Same as Table A-6	Same as Table A-6

[a] EPA changed the name of model scale "National" to "Default" after MOVES2014b, though it functions the same.
[b] The excluded source types are not expected to cross international borders.
[c] The lev_06_20250106 input database was developed for EPA's 2022v2 platform and was applied in California's run. It contains alternative emission rates to model the state's Low Emission Vehicle (LEV) programs, which are lower than federal emissions requirements.

Table A-8 summarizes vehicle activity at each border crossing in the three states of Baja California, Sonora, and Chihuahua. The average wait time reflects all seven days of the week for hours between 8:00 AM and 8:00 PM during July 2024. The vehicle volumes are year-specific and reflect total crossings from April 1 through September 30. The total volumes for this period were divided by 183 days to arrive at the number vehicles per day in 2017 and 2023. The total number of vehicles at border crossings in the three-state area were approximately 95 percent personal vehicles, 5 percent trucks, and <0.2 percent buses.

Table A-8. Border idling activity summary.

State	Border Crossing Name	Average Wait Time (minutes)	2017 Vehicles Per Day [a]	2023 Vehicles Per Day [a]
Baja California	San Ysidro	120	38,216	44,284
	Otay Mesa	90	24,359	18,773
	Tecate	62	3,091	2,999
	Calexico - West	48	11,948	13,706
	Calexico - East	39	11,328	9,180
	Andrade	17	1,584	1,503
Sonora	San Luis	34	8,501	8,718
	Lukeville	4	1,126	1,299
	Sasabe	4	64	77
	Nogales	71	11,383	11,299
	Naco	9	839	915
	Douglas	30	4,926	4,533
Chihuahua	Columbus	9	1,139	1,145
	Santa Teresa	54	2,030	2,581
	El Paso - Bridge of the Americas	65	37,072	23,204
	El Paso - Ysleta	44	N/A [b]	1,757
	Tornillo	4	891	1,378
	Presidio	14	1,925	1,986
Total (excluding Ysleta) *Personal Vehicles* *Trucks* *Buses*		**75** [c]	**160,421** *152,824* *7,319* *278*	**147,581** *140,970* *6,420* *180*

[a] Day corresponds to an average day during months of April to September.
[b] Ysleta crossing data were missing in 2017; therefore, this crossing is excluded from the emissions analysis.
[c] The overall wait time of 75 minutes reflects the average wait time at each crossing, excluding Ysleta, weighted by total volume of vehicles. The weighted average wait time in 2017 and 2023 was 74 and 76 minutes, respectively.

The analysis paired MOVES emission factors (grams/hour) with the average wait time (converted to hours) and the number of vehicles per day according to:

$$Emissions_{Y,S,P,V} = \sum\left(EF_{Y,P,C,V} \; x \; Wait\ Time_{B,V} \; x \; Volume_{Y,B,V}\right)$$

Where:

Emissions = short tons of pollutant emitted per Ozone Season Day (Apr-Sep);
Y = year (2017, 2023);
S = state (Baja California, Sonora, Chihuahua);
P = pollutant (VOC, NOX);
V = vehicle type (Personal Vehicles, Buses, Trucks);
EF = emission factor in grams of pollutant per hour of idle;
C = country of vehicle origin (50% Mexico, 50% US).
Wait Time = average hours of idle per vehicle, July daytime
B = border crossing (listed by state S in Table A-8)
Volume = number of vehicles

907184 = unit conversion, number of grams per short ton

Calculated emissions for both on-road and border crossings are presented in Table A-9.

Table A-9. 2017 and 2023 three-state total on-road and border crossing idling emissions by vehicle group.

Vehicle Group	State	VOC (Tons/Day)			NOx (Tons/Day)		
		2017	2023	Percent Change	2017	2023	Percent Change
General On-Road Inventory							
Motorcycles and Light-Duty Vehicles	Baja California	75.6	83.0	10%	205.6	216.7	5%
	Chihuahua	75.0	83.7	12%	216.5	228.8	6%
	Sonora	52.1	57.7	11%	132.4	139.3	5%
Buses	Baja California	16.2	12.9	-20%	16.4	14.3	-13%
	Chihuahua	16.9	13.4	-20%	16.6	14.5	-13%
	Sonora	10.1	8.0	-20%	9.8	8.5	-13%
Heavy-Duty Trucks	Baja California	47.3	43.5	-8%	57.3	62.9	10%
	Chihuahua	49.2	45.3	-8%	58.2	63.9	10%
	Sonora	29.3	27.0	-8%	34.3	37.7	10%
Border Crossing Idling Inventory							
Personal Vehicles [a]	Baja California	1.03	1.17	14%	0.91	0.82	-10%
	Chihuahua	0.32	0.24	-24%	0.28	0.17	-40%
	Sonora	0.16	0.17	9%	0.14	0.12	-14%
Buses [b]	Baja California	0.032	0.018	-44%	0.041	0.023	-44%
	Chihuahua	0.005	0.003	-38%	0.006	0.004	-38%
	Sonora	0.004	0.002	-36%	0.005	0.003	-36%
Trucks [c]	Baja California	0.48	0.39	-19%	0.60	0.56	-6%
	Chihuahua	0.27	0.06	-79%	0.33	0.08	-76%
	Sonora	0.11	0.09	-16%	0.13	0.13	-2%
Total		**374.0**	**376.7**	**1%**	**749.7**	**788.6**	**5%**

[a] "Personal Vehicles" is BTS nomenclature and includes Motorcycles and Light-Duty Vehicles.
[b] "Buses" in the Border Crossing Idling Inventory are assumed to be 100% of Intercity/Other Bus source type.
[c] "Trucks" is BTS nomenclature and includes Single Unit and Combination Unit Short- and Long-haul Trucks.

APPENDIX B

Example HYSPLIT Control File

APPENDIX B Example HYSPLIT Control File for May 5, 2021, 19 UTC (12 PM 100 m initiation height, Maricopa NAA northeast corner initiation point)

```
2021 05 05 19
1
33.751874 -111.574461 100
-72
2
15500
4
./NAM12/
20210505_hysplit.t00z.namsa
./NAM12/
20210504_hysplit.t00z.namsa
./NAM12/
20210503_hysplit.t00z.namsa
./NAM12/
20210502_hysplit.t00z.namsa
./hysplit_output_100/
hysplit.ne.20210505.12.100m.72.bt
```

APPENDIX C

Plots of HYSPLIT 3-day Ensemble Trajectories from Each Maricopa NAA Ozone Exceedance Day in 2021–2023

APPENDIX C Plots of HYSPLIT 3-day Ensemble Trajectories from Each Maricopa NAA Ozone Exceedance Day in 2021–2023

All Exceedance Days			All Possible wildfire-impacted days Removed			Atypical Days Removed		
2021	2022	2023	2021	2022	2023	2021	2022	2023
5/5/2021	4/25/2022	4/11/2023	5/5/2021	5/6/2022	4/11/2023	5/5/2021	4/25/2022	4/11/2023
5/6/2021	4/26/2022	4/16/2023	5/6/2021	5/12/2022	4/16/2023	5/6/2021	4/26/2022	4/16/2023
5/12/2021	4/29/2022	4/20/2023	5/12/2021	5/13/2022	4/20/2023	5/12/2021	4/29/2022	4/20/2023
5/13/2021	4/30/2022	5/8/2023	5/13/2021	5/15/2022	5/8/2023	5/13/2021	4/30/2022	5/8/2023
5/24/2021	5/6/2022	5/9/2023	5/24/2021	5/25/2022	5/9/2023	5/24/2021	5/6/2022	5/9/2023
5/26/2021	5/12/2022*	5/11/2023	5/26/2021	5/26/2022	5/11/2023	5/26/2021	5/12/2022	5/11/2023
5/27/2021	5/13/2022	5/12/2023	5/27/2021	6/1/2022	5/12/2023	5/27/2021	5/13/2022	5/12/2023
5/28/2021	5/15/2022	5/14/2023	5/28/2021	6/2/2022	5/17/2023	5/28/2021	5/15/2022	5/14/2023
6/9/2021	5/25/2022	5/15/2023	6/9/2021	6/27/2022	5/20/2023	6/9/2021	5/25/2022	5/15/2023
6/11/2021	5/26/2022	5/16/2023	6/24/2021	6/28/2022	5/22/2023	6/11/2021	5/26/2022	5/16/2023
6/12/2021	6/1/2022	5/17/2023	6/26/2021	6/29/2022	6/1/2023	6/12/2021	6/1/2022	5/17/2023
6/15/2021	6/2/2022	5/20/2023	7/2/2021	6/30/2022	6/4/2023	6/18/2021	6/2/2022	5/20/2023
6/16/2021	6/15/2022	5/21/2023	7/4/2021	7/10/2022	6/8/2023	6/24/2021	6/21/2022	5/21/2023
6/18/2021	6/16/2022	5/22/2023	7/8/2021	8/4/2022	6/9/2023	6/26/2021	6/22/2022	5/22/2023
6/24/2021	6/21/2022	6/1/2023	7/9/2021	8/5/2022	6/13/2023	7/2/2021	6/27/2022	6/1/2023
6/26/2021	6/22/2022	6/4/2023	8/1/2021	8/6/2022	6/14/2023	7/4/2021	6/28/2022	6/4/2023
6/28/2021	6/27/2022	6/8/2023	8/2/2021	8/8/2022	6/15/2023	7/8/2021	6/29/2022	6/8/2023
6/29/2021	6/28/2022	6/9/2023	8/28/2021	8/10/2022	6/29/2023	7/9/2021	6/30/2022	6/9/2023
7/1/2021	6/29/2022	6/13/2023	8/29/2021	8/11/2022	7/3/2023	7/13/2021	7/10/2022	6/13/2023
7/2/2021	6/30/2022	6/14/2023	8/30/2021	8/13/2022	8/15/2023	7/14/2021	7/13/2022	6/14/2023
7/4/2021	7/10/2022	6/15/2023	9/3/2021	8/15/2022	8/16/2023	7/17/2021	7/14/2022	6/15/2023
7/8/2021	7/13/2022	6/17/2023	9/4/2021	8/16/2022	8/24/2023	7/19/2021	7/18/2022	6/17/2023
7/9/2021	7/14/2022	6/22/2023		8/17/2022	8/25/2023	7/27/2021	7/22/2022	6/29/2023
7/13/2021	7/15/2022	6/23/2023		8/18/2022	8/26/2023	7/28/2021	7/23/2022	7/1/2023
7/14/2021	7/16/2022	6/24/2023		8/22/2022	8/28/2023	7/30/2021	8/4/2022	7/2/2023
7/17/2021	7/17/2022	6/25/2023		8/23/2022	8/29/2023	7/31/2021	8/5/2022	7/3/2023
7/19/2021	7/18/2022	6/26/2023		8/24/2022	8/30/2023	8/1/2021	8/6/2022	7/7/2023
7/20/2021	7/22/2022	6/29/2023		8/25/2022		8/2/2021	8/8/2022	7/8/2023
7/21/2021	7/23/2022	6/30/2023		8/26/2022		8/5/2021	8/10/2022	7/18/2023
7/22/2021	8/4/2022	7/1/2023		8/30/2022		8/6/2021	8/11/2022	7/19/2023
7/27/2021	8/5/2022	7/2/2023		8/31/2022		8/17/2021	8/13/2022	7/21/2023
7/28/2021	8/6/2022	7/3/2023		9/1/2022		8/24/2021	8/15/2022	7/22/2023
7/30/2021	8/8/2022	7/7/2023		9/2/2022		8/25/2021	8/16/2022	7/23/2023
7/31/2021	8/10/2022	7/8/2023		9/7/2022		8/26/2021	8/17/2022	8/15/2023
8/1/2021	8/11/2022	7/18/2023		9/8/2022		8/27/2021	8/18/2022	8/16/2023
8/2/2021	8/13/2022	7/19/2023				8/28/2021	8/22/2022	8/22/2023
8/3/2021	8/15/2022	7/21/2023				8/29/2021	8/23/2022	8/24/2023
8/4/2021	8/16/2022	7/22/2023				8/30/2021	8/24/2022	8/25/2023
8/5/2021	8/17/2022	7/23/2023				9/3/2021	8/25/2022	8/26/2023
8/6/2021	8/18/2022	7/24/2023				9/4/2021	8/26/2022	8/28/2023
8/17/2021	8/22/2022	7/25/2023				9/5/2021	8/30/2022	8/29/2023
8/24/2021	8/23/2022	7/26/2023					8/31/2022	8/30/2023
8/25/2021	8/24/2022	7/27/2023					9/1/2022	
8/26/2021	8/25/2022	7/28/2023					9/2/2022	
8/27/2021	8/26/2022	7/29/2023					9/7/2022	
8/28/2021	8/30/2022	7/31/2023					9/8/2022	
8/29/2021	8/31/2022	8/1/2023						
8/30/2021	9/1/2022	8/15/2023						
9/3/2021	9/2/2022	8/16/2023						
9/4/2021	9/7/2022	8/17/2023						
9/5/2021	9/8/2022	8/18/2023						
		8/22/2023						
		8/24/2023						
		8/25/2023						
		8/26/2023						
		8/28/2023						
		8/29/2023						
		8/30/2023						

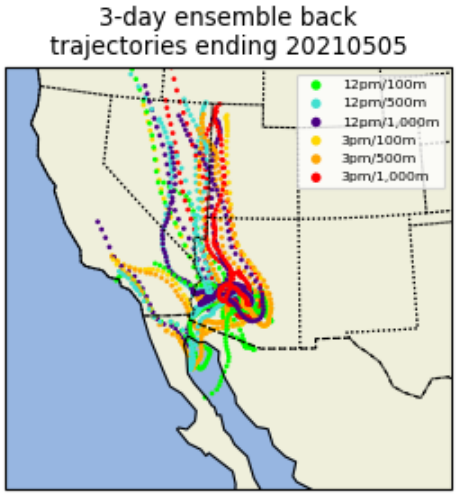
3-day ensemble back trajectories ending 20210505
12pm/100m
12pm/500m
12pm/1,000m
3pm/100m
3pm/500m
3pm/1,000m

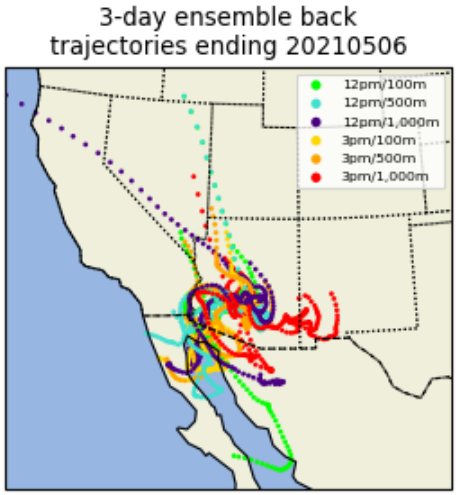
3-day ensemble back trajectories ending 20210506
12pm/100m
12pm/500m
12pm/1,000m
3pm/100m
3pm/500m
3pm/1,000m

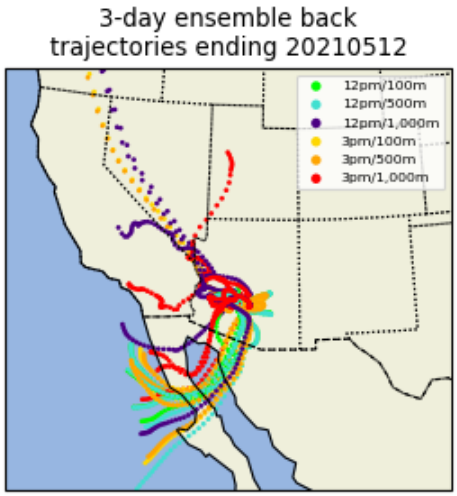
3-day ensemble back trajectories ending 20210512
12pm/100m
12pm/500m
12pm/1,000m
3pm/100m
3pm/500m
3pm/1,000m

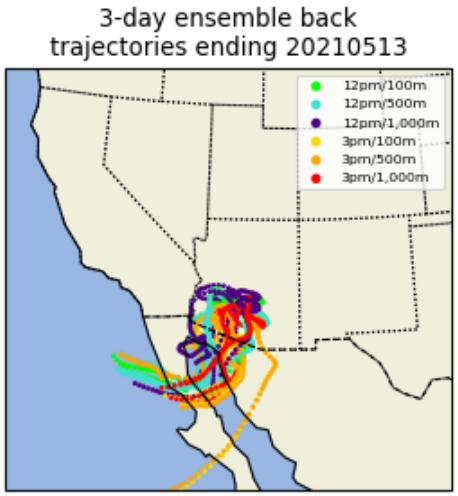
3-day ensemble back trajectories ending 20210513
12pm/100m
12pm/500m
12pm/1,000m
3pm/100m
3pm/500m
3pm/1,000m

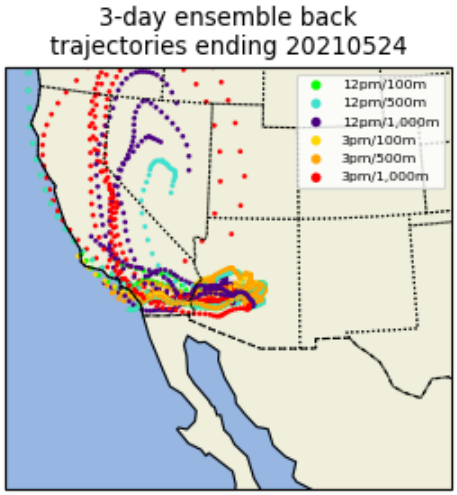
3-day ensemble back trajectories ending 20210524
12pm/100m
12pm/500m
12pm/1,000m
3pm/100m
3pm/500m
3pm/1,000m

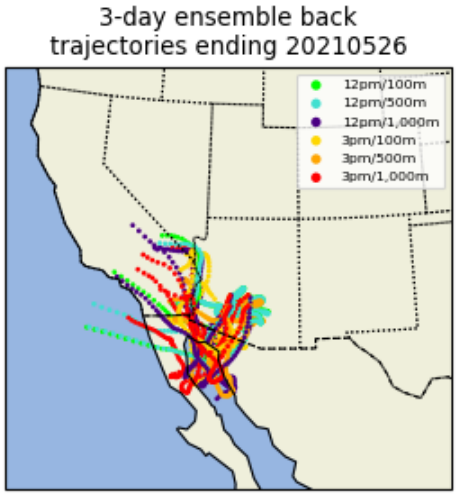
3-day ensemble back trajectories ending 20210526
12pm/100m
12pm/500m
12pm/1,000m
3pm/100m
3pm/500m
3pm/1,000m

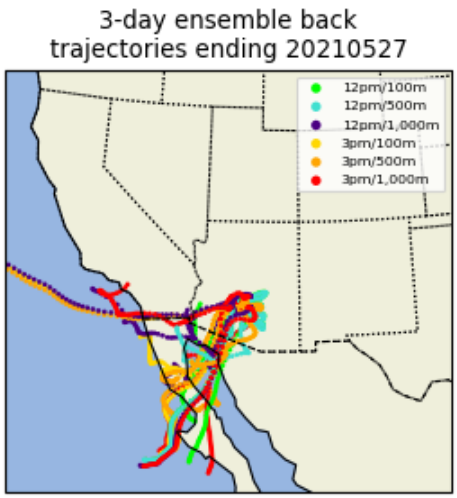
3-day ensemble back trajectories ending 20210527
12pm/100m
12pm/500m
12pm/1,000m
3pm/100m
3pm/500m
3pm/1,000m

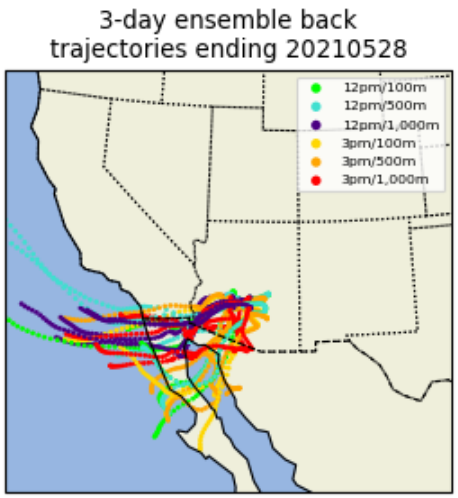
3-day ensemble back trajectories ending 20210528
12pm/100m
12pm/500m
12pm/1,000m
3pm/100m
3pm/500m
3pm/1,000m

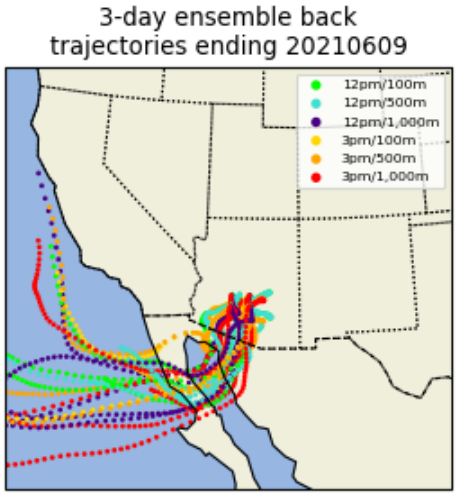
3-day ensemble back trajectories ending 20210609
12pm/100m
12pm/500m
12pm/1,000m
3pm/100m
3pm/500m
3pm/1,000m

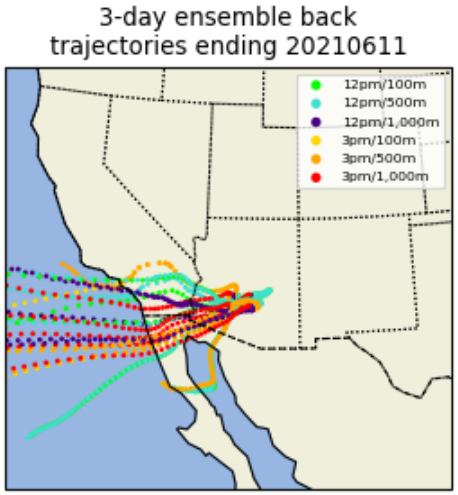
3-day ensemble back trajectories ending 20210611
12pm/100m
12pm/500m
12pm/1,000m
3pm/100m
3pm/500m
3pm/1,000m

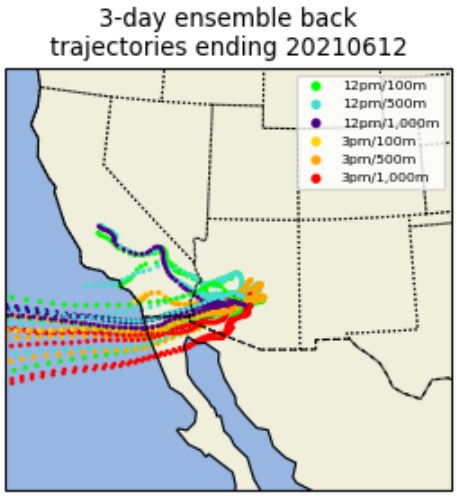
3-day ensemble back trajectories ending 20210612
12pm/100m
12pm/500m
12pm/1,000m
3pm/100m
3pm/500m
3pm/1,000m

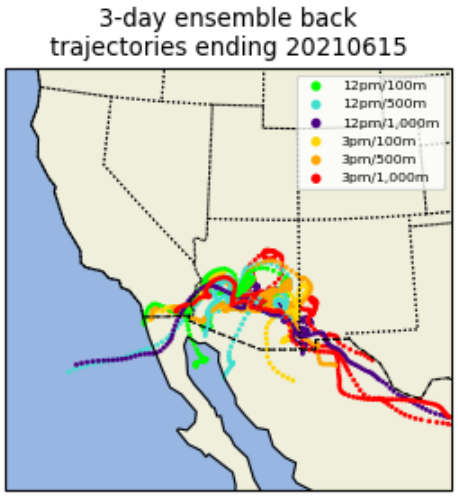
3-day ensemble back trajectories ending 20210615
12pm/100m
12pm/500m
12pm/1,000m
3pm/100m
3pm/500m
3pm/1,000m

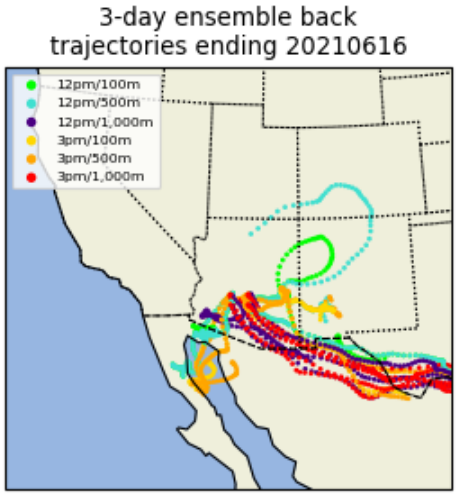
3-day ensemble back trajectories ending 20210616
12pm/100m
12pm/500m
12pm/1,000m
3pm/100m
3pm/500m
3pm/1,000m

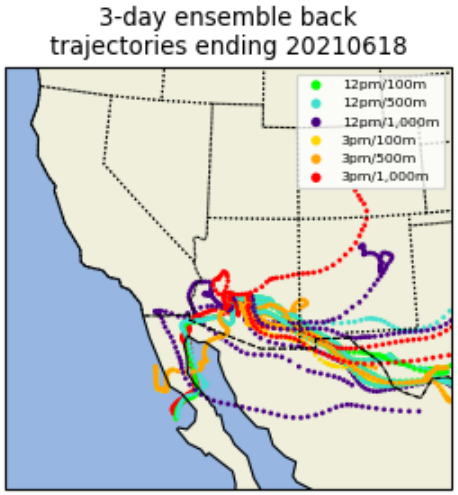
3-day ensemble back trajectories ending 20210618
12pm/100m
12pm/500m
12pm/1,000m
3pm/100m
3pm/500m
3pm/1,000m

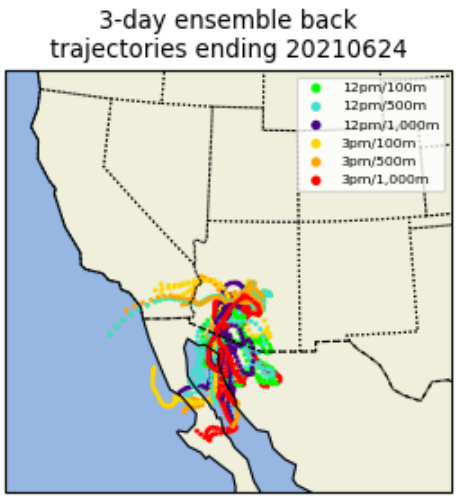
3-day ensemble back trajectories ending 20210624
12pm/100m
12pm/500m
12pm/1,000m
3pm/100m
3pm/500m
3pm/1,000m

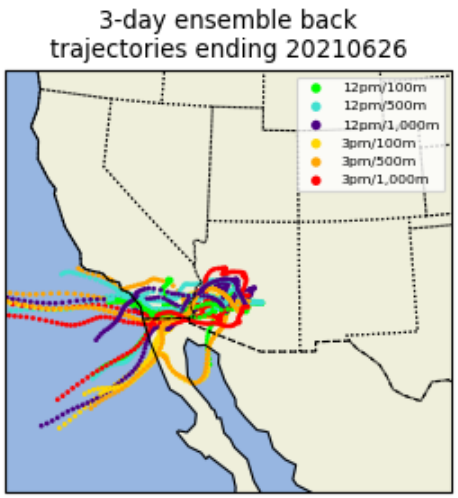
3-day ensemble back trajectories ending 20210626
12pm/100m
12pm/500m
12pm/1,000m
3pm/100m
3pm/500m
3pm/1,000m

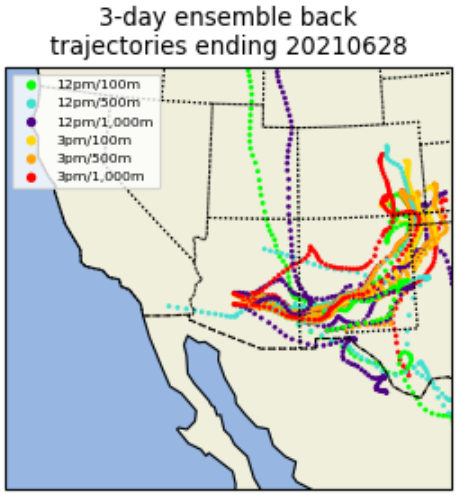
3-day ensemble back trajectories ending 20210628
12pm/100m
12pm/500m
12pm/1,000m
3pm/100m
3pm/500m
3pm/1,000m

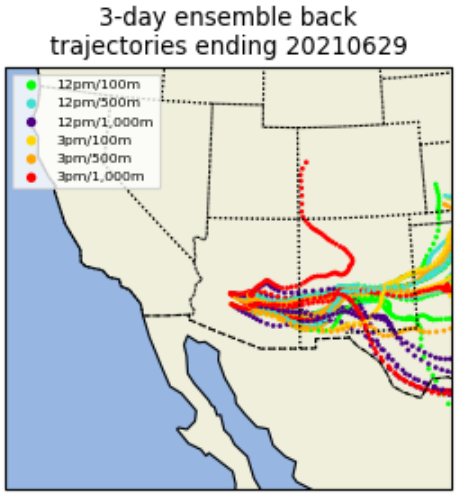
3-day ensemble back trajectories ending 20210629
12pm/100m
12pm/500m
12pm/1,000m
3pm/100m
3pm/500m
3pm/1,000m

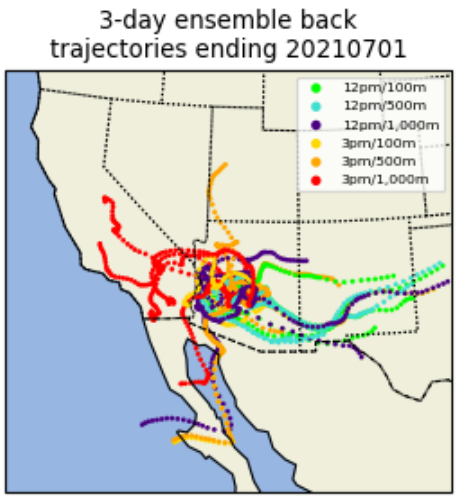
3-day ensemble back trajectories ending 20210701
12pm/100m
12pm/500m
12pm/1,000m
3pm/100m
3pm/500m
3pm/1,000m

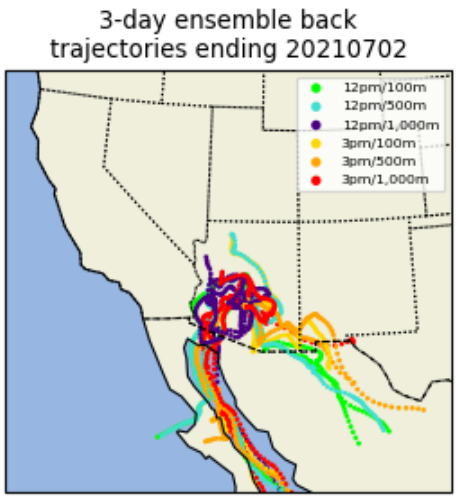
3-day ensemble back trajectories ending 20210702
12pm/100m
12pm/500m
12pm/1,000m
3pm/100m
3pm/500m
3pm/1,000m

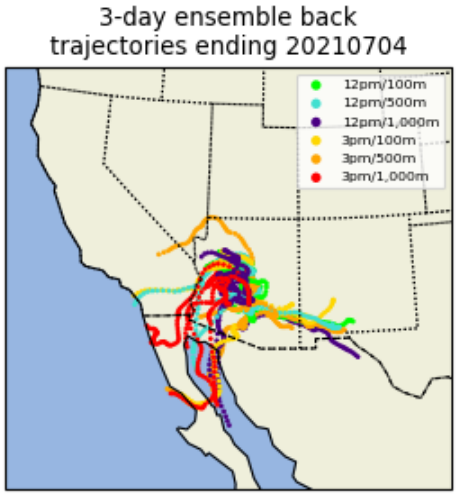
3-day ensemble back trajectories ending 20210704
12pm/100m
12pm/500m
12pm/1,000m
3pm/100m
3pm/500m
3pm/1,000m

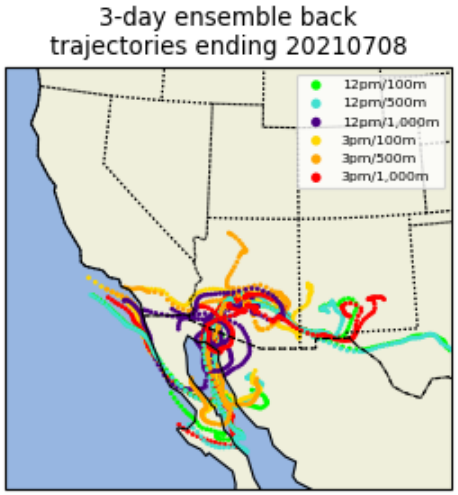
3-day ensemble back trajectories ending 20210708
12pm/100m
12pm/500m
12pm/1,000m
3pm/100m
3pm/500m
3pm/1,000m

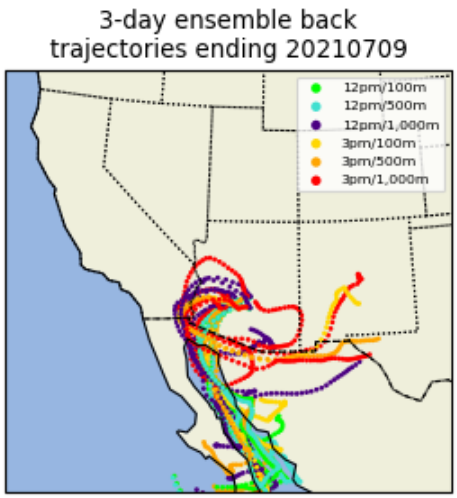
3-day ensemble back trajectories ending 20210709
12pm/100m
12pm/500m
12pm/1,000m
3pm/100m
3pm/500m
3pm/1,000m

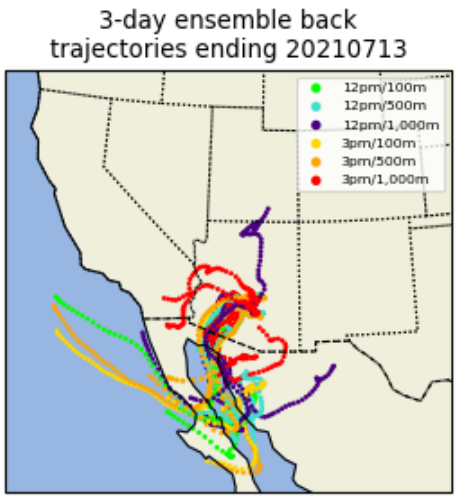
3-day ensemble back trajectories ending 20210713
12pm/100m
12pm/500m
12pm/1,000m
3pm/100m
3pm/500m
3pm/1,000m

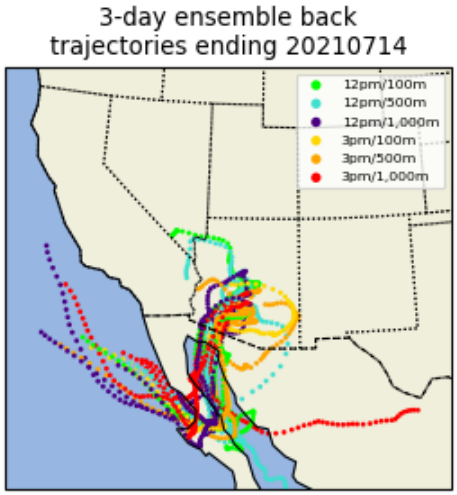
3-day ensemble back trajectories ending 20210714
12pm/100m
12pm/500m
12pm/1,000m
3pm/100m
3pm/500m
3pm/1,000m

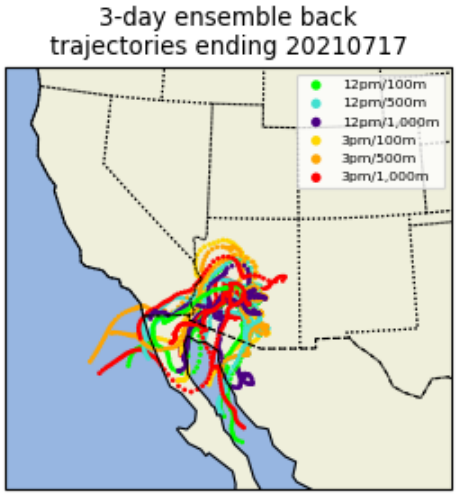
3-day ensemble back trajectories ending 20210717
12pm/100m
12pm/500m
12pm/1,000m
3pm/100m
3pm/500m
3pm/1,000m

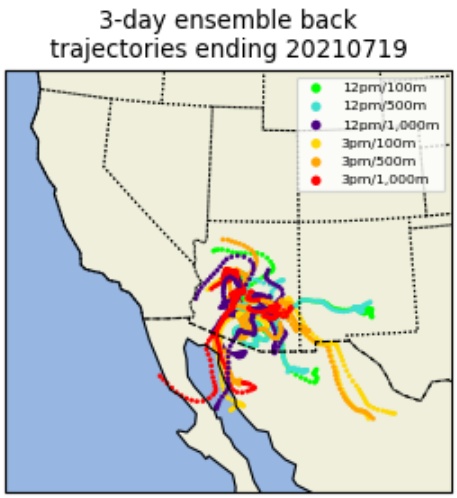
3-day ensemble back trajectories ending 20210719
12pm/100m
12pm/500m
12pm/1,000m
3pm/100m
3pm/500m
3pm/1,000m

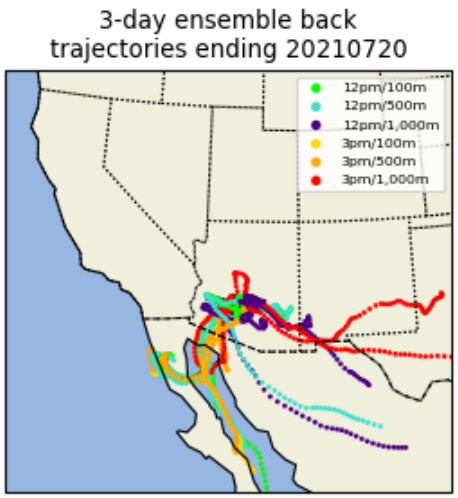
3-day ensemble back trajectories ending 20210720
12pm/100m
12pm/500m
12pm/1,000m
3pm/100m
3pm/500m
3pm/1,000m

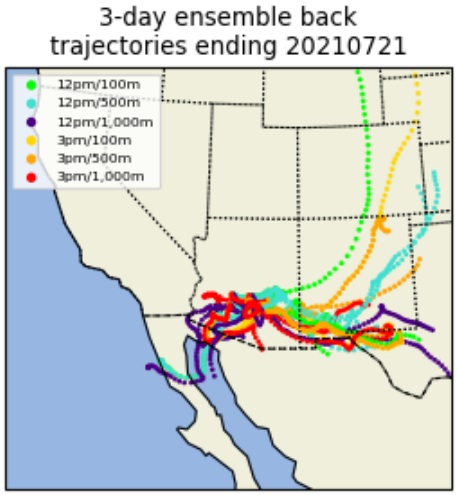
3-day ensemble back trajectories ending 20210721
12pm/100m
12pm/500m
12pm/1,000m
3pm/100m
3pm/500m
3pm/1,000m

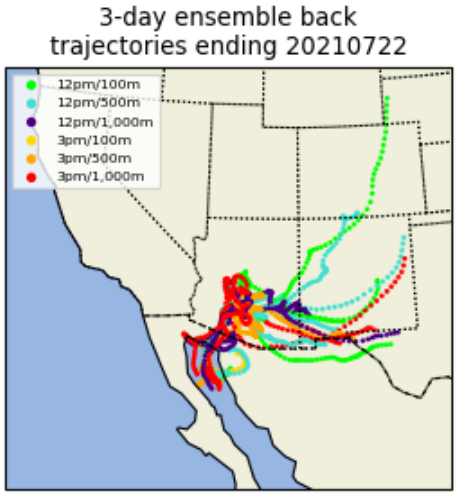
3-day ensemble back trajectories ending 20210722
12pm/100m
12pm/500m
12pm/1,000m
3pm/100m
3pm/500m
3pm/1,000m

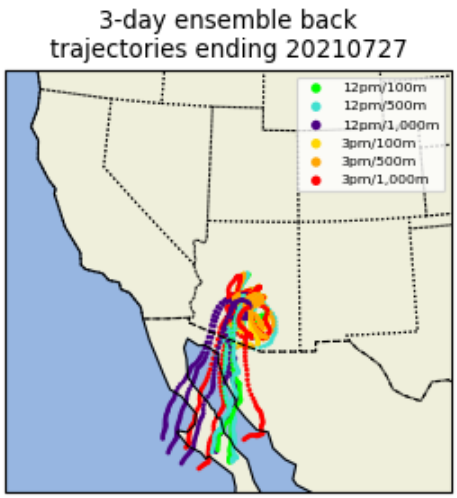
3-day ensemble back trajectories ending 20210727
12pm/100m
12pm/500m
12pm/1,000m
3pm/100m
3pm/500m
3pm/1,000m

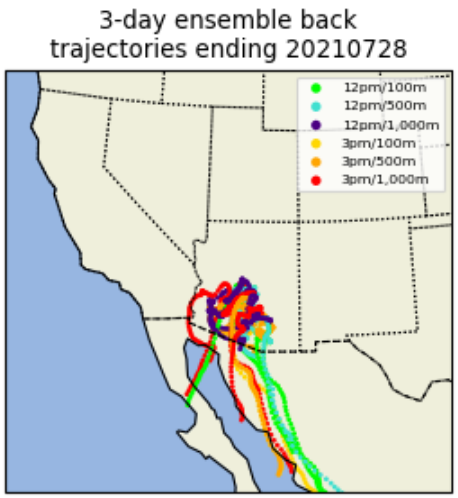
3-day ensemble back trajectories ending 20210728
12pm/100m
12pm/500m
12pm/1,000m
3pm/100m
3pm/500m
3pm/1,000m

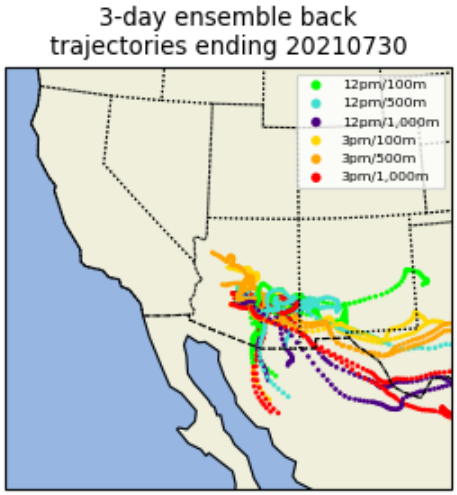
3-day ensemble back trajectories ending 20210730
12pm/100m
12pm/500m
12pm/1,000m
3pm/100m
3pm/500m
3pm/1,000m

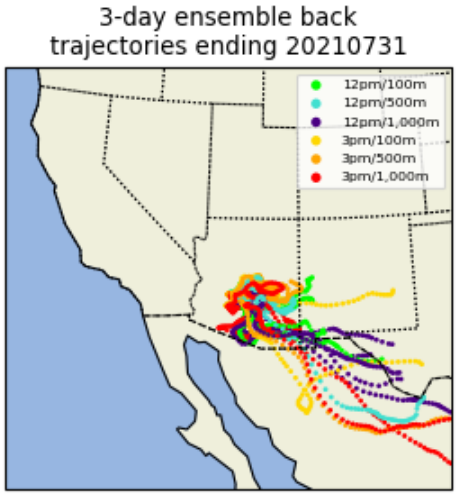
3-day ensemble back trajectories ending 20210731
12pm/100m
12pm/500m
12pm/1,000m
3pm/100m
3pm/500m
3pm/1,000m

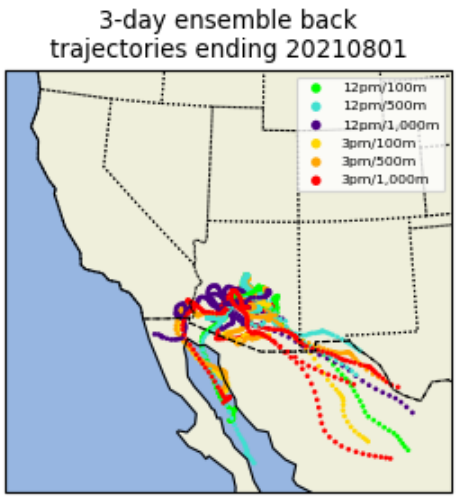
3-day ensemble back trajectories ending 20210801
12pm/100m
12pm/500m
12pm/1,000m
3pm/100m
3pm/500m
3pm/1,000m

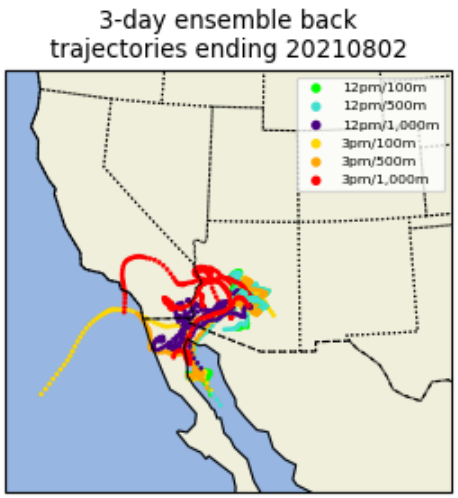
3-day ensemble back trajectories ending 20210802
12pm/100m
12pm/500m
12pm/1,000m
3pm/100m
3pm/500m
3pm/1,000m

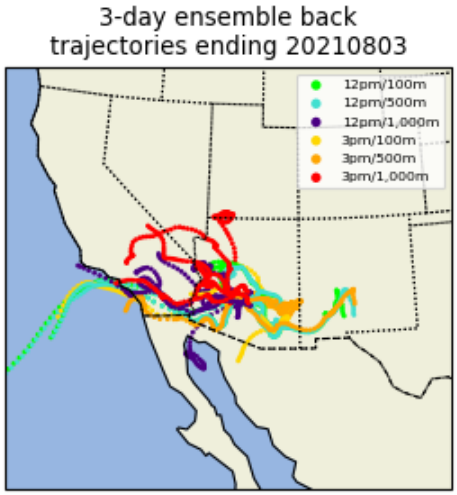
3-day ensemble back trajectories ending 20210803
12pm/100m
12pm/500m
12pm/1,000m
3pm/100m
3pm/500m
3pm/1,000m

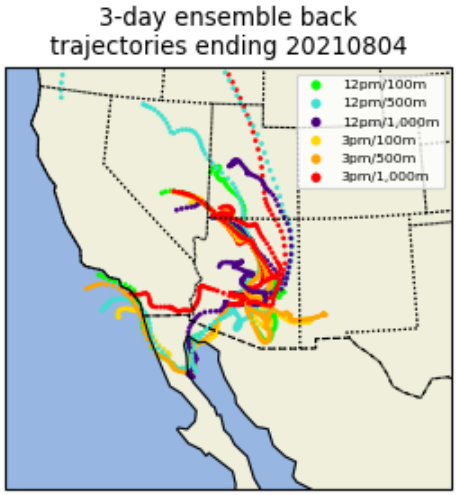
3-day ensemble back trajectories ending 20210804
12pm/100m
12pm/500m
12pm/1,000m
3pm/100m
3pm/500m
3pm/1,000m

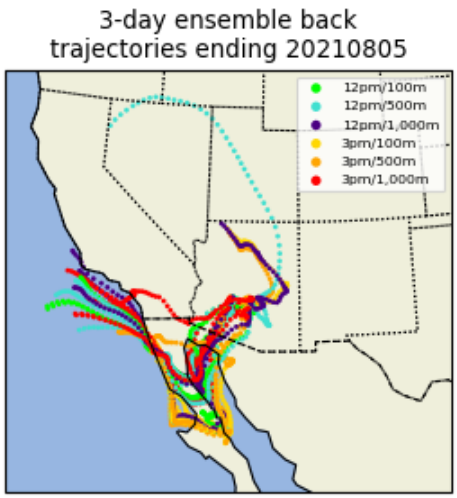
3-day ensemble back trajectories ending 20210805
12pm/100m
12pm/500m
12pm/1,000m
3pm/100m
3pm/500m
3pm/1,000m

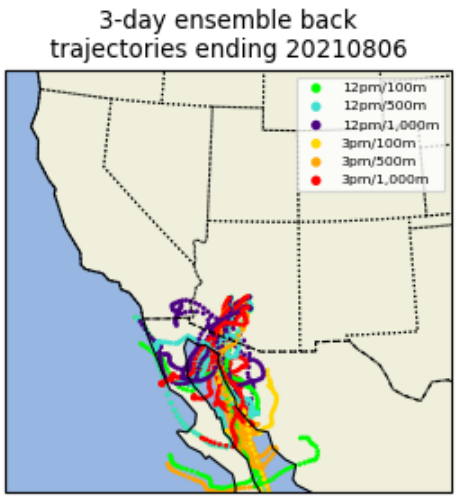
3-day ensemble back trajectories ending 20210806
12pm/100m
12pm/500m
12pm/1,000m
3pm/100m
3pm/500m
3pm/1,000m

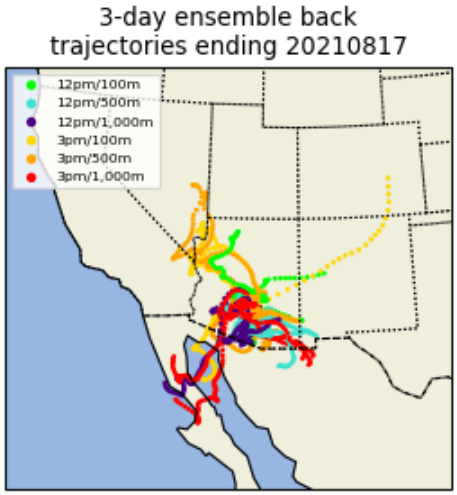
3-day ensemble back trajectories ending 20210817
12pm/100m
12pm/500m
12pm/1,000m
3pm/100m
3pm/500m
3pm/1,000m

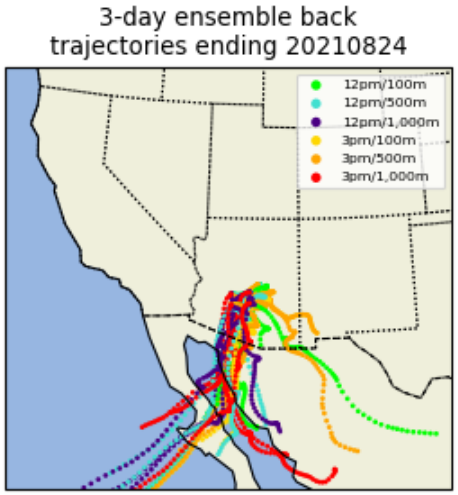
3-day ensemble back trajectories ending 20210824
12pm/100m
12pm/500m
12pm/1,000m
3pm/100m
3pm/500m
3pm/1,000m

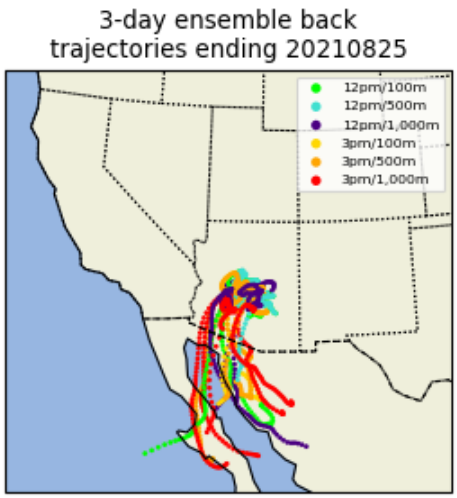
3-day ensemble back trajectories ending 20210825
12pm/100m
12pm/500m
12pm/1,000m
3pm/100m
3pm/500m
3pm/1,000m

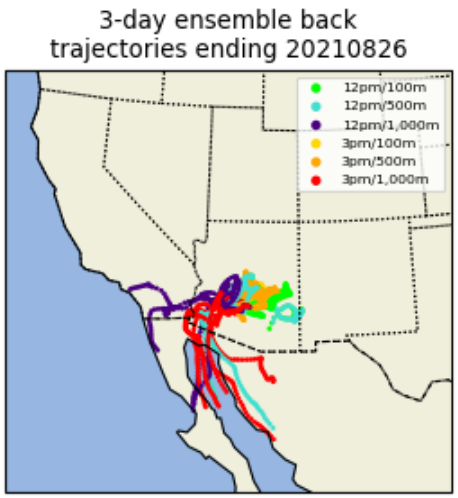
3-day ensemble back trajectories ending 20210826
12pm/100m
12pm/500m
12pm/1,000m
3pm/100m
3pm/500m
3pm/1,000m

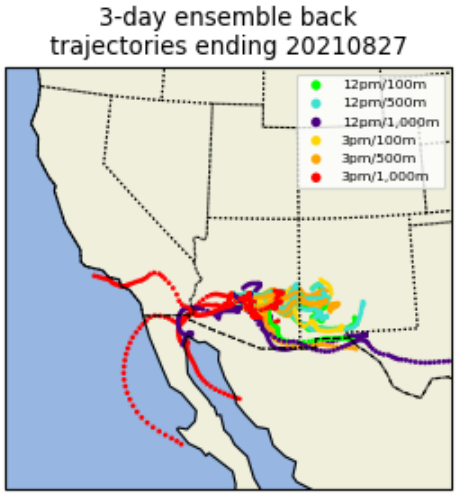
3-day ensemble back trajectories ending 20210827
12pm/100m
12pm/500m
12pm/1,000m
3pm/100m
3pm/500m
3pm/1,000m

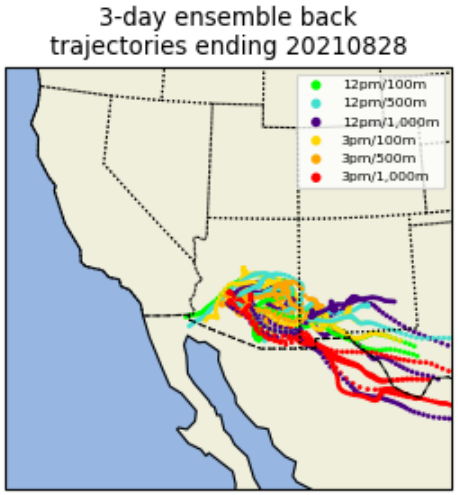
3-day ensemble back trajectories ending 20210828
12pm/100m
12pm/500m
12pm/1,000m
3pm/100m
3pm/500m
3pm/1,000m

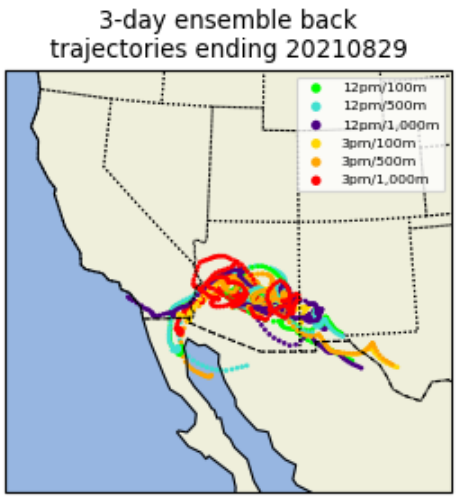
3-day ensemble back trajectories ending 20210829
12pm/100m
12pm/500m
12pm/1,000m
3pm/100m
3pm/500m
3pm/1,000m

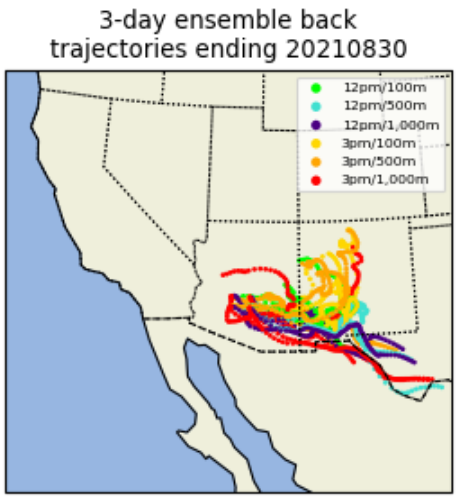
3-day ensemble back trajectories ending 20210830
12pm/100m
12pm/500m
12pm/1,000m
3pm/100m
3pm/500m
3pm/1,000m

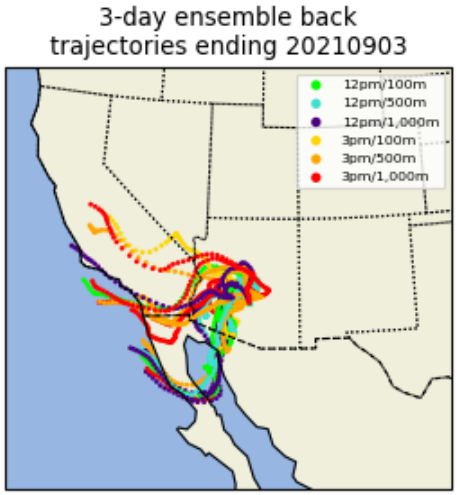
3-day ensemble back trajectories ending 20210903
12pm/100m
12pm/500m
12pm/1,000m
3pm/100m
3pm/500m
3pm/1,000m

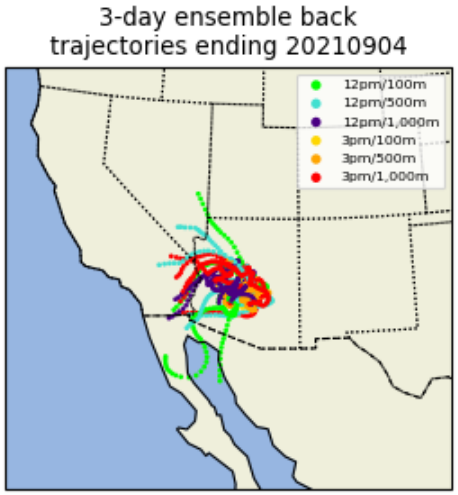
3-day ensemble back trajectories ending 20210904
12pm/100m
12pm/500m
12pm/1,000m
3pm/100m
3pm/500m
3pm/1,000m

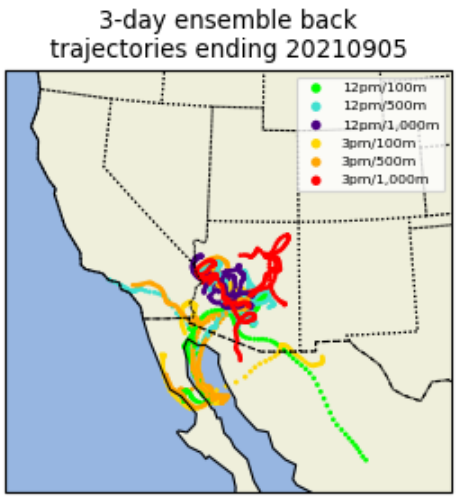
3-day ensemble back trajectories ending 20210905
12pm/100m
12pm/500m
12pm/1,000m
3pm/100m
3pm/500m
3pm/1,000m

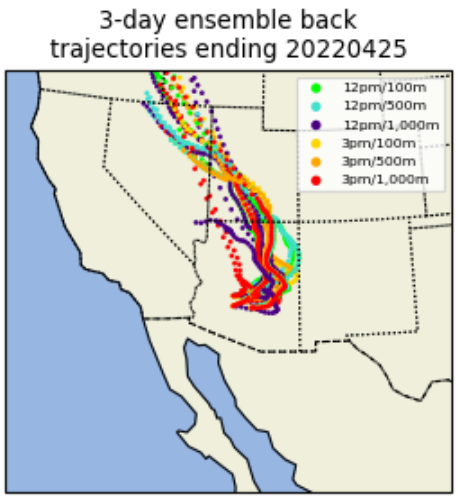
3-day ensemble back trajectories ending 20220425
12pm/100m
12pm/500m
12pm/1,000m
3pm/100m
3pm/500m
3pm/1,000m

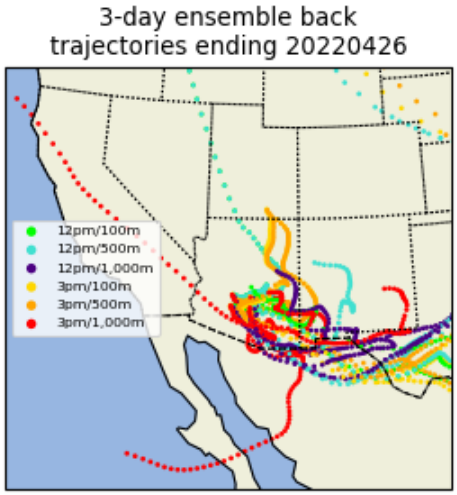
3-day ensemble back trajectories ending 20220426
12pm/100m
12pm/500m
12pm/1,000m
3pm/100m
3pm/500m
3pm/1,000m

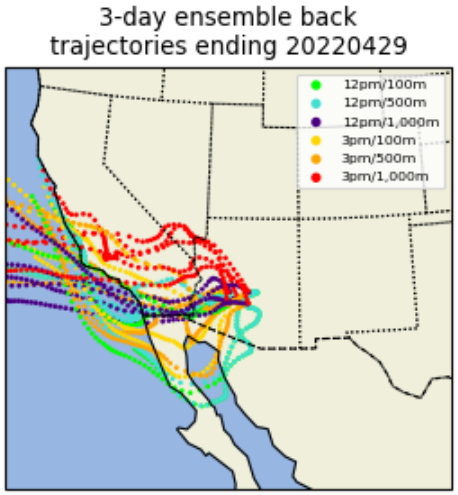
3-day ensemble back trajectories ending 20220429
12pm/100m
12pm/500m
12pm/1,000m
3pm/100m
3pm/500m
3pm/1,000m

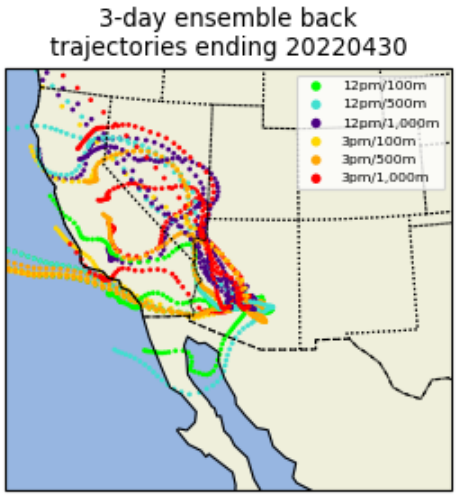
3-day ensemble back trajectories ending 20220430
12pm/100m
12pm/500m
12pm/1,000m
3pm/100m
3pm/500m
3pm/1,000m

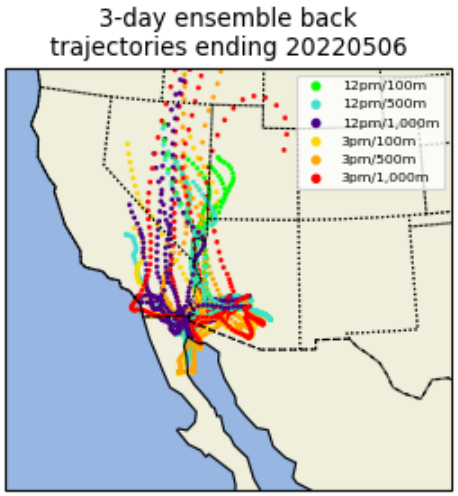
3-day ensemble back trajectories ending 20220506
12pm/100m
12pm/500m
12pm/1,000m
3pm/100m
3pm/500m
3pm/1,000m

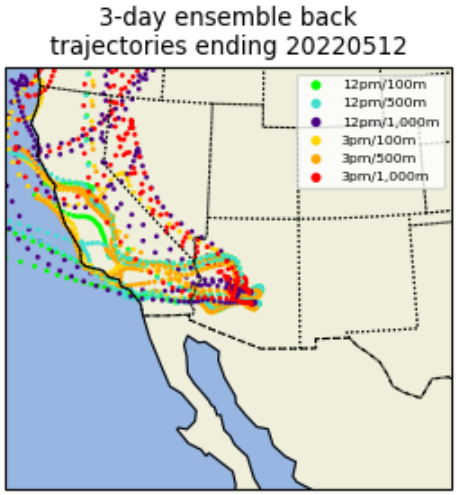
3-day ensemble back trajectories ending 20220512
12pm/100m
12pm/500m
12pm/1,000m
3pm/100m
3pm/500m
3pm/1,000m

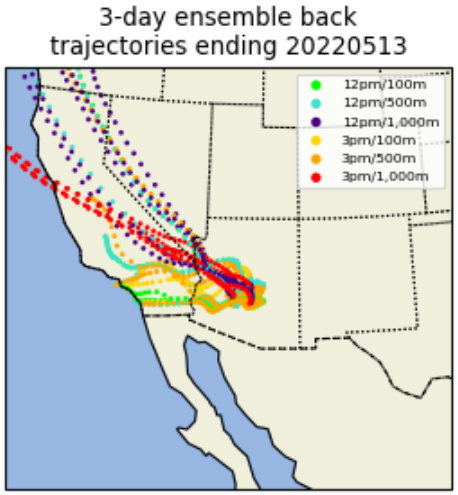
3-day ensemble back trajectories ending 20220513
12pm/100m
12pm/500m
12pm/1,000m
3pm/100m
3pm/500m
3pm/1,000m

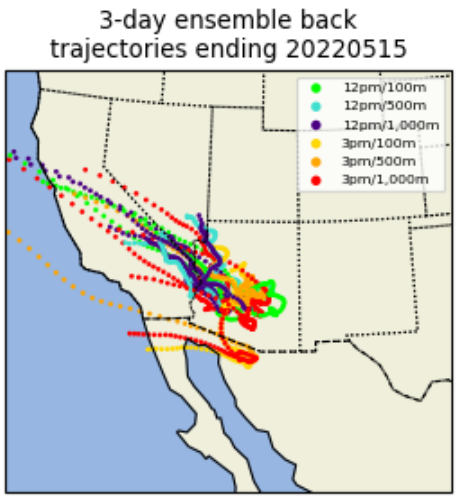
3-day ensemble back trajectories ending 20220515
12pm/100m
12pm/500m
12pm/1,000m
3pm/100m
3pm/500m
3pm/1,000m

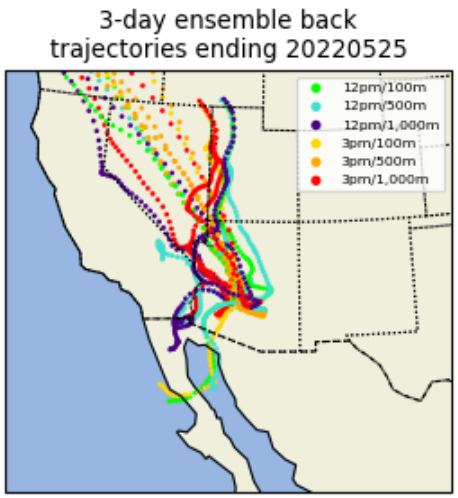
3-day ensemble back trajectories ending 20220525
12pm/100m
12pm/500m
12pm/1,000m
3pm/100m
3pm/500m
3pm/1,000m

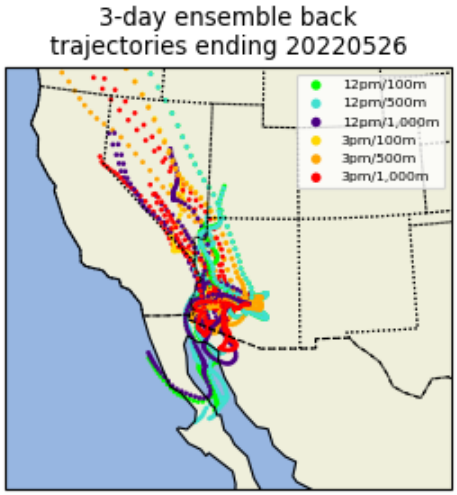
3-day ensemble back trajectories ending 20220526
12pm/100m
12pm/500m
12pm/1,000m
3pm/100m
3pm/500m
3pm/1,000m

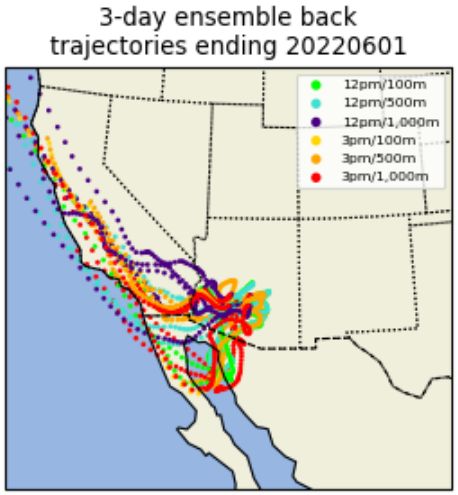
3-day ensemble back trajectories ending 20220601
12pm/100m
12pm/500m
12pm/1,000m
3pm/100m
3pm/500m
3pm/1,000m

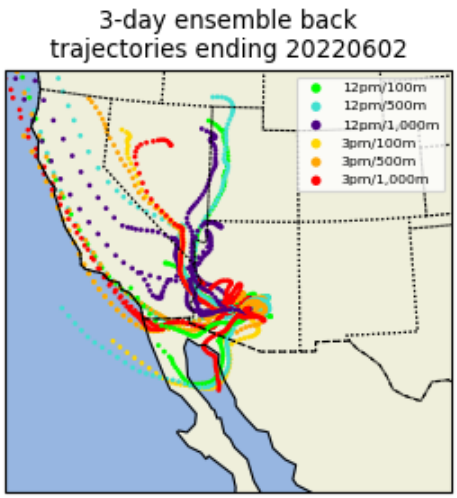
3-day ensemble back trajectories ending 20220602
12pm/100m
12pm/500m
12pm/1,000m
3pm/100m
3pm/500m
3pm/1,000m

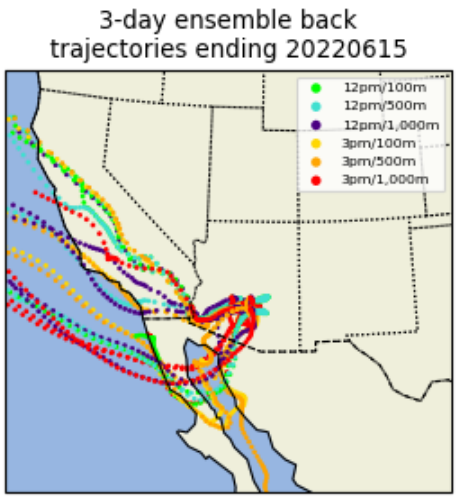
3-day ensemble back trajectories ending 20220615
12pm/100m
12pm/500m
12pm/1,000m
3pm/100m
3pm/500m
3pm/1,000m

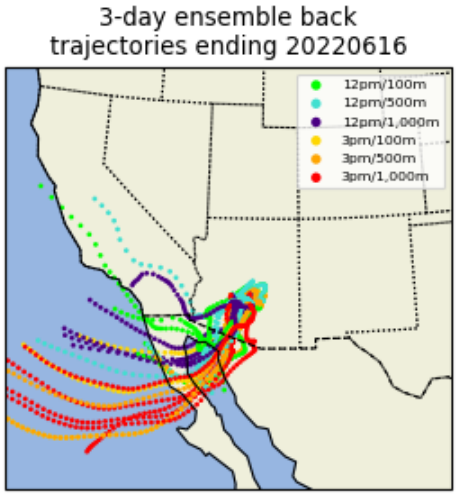
3-day ensemble back trajectories ending 20220616
12pm/100m
12pm/500m
12pm/1,000m
3pm/100m
3pm/500m
3pm/1,000m

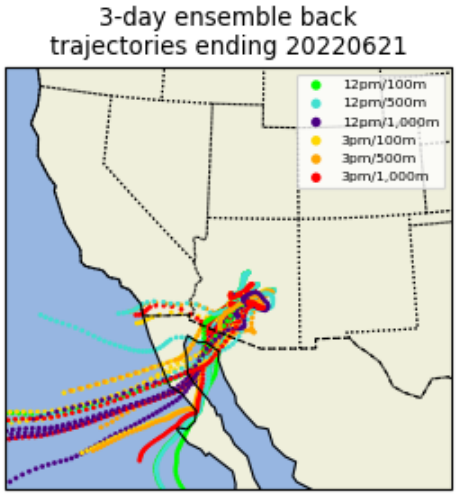
3-day ensemble back trajectories ending 20220621
12pm/100m
12pm/500m
12pm/1,000m
3pm/100m
3pm/500m
3pm/1,000m

3-day ensemble back trajectories ending 20220622
12pm/100m
12pm/500m
12pm/1,000m
3pm/100m
3pm/500m
3pm/1,000m

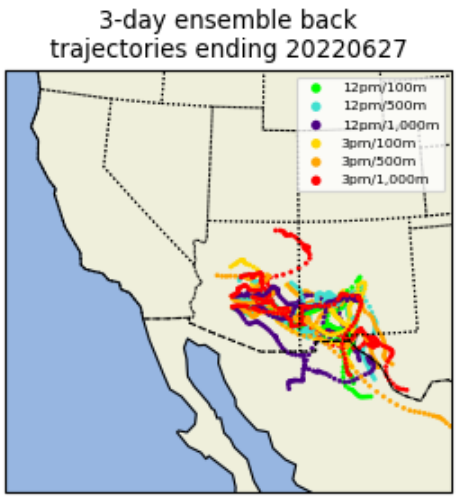
3-day ensemble back trajectories ending 20220627
12pm/100m
12pm/500m
12pm/1,000m
3pm/100m
3pm/500m
3pm/1,000m

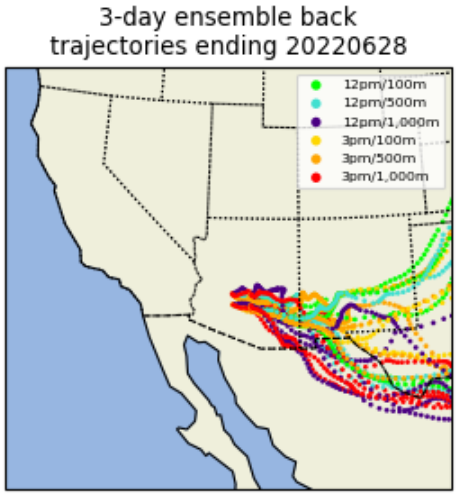
3-day ensemble back trajectories ending 20220628
12pm/100m
12pm/500m
12pm/1,000m
3pm/100m
3pm/500m
3pm/1,000m

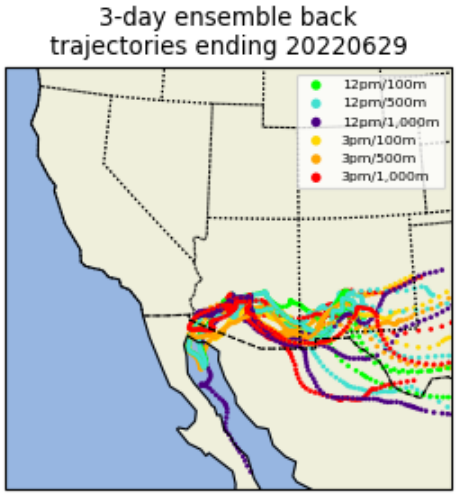
3-day ensemble back trajectories ending 20220629
12pm/100m
12pm/500m
12pm/1,000m
3pm/100m
3pm/500m
3pm/1,000m

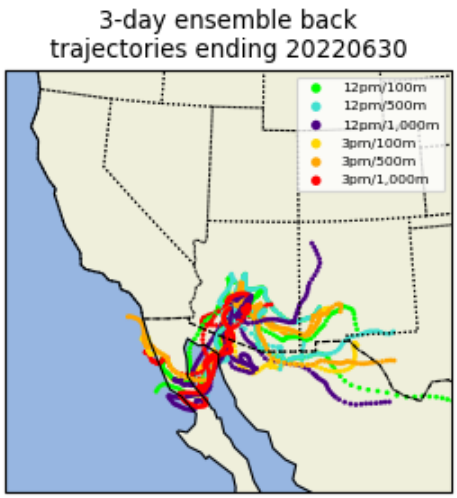
3-day ensemble back trajectories ending 20220630
12pm/100m
12pm/500m
12pm/1,000m
3pm/100m
3pm/500m
3pm/1,000m

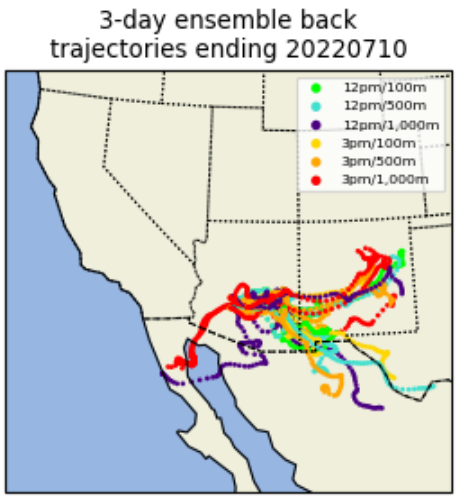
3-day ensemble back trajectories ending 20220710
12pm/100m
12pm/500m
12pm/1,000m
3pm/100m
3pm/500m
3pm/1,000m

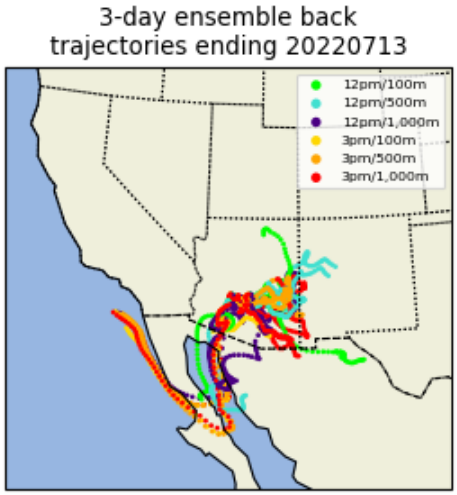
3-day ensemble back trajectories ending 20220713
12pm/100m
12pm/500m
12pm/1,000m
3pm/100m
3pm/500m
3pm/1,000m

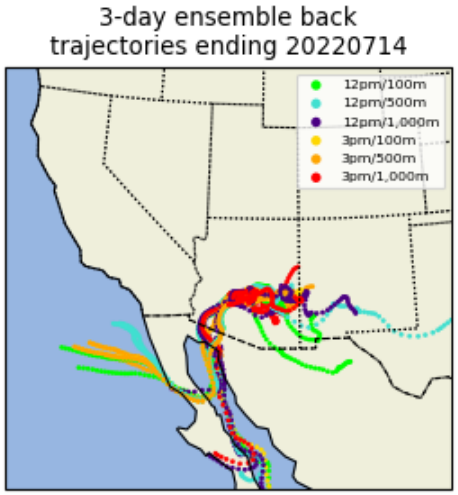
3-day ensemble back trajectories ending 20220714
12pm/100m
12pm/500m
12pm/1,000m
3pm/100m
3pm/500m
3pm/1,000m

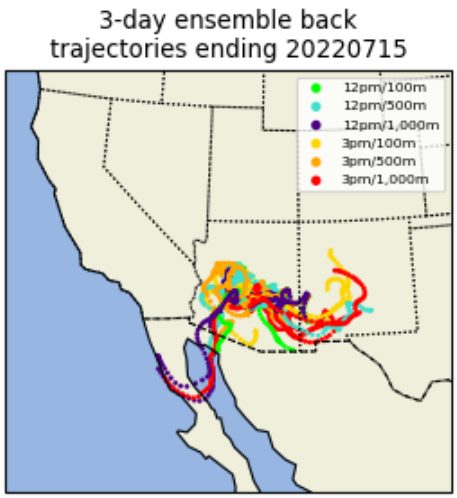
3-day ensemble back trajectories ending 20220715
12pm/100m
12pm/500m
12pm/1,000m
3pm/100m
3pm/500m
3pm/1,000m

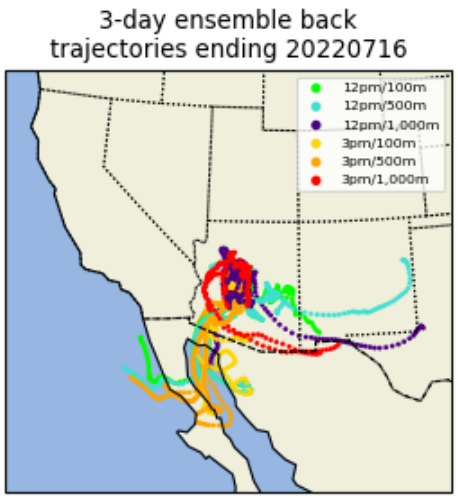
3-day ensemble back trajectories ending 20220716
12pm/100m
12pm/500m
12pm/1,000m
3pm/100m
3pm/500m
3pm/1,000m

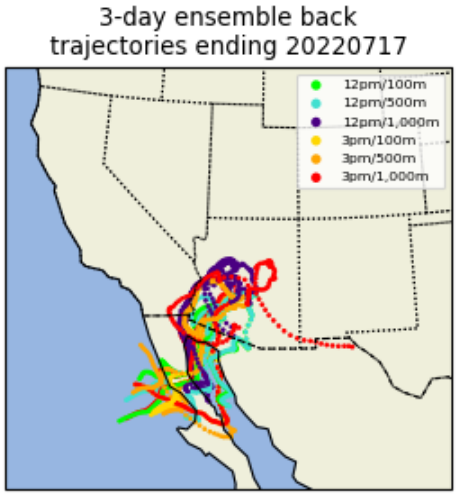
3-day ensemble back trajectories ending 20220717
12pm/100m
12pm/500m
12pm/1,000m
3pm/100m
3pm/500m
3pm/1,000m

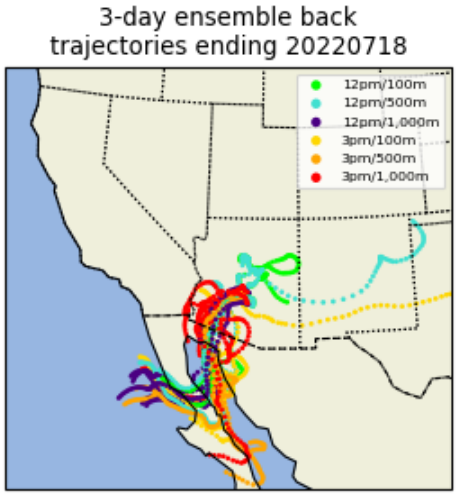
3-day ensemble back trajectories ending 20220718
12pm/100m
12pm/500m
12pm/1,000m
3pm/100m
3pm/500m
3pm/1,000m

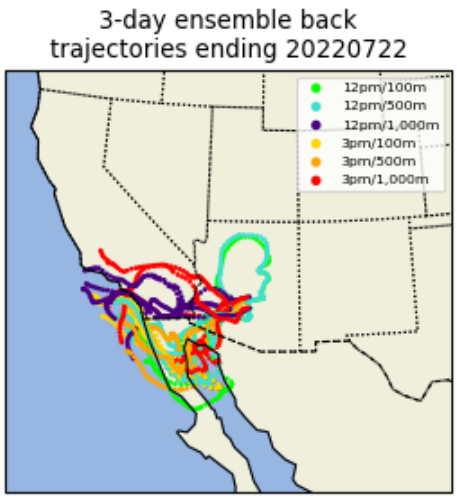
3-day ensemble back trajectories ending 20220722
12pm/100m
12pm/500m
12pm/1,000m
3pm/100m
3pm/500m
3pm/1,000m

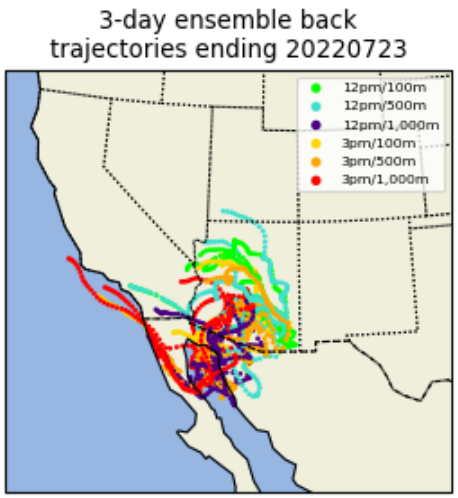
3-day ensemble back trajectories ending 20220723
12pm/100m
12pm/500m
12pm/1,000m
3pm/100m
3pm/500m
3pm/1,000m

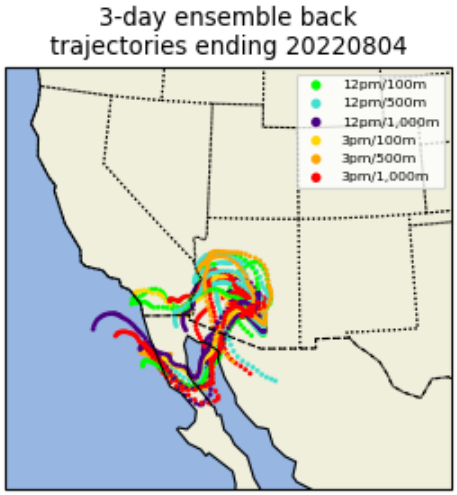
3-day ensemble back trajectories ending 20220804
12pm/100m
12pm/500m
12pm/1,000m
3pm/100m
3pm/500m
3pm/1,000m

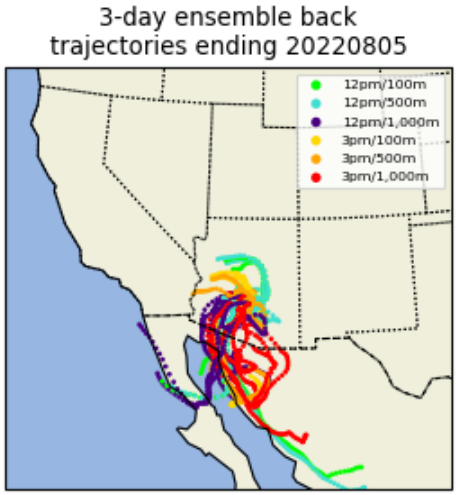
3-day ensemble back trajectories ending 20220805
12pm/100m
12pm/500m
12pm/1,000m
3pm/100m
3pm/500m
3pm/1,000m

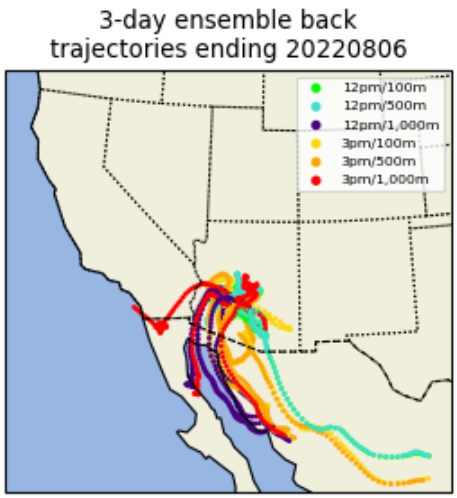
3-day ensemble back trajectories ending 20220806
12pm/100m
12pm/500m
12pm/1,000m
3pm/100m
3pm/500m
3pm/1,000m

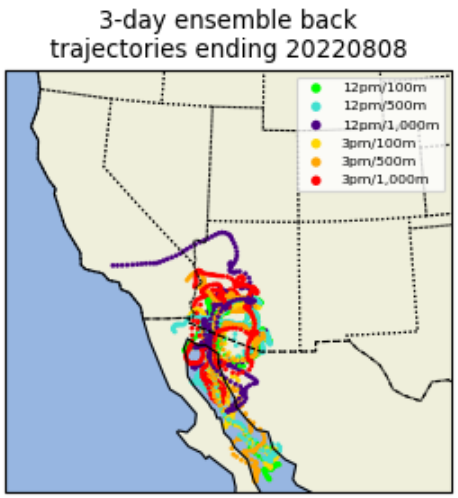
3-day ensemble back trajectories ending 20220808
12pm/100m
12pm/500m
12pm/1,000m
3pm/100m
3pm/500m
3pm/1,000m

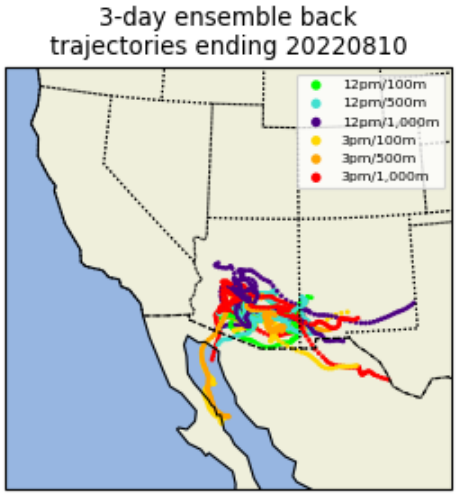
3-day ensemble back trajectories ending 20220810
12pm/100m
12pm/500m
12pm/1,000m
3pm/100m
3pm/500m
3pm/1,000m

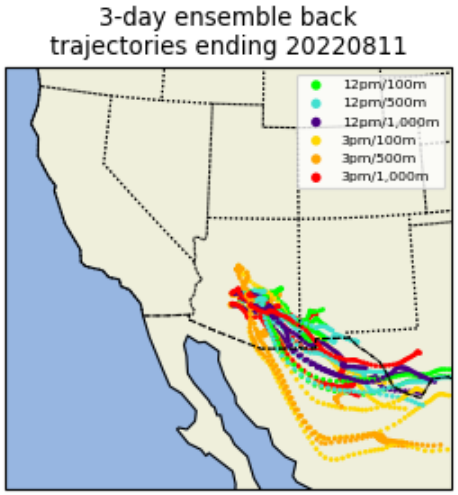
3-day ensemble back trajectories ending 20220811
12pm/100m
12pm/500m
12pm/1,000m
3pm/100m
3pm/500m
3pm/1,000m

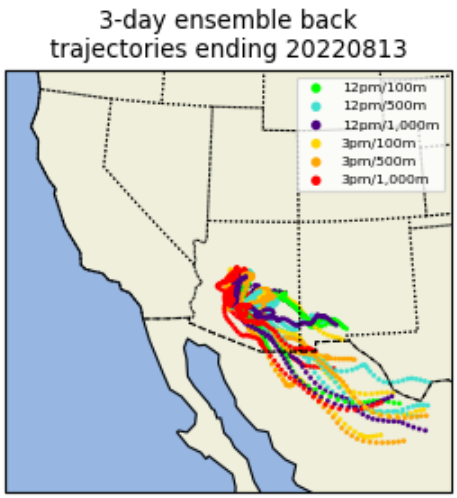
3-day ensemble back trajectories ending 20220813
12pm/100m
12pm/500m
12pm/1,000m
3pm/100m
3pm/500m
3pm/1,000m

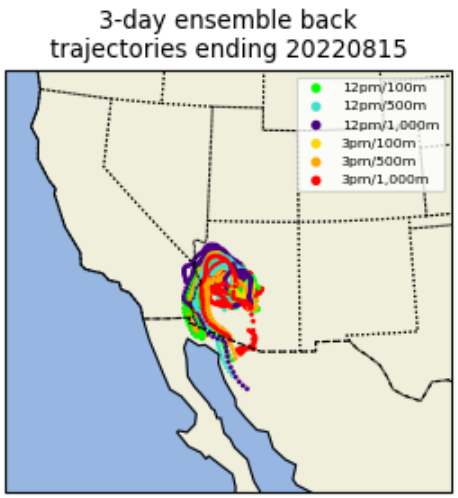
3-day ensemble back trajectories ending 20220815
12pm/100m
12pm/500m
12pm/1,000m
3pm/100m
3pm/500m
3pm/1,000m

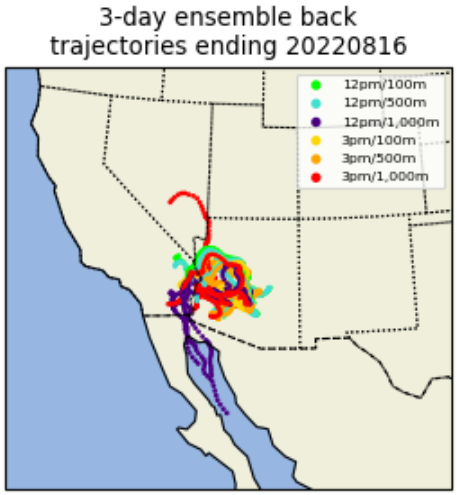
3-day ensemble back trajectories ending 20220816
12pm/100m
12pm/500m
12pm/1,000m
3pm/100m
3pm/500m
3pm/1,000m

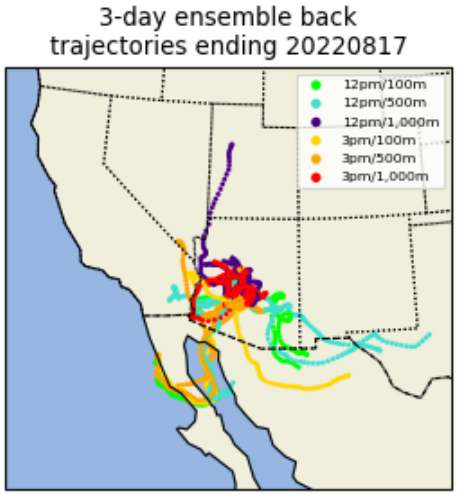
3-day ensemble back trajectories ending 20220817
12pm/100m
12pm/500m
12pm/1,000m
3pm/100m
3pm/500m
3pm/1,000m

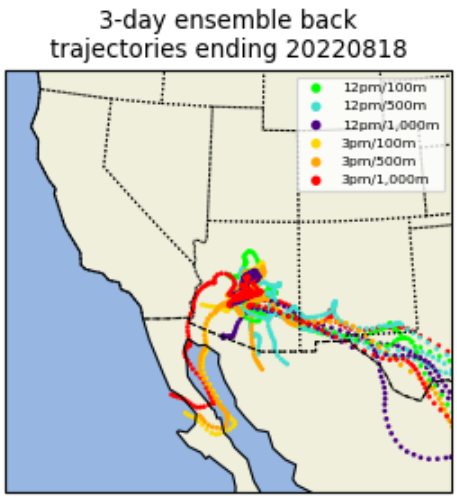
3-day ensemble back trajectories ending 20220818
12pm/100m
12pm/500m
12pm/1,000m
3pm/100m
3pm/500m
3pm/1,000m

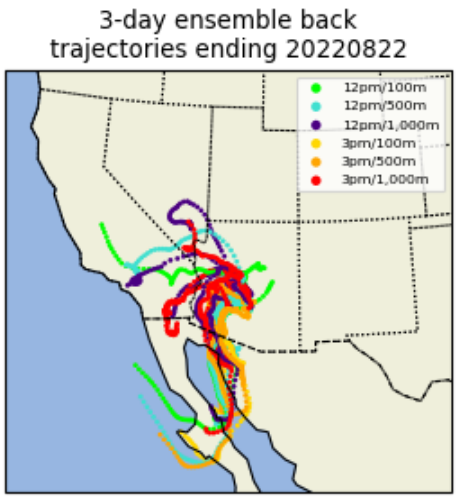
3-day ensemble back trajectories ending 20220822
12pm/100m
12pm/500m
12pm/1,000m
3pm/100m
3pm/500m
3pm/1,000m

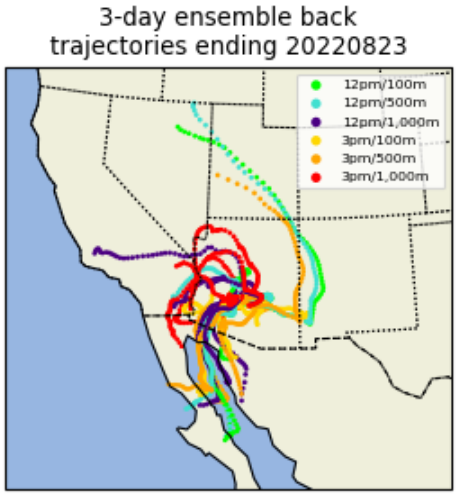
3-day ensemble back trajectories ending 20220823
12pm/100m
12pm/500m
12pm/1,000m
3pm/100m
3pm/500m
3pm/1,000m

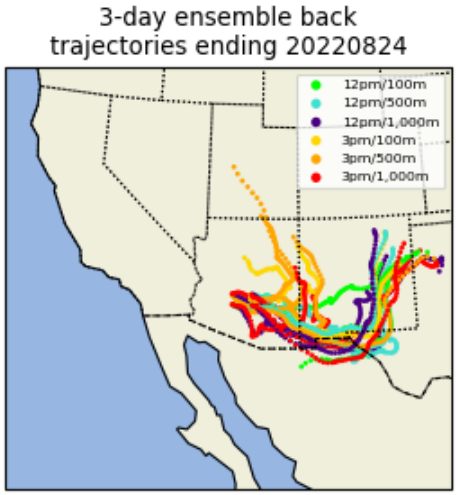
3-day ensemble back trajectories ending 20220824
12pm/100m
12pm/500m
12pm/1,000m
3pm/100m
3pm/500m
3pm/1,000m

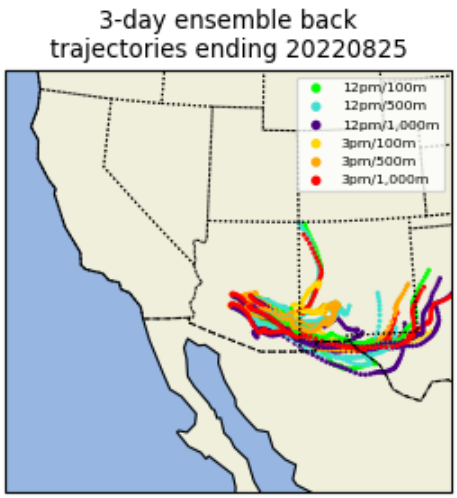
3-day ensemble back trajectories ending 20220825
12pm/100m
12pm/500m
12pm/1,000m
3pm/100m
3pm/500m
3pm/1,000m

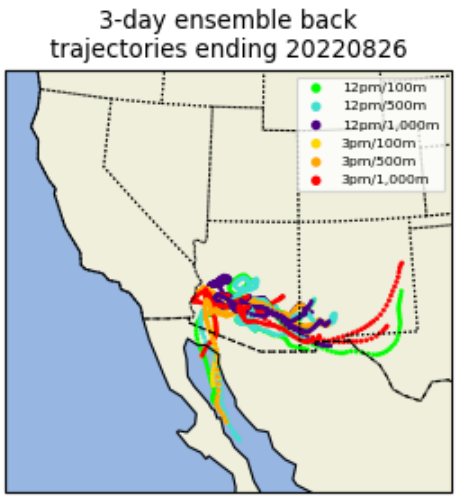
3-day ensemble back trajectories ending 20220826
12pm/100m
12pm/500m
12pm/1,000m
3pm/100m
3pm/500m
3pm/1,000m

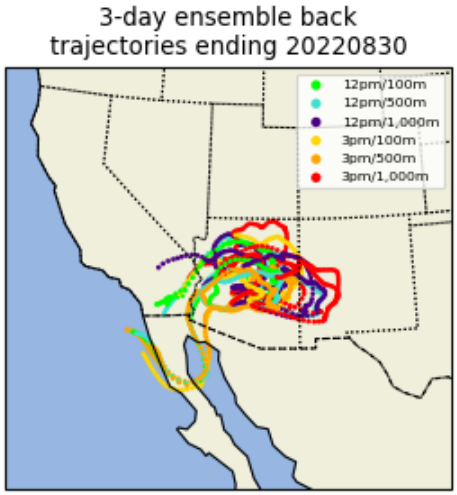
3-day ensemble back trajectories ending 20220830
12pm/100m
12pm/500m
12pm/1,000m
3pm/100m
3pm/500m
3pm/1,000m

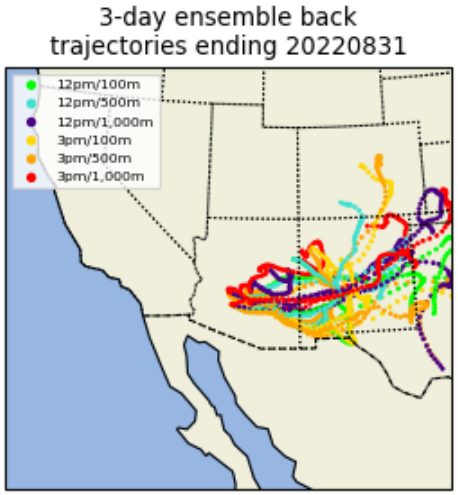
3-day ensemble back trajectories ending 20220831
12pm/100m
12pm/500m
12pm/1,000m
3pm/100m
3pm/500m
3pm/1,000m

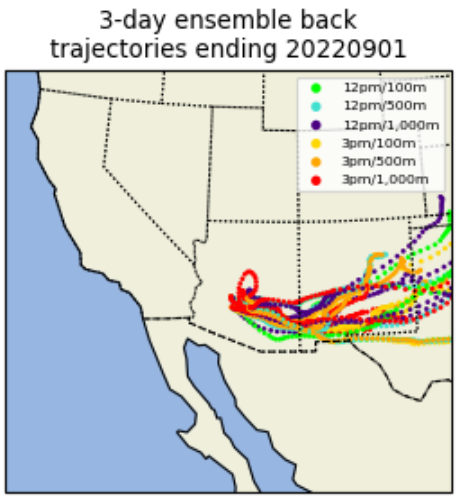
3-day ensemble back trajectories ending 20220901
12pm/100m
12pm/500m
12pm/1,000m
3pm/100m
3pm/500m
3pm/1,000m

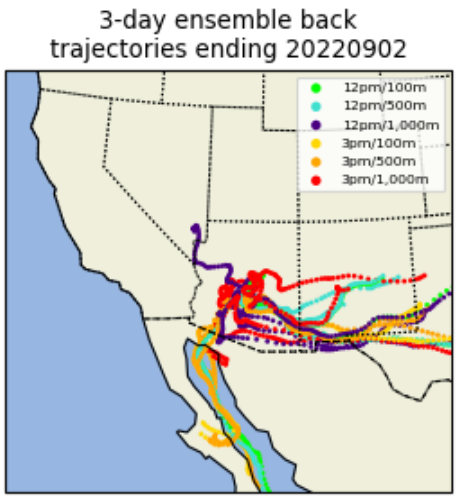
3-day ensemble back trajectories ending 20220902
12pm/100m
12pm/500m
12pm/1,000m
3pm/100m
3pm/500m
3pm/1,000m

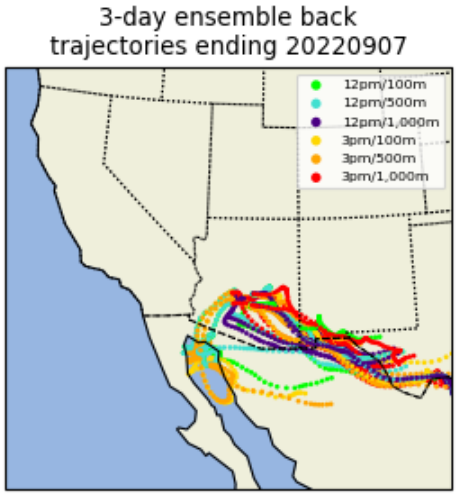
3-day ensemble back trajectories ending 20220907
12pm/100m
12pm/500m
12pm/1,000m
3pm/100m
3pm/500m
3pm/1,000m

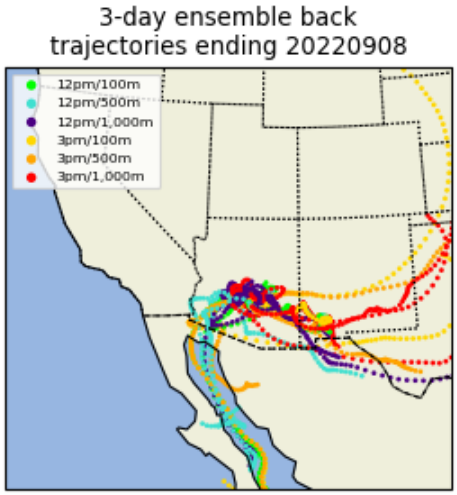
3-day ensemble back trajectories ending 20220908
12pm/100m
12pm/500m
12pm/1,000m
3pm/100m
3pm/500m
3pm/1,000m

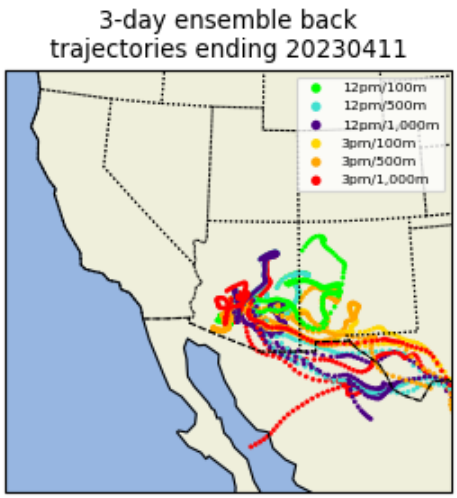
3-day ensemble back trajectories ending 20230411
12pm/100m
12pm/500m
12pm/1,000m
3pm/100m
3pm/500m
3pm/1,000m

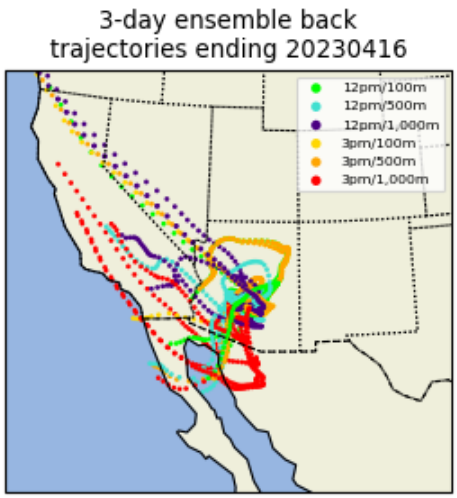
3-day ensemble back trajectories ending 20230416
12pm/100m
12pm/500m
12pm/1,000m
3pm/100m
3pm/500m
3pm/1,000m

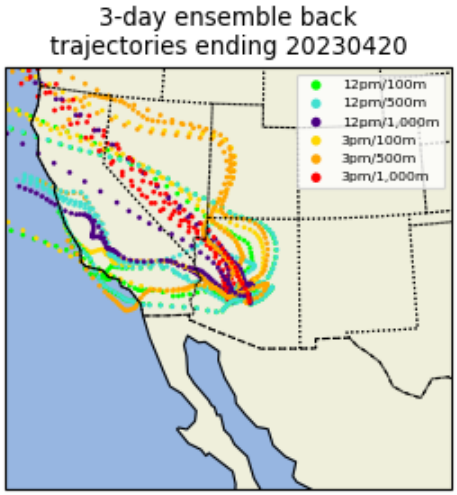
3-day ensemble back trajectories ending 20230420
12pm/100m
12pm/500m
12pm/1,000m
3pm/100m
3pm/500m
3pm/1,000m

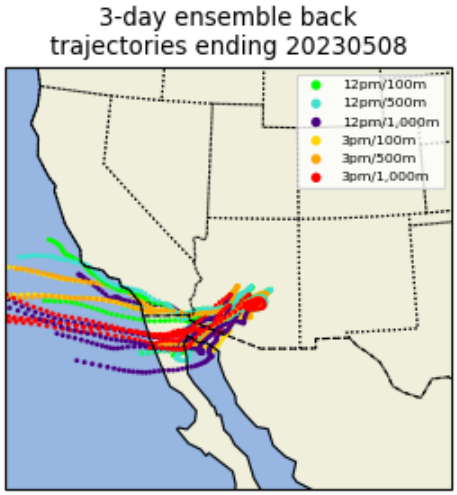
3-day ensemble back trajectories ending 20230508
12pm/100m
12pm/500m
12pm/1,000m
3pm/100m
3pm/500m
3pm/1,000m

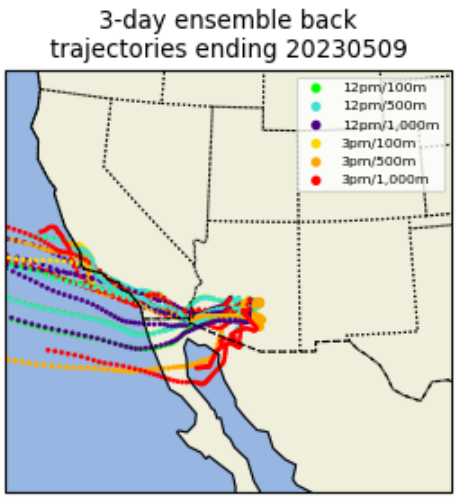
3-day ensemble back trajectories ending 20230509
12pm/100m
12pm/500m
12pm/1,000m
3pm/100m
3pm/500m
3pm/1,000m

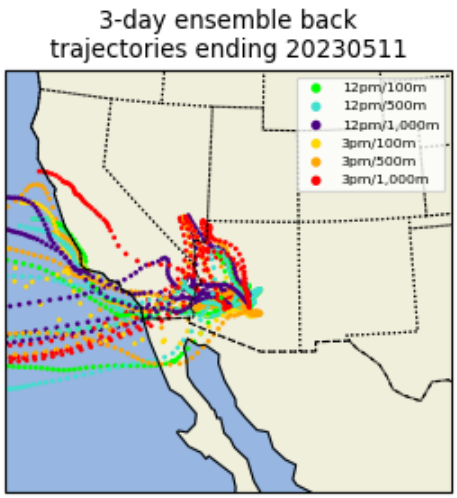
3-day ensemble back trajectories ending 20230511
12pm/100m
12pm/500m
12pm/1,000m
3pm/100m
3pm/500m
3pm/1,000m

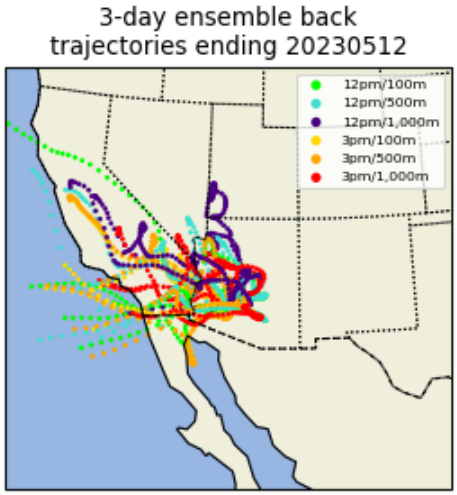
3-day ensemble back trajectories ending 20230512
12pm/100m
12pm/500m
12pm/1,000m
3pm/100m
3pm/500m
3pm/1,000m

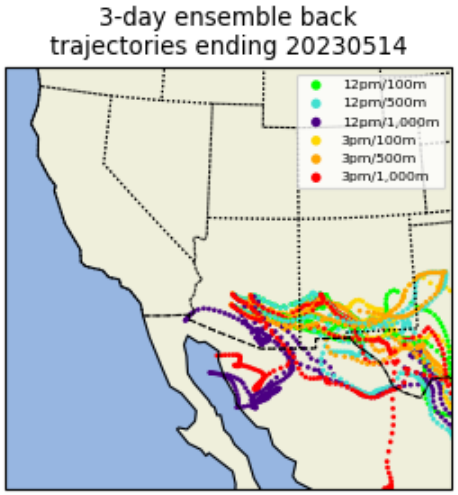
3-day ensemble back trajectories ending 20230514
12pm/100m
12pm/500m
12pm/1,000m
3pm/100m
3pm/500m
3pm/1,000m

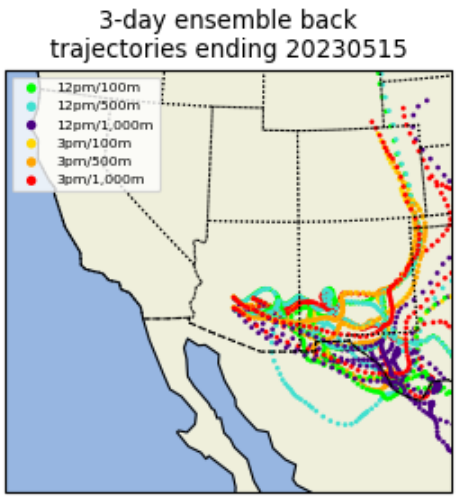
3-day ensemble back trajectories ending 20230515
12pm/100m
12pm/500m
12pm/1,000m
3pm/100m
3pm/500m
3pm/1,000m

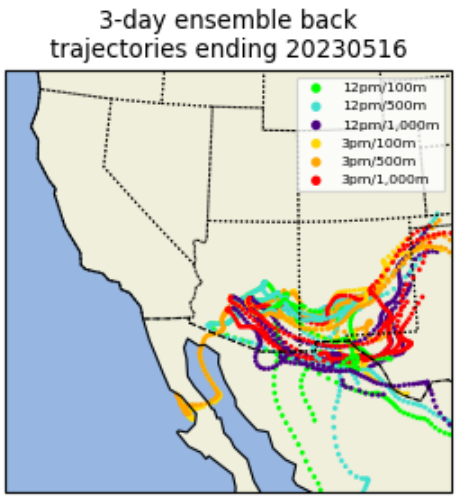
3-day ensemble back trajectories ending 20230516
12pm/100m
12pm/500m
12pm/1,000m
3pm/100m
3pm/500m
3pm/1,000m

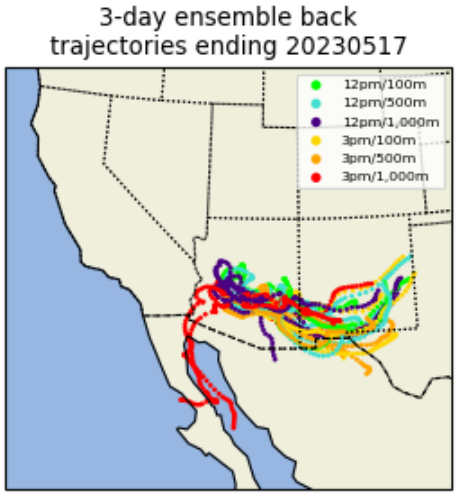
3-day ensemble back trajectories ending 20230517
12pm/100m
12pm/500m
12pm/1,000m
3pm/100m
3pm/500m
3pm/1,000m

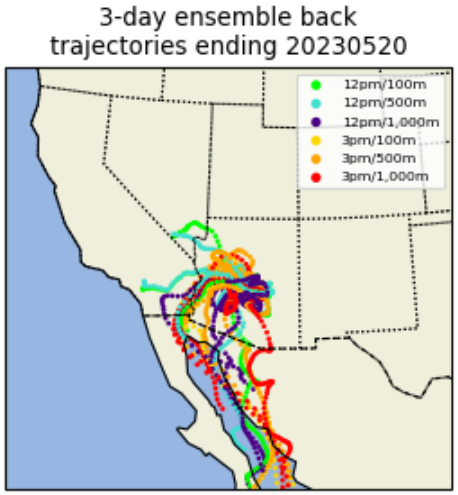
3-day ensemble back trajectories ending 20230520
12pm/100m
12pm/500m
12pm/1,000m
3pm/100m
3pm/500m
3pm/1,000m

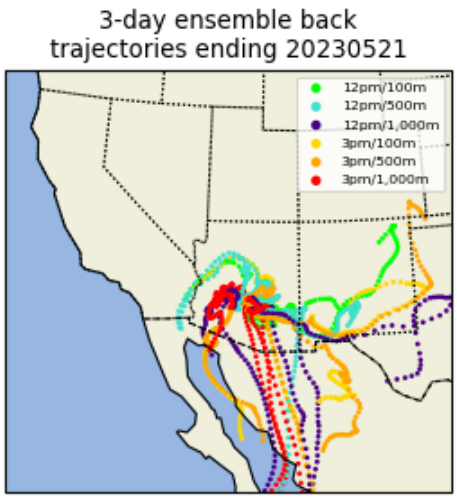
3-day ensemble back trajectories ending 20230521
12pm/100m
12pm/500m
12pm/1,000m
3pm/100m
3pm/500m
3pm/1,000m

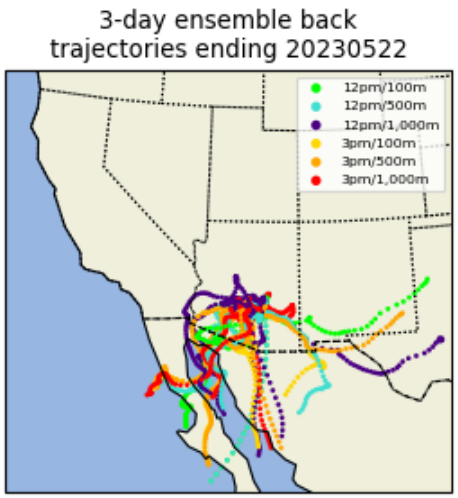
3-day ensemble back trajectories ending 20230522
12pm/100m
12pm/500m
12pm/1,000m
3pm/100m
3pm/500m
3pm/1,000m

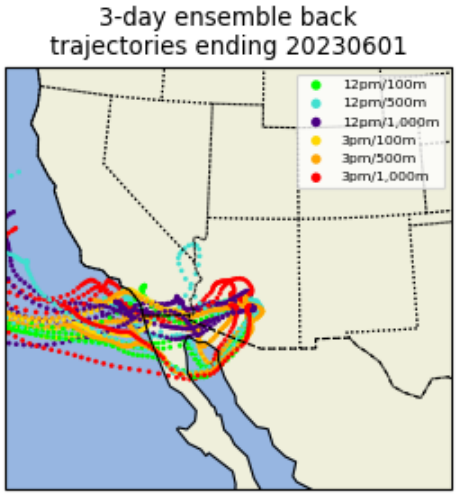
3-day ensemble back trajectories ending 20230601
12pm/100m
12pm/500m
12pm/1,000m
3pm/100m
3pm/500m
3pm/1,000m

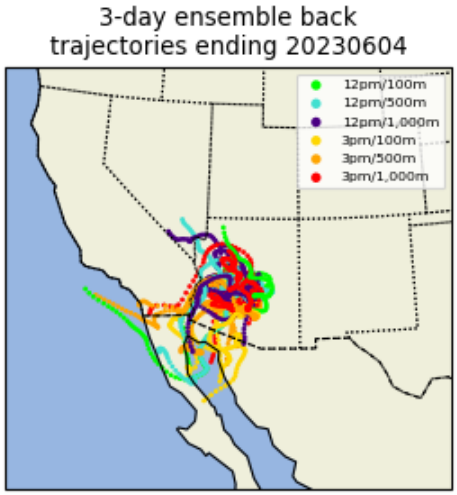
3-day ensemble back trajectories ending 20230604
12pm/100m
12pm/500m
12pm/1,000m
3pm/100m
3pm/500m
3pm/1,000m

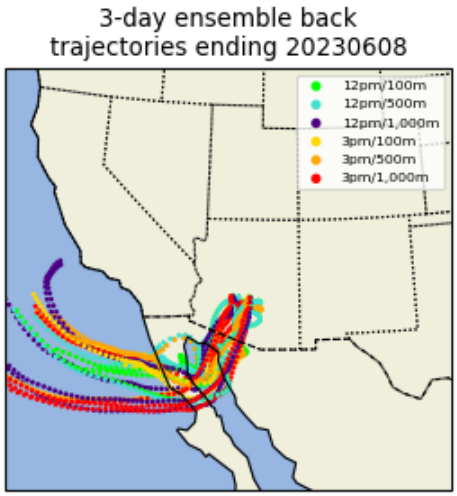
3-day ensemble back trajectories ending 20230608
12pm/100m
12pm/500m
12pm/1,000m
3pm/100m
3pm/500m
3pm/1,000m

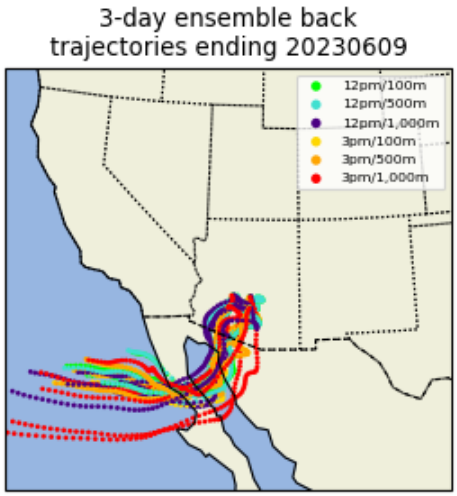
3-day ensemble back trajectories ending 20230609
12pm/100m
12pm/500m
12pm/1,000m
3pm/100m
3pm/500m
3pm/1,000m

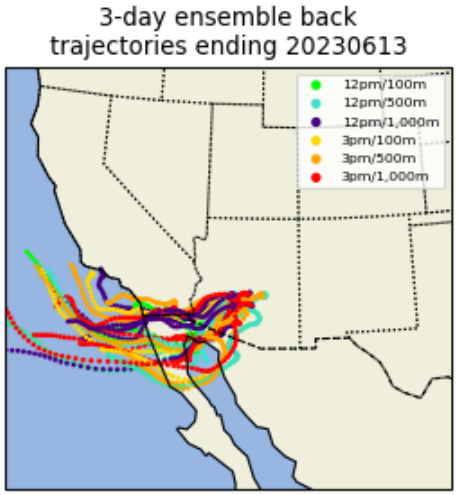
3-day ensemble back trajectories ending 20230613
12pm/100m
12pm/500m
12pm/1,000m
3pm/100m
3pm/500m
3pm/1,000m

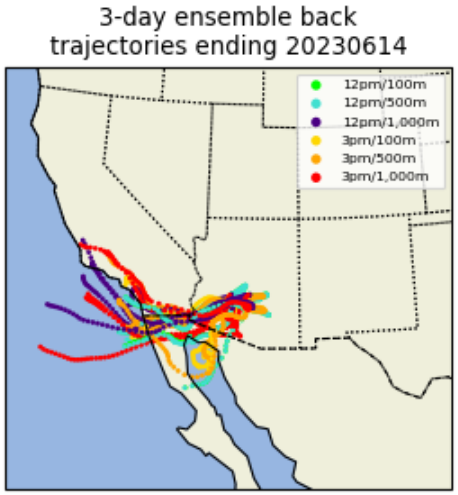
3-day ensemble back trajectories ending 20230614
12pm/100m
12pm/500m
12pm/1,000m
3pm/100m
3pm/500m
3pm/1,000m

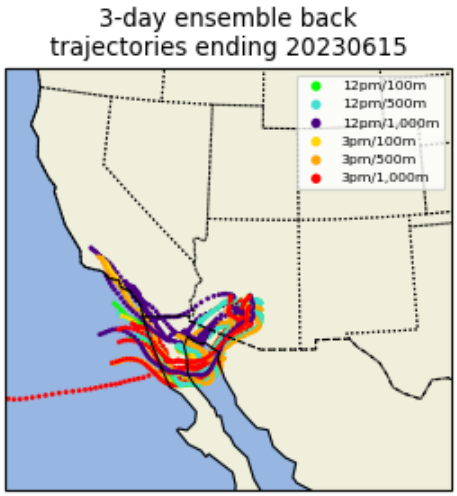
3-day ensemble back trajectories ending 20230615
12pm/100m
12pm/500m
12pm/1,000m
3pm/100m
3pm/500m
3pm/1,000m

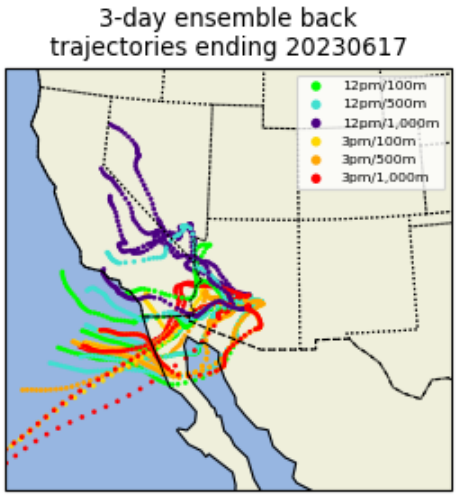
3-day ensemble back trajectories ending 20230617
12pm/100m
12pm/500m
12pm/1,000m
3pm/100m
3pm/500m
3pm/1,000m

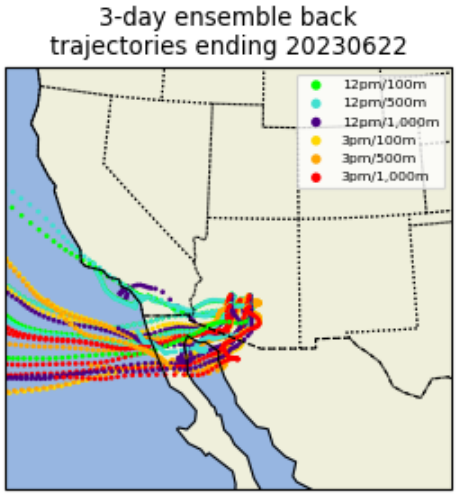
3-day ensemble back trajectories ending 20230622
12pm/100m
12pm/500m
12pm/1,000m
3pm/100m
3pm/500m
3pm/1,000m

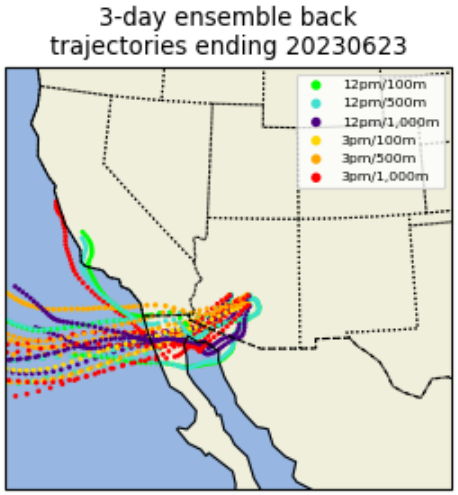
3-day ensemble back trajectories ending 20230623
12pm/100m
12pm/500m
12pm/1,000m
3pm/100m
3pm/500m
3pm/1,000m

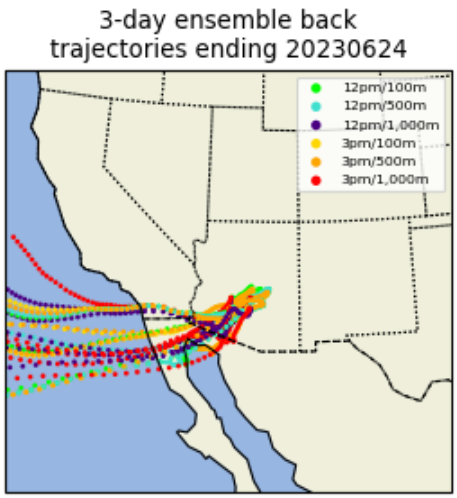
3-day ensemble back trajectories ending 20230624
12pm/100m
12pm/500m
12pm/1,000m
3pm/100m
3pm/500m
3pm/1,000m

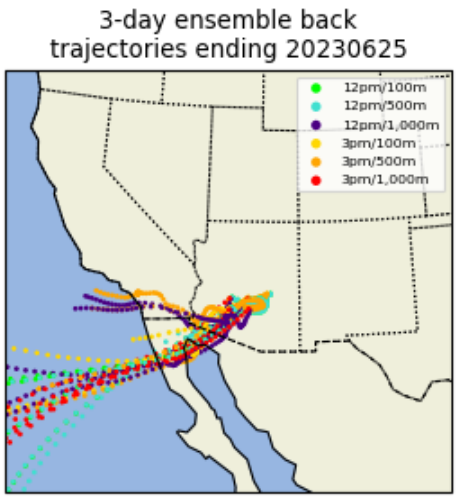
3-day ensemble back trajectories ending 20230625
12pm/100m
12pm/500m
12pm/1,000m
3pm/100m
3pm/500m
3pm/1,000m

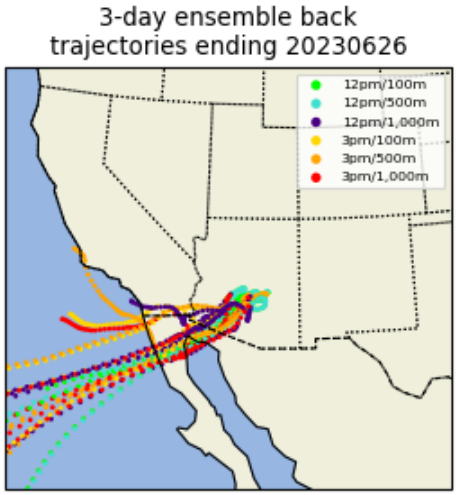
3-day ensemble back trajectories ending 20230626
12pm/100m
12pm/500m
12pm/1,000m
3pm/100m
3pm/500m
3pm/1,000m

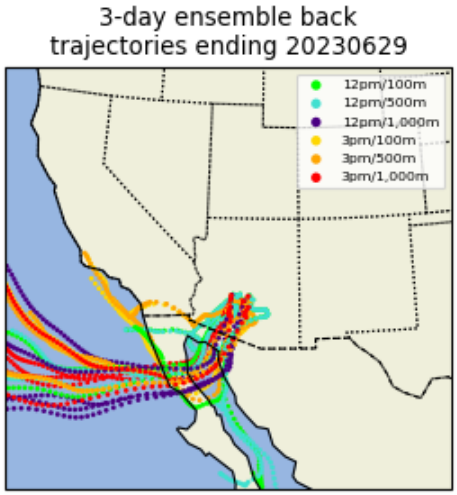
3-day ensemble back trajectories ending 20230629
12pm/100m
12pm/500m
12pm/1,000m
3pm/100m
3pm/500m
3pm/1,000m

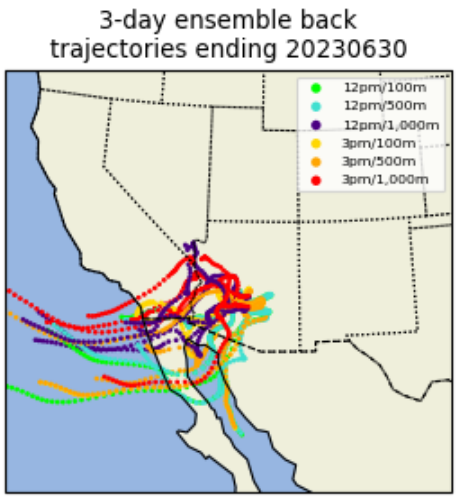
3-day ensemble back trajectories ending 20230630
12pm/100m
12pm/500m
12pm/1,000m
3pm/100m
3pm/500m
3pm/1,000m

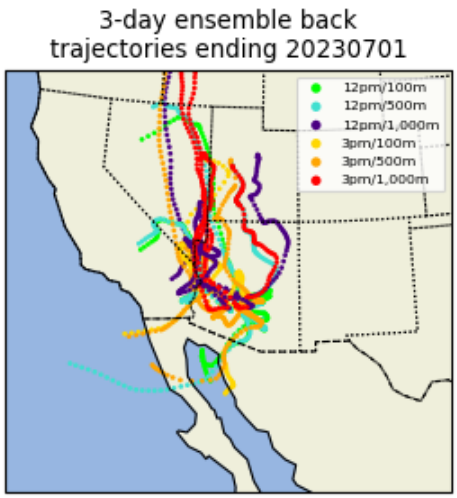
3-day ensemble back trajectories ending 20230701
12pm/100m
12pm/500m
12pm/1,000m
3pm/100m
3pm/500m
3pm/1,000m

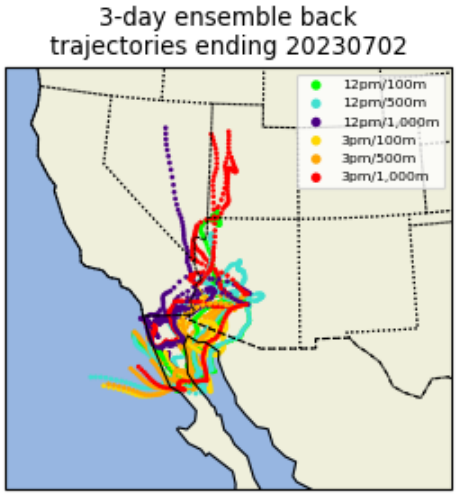
3-day ensemble back trajectories ending 20230702
12pm/100m
12pm/500m
12pm/1,000m
3pm/100m
3pm/500m
3pm/1,000m

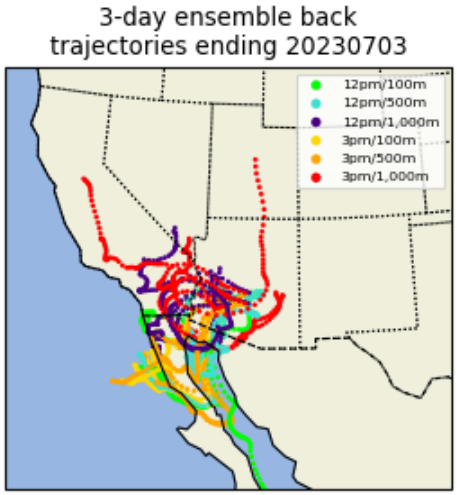
3-day ensemble back trajectories ending 20230703
12pm/100m
12pm/500m
12pm/1,000m
3pm/100m
3pm/500m
3pm/1,000m

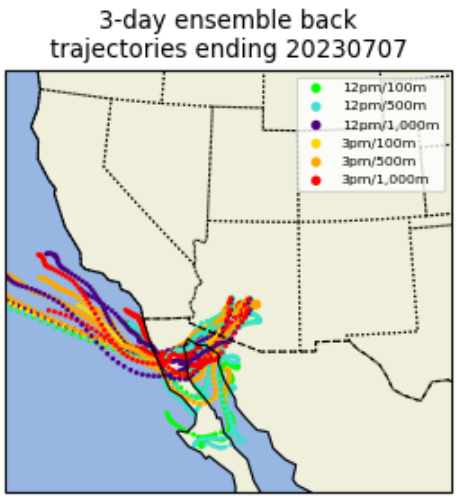
3-day ensemble back trajectories ending 20230707
12pm/100m
12pm/500m
12pm/1,000m
3pm/100m
3pm/500m
3pm/1,000m

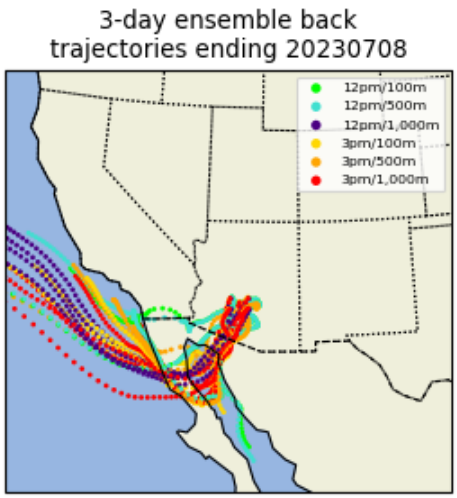
3-day ensemble back trajectories ending 20230708
12pm/100m
12pm/500m
12pm/1,000m
3pm/100m
3pm/500m
3pm/1,000m

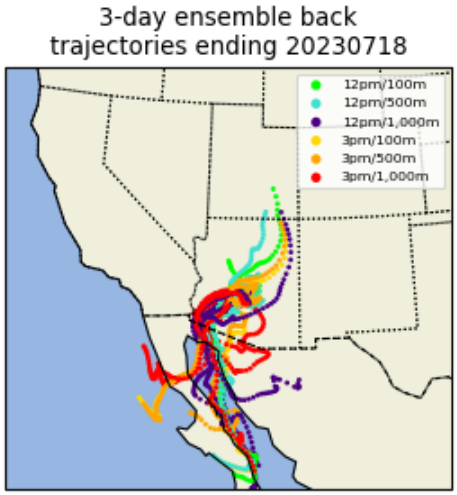
3-day ensemble back trajectories ending 20230718
12pm/100m
12pm/500m
12pm/1,000m
3pm/100m
3pm/500m
3pm/1,000m

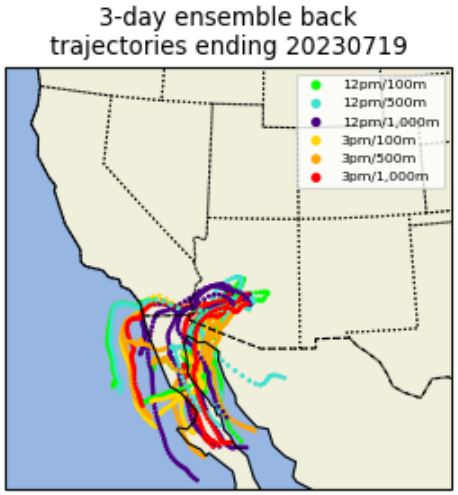
3-day ensemble back trajectories ending 20230719
12pm/100m
12pm/500m
12pm/1,000m
3pm/100m
3pm/500m
3pm/1,000m

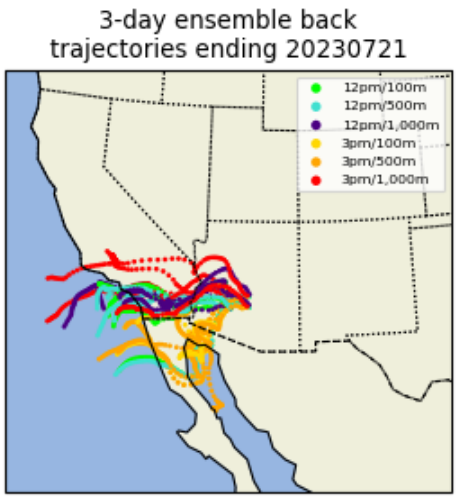
3-day ensemble back trajectories ending 20230721
12pm/100m
12pm/500m
12pm/1,000m
3pm/100m
3pm/500m
3pm/1,000m

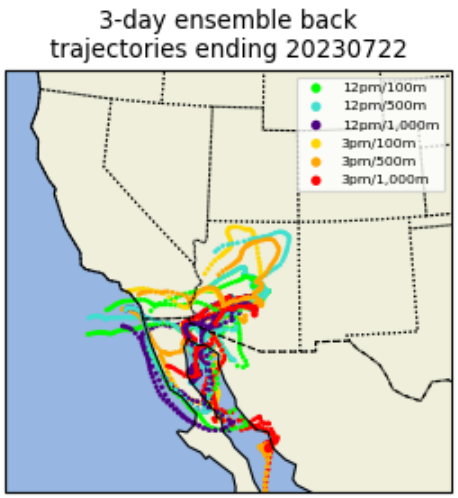
3-day ensemble back trajectories ending 20230722
12pm/100m
12pm/500m
12pm/1,000m
3pm/100m
3pm/500m
3pm/1,000m

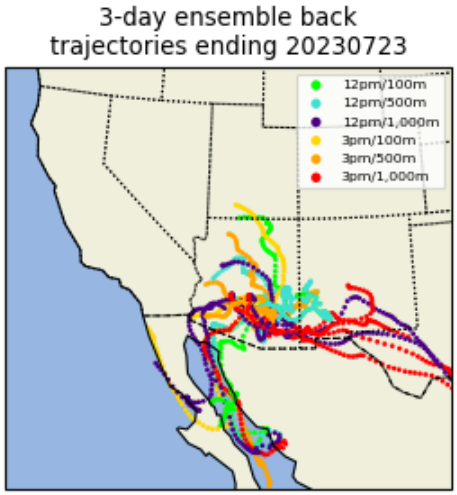
3-day ensemble back trajectories ending 20230723
12pm/100m
12pm/500m
12pm/1,000m
3pm/100m
3pm/500m
3pm/1,000m

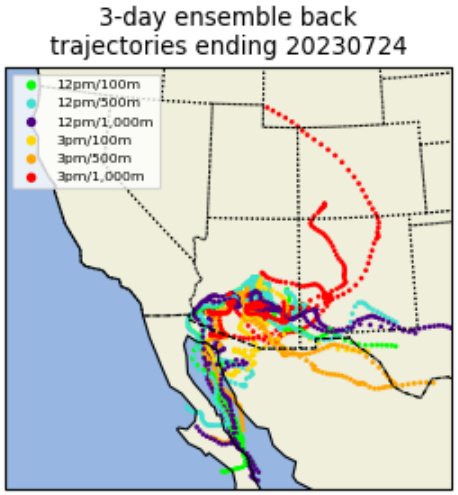
3-day ensemble back trajectories ending 20230724
12pm/100m
12pm/500m
12pm/1,000m
3pm/100m
3pm/500m
3pm/1,000m

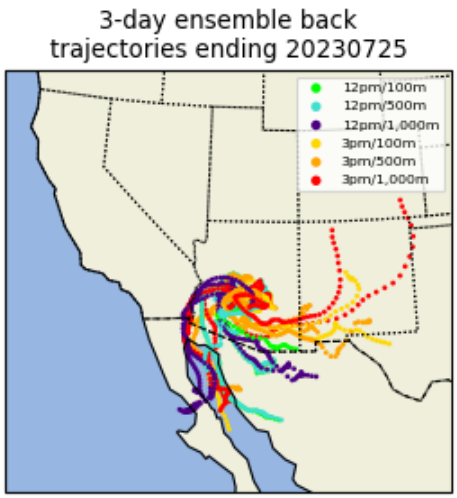
3-day ensemble back trajectories ending 20230725
12pm/100m
12pm/500m
12pm/1,000m
3pm/100m
3pm/500m
3pm/1,000m

3-day ensemble back trajectories ending 20230726
12pm/100m
12pm/500m
12pm/1,000m
3pm/100m
3pm/500m
3pm/1,000m

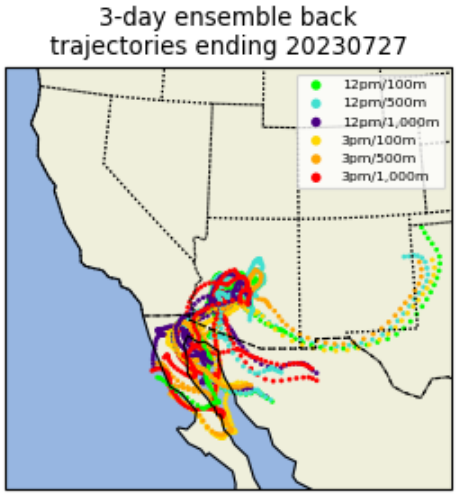
3-day ensemble back trajectories ending 20230727
12pm/100m
12pm/500m
12pm/1,000m
3pm/100m
3pm/500m
3pm/1,000m

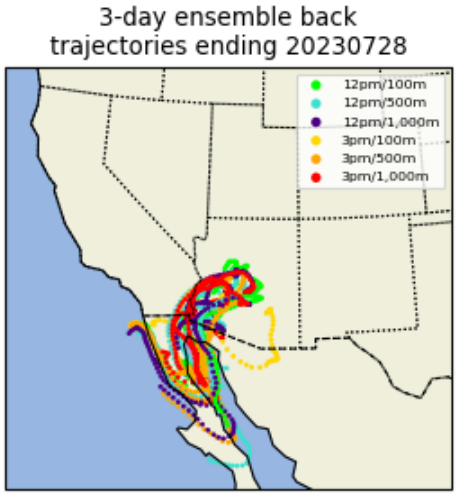
3-day ensemble back trajectories ending 20230728
12pm/100m
12pm/500m
12pm/1,000m
3pm/100m
3pm/500m
3pm/1,000m

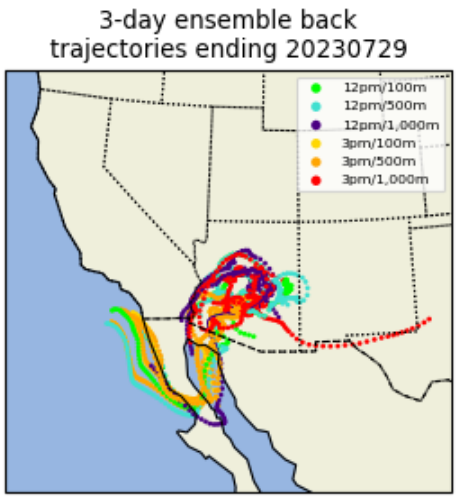
3-day ensemble back trajectories ending 20230729
12pm/100m
12pm/500m
12pm/1,000m
3pm/100m
3pm/500m
3pm/1,000m

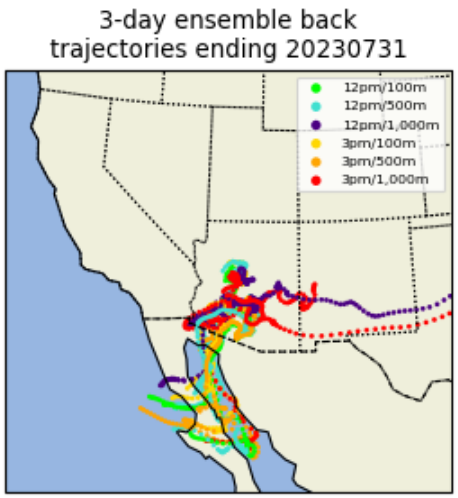
3-day ensemble back trajectories ending 20230731
12pm/100m
12pm/500m
12pm/1,000m
3pm/100m
3pm/500m
3pm/1,000m

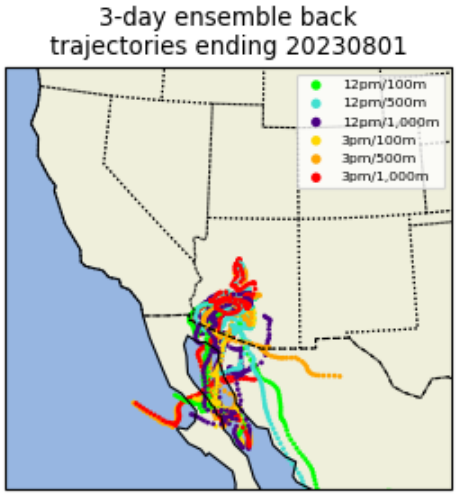
3-day ensemble back trajectories ending 20230801
12pm/100m
12pm/500m
12pm/1,000m
3pm/100m
3pm/500m
3pm/1,000m

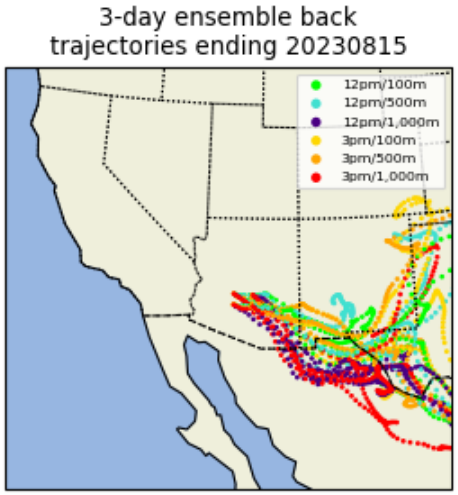
3-day ensemble back trajectories ending 20230815
12pm/100m
12pm/500m
12pm/1,000m
3pm/100m
3pm/500m
3pm/1,000m

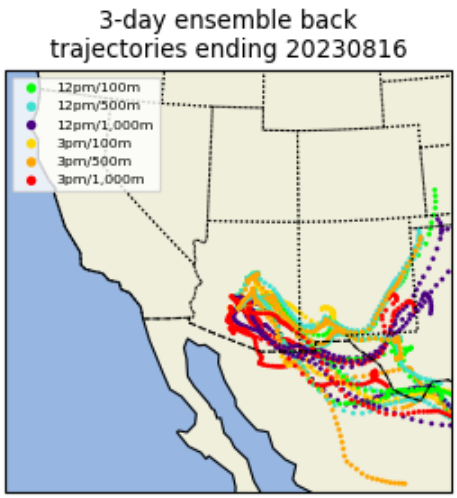
3-day ensemble back trajectories ending 20230816
12pm/100m
12pm/500m
12pm/1,000m
3pm/100m
3pm/500m
3pm/1,000m

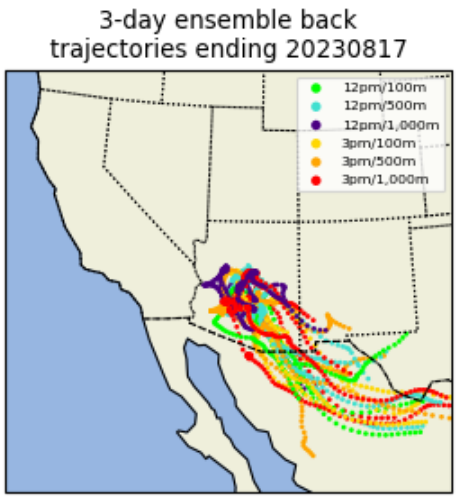
3-day ensemble back trajectories ending 20230817
12pm/100m
12pm/500m
12pm/1,000m
3pm/100m
3pm/500m
3pm/1,000m

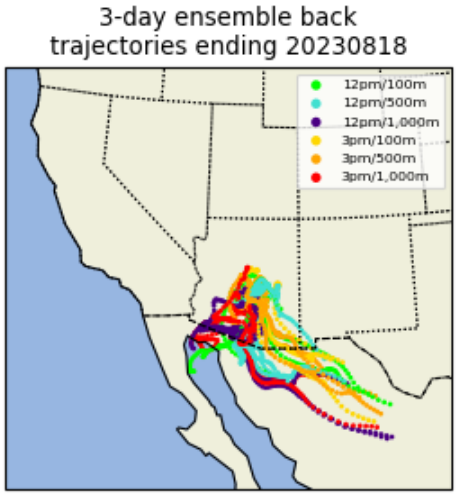
3-day ensemble back trajectories ending 20230818
12pm/100m
12pm/500m
12pm/1,000m
3pm/100m
3pm/500m
3pm/1,000m

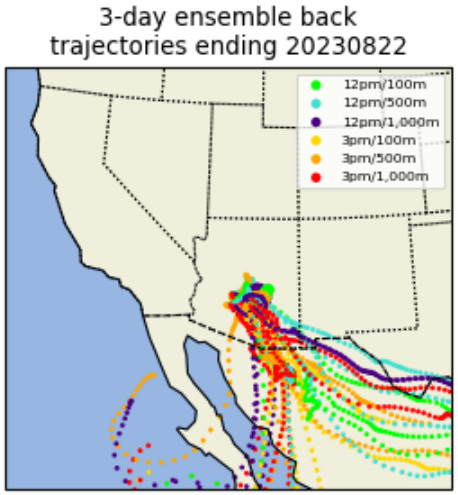
3-day ensemble back trajectories ending 20230822
12pm/100m
12pm/500m
12pm/1,000m
3pm/100m
3pm/500m
3pm/1,000m

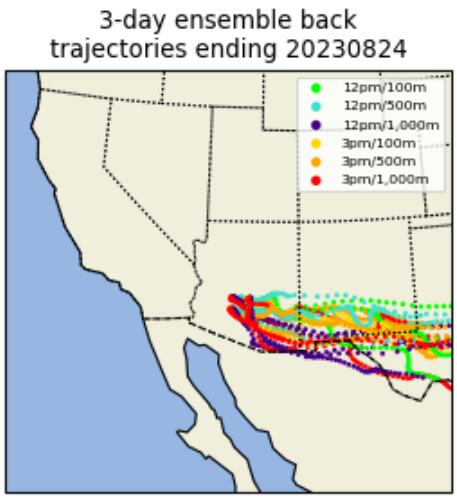
3-day ensemble back trajectories ending 20230824
12pm/100m
12pm/500m
12pm/1,000m
3pm/100m
3pm/500m
3pm/1,000m

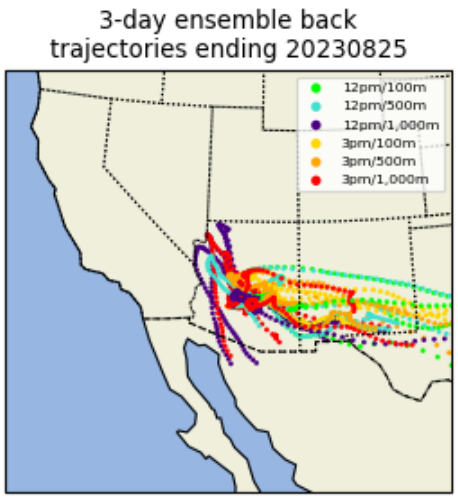
3-day ensemble back trajectories ending 20230825
12pm/100m
12pm/500m
12pm/1,000m
3pm/100m
3pm/500m
3pm/1,000m

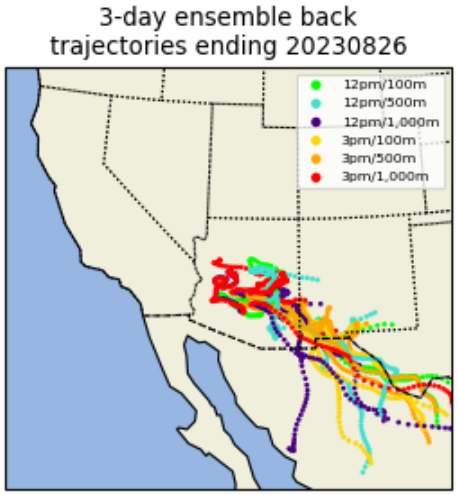
3-day ensemble back trajectories ending 20230826
12pm/100m
12pm/500m
12pm/1,000m
3pm/100m
3pm/500m
3pm/1,000m

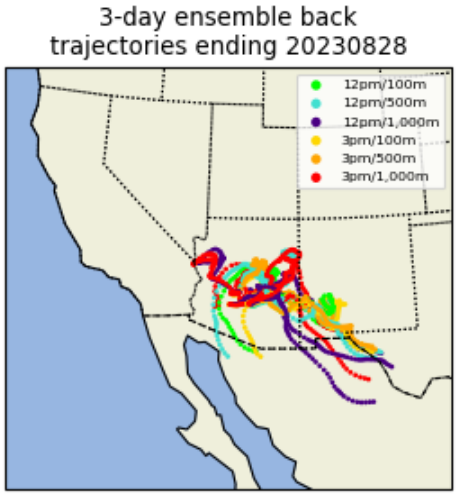
3-day ensemble back trajectories ending 20230828
12pm/100m
12pm/500m
12pm/1,000m
3pm/100m
3pm/500m
3pm/1,000m

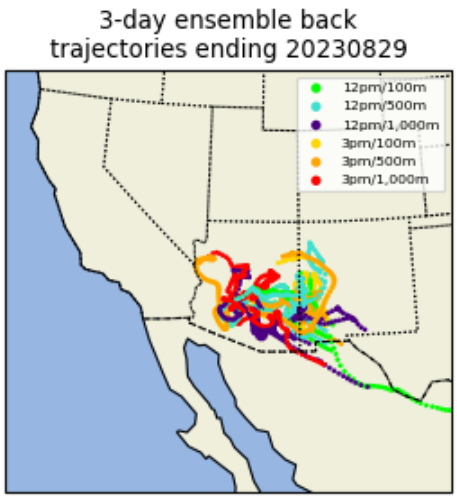
3-day ensemble back trajectories ending 20230829
12pm/100m
12pm/500m
12pm/1,000m
3pm/100m
3pm/500m
3pm/1,000m

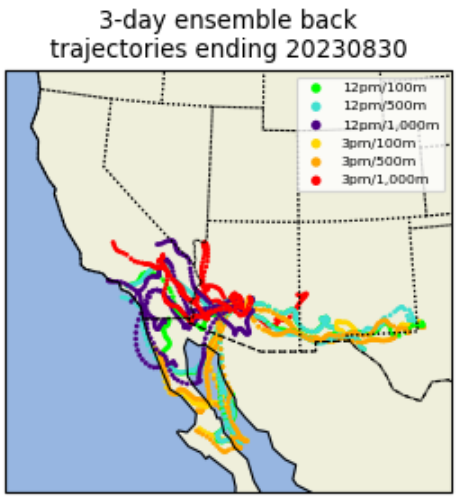
3-day ensemble back trajectories ending 20230830
12pm/100m
12pm/500m
12pm/1,000m
3pm/100m
3pm/500m
3pm/1,000m

MAG 2025 CLEAN AIR ACT SECTION 179B(b) RETROSPECTIVE DEMONSTRATION OF THE IMPACT OF INTERNATIONAL EMISSIONS ON OZONE CONCENTRATIONS IN THE MARICOPA NONATTAINMENT AREA

APPENDIX B –
Technical Modeling Support Document for the MAG 2025 Clean Air Act Section 179B(b) Retrospective Demonstration of the Impact of International Emissions on Ozone Concentrations i n the Maricopa Nonattainment Area

SEPTEMBER 2025

MARICOPA ASSOCIATION of GOVERNMENTS

TECHNICAL MODELING SUPPORT DOCUMENT

FOR

THE MAG 2025 CLEAN AIR ACT SECTION 179B(b) RETROSPECTIVE DEMONSTRATION OF THE IMPACT OF INTERNATIONAL EMISSIONS ON OZONE CONCENTRATIONS IN THE MARICOPA NONATTAINMENT AREA

September 2025

Maricopa Association of Governments

302 North 1st Avenue, Suite 200

Phoenix, Arizona 85003

MARICOPA ASSOCIATION of GOVERNMENTS

Table of Contents

List of Tables v

List of Figures vii

1. INTRODUCTION 1

1.1. Purpose 1

1.2. Overview of the Modeling Analysis 1

1.3. Structure of This Document 5

2. CONCEPTUAL MODEL AND EPISODE SELECTION 6

3. EMISSIONS INVENTORY AND PROCESSING 7

3.1. Introduction to the Emissions Inventory Development Process 7

3.2. 2023 Local Anthropogenic Emissions Inventory 8

3.2.1. Point Sources 8

3.2.2. Area Sources 11

3.2.3. Nonroad Mobile Sources 16

3.2.4. Aircraft 18

3.2.5. Onroad Mobile Sources 23

3.3. Continental USA and Mexico Anthropogenic Emissions Inventory 30

3.4. Biogenic and Other Natural Source Emissions Inventory 34

3.4.1. Biogenic Emissions 34

3.4.2. US Wild, Prescribed, and Agricultural Fires Emissions 36

3.4.3. Mexico Fire Emissions 37

3.4.4. Lightning Emissions 38

3.5. Emissions Processing for Photochemical Modeling (SMOKE) 38

3.5.1. Spatial Allocation and Surrogates 39

3.5.2. Chemical Speciation 60

3.5.3. Temporal Allocation 61

3.5.4. Emissions Summaries for the 4 km Modeling Domain and the Maricopa NAA 69

4. METEOROLOGICAL MODELING 73

4.1. Overview of the Weather Research and Forecasting (WRF) Model 73

4.2. Domains, Vertical Layering, and Physics Configuration 73

4.3. Model Inputs and Initial/Boundary Conditions 76
4.4. Meteorological Model Performance Evaluation 77
4.4.1. Comparison against Ground-Based Observations 78
4.4.2. Upper-Air/Vertical Structure and PBLH 81
4.4.3. Justification of WRF Vertical Layer Configuration Choices 86
4.5. Meteorology and Chemistry Interface Processing 94
5. PHOTOCHEMICAL GRID MODELING PLATFORM 95
5.1. Modeling System Overview 95
5.2. Photochemical Model Configurations 95
5.3. Modeling Domains, Grid Resolution, and Layer Structure 99
5.4. Chemical Mechanisms 102
5.5. Initial and Boundary Conditions (IC/BCs) 102
5.5.1. GEOS-Chem Global Chemical Transport Model 102
5.5.2. GEOS-Chem Model Evaluation 104
5.5.3. Comparison of the IC/BCs between the Base and Zero-Out Cases 109
5.5.4. GOES-Chem Conversion Tools for CAMx and CMAQ 109
6. MODEL PERFORMANCE EVALUATION 111
6.1. Methodology and Goals 111
6.2. Operational Evaluation 113
6.2.1. Statistical Performance Metrics 113
6.2.2. Graphical Analysis 118
6.2.3. Evaluation of Ozone Precursors in the Maricopa NAA and Ozone in Mexico 128
6.3. Diagnostic Evaluation 131
6.3.1. Satellite Data Comparison 131
6.3.2. Upper-Air Data Comparison 132
6.4. Performance Evaluation Summary and Conclusions 135
7. SOURCE APPORTIONMENT AND ZERO-OUT DEMONSTRATION 136
7.1. Demonstration of Zeroing-Out International Anthropogenic Sources 136
7.1.1. Calculation of Relative Response Factors (RRFs) 136
7.1.2. Calculation of Design Values without International Anthropogenic 137
7.2. Demonstration of Source Apportionment 140

7.3. Demonstration Results and Conclusion 150
7.4. Weight of Evidence Analysis 152
8. REFERENCES 155
Appendix 1 160
Sensitivity Analysis for Solana Generating Station Emissions 160
Appendix 2 165
Specification for Spatial Surrogates in the 4 km Modeling Domain 165
Appendix 3A 168
2023 Monthly Profiles for the EGUs in Maricopa and Pinal Counties 168
Appendix 3B 170
2023 Daily Profiles for the EGUs in Maricopa and Pinal Counties 170
Appendix 3C1 172
2023 Weekday Hourly Profiles (UTC from 0 to 11) for the EGUs in Maricopa and Pinal Counties 172
Appendix 3C2 174
2023 Weekday Hourly Profiles (UTC from 12 to 23) for the EGUs in Maricopa and Pinal Counties 174
Appendix 3C3 176
2023 Weekend Hourly Profiles (UTC from 0 to 11) for the EGUs in Maricopa and Pinal Counties 176
Appendix 3C4 178
2023 Weekend Hourly Profiles (UTC from 12 to 23) for the EGUs in Maricopa and Pinal Counties 178
Appendix 4 180
Ozone Modeling Protocol in Support of the Revised MAG 2025 Moderate Area Plan for the Maricopa Eight-Hour Ozone Nonattainment Area 180

List of Tables

Table 3-1. 2023 Annual point source emissions in Maricopa County (units: short tons/year) 9
Table 3-2. 2023 Annual point source emissions in Pinal County (units: short tons/year) 10
Table 3-3. Maricopa County Emission Reduction Credits (ERCs) and Mobile Emission Reduction Credits (MERCs) and annual emissions in Salt River Pima-Maricopa Indian Community (units: short tons/year) 10
Table 3-4. 2023 annual area source emissions in Maricopa County (units: short tons/year) 11
Table 3-5. 2023 annual area source emissions in Pinal County (units: short tons/year) 14
Table 3-6. 2023 annual locomotives emissions in Maricopa and Pinal counties (units: short tons/year) 17
Table 3-7. Ozone season (April-September) average daily nonroad mobile source emissions for Maricopa and Pinal counties in 2023 (unit: short tons/day) 18
Table 3-8. 2023 annual airport operations (by aircraft category) and related data sources for 20 airports in the 4 km modeling domain 21
Table 3-9. Aircraft type activity distribution at Chandler Municipal airport 22
Table 3-10. MOVES compliance factors for the local I/M programs in 2023 25
Table 3-11. Match table for ABM area/facility types and MOVES road types 28
Table 3-12. Match table for ABM vehicle classes and MOVES source types 29
Table 3-13. Regulatory RVP by month for gasoline in Area A and Area C 29
Table 3-14. EPA's 2022 v1/v2 platform sectors used in the emissions modeling process for 36 and 12 km modeling domains 31
Table 3-15. Fire emissions for the U.S. (2023 EPA NEI) and Mexico (2023 FINN) 37
Table 3-16. Spatial surrogates used for the 4 km domain 41
Table 3-17. Inventory resolutions for different categories in the 4 km modeling domain 61
Table 3-18. Summary of average daily emissions used for each category in the 4 km modeling domain and the Maricopa NAA (unit: short tons/day) 70
Table 4-1. Configuration of WRF modeling domains (Lambert Conformal Conic projection with 33° N and 45° N true latitudes and 112° W and 33.5° N central longitude and latitude) 74
Table 4-2. Typical pressures and heights for the 23 vertical layers in WRF 75
Table 4-3. Statistical comparison of WRF performance for temperature, water vapor mixing ratio, wind direction, and wind speed during the modeling period (April 1–September 30) over the 4 km domain 79
Table 4-4. Typical pressures and heights for the 35 vertical layers in WRF 87
Table 4-5. Statistical comparison of WRF performance for temperature, water vapor mixing ratio, wind direction, and wind speed during the modeling period (April 1–September 30) over the 12 km domain for the base case (WRF_L23_MAG) and two sensitivity tests (WRF_L35_MAG and WRF_L35_EPA) 89

Table 4-6. Statistical comparison of WRF performance for temperature, water vapor mixing ratio, wind direction, and wind speed during the modeling period (April 1–September 30) over the 4 km domain for the WRF_L35_MAG sensitivity test 90
Table 5-1. CAMx modeling configuration 97
Table 5-2. CMAQ modeling configuration 98
Table 5-3. Configuration of CAMx/CMAQ modeling domains (LCC projection with 33° N and 45° N true latitudes and 112° W and 33.5° N central longitude and latitude) 100
Table 5-4. Average pressures and heights of CAMx/CMAQ vertical layers 101
Table 6-1. Statistical performance metrics for model performance evaluation 112
Table 6-2. Statistical metrics by month for CAMx modeled one-hour ozone values for monitors in the Maricopa NAA 114
Table 6-3. Statistical metrics by month for CMAQ modeled one-hour ozone values for monitors in the Maricopa NAA 114
Table 6-4. Statistical metrics by month for CAMx modeled MDA8 ozone values for monitors in the Maricopa NAA 115
Table 6-5. Statistical metrics by month for CMAQ modeled MDA8 ozone values for monitors in the Maricopa NAA 115
Table 6-6. Statistical metrics by month for CAMx modeled MDA8 ozone values paired with observed MDA8 ozone values greater than 60 ppb for monitors in the Maricopa NAA 116
Table 6-7. Statistical metrics by month for CMAQ modeled MDA8 ozone values paired with observed MDA8 ozone values greater than 60 ppb for monitors in the Maricopa NAA 116
Table 6-8. Statistical metrics for CAMx modeled MDA8 ozone values for controlling monitors. 117
Table 6-9. Statistical metrics for CMAQ modeled MDA8 ozone values for controlling monitors 117
Table 7-1. Wildfire atypical events for 2021-2023 137
Table 7-2. 2023 DVBs for the ozone monitoring sites in the Maricopa NAA (unit: ppb) 138
Table 7-3. Unadjusted RRF and DVF of CAMx sensitivity runs excluding IA emissions using zero-out method, as well as the EPA DVB 139
Table 7-4. MAG RRF and DVF of CAMx sensitivity runs excluding IA emissions using zero-out method, as well as the MAG DVB 140
Table 7-5. Emission source groups for the source apportionment analysis 142
Table 7-6. Unadjusted RRF and DVF of CAMx sensitivity runs excluding IA emissions and NAA emissions using OSAT, as well as the EPA DVB 149
Table 7-7. MAG RRF and DVF of CAMx sensitivity runs excluding IA emissions and NAA emissions using OSAT, as well as the MAG DVB 150
Table 7-8. Modeled contributions from international anthropogenic emissions to DVBs and resulting DVs with IA contributions removed based on zero-out method 151
Table 7-9. Modeled contributions from international anthropogenic emissions to DVBs and resulting DVs with IA contributions removed based on OSAT 151

Table 7-10. Unadjusted RRF and DVF of CMAQ sensitivity runs excluding IA emissions using zero-out method, as well as the EPA DVB 153
Table 7-11. MAG RRF and DVF of CMAQ sensitivity runs excluding IA emissions using zero-out method, as well as the MAG DVB 154
Table 7-12. Modeled contributions from international anthropogenic emissions to DVBs and resulting DVs with IA contributions removed based on CMAQ zero-out scenario 154

List of Figures

Figure 3-1. Locations of 20 airports within the 4 km modeling domain (black box). The gray polygon indicates the Maricopa County boundary 20
Figure 3-2. The spatial allocation for MERCs emissions in Maricopa County 43
Figure 3-3. Spatial surrogate (ID = 999) for the MERCs in Maricopa County 44
Figure 3-4. MDA8 ozone concentrations (ppb) on May 17, 2023 (Wednesday) 45
Figure 3-5. Spatial distribution of daily VOC emissions from point sources (kg/day) for May 17, 2023 46
Figure 3-6. Spatial distribution of daily NO_x emissions from point sources (kg/day) for May 17, 2023 47
Figure 3-7. Spatial distribution of daily CO emissions from point sources (kg/day) for May 17, 2023 47
Figure 3-8. Spatial distribution of daily VOC emissions from MERCs (kg/day) for May 17, 2023 48
Figure 3-9. Spatial distribution of daily NO_x emissions from MERCs (kg/day) for May 17, 2023 48
Figure 3-10. Spatial distribution of daily VOC emissions from AREA (kg/day) for May 17, 2023 49
Figure 3-11. Spatial distribution of daily NO_x emissions from AREA (kg/day) for May 17, 2023 49
Figure 3-12. Spatial distribution of daily CO emissions from AREA (kg/day) for May 17, 2023 50
Figure 3-13. Spatial distribution of daily VOC emissions from NONROAD (kg/day) for May 17, 2023 50
Figure 3-14. Spatial distribution of daily NO_x emissions from NONROAD (kg/day) for May 17, 2023 51
Figure 3-15. Spatial distribution of daily CO emissions from NONROAD (kg/day) for May 17, 2023 51
Figure 3-16. Spatial distribution of daily VOC emissions from ONROAD (kg/day) for May 17, 2023 52
Figure 3-17. Spatial distribution of daily NO_x emissions from ONROAD (kg/day) for May 17, 2023 52
Figure 3-18. Spatial distribution of daily CO emissions from ONROAD (kg/day) for May 17, 2023 53
Figure 3-19. Spatial distribution of daily VOC emissions from Airports (kg/day) for May 17, 2023 53

Figure 3-20. Spatial distribution of daily NO_x emissions from Airports (kg/day) for May 17, 2023 54
Figure 3-21. Spatial distribution of daily CO emissions from Airports (kg/day) for May 17, 2023 54
Figure 3-22. Spatial distribution of daily VOC emissions from Biogenics (kg/day) for May 17, 2023 55
Figure 3-23. Spatial distribution of daily NO_x emissions from Biogenics (kg/day) for May 17, 2023 55
Figure 3-24. Spatial distribution of daily CO emissions from Biogenics (kg/day) for May 17, 2023 56
Figure 3-25. Spatial distribution of daily VOC emissions from Fires (kg/day) for May 17, 2023 ... 56
Figure 3-26. Spatial distribution of daily NO_x emissions from Fires (kg/day) for May 17, 2023 57
Figure 3-27. Spatial distribution of daily CO emissions from Fires (kg/day) for May 17, 2023 57
Figure 3-28. Spatial distribution of daily NO_x emissions from Lightning (kg/day) for May 17, 2023 58
Figure 3-29. Spatial distribution of daily VOC emissions from all sources (kg/day) for May 17, 2023 58
Figure 3-30. Spatial distribution of daily NO_x emissions from all sources (kg/day) for May 17, 2023 59
Figure 3-31. Spatial distribution of daily CO emissions from all sources (kg/day) for May 17, 2023 59
Figure 3-32. Normalized 2023 temporal profiles for EGU facilities in Maricopa County, showing monthly and weekly patterns, and daily patterns in UTC 63
Figure 3-33. Normalized 2023 temporal profiles for EGU facilities in Pinal County, showing monthly and weekly patterns, and daily patterns in UTC 64
Figure 3-34. Normalized 2023 temporal profiles (monthly, weekly, daily) for county-wide facilities in Maricopa and Pinal Counties versus the EPA 2022hc modeling platform defaults. 65
Figure 3-35. Weekly profile for MERCs 66
Figure 3-36. Diurnal variation of hourly VOC emission fractions within the 4 km domain on May 17, 2023 67
Figure 3-37. Diurnal variation of hourly NO_x emission fractions within the 4 km modeling domain on May 17, 2023 68
Figure 3-38. Diurnal variation of hourly CO emission fractions within the 4 km modeling domain on May 17, 2023 68
Figure 3-39. 2023 ozone season daily average NO_x emissions (short ton) for the EGUs in the 4 km modeling domain 70
Figure 3-40. 2023 ozone season daily VOC and NO_x emissions (short ton) for all sources in the 4 km modeling domain 71
Figure 3-41. Pie charts for 2023 ozone season average daily VOC, NO_x, and CO emissions by source category in the 4 km modeling domain (left set) and the Maricopa NAA (right set) 72

Figure 4-1. Modeling domains used in this study with horizontal resolutions of 36, 12, and 4 km; CAMx/CMAQ domains (red) and WRF domains (blue) 74
Figure 4-2. Time series comparison of observed and simulated near-surface meteorological variables (2-m mixing ratio, 2-m temperature, 10-m wind speed, and 10-m wind direction) for July 2023 80
Figure 4-3. Vertical profiles for relative humidity at KTUS site in the 4 km domain 82
Figure 4-4. Vertical profiles for temperature at KTUS site in the 4 km domain 82
Figure 4-5. Vertical profiles for wind direction at KTUS site in the 4 km domain 83
Figure 4-6. Vertical profiles for wind speed at KTUS site in the 4 km domain 83
Figure 4-7. Ceilometer attenuated backscatter over Phoenix with WRF-predicted PBL height and AERMET-derived mixing height, shown for four days: two representative cases highlighted in the text (pre-monsoon season: June 24, 2023; monsoon season: August 2, 2023), and two supplementary examples (June 28 and August 7, 2023) illustrating consistent seasonal patterns 85
Figure 4-8. Time series comparison of observed and simulated near-surface meteorological variables (2-m mixing ratio, 2-m temperature, 10-m wind speed, and 10-m wind direction) in July for the WRF_L35_MAG sensitivity test 91
Figure 4-9. Vertical profiles for relative humidity for the WRF_L35_MAG sensitivity test 92
Figure 4-10. Vertical profiles for temperature for the WRF_L35_MAG sensitivity test 92
Figure 4-11. Vertical profiles for wind direction for the WRF_L35_MAG sensitivity test 93
Figure 4-12. Vertical profiles for wind speed for the WRF_L35_MAG sensitivity test 93
Figure 5-1. MAG air quality modeling system flowchart 96
Figure 5-2. CAMx/CMAQ and WRF modeling boundaries 100
Figure 5-3. Scatterplot comparing GEOS-Chem simulated daily mean ozone with CASTNET observations across the 10 CASTNET sites in California and Arizona for April–September 2023. Performance statistics are shown in the lower right 105
Figure 5-4. Time series of daily mean ozone from GEOS-Chem and CASTNET observations averaged across the 10 sites in California and Arizona for April–September 2023 105
Figure 5-5. Comparison of GEOS-Chem and ozonesonde vertical ozone profiles at Trinidad Head, California, on June 12 and July 22, 2023. Left panels: observed ozone partial pressure from ozonesondes. Middle panels: stratospheric profile comparisons. Right panels: tropospheric profile comparisons 107
Figure 5-6. Comparison of GEOS-Chem and ozonesonde vertical ozone profiles at Boulder, Colorado on May 4 and June 15, 2023 108
Figure 5-7. Daily mean ozone at 721 hPa along the four lateral boundaries of the 36 km domain from the GEOS-Chem base (blue) and zero-out (orange) simulations for April–September 2023. Average differences between the two cases are shown for April–June and July– September 110
Figure 6-1. Time series plots of modeled MDA8 ozone over observed concentrations for each monitor; observed (grey), CAMx (red), CMAQ (blue) 119

Figure 6-2. Time series of observed and modeled MDA8 ozone concentrations for monitors in the Maricopa NAA; observed (grey), CAMx (red), CMAQ (blue) 125
Figure 6-3. Spatial distribution of mean errors for modeled MDA8 ozone; CAMx (left), CMAQ (right) 125
Figure 6-4. Spatial distribution of mean biases for modeled MDA8 ozone; CAMx (left), CMAQ (right) 125
Figure 6-5. Scatter plot of observed and modeled MDA8 ozone concentrations for monitors in the Maricopa NAA; CAMx (gray), CMAQ (red) 126
Figure 6-6. Soccer plots of MDA8 ozone normalized mean bias and error; (a) CAMx and (b) CMAQ 126
Figure 6-7. Box plots of modeled MDA8 ozone distribution for entire modeling period (top left), monthly distribution of modeled MDA8 ozone (top right), day of week distribution of modeled MDA8 ozone (bottom left), and diurnal distribution of modeled one-hour ozone (bottom right) 127
Figure 6-8. Hourly NO_2 time series for July 2023 at four AQS sites in the Maricopa nonattainment area (Buckeye, Central Phoenix, JLG Supersite, and West Phoenix). Observations are compared with CAMx base case 129
Figure 6-9. Formaldehyde (HCHO) at JLG Supersite for July 2023. AQS observations are reported as three metrics: a 24-hr sample collected every six days ("24-hr 6-day"), an 8-hr sample collected every three days ("8-hr 3-day"), and the daily maximum 8-hr sample ("8-hr max"). Observations are compared with CAMx base case 130
Figure 6-10. Hourly ozone for Guadalajara (top), Mexico City (middle), and Monterrey (bottom) averaged across monitoring sites for July 2023: comparison of SINAICA observations and CAMx base case 131
Figure 6-11. Comparison of CAMx and CMAQ simulated tropospheric NO_2 vertical column densities (VCDs) against TROPOMI observations over the 4 km domain during April–September 2023. Bars indicate monthly mean percent differences relative to TROPOMI 132
Figure 6-12. Comparison of CMAx/CMAQ and ozonesonde vertical ozone profiles at Trinidad Head, California, for June 12 and July 22, 2023 134
Figure 6-13. Comparison of CMAx/CMAQ and ozonesonde vertical ozone profiles at Boulder, Colorado, on May 4 and June 15, 2023 134
Figure 7-1. Emission source regions for the source apportionment analysis 142
Figure 7-2. Daily source contributions to the CAMx modeled MDA8 ozone in the Maricopa NAA 143
Figure 7-3. Daily international anthropogenic source contributions to the CAMx modeled MDA8 ozone in the Maricopa NAA 144
Figure 7-4. Daily international anthropogenic source contributions to the CAMx modeled MDA8 ozone in the Maricopa NAA 145

Figure 7-5. Monthly anthropogenic source contributions to the CAMx modeled MDA8 ozone in the Maricopa NAA; total IA (BC IA + Mexico IA) vs. local (NAA Anthro) 145
Figure 7-6. Anthropogenic source contributions to the CAMx modeled MDA8 ozone in the Maricopa NAA for all modeled days and modeled top 10 days 147
Figure 7-7. Regional source contributions to the CAMx modeled MDA8 ozone in the Maricopa NAA for all modeled days and modeled top 10 days 148
Figure 7-8. Source group contributions to the CAMx modeled MDA8 ozone in the Maricopa NAA for all modeled days and modeled top 10 days 148

1. INTRODUCTION

1.1. Purpose

The purpose of this technical modeling support document (TSD) is to provide an in-depth and comprehensive description of the modeling tasks and techniques performed in support of the MAG 2025 Clean Air Act Section 179B(b) Retrospective Demonstration of the Impact of International Emissions on Ozone Concentrations in the Maricopa Nonattainment Area. The modeling work described in this TSD establishes the platform from which Ramboll Americas performed the photochemical modeling and supporting analyses included in the MAG 2025 Clean Air Act Section 179B(b) Retrospective Demonstration and their supporting report (Appendix A to the MAG 2025 Clean Air Act Section 179B(b) Retrospective Demonstration). This TSD also serves as the primary source material for a conceptual model of ozone formation in the Maricopa Nonattainment Area.

While the modeling analyses performed by Ramboll serve as the primary evidence that the Maricopa Nonattainment Area would have attained the EPA 2015 ozone standard by August 3, 2024, but for the impact from manmade international emissions, MAG also performed internal photochemical modeling to validate Ramboll's results as presented in this TSD. MAG replicated the modeling performed by Ramboll, so the model performance evaluation and metrics presented here can be applied to the work performed by Ramboll. Additionally, MAG evaluated photochemical modeling with two models (CAMx and CMAQ) and also performed additional modeling techniques such as zero-out modeling in addition to the source apportionment performed by Ramboll. All of this additional work is presented below and provides substantial weight-of-evidence to primary modeling work performed by Ramboll.

1.2. Overview of the Modeling Analysis

This 179B(b) retrospective demonstration is supported by a comprehensive technical modeling analysis. The analysis evaluates 8-hour ozone formation in the Maricopa nonattainment area using state-of-the-science methods, and explicitly quantifies the contribution of international emissions to local ozone levels. The primary objective is to demonstrate that the area would attain the 2015 ozone NAAQS by August 3, 2024, but for the influence of international anthropogenic emissions. To achieve this, MAG designed a modeling platform to function as a targeted experiment isolating the impact of international anthropogenic emissions on local air quality. All modeling procedures were

developed in accordance with EPA's Guidance on Air Quality Models and ozone attainment demonstration guidelines, ensuring that regulatory criteria for technical soundness are met.

Base Year and Modeling Tools: The analysis employs a 2023 base year photochemical modeling platform, which serves as the foundation for all simulations and calculations. Ozone concentrations during the 2023 ozone season (April–September) were simulated using two distinct photochemical grid models in parallel: the Comprehensive Air Quality Model with Extensions (CAMx) and the Community Multiscale Air Quality (CMAQ) model. Both models are peer-reviewed, EPA-approved models that have been widely used for regulatory ozone studies and meet the Agency's criteria for SIP modeling applications (e.g., having appropriate scientific formulation and published performance evaluations). Using a dual-model approach provides an important inter-model comparison to bolster confidence in the results – any attainment determination or conclusion about international impacts is more robust if confirmed by two independent models, thereby reducing uncertainty associated with any single model formulation. The modeling domain consists of a nested grid system with fine resolution over the Phoenix area (details are provided in Section 4.2), and meteorological inputs are generated by the Weather Research and Forecasting (WRF) model. The WRF model was run for the full April–September 2023 period to provide hourly weather data (wind fields, temperature, humidity, etc.) needed for chemistry simulations. Key model inputs, including emissions and boundary conditions, were prepared as described below.

Emissions Inputs: A comprehensive 2023 emissions inventory was developed to drive the modeling. The inventory covers all source categories (anthropogenic and natural) and was prepared using the latest available tools and data. For on-road and non-road mobile sources, EPA's Motor Vehicle Emission Simulator was used (the latest versions, referred to here as MOVES4.0 for local-scale modeling and MOVES5 for national-scale data) along with MAG's specialized MOVESLINK4 tool for generating hour-by-hour, gridded emissions from transportation activity. Point (industrial) and area source emissions within the 4 km local domain were compiled by Maricopa Air Quality Department (MCAQD) and Pinal County Air Control District (PCAQCD) from facility reports and other local data. The on-road motor vehicle inventory for the Maricopa area was developed with locally specific inputs – including 2023 vehicle registration counts from the Arizona Department of Transportation (ADOT), travel activity (vehicle miles traveled and speeds) from MAG's regional travel demand model, and local fuel specifications and inspection/maintenance program data. Non-road equipment emissions were similarly calculated with MOVES4.0 using local equipment population and activity adjustments. Emissions from aviation

sources (aircraft, airport ground support equipment, etc.) were estimated using the Federal Aviation Administration's Aviation Environmental Design Tool (AEDT) version 3g, with 2023 operational data (flight counts, aircraft types, etc.) for all airports in the region. Natural emissions that can contribute to ozone formation were also included: biogenic volatile organic compound (VOC) emissions from vegetation and soils were modeled using the Model of Emissions of Gases and Aerosols from Nature (MEGAN) v3.2 driven by the 2023 meteorological data, wildfire emissions for 2023 were obtained from the EPA's National Emissions Inventory (for U.S. fires) and from the NCAR FINN database (for fires in Mexico), and lightning-generated NOx was accounted for using CMAQ's in-line lightning module informed by observed lightning flash data for 2023. All emissions data (local and regional) were processed through the Sparse Matrix Operator Kernel Emissions (SMOKE) modeling system to perform temporal allocation (e.g. hourly profiles), chemical speciation into model species, and spatial gridding of county-level data to the 4 km and larger grids. The final output was a set of model-ready emissions files, which were processed and formatted for direct input into the CAMx and CMAQ photochemical models. These files provide comprehensive data for three nested modeling domains: a broad 36 km regional grid, an intermediate 12 km grid, and a high-resolution 4 km grid focused on the Maricopa 8-hour ozone nonattainment area (A detailed description of the base year emissions development is provided in Section 3 below).

Modeling Approach and Regulatory Tests: The core of the attainment demonstration is a comparison of modeled ozone concentrations to the NAAQS, with and without international emissions influence. In coordination with EPA guidance, MAG selected a full ozone-season simulation (April 1 – September 30, 2023) as the modeling period, rather than a few selected episodes, to ensure that a wide range of meteorological conditions is represented. This six-month period covers the entire ozone season when high ozone is observed, thereby capturing multiple pollution buildup and cleanup cycles, as recommended by EPA's modeling guidance. Within this timeframe, the first two weeks of April 2023 were treated as model spin-up – an initialization period allowing the model to stabilize – and were not used in model performance evaluation or attainment calculations. Ozone model performance was evaluated against observed ozone monitor data for 2023 to ensure the models are reproducing actual ozone patterns within acceptable accuracy (model performance results are discussed in Section 6 below). Once the base modeling was validated, MAG conducted specialized modeling analyses to isolate the impact of international emissions. Specifically, a global chemical transport model (GEOS-Chem v14.6.1) was used to generate boundary condition inputs for the regional model under two scenarios:

- Base Case: representing typical 2023 conditions with all global emissions included (providing "normal" boundary conditions reflecting actual transported pollution from outside the modeling domain), and
- International "Zero-Out" Case: a scenario in which all international anthropogenic emissions (i.e., emissions originating outside the U.S.) were removed from the global model. This yields an alternate set of boundary conditions depicting a world where foreign anthropogenic pollution is absent.

CAMx and CMAQ were then run for 2023 with each set of boundary conditions, while holding all domestic emissions constant, to quantify the difference in ozone outcomes with vs. without international contributions. This comparative modeling strategy – often termed a "but-for international" analysis – directly addresses the requirement of CAA §179B by simulating what ozone concentrations in the Maricopa area would have been if overseas anthropogenic emissions did not impact the region. In addition, CAMx's Ozone Source Apportionment Technology (OSAT) tool was applied to attribute portions of the ozone concentration to various source regions, including international sources. These techniques provide a robust weight-of-evidence that separates local vs. transported ozone contributions.

Key Findings: The modeling results indicate that international emissions are a determining factor in the Maricopa area's ozone levels. When the contribution of international anthropogenic emissions is removed in the modeling analysis, the highest conservative simulated 8-hour ozone design value within the nonattainment area is 66 ppb. A more refined estimate of 62 ppb is achieved when a reasonable number of wildfire days (atypical events) are excluded. Both values demonstrate attainment by falling below the 70 ppb national standard. In other words, the local and U.S. domestic emissions by themselves (absent foreign pollution) are not projected to cause a NAAQS violation – the area would attain the 2015 ozone NAAQS by the attainment deadline but for the internationally transported portion of ozone. This is a crucial conclusion. It means the statutory attainment test is passed under the modeled no-international scenario, thereby forming the technical basis of the §179B demonstration. Detailed modeling outputs, including concentration projections and source contribution breakdowns, are presented in Section 7 below, which covers the modeled attainment demonstration and weight-of-evidence analysis.

Data Access: All input and output files from the modeling analysis have been archived and will be made available to EPA and stakeholders upon request.

1.3. Structure of This Document

This technical support document (TSD) is organized as follows to present the regulatory context, modeling approach, results, and conclusions in a logical and comprehensive manner:

- **Section 1 – Introduction:** Outlines the regulatory background, purpose of the SIP revision, and an overview of the technical analysis and key findings.
- **Section 2 – Modeling Protocol and Conceptual Model:** A complete description of MAG's modeling protocol and conceptual model has been included in this TSD as Appendix 4.
- **Section 3 – Emissions Inventory Development:** Details the development of the 2023 base year emissions inventories for all source categories (industry, mobile sources, natural sources, etc.) that feed into the modeling analysis.
- **Section 4 – Meteorological Modeling:** Describes the configuration of the WRF meteorological simulation, its performance evaluation against observed weather data, and any observation-based adjustments or data assimilation (e.g., nudging) applied to improve model accuracy.
- **Section 5 – Photochemical Modeling Configuration:** Provides specifics on the configuration of the CAMx and CMAQ air quality models, including chemical mechanisms and the development of initial/boundary conditions using the GEOS-Chem global model.
- **Section 6 – Air Quality Model Performance Evaluation:** Presents an evaluation of CAMx and CMAQ performance by comparing modeled ozone (and precursor) concentrations to observations, as well as diagnostic analyses to ensure the models are suitable for use in the attainment test.
- **Section 7 – Attainment Demonstration and 179B(b) Analysis:** Provides the modeling demonstration, including calculated ozone design values for the year 2023, and the outcomes of the source apportionment and "zero-out" sensitivity analyses quantifying international contributions. This Section demonstrates that the area would attain the 2015 ozone NAAQS "but for" the international emissions.

Supporting details, such as detailed model inputs/outputs, are provided in appendices to this TSD.

2. CONCEPTUAL MODEL AND EPISODE SELECTION

MAG had previously developed a draft modeling protocol, which includes a comprehensive conceptual model of ozone formation in the Maricopa Nonattainment Area. This modeling protocol was shared with EPA for review and comment on May 23, 2025. For ease of documentation, the complete modeling protocol and associated conceptual model are included as an Appendix 4 to this TSD.

Please note that when the modeling protocol was developed, it was intended to serve as a broad basis for both a possible retrospective CAA Section 179B(b) demonstration and also as a basis for a possible prospective CAA Section 179B(a) attainment demonstration that would be included in a more traditional State Implementation Plan revision. While references to attainment demonstrations in the modeling protocol are not necessarily strictly relevant to a retrospective CAA Section 179B(b) demonstration, those statements are not in conflict with the technical work performed for the MAG 2025 Clean Air Act Section 179B(b) Retrospective Demonstration.

3. EMISSIONS INVENTORY AND PROCESSING

3.1. Introduction to the Emissions Inventory Development Process

The anthropogenic emissions inventory for the 12 and 36 km modeling domains was derived primarily from the EPA's Air Quality Modeling Platform (AQMP) 2022 version 1 (U.S. EPA, 2025a). This platform provided year 2022 emissions for point, area, and nonroad source categories across the continental United States and Mexico.

The baseline emissions inventory was enhanced by incorporating two critical updates. First, onroad mobile source emissions were updated using the EPA's latest onroad model, MOVES5, as provided in the EPA's AQMP 2022v2. Second, to capture actual 2023 performance, hourly data from Continuous Emissions Monitoring Systems (CEMS) were incorporated for all major U.S. Electric Generating Unit (EGU) point sources (U.S. EPA, 2025c). The methodology used to develop the anthropogenic emissions for the 4 km domain is detailed in Section 3.2.

The natural emissions inventory was developed for the 36, 12, and 4 km modeling domains and includes biogenic, wildfire, and lightning-generated sources.

- Biogenic Emissions: These emissions were modeled using the latest Model of Emissions of Gases and Aerosols from Nature (MEGAN) v3.2. MEGAN estimates biogenic emissions by combining hourly gridded meteorological inputs (e.g., temperature, radiation, humidity, wind), land cover and vegetation distributions, leaf area index (LAI), and species-specific emission factors. These inputs are used to scale baseline emission factors through environmental activity algorithms (light, temperature, LAI, soil moisture, etc.), producing gridded fluxes of biogenic volatile organic compounds (BVOCs) and soil NO.
- Wildfire Emissions: 2023 wildfire emissions were compiled from two primary sources. Fires within the U.S. were based on the EPA's 2023 National Emissions Inventory (NEI) (U.S. EPA, 2025d), while emissions for Mexico were extracted from the Fire Inventory from NCAR (FINN) version 2.5 (Wiedinmyer et al., 2023; UCAR, 2025).
- Lightning Emissions: Lightning-generated nitrogen oxides (NO_x) were calculated by EPA scientists for each modeling domain. The calculations were based on processing 2023 flash data from the National Lightning Detection Network (NLDN) and the World Wide Lightning Location Network (WWLLN) (Kang et al., 2022).

3.2. 2023 Local Anthropogenic Emissions Inventory

The 2023 anthropogenic emissions inventory for the 4 km domain was developed for this plan. Specifically, point and area source emissions inventories were compiled by the Maricopa County Air Quality Department (MCAQD) and the Pinal County Air Quality Control District (PCAQCD). Nonroad and onroad mobile source emissions were estimated using the EPA's Motor Vehicle Emission Simulator (MOVES4). Aviation emissions from aircraft, Ground Support Equipment (GSE), and Auxiliary Power Units (APUs) at all airports within the 4 km domains, except for Luke Air Force base, were calculated using the latest version of the Federal Aviation Administration's Aviation Environmental Design Tool (AEDT 3g). Additionally, the EPA Spatial Allocator tool was applied to distribute emissions geographically for each Source Classification Code (SCC) in the area and nonroad source categories.

3.2.1. Point Sources

Point sources refer to major stationary sources that emit significant quantities of air pollutants. A point source is required to report emissions if it meets the definition of a major source under 40 CFR Part 70. For this emissions inventory, point sources within the 4 km domain were classified as either EGU or non-EGU sources. EGUs refer to power plants, while non-EGUs include other major stationary sources such as landfills, petroleum storage and transfer facilities, and large industrial operations. MCAQD identified point sources within the county using its inventory, permitting, and compliance tracking (IMPACT) database. As shown in Table 3-1, emissions data for a total of 22 stationary sources, including both EGU and non-EGU point sources, were collected for 2023.

Pinal County provided emissions for a list of 20 point source facilities, including the EGU and nonEGU sources as shown in Table 3-2. Apache Junction Landfill is the only one located within the boundary of Maricopa 8-hour ozone nonattainment area (NAA).

MCAQD manages two types of emission credits. In 2023, MCAQD certified Emission Reduction Credits (ERCs) for two facilities, totaling 1.8 tons of NO_x and 11.1 tons of volatile organic compounds (VOCs). In 2025, MCAQD also proposed an annual pool of Mobile Emission Reduction Credits (MERCs) that can be utilized under Maricopa Rule 204 or 205. MERCs represent banked mobile source emission reductions that could be used by new sources; for modeling, these potential emissions were spatially allocated as a separate 'MERC' category to examine their impact. This pool consists of 500 tons of VOCs and 1,000 tons of NO_x for distribution within the Maricopa County portion of the 2015 8-hour ozone NAA.

Finally, the emissions data for the Salt River Pima-Maricopa Indian Community (SRPMIC) were obtained from the EPA's 2017 modeling platform (U.S. EPA, 2022) and reviewed by the tribal environmental agency. Emissions for 2023 were assumed to remain unchanged from 2017 levels.

Table 3-3 lists the Maricopa County's two emission reduction credits and the annual emissions in the Salt River Pima-Maricopa Indian Community.

Table 3-1. 2023 Annual point source emissions in Maricopa County (units: short tons/year)

Count	Facility Name	VOC	NO_x	CO
1	APS West Phoenix Power Plant	21.98	392.47	113.17
2	Arlington Valley LLC	0.24	101.74	32.81
3	Gila River Power Station	2.38	305.02	70.35
4	Mesquite Generating Station	24.73	240.06	27.03
5	New Harquahala Generating Co	6.31	79.24	28.48
6	Ocotillo Power Plant	5.85	85.83	28.93
7	Redhawk Generating Facility	6.35	141.96	191.79
8	SRP Agua Fria Generating Station	5.65	227.25	68.74
9	SRP Kyrene Generating Station	0.48	55.29	13.20
10	Santan Generating Station	10.93	274.38	109.87
11	Butterfield Station Facility	17.11	22.48	33.73
12	CMC STEEL FABRICATORS	12.96	65.63	900.93
13	Glendale Municipal Sanitary Landfill	2.23	4.78	8.37
14	Honeywell	116.90	31.77	11.23
15	Intel Corp-Ocotillo Campus	76.32	134.44	200.42
16	Luke AFB - 56th Fighter Wing	8.72	3.02	2.63
17	New Wincup Holdings Inc	92.46	2.69	0.11
18	Northwest Regional Landfill	30.19	21.04	87.17
19	Oak Canyon Manufacturing Inc	33.61	0.00	0.00
20	SFPP LP Phoenix Terminal	133.00	14.88	13.22
21	Trendwood Inc	14.67	0.00	0.00
22	Solana Generating Station*	421.58	0.81	0.38
Total		**1,044.65**	**2,204.78**	**1,942.56**

* Solana Generating Station is located outside of the Maricopa NAA. Emissions from this facility were all fugitive and omitted from Ramboll's CAA §179B(b) modeling demonstration. After incorporating this source into the updated inventory, MAG re-executed CAMx and CMAQ baseline and zero-out simulations to assess sensitivity to the added emissions; the modeled eight-hour ozone design values and relative response factors were unchanged. CAMx source-apportionment likewise indicated no change to the results. The conclusions from Ramboll's §179B(b) demonstration remain unchanged, whereas all results from MAG's work in this document incorporate the updated emissions. (See Appendix 1 for sensitivity analysis).

Table 3-2. 2023 Annual point source emissions in Pinal County (units: short tons/year)

Count	Facility Name	VOC	NO_x	CO
1	Apache Junction Landfill*	3.88	5.87	18.73
2	Saguaro Power Plant	2.50	147.12	50.69
3	APS - Sundance Power Plant	9.66	44.18	14.85
4	Arizona Environmental Container Corporation	36.28	0.03	0.00
5	ASARCO - Ray Complex, Ray Operations**	12.98	88.51	306.40
6	Cactus Landfill	11.06	35.40	10.67
7	Casa Grande Municipal Solid Waste Landfill	350.00	2.38	6.96
8	Casa Grande Plant (Foundation - Prowall Foam Plant)	124.69	0.97	0.81
9	Mesa Fully Formed - Coolidge Plant	0.18	0.00	0.00
10	Durham Regional Landfill	9.16	2.87	0.62
11	Casa Grande Compressor Station	1.10	6.97	0.61
12	Oracle Compressor Station	1.44	164.17	5.04
13	Frito-Lay Plant	4.43	28.99	46.56
14	Hexcel Corporation	113.52	29.74	8.28
15	Kohler Co	0.00	0.25	0.08
16	Republic Plastics - Eloy Foam Plant	204.10	0.00	0.00
17	Sierra Estrella Landfill	5.32	0.00	0.00
18	Coolidge Generating Station	2.20	45.00	33.10
19	Desert Basin Generating Station	0.40	122.60	146.00
20	Tom Mix Compressor Station	0.00	19.44	7.88
Total		**892.90**	**744.49**	**657.28**

* Apache Junction Landfill is the only point source from Pinal County located within the Maricopa NAA.

** The facility for "ASARCO - Ray Complex" is located outside of the 4 km modeling domain.

Table 3-3. Maricopa County Emission Reduction Credits (ERCs) and Mobile Emission Reduction Credits (MERCs) and annual emissions in Salt River Pima-Maricopa Indian Community (units: short tons/year)

Count	Name	VOC	NO_x	CO
1	Maricopa County Emission Reduction Credits (ERCs)	11.10	1.80	n/a
2	Maricopa County Mobile Emission Reduction Credits (MERCs)	500.00	1,000.00	n/a
3	Salt River Pima-Maricopa Indian Community	97.40	177.55	148.82

3.2.2. Area Sources

Area sources are stationary sources that are either too small or too numerous to be classified as point sources. MCAQD developed annual emissions for area sources for 2023 using data from the MCAQD IMPACT database, EPA guidance documents, and the EPA's Wagon Wheel tools. Tables 3-4 lists the 2023 annual area source emissions in Maricopa County. As shown in Table 3-5, Pinal County Air Quality Control District (PCAQCD) followed similar methods for Pinal County's area sources, with appropriate local data and scaling where necessary.

Table 3-4. 2023 annual area source emissions in Maricopa County (units: short tons/year)

SCC	SCC Description	VOC	NO_x	CO
2102004001	Industrial Distillate Oil: Boilers	0.70	71.37	17.82
2102004002	Industrial Distillate Oil: Engines	99.90	1,436.23	309.11
2102006000	Industrial Natural Gas	21.53	391.47	328.83
2102007000	Industrial Liquefied Petroleum Gas	1.70	47.75	26.73
2103004001	Commercial/institutional distillate oil: Boilers	0.07	3.30	0.80
2103004002	Commercial/institutional distillate oil: Engines	0.42	5.48	1.16
2103006000	Commercial/institutional natural gas	47.38	861.07	723.32
2103007000	Comm/Inst Fuel Combustion: All Combustor Types (LPG)	4.70	128.60	72.00
2104004000	Residential distillate oil	0.01	0.19	0.05
2104006000	Residential natural gas	59.30	1,013.41	431.24
2104007000	Residential liquefied petroleum gas (LPG)	2.10	70.23	19.86
2301000000	Chemical manufacturing	149.55	n/a	0.00
2302002100	-Commercial cooking: Conveyorized charbroiling	14.72	n/a	46.99
2302002200	-Commercial cooking: Under-fired charbroiling	62.11	n/a	186.95
2302003000	-Commercial cooking: Deep fat frying	14.87	n/a	53.52
2302003100	-Commercial cooking: Flat griddle frying	11.71	n/a	17.31
2302003200	-Commercial cooking: Clamshell griddle frying	0.14	n/a	3.91
2302050000	Bakeries	71.37	n/a	0.00
2304000000	Secondary metal production	46.15	20.52	109.41
2308000000	Rubber/Plastic product mfg.	978.78	n/a	0.00
2309000000	Fabricated metals	7.21	1.20	0.30
2312000000	Electrical equipment mfg.	161.76	37.94	8.51
2399000000	Industrial processes, not elsewhere classified (NEC)	65.57	13.91	49.05
2850000010	Commercial Sterilization	1.60	n/a	n/a
2401001000	Architectural coatings	2,436.21	n/a	n/a
2401005000	Auto refinishing	498.30	n/a	n/a
2401008000	Traffic markings	555.68	n/a	n/a
2401020000	Wood furniture	830.43	n/a	n/a

SCC	SCC Description	VOC	NO_x	CO
2401025000	Metal Furniture: SIC 25	49.95	n/a	n/a
2401030000	Paper: SIC 26	19.32	n/a	n/a
2401055000	Machinery and Equipment: SIC 35	41.34	n/a	n/a
2401060000	Large Appliances: SIC 363	11.41	n/a	n/a
2401065000	Electronic and Other Electrical: SIC 36 - 363	24.32	n/a	n/a
2401070000	Motor Vehicles: SIC 371	53.85	n/a	n/a
2401075000	Aircraft surface coating	6.71	n/a	n/a
2401080000	Marine: SIC 373	8.01	n/a	n/a
2401085000	Railroad: SIC 374	5.86	n/a	n/a
2401090000	Misc. surface coating	101.30	n/a	n/a
2401100000	Industrial Maintenance Coatings	756.26	n/a	n/a
2401200000	Other Special Purpose Coatings	479.18	n/a	n/a
2415000000	Degreasing	527.83	n/a	n/a
2420000000	Dry cleaning	18.10	n/a	n/a
2425000000	Graphics arts	285.09	n/a	n/a
2440000000	Misc. Industrial Solvent Use	56.76	n/a	n/a
2460100000	-Personal care products	4,558.68	n/a	n/a
2460200000	-Household products	4,642.08	n/a	n/a
2460400000	-Automotive aftermarket products	439.71	n/a	n/a
2460500000	-Coatings and related products	2,295.48	n/a	n/a
2460600000	-Adhesives and sealants	4,407.35	n/a	n/a
2460800000	-FIFRA related products	4,142.37	n/a	n/a
2460900000	-Miscellaneous products, NEC	162.85	n/a	n/a
2461022000	Emulsified Asphalt	170.10	n/a	n/a
2461025100	Hot Mix Asphalt	839.16	n/a	n/a
2461025200	Warm Mix Asphalt	14.69	n/a	n/a
2461850000	Agricultural Pesticides	212.70	n/a	n/a
2501011011	Residential Portable Gas Cans (RPGC): Permeation	80.29	n/a	n/a
2501011012	RPGC: Evaporation (incl. diurnal losses)	90.09	n/a	n/a
2501011013	RPGC: Spillage During Transport	301.96	n/a	n/a
2501011014	RPGC: Refilling at the Pump - Vapor Displacement	28.35	n/a	n/a
2501011015	RPGC: Refilling at the Pump – Spillage	8.81	n/a	n/a
2501012011	Commercial Portable Gas Cans (CPGC): Permeation	5.20	n/a	n/a
2501012012	CPGC: Evaporation (incl. diurnal losses)	4.27	n/a	n/a
2501012013	CPGC: Spillage During Transport	411.93	n/a	n/a
2501012014	CPGC: Refilling at the Pump - Vapor Displacement	121.15	n/a	n/a

SCC	SCC Description	VOC	NO_x	CO
2501012015	CPGC: Refilling at the Pump - Spillage	16.95	n/a	n/a
2501050120	Bulk terminals	103.23	n/a	n/a
2501055120	Bulk plants	28.03	n/a	n/a
2501060051	Gasoline Stations Stage 1: Submerged Filling	102.05	n/a	n/a
2501060053	Gasoline Stations Stage 1: Balanced Submerged Filling	330.85	n/a	n/a
2501060201	Gasoline Stations Underground Tank: Breathing&Emptying	671.67	n/a	n/a
2501080050	Airports: Aviation Gasoline Stage 1: Total	1.54	n/a	n/a
2501080100	Airports: Aviation Gasoline Stage 2: Total	564.58	n/a	n/a
2505030120	Truck: Gasoline (Tank Trucks in Transit)	57.84	n/a	n/a
2505040120	Pipeline Gasoline	66.15	n/a	n/a
2510000000	VOL storage/transport	10.83	n/a	n/a
2610000500	ALL Open Burning	24.58	10.93	229.38
2620000000	Landfills	9.60	16.60	17.60
2630020000	Publicly Owned Treatment Works (POTWs)	59.84	n/a	n/a
2650000000	Other waste	2.10	6.80	4.40
2660000000	Leaking Underground Storage Tanks	4.52	n/a	n/a
2680003000	Composting	752.50	n/a	n/a
2805002000	-Beef cattle production composite; NEC	101.00	n/a	n/a
2805007100	-Poultry: layers with dry shit management; confinement	102.61	n/a	n/a
2805009100	-Poultry: broilers; confinement	0.01	n/a	n/a
2805010100	Agriculture Production - Livestock (confinement)	0.02	n/a	n/a
2805018000	-Dairy cattle composite; NEC	791.33	n/a	n/a
2805025000	-Swine composite; NEC (see also 2805-039,-047,-053)	50.96	n/a	n/a
2805035000	Agriculture Production - Livestock (Horses and Ponies Waste Emissions)	10.61	n/a	n/a
2805040000	Agriculture Production - Livestock (Sheep and lambs Emissions)	0.45	n/a	n/a
2805045000	Agriculture Production - Livestock (Goats Emissions)	1.39	n/a	n/a
2810015000	Prescribed fires	0.20	0.20	2.50
2810025000	Backyard BBQs (Residential Grilling)	88.06	23.18	1,120.89
2810030000	Structure fires	17.30	2.20	94.10
2810040000	Aircraft engine testing	0.04	1.72	1.36
2810050000	Vehicle fires	6.50	0.80	25.40
2810060100	Crematories - Human	1.02	35.28	1.94
2810060200	Crematories - Animal	0.20	8.80	0.50
2830001000	Accidental releases	10.42	0.05	0.18
Total		**35,515.46**	**4,209.23**	**3,905.11**

Table 3-5. 2023 annual area source emissions in Pinal County (units: short tons/year)

SCC	SCC Description	VOC	NO_x	CO
2102004002	Industrial Distillate Oil: Engines	7.70	107.85	n/a
2102006000	Industrial Natural Gas	3.08	147.91	n/a
2102007000	Industrial Liquefied Petroleum Gas	0.17	4.54	2.54
2102008000	Industrial wood	0.05	0.61	1.66
2103006000	Commercial/institutional natural gas	1.99	36.12	30.34
2103007000	Fuel Combustion: All Combustor Types (LPG)	0.16	4.38	2.45
2103008000	Commercial/institutional wood	0.08	0.98	2.67
2104006000	Residential natural gas	5.70	97.35	41.43
2302002100	-Commercial cooking: Conveyorized charbroiling	5.49	n/a	18.30
2302002200	-Commercial cooking: Under-fired charbroiling	12.06	n/a	39.44
2302003000	-Commercial cooking: Deep fat frying	3.11	n/a	n/a
2302003100	-Commercial cooking: Flat griddle frying	1.79	n/a	3.72
2302003200	-Commercial cooking: Clamshell griddle frying	0.09	n/a	n/a
2302050000	Bakeries	14.58	n/a	n/a
2305070000	Non-metallic Mineral processing	1.13	34.84	8.86
2309000000	Fabricated metals	26.21	0.02	0.00
2325000000	Mining/quarrying	n/a	1.77	0.38
2401001000	Architectural coatings	306.56	n/a	n/a
2401005000	Auto refinishing	29.38	n/a	n/a
2401008000	Traffic markings	65.83	n/a	n/a
2401015000	Factory finished wood	1.33	n/a	n/a
2401020000	Wood furniture	12.90	n/a	n/a
2401055000	Machinery and Equipment: SIC 35	1.74	n/a	n/a
2401065000	Electronic and Other Electrical: SIC 36 - 363	0.47	n/a	n/a
2401070000	Motor Vehicles: SIC 371	1.08	n/a	n/a
2401075000	Aircraft surface coating	0.10	n/a	n/a
2401090000	Misc. surface coating	25.06	2.19	0.47
2401100000	Industrial Maintenance Coatings	49.72	n/a	n/a
2401200000	Other Special Purpose Coatings	1.95	n/a	n/a
2415000000	Degreasing	75.77	n/a	n/a
2420000000	Dry cleaning	0.57	n/a	n/a
2425000000	Graphics arts	18.21	n/a	n/a
2460100000	-Personal care products	474.80	n/a	n/a
2460200000	-Household products	483.49	n/a	n/a
2460400000	-Automotive aftermarket products	45.80	n/a	n/a
2460500000	-Coatings and related products	230.26	n/a	n/a
2460600000	-Adhesives and sealants	442.10	n/a	n/a

SCC	SCC Description	VOC	NO_x	CO
2460800000	-FIFRA related products	431.44	n/a	n/a
2460900000	-Miscellaneous products, NEC	16.97	n/a	n/a
2461022000	Emulsified Asphalt	24.88	n/a	n/a
2461850000	Agricultural Pesticides	111.19	n/a	n/a
2501011011	Residential Portable Gas Cans (RPGC): Permeation	5.14	n/a	n/a
2501011012	RPGC: Evaporation (incl. diurnal losses)	5.77	n/a	n/a
2501011013	RPGC: Spillage During Transport	10.01	n/a	n/a
2501011014	RPGC: Refilling at the Pump - Vapor Displacement	1.82	n/a	n/a
2501011015	RPGC: Refilling at the Pump - Spillage	0.29	n/a	n/a
2501012011	Commercial Portable Gas Cans (CPGC): Permeation	0.22	n/a	n/a
2501012012	CPGC: Evaporation (incl. diurnal losses)	0.18	n/a	n/a
2501012013	CPGC: Spillage During Transport	13.65	n/a	n/a
2501012014	CPGC: Refilling at the Pump - Vapor Displacement	5.23	n/a	n/a
2501012015	CPGC: Refilling at the Pump - Spillage	0.56	n/a	n/a
2501050120	Bulk terminals	9.68	n/a	n/a
2501060051	Gasoline Stations Stage 1: Submerged Filling	63.85	n/a	n/a
2501060053	Gasoline Stations Stage 1: Balanced Submerged Filling	111.67	n/a	n/a
2501060201	Gasoline Stations Undergrnd Tank: Breathing & Emptying	109.56	n/a	n/a
2501080050	Airports: Aviation Gasoline Stage 1: Total	97.72	n/a	n/a
2501080100	Airports: Aviation Gasoline Stage 2: Total	0.19	n/a	n/a
2505030120	Truck: Gasoline (Tank Trucks in Transit)	7.17	n/a	n/a
2505040120	Pipeline Gasoline	2.41	n/a	n/a
2610000500	All Open Burning	18.04	8.02	167.21
2630020000	Publicly Owned Treatment Works (POTWs)	6.43	354.15	77.93
2660000000	Leaking Underground Storage Tanks	22.74	n/a	n/a
2680003000	Composting	91.49	n/a	n/a
2801500000	Agricultural Field Burning - whole field set on fire (unspecified)	11.70	2.74	116.03
2801500150	Agricultural Field Burning - whole field set on fire (Corn)	11.41	2.85	65.68
2801500160	Agricultural Field Burning: Cotton	1.03	0.38	8.14
2801500171	Agricultural Field Burning: Fallow	8.32	2.52	57.52
2805002000	-Beef cattle production composite; NEC	52.06	n/a	n/a
2805007100	-Poultry: layers with dry shit management; confinement	11.00	n/a	n/a
2805018000	-Dairy cattle composite; NEC	314.59	n/a	n/a
2805025000	-Swine composite; NEC (see also 2805-039, -047, -053)	1.81	n/a	n/a

SCC	SCC Description	VOC	NO_x	CO
2805035000	Agriculture Production - Livestock (Horses and Ponies Waste Emissions)	4.75	n/a	n/a
2805040000	Agriculture Production - Livestock (Sheep and lambs Emissions)	0.72	n/a	n/a
2805045000	Agriculture Production - Livestock (Goats Emissions)	0.68	n/a	n/a
2810025000	Backyard BBQs	8.48	2.23	107.91
2810030000	Structure fires	1.83	0.23	10.01
2810050000	Vehicle fires	0.66	0.08	2.58
2810060100	Crematories - Human	0.03	0.38	0.31
2830001000	Accidental releases	1.78	0.01	0.05
Total		**3,949.64**	**812.16**	**765.67**

3.2.3. Nonroad Mobile Sources

Nonroad mobile sources include off-highway recreational vehicles and pleasure craft, locomotives, aircraft and airport support vehicles, and equipment from commercial, industrial, agricultural, lawn maintenance and construction activities.

The nonroad emissions inventory was developed using MOVES4. There were no emissions from logging equipment or underground mining/oil field equipment in Maricopa and Pinal Counties. Locomotive emissions are from EPA rail estimates based on national locomotive fuel usage, locomotive fleet data, the amount of track in each state and county, along with usage and grade data for each track section. Season-day rail estimates were calculated assuming that rail activity is consistent throughout the year. Table 3-6 summarizes the 2023 annual locomotive emissions in both Maricopa and Pinal Counties. Airport ground support equipment, aircraft, and auxiliary power unit emissions were developed with the Federal Aviation Administration (FAA)'s Aviation Environmental Design Tool (AEDT 3g), as will be discussed in detail in Section 3.2.4.

MOVES4 Nonroad Equipment Emissions

For most nonroad mobile source categories (except airport GSE, APUs, aircraft and locomotives), the EPA Motor Vehicle Emission Simulator (MOVES 4) model was used to produce emission estimates for Maricopa and Pinal counties.

Local population and activity levels were used for lawn and garden equipment in Maricopa County. For the local commercial lawn and garden industry, ENVIRON performed a survey as a part of the Cap and Trade Oversight Committee work (ENVIRON, 2003). Survey results

Table 3-6. 2023 annual locomotives emissions in Maricopa and Pinal counties (units: short tons/year)

County	SCC	SCC Description	VOC	NO_x	CO
Maricopa	2285002006	Locomotives: Line haul class I	31.45	780.50	172.47
	2285002007	Line haul locomotives: Class II/III Operations	2.37	49.83	6.49
	2285002008	Locomotives: Passenger trains	2.03	37.70	6.47
	2285002010	Locomotives: Yard locomotives	16.97	261.28	36.37
	County Total		**52.82**	**1,129.31**	**221.80**
Pinal	2285002006	Locomotives: Line haul class I	38.04	825.05	162.99
	2285002007	Line haul locomotives: Class II/III Operations	5.41	117.24	14.42
	2285002008	Locomotives: Passenger trains	2.10	37.71	5.48
	County Total		**45.55**	**980.00**	**182.89**

showed that equipment populations for most categories of this sector in Maricopa County were significantly lower than EPA default values, while the average annual hours of operation for most equipment in this sector were slightly higher than EPA defaults. Thus, equipment population numbers and activity levels for commercial lawn and garden equipment were adjusted based on the ENVIRON survey results. Populations for agriculture and construction equipment in both Maricopa and Pinal counties were updated with spatial surrogates developed by EPA for the 2016 NEI and subsequent EPA modeling platforms. Logging, oil fields and underground mining are not present in the Maricopa NAA.

Hourly profiles of daily average temperature observations at the Phoenix Sky Harbor Airport weather station were obtained from National Oceanic and Atmospheric Administration (NOAA) National Centers for Environmental Information (NCEI) Local Climatological Data (NCEI, 2023). MOVES4 was run for each day of the year in 2023 using day-specific meteorology. The 2023 calendar was used to select appropriate weekday or weekend emission factors for each day.

MOVES4 default fuels were used, with Arizona Retail RVP Standards for Area A (AZDA, 2024) applied using the Fuel Wizard, identical to the fuel data used in modeling onroad mobile source emissions. Table 3-7 shows the average daily nonroad emissions by category for Maricopa and Pinal counties during the ozone season. For Maricopa County, the "Lawn and Garden" category is the dominant source of VOC emissions, while "Construction" is the main contributor to NO_x emissions.

Table 3-7. Ozone season (April-September) average daily nonroad mobile source emissions for Maricopa and Pinal counties in 2023 (unit: short tons/day)

Source Category	Maricopa County			Pinal County		
	VOC	NO_x	CO	VOC	NO_x	CO
Agricultural	0.05	0.51	0.57	0.04	0.44	0.48
Commercial	3.38	1.96	88.25	0.06	0.04	1.63
Construction	3.58	14.67	39.04	0.25	1.02	2.68
Industrial	0.37	2.44	10.22	0.01	0.09	0.24
Lawn and Garden	10.28	1.58	176.85	0.76	0.12	13.05
Pleasure craft	0.57	0.25	3.00	0.12	0.06	0.66
Railroad	0.00	0.01	0.04	0.00	0.01	0.03
Recreational	1.59	0.14	19.82	0.70	0.05	4.80
Total	**19.82**	**21.56**	**337.79**	**1.94**	**1.83**	**23.57**

3.2.4. Aircraft

The AEDT 3g model was used to produce emission estimates for airports located within the 4 km modeling domain in both Maricopa and Pinal Counties. AEDT models aircraft performance in space and time to estimate noise, fuel consumption, emissions, and air quality consequences. AEDT leverages geographic information system (GIS) and relational database technology to support individual studies ranging in scope from a single flight at an airport to scenarios at the regional, national, and global levels. AEDT is actively used by the U.S. government for regulatory studies, research, and domestic aviation system planning and aviation environmental policy analysis.

The AEDT 3g model was used to calculate aircraft, GSE, and APU emissions of VOC, NO_x, $PM_{2.5}$ and PM_{10}, SO_2, and CO using airport operational data for 2023 as discussed below. The model computes emissions individually for each combination of aircraft and engine type, and the AEDT model outputs aggregated emissions for four main aircraft categories:

- Air carriers (AC): Larger commercial aircraft with at least 60 seats or 18,000 pounds of payload capacity, used for scheduled service to transport passengers and/or freight;

- Air taxis (AT): Smaller commercial turbine- or piston-powered aircraft with less than 60 seats or 18,000 pounds of payload capacity;
- General aviation (GA): Aircraft used on an unscheduled basis for recreational flying, personal transportation, and other activities, including business travel; and
- Military (ML): Aircraft used to support military operations.

The AEDT model utilizes three main input databases to estimate annual or seasonal emission inventories at each airport:

- Airport database: Relevant airport information, such as latitude, longitude, runway, taxi-in and taxi-out time, country, and weather data;
- Fleet database: Aircraft/engine models and flight tracking profiles for arrival, departure, and touch-and-go (T&G) operations; and
- Local activity database: Number of aircraft operations for landing/takeoffs (LTO), and fleet mix at each airport.

Local aircraft activity data is a critical input to the AEDT 3g model. The FAA Operations Network (OPSNET) database (FAA, 2024a) provided daily activity data on 2023 aircraft operations for the eight larger commercial and general aviation airports in the Maricopa County (Chandler Municipal, Falcon Field, Glendale Municipal, Phoenix Deer Valley, Phoenix Goodyear, Phoenix-Mesa Gateway, Phoenix Sky Harbor, and Scottsdale airports). FAA 5010 Airport Master Records database (airportiq5010.com) provided operations data for five smaller general aviation airports in the Maricopa County (Buckeye Municipal, Gila Bend Municipal, Stellar Airpark, and Wickenburg Municipal airports) and six airports in Pinal County (Ak-Chin Regional, Casa Grande Municipal, Eloy Municipal, Arizona Soaring, Pinal Airpark, and Coolidge Municipal). 2023 operations for Sky Ranch at Carefree came from the MCAQD 2024 survey. Luke Air Force Base (AFB) personnel provided counts of F-16 and F-35 military aircraft based at Luke AFB in 2023. Figure 3-1 illustrates locations of twenty airports within the 4 km modeling domain.

The FAA Traffic Flow Management System Counts (TFMSC) database supplied 2023 fleet mix for 15 commercial and general aviation airports, except for three airports in Pinal County (Ak-Chin Regional, Eloy Municipal, and Coolidge Municipal), which use 2017 data. The fleet information for Arizona Soaring was taken from its airport website (https://azsoaring.com/training/). Table 3-8 summarizes the activity level for each aircraft category at each airport included in the inventory and indicates the data sources for activity and fleet mix.

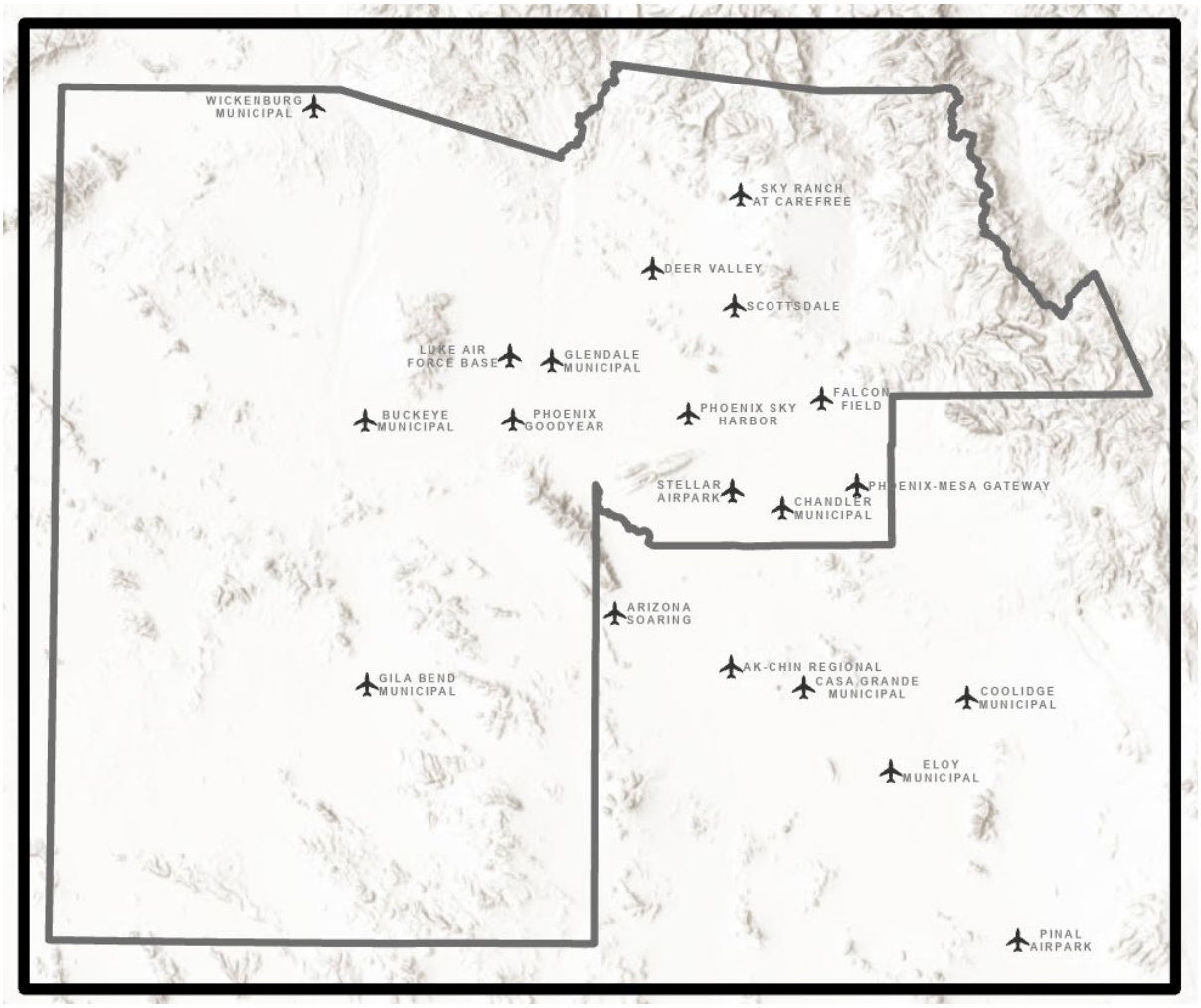

Figure 3-1. Locations of 20 airports within the 4 km modeling domain (black box). The gray polygon indicates the Maricopa County boundary

The following section describes the derivation of activity and emission estimates for general aviation activity at a representative airport: Chandler Municipal (CHD). The OPSNET database reported 212,616 general aviation operations at this airport in 2023, as listed in Table 3-9. The TFMSC database of general aviation activity and fleet mix at Chandler Municipal airport in 2023 comprised 99 different aircraft types recognized by AEDT 3g, with a combined 2,634 operations. The smaller numbers reported in TFMSC are a representative sample of the total general aviation operations. The number of operations for each type in the sample divided by the combined number of operations in the sample gives a relative frequency distribution of aircraft types at this airport. This frequency distribution, multiplied by the total number of operations reported by OPSNET, provides the number of operations allocated to each aircraft type for input to the AEDT

3g model. Table 3-9 demonstrates this calculation for the general aviation activity at Chandler Municipal Airport. When applied to each aircraft category at each airport, this procedure typically resulted in 10 to 100 aircraft types representing 98.6 to 100% of all reported activity.

Table 3-8. 2023 annual airport operations (by aircraft category) and related data sources for 20 airports in the 4 km modeling domain

Airport Name	2023 Operations						
	FAA LID	Operations Data Source[1]	Fleet Mix Data Source[2]	AC	AT	GA	ML
Buckeye Municipal	BXK	AirportIQ 5010	TFMSC	0	100	54,000	100
Chandler Municipal	CHD	OPSNET	TFMSC	0	21,172	212,616	114
Falcon Field	FFZ	OPSNET	TFMSC	18	78,498	268,909	1,447
Gila Bend Municipal	E63	AirportIQ 5010	TFMSC	0	624	41,317	59
Glendale Municipal	GEU	OPSNET	TFMSC	0	718	114,955	882
Phoenix Deer Valley	DVT	OPSNET	TFMSC	15	57,552	286,551	275
Phoenix Goodyear	GYR	OPSNET	TFMSC	156	62,033	156,179	152
Phoenix-Mesa Gateway	IWA	OPSNET	TFMSC	12,068	61,898	185,280	2,851
Phoenix Sky Harbor	PHX	OPSNET	TFMSC	394,482	35,088	22,814	2,281
Scottsdale	SDL	OPSNET	TFMSC	22	55,565	119,690	549
Sky Ranch at Carefree	18AZ	Survey	TFMSC	0	0	4,416	0
Stellar Airpark	P19	AirportIQ 5010	TFMSC	0	0	40,000	0
Wickenburg Municipal	E25	AirportIQ 5010	TFMSC	0	400	35,700	50
Ak-Chin Regional	A39	AirportIQ 5010	TFMSC	0	0	34,675	0
Casa Grande Municipal	CGZ	AirportIQ 5010	TFMSC	0	2,038	119,552	410
Eloy Municipal	E60	AirportIQ 5010	TFMSC	0	0	29,900	100
Arizona Soaring	E68	AirportIQ 5010	Website[3]	0	0	25,200	0
Pinal Airpark	MZJ	AirportIQ 5010	TFMSC	0	0	8,200	50,000
Coolidge Municipal	P08	AirportIQ 5010	TFMSC	0	0	56,000	50
Luke Air Force Base	LUF	[Emissions for 2023 were estimated by scaling based on numbers of F-16 and F-35 fighter jets, see text for details]					

[1] AirportIQ 5010: online database of FAA Form 5010 information (http://airportiq5010.com)
OPSNET: Operational Network (FAA, 2024a)
Survey: 2024 MCAQD survey of operations for Sky Ranch at Carefree

[2] TFMSC: Traffic Management System Counts are from 2023, except for airports P08, E60, and A39, which use 2017 data (FAA, 2024b).

[3] Website for air fleet mixing (https://azsoaring.com/training/)

Table 3-9. Aircraft type activity distribution at Chandler Municipal airport

Rank	Aircraft Type	TFMSC Reported Operations	Relative Frequency (%)	Cumulative Frequency (%)	Total Operations for AEDT
1	BE20 - Beech 200 Super King	461	17.502%	17.502%	37,206
2	C25C - Cessna Citation CJ4	172	6.530%	24.032%	13,884
3	C172 - Cessna Skyhawk 172/Cutlass	159	6.036%	30.068%	12,834
4	P28A - Piper Cherokee	147	5.581%	35.649%	11,866
5	PC12 - Pilatus PC-12	122	4.632%	40.281%	9,848
6	SF50 - Cirrus Vision SF50	110	4.176%	44.457%	8,880
7	BE33 - Beech Bonanza 33	109	4.138%	48.595%	8,798
8	C560 - Cessna Citation V/Ultra/Encore	106	4.024%	52.620%	8,556
9	S22T - Cirrus SR-22 Turbo	97	3.683%	56.302%	7,830
10	C182 - Cessna Skylane 182	69	2.620%	58.922%	5,570
11	C425 - Cessna 425 Corsair	68	2.582%	61.503%	5,488
12	P46T - Piper Malibu Meridian	60	2.278%	63.781%	4,844
13	EA50 - Eclipse 500	58	2.202%	65.983%	4,682
14	AC90 - Gulfstream Commander	49	1.860%	67.844%	3,956
15	M20P - Mooney M-20C Ranger	49	1.860%	69.704%	3,956
16	BE9L - Beech King Air 90	47	1.784%	71.488%	3,794
17	BE36 - Beech Bonanza 36	42	1.595%	73.083%	3,390
18	C56X - Cessna Excel/XLS	40	1.519%	74.601%	3,228
19	SR22 - Cirrus SR 22	40	1.519%	76.120%	3,228
20	BE58 - Beech 58	39	1.481%	77.601%	3,148
21	C421 - Cessna Golden Eagle 421	38	1.443%	79.043%	3,068
22	C340 - Cessna 340	25	0.949%	79.992%	2,018
⋮	⋮	⋮	⋮	⋮	⋮
93	C335 - Cessna 335	1	0.038%	99.772%	80
94	C750 - Cessna Citation X	1	0.038%	99.810%	80
95	COL3 - Lancair LC-40 Columbia 400	1	0.038%	99.848%	80
96	DA62 - Diamond DA62	1	0.038%	99.886%	80
97	GLAS - New Glasair	1	0.038%	99.924%	80
98	KODI - Quest Kodiak	1	0.038%	99.962%	80
99	PA31 - Piper Navajo PA-31	1	0.038%	100.000%	80
TOTAL		**2,634**			**212,616**

Note: Computations rounded to produce even multiples of LTO, with adjustments to account for accumulated rounding error added to the dominant aircraft type.

There are three types of aircraft with emissions at Luke AFB: F-16 fighter jets, F-35 fighter jets and transient aircraft. There are also emissions from associated GSE. The ratio of 0.252 between the number of F-16s based at Luke AFB in 2023 and the number of F-16s based there in 2008 (Weston, 2010) provides an estimate of aircraft and associated GSE emissions. Emissions from F-35 aircraft and their associated GSE were scaled using a ratio of 0.868 between the number of F-35 aircraft based at Luke AFB in 2023 and the future total number of F-35 aircraft in the L6 scenario emissions as obtained from the base's 2012 environmental impact statement report (USAF, 2012). Transient aircraft emissions for 2023 are similar to those for 2008, based on discussions with Luke AFB personnel.

Particulate Matter Emissions: The emissions inventory for anthropogenic particulate matter (PM) within the 4 km domain was based on the EPA's 2021v1 platform, except for the aviation and nonroad source categories, for which locally developed inventories were substituted.

3.2.5. Onroad Mobile Sources

This section describes how onroad mobile source emissions were estimated using local travel activity data and EPA's MOVES model. Motor Vehicle Emission Simulator (MOVES4) is the state-of-the-art emissions modeling tool developed by the U.S. Environmental Protection Agency (EPA) for the purpose of estimating onroad and off-network motor vehicle emission factors. Onroad emissions inventory for the 4 km modeling domain were developed using MOVES4 and MAG MOVESLINK4, which is a tool preparing MOVES4 inputs, executing MOVES4, and generating gridded emission files for photochemical modeling. Note that onroad emissions for national domains of 36 km and 12 km used an updated MOVES5-based 2022 platform inventory (per EPA 2022v2), while local 4 km domain onroad emissions were developed with MOVES4 with local data. This SIP development began in July 2024, which preceded EPA's MOVES5 release (December 11, 2024), so MOVES4 was applied for the local inventory.

The MAG MOVESLINK4 model processes transportation network assignment results for Maricopa and Pinal counties derived by ABM and develops the onroad emissions inventory using MOVES emission factors for the photochemical air quality modeling analysis. The MOVESLINK4 utilizes Geographic Information Systems (GIS) technology in processing geospatial network and emissions data. It was coded with the Python programming language.

To estimate onroad exhaust, evaporative, refueling, and extended idling emissions for 2023, MOVES4 was executed using local input data for individual modeling episode days.

MOVES4 modeling scenarios were created using the County Domain option, the Emissions Rates mode for the MOVES onroad network emissions, and the Inventory mode for the MOVES off-network emissions.

MOVES4 requires local data such as the presence of inspection and maintenance (I/M) programs, meteorological data, vehicle populations, source type age distribution, annual vehicle miles traveled (VMT), monthly/daily/hourly fractions, road type distribution, average speed distribution, fuel data, and alternative vehicle and fuel technologies (AVFT) (U.S. EPA, 2023a).

The MOVES4 inputs were developed using local data from multiple sources such as the Arizona Department of Transportation (ADOT), the Arizona Department of Agriculture (AZDA), the Maricopa Association of Governments (MAG) Transportation Division, and the National Centers for Environmental Information (NCEI).

Since the 4 km modeling domain contains a subarea (i.e., Area A) where control measures such as I/M programs and fuel programs were enforced, MOVES4 were run separately for the subarea and outside the subarea. The Area A boundary was defined in Arizona Senate Bill 1427 (SB 1427), and expanded in Arizona House Bill 2538 (HB 2538). The air quality measures described in HB 2538 were implemented in Area A. The Area A boundary (HB 2538) covers portions of Maricopa, Pinal, and Yavapai Counties. Onroad vehicles registered and operating in Area A are subject to the vehicle emissions inspection programs and the Cleaner Burning Gasoline (CBG) fuel requirements. Input data for Area A and outside Area A were prepared separately.

I/M Programs

MOVES4 has an [IMCoverage] table for I/M programs, which reflects the actual proportions of vehicles subject to the specified levels of inspection. MOVES I/M program input was derived from the existing I/M program operated in Area A. The compliance factors for MOVES were derived from gasoline regulatory class coverage adjustments, compliance rates, waiver rates, and vehicle emissions testing failure rates. The gasoline regulatory class coverage adjustments were obtained from the MOVES4 Technical Guidance (U.S. EPA, 2023b). Compliance rate, waiver rate, and failure rate were calculated using the ADEQ 2018 vehicle inspection data. Table 3-10 shows the MOVES compliance factors for the local I/M programs in 2023. For outside Area A, the No I/M Program option was applied.

Table 3-10. MOVES compliance factors for the local I/M programs in 2023

I/M Test Type	MOVES Test StandardID	Model Years		Test Frequency	MOVES Regulatory Class ID	Compliance Factor
		From	To			
Exhaust Loaded / Idle Test	13	1967	1980	Annual	21	85.65%
					31	88.45%
					32	87.85%
Exhaust IM147	33	1981	1995	Biennial	21	91.78%
					31	91.93%
					32	86.14%
Exhaust OBD Check	51	1996	2018	Biennial	21	99.48%
					31	99.30%
					32	97.37%
Exhaust Loaded / Idle Test	13	1967	2018	Annual	41	98.86%
					42	98.99%
					43	97.83%
					51	96.24%
					52	98.99%
					53	98.94%
					54	97.98%
					61	88.84%
					62	88.84%
Evaporative Gas Cap Check	41	1967	1980	Annual	21	85.57%
					31	88.41%
					32	87.82%
Evaporative Gas Cap and Pressure Check	44	1981	1995	Biennial	21	91.77%
					31	91.93%
					32	86.13%
Evaporative Gas Cap and OBD Check	45	1996	2018	Biennial	21	99.48%
					31	99.13%
					32	95.94%
Evaporative Gas Cap Check	41	1967	2018	Annual	41	98.85%
					42	98.99%
					43	97.83%
					51	96.20%
					52	98.99%
					53	98.94%
					54	97.98%
					61	88.09%
					62	88.09%

Meteorological Data

MOVES4 requires hourly temperature and relative humidity data by specific month of the year. Meteorological data at the Phoenix Sky Harbor International Airport and the Casa Grande Municipal Airport in 2023 were obtained from the National Centers for Environmental Information Local Climatological Data (NCEI, 2023), and used for Area A and outside Area A, respectively.

Source Type Population

In MOVES4, off-network emissions including start, evaporative, and extended idle emissions are directly determined by population of vehicles in an area. The Maricopa Association of Governments (MAG) contracted with Eastern Research Group, Inc. (ERG) to decode vehicle identification numbers (VINs) from Arizona registration data and classify vehicles registered in Maricopa County into the vehicle types, fuel types, and model years needed as inputs to MOVES model. The vehicle source type population was derived using ERG's vehicle classification script, the Arizona Department of Transportation (ADOT) December 2023 vehicle registration data, and the transit bus data from Valley Metro, City of Phoenix, City of Scottsdale, and City of Glendale. The ERG's vehicle classification script decoded a VIN for each vehicle in the ADOT vehicle registration data, extract vehicles registered in Maricopa, Pinal, and Gila Counties, remove non-road equipment or trailers, remove duplicate entries, classify the VIN decoded data into MOVES source type categories, and generate the MOVES source type population input for each county in 2023 by totaling populations grouped by source type. The vehicle population in a subarea was estimated by multiplying the vehicle population in each county by the ratio of the population in between a specific geographical subarea and county.

Source Type Age Distribution

The source type age distribution was derived using the ERG's vehicle classification scripts, the ADOT December 2023 vehicle registration data, the transit bus data from public transit providers, and the MOVES4 national default age distributions. The ERG's vehicle classification scripts generated the source type age distributions from the VIN decoded registration data for most of source types, except transit bus (source type 42) and long-haul truck (source types 53 and 62). Age distribution for transit bus was developed using the local transit bus data from Valley Metro, City of Phoenix, City of Scottsdale, and City of Glendale. Age distribution for the long-haul truck was obtained from the MOVES4 national default age distribution.

Annual Vehicle Miles Traveled (VMT)

VMT was used to estimate onroad exhaust and evaporative emissions. Annual average daily VMTs were derived from the average weekday VMTs of the MAG Activity-Based Model (ABM) results provided by the MAG transportation modeling staff. The traffic assignment data were clipped using GIS to calculate VMTs for Area A and outside Area A. The annual average daily VMTs were multiplied by number of days in 2023 to obtain the annual VMTs.

Road Type Distribution

The local road type distributions were derived from the MAG ABM transportation network assignment data that provide VMTs for local road types and ABM vehicle classes. The MAG ABM transportation network assignment data provided all road type distributions for the MOVES runs. The matchup methods to map the ABM area/facility types to the MOVES road types and the ABM vehicle classes to the MOVES source types are provided in Tables 3-11 and 3-12, respectively.

VMT Fraction

Since VMT varies by month, day of week, and hour, MOVES4 requires month/day/hour VMT fractions as a local input to derive hourly VMT for each weekday/weekend and month from the annual VMT.

For the development of freeway VMT fractions, the 2022 ADOT Transportation Data Management System data were collected from https://adot.public.ms2soft.com/tcds/. The data from the permanent traffic count stations providing the full records for the 12-month period were used in developing the freeway VMT fractions.

For the development of arterial VMT fractions, the MAG transportation modeling team provided the weekday time of day factors for arterials from the MAG 2018-2019 counts that are the latest data available for arterials. The arterial VMT fractions were developed based on the weekday time of day factor for arterials.

Average Speed Distribution

In MOVES4, vehicle power, speed, and acceleration have a significant effect on vehicle emissions for all pollutants. MOVES4 estimates those emission effects by assigning activity to operating mode distributions, which are determined by the distribution of vehicle hours traveled (VHT) in sixteen speed bins. Local estimates of average speed were developed by post-processing the output from the MAG ABM transportation network assignment data, which provide link-specific data in the four time periods: AM (6:00-8:59), MD (9:00-13:59), PM (14:00-17:59), and NT (0:00-5:59 and 18:00-23:59). To develop the average speed

distribution, VHTs in sixteen speed bins were accumulated separately for each hour of the day, source type, and road type. Then, the average speed distribution was calculated by normalizing VHTs in sixteen speed bins for each hour of the day, source type, and road type. The same methodology was applied to develop the speed estimates for Area A and outside Area A.

Table 3-11. Match table for ABM area/facility types and MOVES road types

MAG ABM Area Type	MAG ABM Facility Type	MOVES Road Type
5. Rural	00. Freeway HOV Lane 01. Freeway 07. Unmetered Ramp 08. Freeway Metered Ramp 16. Freeway HOV Link	2. Rural Restricted Access
	02. Expressway 03. Collector 04. 6 Legged Arterial 05. Centroid Connector 06. Major Arterial 09. CD Road 10. Parkway 11. Unpaved Road	3. Rural Unrestricted Access
1. CBD 2. Urban 3. Urban Fringe 4. Suburban	00. Freeway HOV Lane 01. Freeway 07. Unmetered Ramp 08. Freeway Metered Ramp 16. Freeway HOV Link	4. Urban Restricted Access
	02. Expressway 03. Collector 04. 6 Legged Arterial 05. Centroid Connector 06. Major Arterial 09. CD Road 10. Parkway 11. Unpaved Road	5. Urban Unrestricted Access

Table 3-12. Match table for ABM vehicle classes and MOVES source types

MAG ABM Vehicle Class	Source Type
MC (Motorcycle)	11. Motorcycle
LDV (Light Duty Vehicle)	21. Passenger Car 31. Passenger Truck
LGT (Light Commercial Truck)	32. Light Commercial Truck
BUS (Transit Bus)	42. Transit Bus
MED (Medium Duty Vehicle)	51. Refuge Truck 52. Single Unit Short-haul Truck 53. Single Unit Long-haul Truck 54. Motor Home
HVY (Heavy Duty Vehicle)	41. Other Buses 43. School Bus 61. Combination Short-haul Truck 62. Combination Long-haul Truck

Fuel Data

Regarding the local fuel input data, MOVES4 provides three MOVES tables, which are fuelsupply, fuelformulation, and fuelusagefraction. The MOVES4 default fuel data for Maricopa and Pinal counties were used for Area A and outside Area A, respectively. There was an additional adjustment for the fuelformulation data to comply with the regulatory Reid Vapor Pressure (RVP) values in this region. The MOVES4 Fuels Wizard was applied to adjust the MOVES4 default gasoline fuel parameters with the regulatory RVP values provided by the Arizona Department of Agriculture (AZDA) Department of Weights and Measures Services Division (WMSD). The regulatory RVPs for Area A and Area C shown in Table 3-13 were applied for Area A and outside Area A, respectively.

Table 3-13. Regulatory RVP by month for gasoline in Area A and Area C

Month	Averaged RVP (psi)	
	Area A	Area C
April	10	10
May	9	10
June	7	7
July	7	7
August	7	7
September	7	7

Alternative Vehicle and Fuel Technologies (AVFT) Strategy

The AVFT table is used to adjust fuel type distributions to reflect local information, such as vehicle registration data. The AVFT table was derived using the ERG's vehicle classification scripts, the ADOT December 2023 vehicle registration data, the transit bus data from public transit providers, and the MOVES4 national default AVFT.

The ERG's vehicle classification scripts generated the AVFT table from the VIN decoded registration data for most source types, except transit bus (source type 42) and long-haul truck (source types 53 and 62). The AVFT table for transit bus was developed using the local transit bus data from Valley Metro, City of Phoenix, City of Scottsdale, and City of Glendale. The AVFT table for the long-haul truck was obtained from the MOVES4 national default AVFT.

3.3. Continental USA and Mexico Anthropogenic Emissions Inventory

The anthropogenic emissions inventory for the 12 and 36 km domains originated with the EPA's 2022v1 modeling platform baseline (see Section 3.1). To more accurately represent the 2023 modeling year, two key updates were incorporated:

1. Onroad mobile emissions for the U.S. and Mexico were updated. For the United States, the MOVES5 model (from EPA 2022v2) was used to generate monthly emissions data, which were then formatted as nonpoint sources by county and Source Classification Code (SCC). Updated Mexico onroad emissions incorporates new inventories for five non-border states (Baja California Sur, Durango, San Luis Potosi, Sinaloa, and Zacatecas).
2. Actual hourly 2023 CEMS data were used for major U.S. Electric Generating Units.

Table 3-14 summarizes final anthropogenic emission inventories used for each category in the model for the 36 and 12 km domains and their temporal resolutions.

Table 3-14. EPA's 2022 v1/v2 platform sectors used in the emissions modeling process for 36 and 12 km modeling domains

Platform Sector (Abbreviation)	Data Category	Description and Resolution of the Data Input to SMOKE
EGU units (ptegu)	Point	2023 hourly Continuous Emissions Monitoring System (CEMS) values for NO_x and SO_2, and the remaining pollutants temporally allocated according to CEMS heat input where the units are matched to the 2022 modeling platform data. Annual resolution for sources not matched to CEMS data, hourly for CEMS sources. https://gaftp.epa.gov/Air/emismod/2022/v1/2022emissions/2023CEMS/2022hc_ptegu_with_2023_CEMS_inventory_19jun2025.zip
Point oil and gas (pt_oilgas)	Point	2022 NEI point sources that include oil and gas production emissions processes for facilities with North American Industry Classification System (NAICS) codes related to Oil and Gas Extraction, Natural Gas Distribution, Drilling Oil and Gas Wells, Support Activities for Oil and Gas Operations, Pipeline Transportation of Crude Oil, and Pipeline Transportation of Natural Gas. Includes U.S. offshore oil production. Annual resolution.
Aircraft and ground support equipment (airports)	Point	EPA estimated 2022 emissions, including aircraft and airport ground support for the top 51 airports. Smaller airports, including aircraft and airport ground support were projected from 2020 NEI to 2022 based on the 2023 Terminal Area Forecast (TAF). Georgia provided emissions for HJAIA. Annual resolution. Note that the airport emissions in this category were used for the 36 and 12 km modeling domains, not the 4 km domain.
Remaining non-EGU point (ptnonipm)	Point	All 2022 NEI point source records not matched to the airports, ptegu, or pt_oilgas sectors. Includes 2020 NEI rail yard emissions projected to 2022 using updated R-1 reported yard fuel usage. Annual resolution.
Livestock (livestock)	Nonpoint	2022 nonpoint livestock emissions developed using a similar method to 2020 NEI but with adjusted animal counts and using 2022 meteorology. Livestock includes ammonia and other pollutants (except $PM_{2.5}$). County and annual resolution.
Agricultural fertilizer (fertilizer)	Nonpoint	2022 agricultural fertilizer ammonia emissions based on bidirectional flux calculations

Platform Sector (Abbreviation)	Data Category	Description and Resolution of the Data Input to SMOKE
Area fugitive dust (afdust_adj)	Nonpoint	PM_{10} and $PM_{2.5}$ nonpoint fugitive dust sources including building construction, road construction, agricultural dust from crops, and mining and quarrying which were all held constant. Additional dust sources not held constant include paved road dust and agricultural dust from livestock, where paved road dust emissions were adjusted to 2022 based on VMT and dust from livestock based on animal count differences. The emissions modeling system applies a transportable fraction reduction and zero-out adjustments based on the year-specific gridded hourly meteorology (precipitation and snow/ice cover). County and annual resolution.
Category 1, 2 CMV (cmv_c1c2_36)	Nonpoint	2022 Category 1 (C1) and Category 2 (C2), commercial marine vessel (CMV) emissions based on 2022 Automatic Identification System (AIS) data categorized using SCCs specific to ship type. Point and hourly resolution.
Category 3 CMV (cmv_c3_36)	Nonpoint	2022 Category 3 (C3) commercial marine vessel (CMV) emissions based on 2022 AIS data categorized using SCCs specific to ship type. Point and hourly resolution.
Locomotives (rail)	Nonpoint	Class I line haul rail locomotives emissions from 2020 NEI projected to 2022 using R-1 reported fuel usage. County and annual resolution. Class II and III locomotive emissions were projected from 2020 based on the 2021 U.S. Energy Information Administration's Annual Energy Outlook. Commuter rail was projected from 2020 using fuel use per company from the Federal Transit Administration's (FTA) 2022 National Transit Database. Amtrak emissions were adjusted down based on 2020 fuel use reported in Amtrak's FY22 AMTRAK Sustainability Report. County and annual resolution.
Nonpoint source oil and gas (np_oilgas)	Nonpoint	2022 well activity data (production and exploration of oil, gas, etc.) run through Oil and Gas tool. Abandoned wells based on 2022, plus other state-specific inputs. County and annual resolution.

Platform Sector (Abbreviation)	Data Category	Description and Resolution of the Data Input to SMOKE
Open Burning (openburn)	Nonpoint	This new sector for the 2022v1 platform was split out from the prior nonpt sector and includes emissions from yard waste, land clearing, and residential household waste burning. These are SCCs starting with 261. County and annual resolution.
Residential Wood Combustion (rwc)	Nonpoint	2020 NEI nonpoint sources with residential wood combustion (RWC) processes, projected to 2022 with state-level adjustment factors derived from the State Energy Data System (SEDS) plus specific adjustments for California and Idaho. County and annual resolution.
Solvents (np_solvents)	Nonpoint	Emissions of solvents based on methods used for the 2020 NEI. 2021 emissions are used to represent 2022. Includes household cleaners, personal care products, adhesives, architectural and aerosol coatings, printing inks, and pesticides. Annual and county resolution.
Remaining nonpoint (nonpt)	Nonpoint	Nonpoint sources not included in other platform sectors. Mostly held constant at 2020 levels, but with some SCCs adjusted to 2022 based on population, energy consumption ratios and employment data. County and annual resolution.
Nonroad (nonroad)	Nonroad	2022 nonroad equipment emissions developed with MOVES4, including the updates made to spatial apportionment that were developed with the 2016v1 platform. MOVES4 was used for all states except California, which submitted their own emissions for 2020 and 2023 that were then interpolated to 2022. County and monthly resolution.
Updated Onroad (onroad)	Onroad	The MOVES5 model was used to create new 2022 emission, incorporating several key updates. Vehicle data was refreshed using 2023 figures for registration, age distribution, and vehicle population (VPOP) by source and fuel type. Activity data such as Vehicle Miles Traveled (VMT), hoteling, off-network idling, and starts were updated to reflect these new splits. Additionally, telematics data from 2022-2023 was used to refine temporal patterns, VMT fractions, and speeds. The model also incorporated updates from state and local agencies, added total energy consumption to outputs, and improved spatial surrogates using 2022 traffic data. MOVES5 was run for v2022hd. Source: https://gaftp.epa.gov/Air/emismod/2022/v2/2022emissions/draft/2022hd_onroad_SMOKE-MOVES_inventory_19jun2025.zip

Platform Sector (Abbreviation)	Data Category	Description and Resolution of the Data Input to SMOKE
Mexico stationary point sources (canmex_point)	Point	Mexico point source emissions not included in other sectors. Mexico point source emissions for six border states represent 2018 and were developed by SEMARNAT in collaboration with EPA, while emissions for all other states were carried forward from 2019ge (U.S. EPA, 2022b). Annual and monthly point resolution.
Mexico agricultural sources (canmex_ag)	Nonpoint	Mexico agricultural emissions were provided by SEMARNAT and include updated emissions for six border states representing 2018 developed by SEMARNAT in collaboration with EPA, while emissions for all other states were carried forward from 2019ge. Annual municipio and province resolution.
Mexico nonpoint (canmex_area)	Nonpoint	Mexico nonpoint source emissions. The emissions included updated emissions for six border states representing 2018 developed by SEMARNAT in collaboration with EPA, while emissions for all other states were carried forward from 2019ge. Annual and monthly municipio and province resolution.
Mexico nonroad (canmex_nonroad)	Nonroad	Mexico nonroad source emissions. The emissions included updated emissions for six border states representing 2018 developed by SEMARNAT in collaboration with EPA, while emissions for all other states were carried forward from 2019ge. Annual and monthly municipio and province resolution.
Updated Mexico onroad sources (mexico_onroad)	Onroad	Mexico onroad emissions. 2020 and 2023 emissions output from MOVES-Mexico were interpolated to 2022. Municipio monthly resolution. Incorporate new inventories for five non-border states (Baja California Sur, Durango, San Luis Potosi, Sinaloa, Zacatecas).

3.4. Biogenic and Other Natural Source Emissions Inventory

3.4.1. Biogenic Emissions

Emission of ozone precursors, which include volatile organic compounds (VOC), carbon monoxide (CO) from vegetation, and nitrogen monoxide (NO) from soil, were estimated for the 36, 12, and 4 km modeling domains using the Model of Emissions of Gases and Aerosols from Nature (MEGAN) v3.2. MEGAN is a state-of-the-art biogenic emissions

model developed initially at the National Center for Atmospheric Research (NCAR) and maintained at the University of California, Irvine (Guenther et al., 2012 and 2018; Jiang et al., 2011; Guenther, 2006a, 2006b, and 2007; Guenther et al., 2006). MEGAN v3.2 contains some corrections and improvements (Jiang et al., 2018; Guenther et al., 2017).

Compared to its previous versions, MEGAN v3.2 contains improved vegetation data, updated emission factors, enhanced canopy processes, expanded chemical components (Guenther et al., 2020; Jiang et al., 2018; Guenther et al., 2017, 2012), and integrated two different soil nitrogen monoxide (NO) emission algorithms: BDSNP (Human, R. C., et al., 2012) and YL (Younger, Levy, 1995). BDSNP is used in this work because it aligns better with observed NOx columns and improved ozone and N deposition modeling. Notably, the soil NO emission algorithm has been substantially updated in MEGAN. BDSNP algorithm in v3.2 is considered as more dynamic and responsive to soil temperature and moisture conditions, as well as interactions with the vegetation canopy. These processes are influenced by meteorological drivers such as air temperature, humidity, solar radiation, wind speed, and precipitation.

The biogenic VOC (BVOC) emission calculations in MEGAN v3.2 are driven by a detailed database of emission factors that are mapped to gridded emission vegetation types and growth-form-specific speciation tables. This database is informed by thousands of observations across different vegetation species (Guenther et al., 2012; Guenther et al., 2018). The model applies these base emission factors to spatially resolved maps of vegetation and adjusts them using light-dependent activity corrections.

MEGAN v3.2 is integrated in-line within the Community Multiscale Air Quality (CMAQ) model v5.5. This in-line coupling enables MEGAN to compute gridded biogenic emissions dynamically during CMAQ execution, ensuring direct integration with atmospheric chemistry processes. The accuracy of these emissions is improved when the meteorological fields used as input for the MEGAN model are enhanced using the Weather Research and Forecasting (WRF) model's data assimilation capabilities. The WRF Data Assimilation (WRFDA) system was implemented to incorporate observational data through surface and gridded analysis nudging. This technique combines surface and upper-air data from the National Centers for Environmental Prediction (NCEP) with the model's simulation to continuously update its state. This process yields a more accurate estimate of the atmospheric state and improves the overall performance of the meteorological simulation, as will be discussed in detail in Section 4. Specifically, the meteorological inputs for MEGAN v3.2 are photosynthetically active radiation (PAR), 2-meter air temperature, humidity, wind speed, top-layer soil moisture, and precipitation.

MEGAN v3.2 also requires critical land cover inputs like the leaf area index (LAI) and fractional vegetation cover, which are derived from both satellite and ground-based observations. In this plan, the LAI input is based on the 2023 Copernicus Global Land Service (CGLS) Collection 300m LAI Version 1 product at a ten-day temporal resolution. These data were regridded to a 0.01° spatial resolution and processed using the MEGAN LAI preprocessor to align with the model domains.

By updating CMAQ run script, the CMAQ v5.5 is able to provide diagnostic outputs including hourly gridded biogenic emissions used for CAMx photochemical modeling.

3.4.2. US Wild, Prescribed, and Agricultural Fires Emissions

Emissions from U.S. wild, prescribed, and agricultural fires were sourced directly from the EPA's 2023 National Emission Inventory (NEI) beta version (U.S. EPA, 2025d). This dataset provided day-specific, point-source emissions for key ozone precursors and particulate matter, including VOC, NO_x, NH_3, PM_{10}, $PM_{2.5}$, SO_2, and CO. The data files also contained critical parameters for plume rise modeling, such as acres burned and heat flux (HFLUX). While the inventory is for the year 2023, the underlying methodology used by the EPA to generate these emissions is consistent with the process documented for the 2022v1 emissions platform (U.S. EPA, 2025a).

The EPA's methodology for wild and prescribed fires involves a comprehensive, two-step modeling framework. First, input activity data is processed and reconciled using a modified Python-based Satellite Mapping Automated Reanalysis Tool for Fire Incident Reconciliation version 2 (SmartFire2) to generate daily fire acres by location and type. This system consolidates information from numerous sources, including NOAA's Hazard Mapping System (HMS), Wildland Fire Interagency Geospatial Services (WFIGS) perimeters, Incident Status Summary (ICS-209) reports, and activity data from the U.S. Forest Service, the Department of the Interior, and 33 state, local, and tribal agencies.

Emissions are calculated in the BlueSky Pipeline (BSP), which uses Landfire and FCCS data to determine fuel loading, CONSUME to calculate biomass consumption, and SERA to apply emission factors. The final inventory is then post-processed to geocode fire locations and assign emissions to flaming and smoldering categories.

Agricultural fire emissions are computed within a new BlueSky Pipeline (BSP) agricultural burn module. This process uses 2023 HMS satellite detections that are identified as crop residue over agricultural lands using the USDA Cropland Data Layer (CDL). For most crops, the area burned is estimated using state-specific field size tables, and emissions are then calculated as the product of this area, fuel loading, combustion completeness, and specific

emission factors. The inventory is further refined by excluding detections under certain conditions, such as for specific crops like corn and soybeans in nine Midwestern states, in areas with daily snow cover, and from inconsistent VIIRS satellite data.

The final output from all fire processes is a SMOKE-ready, daily point-source emission inventory in the FF10 format, which was processed by SMOKE for both the CMAQ and CAMx photochemical models.

3.4.3. Mexico Fire Emissions

Annual 2023 wildfire emissions for Mexico are included in the ptfire_othna sector and were developed from the Fire Inventory from NCAR (FINN) v2.5 daily fire emissions (Wiedenmyer, 2023). For FINN fires, listed vegetation type codes of 1 and 9 are defined as agricultural burning, all other fire detections are assumed to be wildfires. All wildland fires that are not defined as agricultural are assumed to be wildfires rather than prescribed. FINN fire detects of less than 50 square meters (0.012 acres) are removed from the inventory. The locations of FINN fires are geocoded from latitude and longitude to FIPS code. Table 3-15 summarizes all fire emissions used for this plan.

Table 3-15. Fire emissions for the U.S. (2023 EPA NEI) and Mexico (2023 FINN)

Platform Sector (Abbreviation)	Data Category	Description and Resolution of the Data Input to SMOKE
Point source wildfires (ptfire-wild)	Point	Point source day-specific wildfires for 2023 computed using SMARTFIRE 2 and BlueSky Pipeline. Point and daily resolution
Point source prescribed fires (ptfire-rx)	Point	Point source day-specific prescribed fires for 2023 computed using SMARTFIRE 2 and BlueSky Pipeline. The ptfire emissions were run as two separate sectors: ptfire-rx (prescribed, including Flint Hills/grasslands) and ptfire-wild. Point and daily resolution.
Point source agricultural fires (ptagfire)	Point	Agricultural fire sources for 2023 NEI (beta version) developed by EPA as point and day-specific emissions. Point and daily resolution.
Mexico fires (ptfire_othna)	Point	Point source day-specific wildfires and agricultural fires in Mexico for 2023. Mexico fire data are from v2.5 of the Fire INventory (FINN) from National Center for Atmospheric Research (Wiedinmyer, 2023). Point and daily resolution.

3.4.4. Lightning Emissions

For applications over the continental North America, lightning data from the National Lightning Detection Network (NLDN) or scaled data from the World Wide Lightning Location Network (WWLLN) (Kang et al., 2022) can be used directly to generate lightning-produced NO (LNO) in CMAQ. While data from the commercial NLDN is an alternative, scaled WWLLN data was selected as it provides LNOx estimates that are comparable in both time and space to those derived from NLDN data (Kang et al., 2022).

The CMAQ in-line lightning module requires two primary input files: (1) an hourly lightning strike NetCDF file and (2) a lightning parameters NetCDF file. The parameter file defines key characteristics such as cloud-to-ground (CG) to inter-cloud/intra-cloud (IC) flash ratios and the number of moles of NO produced per flash (for both CG and IC flashes). Once the total column LNOx is calculated for a grid cell, CMAQ vertically distributes the emissions throughout the atmospheric column. This allocation is based on meteorological data from the accompanying Weather Research and Forecasting (WRF) model simulation, such as convective precipitation and cloud-top height, ensuring the emissions are placed at realistic altitudes where lightning occurs.

For this modeling effort, CMAQ-ready hourly lightning data based on the 2023 WWLLN observations, along with the required parameter NetCDF files, were provided by the EPA research group for all modeling domains. The resulting LNOx emissions are generated as diagnostic model outputs, which were then processed for use as inputs to the CAMx photochemical model.

3.5. Emissions Processing for Photochemical Modeling (SMOKE)

The 2023 emissions inventories, as described in Sections 3.3 and 3.4, must be processed for use within the selected photochemical grid models, CAMx and CMAQ. This critical data processing step was accomplished using the Sparse Matrix Operator Kernel Emissions (SMOKE) modeling system.

SMOKE transforms the raw emissions inventory data from its native format into the hourly, gridded, and chemically speciated inputs required by the air quality models. This transformation involves three primary functions:

- **Spatial Allocation:** Emissions data, originally provided at various spatial resolutions (e.g., county totals for area sources or specific latitude/longitude coordinates for point sources), are allocated onto the specific horizontal grid

structure of the modeling domain. This ensures that emissions are correctly placed within each grid cell.

- **Temporal Allocation:** The annual, monthly, or daily emission totals from the inventory are disaggregated into hourly emission profiles. This is achieved by applying source-category-specific temporal profiles that account for diurnal, day-of-week, and seasonal variations in emissions activity.
- **Chemical Speciation:** Precursor pollutants, such as Volatile Organic Compounds (VOCs), Oxides of Nitrogen (NO_x), and Particulate Matter (PM), are disaggregated into the individual chemical species recognized by the photochemical model's gas-phase chemical mechanism (e.g., CB6ae7). This speciation is essential for accurately simulating atmospheric ozone formation.

The final output of the SMOKE processing system consists of model-ready emissions files that serve as direct inputs for the CAMx and CMAQ modeling simulations.

3.5.1. Spatial Allocation and Surrogates

The EPA's Surrogate Tools DB v1.3 is a specialized, standalone toolkit for creating the spatial surrogates used in emissions modeling. Written in Java, it leverages the power of a Postgres database with the PostGIS extension to handle complex spatial data processing. This database-centric approach distinguishes it from the original Spatial Allocator, allowing it to efficiently manage the creation of large sets of surrogates without relying on the C-code of the original tool. Notably, the Surrogate Tools DB v1.3 fixed a bug that caused incorrect surrogate fractions in edge grid cells when the grid doesn't fully cover all the counties in the modeling domain.

A key function of the toolkit is to not only generate these critical files but also to manage the entire workflow. This includes essential quality assurance functions like merging surrogates from different data sources and "gap-filling," a process that intelligently fills in missing data for certain areas to ensure a complete and robust dataset. The result is a more streamlined and powerful system for developing the precise spatial inputs required by air quality models like SMOKE and CMAQ.

The Surrogate Tools DB generates spatial surrogates using three primary components:

1. A weighted shapefile representing the location of emissions, such as roadways (line), population density (polygon), or airports (point).
2. A boundary shapefile for the relevant geopolitical areas (e.g., counties).

3. The target modeling grid configuration.

The tool processes these components for regularly spaced air quality model grids across various map projections, including Universal Transverse Mercator (UTM), Lambert Conformal, and latitude-longitude.

The shapefiles and configurations for the 36 and 12 km modeling domains were sourced directly from the EPA's 2022 v1 modeling platform, covering the continental U.S. and Mexico (https://gaftp.epa.gov/Air/emismod/2022/v1/spatial_surrogates/). These inputs were then processed with the Surrogate Tools DB v1.3 to generate spatial surrogates, following the specific MAG domain configurations detailed in Section 5.3.

To improve the accuracy of the spatial surrogates for the 4 km modeling domain, default national datasets were replaced with higher-resolution local data for Maricopa and Pinal Counties. This local refinement provides a more precise spatial distribution of emissions, as shown in Table 3-16. Details regarding the specification for the spatial surrogates are provided in Appendix 2.

Key datasets used include:

- MAG 2023 regional traffic data
- MAG 2022 regional land use and land cover data
- MAG 2023 regional employment data
- MAG region residential housing completion data (2022–2024)
- Updated Arizona railroad network data
- Locations of gasoline dispensing facilities

The following steps detail the methodology used to develop the spatial surrogate for MERCs (as referenced in Section 3.2.1). To establish plausible locations for new or expanded emission sources, the Mobile Emission Reduction Credits (MERCs) tonnage is allocated to specific land types. Eligible areas include existing industrial, commercial, and suitable vacant lands. Excluded areas are residential zones, mountainous terrain, and forest land. This siting method ensures that potential emissions fall within the model's defined area of ozone influence. Figure 3-2 illustrates the spatial allocation for MERCs emissions in Maricopa County.

Table 3-16. Spatial surrogates used for the 4 km domain

No.	Surrogate	Surrogate Code
1	Population	100
2	Housing	110
3	Detached Housing	135
4	Single and Dual Unit Housing	136
5	Single + Dual Unit + Manufactured Housing	137
6	Local House Change	138
7	Construction	141
8	Residential Heating - Natural Gas	150
9	Residential Heating - Distillate Oil	170
10	Residential Heating - Coal	180
11	Residential Heating - LP Gas	190
12	Extended Idle Locations	205
13	Total Road AADT	239
14	Total Road Miles	240
15	Total Restricted Road Miles	241
16	Total Restricted AADT	242
17	Total Unrestricted Road Miles	243
18	Total Unrestricted AADT	244
19	Intercity Bus Terminals	258
20	Transit Bus Terminals	259
21	Total Railroad Miles	260
22	NTAD Total Railroad Density	261
23	NTAD Class 1 2 3 Railroad Density	271
24	ERTAC Rail Yards	275
25	NLCD Low	300
26	NLCD Open + Low	304
27	NLCD Low + Med	305
28	NLCD Med + High	306
29	NLCD All Development	307
30	NLCD Low + Med + High	308
31	NLCD Open + Low + Med	309
32	NLCD Total Agriculture	310
33	NLCD Crop Land	319
34	NLCD Forest Land	320
35	NLCD Recreational Land	321
36	NLCD Land	340
37	NLCD Water	350
38	FAO 2010 Cattle	401
39	FAO 2010 Pig	402
40	FAO 2010 Chicken	403

No.	Surrogate	Surrogate Code
41	FAO 2010 Goat	404
42	FAO 2010 Horse	405
43	FAO 2010 Sheep	406
44	Commercial Land	500
45	Aircraft Engine Manufacturers	504
46	Industrial Land	505
47	Education	506
48	Public Schools	508
49	Commercial plus Industrial	510
50	Single Family Residential	527
51	Residential+Commercial+Industrial+Institutional+Government	535
52	Retail Trade (COM1)	540
53	Auto refinish	544
54	Hospital (COM6)	560
55	Gas Stations	600
56	Refineries and Tank Farms	650
57	Airport Points	710
58	Airport Areas	711
59	Golf Courses	850
60	Mines	860
61	Sand and Gravel Mines	861
62	Lead Mines	862
63	Crushed Stone Mines	863
64	Wastewater Treatment Facilities	870
65	Landfills	871
66	Crematories	872
67	Drycleaners	880
68	OSM Fuel	900
69	OSM Asphalt Surfaces	901
70	OSM Unpaved Roads	902
71	FAO 2010 Large Cattle Operations	4011
72	NPDES 2020 Beef Cattle	4012
73	NPDES 2020 Dairy Cattle	4013
74	NPDES 2020 Swine	4021
75	NPDES 2020 Chicken	4031
76	NPDES 2020 Goat	4041
77	NPDES 2020 Turkey	4071
78	MERC	999

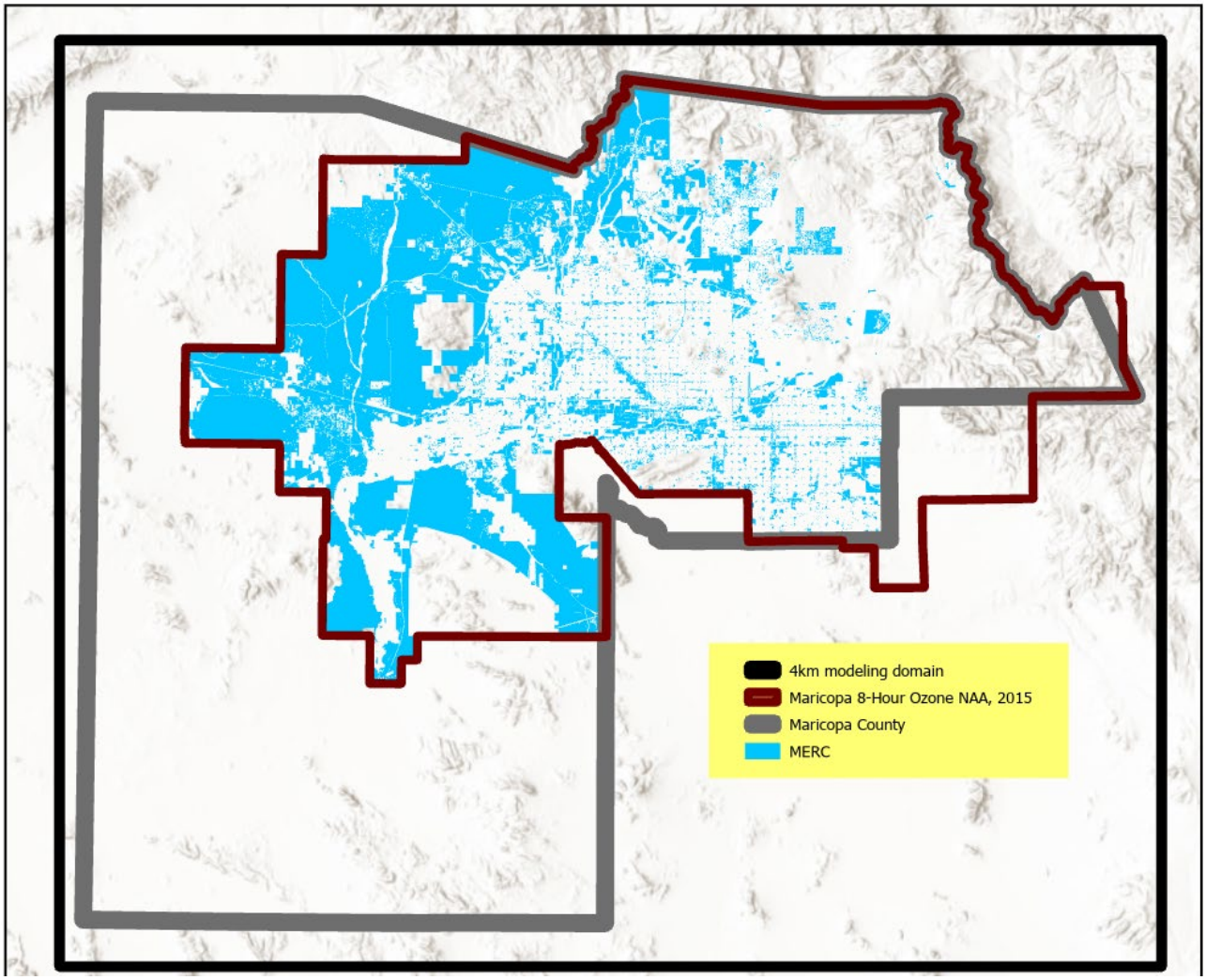

Figure 3-2. The spatial allocation for MERCs emissions in Maricopa County

Specifically, the process involved overlaying a shapefile of MAG's 2022 land use data with shapefiles for the Maricopa County boundary and the Maricopa NAA. The 2022 land use data was limited to several categories, including Industrial, Commercial, Public Land, Vacant, Vacant State Trust, Developing Employment, Other Employment, and Mixed Use. The areas colored aqua in Figure 3-2 indicate the zones eligible for this spatial allocation and Figure 3-3 indicates the derived spatial surrogate.

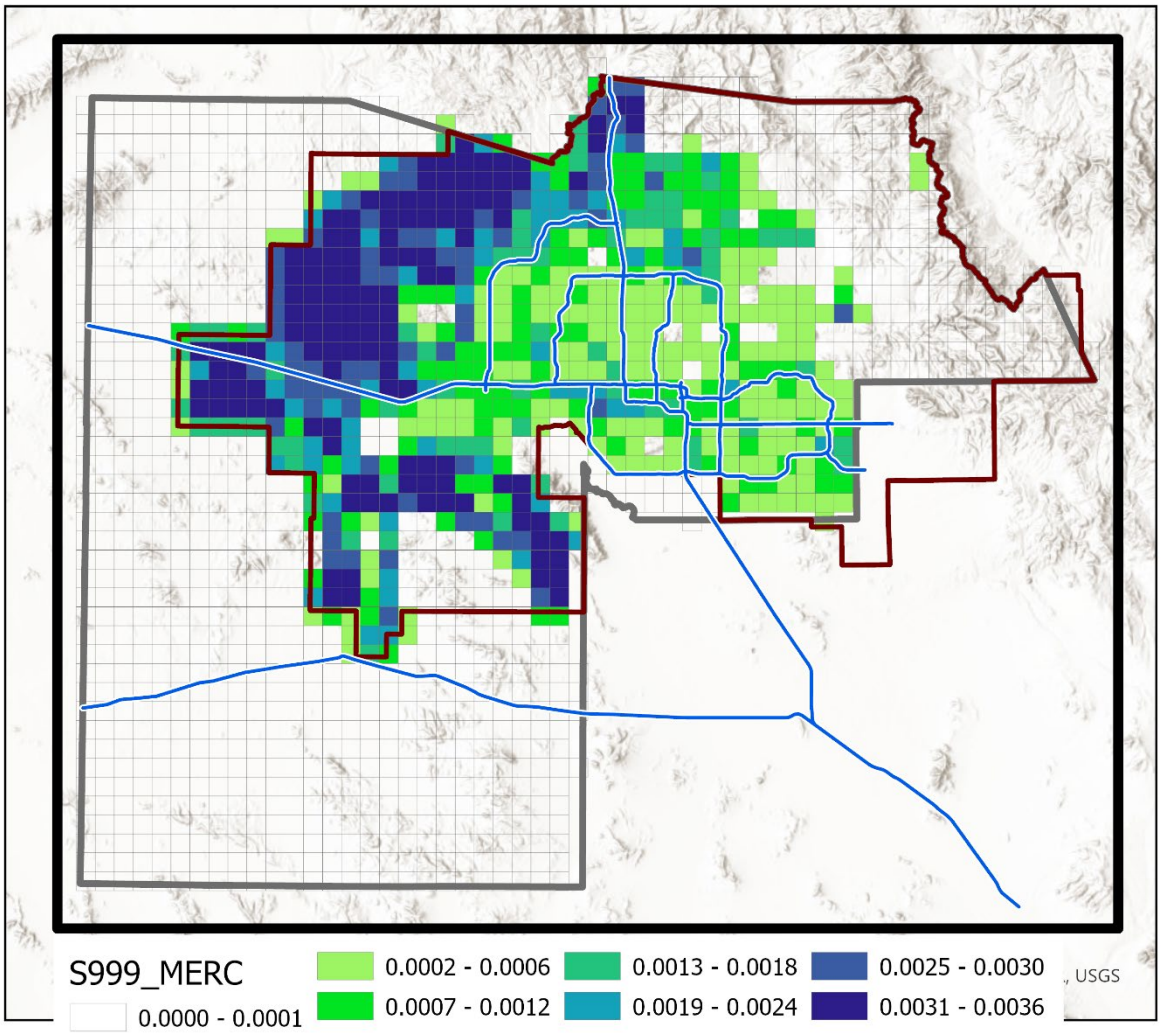

Figure 3-3. Spatial surrogate (ID = 999) for the MERCs in Maricopa County

Ozone Day Analysis and Emissions Distribution

As an example of quality assurance (QA) and verification of the spatial allocation of the gridded emissions inventory, the following is an in-depth look at the emissions distribution on a representative exceedance day.

Figure 3-4 illustrates the daily maximum 8-hour average (MDA8) ozone concentrations across the Maricopa NAA on Wednesday, May 17, 2023. This day was selected as a representative high-ozone event for the emissions analysis because of the widespread exceedances observed. On this day, daily maximum 8-hour average ozone concentrations peaked at 90 ppb, with all but five monitoring sites in the area recording levels above the standard.

Figures 3-5 through 3-31 display emission density plots for VOCs, NO_x, and CO across the 4 km modeling domain on May 17, 2023. These plots, generated from the SMOKE modeling platform, show the geographic distribution of emissions from various source sectors. These highlight that VOC emissions are heavily concentrated in urbanized areas (e.g., central Phoenix and major roadways, especially in the onroad and area source maps), whereas NO_x emissions have hotspots at power plants and along highways. Biogenic VOC emissions (Figure 3-22) are widespread but highest in agricultural and forest areas. Collectively, these QA maps confirm that emissions were allocated to expected locations (e.g., onroad emissions along transportation corridors, airports at known airport locations, etc.).

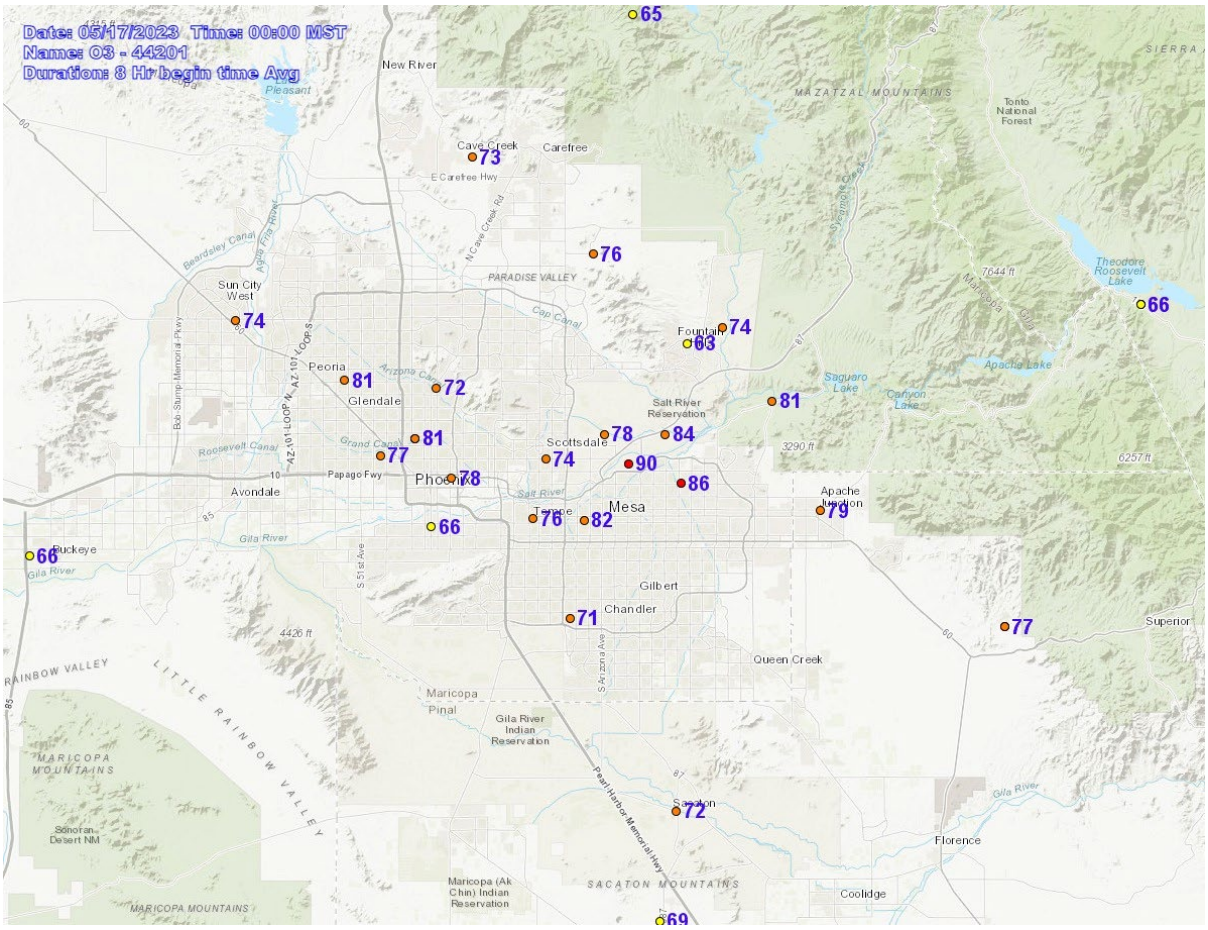

Figure 3-4. MDA8 ozone concentrations (ppb) on May 17, 2023 (Wednesday)

Spatial Allocation Methodology

The methodology for spatially allocating emissions to the model grid varied by source category:

- **Point, Airport, and Fire Sources:** Emissions were assigned to specific grid cells based on their precise geographic coordinates (latitude and longitude).
- **Area, Nonroad, and MERCs Sources:** Emissions were distributed using appropriate spatial surrogates, as described elsewhere in this document.
- **Onroad, Biogenic, and Lightning Sources:** These emissions were incorporated directly as pre-gridded model inputs. Onroad emissions were developed using MAG's MOVES4LINK tool (see Section 3.2.5), while biogenic and lightning emissions were derived from CMAQ model outputs.

It is important to note that anthropogenic emissions from the neighboring portions of Maricopa and Pinal Counties were sourced from the EPA's 2021v1 modeling platform and processed through SMOKE using default spatial surrogates.

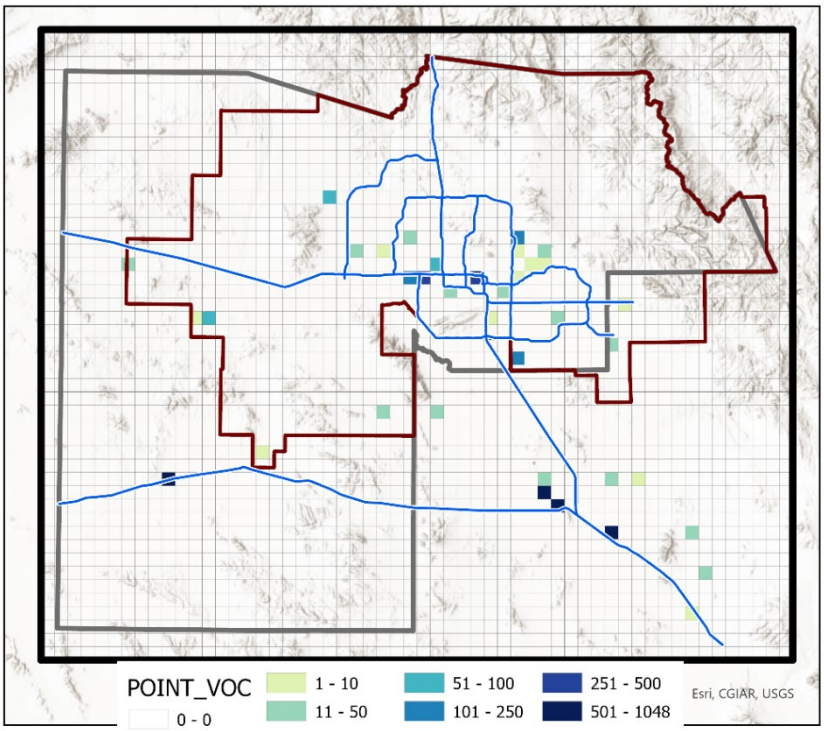

Figure 3-5. Spatial distribution of daily VOC emissions from point sources (kg/day) for May 17, 2023

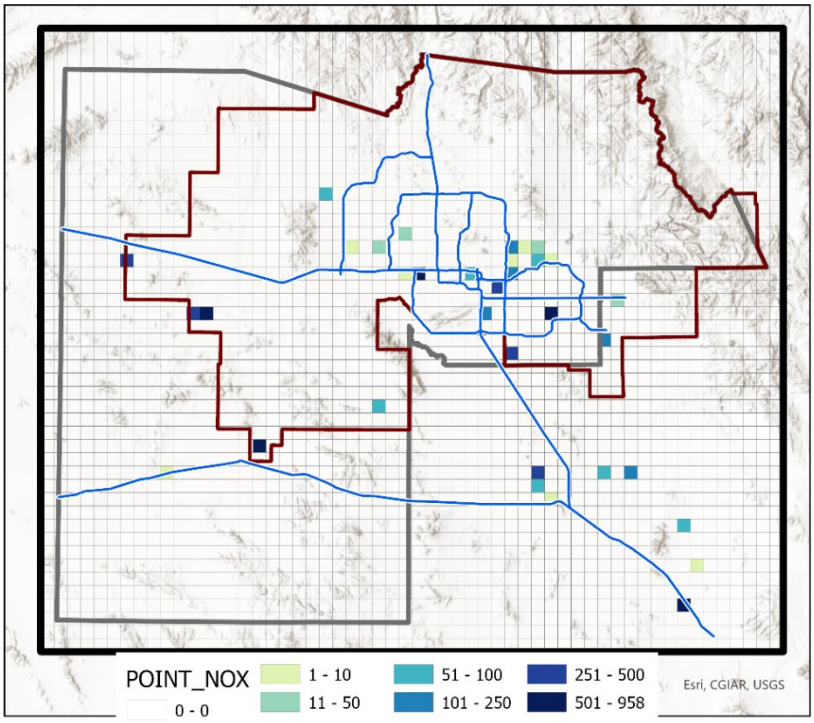

Figure 3-6. Spatial distribution of daily NO_x emissions from point sources (kg/day) for May 17, 2023

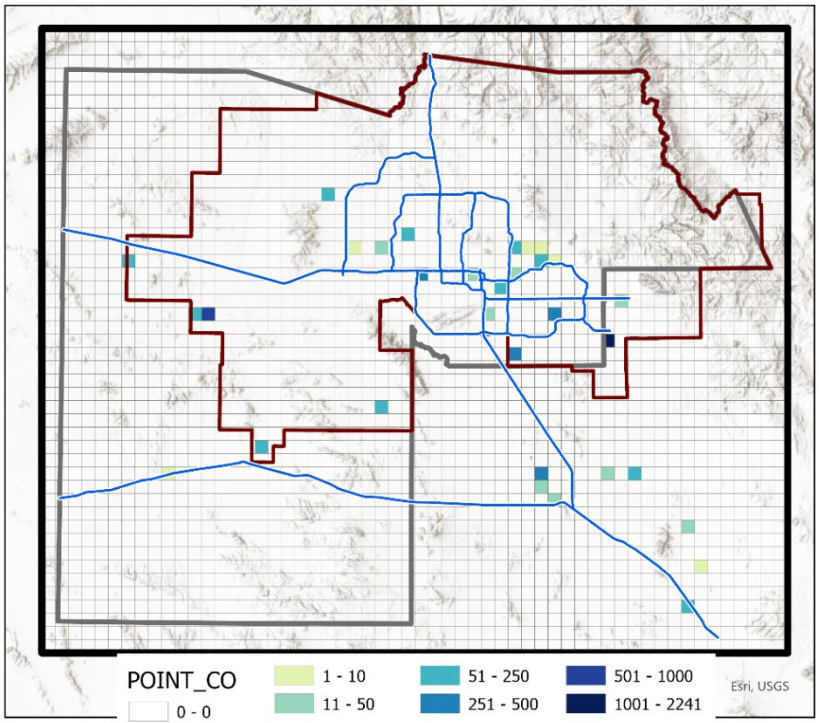

Figure 3-7. Spatial distribution of daily CO emissions from point sources (kg/day) for May 17, 2023

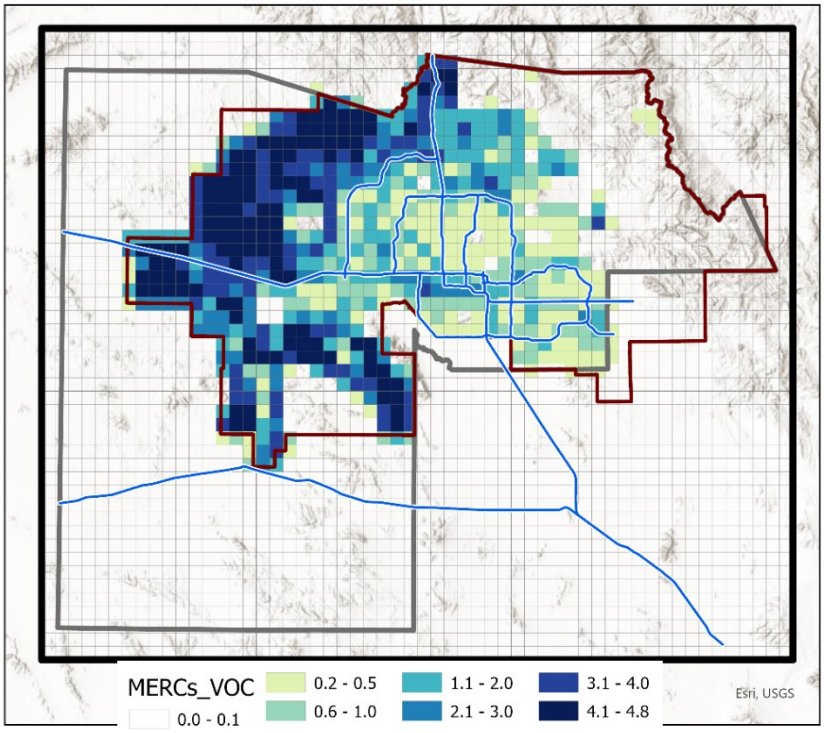

Figure 3-8. Spatial distribution of daily VOC emissions from MERCs (kg/day) for May 17, 2023

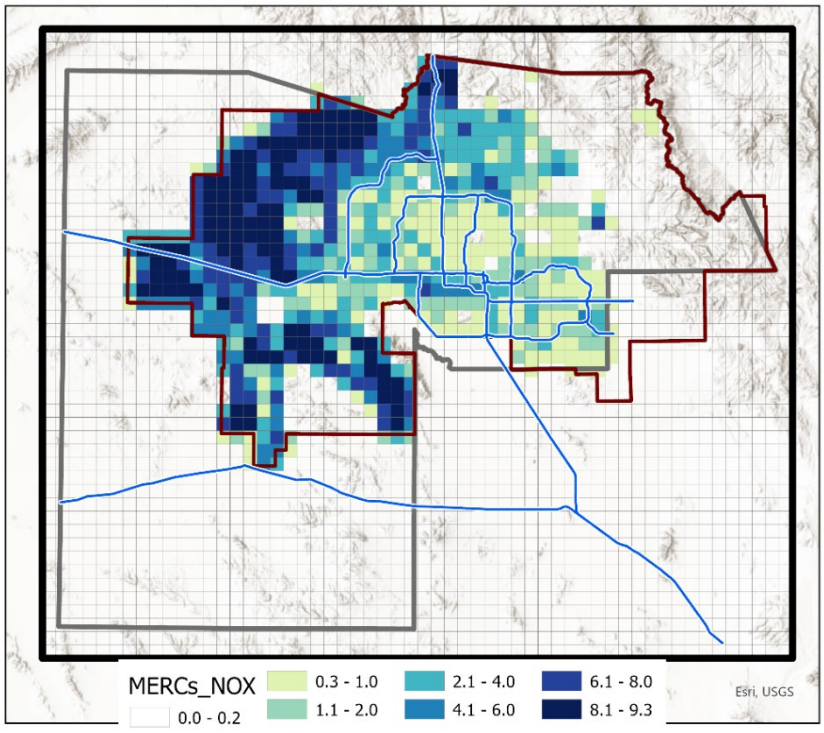

Figure 3-9. Spatial distribution of daily NO_x emissions from MERCs (kg/day) for May 17, 2023

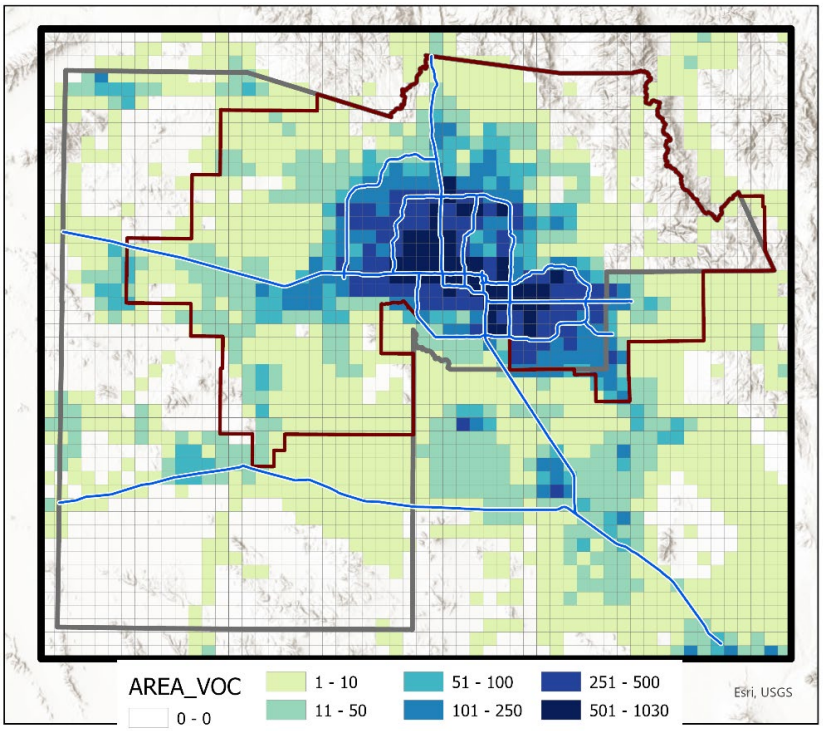

Figure 3-10. Spatial distribution of daily VOC emissions from AREA (kg/day) for May 17, 2023

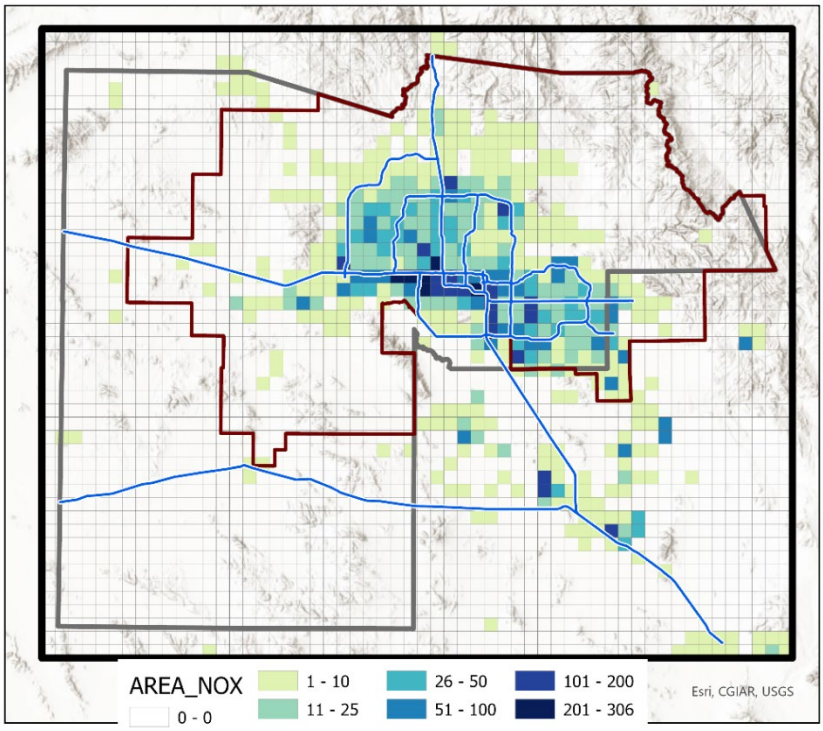

Figure 3-11. Spatial distribution of daily NO_x emissions from AREA (kg/day) for May 17, 2023

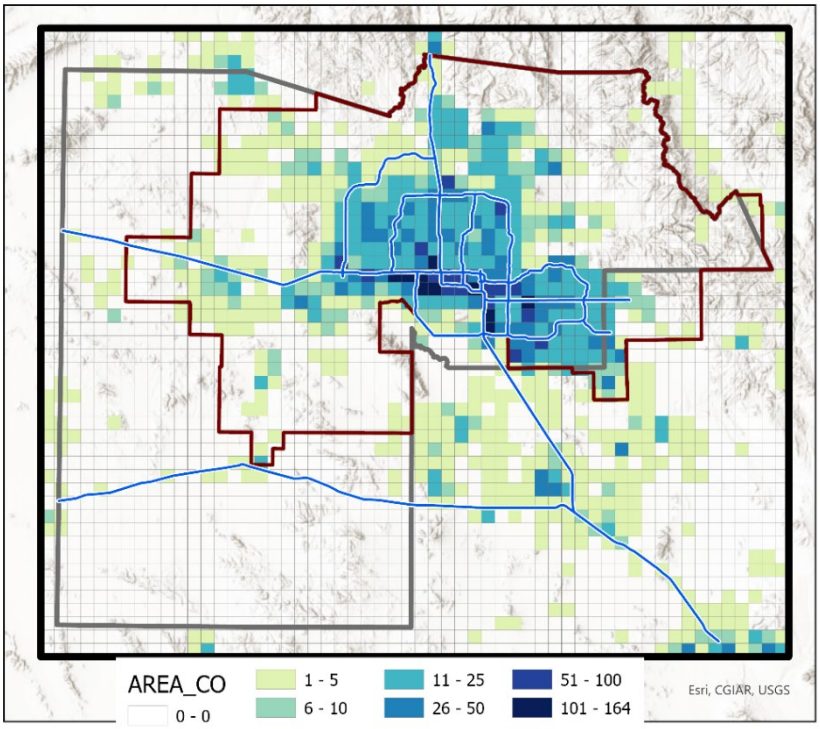

Figure 3-12. Spatial distribution of daily CO emissions from AREA (kg/day) for May 17, 2023

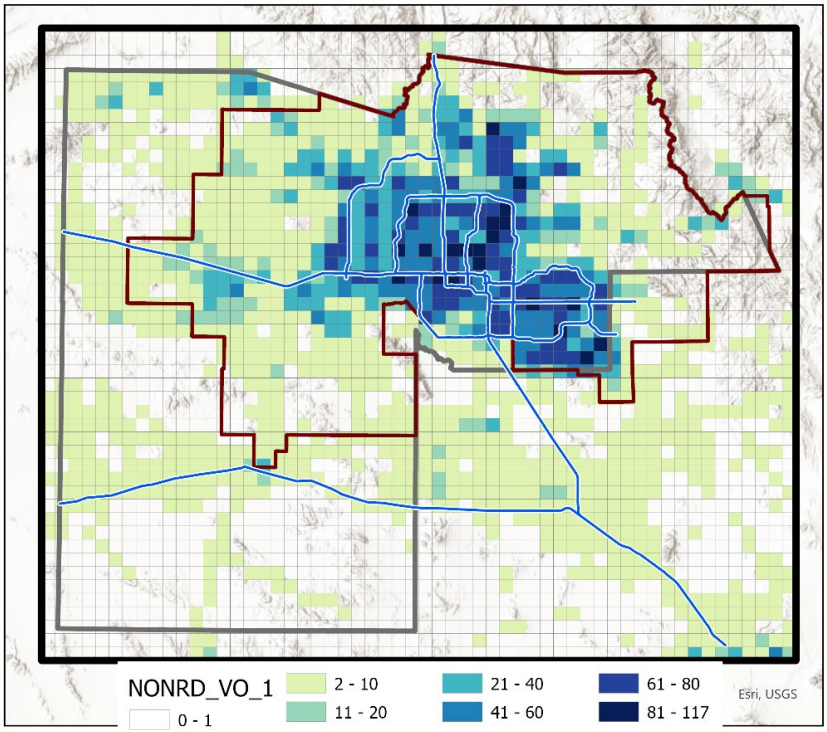

Figure 3-13. Spatial distribution of daily VOC emissions from NONROAD (kg/day) for May 17, 2023

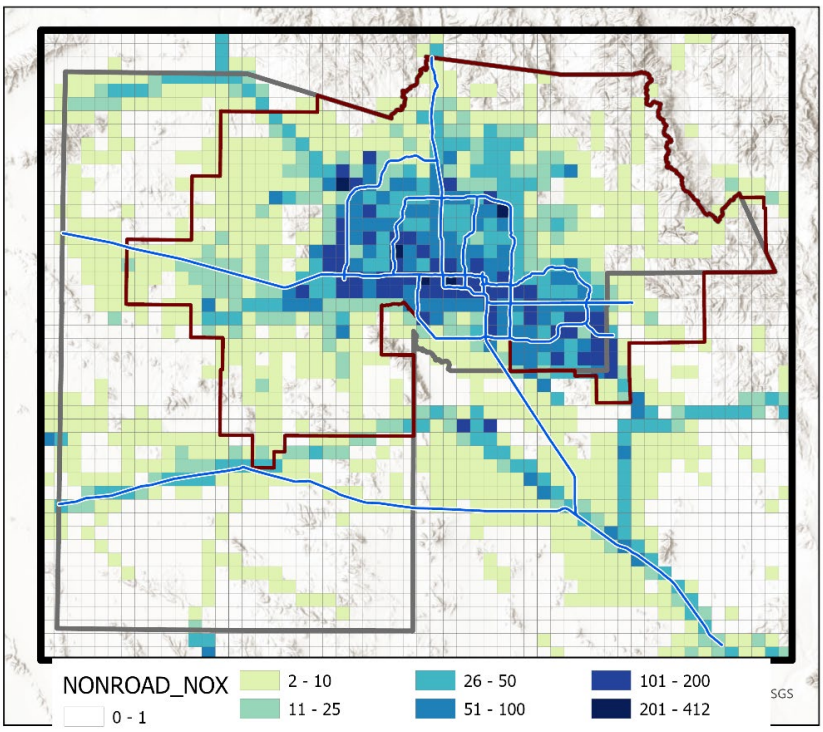

Figure 3-14. Spatial distribution of daily NO_x emissions from NONROAD (kg/day) for May 17, 2023

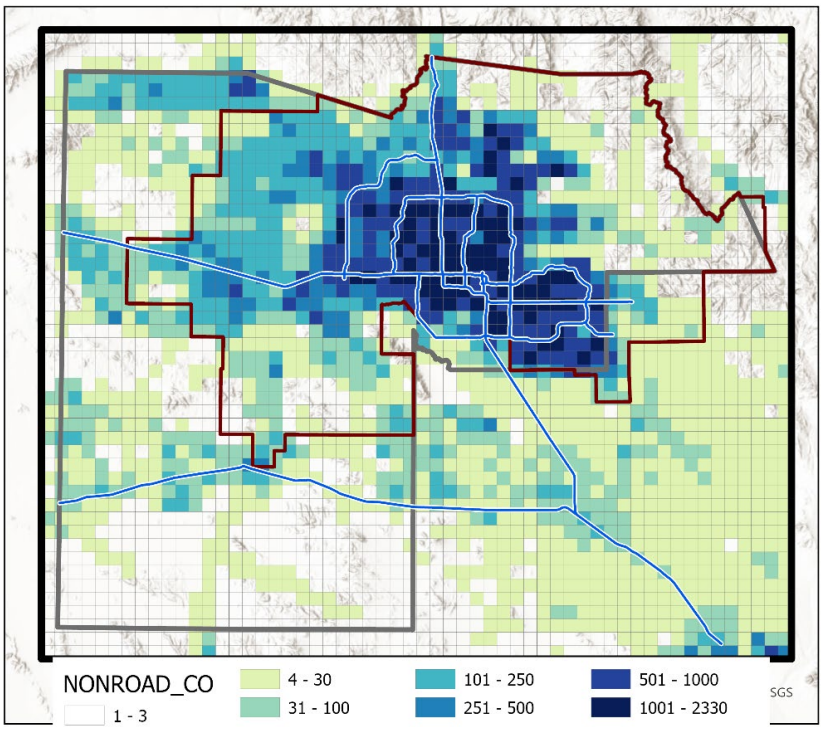

Figure 3-15. Spatial distribution of daily CO emissions from NONROAD (kg/day) for May 17, 2023

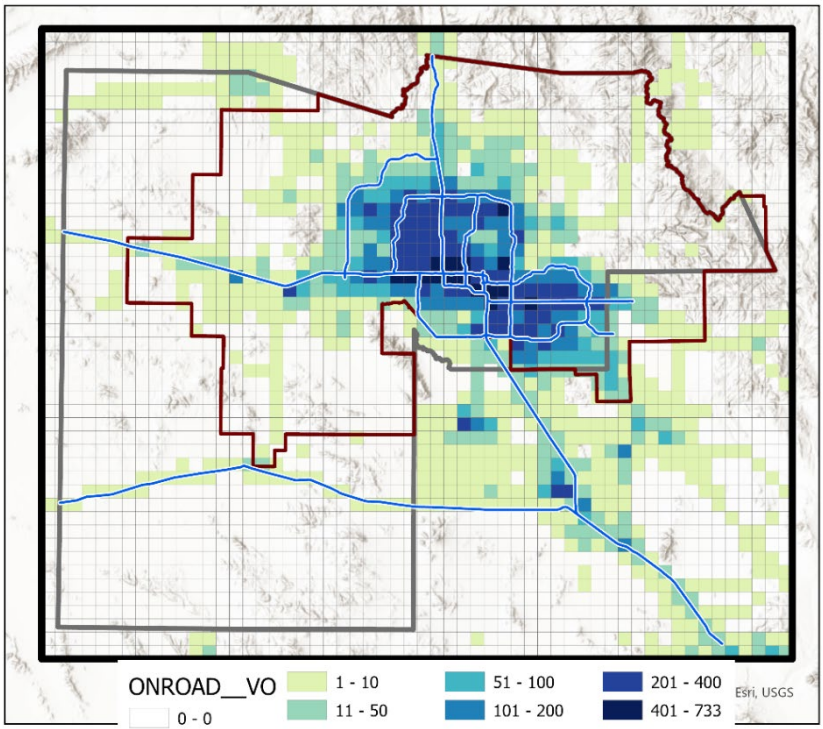

Figure 3-16. Spatial distribution of daily VOC emissions from ONROAD (kg/day) for May 17, 2023

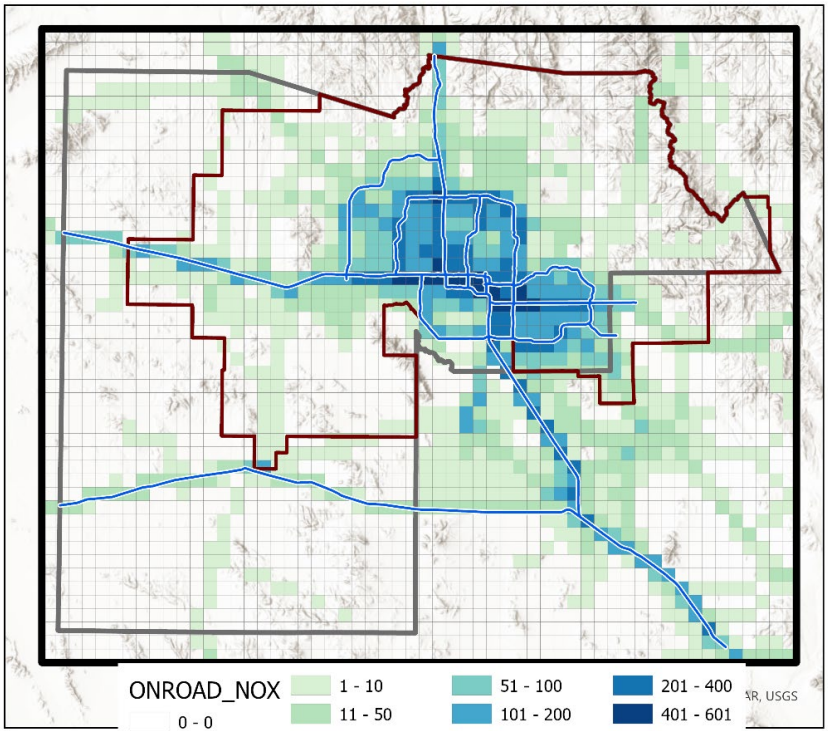

Figure 3-17. Spatial distribution of daily NO_x emissions from ONROAD (kg/day) for May 17, 2023

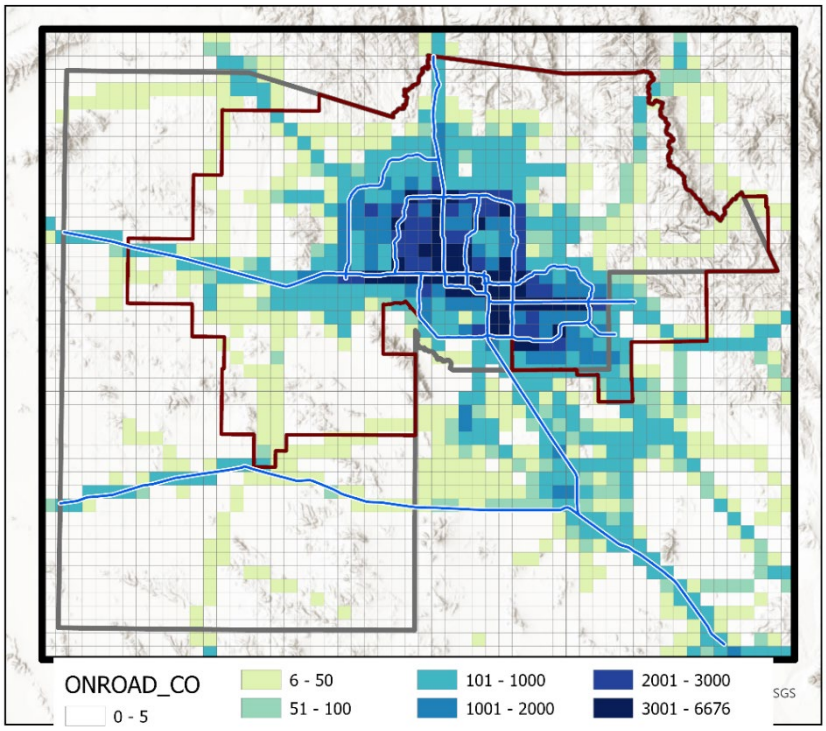

Figure 3-18. Spatial distribution of daily CO emissions from ONROAD (kg/day) for May 17, 2023

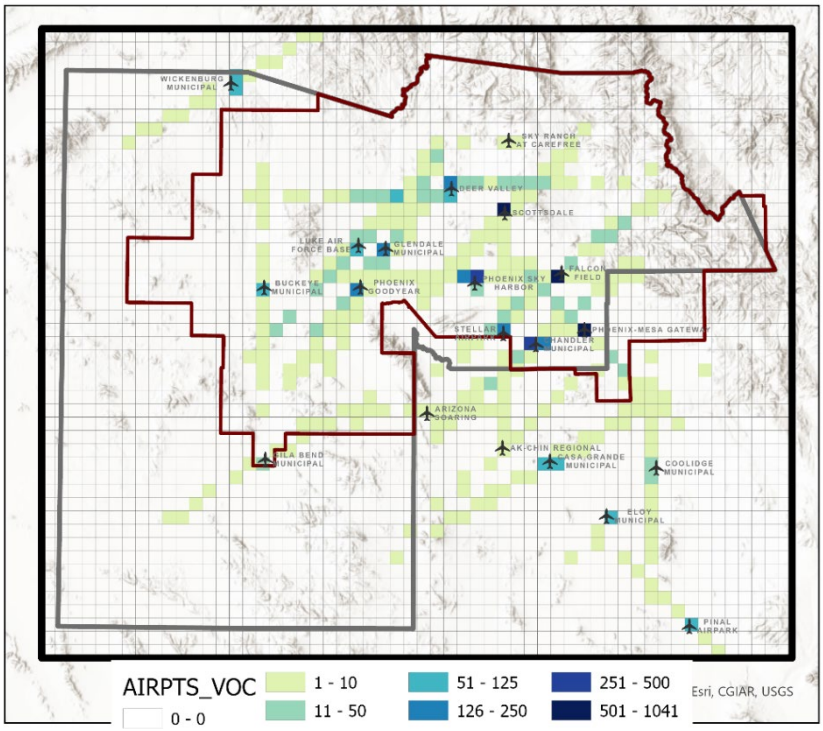

Figure 3-19. Spatial distribution of daily VOC emissions from Airports (kg/day) for May 17, 2023

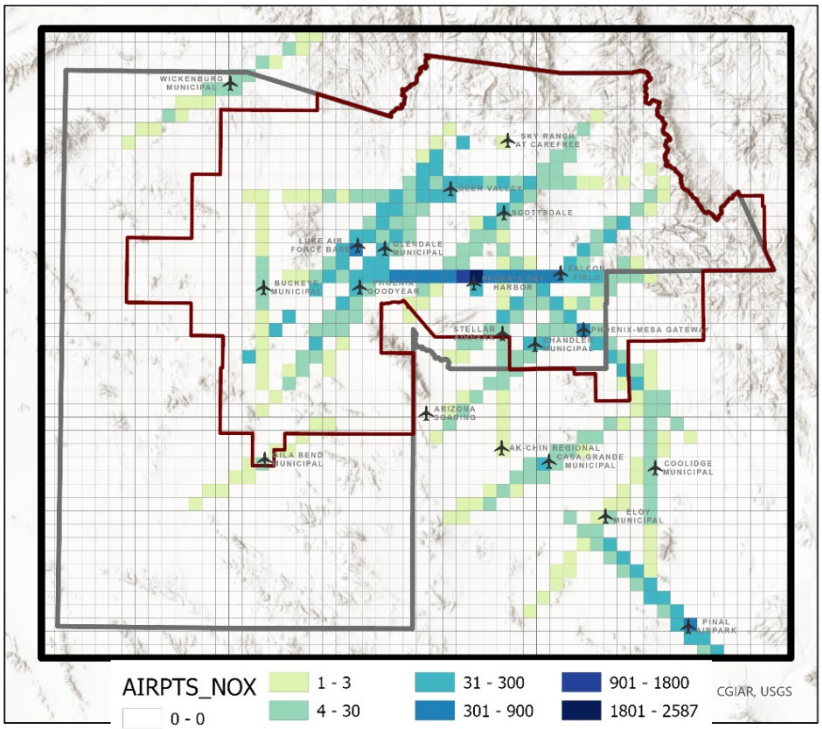

Figure 3-20. Spatial distribution of daily NO_x emissions from Airports (kg/day) for May 17, 2023

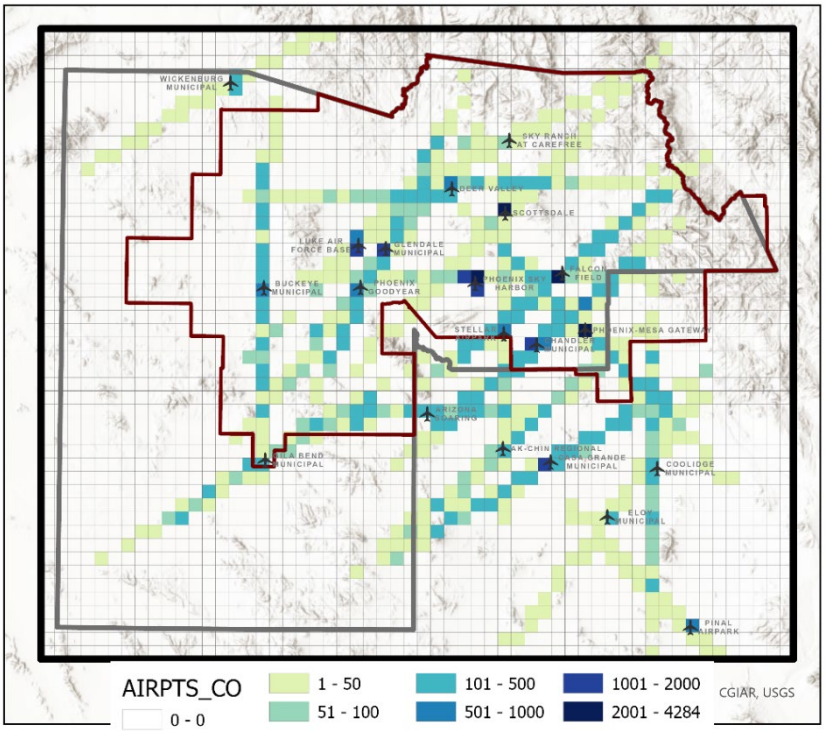

Figure 3-21. Spatial distribution of daily CO emissions from Airports (kg/day) for May 17, 2023

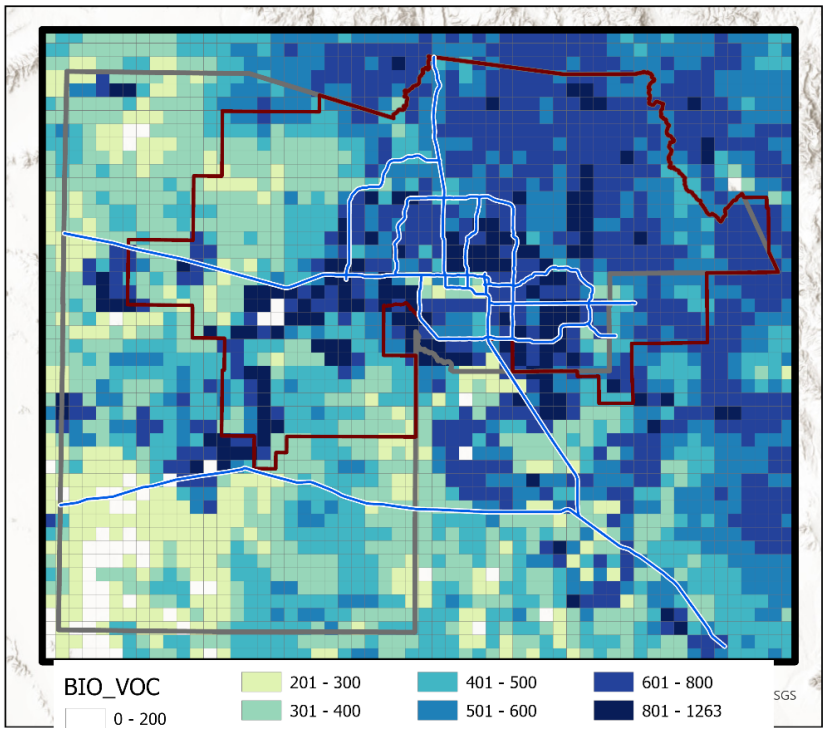

Figure 3-22. Spatial distribution of daily VOC emissions from Biogenics (kg/day) for May 17, 2023

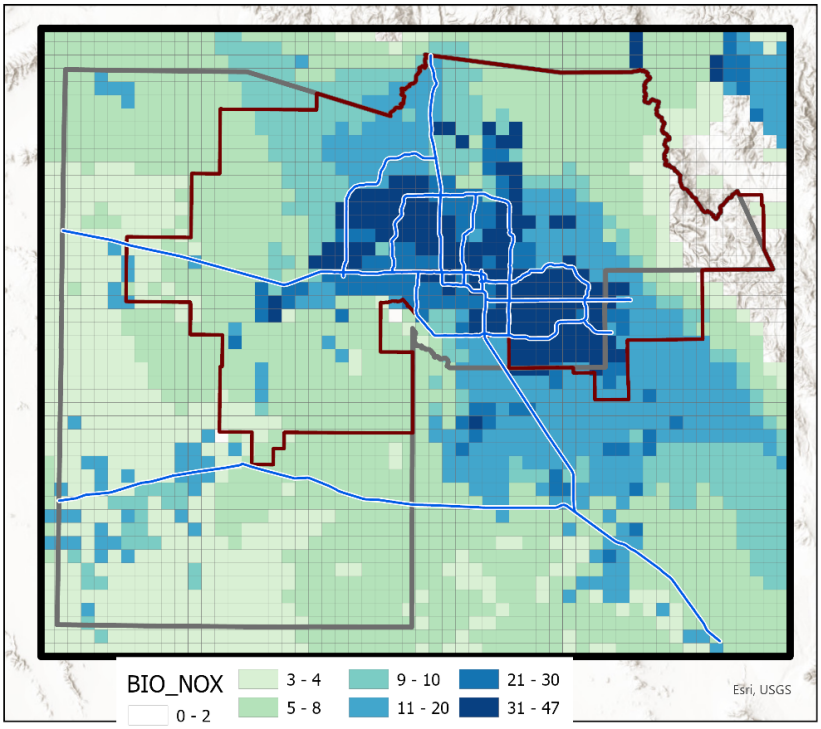

Figure 3-23. Spatial distribution of daily NO_x emissions from Biogenics (kg/day) for May 17, 2023

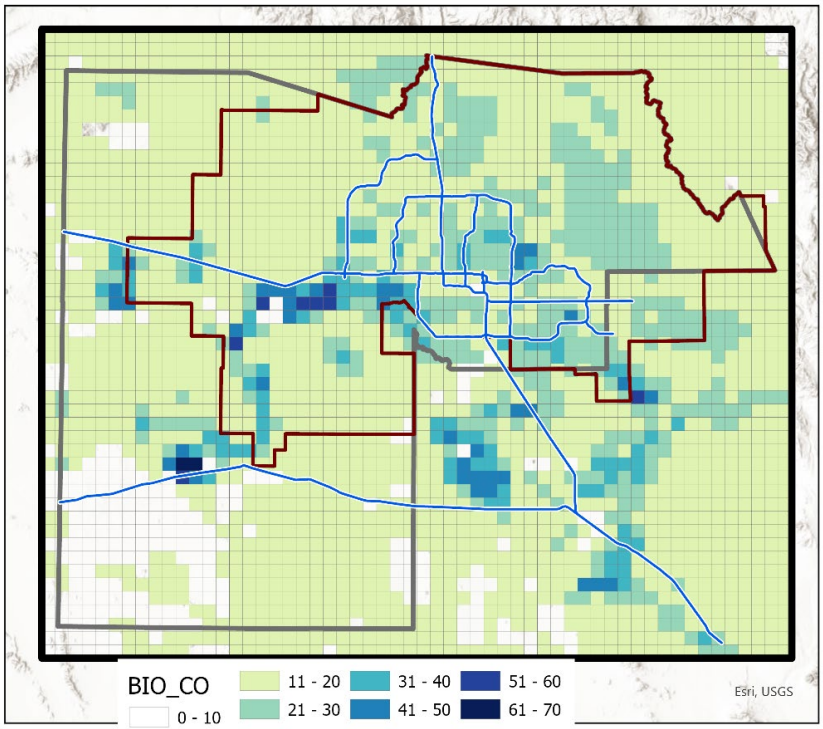

Figure 3-24. Spatial distribution of daily CO emissions from Biogenics (kg/day) for May 17, 2023

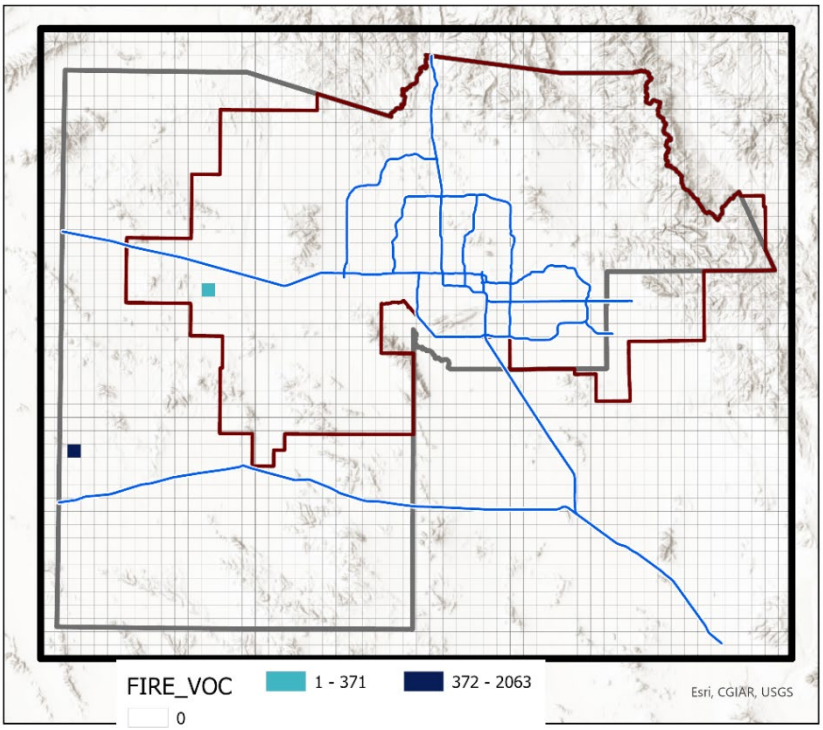

Figure 3-25. Spatial distribution of daily VOC emissions from Fires (kg/day) for May 17, 2023

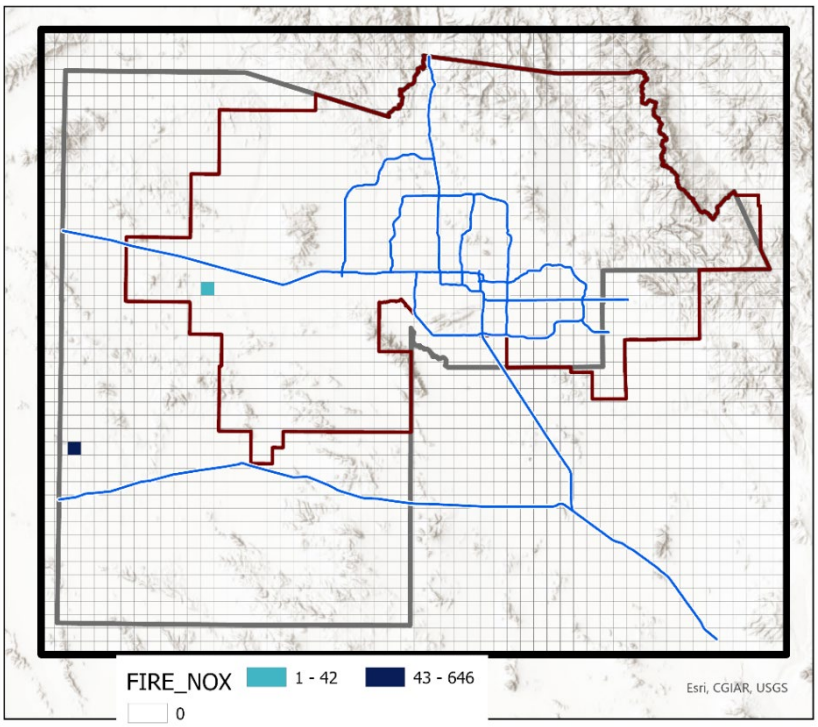

Figure 3-26. Spatial distribution of daily NO_x emissions from Fires (kg/day) for May 17, 2023

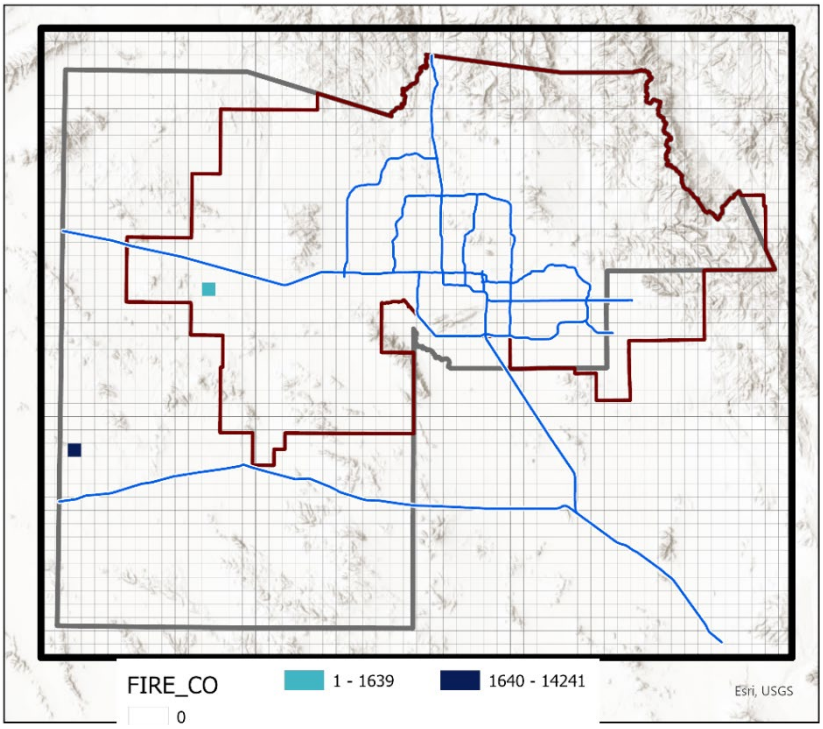

Figure 3-27. Spatial distribution of daily CO emissions from Fires (kg/day) for May 17, 2023

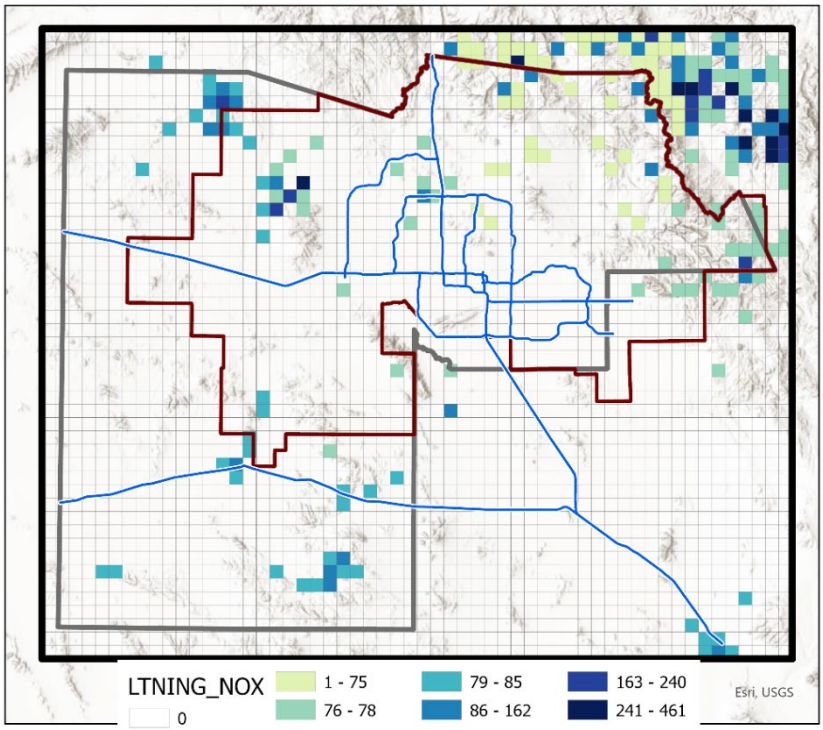

Figure 3-28. Spatial distribution of daily NO_x emissions from Lightning (kg/day) for May 17, 2023

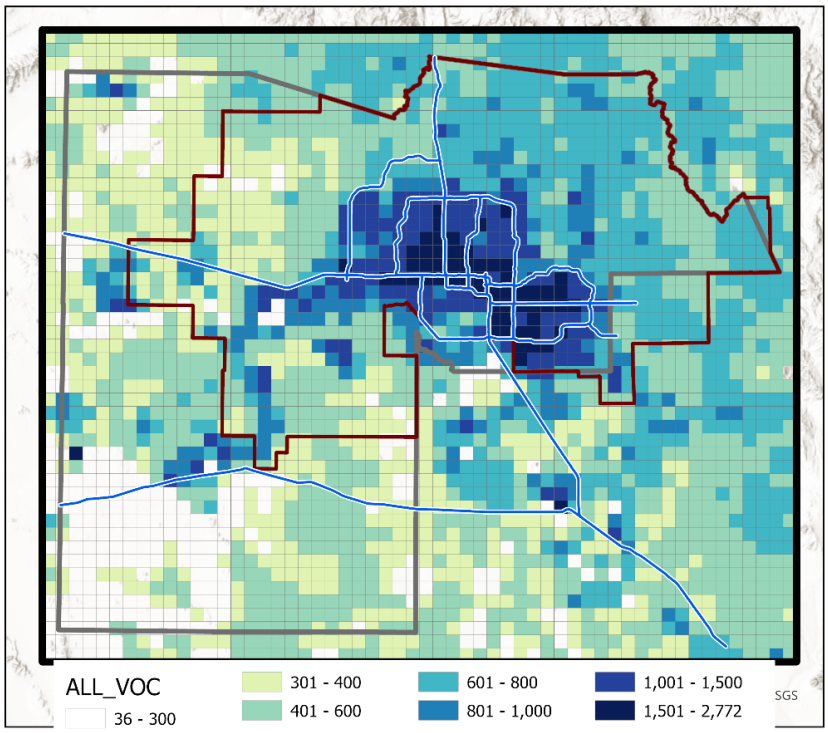

Figure 3-29. Spatial distribution of daily VOC emissions from all sources (kg/day) for May 17, 2023

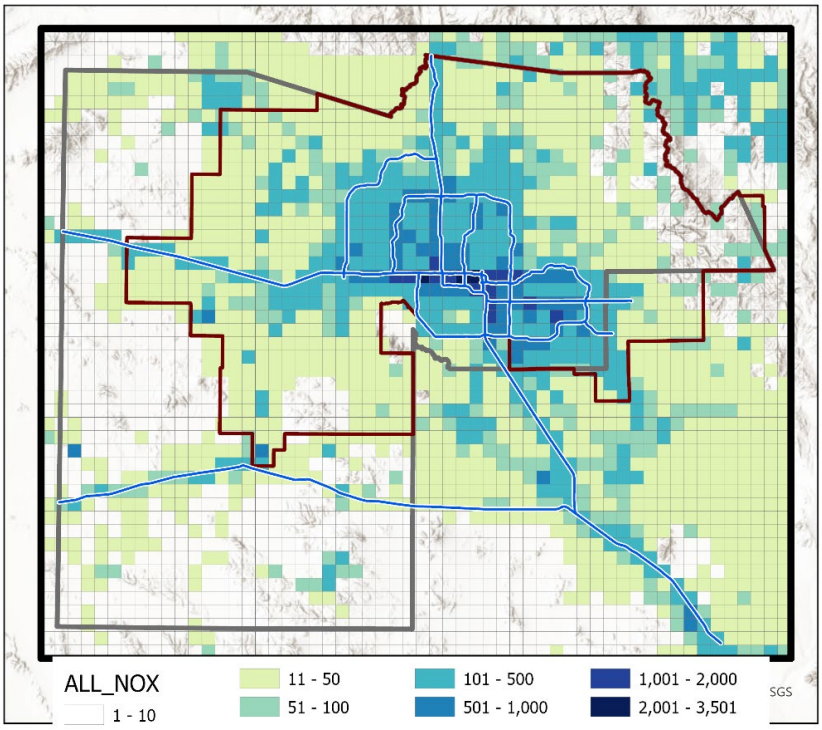

Figure 3-30. Spatial distribution of daily NO_x emissions from all sources (kg/day) for May 17, 2023

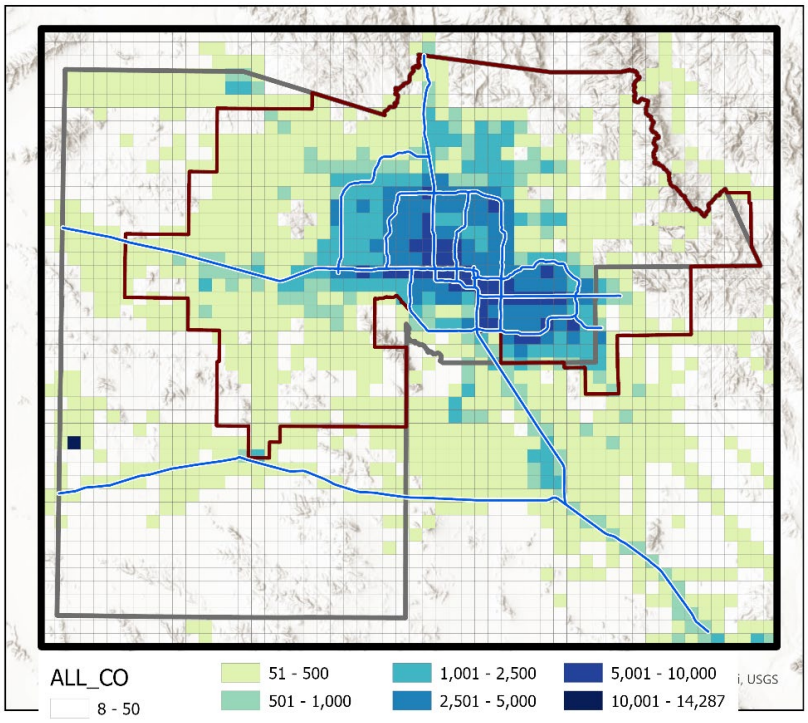

Figure 3-31. Spatial distribution of daily CO emissions from all sources (kg/day) for May 17, 2023

3.5.2. Chemical Speciation

To prepare the emissions inventory for air quality modeling, chemical speciation from the SMOKE modeling system is performed to convert broad pollutant categories into the specific model species required by the chemical mechanism. First, speciation is performed according to the CMAQ CB6 mechanism, then further refined for the CAMx CB7 mechanism.

In the first step, files are prepared for CMAQ using the Carbon Bond 6 revision 5 with AERO7 aerosol module (CB6R5_AE7). VOC emissions are speciated into either explicit chemical compounds like benzene (BENZ) and ethanol (ETOH) or lumped groups representing similar chemical properties, such as paraffins (PAR) and olefins (OLE). The basis for this process is the EPA's SPECIATE v5.3 database, which provides profiles that are processed through the S2S-Tool to generate the necessary input files for the SMOKE modeling platform.

A key aspect of the VOC speciation methodology is the handling of Hazardous Air Pollutants (HAPs) that are also VOCs, ensuring mass is not double-counted. For many sectors, key HAPs such as naphthalene, benzene, acetaldehyde, formaldehyde, and methanol (collectively referred to as NBAFM) are explicitly accounted for by subtracting their mass from the total VOC inventory. The remaining non-HAP VOC mass is then speciated using profiles that have been renormalized. For mobile sources, the MOVES4 model calculates certain integrated species (e.g., ethanol, benzene, formaldehyde) directly, while the remaining organic gas mass, termed NONHAPTOG (Non-HAP Total Organic Gas), is speciated outside of MOVES using updated, region-specific profiles for both onroad and nonroad categories.

The speciation methodology is tailored to different emission source categories to improve accuracy. For instance, the oil and gas sector uses variable, county-specific profiles that reflect regional differences in gas composition and controls. Likewise, the approach for integrating HAPs varies by sector, with some sources undergoing full integration while others do not. These detailed speciation procedures ensure that the chemical composition of VOC emissions is accurately represented in the model, which is critical for correctly simulating photochemical ozone formation.

In the second step, files are prepared for CAMx utilizing the Carbon Bond 7, revision 1 (CB7r1) chemical mechanism, a significant update over previous versions. This mechanism features a comprehensive revision of ozone chemistry, with major updates to the reactions involving biogenic VOCs, such as isoprene and terpenes, as well as key

anthropogenic VOCs like larger alkanes. While the CB7r1 mechanism is compatible with existing speciation profiles for anthropogenic emissions, its updated biogenic chemistry requires a different approach. Specifically, α-pinene must be separated from other terpenes, and sesquiterpene emissions must be explicitly included. To prepare the data for the CAMx model, a conversion tool from the EPA's 2021v1 platform was used to process and adapt the CMAQ-ready emissions files.

3.5.3. Temporal Allocation

Emissions inventories were prepared at multiple temporal resolutions (hourly, daily, monthly, and annual). Table 3-17 summarizes the temporal resolution of all inventory datasets used for the CAMx/CMAQ 4 km modeling domain. Annual emissions were disaggregated to monthly, daily, and hourly values by Source Classification Code (SCC). In SMOKE, this temporal allocation was performed by applying profiles in the following sequence: monthly, day-of-week, then hourly. Temporal profiles varied by county, sector, and season.

Table 3-17. Inventory resolutions for different categories in the 4 km modeling domain

Category	Maricopa County	Pinal County	Other Counties
Point (EGU-CEMS)	Hourly	Hourly	N/A
Point (EGU-nonCEMS)	Monthly	Monthly	N/A
Point (ptnonipm)	Annual	Annual	N/A
MERCs	Annual	Annual	N/A
Area	Annual	Annual	Annual
Airports (AEDT 3g)	Hourly	Hourly	N/A
Rail	Annual	Annual	Annual
Nonroad (MOVES4)	Daily	Daily	Monthly
Onroad (MOVES4)	Hourly	Hourly	Annual
Biogenic (MEGAN v3.2)	Hourly	Hourly	Hourly
Fires (2023 NEI)	Daily	Daily	Daily
Lightning	Hourly	Hourly	Hourly

EGU Temporal Profile Development

Temporal profiles for Electrical Generating Unit (EGU) point sources in Maricopa and Pinal Counties were developed from 2023 hourly Continuous Emission Monitoring Systems (CEMS) data using a hierarchical approach to assign the most representative profiles.

Where CEMS data were available for at least one unit at a facility, that information was used to create a facility-specific profile that was applied to all other unmonitored units at that site. Facilities lacking CEMS data, such as the Ocotillo Power Plant, were assigned a county-wide profile developed by aggregating CEMS data from all other reporting EGUs within the respective county.

While monthly profiles were developed, the weekday/weekend and daily profiles were specifically based on CEMS data from the ozone season from April 1 to September 30, 2023. All profiles were normalized to preserve the mass balance of the inventory, ensuring that the temporal allocation process did not alter total annual emissions. Tables for each monthly/weekly/daily profile from the EGUs are provided in Appendices 3A through 3C4.

Figures 3-32 through 3-34 present the resulting normalized monthly, weekly, and daily temporal profiles for EGU point sources in both counties. Most EGUs from Maricopa County show flatter profiles of the monthly and hourly profiles than those from Pinal County.

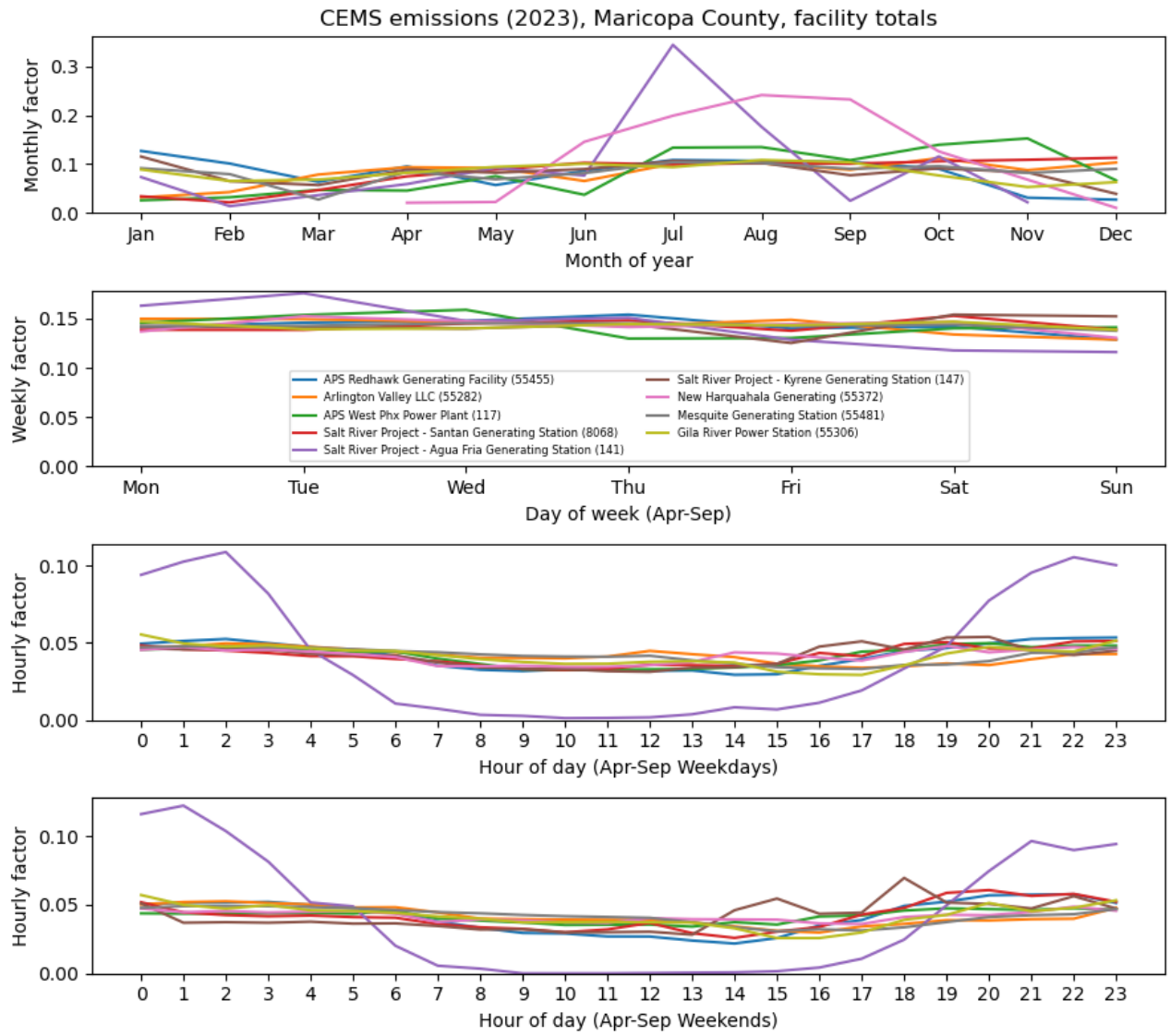

Figure 3-32. Normalized 2023 temporal profiles for EGU facilities in Maricopa County, showing monthly and weekly patterns, and daily patterns in UTC

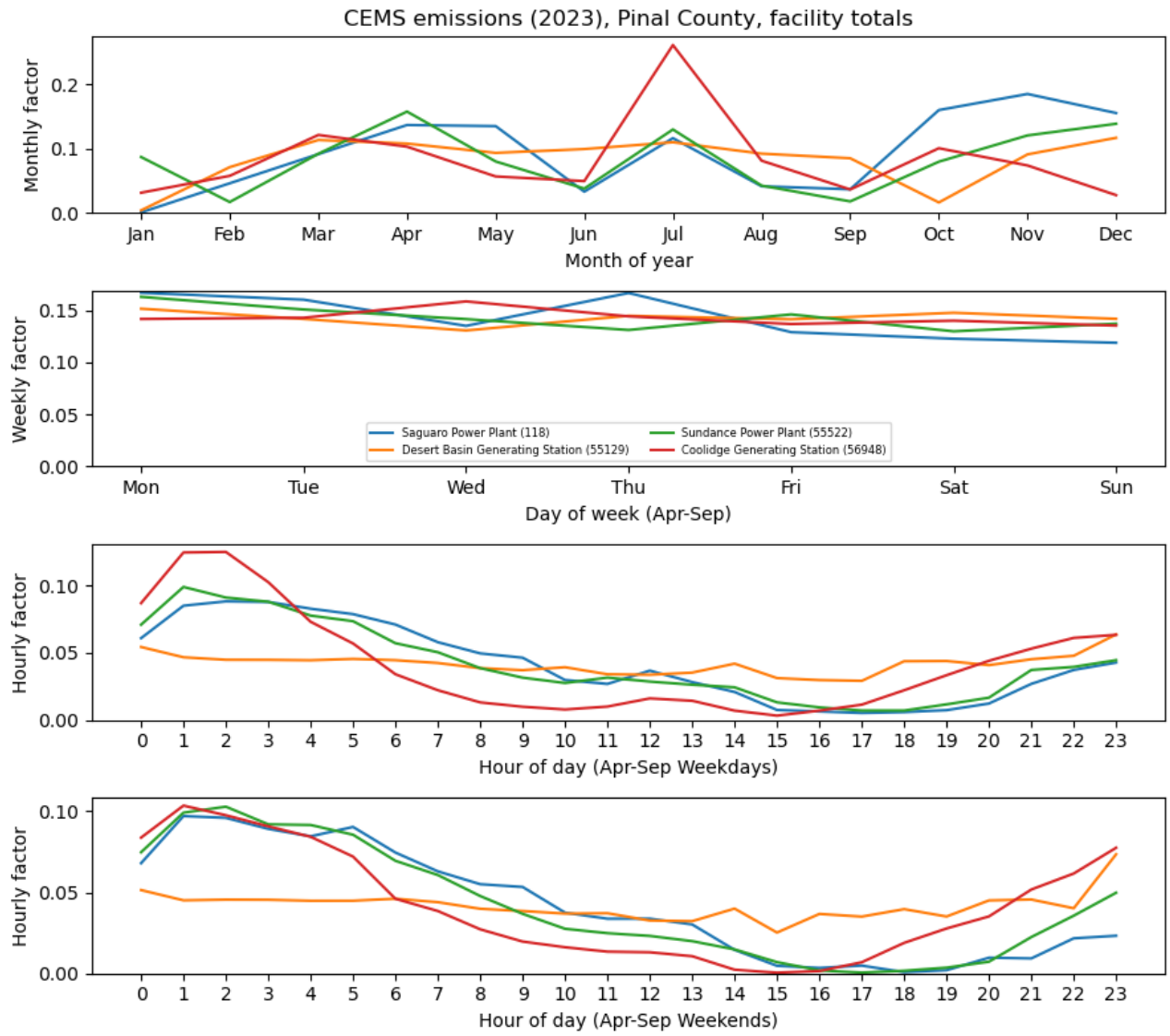

Figure 3-33. Normalized 2023 temporal profiles for EGU facilities in Pinal County, showing monthly and weekly patterns, and daily patterns in UTC

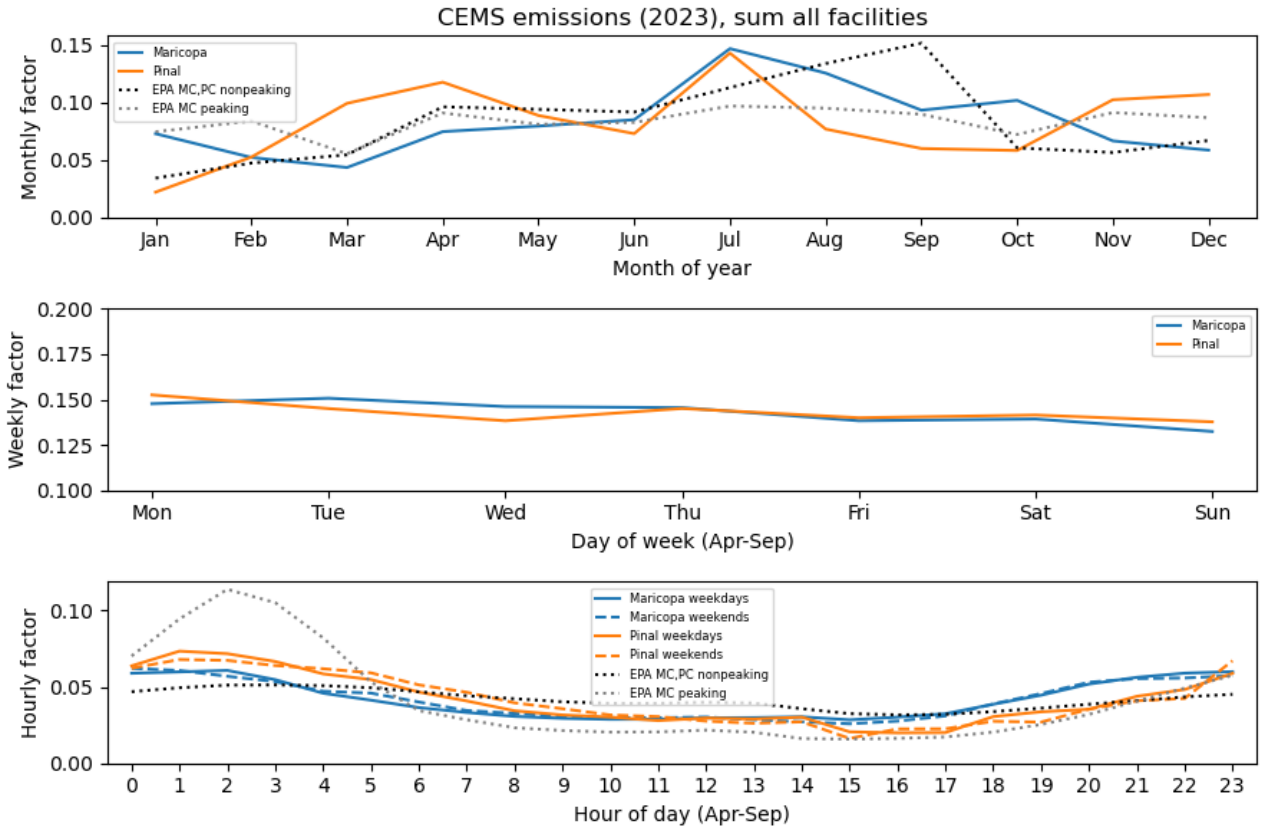

Figure 3-34. Normalized 2023 temporal profiles (monthly, weekly, daily) for county-wide facilities in Maricopa and Pinal Counties versus the EPA 2022hc modeling platform defaults

MERCs Temporal Profiles

Similar to other industrial point sources, MERCs emissions are modeled with specific temporal profiles from the EPA's 2022v1 modeling platform. The monthly distribution is assumed to be uniform, using Profile #262 from the file of "tpro_monthly_general _2022platform_03jun2024_v0". Furthermore, the weekly and daily profiles reflect typical industrial activity, using Profile #8 from "amptpro_general_2011platform_tpro_weekly _6nov2014_09sep2016_v2" and Profile #26 from "amptpro_general_2011platform_tpro _hourly_6nov2014_18apr2022_v11" respectively. The weekly and daily profiles for MERCs used in this plan are displayed in Figures 3-35 through 3-38.

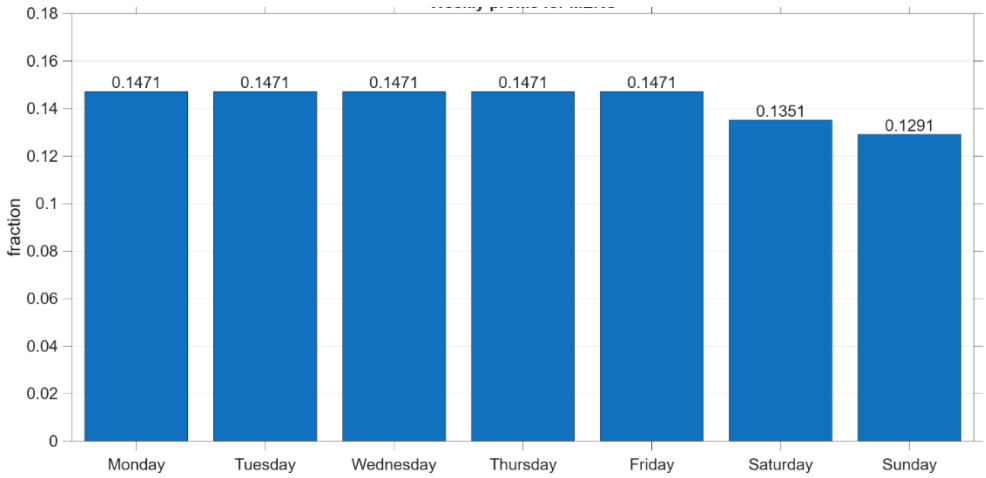

Figure 3-35. Weekly profile for MERCs

Summary of diurnal profiles

Figures 3-36 through 3-38 display the diurnal changes of hourly emission fractions for VOC, NO_x, and CO for the 4 km modeling domain on May 17, 2023. The profiles aggregate emissions from point, area, nonroad, onroad, airport, MERCs (equivalent to ERC), biogenic, wildfire, and lightning source categories. Diurnal patterns differ by pollutant and source:

- **VOC:** Biogenic VOC emissions dominate the daytime, with a broad late-morning to mid-afternoon peak driven by temperature and sunlight (isoprene and terpene emissions). Anthropogenic VOC sources follow activity patterns: on-road VOC peaks during morning commute and remains elevated into evening; nonroad equipment peaks midday during work hours; airports show brief midday spikes; MERCs (mobile credits, treated as industrial) emissions are relatively flat; traditional point sources are nearly flat, indicating steady operations. Wildfire VOC, on this date, is minimal.
- **NO_x:** NO_x is overwhelmingly from combustion sources. On-road and nonroad NO_x exhibit pronounced morning and early-evening surges corresponding to traffic patterns and daily work schedules. Airports contribute midday NO_x spikes (from aircraft LTO cycles). Point sources appear as steady but localized NO_x contributions. Notably, natural NO_x shows up as an evening "flash" of lightning-generated NO_x after ~18:00–20:00 local standard time (LST) in the model, corresponding to convective thunderstorms. Biogenic soil NO also adds a smaller, broad daytime signal in vegetated areas. Fire NO_x is negligible on this particular day.
- **CO:** CO temporal behavior closely mirrors that of NO_x, as it is also dominated by on-road and nonroad mobile combustion. CO emissions peak during daytime travel and work hours and drop off overnight. The highest CO fractions occur

around major roadways and urban centers (similar spatially to NO_x). Point-source CO (e.g., industrial combustion) is steady and minor in the total mix. Biogenic CO is negligible, and wildfire CO is very low on May 17.

Each set of category-specific diurnal fractions sums to 1.0 for that day and is applied to the corresponding source's daily total to distribute emissions by hour in the model. These profiles demonstrate that ozone precursor timing in the Phoenix area is driven by (1) abundant biogenic VOC released during daytime heat and (2) anthropogenic NO_x (and CO) peaking during human activity periods, with substantial emissions continuing into the evening. Capturing these temporal patterns with high fidelity is essential for accurate photochemical modeling of 8-hour ozone exceedances.

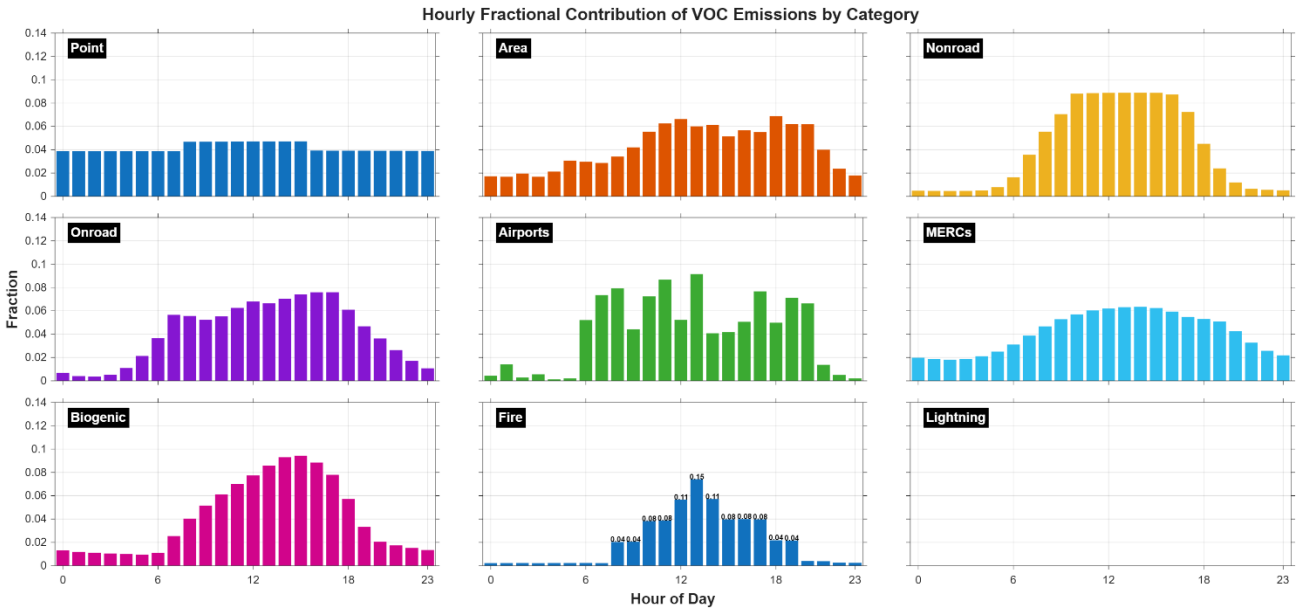

Figure 3-36. Diurnal variation of hourly VOC emission fractions within the 4 km domain on May 17, 2023

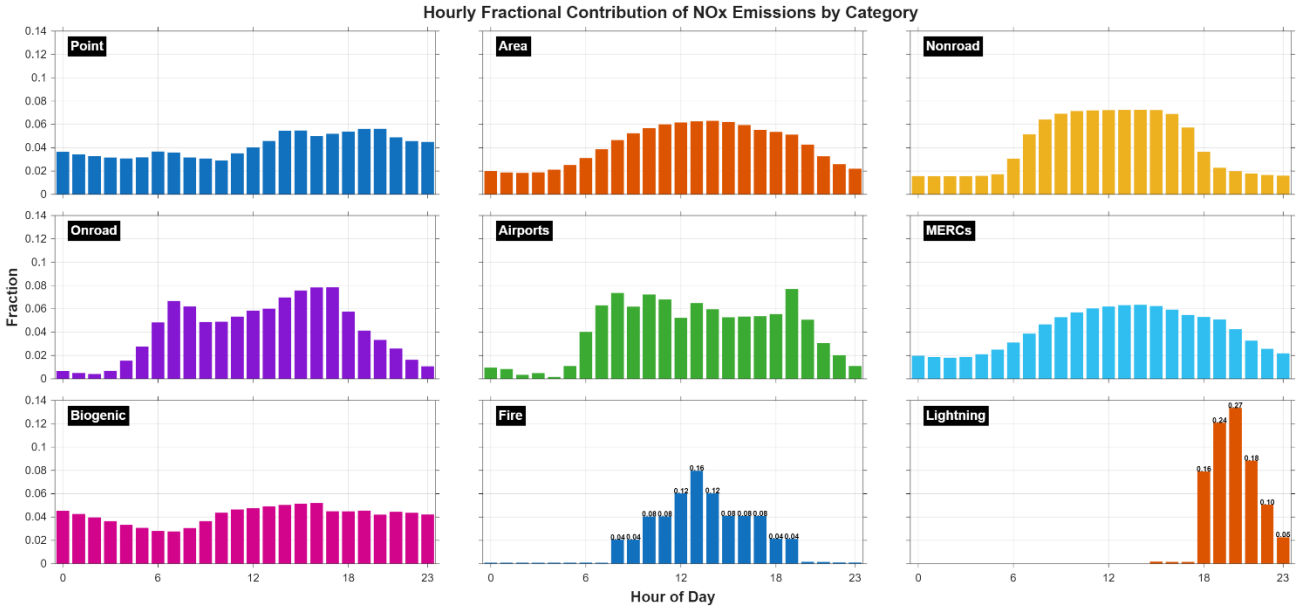

Figure 3-37. Diurnal variation of hourly NO_x emission fractions within the 4 km modeling domain on May 17, 2023

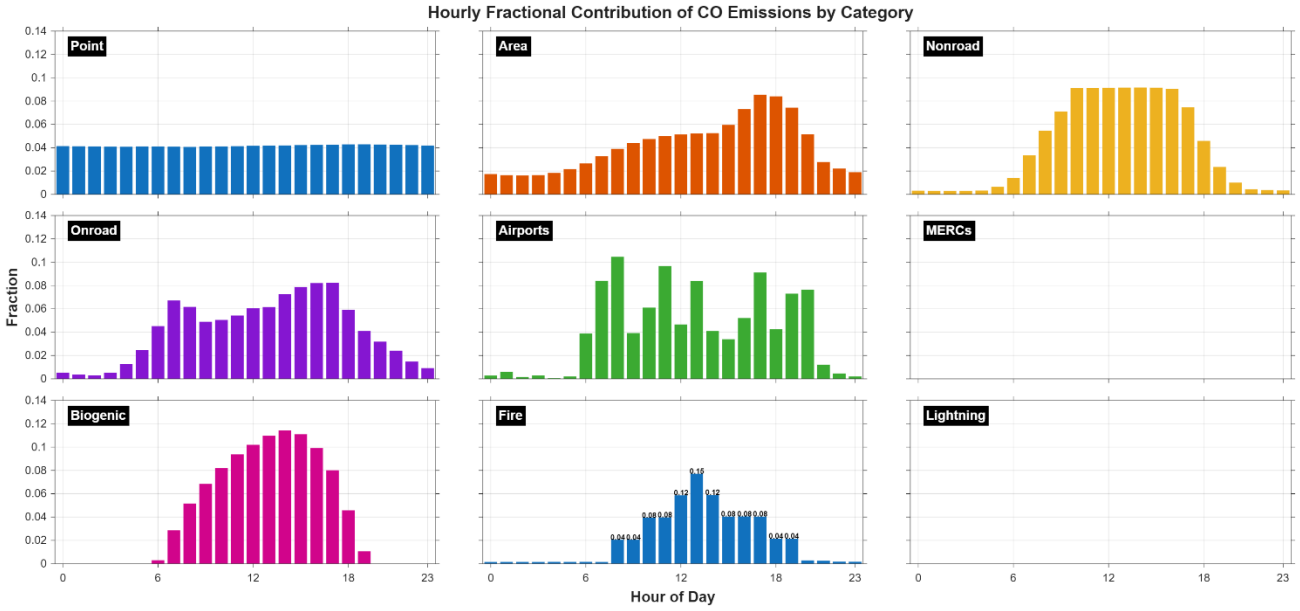

Figure 3-38. Diurnal variation of hourly CO emission fractions within the 4 km modeling domain on May 17, 2023

3.5.4. Emissions Summaries for the 4 km Modeling Domain and the Maricopa NAA

Table 3-18 reports the 2023 ozone-season daily average emissions for VOC, NO_x, and CO in both the regional 4 km modeling domain and the Maricopa NAA across 11 source categories, and the data reveal distinct primary and secondary contributors for each pollutant. In the 4 km domain, the totals are 1,706.67 tpd for VOC, 165.72 tpd for NO_x, and 1,042.56 tpd for CO. The corresponding totals for the Maricopa NAA are 720.49 tpd for VOC, 111.69 tpd for NO_x, and 870.57 tpd for CO.

VOC is overwhelmingly biogenic in both domains (1,507.74 tpd in the 4 km domain; 552.72 tpd in the Maricopa NAA), with area sources a distant second (113.60 tpd in the 4 km domain; 97.32 tpd in the Maricopa NAA). NO_x is led by on-road and nonroad mobile sources (51.50 and 29.91 tpd in the 4 km domain; 39.59 and 22.80 tpd in the Maricopa NAA), supplemented by biogenic emissions (42.03 tpd; 17.64 tpd) and a smaller lightning component (8.83 tpd; 2.06 tpd). CO is dominated by mobile sources, with on-road and nonroad contributions of 530.83 and 368.12 tpd in the 4 km domain and 466.86 and 312.34 tpd in the Maricopa NAA; airports contribute moderately (41.99 tpd; 33.96 tpd), and biogenic CO is smaller but non-negligible (56.44 tpd; 20.68 tpd). Wildfire adds modest VOC and CO and very little NO_x (7.73/26.91/0.45 tpd in the 4 km domain; 6.59/21.36/0.33 tpd in the Maricopa NAA), while point, MERC, and ERC categories are minor for all pollutants.

Figure 3-39 shows the daily fluctuations in NO_x emissions from power plants within the 4 km modeling domain. As detailed in Section 3.5.3, the emissions data are derived from two methods. The majority of units are equipped with CEMS that provide direct measurements. For a few unmonitored facilities and units, emissions were estimated using local daily, weekly, and monthly profiles.

EGU NO_x emissions show a clear seasonal pattern. From April to early July, daily totals typically range from 4–7 tpd, with a notable spike to over 10 tpd in the middle of May. The highest emissions occur in early to mid-July, with a sharp peak reaching nearly 15 tpd. Levels then remain high through August, mostly between 6–10 tpd, before gradually decreasing to 5-7 tpd in September. This pattern suggests emissions are driven by electrical demand, particularly during extreme heat, rather than a simple weekday/weekend cycle.

Table 3-18. Summary of average daily emissions used for each category in the 4 km modeling domain and the Maricopa NAA (unit: short tons/day)

Category	4 km Domain			Maricopa NAA		
	VOC	NO_x	CO	VOC	NO_x	CO
Point	5.57	8.89	6.72	1.99	7.49	5.82
Airports[1]	5.42	10.50	41.99	4.90	9.79	33.96
Area	113.60	10.88	11.55	97.32	9.25	9.56
Nonroad	23.40	29.91	368.12	18.40	22.80	312.34
Onroad	41.82	51.50	530.83	37.16	39.59	466.86
MERCs	1.37	2.74	0.00	1.37	2.74	0.00
ERC	0.03	0.005	0.00	0.03	0.005	0.00
Biogenic	1,507.74	42.03	56.44	552.72	17.64	20.68
Lightning	0.00	8.83	0.00	0.00	2.06	0.00
Wildfire	7.73	0.45	26.91	6.59	0.33	21.36
Total	**1,706.67**	**165.72**	**1,042.56**	**720.49**	**111.69**	**870.57**

[1] Only emissions occurring at or below 3,000 feet above ground level (AGL) are summarized here, using FAA's AEDT 3g.

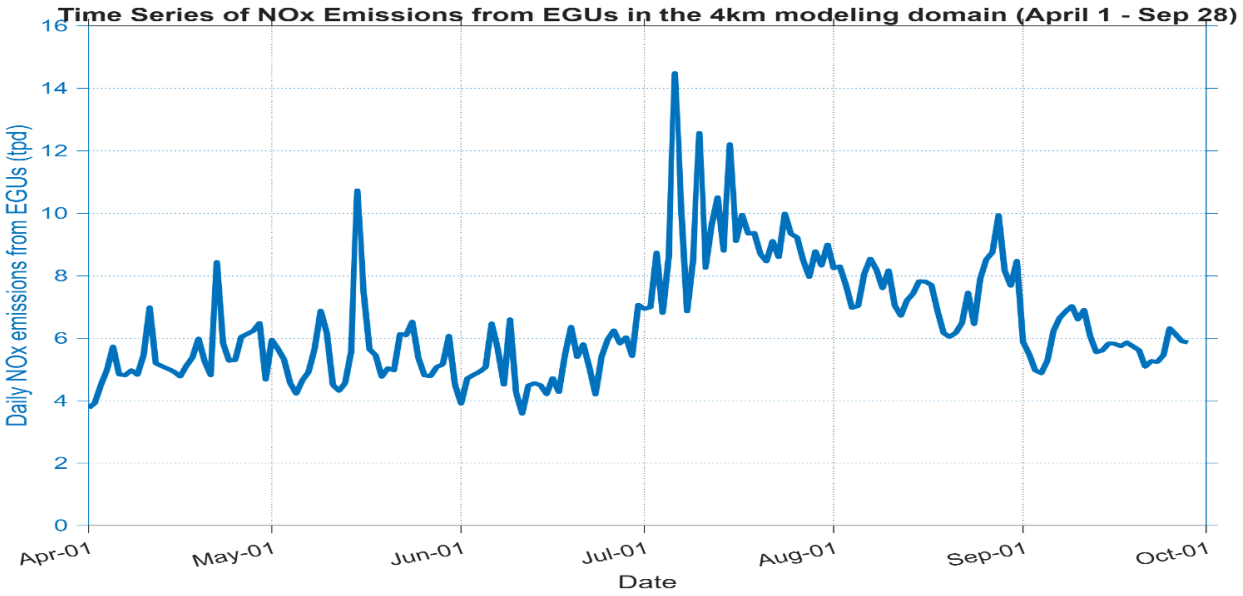

Figure 3-39. 2023 ozone season daily average NO_x emissions (short ton) for the EGUs in the 4 km modeling domain

Figure 3-40 shows the daily total VOC and NO_x emissions within the 4 km modeling domain. From April through September, domain-wide VOC totals exhibit a pronounced summertime ramp: values oscillate between ~400–1,200 tpd in April–May, surge in late June–July to 2,500–3,500 tpd with multi-day plateaus, then ease through August–September with episodic spikes. NO_x totals are comparatively stable (≈130–190 tpd) with a clear weekday–weekend cycle and slightly higher midsummer levels. Two brief late-August/early-September bursts exceed 400 tpd from lightning. Overall, the series shows strong seasonal VOC forcing and steadier anthropogenic NO_x emissions.

Figure 3-41 summarizes source shares vie pie charts. VOC is dominated by biogenics, with area next and mobile minor. NO_x is dominated by mobile (on-road then nonroad); airports/point secondary; natural (soil/lightning) nontrivial. CO is transportation-driven (on-road/nonroad), with airports/wildfire small. Patterns are similar across geographies, with slightly higher biogenic VOC outside the Maricopa NAA overall.

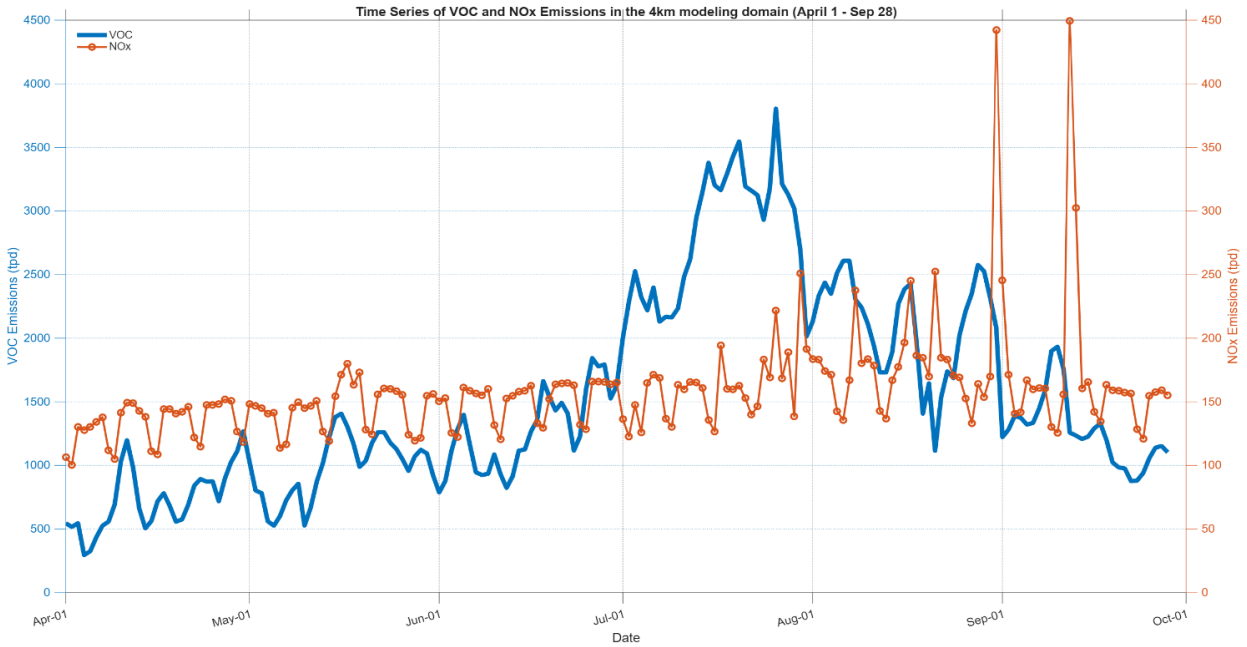

Figure 3-40. 2023 ozone season daily VOC and NO_x emissions (short ton) for all sources in the 4 km modeling domain

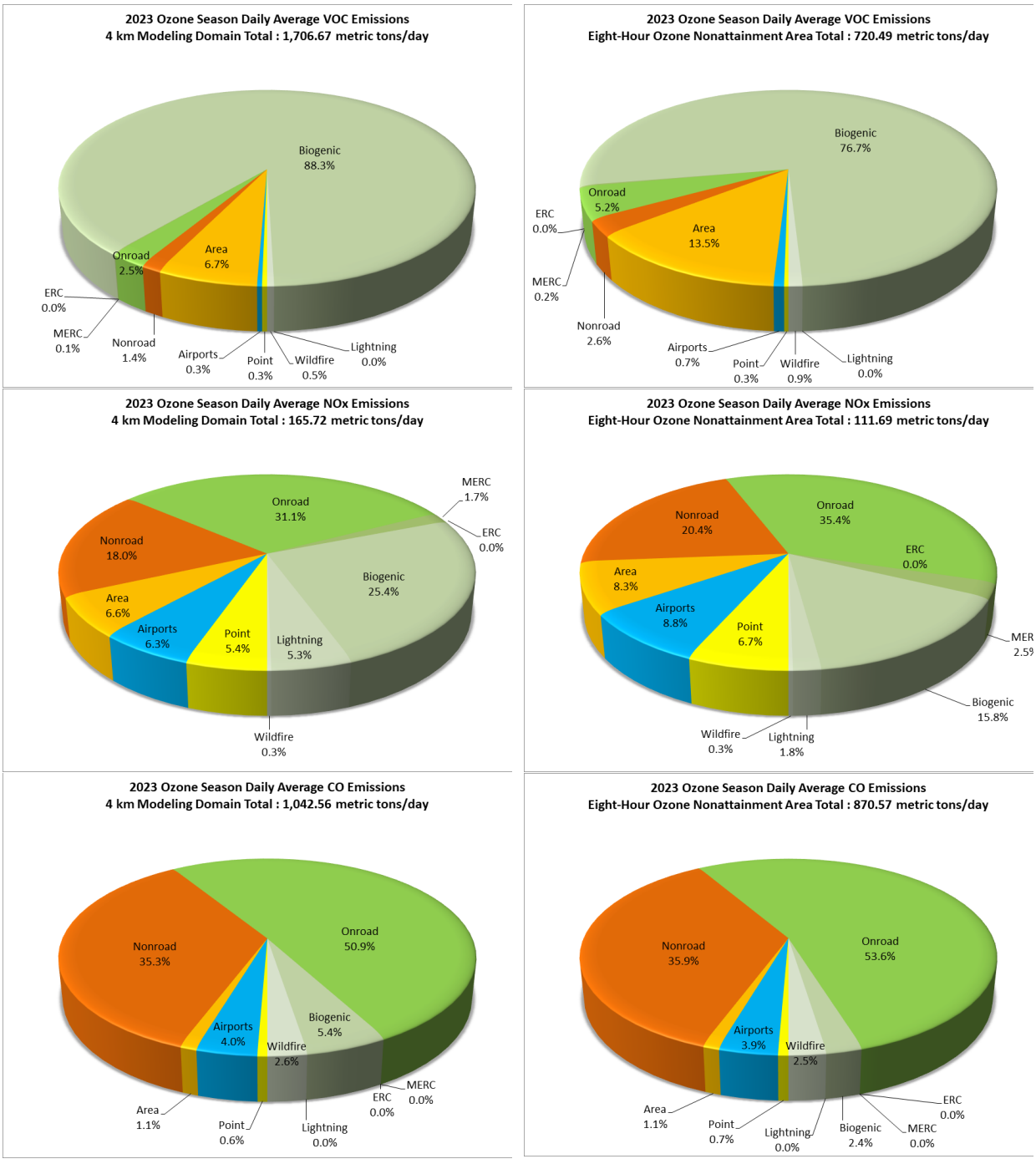

Figure 3-41. Pie charts for 2023 ozone season average daily VOC, NO_x, and CO emissions by source category in the 4 km modeling domain (left set) and the Maricopa NAA (right set)

4. METEOROLOGICAL MODELING

4.1. Overview of the Weather Research and Forecasting (WRF) Model

The Weather Research and Forecasting (WRF) model is an offline, mesoscale meteorological model that simulates wind, vertical mixing, temperature, humidity, solar radiation, and related variables. The latest WRF version 4.7.0 with the Advanced Research WRF (ARW) dynamic core was applied to generate meteorological input fields for CAMx and CMAQ in this work. A detailed description of the WRF model is available on the WRF user webpage (http://www2.mmm.ucar.edu/wrf/users/) and in Skamarock et al. (2019). Given the complex weather and terrain patterns in Maricopa County, particularly in the Phoenix area, a customized model configuration with locally tailored physical parameterizations was developed as described below. The simulation was initialized at 12:00 Coordinated Universal Time (UTC) and covered the period from April through September 2023.

4.2. Domains, Vertical Layering, and Physics Configuration

The WRF model was configured with three two-way nested domains at horizontal resolutions of 36, 12, and 4 km (Figure 4-1). The selection of nested modeling domains considered the boundaries of the Maricopa NAA, the distribution of major emission sources, the locations of meteorological and air quality monitoring sites, prevailing winds associated with elevated ozone, and regional pollutant transport. Since ozone concentrations in the Maricopa NAA can be substantially influenced by transported ozone and ozone precursor emissions from outside the Maricopa NAA (U.S. EPA, 2015), the outermost 36 km domain covers the southwestern U.S. and Mexico. In the two-way nested WRF run, the child domains (12 km and 4 km) receive their boundary conditions from their respective parent domains (36 km and 12km). In turn, the child domains feedback their fine-scale solutions to replace the parent solutions over the nested regions, with smoothing applied to maintain numerical stability. The WRF modeling domains are larger than the CAMx/CMAQ modeling domains in order to develop meteorological data for simulation of ozone concentrations around the boundaries of the CAMx/CMAQ modeling domains. The WRF domain configurations are summarized in Table 4-1.

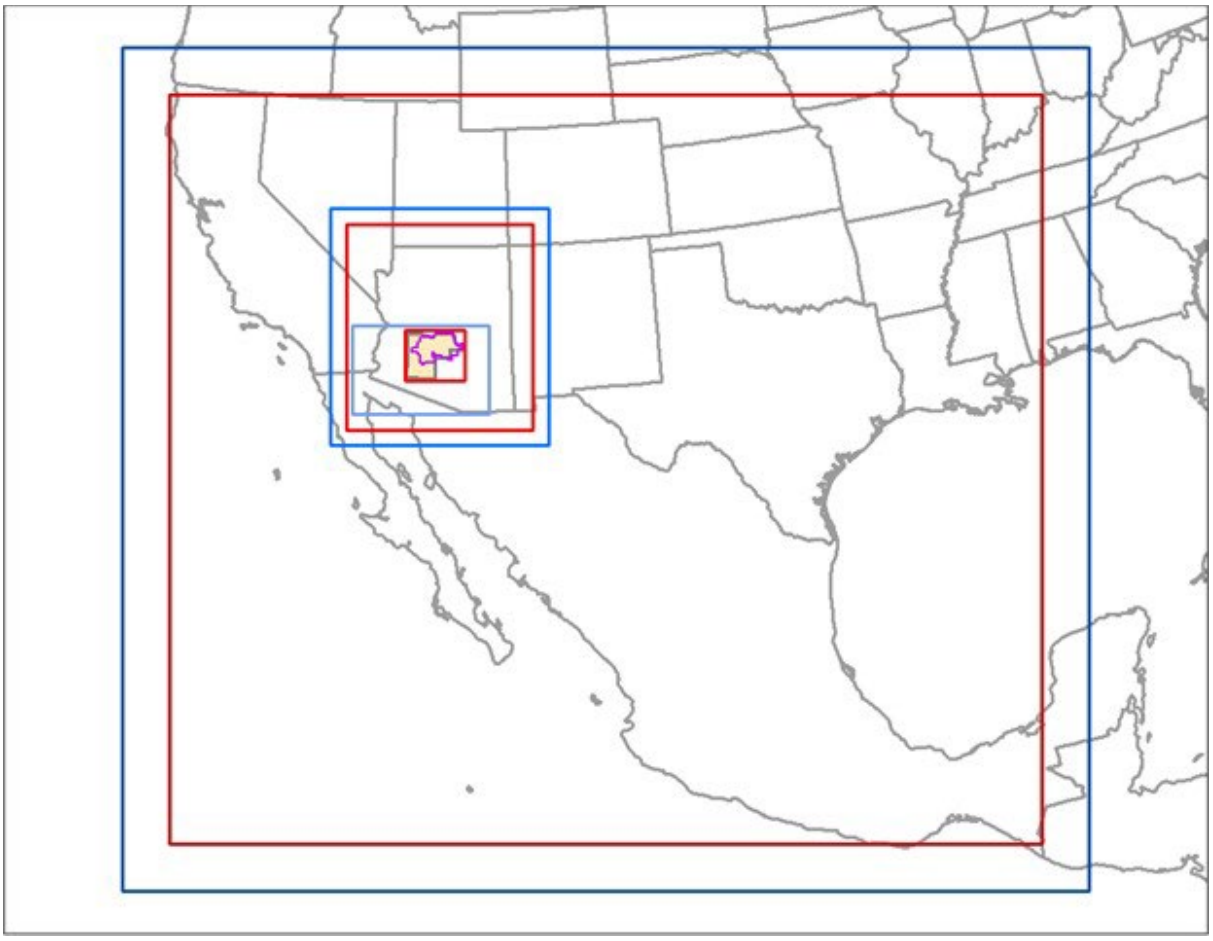

Figure 4-1. Modeling domains used in this study with horizontal resolutions of 36, 12, and 4 km; CAMx/CMAQ domains (red) and WRF domains (blue)

Table 4-1. Configuration of WRF modeling domains (Lambert Conformal Conic projection with 33° N and 45° N true latitudes and 112° W and 33.5° N central longitude and latitude)

Domain	Grid Resolution	Origin (SW, km)	Extent (NE, km)	NX	NY	NZ
36 km Grid Domain	36 km x 36 km	(-1,206, -2,059.2)	(2,466, 1,144.8)	102	89	23
12 km Grid Domain	12 km x 12 km	(-414, -367.2)	(414, 532.8)	69	75	23
4 km Grid Domain	4 km x 4 km	(-330, -247.2)	(186, 88.8)	129	84	23

The vertical resolution and coordinates for the WRF modeling are based on the terrain-following sigma coordinate system, which ranges from 1 at the surface to 0 at the model top. A total of 23 vertical layers is used, with the upper boundary corresponding to a reference pressure of 100 hPa. The seasonal average pressure and height of each vertical

layer are presented in Table 4-2. The vertical layer structures of the 12 and 4 km domains are consistent with those of the 36 km domain. Tests of various layer structures were performed and the 23-layer case was found to provide the best overall performance. See section 4.4.3 below for further details.

The WRF model simulations employed the following physical parameterization schemes: the New Yonsei University (YSU) scheme for planetary boundary layer physics, the Unified Noah Land Surface Model (LSM) for land surface physics, the WRF Signle-Moment 6-Class (WSM6) Scheme for cloud microphysics, the New Tiedtke scheme for cumulus parameterization, identified by cu_physics = 16, as a newer, improved version of the original Tiedtke cumulus parameterization for simulating deep convection, the MM5 similarity scheme for the surface layer, and the more advanced of Rapid Radiative Transfer Model (RRTM) for longwave and shortwave radiation.

Table 4-2. Typical pressures and heights for the 23 vertical layers in WRF

Layer	Vertical Layer Pressure (hPa)	Vertical Layer Height (m)
23	121	16,048
22	227	13,946
21	395	8,793
20	501	5,576
19	543	4,921
18	586	4,307
17	628	3,729
16	670	3,183
15	721	2,664
14	772	1,979
13	811	1,516
12	836	1,160
11	853	987
10	870	816
9	887	648
8	900	482
7	909	400
6	917	319
5	926	238
4	932	158
3	936	119
2	941	79
1	945	39

4.3. Model Inputs and Initial/Boundary Conditions

The fifth generation of ECMWF atmospheric reanalysis dataset (ERA5; ID: ds633.0) was obtained from the National Center for Atmospheric Research (NCAR) Computational Information Systems Laboratory (CISL) and used as input to the WRF modeling. The WRF Preprocessing System (WPS) was employed to prepare the ERA5 data for real-data simulations. A customized shell script was used to automate the WPS workflow, which included the following steps: 1) Defining the coarse parent domain and fine nested domains; 2) Computing geospatial parameters such as latitude, longitude, map scale factors, and Coriolis parameters at each grid point; 3) Interpolating static terrestrial datasets to the simulation grids; 4) Using a NCAR-developed Python package to convert the ERA5 data into immediate files compatible with metgrid.exe program; and 5) Transferring time-varying meteorological data at standard hourly or 3-hour intervals.

Land use and land cover data inputs were primarily sourced from the National Land Cover Database (NLCD) CONUS 30-meter dataset, provided by the Multi-Resolution Land Characteristics (MRLC) consortium (https://www.mrlc.gov). As a secondary source, MODIS MCD12Q1 2023 annual land cover at 500-meter resolution was obtained from NASA Earthdata (https://earthdata.nasa.gov).

Two observational datasets were ingested for data assimilation: 1) NCEP ADP Global Surface Observational Weather Data, and 2) NCEP ADP Global Upper Air Observational Weather Data. These datasets were processed using OBSGRID utility, which performed quality control and converted the observations into little-R format files (OBS_DOMAINS101, OBS_DOMAINS201, and OBS_DOMAINS301) corresponding to each modeling domain. Grid analysis and observational nudging were subsequently applied across all modeling domains, presumably through Four-Dimensional Data Assimilation (FDDA) to guide the model toward observed atmospheric states.

Additionally, the surface FDDA option in OBSGRID was used to generate surface analysis files (wrfsfdda_d01, wrfsfdda_d02, and wrfsfdda_d01), which were incorporated during the WRF simulation to enhance surface-level assimilation.

The meteorological initial conditions for each modeling domain, along with lateral boundary conditions for the outmost domain (36 km resolution) were generated by the "real.exe" program using the data prepared by WPS. During WRF.exe simulation, two-way nesting was employed, allowing the parent domain to dynamically provide lateral boundary conditions to its nested (child) domains in real time.

4.4. Meteorological Model Performance Evaluation

Meteorological performance evaluation focuses on four key variables: temperature and water vapor mixing ratio at 2 m above ground level, and wind speed (WS) and wind direction (WD) at 10 m above ground level. The hourly surface observational database (i.e., METAR) and upper-air sounding data from the Meteorological Assimilation Data Ingest System (MADIS) within the modeling domain will serve as the primary WRF validation dataset. METAR includes observations from the Automated Surface Observing System (ASOS), Automated Weather Observing System (AWOS) and non-automated reports. MADIS RAdiosonde Observation (RAOB) dataset provides wind, temperature, moisture and geopotential height at multiple atmospheric pressure levels from stations across North America.

To evaluate planetary boundary layer height (PBLH), data were utilized from the Unified Ceilometer Network, a ground-based lidar system primarily designed for cloud detection but capable of resolving the vertical structure of the lower atmosphere. Ceilometers provide valuable measurements of mixing layer height (MLH), a critical variable for pollutant dilution and accurate air quality forecasts. For this study, MLH was measured hourly at the JLG Supersite in Arizona, supporting a three-dimensional assessment of chemical and dynamical processes in the lower atmosphere.

For comparison, a separate PBLH was also calculated with the AERMET model using three 2023 datasets: 1) 1- and 5-minute wind data from the Automated Surface Observing Systems (ASOS) network at Phoenix Sky Harbor; 2) hourly surface meteorological data from the National Weather Service (NWS) at Phoenix Sky Harbor; and 3) upper air radiosonde data (WMO ID: 74626) located near the Phoenix Zoo from the Integrated Global Radiosonde Archive (IGRA) dataset for the period of June 19 to September 15, 2023.

Model performance is quantified using standard statistical metrics, including correlation coefficient (R), standard deviation (SD), mean absolute error (MAE), mean bias (MB), and root mean square error (RMSE). The latest version of the Atmospheric Model Evaluation Tool (AMET v1.5) was used for WRF evaluation. AMET scripts first pair observations and gridded model output in space and time, then provide a suite of analysis methods to assess model skill for both predicted and derived atmospheric fields.

4.4.1. Comparison against Ground-Based Observations

Table 4-3 summarizes the statistical performance of WRF for near-surface meteorological variables during the modeling period (April 1–September 30), while Figure 4-2 provides a time series comparison for July to further illustrate these results. We focus on July because it represents the most challenging month for meteorological modeling in the region. This period corresponds to the peak of the North American monsoon, characterized by frequent monsoon thunderstorms, elevated humidity, and extreme heat events that frequently coincide with ozone exceedances. Central and southern Arizona, including Phoenix, Tucson, and the surrounding desert regions, are strongly affected by these conditions.

As shown in Table 4-3, the model reproduces temperature and water vapor mixing ratio with high skill. Correlations with observations are strong (R = 0.94 for temperature and 0.95 for mixing ratio), with only a modest cold bias for temperature (–1.55 K) and negligible bias for mixing ratio (+0.10 g/kg). The RMSE values are within acceptable ranges (3.28 K and 1.18 g/kg, respectively). In the July time series (Figure 4-2), water vapor mixing ratio closely tracks daily and synoptic variations with minimal systematic bias. Temperature is also well represented, showing high correlation and realistic diurnal and day-to-day variability. However, the model exhibits a systematic cold bias at night, with nocturnal minima consistently underestimated by about 1–2 K. Overall, these results indicate that the model reproduces the thermodynamic state near the surface reasonably well.

The 10 m wind fields are less consistent. Wind speed shows only a modest correlation (R = 0.59), with a small negative bias (–0.40 m/s) and an RMSE of 1.89 m/s. This indicates that the model reproduces mean magnitudes reasonably well but struggles with temporal variability. The July time series shows that the model reproduces the diurnal pattern of stronger winds during the day and weaker winds at night, but tends to underpredict both daytime maxima and nighttime minima, resulting in a systematic low bias. Consequently, the overall correlation remains moderate (R ≈ 0.5), indicating limited skill in representing short-term variability despite capturing the general cycle.

Correlation is not reported for wind direction due to its circular nature. Wind direction exhibits the largest errors, with substantial variability (SD ≈ 54°) and large discrepancies (MAE ≈ 38°; RMSE ≈ 54°). Reported RMSE values for wind direction typically range from 60° to 80° in complex topographies (Jimenez et al., 2013), placing our results in a similar magnitude. Although the mean bias is small (+1.25° in July), the errors remain large, with frequent phase shifts between modeled and observed cycles. The model reproduces the

general diurnal rotation between daytime westerlies and nighttime easterlies, although the timing of transitions occasionally lags or leads the observations, reflecting the difficulty of representing localized circulations and directional shifts in the region.

Table 4-3. Statistical comparison of WRF performance for temperature, water vapor mixing ratio, wind direction, and wind speed during the modeling period (April 1–September 30) over the 4 km domain

Variables	R	SD	MAE	MB	RMSE
Temperature (K)	0.94	2.89	2.35	-1.55	3.28
Mixing Ratio (g/kg)	0.95	1.17	0.84	0.10	1.18
Wind Direction (deg)	-	54.24	38.20	3.86	54.38
Wind Speed (m/s)	0.59	1.85	1.43	-0.40	1.89

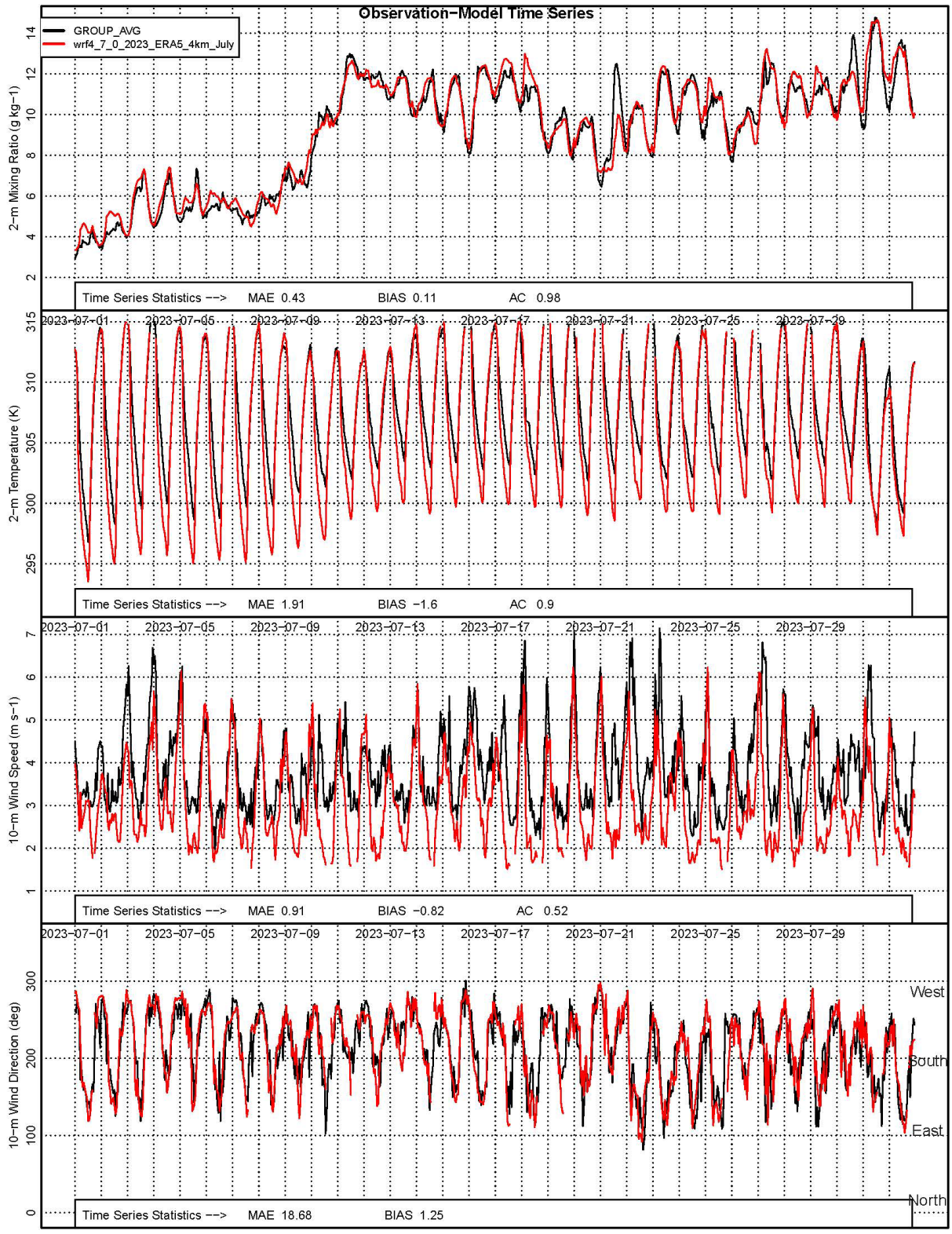

Figure 4-2. Time series comparison of observed and simulated near-surface meteorological variables (2-m mixing ratio, 2-m temperature, 10-m wind speed, and 10-m wind direction) for July 2023

4.4.2. Upper-Air/Vertical Structure and PBLH

Since surface conditions alone cannot fully explain model performance, it is also important to evaluate vertical profiles aloft, as they strongly influence boundary-layer mixing and the transport of ozone precursors. Figures 4-3 through 4-6 compare modeled and observed vertical profiles of relative humidity, temperature, wind direction, and wind speed at one valid sounding site (KTUS) located at Tucson, respectively.

Relative humidity is reasonably well reproduced by the model. Biases are within about −2% to +4% across most levels. RMSE is ~5–8% below ~700 hPa and increases to ~10–18% above 500 hPa. The IOA is around 0.8 in the boundary layer but decreases to 0.4–0.6 at mid- to upper-levels, suggesting some difficulties in capturing upper-level humidity variability. Overall, the model captures the vertical moisture structure near the surface, with reduced skill higher in the column.

Among the four variables, temperature shows the best agreement. Biases are small at all levels (generally within ±0.5 K), and the spread is narrow below ~500 hPa. RMSE is ~0.5–0.8 K in the boundary layer, increases to ~1–1.5 K in the mid-troposphere, and reaches ~2–3 K near 300 hPa. The IOA remains high (≥0.9) through most of the column, with only a slight reduction aloft. These results indicate that the model captures the vertical thermal structure well, with modest degradation only at upper levels.

The consistency between modeled and observed wind direction is relatively weak. The model shows little systematic bias (most values within ±2°). RMSE is largest in the boundary layer (~30° below 700 hPa) and decreases to ~10–20° at mid- and upper levels. Correlation/IOA is not reported for wind direction due to its circular nature. Thus, although the model avoids large directional shifts, it exhibits substantial variability, especially lower levels, which may contribute to frequently low wind speeds and highly stable conditions, complex terrain, and uncertainties in simulating vertical mixing.

Wind speed, which plays a key role in vertical mixing and ozone formation, is well represented in the lower troposphere. Below ~500 hPa, biases are minimal (within ±1 m/s) and RMSE values remain small (≤2 m/s), with IOA greater than 0.8, indicating very good agreement with observations. At higher levels (above ~500 hPa), the model shows larger deviations, with biases ranging from –3 to +1 m/s and RMSE increasing to 3–5 m/s. Overall, the model captures near-surface winds reliably, though biases and errors increase aloft.

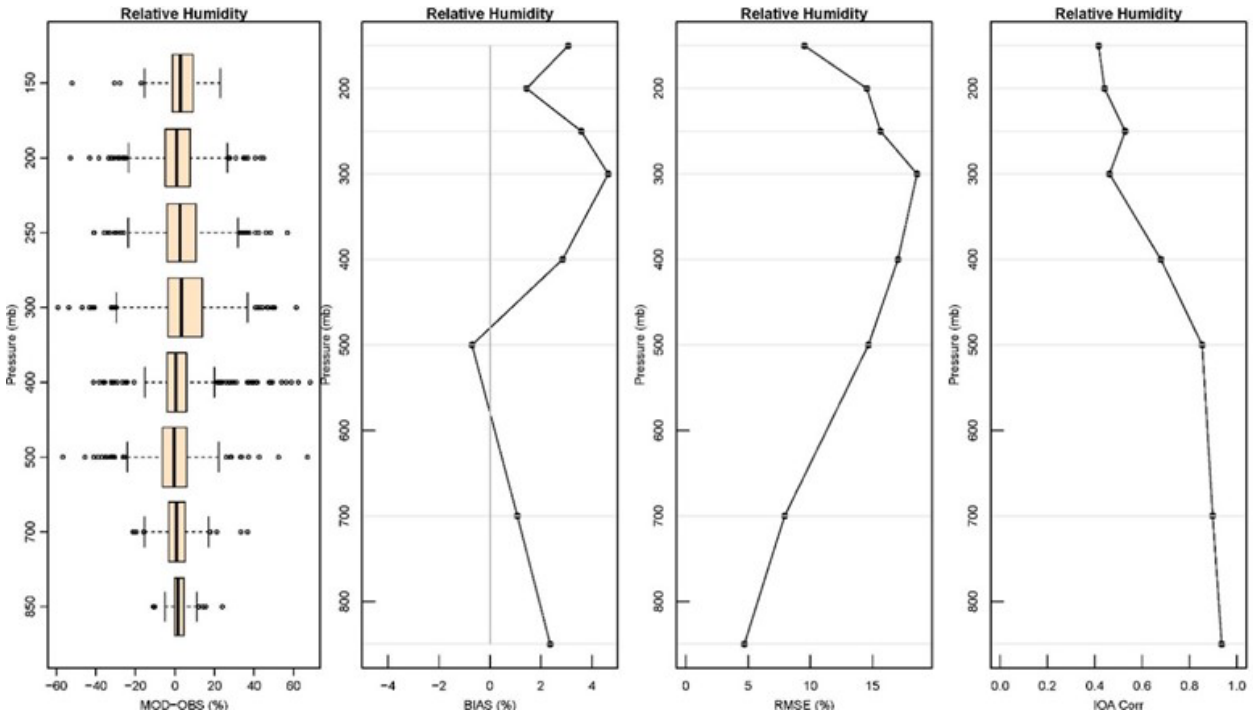

Figure 4-3. Vertical profiles for relative humidity at KTUS site in the 4 km domain

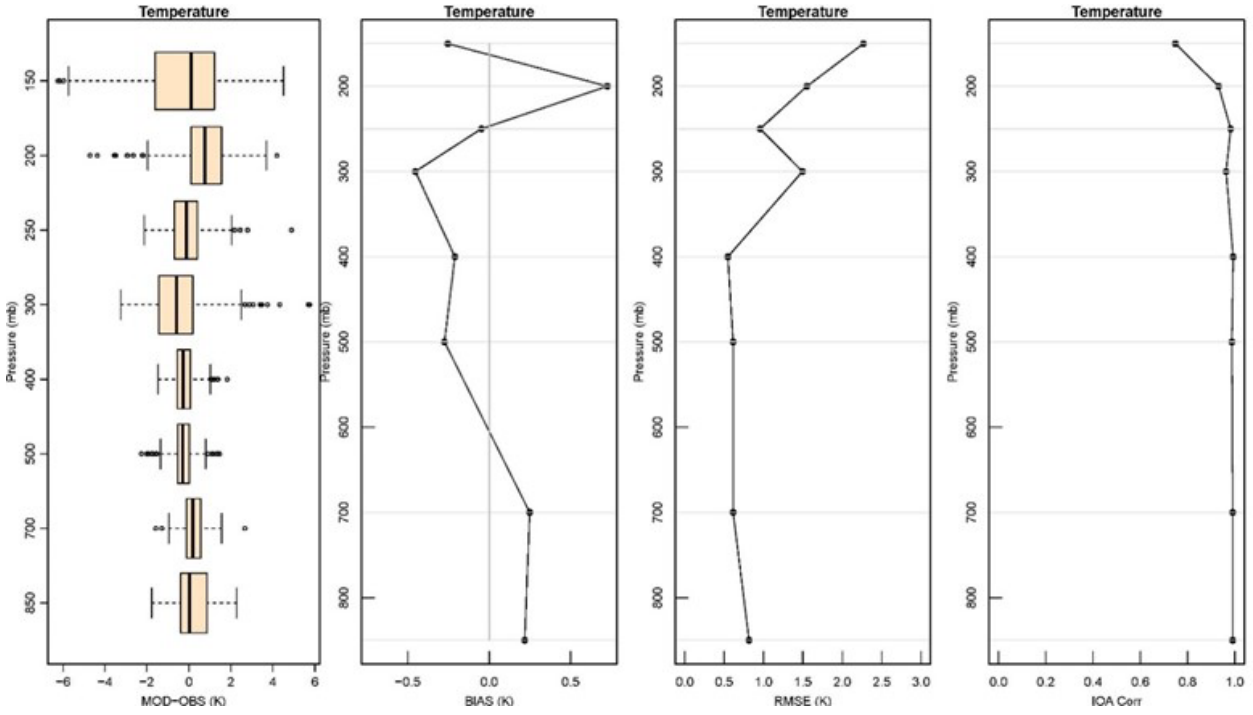

Figure 4-4. Vertical profiles for temperature at KTUS site in the 4 km domain

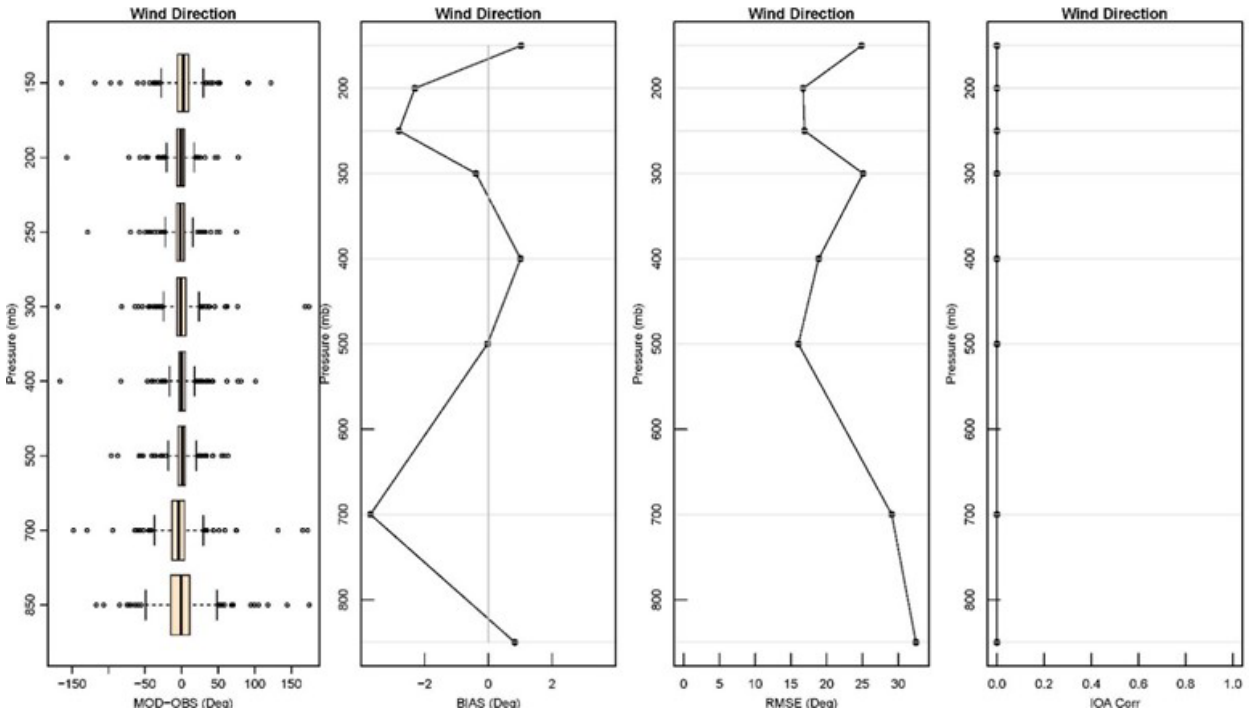

Figure 4-5. Vertical profiles for wind direction at KTUS site in the 4 km domain

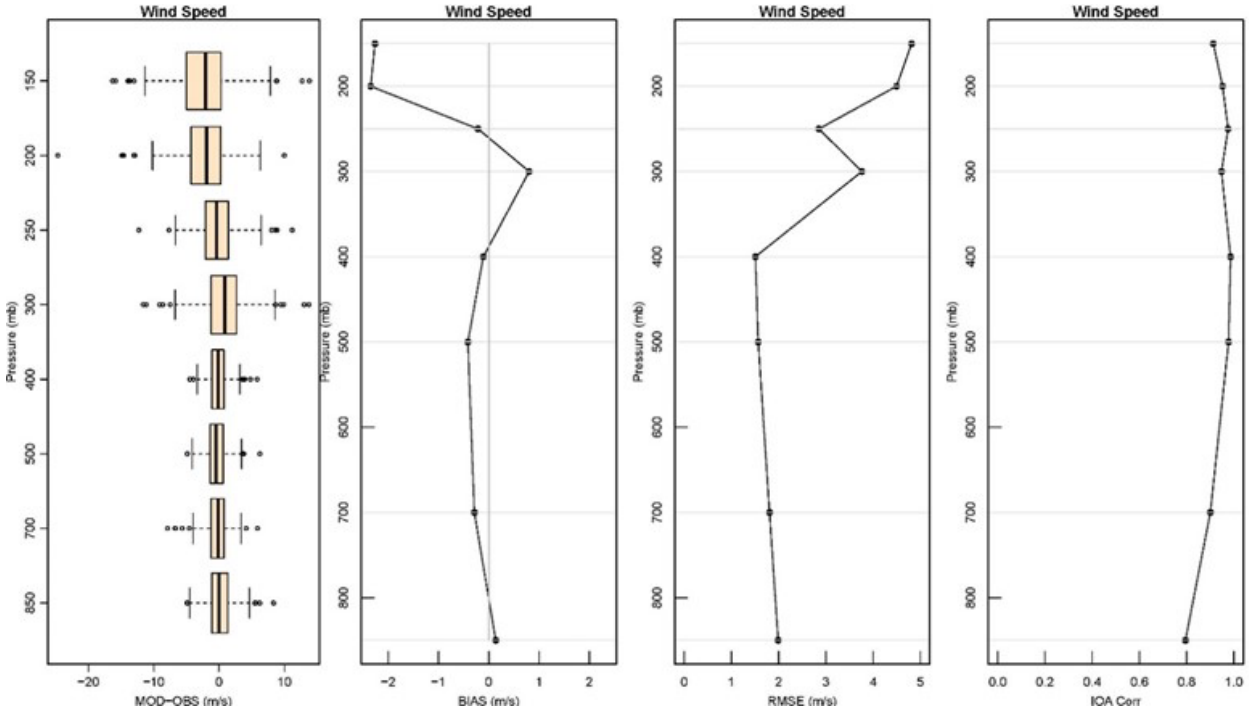

Figure 4-6. Vertical profiles for wind speed at KTUS site in the 4 km domain

Figure 4-7 shows ceilometer attenuated backscatter profiles over Phoenix with boundary layer height estimates from WRF and mixing heights derived from AERMET. The first part of the summer (April-June) is the pre-monsoon season with typically dry conditions, while the monsoon season begins in July, bringing moisture to the region with the change of circulation patterns. Two representative days are highlighted in the discussion: a pre-monsoon season case (June 24, 2023) and a monsoon season case (August 2, 2023). To provide additional context, two supplementary days (June 28 and August 7, 2023) are also included in the figure, which exhibit similar seasonal characteristics and support the comparisons drawn between pre-monsoon and monsoon conditions. These examples illustrate how boundary layer growth differs under contrasting seasonal regimes and how WRF compares with reference data.

Under pre-monsoon conditions, relatively clear and dry skies limited aerosol and moisture in the lower atmosphere, resulting in weaker and more confined backscatter signals. The ceilometer suggests that the morning mixing depth remained shallow (<500 m) until ~11 LST, then steadily deepened through midday (reaching ~2 km by early afternoon) before collapsing after ~18 LST. WRF captured the overall diurnal pattern but showed earlier morning growth than observed, with boundary layer heights beginning to rise by ~07 LST (~800–1000 m by 09 LST). The afternoon maximum (~2 km) was generally comparable to ceilometer retrievals but remained lower than AERMET estimates, which indicated a deeper and more sustained boundary layer (~3 km by 18 LST).

In contrast, the monsoon case shows stronger and vertically more extended backscatter returns, consistent with higher aerosol concentrations and elevated humidity. From the ceilometer retrievals, boundary layer growth was more vigorous, with mixing depths reaching ~1 km by ~09 LST and continuing to deepen through the afternoon (~3 km or more). Some attenuation in the profiles reflects the influence of water vapor, a known limitation of ceilometer retrievals under moist conditions. WRF reproduced the main features of the diurnal cycle, though with a slight delay in the morning growth compared to both ceilometer and AERMET. In the afternoon, WRF tracked the observed deepening more closely, with maximum heights (~3 km) similar to AERMET.

Overall, the two cases demonstrate that WRF provides a reasonable representation of the diurnal boundary layer cycle, although discrepancies remain in the timing and magnitude of growth, particularly under dry pre-monsoon conditions. Additional days (June 28 and August 7, 2023; see Figure 4-7) show similar pre-monsoon and monsoon characteristics, further supporting these conclusions. Accurate simulation of boundary layer dynamics is critical for surface ozone modeling in Phoenix.

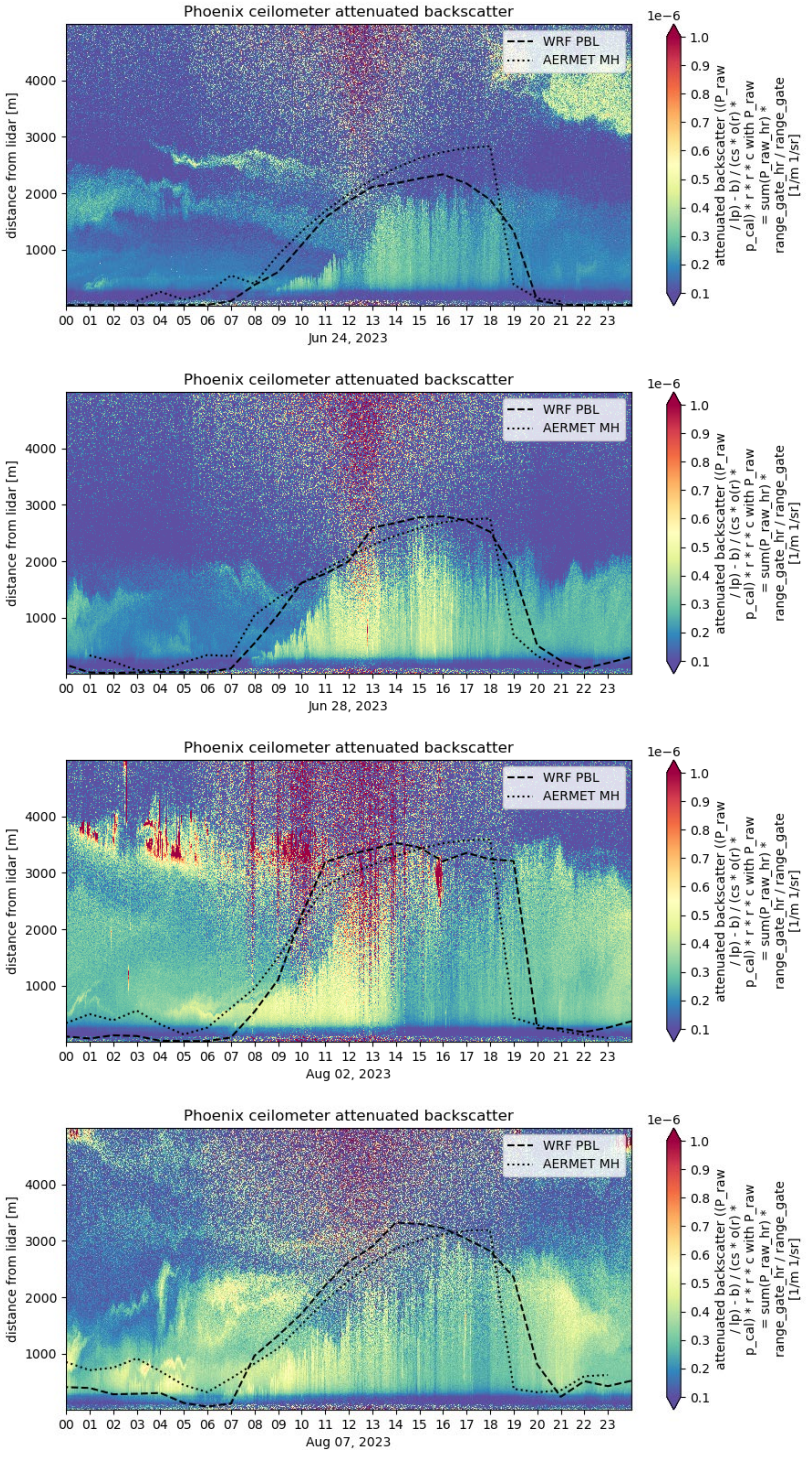

Figure 4-7. Ceilometer attenuated backscatter over Phoenix with WRF-predicted PBL height and AERMET-derived mixing height, shown for four days: two representative cases highlighted in the text (pre-monsoon season: June 24, 2023; monsoon season: August 2, 2023), and two supplementary examples (June 28 and August 7, 2023) illustrating consistent seasonal patterns

4.4.3. Justification of WRF Vertical Layer Configuration Choices

Another commonly applied WRF configuration is for 35 vertical layers extending up to 50 mb. Table 4-4 represents this structure, which has been used in previous studies (e.g., U.S. EPA, 2014 and 2021). This configuration provides enhanced resolution of the planetary boundary layer (PBL) by placing the lowest model layer near 19 m above ground level, compared with the 23-layer configuration used in this study, which has a first-layer height of approximately 40 m. To evaluate the sensitivity of the modeling results to vertical structure and physics options, two additional WRF sensitivity simulations were conducted, with the 23-layer base case denoted as WRF_L23_MAG:

- **WRF_L35_MAG:** Applied 35 vertical layers for all three nested domains, while retaining the same physics options as the base case (WRF_L23_MAG).
- **WRF_L35_EPA:** The physics configuration described in U.S. EPA (2021) was adopted, with 35 vertical layers applied to two nested domains (36 km and 12 km). Only two nested domains are used because WRF crashed and failed to complete within the inclusion of the 4 km domain as a third nested domain no matter using hybrid vertical coordinate or original WRF terrain-following coordinate, due to numerical instability, overly restrictive physical scheme constrains, and an improper first-layer configuration. Further testing and investigation is required to identify the specific causes and develop robust solutions, so the 4 km domain is excluded from this test. The physics differences from the base case WRF include:
    - **Microphysics:** Morrison Double-moment scheme (WRF_L35_EPA) vs. WRF Single-moment 6-class scheme (WRF_L23_MAG).
    - **Planetary boundary layer:** ACM2 scheme (WRF_L35_EPA) vs. YSU scheme (WRF_L23_MAG).
    - **Surface layer:** Pleim-Xiu scheme (WRF_L35_EPA) vs. MM5 Similarity scheme (WRF_L23_MAG).
    - **Land surface model:** Pleim-Xiu LSM (WRF_L35_EPA) vs. Unified Noah LSM (WRF_L23_MAG).

Results from these two sensitivity simulations are presented below to evaluate the impacts of vertical resolution and physics options and to support the selection of the 23-layer configuration used in this study.

Table 4-4. Typical pressures and heights for the 35 vertical layers in WRF

Layer	Vertical Layer Pressure (Pa)	Vertical Layer Height (m)
35	72	20,037
34	117	16,369
33	162	14,106
32	206	12,383
31	251	10,970
30	296	9,758
29	340	8,692
28	385	7,738
27	430	6,873
26	474	6,082
25	519	5,352
24	564	4,674
23	609	4,039
22	653	3,442
21	694	2,877
20	725	2,446
19	752	2,134
18	775	1,830
17	793	1,633
16	811	1,438
15	829	1,248
14	847	1,060
13	860	876
12	869	785
11	878	695
10	887	605
9	896	517
8	906	429
7	915	342
6	924	255
5	930	169
4	935	127
3	939	84
2	943	42
1	945	21

Table 4-5 summarizes the statistical comparison of WRF performance over the 12 km domain for the base case and two sensitivity tests. All simulations show high correlations (R = 0.92–0.97) and low biases for temperature and water vapor mixing ratio, indicating good agreement between modeled and observed values. The WRF_L35_EPA case provides the best performance for temperature (MB = –0.73 K, RMSE = 2.52 K) but the worst performance for mixing ratio (MB = 0.79 g/kg, RMSE = 1.64 g/kg). Wind direction is relatively poorly simulated in all cases, with RMSE ranging from 56° to 59°, while wind speed performance is moderate. Performance for wind speed and direction is generally comparable across the three cases. The complex terrain of the Phoenix region makes simulating local wind fields particularly challenging, as it strongly affects local circulation patterns.

Specifically comparing WRF_L23_MAG and WRF_L35_MAG over the 12 km domain, the two cases are configured with identical physics schemes and differ only in the number of vertical layers. Overall, their performance is nearly indistinguishable. WRF_L35_MAG shows marginal improvements for all four variables. For temperature, the errors are slightly reduced relative to WRF_L23_MAG (MAE = 2.37 K vs. 2.41 K; MB = –1.40 K vs. –1.41 K; RMSE = 3.19 K vs. 3.23 K). For wind direction, WRF_L35_MAG reduces RMSE by about 2.6° (56.35° vs. 58.96°) and slightly lowers MAE and MB as well. For wind speed, performance is also marginally better (RMSE = 1.98 m/s vs. 2.03 m/s). For mixing ratio, the performance is essentially identical, with the same MAE (0.80 g/kg) and negligible differences in MB (–0.07 g/kg vs. –0.04 g/kg) and RMSE (1.15 g/kg vs. 1.18 g/kg). These results suggest that increasing the vertical layers from 23 to 35 provides only minimal improvement for the 12 km domain, with nearly equivalent overall performance across the two configurations.

It should be noted that the WRF_L35_EPA case successfully completed for the two nested 36 and 12 km domains, outperforming the other cases in temperature and showing slight improvements in wind speed, though underperforming in mixing ratio and introducing a noticeable positive bias in 12 km domain. However, it failed to complete for the 4 km domain due to numerical instabilities. Accordingly, the configuration with 35 vertical layers and EPA physics is not adopted in this work, and model performance results for WRF_L35_EPA on the 4 km domain are excluded from the following discussion.

Table 4-5. Statistical comparison of WRF performance for temperature, water vapor mixing ratio, wind direction, and wind speed during the modeling period (April 1–September 30) over the 12 km domain for the base case (WRF_L23_MAG) and two sensitivity tests (WRF_L35_MAG and WRF_L35_EPA)

Variables	Scenarios	R	SD	MAE	MB	RMSE
Temperature (K)	WRF_L23_MAG	0.95	2.91	2.41	-1.41	3.23
	WRF_L35_MAG	0.95	2.87	2.37	-1.40	3.19
	WRF_L35_EPA	0.97	2.41	1.88	-0.73	2.52
Mixing Ratio (g/kg)	WRF_L23_MAG	0.95	1.15	0.80	-0.04	1.18
	WRF_L35_MAG	0.95	1.14	0.80	-0.07	1.15
	WRF_L35_EPA	0.92	1.43	1.15	0.79	1.64
Wind Direction (deg)	WRF_L23_MAG	-	58.48	42.21	7.51	58.96
	WRF_L35_MAG	-	57.99	41.57	6.40	56.35
	WRF_L35_EPA	-	57.64	41.34	6.30	57.98
Wind Speed (m/s)	WRF_L23_MAG	0.63	2.01	1.53	-0.22	2.03
	WRF_L35_MAG	0.62	1.97	1.50	-0.17	1.98
	WRF_L35_EPA	0.66	1.80	1.41	-0.56	1.89

WRF model performance was evaluated further for WRF_L23_MAG and WRF_L35_MAG on the 4 km domain. Table 4-6 shows that WRF_L35_MAG performs comparably to WRF_L23_MAG (Table 4-3). Minor differences were observed: temperature performance was slightly degraded (MB more negative by 0.09 K, RMSE increased by 0.05 K); mixing ratio performance was slightly improved (MB decreased by 0.04 g/kg, RMSE nearly unchanged); and wind direction and wind speed showed small improvements (wind direction MB decreased by 1.02°, RMSE decreased by 0.54°; wind speed MB increased by 0.08, RMSE decreased by 0.03). The time series in Figure 4-8 shows very comparable performance for all parameters relative to Figure 4-2.

Figures 4-9 through 4-12 present the vertical profile evaluation for WRF_L35_MAG, for comparison with Figures 4-3 through 4-6 (WRF_L23_MAG). Relative humidity shows a slight improvement in capturing upper-level variability, particularly above ~500 hPa, while model skill in lower levels remains comparable. RMSE values are similar in the lower troposphere but slightly reduced aloft, and the index of agreement remains high in lower levels with modest improvement at mid-levels. For temperature, the WRF_L35_MAG

simulation exhibits marginally smaller biases across most levels. RMSE values are slightly larger near the surface but reduced in the mid- to upper troposphere. The IOA stays very high (≥0.9) throughout the column, with even less degradation aloft, indicating that the vertical thermal structure is captured equally well, with modest improvements relative to WRF_L23_MAG. For wind direction, the WRF_L35_MAG case shows slightly larger biases at several lower levels (up to ~5–10°). RMSE increases notably in the boundary layer (reaching ~40–50°), while mid- and upper-level errors remain comparable. For wind speed, WRF_L35_MAG exhibits more consistent performance throughout the vertical profile, though it slightly overestimates wind speed at the surface and underestimates it in the lower levels compared with WRF_L23_MAG.

Table 4-6. Statistical comparison of WRF performance for temperature, water vapor mixing ratio, wind direction, and wind speed during the modeling period (April 1–September 30) over the 4 km domain for the WRF_L35_MAG sensitivity test

Variables	R	SD	MAE	MB	RMSE
Temperature (K)	0.94	2.90	2.36	-1.64	3.33
Mixing Ratio (g/kg)	0.95	1.17	0.83	0.06	1.18
Wind Direction (deg)	-	53.76	37.63	2.84	53.84
Wind Speed (m/s)	0.57	1.84	1.41	-0.32	1.86

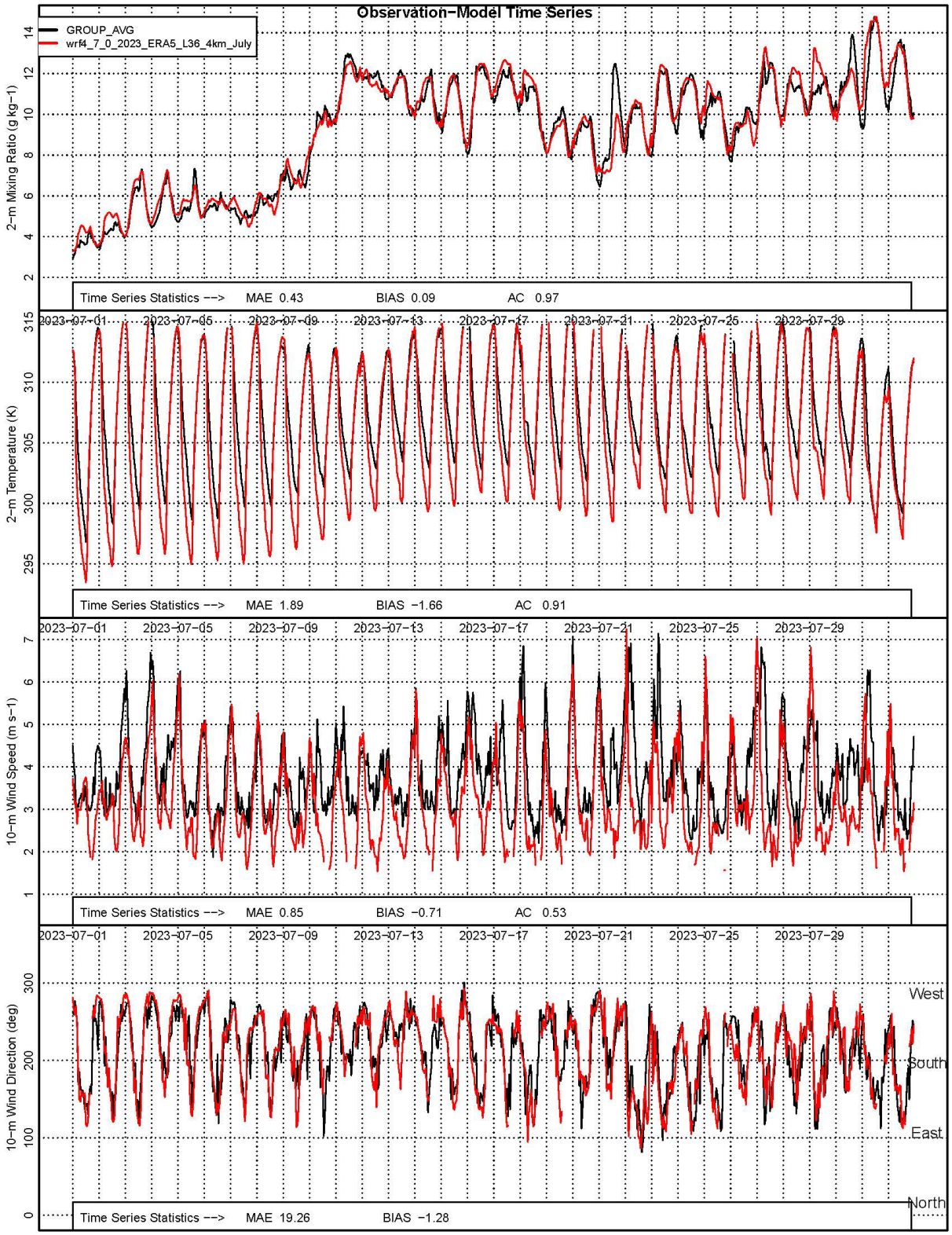

Figure 4-8. Time series comparison of observed and simulated near-surface meteorological variables (2-m mixing ratio, 2-m temperature, 10-m wind speed, and 10-m wind direction) in July for the WRF_L35_MAG sensitivity test

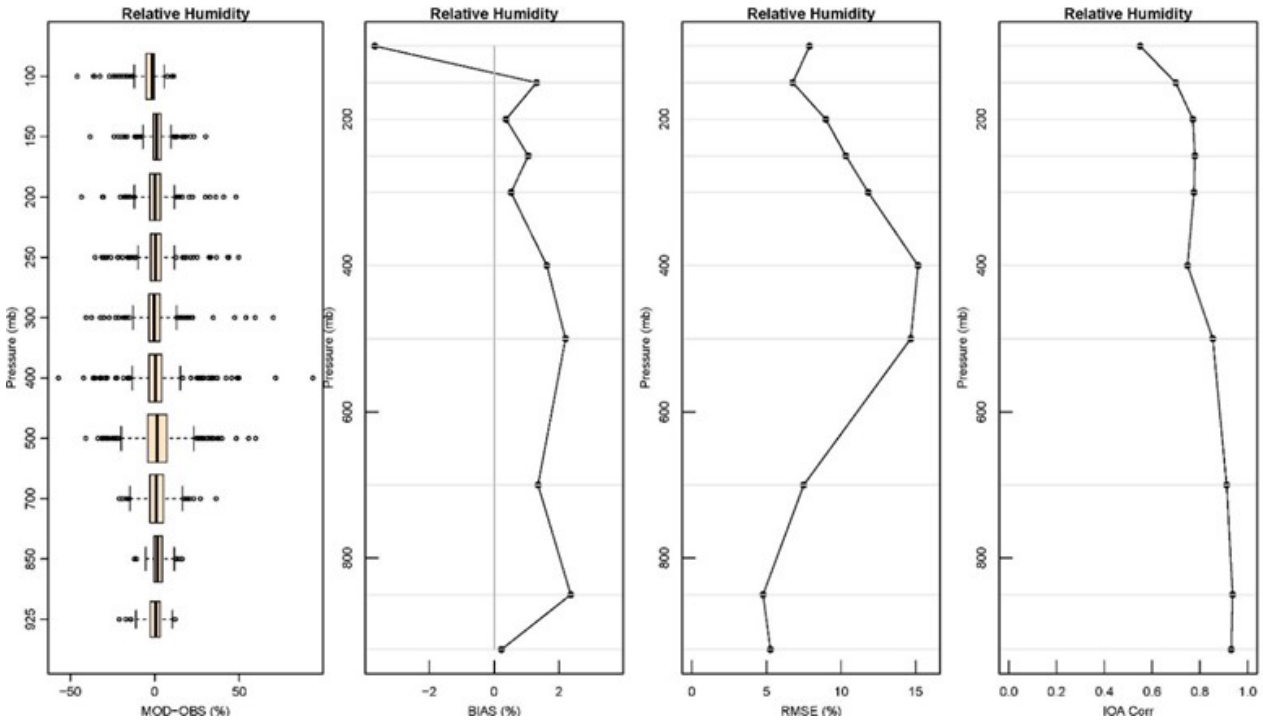

Figure 4-9. Vertical profiles for relative humidity for the WRF_L35_MAG sensitivity test

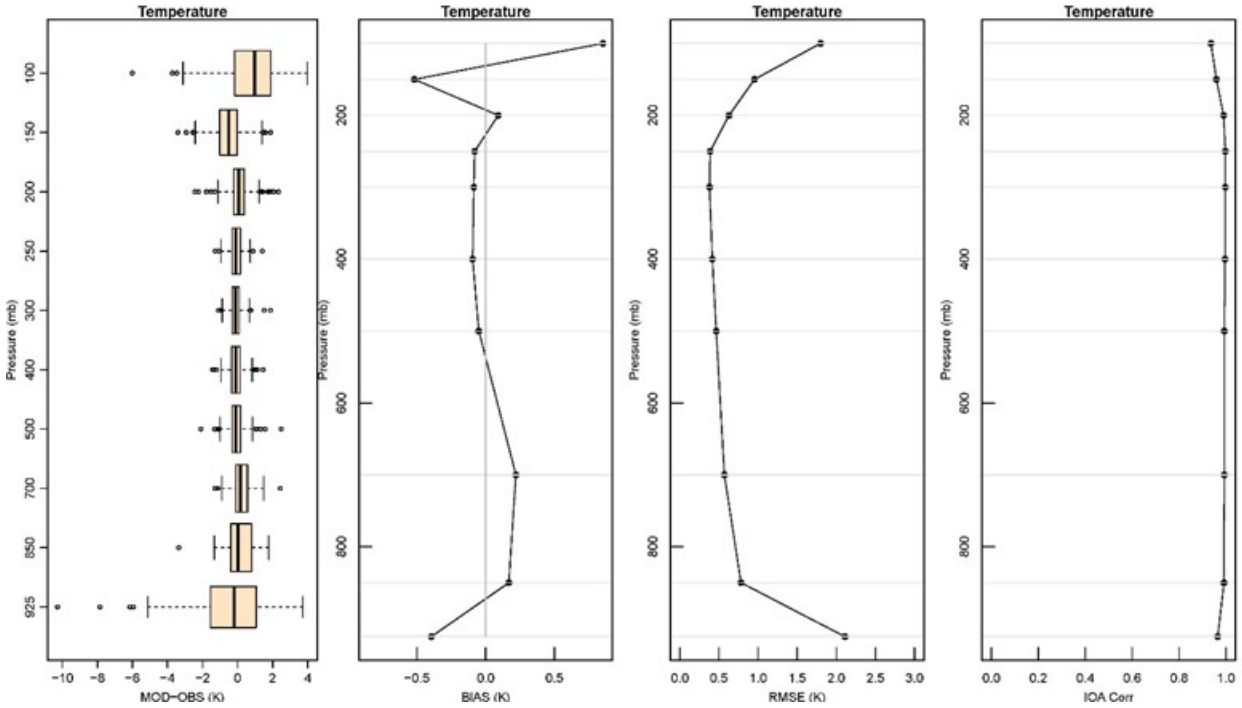

Figure 4-10. Vertical profiles for temperature for the WRF_L35_MAG sensitivity test

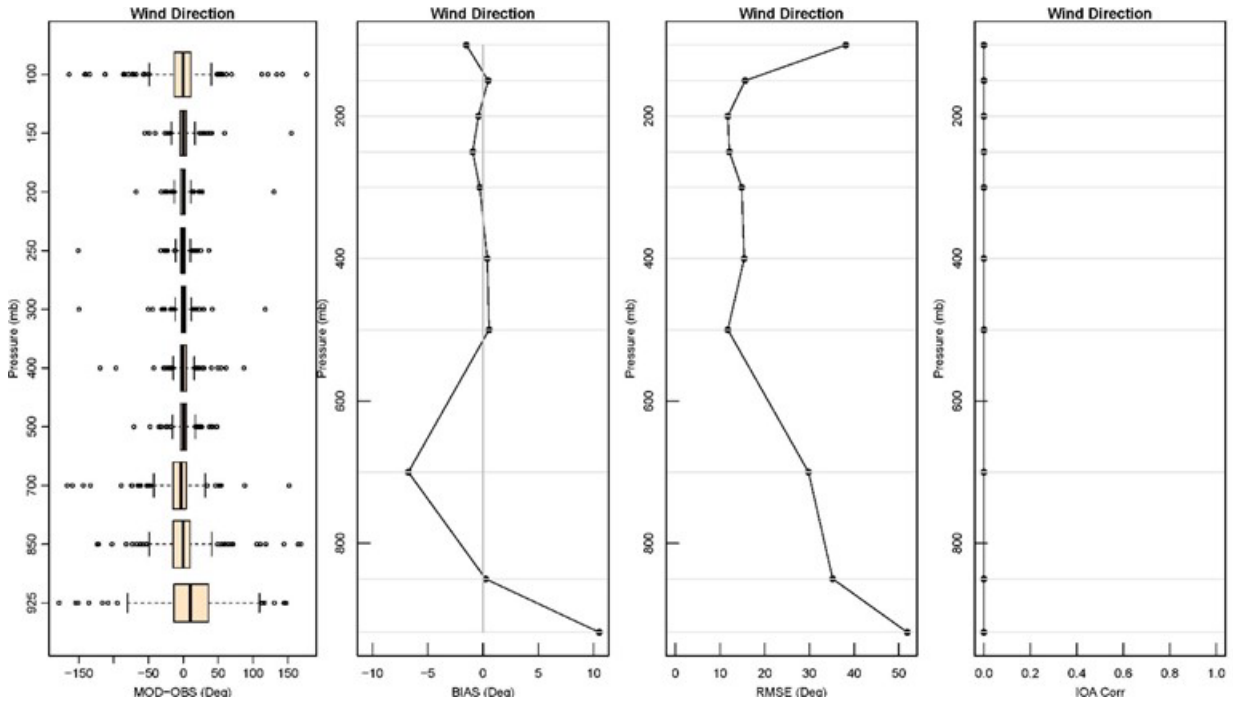

Figure 4-11. Vertical profiles for wind direction for the WRF_L35_MAG sensitivity test

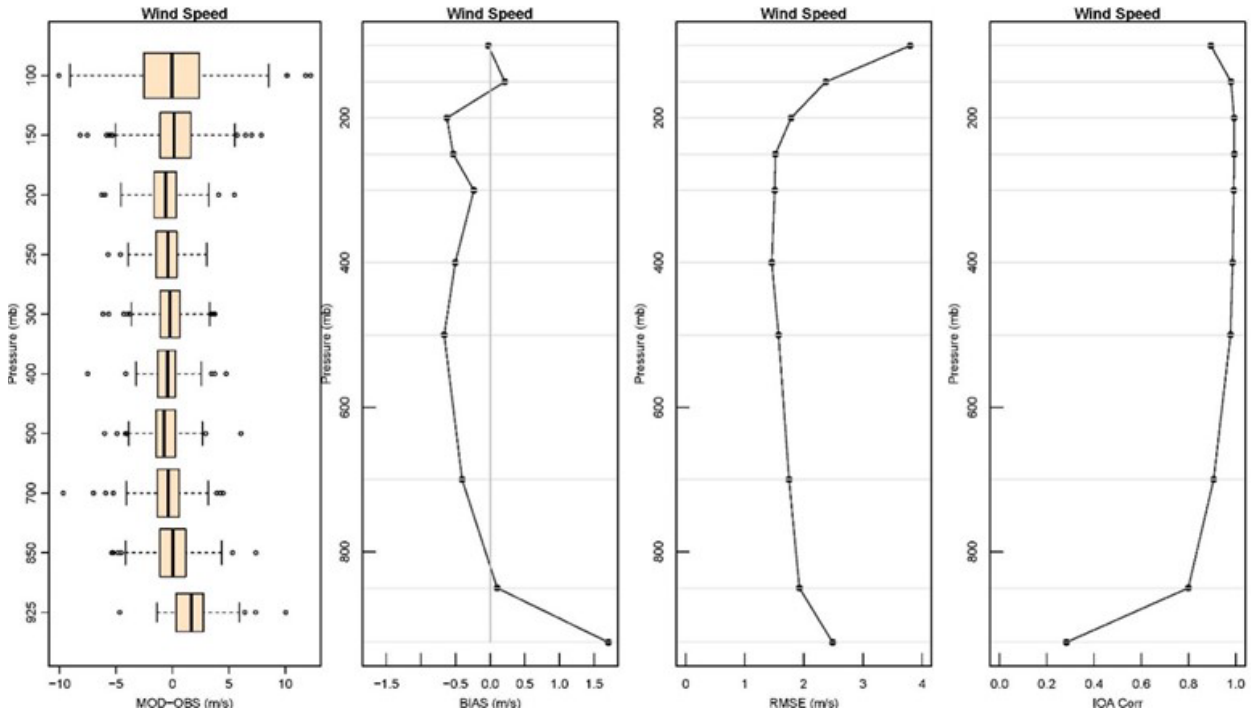

Figure 4-12. Vertical profiles for wind speed for the WRF_L35_MAG sensitivity test

4.5. Meteorology and Chemistry Interface Processing

Outputs from the WRF model require specific preprocessing before utilization in air quality and emissions modeling systems. For use with CAMx, WRF outputs are processed using a suite of CAMx-specific preprocessing tools, which include *wrfcamx_v5.2*, *watermask_ncf*, and *kvpatch_v6nc*. These tools adapt the WRF meteorological data to meet the input format and structural requirements of CAMx.

Similarly, for simulations with the CMAQ model, WRF outputs are processed by the Meteorology-Chemistry Interface Processor (MCIP v5.5). This step is critical for maintaining dynamic consistency between the WRF-generated meteorological fields and the CMAQ chemical transport model.

The processed meteorological data fields derived from these respective pathways (i.e., data processed by *wrfcamx_v5.2* et al. for CAMx and MCIP-processed data for CMAQ) serve as essential inputs for:

- The CAMx and CMAQ photochemical air quality models.
- The Model of Emissions of Gases and Aerosols from Nature (MEGAN) for the characterization of biogenic emissions.
- The Sparse Matrix Operator Kernel Emissions (SMOKE) system

5. PHOTOCHEMICAL GRID MODELING PLATFORM

5.1. Modeling System Overview

A variety of emissions, meteorology, and air quality models are needed to perform a full modeling evaluation and source apportionment analyses. The models used in this study meet EPA's guidance criteria: they have undergone peer review, are based on sound theory, have demonstrated good performance in past studies, and are well documented. The most commonly used photochemical air quality models for ozone attainment demonstration are CAMx and CMAQ. Both models provide useful tools such as the Ozone Source Apportionment Technology (OSAT) in CAMx and the Integrated Source Apportionment Method (ISAM) in CMAQ, as well as the Decoupled Direct Method (DDM), which have been used in many photochemical modeling applications to evaluate the contributions of pollutants, source categories, and source regions to local ozone concentrations as well as emissions sensitivities. Figure 5-1 illustrates the MAG air quality modeling system flowchart with CAMx version 7.32 as the core model and CMAQ version 5.5 as the secondary model. All anthropogenic, biogenic, and fire emissions inventories for CAMx and CMAQ were developed using multiple emissions processing tools such as SMOKE 5.1, MOVES 4.0, AEDT 3g, and MEGAN 3.2. The WRF version 4.7.0 was used to develop meteorological input data for CAMx and CMAQ.

5.2. Photochemical Model Configurations

In this study, CAMx was used as the core photochemical model and CMAQ as the secondary photochemical model. CAMx requires a namelist control file specifying input files and model configuration such as model clock control, map projection parameters, modeling grid parameters, model options, and output specifications. Tables 5-1 and 5-2 summarize the CAMx and CMAQ model configurations applied for the study, respectively. The CAMx configuration was set up to perform two-way grid nesting on the 36, 12, and 4 km modeling domains. Three-dimensional initial and boundary conditions (ICBC) for the 36 km master domain were developed from the GEOS-Chem version 14.6.1 global chemistry model and extracted using GEOS2CAMx version 4.1. The WRF meteorological fields were processed for CAMx using WRFCAMx version 5.2 pre-processor. The O3MAP pre-processor was used to prepare albedo/haze/ozone column inputs for CAMx from TOMS data. The photolysis inputs were generated using TUV pre-processor.

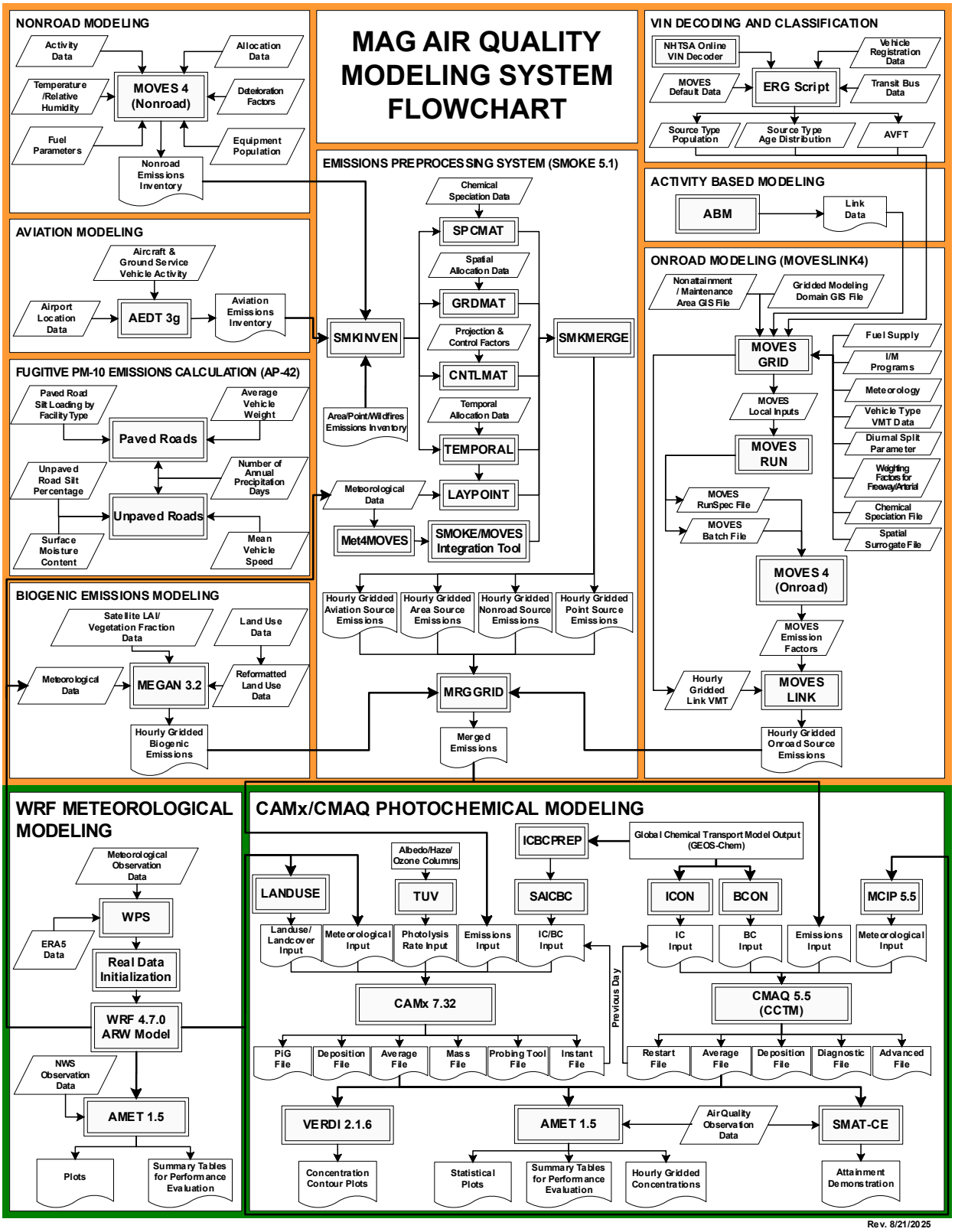

Figure 5-1. MAG air quality modeling system flowchart

Table 5-1. CAMx modeling configuration

Science Options	CAMx Modeling Schemes	Comment
Photochemical Model	CAMx v7.32 – August 2025	
Horizontal Grid	36/12/4 km	LCC Projection
• 36 km Grid	92 x 79 cells	
• 12 km Grid	59 x 65 cells	
• 4 km Grid	56 x 47 cells	
Vertical Grid	23 vertical layers	
Grid Interaction	36/12/4 km two-way nesting	
Initial Condition	GEOS-Chem, GEOS2CAMX v4.1	
Boundary Condition	GEOS-Chem, GEOS2CAMX v4.1	
Emissions	EPA's 2022 Emissions Modeling Platform, MAG 2023 emissions inventory, SMOKE v5.1	
Meteorological Data	WRF 4.7.0	
Meteorological Processor	WRFCAMx v5.2, YSU Kv, KVPATCH v6	Compatible with CAMx v7.32
Chemistry Parameters	CB7r1_CF3_SIMPLE_NoEvap	CB7 revision 1 Coarse/Fine aerosol treatment
Chemistry Solver	Euler Backward Iterative (EBI)	Efficient and accurate solver
Horizontal Advection	Piecewise Parabolic Method (PPM)	Eulerian continuity equation
Horizontal Diffusion	Explicit simultaneous 2-D solver	K-theory 1st order closure
Vertical Advection	Implicit backward-Euler hybrid centered/upstream solver	Eulerian continuity equation
Vertical Diffusion	Implicit backwards-Euler centered solver	Standard K-theory approach
Dry Deposition Scheme	Resistance model for gases and aerosols (ZHANG dry deposition)	ZHANG03
Wet Deposition Scheme	Exponential decay as a function of scavenging coefficient	Scavenging model for gases and aerosols

Table 5-2. CMAQ modeling configuration

Science Options	CMAQ Modeling Schemes	Comment
Photochemical Model	CMAQ v5.5 – September 9 2024	
Horizontal Grid	36/12/4 km	LCC Projection
• 36 km Grid	92 x 79 cells	
• 12 km Grid	59 x 65 cells	
• 4 km Grid	56 x 47 cells	
Vertical Grid	23 vertical layers	
Grid Interaction	36/12/4 km one-way nesting	
Initial and Boundary Condition	aqmbc for GEOS-Chem v14	aqmbc: a python tool to make initial and boundary conditions for CMAQ.
Emissions	EPA's 2022 Emissions Modeling Platform, MAG 2023 emissions inventory, SMOKE v5.1	
Meteorological Data	WRF 4.7.0	
Meteorological Processor	Meteorology-Chemistry Interface Processor (MCIP v5.5)	Compatible with CMAQ v5.5
Chemistry Mechanism	cb6r5_ae7_aq	aero7: aerosol chemistry module
Gas Phase Chemistry Solver	Euler Backward Iterative (EBI)	Efficient and accurate solver
Horizontal/Vertical Advection	3-D Advection Scheme (wrf_cons)	piecewise parabolic method (PPM)
Horizontal Diffusion	hdiff/multiscale	the approach of Smagorinsky
Vertical Diffusion	vdiff/acm2_m3dry	the Asymmetrical Convective Model Version 2 (ACM2) with m3dry
Dry Deposition Scheme	m3dry	Multi-layer Model for Dry Deposition
Wet Deposition Scheme	Wet deposition is calculated through in-cloud and below-cloud scavenging.	

The modeling period extends from April through September of 2023 since ozone exceedances have occurred mostly during April to September over the past 25 years. As suggested in EPA's modeling guidance, the length of the model spin-up period was set to two weeks (April 1 to 14) to minimize the influence of initial conditions (IC).

5.3. Modeling Domains, Grid Resolution, and Layer Structure

Horizontal Domain

Selection of the modeling domains takes into account the Maricopa NAA boundaries, the distribution of major emissions sources, the location of the meteorological and air quality monitoring sites, and the prevailing winds associated with elevated ozone concentrations as well as regional air pollutant transport. Figure 5-2a shows the spatial relationship among the master (36 km grid resolution), the first-nested (12 km grid resolution), and the second-nested (4 km grid resolution) modeling domains of CAMx and CMAQ models. Figure 5-2b illustrates the inner modeling domain comprised of 4-by-4 km grid cells that cover the Maricopa NAA, Maricopa County, and portions of Pinal, Gila, and Yavapai counties.

Since ozone concentrations in the Maricopa NAA can be substantially influenced by transported ozone and ozone precursor emissions from outside the Maricopa NAA (U.S. EPA, 2015), the master 36 km grid modeling domain (36 km domain) covers the southwestern U.S. and Mexico. The extensive coverage of the master modeling domain of CAMx/CMAQ is designed to capture the characteristics of long-range transport of ozone and ozone precursor emissions from neighboring states and Mexico to the Maricopa NAA. The 36 km domain is used to generate initial and boundary conditions to the 12 km grid modeling domain (12 km domain). The 12 km modeling domain is used to provide boundary and initial condition data to the core 4 km grid modeling domain (4 km domain). The CAMx/CMAQ model evaluation is performed at the monitors in the Maricopa NAA in the 4 km domain. The CAMx/CMAQ modeling domain configurations are provided in Table 5-3.

The CAMx/CMAQ inner 4 km domain encompasses the Maricopa NAA, consisting of 56 grid cells in the west-east direction and 47 grid cells in the south-north direction. The origin of the modeling domain (the southwest corner of the inner domain) is located at -130.000 km easting and -119.200 km northing, relative to the central point at 112° W and 33.5° N, using the Lambert Conformal Conic (LCC) projection. The domain comprises approximately 16,260 square miles and includes potential emission sources within Maricopa and Pinal counties, which play a role in ozone formation in the Maricopa NAA.

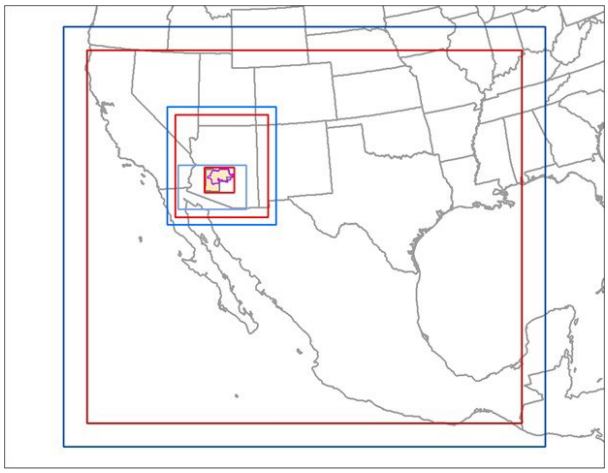

a) CAMx/CMAQ modeling domains (red) and WRF modeling domains (blue): 36, 12, and 4 km grid modeling domains

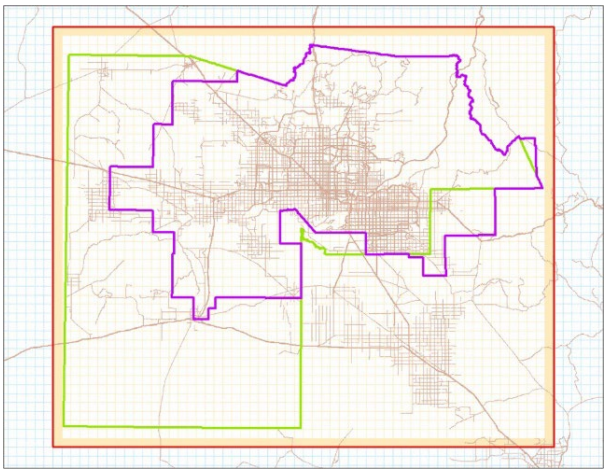

b) CAMx/CMAQ (red) 4 km grid modeling domains, Maricopa County (green), and the Maricopa NAA (purple)

Figure 5-2. CAMx/CMAQ and WRF modeling boundaries

Table 5-3. Configuration of CAMx/CMAQ modeling domains (LCC projection with 33° N and 45° N true latitudes and 112° W and 33.5° N central longitude and latitude)

Domain	Grid Resolution	Origin (SW, km)	Extent (NE, km)	NX	NY	NZ
36 km Grid Domain	36 km x 36 km	(-1,026, -1,879.2)	(2,286, 964.8)	92	79	23
12 km Grid Domain	12 km x 12 km	(-354, -307.2)	(354, 472.8)	59	65	23
4 km Grid Domain	4 km x 4 km	(-130, -119.2)	(94, 68.8)	56	47	23

Vertical Layer Configuration

The vertical layer resolution and coordinates for CAMx/CMAQ modeling are based on the sigma coordinate system. The sigma coordinate system uses the terrain-following hydrostatic pressure vertical coordinates ranging from 1 at the surface to 0 at the upper top boundary of the modeling domain. The 23 vertical layer configuration is used for CAMx/CMAQ modeling. The upper top boundary is based on the reference pressure of 100 hPa. The seasonal average pressure and height of vertical layers for CAMx/CMAQ modeling are presented in Table 5-4. The vertical depth and vertical layer structures of the 12 and 4 km domains are consistent with those of the 36 km domain.

Table 5-4. Average pressures and heights of CAMx/CMAQ vertical layers

Layer	Vertical Layer Pressure (hPa)	Vertical Layer Height (m)
23	121	16,048
22	227	13,946
21	395	8,793
20	501	5,576
19	543	4,921
18	586	4,307
17	628	3,729
16	670	3,183
15	721	2,664
14	772	1,979
13	811	1,516
12	836	1,160
11	853	987
10	870	816
9	887	648
8	900	482
7	909	400
6	917	319
5	926	238
4	932	158
3	936	119
2	941	79
1	945	39

5.4. Chemical Mechanisms

In this study, CAMx and CMAQ modeling used the most up-to-date chemical mechanism available for each model's photochemical reactions of ozone precursor emissions. The most up-to-date chemical mechanisms available for CAMx and CMAQ are Carbon Bond Version 7 revision 1 (CB7r1) and Carbon Bond Version 6 (CB6R3AE7), respectively.

CB7r1_CF3_SIMPLE_NoEvap in CAMx is updated from CB6r5 to focus on ozone chemistry of biogenic VOC, to reflect current information on alkane chemistry and organic peroxy radical reactions, and to support formation of Coarse/Fine (CF) aerosol chemistry scheme with ISORROPIA inorganic PM chemistry and SOAP3_SIMPLE_NOEVAP organic PM chemistry. The SOAP scheme is an organic chemistry/partitioning module, which consists of gas-phase VOC/IVOC/SVOC oxidation chemistry and equilibrium partitioning between gas and aerosol phases. SIMPLE is one of two module options for the SOAP version 3 (SOAP3) scheme and assumes VOC oxidation only produces non-volatile products (AOA0 or BOA0), so aerosol mass yields are zero for AOA1, ASOA2, BOA1, and BOA2.

CB6R3AE7 in CMAQ is updated from the previous version of CB6 to support formation of secondary organic aerosols by including four new species (AACD, FACD, APIN, and IVOC) and mapping low volatility compounds.

CAMx and CMAQ modeling require ozone precursor emissions (i.e., VOC and NO_x) in the model species emissions for ozone chemistry. The SMOKE modeling system is used for the chemical speciation process of emissions according to CB6R3AE7 chemical speciation profiles for emission source categories. Since CB7r1 in CAMx is backwards compatible with CB6, the model species emissions converted by SMOKE CB6R3AE7 speciation profiles were used for CAMx modeling without any additional process.

5.5. Initial and Boundary Conditions (IC/BCs)

5.5.1. GEOS-Chem Global Chemical Transport Model

Initial and boundary conditions for CAMx and CMAQ were generated using the GEOS-Chem chemical transport model (v14.6.1; https://doi.org/10.5281/zenodo.15548267). GEOS-Chem is a global 3-D chemical transport model driven by assimilated meteorological data from NASA's Goddard Earth Observing System, and version 14.6.1 was the most recent release available at the time of model preparation. Simulations were conducted for the period January 1, 2022 through September 30, 2023. The 2022 simulation (spin-up) was performed on a global 4° latitude × 5° longitude grid, while the 2023 simulation was performed at higher resolution on a 2° latitude × 2.5° longitude grid.

For this study, initial and boundary conditions were obtained from GEOS-Chem simulations specifically for the period of April 1 to September 30, 2023. The model employed 72 vertical layers extending from the surface to approximately 0.01 hPa. The lowest layer of the model reaches about 58 m above the surface, corresponding to roughly 1005.65 hPa.

Meteorological inputs were obtained from the second Modern-Era Retrospective analysis for Research and Applications (MERRA-2; GMAO - Global Modeling and Assimilation Office Research Site), a NASA atmospheric reanalysis starting in 1980 that employs GEOS-5 (Version 5.12.4) to assimilate newer satellite observations.

The chemical mechanism used was the full chemistry configuration, which includes a detailed NO_x–O_x–hydrocarbons–aerosols–halogens mechanism, a simplified secondary organic aerosol scheme, and the Unified Chemistry Extension (UCX) for stratospheric processes. This setup allows for a comprehensive representation of tropospheric and stratospheric chemistry, including oxidant reactions and aerosol–gas partitioning relevant to ozone and particulate matter formation.

Anthropogenic emissions over the United States were derived from the 2016 National Emissions Inventory (NEI) and projected to 2023 using sector-specific scaling factors from the EPA Trends Report for Tier 1 CAPS. Global anthropogenic sources were represented by the Community Emissions Data System (CEDS v2; Hoesly et al., 2018) at 0.1° × 0.1° resolution for 1980–2019. Shipping emissions were taken from CEDS, and aircraft contributions were prescribed using the AEIC 2019 inventory (Simone et al., 2013).

Natural emissions included biogenic VOCs from the offline MEGAN v2.1 inventory (Guenther et al., 2012) and soil NO_x parameterized following Hudman et al. (2012). Lightning and volcanic emissions were introduced following Murray et al. (2012) and Carn et al. (2015), respectively. Biomass burning emissions were represented by the Global Fire Emissions Database version 4s (GFED v4s; van der Werf et al., 2017). Mineral dust emissions were simulated using the offline DEAD scheme (Zender et al., 2003) with a high-resolution dust source function from Meng et al. (2021), while sea salt emissions were parameterized based on wind speed and sea surface temperature following Jaeglé et al. (2011). Additional natural hydrocarbon emissions included ethane (Tzompa-Sosa et al., 2017) and propane (Xiao et al., 2008).

This modeling configuration provides a consistent global representation of ozone, aerosols, and their precursors to supply chemical boundary conditions for the regional modeling system. Two boundary condition scenarios were prepared: (1) the base case, which includes a full representation of global ozone, PM, and precursors, and (2) the zero-

out case, a sensitivity simulation in which international anthropogenic emissions were excluded.

5.5.2. GEOS-Chem Model Evaluation

CASTNET data (https://www.epa.gov/castnet) were used to evaluate surface ozone simulated by GEOS-Chem. The Clean Air Status and Trends Network (CASTNET) is a long-term, rural air quality monitoring network managed by the U.S. Environmental Protection Agency (EPA) in partnership with federal, state, tribal, and local agencies. CASTNET sites are located away from major emission sources to capture background air quality and assess trends in pollutant concentrations over time. The network monitors multiple pollutants, including ground-level ozone, and its data have been used to evaluate the effectiveness of emission reduction programs, support National Ambient Air Quality Standards (NAAQS) assessments, and inform environmental management decisions. Hourly ozone concentrations for April–September 2023 were extracted from the U.S. EPA database for seven CASTNET monitoring sites in California and three sites in Arizona. These sites were selected for their relevance to ozone patterns in the Maricopa NAA. The site coordinates were matched to the corresponding GEOS-Chem model grid cells, and hourly observations were compared with simulated ozone and aggregated to daily values to evaluate model performance.

In addition to surface observations, vertical ozone profiles from NOAA's Global Monitoring Laboratory (GML) ozonesonde program (https://gml.noaa.gov/ozwv/ozsondes/index.html) were used to evaluate GEOS-Chem simulations. Ozonesondes are balloon-borne instruments paired with meteorological radiosondes that measure ozone, pressure, temperature, and humidity as the balloon ascends to about 35 km, transmitting the data to a ground station. These high-resolution profiles characterize ozone throughout the troposphere and lower stratosphere and are also used to estimate total column ozone. For this study, ozonesonde launches from Boulder, Colorado, and Trinidad Head, California, both located within the CAMx/CMAQ 36 km domain, were obtained for April–September 2023 to assess GEOS-Chem's ability to reproduce observed vertical ozone structure in the western United States. During this period, 23 profiles were available from Boulder and 18 from Trinidad Head.

Figures 5-3 and 5-4 evaluate GEOS-Chem surface ozone against CASTNET observations from 10 monitoring sites in California and Arizona for April–September 2023. The scatterplot (Figure 5-3) shows that GEOS-Chem reproduces the observed daily mean variability with a correlation coefficient of 0.73. The mean bias (0.6 ppb) is small, and error

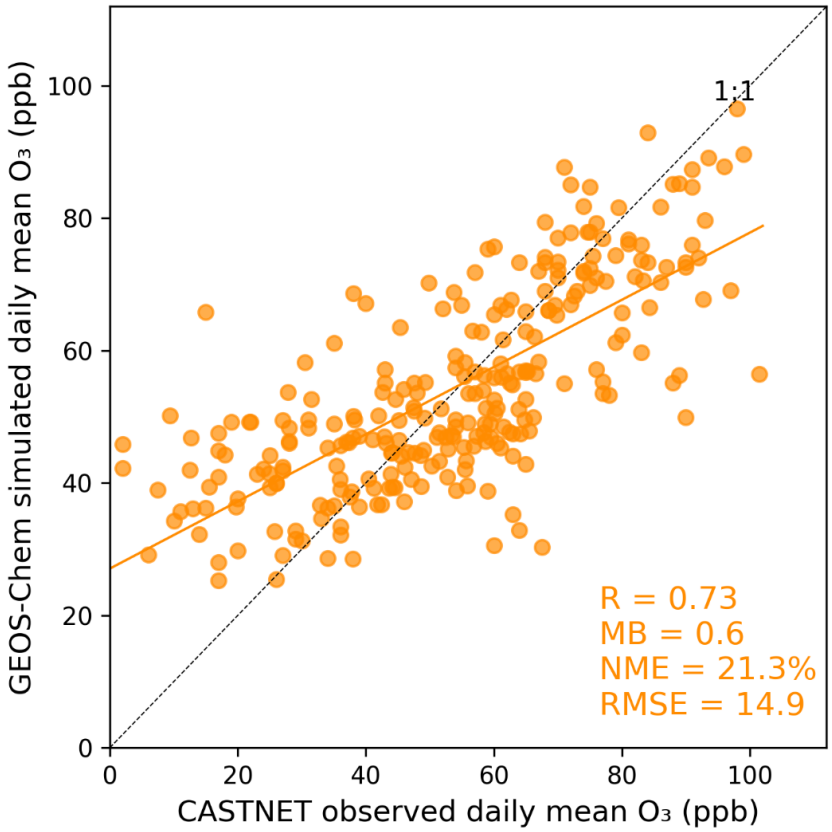

Figure 5-3. Scatterplot comparing GEOS-Chem simulated daily mean ozone with CASTNET observations across the 10 CASTNET sites in California and Arizona for April–September 2023. Performance statistics are shown in the lower right

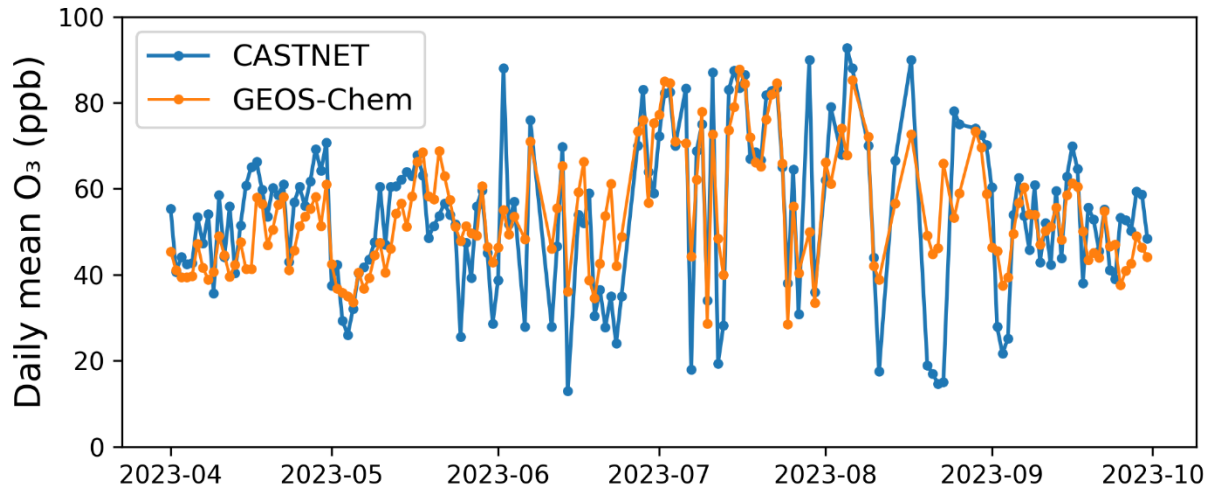

Figure 5-4. Time series of daily mean ozone from GEOS-Chem and CASTNET observations averaged across the 10 sites in California and Arizona for April–September 2023

metrics (NME = 21.3%, RMSE = 14.9 ppb) indicate that model performance is within an acceptable range for regional boundary-condition applications.

The time series (Figure 5-4) demonstrates that GEOS-Chem captures the observed seasonal cycle and synoptic-scale fluctuations, including elevated ozone episodes in June–August. Peak values are generally underestimated, consistent with the scatterplot, but the phasing of ozone episodes is well reproduced. Some abrupt drops and rebounds in the observed series are evident. These are attributed to variations in the number of active CASTNET sites contributing to the daily mean, an artifact of network averaging, rather than true atmospheric signals. Despite these fluctuations, the overall model–observation agreement supports the suitability of GEOS-Chem for providing ozone boundary conditions to the regional modeling system.

Figures 5-5 and 5-6 evaluate GEOS-Chem vertical ozone profiles against ozonesonde measurements from Trinidad Head, California, and Boulder, Colorado for selected representative dates. At both sites, the model reproduces the broad vertical structure, with relatively low mixing ratios near the surface, a mid-tropospheric minimum, and increasing concentrations toward the upper troposphere and lower stratosphere. The shape and seasonal variability of the profiles are generally consistent with observations, supporting the suitability of GEOS-Chem for representing background ozone levels in boundary condition applications.

Quantitatively, in the lower troposphere (~800 hPa), GEOS-Chem closely matches the ozonesonde profiles at Boulder, with differences generally less than 5 ppb. At Trinidad Head, the model shows larger positive biases of ~10–20 ppb during summer, likely reflecting challenges in representing coastal boundary-layer processes. The July 22 profile at Trinidad Head is notable for its pronounced fine-scale variability, which the model does not capture, leading to larger departures than in the other three cases. Differences in the mid-troposphere (~500–600 hPa) are typically around 10 ppb. In the lower stratosphere (100–70 hPa), GEOS-Chem exhibits a systematic high bias on the order of 100–300 ppb, excluding the Trinidad Head profile from June 12, 2023.

These deviations are within a range acceptable for boundary condition applications. The comparisons confirm that GEOS-Chem provides a reasonable representation of ozone vertical structure. Despite modest biases aloft, the model skill is sufficient to support its use in generating chemical boundary conditions for the regional photochemical modeling system.

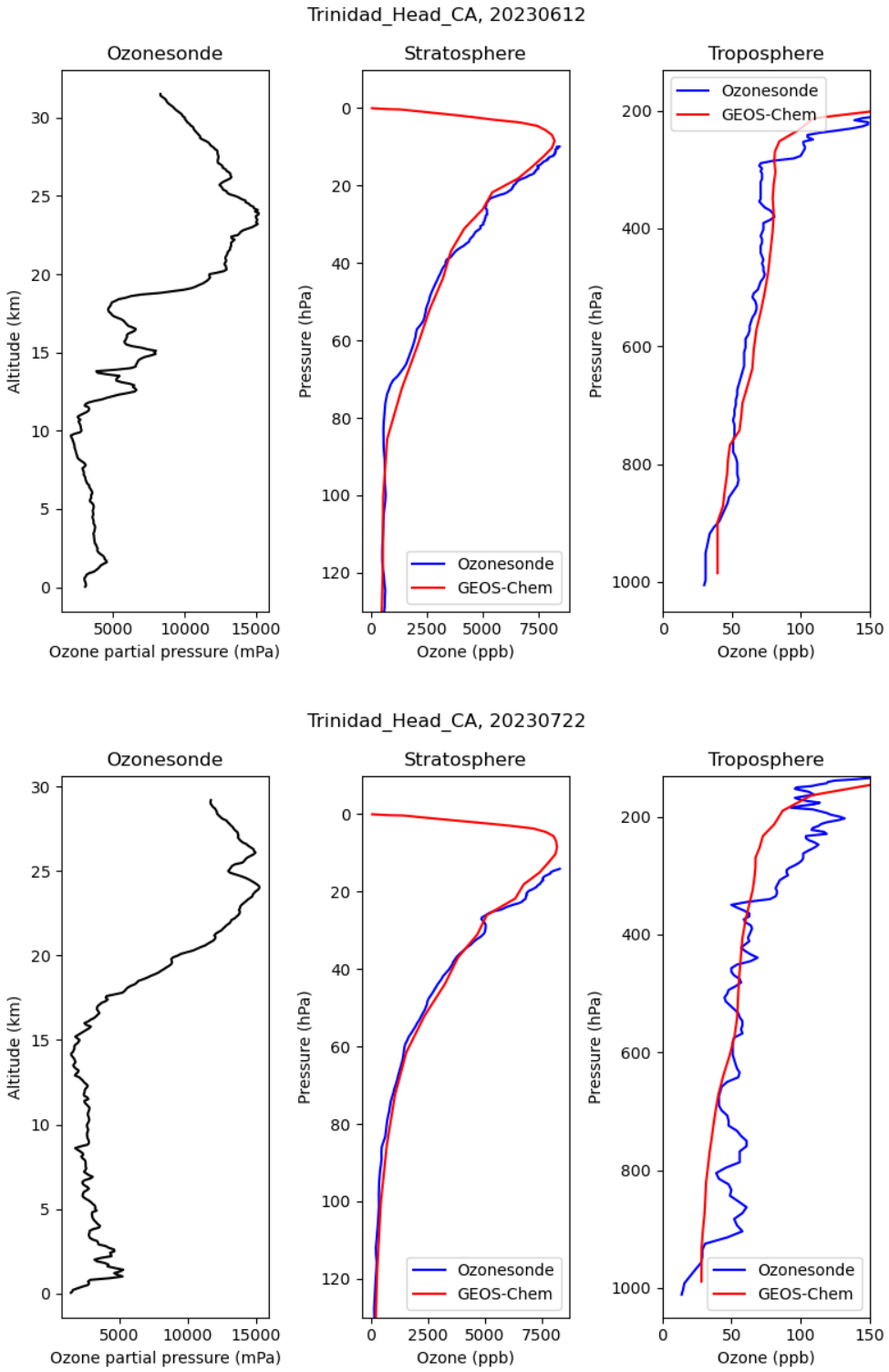

Figure 5-5. Comparison of GEOS-Chem and ozonesonde vertical ozone profiles at Trinidad Head, California, on June 12 and July 22, 2023. Left panels: observed ozone partial pressure from ozonesondes. Middle panels: stratospheric profile comparisons. Right panels: tropospheric profile comparisons

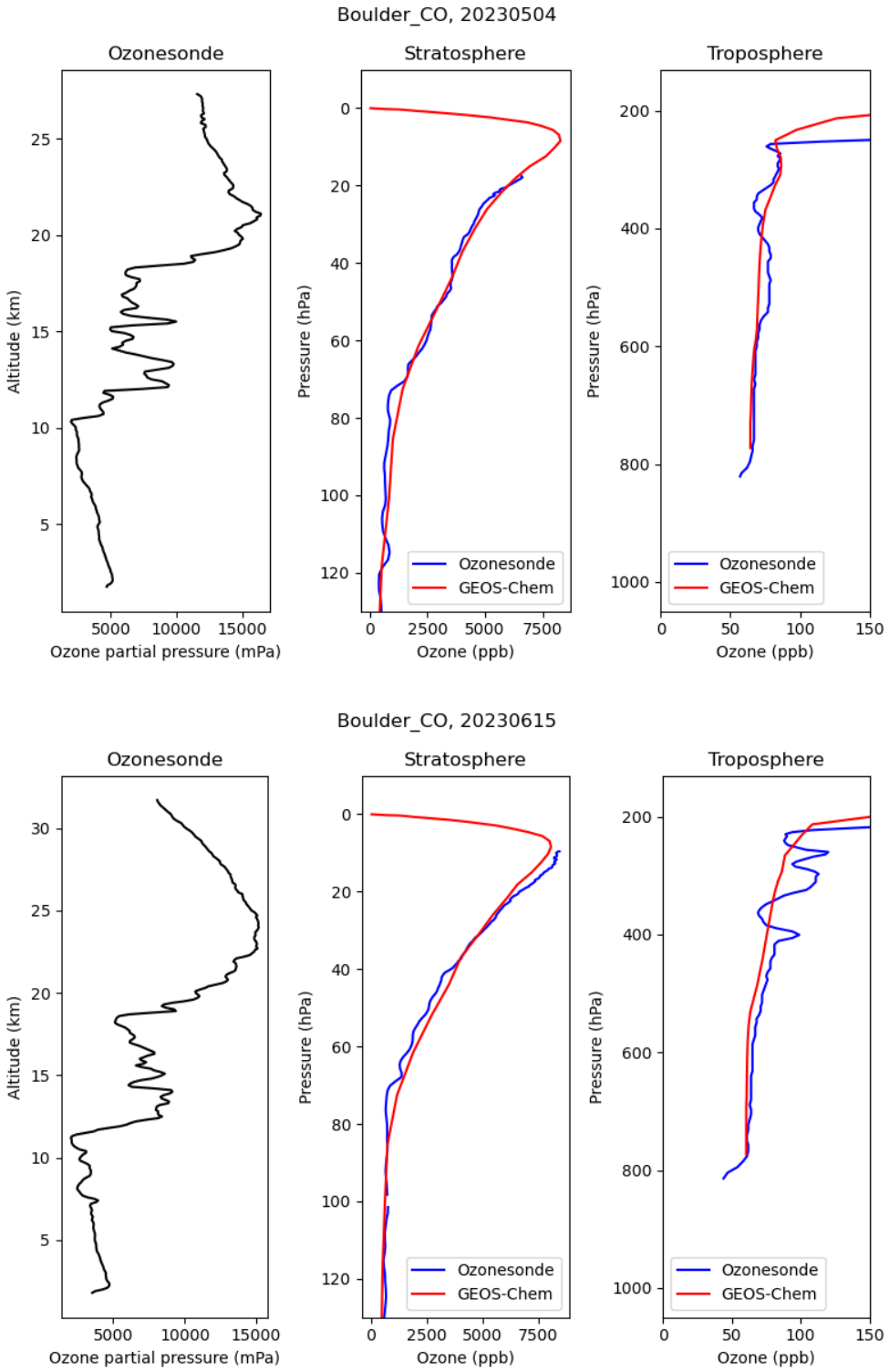

Figure 5-6. Comparison of GEOS-Chem and ozonesonde vertical ozone profiles at Boulder, Colorado on May 4 and June 15, 2023

5.5.3. Comparison of the IC/BCs between the Base and Zero-Out Cases

To further characterize the model inputs, we examined the boundary conditions from the GEOS-Chem base and zero-out simulations to summarize their seasonal and spatial characteristics (Figure 5-7). Across all four lateral boundaries at 721 hPa, ozone levels in the base case are consistently higher than in the zero-out case, but the magnitude of the differences varies by season and boundary location.

The largest case difference across all boundaries and seasons occurs along the west boundary in spring (April–June), with an average enhancement of 17.9 ppb. This substantial increase indicates strong inflow and is nearly double the summer difference (9.3 ppb). A similar pattern is evident along the north and east boundaries, where springtime differences (~13 ppb) are about twice those in summer (~6 ppb). In contrast, the south boundary shows more consistent seasonal differences, with enhancements of 11.8 ppb in spring and 8.1 ppb in summer. While the focus of this comparison is the relative magnitude of the two cases, it is noteworthy that absolute ozone levels along the north and east boundaries rise substantially in summer. This enhancement is consistent with long-range transport and may partly reflect the influence of Canadian wildfires during 2023 season, which were documented to impact air quality across the continental U.S. These results provide important context for interpreting the role of boundary inflow in subsequent regional model applications.

5.5.4. GOES-Chem Conversion Tools for CAMx and CMAQ

The GEOS2CAMx tool (version 4.1; https://www.camx.com/download/support-software/) was used to generate initial and boundary condition (IC/BC) inputs for the CAMx simulations. The program converts GEOS-Chem outputs into CAMx-ready files through a combination of species mapping, horizontal regridding, and vertical interpolation. Supported CAMx grid projections include latitude–longitude, Lambert conformal, UTM, and polar stereographic. A species mapping table (e.g., geoschem_*.txt) defines the relationship between GEOS-Chem species and the CAMx chemical mechanism species. GEOS2CAMx can create multiple output file types, including lateral boundary conditions, initial conditions, top boundary conditions, and surface-layer fields. The tool interpolates concentrations to the CAMx vertical structure using either above-ground-level (AGL) or mean-sea-level (MSL) coordinates if topography is available.

The aqmbc tool (https://github.com/barronh/aqmbc) was used to generate boundary conditions for CMAQ. This Python-based tool streamlines boundary condition processing by supporting multiple global and regional models through a unified framework. It

currently supports GEOS-Chem (versions 12 and 14), NASA GMAO's GEOS-CF, RAQMS, and both hemispheric and regional CMAQ configurations. The tool wraps standard SpeciesConc files into boundary condition files (SpeciesBC). Additionally, it provides functionality for converting between latitude/longitude and model grid indices and for interpolating concentrations to sigma levels.

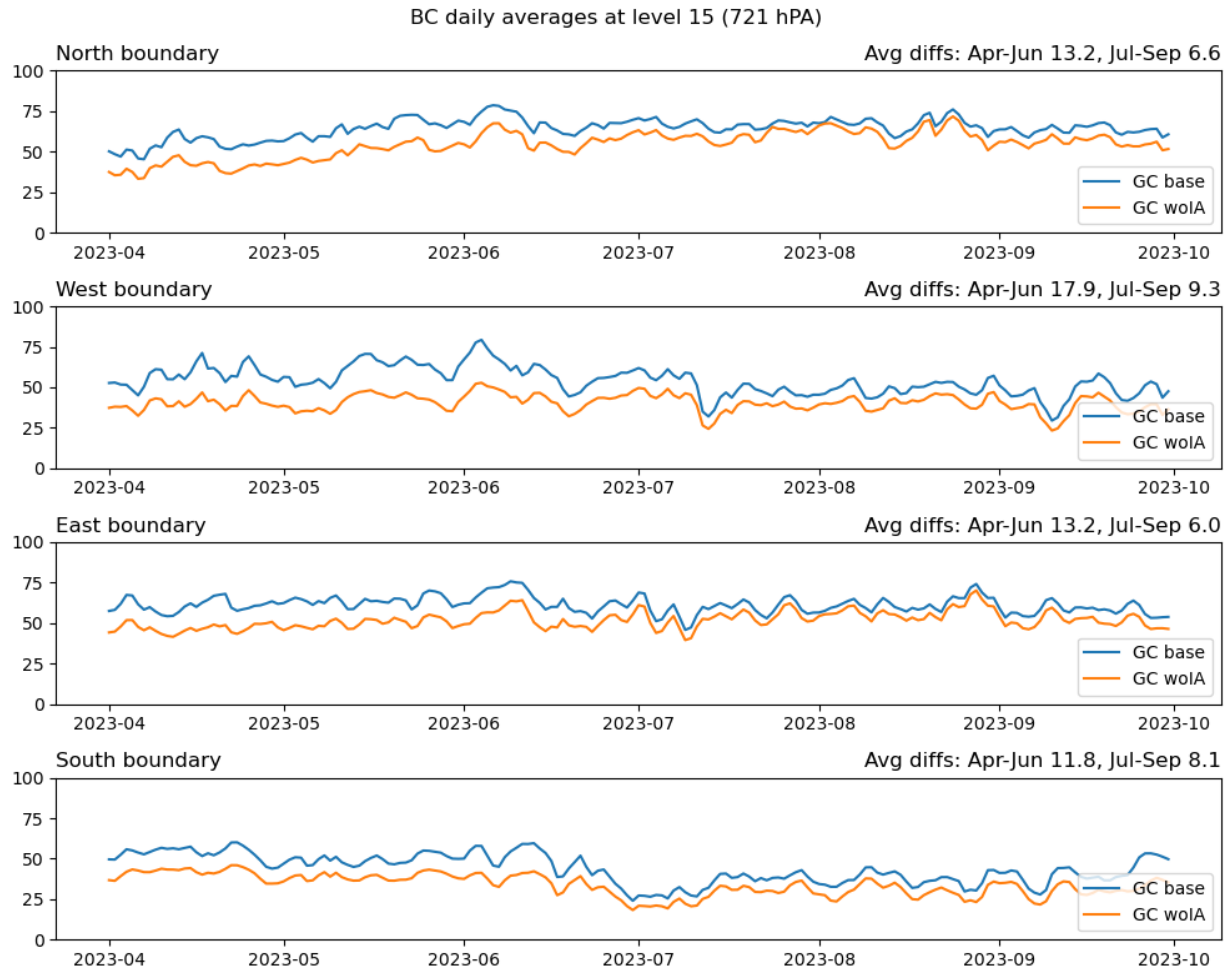

Figure 5-7. Daily mean ozone at 721 hPa along the four lateral boundaries of the 36 km domain from the GEOS-Chem base (blue) and zero-out (orange) simulations for April–September 2023. Average differences between the two cases are shown for April–June and July– September

6. MODEL PERFORMANCE EVALUATION

6.1. Methodology and Goals

EPA provides guidance and tools for model performance evaluation, which assess relevant variables paired in time and space for recommended statistical metrics for CAMx/CMAQ model performance evaluations. The Atmospheric Model Evaluation Tool (AMET) is one of the evaluation tools for CAMx/CMAQ model performance, which allows tests to be performed on a site-by-site and/or network aggregate basis, for any duration or frequency of interest (Appel, 2011). AMET is built on a set of R scripts communicating with MySQL databases to create various types of plots and statistics using paired observation and model output data. The key statistical performance metrics available in AMET and used in this study are listed in Table 6-1.

Statistical metrics of mean bias, mean error, root mean square error and index of agreement were computed to satisfy the operational model performance evaluation. Hourly time series plots, paired and summary scatter-density plots, diurnal box-and-whisker plots, soccer goal diagrams, and Taylor diagrams were generated to support the graphical model performance evaluation.

The CAMx/CMAQ air quality model performance was evaluated using AMET v1.5 with the statistical metrics in Table 6-1 and the following statistical metrics:

- Normalized bias test: The metric provides a measure of the ability of the model to replicate observed patterns during the times of day when available monitoring and modeled data are most likely to represent similar spatial scales. EPA's recommended acceptable range is ±15%.
- Gross error of all pairs above 60 ppb: In conjunction with bias, this metric provides an overall assessment of base case performance and may be used as a reference to other modeling applications. Gross error may be interpreted as precision. EPA recommended range for the metric is ±35%.

In general, the performance metrics that fall within or below these ranges are considered acceptable by EPA.

Table 6-1. Statistical performance metrics for model performance evaluation

Metric Name	Definition
Mean Bias (MB)	$MB = \frac{1}{N}\sum(M_i - O_i)$
Mean Error (ME)	$ME = \frac{1}{N}\sum\lvert M_i - O_i\rvert$
Root Mean Square Error (RMSE)	$RMSE = \sqrt{\frac{\sum(M_i - O_i)^2}{N}}$
Fractional Bias (FB)	$FB = 100\% \times \frac{2}{N}\sum\frac{(M_i - O_i)}{(M_i + O_i)}$
Fractional Error (FE)	$FE = 100\% \times \frac{2}{N}\sum\frac{\lvert M_i - O_i\rvert}{(M_i + O_i)}$
Normalized Mean Bias (NMB)	$NMB = 100\% \times \frac{\sum(M_i - O_i)}{\sum O_i}$
Normalized Mean Error (NME)	$NME = 100\% \times \frac{\sum\lvert M_i - O_i\rvert}{\sum O_i}$
Correlation Coefficient (R)	$R = \frac{\sum_1^N\left((M_i - \bar{M}) \times (O_i - \bar{O})\right)}{\sqrt{\sum_1^N(M_i - \bar{M})^2 \sum_1^N(O_i - \bar{O})^2}}$
Index of Agreement	$IoA = 1 - \frac{\sum(O_i - M_i)^2}{\sum(\lvert M_i - \bar{O}\rvert + \lvert O_i - \bar{O}\rvert)^2}$

6.2. Operational Evaluation

For the CAMx/CMAQ model performance evaluation, operational evaluation was conducted to assess how accurately the CAMx/CMAQ model replicates observed ozone concentrations for the 2023 base year. Statistical metrics and graphical analysis were provided for the operational evaluation. The operational evaluation for the CAMx/CMAQ model may identify limitations and uncertainties in the model and model inputs that may require further improvements.

6.2.1. Statistical Performance Metrics

For the statistical performance evaluation, the observed and modeled ozone values for all ozone monitoring sites in the 8-hour ozone NAA in 2023 were evaluated for the statistical metrics provided in Table 6-1. Two quantitative criteria were applied to judge whether the CAMx/CMAQ model met the desired performance: NMB within ±15%, and NME < 35%. A positive NMB means that the model tends to overestimate the observation on average and a negative NMB means the model tends to underestimate. The Index of Agreement is the standardized measure of the degree of model prediction error and varies between zero and one. A value of zero indicates the poorest agreement between modeled and observed values, and one is the perfect match.

For all monitors in the 8-hour ozone NAA, normalized mean biases and errors for modeled one-hour ozone, modeled MDA8 ozone, and modeled MDA8 ozone paired with observed MDA8 values exceeding 60 ppb during the April–September 2023 modeling period were generally within the statistical goals, as shown in Tables 6-2 through 6-7. All normalized mean biases met the ±15% goal, except for CAMx modeled one-hour ozone in June. All normalized mean errors were within the 35% goal. The Index of Agreement indicated good overall agreement between modeled and observed values for both one-hour and MDA8 ozone. However, agreement was weaker for modeled MDA8 ozone paired with observed values above 60 ppb. In general, both CAMx and CMAQ models showed satisfactory statistical performance.

Additionally, statistical metrics for modeled MDA8 ozone for the five controlling monitors, which showed the highest 2023 base year design values, are listed in Tables 6-8 and 6-9. These monitors showed statistical performance comparable to network average in the Maricopa NAA. All controlling monitors sufficiently met the statistical goals for NMB and NME.

Table 6-2. Statistical metrics by month for CAMx modeled one-hour ozone values for monitors in the Maricopa NAA

Metric	Apr	May	Jun	Jul	Aug	Sep	Apr-Sep
Number of Pairs (#)	8,876	17,491	16,583	17,463	17,498	16,893	95,636
Avg. Observed Value (ppb)	44.5	45.5	46.4	44.3	41.7	33.8	42.6
Avg. Modeled Value (ppb)	45.1	48.2	53.7	44.7	38.9	36.8	44.5
MB (ppb)	0.6	2.7	7.3	0.4	-2.9	3.1	1.9
ME (ppb)	7.6	8.8	10.0	7.9	7.8	8.0	8.4
RMSE (ppb)	9.9	11.1	12.8	10.1	10.0	10.2	10.8
FB (%)	5.0	7.8	18.3	2.0	-6.2	13.6	6.7
FE (%)	21.1	21.8	23.9	20.9	23.0	30.7	23.8
NMB (%)	1.2	6.0	15.6	1.0	-6.9	9.1	4.4
NME (%)	17.0	19.4	21.5	17.8	18.6	23.6	19.7
Correlation Coefficient (R)	0.77	0.73	0.80	0.83	0.82	0.79	0.79
Index of Agreement	0.86	0.84	0.85	0.91	0.89	0.88	0.88

Table 6-3. Statistical metrics by month for CMAQ modeled one-hour ozone values for monitors in the Maricopa NAA

Metric	Apr	May	Jun	Jul	Aug	Sep	Apr-Sep
Number of Pairs (#)	8,876	17,491	16,583	17,463	17,498	16,893	95,636
Avg. Observed Value (ppb)	44.5	45.5	46.4	44.3	41.7	33.8	42.6
Avg. Modeled Value (ppb)	47.4	50.0	52.4	44.7	42.0	38.6	45.7
MB (ppb)	2.9	4.5	6.0	0.3	0.3	4.9	3.1
ME (ppb)	7.3	7.9	9.1	7.4	7.3	8.1	7.9
RMSE (ppb)	9.7	10.2	11.7	9.6	9.3	10.4	10.2
FB (%)	10.8	11.8	16.2	2.9	2.9	20.0	10.6
FE (%)	20.4	19.7	22.3	19.5	20.6	29.9	22.1
NMB (%)	6.5	9.8	12.9	0.8	0.7	14.4	7.3
NME (%)	16.5	17.5	19.5	16.6	17.4	23.8	18.5
Correlation Coefficient (R)	0.80	0.80	0.81	0.84	0.83	0.81	0.82
Index of Agreement	0.86	0.87	0.86	0.91	0.90	0.87	0.89

Table 6-4. Statistical metrics by month for CAMx modeled MDA8 ozone values for monitors in the Maricopa NAA

Metric	Apr	May	Jun	Jul	Aug	Sep	Apr-Sep
Number of Pairs (#)	373	741	703	740	738	683	3,978
Avg. Observed Value (ppb)	59.1	58.4	63.0	61.0	55.7	49.7	57.8
Avg. Modeled Value (ppb)	58.2	62.0	69.2	61.9	52.7	50.7	59.2
MB (ppb)	-0.9	3.6	6.3	0.8	-3.0	1.0	1.5
ME (ppb)	5.0	6.8	8.0	6.7	5.7	4.7	6.3
RMSE (ppb)	6.4	8.7	10.7	8.4	7.3	5.8	8.2
FB (%)	-1.4	6.3	9.5	1.6	-5.1	1.5	2.3
FE (%)	8.6	11.6	11.9	10.9	10.7	9.6	10.7
NMB (%)	-1.5	6.2	10.0	1.4	-5.4	2.0	2.5
NME (%)	8.5	11.6	12.6	10.9	10.3	9.4	10.8
Correlation Coefficient (R)	0.22	0.55	0.44	0.63	0.83	0.72	0.70
Index of Agreement	0.53	0.71	0.59	0.79	0.88	0.83	0.83

Table 6-5. Statistical metrics by month for CMAQ modeled MDA8 ozone values for monitors in the Maricopa NAA

Metric	Apr	May	Jun	Jul	Aug	Sep	Apr-Sep
Number of Pairs (#)	373	741	703	740	738	683	3,978
Avg. Observed Value (ppb)	59.1	58.4	63.0	61.0	55.7	49.7	57.8
Avg. Modeled Value (ppb)	59.5	62.2	67.0	60.7	54.6	52.2	59.4
MB (ppb)	0.3	3.7	4.1	-0.4	-1.1	2.5	1.6
ME (ppb)	4.6	5.8	6.5	6.0	5.1	4.6	5.5
RMSE (ppb)	5.7	7.3	8.4	7.8	6.7	5.7	7.1
FB (%)	0.7	6.7	6.5	-0.2	-1.4	4.7	3.0
FE (%)	7.9	10.1	10.0	9.8	9.4	9.2	9.5
NMB (%)	0.6	6.4	6.5	-0.6	-2.0	5.0	2.8
NME (%)	7.8	10.0	10.3	9.8	9.2	9.3	9.6
Correlation Coefficient (R)	0.32	0.71	0.52	0.67	0.83	0.72	0.74
Index of Agreement	0.58	0.79	0.67	0.81	0.90	0.82	0.85

Table 6-6. Statistical metrics by month for CAMx modeled MDA8 ozone values paired with observed MDA8 ozone values greater than 60 ppb for monitors in the Maricopa NAA

Metric	Apr	May	Jun	Jul	Aug	Sep	Apr-Sep
Number of Pairs (#)	155	317	455	389	290	37	1,643
Avg. Observed Value (ppb)	64.2	66.8	67.5	68.7	67.9	63.5	67.3
Avg. Modeled Value (ppb)	59.0	65.7	71.8	66.8	60.8	62.1	66.1
MB (ppb)	-5.2	-1.1	4.3	-2.0	-7.1	-1.4	-1.2
ME (ppb)	6.0	4.4	6.8	7.2	8.0	3.0	6.5
RMSE (ppb)	7.6	5.5	9.5	9.2	9.6	3.6	8.5
FB (%)	-8.7	-1.8	5.9	-3.1	-11.2	-2.3	-2.3
FE (%)	10.1	6.7	9.5	10.7	12.6	4.8	9.7
NMB (%)	-8.0	-1.6	6.4	-2.8	-10.4	-2.2	-1.8
NME (%)	9.4	6.5	10.1	10.4	11.8	4.7	9.6
Correlation Coefficient (R)	0.19	0.58	0.15	0.19	0.43	0.45	0.29
Index of Agreement	0.33	0.75	0.41	0.50	0.53	0.61	0.54

Table 6-7. Statistical metrics by month for CMAQ modeled MDA8 ozone values paired with observed MDA8 ozone values greater than 60 ppb for monitors in the Maricopa NAA

Metric	Apr	May	Jun	Jul	Aug	Sep	Apr-Sep
Number of Pairs (#)	155	317	455	389	290	37	1,643
Avg. Observed Value (ppb)	64.2	66.8	67.5	68.7	67.9	63.5	67.3
Avg. Modeled Value (ppb)	60.7	66.9	69.4	65.3	63.1	61.9	65.8
MB (ppb)	-3.4	0.1	1.9	-3.4	-4.8	-1.7	-1.5
ME (ppb)	4.7	4.0	5.4	6.9	6.0	3.7	5.5
RMSE (ppb)	5.8	4.9	6.9	9.0	7.7	4.6	7.2
FB (%)	-5.7	0.1	2.6	-5.2	-7.5	-2.9	-2.4
FE (%)	7.6	6.0	7.8	10.3	9.2	6.0	8.2
NMB (%)	-5.4	0.2	2.8	-4.9	-7.1	-2.6	-2.2
NME (%)	7.3	5.9	8.0	10.0	8.8	5.9	8.1
Correlation Coefficient (R)	0.24	0.63	0.27	0.27	0.48	0.45	0.37
Index of Agreement	0.42	0.79	0.55	0.53	0.62	0.58	0.61

Table 6-8. Statistical metrics for CAMx modeled MDA8 ozone values for controlling monitors

Metric	Mesa	North Phoenix	Glendale	Lehi	JLG Supersite
Number of Pairs (#)	166	165	168	164	166
Avg. Observed Value (ppb)	60.1	57.5	60.0	62.6	61.1
Avg. Modeled Value (ppb)	59.1	60.6	59.6	61.0	59.0
MB (ppb)	-1.0	3.1	-0.4	-1.6	-2.1
ME (ppb)	6.1	7.2	5.9	5.9	6.3
RMSE (ppb)	7.8	9.1	7.7	7.5	8.3
FB (%)	-1.9	5.0	-0.8	-2.8	-3.6
FE (%)	10.4	12.1	9.9	9.6	10.5
NMB (%)	-1.6	5.4	-0.7	-2.5	-3.4
NME (%)	10.2	12.5	9.8	9.4	10.3
Correlation Coefficient (R)	0.73	0.62	0.72	0.75	0.72
Index of Agreement	0.85	0.76	0.84	0.86	0.84

Table 6-9. Statistical metrics for CMAQ modeled MDA8 ozone values for controlling monitors

Metric	Mesa	North Phoenix	Glendale	Lehi	JLG Supersite
Number of Pairs (#)	166	165	168	164	166
Avg. Observed Value (ppb)	60.1	57.5	60.0	62.6	61.1
Avg. Modeled Value (ppb)	58.9	60.2	59.2	61.1	58.8
MB (ppb)	-1.2	2.7	-0.8	-1.4	-2.3
ME (ppb)	5.4	6.2	5.0	5.1	5.6
RMSE (ppb)	6.9	7.8	6.4	6.4	7.6
FB (%)	-1.7	4.8	-1.1	-2.1	-3.5
FE (%)	9.3	10.5	8.5	8.3	9.4
NMB (%)	-1.9	4.7	-1.4	-2.3	-3.8
NME (%)	9.1	10.8	8.3	8.2	9.2
Correlation Coefficient (R)	0.76	0.68	0.79	0.79	0.76
Index of Agreement	0.86	0.80	0.88	0.88	0.85

6.2.2. Graphical Analysis

Graphical analysis provides a visual and intuitive way to complement statistical metrics and assess the modeling performance with a qualitative summary.

To examine how well the CAMx/CMAQ model replicates day-to-day fluctuations in observed MDA8 ozone concentrations, time series of modeled MDA8 ozone are plotted against observations for each monitoring site in the Maricopa NAA are given in Figure 6-1. In addition to this site-specific analysis, a time series plot of the network average MDA8 ozone over the observed values is provided in Figure 6-2. The results indicate that the CAMx/CMAQ model generally replicates the day-to-day variability in ozone during the modeling period at these sites, but it tends to overestimate the observed ozone in June (a pre-monsoon period) and underestimate in August (a monsoon period). This seasonal bias may be related to challenges in simulating the distinct meteorological regimes and their influence on biogenic emissions and transport pathways.

Figures 6-3 and 6-4 illustrate the spatial variability in mean error and mean bias at monitor locations for the modeled MDA8 ozone values. At most monitoring sites in the 8-hour ozone NAA, the CAMx/CMAQ model generally captures the spatial patterns of MDA8 ozone uniformly. In this area, the mean error is mainly between 4 and 7 ppb and the mean bias is between -3 and 4 ppb. The exception is at the Fountain Hills monitor where the mean bias is 8 ppb and the mean bias is 9 ppb.

A scatter plot of modeled and observed MDA8 ozone for all monitors in the 8-hour ozone NAA are provided in Figure 6-5. The plot indicates that the CAMx/CMAQ modeled ozone generally clustered around the best-fit-line and had a slightly larger bias at higher ozone above 60 ppb than at lower ozone.

One of the available statistical visualization methods in AMET is a soccer goal plot, which is a quick visual assessment of how closely the model predicts observations within an intuitive target shape composed of normalized mean bias and normalized mean error. Soccer goal plots in Figure 6-6 show that the CAMx/CMAQ model performance underlies center of the goal, which indicates minimal systematic error and reasonable magnitude of deviation of model predictions relative to observations.

Figure 6-7 shows the periodic, monthly, and day of week distributions of modeled MDA8 ozone for the 8-hour ozone NAA, as well as the diurnal distributions of one-hour ozone. The distribution of CAMx/CMAQ predictions generally corresponds well with that of the observed concentrations over the entire modeling period. The distribution of predicted concentrations tends to be close to that of the observed concentration at the 25th

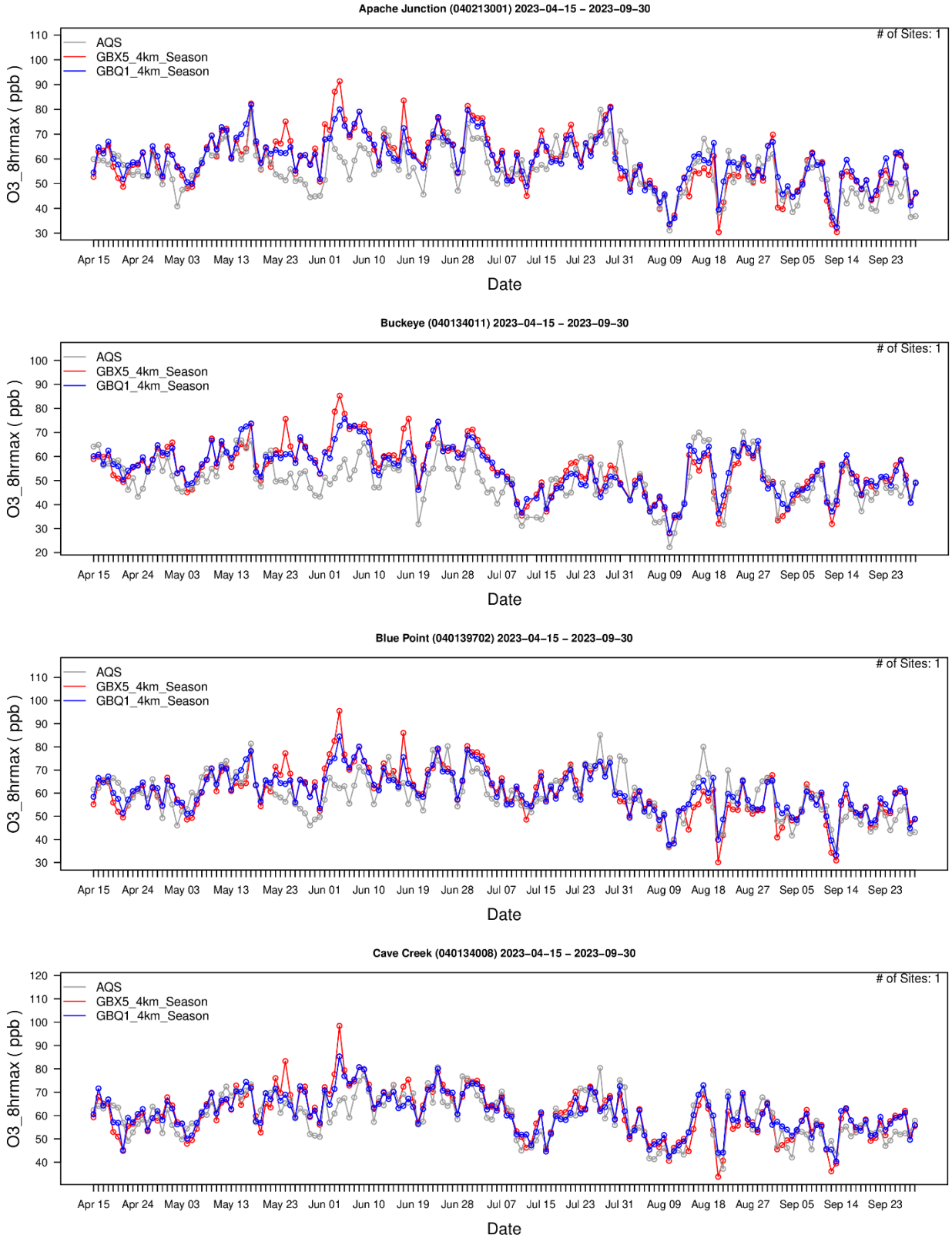

Figure 6-1. Time series plots of modeled MDA8 ozone over observed concentrations for each monitor; observed (grey), CAMx (red), CMAQ (blue)

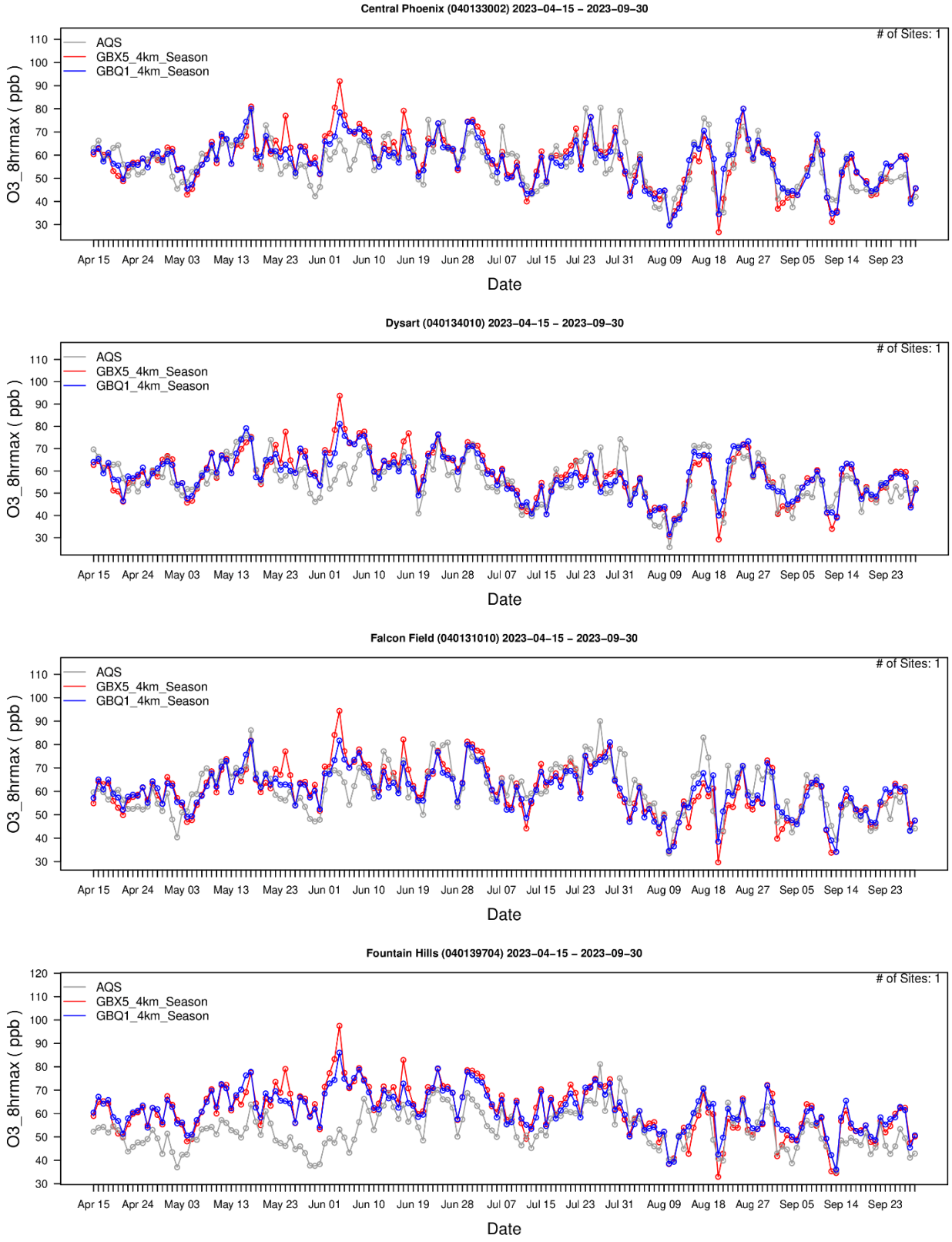

Figure 6-1. (Continued)

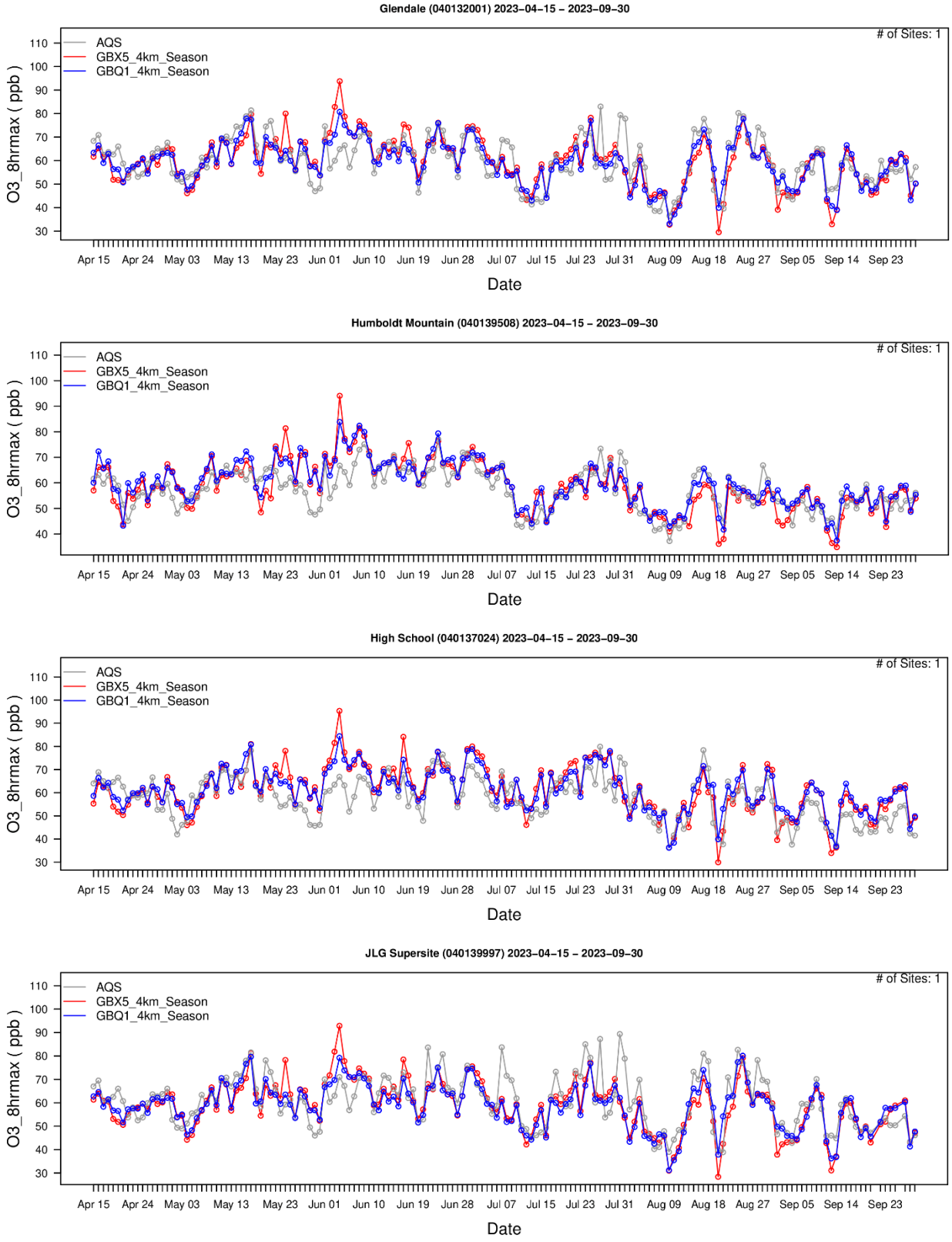

Figure 6-1. (Continued)

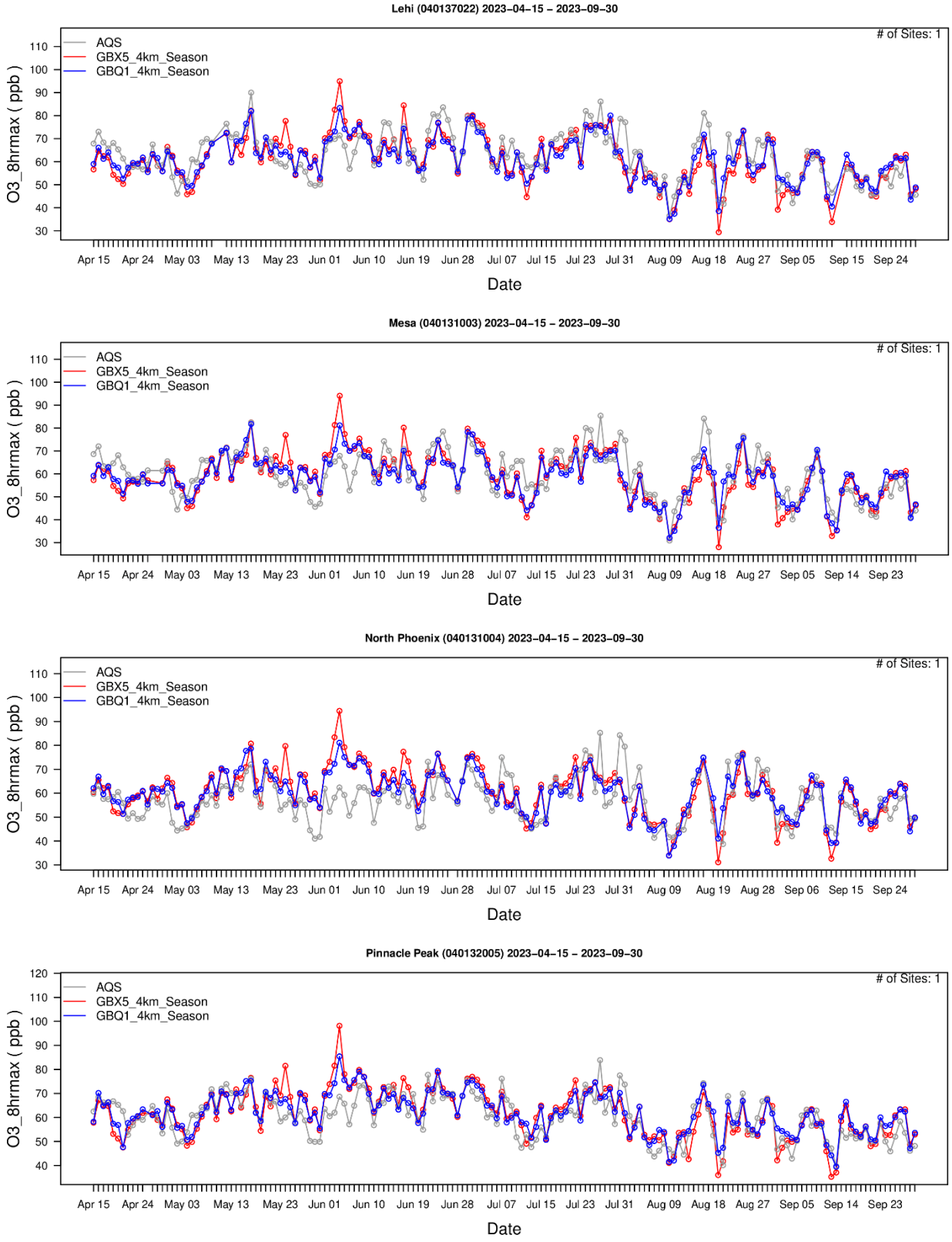

Figure 6-1. (Continued)

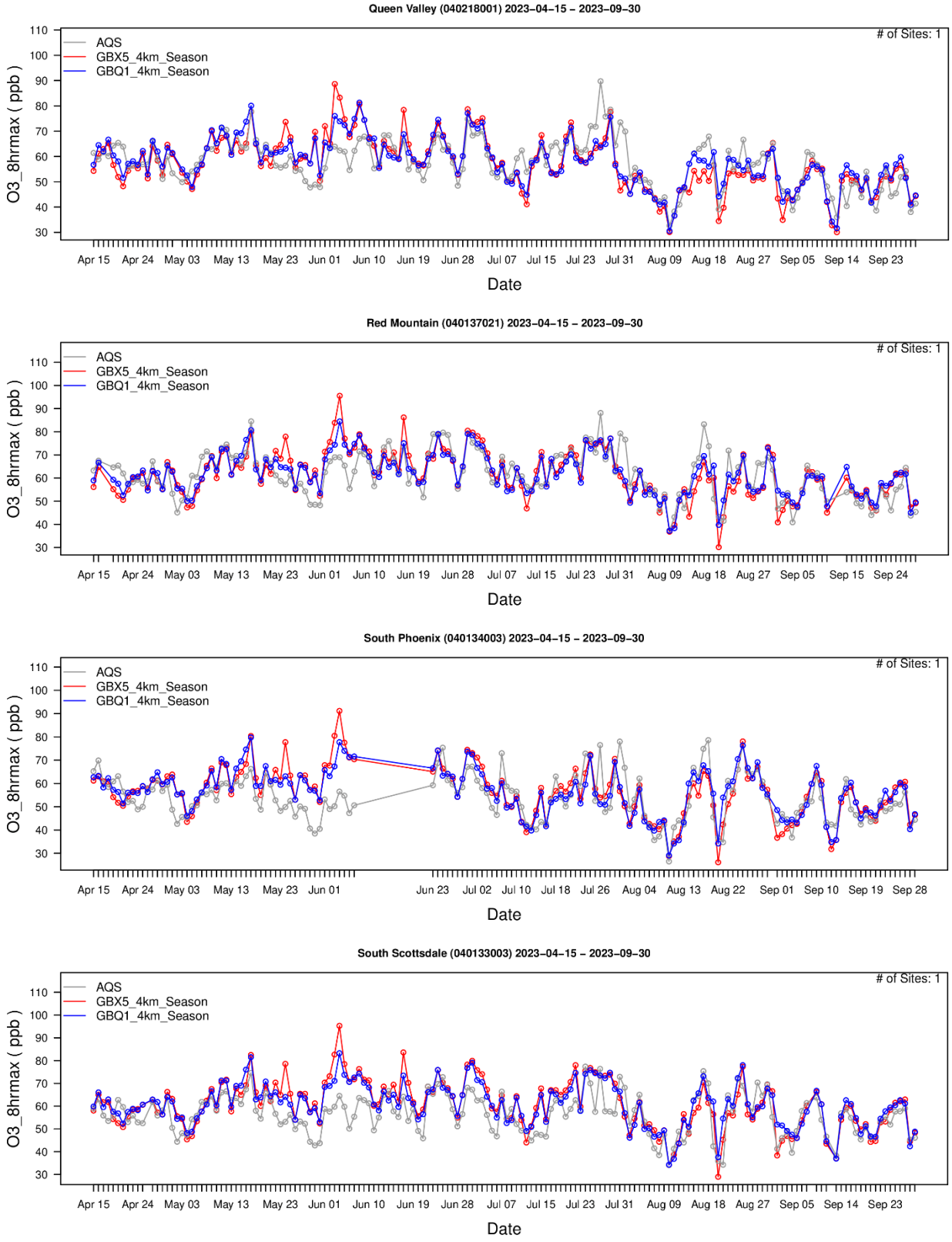

Figure 6-1. (Continued)

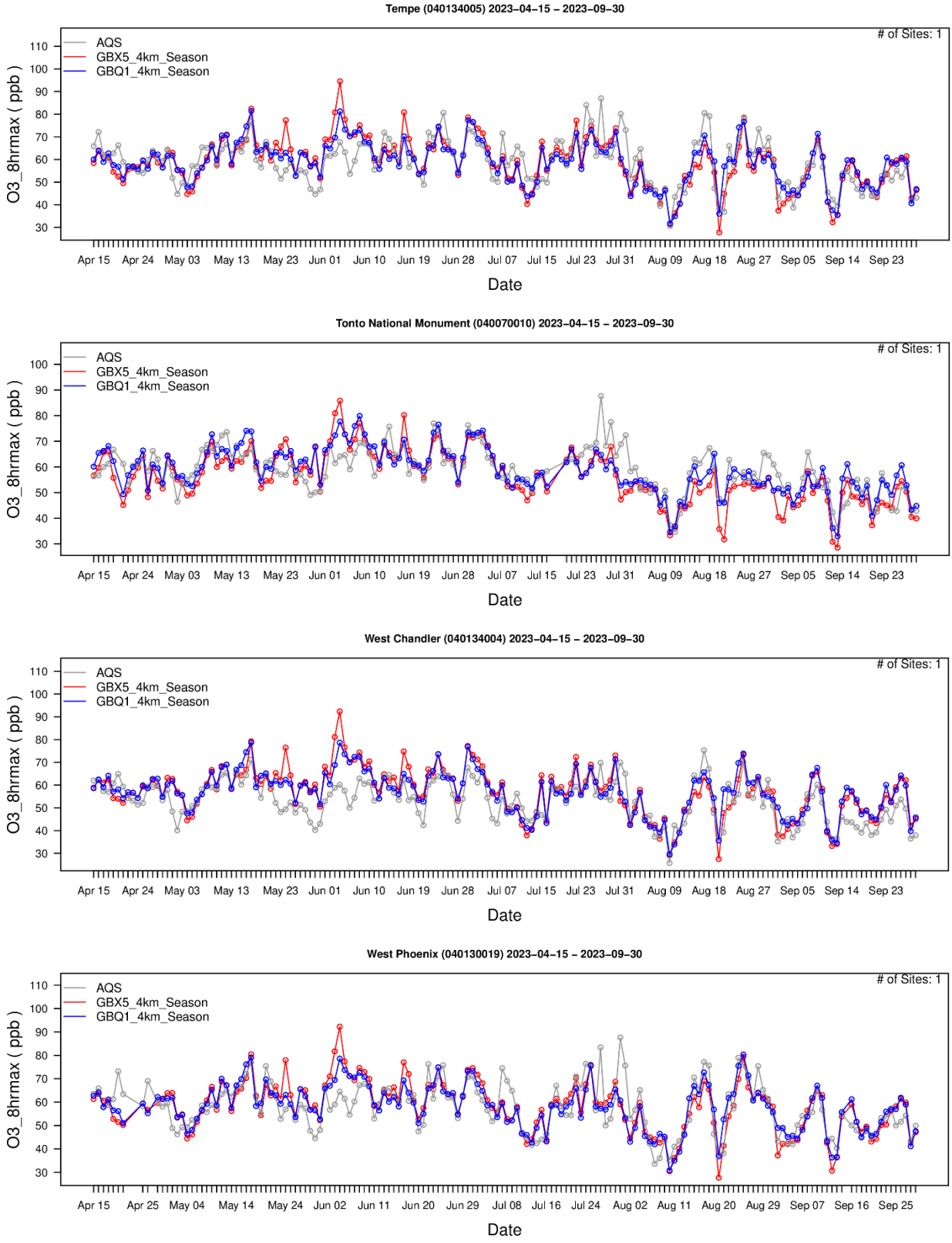

Figure 6-1. (Continued)

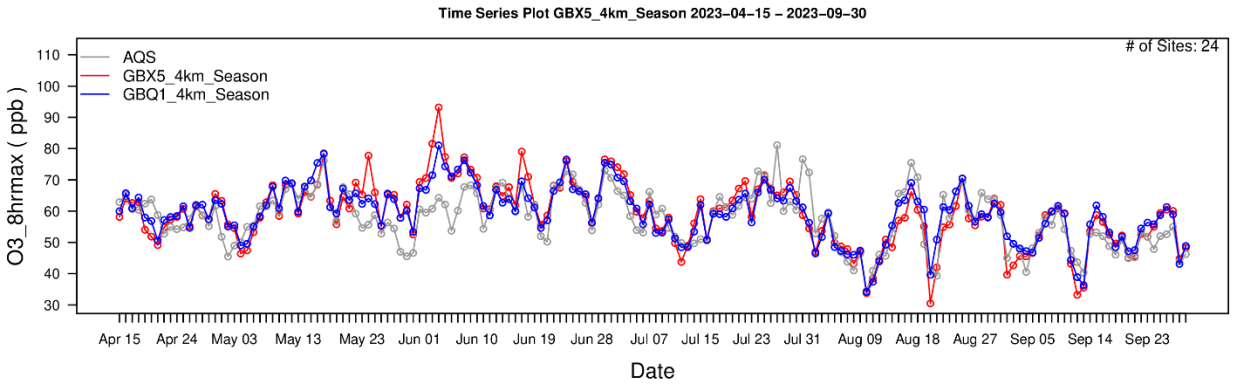

Figure 6-2. Time series of observed and modeled MDA8 ozone concentrations for monitors in the Maricopa NAA; observed (grey), CAMx (red), CMAQ (blue)

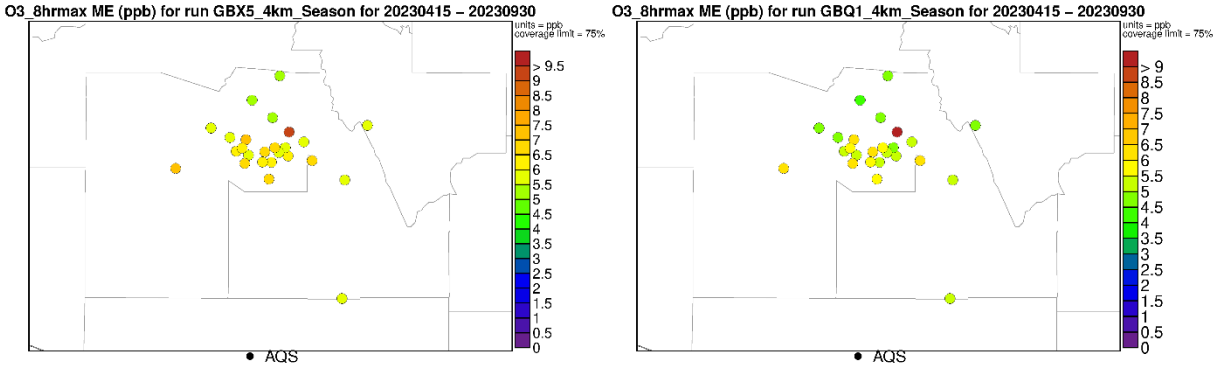

Figure 6-3. Spatial distribution of mean errors for modeled MDA8 ozone; CAMx (left), CMAQ (right)

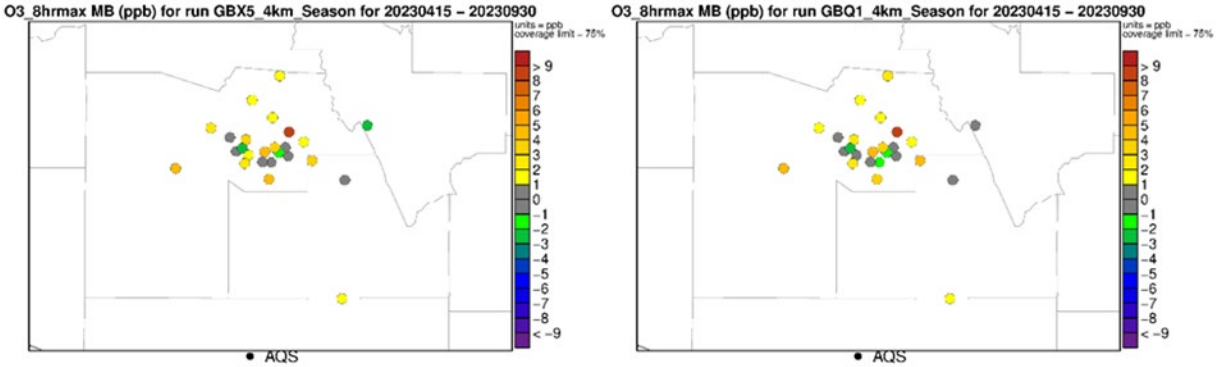

Figure 6-4. Spatial distribution of mean biases for modeled MDA8 ozone; CAMx (left), CMAQ (right)

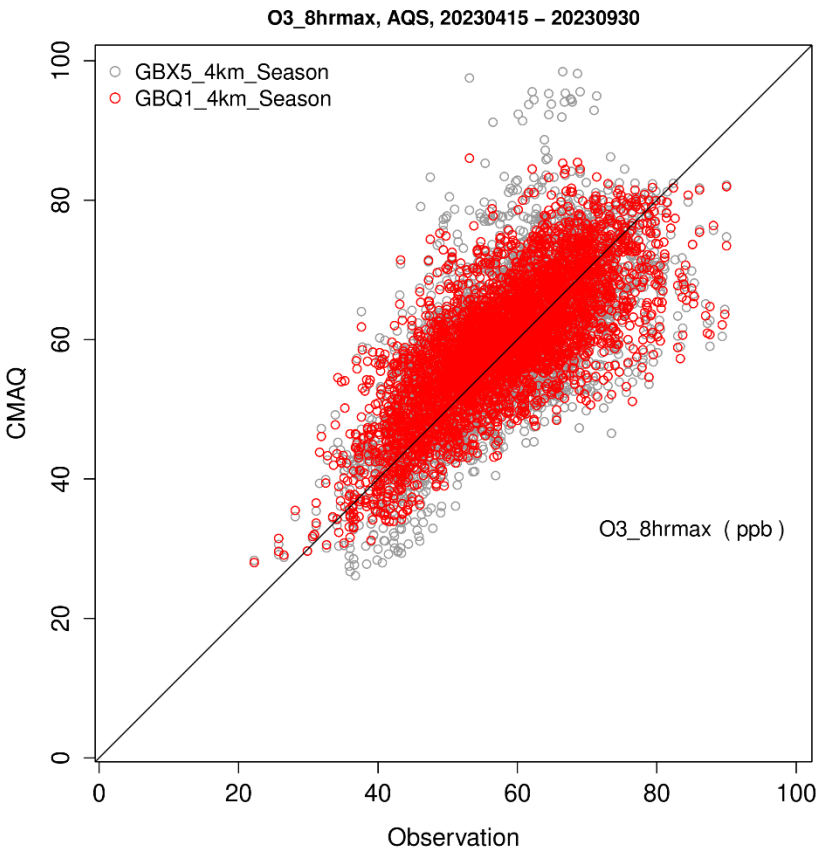

Figure 6-5. Scatter plot of observed and modeled MDA8 ozone concentrations for monitors in the Maricopa NAA; CAMx (gray), CMAQ (red)

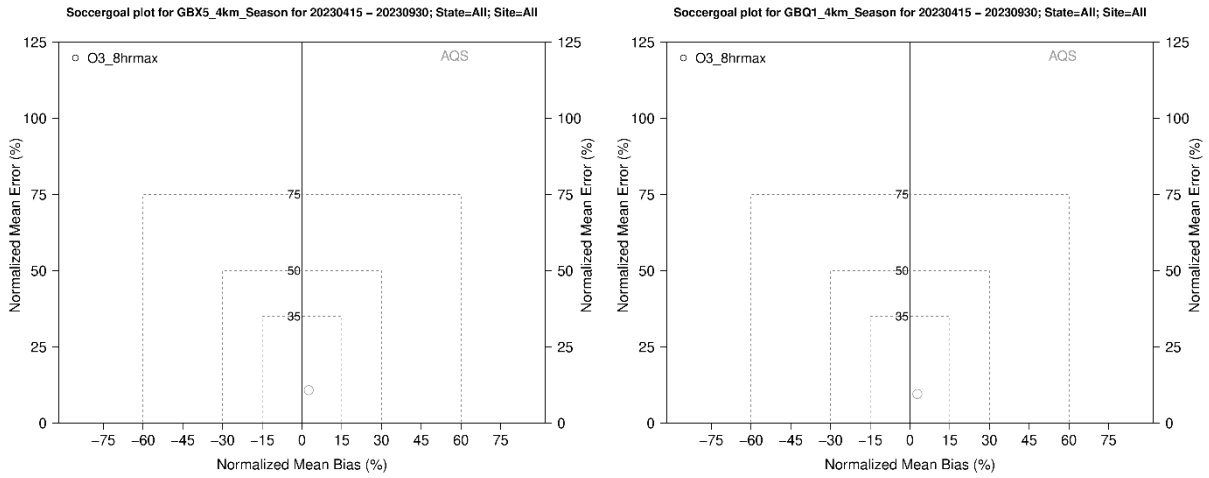

Figure 6-6. Soccer plots of MDA8 ozone normalized mean bias and error; (a) CAMx and (b) CMAQ

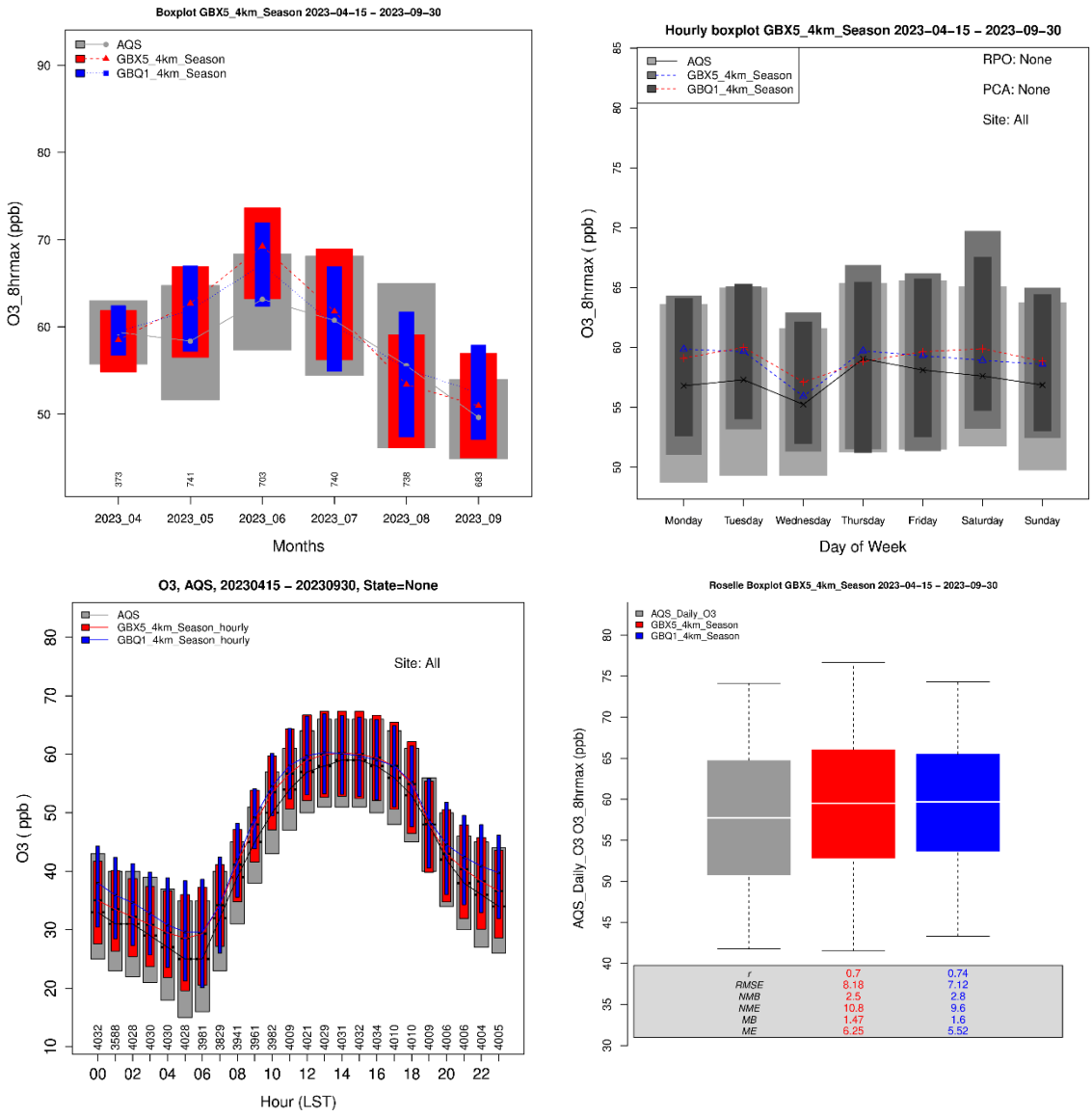

Figure 6-7. Box plots of modeled MDA8 ozone distribution for entire modeling period (top left), monthly distribution of modeled MDA8 ozone (top right), day of week distribution of modeled MDA8 ozone (bottom left), and diurnal distribution of modeled one-hour ozone (bottom right)

percentile, median, and 75th percentile values. For the monthly distribution of modeled MDA8 ozone, the CAMx/CMAQ model under predicts in April and August followed by over prediction in the remainder of the months. The day of week distribution indicates that the CAMx/CMAQ model closely tracks the observed values on Thursday and Friday but over predicts on the remainder of the days. For the diurnal distribution of one-hour ozone, the CAMx/CMAQ model closely tracks the observed concentrations during the afternoon but over predicts the remainder of the hours.

6.2.3. Evaluation of Ozone Precursors in the Maricopa NAA and Ozone in Mexico

Model performance was also evaluated for NO_2 and HCHO within the Maricopa nonattainment area, and for ozone observations from Mexico. July 2023 was selected as a representative midsummer period with strong photochemical activity.

Figure 6-8 compares observed and simulated hourly NO_2 at four AQS sites in the Maricopa nonattainment area (Buckeye, Central Phoenix, JLG Supersite, and West Phoenix) for July 2023. Buckeye, which represents a rural setting, shows generally low observed concentrations with occasional spikes of 10–20 ppb. CAMx reproduces the overall diurnal cycle but simulated daytime peaks are often below 5 ppb, much lower than observed, and day-to-day variability is reduced. Central Phoenix, located in the urban core, shows higher concentrations with pronounced morning and evening rush-hour peaks often reaching 20–40 ppb or higher. The model captures the timing of these events but underestimates their magnitude by 15–30 ppb. At JLG Supersite, also in an urban area, observed NO_2 includes frequent spikes of 10–25 ppb on top of a moderate background. CAMx follows the diurnal pattern reasonably well but remains consistently lower than observations, particularly during the morning build-up. At West Phoenix, observed concentrations are generally between the rural and central sites, with several peaks above 20 ppb. CAMx captures the diurnal pattern but remains lower than observations, and only limited comparison is possible after July 24 due to missing data. Overall, CAMx captures the timing of the NO_2 diurnal cycle across all four sites but generally underestimates the magnitude, with the largest bias at Central Phoenix.

Formaldehyde (HCHO) observations are available only at JLG Supersite through AQS. Figure 6-9 compares CAMx with three reported metrics: a 24-hr sample collected every six days ("24-hr 6-day"), an 8-hr sample collected every three days ("8-hr 3-day"), and the daily maximum 8-hr sample ("8-hr max"). Observed HCHO during July generally ranges from 4–8 ppb with modest variability across the month. CAMx values are consistently lower, mostly between 2–4 ppb, and unlike the observations they show a gradual upward trend through the month. The largest gap appears in the daily maximum 8-hr sample. The persistent low bias is consistent with known uncertainties in VOC emissions and secondary formaldehyde chemistry, and highlights the difficulty of simulating HCHO accurately at the regional scale.

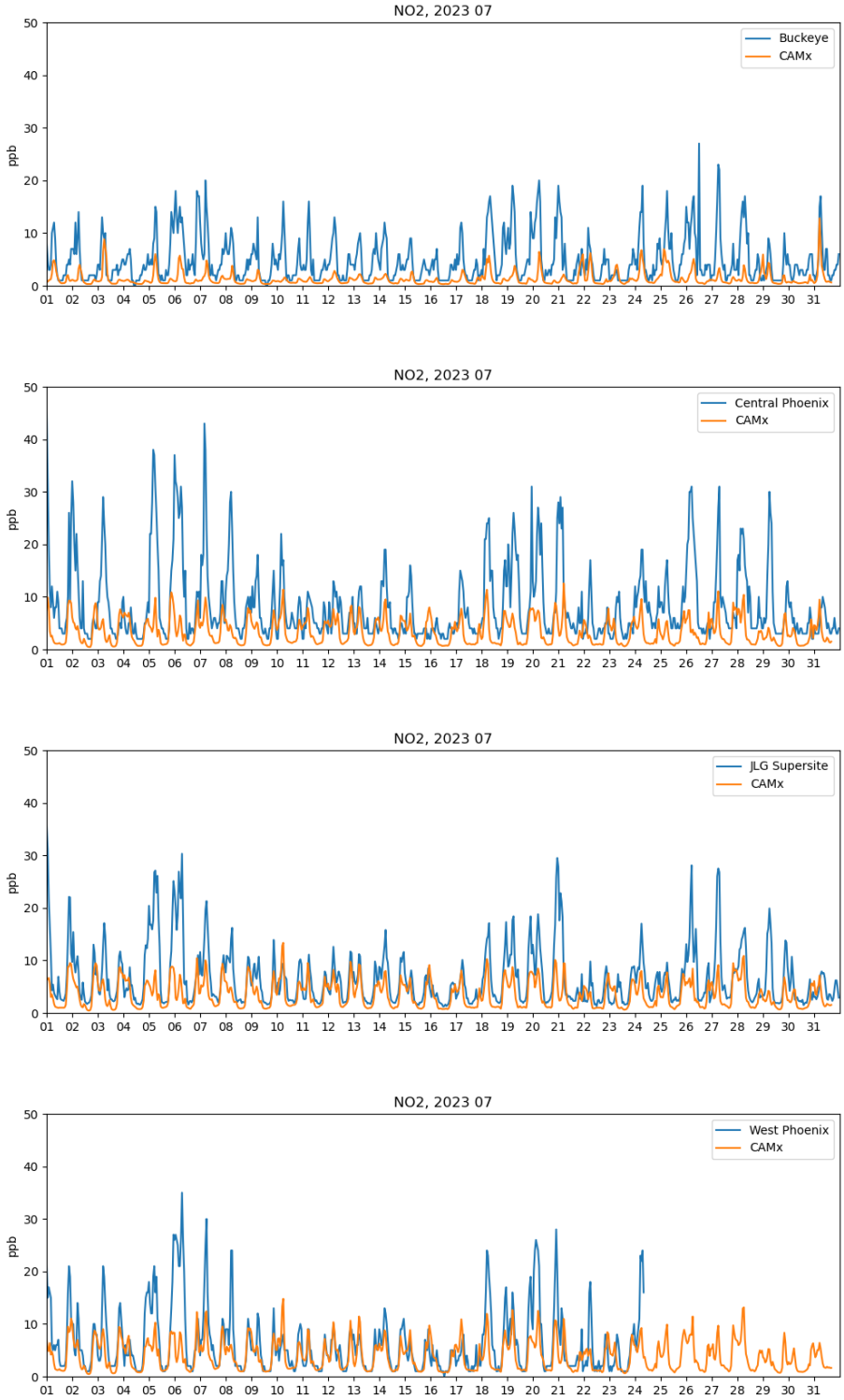

Figure 6-8. Hourly NO_2 time series for July 2023 at four AQS sites in the Maricopa nonattainment area (Buckeye, Central Phoenix, JLG Supersite, and West Phoenix). Observations are compared with CAMx base case

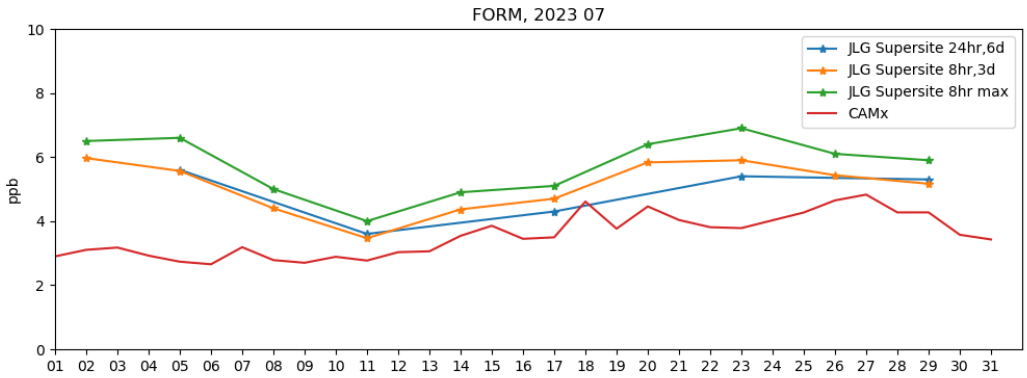

Figure 6-9. Formaldehyde (HCHO) at JLG Supersite for July 2023. AQS observations are reported as three metrics: a 24-hr sample collected every six days ("24-hr 6-day"), an 8-hr sample collected every three days ("8-hr 3-day"), and the daily maximum 8-hr sample ("8-hr max"). Observations are compared with CAMx base case

As a complementary evaluation, ozone observations from Mexican monitoring networks were examined. Data were obtained from the Mexican National Air Quality Information System (SINAICA) using the rsinaica R package, and sites within Guadalajara, Mexico City, and Monterrey were averaged to the city scale.

As shown in Figure 6-10, in Guadalajara, observations show a pronounced diurnal cycle with afternoon peaks commonly in the 60–100 ppb range. CAMx follows the daily timing but is generally 10–25 ppb lower at the afternoon maximum, and simulated overnight values often drop near zero while observations usually remain ~10–25 ppb. This produces an exaggerated diurnal range with too-low minima, likely reflecting limitations in nighttime chemistry or mixing and a possible underestimation of local emissions. In Mexico City, observed peaks are in a range similar to Guadalajara. CAMx captures the phase but underestimates the afternoon maximum by about 10–25 ppb on most days, while nighttime minima are closer to observations. The persistent low bias at peak hours may be linked to underestimated precursor emissions or photochemical activity during high-ozone episodes. In Monterrey, observed afternoon peaks are fairly regular, typically 50–75 ppb. CAMx reproduces the timing and shape of the diurnal cycle well, with peaks often within 5–10 ppb of the observations. Simulated values tend to be slightly higher, especially during the afternoon maximum, but overall Monterrey shows the best agreement between CAMx and observations among the three cities.

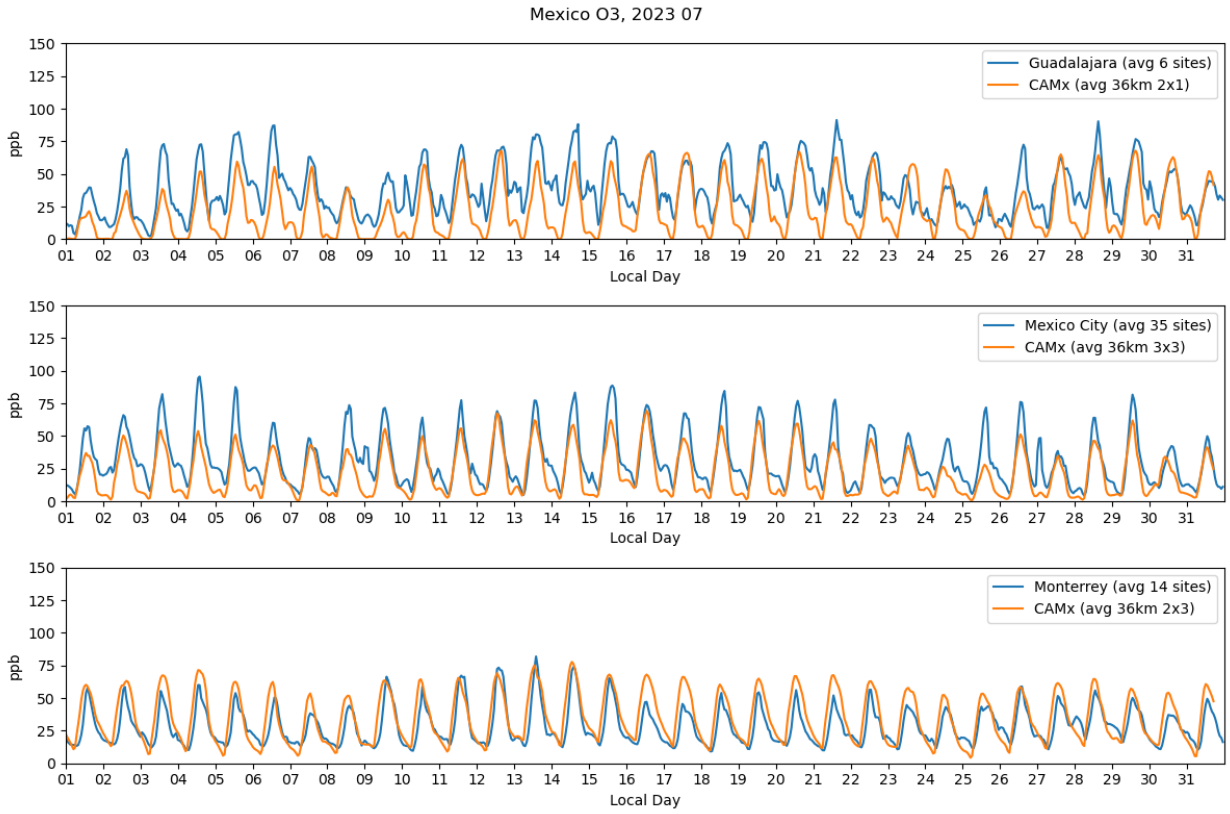

Figure 6-10. Hourly ozone for Guadalajara (top), Mexico City (middle), and Monterrey (bottom) averaged across monitoring sites for July 2023: comparison of SINAICA observations and CAMx base case

6.3. Diagnostic Evaluation

6.3.1. Satellite Data Comparison

In addition to ground-based monitors, we also evaluated the CAMx and CMAQ simulations using satellite observations of tropospheric NO_2 vertical column densities (VCDs) from the Tropospheric Monitoring Instrument (TROPOMI) onboard the Sentinel-5 Precursor (S5P) satellite operated by the European Space Agency (ESA). To ensure comparability between model outputs and satellite retrievals, we processed model concentrations into Level 3–like gridded products following the cmaqsatproc workflow (Henderson, 2023; https://github.com/barronh/cmaqsatproc), which facilitates direct comparison with TROPOMI. In this process, TROPOMI pixels were screened using a qa_value threshold of 0.75, which effectively removes cloud-contaminated scenes (cloud radiance fraction > 0.5), scenes partially covered by snow or ice, and retrievals flagged

with errors or other quality issues. Vertical concentration profiles from both CMAQ and CAMx were then integrated at satellite overpass times to produce total column densities on the model grids, extending from the surface to the model top (e.g., VGTOP = 5000 Pa for CMAQ).

Figure 6-11 presents monthly mean percent differences of CAMx and CMAQ NO_2 VCDs relative to TROPOMI in the 4 km domain for April–September 2023. CAMx shows small positive biases in spring and early summer (e.g., +7% in April and +10% in June), but shifts to modest underestimation later in the season (e.g., −13% in July). The transition from positive to negative biases in CAMx reflects more pronounced underestimation during high photochemical activity in midsummer. In contrast, CMAQ consistently underestimates TROPOMI column densities throughout the period, with differences exceeding −30% in midsummer. Overall, both models underpredict NO_2 columns compared to satellite retrievals of TROPOMI, with CAMx generally showing smaller negative biases than CMAQ over the study period.

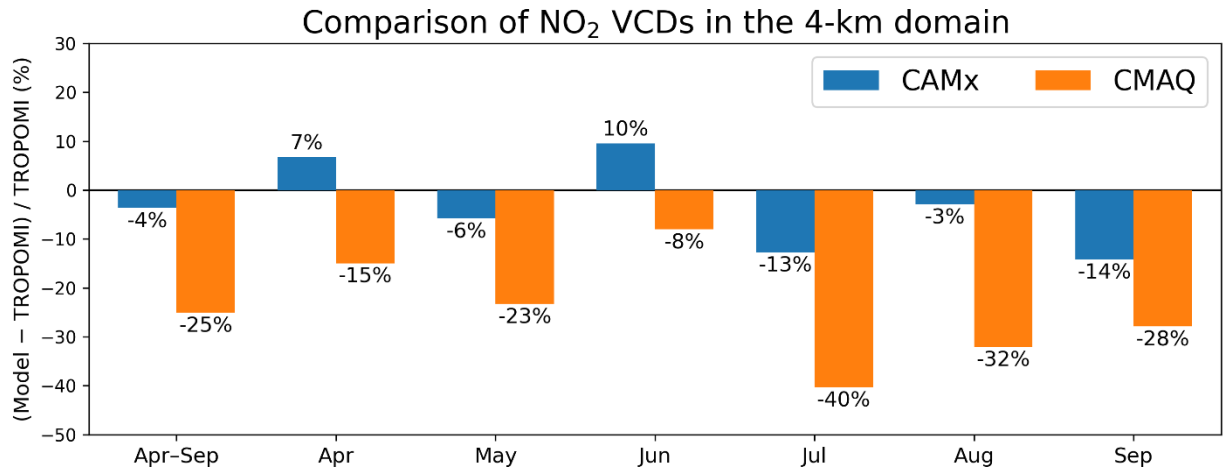

Figure 6-11. Comparison of CAMx and CMAQ simulated tropospheric NO_2 vertical column densities (VCDs) against TROPOMI observations over the 4 km domain during April–September 2023. Bars indicate monthly mean percent differences relative to TROPOMI

6.3.2. Upper-Air Data Comparison

As described in Section 5.5.2, ozonesonde profiles from NOAA's Global Monitoring Laboratory provide high-resolution vertical measurements of ozone from the surface through the lower stratosphere. These data are applied here to evaluate CAMx for selected launches at Trinidad Head, California, and Boulder, Colorado, on the same days

used for the GEOS-Chem evaluation (Figures 6-12 and 6-13). In contrast to surface observations that capture only near-ground conditions and satellite vertical column densities that represent integrated totals, ozonesondes offer layer-by-layer information. This allows a direct check on how CAMx represents ozone structure through the depth of the atmosphere.

At Boulder, CAMx matches the observed profiles reasonably well in the lower and middle troposphere. On May 4, differences below about 400 hPa are within 5–10 ppb, and the June 15 profile shows similar agreement. Larger differences occur higher up, which may reflect small errors in the placement of the tropopause, smoothing from the model's coarser vertical layers, and how stratospheric ozone and upper boundary conditions are handled. At Trinidad Head, the model exhibits noticeable differences near the boundary layer. On June 12, ozone is overestimated by about 10–25 ppb around 1000–800 hPa, with larger offset near the surface. The July 22 profile shows pronounced small-scale variability in the ozonesonde record that CAMx does not reproduce, leading to mismatches exceeding 20 ppb between 400 and 700 hPa. In the lower stratosphere, CAMx is again substantially higher than the observations.

CAMx captures the main vertical features and seasonal patterns of ozone at both sites, though it tends to be high in the coastal boundary layer at Trinidad Head and aloft near and above the tropopause. Its overall performance is comparable to that of GEOS-Chem and provides a reasonable representation of ozone at these locations.

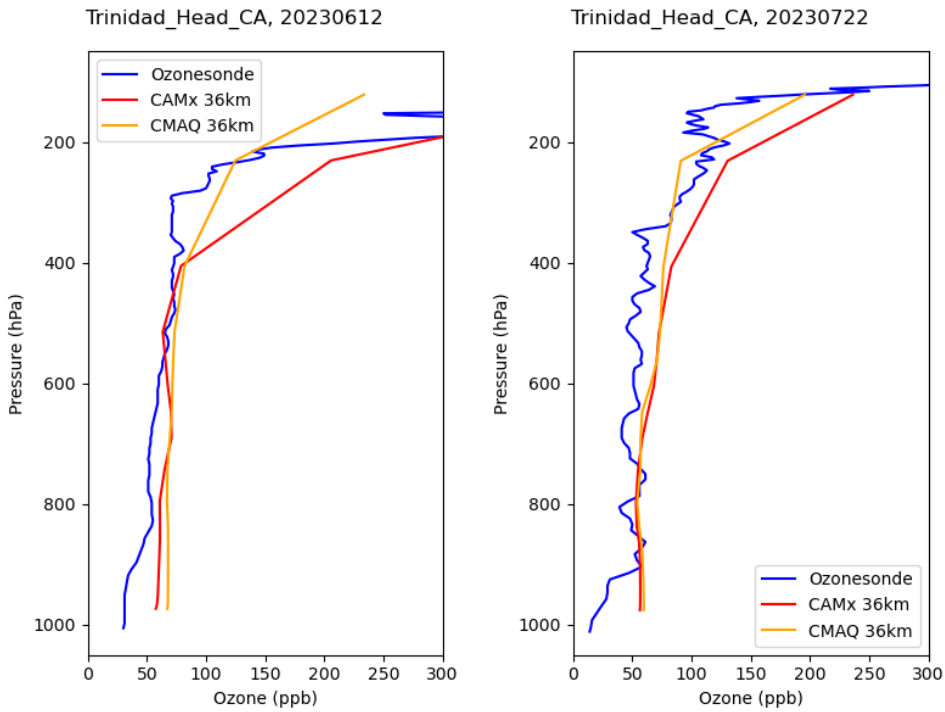

Figure 6-12. Comparison of CMAx/CMAQ and ozonesonde vertical ozone profiles at Trinidad Head, California, for June 12 and July 22, 2023

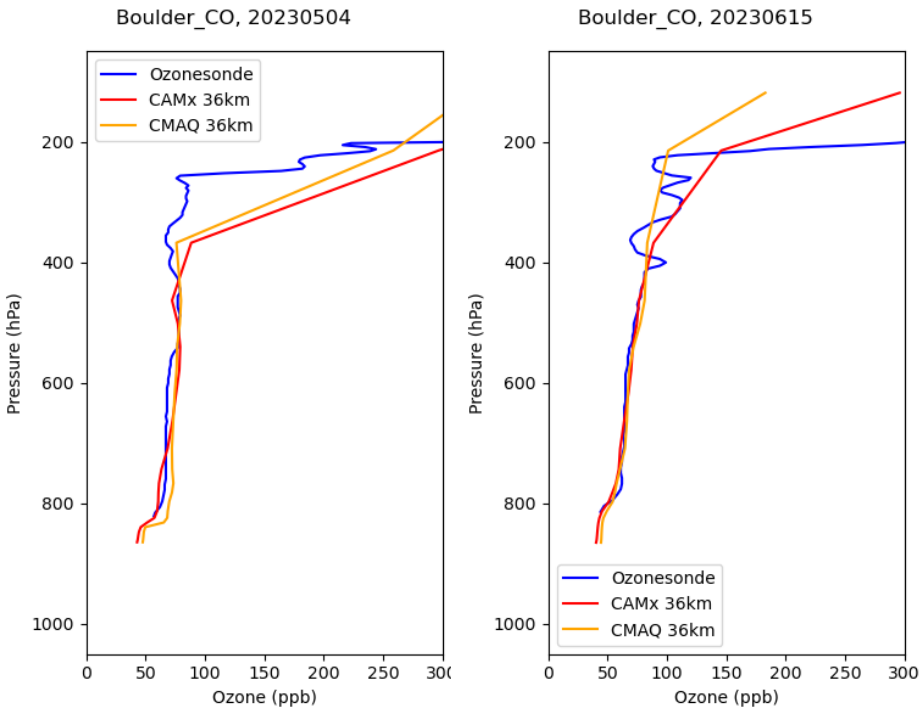

Figure 6-13. Comparison of CMAx/CMAQ and ozonesonde vertical ozone profiles at Boulder, Colorado, on May 4 and June 15, 2023

6.4. Performance Evaluation Summary and Conclusions

In evaluating the CAMx/CMAQ model performance for 2023 ozone data in the Maricopa NAA, statistical metrics such as normalized mean bias (NMB), normalized mean error (NME), and Index of Agreement were used. The target goals were ±15% for NMB and <35% for NME. Most model results met these goals, except for CAMx one-hour ozone in June, which slightly exceeded the NMB limit. The Index of Agreement showed good model-observation alignment overall, though it was weaker for high ozone levels (MDA8 > 60 ppb). Additionally, the five controlling monitors, which are those with the highest 2023 ozone values, also met the statistical goals and performed similarly to the overall network. Both models demonstrated acceptable and consistent performance.

Graphical analyses were used to visually assess the CAMx/CMAQ model's performance in simulating MDA8 ozone levels across the Maricopa NAA. Time series plots show that the model generally captures daily ozone variability but tends to overpredict in June and underpredict in August. Spatial plots reveal that the model performs consistently across most sites, with typical mean errors of 4–7 ppb and mean biases between -3 and 4 ppb, except at Fountain Hills, where biases were notably higher (8–9 ppb).

A scatter plot indicates that modeled ozone values align well with observed data, though with slightly higher bias at ozone levels above 60 ppb. Soccer goal plots demonstrate that model performance is within acceptable limits, indicating low systematic error and reasonable variability.

Finally, distribution plots show that predicted ozone levels closely match observed data across various percentiles, days of the week, and hours of the day. However, the model tends to underpredict in April and August, overpredict during other months, and overpredict on most days except Thursday and Friday. It tracks afternoon ozone well but overestimates during other times of the day.

7. SOURCE APPORTIONMENT AND ZERO-OUT DEMONSTRATION

This section presents the results of a source apportionment analysis and a zero-out analysis to corroborate an impact of international anthropogenic sources to the Maricopa NAA.

7.1. Demonstration of Zeroing-Out International Anthropogenic Sources

The zero-out simulations (i.e, brute force methods) are a traditional method to identify the contributions from specific pollutants, source groups/categories, and source regions. Although zero-out methods have some limitations due to chemical nonlinearities and unrealistic assumptions, they are commonly used as supporting tools in source apportionment analysis to cross-validate results. To quantify the contribution of international anthropogenic emissions to ozone concentrations of the monitoring sites in the Maricopa NAA in 2023, CAMx zero-out simulations were performed using the GEOS-Chem zero-out IA scenario as IC/BC and removing Mexico anthropogenic emissions within the CAMx modeling domains.

7.1.1. Calculation of Relative Response Factors (RRFs)

For the modeled attainment demonstration, the EPA guidance recommends using modeled base year and future (or sensitivity) ozone concentrations in a relative manner to estimate future year design values (U.S. EPA, 2018). The relative response factors (RRF) are the ratios calculated from the fractional changes in ozone concentrations between the sensitivity and base case scenarios at each ozone monitoring site in the Maricopa NAA.

Given the more stringent ozone NAAQS, EPA guidance calls for calculating RRFs using the 10 highest modeled ozone days for each monitor, including the grid cell containing the monitor and its surrounding 3×3 array of cells. Modeled MDA8 ozone concentrations were averaged over the 10 highest MDA8 ozone near the monitor without additional consideration since all base MDA8 ozone concentrations were greater than or equal to 60 ppb. These RRFs (unadjusted RRFs) were calculated by the Software for Model Attainment Test – Community Edition (SMAT-CE; U.S. EPA, 2024) and paired with the EPA base year design values.

In addition, following the EPA guidance, which also recommends considering removal of atypical events from the RRF calculation, another set of RRFs was calculated by removing the 16 wildfire atypical events in 2023 and adding the next-highest modeled days from outside the top 10 to maintain the use of 10 days in the RRF calculation. These RRFs (MAG

RRFs) were paired with the MAG base year design values, which were derived by excluding the 31 wildfire atypical events in 2021-2023. The wildfire atypical events for 2021-2023 are listed in Table 7-1. The calculated RRFs for each site are listed in the next section.

Table 7-1. Wildfire atypical events for 2021-2023

2021	2022	2023
6/15/2021	6/15/2022	6/22/2023
6/16/2021	6/16/2022	6/23/2023
6/28/2021	7/15/2022	6/24/2023
6/29/2021	7/16/2022	6/25/2023
7/1/2021	7/17/2022	6/26/2023
7/20/2021		6/30/2023
7/21/2021		7/24/2023
7/22/2021		7/25/2023
8/3/2021		7/26/2023
8/4/2021		7/27/2023
		7/28/2023
		7/29/2023
		7/31/2023
		8/1/2023
		8/17/2023
		8/18/2023

7.1.2. Calculation of Design Values without International Anthropogenic

Following the SMAT-CE procedure described in EPA's modeling guidance for the attainment demonstration (U.S. EPA, 2018), the modeled base and zero-out scenarios were used to quantify IA impacts on all ozone monitoring sites in the Maricopa NAA based on the 2023 base year design values (DVB). When the projected design values without international anthropogenic emissions (DVF) are less than or equal to the current NAAQS level, the modeled retrospective demonstration indicates that the Maricopa NAA would have attained the 2015 ozone NAAQS by the attainment date of August 3, 2024, but for international anthropogenic contributions. DVF for monitoring site *i* was calculated using Equation 1 below:

$$(DVF)_i = (RRF)_i(DVB)_i \quad (1)$$

where $(DVF)_i$ is the estimated design value without international anthropogenic emissions at monitoring site *i*; $(RRF)_i$ is the relative response factor for monitoring site *i*; and $(DVB)_i$ is the base year design value monitored at monitoring site *i*.

The 2023 EPA 8-hour ozone DVBs were established as the 3-year average of the annual fourth highest MDA8 ozone for a specific monitor from observations during 2021-2023. Also, the 2023 MAG DVBs were calculated in the same manner as the 2023 EPA DVBs but excluding the 31 wildfire atypical events for 2021-2023 from the annual fourth highest MDA8 ozone selection. As presented in Table 7-2, the highest 2023 EPA DVB of 80 ppb appeared at two monitoring sites (Mesa and JLG Supersite) and the highest 2023 MAG DVB of 77 ppb appeared at four monitoring sites (North Phoenix, Glendale, Lehi, and JLG Supersite). For the DVF calculation, the EPA DVBs were paired with the unadjusted RRFs and the MAG DVBs were paired with the MAG RRFs.

Table 7-2. 2023 DVBs for the ozone monitoring sites in the Maricopa NAA (unit: ppb)

Site ID	Site Name	County	EPA DVB*	MAG DVB**
40070010	Tonto NM	Gila	75.0	72.0
40130019	West Phoenix	Maricopa	77.0	74.0
40131003	Mesa	Maricopa	**80.0**	76.0
40131004	North Phoenix	Maricopa	78.0	**77.0**
40131010	Falcon Field	Maricopa	79.0	76.0
40132001	Glendale	Maricopa	79.0	**77.0**
40132005	Pinnacle Peak	Maricopa	77.0	76.0
40133002	Central Phoenix	Maricopa	77.0	73.0
40133003	South Scottsdale	Maricopa	74.0	72.0
40134003	South Phoenix	Maricopa	73.0	68.0
40134004	West Chandler	Maricopa	71.0	70.0
40134005	Tempe	Maricopa	77.0	73.0
40134008	Cave Creek	Maricopa	73.0	71.0
40134010	Dysart	Maricopa	75.0	74.0
40134011	Buckeye	Maricopa	69.0	67.0
40137021	Red Mountain	Maricopa	77.0	75.0
40137022	Lehi	Maricopa	79.0	**77.0**
40137024	High School	Maricopa	75.0	72.0
40139508	Humboldt Mountain	Maricopa	70.0	69.0
40139702	Blue Point	Maricopa	76.0	73.0
40139704	Fountain Hills	Maricopa	74.0	72.0
40139997	JLG Supersite	Maricopa	**80.0**	**77.0**
40213001	Apache Junction	Pinal	72.0	71.0
40218001	Queen Valley	Pinal	75.0	72.0

* Based on the EPA's 2023 design values (average of the annual 4th highest MDA8 in 2021-2023).
** Based on the MAG's 2023 design values excluding the wildfire atypical events in 2021-2023.

Lastly, following Equation 1, two sets of DVFs were calculated to quantify the IA emissions impact for individual ozone monitoring sites in the 8-hour ozone NAA based on the CAMx zero-out scenario. One set of DVFs was calculated using the EPA DVBs and unadjusted RRFs as shown in Table 7-3. The other set of DVFs was calculated using the MAG DVBs paired with the MAG RRFs as listed in Table 7-4. According to the unadjusted RRFs and MAG RRFs, the most influential site from the IA emissions (the lowest RRF) was Buckeye. The least influential sites from the IA emissions (the highest RRF) were Central Phoenix and JLG Supersite (0.873) among the unadjusted RRFs, and South Scottsdale (0.857) among the MAG RRFs. For the DVF, the maximum 2023 DVF appeared at JLG Supersite (70 ppb) based on the EPA DVBs paired with unadjusted RRFs and North Phoenix (65.8 ppb) based on the MAG DVBs paired with the MAG RRFs.

Table 7-3. Unadjusted RRF and DVF of CAMx sensitivity runs excluding IA emissions using zero-out method, as well as the EPA DVB

Site ID	Site Name	EPA DVB	Unadjusted RRF	DVF
40070010	Tonto NM	75.0	0.827	62.0
40130019	West Phoenix	77.0	0.859	66.1
40131003	Mesa	**80.0**	0.872	69.7
40131004	North Phoenix	78.0	0.841	65.5
40131010	Falcon Field	79.0	0.862	68.0
40132001	Glendale	79.0	0.842	66.4
40132005	Pinnacle Peak	77.0	0.823	63.3
40133002	Central Phoenix	77.0	**0.876**	67.4
40133003	South Scottsdale	74.0	0.872	64.5
40134003	South Phoenix	73.0	0.864	63.0
40134004	West Chandler	71.0	0.847	60.1
40134005	Tempe	77.0	0.871	67.0
40134008	Cave Creek	73.0	0.803	58.6
40134010	Dysart	75.0	0.806	60.4
40134011	Buckeye	69.0	0.770	53.1
40137021	Red Mountain	77.0	0.854	65.7
40137022	Lehi	79.0	0.853	67.3
40137024	High School	75.0	0.854	64.0
40139508	Humboldt Mountain	70.0	0.796	55.7
40139702	Blue Point	76.0	0.845	64.2
40139704	Fountain Hills	74.0	0.847	62.6
40139997	JLG Supersite	**80.0**	**0.876**	**70.0**
40213001	Apache Junction	72.0	0.868	62.5
40218001	Queen Valley	75.0	0.831	62.2

Table 7-4. MAG RRF and DVF of CAMx sensitivity runs excluding IA emissions using zero-out method, as well as the MAG DVB

Site ID	Site Name	MAG DVB	MAG RRF	MAG DVF
40070010	Tonto NM	72.0	0.822	59.1
40130019	West Phoenix	74.0	0.832	61.5
40131003	Mesa	76.0	0.856	65.0
40131004	North Phoenix	**77.0**	0.855	**65.8**
40131010	Falcon Field	76.0	0.843	64.0
40132001	Glendale	**77.0**	0.832	64.0
40132005	Pinnacle Peak	76.0	0.831	63.1
40133002	Central Phoenix	73.0	0.854	62.3
40133003	South Scottsdale	72.0	**0.857**	61.6
40134003	South Phoenix	68.0	0.829	56.3
40134004	West Chandler	70.0	0.854	59.7
40134005	Tempe	73.0	0.855	62.4
40134008	Cave Creek	71.0	0.798	56.6
40134010	Dysart	74.0	0.817	60.4
40134011	Buckeye	67.0	0.782	52.4
40137021	Red Mountain	75.0	0.838	62.8
40137022	Lehi	**77.0**	0.843	64.9
40137024	High School	72.0	0.838	60.3
40139508	Humboldt Mountain	69.0	0.798	55.0
40139702	Blue Point	73.0	0.837	61.0
40139704	Fountain Hills	72.0	0.839	60.3
40139997	JLG Supersite	**77.0**	0.853	65.7
40213001	Apache Junction	71.0	0.842	59.7
40218001	Queen Valley	72.0	0.824	59.2

7.2. Demonstration of Source Apportionment

Source apportionment methods are complementary techniques used to identify emission sources and geographic regions that contribute to elevated ozone concentrations. These tools are valuable for characterizing the sources that most significantly influence ozone levels within the model. The CAMx air quality model offers source apportionment capabilities to help identify the origins of ozone formation. Source apportionment methods available for CAMx are the Ozone Source Apportionment Technology (OSAT). This tool uses reactive tracers operated in parallel to the main photochemical model to link ozone concentrations to specific emission source sectors and geographic regions selected by the user. Without perturbing the underlying relationships between all sources

and concentrations, these sets of tracer species track the fate of precursors from different emission sources and geographic regions, as well as the ozone formed from those precursors under VOC-sensitive or NO_x-sensitive conditions. These methods are useful both as a diagnostic tool for identifying key contributors to ozone levels and as a support for regulatory analysis by pinpointing effective emission control strategies for meeting air quality standards. A key advantage of source apportionment techniques is their use of tracers to quantify the mass contribution of each source to a receptor, making them less affected by the non-linear chemical interactions that can complicate the interpretation of sensitivity simulations.

CAMx OSAT was utilized to quantify the contribution of international anthropogenic emissions to ozone concentrations at the monitoring sites in the Maricopa NAA in 2023. For this source apportionment analysis, four source regions as shown in Figure 7-1 were identified and nine emission source groups as defined in Table 7-5 were tracked by reactive tracers.

To evaluate international anthropogenic impact for the 179B demonstration, it is critical to transfer apportionment information derived from global chemistry models to CAMx source apportionment applications. Within traditional IC/BC tracers used in typical applications, source apportionment techniques could not transfer apportionment information from global chemistry models to the master domain. However, CAMx has introduced SAT IC/BC files (since version 7.0) which accommodate the ability to transfer apportionment information from global chemistry models to the CAMx OSAT application. In this analysis, IC/BC derived from GEOS-Chem were provided to CAMx in two groups. One group represents IA ozone and precursors and the other represents global natural and US emissions outside the 36 km master domain.

The 2023 CAMx OSAT results were extracted at the locations of all ozone monitoring sites in the Maricopa NAA from the 4 km grid output files. The hourly ozone tracers and ozone concentrations were post-processed to calculate MDA8 values each day. For each grid cell on each day, the MDA8 hour corresponding to the base case MDA8 ozone was used to calculate MDA8 values for all ozone tracers. Using an R script developed by MAG, the post-processed MDA8 values of all ozone tracers were compiled into a spreadsheet and reorganized to visualize the source apportionment contribution plots presented below.

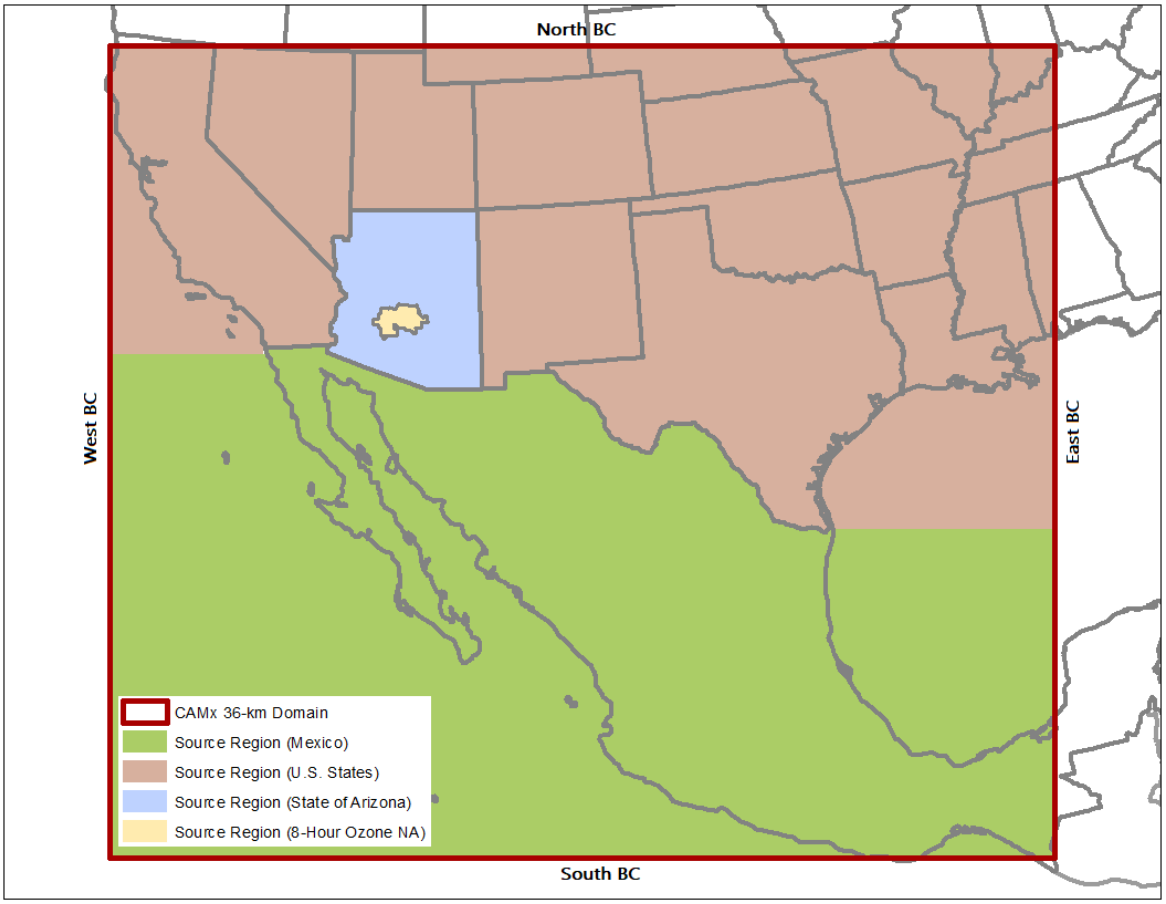

Figure 7-1. Emission source regions for the source apportionment analysis

Table 7-5. Emission source groups for the source apportionment analysis

Group ID	Group Name	Description
IC/BC IA	International Anthropogenic	Non-US anthropogenic emissions estimated based on 2023 GEOS-Chem base case and zero-out simulations
IC/BC Rem	Global Natural & US Anthropogenic	Global natural emissions plus US biogenic and anthropogenic emissions from outside the 36 km grid, based on 2023 GEOS-Chem base case and zero-out simulations
1	Biogenic	Biogenic emissions for each source region
2	Area	Area emissions for each source region
3	Onroad	Onroad emissions for each source region
4	Nonroad	Nonroad emissions for each source region
5	Point	Point emissions for each source region
6	Wildfire	Wildfire emissions for each source region
7	Lightning NO_x	Lightning NO_x emissions for each source region

Figure 7-2 presents a stacked area plot showing source contributions from natural and anthropogenic source groups of each source region compared to the 2023 site-averaged MDA8 ozone in the Maricopa NAA, for the period April 15th to September 30th. The stacked area plot indicates that the transported boundary condition of the 36 km master domain (BC IA + BC Rem) was the major contributor (about 79%) to site-averaged MDA8 ozone in the Maricopa NAA over April to June and its contribution reduced to about 51% for the later months. Local contribution (anthropogenic and natural) within the Maricopa NAA showed the opposite pattern, which was about 16% contribution over April to June and about 33% contribution for the later months. In this figure, natural sources includes three source groups, which are biogenic, wildfire, and lightning NO_x.

Focusing on the international anthropogenic source contributions to 2023 site-averaged MDA8 ozone in the Maricopa NAA, Figure 7-3 presents daily anthropogenic source contributions from Asia/Intercontinental anthropogenic sources (BC IA) and Mexico anthropogenic sources (Mexico IA). The contributions from BC IA and Mexico IA showed similar patterns to total BC (BC IA + BCRem) and local contributions, respectively. Interestingly, Mexico IA became larger than BC IA contribution during July through August, coinciding with southerly monsoonal flow.

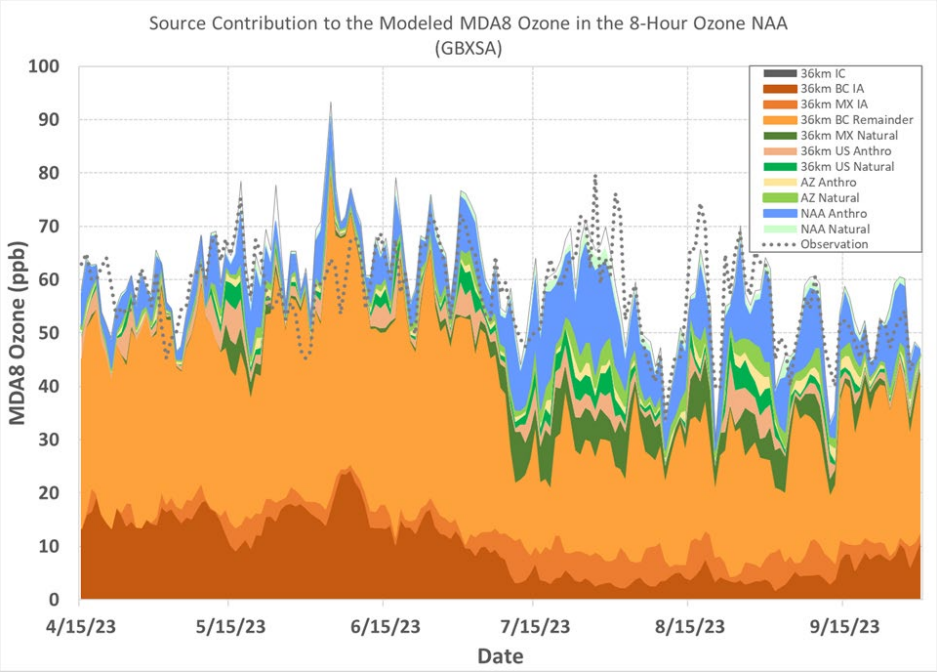

Figure 7-2. Daily source contributions to the CAMx modeled MDA8 ozone in the Maricopa NAA

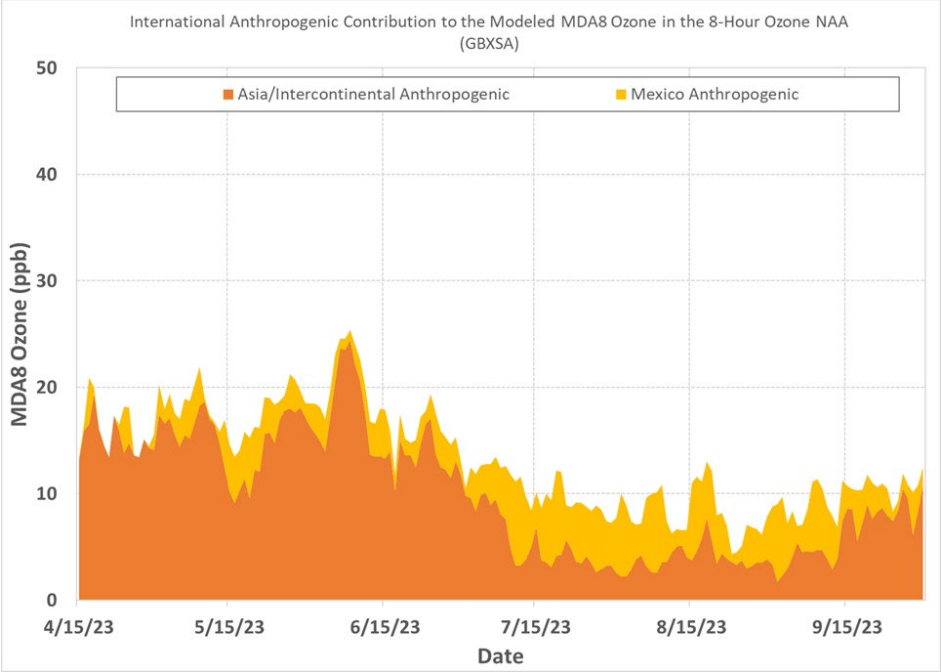

Figure 7-3. Daily international anthropogenic source contributions to the CAMx modeled MDA8 ozone in the Maricopa NAA

Augmenting the international anthropogenic source contributions, the four NAA anthropogenic source groups were added in Figure 7-4 to compare the evolution of relative contributions from international versus local anthropogenic sources. Local anthropogenic contributions were much smaller than total IA contributions during April through June and became comparable to total IA during July through August. Among the four NAA anthropogenic source groups, the onroad source contributed most to MDA8 ozone in the Maricopa NAA over the entire modeling period, followed by nonroad, area, and point sources. The Maricopa NAA onroad source contributions were comparable to the Mexico IA contributions.

The contributions from total IA and NAA anthropogenic sources were averaged by month in Figure 7-5 to illustrate clearer monthly comparison of relative contributions from total IA versus local anthropogenic sources. The relative contributions from total IA were the highest in May (29%) and the lowest in August (16%), while the relative contributions from NAA anthropogenic sources were the highest in July (19%) and the lowest in May (6%). The seasonal average contributions from total IA and NAA anthropogenic sources were 22% and 12%, respectively. This indicates that the transported IA contributions were almost double the local anthropogenic contributions over the entire modeling period from April through September 2023.

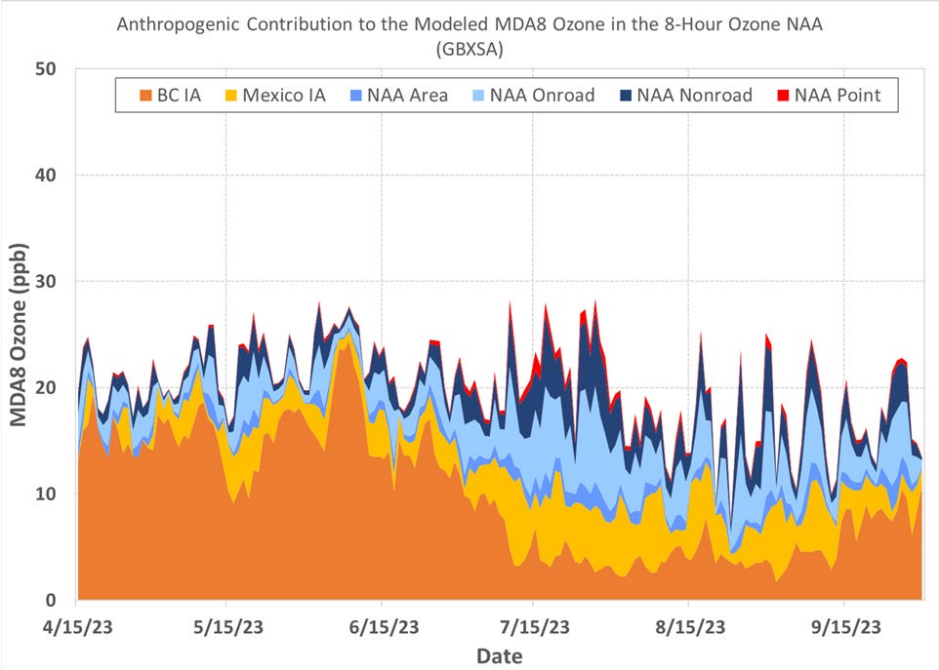

Figure 7-4. Daily international anthropogenic source contributions to the CAMx modeled MDA8 ozone in the Maricopa NAA

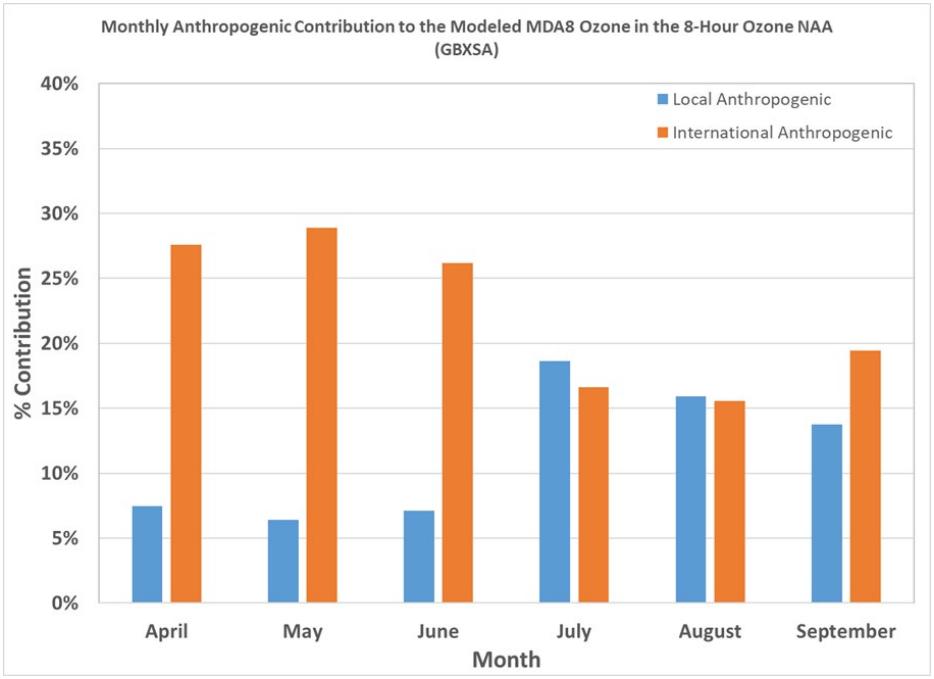

Figure 7-5. Monthly anthropogenic source contributions to the CAMx modeled MDA8 ozone in the Maricopa NAA; total IA (BC IA + Mexico IA) vs. local (NAA Anthro)

For the entire modeling period and for the modeled top 10 days, the overall contributions from NAA anthropogenic sources, BC IA, and Mexico IA are presented in Figure 7-6. The modeled top 10 days for each monitoring site were selected and the contributions on those top 10 days at each monitoring site were averaged to calculate the site-averaged contributions. For both selections of modeled days, the relative contributions among these three sources showed similar patterns, which are in order of BC IA (17-18%), NAA anthropogenic sources (10-12%), and Mexico IA (3-6%). Since most of the modeled top 10 days occurred during May through June, the BC IA contributions for the modeled top 10 days were higher than those for the entire modeling period.

For the entire modeling domains, the regional source contributions (anthropogenic + natural) from all four regions and BC to the site-averaged MDA8 ozone in the 8-hour ozone NAA are presented in Figure 7-7. For the entire modeling period, the total BC contributed most to the Maricopa NAA with 64%, followed by NAA (13%), Mexico (10%), 36 km U.S. (6%), and Arizona (5%). This contribution order for the modeled top 10 days slightly changes to the order of total BC (71%), NAA (12%), 36 km U.S. (7%), Mexico (5%), and Arizona (3%).

Also, the contributions from all source groups and BC IA and BC Rem to the site-averaged MDA8 ozone in the 8-hour ozone NAA were illustrated in Figure 7-8. For the entire modeled days, the BC Rem contributed most to the Maricopa NAA with 48%, followed by the BC IA (17%), onroad (12%), natural (11%), nonroad (6%), area (3%), and point (2%). The contribution order for the modeled top 10 days remained the same in the order of BC Rem (54%), BC IA (18%), onroad (10%), natural (7%), nonroad (6%), area (2%), and point (2%).

Lastly, the same RRF calculation methods used for the zero-out analysis were applied to the post-processed CAMx OSAT results, which were hourly cumulative ozone concentrations excluding ozone tracers for the sources of interest, which were the total IA (BC IA + Mexico IA) and NAA anthropogenic emissions. Two sets of DVFs were calculated to quantify the IA emissions impact for individual ozone monitoring sites in the Maricopa NAA, as well as additional two sets of DVFs to quantify the Maricopa NAA anthropogenic impact. Table 7-6 lists DVFs calculated using the EPA DVBs and unadjusted RRFs and Table 7-7 presents DVFs calculated using the MAG DVBs paired with the MAG RRFs.

According to the unadjusted RRFs, the most influenced sites (the lowest RRF) from the IA emissions and NAA anthropogenic emissions were Buckeye (0.724) and Central Phoenix (0.835), respectively. The least influenced sites (the highest RRF) from the IA emissions

and NAA anthropogenic emissions were totally opposite from the most influenced sites, which were Central Phoenix (0.830) and Buckeye (0.978), respectively.

For the MAG RRFs, the most influenced sites (the lowest RRF) from the IA emissions and NAA anthropogenic emissions were Buckeye (0.734) and South Scottsdale (0.860), respectively. The least influenced sites (the highest RRF) from the IA emissions and NAA anthropogenic emissions were Mesa/South Scottsdale/Tempe (0.811) and Buckeye (0.978), respectively.

For the retrospective demonstration for the excluding IA scenario, the maximum 2023 DVF appeared at JLG Supersite (66.2 ppb) based on the EPA DVBs paired with unadjusted RRFs and North Phoenix (62.2 ppb) based on the MAG DVBs paired with the MAG RRFs. The maximum 2023 DVF appeared at the same sites as the zero-out scenario in the previous section but values were lower about 4 ppb.

For the OSAT scenario excluding NAA anthropogenic emissions, the maximum 2023 DVF appeared at Tonto National Monument (70.9 ppb) based on the EPA DVBs paired with unadjusted RRFs and Glendale (68.8 ppb) based on the MAG DVBs paired with the MAG RRFs.

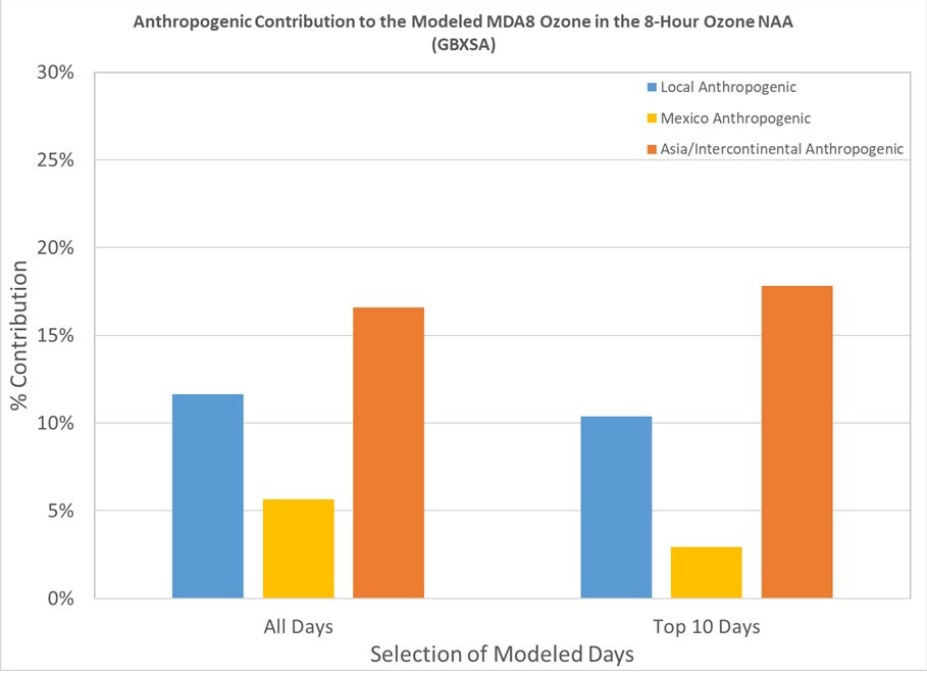

Figure 7-6. Anthropogenic source contributions to the CAMx modeled MDA8 ozone in the Maricopa NAA for all modeled days and modeled top 10 days

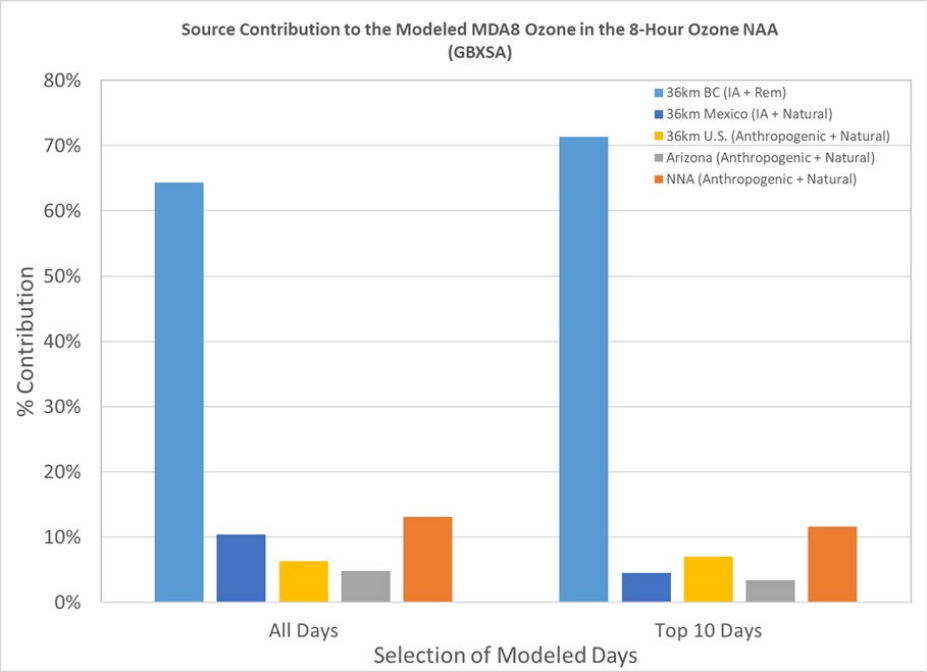

Figure 7-7. Regional source contributions to the CAMx modeled MDA8 ozone in the Maricopa NAA for all modeled days and modeled top 10 days

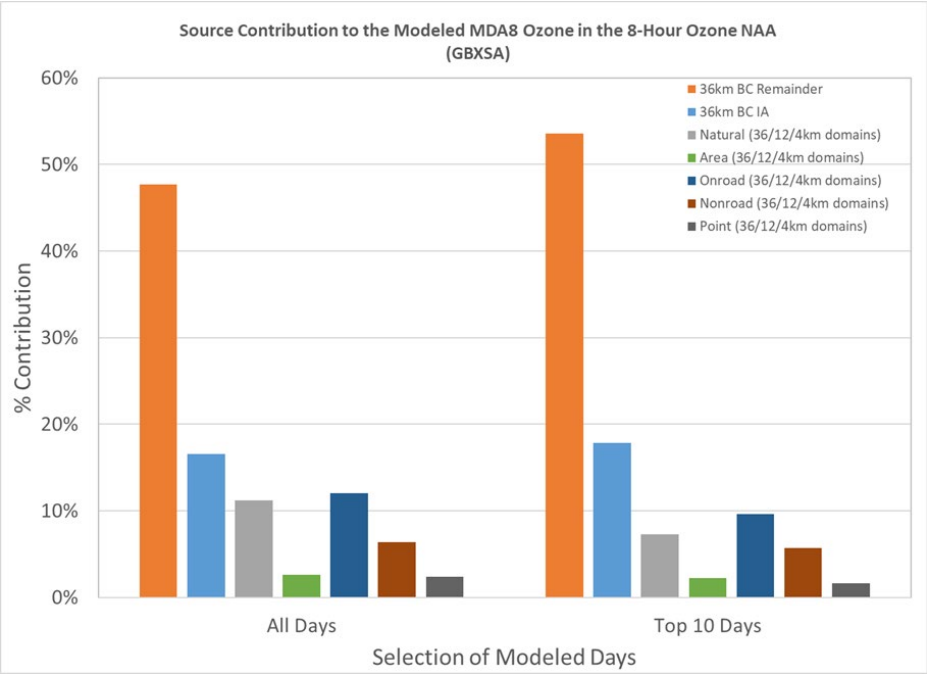

Figure 7-8. Source group contributions to the CAMx modeled MDA8 ozone in the Maricopa NAA for all modeled days and modeled top 10 days

Table 7-6. Unadjusted RRF and DVF of CAMx sensitivity runs excluding IA emissions and NAA emissions using OSAT, as well as the EPA DVB

Site ID	Site Name	EPA DVB	Excluding IA		Excluding NAA Anthro	
			Unadjusted RRF	DVF	Unadjusted RRF	DVF
40070010	Tonto NM	75.0	0.784	58.7	0.945	**70.9**
40130019	West Phoenix	77.0	0.814	62.6	0.862	66.3
40131003	Mesa	**80.0**	0.826	66.0	0.852	68.1
40131004	North Phoenix	78.0	0.797	62.1	0.885	69.0
40131010	Falcon Field	79.0	0.821	64.8	0.837	66.1
40132001	Glendale	79.0	0.796	62.8	0.870	68.6
40132005	Pinnacle Peak	77.0	0.776	59.7	0.903	69.5
40133002	Central Phoenix	77.0	**0.830**	63.9	0.835	64.3
40133003	South Scottsdale	74.0	0.826	61.1	0.849	62.7
40134003	South Phoenix	73.0	0.819	59.8	0.869	63.4
40134004	West Chandler	71.0	0.801	56.8	0.889	63.1
40134005	Tempe	77.0	0.826	63.5	0.853	65.6
40134008	Cave Creek	73.0	0.757	55.2	0.914	66.7
40134010	Dysart	75.0	0.764	57.3	0.926	69.4
40134011	Buckeye	69.0	0.724	49.9	**0.978**	67.4
40137021	Red Mountain	77.0	0.810	62.3	0.867	66.7
40137022	Lehi	79.0	0.810	63.9	0.868	68.6
40137024	High School	75.0	0.810	60.7	0.866	64.9
40139508	Humboldt Mountain	70.0	0.748	52.3	0.931	65.1
40139702	Blue Point	76.0	0.802	60.9	0.891	67.7
40139704	Fountain Hills	74.0	0.804	59.4	0.888	65.7
40139997	JLG Supersite	**80.0**	0.828	**66.2**	0.838	67.0
40213001	Apache Junction	72.0	0.827	59.5	0.850	61.2
40218001	Queen Valley	75.0	0.785	58.8	0.920	68.9

Table 7-7. MAG RRF and DVF of CAMx sensitivity runs excluding IA emissions and NAA emissions using OSAT, as well as the MAG DVB

Site ID	Site Name	MAG DVB	Excluding IA		Excluding NAA Anthro	
			MAG RRF	DVF	MAG RRF	DVF
40070010	Tonto NM	72.0	0.780	56.1	0.952	68.5
40130019	West Phoenix	74.0	0.787	58.2	0.896	66.2
40131003	Mesa	76.0	**0.811**	61.6	0.864	65.6
40131004	North Phoenix	**77.0**	0.809	**62.2**	0.867	66.7
40131010	Falcon Field	76.0	0.799	60.6	0.893	67.8
40132001	Glendale	**77.0**	0.787	60.5	0.894	**68.8**
40132005	Pinnacle Peak	76.0	0.783	59.5	0.903	68.6
40133002	Central Phoenix	73.0	0.810	59.1	0.866	63.2
40133003	South Scottsdale	72.0	**0.811**	58.4	0.860	61.9
40134003	South Phoenix	68.0	0.784	53.2	0.910	61.8
40134004	West Chandler	70.0	0.808	56.5	0.877	61.3
40134005	Tempe	73.0	**0.811**	59.1	0.865	63.1
40134008	Cave Creek	71.0	0.752	53.3	0.916	65.0
40134010	Dysart	74.0	0.772	57.0	0.920	68.0
40134011	Buckeye	67.0	0.734	49.1	**0.978**	65.5
40137021	Red Mountain	75.0	0.792	59.3	0.890	66.7
40137022	Lehi	**77.0**	0.800	61.5	0.890	68.5
40137024	High School	72.0	0.792	57.0	0.888	63.9
40139508	Humboldt Mountain	69.0	0.749	51.6	0.924	63.7
40139702	Blue Point	73.0	0.790	57.6	0.897	65.4
40139704	Fountain Hills	72.0	0.792	56.9	0.892	64.2
40139997	JLG Supersite	**77.0**	0.808	**62.2**	0.869	66.9
40213001	Apache Junction	71.0	0.795	56.4	0.909	64.5
40218001	Queen Valley	72.0	0.780	56.1	0.941	67.7

7.3. Demonstration Results and Conclusion

For sensitivity runs using zero-out method and OSAT as described above, retrospective demonstration results for the site-averaged and site-maximum DVFs in the Maricopa NAA are summarized in Tables 7-8 a nd 7-9, respectively.

For the retrospective demonstration based on zero-out results, all IA sources contributed about 12 ppb to site-averaged DVB and about 10 ppb to site-maximum DVB at JLG

Supersite. Site-specific DVFs for zeroing-out all IA contributions ranged from 53 to 70 ppb based on EPA 2023 DVBs with unadjusted RRFs and 52-65 ppb based on MAG DVBs (31 atypical wildfire impact days in 2021-2023 were removed from DVB calculation) with MAG RRFs (coincident atypical wildfire impact days in 2023 were removed from RRF calculation with modeled top 10 days).

For the retrospective demonstration based on OSAT results —which is considered more scientifically robust for apportionment as it avoids the non-linearities of the zero-out method— all IA sources contributed about 15 ppb to site-averaged DVB and about 14-15 ppb to site-maximum DVB at JLG Supersite. Site-specific DVFs for excluding all IA contributions from OSAT results ranged from 50 to 66 ppb based on EPA 2023 DVBs with unadjusted RRFs and 49-62 ppb based on MAG DVBs with MAG RRFs.

These findings from zero-out methods and OSAT consistently demonstrate that the international transport from Mexico, Asia, and intercontinental anthropogenic sources contributed significantly to ozone levels in the Maricopa NAA. Consequently, the weight of evidence strongly supports the conclusion that the Maricopa NAA would have attained the 2015 ozone NAAQS by the moderate attainment date of August 3, 2024, but for international anthropogenic contributions.

Table 7-8. Modeled contributions from international anthropogenic emissions to DVBs and resulting DVs with IA contributions removed based on zero-out method

	Source	DVB (ppb)	DVF w/o IA (ppb)	Total IA Contribution (ppb)
Site Average	EPA	**75**	**63**	11.8
	MAG	**73**	**60**	12.1
Site Max at JLG	EPA	**80**	**70**	10.0
	MAG	**77**	**65**	11.3

Table 7-9. Modeled contributions from international anthropogenic emissions to DVBs and resulting DVs with IA contributions removed based on OSAT

	Source	DVB (ppb)	DVF w/o IA (ppb)	Total IA Contribution (ppb)
Site Average	EPA	**75**	**60**	15.2
	MAG	**73**	**57**	15.5
Site Max at JLG	EPA	**80**	**66**	13.8
	MAG	**77**	**62**	14.8

7.4. Weight of Evidence Analysis

Additional retrospective demonstration of CMAQ with zero-out scenario was conducted to corroborate the CAMx retrospective demonstration presented in the previous section. Like the CAMx zero-out scenario, two sets of DVFs were calculated to quantify the IA emissions impact for individual ozone monitoring sites in the 8-hour ozone NAA based on the CMAQ zero-out scenario. One set of DVFs was calculated using the EPA DVBs and unadjusted RRFs as shown in Table 7-10. The other set of DVFs was calculated using the MAG DVBs paired with the MAG RRFs as listed in Table 7-11. According to the unadjusted RRFs and MAG RRFs, the most influential site from the IA emissions (the lowest RRF) was Buckeye. The least influential sites from the IA emissions (the highest RRF) were South Scottsdale and Tempe (0.881) among the unadjusted RRFs, and Central Phoenix (0.854) among the MAG RRFs. For the DVF, the maximum 2023 DVF appeared at JLG Supersite (70.2 ppb) based on the EPA DVBs paired with unadjusted RRFs and Glendale (64.4 ppb) based on the MAG DVBs paired with the MAG RRFs.

The retrospective demonstration results of CMAQ for the site-averaged and site-maximum DVFs in the Maricopa NAA are summarized in Table 7-12. Site-averaged contributions from all IA were about 13 ppb based on EPA 2023 DVBs with unadjusted RRFs and about 14 ppb based on MAG DVBs with MAG RRFs. Site-specific DVFs for zeroing-out all IA contributions ranged from 51 to 70 ppb based on EPA 2023 DVBs with unadjusted RRFs, and from 49 to 64 ppb using MAG DVBs with MAG RRFs.

Comparable to the retrospective demonstration results from the CAMx zero-out scenario, these CMAQ results corroborate the conclusion presented in the previous section: the Maricopa NAA would have attained the 2015 ozone NAAQS by the moderate attainment date of August 3, 2024, but for international anthropogenic contributions.

Table 7-10. Unadjusted RRF and DVF of CMAQ sensitivity runs excluding IA emissions using zero-out method, as well as the EPA DVB

Site ID	Site Name	EPA DVB	Unadjusted RRF	DVF
40070010	Tonto NM	75.0	0.782	58.6
40130019	West Phoenix	77.0	0.862	66.3
40131003	Mesa	**80.0**	0.855	68.4
40131004	North Phoenix	78.0	0.843	65.7
40131010	Falcon Field	79.0	0.866	68.3
40132001	Glendale	79.0	0.845	66.7
40132005	Pinnacle Peak	77.0	0.788	60.6
40133002	Central Phoenix	77.0	0.856	65.8
40133003	South Scottsdale	74.0	**0.881**	65.2
40134003	South Phoenix	73.0	0.850	62.0
40134004	West Chandler	71.0	0.800	56.7
40134005	Tempe	77.0	**0.881**	67.8
40134008	Cave Creek	73.0	0.798	58.2
40134010	Dysart	75.0	0.809	60.6
40134011	Buckeye	69.0	0.745	51.3
40137021	Red Mountain	77.0	0.855	65.8
40137022	Lehi	79.0	0.855	67.5
40137024	High School	75.0	0.855	64.0
40139508	Humboldt Mountain	70.0	0.746	52.2
40139702	Blue Point	76.0	0.826	62.7
40139704	Fountain Hills	74.0	0.807	59.7
40139997	JLG Supersite	**80.0**	0.878	**70.2**
40213001	Apache Junction	72.0	0.826	59.4
40218001	Queen Valley	75.0	0.787	59.0

Table 7-11. MAG RRF and DVF of CMAQ sensitivity runs excluding IA emissions using zero-out method, as well as the MAG DVB

Site ID	Site Name	MAG DVB	MAG RRF	MAG DVF
40070010	Tonto NM	72.0	0.778	56.0
40130019	West Phoenix	74.0	0.837	61.9
40131003	Mesa	76.0	0.830	63.0
40131004	North Phoenix	**77.0**	0.827	63.7
40131010	Falcon Field	76.0	0.801	60.8
40132001	Glendale	**77.0**	0.837	**64.4**
40132005	Pinnacle Peak	76.0	0.789	59.9
40133002	Central Phoenix	73.0	**0.854**	62.3
40133003	South Scottsdale	72.0	0.851	61.3
40134003	South Phoenix	68.0	0.826	56.1
40134004	West Chandler	70.0	0.824	57.7
40134005	Tempe	73.0	0.849	61.9
40134008	Cave Creek	71.0	0.771	54.7
40134010	Dysart	74.0	0.799	59.1
40134011	Buckeye	67.0	0.737	49.4
40137021	Red Mountain	75.0	0.802	60.1
40137022	Lehi	**77.0**	0.816	62.8
40137024	High School	72.0	0.824	59.3
40139508	Humboldt Mountain	69.0	0.748	51.5
40139702	Blue Point	73.0	0.800	58.3
40139704	Fountain Hills	72.0	0.788	56.7
40139997	JLG Supersite	**77.0**	0.827	63.6
40213001	Apache Junction	71.0	0.797	56.5
40218001	Queen Valley	72.0	0.774	55.7

Table 7-12. Modeled contributions from international anthropogenic emissions to DVBs and resulting DVs with IA contributions removed based on CMAQ zero-out scenario

	Source	DVB (ppb)	DVF w/o IA (ppb)	Total IA Contribution (ppb)
Site Average	EPA	**75**	**62**	12.9
	MAG	**73**	**59**	14.1
Site Max	EPA	**80**	**70**	9.8
	MAG	**77**	**64**	12.6

8. REFERENCES

Appel, K. W., K. Foley, J. Bash, R. Pinder, R. Dennis, D. Allen, and K. Pickering (2011). A Multi-Resolution Assessment of the Community Multiscale Air Quality (CMAQ) Model v4.7 Wet Deposition Estimates for 2002-2006. *Geoscientific Model Development*, 4, 357-371.

AZDA (2024). Arizona Retail RVP Standards. Arizona Department of Agriculture (AZDA). https://agriculture.az.gov/sites/default/files/Arizona%20Retail%20RVP%20Standards%20%28Updated%20March%202024%29.pdf.

Bertram, T. H., A. Heckel, A. Richter, J. P. Burrows, and R. C. Cohen (2005). Satellite measurements of daily variations in soil NO_x emissions. *Geophys. Res. Lett.*, 32, L24812, doi:10.1029/2005GL024640.

Boyer, D. (2018). Biogenic Emission Modeling with MEGAN, TCEQ.

Carn, S. A., K. Yang, A. J. Prata, and N. A. Krotkov (2015). Extending the long-term record of volcanic SO_2 emissions with the Ozone Mapping and Profiler Suite (OMPS) Nadir Mapper. *Geophysical Research Letters*, 42:925-932. https://doi.org/10.1002/2014GL062437.

ENVIRON et al. (2003). Maricopa County 2002 Comprehensive Emission Inventory for the Cap and Trade Oversight Committee, Final Rep. Oct. 9, 2003. Prepared for Arizona Department of Environmental Quality.

FAA (2024a). Operational Network (OPSNET) database. Federal Aviation Administration. https://aspm.faa.gov/opsnet/sys/Airport.asp.

FAA (2024b). Traffic Flow Management System Counts (TFMSC) database. Federal Aviation Administration. https://aspm.faa.gov/tfms/sys/Airport.asp.

Guenther, A. (2006a). User's Guide to Processing Driving Variables for Model of Emissions of Gases and Aerosols from Nature (MEGAN).

Guenther, A. (2006b). User's Guide to the Model of Emissions of Gases and Aerosols from Nature (MEGAN) Version MEGAN-VBA-2.0.

Guenther, A. (2007). Corrigendum to "Estimates of global terrestrial isoprene emissions using MEGAN (Model of Emissions of Gases and Aerosols from Nature)". *Atmos. Chem. Phys.*, 7, 4327–4327.

Guenther, A., T. Karl, P. Harley, C. Wiedinmyer, P. I. Palmer, and C. Geron (2006). Estimates of global terrestrial isoprene emissions using MEGAN (Model of Emissions of Gases and Aerosols from Nature). *Atmos. Chem. Phys.*, 6, 1–30.

Guenther, A. B., X. Jiang, C. L. Heald, T. Sakulyanontvittaya, T. Duhl, L. K. Emmons, and X. Wang (2012). The Model of Emissions of Gases and Aerosols from Nature version 2.1 (MEGAN2.1): an extended and updated framework for modeling biogenic emissions. *Geoscientific Model Development*, 5:1471–1492. https://doi.org/10.5194/gmd-5-1471-2012.

Guenther, A. B., S. Tejas, L. Huang, A. Wentland, J. Jung, R. Beardsley, J. Johnson, W. Chun, W. Hsieh, S. Kemball-Cook, G. Yarwood (2017). A Next Generation Modelling System for Estimating Texas Biogenic VOC Emissions. Project Report of Texas Commission on Environmental Quality.

Guenther, A., X. Jiang, T. Shah, L. Huang, S. Kemball-Cook, and G. Yarwood (2018). Model of Emissions of Gases and Aerosol from Nature Version 3 (MEGAN3) for Estimating Biogenic Emissions, International Technical Meeting on Air Pollution Modelling and its Application, 187–192, 14–18 May 2018, Ottawa, ON, Canada, https://doi.org/10.1007/978-3-030-22055-6_29, 2018.

Henderson, B. H. (2022). cmaqsatproc v2: Satellite data processing for CMAQ [Poster]. 21st Annual Community Modeling and Analysis System Conference, Chapel Hill, NC, October 2022. Retrieved from https://www.cmascenter.org/conference/2022/slides/Henderson_satellite-data-CMAS2022.pdf.

Hoesly, R. M., S. J. Smith, L. Feng, Z. Klimont, G. Janssens-Maenhout, T. Pitkanen, J. J. Seibert, L. Vu, R. J. Andres, R. M. Bolt, T. C. Bond, L. Dawidowski, N. Kholod, J.-I. Kurokawa, M. Li, L. Liu, Z. Lu, M. C. P. Moura, P. R. O'Rourke, and Q. Zhang (2018). Historical (1750–2014) anthropogenic emissions of reactive gases and aerosols from the Community Emissions Data System (CEDS). *Geoscientific Model Development*, 11:369–408. https://doi.org/10.5194/gmd-11-369-2018.

Hudman, R. C., N. E. Moore, A. K. Mebust, R. V. Martin, A. R. Russell, L. C. Valin, and R. C. Cohen (2012). Steps towards a mechanistic model of global soil nitric oxide emissions: implementation and space-based constraints. *Atmospheric Chemistry and Physics*, 12:7779–7795. https://doi.org/10.5194/acp-12-7779-2012.

Jaeglé, L., P. K. Quinn, T. S. Bates, B. Alexander, and J.-T. Lin (2011). Global distribution of sea salt aerosols: new constraints from in situ and remote sensing observations.

Atmospheric Chemistry and Physics, 11:3137–3157. https://doi.org/10.5194/acp-11-3137-2011.

Jiang, X., A. Guenther, T. Duhl, and T. Sakulyanontvittaya (2011). MEGAN version 2.10 User's Guide. NCAR Earth Systems Laboratory, Atmosperhic Chemistry Division. www.acom.ucar.edu/webt/MEGAN/MEGAN2.1_User_Guide_05-07-2012.pdf.

Jiang, X., A. Guenther, M. Potosnak, C. Geron, R. Seco, T. Karl, S. Kim, L. Gu, and S. Pallardy (2018). Isoprene emission response to drought and the impact on global atmospheric chemistry. *Atmospheric Environment*, 183, pp.69-83.

Jimenez, J. A. and J. Dudhia (2013). On the Ability of the WRF Model to Reproduce the Surface Wind Direction over Complex Terrain. *Journal of Applied Meteorology and Climatology*, 52, pp. 1610-1617.

Kang, D., C. Hogrefe, G. Sarwar, J. D. East, J. M. Madden, R. Mathur, and B. H. Henderson (2022). Assessing the Impact of Lightning NO_x Emissions in CMAQ Using Lightning Flash Data from WWLLN over the Contiguous United States. *Atmosphere*, 13(8), 1248. https://doi.org/10.3390/atmos13081248.

Mansell, G. E., G. Yarwood (ENVIRON), A. Guenther (NCAR), and C. Wiedinmyer (Golden CO) (2006). Final Report Maricopa Association of Governments 2006 Biogenics Study.

Meng, J., R. V. Martin, P. Ginoux, M. Hammer, M. P. Sulprizio, D. A. Ridley, and A. van Donkelaar (2021). Grid-independent high-resolution dust emissions (v1.0) for chemical transport models: application to GEOS-Chem (12.5.0). *Geoscientific Model Development*, 14:4249–4260. https://doi.org/10.5194/gmd-14-4249-2021.

Murray, L. T., D. J. Jacob, J. A. Logan, R. C. Hudman, and W. J. Koshak (2012). Optimized regional and interannual variability of lightning in a global chemical transport model constrained by LIS/OTD satellite data. *Journal of Geophysical Research: Atmospheres*, 117:D20307. https://doi.org/10.1029/2012JD017934.

NCEI (2023). Local Climatological Data. NOAA National Centers for Environmental Information. https://www.ncei.noaa.gov.

Ramboll (2021). 2017 GEOS-Chem application to support US regional modeling. Prepared for the Western States Air Resources Council, Santa Fe, New Mexico, 8 April 2021. https://views.cira.colostate.edu/docs/IWDW/Modeling/WRAP/2017/Ramboll_WESTAR_GEOSChem_Report_8Apr_2021.pdf.

Simone, N. W., M. E. J. Stettler, and S. R. H. Barrett (2013). Rapid estimation of global civil aviation emissions with uncertainty quantification. *Transportation Research Part D: Transport and Environment*, 25:33–41. https://doi.org/10.1016/j.trd.2013.07.001.

Skamarock, W. C., J. B. Klemp, J. Dudhia, D. O. Gill, Z. Liu, J. Berner, W. Wang, J. G. Powers, M. G. Duda, D. M. Barker, and X.-Y. Huang (2019). A description of the Advanced Research WRF version 4. *NCAR Technical Note NCAR/TN-556+STR*, 145 pp., doi:10.5065/1dfh-6p97.

Tzompa-Sosa, Z. A., E. Mahieu, B. Franco, C. A. Keller, A. J. Turner, D. Helmig, A. Fried, D. Richter, P. Weibring, J. Walega, T. I. Yacovitch, S. C. Herndon, D. R. Blake, F. Hase, J. W. Hannigan, S. Conway, K. Strong, M. Schneider, and E. V. Fischer (2017). Revisiting global fossil fuel and biofuel emissions of ethane. *Journal of Geophysical Research: Atmospheres*, 122:2493–2512. https://doi.org/10.1002/2016JD025767.

UCAR (2025). https://www.acom.ucar.edu/acresp/MODELING/finn_emis_txt/final_2023/ (modvrs_base).

USAF (2012). Final F-35A Training Basing Environmental Impact Statement. http://www.dtic.mil/dtic/tr/fulltext/u2/a612501.pdf.

U.S. EPA (2014). Meteorological Model Performance for Annual 2011 WRF v3.4 Simulation. Technical report. *U.S. Environmental Protection Agency*, November 2014.

U.S. EPA (2015). Air Quality Modeling Technical Support Document for the 2008 Ozone NAAQS Transport Assessment. Technical report, *U.S. Environmental Protection Agency*, January 2015.

U.S. EPA (2018). Modeling Guidance for Demonstrating Attainment of Air Quality Goals for Ozone, PM2.5 and Regional Haze. EPA 454/R-18-009, November 2018. https://www3.epa.gov/ttn/scram/guidance/guide/O3-PM-RH-Modeling_Guidance-2018.pdf.

U.S. EPA (2021). An Expert Report on the WRF Vertical Layer Configuration of the EPA's 2021 and 2022 Air Quality Modeling Platforms. Technical report, *U.S. Environmental Protection Agency*.

U.S. EPA (2022). Technical Support Document (TSD): Preparation of Emissions Inventories for the 2017 North American Emissions Modeling Platform, https://gaftp.epa.gov/Air/emismod/2017/2017emissions/.

U.S. EPA (2023a). Using MOVES to Prepare Emission Inventories for State Implementation Plans and Transportation Conformity. Technical report. U.S. Environmental Protection Agency, August 2023.

U.S. EPA (2023b). MOVES4 Technical Guidance: Using MOVES to Prepare Emission Inventories for State Implementation Plans and Transportation Conformity. U.S. Environmental Protection Agency, EPA-420-B-23-011, August 2023.

U.S. EPA (2024). Photochemical Modeling Tools: SMAT-CE. https://www.epa.gov/scram/photochemical-modeling-tools.

U.S. EPA (2025a). Technical Support Document (TSD): Preparation of Emissions Inventories for the 2022v1 North American Emissions Modeling Platform, https://gaftp.epa.gov/Air/emismod/2022/v1/.

U.S. EPA (2025b). https://gaftp.epa.gov/Air/emismod/2022/v2/2022emissions/draft/.

U.S. EPA (2025c). https://gaftp.epa.gov/Air/emismod/2022/v1/2022emissions/2023CEMS/.

U.S. EPA (2025d). https://gaftp.epa.gov/Air/nei/2023/doc/supporting_data/events/beta/ff10/.

U.S. EPA (2025e). https://gaftp.epa.gov/Air/nei/2023/doc/supporting_data/events/beta/ff10/, https://gaftp.epa.gov/Air/nei/2023/doc/supporting_data/events/beta/2023NEI_beta_version_Wildland_and_ag_fires_memo.pdf.

Van der Werf, G. R., J. T. Randerson, L. Giglio, T. T. van Leeuwen, Y. Chen, B. M. Rogers, M. Mu, M. J. E. van Marle, D. C. Morton, G. J. Collatz, R. J. Yokelson, and P. S. Kasibhatla (2017). Global fire emissions estimates during 1997–2016. *Earth System Science Data*, 9:697–720. https://doi.org/10.5194/essd-9-697-2017.

Weston (2010). 2008 Mobile Source Air Emissions Inventory for Luke Air Force Base. Weston Solutions, Inc. Prepared for Air Education and Training Command (AETC), US Air Force, Randolph AFB, TX. June 2010.

Wiedinmyer, C., Y. Kimura, E. C. McDonald-Buller, L. K. Emmons, R. R. Buchholz, W. Tang, K. Seto, M. B. Joseph, K. C. Barsanti, A. G. Carlton, and R. Yokelson (2023). The Fire Inventory from NCAR version 2.5: an updated global fire emissions model for climate and chemistry applications. *Geoscientific Model Development*, Submitted (DOI: 10.5194/egusphere-2023-124).

Xiao, Y., J. A. Logan, D. J. Jacob, R. C. Hudman, R. Yantosca, and D. R. Blake (2008). Global budget of ethane and regional constraints on U.S. sources. *Journal of Geophysical Research: Atmospheres*, 113:D21306. https://doi.org/10.1029/2007JD009415.

Zender, C. S., H. Bian, and D. Newman (2003). Mineral Dust Entrainment and Deposition (DEAD) model: Description and 1990s dust climatology. *Journal of Geophysical Research: Atmospheres*, 108:D14:4416. https://doi.org/10.1029/2002JD002775.

Appendix 1

Sensitivity Analysis for Solana Generating Station Emissions

As mentioned in Section 3.2.1, fugitive point source emissions from one facility located outside of the Maricopa NAA, Solana Generating Station, were omitted from Ramboll's CAA §179B(b) modeling demonstration. After incorporating this source into the updated inventory, CAMx sensitivity test was conducted for baseline and source apportionment simulations. The purpose of this sensitivity test is to assess model sensitivity to the added emissions. This appendix evaluates whether adding previously omitted Solana emissions affects model performance, design values, RRFs, or source apportioned contributions.

For the CAMx simulations, the reference case is GBX4, which incorporates the same inputs used for Ramboll's CAA §179B(b) modeling demonstration and the sensitivity case is GBX5, which incorporates the updated inventory.

To check the model sensitivity to the added emissions, statistical metrics between the reference and sensitivity cases (GBX4 and GBX5) were compared based on the modeled site-average MDA8 ozone values for the Maricopa NAA. The results indicate that all statistical metrics are identical as shown in Table 1A-1 below.

Table 1A-1. Comparison of statistical metrics between two CAMx scenarios (GBX4 and GBX5) based on the modeled site-average MDA8 ozone values for the Maricopa NAA

Metric	GBX4	GBX5	Difference
Number of Pairs (#)	4,312	4,312	0
Avg. Observed Value (ppb)	57.7	57.7	0.0
Avg. Modeled Value (ppb)	58.8	58.8	0.0
MB (ppb)	1.1	1.1	0.0
ME (ppb)	6.2	6.2	0.0
RMSE (ppb)	8.1	8.1	0.0
FB (%)	1.6	1.6	0.0
FE (%)	10.7	10.7	0.0
NMB (%)	1.9	1.9	0.0
NME (%)	10.7	10.7	0.0
Correlation Coefficient (R)	0.69	0.69	0.00
Index of Agreement	0.82	0.82	0.00

In addition to statistical metrics comparison, the reference and sensitivity cases (GBX4 and GBX5) were compared using time series and model to model scatter plot as shown below in Figures 1A-1 and 1A-2. These graphical analyses also indicate that two CAMx scenarios provide identical results.

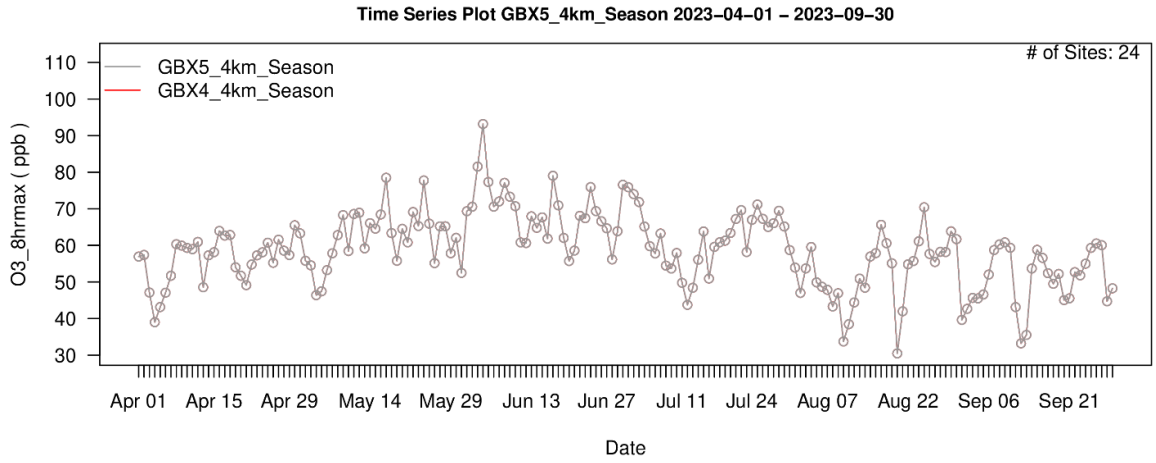

Figure 1A-1. Time series plot between reference and sensitivity cases (GBX4 and GBX5)

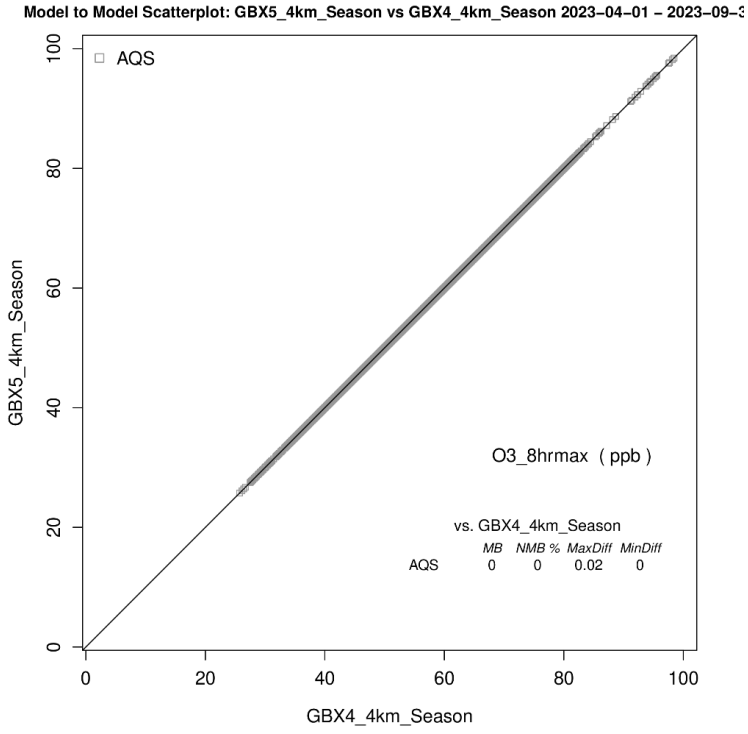

Figure 1A-2. Scatter plot between reference and sensitivity cases (GBX4 and GBX5)

Also, SMAT was conducted to compare the reference and sensitivity cases (GBX4 and GBX5) since Ramboll's §179B(b) demonstration results are derived from SMAT results. By setting GBX4 as modeled base case and GBX5 as modeled sensitivity case, SMAT results indicate that there is no difference between two modeled cases with RRF 1 and unchanged design values for all monitoring sites in Table 1A-2.

Table 1A-2. SMAT results based on EPA DVB using GBX4 as modeled base case and GBX5 as modeled sensitivity case

Site ID	Site Name	DVB (ppb)	DVF (ppb)	RRF
40070010	Tonto NM	75	75	1.000
40130019	West Phoenix	77	77	1.000
40131003	Mesa	80	80	1.000
40131004	North Phoenix	78	78	1.000
40131010	Falcon Field	79	79	1.000
40132001	Glendale	79	79	1.000
40132005	Pinnacle Peak	77	77	1.000
40133002	Central Phoenix	77	77	1.000
40133003	South Scottsdale	74	74	1.000
40134003	South Phoenix	73	73	1.000
40134004	West Chandler	71	71	1.000
40134005	Tempe	77	77	1.000
40134008	Cave Creek	73	73	1.000
40134010	Dysart	75	75	1.000
40134011	Buckeye	69	69	1.000
40137021	Red Mountain	77	77	1.000
40137022	Lehi	79	79	1.000
40137024	High School	75	75	1.000
40139508	Humboldt Mountain	70	70	1.000
40139702	Blue Point	76	76	1.000
40139704	Fountain Hills	74	74	1.000
40139997	JLG Supersite	80	80	1.000
40213001	Apache Junction	72	72	1.000
40218001	Queen Valley	75	75	1.000

Lastly, the IA emissions impacts for individual ozone monitoring sites in the Maricopa NAA were evaluated for both CAMx cases (GBX4 and GBX5) using their OSAT results and the SMAT tool. The comparison results indicate that there is no change on the IA emissions impacts in Table 1A-3.

Table 1A-3. SMAT results of two CAMx cases (GBX4 and GBX5) excluding IA emissions using OSAT

Site ID	Site Name	EPA DVB	GBX4 Excluding IA		GBX5 Excluding IA		Difference (GBX5 – GBX4)	
			RRF	DVF	RRF	DVF	RRF	DVF
40070010	Tonto NM	75.0	0.784	58.7	0.784	58.7	0.000	0.0
40130019	West Phoenix	77.0	0.814	62.6	0.814	62.6	0.000	0.0
40131003	Mesa	**80.0**	0.826	66.0	0.826	66.0	0.000	0.0
40131004	North Phoenix	78.0	0.797	62.1	0.797	62.1	0.000	0.0
40131010	Falcon Field	79.0	0.821	64.8	0.821	64.8	0.000	0.0
40132001	Glendale	79.0	0.796	62.8	0.796	62.8	0.000	0.0
40132005	Pinnacle Peak	77.0	0.776	59.7	0.776	59.7	0.000	0.0
40133002	Central Phoenix	77.0	**0.830**	63.9	**0.830**	63.9	0.000	0.0
40133003	South Scottsdale	74.0	0.826	61.1	0.826	61.1	0.000	0.0
40134003	South Phoenix	73.0	0.819	59.8	0.819	59.8	0.000	0.0
40134004	West Chandler	71.0	0.801	56.8	0.801	56.8	0.000	0.0
40134005	Tempe	77.0	0.826	63.5	0.826	63.5	0.000	0.0
40134008	Cave Creek	73.0	0.757	55.2	0.757	55.2	0.000	0.0
40134010	Dysart	75.0	0.764	57.3	0.764	57.3	0.000	0.0
40134011	Buckeye	69.0	0.724	49.9	0.724	49.9	0.000	0.0
40137021	Red Mountain	77.0	0.810	62.3	0.810	62.3	0.000	0.0
40137022	Lehi	79.0	0.810	63.9	0.810	63.9	0.000	0.0
40137024	High School	75.0	0.810	60.7	0.810	60.7	0.000	0.0
40139508	Humboldt Mountain	70.0	0.748	52.3	0.748	52.3	0.000	0.0
40139702	Blue Point	76.0	0.802	60.9	0.802	60.9	0.000	0.0
40139704	Fountain Hills	74.0	0.804	59.4	0.804	59.4	0.000	0.0
40139997	JLG Supersite	**80.0**	0.828	**66.2**	0.828	**66.2**	0.000	0.0
40213001	Apache Junction	72.0	0.827	59.5	0.827	59.5	0.000	0.0
40218001	Queen Valley	75.0	0.785	58.8	0.785	58.8	0.000	0.0

In summary, incorporation of fugitive emissions from Solana Generating Station does not make any impact on the statistical metrics, modeled 8-hour ozone design values, and relative response factors as well as the CAMx source-apportionment results. Consequently, this emissions update does not change the conclusions from Ramboll's §179B(b) demonstration.

As a quality-assurance check, a CMAQ sensitivity (with vs. without Solana emissions) confirms that ozone responses are negligible. Across bins of baseline MDA8 ozone, differences (Included − Excluded) are centered near zero with a median of 0.0010 ppb, P95 of 0.0080 ppb, and maximum of 0.0130 ppb as shown in Figure 1A-3. These changes are hundreds of times smaller than typical model performance error (ME ≈ 6.2 ppb; RMSE ≈ 8.1 ppb; Table 1A-1) and therefore have no effect on RRFs or projected design values. Consistent with CAMx, the CMAQ check shows no concentration-dependent pattern across the 40–90 ppb baseline range. This CMAQ result is presented only as a QA corroboration. CAMx remains the sole basis for the modeled attainment test (SMAT-CE).

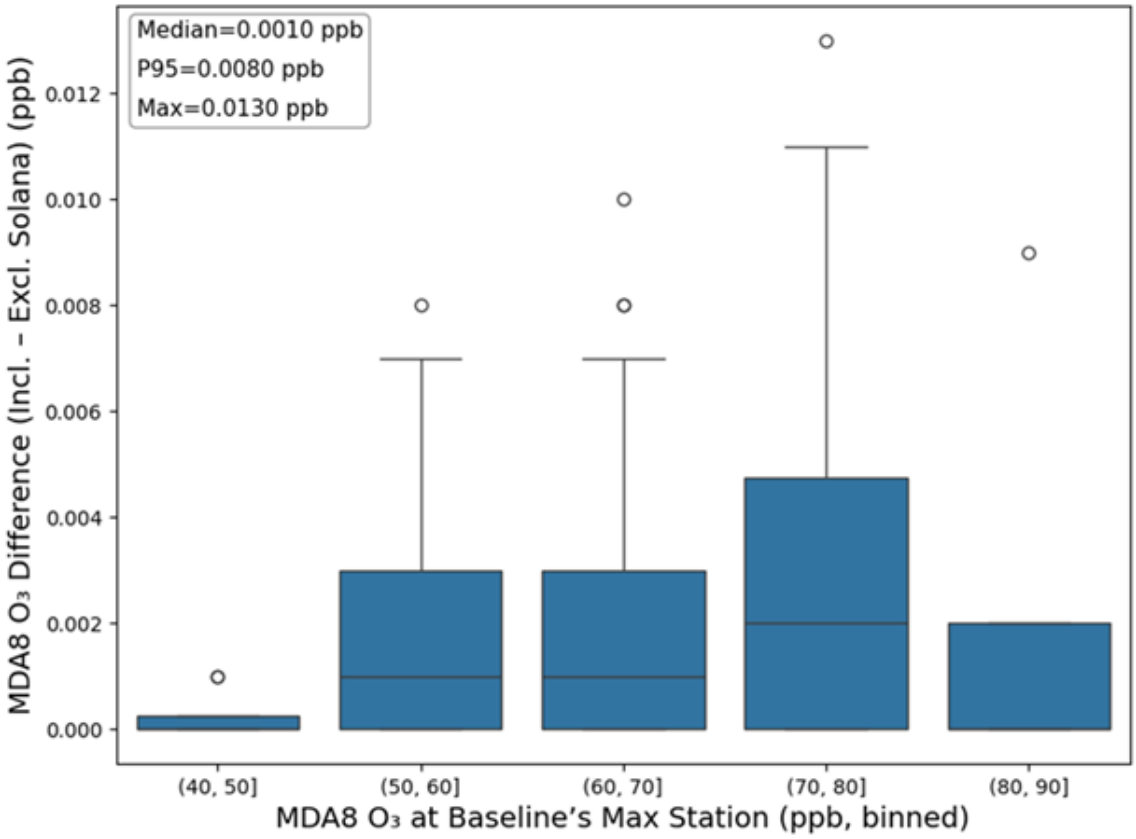

Figure 1A-3. CMAQ QA corroboration—Distribution of MDA8 ozone differences (Included − Excluded Solana, ppb) binned by baseline MDA8 ozone at the max station (April-September 2023)

Appendix 2

Specification for Spatial Surrogates in the 4 km Modeling Domain

No.	Region	Surrogate	Surrogate Code	Data Shapefile	Data Attribute	Weight Shapefile	Weight Attribute	Weight Function	Filter Function	Merge Function	Secondary Surrogate	Tertiary Surrogate	Quaternary Surrogate
1	USA	Population	100	cb_2020_us_county_500k	GEOID	ACS_2020_5YR_BG_pop_hu_mobile	POP2020						
2	USA	Housing	110	cb_2020_us_county_500k	GEOID	ACS_2020_5YR_BG_pop_hu_mobile	HU2020				Population		
3	USA	Detached Housing	135	cb_2020_us_county_500k	GEOID	ACS_2020_5YR_BG_pop_hu_mobile	DETACHEDH				NLCD Low Intensity Development		
4	USA	Single and Dual Unit Housing	136	cb_2020_us_county_500k	GEOID	ACS_2020_5YR_BG_pop_hu_mobile	LTTRIUNIT				NLCD Low Intensity Development		
5	USA	Single + Dual Unit + Manufactured Housing	137	cb_2020_us_county_500k	GEOID	ACS_2020_5YR_BG_pop_hu_mobile	SNGDLMOBL				NLCD Low Intensity Development	NLCD Land	
6	USA	Local House Change	138	cb_2020_us_county_500k	GEOID	MCPC_RESIDENTIAL_complt2022_2024	SQFT						
7	USA	Construction	141	cb_2020_us_county_500k	GEOID					0.5*Local House Change+0.5*Total Road Miles	Housing Change and Population	Population	
8	USA	Residential Heating - Natural Gas	150	cb_2020_us_county_500k	GEOID	ACS_2020_5YR_BG_pop_hu_mobile	UTIL_GAS				Population		
9	USA	Residential Heating - Distillate Oil	170	cb_2020_us_county_500k	GEOID	ACS_2020_5YR_BG_pop_hu_mobile	FUEL_OIL				Housing		
10	USA	Residential Heating - Coal	180	cb_2020_us_county_500k	GEOID	ACS_2020_5YR_BG_pop_hu_mobile	COAL				Housing		
11	USA	Residential Heating - LP Gas	190	cb_2020_us_county_500k	GEOID	ACS_2020_5YR_BG_pop_hu_mobile	LP_GAS				Housing		
12	USA	Extended Idle Locations	205	cb_2020_us_county_500k	GEOID	oil_2019_06_24_rev_truck	rev_truck				Total Road Miles		
13	USA	Total Road AADT	239	cb_2020_us_county_500k	GEOID	vol_all_2023_build_ll	VMT				Total Road Miles		
14	USA	Total Road Miles	240	cb_2020_us_county_500k	GEOID	vol_all_2023_build_ll	LINKLEN						
15	USA	Total Restricted Road Miles	241	cb_2020_us_county_500k	GEOID	vol_all_2023_build_ll_FW	LINKLEN				Total Road Miles		
16	USA	Total Restricted AADT	242	cb_2020_us_county_500k	GEOID	vol_all_2023_build_ll_FW	VMT				Total Road AADT		
17	USA	Total Unrestricted Road Miles	243	cb_2020_us_county_500k	GEOID	vol_all_2023_build_ll_LC	LINKLEN				Total Road Miles		
18	USA	Total Unrestricted AADT	244	cb_2020_us_county_500k	GEOID	vol_all_2023_build_ll_LC	VMT				Total Road AADT		
19	USA	Intercity Bus Terminals	258	cb_2020_us_county_500k	GEOID	NTAD_2016_ipcd_BUS_I_1	NONE				Commercial plus Industrial	Population	NLCD Land
20	USA	Transit Bus Terminals	259	cb_2020_us_county_500k	GEOID	NTAD_2016_ipcd_BUS_T_1	NONE				Commercial plus Industrial	Population	NLCD Land
21	USA	Total Railroad Miles	260	cb_2020_us_county_500k	GEOID	ARIZONA_RAILROAD_latlon_mainline	NONE				Total Road Miles	Population	
22	USA	NTAD Total Railroad Density	261	cb_2020_us_county_500k	GEOID	ntad_2014_rail_fixed	DENS				Total Railroad Miles	Total Road Miles	Population
23	USA	NTAD Class 1 2 3 Railroad Density	271	cb_2020_us_county_500k	GEOID	ntad_2014_rail_fixed	DENS		RAILTYPE=1		NTAD Total Railroad Density	Total Railroad Miles	Total Road Miles
24	USA	ERTAC Rail Yards	275	cb_2020_us_county_500k	GEOID	ARIZONA_RAILROAD_latlon_Spur	NONE				NTAD Total Railroad Density	Total Railroad Miles	Population
25	USA	NLCD Low	300	cb_2020_us_county_500k	GEOID	MCPC2022_Land_Use_ll_LowDensity	NONE				Housing	Population	NLCD Land
26	USA	NLCD Open + Low	304	cb_2020_us_county_500k	GEOID	MCPC2022_Land_Use_ll_LowOpen	NONE				Housing	Population	NLCD Land
27	USA	NLCD Low + Med	305	cb_2020_us_county_500k	GEOID	MCPC2022_Land_Use_ll_LowMedium	NONE				Housing	Population	NLCD Land
28	USA	NLCD Med + High	306	cb_2020_us_county_500k	GEOID	MCPC2022_Land_Use_ll_MediumHigh	NONE				Housing	Population	NLCD Land
29	USA	NLCD All Development	307	cb_2020_us_county_500k	GEOID	MCPC2022_Land_Use_ll_AllDevelopment	NONE				Housing	Population	NLCD Land
30	USA	NLCD Low + Med + High	308	cb_2020_us_county_500k	GEOID	MCPC2022_Land_Use_ll_LowMediumHigh	NONE				Population	NLCD Land	
31	USA	NLCD Open + Low + Med	309	cb_2020_us_county_500k	GEOID	MCPC2022_Land_Use_ll_LowMediumOpen	NONE				Housing	Population	NLCD Land
32	USA	NLCD Total Agriculture	310	cb_2020_us_county_500k	GEOID	MCPC2022_Land_Use_ll_agriculture	NONE				Housing	NLCD Land	
33	USA	NLCD Crop Land	319	cb_2020_us_county_500k	GEOID	MCPC2022_Land_Use_ll_agriculture	NONE				Housing	NLCD Land	
34	USA	NLCD Forest Land	320	cb_2020_us_county_500k	GEOID	nlcd_2019_land_cover_l48_20210604_500m_ll_forest	NONE				Housing	NLCD Land	
35	USA	NLCD Recreational Land	321	cb_2020_us_county_500k	GEOID	nlcd_2019_land_cover_l48_20210604_500m_ll_recreation	NONE				Housing	NLCD Land	

No.	Region	Surrogate	Surrogate Code	Data Shapefile	Data Attribute	Weight Shapefile	Weight Attribute	Weight Function	Filter Function	Merge Function	Secondary Surrogate	Tertiary Surrogate	Quaternary Surrogate
36	USA	NLCD Land	340	cb_2020_us_county_500k	GEOID	nlcd_2019_land_cover_l48_20210604_500m_ll_land	NONE						
37	USA	NLCD Water	350	cb_2020_us_county_500k	GEOID	Maricopa_only_lakes_latlon	NONE						
38	USA	FAO 2010 Cattle	401	cb_2020_us_county_500k	GEOID	fao_Cattle_2010_Da_nlcdproj_masked_ll	DN				NLCD Total Agriculture	NLCD Open + Low	
39	USA	FAO 2010 Pig	402	cb_2020_us_county_500k	GEOID	fao_Pig_2010_Da_nlcdproj_masked_ll	DN				NLCD Total Agriculture	NLCD Open + Low	
40	USA	FAO 2010 Chicken	403	cb_2020_us_county_500k	GEOID	fao_Chicken_2010_Da_nlcdproj_masked_ll	DN				NLCD Total Agriculture	NLCD Open + Low	
41	USA	FAO 2010 Goat	404	cb_2020_us_county_500k	GEOID	fao_Goat_2010_Da_nlcdproj_masked_ll	DN				NLCD Total Agriculture	NLCD Open + Low	
42	USA	FAO 2010 Horse	405	cb_2020_us_county_500k	GEOID	fao_Horse_2010_Da_nlcdproj_masked_ll	DN				NLCD Total Agriculture	NLCD Open + Low	
43	USA	FAO 2010 Sheep	406	cb_2020_us_county_500k	GEOID	fao_Sheep_2010_Da_nlcdproj_masked_ll	DN				NLCD Total Agriculture	NLCD Open + Low	
44	USA	Commercial Land	500	cb_2020_us_county_500k	GEOID	MCPC2022_Land_Use_ll_commercial	NONE				Population	NLCD Land	
45	USA	Aircraft Engine Manufacturers	504	cb_2020_us_county_500k	GEOID	EMPLOYERS_2023_MCPC_ll_aircraft_engine	Employees				Industrial Land	Population	
46	USA	Industrial Land	505	cb_2020_us_county_500k	GEOID	MCPC2022_Land_Use_ll_Industrial	NONE				Population	NLCD Land	
47	USA	Education	506	cb_2020_us_county_500k	GEOID	MCPC2022_Land_Use_ll_education	NONE				Population	NLCD Land	
48	USA	Public Schools	508	cb_2020_us_county_500k	GEOID	public_schools_2018_2019_latlon	TOTAL				Population	NLCD Land	
49	USA	Commercial plus Industrial	510	cb_2020_us_county_500k	GEOID	MCPC2022_Land_Use_ll_commercial_industrial	NONE				Population	NLCD Land	
50	USA	Single Family Residential	527	cb_2020_us_county_500k	GEOID	MCPC2022_Land_Use_ll_SingleFamily	NONE				Housing	Population	NLCD Land
51	USA	Residential + Commercial + Industrial + Institutional + Government	535	cb_2020_us_county_500k	GEOID	MCPC2022_Land_Use_ll_535	NONE				Population	NLCD Land	
52	USA	Retail Trade (COM1)	540	cb_2020_us_county_500k	GEOID	EMPLOYERS_2023_MCPC_ll_retail_trade	Employees				Housing	Commercial Land	Population
53	USA	Auto refinish	544	cb_2020_us_county_500k	GEOID	EMPLOYERS_2023_MCPC_ll_autorefinish_811121	Employees				Commercial Land	Population	
54	USA	Hospital (COM6)	560	cb_2020_us_county_500k	GEOID	AZ_all_hospital_latlon	CAPACITY				Commercial Land	Population	
55	USA	Gas Stations	600	cb_2020_us_county_500k	GEOID	XY_Fueling_Facilities_MC_and_PC_latlon	NONE				Commercial Land	Population	NLCD Land
56	USA	Refineries and Tank Farms	650	cb_2020_us_county_500k	GEOID	EIA_2015_US_Oil	NONE				NLCD Low + Med	Population	NLCD Land
57	USA	Airport Points	710	cb_2020_us_county_500k	GEOID	MC_PC_Airport_NOx_emissions_v2	NOX_EMIS				Population	NLCD Land	
58	USA	Airport Areas	711	cb_2020_us_county_500k	GEOID	airport_area	AREA				Population	NLCD Land	
59	USA	Golf Courses	850	cb_2020_us_county_500k	GEOID	MCPC2022_Land_Use_ll_golf	NONE				Housing	Population	NLCD Land
60	USA	Mines	860	cb_2020_us_county_500k	GEOID	usgs_mrds_active_mines	NONE				NLCD Open + Low	NLCD Land	
61	USA	Sand and Gravel Mines	861	cb_2020_us_county_500k	GEOID	usgs_mrds_active_mines	NONE		CAT=Gravel		Mines	NLCD Open + Low	NLCD Land
62	USA	Lead Mines	862	cb_2020_us_county_500k	GEOID	usgs_mrds_active_mines	NONE		CAT=Lead		Mines	NLCD Open + Low	NLCD Land
63	USA	Crushed Stone Mines	863	cb_2020_us_county_500k	GEOID	usgs_mrds_active_mines	NONE		CAT=Stone		Mines	NLCD Open + Low	NLCD Land
64	USA	Wastewater Treatment Facilities	870	cb_2020_us_county_500k	GEOID	MC_PC_WWTR_wastewater	Capacity				Commercial plus Industrial	NLCD Water	NLCD Land
65	USA	Landfills	871	cb_2020_us_county_500k	GEOID	MC_PC_landfill_wo_NW_Glendale	EMIS				Commercial plus Industrial	NLCD Water	NLCD Land
66	USA	Crematories	872	cb_2020_us_county_500k	GEOID	EMPLOYERS_2023_MCPC_ll_cemeteries_812220	Employees				Population	NLCD Land	
67	USA	Drycleaners	880	cb_2020_us_county_500k	GEOID	EMPLOYERS_2023_MCPC_ll_drycleaner_812320	Employees				Commercial Land	Population	NLCD Land
68	USA	OSM Fuel	900	cb_2020_us_county_500k	GEOID	osm_fuel_points_us_mar2023	NONE				Total Road AADT	Total Road Miles	
69	USA	OSM Asphalt Surfaces	901	cb_2020_us_county_500k	GEOID	osm_asphalt_surfaces_us_mar2023	NONE				NLCD All Development		
70	USA	OSM Unpaved Roads	902	cb_2020_us_county_500k	GEOID	osm_unpaved_roads_us_mar2023	NONE				NLCD Open + Low		
71	USA	FAO 2010 Large Cattle Operations	4011	cb_2020_us_county_500k	GEOID	fao_LargeCattle_2010_Da_nlcdproj_masked_ll	DN				FAO 2010 Cattle	NLCD Total Agriculture	NLCD Open + Low
72	USA	NPDES 2020 Beef Cattle	4012	cb_2020_us_county_500k	GEOID	livestock_npdes_state_permits_subset_ll_beef	Population				FAO 2010 Cattle	NLCD Total Agriculture	NLCD Open + Low
73	USA	NPDES 2020 Dairy Cattle	4013	cb_2020_us_county_500k	GEOID	livestock_npdes_state_permits_subset_ll_dairy	Population				FAO 2010 Large Cattle Operations	NLCD Total Agriculture	NLCD Open + Low
74	USA	NPDES 2020 Swine	4021	cb_2020_us_county_500k	GEOID	livestock_npdes_state_permits_subset_ll_swine	Population				FAO 2010 Pig	NLCD Total Agriculture	NLCD Open + Low

No.	Region	Surrogate	Surrogate Code	Data Shapefile	Data Attribute	Weight Shapefile	Weight Attribute	Weight Function	Filter Function	Merge Function	Secondary Surrogate	Tertiary Surrogate	Quaternary Surrogate
75	USA	NPDES 2020 Chicken	4031	cb_2020_us_county_500k	GEOID	livestock_npdes_state_permits_subset_ll_chicken	Population				FAO 2010 Chicken	NLCD Total Agriculture	NLCD Open + Low
76	USA	NPDES 2020 Goat	4041	cb_2020_us_county_500k	GEOID	livestock_npdes_state_permits_subset_ll_goat	Population				FAO 2010 Goat	NLCD Total Agriculture	NLCD Open + Low
77	USA	NPDES 2020 Turkey	4071	cb_2020_us_county_500k	GEOID	livestock_npdes_state_permits_subset_ll_turkey	Population				NLCD Total Agriculture	NLCD Open + Low	
78	USA	MERC	999	cb_2020_us_county_500k	GEOID	MERC	NONE				Industrial Land	Commercial Land	

Appendix 3A

2023 Monthly Profiles for the EGUs in Maricopa and Pinal Counties

County	Facility	Unit	Jan	Feb	Mar	Apr	May	Jun	Jul	Aug	Sep	Oct	Nov	Dec
Maricopa	All	All	0.072798	0.052108	0.043322	0.074606	0.07945	0.084968	0.146971	0.125624	0.093301	0.101858	0.066522	0.058472
Pinal	All	All	0.021827	0.052378	0.099272	0.117701	0.088665	0.072854	0.143076	0.076834	0.059883	0.05814	0.102415	0.106954
Maricopa	545911	All	0.127158	0.101292	0.063665	0.09541	0.057168	0.086412	0.108579	0.106816	0.10457	0.090401	0.031261	0.027266
Maricopa	546011	All	0.031671	0.042767	0.078818	0.093774	0.092178	0.065567	0.100949	0.101896	0.088392	0.112718	0.087795	0.103474
Maricopa	1139111	All	0.025824	0.032052	0.047131	0.045765	0.075414	0.037217	0.133983	0.135066	0.108175	0.139841	0.152888	0.066644
Maricopa	1139211	All	0.034095	0.021723	0.046835	0.075044	0.088904	0.102872	0.099072	0.102306	0.100962	0.105927	0.109112	0.113146
Maricopa	1139311	All	0.073539	0.013812		0.059257	0.092455	0.076676	0.34483	0.176621	0.024922	0.115963	0.021925	
Maricopa	1139411	All	0.115668	0.065219	0.057083	0.088998	0.082552	0.089964	0.106479	0.102838	0.077261	0.091544	0.083227	0.039166
Maricopa	10704011	All				0.020849	0.022538	0.14594	0.199398	0.241835	0.232841	0.126183		0.010417
Maricopa	10704311	All	0.091718	0.079626	0.027531	0.085076	0.068999	0.081719	0.104126	0.102349	0.090525	0.095827	0.082067	0.090437
Maricopa	10704411	All	0.089057	0.065484	0.068341	0.08229	0.094414	0.100803	0.093944	0.108616	0.103879	0.076817	0.053194	0.06316
Pinal	998011	All	0.00078			0.136673	0.134982	0.033047	0.116213	0.041497	0.036728	0.15989	0.184897	0.155293
Pinal	998111	All	0.003997	0.071138	0.113375	0.10782	0.093353	0.099269	0.109832	0.092169	0.084988	0.016284	0.091005	0.116769
Pinal	1032711	All	0.086943	0.016923	0.091979	0.157529	0.08002	0.037819	0.129703	0.042492	0.017866	0.079645	0.120476	0.138605
Pinal	11310611	All	0.031382	0.057625	0.121235	0.102953	0.056703	0.04952	0.260925	0.081206	0.036443	0.100551	0.073794	0.027663
Maricopa	545911	48317513	0.137071	0.094158	2.99E-06	0.121295	0.100616	0.096161	0.110816	0.107894	0.117706	0.11428		
Maricopa	545911	48317613	0.122142	0.106726	0.126407	0.07808	0.024517	0.081004	0.112087	0.109563	0.097628	0.127266	0.014579	
Maricopa	545911	48318013	0.131144	0.108981	0.130449	0.080306	0.005958	0.081021	0.111266	0.109874	0.098176	0.127644	0.01518	
Maricopa	545911	48318413	0.119504	0.095457	2.62E-06	0.10267	0.096293	0.087834	0.100897	0.100522	0.105366	0.001128	0.088873	0.101453
Maricopa	546011	48316913	0.03552	0.04326	0.071021	0.086731	0.089362	0.064652	0.097156	0.10084	0.092337	0.114809	0.096048	0.108265
Maricopa	546011	48317013	0.027313	0.042209	0.087647	0.10175	0.095367	0.066603	0.105245	0.103092	0.083926	0.110351	0.078449	0.098049
Maricopa	1139111	46679113	0.007268	0.089311	0.097659		0.000396	0.047418	0.128164	0.132655	0.104695	0.149155	0.160646	0.082633
Maricopa	1139111	105572013	0.04441		0.029141	0.063369	0.118165	0.02709	0.140265	0.138659	0.125402	0.123768	0.138232	0.051498
Maricopa	1139111	105572113	0.027348		0.00772	0.080045	0.116587	0.03628	0.133971	0.13399	0.093608	0.146366	0.159694	0.06439
Maricopa	1139211	105573113	0.003303		0.022866	0.09363	0.09422	0.111701	0.104486	0.111151	0.111664	0.107552	0.118987	0.120439
Maricopa	1139211	105573213	0.003194		0.022902	0.082341	0.084922	0.111237	0.101876	0.112537	0.11672	0.119496	0.118911	0.125863
Maricopa	1139211	105573313	0.084105	0.056943	0.085666	0.054056	0.087817	0.088933	0.092408	0.086844	0.079516	0.093618	0.093164	0.096929
Maricopa	1139311	142939613	0.106945	0.00757		0.054284	0.072494	0.02837	0.268807	0.251364	0.03562	0.143473	0.031073	
Maricopa	1139311	142939713	0.074056	0.018238		0.046812	0.081713	0.018181	0.285944	0.23235	0.032583	0.181108	0.029013	
Maricopa	1139311	142939813	0.022444	0.018198		0.080983	0.134895	0.216488	0.526991					
Maricopa	1139411	142941413	0.115668	0.065219	0.057083	0.088998	0.082552	0.089964	0.106479	0.102838	0.077261	0.091544	0.083227	0.039166
Maricopa	10704011	58571513				0.021365	0.031762	0.138973	0.217298	0.228485	0.232295	0.117982		0.01184
Maricopa	10704011	58571613				0.022298	0.015648	0.139669	0.16592	0.251503	0.256678	0.135655		0.012628
Maricopa	10704011	58571713				0.01907	0.019594	0.158262	0.211386	0.246362	0.212394	0.125853		0.00708
Maricopa	10704311	58618813	0.114269	0.094048	0.017533	0.085678	0.04794	0.080976	0.106427	0.101848	0.090265	0.098688	0.072424	0.089905
Maricopa	10704311	58618913	0.107447	0.087347	0.013586	0.07752	0.065837	0.082481	0.112172	0.104708	0.094959	0.10084	0.063557	0.089545
Maricopa	10704311	58713613	0.075054	0.070351	0.033011	0.088438	0.079705	0.082033	0.100531	0.102639	0.089248	0.093303	0.094751	0.090936
Maricopa	10704311	58713713	0.074841	0.06947	0.042223	0.087598	0.079894	0.081466	0.098965	0.100646	0.088353	0.091652	0.093735	0.091156
Maricopa	10704411	58713913	0.101795	0.013674	0.094244	0.090462	0.08465	0.087754	0.073225	0.093868	0.093532	0.081024	0.089059	0.096714
Maricopa	10704411	58714513	0.109038	0.013822	0.08522	0.087513	0.075568	0.081129	0.095534	0.097199	0.094509	0.071283	0.091733	0.097452
Maricopa	10704411	58714613	0.097501	0.081783		0.011904	0.09416	0.107395	0.101739	0.102911	0.104432	0.082011	0.104144	0.112021
Maricopa	10704411	58714713	0.106299	0.081227		0.022941	0.086712	0.107717	0.08871	0.11304	0.105816	0.076976	0.101575	0.108987
Maricopa	10704411	58714813	0.040422	0.092946	0.122468	0.113696	0.09479	0.112731	0.079331	0.110436	0.091705	0.09032		0.051155
Maricopa	10704411	58714913	0.055659	0.086877	0.104077	0.104968	0.104413	0.101414	0.108291	0.109463	0.10375	0.110041	0.005334	0.005713
Maricopa	10704411	58715013	0.088806	0.079331	0.078439	0.120328	0.115689	0.105672	0.113714	0.126315	0.123088	0.048618		
Maricopa	10704411	58715113	0.106433	0.100985	0.060443	0.119239	0.110068	0.111159	0.096603	0.125609	0.12258	0.046882		
Pinal	998011	67644213	0.00078			0.136673	0.134982	0.033047	0.116213	0.041497	0.036728	0.15989	0.184897	0.155293
Pinal	998111	48101713	0.003531	0.066224	0.108509	0.102414	0.088684	0.101658	0.117652	0.095861	0.083442	0.016599	0.094779	0.120646
Pinal	998111	48101813	0.00443	0.0757	0.117892	0.112839	0.097687	0.097051	0.102571	0.088742	0.086424	0.015993	0.087502	0.113169
Pinal	1032711	48098813	0.076027	0.022435	0.0263	0.160699	0.113871	0.05179	0.128993	0.006738	0.017577	0.040612	0.213952	0.141007
Pinal	1032711	62911013	0.076734	0.019209	0.015606	0.158056	0.089825	0.049955	0.136176	0.018406	0.026598	0.05011	0.219676	0.13965

County	Facility	Unit	Jan	Feb	Mar	Apr	May	Jun	Jul	Aug	Sep	Oct	Nov	Dec
Pinal	1032711	62911113	0.077815	0.02679	0.038247	0.195314	0.053868	0.044277	0.143571	0.061219	0.013984	0.098461	0.063717	0.182737
Pinal	1032711	62911213	0.087836	0.012972	0.122315	0.172422	0.083555	0.002476	0.107203	0.045336	0.011553	0.091008	0.066998	0.196328
Pinal	1032711	62911313	0.103422	0.012789	0.171104	0.159992	0.088195	0.014657	0.087056	0.025104	0.009085	0.050492	0.149862	0.128241
Pinal	1032711	62911413	0.1043	0.057949	0.061188	0.047161	0.066969	0.073227	0.122708	0.041345	0.018334	0.047235	0.186658	0.172925
Pinal	1032711	62911513	0.088418	0.000226	0.122655	0.082938	0.090141	0.059011	0.147486	0.07678	0.030169	0.105339	0.069237	0.127599
Pinal	1032711	62911613	0.126648	0.000668	0.175632	0.111329	0.060875	0.07842	0.150249	0.036471	0.034156	0.041147	0.069825	0.11458
Pinal	1032711	62911713	0.094116	0.015656	0.142719	0.242195	0.017503	0.015837	0.14175	0.068467	0.013566	0.128183	0.087484	0.032523
Pinal	1032711	62911813	0.063928	0.006771	0.088833	0.195267	0.108463	0.015955	0.134307	0.046328	0.010594	0.115767	0.076894	0.136892
Pinal	11310611	118549313				0.255187	0.077223	0.017355	0.426141	0.097631	0.0212	0.050879	0.034259	0.020126
Pinal	11310611	118549413	0.001996	0.043636	0.221806	0.193856	0.054963	0.018986	0.300277	0.077331	0.009289	0.039521	0.026483	0.011856
Pinal	11310611	118549513	0.002422	0.035752	0.209096	0.186151	0.055825	0.017322	0.302767	0.083532	0.010221	0.052787	0.03173	0.012396
Pinal	11310611	118549613	0.077266	0.089947	0.080939	0.021759	0.045135	0.065139	0.227455	0.074356	0.051233	0.14125	0.088423	0.037097
Pinal	11310611	118549713	0.096074	0.115773	0.083287	0.026265	0.056009	0.071122	0.224288	0.069233	0.049235	0.104253	0.07626	0.0282
Pinal	11310611	118549813	0.093096	0.101987	0.089485	0.027222	0.047021	0.072126	0.234957	0.063459	0.043559	0.105748	0.085201	0.036138
Pinal	11310611	118549913	0.031825	0.050455	0.093389	0.031049	0.048314	0.070075	0.276847	0.069513	0.046975	0.161055	0.08833	0.032173
Pinal	11310611	118550013	0.005383	0.036666	0.017319	0.12484	0.068264	0.053287	0.283102	0.111236	0.046621	0.102453	0.111754	0.039076
Pinal	11310611	118550113	0.006184	0.035406	0.173346	0.125694	0.059857	0.052731	0.227019	0.082629	0.034157	0.094813	0.079762	0.028403
Pinal	11310611	118550213	0.004449	0.046386	0.16957	0.120403	0.060246	0.042181	0.235356	0.079846	0.032815	0.107299	0.076042	0.025407
Pinal	11310611	118550313	0.009602	0.042441	0.174747	0.104131	0.055514	0.043749	0.236347	0.089977	0.0371	0.109496	0.072757	0.02414
Pinal	11310611	118550413	0.000209	0.043127	0.153225	0.215929	0.063415	0.010834	0.323266	0.080482	0.015268	0.043838	0.036644	0.013762

Appendix 3B

2023 Daily Profiles for the EGUs in Maricopa and Pinal Counties

County	Facility	Unit	Mon	Tue	Wed	Thu	Fri	Sat	Sun
Maricopa	All	All	0.147692	0.150717	0.146126	0.145512	0.138314	0.139247	0.132391
Pinal	All	All	0.15255	0.145001	0.138292	0.145062	0.139939	0.141446	0.137709
Maricopa	545911	All	0.141381	0.145915	0.147763	0.154124	0.140123	0.14193	0.128763
Maricopa	546011	All	0.149795	0.149485	0.146523	0.142695	0.148872	0.133908	0.128721
Maricopa	1139111	All	0.145765	0.153761	0.158967	0.129852	0.130341	0.140161	0.141153
Maricopa	1139211	All	0.138723	0.138622	0.145124	0.148258	0.137681	0.152866	0.138726
Maricopa	1139311	All	0.163152	0.175876	0.147597	0.1509	0.128618	0.117793	0.116064
Maricopa	1139411	All	0.142341	0.141374	0.13995	0.144612	0.12528	0.154102	0.15234
Maricopa	10704011	All	0.136956	0.15253	0.147279	0.141516	0.144462	0.14675	0.130507
Maricopa	10704311	All	0.142455	0.142672	0.145344	0.145228	0.142546	0.14405	0.137705
Maricopa	10704411	All	0.14709	0.139348	0.140113	0.144516	0.143303	0.146914	0.138716
Pinal	998011	All	0.166998	0.160338	0.135128	0.166743	0.129093	0.122803	0.118897
Pinal	998111	All	0.151616	0.141798	0.130732	0.144787	0.141471	0.14772	0.141874
Pinal	1032711	All	0.163021	0.15087	0.141629	0.131218	0.146175	0.12988	0.137207
Pinal	11310611	All	0.141728	0.142942	0.158662	0.144261	0.136903	0.140129	0.135374
Maricopa	545911	48317513	0.132081	0.146239	0.154309	0.159528	0.143993	0.138805	0.125045
Maricopa	545911	48317613	0.144798	0.140233	0.142204	0.160475	0.135169	0.145475	0.131646
Maricopa	545911	48318013	0.139325	0.143491	0.143025	0.157534	0.141939	0.144541	0.130144
Maricopa	545911	48318413	0.14921	0.151901	0.149374	0.14134	0.138932	0.140196	0.129047
Maricopa	546011	48316913	0.147266	0.149541	0.146656	0.14416	0.148673	0.136019	0.127684
Maricopa	546011	48317013	0.152531	0.149424	0.14638	0.14111	0.149087	0.131625	0.129843
Maricopa	1139111	46679113	0.161042	0.158182	0.13738	0.121083	0.133471	0.139726	0.149118
Maricopa	1139111	105572013	0.140004	0.147412	0.162018	0.13021	0.135437	0.140671	0.144248
Maricopa	1139111	105572113	0.139814	0.157258	0.173051	0.136554	0.122126	0.139945	0.131252
Maricopa	1139211	105573113	0.136324	0.136854	0.156729	0.150699	0.140848	0.143497	0.135049
Maricopa	1139211	105573213	0.134717	0.139669	0.140563	0.154049	0.135435	0.154105	0.141463
Maricopa	1139211	105573313	0.145254	0.139403	0.13767	0.139882	0.136656	0.161349	0.139785
Maricopa	1139311	142939613	0.152457	0.184393	0.142255	0.150315	0.131452	0.116115	0.123011
Maricopa	1139311	142939713	0.159934	0.148237	0.161349	0.124142	0.138088	0.150246	0.118005
Maricopa	1139311	142939813	0.177806	0.189275	0.142167	0.173766	0.117581	0.092734	0.10667
Maricopa	1139411	142941413	0.142341	0.141374	0.13995	0.144612	0.12528	0.154102	0.15234
Maricopa	10704011	58571513	0.134833	0.156906	0.14918	0.13722	0.131673	0.15329	0.136898
Maricopa	10704011	58571613	0.135902	0.144239	0.148436	0.138079	0.163177	0.145073	0.125095
Maricopa	10704011	58571713	0.139947	0.155411	0.144416	0.148696	0.140815	0.141793	0.128922
Maricopa	10704311	58618813	0.139433	0.140006	0.143679	0.148155	0.143534	0.14548	0.139713
Maricopa	10704311	58618913	0.147306	0.142081	0.144762	0.146557	0.141768	0.141144	0.136382
Maricopa	10704311	58713613	0.14141	0.145006	0.145716	0.143551	0.142059	0.144883	0.137376
Maricopa	10704311	58713713	0.141975	0.143221	0.146821	0.1433	0.142798	0.144459	0.137426
Maricopa	10704411	58713913	0.145561	0.140413	0.140865	0.153509	0.140955	0.143415	0.135281
Maricopa	10704411	58714513	0.147335	0.133733	0.143876	0.140764	0.147749	0.144861	0.141682
Maricopa	10704411	58714613	0.146747	0.137879	0.12999	0.134466	0.159106	0.151267	0.140545
Maricopa	10704411	58714713	0.149489	0.139643	0.141041	0.13822	0.140852	0.14632	0.144434
Maricopa	10704411	58714813	0.148827	0.130968	0.147142	0.14849	0.13413	0.152967	0.137476
Maricopa	10704411	58714913	0.146329	0.1451	0.135566	0.146539	0.145054	0.148355	0.133058
Maricopa	10704411	58715013	0.144426	0.140367	0.13948	0.142148	0.139956	0.150275	0.143348
Maricopa	10704411	58715113	0.148439	0.146351	0.142379	0.150482	0.139215	0.138388	0.134745
Pinal	998011	67644213	0.166998	0.160338	0.135128	0.166743	0.129093	0.122803	0.118897
Pinal	998111	48101713	0.146851	0.138829	0.13168	0.138649	0.149617	0.146302	0.148073

County	Facility	Unit	Mon	Tue	Wed	Thu	Fri	Sat	Sun
Pinal	998111	48101813	0.156073	0.144576	0.129846	0.150529	0.133853	0.149047	0.136076
Pinal	1032711	48098813	0.16291	0.139279	0.148318	0.164652	0.12632	0.115975	0.142546
Pinal	1032711	62911013	0.177238	0.161922	0.122416	0.1117	0.145741	0.138543	0.14244
Pinal	1032711	62911113	0.169684	0.140086	0.126072	0.154605	0.107181	0.137283	0.165088
Pinal	1032711	62911213	0.170827	0.136588	0.129387	0.14318	0.152762	0.129143	0.138114
Pinal	1032711	62911313	0.163768	0.182807	0.117778	0.087365	0.158741	0.131295	0.158246
Pinal	1032711	62911413	0.170268	0.150154	0.139301	0.126257	0.141193	0.146968	0.125859
Pinal	1032711	62911513	0.175986	0.151542	0.169889	0.119724	0.134587	0.102421	0.145851
Pinal	1032711	62911613	0.182943	0.138648	0.128636	0.117491	0.149698	0.14422	0.138364
Pinal	1032711	62911713	0.130147	0.159804	0.16514	0.129541	0.163382	0.133847	0.118139
Pinal	1032711	62911813	0.142893	0.151923	0.153595	0.134824	0.176965	0.131647	0.108152
Pinal	11310611	118549313	0.134391	0.140267	0.156757	0.169647	0.135402	0.13458	0.128957
Pinal	11310611	118549413	0.122534	0.13691	0.189495	0.153214	0.142884	0.129877	0.125086
Pinal	11310611	118549513	0.12881	0.131001	0.177881	0.159291	0.153283	0.12662	0.123114
Pinal	11310611	118549613	0.135857	0.167714	0.142714	0.171095	0.132619	0.115143	0.134857
Pinal	11310611	118549713	0.133364	0.164569	0.141026	0.159322	0.142512	0.120966	0.13824
Pinal	11310611	118549813	0.150245	0.144482	0.133415	0.156161	0.138413	0.132854	0.144431
Pinal	11310611	118549913	0.143407	0.150212	0.148683	0.148634	0.131275	0.13956	0.138229
Pinal	11310611	118550013	0.14604	0.133687	0.172352	0.136898	0.127462	0.144467	0.139094
Pinal	11310611	118550113	0.146948	0.13569	0.160352	0.127036	0.138646	0.157819	0.133509
Pinal	11310611	118550213	0.146381	0.14112	0.154176	0.123582	0.13317	0.161893	0.139678
Pinal	11310611	118550313	0.156434	0.147089	0.160052	0.120089	0.124225	0.160569	0.131541
Pinal	11310611	118550413	0.139613	0.119205	0.173646	0.135838	0.158901	0.131414	0.141383

Appendix 3C1

2023 Weekday Hourly Profiles (UTC from 0 to 11) for the EGUs in Maricopa and Pinal Counties

County	Facility	Unit	0	1	2	3	4	5	6	7	8	9	10	11
Maricopa	All	All	0.058908	0.059824	0.060761	0.054728	0.045856	0.041284	0.036443	0.03326	0.030673	0.029426	0.028767	0.028836
Pinal	All	All	0.063758	0.073377	0.071708	0.066598	0.058503	0.054771	0.046602	0.040778	0.034358	0.031613	0.030203	0.027934
Maricopa	545911	All	0.049482	0.051255	0.052565	0.049906	0.047327	0.044894	0.041826	0.035234	0.032583	0.031745	0.032867	0.032381
Maricopa	546011	All	0.046475	0.047889	0.049672	0.049168	0.04743	0.045801	0.043939	0.042393	0.040319	0.040279	0.039994	0.041141
Maricopa	1139111	All	0.045671	0.046477	0.046174	0.045778	0.046269	0.044262	0.044439	0.039778	0.036339	0.032907	0.032605	0.032605
Maricopa	1139211	All	0.048367	0.045884	0.045081	0.043476	0.041434	0.041368	0.039592	0.038048	0.035367	0.033051	0.03255	0.033176
Maricopa	1139311	All	0.094132	0.102732	0.108969	0.08197	0.045333	0.029139	0.010663	0.007297	0.003361	0.002663	0.001202	0.001337
Maricopa	1139411	All	0.046404	0.045843	0.045794	0.04567	0.042969	0.042291	0.041835	0.037327	0.034071	0.033319	0.033066	0.031623
Maricopa	10704011	All	0.045518	0.047311	0.045071	0.045718	0.04437	0.042736	0.040792	0.034969	0.034876	0.03525	0.034524	0.034508
Maricopa	10704311	All	0.047242	0.047704	0.047859	0.047382	0.046934	0.045938	0.044718	0.043938	0.042593	0.041538	0.041142	0.041016
Maricopa	10704411	All	0.055452	0.049639	0.047633	0.048406	0.046536	0.044997	0.044738	0.042042	0.039446	0.037611	0.036396	0.036497
Pinal	998011	All	0.060744	0.08487	0.088102	0.087668	0.082669	0.078614	0.070883	0.057784	0.049456	0.046247	0.029678	0.026761
Pinal	998111	All	0.054204	0.046578	0.044699	0.044643	0.044351	0.045331	0.044393	0.042321	0.038483	0.037	0.039182	0.033936
Pinal	1032711	All	0.070771	0.098818	0.090942	0.087841	0.07754	0.073374	0.057014	0.050322	0.038474	0.031435	0.027472	0.03146
Pinal	11310611	All	0.08678	0.124407	0.124831	0.102377	0.072929	0.056817	0.03397	0.02209	0.013045	0.009823	0.007777	0.009947
Maricopa	545911	48317513	0.048688	0.051111	0.055008	0.04898	0.047731	0.046289	0.044972	0.037919	0.034706	0.033985	0.036135	0.033755
Maricopa	545911	48317613	0.048002	0.047622	0.049567	0.049939	0.046592	0.043996	0.039393	0.032273	0.030273	0.030235	0.030312	0.03063
Maricopa	545911	48318013	0.048624	0.053148	0.051439	0.050121	0.046973	0.04533	0.042043	0.037178	0.034998	0.032272	0.031174	0.031353
Maricopa	545911	48318413	0.052047	0.052821	0.053366	0.05062	0.047772	0.043914	0.040503	0.033489	0.030526	0.03035	0.032938	0.033174
Maricopa	546011	48316913	0.044113	0.046517	0.048461	0.04812	0.046582	0.045767	0.044629	0.043925	0.040461	0.04188	0.041235	0.041442
Maricopa	546011	48317013	0.049021	0.049369	0.050978	0.050297	0.048346	0.045838	0.043196	0.040742	0.040166	0.038552	0.038657	0.040817
Maricopa	1139111	46679113	0.03989	0.041968	0.040798	0.041954	0.044323	0.043202	0.044053	0.042911	0.042181	0.042131	0.041535	0.041301
Maricopa	1139111	105572013	0.045675	0.046613	0.046501	0.046767	0.045373	0.043856	0.044655	0.040893	0.035342	0.032595	0.03222	0.03222
Maricopa	1139111	105572113	0.050235	0.049893	0.050066	0.047718	0.048788	0.045543	0.044506	0.036081	0.032813	0.025958	0.025969	0.026154
Maricopa	1139211	105573113	0.052071	0.046644	0.042469	0.044849	0.040095	0.039429	0.037817	0.034859	0.033302	0.031649	0.031595	0.031534
Maricopa	1139211	105573213	0.04719	0.047011	0.048395	0.042664	0.041143	0.040993	0.03892	0.040928	0.036617	0.032522	0.031754	0.032342
Maricopa	1139211	105573313	0.045592	0.043922	0.044513	0.042829	0.043164	0.043828	0.04218	0.038541	0.036309	0.035091	0.034384	0.035784
Maricopa	1139311	142939613	0.113511	0.110549	0.105051	0.086	0.050543	0.030074	0.007864	0.003479	0	7.38E-05	0.000114	0.000327
Maricopa	1139311	142939713	0.103684	0.103063	0.092984	0.076566	0.044639	0.032553	0.009652	0.00446	0.000145	0.000272	0.000526	0.000651
Maricopa	1139311	142939813	0.06625	0.094158	0.125269	0.081779	0.040311	0.025554	0.014409	0.013516	0.009379	0.007234	0.002872	0.002933
Maricopa	1139411	142941413	0.046404	0.045843	0.045794	0.04567	0.042969	0.042291	0.041835	0.037327	0.034071	0.033319	0.033066	0.031623
Maricopa	10704011	58571513	0.043721	0.042753	0.042526	0.047039	0.047667	0.044908	0.042451	0.037659	0.03818	0.034816	0.034174	0.033781
Maricopa	10704011	58571613	0.047471	0.052637	0.051079	0.049479	0.045013	0.043288	0.041155	0.034039	0.034197	0.034655	0.033797	0.034322
Maricopa	10704011	58571713	0.045543	0.047049	0.042298	0.041203	0.040669	0.040186	0.038895	0.033207	0.032313	0.036177	0.035485	0.035363
Maricopa	10704311	58618813	0.048098	0.048688	0.048051	0.047475	0.047617	0.047023	0.045786	0.044409	0.042068	0.039884	0.039398	0.038978
Maricopa	10704311	58618913	0.047865	0.047637	0.04816	0.047513	0.047594	0.047071	0.046107	0.0449	0.043413	0.041982	0.041645	0.04193
Maricopa	10704311	58713613	0.046645	0.047371	0.047832	0.047465	0.046479	0.045105	0.043752	0.043551	0.042732	0.042314	0.041942	0.04175
Maricopa	10704311	58713713	0.046586	0.047262	0.047489	0.047129	0.046263	0.044899	0.043608	0.043134	0.042237	0.041823	0.041432	0.041273
Maricopa	10704411	58713913	0.047173	0.048607	0.047514	0.048804	0.048917	0.042413	0.040286	0.040991	0.035837	0.035305	0.033197	0.03282
Maricopa	10704411	58714513	0.056419	0.047085	0.049295	0.048816	0.047915	0.045254	0.044149	0.044424	0.042131	0.036874	0.037347	0.036511
Maricopa	10704411	58714613	0.048093	0.046142	0.044649	0.045572	0.043954	0.04301	0.044225	0.043183	0.04201	0.04135	0.040711	0.04126
Maricopa	10704411	58714713	0.053059	0.052428	0.048332	0.049517	0.048437	0.04495	0.045189	0.041829	0.040587	0.039809	0.036771	0.038265
Maricopa	10704411	58714813	0.064228	0.055166	0.049948	0.048725	0.047593	0.051802	0.044829	0.044321	0.038122	0.040457	0.035955	0.035272
Maricopa	10704411	58714913	0.05031	0.041975	0.044403	0.048507	0.043778	0.044146	0.046218	0.043265	0.042249	0.040516	0.040019	0.040533
Maricopa	10704411	58715013	0.060664	0.051444	0.046377	0.045413	0.045036	0.043516	0.048941	0.041804	0.041205	0.035773	0.034741	0.038016
Maricopa	10704411	58715113	0.0636	0.055157	0.050531	0.051706	0.046657	0.045128	0.044164	0.036529	0.03355	0.031536	0.032748	0.02982

County	Facility	Unit	0	1	2	3	4	5	6	7	8	9	10	11
Pinal	998011	67644213	0.060744	0.08487	0.088102	0.087668	0.082669	0.078614	0.070883	0.057784	0.049456	0.046247	0.029678	0.026761
Pinal	998111	48101713	0.045418	0.046462	0.045957	0.04587	0.045755	0.047569	0.046413	0.044139	0.037932	0.034538	0.037808	0.029343
Pinal	998111	48101813	0.062316	0.046685	0.043537	0.043511	0.043055	0.043264	0.042527	0.040644	0.038992	0.039273	0.04045	0.038175
Pinal	1032711	48098813	0.051035	0.090836	0.08944	0.081583	0.079968	0.074167	0.055368	0.052798	0.04215	0.034733	0.031649	0.038699
Pinal	1032711	62911013	0.063751	0.099503	0.10003	0.088589	0.085052	0.080837	0.062848	0.046816	0.042827	0.031913	0.023182	0.034924
Pinal	1032711	62911113	0.079229	0.103415	0.094817	0.089192	0.076577	0.071756	0.054399	0.049096	0.041864	0.033347	0.026918	0.035034
Pinal	1032711	62911213	0.069215	0.105114	0.103532	0.086373	0.074629	0.076462	0.065717	0.052224	0.034316	0.028069	0.02757	0.027403
Pinal	1032711	62911313	0.080278	0.113341	0.077494	0.089095	0.068329	0.061253	0.046868	0.049884	0.042923	0.036891	0.033643	0.039907
Pinal	1032711	62911413	0.085307	0.10393	0.106668	0.114884	0.095166	0.090237	0.051623	0.039162	0.020129	0.011913	0.012461	0.008627
Pinal	1032711	62911513	0.089905	0.117247	0.095389	0.091295	0.081409	0.079401	0.054684	0.050823	0.022785	0.019078	0.017996	0.020082
Pinal	1032711	62911613	0.07346	0.096103	0.098341	0.102554	0.08623	0.083333	0.056477	0.047788	0.024355	0.019089	0.018694	0.02396
Pinal	1032711	62911713	0.068834	0.098265	0.087157	0.078969	0.071996	0.067132	0.055862	0.048646	0.040133	0.034782	0.031377	0.034782
Pinal	1032711	62911813	0.062143	0.076441	0.070832	0.077981	0.067477	0.061153	0.059668	0.057138	0.054168	0.046469	0.03866	0.03789
Pinal	11310611	118549313	0.088538	0.104238	0.108614	0.084077	0.047958	0.04487	0.034489	0.030199	0.017759	0.012612	0.010638	0.015271
Pinal	11310611	118549413	0.090628	0.11009	0.110424	0.079853	0.046859	0.046275	0.037588	0.029736	0.020799	0.014701	0.009856	0.019379
Pinal	11310611	118549513	0.087511	0.108618	0.113957	0.081088	0.04313	0.045382	0.036873	0.027864	0.020022	0.0156	0.013681	0.017102
Pinal	11310611	118549613	0.082349	0.125651	0.131556	0.122095	0.088508	0.056635	0.031302	0.019429	0.009714	0.008635	0.01054	0.010921
Pinal	11310611	118549713	0.088322	0.135335	0.131386	0.116592	0.081928	0.057293	0.028647	0.022441	0.012411	0.007271	0.005516	0.008901
Pinal	11310611	118549813	0.095194	0.136546	0.135982	0.115024	0.077764	0.054336	0.029567	0.019476	0.007057	0.002752	0.005081	0.01122
Pinal	11310611	118549913	0.0831	0.125982	0.141618	0.115125	0.076681	0.060362	0.036053	0.021714	0.007238	0.001502	0.004643	0.011267
Pinal	11310611	118550013	0.095632	0.130345	0.11013	0.097096	0.080448	0.067094	0.035628	0.021404	0.010473	0.008873	0.005031	0.003887
Pinal	11310611	118550113	0.088562	0.136616	0.131851	0.100774	0.080719	0.060415	0.031324	0.019013	0.010971	0.009631	0.005858	0.004964
Pinal	11310611	118550213	0.082417	0.126834	0.131522	0.105351	0.08889	0.065342	0.036382	0.017912	0.01356	0.011885	0.008537	0.005636
Pinal	11310611	118550313	0.08016	0.128918	0.134929	0.111841	0.077969	0.059319	0.033704	0.017021	0.010167	0.009943	0.004157	0.004831
Pinal	11310611	118550413	0.076324	0.100657	0.105199	0.082975	0.052721	0.047611	0.038284	0.027415	0.024495	0.018493	0.015654	0.018412

Appendix 3C2

2023 Weekday Hourly Profiles (UTC from 12 to 23) for the EGUs in Maricopa and Pinal Counties

County	Facility	Unit	12	13	14	15	16	17	18	19	20	21	22	23
Maricopa	All	All	0.029759	0.029888	0.030391	0.028427	0.030199	0.03242	0.038615	0.044553	0.051829	0.056236	0.058978	0.05994
Pinal	All	All	0.029605	0.028971	0.030188	0.020584	0.019921	0.020078	0.030535	0.033681	0.035313	0.043818	0.048264	0.058839
Maricopa	545911	All	0.031897	0.032118	0.029325	0.029656	0.03512	0.039573	0.044711	0.046701	0.049646	0.05255	0.05316	0.053477
Maricopa	546011	All	0.044828	0.042692	0.040793	0.036513	0.034809	0.033885	0.034726	0.036719	0.035595	0.039385	0.042742	0.042812
Maricopa	1139111	All	0.032889	0.033074	0.034083	0.035525	0.0386	0.044367	0.045377	0.04922	0.049821	0.047241	0.048262	0.048238
Maricopa	1139211	All	0.035808	0.035539	0.035114	0.036464	0.04349	0.041361	0.049335	0.050513	0.046422	0.046295	0.051004	0.051262
Maricopa	1139311	All	0.001689	0.003687	0.008238	0.006839	0.011209	0.01919	0.033414	0.047758	0.077506	0.095559	0.10565	0.100465
Maricopa	1139411	All	0.031222	0.033985	0.034213	0.036396	0.047601	0.051042	0.045677	0.05344	0.053921	0.045208	0.042162	0.044924
Maricopa	10704011	All	0.035564	0.037626	0.043874	0.043089	0.040528	0.038529	0.04416	0.047989	0.043904	0.045713	0.047354	0.04603
Maricopa	10704311	All	0.041658	0.038681	0.036523	0.034221	0.033462	0.033072	0.035716	0.035974	0.038212	0.043561	0.043801	0.047116
Maricopa	10704411	All	0.037736	0.038146	0.037233	0.031305	0.029655	0.029244	0.035455	0.043129	0.047393	0.045314	0.044482	0.051515
Pinal	998011	All	0.036618	0.028149	0.020797	0.007417	0.006332	0.005237	0.005855	0.007276	0.01221	0.026815	0.037149	0.042668
Pinal	998111	All	0.033578	0.035178	0.041834	0.03111	0.029641	0.029037	0.043638	0.043812	0.040724	0.045103	0.047682	0.063541
Pinal	1032711	All	0.028528	0.026179	0.024261	0.01309	0.009346	0.006997	0.006997	0.011594	0.016554	0.037148	0.039438	0.044406
Pinal	11310611	All	0.01601	0.01427	0.006928	0.003239	0.006934	0.011375	0.022079	0.033239	0.043959	0.052982	0.060963	0.063229
Maricopa	545911	48317513	0.033457	0.033973	0.031164	0.030772	0.032842	0.032631	0.036775	0.04363	0.049042	0.053392	0.053342	0.049701
Maricopa	545911	48317613	0.030816	0.029158	0.033799	0.038681	0.042067	0.042702	0.050257	0.050644	0.044089	0.047421	0.054542	0.05699
Maricopa	545911	48318013	0.030849	0.030678	0.026741	0.026537	0.031662	0.041067	0.048453	0.046485	0.046062	0.048152	0.056198	0.062462
Maricopa	545911	48318413	0.032001	0.033694	0.025966	0.023844	0.034487	0.042777	0.045323	0.046774	0.057236	0.059001	0.049647	0.04773
Maricopa	546011	48316913	0.045108	0.041894	0.040273	0.037026	0.035055	0.034217	0.036008	0.036409	0.035013	0.038426	0.044307	0.043132
Maricopa	546011	48317013	0.044527	0.043553	0.041353	0.03596	0.034545	0.033527	0.033343	0.037052	0.036223	0.04042	0.041055	0.042466
Maricopa	1139111	46679113	0.041606	0.043393	0.040734	0.041571	0.042422	0.040634	0.041358	0.041152	0.039925	0.039805	0.039627	0.041528
Maricopa	1139111	105572013	0.032964	0.031836	0.031944	0.032502	0.039309	0.041631	0.044384	0.050499	0.05033	0.049607	0.051447	0.050837
Maricopa	1139111	105572113	0.025919	0.026272	0.031165	0.034052	0.034803	0.050307	0.04964	0.054198	0.057084	0.050532	0.051602	0.0507
Maricopa	1139211	105573113	0.034764	0.036471	0.034506	0.037613	0.04472	0.041394	0.050725	0.045753	0.038559	0.043625	0.06423	0.061326
Maricopa	1139211	105573213	0.036546	0.035082	0.037715	0.037335	0.044909	0.042829	0.050676	0.047039	0.049098	0.047893	0.042442	0.047958
Maricopa	1139211	105573313	0.036178	0.035004	0.033122	0.034347	0.040728	0.039831	0.046482	0.059149	0.052134	0.047532	0.045527	0.043828
Maricopa	1139311	142939613	0.00071	0.003409	0.003681	0.004339	0.007259	0.01526	0.030933	0.044643	0.073524	0.097697	0.108115	0.102845
Maricopa	1139311	142939713	0.001147	0.001757	0.007035	0.00765	0.009576	0.015378	0.029413	0.052828	0.089708	0.108338	0.107974	0.100002
Maricopa	1139311	142939813	0.003141	0.005448	0.014003	0.008885	0.016653	0.026267	0.039092	0.047228	0.07249	0.083587	0.101261	0.098282
Maricopa	1139411	142941413	0.031222	0.033985	0.034213	0.036396	0.047601	0.051042	0.045677	0.05344	0.053921	0.045208	0.042162	0.044924
Maricopa	10704011	58571513	0.036751	0.038709	0.042096	0.042799	0.041582	0.04072	0.045044	0.050955	0.041536	0.043978	0.043411	0.042746
Maricopa	10704011	58571613	0.034822	0.036922	0.040538	0.038572	0.036397	0.035314	0.044621	0.045055	0.04423	0.046346	0.047429	0.048621
Maricopa	10704011	58571713	0.035074	0.037201	0.048455	0.047273	0.043099	0.03922	0.042918	0.047698	0.045882	0.046819	0.051051	0.04692
Maricopa	10704311	58618813	0.039752	0.038284	0.035986	0.034203	0.032292	0.033042	0.03726	0.035274	0.039586	0.044522	0.042932	0.049391
Maricopa	10704311	58618913	0.043261	0.040813	0.038694	0.034147	0.03188	0.031162	0.033386	0.035729	0.034436	0.040272	0.044415	0.045988

County	Facility	Unit	12	13	14	15	16	17	18	19	20	21	22	23
Maricopa	10704311	58713613	0.042028	0.038323	0.036006	0.033655	0.034969	0.033723	0.035131	0.035059	0.040389	0.045442	0.041571	0.046765
Maricopa	10704311	58713713	0.041584	0.037616	0.035679	0.034798	0.034327	0.034042	0.036856	0.037547	0.038185	0.043741	0.045993	0.046498
Maricopa	10704411	58713913	0.038978	0.038686	0.037838	0.029117	0.027469	0.026274	0.059489	0.051378	0.045883	0.046982	0.048015	0.048027
Maricopa	10704411	58714513	0.037727	0.040055	0.036406	0.033195	0.029756	0.030189	0.036827	0.042886	0.041956	0.045096	0.040494	0.049196
Maricopa	10704411	58714613	0.041461	0.040905	0.038968	0.036481	0.039468	0.038572	0.036836	0.037926	0.038204	0.044183	0.040718	0.042121
Maricopa	10704411	58714713	0.035656	0.036371	0.034106	0.027189	0.026389	0.025176	0.030395	0.03983	0.05602	0.050373	0.049026	0.050296
Maricopa	10704411	58714813	0.036437	0.034511	0.032488	0.027342	0.019243	0.019314	0.023595	0.045056	0.043755	0.054398	0.042669	0.064774
Maricopa	10704411	58714913	0.043376	0.041193	0.039657	0.033599	0.032384	0.03141	0.028345	0.050404	0.041449	0.042255	0.043364	0.046645
Maricopa	10704411	58715013	0.036267	0.036688	0.035909	0.034593	0.034389	0.031225	0.03665	0.039314	0.052927	0.039783	0.041458	0.047866
Maricopa	10704411	58715113	0.031673	0.036354	0.041988	0.02862	0.028216	0.031778	0.029932	0.036634	0.059565	0.040477	0.05035	0.063289
Pinal	998011	67644213	0.036618	0.028149	0.020797	0.007417	0.006332	0.005237	0.005855	0.007276	0.01221	0.026815	0.037149	0.042668
Pinal	998111	48101713	0.028323	0.031042	0.037858	0.032482	0.030923	0.03112	0.058395	0.050621	0.046002	0.045755	0.04733	0.052945
Pinal	998111	48101813	0.03843	0.038996	0.045504	0.029844	0.028458	0.027114	0.030015	0.037526	0.035851	0.044502	0.048007	0.073324
Pinal	1032711	48098813	0.032016	0.029079	0.024747	0.014907	0.010207	0.011455	0.009546	0.016669	0.018505	0.032971	0.038332	0.039139
Pinal	1032711	62911013	0.026494	0.028903	0.02401	0.016107	0.009935	0.007978	0.003688	0.00715	0.009484	0.030333	0.033193	0.042451
Pinal	1032711	62911113	0.026999	0.026276	0.025231	0.010607	0.009241	0.003857	0.002571	0.008839	0.019124	0.033588	0.034873	0.04315
Pinal	1032711	62911213	0.029402	0.029319	0.028652	0.009079	0.009745	0.008329	0.007746	0.015659	0.014743	0.0329	0.029569	0.034233
Pinal	1032711	62911313	0.034107	0.031323	0.027726	0.012529	0.013109	0.007657	0.005452	0.009165	0.014617	0.033063	0.032019	0.039327
Pinal	1032711	62911413	0.006983	0.002739	0.006436	0.004245	0.004108	0.004245	0.011228	0.01739	0.031905	0.048336	0.058058	0.06422
Pinal	1032711	62911513	0.019232	0.012899	0.013053	0.006797	0.005716	0.004325	0.006411	0.012744	0.017842	0.048583	0.060168	0.052136
Pinal	1032711	62911613	0.019616	0.018826	0.0208	0.015271	0.009347	0.006187	0.005003	0.014613	0.01514	0.048052	0.04476	0.052001
Pinal	1032711	62911713	0.037376	0.034701	0.030323	0.013053	0.00981	0.007864	0.006324	0.011513	0.013621	0.039241	0.036728	0.041511
Pinal	1032711	62911813	0.03822	0.033601	0.031346	0.021282	0.010669	0.006654	0.010779	0.007039	0.016113	0.033821	0.035361	0.045095
Pinal	11310611	118549313	0.026253	0.032515	0.015014	0.006005	0.011839	0.017244	0.027282	0.029255	0.03732	0.052677	0.07361	0.071723
Pinal	11310611	118549413	0.033912	0.037087	0.015035	0.00426	0.009522	0.011777	0.021801	0.028065	0.035416	0.049449	0.071834	0.065653
Pinal	11310611	118549513	0.033703	0.029282	0.013014	0.006173	0.008926	0.010762	0.023108	0.031367	0.043047	0.058814	0.069659	0.061316
Pinal	11310611	118549613	0.011556	0.007937	0.005714	0.000317	0.003302	0.010476	0.018286	0.028317	0.042857	0.052127	0.06	0.061778
Pinal	11310611	118549713	0.007021	0.00514	0.004827	0.00257	0.005203	0.008776	0.016423	0.029023	0.048329	0.054159	0.06375	0.058735
Pinal	11310611	118549813	0.014678	0.00875	0.007339	0.002611	0.004234	0.013408	0.018559	0.027803	0.042693	0.045374	0.061605	0.062945
Pinal	11310611	118549913	0.01509	0.006828	0.004029	0.002595	0.004575	0.014476	0.02663	0.025947	0.044247	0.043428	0.06043	0.066439
Pinal	11310611	118550013	0.007409	0.006632	0.00215	0.001921	0.009056	0.016282	0.027578	0.044729	0.04976	0.055934	0.055385	0.057123
Pinal	11310611	118550113	0.009234	0.007099	0.002234	0.002234	0.005709	0.007099	0.021694	0.042941	0.047012	0.05555	0.055798	0.062699
Pinal	11310611	118550213	0.009542	0.011272	0.006361	0.002734	0.005971	0.005971	0.019977	0.032699	0.039953	0.051783	0.05262	0.066849
Pinal	11310611	118550313	0.010167	0.008145	0.004662	0.004382	0.008314	0.009606	0.021514	0.037412	0.047916	0.055219	0.055275	0.064431
Pinal	11310611	118550413	0.03585	0.033823	0.012978	0.005921	0.008273	0.013221	0.021981	0.029037	0.041123	0.059778	0.066185	0.06359

Appendix 3C3

2023 Weekend Hourly Profiles (UTC from 0 to 11) for the EGUs in Maricopa and Pinal Counties

County	Facility	Unit	0	1	2	3	4	5	6	7	8	9	10	11
Maricopa	All	All	0.06215	0.060731	0.056913	0.053436	0.047133	0.045904	0.040102	0.034519	0.032634	0.030572	0.029868	0.029773
Pinal	All	All	0.062191	0.067903	0.067299	0.063963	0.061876	0.059169	0.051309	0.046489	0.039539	0.0357	0.031606	0.030536
Maricopa	545911	All	0.050537	0.051376	0.051618	0.052033	0.049871	0.047267	0.04428	0.03779	0.03321	0.029459	0.029059	0.026934
Maricopa	546011	All	0.050302	0.051912	0.052502	0.051275	0.050148	0.048034	0.048169	0.044345	0.039903	0.039467	0.039186	0.039011
Maricopa	1139111	All	0.043717	0.043514	0.043767	0.043678	0.04401	0.043534	0.045495	0.039894	0.038419	0.037064	0.035261	0.035435
Maricopa	1139211	All	0.051785	0.044386	0.042488	0.041604	0.042138	0.040996	0.040538	0.035857	0.033558	0.032445	0.029973	0.032032
Maricopa	1139311	All	0.115858	0.122028	0.103518	0.081311	0.051586	0.048798	0.020163	0.005631	0.00352	0.000109	9.63E-05	0.000112
Maricopa	1139411	All	0.051026	0.036916	0.037334	0.036916	0.037683	0.036218	0.036427	0.034515	0.031947	0.032128	0.029867	0.030049
Maricopa	10704011	All	0.047227	0.044507	0.045441	0.044367	0.044927	0.045481	0.043321	0.0374	0.039334	0.038521	0.03722	0.036707
Maricopa	10704311	All	0.047688	0.048948	0.049084	0.04891	0.048222	0.047574	0.046142	0.044618	0.043761	0.042553	0.041642	0.041088
Maricopa	10704411	All	0.057046	0.049898	0.047096	0.049743	0.045888	0.045443	0.044028	0.041472	0.039864	0.03716	0.037266	0.037533
Pinal	998011	All	0.067937	0.096989	0.095867	0.089097	0.084504	0.090287	0.074502	0.062936	0.055009	0.053308	0.037489	0.033747
Pinal	998111	All	0.051386	0.04507	0.045472	0.045395	0.044809	0.044833	0.046034	0.043932	0.039854	0.038468	0.036909	0.037131
Pinal	1032711	All	0.07469	0.099061	0.102771	0.091896	0.091501	0.085496	0.069426	0.060661	0.047722	0.036754	0.027548	0.024835
Pinal	11310611	All	0.083696	0.103426	0.09748	0.090659	0.084204	0.072016	0.046028	0.038487	0.027216	0.019674	0.016171	0.013446
Maricopa	545911	48317513	0.050227	0.051337	0.052221	0.052082	0.057214	0.05203	0.047366	0.04031	0.034519	0.02807	0.032768	0.027237
Maricopa	545911	48317613	0.048489	0.047377	0.048206	0.049884	0.044406	0.044447	0.040869	0.035978	0.031713	0.029146	0.026316	0.026235
Maricopa	545911	48318013	0.051985	0.048569	0.051169	0.055357	0.048312	0.044552	0.044853	0.038151	0.037614	0.036733	0.035036	0.031878
Maricopa	545911	48318413	0.051388	0.056804	0.054161	0.051191	0.048548	0.04712	0.04369	0.0366	0.029822	0.025472	0.023207	0.023437
Maricopa	546011	48316913	0.047975	0.050585	0.051022	0.050135	0.048759	0.047911	0.048052	0.04512	0.039411	0.039347	0.039077	0.038922
Maricopa	546011	48317013	0.052841	0.05336	0.054117	0.052518	0.051662	0.048169	0.048296	0.043498	0.04044	0.039599	0.039304	0.039108
Maricopa	1139111	46679113	0.039519	0.039379	0.039623	0.039781	0.039973	0.039903	0.04247	0.039519	0.039519	0.039327	0.039728	0.03992
Maricopa	1139111	105572013	0.044331	0.043726	0.044035	0.043662	0.043906	0.045681	0.043597	0.044511	0.041938	0.038657	0.036612	0.036046
Maricopa	1139111	105572113	0.046621	0.046832	0.047028	0.047058	0.047615	0.044151	0.050327	0.034812	0.03335	0.033245	0.029826	0.03085
Maricopa	1139211	105573113	0.046042	0.040793	0.041903	0.042308	0.04259	0.041427	0.040441	0.037235	0.035756	0.033924	0.030965	0.031581
Maricopa	1139211	105573213	0.069406	0.051508	0.044482	0.040362	0.040259	0.038772	0.039575	0.034344	0.03137	0.02954	0.028327	0.028515
Maricopa	1139211	105573313	0.039856	0.040787	0.041075	0.042158	0.043563	0.042784	0.041583	0.036032	0.033611	0.033899	0.03065	0.035947
Maricopa	1139311	142939613	0.103851	0.115799	0.101175	0.081819	0.05103	0.025451	0.010439	0.007241	0.00411	9.39E-05	8.72E-05	0.000134
Maricopa	1139311	142939713	0.09619	0.125166	0.107758	0.076353	0.050943	0.043747	0.023894	0.008309	0.005397	0	0	0
Maricopa	1139311	142939813	0.153953	0.126892	0.10193	0.086165	0.05305	0.085805	0.029061	0.000477	0.000631	0.000252	0.000216	0.000207
Maricopa	1139411	142941413	0.051026	0.036916	0.037334	0.036916	0.037683	0.036218	0.036427	0.034515	0.031947	0.032128	0.029867	0.030049
Maricopa	10704011	58571513	0.048091	0.042692	0.042378	0.042711	0.041398	0.046131	0.045706	0.04051	0.04663	0.044227	0.041398	0.038199
Maricopa	10704011	58571613	0.048779	0.048419	0.047473	0.047001	0.046753	0.044997	0.041868	0.035273	0.03534	0.035003	0.034935	0.03471
Maricopa	10704011	58571713	0.044981	0.043039	0.046904	0.043835	0.04706	0.045214	0.042068	0.03597	0.035115	0.035562	0.034804	0.036863
Maricopa	10704311	58618813	0.044406	0.048581	0.048936	0.049054	0.048534	0.048404	0.046736	0.045731	0.044418	0.041828	0.040208	0.039037
Maricopa	10704311	58618913	0.050285	0.050038	0.050446	0.050743	0.050335	0.049951	0.048392	0.046191	0.045696	0.044248	0.042677	0.042554
Maricopa	10704311	58713613	0.048172	0.048758	0.04866	0.048118	0.047195	0.046262	0.044949	0.04356	0.042681	0.042203	0.041856	0.041379
Maricopa	10704311	58713713	0.047909	0.048567	0.048518	0.048064	0.047232	0.046206	0.044958	0.04342	0.042675	0.042133	0.041814	0.041359
Maricopa	10704411	58713913	0.061339	0.049111	0.04942	0.05361	0.046035	0.044103	0.042557	0.039341	0.041336	0.035647	0.032045	0.032942
Maricopa	10704411	58714513	0.053601	0.047995	0.049203	0.055101	0.049291	0.046859	0.044675	0.042884	0.043626	0.038428	0.037904	0.03853
Maricopa	10704411	58714613	0.04404	0.04517	0.044411	0.044731	0.043956	0.043754	0.043737	0.043922	0.042962	0.042473	0.04313	0.042861
Maricopa	10704411	58714713	0.061019	0.045208	0.045208	0.048083	0.04336	0.04425	0.049144	0.041272	0.039407	0.03797	0.039185	0.038398
Maricopa	10704411	58714813	0.065112	0.060742	0.045088	0.053749	0.048044	0.04682	0.043848	0.042211	0.037618	0.037062	0.035711	0.033359
Maricopa	10704411	58714913	0.041108	0.043463	0.044432	0.045103	0.044879	0.04482	0.044313	0.043881	0.043598	0.042614	0.049932	0.051557
Maricopa	10704411	58715013	0.060535	0.045074	0.045981	0.045238	0.044613	0.042919	0.043706	0.040703	0.036927	0.036452	0.035753	0.03724
Maricopa	10704411	58715113	0.070703	0.063307	0.052965	0.052039	0.046495	0.050152	0.040439	0.037345	0.032878	0.026176	0.023761	0.024356

County	Facility	Unit	0	1	2	3	4	5	6	7	8	9	10	11
Pinal	998011	67644213	0.067937	0.096989	0.095867	0.089097	0.084504	0.090287	0.074502	0.062936	0.055009	0.053308	0.037489	0.033747
Pinal	998111	48101713	0.050865	0.047148	0.046694	0.046576	0.046053	0.04701	0.049721	0.043953	0.040295	0.037219	0.034557	0.034774
Pinal	998111	48101813	0.05189	0.043064	0.044292	0.044254	0.043607	0.042731	0.042474	0.043911	0.039427	0.039674	0.039179	0.039408
Pinal	1032711	48098813	0.069082	0.088248	0.105518	0.085299	0.087826	0.088458	0.081087	0.0615	0.049495	0.036436	0.025484	0.025484
Pinal	1032711	62911013	0.077234	0.099384	0.094376	0.09688	0.099576	0.084553	0.069915	0.068952	0.042373	0.025424	0.022149	0.018683
Pinal	1032711	62911113	0.069892	0.091027	0.098813	0.091027	0.088802	0.099926	0.073971	0.060623	0.045977	0.037078	0.029106	0.025399
Pinal	1032711	62911213	0.084723	0.104133	0.091117	0.08792	0.09477	0.092715	0.083124	0.06417	0.056406	0.036081	0.020553	0.018041
Pinal	1032711	62911313	0.078281	0.101623	0.081981	0.088528	0.104469	0.080843	0.060063	0.055223	0.04953	0.052092	0.038998	0.031597
Pinal	1032711	62911413	0.063504	0.10292	0.137956	0.111679	0.09854	0.074088	0.052555	0.05292	0.031752	0.024088	0.015693	0.016423
Pinal	1032711	62911513	0.090037	0.110851	0.128625	0.096819	0.084892	0.081618	0.067587	0.050748	0.040458	0.030402	0.023386	0.019411
Pinal	1032711	62911613	0.078543	0.119318	0.127674	0.108623	0.097928	0.089572	0.067179	0.05381	0.035428	0.023396	0.023396	0.015374
Pinal	1032711	62911713	0.073406	0.090734	0.090734	0.083514	0.084958	0.081829	0.067629	0.068592	0.056799	0.045247	0.041637	0.041637
Pinal	1032711	62911813	0.064505	0.094665	0.093096	0.082985	0.082287	0.076534	0.062238	0.062064	0.05788	0.049686	0.031729	0.031206
Pinal	11310611	118549313	0.095421	0.105251	0.078398	0.062335	0.050108	0.056341	0.024215	0.023496	0.047231	0.052745	0.045553	0.032366
Pinal	11310611	118549413	0.103246	0.103002	0.070539	0.062241	0.05565	0.064437	0.036124	0.04125	0.046375	0.044667	0.036612	0.030754
Pinal	11310611	118549513	0.112782	0.098246	0.062907	0.061654	0.057644	0.063659	0.034085	0.050125	0.045113	0.045113	0.036842	0.030827
Pinal	11310611	118549613	0.074095	0.105524	0.114476	0.088	0.092381	0.073143	0.046857	0.031619	0.015238	0.012762	0.007048	0.006667
Pinal	11310611	118549713	0.072555	0.102651	0.106951	0.099606	0.09029	0.068613	0.043354	0.032963	0.016123	0.007703	0.011465	0.008599
Pinal	11310611	118549813	0.080559	0.098584	0.10686	0.100975	0.092698	0.073018	0.044694	0.030164	0.013427	0.007541	0.002207	0.001655
Pinal	11310611	118549913	0.0861	0.100657	0.112018	0.102077	0.091248	0.074383	0.047932	0.041008	0.019528	0.007811	0.001775	0.00142
Pinal	11310611	118550013	0.071874	0.090594	0.095563	0.085394	0.079501	0.06783	0.049688	0.039635	0.024497	0.013982	0.01144	0.009244
Pinal	11310611	118550113	0.078614	0.113754	0.099988	0.099867	0.094916	0.08284	0.054824	0.042145	0.026567	0.015578	0.012559	0.009902
Pinal	11310611	118550213	0.073275	0.111657	0.108555	0.109977	0.104549	0.080512	0.055311	0.039545	0.028431	0.011631	0.01176	0.011502
Pinal	11310611	118550313	0.081949	0.114892	0.107678	0.102777	0.093793	0.07664	0.055949	0.0422	0.023006	0.011026	0.011163	0.011163
Pinal	11310611	118550413	0.107243	0.087784	0.073297	0.074378	0.068324	0.06573	0.032432	0.044324	0.040216	0.041946	0.034378	0.029189

Appendix 3C4

2023 Weekend Hourly Profiles (UTC from 12 to 23) for the EGUs in Maricopa and Pinal Counties

County	Facility	Unit	12	13	14	15	16	17	18	19	20	21	22	23
Maricopa	All	All	0.03026	0.028478	0.027166	0.025835	0.027596	0.030954	0.038832	0.045612	0.053012	0.055417	0.055795	0.057307
Pinal	All	All	0.027586	0.026171	0.027114	0.016239	0.022483	0.02256	0.027492	0.026943	0.035397	0.040909	0.042407	0.067122
Maricopa	545911	All	0.02685	0.023952	0.021786	0.025755	0.034943	0.038866	0.049144	0.052177	0.056855	0.05733	0.057628	0.051278
Maricopa	546011	All	0.038964	0.0372	0.034208	0.030994	0.02976	0.034241	0.036046	0.038749	0.038542	0.039521	0.039823	0.047699
Maricopa	1139111	All	0.035549	0.034094	0.037312	0.035554	0.041448	0.042233	0.045773	0.047342	0.046766	0.04628	0.047352	0.046508
Maricopa	1139211	All	0.036746	0.02929	0.025878	0.030403	0.03381	0.042803	0.047678	0.058598	0.0606	0.056424	0.057853	0.052117
Maricopa	1139311	All	0.000333	0.000583	0.000799	0.001664	0.004324	0.01077	0.024638	0.049579	0.074467	0.09627	0.089725	0.09412
Maricopa	1139411	All	0.030384	0.028221	0.046001	0.054459	0.043419	0.044271	0.069449	0.051584	0.050537	0.047258	0.05619	0.047202
Maricopa	10704011	All	0.040221	0.039481	0.039341	0.039167	0.036387	0.035947	0.041047	0.042654	0.042367	0.044714	0.048561	0.045661
Maricopa	10704311	All	0.040467	0.037228	0.033659	0.030733	0.032169	0.031229	0.033568	0.037391	0.041018	0.042384	0.043085	0.046837
Maricopa	10704411	All	0.037231	0.036973	0.032856	0.025758	0.025758	0.029824	0.039005	0.042586	0.0513	0.045247	0.047813	0.05321
Pinal	998011	All	0.033781	0.030209	0.01456	0.004729	0.003436	0.004865	0.000816	0.002007	0.00973	0.009287	0.02167	0.023235
Pinal	998111	All	0.032607	0.032225	0.03997	0.025216	0.036691	0.035049	0.039636	0.035102	0.045012	0.045555	0.040197	0.073449
Pinal	1032711	All	0.023142	0.019919	0.014817	0.007003	0.001878	0.00051	0.001693	0.003594	0.007258	0.022446	0.035617	0.049762
Pinal	11310611	All	0.013078	0.010649	0.00233	0.000466	0.001511	0.006921	0.018869	0.027724	0.035153	0.051734	0.061593	0.077467
Maricopa	545911	48317513	0.026145	0.026041	0.02351	0.022383	0.027636	0.029543	0.042026	0.034502	0.04969	0.06382	0.072471	0.05685
Maricopa	545911	48317613	0.0267	0.023143	0.026943	0.038888	0.04287	0.04285	0.048833	0.048247	0.064618	0.05902	0.053077	0.051743
Maricopa	545911	48318013	0.033511	0.029816	0.02045	0.023694	0.033769	0.039354	0.036798	0.047173	0.055701	0.06047	0.052114	0.042941
Maricopa	545911	48318413	0.022551	0.018152	0.016987	0.019859	0.036321	0.044084	0.065568	0.075924	0.058215	0.047416	0.051486	0.051995
Maricopa	546011	48316913	0.03873	0.036788	0.034139	0.034268	0.03122	0.037547	0.036286	0.03963	0.038074	0.040234	0.040273	0.046496
Maricopa	546011	48317013	0.03922	0.037649	0.034283	0.027423	0.028167	0.030635	0.035783	0.037789	0.039052	0.038743	0.039332	0.049011
Maricopa	1139111	46679113	0.039955	0.040043	0.044321	0.043011	0.047569	0.044111	0.043919	0.043308	0.042889	0.042819	0.045823	0.04357
Maricopa	1139111	105572013	0.037024	0.035261	0.03813	0.035107	0.040356	0.03723	0.043083	0.047508	0.044009	0.046569	0.044678	0.044344
Maricopa	1139111	105572113	0.030021	0.027596	0.030308	0.029645	0.037448	0.046471	0.050523	0.050628	0.05334	0.048926	0.051803	0.051577
Maricopa	1139211	105573113	0.031106	0.029292	0.024853	0.030137	0.033942	0.037623	0.040265	0.043453	0.065558	0.063797	0.084229	0.05078
Maricopa	1139211	105573213	0.039233	0.029011	0.026104	0.035507	0.030686	0.041558	0.036139	0.074928	0.061218	0.042328	0.042362	0.064466
Maricopa	1139211	105573313	0.039704	0.029567	0.026639	0.025606	0.036776	0.049012	0.066224	0.056984	0.055224	0.063296	0.047845	0.041177
Maricopa	1139311	142939613	0.000188	0.00057	0.000845	0.001897	0.003299	0.009098	0.019256	0.043105	0.085057	0.113693	0.105212	0.116549
Maricopa	1139311	142939713	0.000315	0.000331	0.00029	0.000952	0.003073	0.01031	0.025758	0.053492	0.080016	0.106048	0.09014	0.091519
Maricopa	1139311	142939813	0.00055	0.000883	0.001306	0.002144	0.007099	0.013531	0.030619	0.053906	0.054041	0.061941	0.068455	0.066887
Maricopa	1139411	142941413	0.030384	0.028221	0.046001	0.054459	0.043419	0.044271	0.069449	0.051584	0.050537	0.047258	0.05619	0.047202
Maricopa	10704011	58571513	0.037663	0.037589	0.036128	0.037515	0.037959	0.038051	0.04101	0.04284	0.041342	0.04284	0.044005	0.042988
Maricopa	10704011	58571613	0.044975	0.041891	0.039055	0.037051	0.035521	0.035138	0.042341	0.043849	0.043894	0.045425	0.045222	0.045087
Maricopa	10704011	58571713	0.038805	0.039388	0.042961	0.042728	0.035484	0.034435	0.03997	0.041427	0.042126	0.046069	0.056227	0.048963
Maricopa	10704311	58618813	0.038328	0.035442	0.033373	0.029813	0.031504	0.031753	0.034721	0.035679	0.049314	0.046074	0.042975	0.045151
Maricopa	10704311	58618913	0.04102	0.037902	0.032014	0.028476	0.030406	0.027351	0.029082	0.035094	0.035663	0.039931	0.045288	0.046215
Maricopa	10704311	58713613	0.041172	0.038264	0.033099	0.029702	0.031232	0.029789	0.033088	0.041031	0.040945	0.044743	0.043571	0.049572
Maricopa	10704311	58713713	0.041156	0.037238	0.03568	0.034171	0.034925	0.035119	0.03656	0.037344	0.038486	0.039182	0.04102	0.046264
Maricopa	10704411	58713913	0.036343	0.029866	0.032571	0.021255	0.023172	0.023852	0.069516	0.048292	0.052976	0.043129	0.047256	0.044288
Maricopa	10704411	58714513	0.038675	0.035137	0.03288	0.026269	0.024915	0.027084	0.038821	0.046539	0.046553	0.043146	0.039345	0.052538
Maricopa	10704411	58714613	0.04313	0.040113	0.038141	0.031669	0.033911	0.04554	0.035411	0.037315	0.042052	0.040535	0.042945	0.044091
Maricopa	10704411	58714713	0.037029	0.047586	0.036002	0.023682	0.02399	0.019798	0.025701	0.037782	0.056416	0.055783	0.048528	0.055201
Maricopa	10704411	58714813	0.03312	0.041448	0.027351	0.020216	0.013588	0.00925	0.026557	0.04059	0.05661	0.046868	0.057436	0.077604
Maricopa	10704411	58714913	0.045565	0.041824	0.035817	0.031018	0.031331	0.033104	0.044581	0.038917	0.036905	0.038023	0.038068	0.045148
Maricopa	10704411	58715013	0.03663	0.033137	0.034266	0.03382	0.028186	0.033493	0.041744	0.052626	0.049192	0.040897	0.051511	0.049356
Maricopa	10704411	58715113	0.02664	0.02755	0.025779	0.017159	0.026971	0.04729	0.026673	0.036783	0.071828	0.055513	0.058806	0.058392

County	Facility	Unit	12	13	14	15	16	17	18	19	20	21	22	23
Pinal	998011	67644213	0.033781	0.030209	0.01456	0.004729	0.003436	0.004865	0.000816	0.002007	0.00973	0.009287	0.02167	0.023235
Pinal	998111	48101713	0.027873	0.026887	0.037831	0.023653	0.047789	0.040384	0.040719	0.033512	0.058821	0.047936	0.03786	0.05187
Pinal	998111	48101813	0.03718	0.03738	0.042036	0.026726	0.025974	0.029896	0.038589	0.036637	0.031677	0.043254	0.042455	0.094287
Pinal	1032711	48098813	0.025695	0.021061	0.017692	0.010952	0.000842	0	0.01011	0.011794	0.009056	0.013269	0.028854	0.046757
Pinal	1032711	62911013	0.014445	0.014253	0.011941	0.004622	0.000385	0	0.004622	0.007126	0.012519	0.035439	0.04141	0.053737
Pinal	1032711	62911113	0.020764	0.020393	0.014831	0.00723	0.000371	0	0	0.002039	0.023545	0.019466	0.035966	0.043752
Pinal	1032711	62911213	0.018041	0.018041	0.017356	0.004567	0	0	0	0.00274	0.008678	0.026262	0.028774	0.04179
Pinal	1032711	62911313	0.032451	0.022773	0.009963	0.000285	0	0	0	0.005408	0.000569	0.009394	0.038713	0.057216
Pinal	1032711	62911413	0.014964	0.009124	0.007664	0.007299	0.007299	0.00073	0	0.007299	0.009854	0.032482	0.055109	0.066058
Pinal	1032711	62911513	0.012161	0.011693	0.009355	0.005145	0.001169	0	0	0	0.000935	0.035547	0.053087	0.046071
Pinal	1032711	62911613	0.015374	0.015374	0.011364	0.006684	0.000334	0	0	0	0.001671	0.031417	0.030749	0.046791
Pinal	1032711	62911713	0.041877	0.032972	0.017329	0.005054	0.000241	0	0	0	0	0.009146	0.0142	0.052467
Pinal	1032711	62911813	0.031904	0.027545	0.023536	0.01447	0.00802	0.003487	0.000174	0	0.000349	0.016562	0.034693	0.050384
Pinal	11310611	118549313	0.031168	0.030688	0.005754	0.007912	0.018701	0.003836	0.018461	0.017742	0.015584	0.028291	0.063054	0.085351
Pinal	11310611	118549413	0.029534	0.036368	0.00659	0	0	0.000244	0.007811	0.012936	0.015621	0.031975	0.066634	0.097388
Pinal	11310611	118549513	0.030075	0.040351	0.006767	0	0	0.001003	0.008521	0.014787	0.02005	0.034586	0.060401	0.084461
Pinal	11310611	118549613	0.004571	0	0	0	0	0.016381	0.023238	0.02781	0.036381	0.070857	0.072952	0.08
Pinal	11310611	118549713	0.00412	0	0	0	0	0.009137	0.034755	0.045683	0.037263	0.061627	0.068434	0.078108
Pinal	11310611	118549813	0.004046	0	0	0	0	0.008828	0.027773	0.041935	0.045246	0.070443	0.074122	0.075225
Pinal	11310611	118549913	0.004438	0	0	0	0	0.006213	0.026274	0.037103	0.042073	0.060004	0.069057	0.06888
Pinal	11310611	118550013	0.009244	0.005778	0.002773	0	0.003351	0.012595	0.024151	0.037093	0.050497	0.061706	0.070257	0.083314
Pinal	11310611	118550113	0.010144	0.004951	0.001449	0	0	0.005917	0.01268	0.033088	0.038643	0.048303	0.042748	0.070523
Pinal	11310611	118550213	0.011372	0.005299	0.001292	0	0	0.003748	0.010856	0.024683	0.039416	0.049754	0.04549	0.061385
Pinal	11310611	118550313	0.011163	0.005173	0.001906	0	0	0.005581	0.015246	0.020419	0.037163	0.052682	0.053771	0.064661
Pinal	11310611	118550413	0.027459	0.031568	0.005838	0	0	0.004541	0.014703	0.000649	0.013622	0.028757	0.068757	0.104865

Appendix 4

Ozone Modeling Protocol in Support of the Revised MAG 2025 Moderate Area Plan for the Maricopa Eight-Hour Ozone Nonattainment Area

OZONE MODELING PROTOCOL

IN SUPPORT OF

THE REVISED MAG 2025 MODERATE AREA PLAN FOR

THE MARICOPA EIGHT-HOUR OZONE NONATTAINMENT AREA

(2015 OZONE STANDARD)

June 2025

Maricopa Association of Governments

302 North 1st Avenue, Suite 300

Phoenix, Arizona 85003

MARICOPA ASSOCIATION of GOVERNMENTS

Table of Contents

Table of Contents ii
List of Tables iv
List of Figures iv
List of Acronyms v
1. OVERVIEW OF MODELING PROTOCOL 1
1.1 Background 1
1.2 Purpose of Modeling Protocol 2
2. CONCEPTUAL DESCRIPTION 2
3. MODELING EPISODE SELECTION 4
3.1. Modeling Year and Modeling Period Selection 4
3.2. Emissions Excluding International Anthropogenic Sources 4
4. MODELING DOMAIN SELECTION 5
4.1. Horizontal Domain 5
4.2. Vertical Layer Configuration 7
5. MODEL SELECTION 9
6. MODEL INPUT 11
6.1. Weather Research and Forecasting Model 11
6.1.1. Physical Parameterization Schemes 11
6.1.2. Input Data Preparation Procedures 11
6.1.3. Initial and Boundary Conditions 12
6.1.4. Meteorology and Chemistry Interface Processing 12
6.2. Ozone Column Data 12
6.3. Observed Ozone Data 12
6.4. Photochemical Modeling Configuration 14
6.4.1. CAMx model configuration 14
6.4.2. CMAQ model configuration 16
7. EMISSIONS INPUT 16
7.1. Point Source Emissions 17
7.2. Area Source Emissions 17

7.3. Onroad Mobile Source Emissions 17
7.4. Nonroad Mobile Source Emissions 19
7.5. Airport Emissions 20
7.6. Biogenic Source Emissions 21
7.7. Emissions Preprocessing 22
7.7.1. Temporal Allocation of Emissions 22
7.7.2. Spatial Allocation of Emissions 22
7.7.3. Chemical Speciation 23
8. MODEL PERFORMANCE EVALUATION 23
8.1. Meteorological Model Performance Evaluation 24
8.2. Air Quality Model Performance Evaluation 25
9. MODELED ATTAINMENT DEMONSTRATION 26
9.1. Base Design Values 26
10. SUPPLEMENTAL ANALYSES 27
11. 179B DEMONSTRATION 28
12. MANAGEMENT STRUCTURE AND COMMITTEES 30
13. PARTICIPATING ORGANIZATIONS 31
14. PROCEDURAL REQUIREMENTS 33
15. SCHEDULE 33
16. REFERENCES 35

List of Tables

Table 1. Configuration of WRF modeling domains (LCC projection with 33 N and 45 N true latitudes and 112 W and 33.5 N central longitude and latitude) 7
Table 2. Configuration of CAMx/CMAQ modeling domains (LCC projection with 33 N and 45 N true latitudes and 112 W and 33.5 N central longitude and latitude) 7
Table 3. Average pressures and heights of WRF and CAMx/CMAQ vertical layers 8
Table 4. Characteristics of ozone monitoring sites in the Maricopa eight-hour ozone nonattainment area 13
Table 5. CAMx modeling configuration 15
Table 6. Operations for airports in the 4 km domain in 2023 21
Table 7. Statistical metrics for model performance evaluation 24
Table 8. 2023 base design value (DVB2023) in ppm 26
Table 9. Schedule 34

List of Figures

Figure 1. CAMx/CMAQ and WRF modeling boundaries 6
Figure 2. MAG air quality modeling system flow chart 10
Figure 3. Locations of ozone monitoring sites in the Maricopa eight-hour ozone nonattainment area 14
Figure 4. MAG policy structure 31
Figure 5. MAG committee structure 32

List of Acronyms

ABM	Activity-Based Model
AC	Air Commercial
ADEQ	Arizona Department of Environmental Quality
ADOT	Arizona Department of Transportation
AEDT	Aviation Environmental Design Tool
AFB	Air Force Base
AMET	Atmospheric Model Evaluation Tool
APCA	Anthropogenic Precursor Culpability Assessment
APM	Aviation Performance Metrics
APU	Auxiliary Power Units
AQMP	Air Quality Modeling Platform
AQTAC	Air Quality Technical Advisory Committee
ASOS	Automated Surface Observing System
AT	Air Taxi
ATADS	Air Traffic Activity Data System
AVFT	Alternative Vehicle and Fuel Technologies
AWOS	Automated Weather Observing System
AZDA	Arizona Department of Agriculture
BADA 3	Base of Aircraft Data Family 3
BADA 4	Base of Aircraft Data Family 4
CAA	Clean Air Act
CAMx	Chemical Atmospheric Model with Extensions
CEMS	Continuous Emissions Monitoring System
CGLS	Copernicus Global Land Service
CISL	Computational Information Systems Laboratory
CMAQ	Community Multiscale Air Quality
CPA	Chemical Process Analysis
DDM	Decoupled Direct Method
EBI	Euler Backward Iterative
EIS	Environmental Impact Statement
ERA5	ECMWF Reanalysis v5
ETMSC	Enhanced Traffic Management System Counts

FAA	Federal Aviation Administration
FB	Fractional Bias
FDDA	Four-Dimensional Data Assimilation
FE	Fractional Error
GA	General Aviation
GIS	Geographic Information Systems
GSE	Ground Support Equipment
H-CMAQ	Hemispheric CMAQ
HDDM	Higher-order Decoupled Direct Method
I/M	Inspection and Maintenance
IATA	International Air Transport Association
ICAO	International Civil Aviation Organization
ICBC	Initial Condition and Boundary Condition
ISAM	Integrated Source Apportionment Method
LAI	leaf area index
LCC	Lambert Conformal Conic
LSM	Land Surface Model
LTO	Landing and Take-Off
MADIS	Meteorological Assimilation Data Ingest System
MB	Mean Bias
MCAQD	Maricopa County Air Quality Department
MCIP	Meteorology-Chemistry Interface Processor
ME	Mean Error
MEGAN	Model of Emissions of Gases and Aerosols from Nature
MERC	Mobile Emission Reduction Credit
ML	Military
MOVES	Motor Vehicle Emission Simulator
NAAQS	National Ambient Air Quality Standard
NCAR	National Center for Atmospheric Research
NCDC	National Climatic Data Center
NCEP	National Center for Environmental Prediction
NEI	National Emissions Inventory
NMB	Normalized Mean Bias

NME	Normalized Mean Error
NOx	Nitrogen Oxides
OSAT	Ozone Source Apportionment Technology
PAR	Photosynthetically Active Radiation
PCAQCD	Pinal County Air Quality Control District
PEI	Periodic Emissions Inventory
ppm	parts per million
PPM	Piecewise Parabolic Method
RAOB	RAdiosonde Observation
RCEI	Regional Climate Extremes Index
RMSE	Root Mean Square Error
RRTM	Rapid Radiative Transfer Model
RVP	Reid Vapor Pressure
SA	Spatial Allocator
SCC	Source Classification Code
SIP	State Implementation Plan
SMOKE	Sparse Matrix Operator Kernel Emissions
TAF	Terminal Area Forecast
TOMS	Total Ozone Mapping Spectrometer
TROPOMI	TROPOspheric Monitoring Instrument
TSD	Technical Support Document
TUV	Tropospheric Ultraviolet Visible
U.S. DOT	United States Department of Transportation
U.S. EPA	United States Environmental Protection Agency
UHI	Urban Heat Island
UTC	Universal Time Coordinate
VOC	Volatile Organic Compounds
WPS	WRF Preprocessing System
WRF	Weather Research and Forecasting
YSU	Yonsei University

1. OVERVIEW OF MODELING PROTOCOL

1.1 Background

In accordance with the Clean Air Act (CAA), the United States Environmental Protection Agency (U.S. EPA) designated the Maricopa eight-hour ozone nonattainment area as a Marginal area on June 4, 2018, for the 2015 ozone National Ambient Air Quality Standard (NAAQS) of 0.070 parts per million (ppm). The Maricopa eight-hour ozone nonattainment area extends for the 5,288 square mile area that includes a predominant area of Maricopa County, and portions of the Tonto National Monument monitor in Gila County and the Queen Valley monitor in Pinal County. The Marginal designation became effective on August 3, 2018, setting an attainment date of August 3, 2021.

The MAG 2020 Eight-Hour Ozone Plan - Submittal of Marginal Area Requirements was submitted to EPA in June 2020. The plan addresses requirements for a Marginal area, such as Emissions Statements, Baseline Emissions Inventory, Periodic Emissions Inventory, New Source Review, and Transportation Conformity. On September 15, 2022, EPA signed a final rule determining that the Maricopa eight-hour ozone nonattainment area did not attain the 2015 ozone standard by August 3, 2021, attainment date and is reclassified as a Moderate area. The attainment date for Moderate areas is August 3, 2024.

On October 18, 2023, EPA published a Finding of Failure to Submit a plan revision addressing Moderate Area requirements for the Maricopa Nonattainment Area by the January 1, 2023, due date. A Finding of Failure to Submit triggers the imposition of CAA sanctions and Federal Implementation Plan (FIP) requirements.

Between December 2024 and April 2025, ADEQ submitted four SIP revisions for the Maricopa Nonattainment Area - covering contingency measures (December 23, 2024), RACT for Gila County (March 26, 2025) and Pinal County (April 14, 2025) and additional Moderate-area plan ("MAG 2025 Eight-Hour Ozone Plan – Submittal of Applicable Moderate Area Requirements for the Maricopa Nonattainment Area" including appendices) with a parallel-processing request (April 25, 2025). EPA has reviewed all submissions, found them complete under 40 CFR 51 Appendix V (including the parallel-processing attachment), and terminated the sanctions clocks initiated on October 18, 2023.

This revised plan, together with the accompanying CAA §179B(b) demonstration, supersedes the April 25, 2025, submittal and demonstrates that this area would attain the

2015 eight-hour ozone NAAQS in the absence of significant international emission influences.

1.2 Purpose of Modeling Protocol

The objectives of this modeling protocol are to describe modeling methodologies and assumptions that will be used to determine whether the Maricopa eight-hour ozone nonattainment area would attain the 2015 ozone standard if without significant international emission influences through §179B(b) demonstration, and to establish the conformity budget for onroad mobile source emissions using the EPA Motor Vehicle Emission Simulator (MOVES) model.

The protocol is viewed as a set of general guidelines that provide focus, consistency, and a basis for consensus for all parties involved in this analysis. This modeling protocol will be reviewed and approved by members of the Air Quality Planning Team prior to commencement of modeling. This team includes staff representatives from MAG, the Arizona Department of Environmental Quality (ADEQ), the Arizona Department of Transportation (ADOT), the Maricopa County Air Quality Department (MCAQD), and the Pinal County Air Quality Control District (PCAQCD). Representatives of other agencies, including the U.S. EPA and the United States Department of Transportation (U.S. DOT), will be consulted on technical matters, as needed.

2. CONCEPTUAL DESCRIPTION

During the summer ozone season in the Maricopa 8-hour ozone nonattainment area, ozone levels are influenced by meteorological systems operating at multiple scales, including deep vertical mixing caused by stratospheric intrusion and blocking high-pressure systems, lower-level vertical mixing due to the development and dissipation of nocturnal inversion layers, long-range transport of upwind pollutants, and local mountain-valley breezes driven by terrain and topographic features. Additionally, strong solar radiation and drier air enhance ozone formation. Ozone exceedances are typically linked to the interaction of these large- and small-scale meteorological systems, in conjunction with local emissions. Note that urban heat flux has shown a strong upward trend since 2000, driven by the rapid growth of urbanization.

Characteristics of exceedances:

- Since 2000, extreme weather events in the Southwest, as indicated by the Regional Climate Extremes Index (RCEI), have increased, and wildfire events, which are linked

to these extreme conditions, have become more frequent. The variation in ozone exceedances has mirrored this trend. This suggests that changes in large-scale atmospheric systems are altering regional meteorological conditions, which in turn influence regional ozone levels. These extreme weather patterns, including increased wildfires, may exacerbate ozone pollution, as smoke and other pollutants can contribute to higher concentrations of ozone in the atmosphere.

- The combination and interaction of favorable large- and local-scale systems contribute to extreme ozone concentrations and widespread exceedances, which result in the occurrence of the top 10 high ozone days for each year.
- Monitors with the highest frequency of exceedances are located downwind of the urban core.

Key formation factors:

- Local photochemical buildup due to intense solar radiation, high temperatures and stagnant conditions, combined with natural and anthropogenic emissions.
- Daytime temperatures are often above 100℉, with urban heat island effect causing overnight temperatures to remain elevated.
- Sustained valley breeze/mountain breeze circulation pattern traps ozone in basin.
- Westerly regional and long-range transport patterns bring pollution from California and wildfire smoke from the western states.
- Frequent long-range transport due to wind shifts during the summer monsoon season brings ozone and ozone precursors from Mexico into the region.
- Stratospheric intrusion contributes to downward transport of ozone-rich air mass from upper levels.
- The inversion layer traps ozone and ozone precursors from the previous day, enhancing ozone concentration due to strong vertical mixing after sunrise.
- Long-term OMI data confirm a significant regional NO_2 decrease, strongest 2005-2014 (likely reflecting emission controls), but the reduction rate has slowed considerably in recent years.
- High-resolution TROPOMI/TEMPO link summer ozone exceedances to consistently higher NO_2 levels (especially morning/early afternoon) and reveal profound, distinct impacts of wildfire smoke on NO_2/HCHO.

3. MODELING EPISODE SELECTION

3.1. Modeling Year and Modeling Period Selection

The EPA modeling guidance (U.S. EPA, 2018) suggests the consideration of the following criteria in selecting the modeling episode period: 1) The modeling episode should encompass full synoptic cycles of a ramp-up to a high ozone period and a ramp-down to cleaner conditions under a variety of meteorological conditions, 2) the most recently compiled and quality-assured national emissions inventory databases should be available for the modeling episode, 3) a sufficient number of days should be available so that the modeled attainment test applied at each monitor is based on multiple days, 4) the modeling episode must ensure that the modeling system appropriately characterizes low pollution periods, development of elevated periods, and transition back to low pollution periods through synoptic cycles, and 5) the modeling episode should cover a variety of meteorological conditions conducive to elevated or poor ozone concentrations.

The year 2023 is selected for the development of the emissions inventory and base design values because point and area source emissions inventories were prepared by both the Maricopa County Air Quality Department (MCAQD) and the Pinal County Air Quality Control District (PCAQCD).

The base design values of monitors in 2023 are developed using ozone observations at monitors during the three-year period of 2021-2023. Since the full ozone season from April 1 through September 30 provides a sufficient amount of days (i.e., 183 days) for the development of the ten highest modeled days for ozone concentrations, covers a variety of meteorological conditions, and characterizes high-low and transitional conditions of ozone concentrations in the Maricopa eight-hour ozone nonattainment area, the period of April 1 through September 30 in 2023 is selected for the modeling episode in this study.

For the source apportionment analysis, the initial three days of the modeling episode will be used as the spin-up period of the modeling to minimize the impact of fluctuations in the initial condition data. The modeling results from the spin-up period of April 1-3 will not be used for the modeled attainment demonstration.

3.2. Emissions Excluding International Anthropogenic Sources

For the Clean Air Act §179B(b) retrospective demonstration, we prepare two global/hemispheric simulations to supply initial and boundary conditions (IC/BC) to the

36 km Chemical Atmospheric Model with Extensions (CAMx) and the Community Multiscale Air Quality (CMAQ) regional models as follows:

1. **Baseline scenario.** GEOS-Chem (and/or Hemispheric CMAQ) is driven by the complete 2023 emissions inventory—including all anthropogenic, biomass-burning, biogenic, and other natural sources worldwide.
2. **International-anthropogenic-off sensitivity.** The same model is rerun with every anthropogenic source outside the United States removed; U.S. anthropogenic emissions and all natural sources are retained. To stay consistent, Mexican anthropogenic emissions are also set to zero inside the 36 km and 12 km grids.

Comparing the model outputs between the two aforementioned simulations would quantify the impact of ozone attributable to foreign anthropogenic pollution; these findings would provide the evidence required for the §179B(b) demonstration.

4. MODELING DOMAIN SELECTION

4.1. Horizontal Domain

Selection of the modeling domains should take into account the Maricopa eight-hour ozone nonattainment area boundaries, the distribution of major emissions sources, the location of the meteorological and air quality monitoring sites, and the prevailing winds associated with elevated ozone concentrations, as well as regional air pollutant transport. Figure 1a shows the spatial relationship among the master (36 km grid resolution), the first-nested (12 km grid resolution), and the second-nested (4 km grid resolution) modeling domains of CAMx, CMAQ, and the Weather Research and Forecasting (WRF) models. Figure 1b illustrates the inner modeling domain comprised of 4-by-4 km grid cells that cover the Maricopa eight-hour ozone nonattainment area, Maricopa County, and portions of Pinal, Gila, and Yavapai counties.

Since ozone concentrations in the Maricopa eight-hour ozone nonattainment area can be substantially influenced by transported ozone and ozone precursor emissions from outside the Maricopa eight-hour ozone nonattainment area (U.S. EPA, 2015), the master 36 km grid modeling domain (36 km domain) covers the southwestern U.S. and Mexico. The extensive coverage of the master modeling domain of CAMx/CMAQ and WRF is designed to capture the characteristics of long-range transport of ozone and ozone precursor emissions from neighboring states and Mexico to the Maricopa eight-hour ozone nonattainment area. The 36 km domain will be used to generate initial and boundary conditions to the 12 km grid modeling domain (12 km domain). The 12 km

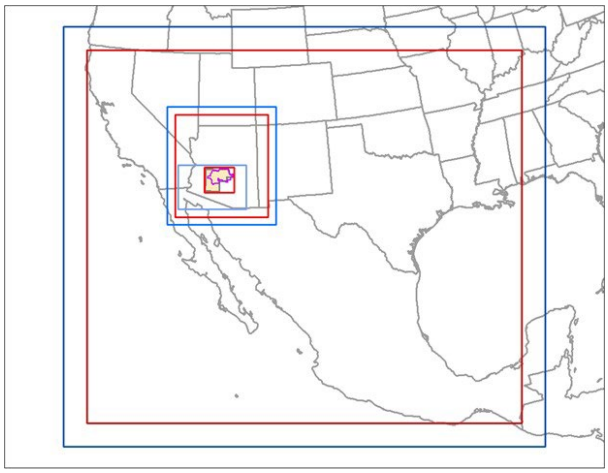

a) CAMx/CMAQ modeling domains (red) and WRF modeling domains (blue): 36-km, 12-km and 4-km grid modeling domains

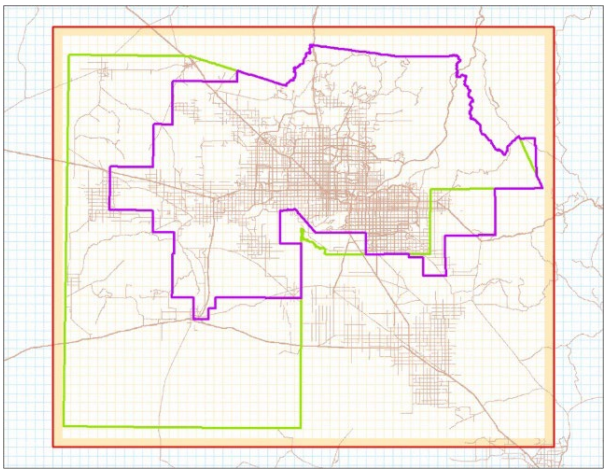

b) CAMx/CMAQ (red) 4-km grid modeling domains, Maricopa County (green), and the Maricopa eight-hour ozone nonattainment area (purple)

Figure 1. CAMx/CMAQ and WRF modeling boundaries

modeling domain will be used to provide boundary and initial condition data to the core 4 km grid modeling domain (4 km domain). The CAMx and CMAQ model evaluation and source apportionment analyses will be performed at the monitors in the Maricopa eight-hour ozone nonattainment area in the 4 km domain.

The WRF modeling domains are larger than the CAMx/CMAQ modeling domains to develop meteorological data to simulate ozone concentrations around the boundaries of the CAMx/CMAQ modeling domains. The boundaries of CAMx/CMAQ and WRF modeling domains are illustrated in Figure 1a. The WRF and CAMx/CMAQ modeling domain configurations are provided in Table 1 and Table 2. The CAMx/CMAQ inner 4 km domain encompasses the Maricopa eight-hour ozone nonattainment area, consisting of 56 grid cells in the west-east direction and 47 grid cells in the south-north direction. The origin of the modeling domain (the southwest corner of the inner domain) is located at -130.000 km easting and -119.200 km northing, relative to the central point at 112°W and 33.5°N, using the Lambert conformal conic (LCC) projection. The domain comprises approximately 16,260 square miles and includes potential emission sources within Maricopa and Pinal counties, which play a role in ozone formation in the Maricopa eight-hour ozone nonattainment area.

Table 1. Configuration of WRF modeling domains (LCC projection with 33 N and 45 N true latitudes and 112 W and 33.5 N central longitude and latitude)

Domain	Grid Resolution	Origin (SW, km)	Extent (NE, km)	NX	NY	NZ
36 km Grid Domain	36 km x 36 km	(-1,206, -2,059.2)	(2,466, 1,144.8)	102	89	23
12 km Grid Domain	12 km x 12 km	(-414, -367.2)	(414, 532.8)	69	75	23
4 km Grid Domain	4 km x 4 km	(-330, -247.2)	(186, 88.8)	129	84	23

Table 2. Configuration of CAMx/CMAQ modeling domains (LCC projection with 33 N and 45 N true latitudes and 112 W and 33.5 N central longitude and latitude)

Domain	Grid Resolution	Origin (SW, km)	Extent (NE, km)	NX	NY	NZ
36 km Grid Domain	36 km x 36 km	(-1,026, -1,879.2)	(2,286, 964.8)	92	79	23
12 km Grid Domain	12 km x 12 km	(-354, -307.2)	(354, 472.8)	59	65	23
4 km Grid Domain	4 km x 4 km	(-130, -119.2)	(94, 68.8)	56	47	23

4.2. Vertical Layer Configuration

The vertical layer resolution and coordinates for WRF and CAMx/CMAQ modeling are based on the sigma coordinate system. The sigma coordinate system uses the terrain-following hydrostatic pressure vertical coordinates ranging from 1 at the surface to 0 at the upper top boundary of the modeling domain. The 23 vertical layers configuration is used for both CAMx/CMAQ and WRF modeling. The upper top boundary is based on the reference pressure of 100 hPa. The seasonal average pressure and height of vertical layers for the CAMx/CMAQ and WRF modeling are presented in Table 3. The vertical depth and vertical layer structures of the 12 km and 4 km domains are consistent with those of the 36 km domain.

Table 3. Average pressures and heights of WRF and CAMx/CMAQ vertical layers

Layer	Vertical Layer Pressure (hPa)	Vertical Layer Height (m)
23	121	16,048
22	227	13,946
21	395	8,793
20	501	5,576
19	543	4,921
18	586	4,307
17	628	3,729
16	670	3,183
15	721	2,664
14	772	1,979
13	811	1,516
12	836	1,160
11	853	987
10	870	816
9	887	648
8	900	482
7	909	400
6	917	319
5	926	238
4	932	158
3	936	119
2	941	79
1	945	39

5. MODEL SELECTION

A variety of emissions, meteorology, and air quality models are needed to perform a full modeling evaluation and source apportionment analyses. The models used in this study meet the EPA guidance requirements of having prior peer reviews, appropriate theoretical bases, good performance in previous studies, and available documentation. The most commonly used photochemical air quality models for ozone attainment demonstration are CAMx and CMAQ. Both models provide useful tools such as the Ozone Source Apportionment Technology (OSAT) in CAMx and the Integrated Source Apportionment Method (ISAM) in CMAQ, as well as the Decoupled Direct Method (DDM), which have been used in many photochemical modeling applications to evaluate the contributions of pollutants, source categories, and source regions to local ozone concentrations as well as emissions sensitivities. The latest CAMx version 7.31 and CMAQ version 5.5 are used in the study. Figure 2 illustrates the MAG air quality modeling system flowchart with CAMx as the core model and CMAQ as the secondary model. Onroad mobile source emissions are generated by the MOVES4.0 and MAG MOVESLINK4 models. MOVESLINK4 was developed by MAG to estimate hourly gridded emissions for the photochemical air quality modeling analysis using the Activity-Based Model (ABM) outputs. Nonroad mobile source emissions are developed using the MOVES4.0 model and the Federal Aviation Administration (FAA) Aviation Environmental Design Tool (AEDT) version 3g. Biogenic source emissions are computed using the Model of Emissions of Gases and Aerosols from Nature (MEGAN) version 3.2. The WRF version 4.7.0 is used to develop meteorological input data for CAMx and CMAQ. The Sparse Matrix Operator Kernel Emissions (SMOKE) version 5.1 is used to develop emissions input data for CAMx and CMAQ. More detailed discussions on the preparation of meteorological inputs and emissions inventory are provided in Sections 6 and 7.

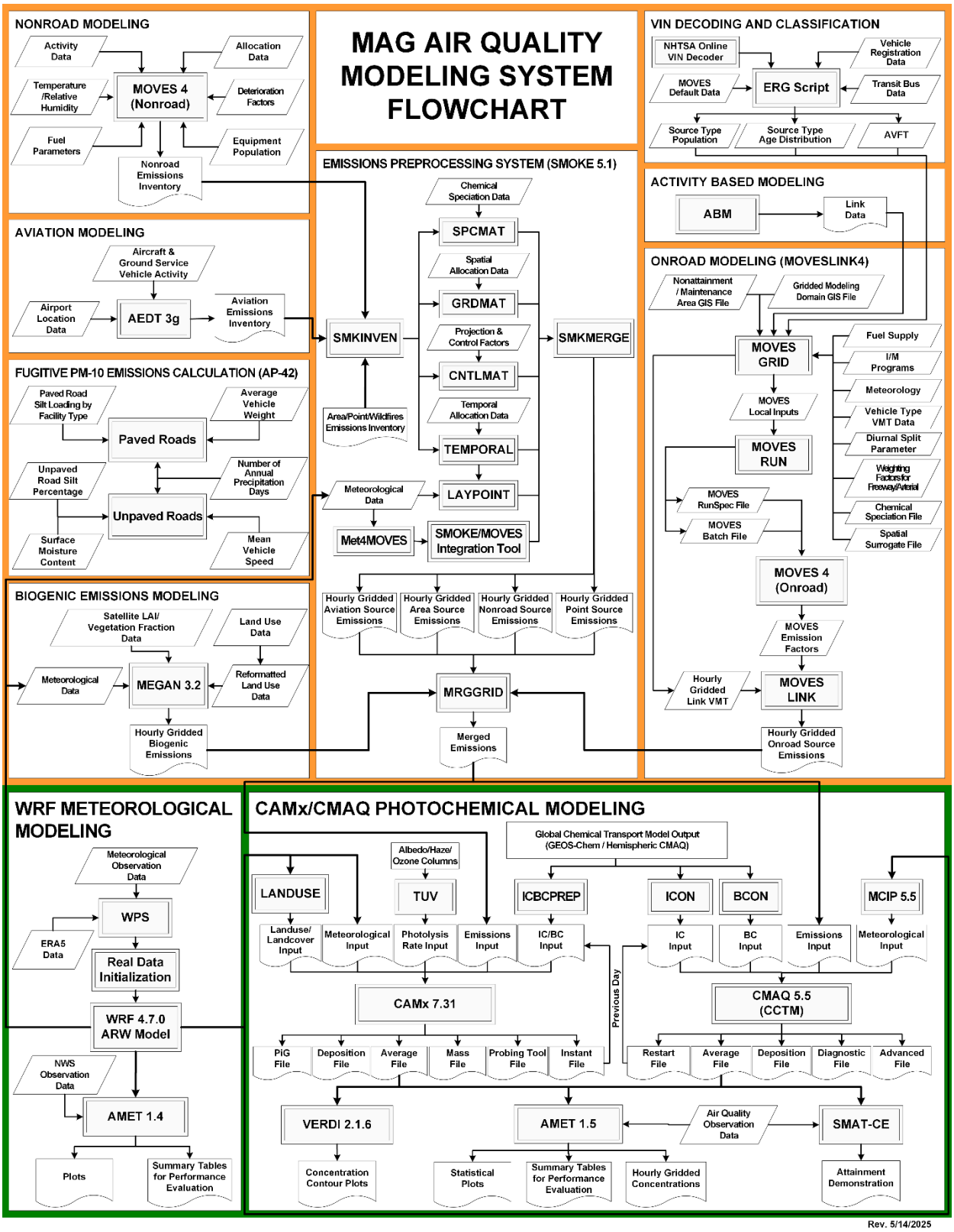

Figure 2. MAG air quality modeling system flow chart

6. MODEL INPUT

6.1. Weather Research and Forecasting Model

6.1.1. Physical Parameterization Schemes

The WRF model is an off-line, dynamic grid model that simulates wind, vertical mixing, temperature, humidity and solar radiation etc. The physical parameterization schemes used in the WRF model runs are as follows:

3. New Yonsei University (YSU) planetary boundary layer physics.
4. Noah Land Surface Model (LSM) surface physics.
5. Thompson microphysics scheme for cloud microphysics.
6. New Tiedtke scheme for cumulus parameterization.
7. MM5 similarity surface layer scheme.
8. Rapid Radiative Transfer Model (RRTM) for longwave and shortwave radiation.

The simulation starting time is 12:00 Universal Time Coordinate (UTC), and the model is initialized at the same time. For the full season simulation through April to September, the first 72 hours are considered as spin-up. In addition, grid analysis and observational nudging based on OBSGRID are applied to all modeling domains, presumably via Four-Dimensional Data Assimilation (FDDA).

6.1.2. Input Data Preparation Procedures

The fifth generation of ECMWF atmospheric reanalysis of the global climate (ERA5) archived data (ds633000) are obtained from the National Center for Atmospheric Research (NCAR) Computational Information Systems Laboratory (CISL) and used as input to the WRF modeling. A customized shell program is used to read input files processed by the WRF Preprocessing System (WPS). The procedures of the WPS to prepare input to WRF for real-data simulations include: 1) defining coarse parent domain and fine nested domains; 2) computing latitude, longitude, map scale factors, and Coriolis parameters at every grid point; 3) interpolating time-invariant terrestrial data to simulation grids; 4) using a Python package from NCAR to process the ERA5 data to generate immediate files for metgrid program application; and 5) transferring time-variant data at a standard hourly or 3-hour interval.

6.1.3. Initial and Boundary Conditions

In WRF two-way nesting simulation, the input files are generated by *real.exe*, the program uses the data from WPS output to generate initial and boundary conditions for all nested domains.

6.1.4. Meteorology and Chemistry Interface Processing

Outputs from the WRF model require specific preprocessing before utilization in air quality and emissions modeling systems. For application with the CAMx, WRF outputs are processed using a suite of CAMx-specific preprocessing tools, which include *wrfcamx_v5.2*, *watermask_ncf*, and *kvpatch_v6nc*. These tools adapt the WRF meteorological data to meet the input format and structural requirements of CAMx.

Similarly, for simulations with the CMAQ model, WRF outputs are processed by the Meteorology-Chemistry Interface Processor (MCIP). This step is critical for maintaining dynamic consistency between the WRF-generated meteorological fields and the CMAQ chemical transport model.

The processed meteorological data fields derived from these respective pathways (i.e., data processed by *wrfcamx_v5.2* et al. for CAMx and MCIP-processed data for CMAQ) serve as essential inputs for:

- The CAMx and CMAQ photochemical air quality models.
- The Model of Emissions of Gases and Aerosols from Nature (MEGAN) for the characterization of biogenic emissions.
- The Sparse Matrix Operator Kernel Emissions (SMOKE) system

6.2. Ozone Column Data

The CAMx photochemical mechanism requires ozone column and clear-sky photolysis rate data. Day-specific ozone column data are obtained from the Total Ozone Mapping Spectrometer (TOMS) satellite platform. The CAMx Tropospheric Ultraviolet Visible (TUV) radiative transfer model uses TOMS ozone column data to calculate clear-sky photolysis rates and to adjust the clear-sky photolysis rates in presence of clouds and aerosols.

6.3. Observed Ozone Data

Observed ozone concentrations collected from the air quality monitoring sites in Table 4 will be used in evaluating the CAMx/CMAQ model performance and developing the

baseline design values for the monitoring sites. The locations of the monitoring sites are illustrated in Figure 3.

Table 4. Characteristics of ozone monitoring sites in the Maricopa eight-hour ozone nonattainment area

AQS ID	Site Name	Owning Agency	Elev. (m)	Land Use	Date Established	ID
04-007-0010	Tonto National Monument	ADEQ	786	Desert	1988-04-01	TN
04-013-0019	West Phoenix	MCAQD	333	Residential	1984-01-01	WP
04-013-1003	Mesa	MCAQD	383	Commercial	1976-01-01	ME
04-013-1004	North Phoenix	MCAQD	378	Residential	1968-01-01	NP
04-013-1010	Falcon Field	MCAQD	384	Desert	1989-06-01	FF
04-013-2001	Glendale	MCAQD	350	Residential	1974-01-01	GL
04-013-2005	Pinnacle Peak	MCAQD	733	Residential	1988-02-01	PP
04-013-3002	Central Phoenix	MCAQD	339	Residential	1961-01-01	CP
04-013-3003	South Scottsdale	MCAQD	368	Residential	1973-01-01	SS
04-013-4003	South Phoenix	MCAQD	326	Residential	1999-10-01	SP
04-013-4004	West Chandler	MCAQD	366	Residential	2000-07-01	WC
04-013-4005	Tempe	MCAQD	352	Residential	2000-07-01	TE
04-013-4008	Cave Creek	MCAQD	587	Residential	2001-07-20	CC
04-013-4010	Dysart	MCAQD	359	Commercial	2003-07-01	DY
04-013-4011	Buckeye	MCAQD	258	Agricultural	2004-08-01	BE
04-013-7020	Senior Center	SRP-MIC	377	Residential	2004-05-01	SC
04-013-7021	Red Mountain	SRP-MIC	394	Desert	2002-05-27	RM
04-013-7022	Lehi	SRP-MIC	412	Residential	2003-05-01	LE
04-013-7024	High School	SRP-MIC	366	Residential	2006-03-30	HS
04-013-9508	Humboldt Mountain	MCAQD	1582	Forest	1995-08-01	HM
04-013-9702	Blue Point	MCAQD	436	Desert	1993-01-01	BP
04-013-9704	Fountain Hills	MCAQD	505	Residential	1996-04-01	FH
04-013-9706	Rio Verde*	MCAQD	478	Residential	1997-01-01	RV
04-013-9997	JLG Supersite	ADEQ	346	Residential	1993-07-01	JLG
04-021-3001	Apache Junction	PCAQCD	525	Commercial	1987-01-01	AJ
04-021-8001	Queen Valley	ADEQ	634	Desert	2001-01-01	QV

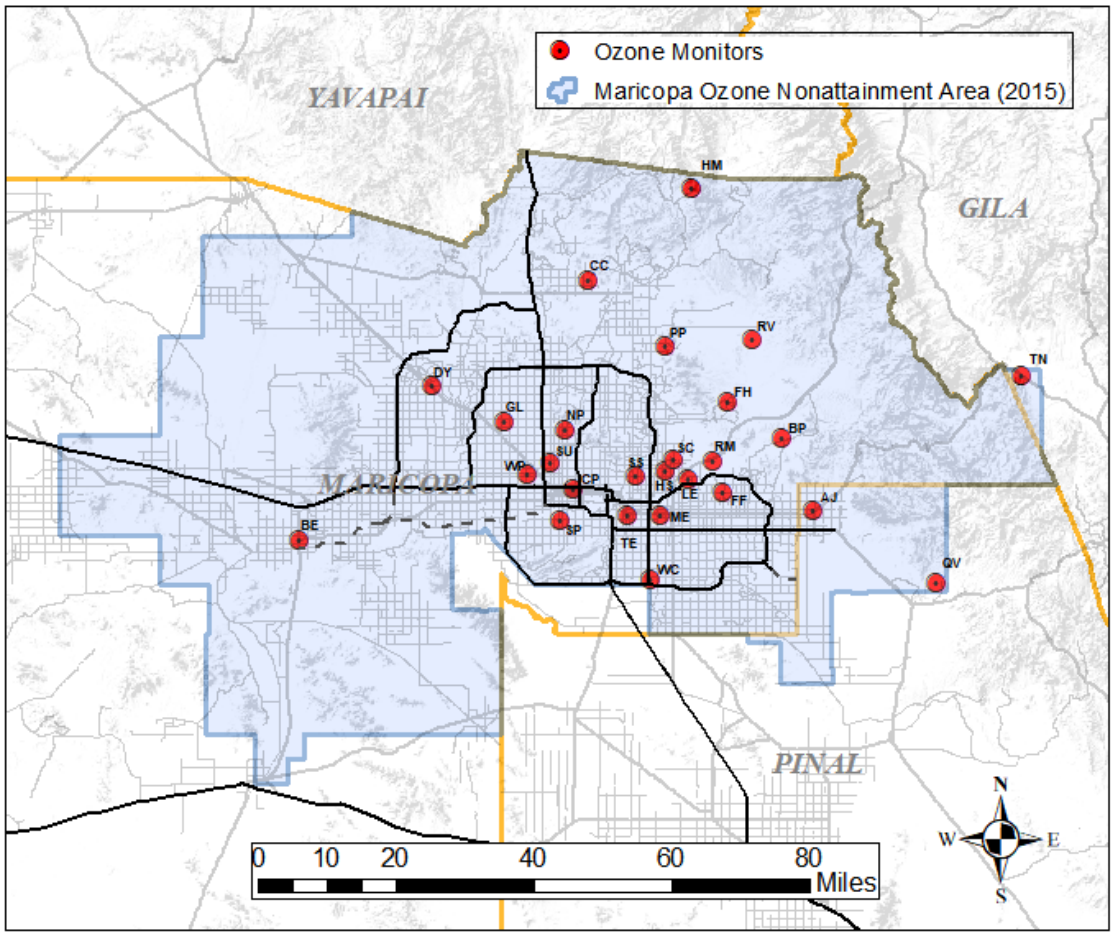

Figure 3. Locations of ozone monitoring sites in the Maricopa eight-hour ozone nonattainment area

6.4. Photochemical Modeling Configuration

6.4.1. CAMx model configuration

CAMx requires a namelist control file specifying input files and model configuration such as model clock control, map projection parameters, modeling grid parameters, model options, and output specifications. Table 5 summarizes the CAMx model configuration. The CAMx configuration is set up to perform two-way grid nesting on the 36 km, 12 km, and 4 km modeling domains. Initial and boundary conditions (ICBC) for the 36 km domain are extracted from the GEOS-Chem or Hemispheric CMAQ global chemistry model. The meteorological fields developed by WRF are processed for CAMx using WRFCAMx pre-processor. The O3MAP pre-processor is used to prepare albedo/haze/ozone column inputs for CAMx from TOMS data. The photolysis inputs are generated using TUV pre-processor.

Table 5. CAMx modeling configuration

Science Options	CAMx Modeling Schemes	Comment
Photochemical Model	CAMx v7.31 – August 2024	
Horizontal Grid	36-km/12-km/4-km	LCC Projection
• 36-km Grid	92 x 79 cells	
• 12-km Grid	59 x 65 cells	
• 4-km Grid	56 x 47 cells	
Vertical Grid	23 vertical layers	
Grid Interaction	36-km/12-km/4-km two-way nesting	
Initial Condition	GEOS-Chem/Hemispheric CMAQ results, GEOS2CAMX v4.0	
Boundary Condition	GEOS-Chem/Hemispheric CMAQ results, GEOS2CAMX v4.0	
Emissions	EPA's 2022 Emissions Modeling Platform, MAG 2023 emissions inventory, SMOKE v5.1, LNOx v2.0	
Meteorological Data	WRF 4.7.0	
Meteorological Processor	WRFCAMx v5.2, YSU Kv, KVPATCH v6	Compatible with CAMx v7.31
Chemistry Parameters	CB7r1	CB7 revision 1
Chemistry Solver	Euler Backward Iterative (EBI)	Efficient and accurate solver
Horizontal Advection	Piecewise Parabolic Method (PPM)	Eulerian continuity equation
Horizontal Diffusion	Explicit simultaneous 2-D solver	K-theory 1st order closure
Vertical Advection	Implicit backward-Euler hybrid centered/upstream solver	Eulerian continuity equation
Vertical Diffusion	Implicit backwards-Euler centered solver	Standard K-theory approach
Deposition Schemes		
• Dry Deposition	Resistance model for gases and aerosols (ZHANG dry deposition)	ZHANG03
• Wet Deposition	Exponential decay as a function of scavenging coefficient	Scavenging model for gases and aerosols

6.4.2. CMAQ model configuration

CMAQ simulations for the supplemental analyses are performed using a one-way nesting approach in which continental CMAQ simulations are first performed for the 36 km domain. Initial and boundary conditions for the 36 km domain are extracted from GEOS-Chem or Hemispheric CMAQ in a process similar to the CAMx model. Meteorological data from WRF are processed using the Meteorology-Chemistry Interface Processor (MCIP v5.5), and the resulting MCIP outputs are used to provide meteorological inputs for the CMAQ model. The CMAQ 36 km simulation is initialized for April 1, 2023, with 3-5 days as the spin-up period and conducted for April 1 through September 30, 2023. The 12 and 4 km modeling domain simulations for both base and future years are subsequently conducted using the boundary and initial conditions derived from the 36 and 12 km CMAQ simulations, respectively. The hourly boundary and initial fields for the 12 and 4 km domains are obtained by application of the BCON and ICON processing tools to the 3-D concentration fields generated by the CMAQ simulation of the 36 km and 12 km domains, respectively. CMAQv5.5 is used for the CMAQ Integrated Source Apportionment Method (ISAM) and the CMAQ Higher-order Decoupled Direct Method in Three Dimensions (HDDM-3D). The CMAQv5.5 chemistry mechanism cb6r3_ae7_aq with pNO3 photolysis (Sarwar et al., 2024) is used in CMAQ simulations.

7. EMISSIONS INPUT

Anthropogenic emissions inventories for 2023 covering the period of April 1 through September 30 are developed for Maricopa and Pinal counties for the 4 km domain. Due to EPA's emission platform data availability, the 2022 U.S. and Mexico anthropogenic emissions inventory for the 12 km and 36 km domains are obtained from the EPA 2022v1 Air Quality Modeling Platform (AQMP) (U.S. EPA, 2024). The differences between 2022 and 2023 in background emissions are negligible for modeling purposes since emissions trends are generally flat or downward in a short span.

Biogenic emissions for all three domains are generated with MEGAN 3.2, driven by 2023 land-cover and meteorological inputs. Wildfire emissions from the EPA 2023 NEI beta release (U.S. EPA, 2025) are used for the United States and from the 2023 Fire Inventory of NCAR (FINN) data for regions outside of the country. The 2023 grid-cell lightning-flash-rate data for each domain are provided by EPA scientists and converted to lightning-NOx emissions through CMAQ's in-line lightning module. The subsections that follow provide a detailed description of the 4 km emission-inventory development.

7.1. Point Source Emissions

Point sources include major stationary sources that emit a large amount of air pollutants (i.e., VOC, NOx, CO, SO_2, PM-10, PM-2.5, lead, and NH_3) into the air. Point sources are required to report emissions and obtain permits under 40 CFR Part 70. MCAQD identified a total of 24 stationary sources in 2023 as point sources through a search of the electric permit system database. Pinal County point source emissions inventory for 2023 is developed by Pinal County Air Quality Control District (PCAQCD). A total of 21 facilities are listed as point sources in Pinal County. For the Salt River Pima-Maricopa Indian Community (SRPMIC), point source emissions are adopted from the 2017 EPA modeling platform, which contains the best available emissions data for this region.

In addition, 2023 traditional emission reduction credit (ERCs) from Maricopa County will be included as point sources in the plan.

7.2. Area Source Emissions

Area sources are stationary sources that are either too small or too numerous to be classified as point sources. The Maricopa County Air Quality Department (MCAQD) developed annual emissions for area sources for 2023 using data from the MCAQD IMPACT database, various EPA guidance documents, and the EPA's Wagon Wheel tools. The 2023 area source emissions in Pinal County were primarily developed using the 2017 EPA modeling platform. For some categories, emissions were scaled using socioeconomic data comparing Pinal County to Maricopa County for the base years of 2017 and 2023. Additionally, certain area source emissions were derived from permits issued within the Pinal County.

In addition, 1,000 tons/year of NOx and 500 tons/year of VOC, intended for potential non-traditional mobile emission reduction credits (MERCs), will be allocated as area sources to the Maricopa County portion of the Maricopa 8-hour ozone nonattainment area.

7.3. Onroad Mobile Source Emissions

EPA released MOVES4.0 onroad model in September 2023. Onroad network and off-network emissions for the 4 km modeling domain will be calculated using the MOVES4.0 onroad and MAG MOVESLINK4 models. The MAG MOVESLINK4 model processes transportation network assignment results for Maricopa and Pinal counties derived by ABM and develops the onroad emissions inventory using MOVES emission factors for the photochemical air quality modeling analysis. The MOVESLINK4 utilizes Geographic

Information Systems (GIS) technology in processing geospatial network and emissions data. It was coded with the Python programming language.

To calculate onroad and off-network vehicle-fleet emissions for 2023, MOVES4.0 is executed using local input data for individual modeling episode days. MOVES modeling scenarios are created using the County Domain option, the Emissions Rates mode for the MOVES onroad network emissions, and the Inventory mode for the MOVES off-network emissions. Local input data for MOVES4.0 model runs are compiled and developed for the Inspection and Maintenance (I/M) program, meteorological data, vehicle population, source type age distribution, annual VMT, monthly/daily/hourly VMT temporal profile, road type VMT distribution, average speed distribution, fuel parameter data, and transit bus data for Alternative Vehicle and Fuel Technologies (AVFT) (U.S. EPA, 2023):

- I/M programs: The I/M types and model years, frequency, compliance factors, cutpoints in place are provided by ADEQ.
- Meteorological data: Temperature and humidity data measured at the Phoenix Sky Harbor International Airport and Casa Grande in 2023 are obtained from NOAA/NCEI for the modeling episode days.
- Vehicle population: MOVES vehicle population inputs are generated by the Eastern Research Group Inc. (ERG) script with the 2023 vehicle registration data provided by ADOT.
- Source type age distribution: MOVES source type age distribution inputs are generated by the ERG script with the 2023 vehicle registration data provided by ADOT.
- Annual VMT: The annual VMT data are calculated using the average weekday VMTs from the ABM transportation network assignment results provided by the MAG transportation modeling staff.
- Road type VMT distribution: The road type VMT distributions are derived from the ABM transportation network assignment results provided by the MAG transportation modeling staff.
- VMT fraction: The monthly/daily/hourly VMT temporal profiles developed from the ADOT traffic count data are provided by the MAG transportation modeling staff.
- Average speed distribution: Local average speeds for individual links are derived from the ABM transportation network assignment results provided by the MAG transportation modeling staff.
- Fuel data: The fuel formulation data are developed based on the MOVES4.0 default fuel parameters, the local gasoline Reid Vapor Pressure (RVP) regulatory values

from the Arizona Department of Agriculture (AZDA), and the MOVES4.0 Fuel Wizard.

- AVFT strategy: MOVES AVFT inputs are generated by the ERG script with the 2023 vehicle registration data provided by ADOT and local transit bus data from the Valley Metro, City of Phoenix, City of Scottsdale, City of Glendale, and ADOT.

7.4. Nonroad Mobile Source Emissions

Nonroad mobile sources are vehicles or equipment that move (or are moved) within the 12-month period and are not licensed or certified as highway vehicles. Nonroad vehicles and equipment fall into the following categories:

- Agricultural equipment, such as tractors, combines and balers;
- Airport ground support equipment (GSE), such as baggage tugs and terminal tractors, and auxiliary power units (APU);
- Commercial equipment, such as generators and pumps;
- Construction equipment, such as graders, back hoes and trenchers;
- Industrial equipment, such as forklifts and sweepers;
- Lawn and garden equipment, such as leaf blowers and lawn mowers;
- Logging equipment;
- Oil field equipment;
- Pleasure craft, such as power boats and personal watercraft;
- Railway maintenance equipment, such as rail straighteners;
- Recreational equipment, such as all-terrain vehicles and off-road motorcycles;
- Underground mining equipment;
- Aircraft, such as jet- and piston-engine planes; and
- Locomotives, such as switching and line-haul trains.

For most nonroad mobile source categories (except airport GSE, APUs, aircraft and locomotives), the EPA MOVES4.0 nonroad model is used to produce emission estimates for Maricopa and Pinal counties, with MOVES default fuel parameters adjusted for local RVP regulations, and with local day-specific meteorological profiles from Sky Harbor and Casa Grande NWS stations. Local population and activity levels are used for lawn & garden equipment in Maricopa County. Populations for agriculture and construction equipment are updated using the new spatial surrogates developed for the EPA 2016 modeling platform that were distributed with the EPA 2020 modeling platform as updates to the default MOVES database. Logging, oil fields, and underground mining are not present in the nonattainment area. For aircraft, APUs, and airport GSE categories, AEDT 3g is used to compute emissions related to aircraft operation, with local airport activity and fleet mix

inputs. In addition, a local survey of the railroad companies having operations within the county (Burlington Northern Santa Fe, Union Pacific and Amtrak) provides locomotive emissions estimates.

7.5. Airport Emissions

The FAA's AEDT 3g model is going to be used to estimate emissions for aircraft at 19 airports within the 4 km modeling domain, except Luke Air Force Base. AEDT calculates emissions, noise, and fuel use, supporting aviation studies at local, regional, and global scales, as well as U.S. regulatory analysis.

The model computes VOC and NOx emissions from aircraft, ground support equipment (GSE), and auxiliary power units (APUs). Emissions are calculated for each combination of aircraft and engine type and aggregated into four categories: air carriers (large commercial aircraft), air taxis (smaller commercial aircraft), general aviation (unscheduled recreational and business aircraft), and military aircraft.

AEDT relies on two main databases for its estimates: an airport database (including location, runways, and weather) and a local activity database (fleet mix and landing/takeoff operations).

Local aircraft activity data (number of LTOs or Touch & Go operations) is a critical input to the AEDT model. The FAA Operations Network (OPSNET) database provided day-specific activity data on 2023 aircraft operations for eight major airports in the Maricopa County (Chandler Municipal, Falcon Field, Glendale Municipal, Phoenix Deer Valley, Phoenix Goodyear, Phoenix-Mesa Gateway, Phoenix Sky Harbor, and Scottsdale airports). MCAQD conducted a survey of 2023 airport operations and fleet mix at Sky Ranch at Carefree in 2024. Additionally, operations data for three smaller general aviation airports - Buckeye Municipal, Gila Bend Municipal, and Stellar Airpark - were sourced from AirNav (airnav.com) and AirportIQ.com for 2023. Base personnel provided the number of F-16s and F-35s military aircraft based at Luke AFB in 2023. All 21 airports located in Maricopa and Pinal counties within the 4 km domain are listed in Table 6.

The FAA Traffic Flow Management System Counts (TFMSC) database provided the aircraft fleet mix for 15 of the 19 commercial and general aviation airports. Because the operational data are day-specific, determining ozone season operations and emissions (from April 1 to September 30) for each category at each airport was straightforward.

Note that the Luke AFB emissions for the F-16 aircraft in 2023 are developed separately by scaling the 2008 emissions (Weston, 2010) with the numbers of F-16 aircraft in 2008

and 2023. Similarly, the emissions for the F-35 aircraft in 2023 are scaled based on emissions reported for the 144 F-35 aircraft from the 2012 Environmental Impact Statement (EIS) report (USAF, 2012) with the numbers of F-35 aircraft in 2023.

Table 6. Operations for airports in the 4 km domain in 2023

No	Airport Name	Code	County	Latitude	Longitude	2023
1	Chandler Municipal Airport	CHD	Maricopa	33.269	-111.811	222,932
2	Deer Valley Airport	DVT	Maricopa	33.688	-112.083	358,518
3	Falcon Field Airport	FFZ	Maricopa	33.461	-111.728	336,441
4	Glendale Municipal Airport	GEU	Maricopa	33.527	-112.295	89,084
5	Phoenix Goodyear Airport	GYR	Maricopa	33.423	-112.376	79,383
6	Phoenix-Mesa Gateway Airport	IWA	Maricopa	33.308	-111.655	267,103
7	Phoenix Sky Harbor Airport	PHX	Maricopa	33.434	-112.008	498,081
8	Scottsdale Airport	SDL	Maricopa	33.623	-111.911	186,812
9	Sky Ranch at Carefree Airport	18AZ	Maricopa	33.818	-111.898	4,291
10	Buckeye Municipal Airport	BXK	Maricopa	33.42	-112.686	54,200
11	Wickenburg Municipal Airport	E25	Maricopa	33.969	-112.799	36,150
12	Gila Bend Municipal Airport	E63	Maricopa	32.958	-112.678	42,000
13	Stellar Airpark	P19	Maricopa	33.299	-111.916	40,000
14	Pleasant Valley Airport	P48	Maricopa	33.801	-112.251	30,000
15	Luke Air Force Base	LUF	Maricopa	33.535	-112.383	n/a
16	Ak-Chin Regional Airport	A39	Pinal	32.991	-111.919	34,675
17	Casa Grande Municipal Airport	CGZ	Pinal	32.955	-111.767	122,000
18	Eloy Municipal Airport	E60	Pinal	32.807	-111.587	30,000
19	Arizona Soaring	E68	Pinal	33.084	-112.161	25,200
20	Pinal Airpark	MZJ	Pinal	32.51	-111.325	58,200
21	Coolidge Municipal Airport	P08	Pinal	32.936	-111.427	56,050

7.6. Biogenic Source Emissions

Emissions from biogenic sources for all three nested domains are estimated using MEGAN. MEGAN is a state-of-the-art biogenic emissions model developed by Alex Guenther, NCAR, and maintained by the University of California, Irvine. Corrections and improvements were made in MEGAN v3.2 (Jiang et al., 2018; Guenther et al., 2017). MEGAN requires both land cover and meteorological data as inputs. Land cover data such as leaf area index (LAI) and the fraction of surface area covered by vegetation are typically based on satellite and ground observations.

The LAI input to MEGAN is based on the Copernicus Global Land Service (CGLS) Collection 300m LAI Version 1 product for 2023 (ten-day resolution). The CGLS data is re-gridded to 0.01 degree resolution for input to the MEGAN LAI preprocessor which maps it to the modeling domains. Emission factors and vegetation light dependence fractions are specified from gridded maps based on observations of emissions from all vegetation types and tree species.

MEGAN calculates gridded biogenic emission rates using the aforementioned inputs along with the meteorological conditions in each grid cell. Meteorological input data are obtained from WRF model simulation results postprocessed with MCIP v5.5 and then input to the MET2MGN tool which prepares the meteorological input data for MEGAN. The MET2MGN output includes photosynthetically active radiation (PAR) at the surface, air temperature at 2 meters above surface, air pressure, humidity, wind speed, top-layer soil moisture and temperature, and accumulated precipitation for each grid cell for each hour.

7.7. Emissions Preprocessing

The emissions inventories are preprocessed for input to CAMx and CMAQ by using SMOKE v5.1 to develop temporally allocated, spatially gridded, and chemically speciated emissions as discussed in the following sections.

7.7.1. Temporal Allocation of Emissions

Emissions inventories are provided at various temporal levels (i.e., daily, monthly, or annual). SMOKE develops day-specific hourly emissions using temporal profiles. The monthly profiles for each EGU point source in both Maricopa and Pinal counties are developed using the EPA monthly emission data from 2019 to 2023. Weekly and diurnal profiles for EGU sources will be developed using Continuous Emissions Monitoring System (CEMS) data from 2022 AQMP. Monthly, weekly, and diurnal profiles for other point sources are taken from EPA 2022 AQMP directly. For the temporal allocation of area and nonroad sources, the EPA temporal profiles are used to develop day-specific hourly emissions by Source Classification Code (SCC).

7.7.2. Spatial Allocation of Emissions

Most anthropogenic emissions, except point sources, are reported as county-level. These emissions are to be spatially allocated to grid cells for photochemical air quality modeling. For example, gridded agricultural land use is used to spatially distribute agricultural

pesticide emissions to grid cells. The EPA Spatial Allocator (SA) v4.4 is used in generating geo-referenced spatial surrogates that are inputs to the SMOKE modeling system. Three components are required for developing spatial surrogates as follows:

- Weight shapefile: This geospatial dataset is used for allocating (or weighting) county-level emissions to grid cells, for example roadways, population density, or golf courses.
- Data shapefile: This geospatial dataset includes county and municipal boundary layers.
- Output grid or polygon: This geospatial dataset includes the grid or polygon configuration for the modeling domains.

A total of 56 spatial surrogates are developed for Maricopa and Pinal counties by using MAG GIS shapefiles covering the 4 km modeling domain in 2023. These shapefiles contain population data, regional traffic data, land use and land cover, and employment data. The spatial surrogates for the 12 km and 36 km domains over the U.S. and Mexico are developed using shapefiles and settings from the EPA defaults provided in the 2022 AQMP.

7.7.3. Chemical Speciation

The CAMx and CMAQ modeling in this study uses the most up-to-date chemical mechanism, Carbon Bond Version 6 (CB6R3AE7), as photochemical reactions of ozone precursor emissions. This version of chemical mechanism includes four new species that were not in the previous version of CB6: AACD, FACD, APIN, and IVOC. This updated mechanism supports formation of secondary organic aerosols by mapping low volatility compounds. The SMOKE modeling system is used for the chemical speciation process, which converts ozone precursor emissions (i.e., VOC and NOx) to the model species emissions for ozone chemistry according to chemical speciation profiles for emission source categories. The SMOKE CB6R3AE7 speciation profiles are used to perform the chemical speciation process for both CAMx and CMAQ modeling.

8. MODEL PERFORMANCE EVALUATION

EPA provides the model performance evaluation methods and a tool that assess relevant variables paired in time and space for recommended statistical metrics for WRF and CAMx/CMAQ model performance evaluations. The Atmospheric Model Evaluation Tool (AMET) is used to evaluate WRF and CAMx/CMAQ model performance, which allows tests

to be performed on a site-by-site and/or network aggregate basis, for any duration or frequency of interest. A list of the statistical metrics used in AMET is provided in Table 7.

Table 7. Statistical metrics for model performance evaluation

Metric Name	Definition
Mean Bias (MB)	$MB = \frac{1}{N}\sum(M_i - O_i)$
Mean Error (ME)	$ME = \frac{1}{N}\sum\lvert M_i - O_i\rvert$
Root Mean Square Error (RMSE)	$RMSE = \sqrt{\frac{\sum(M_i - O_i)^2}{N}}$
Fractional Bias (FB)	$FB = 100\% \times \frac{2}{N}\sum\frac{(M_i - O_i)}{(M_i + O_i)}$
Fractional Error (FE)	$FB = 100\% \times \frac{2}{N}\sum\frac{\lvert M_i - O_i\rvert}{(M_i + O_i)}$
Normalized Mean Bias (NMB)	$NMB = 100\% \times \frac{\sum(M_i - O_i)}{\sum O_i}$
Normalized Mean Error (NME)	$NMB = 100\% \times \frac{\sum\lvert M_i - O_i\rvert}{\sum O_i}$
Correlation Coefficient	$R^2 = \left(\frac{\sum_1^N\left((M_i - \bar{M}) \times (O_i - \bar{O})\right)}{\sqrt{\sum_1^N(M_i - \bar{M})^2 \sum_1^N(O_i - \bar{O})^2}}\right)^2$
Index of Agreement	$IoA = 1 - \frac{\sum(O_i - M_i)^2}{\sum(\lvert M_i - \bar{O}\rvert + \lvert O_i - \bar{O}\rvert)^2}$

Statistical metrics of mean bias, mean error bias, root mean square error and index of agreement will be computed to satisfy the operational model performance evaluation. Hourly time-series plots, paired and summary scatter-density plots, diurnal box-and-whisker plots, soccer goal diagrams, and Taylor diagrams will be generated.

8.1. Meteorological Model Performance Evaluation

A meteorological performance evaluation will be conducted using AMET v1.5, focusing on four key variables: temperature, water vapor mixing ratio, wind speed, and wind

direction. The hourly surface observational database (i.e., METAR) and sounding data in the Meteorological Assimilation Data Ingest System (MADIS) within the modeling domain will serve as the primary WRF validation and performance evaluation data set. METAR data includes the Automated Surface Observing System (ASOS), Automated Weather Observing System (AWOS) and non-automated reports. MADIS RAdiosonde Observation (RAOB) dataset provides wind, temperature, moisture and geopotential height at different atmospheric pressure levels from all stations in North America. Correlation coefficient, mean bias (fractional and normalized), mean error bias (fractional and normalized), root mean square error and index of agreement will be computed for the operational performance evaluation of meteorological model. Hourly time series plots, paired scatter-density plots, summary plots of scatter-density, diurnal box-and-whisker, soccer goal and Taylor diagrams will be generated.

For the phenomenological meteorological model performance evaluation, emphasis will be put on validation of the simulated valley breeze. Wind vector spatial and temporal distributions will be derived for modeled and observed wind information, as well as 2-D maps of wind fields overlaid on topography. Observed radiosonde data may be evaluated against simulated vertical profiles to assess boundary layer heights, inversion locations and wind shear.

8.2. Air Quality Model Performance Evaluation

The CAMx/CMAQ air quality model performance will be evaluated using AMET v1.5 with the aforementioned statistical metrics in Table 7 and the following statistical metrics:

- Normalized bias test: The metric provides a measure of the ability of the model to replicate observed patterns during the times of day when available monitoring and modeled data are most likely to represent similar spatial scales. The EPA recommended range for the metric is ±15%.
- Gross error of all pairs above 60 ppb: In conjunction with bias, this metric provides an overall assessment of base case performance and may be used as a reference to other modeling applications. Gross error may be interpreted as precision. EPA recommended range for the metric is ±35%.

In general, the performance metrics that fall within or below these ranges will be considered acceptable. Furthermore, the CAMx/CMAQ model performance evaluation may include additional numerical and graphical measures if needed.

9. MODELED ATTAINMENT DEMONSTRATION

9.1. Base Design Values

The base design value for each monitoring site was developed by averaging three-year design values derived from annual fourth-highest daily maximum ozone concentrations from 2021 to 2023. It should be noted that the ozone exceedances known to be impacted by wildfires were excluded when calculating the base design values given in Table 8.

Table 8. 2023 base design value (DVB2023) in ppm

AQS ID	Site Name	Annual 4th Highest MDA8 Ozone (ppm)			3-Year Average Ozone Design Value (ppm)
		2021	2022	2023	
04-007-0010	Tonto NM	0.069	0.074	0.070	0.071
04-013-0019	West Phoenix	0.066	0.076	0.075	0.072
04-013-1003	Mesa	0.077	0.076	0.072	0.075
04-013-1004	North Phoenix	0.075	0.077	0.072	0.074
04-013-1010	Falcon Field	0.075	0.078	0.073	0.075
04-013-2001	Glendale	0.072	0.078	0.074	0.074
04-013-2005	Pinnacle Peak	0.073	0.077	0.073	0.074
04-013-3002	Central Phoenix	0.071	0.072	0.070	0.071
04-013-3003	South Scottsdale	0.079	0.067	0.069	0.071
04-013-4003	South Phoenix	0.067	0.067	0.066	0.066
04-013-4004	West Chandler	0.070	0.068	0.065	0.067
04-013-4005	Tempe	0.073	0.071	0.072	0.072
04-013-4008	Cave Creek	0.070	0.070	0.073	0.071
04-013-4010	Dysart	0.068	0.075	0.070	0.071
04-013-4011	Buckeye	0.063	0.067	0.066	0.065
04-013-7020	Senior Center	0.073	0.074	n/a	n/a
04-013-7021	Red Mountain	0.070	0.074	0.073	0.072
04-013-7022	Lehi	0.073	0.079	0.076	0.076
04-013-7024	High School	0.068	0.076	0.069	0.071
04-013-9508	Humboldt Mountain	0.065	0.069	0.070	0.068
04-013-9702	Blue Point	0.071	0.076	0.072	0.073
04-013-9704	Fountain Hills	0.069	0.076	0.063	0.069
04-013-9997	JLG Supersite	0.076	0.076	0.078	0.076
04-021-3001	Apache Junction	0.068	0.071	0.069	0.069
04-021-8001	Queen Valley	0.070	0.071	0.069	0.070

10. SUPPLEMENTAL ANALYSES

EPA requires supplemental analyses to support the modeled attainment demonstration results since the modeling analyses may contain some uncertainty in elements such as meteorological input data and science formulation. The following sections outline the supplemental analyses that will be performed to confirm the conclusions from the modeled attainment demonstration for the 2015 ozone standard.

Absolute Model Forecasts

Absolute model forecast results may be useful in assessing general progress towards attainment from the baseline emissions inventory to the future emissions inventory. Absolute model forecast analysis compares the future year modeled ozone concentrations to the base year modeled ozone concentrations, and calculates the frequency, magnitude, and relative amount of ozone reductions. Metrics for the absolute model forecast analysis are as follows:

- Percent change in total amount of modeled ozone concentrations greater than or equal to 71 ppb in the nonattainment area;
- Percent change in number of grid cells greater than or equal to 71 ppb in the nonattainment area;
- Percent change in grid cell-hours greater than or equal to 71 ppb in the nonattainment area; and
- Percent change in maximum modeled eight-hour ozone concentrations in the nonattainment area.

Chemical Process Analysis

To assess which ozone precursor (e.g., VOC or NOx) will limit ozone production, the CAMx Chemical Process Analysis (CPA) will be used. This analysis provides detailed reaction rate information over groups of reactions in the chemical mechanism for a selected area. This makes it possible to quantify chemically meaningful attributes such as ozone and oxidant production/loss rates, radical initiation rates, radical propagation efficiencies, radical termination rates, hydrocarbon chaining lengths, formaldehyde production rates, and odd-nitrogen (NOy) reaction rates. This analysis will be used to determine the VOC-limited or NOx-limited area and to develop more appropriate, effective emission control strategies for the attainment of the 2015 ozone standard.

Ozone Source Apportionment Analysis

To confirm and validate the results of the CAMx modeling, other corroboratory analyses may include use of the CAMx Ozone Source Apportionment Technology/Anthropogenic Precursor Culpability Assessment (OSAT/APCA). These analyses will identify and quantify the contributions of multiple upwind source areas, emissions source categories, and individual ozone precursors to local ozone concentrations.

Higher-order Decoupled Direct Method

The higher-order decoupled direct method (HDDM) will be used for the analysis of model sensitivity of ozone to change in precursor emissions. Sensitivity coefficients will be evaluated to predict ozone concentrations to pollutant sources such as initial conditions, boundary conditions, top concentrations, and anthropogenic emissions. The sensitivity analysis tool includes options for varying emission inputs to the model, scaling emissions by a factor, additively increasing emissions by a constant amount, and zeroing-out emissions by source category and geographic region.

Trends in Ambient Air Quality

Progress towards attainment of the ozone standard will be evaluated based on measured historical trends of air quality and emissions. Air quality trends will be established using meteorologically adjusted ozone concentrations at the monitors. Trends in ozone precursor emissions will be examined using monitor data along with satellite observations where available.

Additional Analyses

A few ozone episodes lasting fewer than 20 days in 2023 may be selected for investigation of potential stratospheric intrusion. Refined meteorological inputs could include alternative physical parameterization schemes and additional vertical layers, extending up to 50 hPa. Given the uncertainty in emissions from Mexico, ozone column densities predicted by CAMx/CMAQ will be compared with TROPOspheric Monitoring Instrument (TROPOMI) satellite data. As a result, baseline emissions for Mexico may be adjusted based on comparisons with satellite-derived NO_2 and/or HCHO concentrations.

11. 179B DEMONSTRATION

Under §179B, EPA allows a nonattainment area to be judged on the air quality it would experience "but for" pollution transported from outside the United States. To meet that stringent test for Maricopa County, the weight of evidence case will be built that is

scientifically sound, internally consistent, and transparent. The following is a draft outline of the work to be performed by the selected consultant Ramboll:

1 Overview
  1.1 Introduction
  1.2 Report Organization
  1.3 Summary
2 Conceptual Model
  2.1 The Maricopa Airshed
  2.2 Summary of Ozone Air Quality
  2.3 Ozone and Precursor Monitoring
  2.4 Analyses Specific to the 179B Demonstration
    2.4.1 Exceedances During the 2021-2023 Design Value Period
    2.4.2 Surface Synoptic Analysis
    2.4.3 Upper Air Synoptic Analysis
    2.4.4 International Transport
    2.4.5 Vertical Wind Profiles and Roses
    2.4.6 Recent EPA Modeling Results
      2.4.6.1 2021 Ozone Determination of Attainment by the Attainment Date
      2.4.6.2 Disapproval of "Good Neighbor" State Implementation Plans
3 Precursor and Ozone Trends
  3.1 Maricopa NAA vs. Northern Mexico
    3.1.1 Mexico EI updates
    3.1.2 Results
4 Transport Analysis
  4.1 HYSPLIT Back Trajectories during 2021-2023
    4.1.1 All Days
    4.1.2 No Exceptional Event Days
5 Modeling to Quantify International Contribution
  5.1 EPA Recommended Ozone Design Value Projection Procedure
  5.2 Source Apportionment Modeling
    5.2.1 Model Configuration
    5.2.2 Boundary Conditions via GEOS-Chem or H-CMAQ
    5.2.3 OSAT Configuration (Mexico + BCs Representing Global)
    5.2.4 Model Results: DV Scaling
    5.2.5 Model Results: Removal of Transport Days from DV Calculation
6 Conclusions

12. MANAGEMENT STRUCTURE AND COMMITTEES

MAG has responsibilities for regional involvement in a number of planning issues, and has established an extensive mechanism for ensuring coordinated policy direction from elected officials, coordinated management and technical input, and advice from the appropriate agency staff, as well as direct citizen input. Figure 4 displays the MAG Policy Structure and Figure 5 presents the MAG Committee Structure. All policy committees and formal technical committees follow the Arizona open meeting law which requires, among other requirements, the posting of meeting notices and agendas at least 24 hours prior to any meeting. The MAG Regional Council is the governing body of MAG. It is composed of elected officials from each member agency, and two ex officio members representing the Arizona State Transportation Board. This composition of elected officials is a reflection of citizen input at the local government level. The MAG Regional Council agenda includes a call to the audience, providing the opportunity for public comments at each monthly meeting. MAG holds at least one formal public meeting prior to the adoption of any new or updated nonattainment area plan. Formal public hearings are advertised locally at least 30 days prior to the hearing date and documentation is available for public review during this 30-day period. Draft documents are distributed to appropriate federal, state, and local agencies for review and comment during this period. Comments received are analyzed with a staff response for consideration by the MAG Air Quality Technical Advisory Committee and MAG Regional Council before taking approval action. Documentation of the comments and responses are incorporated into the plan document. Due to the technical complexity of many MAG programs, committees consisting of professional experts are often needed to assist in program development. The Air Quality Technical Advisory Committee is composed of representatives from eight MAG member agencies, citizens, environmental interests, health interests, automobile industry, fuel industry, utilities, public transit, trucking industry, rock products industry, construction firms, housing industry, architecture, agriculture, industry, business, parties to the Air Quality Memorandum of Agreement, and various State and Federal agencies. The role of the Technical Advisory Committee is to review and comment on technical information generated during the planning process and make recommendations to the MAG Management Committee.

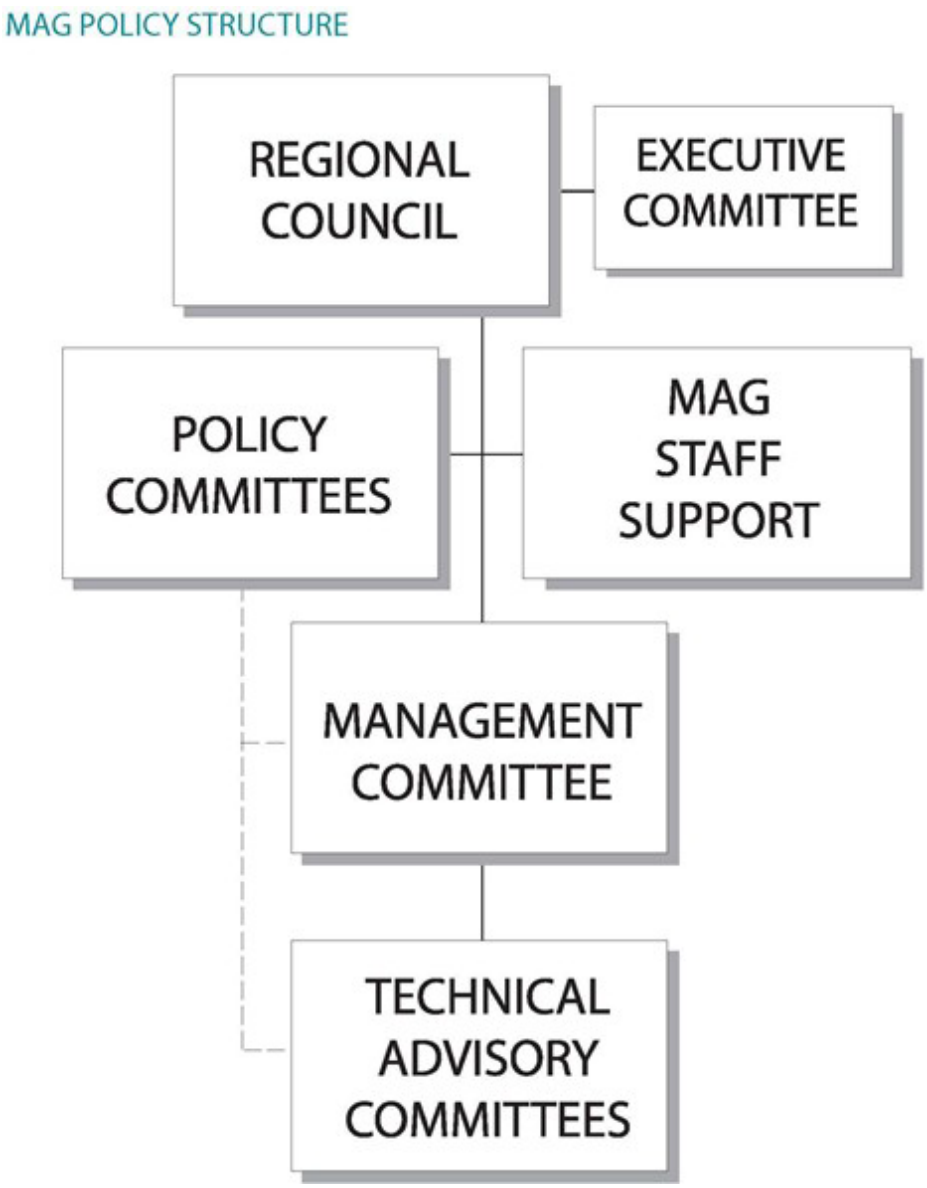

Figure 4. MAG policy structure

13. PARTICIPATING ORGANIZATIONS

Technical oversight for this project will be provided by the Air Quality Planning Team. This team includes staff representatives from MAG, ADEQ, ADOT, MCAQD, and PCAQCD. The Air Quality Planning Team will meet as necessary during the ozone modeling effort. Periodic reports on the status and progress of various phases of the modeling work will be presented at these meetings, and technical issues will be discussed and resolved.

MAG COMMITTEE STRUCTURE

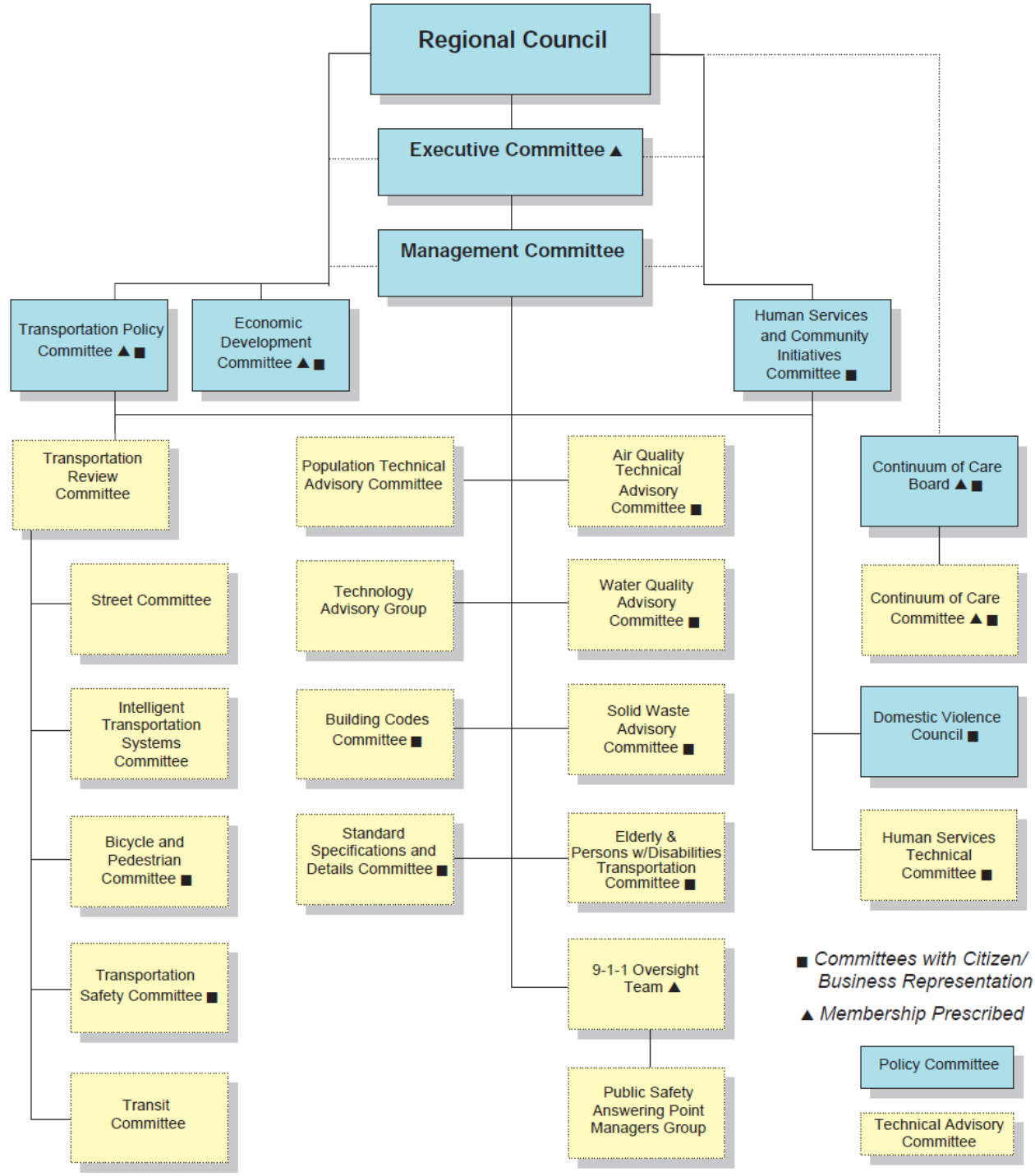

Figure 5. MAG committee structure

14. PROCEDURAL REQUIREMENTS

The following items will be delivered in draft form to the EPA regional office for review and comments during the modeling study. MAG will also provide draft versions of these items to the Air Quality Planning Team for review and comments.

- Modeling Protocol
- Technical Support Document

Technical support document (TSD) will address the modeled attainment demonstration, attainment measures, and the supplemental analyses as the weight of evidence.

15. SCHEDULE

The ozone modeling analysis for the Maricopa eight-hour ozone nonattainment area will include the following tasks. The schedule for the tasks is presented in Table 9.

1. Develop the 2023 emissions inventory, including biogenic emissions. (Completion Date: May 2025)
2. Develop meteorology for 2023 using WRF model. (Completion Date: May 2025)
3. Develop the 2023 global model outputs. (Completion Date: June 2025)
4. Prepare a modeling protocol document (this document) describing the historical background, modeling domain, modeling period, and procedures to be followed in the modeling analysis. (Completion Date: May 2025)
5. Provide technical support for 179B demonstration. (Completion Date: July 2025)
6. Evaluate WRF, CAMx, and CMAQ model performance using EPA recommended model evaluation methodologies. (Completion Date: July 2025)
7. Assess source contributions through OSAT/ISAM and HDDM. (Completion Date: August 2025)
8. Perform weight-of-evidence analyses. (Completion Date: August 2025)
9. Develop Technical Support Document (TSD). (Completion Date: September 2025)
10. Submit the TSD to Air Quality Technical Advisory Committee (AQTAC), Management Committee, and Regional Council for approval. (Completion Date: September 2025)
11. Submit the TSD and Plan to EPA. (Completion Date: September 2025)

Table 9. Schedule

Action Plan	2025						
	Mar	Apr	May	Jun	Jul	Aug	Sep
Develop 2023 raw emissions inventory							
Develop 2023 WRF meteorological data							
Develop 2023 global model outputs							
Develop modeling protocol							
Provide technical support for 179B demonstration							
Evaluate WRF, CAMx, and CMAQ model performance							
Assess source contributions through OSAT/ISAM and HDDM							
Perform weight-of-evidence analyses							
Develop TSD							
Submit TSD to AQTAC, Management Committee, and Regional Council							
Submit TSD/SIP to EPA							

16. REFERENCES

Guenther, A. B., T. Shah, L. Huang, et al. (2017). A next generation modeling system for estimating Texas biogenic VOC emissions, AQRP Project 16–011.

Jiang, X., A. Guenther, M. Potosnak, C. Geron, R. Seco, T. Karl, S. Kim, L. Gu, and S. Pallardy (2018). Isoprene emission response to drought and the impact on global atmospheric chemistry. *Atmospheric Environment*, 183:69–83.

Sarwar, G., C. Hogrefe, B. H. Henderson, R. Mathur, R. Gilliam, A. B. Callaghan, and L. J. Carpenter (2024). Impact of particulate nitrate photolysis on air quality over the Northern Hemisphere. *Science of The Total Environment*, 917, 170406.

U.S. EPA (2015). Air Quality Modeling Technical Support Document for the 2008 Ozone NAAQS Transport Assessment. Technical report, *U.S. Environmental Protection Agency*, January 2015.

U.S. EPA (2023). Using MOVES to Prepare Emission Inventories for State Implementation Plans and Transportation Conformity. Technical report, *U.S. Environmental Protection Agency*, August 2023.

U.S. EPA (2024). The 2022v1 Emissions Modeling Platform. URL http://gaftp.epa.gov/Air/emismod/2022/v1/.

U.S. EPA (2025). The 2023 NEI beta release. URL https://gaftp.epa.gov/Air/nei/2023/doc/supporting_data/events/beta/ff10/.

USAF (2012). Final F-35A Training Basing Environmental Impact Statement. Technical report, *United State Air Force*. URL http://www.dtic.mil/dtic/tr/fulltext/u2/a612501.pdf.

Weston (2010). 2008 Mobile Source Air Emissions Inventory for Luke Air Force Base. Technical report, *Weston Solutions Inc*, June 2010. Prepared for Air Education and Training Command (AETC).

Appendix A Conceptual Model for Ozone

Conceptual Model for Ozone

June 2025

Table of Contents

1 Introduction 1
1.1 2015 8-hour ozone standard 1
1.2 Current status of nonattainment area 1
2 Monitoring network 2
2.1 AQS monitor locations 2
2.2 Site characteristics 3
3 Current air quality 5
3.1 Exceedances impacted by wildfires 5
3.2 Design values 6
3.3 Exceedances 8
3.4 Spatial analysis 9
3.5 Temporal analysis 17
3.5.1 Seasonal patterns 17
3.5.2 Daily patterns 18
3.5.3 Diurnal patterns 18
4 Emissions 22
4.1 Anthropogenic emissions 22
4.2 Biogenic sources 23
4.3 Wildfires 23
4.4 Regional background emissions 23
4.5 Precursor trends 23
4.5.1 Nitrogen dioxide 23
4.5.2 Formaldehyde 24
4.5.3 Carbon monoxide 25
4.5.4 Formation sensitivity 26
4.6 Existing emission control programs 27
5 Meteorological influences 28
5.1 Mesoscale systems 28
5.1.1 Stratospheric ozone intrusions 28
5.1.2 High-pressure systems 31
5.1.3 Cyclones and fronts 32

5.1.4 North American monsoon 33
5.1.5 Extreme climate 33
5.2 Terrain effects 35
5.3 Local weather 36
5.3.1 Wind speed and direction 37
5.3.2 Temperature 40
5.3.3 Relative humidity 42
5.3.4 Surface pressure 43
5.3.5 Nocturnal inversions 44
5.3.6 Surface heat flux and urban heat island effect 46
5.4 Long-range transport 48
6 Satellite NO_2 and HCHO 50
6.1 OMI 51
6.2 TROPOMI 52
6.3 TEMPO 58
6.4 Model evaluation using satellite data 61
7 Conclusions 62
8 References 64

1 Introduction

1.1 2015 8-hour ozone standard

In 2015, the Environmental Protection Agency (EPA) revised the 8-hour ozone standard from 0.075 parts per million to 0.070 parts per million. The 2015 standard is met when the three-year average of the annual fourth-highest daily maximum 8-hour average ozone concentrations measured at each monitor over each year is less than or equal to 0.070 parts per million.

1.2 Current status of nonattainment area

In accordance with the Clean Air Act (CAA), EPA designated the Maricopa Eight-Hour Ozone Nonattainment area as a Marginal Area on June 4, 2018, for the 2015 ozone standard. As a Marginal Area, the Maricopa nonattainment area had an August 3, 2021 attainment date.

On September 15, 2022, EPA signed a notice determining that the Maricopa Eight-Hour Ozone Nonattainment Area did not meet the 2015 ozone standard by the August 3, 2021 attainment date and is reclassified as a Moderate Area. The attainment date for Moderate areas is August 3, 2024.

The current status of ozone air quality in the Maricopa 8-hour ozone nonattainment area is given in Table 1-1. [1] The maximum three-year average of the annual fourth-highest maximum daily 8-hour (MDA8) ozone concentrations from 2021 to 2023 is 0.08 ppm, occurring at Mesa and JLG Supersite.

Table 1-1 Annual fourth-highest MDA8 ozone concentrations (2021 – 2023) and three-year average ozone design values of monitoring sites.

AQS ID	Site Name	Annual 4th Highest MDA8 Ozone (ppm)			3-Year Average Ozone Design Value (ppm)
		2021	2022	2023	
04-007-0010	Tonto NM	0.075	0.074	0.076	0.075
04-013-0019	West Phoenix	0.078	0.076	0.077	0.077
04-013-1003	Mesa	0.083	0.078	0.080	0.080
04-013-1004	North Phoenix	0.081	0.077	0.077	0.078
04-013-1010	Falcon Field	0.080	0.078	0.080	0.079
04-013-2001	Glendale	0.079	0.081	0.079	0.079
04-013-2005	Pinnacle Peak	0.079	0.077	0.076	0.077
04-013-3002	Central Phoenix	0.081	0.072	0.078	0.077
04-013-3003	South Scottsdale	0.081	0.068	0.074	0.074
04-013-4003	South Phoenix	0.074	0.069	0.076	0.073

[1] U.S. EPA, 2025, *Air Quality Design Values*, 2023 Design Value Reports, Retrieved March 31, 2025, from https://www.epa.gov/air-trends/air-quality-design-values.

04-013-4004	West Chandler	0.073	0.071	0.069	0.071
04-013-4005	Tempe	0.079	0.073	0.080	0.077
04-013-4008	Cave Creek	0.074	0.071	0.076	0.073
04-013-4010	Dysart	0.077	0.075	0.074	0.075
04-013-4011	Buckeye	0.071	0.071	0.067	0.069
04-013-7020	Senior Center	0.077	0.075	n/a	n/a
04-013-7021	Red Mountain	0.078	0.075	0.079	0.077
04-013-7022	Lehi	0.076	0.079	0.082	0.079
04-013-7024	High School	0.074	0.077	0.076	0.075
04-013-9508	Humboldt Mountain	0.066	0.072	0.073	0.070
04-013-9702	Blue Point	0.072	0.077	0.080	0.076
04-013-9704	Fountain Hills	0.076	0.076	0.070	0.074
04-013-9706	Rio Verde	n/a	n/a	n/a	n/a (closed in 2017)
04-013-9997	JLG Supersite	0.082	0.076	0.083	0.080
04-021-3001	Apache Junction	0.074	0.072	0.072	0.072
04-021-8001	Queen Valley	0.073	0.077	0.075	0.075

2 Monitoring network

2.1 AQS monitor locations

A network of 26 state and local ozone monitoring stations (SLAMS) located within or near the nonattainment area is used for this study. Stations without significant coverage of the period of the study are excluded. The operating agencies for the monitors include the Arizona Department of Environmental Quality (ADEQ), Maricopa County Air Quality Department (MCAQD), Pinal County Air Quality Control District (PCAQCD) and the Salt River Pima-Maricopa Indian Community (SRP-MIC). One of the locations (JLG Supersite) is operated under the Photochemical Assessment Monitoring Stations (PAMS) program, providing measurements of ozone concentrations as well as volatile organic compounds (VOC) which are ozone precursors that contribute to the formation of ozone. The Queen Valley site was also operated under the PAMS program through 2016.

Hourly and daily summary measurements of air pollutants from these monitoring stations were obtained from the Air Quality System (AQS) for the period 2000-2024. The locations of the monitoring stations are illustrated in Figure 2-1, and the site characteristics of each monitor are listed in Table 2-1. A subset of these monitoring stations also measured nitrogen dioxide (NO_2), VOCs and/or carbon monoxide (CO) as indicated in the table. Additional site information is available in the owning agency monitoring network plans (ADEQ, 2023; MCAQD, 2024; PCAQCD, 2024; SRPMIC, 2024).

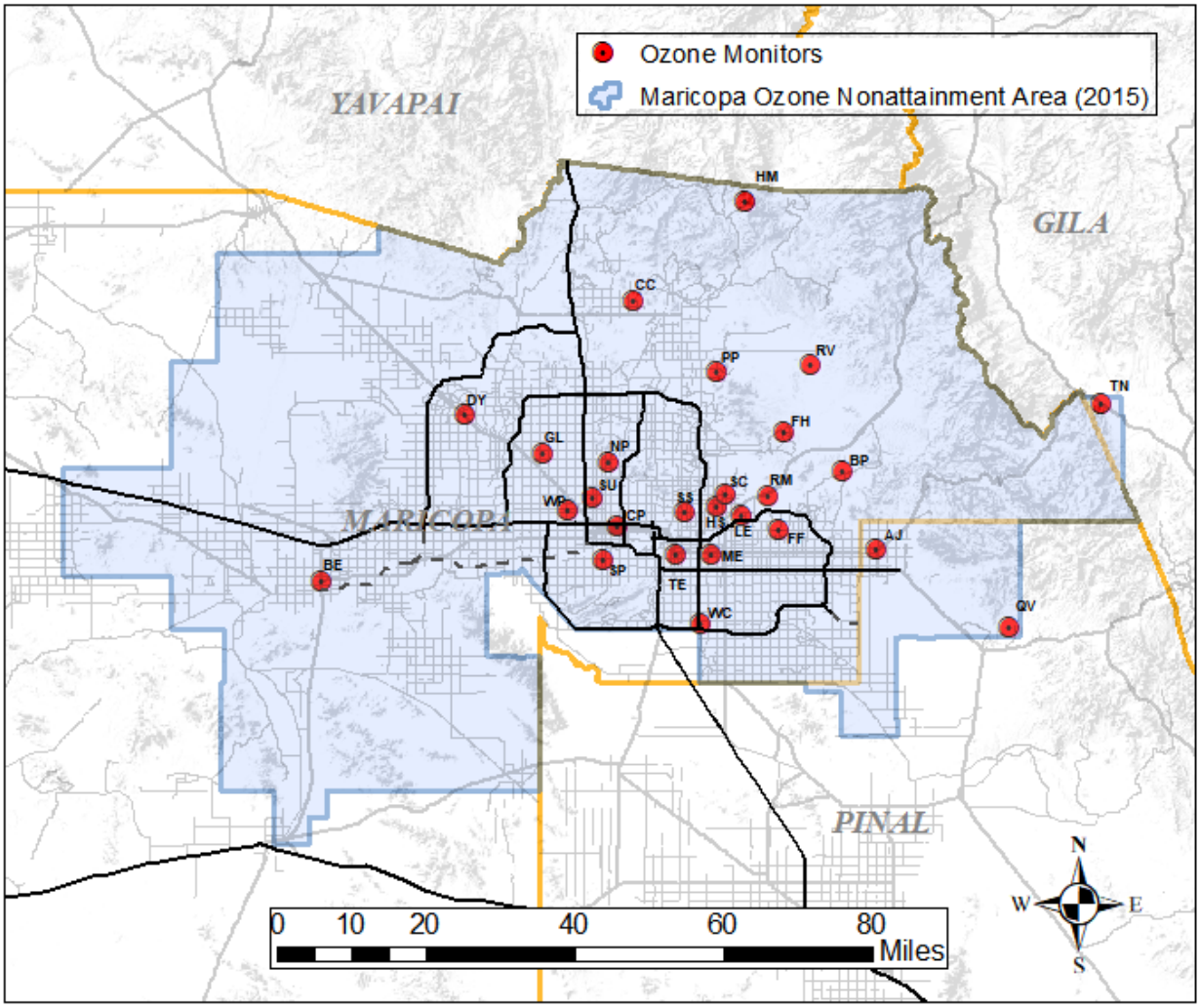

Figure 2-1 Locations of air quality monitoring stations in the Maricopa County Moderate Ozone Nonattainment Area (2015 NAAQS).

2.2 Site characteristics

The characteristics of each monitoring site, such as AQS ID, owning agency, elevation, land use, and pollutants measured during the 2000-2024 period, are listed in Table 2-1.

Table 2-1 State and local active air quality monitor site characteristics.

AQS ID	Site Name	Owning Agency	Elev. (m)	Land Use	O_3	NO_2	VOC	CO	Date Established	ID
04-007-0010	Tonto National Monument	ADEQ	786	Desert	✓				1988-04-01	TN
04-013-0019	West Phoenix	MCAQD	333	Residential	✓	✓		✓	1984-01-01	WP
04-013-1003	Mesa	MCAQD	383	Commercial	✓			✓	1976-01-01	ME
04-013-1004	North Phoenix	MCAQD	378	Residential	✓			✓	1968-01-01	NP

04-013-1010	Falcon Field	MCAQD	384	Desert	✓				1989-06-01	FF
04-013-2001	Glendale	MCAQD	350	Residential	✓			✓	1974-01-01	GL
04-013-2005	Pinnacle Peak	MCAQD	733	Residential	✓				1988-02-01	PP
04-013-3002	Central Phoenix	MCAQD	339	Residential	✓	✓		✓	1961-01-01	CP
04-013-3003	South Scottsdale	MCAQD	368	Residential	✓			✓	1973-01-01	SS
04-013-4003	South Phoenix	MCAQD	326	Residential	✓		✓	✓	1999-10-01	SP
04-013-4004	West Chandler	MCAQD	366	Residential	✓			✓	2000-07-01	WC
04-013-4005	Tempe	MCAQD	352	Residential	✓			✓	2000-07-01	TE
04-013-4008	Cave Creek	MCAQD	587	Residential	✓				2001-07-20	CC
04-013-4010	Dysart	MCAQD	359	Commercial	✓			✓	2003-07-01	DY
04-013-4011	Buckeye	MCAQD	258	Agricultural	✓	✓		✓	2004-08-01	BE
04-013-7020	Senior Center	SRP-MIC	377	Residential	✓				2004-05-01	SC
04-013-7021	Red Mountain	SRP-MIC	394	Desert	✓				2002-05-27	RM
04-013-7022	Lehi	SRP-MIC	412	Residential	✓				2003-05-01	LE
04-013-7024	High School	SRP-MIC	366	Residential	✓				2006-03-30	HS
04-013-9508	Humboldt Mountain	MCAQD	1582	Forest	✓				1995-08-01	HM
04-013-9702	Blue Point	MCAQD	436	Desert	✓				1993-01-01	BP
04-013-9704	Fountain Hills	MCAQD	505	Residential	✓				1996-04-01	FH
04-013-9997	JLG Supersite	ADEQ	346	Residential	✓	✓	✓	✓	1993-07-01	JLG
04-021-3001	Apache Junction	PCAQCD	525	Commercial	✓				1987-01-01	AJ
04-021-8001	Queen Valley	ADEQ	634	Desert	✓		✓		2001-01-01	QV

3 Current air quality

3.1 Exceedances impacted by wildfires

Table 3-1 lists the dates that were possibly impacted by wildfire smoke in recent years. These dates have been agreed upon by all agencies in the region (ADEQ, MAG, MCAQD and PCAQCD), and may be excluded from some analyses.

Table 3-1 Possible wildfire-impacted ozone exceedance dates occurring in 2017-2024.

2017	2018	2019	2020	2021	2022	2023	2024
6/16/2017	7/26/2018	6/8/2019	6/1/2020	6/11/2021	4/25/2022	5/14/2023	5/12/2024
6/19/2017	7/27/2018	6/9/2019	6/11/2020	6/12/2021	4/26/2022	5/15/2023	5/22/2024
6/20/2017	7/28/2018	6/12/2019	8/17/2020	6/15/2021	4/29/2022	5/16/2023	6/3/2024
6/21/2017	7/29/2018	6/14/2019	8/18/2020	6/16/2021	4/30/2022	5/21/2023	6/5/2024
7/7/2017	7/31/2018	6/15/2019	8/19/2020	6/18/2021	6/15/2022	6/17/2023	6/6/2024
8/30/2017	8/1/2018	6/23/2019	8/20/2020	6/28/2021	6/16/2022	6/22/2023	6/14/2024
9/1/2017	8/2/2018	6/24/2019	8/21/2020	6/29/2021	6/21/2022	6/23/2023	6/15/2024
9/7/2017	8/3/2018	6/25/2019	8/23/2020	7/1/2021	6/22/2022	6/24/2023	07/08/24
	8/6/2018		8/24/2020	7/13/2021	7/13/2022	6/25/2023	07/09/24
	8/7/2018		8/25/2020	7/14/2021	7/14/2022	6/26/2023	07/10/24
	8/8/2018		8/26/2020	7/17/2021	7/15/2022	6/30/2023	07/11/24
	8/9/2018		8/27/2020	7/19/2021	7/16/2022	7/1/2023	07/12/24
	8/10/2018		8/28/2020	7/20/2021	7/17/2022	7/2/2023	07/13/24
	8/11/2018		9/15/2020	7/21/2021	7/18/2022	7/7/2023	07/15/24
	8/12/2018		9/16/2020	7/22/2021	7/22/2022	7/8/2023	07/17/24
	8/13/2018		9/18/2020	7/27/2021	7/23/2022	7/18/2023	07/18/24
			9/20/2020	7/28/2021		7/19/2023	07/19/24
			9/21/2020	7/30/2021		7/21/2023	07/22/24
				7/31/2021		7/22/2023	07/23/24
				8/3/2021		7/23/2023	07/24/24
				8/4/2021		7/24/2023	07/25/24
				8/5/2021		7/25/2023	07/26/24
				8/6/2021		7/26/2023	07/30/24
				8/17/2021		7/27/2023	07/31/24
				8/24/2021		7/28/2023	8/5/2024
				8/25/2021		7/29/2023	8/7/2024
				8/26/2021		7/31/2023	8/9/2024
				8/27/2021		8/1/2023	9/11/2024
				9/5/2021		8/17/2023	10/3/2024
						8/18/2023	
						8/22/2023	

3.2 Design values

Figure 3-1 presents the annual peak 8-hour ozone design values in the Maricopa 8-hour ozone nonattainment area from 2000 through 2024, as well as the design value (DV) trends. Although the annual peak DV has bounced back recently, the DV has decreased at a rate of 0.3 ppb per year over the past 25 years. Excluding wildfire-impacted days (see Section 3.1) from the design value calculation, the DV has a more rapidly decreasing trend at a rate of 0.5 ppb per year.

The 8-hour ozone design values at the 26 ozone monitors in the Maricopa 8-hour ozone nonattainment area from 2000 to 2024 are illustrated in Figure 3-2. Since 2000, annual peak design values have occurred at the following eight sites: North Phoenix (11 times), Pinnacle Peak (7 times), Mesa (5 times), Humboldt Mountain (4 times), JLG Supersite (2 times), Red Mountain (2 times), Glendale (1 time), Lehi (1 time), and Rio Verde (1 time). Excluding wildfire-impacted days from the design value calculation, annual peak design values have occurred at the following seven sites: North Phoenix (9 times), Mesa (6 times), Humboldt Mountain (4 times), Pinnacle Peak (3 times), Red Mountain (2 times), Falcon Field (2 times), Lehi (2 times), JLG Supersite (1 time), South Scottsdale (1 time), and Rio Verde (1 time). Buckeye has consistently recorded the regional minimum design values. Among the 14 ozone monitors operating for the entire period of 2000-2024, the highest elevation site Humboldt Mountain had the largest ozone decrease of 0.012 ppm and JLG Supersite had an ozone increase of 0.002 ppm. Excluding wildfire-impacted days, Humboldt Mountain had the largest ozone decrease of 0.016 ppm and JLG Supersite had the smallest ozone decrease of 0.002 ppm.

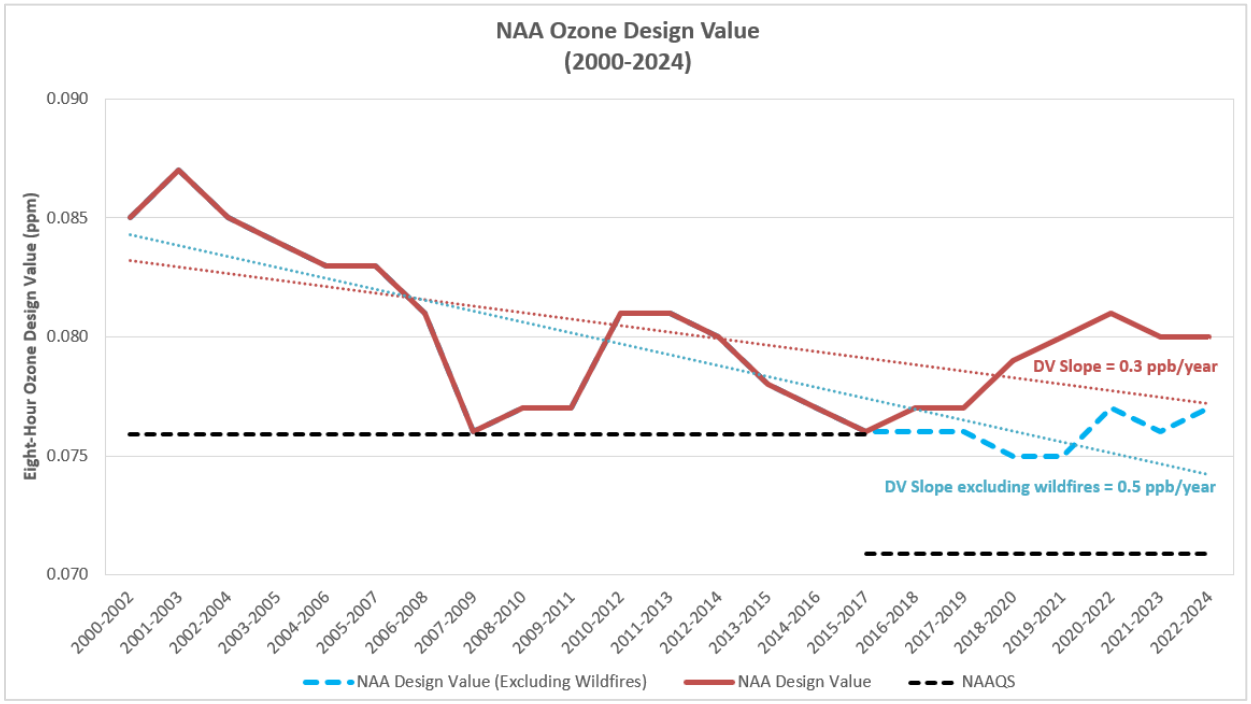

Figure 3-1 Peak 8-hour ozone design values in the Maricopa 8-hour ozone nonattainment area from 2000 through 2024.

a)

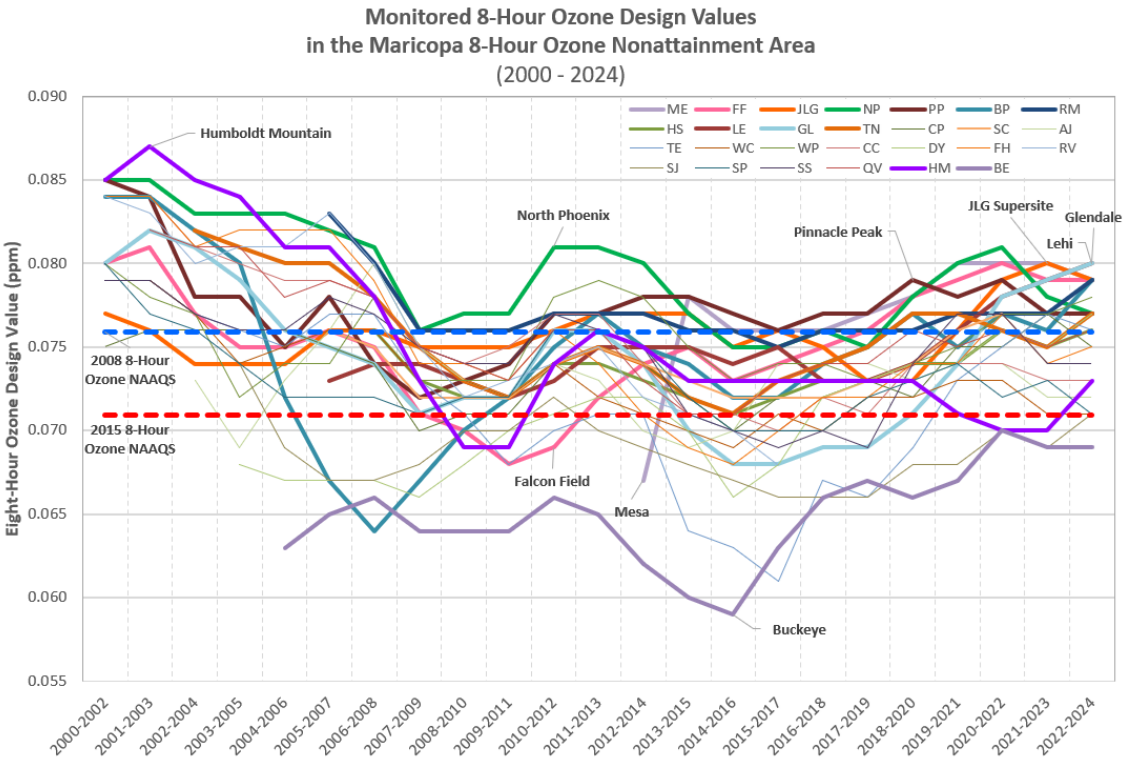

b)

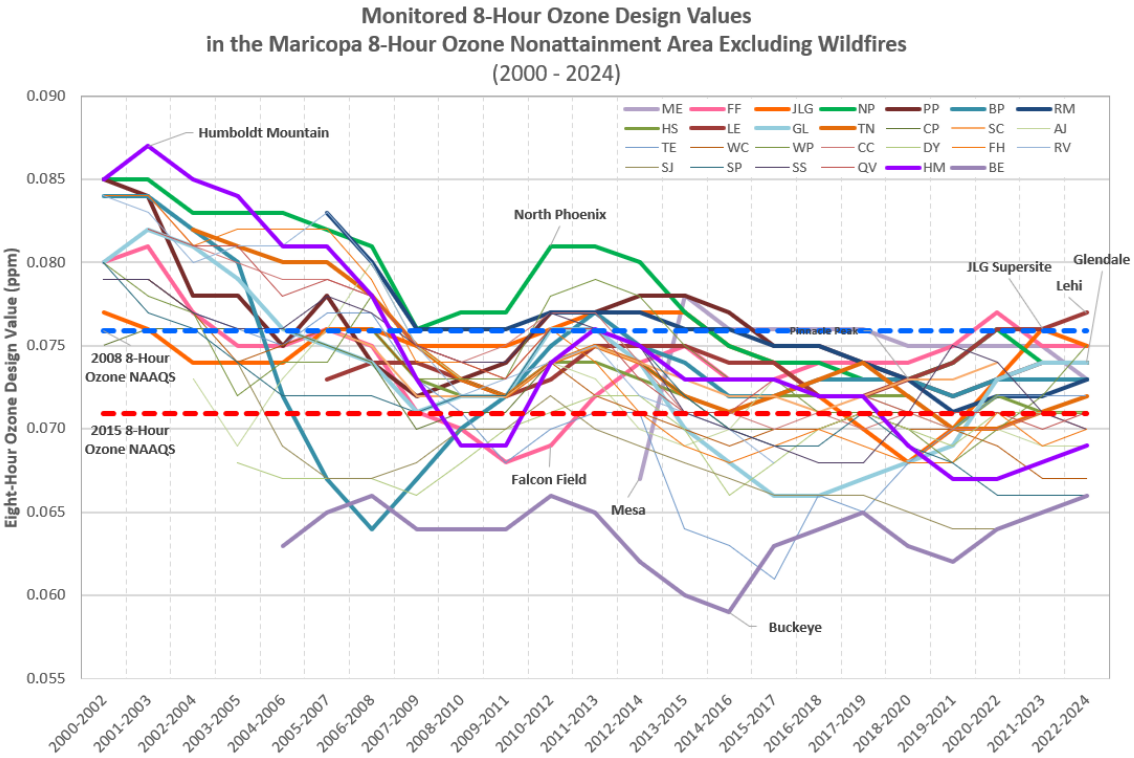

Figure 3-2 8-hour ozone design values of monitors in the Maricopa 8-hour ozone nonattainment area from 2000 through 2024, for a) all days and b) excluding exceedance days impacted by wildfires.

3.3 Exceedances

Due to continuous efforts to reduce anthropogenic emissions by applying federal and local emissions control measures, the number of high-ozone days (MDA8 ozone above 70 ppb) at any monitoring site in the Maricopa 8-hour ozone nonattainment area has continued to decrease over the past 25 years as shown in Figure 3-3. The number of exceedances was highest in 2000 and lowest in 2009. Although the number of high-ozone days fluctuates from year to year, there is a decreasing trend. Splitting the record into five averaging periods (5 years each), as shown in Figure 3-4, reveals a clear downward trend. Comparing 2000-2004 averages with 2020-2024 averages, the number of exceedances has decreased by 62%.

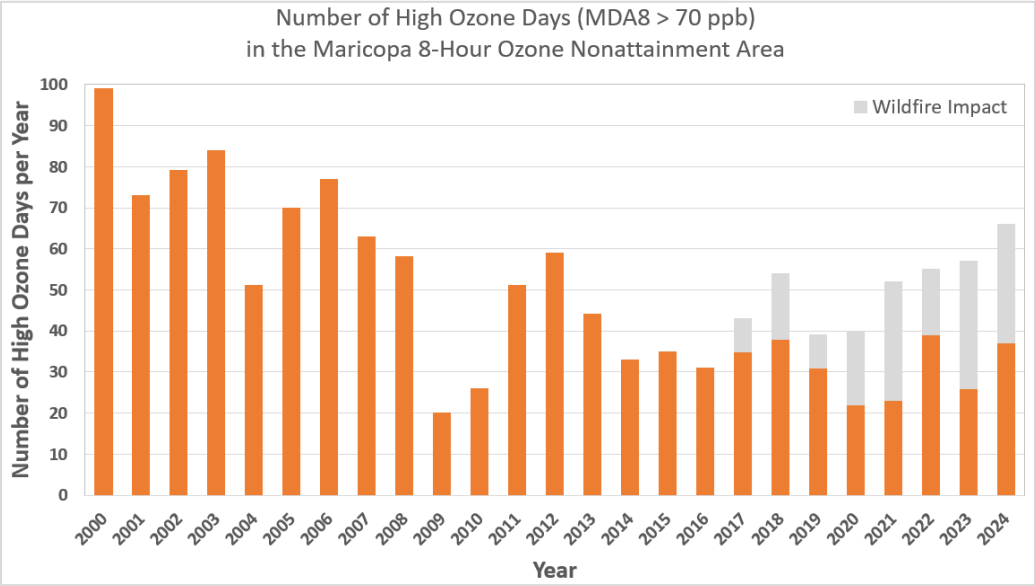

Figure 3-3 Number of 8-hour ozone exceedances (MDA8 ozone above 70 ppb) at monitors in the Maricopa 8-hour ozone nonattainment area.

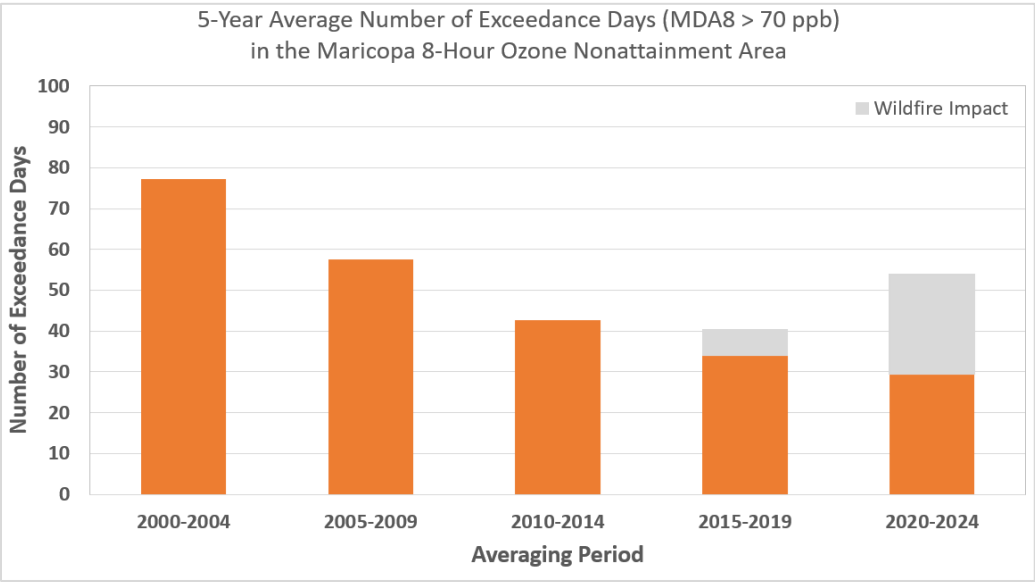

Figure 3-4 Periodic (five-year) average number of ozone exceedances (MDA8 ozone above 70 ppb) at monitors in the Maricopa 8-hour ozone nonattainment area.

3.4 Spatial analysis

For each monitoring site, the annual average number of high-ozone days (MDA8 ozone above 70 ppb) from 2000 through 2024 is shown in Figure 3-5. The high-ozone days occurred most frequently at the North Phoenix site and least frequently at the Buckeye site. Figure 3-5 arranges the monitoring sites in ascending order of annual frequency of high-ozone days, and categorizes them into three groups: 1) low frequency of occurrence (less than 5 days/year); 2) middle frequency; and 3) high frequency (greater than or equal to 15 days/year), shown as blue, green and orange bars respectively. The monitoring sites in each group appear to be spatially related, and can be classified according to their location relative to the daytime prevailing wind pattern from west to east. Monitors with a low frequency of high-ozone days are located in areas upwind of the urban core (west and south of Phoenix), middle frequency monitors are located in the urban core, and high frequency monitors are located in areas downwind of the urban core (east or northeast of Phoenix), with the exception of North Phoenix. Although the North Phoenix site is located in the urban core, the number of high-ozone days at that site is significantly higher than other urban sites. The reason for this is an area for further research.

a)

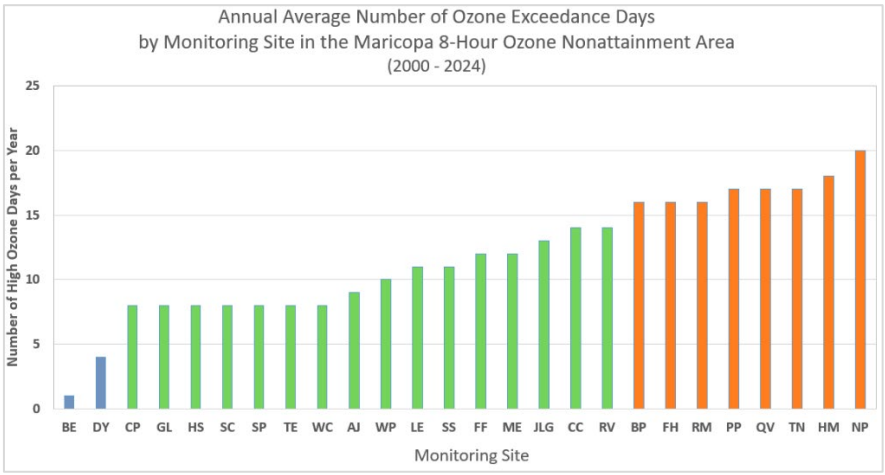

b)

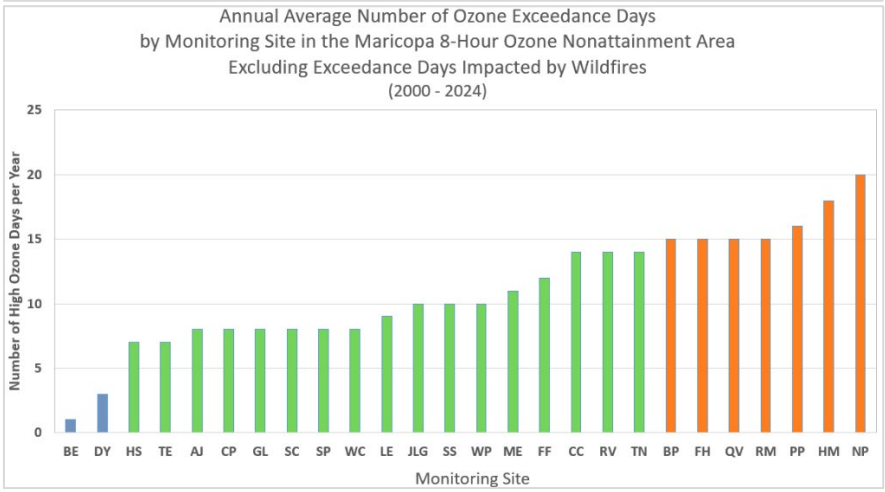

Figure 3-5 Annual average number of high-ozone days with MDA8 ozone above 70 ppb by monitoring site and the Maricopa 8-hour ozone nonattainment area from 2000 to 2024, for a) all days and b) excluding exceedance days impacted by wildfires.

Poor air quality in the area due to elevated ozone is rarely localized to a single monitor and often occurs at many monitors on the same day. The Phoenix metropolitan area includes several major cities and is the core of the nonattainment area. Networks of freeways and arterial roads and several significant point sources exist in the urban core. The edges of the nonattainment area are considered suburban or rural, and monitoring sites in these zones are typically in more remote or mountainous locations. Ozone can be transported by advection downwind of the urban core to surrounding rural and suburban sites and these regions can have different profiles than those in the urban core. The coupling of the urban and downwind sites depends greatly on how the daily weather conditions interact with local emissions.

In order to improve understanding of high ozone situations in this region, high-ozone days having regional peak MDA8 ozone concentrations above 70 ppb in the Maricopa 8-hour ozone nonattainment area were categorized based on how many sites have exceedances: a) single site; b) ≤ 50% of sites; and c) > 50% of sites. To evaluate the relationship between the number of site exceedances and ozone concentration, the annual average of regional peak MDA8 ozone concentrations was computed for these three groups as shown in Figure 3-6. There is a strong

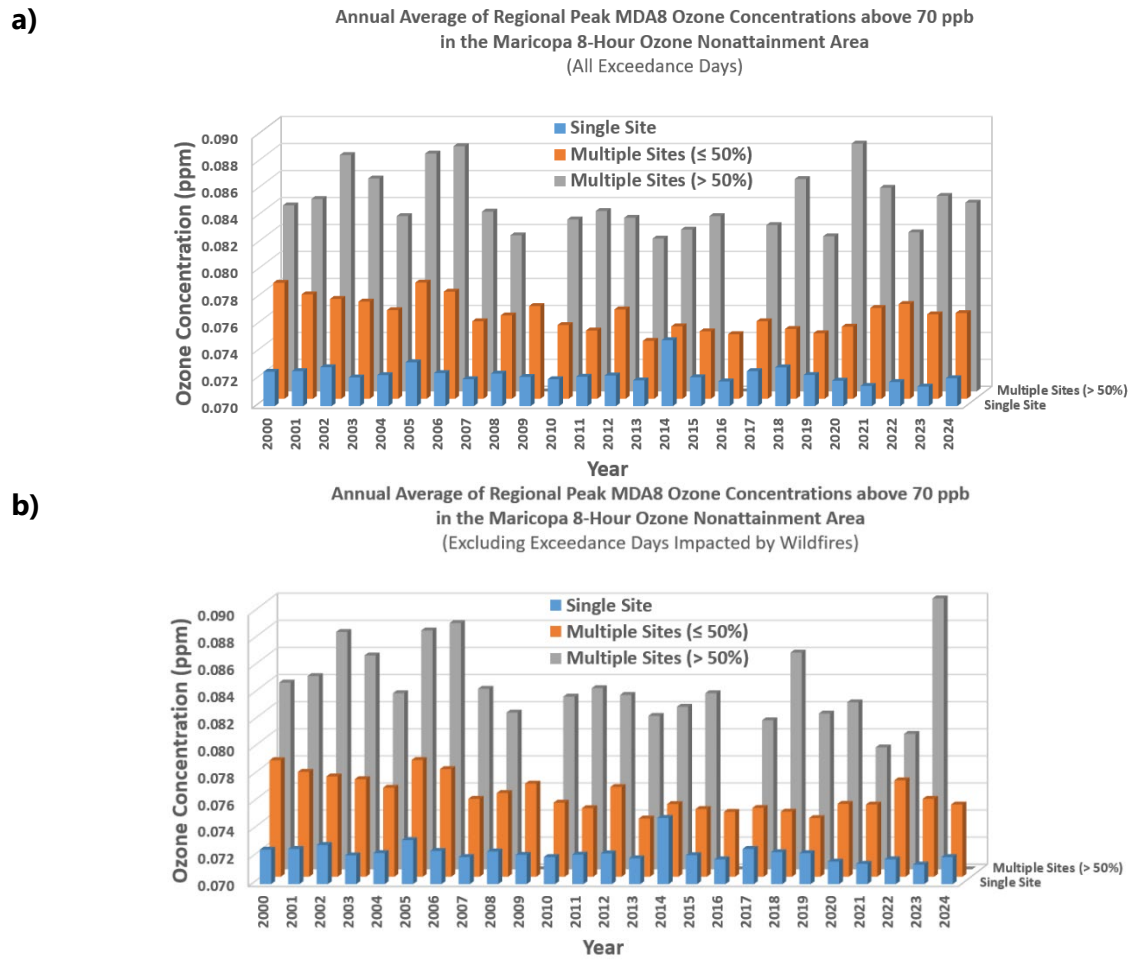

Figure 3-6 Annual average of regional peak MDA8 ozone concentrations above 70 ppb in the Maricopa 8-hour ozone nonattainment area (grouped by number of sites with exceedance), for a) all days and b) excluding exceedance days impacted by wildfires.

correlation between the number of site exceedances and ozone concentrations. In the Maricopa 8-hour nonattainment area, the highest regional peak MDA8 ozone concentrations were recorded on days where exceedances occurred at the largest numbers of sites. Such widespread exceedance conditions indicate that the degree of ozone concentration on ozone exceedance days is highly associated with regional ozone transport and impacted by large-scale weather regimes. This is an area for further research. But in 2009 and 2016, there are no multiple-site exceedances involving more than 50% of all sites due to weakness of transported ozone events.

For the annual peak-ozone days in the Maricopa 8-hour ozone nonattainment area (listed in Table 3-2), the MDA8 ozone data for all ozone monitors in the United States were obtained from AQS, annual percentile rank of MDA8 ozone for each site was calculated, and annual percentiles were spatially interpolated to generate raster surface maps using an inverse distance weighted (IDW) interpolation technique in ArcGIS. Spatial surface maps for the contiguous United States on the annual peak-ozone days in the Maricopa 8-hour ozone nonattainment area from 2000 through 2024 are shown in Figure 3-7.

These spatial surface maps provide detailed information regarding spatial variability in terms of the factors contributing to high ozone levels.

Comparing spatial surface maps over the years, there is a notable feature: when the annual peak-ozone day occurs in the Maricopa 8-hour ozone nonattainment area, multiple states record substantially elevated ozone levels. This spatial pattern may indicate elevated ozone levels are highly correlated with the regional weather conditions.

On peak-ozone days, elevated ozone levels occurred mostly in the central Phoenix urban area and downwind rural areas in the northwestern portion of Maricopa County, and ozone exceedances were observed at multiple monitoring sites. Ozone levels at Buckeye, in an upwind rural area, are consistently the lowest in the Maricopa 8-hour ozone nonattainment area. However, this does not imply that airflows in the upwind area are always clean as there may be impacts from long-range transport for California on local ozone levels. The surface monitor data is not sufficient to evaluate long-range transport impacts.

Table 3-2 Annual peak-ozone days in the Maricopa 8-hour ozone nonattainment area excluding exceedance days impacted by wildfires.

Year	Date	Regional Peak MDA8 Ozone Site	Peak MDA8 Ozone (ppm)
2000	August 10	JLG Supersite	0.093
2001	August 10	Cave Creek	0.099
2002	July 11	West Phoenix	0.102
2003	July 22	Blue Point	0.103
2004	July 27	North Phoenix	0.087
2005	July 20	Tonto National Monument	0.098
2006	July 19	West Phoenix	0.096
2007	August 15	Red Mountain	0.085
2008	June 13	Queen Valley	0.085
2009	July 2	West Phoenix	0.082
2010	June 23	North Phoenix	0.085
2011	June 9	Blue Point	0.092
2012	May 14	North Phoenix	0.091
2013	July 17	Mesa	0.086
2014	June 6	Falcon Field	0.088
2015	June 29	Falcon Field	0.084
2016	July 21	Mesa	0.079
2017	June 14	Tonto National Monument	0.090
2018	July 17	West Phoenix	0.086
2019	July 25	Mesa	0.084
2020	May 6	Falcon Field	0.084
2021	August 28	Mesa	0.082
2022	August 23	JLG Supersite	0.089
2023	May 17	Lehi	0.090
2024	May 30	Tonto National Monument	0.082

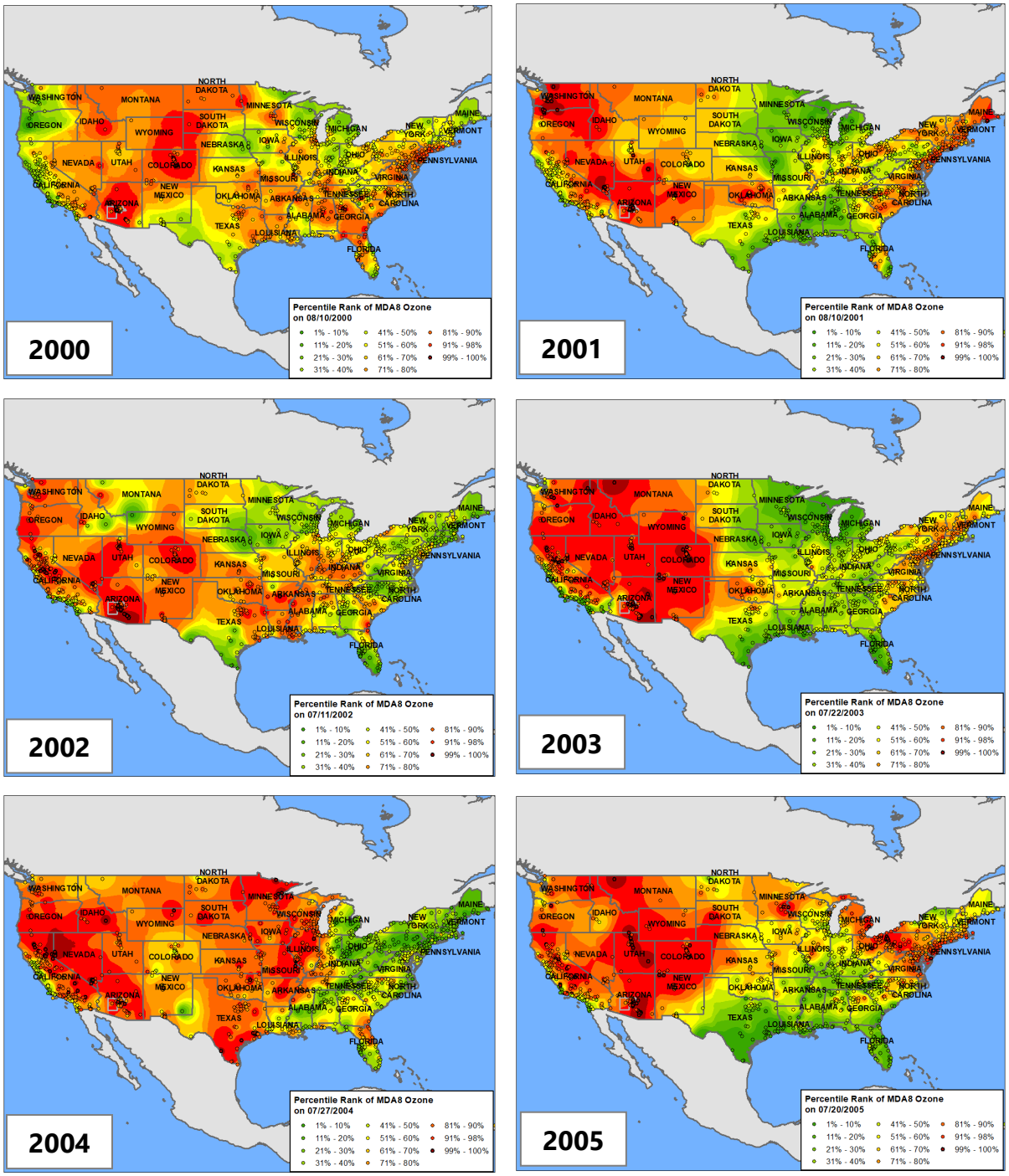

Figure 3-7 Contour plots of annual percentile rank of MDA8 ozone concentration on annual peak-ozone day in the Maricopa 8-hour ozone nonattainment area from 2000 through 2024.

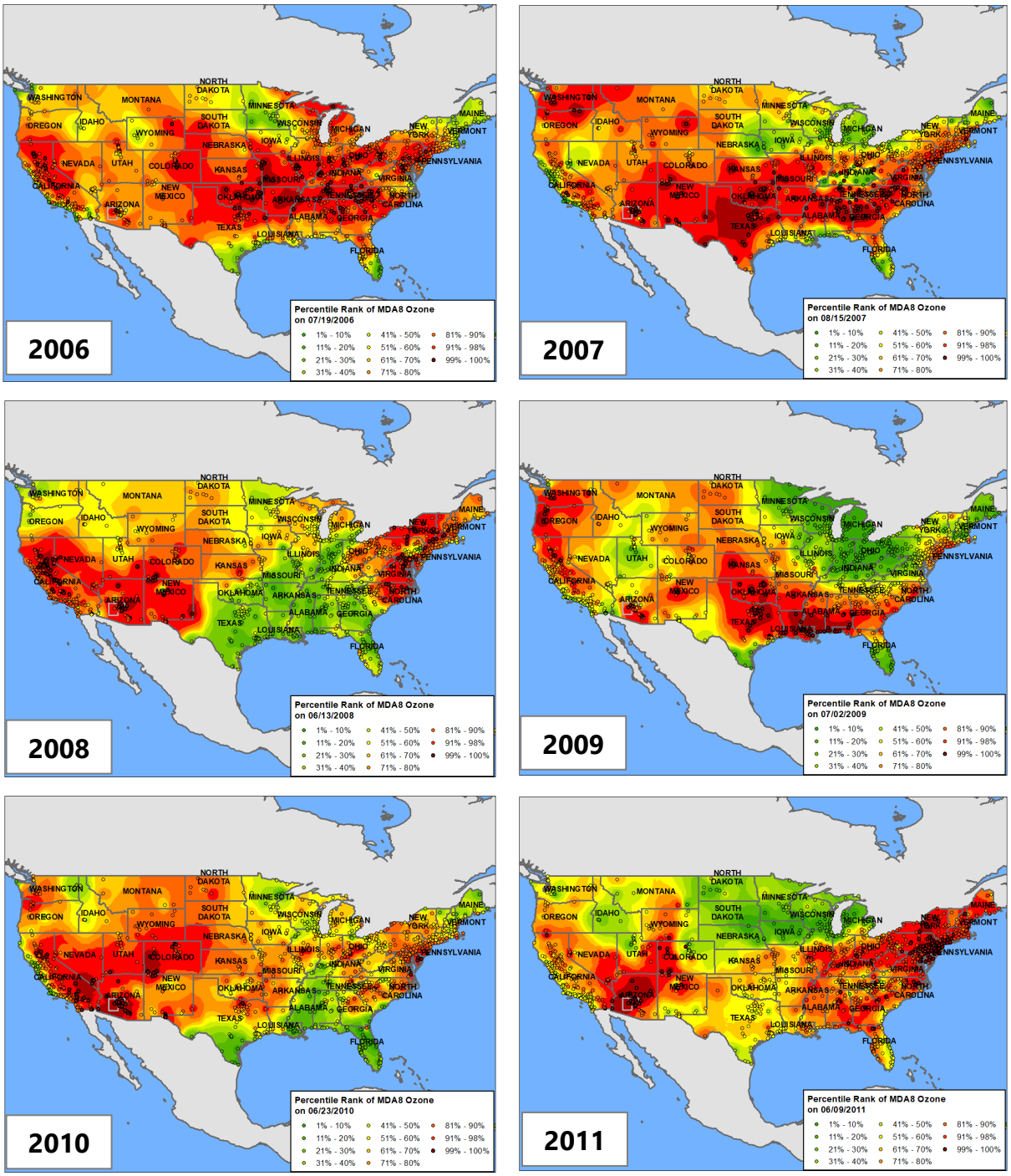

Figure 3-7 Continued.

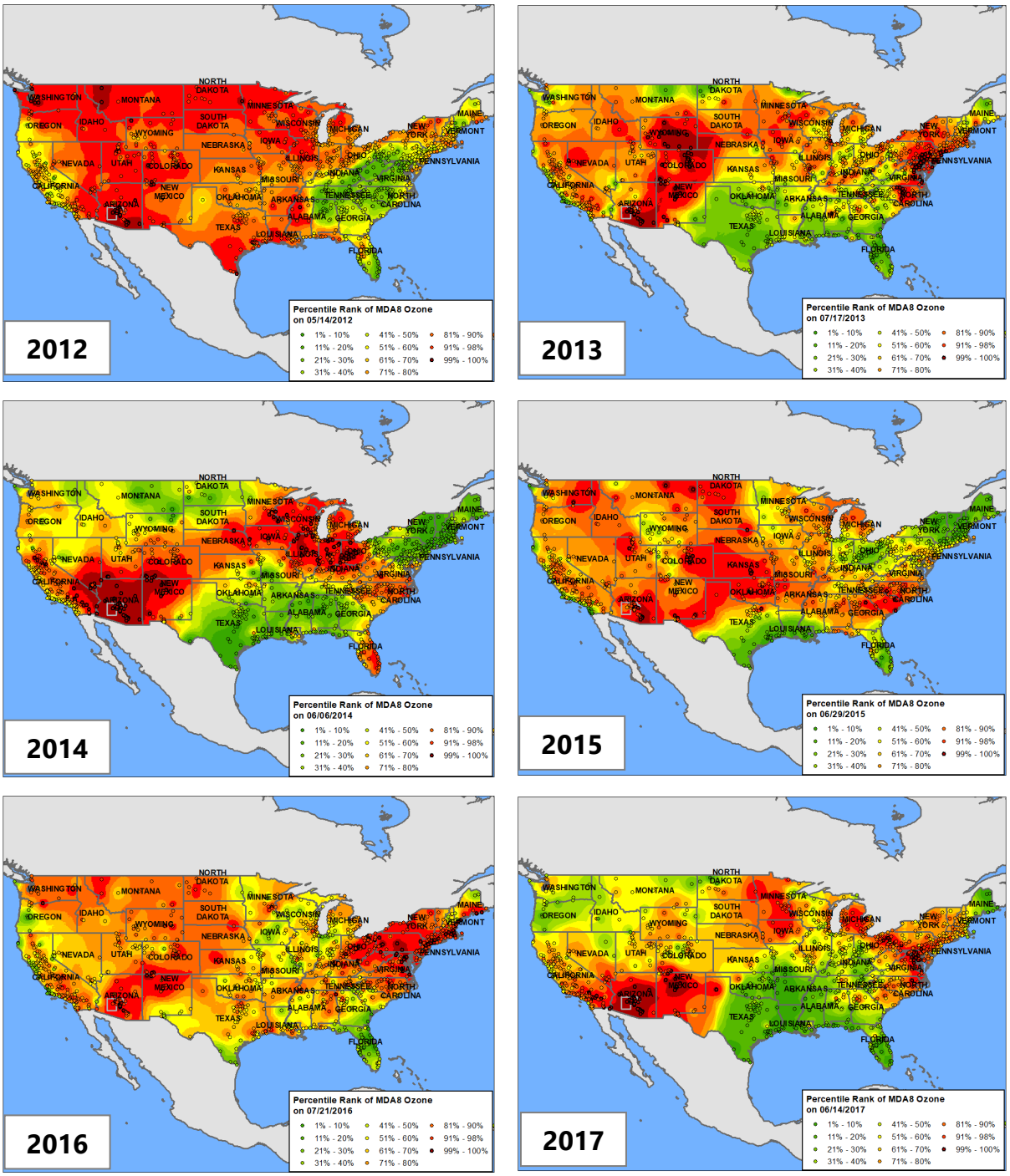

Figure 3-7 Continued.

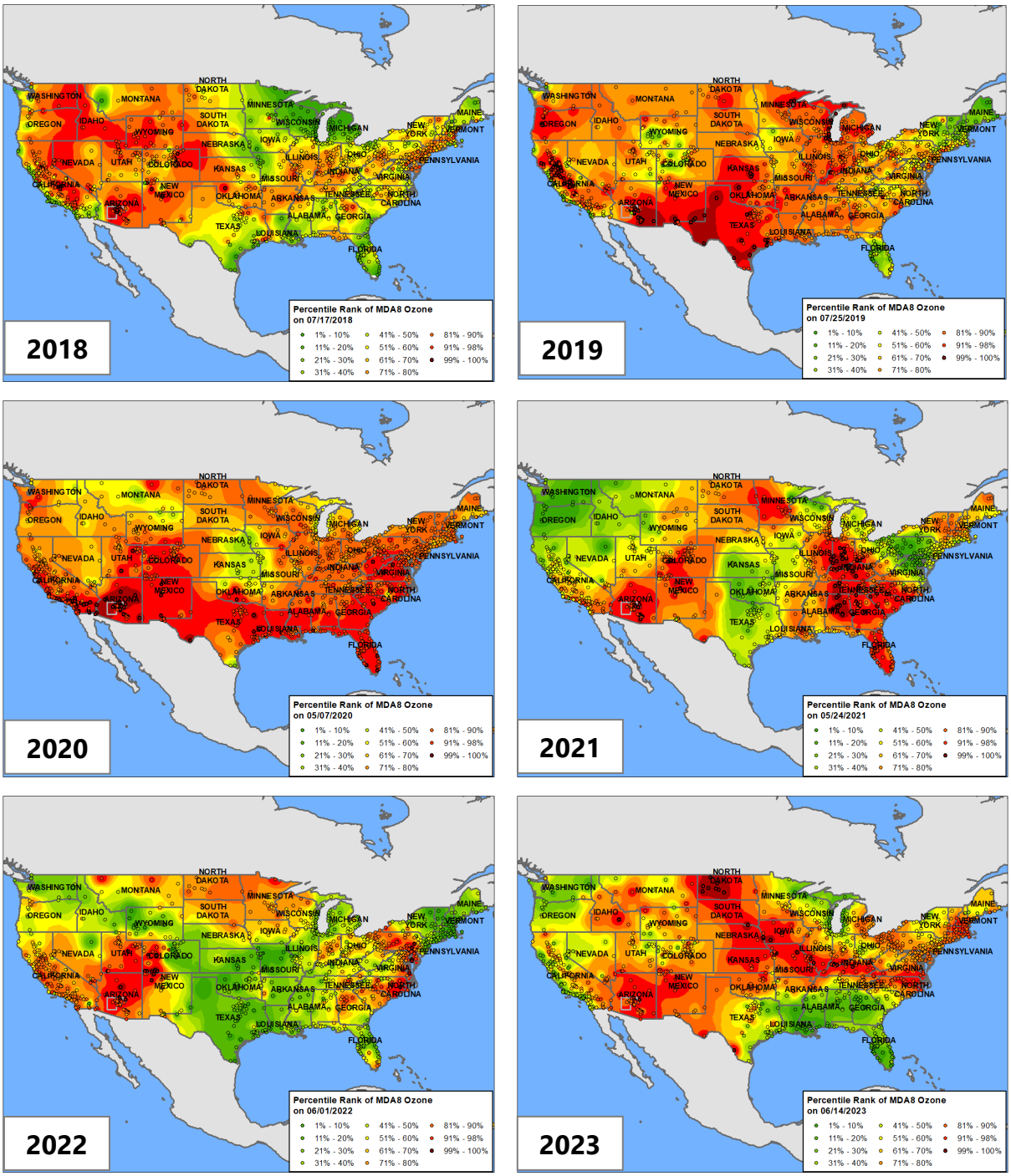

Figure 3-7 Continued.

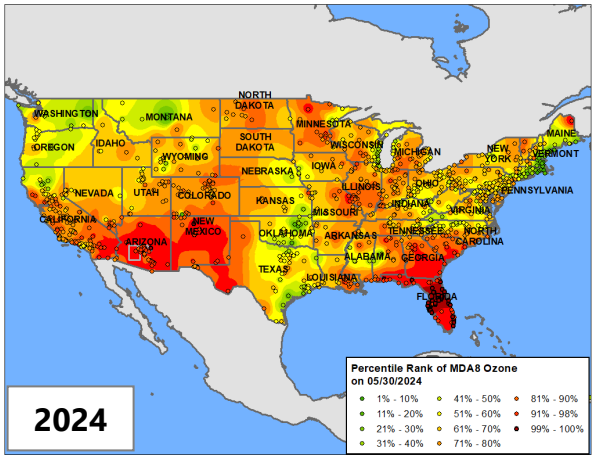

Figure 3-7 Continued.

3.5 Temporal analysis

3.5.1 Seasonal patterns

The accumulated number of high-ozone days by month at ozone monitors in the Maricopa 8-hour ozone nonattainment area is shown in Figure 3-8. Over the past 21 years, ozone exceedances (MDA8 ozone above 70 ppb) occurred not only in the ozone season, which extends from April through September, but also in February, March, and October. However, ozone exceedances outside of the ozone season have not occurred since 2008, except 2024.

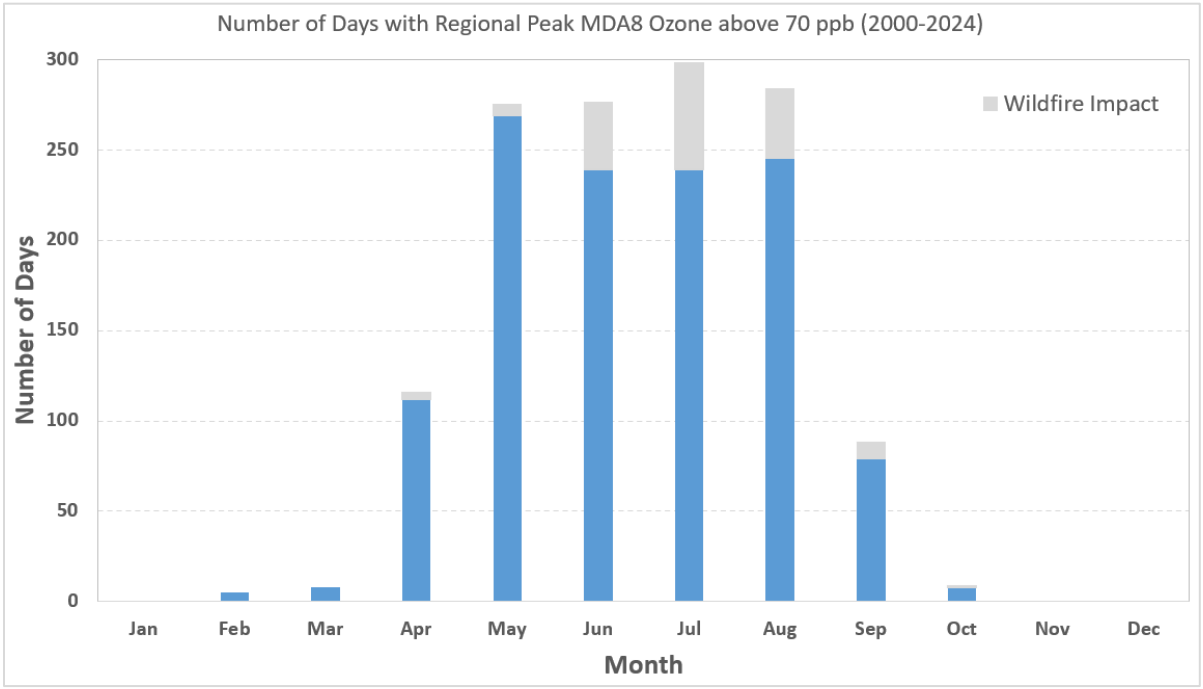

Figure 3-8 Number of days in the 2000-2024 period with regional peak MDA8 ozone concentration above 70 ppb.

3.5.2 Daily patterns

Ozone exceedances are highly influenced by anthropogenic emissions, which vary by day of week, and exhibit lower emissions on the weekends due to fewer industrial, commercial and traffic activities.

The number of high-ozone days (MDA8 above 70 ppb) on each day of the week from 2000 through 2024 is shown in Figure 3-9. The red line on the chart indicates the average number of high-ozone days, which is 172 days. High-ozone days occur most frequently on Thursdays and least frequently on Sundays. Over the past 25 years, only Sunday experienced substantially below-average numbers of ozone exceedance days. Although Saturday belongs to the weekend, it experienced comparable numbers of high-ozone days to Monday. This indicates that the level of anthropogenic activity occurring on Saturday is similar to that of a weekday.

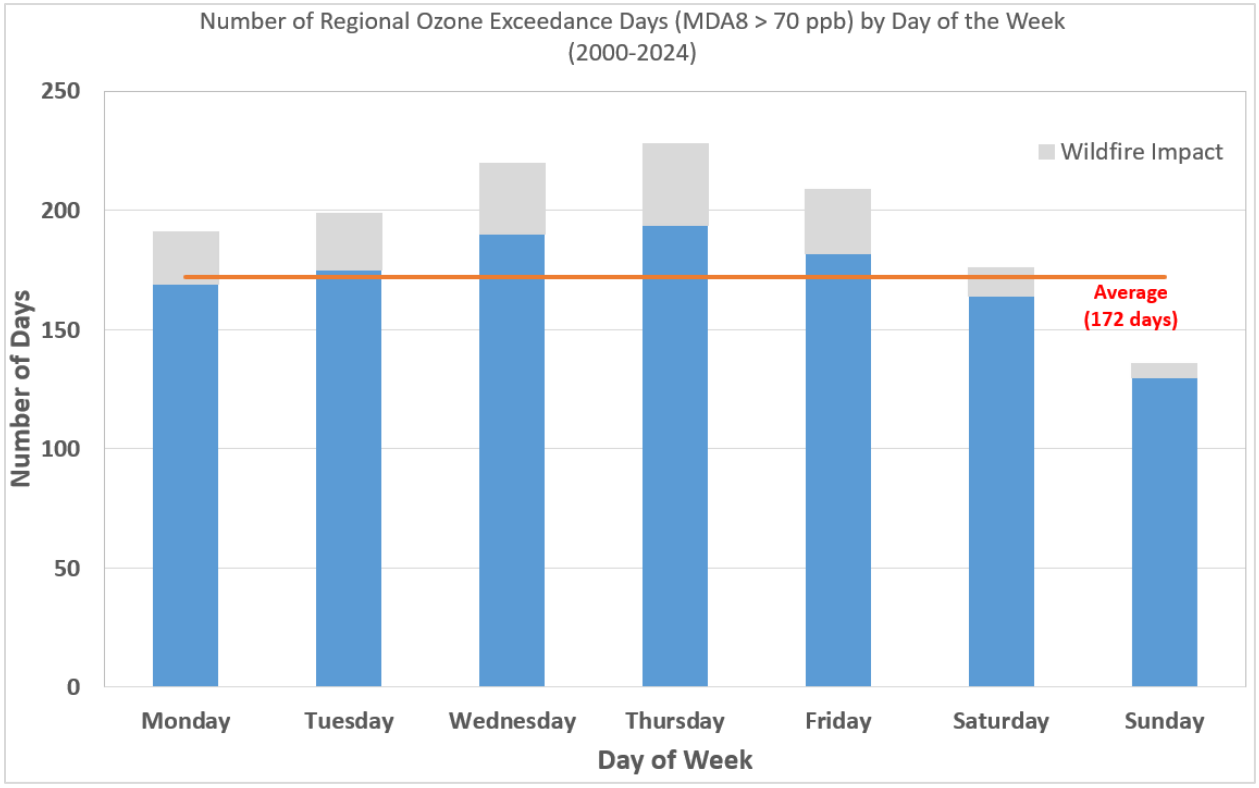

Figure 3-9 Number of regional high-ozone days (MDA8 ozone > 70 ppb) for each day of the week.

3.5.3 Diurnal patterns

Each monitoring site within the nonattainment area exhibits a diurnal pattern in ozone levels, but the timing and magnitude depend on locations. Urban sites exhibit a more pronounced diurnal cycle in ozone, with the maximum occurring in late afternoon before sunset and the minimum just prior to sunrise. Ozone can be consumed by titration from locally generated NO_X in the urban core and also removed by dry deposition during night. In contrast, maximum ozone concentrations have been measured hours later at downwind rural sites. Most anthropogenic

precursors are emitted from the urban core and follow a diurnal pattern related to traffic patterns that peak twice daily with the AM and PM rush hours.

The average 1-hour ozone concentrations at each monitoring site when MDA8 is above 70 ppb is shown in Figure 3-10. All monitors observe the lowest 1-hour ozone just before sunrise at 5 AM or 6 AM, except Humboldt Mountain, which has the lowest 1-hour ozone at 8 AM. The ozone monitor at Humboldt Mountain is located at the highest altitude of 1,582 m and is above the nocturnal inversion (see Section 5.3.4). This site experienced relatively high ozone concentrations above 60 ppb during nighttime, which were much higher than other monitors located at lower elevations. Considering the lack of sunlight required for photochemical ozone production, the high ozone levels at Humboldt Mountain during nighttime hours indicate the presence of a significant ozone reservoir above the nocturnal inversion layer, which was produced over other areas during daytime and then transported to Humboldt Mountain. Compared with rural monitoring sites, the urban monitoring sites have lower ozone profiles during the nighttime and more rapid ozone elevation after sunrise. This may reflect that photochemical production was induced by residual primary and secondary pollutants accumulated overnight from urbanized sources, and new emissions produced locally after sunrise, along with the down-mixing of the ozone reservoir from higher altitudes to the surface.

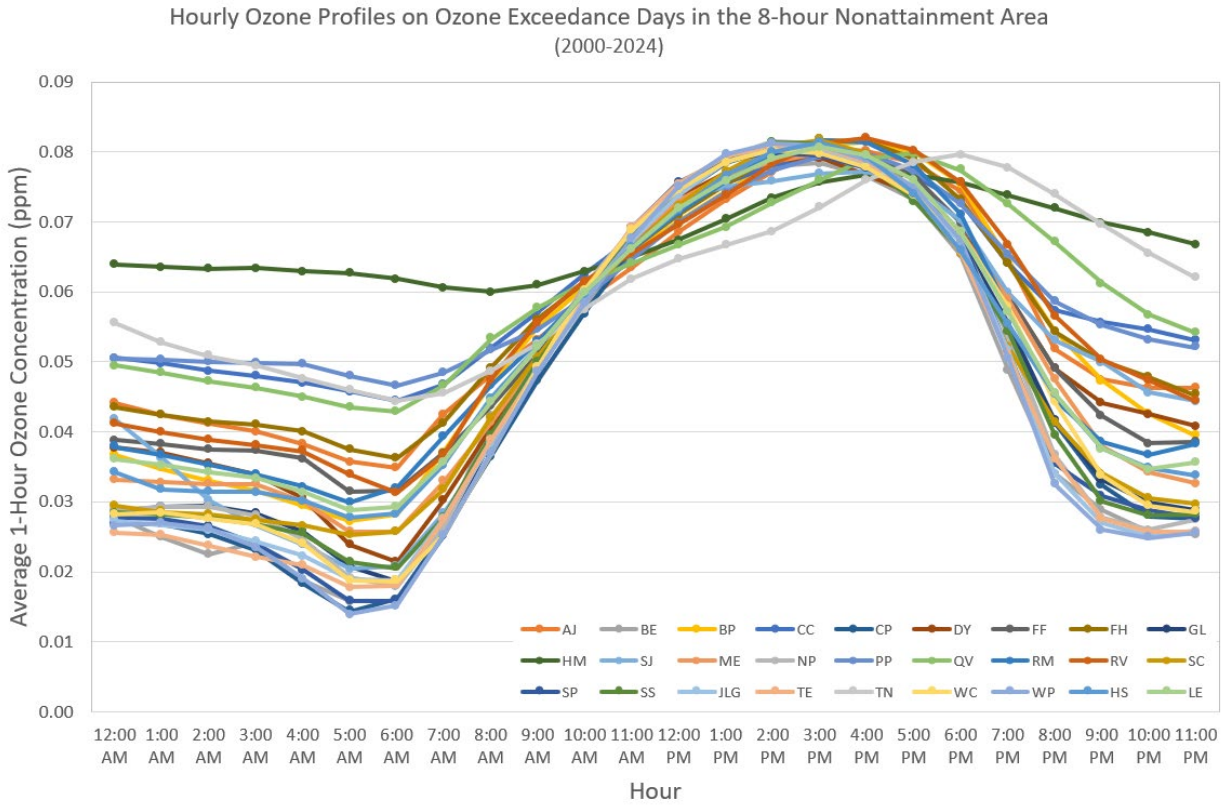

Figure 3-10 Average 1-hour ozone concentration by hour when MDA8 > 70 ppb by monitoring site, excluding exceedance days impacted by wildfires.

To determine the reason for the difference in patterns for rural and urban monitoring sites, MDA1 NO_2 concentrations during ozone season (April-September) were compared with MDA8 ozone concentrations for two representative monitoring sites: JLG Supersite in the urban area and Tonto National Monument in a rural area. Since only a few monitoring sites measure NO_2 in this region, those two representative sites were selected based on NO_2 data availability. As shown in Figure 3-11, over the entire 2000-2024 period, weekend NO_2 concentrations were lower than weekdays at all monitoring sites, while JLG Supersite had higher ozone concentrations on weekends than weekdays and Tonto National Monument had lower ozone concentrations on weekends. JLG Supersite experiences a typical pattern for a VOC-limited area, where ozone increases as NO_X decreases. Conversely, Tonto National Monument experiences a typical pattern for NO_X-limited areas, where ozone decreases as NO_X decreases.

a)

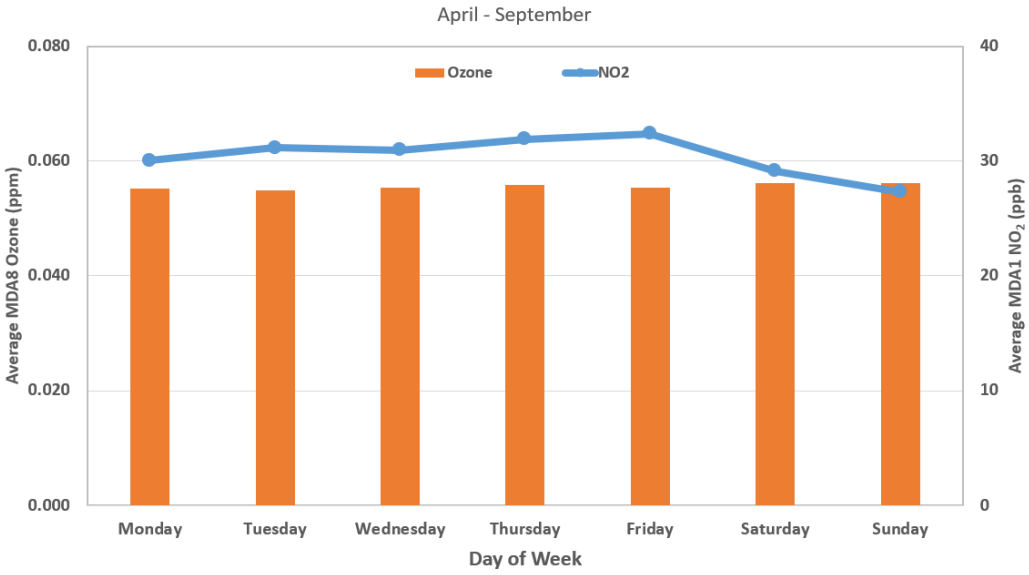

b)

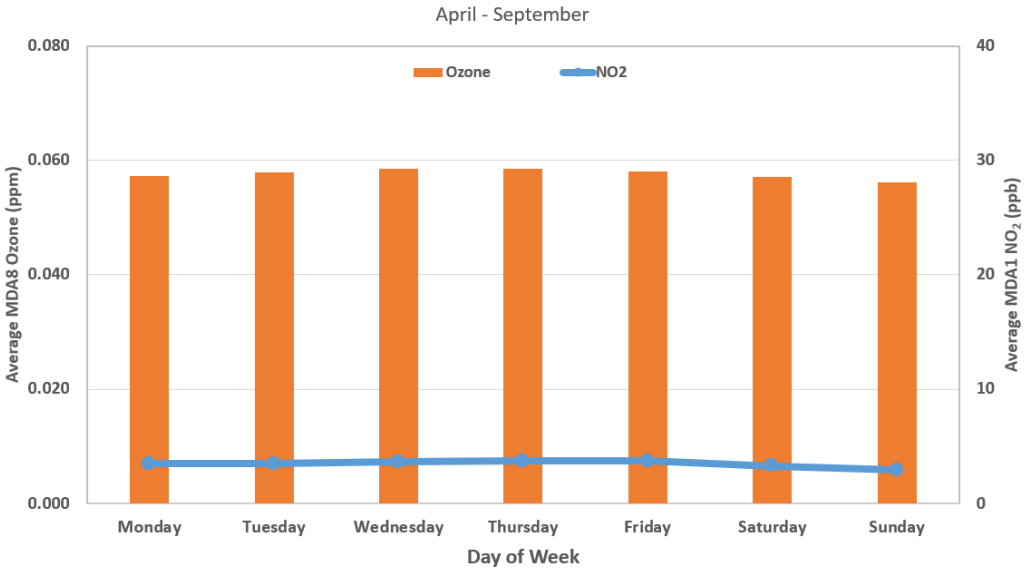

Figure 3-11 Seasonal average MDA8 ozone and MDA1 NO_2 in the ozone season (April-September) at a) JLG Supersite and b) Tonto National Monument, excluding exceedance days impacted by wildfires.

A significant difference exists between daytime and nighttime ozone in the city because of intensive local emissions of NO_X. The nighttime ozone concentration may drop to very low levels due to strong NO_X titration.

MDA8 ozone concentrations are first observed at upwind monitors (Buckeye and Dysart) around 10 AM, then at urban core area monitors (Central Phoenix and JLG Supersite) in late morning about 11 AM, and at downwind monitors (Humboldt Mountain and Tonto Monument) in early afternoon at 1 PM. The time of daily maximum 8-hour average ozone concentrations shifts about 3 hours from the West Valley to the East Valley.

4 Emissions

4.1 Anthropogenic emissions

Anthropogenic sources include stationary point sources such as power plants and industrial facilities, onroad and nonroad mobile sources, and various area sources. Based on data from previous Periodic Emissions Inventory (PEI) for Ozone Precursors (covering the years 2005, 2008, 2011, 2014, 2017, and 2020) and the draft emission inventory for 2023, the total VOC and NOx from all these anthropogenic sources are summarized in Table 4-1 for the Maricopa County during the ozone season. The ozone season daily anthropogenic emissions trends in Maricopa County from 2005 to 2023 are illustrated in Figure 4-1.

Table 4-1 Ozone season daily anthropogenic emissions (tons/day) for Maricopa County for 2005, 2008, 2011, 2014, 2017, 2020 and 2023.

Pollutant	2005	2008	2011	2014	2017	2020	2023
VOC	311.98	287.14	246.13	201.93	194.05	175.04	163.10
NOx	311.54	259.70	252.02	177.72	158.27	126.10	92.75

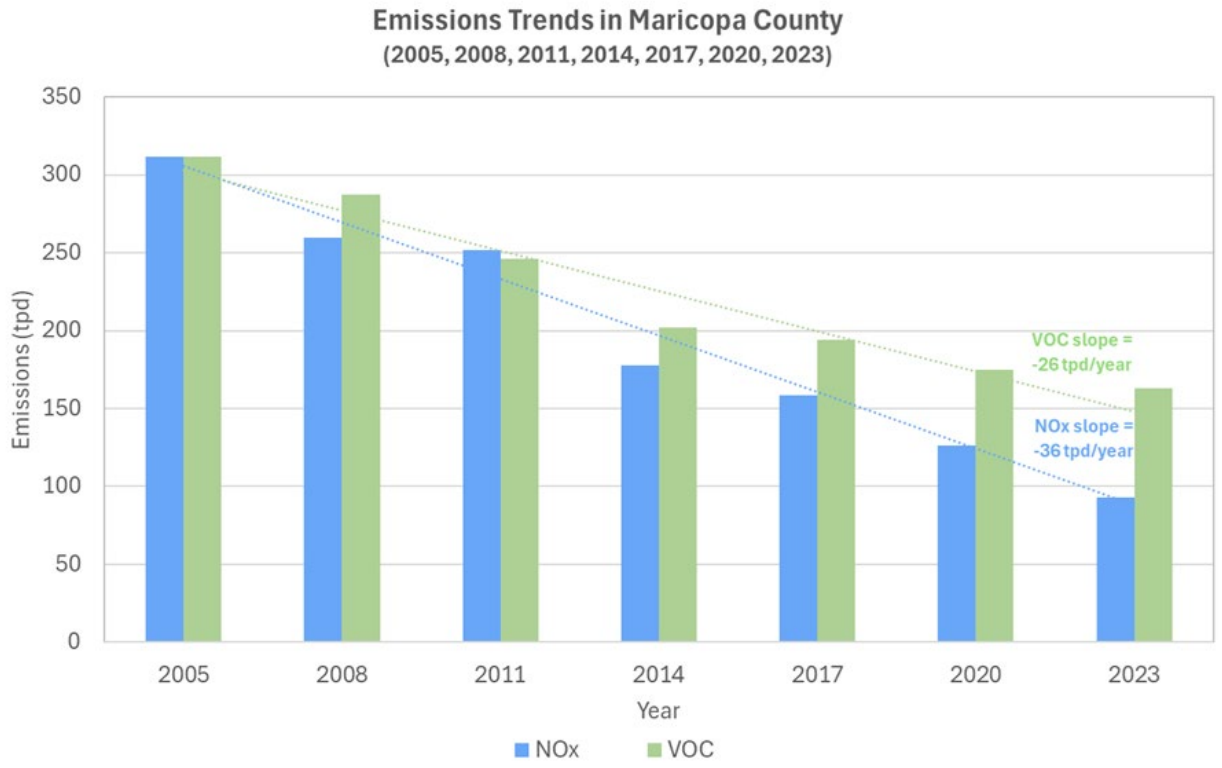

Figure 4-1 Ozone season daily anthropogenic emissions trends in Maricopa County from 2005 to 2023.

4.2 Biogenic sources

Biogenic emissions are the largest VOC source, and are mostly from forests and agricultural areas. These emissions mix with significant urban anthropogenic VOC sources. Naturally occurring VOC levels vary over the course of the ozone season, and biogenic emissions highly depend on meteorology (i.e. sunlight, temperature, and relative humidity).

4.3 Wildfires

Wildfires are considered to be in the nonpoint category for PEI reporting, however for air quality modeling they may be considered as temporary point sources whose transported plumes can disperse ozone precursors from very distant downwind locations. The western United States was heavily impacted by multiple large wildfires in 2020, including the Bush fire that burned over 190,000 acres in Maricopa and Gila Counties. This was the fifth largest wildfire in Arizona history and it had a tremendous impact on total VOC emissions in 2020.

4.4 Regional background emissions

U.S. Background (USB) includes all global natural sources (like stratospheric intrusion, lightning, wildfires, and biogenics) and anthropogenic sources of ozone from outside the United States. High background contributions make local ozone less responsive to local emission controls. CAMx and CMAQ source apportionment modeling done by MAG estimates that contributions from USB are in the range of 57-64% for 2017 ozone concentrations across all monitoring sites in Maricopa County from April through September. The EPA's air quality modeling for the Cross State Air Pollution Rule (CSAPR) (U.S. EPA, 2016) also indicates that the 2017 ozone contributions from USB are 52% averaged across all Maricopa County sites. These results confirm that there is a significant impact from USB ozone and precursor pollutants in Maricopa County.

4.5 Precursor trends

4.5.1 Nitrogen dioxide

Nitrogen dioxide (NO_2) is measured by a subset of four monitor sites in the region. The Buckeye site is an outlying rural area, while Central Phoenix, JLG Supersite and West Phoenix are central urban locations. AQS hourly data (U.S. EPA, 2025) was averaged over the season from April to September of each year. Figure 4-2 shows the annual trend of the mean 1-hour NO_2 for the four monitoring locations. All locations show a decreasing trend, with larger decreases at the more urban locations (Central Phoenix, JLG Supersite, and West Phoenix).

a)

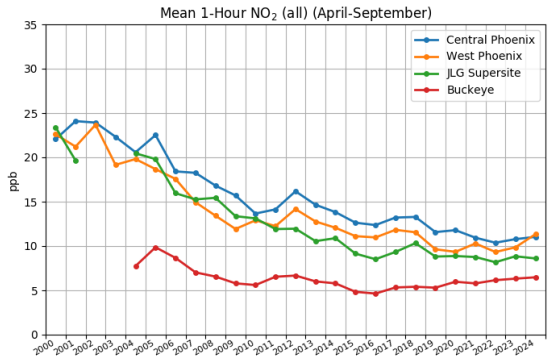

b)

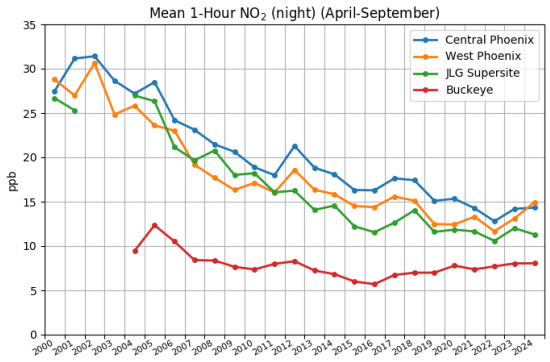

c)

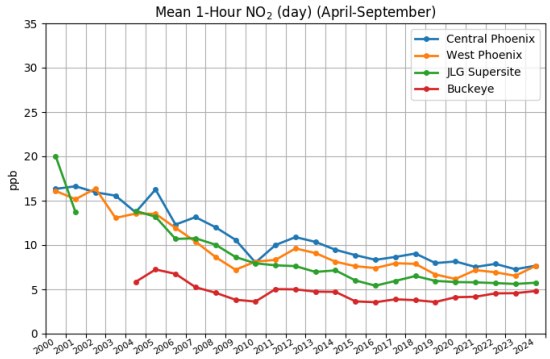

d)

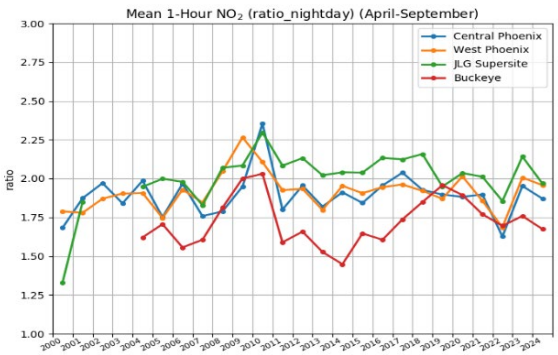

Figure 4-2 Mean 1-hour NO_2 measurements during the ozone season (April-September) in each year from 2000 to 2024, for a) all hours, b) night hours, c) day hours, and d) ratio of NO_2 for night hours to NO_2 for day hours.

4.5.2 Formaldehyde

Formaldehyde (HCHO) is measured at the JLG Supersite monitoring station. AQS daily summary data (U.S. EPA, 2025) was averaged over the season. Figure 4-3 shows the annual trend of the mean 24-hour HCHO over the ozone season (April-September) at the JLG Supersite monitoring location for 2000-2024. There is an unexplained anomaly in the record in 2018 which will be investigated.

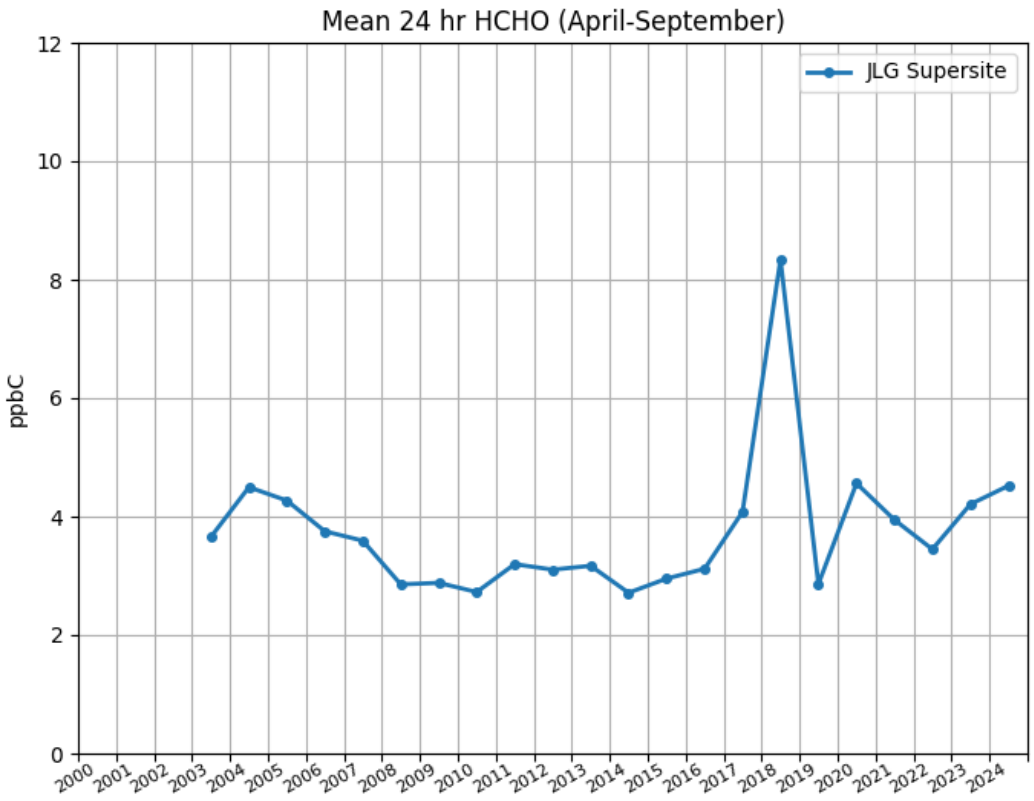

Figure 4-3 Mean 24-hour HCHO measurements at JLG Supersite during the ozone season (April-September) in each year from 2000-2024.

4.5.3 Carbon monoxide

Carbon Monoxide (CO) is measured by a subset of monitoring stations in the network. AQS daily summary data (U.S. EPA, 2025) was averaged over the season. Figure 4-4 shows the annual trend of the mean 1-hour CO over the ozone season (April-September) at each monitoring location for 2000-2024, showing a decrease during that time period.

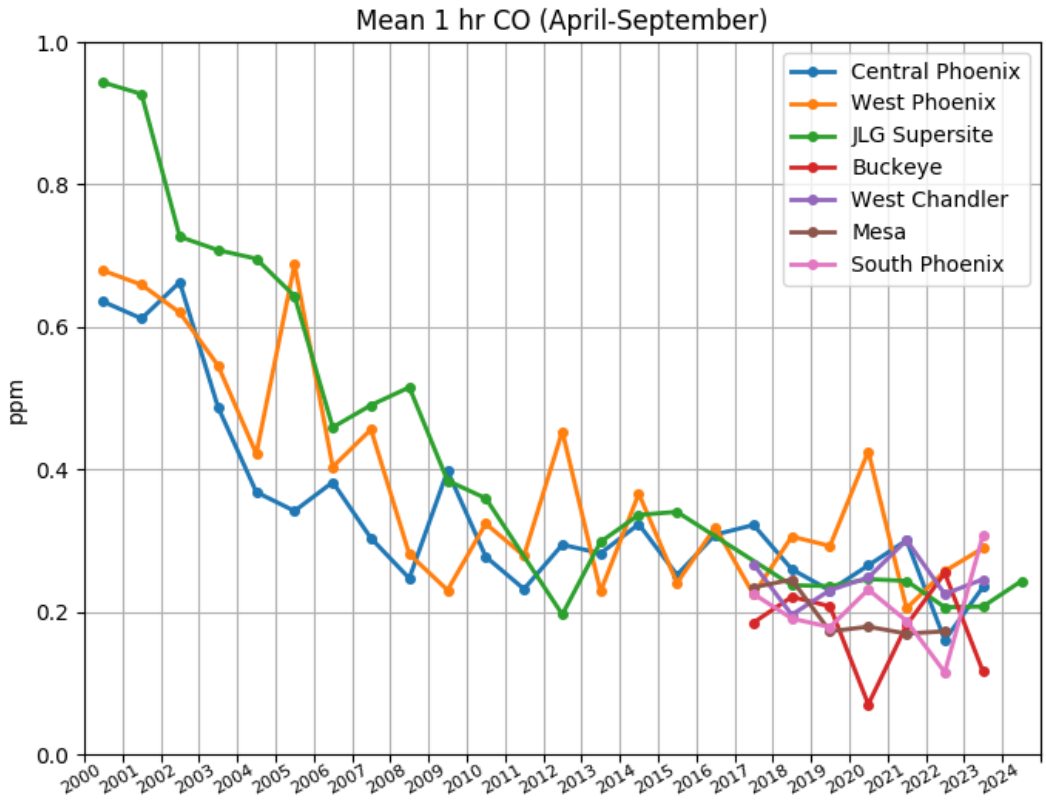

Figure 4-4 Mean 1-hour CO measurements during the ozone season (April-September) in each year from 2000-2024.

4.5.4 Formation sensitivity

Evaluation of ozone response to NO_X and/or VOC emissions reduction is an important sensitivity analysis for determination of which VOC and/or NO_X control strategies are the most effective for reducing ozone. Because of the lowered 2015 ozone standard, the development of emissions control strategies is becoming more important. The CAMx model provides an option for the use of the High-order Direct Decoupled Method (HDDM) to calculate second order sensitivity coefficients along with first-order sensitivity coefficients with respect to predicted ozone concentrations to emission sources. The CAMx HDDM results are discussed in the Weight of Evidence documentation, along with other indicators of ozone formation sensitivity.

4.6 Existing emission control programs

There are 93 existing ozone control measures in the nonattainment area (MAG, 2016). While all of the existing measures in the nonattainment area assist in the improvement of air quality, only a subset of measures have emission reduction benefits that can be quantified. The controls that are currently impacting emissions in the nonattainment area are listed in Table 4-2 below.

Table 4-2 Existing ozone control measures in the nonattainment area.

1	Summer Fuel Reformulation: California Phase 2 and Federal Phase II Reformulated Gasoline with 7 psi from May 1 through September 30
2	Phased-In Emission Test Cutpoints
3	One-Time Waiver from Vehicle Emissions Test
4	Tougher Enforcement of Vehicle Registration and Emissions Test Compliance
5	Expansion of Area A Boundaries
6	Gross Polluter Option for I/M Program Waivers
7	Coordinated Traffic Signal Systems
8	Develop Intelligent Transportation Systems
9	Federal Tier 2 and Tier 3 Motor Vehicle Emissions and Fuel Standards
10	Federal Phase 1 and 2 Light-Duty Vehicle and Phase 1 Medium and Heavy-Duty Vehicle Greenhouse Gas Rules
11	Federal Nonroad Equipment Standards
12	Federal Heavy Duty Diesel Vehicle Emissions Standards
13	Federal Portable Fuel Container Rules

5 Meteorological influences

5.1 Mesoscale systems

Large scale meteorological processes directly determine whether ozone precursors are contained regionally or are transported downwind with the resulting ozone coming from upwind regions or states. Previous studies have demonstrated that local air quality could be degraded by polluted air from up to hundreds of miles upwind of urban and industrial centers (White et al., 1990; Vingarzan, 2004; Venter, 2020). Synoptic scale conditions have an important role in the occurrence of long-range transport of ozone and ozone precursors (Pryor et al., 1992; 1995). Linking ozone air quality at Phoenix local sites with synoptic scale atmospheric circulation can provide information regarding the upwind sources of pollutants and can be used to assess the frequency and trends of conditions conducive to long-range transport. The influence of stratospheric intrusion, high-pressure systems, cyclones, fronts, and the North American Monson on the transport of air pollutants from upper levels and upwind states to the Phoenix area is discussed in the following sections.

5.1.1 Stratospheric ozone intrusions

Stratosphere-to-troposphere transport (STT) primarily impacts the ozone budget in the upper troposphere but can also increase regional surface ozone levels above the legal thresholds set by air quality standards (Danielsen, 1968; Lelieveld et al., 2009; Lefohn et al., 2011; Langford et al., 2012; Zhang et al., 2014; Lin et al., 2015; and Jaeglé et al., 2017). In the western US, for example, deep STT events during spring can add 20-40 ppbv to the ground-level ozone concentration, which can provide over half the ozone needed to exceed the standard set by EPA (Lin et al., 2012; 2015). Estimates of the overall contribution of STT to tropospheric ozone vary widely (Galani et al., 2003; Stohl et al., 2003a; 2003b; Stevenson et al., 2006; Lefohn et al., 2011; Conil, et. al., 2025). Evidence shows large-scale stratospheric intrusions are related to high ozone in Maricopa County (Langford, 2022). For example, widespread 8-hour ozone exceedances in the Maricopa nonattainment area on June 14, 2017 and May 12, 2022 (Table 5-1 and Figure 5-1) are associated with a strong and typical stratospheric intrusion event (Figure 5-2 and Figure 5-3). June 14, 2017, and May 12, 2022, are the top 1st and 4th days for the highest daily 8-hour ozone concentrations in the ozone nonattainment areas for 2017 and 2022, respectively. On June 14, WRF simulations show significant large-scale air mass subsidence over the Phoenix area (Figure 5-2b) when using water vapor as a tracer, while the Model for Prediction Across Scales (MPAS) (the successor to the WRF model) modeling results indicate strong wind shear at upper levels above 10 km (Figure 5-2c), suggesting a clear signal of stratospheric intrusion. Additionally, Amy Butler et al. from NOAA confirmed the occurrence of stratospheric intrusion between June 11-14 based on TOPAZ measurements (Butler et al., 2021). This intrusion also contributed to surface ozone exceedances in Las Vegas and Denver. In addition, Langford et al. (2022) presented the enhancement of surface ozone over Maricopa region associated with stratospheric intrusion based on TOPAZ observations (Figure 5-3) on May 12, 2022. These two typical cases suggest that certain ozone episodes and exceedances are caused by the downward movement of ozone-rich air masses from upper levels due to STT.

Table 5-1 Exceedances of the 8-hour ozone standard of 0.07 ppm on June 14, 2017, and May 12, 2022.

Monitor Site	June 14, 2017	May 12, 2022
Apache Junction	0.089	0.071
Blue Point	0.084	0.077
Falcon Field	0.084	0.078
Fountain Hills	0.085	0.077
Glendale	0.084	0.075
North Phoenix	0.085	0.073
Pinnacle Peak	0.087	0.075
Queen Valley	0.087	0.077
Tonto National Monument	0.090	0.074
West Chandler	0.075	0.075
West Phoenix	0.080	0.072

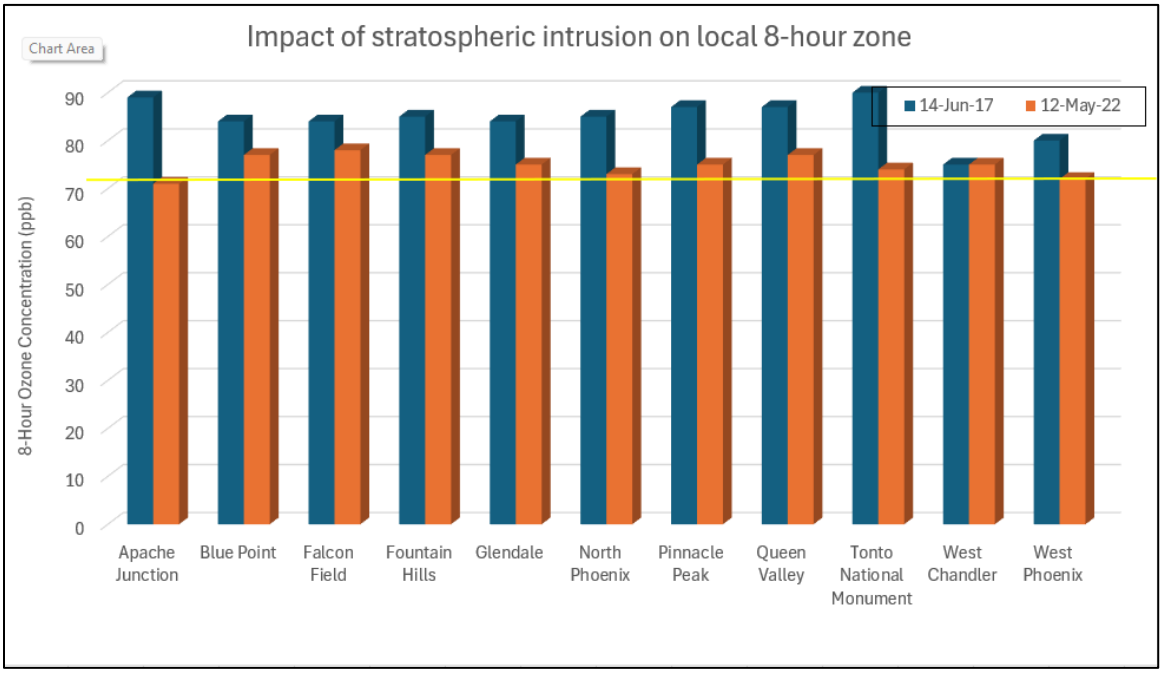

Figure 5-1 Exceedances of the 8-hour ozone standard of 70 ppb at different monitors on June 14, 2017, and May 12, 2022.

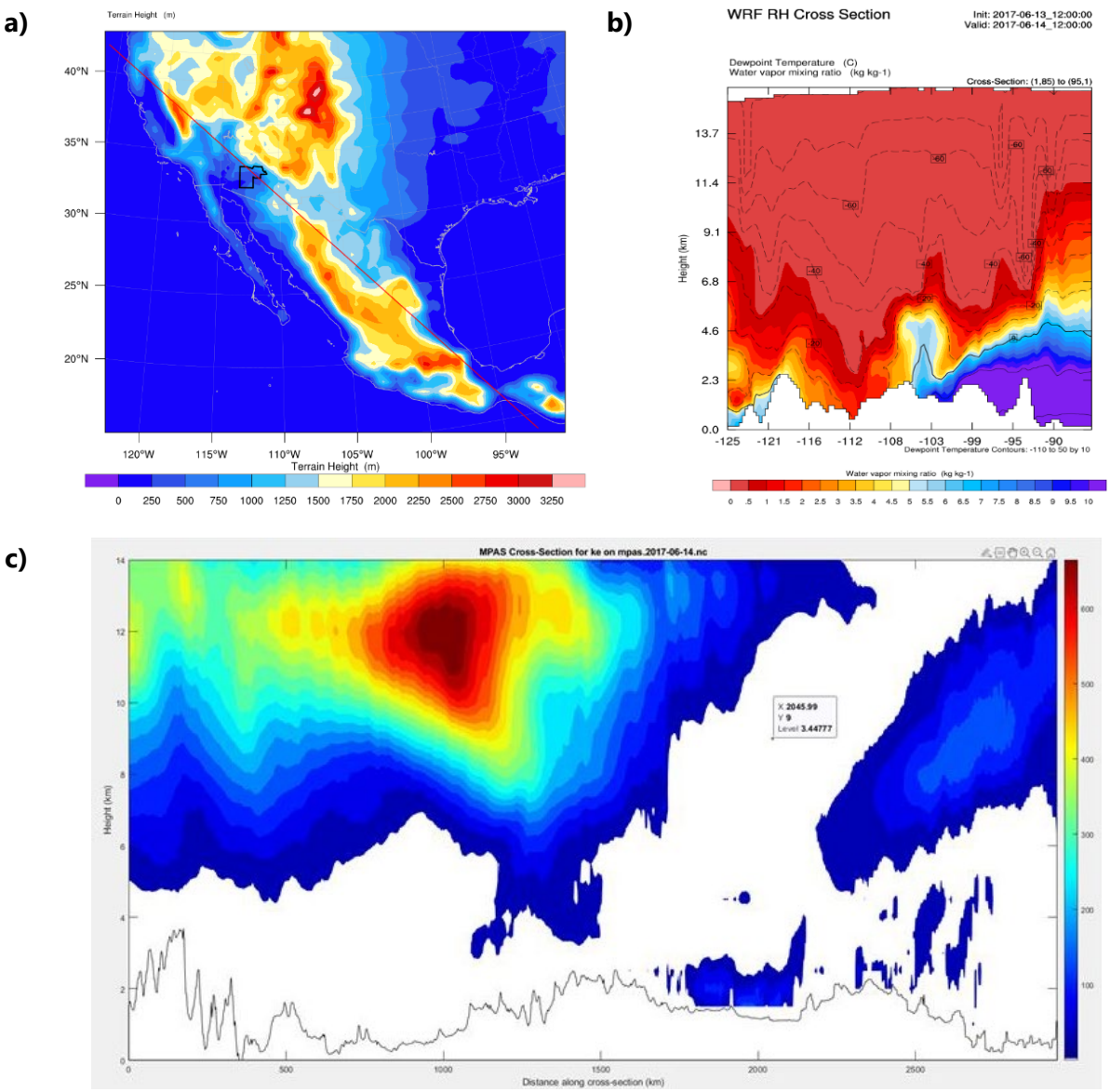

Figure 5-2 WRF and MPAS simulations for the case of June 14, 2017. a) The baseline of vertical cross-section in the WRF 36-km domain. b) The vertical cross-section of water vapor distribution shows the downward movement of dry, cool air over the Phoenix Valley at -112° longitude. c) MPAS simulations reveal a strong upper-level disturbance, with abnormal kinetic energy patterns indicating stratospheric intrusion.

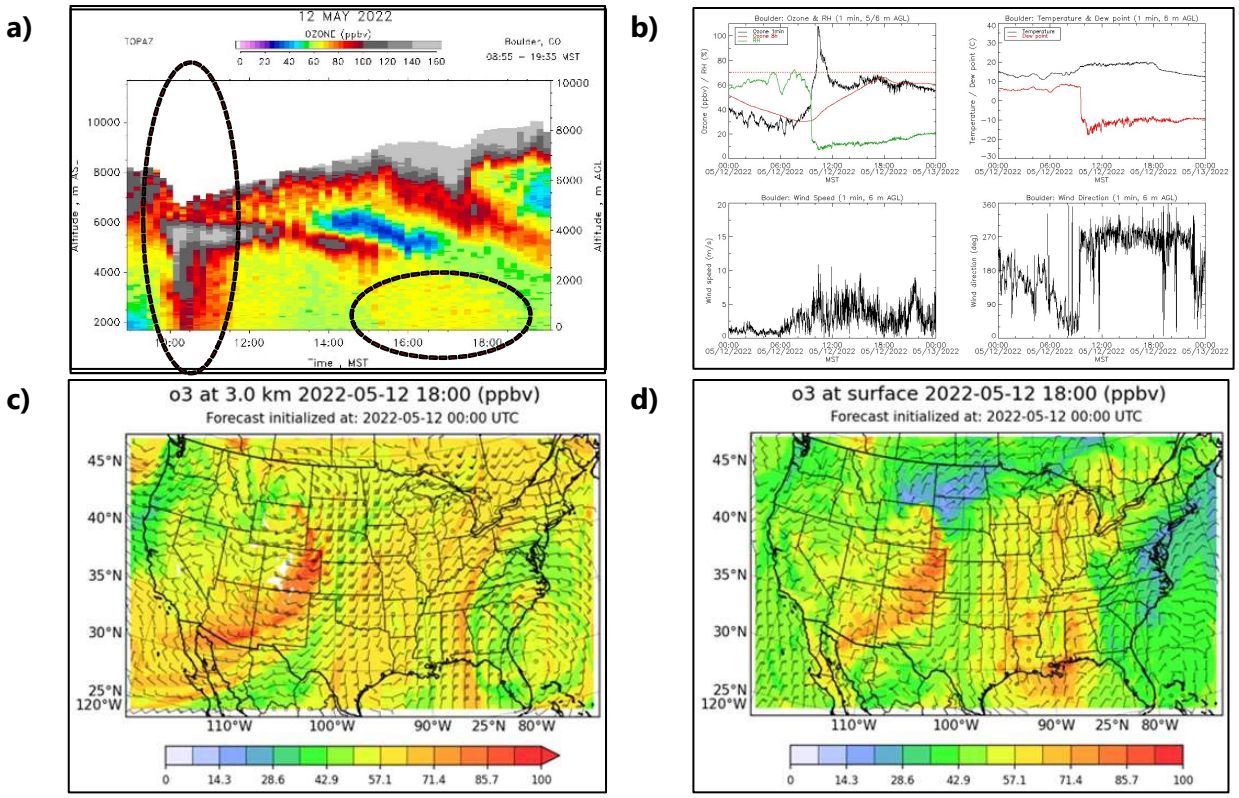

Figure 5-3 Stratospheric intrusion on May 12, 2022 as shown by (a) TOPAZ Lidar ozone measurement in Boulder, CO; (b) in-situ measurements of ozone spike to 108 ppb at 10:25 MST (17:25 UTC); (c) ozone distribution at 3.0 km 18:00 UTC, and (d) at surface 18:00 UTC (cited from presentation by Langford on July 19, 2022).

5.1.2 High-pressure systems

Major episodes of high ozone concentrations are associated with slow-moving and blocking high-pressure (BHP) weather systems. These systems are characterized by widespread layers of air subsidence through most of the troposphere. BHP systems are favorable for the accumulation of ozone precursors such as NOx, CO and VOCs, because the descending air is warmed adiabatically and thus tends to make the troposphere more stable and less conducive to convective mixing. Large scale BHP systems occur most frequently in the springtime over the eastern Pacific Ocean. The surface of the tropical Pacific Ocean cools during these periods. A recent study showed that ozone in the western United States can be increased by these BHP systems (Lin et al., 2015). Strong downward gusts of cold and dry air from the stratosphere trigger the BHP in late spring. The BHP sends the ozone downward due to tropopause folding and stratosphere-troposphere exchange. The air quality of the western United States, much of which sits at high elevations and locations upwind of the state of Arizona, is impacted by these enhanced ozone events. On June 14, 2012, the EPA approved an "exceptional event" demonstration for ozone exceedances at Boulder and Big Piney, Wyoming (Kaldunski et al., 2017). This was the first time since the 1980s that the EPA has recognized a stratospheric intrusion as the cause of a high ozone event. Arizona, a downwind state, is indirectly impacted by ozone intrusions from the stratosphere due to long-range ozone

transport. Late spring high-ozone episodes in Phoenix, for example on April 15 and 16, 2017, are accompanied by cold and dry air transported from the north by the Jet Stream associated with BHP. As shown in Figure 5-4, a meandering polar jet stream influenced by BHP may cause changes in air circulation that drive stratospheric ozone to ground level in the Western United States, including Arizona (Lin et al., 2015).

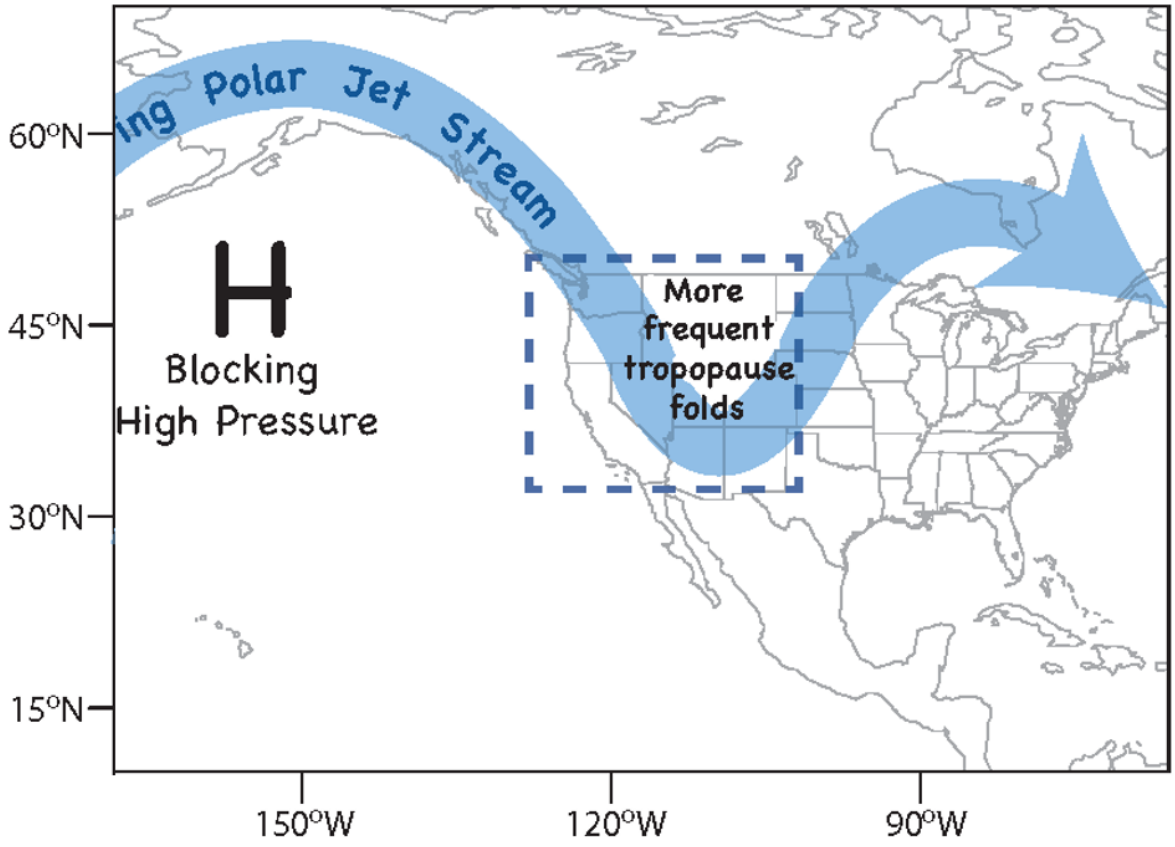

Figure 5-4 Blocking High Pressure over the Pacific Ocean.

In addition, during the summer, persistent high-pressure systems bring cloud-free calm air and high temperatures to Arizona, which are typical conditions conducive to ozone formation. Ozone episodes frequently occur in the summer when there is also strong and lengthy solar radiation, which is the cause of the major air quality issue in Phoenix.

5.1.3 Cyclones and fronts

The southwestern United States is located between the mid-latitude and subtropical atmospheric circulation regimes. This positioning relative to shifts in these regimes is the fundamental reason for the region's circulation variability (Sheppard et al., 2002; Lin, et al., 2012). The change in the circulation leads the air stream to transport ozone and precursor gases from Mexico to Arizona and Phoenix. On the other hand, the circulation shift also functions as a "hard wall", blocking moisture from the Gulf of Mexico, which makes Phoenix have dry air and clear skies. Such conditions are suitable for ozone production by photochemical reactions. The mid-latitude

cyclone air stream is therefore important for the mixing of polluted plumes from upwind and locally generated pollution and is one of the key meteorological conditions conducive to local ozone formation in Phoenix and long-range transport.

5.1.4 North American monsoon

The North American monsoon is most noticeable in Arizona (Sheppard et al., 2002). Up to 50% of the annual precipitation of Arizona occurs in monsoon season from July through September. Because of the intermittent appearance of monsoon, Arizona is dominated by either synoptic high pressure or moist monsoon flow during the monsoon season. The daytime ozone level in Phoenix could be either higher with high pressure or lower with high humidity, cloud cover and precipitation. The distribution of regional NO_X and ozone include signatures from deep convection, lightning production of odd nitrogen, and possible stratospheric intrusions during monsoon season (Ridley et al., 1994). For example, Cooper et al. showed that lightning can contribute 25–30 ppbv of upper tropospheric ozone during the North American Monsoon season (Cooper et al., 2007; Wong, 2013). Modeling studies done by MAG show that the upper air lightning may elevate surface ozone by about 1-3 ppb over the Maricopa 8-hour ozone nonattainment area. In addition, the deep convection associated with monsoon storms could bring the ozone-rich air from the upper troposphere down to the surface and transport it from one region to another. The complexity of interactions of a wide range of atmospheric processes, as well as associated interactions between lightning NO_X emissions and atmospheric chemistry makes it challenging to quantify local ozone concentrations, especially in July when the monsoon season starts.

5.1.5 Extreme climate

The U.S. Climate Extremes Index (CEI) quantifies observed changes in climate within the contiguous United States (Karl et al., 1996). The CEI was developed as a "first-glance" monitoring and communication tool to help policy makers identify possible trends or long-term variations in a variety of climate extremes indicators including those found in observed surface temperature and precipitation across the United States. The CEI provides information on the percentage of the contiguous United States that experienced extreme conditions during any given year or period (Gleason et al., 2008). Individual indicators that comprise the overall index provide details regarding the spatial characteristics of the various parameters over time. In July 2011, a regional CEI (RCEI) was introduced, which computes the CEI across nine U.S. Standard Regions. Arizona belongs to the Southwest region. Year-to-year variations in the Southwest regional index have higher amplitude swings and different percentages of areas affected by extremes, compared with the CEI. There is a good deal of spatial consistency among the RCEI indicators and similar extremes may span across or be absent from a region in any given season. In October 2016, an update was made which improved the resolution and completeness of the climatological inputs. In general, the CEI is an indicator for the trends and variability of temperature, precipitation and drought data as well as tropical system components due to variations of large-scale systems. Ozone production accelerates at high temperatures.

Figure 5-5 (upper panel) shows the long-term variations in summer RCEI for the Southwest US, which represents the percentage of the area experiencing abnormal weather conditions. Since

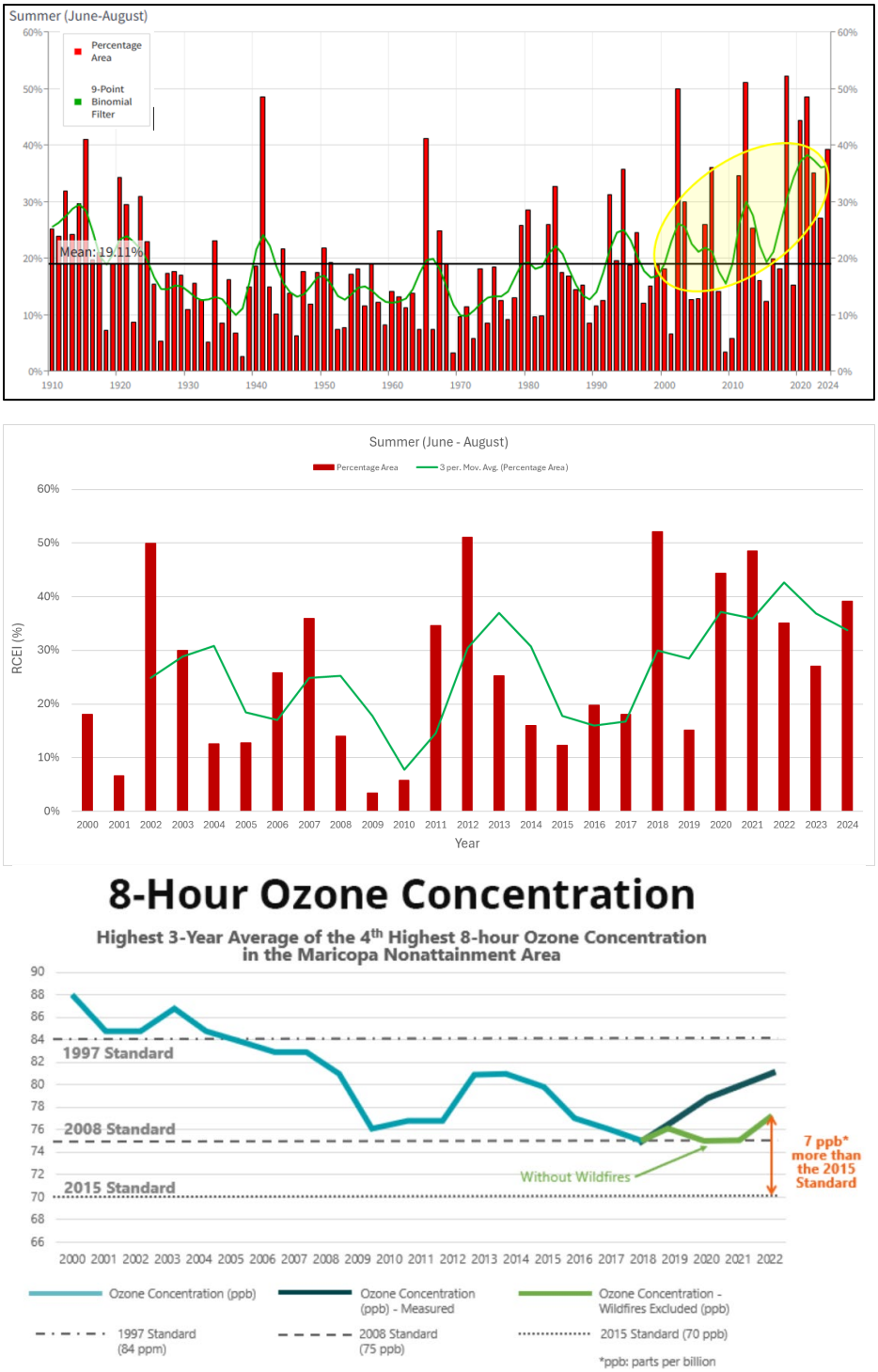

Figure 5-5 Upper Panel: Long-term changes in summer RCEI (%) for the southwestern United States. The green line represents the long-term trend based on a 9-point binomial filter. Middle Panel: Changes in summer RCEI (%) from 2000 to 2024. The green line shows short-term trends using a 3-year moving average. Higher RCEI values indicate greater influence from abnormal weather patterns. Lower panel: Highest 3-year average of the 4th highest ozone concentration in the Maricopa Nonattainment Area.

2000, the variation in ozone exceedances has followed a similar trend to that of the RCEI, suggesting that large atmospheric systems dominate regional meteorological conditions and, consequently, influence regional ozone levels. Prior to 2000, the number of exceedances was high while the RCEI remained relatively low, indicating that high ozone levels during this period were primarily due to local emissions rather than abnormal weather conditions. However, from 2017 to 2024, there has been a significant increasing trend in the RCEI, as shown in Figure 5-5 (middle panel), which may explain the continued rise in ozone levels during the same period (see lower panel) despite substantial reductions in local emissions. This suggests that abnormal weather conditions have played an increasingly important role in the formation of ozone exceedances after 2009.

5.2 Terrain effects

The Phoenix metropolitan area is in central Arizona along the channel and flood plain of the Salt River. The valley is surrounded by flat desert wastelands and by barren, bush, and eastern forest mountains ranging widely in elevation, as illustrated in Figure 5-6 below. The elevation of downtown Phoenix is about 350 meters above mean sea level (AMSL), and surrounding mountain peaks rise as high as 1,400 meters AMSL. The typical daily pattern of mountain/valley up- and down-slope wind flows are constantly observed during daytime (valley breeze) and nighttime (mountain breeze) in the Phoenix Valley. The topographic obstructions to wind flow at the foot of the eastern mountains are a key factor for increasing ozone concentrations in the eastern suburbs. Since Phoenix is in the Sonoran Desert, it typically experiences dry air with clear sky, intense surface heating during daytime, and radiative cooling during nighttime. In addition, the urban heat island (UHI) effect, which pumps air pollutants to upper levels and then circulates them back to the surface the next morning, has become stronger in the Phoenix urban area since 2000 due to rapid growth of the city. The impact of the UHI effect on ozone levels in Phoenix is discussed in Section 5.3.6 below.

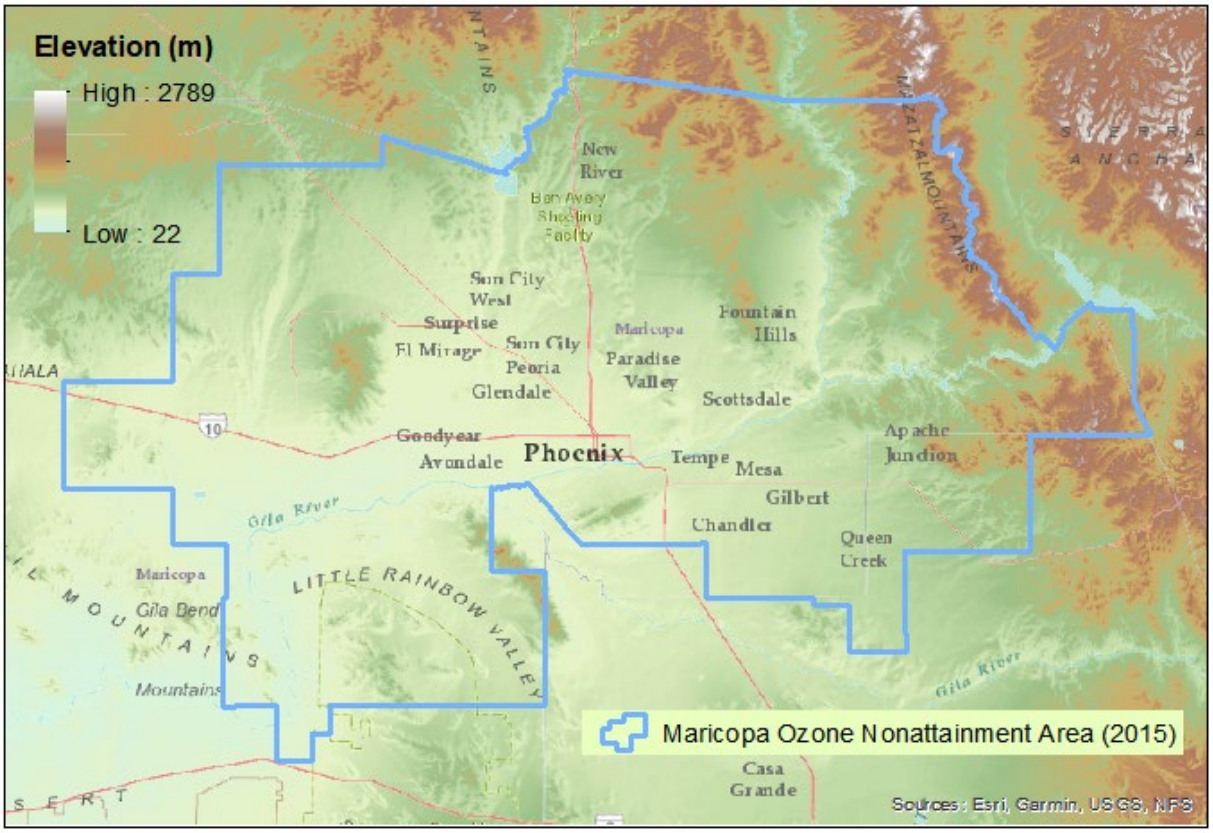

Figure 5-6 Topography of the Maricopa 8-hour ozone nonattainment area.

5.3 Local weather

In May, the Phoenix area typically has relatively lower temperatures, less sunlight, and stronger ventilating westerly winds. While these conditions typically limit ozone production, transport from southern California and Mexico during this time can be enhanced by cold fronts and stratospheric intrusions from low-pressure systems in late spring. Cold fronts and associated westerly transport can recur several times before the monsoonal high-pressure system begins to dominate in the region.

As June is usually much warmer than May, afternoons can be extremely hot (T > 110 °F) and dry (RH < 10%) and have the longest exposure to sunlight near the summer solstice. The month begins with dry air prior to the development of the southwestern monsoon pattern and ends with the dominating monsoonal high-pressure pattern.

July and August have extremely high daytime temperatures and are influenced much more by the regional monsoon pattern. A large-scale upper-level high pressure feature usually aligns over the Four Corners area and pumps moist and unstable air from the southeast. While the synoptic pattern can persist for several weeks, sudden changes in mesoscale weather during this time make ozone formation more complicated. Under monsoonal steering winds, small scale thunderstorms thrive under these favorable dynamics. Days are typically more humid and can exhibit short lived severe weather (intense rain, strong winds and windblown dust). The high pressure often controls

the local flow in between thunderstorm events. Stagnant winds combined with the extreme heat can last long enough to trap pollutants and create the highest ozone concentrations of the season. Additionally, peak biogenic VOC emissions occur in August that might enhance ozone formation.

Elevated ozone in September can occur during the transition from humid unstable conditions to drier autumn-like conditions after the monsoon has dissipated. Elevated ozone is less severe and infrequent due to declining sunlight, a shift back to larger scale westerly wind systems, and decreasing biogenic VOC emissions.

To investigate the relationship between local meteorological conditions and 8-hour ozone concentrations, local meteorological measurements from 2000 through 2020 were compiled and analyzed.

The hourly surface meteorology data was obtained from the Integrated Surface Database (ISD) (TD-3505, NOAA/NCEI). There are 12 ISD stations within the MAG 4-km regional modeling domain. The ISD contains hourly observations, including wind speed and direction, temperature, relative humidity, pressure, etc., compiled from numerous sources (Smith et al., 2011). In the ISD, a calm wind is defined as a wind speed of less than 3 knots, the lower limit of surface observation measurement, and is assigned a value of 0 knots with wind direction reported as missing. Gaps in the ISD records were filled by using AERMET to process 1-minute and 5-minute wind data from Automated Surface Observing System (ASOS) stations (TD-6405, NOAA/NCEI and TD-6401, NOAA/NCEI) into hourly records. Those data are available only through 2022. The historical record length is quite different for the 12 stations. Some stations, such as Phoenix Sky Harbor (KPHX), have over 50 years of continuous reporting, but many other stations have gaps in the record. All parameters, while having different amplitudes, show very similar variability and patterns in the Valley during the overlapping period. The data from KPHX is the primary meteorological data used to analyze relationships between meteorological parameters and ozone concentrations in the Valley.

Each diurnal cycle was normalized by dividing it by its maximum-minimum range in order to highlight the time shifts for the daily variations of eight meteorological parameters, including surface heat flux (SHF), friction velocity (U*), wind speed (WS), wind direction (WD), temperature (TEMP), relative humidity (RH), surface pressure (PRES), and PBL height (PBLH). The normalized diurnal cycles of these eight meteorological parameters are shown in Figure 5-7.

5.3.1 Wind speed and direction

Wind dominates the transport of ozone and ozone precursors and plays an important role in regional and local ozone temporal and spatial distributions. The general pattern of wind speed and direction can be demonstrated by constructing wind roses. Wind roses for the 23-year average show in Figure 5-8 that wind directions in the Valley consist of two dominant flow regimes existing over the diurnal cycle, regardless of the annual or ozone-seasonal average. The daytime period in all seasons is dominated by prevailing winds from the west toward the east (up-valley flow pattern or "valley breeze") while the nighttime hours are generally dominated by prevailing winds from the east toward the west (down-valley flow pattern or "mountain breeze"). These dominant wind patterns are associated with a "valley mountain breeze" flow circulation induced

by terrain. The wind speeds from west to east are greater than from east to west because of the effects of the flat surface of the western Valley and the complex terrain of eastern mountain ranges.

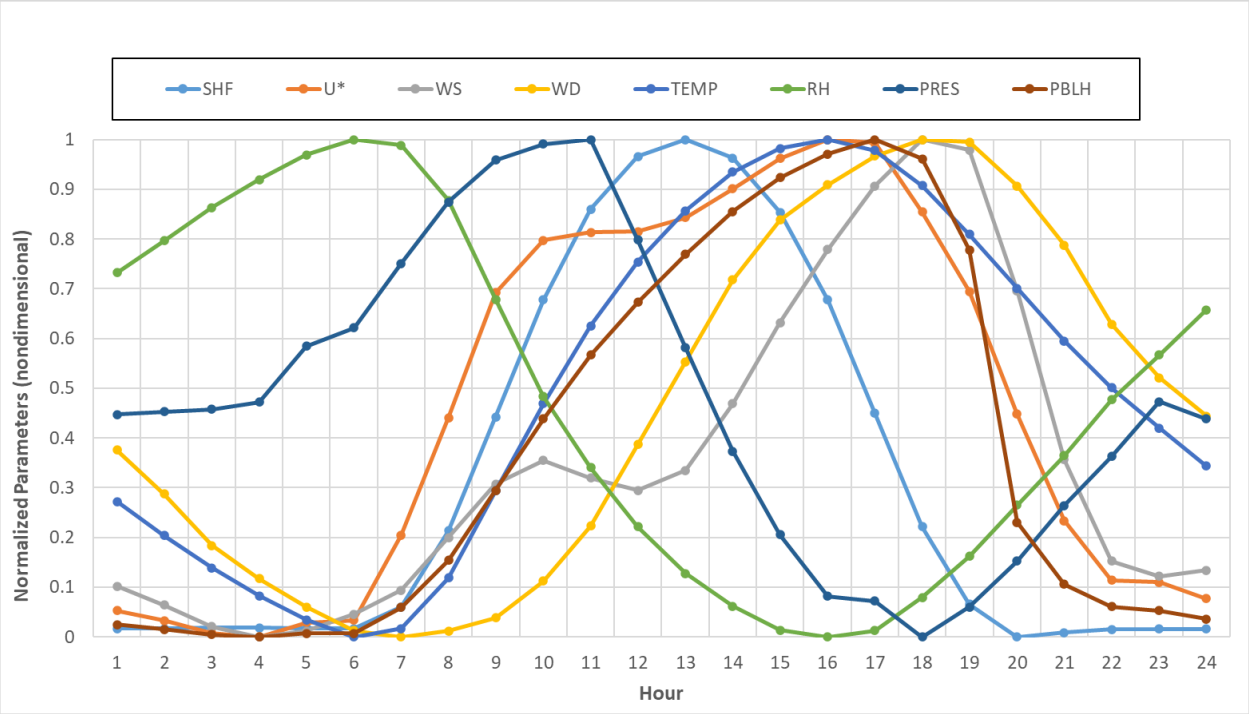

Figure 5-7 Normalized diurnal cycle of all meteorological parameters (SHF, U*, WS, WD, TEMP, RH, PRES and PBLH) during ozone seasons from 2000 to 2022.

This typical local circulation leads to higher ozone concentrations during daytime in the eastern Valley due to transport of ozone and ozone precursors, as measured by downwind monitors located in the eastern parts of the Valley. Wind speed across the Valley and urban core ozone levels determine the distance over which transport will have an influence. The Tonto National Monument monitor measures high ozone during summer daytime even though it is in the east Valley approximately 50 miles from the Phoenix urban core.

a)

b)

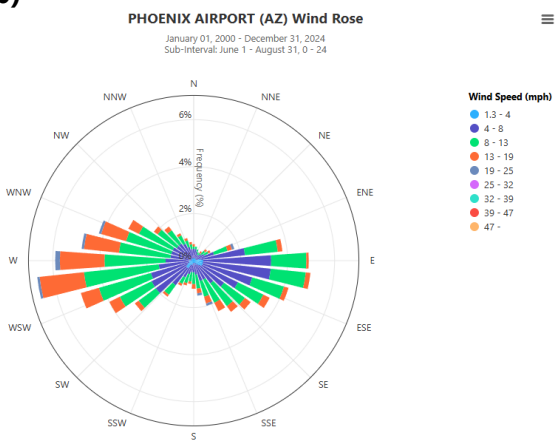

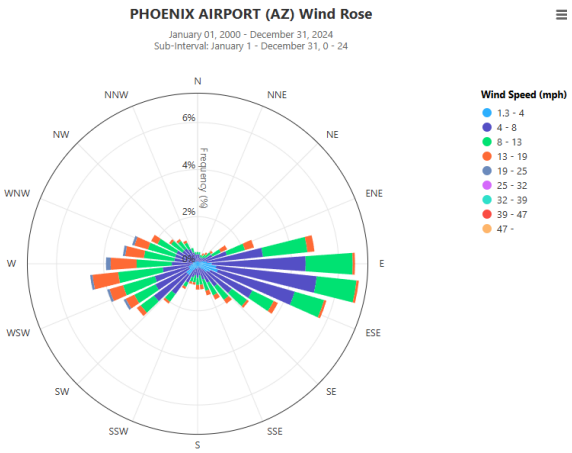

Figure 5-8 Wind roses for (a) 23-year annual average; and (b) 23-year ozone-seasonal mean.

As shown in Figure 5-9, there is a typical pattern for the diurnal cycles of wind speed and wind direction. High winds normally are westerly and observed in late afternoon. Low winds occur in the early morning and blow from the east and southeast. This is a typical mountain/valley wind pattern which indicates the transition between down-slope beginning after sunset (mountain breeze) and up-slope beginning after sunrise (valley breeze). However, wind speed normally drops down sharply after sunset because the surface heating is switched off.

a)

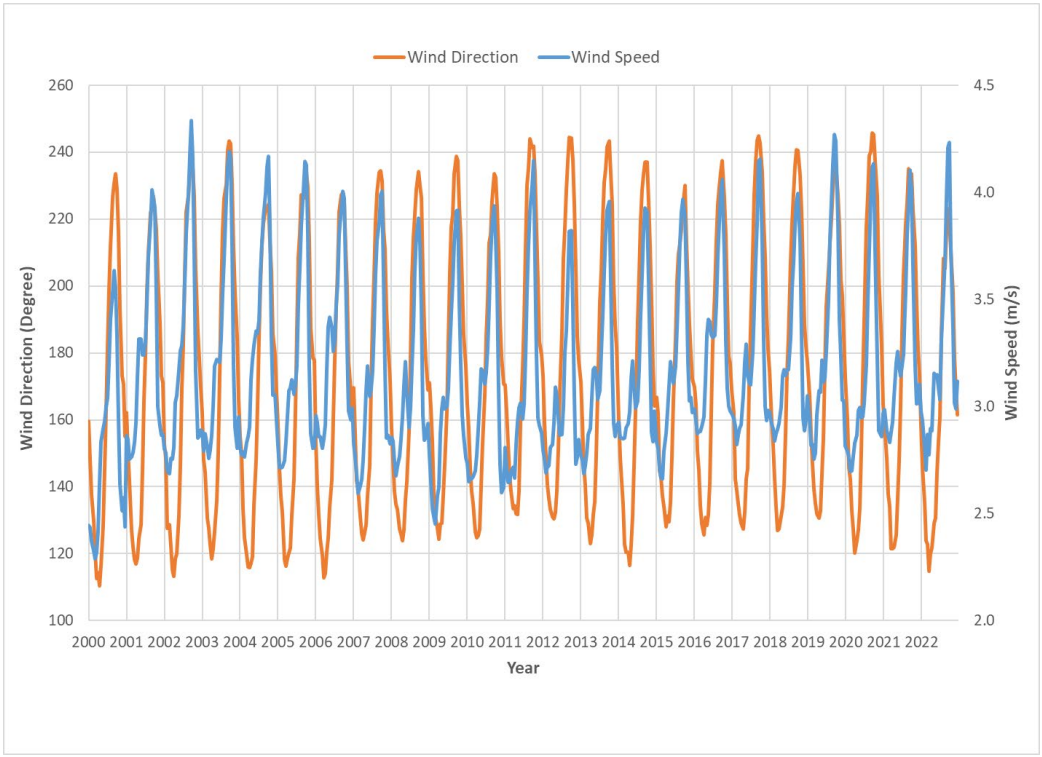

b)

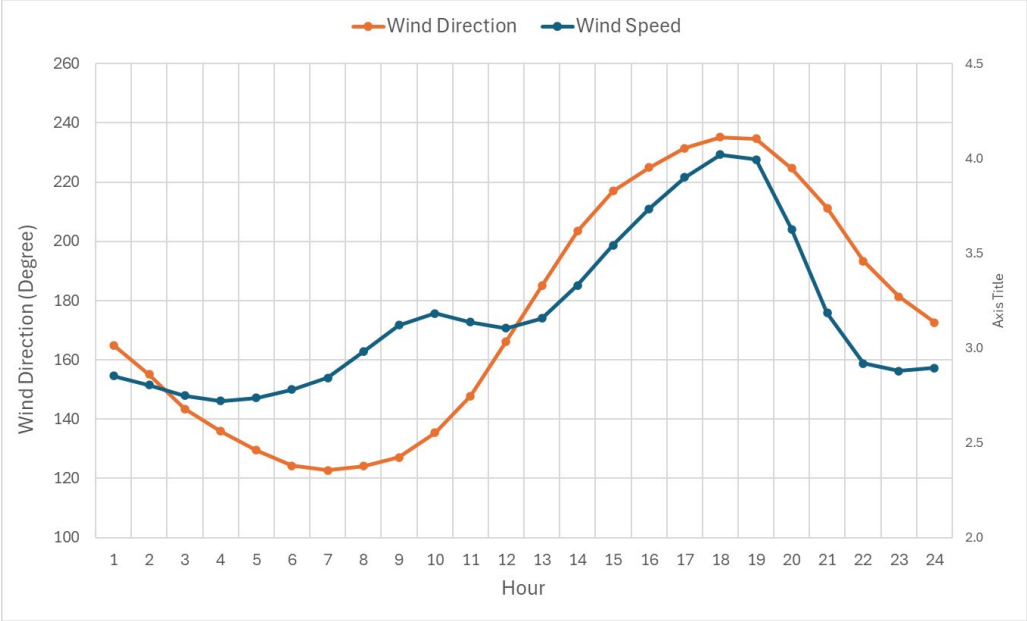

Figure 5-9 Diurnal cycles of wind speed and wind direction for (a) annual average year by year and (b) 23-year average.

5.3.2 Temperature

There is an obvious tendency to observe higher ozone concentrations at higher temperatures; however, high temperatures are not necessarily a sufficient condition for high ozone.

Sunlight is necessary to drive photochemical reactions leading to ozone production and high temperatures are well correlated with strong solar radiation. In addition, warmer temperatures are often associated with overall meteorological conditions such as stagnant high pressure conducive to the formation and accumulation of ozone. Figure 5-10 and Figure 5-11 present the daily maximum and minimum temperatures recorded, along with the annual and summer seasonal averages of maximum and minimum temperatures at the Phoenix Sky Harbor station. Figure 5-12 shows the spatial distribution of air temperatures across Arizona and neighboring states. As depicted in Figure 5-10 and Figure 5-11, daily maximum temperatures consistently exceed 110°F from June to August, and the summer average maximum temperature remains above 100°F, with no significant trend observed over the 23-year period. Figure 5-12 highlights that most areas of Maricopa County experience elevated temperatures during the summer ozone season. Furthermore, the urban core of Phoenix exhibits higher average temperatures than rural areas, a phenomenon primarily driven by the urban heat island effect, especially at night.

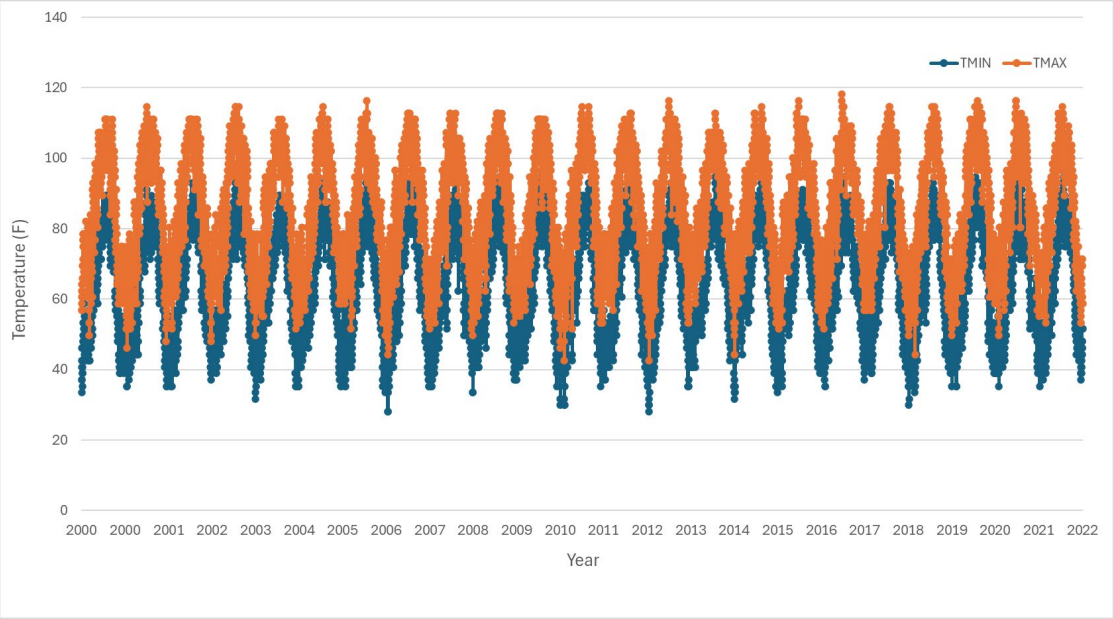

Figure 5-10 Daily averaged maximum and minimum temperatures from 2000 through 2022.

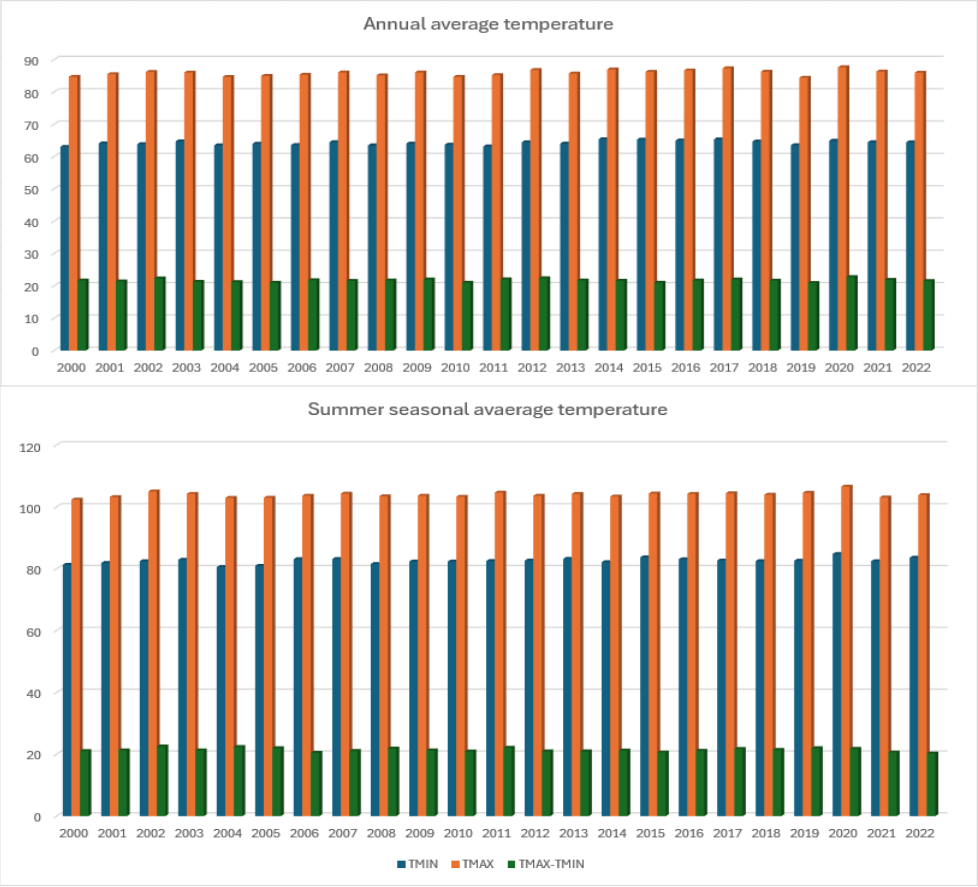

Figure 5-11 Annual and summer seasonal averaged maximum and minimum temperatures from 2000 through 2022.

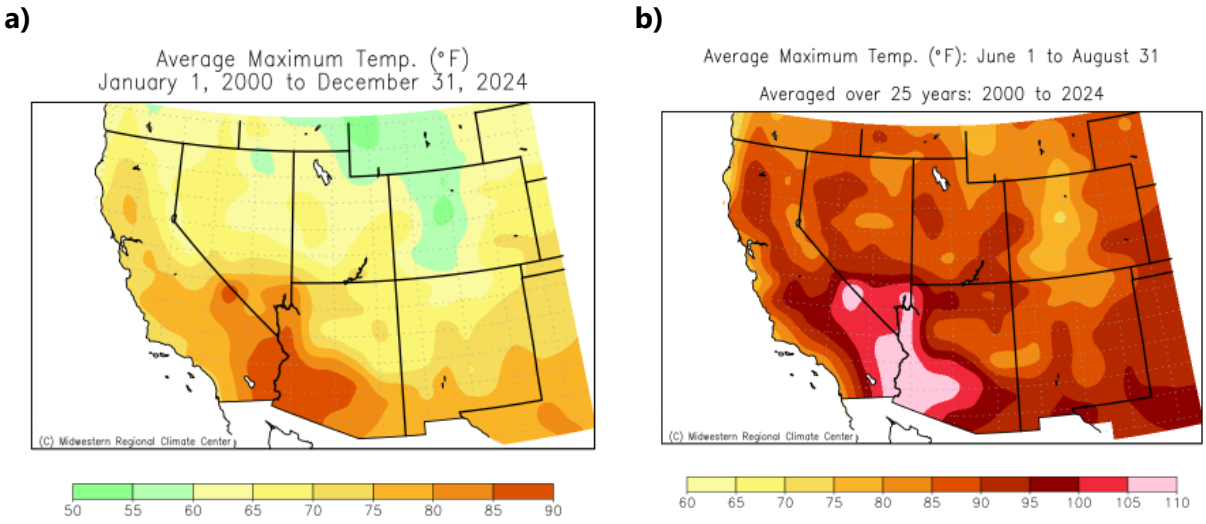

Figure 5-12 Spatial distribution of (a) annual average and (b) ozone-season average temperatures in Arizona and neighboring states.

5.3.3 Relative humidity

There is an obvious tendency to observe relatively higher ozone concentrations under dry air conditions with lower relative humidity values; however, low relative humidity is not necessarily a sufficient condition for high ozone. High-ozone hours occur predominantly during periods characterized by dry air conditions with relatively low atmospheric moisture levels. High-ozone days in the valley typically have either a ridge of cold front that brings cold and dry air from northern regions toward the southern states or a high pressure over the southwest with large-scale clockwise circulation, which blocks the moisture from Gulf of Mexico. This air is often characterized by relatively low relative humidity. In addition, days with higher relative humidity indicate other weather conditions such as cloudy and rainy days that are not conducive to the formation and accumulation of high ozone concentrations.

Figure 5-13 illustrates the annual average diurnal cycle of humidity. Humidity is relatively high in the early morning, and during the day, especially in the late afternoon, the air becomes drier. No significant upward or downward trends have been observed over the past 23 years. The summer ozone season is the driest period of the year, driven by higher temperatures and increased evaporation rates over desert regions.

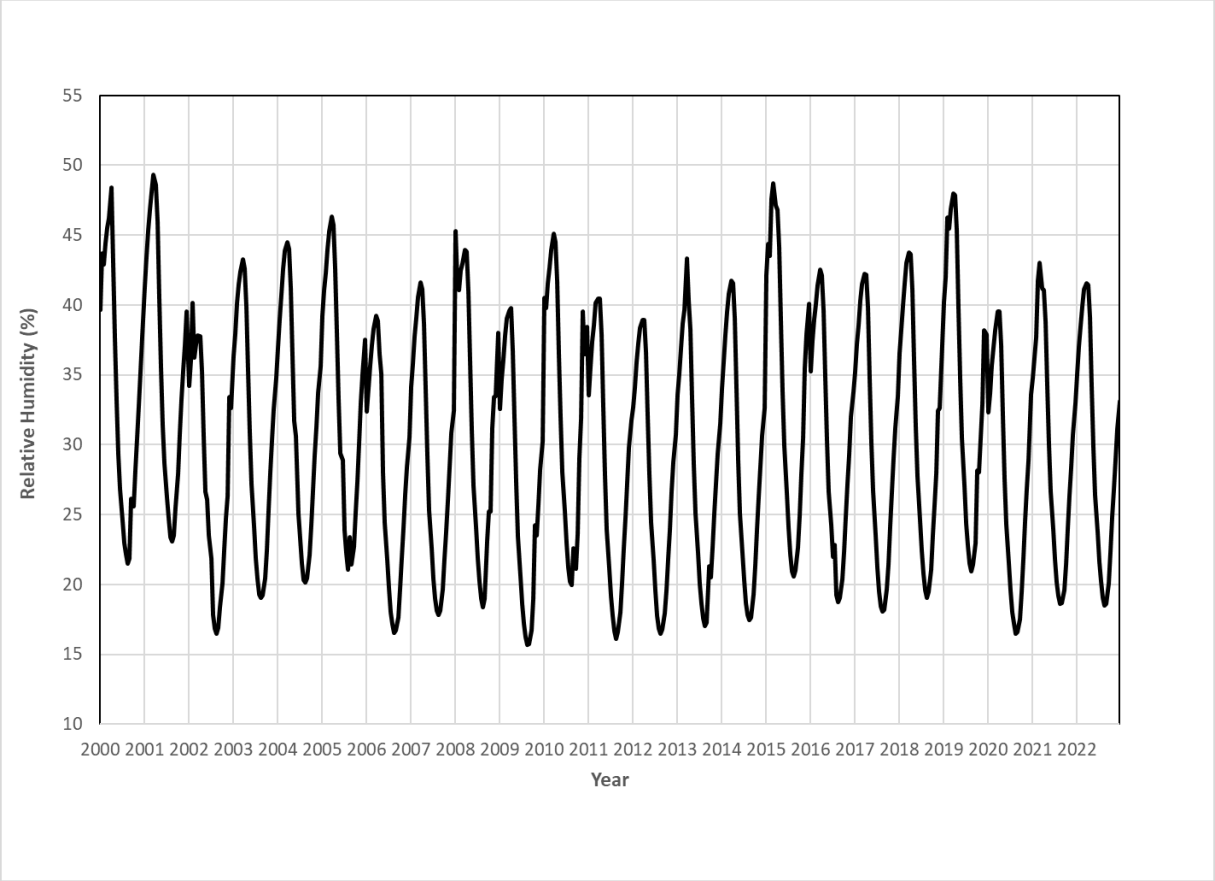

Figure 5-13 Annual averaged diurnal cycle of relative humidity in Phoenix.

5.3.4 Surface pressure

High pressures are associated with slow and northeasterly winds, which blow cold air from mountain ranges down to the valley. Cold air with high density leads to higher surface pressure. However, this normally happens early in morning when the high ozone is not yet established. Higher 8-hour ozone concentrations are actually observed with the surface pressure range between 965 hPa and 975 hPa. These pressures are associated with westerly winds with relatively higher wind speeds. The mild horizontal transport and mixing processes as well as warmer air from the west are more conducive to ozone formation. Note that surface pressure can be affected by either local effects or large weather systems. The variations therefore may be irregular or regular even though surface pressure varies continually. Irregular variations are primarily associated with the development, decay and passage of pressure systems. Sometimes purely local effects can force irregular pressure changes. Wind speed can also be affected by pressure changes because air moves from high to low pressure areas. Consequently, the effect of surface pressure on ozone concentrations is related to the effects of winds and temperature on ozone concentrations.

Regular oscillations of surface pressure have a period of about 12 hours generated by the alternate heating and cooling of the earth's atmosphere by the sun. This produces a rhythmic expansion and contraction of the air. These regular oscillations can be observed as surface pressure diurnal variations. Figure 5-14 illustrates the diurnal variations of surface pressure. In the Phoenix area, surface pressure is lowest in the late afternoon and highest in the late morning. It changes significantly at sunrise and sunset due to the transition of wind direction between down- and up-slopes.

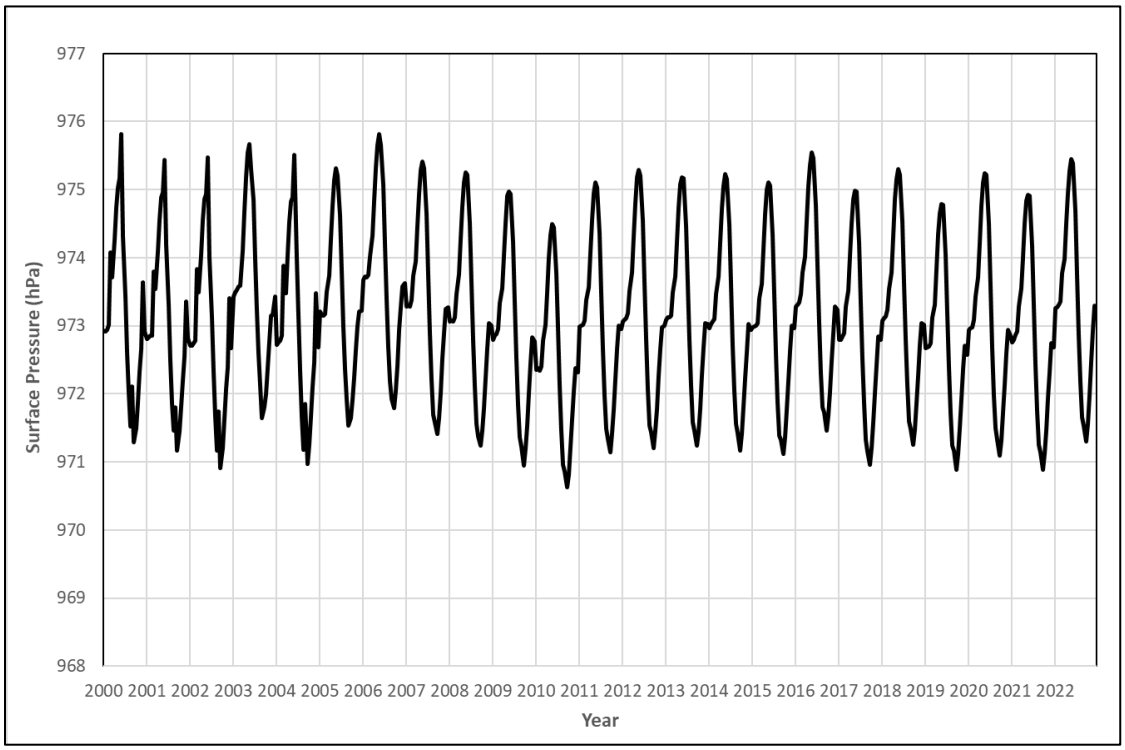

Figure 5-14 Annual averaged diurnal cycles of surface pressure.

5.3.5 Nocturnal inversions

The nocturnal planetary boundary layer is often characterized by a stable layer near the surface with an overlying residual layer. The stable layer develops due to radiative cooling after sunset. Above the stable layer, the remnants of the daytime mixing layer form the residual layer, which initially constitutes uniformly mixed air pollutants remaining from the preceding day (Stull, 1988). Aged ozone from the surface and upper levels is one of these remnant air pollutants in the residual layer, with dry deposition during the night (Sillman, 1999; Xie et al., 2016). This aged ozone can be transported downward through the residual layer during nighttime, and then from the residual layer to the surface due to the convective turbulence in the boundary layer after sunrise. This process is an important mechanism of ozone transport contributing to the formation of ozone pollution in the near surface layer the next day (Caputi et al., 2019; Hu et al., 2018; Morris et al., 2010; Neu et al., 1994; Prabhakar et al., 2017).

The daytime high temperatures in Phoenix make it easier to develop a deep mixing layer, and the rapid nighttime cooling due to the sparsely vegetated desert land makes it easier to build a strong

residual layer over the Valley. Sustained residual layers are decoupled from the surface layer and block surface NO_X, retaining more ozone overnight, thus leading to more fumigation of ozone the following morning. This in turn gives rise to higher ozone concentrations the following afternoon.

The relative significance of this effect is highly dependent on vertical mixing processes, including stratospheric intrusion, blocking high-pressure systems, and deep convective boundary layer developed by thermal dynamics in deserts. Notably, the mixing depth in Phoenix during the summer can exceed 3,000 meters. This unique condition allows the residual layer over Phoenix to retain significant amounts of aged ozone. The full extent of this effect remains an area for future research.

June 14 and July 7 were the top two days among the top 10 ozone days in the Maricopa Nonattainment Area in 2017. The average observed daily maximum 8-hour ozone concentrations in the NAA on these days were 79.63 ppb and 73.29 ppb, respectively. At the Mesa site, ozone levels were even higher, reaching 82.25 ppb on June 14 and 82.0 ppb on July 7. As discussed in Section 5-5-1, the ozone exceedance on June 14 is linked to stratospheric intrusion. Further investigation reveals that the nocturnal inversion exacerbated ozone levels on June 14 and was responsible for the elevated ozone on July 7.

Figure 5-15 (a and c) present examples of nocturnal inversion in the temperature profile measured over Phoenix Sky Harbor at 12:00 UTC on June 14 and July 7, 2017, respectively. Figure 5-15 (b and d) demonstrate that the same nocturnal inversion is well captured by the WRF model.

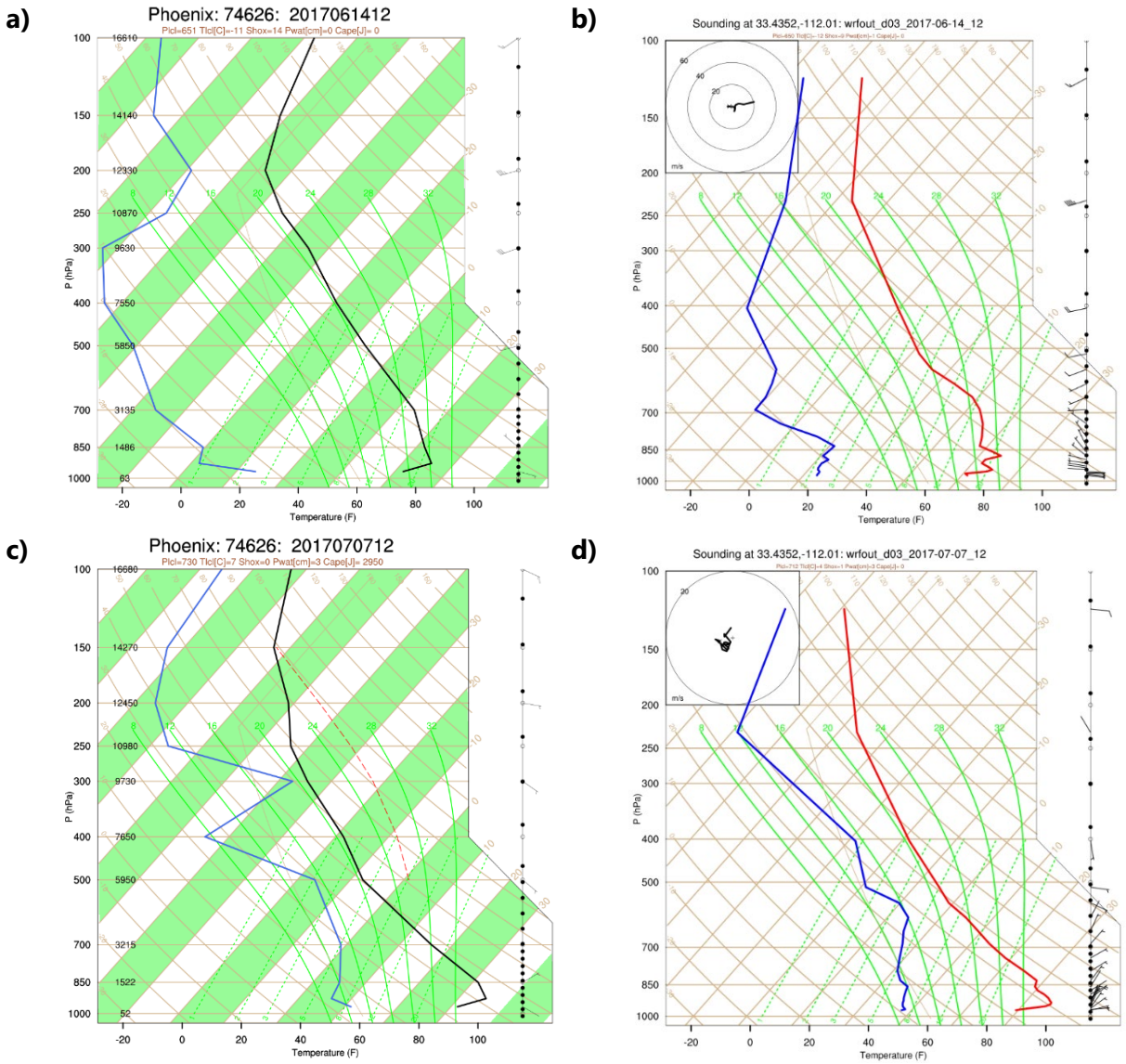

Figure 5-15 Temperature profiles at Phoenix Sky Harbor at 5:00 a.m. local time on June 14 and July 7, 2017, based on (a) and (c) observational data, and (b) and (d) WRF simulations.

5.3.6 Surface heat flux and urban heat island effect

There is an obvious upward trend of the surface heat flux during the last 23 years for both annual average and ozone seasonal mean. The continuous increase of surface heat flux is very likely related to the Urban Heat Island (UHI) effect due to the increasing urbanization of Phoenix. One way to demonstrate this effect is to examine variation of the convective velocity scale (w*) or vertical friction velocity, which depends on surface heat flux, mixing layer height, surface roughness, and air temperature.

Convective velocity scale (or vertical friction velocity w*) indicates the thermal buoyancy. An estimation of w* involves a knowledge of the surface heat flux and the mixing layer height. Combined with surface heat flux it is commonly used to describe the UHI effect. High w* helps to mix and exchange the air vertically which leads to more effective photochemical reactions. The

horizontal friction velocity (u*) is used to represent surface stress and reflects wind shear at the surface layer. Therefore, the relationship between u* and ozone concentration is the same as the relationship between wind speed and ozone concentration. It is less correlated with 8-hour ozone than w*. Vertical mixing processes play a key role in surface ozone levels.

Figure 5-16 demonstrates that the annual mean surface flux has been increasing since 2000 and has an obvious upward trend which may relate to the UHI effect. Although the UHI effect could be present day and night, it tends to be strongest during the daytime when the sun is shining (U.S. EPA, 2008). While the UHI effect is associated with heat flux and thermodynamic driving forces like buoyancy which enhances the vertical mixing, ozone at the Phoenix urban core hardly moves at all horizontally and forms a dome of pollution over the east part of the valley. The vertical mixing process caused by the strong surface heat flux can lead to more efficient photochemical reactions because NO and HNO_3 precursors are favored away from the surface where they are strongly removed. On the other hand, ozone and its precursors that are vertically transported by the vertical mixing process and trapped aloft in the nocturnal residual layer can influence the surface ozone concentrations on the following day as the surface temperature inversion starts to break up (Zhang et al., 1999). It is necessary to identify the relationship between 8-hour ozone concentrations and the UHI effects because heat flux, or w* has significantly increased in the Phoenix urban area since 2000 due to the rapid growth of the city. These UHI effects may offset and even outpace the benefits of emission reductions in Maricopa County.

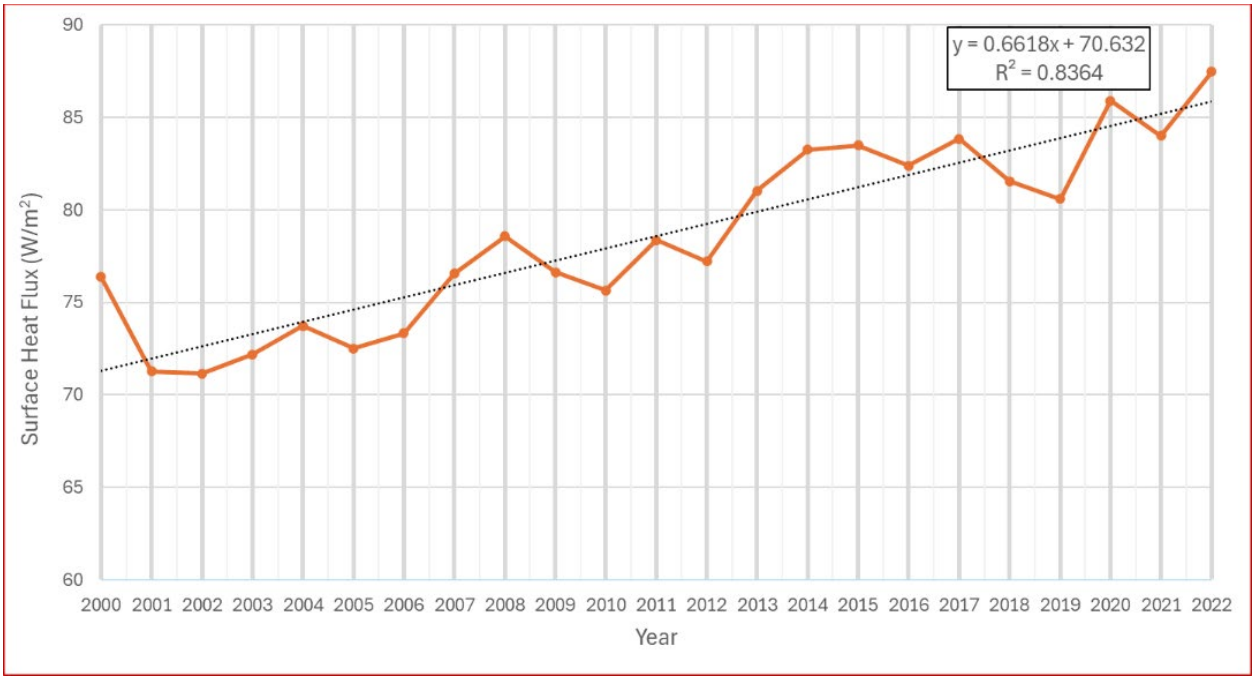

Figure 5-16 Annual average surface heat flux trend from 2000 to 2022.

5.4 Long-range transport

The level of ozone in urban areas is governed by emissions produced locally and by ozone precursors transported over long distances. Transported ozone (international, interstate or stratospheric) can also influence local ozone levels, especially in the late spring and early summer when the transport pathways are conducive to elevated ozone. The Phoenix area is often downwind from source regions in Southern California and Northern Mexico (Gaffney et al., 2002; Li et al., 2015). Trans-Pacific transport of Asian pollution has even been shown to affect surface ozone concentrations across the western United States (Huang et al., 2013). Previous source apportionment studies of ozone for 2016 indicate that cross-boundary transport contributed more than 50% to ozone levels in Phoenix during that year (Hu et al., 2022).

It is important to identify the sources of air parcels transported into the area causing elevated ozone concentrations. The Hybrid Single Particle Lagrangian Integrated Trajectory (HYSPLIT) model is a commonly used tool for the analysis of transport. For a given receptor, back-trajectories from HYSPLIT show the path of the air parcel prior to reaching the destination. For three monitoring sites (North Phoenix, Humboldt Mountain, and Tonto National Monument), transport patterns were analyzed on high-ozone days (MDA8 ozone above 70 ppb) during the 2000-2024 ozone seasons (April-September) by running 72-hour back-trajectories at the height of 100-meter, 500-meter, and 1,000-meter. The starting hour of each back-trajectory corresponds to the hour of the maximum daily average 1-hour (MDA1) ozone at each monitoring site.

Figure 5-17 illustrates the density of hourly back-trajectory endpoints on high-ozone days during the 2000-2024 ozone seasons. Air parcels were mainly transported from southern California, northern Mexico, and other regions within Arizona on high-ozone days. This indicates that the main sources contributing to elevated ozone concentrations in the Maricopa 8-hour ozone nonattainment area are located in these areas. This result is consistent with CAMx source apportionment results from modeling done by MAG. Although back-trajectories for the three monitoring sites show similar transport patterns, there is one notable difference on high-ozone days. Unlike rural downwind monitoring sites, the North Phoenix site is located at the center of the high-density cluster. This may indicate that southwesterly air parcels on high-ozone days tend to have a circular movement within the valley before reaching North Phoenix and trap ozone and ozone-precursor emissions, which elevates ozone levels.

High-ozone days were classified as “stagnant”, “weak transport”, or “transport” based on their movement. The 72-hour back-trajectories with low air mass movement (less than 5 mph over the 72-hour period; total length of the 72-hour back-trajectory/72 hours) are classified as “stagnant.” When there is fast movement, greater than 10 mph over the 72-hour period, the back-trajectory is classified as “transport.” All other back-trajectories are classified as “weak transport.” Table 5-2 shows that high-ozone days occur most often under weak transport conditions (53%), with a significant number (42%) occurring under faster (long-range) transport conditions.

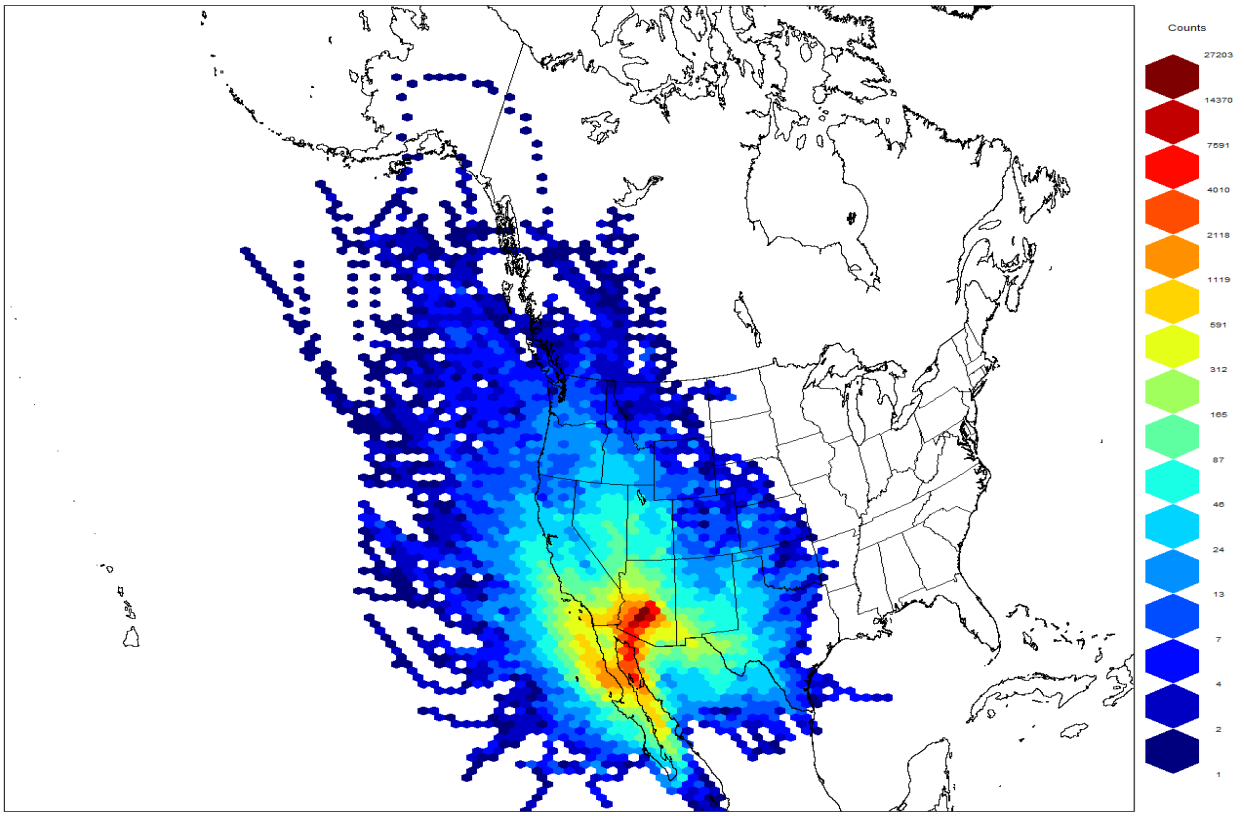

Figure 5-17 Density of back-trajectories on high-ozone days (MDA8 > 70 ppb) during the 2000-2024 ozone seasons at North Phoenix, Humboldt Mountain, or Tonto National Monument.

Table 5-2 Classification of back-trajectories on high-ozone days at Humboldt Mountain, North Phoenix, or Tonto National Monument during 2000-2024 ozone seasons.

Classification	High-ozone days with MDA8 > 70 ppb	
	Number	Percent
Stagnant	171	4%
Weak Transport	2,042	53%
Transport	1,615	42%
Total	3,828	100%

6 Satellite NO_2 and HCHO

Remote sensing data can complement surface measurements by providing more comprehensive spatial coverage of a region than can be obtained from ambient monitors. Among the currently available satellite data products, one of the more useful products for studying ozone formation is tropospheric column NO_2 because the spatial resolution is sufficiently high to distinguish between urban and rural areas and it has a high correspondence with AQS surface measurements. Column Formaldehyde (HCHO) is also available. Satellite data provides information about the density of pollutants in the atmosphere which is not directly comparable to measurements taken at the surface, but can provide additional information for evaluation of regional trends and patterns. Three satellite missions are currently measuring tropospheric NO_2 columns: the Ozone Monitoring Instrument (OMI), the Tropospheric Monitoring Instrument (TROPOMI), and the Tropospheric Emissions: Monitoring of Pollution (TEMPO). OMI has an extensive data record (2005 to present), and therefore is preferable for analyzing long-term regional trends, while TROPOMI has been operating from 2018 to present with enhanced spatial resolution and is more useful for detailed analysis of spatial patterns within the region. Both OMI and TROPOMI pass over Phoenix at approximately 1:30 PM local time. TEMPO, which commenced operations in 2024, is a geostationary instrument providing unprecedented hourly measurements across North America. This capability is crucial for analyzing diurnal cycles of pollutants and emissions, offering enhanced resolution beneficial for source attribution and process studies.

For the analyses presented herein, the following satellite data sets are used:

- **OMI:** Daily gridded Level 3 (L3) data products, specifically L3-OMNO2d_v3 (NO_2) and L3-OMHCHOd_v003 (HCHO), covering the period 2005-2024, were obtained from the GES DISC (https://disc.gsfc.nasa.gov). These products are gridded at a resolution of 0.25 degree x 0.25 degree, and were used for trend analysis. Level 2 swath products (QA4ECV) were obtained from KNMI/TEMIS (https://www.temis.nl). These products feature a spatial resolution of 13km x 24km at nadir and were used for model comparisons..
- **TROPOMI**: Daily swath Level 2 (L2) data products, S5P_RPRO_L2__NO2 (NO_2) and S5P_RPRO_L2__HCHO (HCHO), covering the period 2018-2024, were obtained from the GES DISC (https://disc.gsfc.nasa.gov). The nadir spatial resolution for these products was 3.5 km × 7 km prior to August 6, 2019, and improved to 3.5 km × 5.5 km thereafter.
- **TEMPO:** Hourly gridded Level 3 (L3) data products, TEMPO_NO2_L3_V03 (NO_2) and TEMPO_HCHO_L3_V03 (HCHO), for the year 2024, were obtained from NASA Earthdata (https://search.earthdata.nasa.gov). These products are gridded at a resolution of 0.02 degree x 0.02 degree.

6.1 OMI

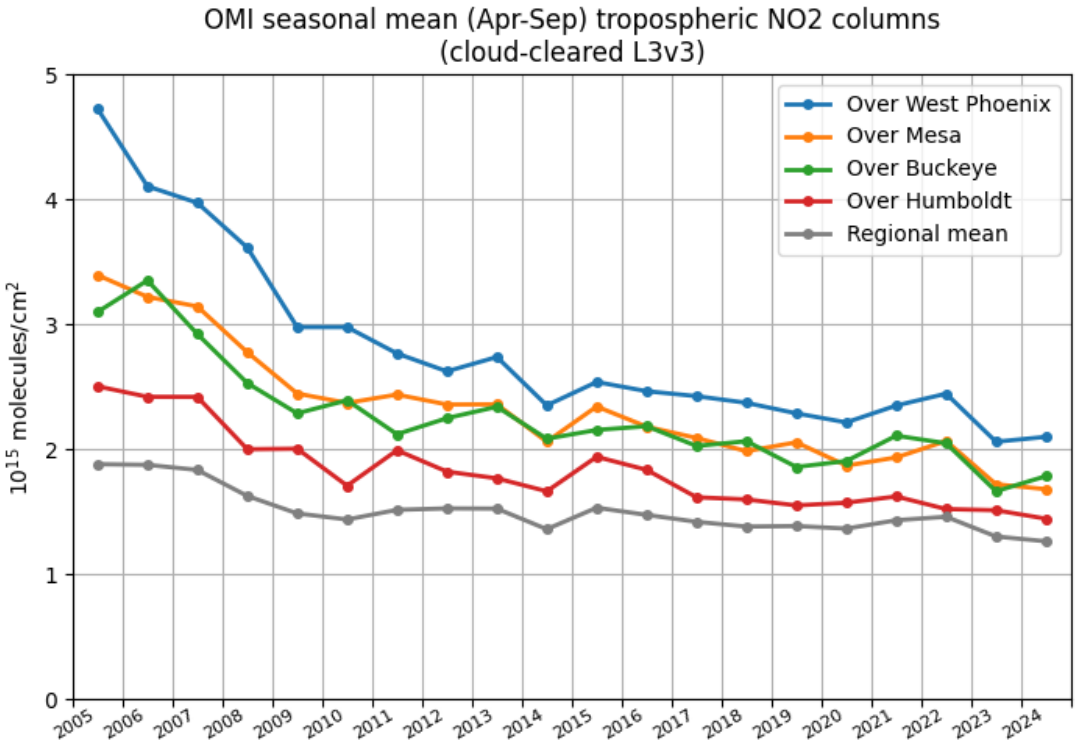

Figure 6-1 Seasonal mean OMI tropospheric NO_2 columns for 2005-2024 (April-September), averaged over selected monitoring locations (West Phoenix, Mesa, Buckeye, Humboldt) and the broader regional mean.

Figure 6-1 displays the long-term trend in OMI seasonal mean (April-September) cloud-cleared Level 3 version 3 (L3v3) tropospheric NO_2 column densities from 2005 to 2024. The time series are presented for spatially averaged data over four specific locations relevant to the Maricopa 8-hour ozone nonattainment area (West Phoenix, Mesa, Buckeye, Humboldt) and for a broader regional mean. Units are expressed as 10^{15} molecules/cm^2.

A predominant feature revealed by this extensive dataset is a significant overall decrease in tropospheric NO_2 columns across all locations and the regional average during the nearly two-decade observation period. The most substantial reductions occurred primarily between 2005 and approximately 2014. Following this period, the rate of decline appears to have attenuated, with trends showing stabilization or slower decreases in more recent years.

Consistent spatial gradients in NO_2 concentrations are maintained throughout the time series. West Phoenix consistently exhibits the highest column densities, reflecting substantial emissions characteristic of the urban core. Mesa and Buckeye show intermediate levels, indicative of significant suburban emission sources. NO_2 columns over Humboldt are considerably lower than the urban/suburban sites, yet remain elevated above the regional mean. The regional mean consistently represents the lowest values, integrating conditions over a wider geographic domain as shown in Figure 6-3.

Superimposed on the long-term downward trend is discernible interannual variability. All time series exhibit fluctuations, with notable relative minima observed around 2009, 2014, and 2020. These variations likely arise from a combination of factors, including year-to-year meteorological variability influencing NO_2 lifetime and dispersion, as well as potential variations in emissions.

In summary, the OMI observations provide robust evidence of a long-term reduction in seasonal mean tropospheric NO_2 over the Maricopa region since 2005, particularly pronounced over urban centers. This trend occurs alongside persistent spatial gradients reflecting emission distributions and significant interannual fluctuations driven by meteorology and emissions variability.

6.2 TROPOMI

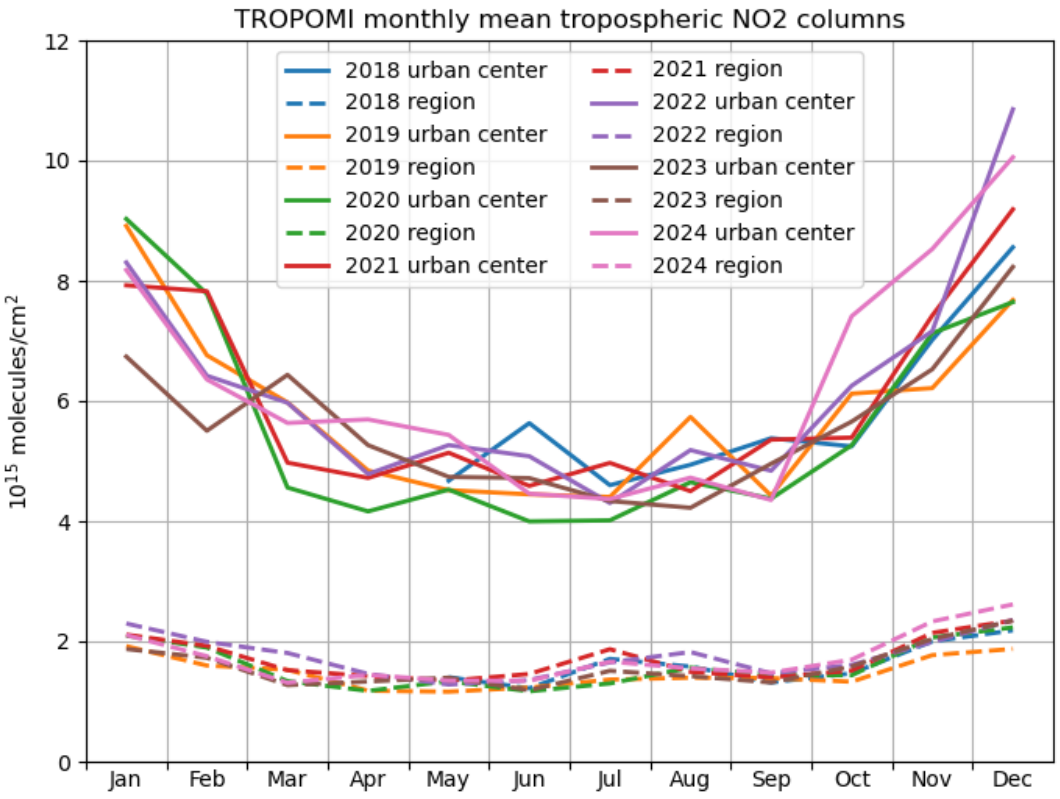

Figure 6-2 Year to year changes in monthly mean NO_2 for 2018-2024.

Figure 6-2 presents the TROPOMI-derived monthly mean tropospheric NO_2 column densities from 2018 through 2024, contrasting average NO_2 levels over the designated "urban center" with the broader surrounding "region".

A primary observation is the consistent and substantial elevation of NO_2 column densities over the urban center compared to the regional background across all months and years analyzed. This magnitude difference underscores the significant contribution of localized emissions within the urban core to the overall regional NO_2 burden.

Both the urban center and regional time series exhibit a pronounced seasonal cycle. Maximum NO_2 column densities typically occur during the winter months (approximately November through February), while minimum levels are observed during the summer months (approximately May through September). This seasonal variation is markedly more pronounced for the urban center, reflecting much larger absolute differences between winter maxima and summer minima compared to the relatively dampened seasonality of the regional background. The seasonality is driven by factors including changes in NOx emission rates, atmospheric lifetime (influenced by photolysis rates and oxidant concentrations), and boundary layer meteorology.

Significant interannual variability is also apparent. Notably, the NO_2 levels, particularly for the urban center, appear generally lower during 2020 compared to the preceding (2019) and subsequent (2021) years, especially during spring and summer months. This is consistent with potential emission reductions associated with the COVID-19 pandemic. Furthermore, there is considerable variability in the magnitude of the winter peaks across different years, for instance, the notably high values observed in late 2024 compared to other recent years, which may reflect specific meteorological conditions or emission changes.

Analysis of Exceedance Conditions, Smoke Influence, and Day-of-Week Patterns using TROPOMI (June-August, JJA 2019 & 2022)

Figure 6-3, Figure 6-4, and Figure 6-5 leverage TROPOMI's enhanced resolution to investigate factors associated with air quality exceedances during the JJA period.

- **Smoke Influence (JJA 2019, Figure 6-3):** Comparing non-smoke exceedance days with smoke-influenced exceedance days in 2019 reveals the profound impact of wildfire emissions. While the urban NO_2 hotspot persists under smoke influence, a distinct, strong secondary hotspot emerges northeast of the main urban area, accompanied by dramatically higher regional HCHO levels. These co-located enhancements are indicative of biomass burning emissions and subsequent photochemistry, significantly altering the regional chemical environment and, particularly for HCHO, overwhelming the typical urban signature. This highlights the critical need to account for episodic events like wildfires when analyzing regional air quality and satellite data.
- **Day-of-Week Exceedance Patterns (JJA 2022, Figure 6-4):** Stratifying exceedance versus non-exceedance days by weekdays and weekends reveals distinct behaviors. On **weekdays (Figure 6-4a)**, peak NO_2 column density over the urban core shows minimal difference between exceedance and non-exceedance conditions, although the plume appears spatially broader on exceedance days. This suggests that while NOx emissions are consistently high, factors beyond peak urban NO_2 levels (e.g., meteorology, transport, VOC availability) are critical drivers of weekday exceedances. Conversely, on **weekends (Figure 6-4b)**, NO_2 Column density are substantially lower on non-exceedance days compared to exceedance days across the urban core. This implies that elevated NO_2 levels themselves

are a more prominent characteristic and potentially a stronger contributing factor to weekend exceedances compared to weekdays.

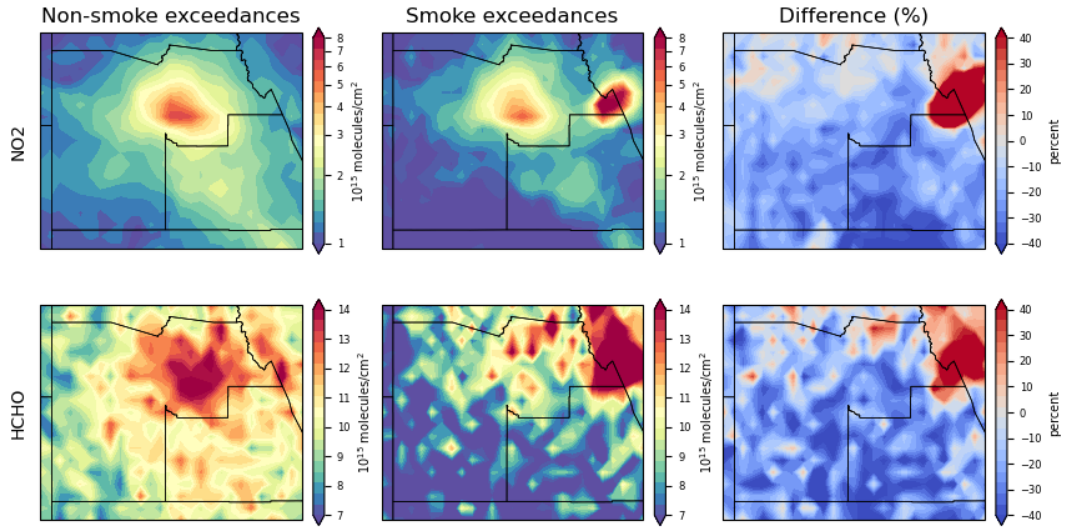

Figure 6-3 TROPOMI NO_2 and HCHO spatial distributions averaged for non-smoke exceedance days versus smoke-influenced exceedance days during June-August (JJA) 2019.

a)

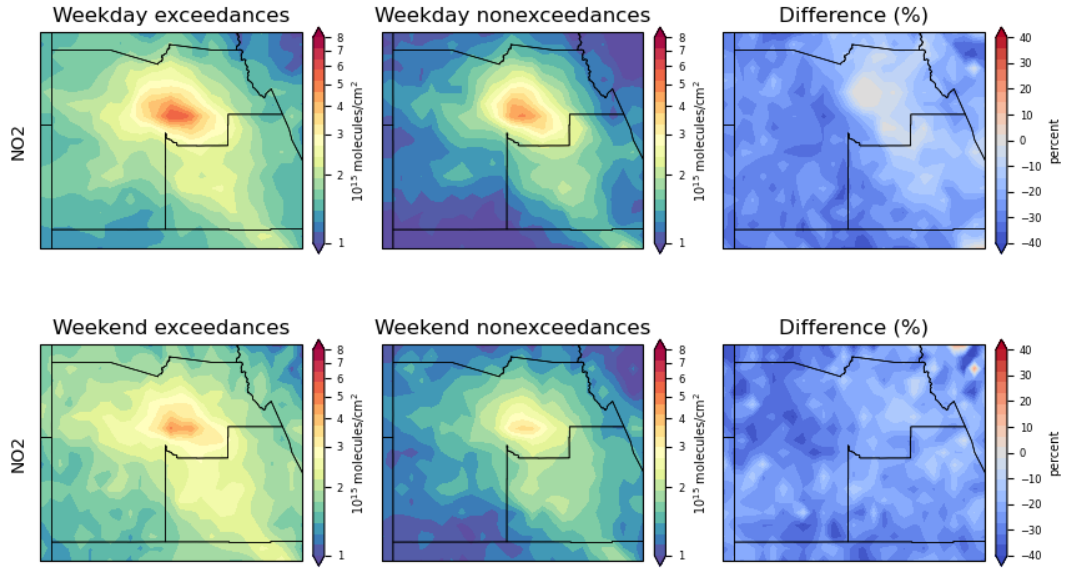

b)

Figure 6-4 TROPOMI NO_2 spatial distributions averaged during June-August (JJA) 2022, comparing: (a) weekday exceedance versus non-exceedance days, and (b) weekend exceedance versus non-exceedance days.

a)

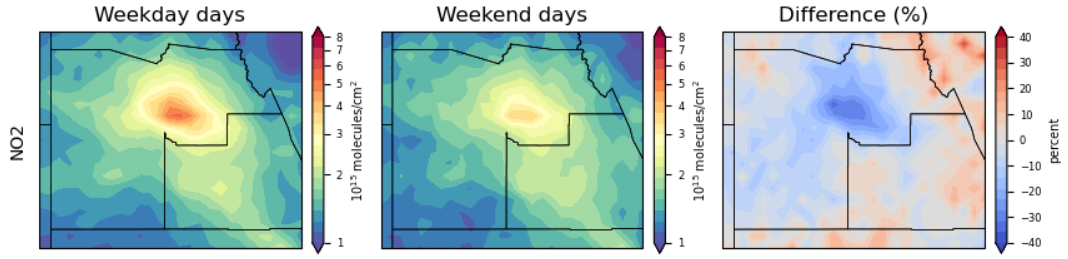

b)

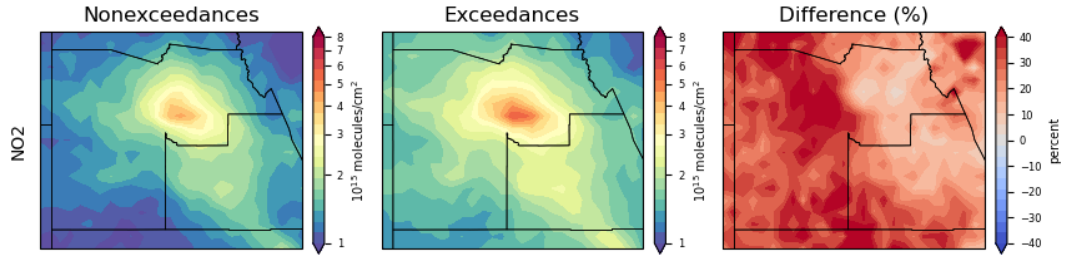

Figure 6-5 TROPOMI NO_2 spatial distributions averaged during June-August (JJA) 2022, comparing: (a) weekdays versus weekends, and (b) non-exceedance versus exceedance days.

- **Weekday vs. Weekend and Aggregate Exceedance Comparison (JJA 2022, Figure 6-5):** Contrasting average weekdays and weekends **(Figure 6-5a)** confirms the expected "weekend effect," with significantly lower NO_2 column density (often > 20-30% reduction) over the urban core on weekends due to reduced traffic/industrial activity. Interestingly, slight positive differences in surrounding areas may suggest altered spatial activity patterns or transport. The aggregate comparison between all exceedance and non-exceedance days **(Figure 6-5b)** reinforces the overall association, showing significantly higher NO_2 across the region, particularly the urbanized area (often > 20-30% increase), on exceedance days.

<u>Interannual TROPOMI NO_2 and HCHO Variations (JJA 2018-2024)</u>

- **NO_2 (Figure 6-6):** The TROPOMI seasonal JJA means from 2018-2024 confirm the persistent urban NO_2 hotspot. Significant interannual variability is evident, dominated by the distinct 2020 minimum (linked to pandemic response) and subsequent rebound towards pre-pandemic levels by 2021/2022, followed by relative stability with minor fluctuations through 2024. Subtle variations in plume shape and occasional enhancements in peripheral areas (e.g., northeast) could reflect other influences, such as episodic events (wildfires).

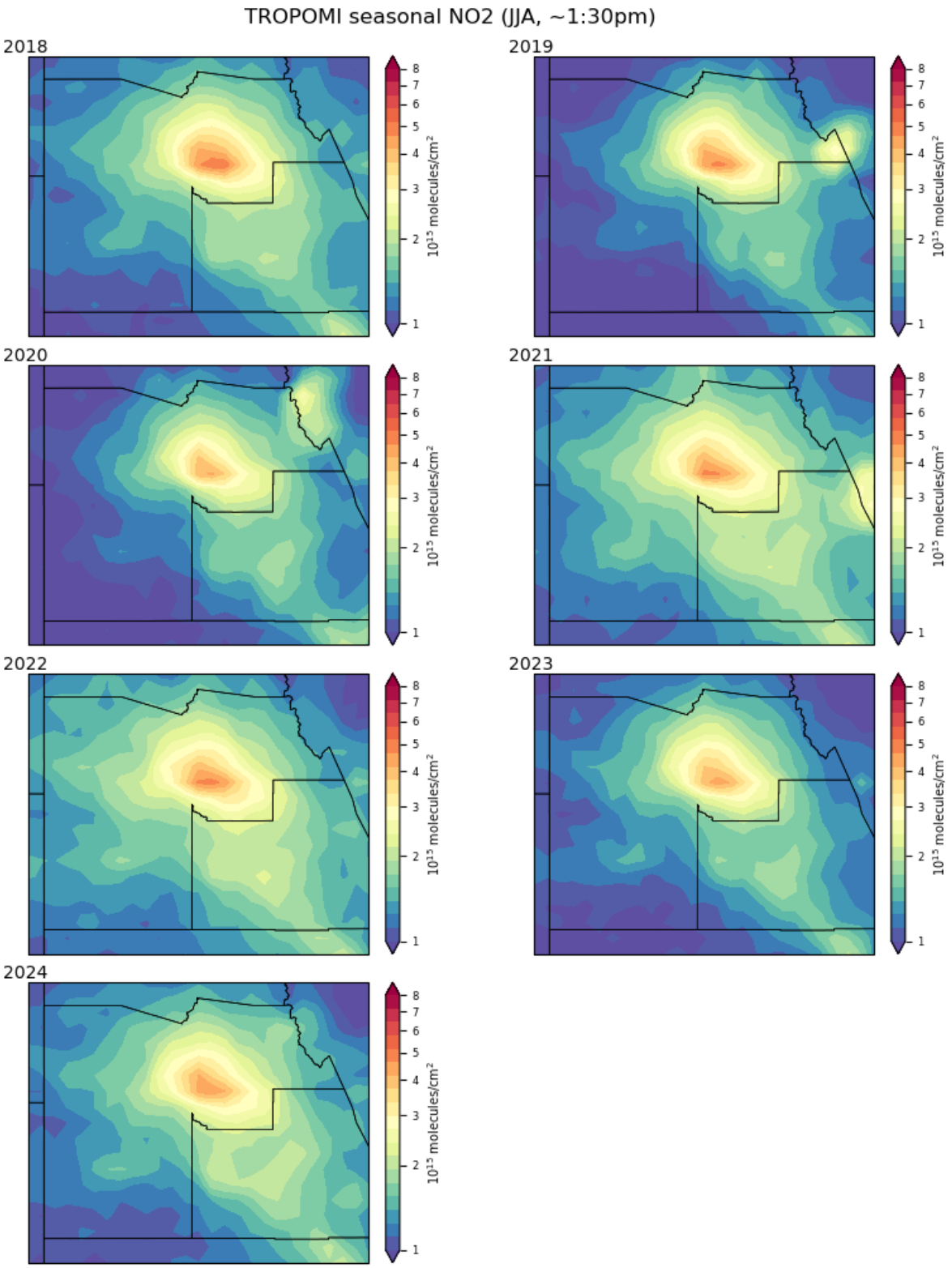

Figure 6-6 TROPOMI NO_2 spatial distributions averaged during June-August (JJA) from 2018 to 2024.

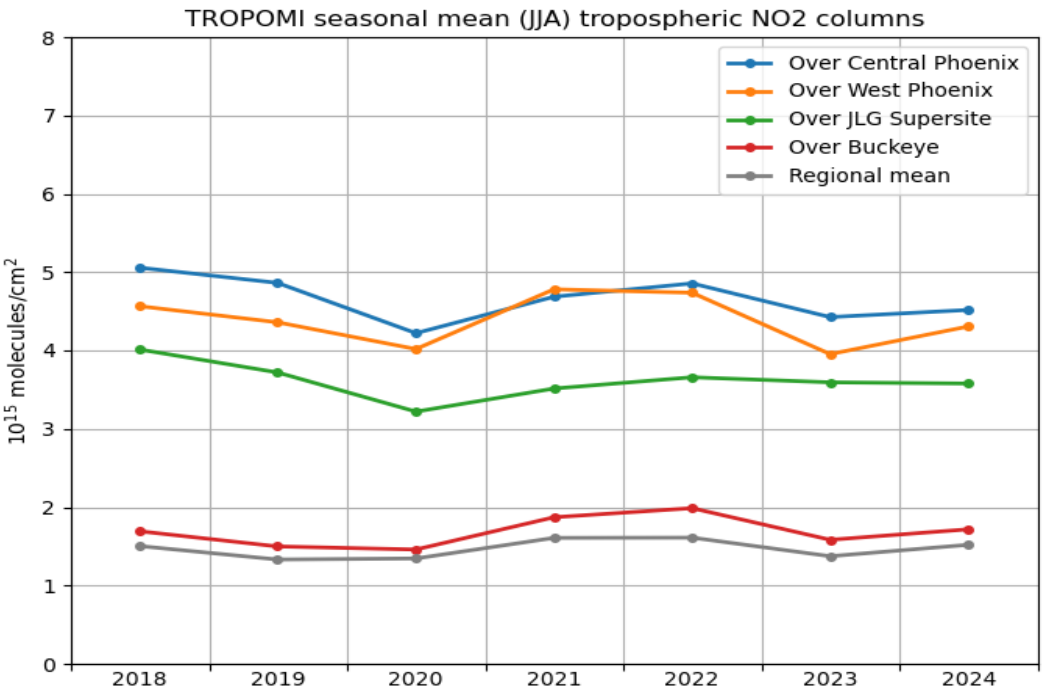

Figure 6-7 Seasonal mean NO_2 column density over four monitoring stations and the region from 2018-2024 (June- August) from TROPOMI.

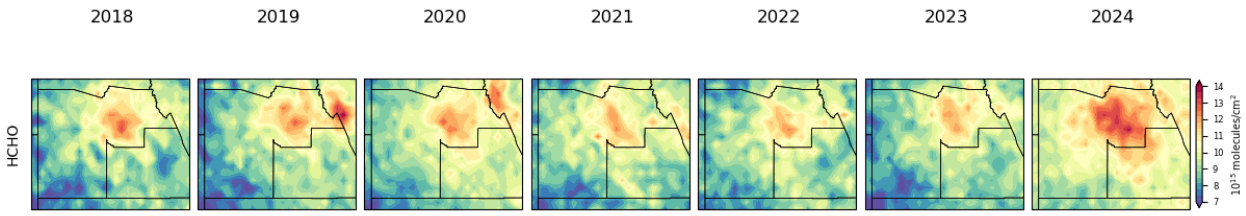

Figure 6-8 Spatial distributions of seasonal mean HCHO column density averaged during June-August (JJA) from 2018 to 2024.

- **NO_2 Time Series (Figure 6-7):** Time series averaged over specific monitor locations reiterate the findings from the spatial plots: a consistent urban-to-rural gradient (Central Phx > West Phx > JLG > Buckeye > Regional), the pronounced 2020 minimum, and the lack of a strong monotonic trend within this 2018-2024 timeframe, unlike the longer OMI record. It should be noted that differences in the observed relative levels between specific locations, as well as the overall absolute magnitudes, are apparent when comparing OMI and TROPOMI data. These differences are attributable to variations in their respective retrieval algorithms and, importantly, their distinct spatial resolutions.

- **HCHO (Figure 6-8):** In contrast to NO_2, HCHO exhibits a more diffuse spatial pattern, reflecting its mixed sources (anthropogenic, biogenic, secondary production, biomass burning). Significant interannual variability is observed, with JJA 2019 and 2024 showing notably higher HCHO concentrations, particularly over and northeast of Maricopa County. These enhancements likely reflect contributions from wildfire smoke (established for 2019) and/or favorable photochemical conditions. The influence of the 2020 activity reduction is less distinct for HCHO compared to NO_2, highlighting the strong role of natural emissions and photochemistry.

6.3 TEMPO

Diurnal NO_2 and HCHO Observations from TEMPO (July/JJA 2024)

TEMPO's geostationary perspective provides hourly observations, revealing crucial diurnal dynamics inaccessible to polar-orbiting satellites.

- **NO_2 Diurnal Cycle and Exceedance Comparison (JJA 2024, Figure 6-9):** TEMPO clearly captures the typical NO_2 diurnal profile: accumulation during morning rush hour (07:00 LT), peaking mid-morning (around 10:00 LT), followed by a steady decline through the afternoon (13:00, 16:00 LT) due to photochemical loss and boundary layer expansion. Critically, comparing exceedance versus non-exceedance days shows consistently and significantly higher NO_2 column density on ozone exceedance days across all observed daylight hours (07:00-16:00 LT). This persistent elevation suggests that higher overall NOx loading (from emissions and/or meteorology) is a key characteristic distinguishing ozone exceedance days during this period.

- **NO_2 and HCHO Diurnal Evolution (July 2024, Figure 6-10):** Comparing the diurnal patterns of NO_2 and HCHO highlights their distinct controlling processes. NO_2 (panels a, c, e, g) shows a sharp urban hotspot, peaking early (07:00-10:00 LT) and decaying rapidly due to photolysis. HCHO (panels b, d, f, h), conversely, starts low and spatially uniform (07:00 LT), then increases substantially by mid-morning (10:00 LT) over broad areas as photochemical production from VOCs dominates. HCHO levels generally peak around midday/early afternoon (13:00 LT) and remain elevated into the late afternoon (16:00 LT), exhibiting a more diffuse pattern than NO_2 and showing evidence of eastward transport influencing its distribution later in the day. These contrasting behaviors underscore the differing dominant sources and atmospheric fates of these key ozone precursors.

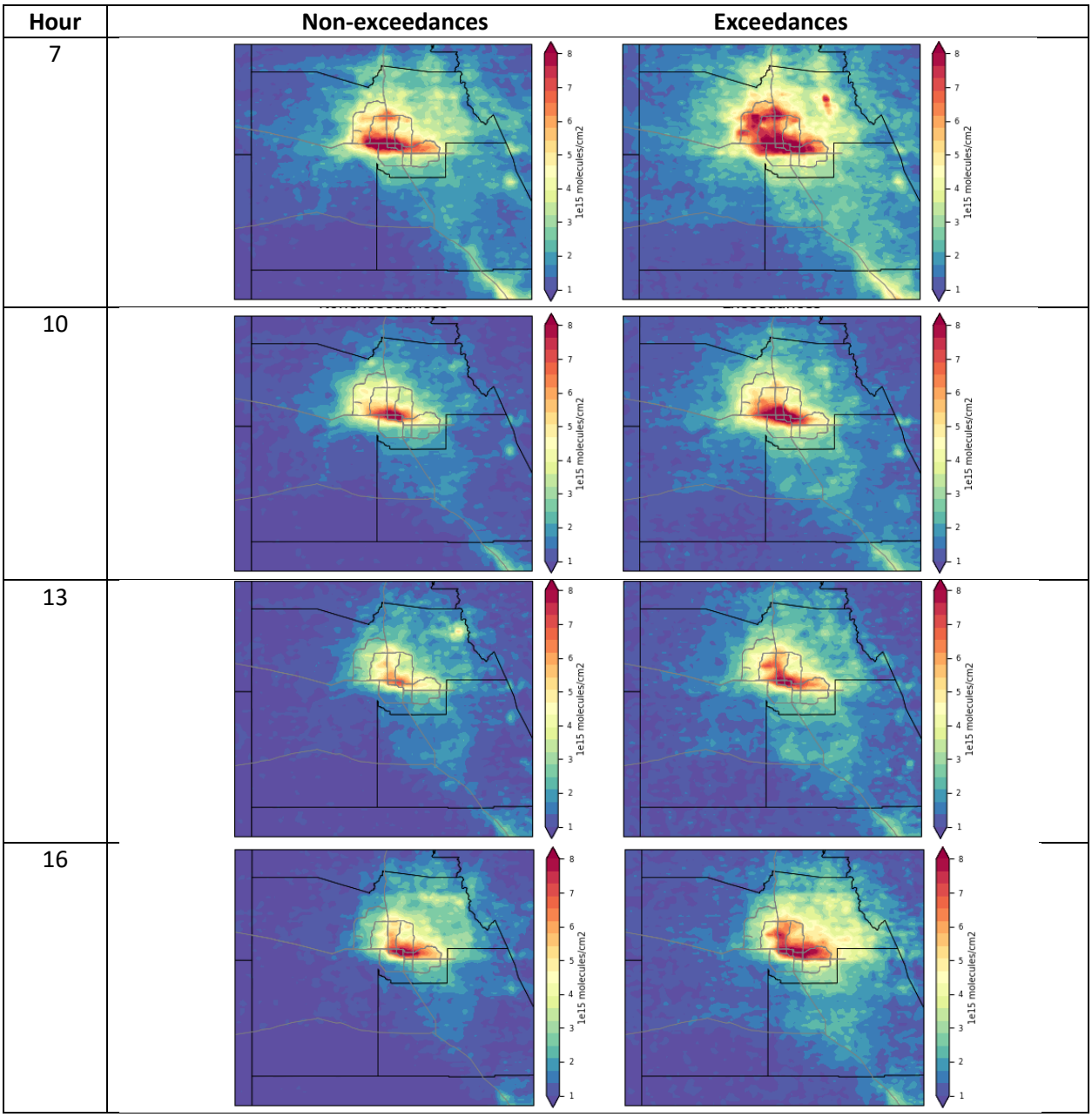

Figure 6-9 Comparison of spatial distributions of seasonal mean NO_2 column density for the non-exceedances versus exceedances days at four specific hours (07:00, 10:00, 13:00, and 16:00 Local Time) in July 2024.

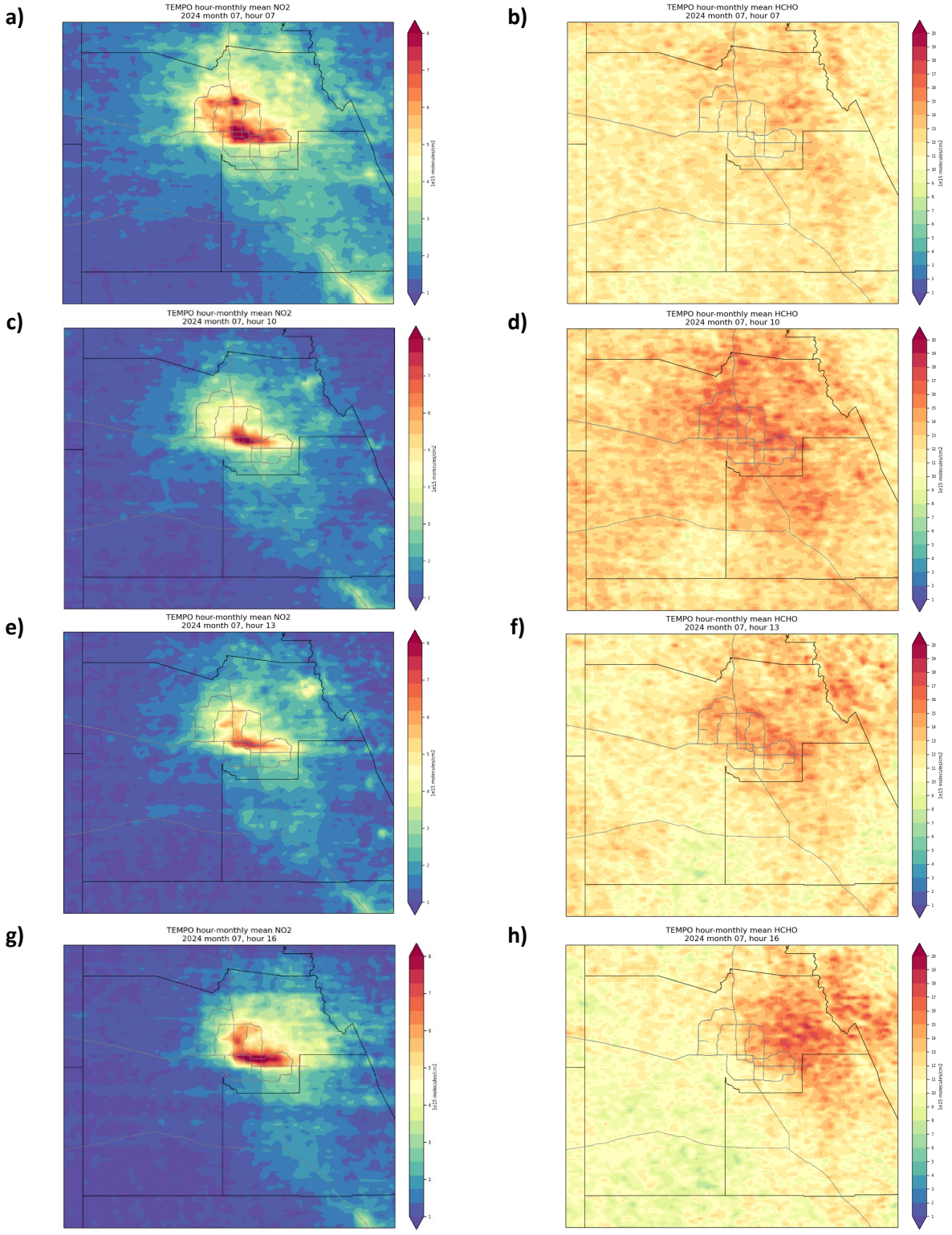

Figure 6-10 TEMPO hourly mean tropospheric column densities for NO_2 (panels a, c, e, g) and HCHO (panels b, d, f, h) for July 2024 at Hour 07, 10, 13 and 16 local time.

6.4 Model evaluation using satellite data

Figure 6-11 facilitates an evaluation of prior air quality model performance by comparing simulated seasonal mean (April-September 2017) tropospheric NO_2 column density from the CMAQ and CAMx models against corresponding satellite retrievals from the OMI product. Model output was resampled to match OMI coverage both temporally and spatially. The OMI averaging kernel was applied to the model columns to compute vertical column densities for comparison to the OMI columns. This comparison assesses the models' ability to replicate observed NO_2 spatial distributions and magnitudes over the southwestern US region.

- **Evaluation of Spatial Patterns:** Visual inspection reveals that both CMAQ and CAMx successfully capture the dominant spatial features evident in the OMI observations. Key anthropogenic source regions, manifested as distinct hotspots of elevated NO_2 column density, are correctly identified by both models over major urban centers (Phoenix, Las Vegas, and Mexicali). The models reproduce the general location and extent of these urban plumes relative to lower background concentrations, indicating a reasonable representation of the spatial distribution of NOx emissions and atmospheric processing on a regional scale.
- **Evaluation of Magnitude and Inter-Model Differences:** While capturing hotspot locations, both CMAQ and CAMx exhibit a positive bias in the magnitude of peak NO_2 column density within these urban areas compared to OMI retrievals. The simulated peak urban NO_2 levels are generally overestimated. Comparing the two models, CMAQ and CAMx produce largely similar spatial patterns and magnitudes. CMAQ shows slightly higher NO_2 than CAMx in the localized high-intensity pixel near the Four Corners region.

In summary, OMI satellite data provide valuable spatial context for evaluating the 2017 modeling simulations. Both CMAQ and CAMx demonstrated proficiency in capturing the location of major NO_2 sources but tended to overestimate peak urban concentrations compared to OMI retrievals for the April-September 2017 period.

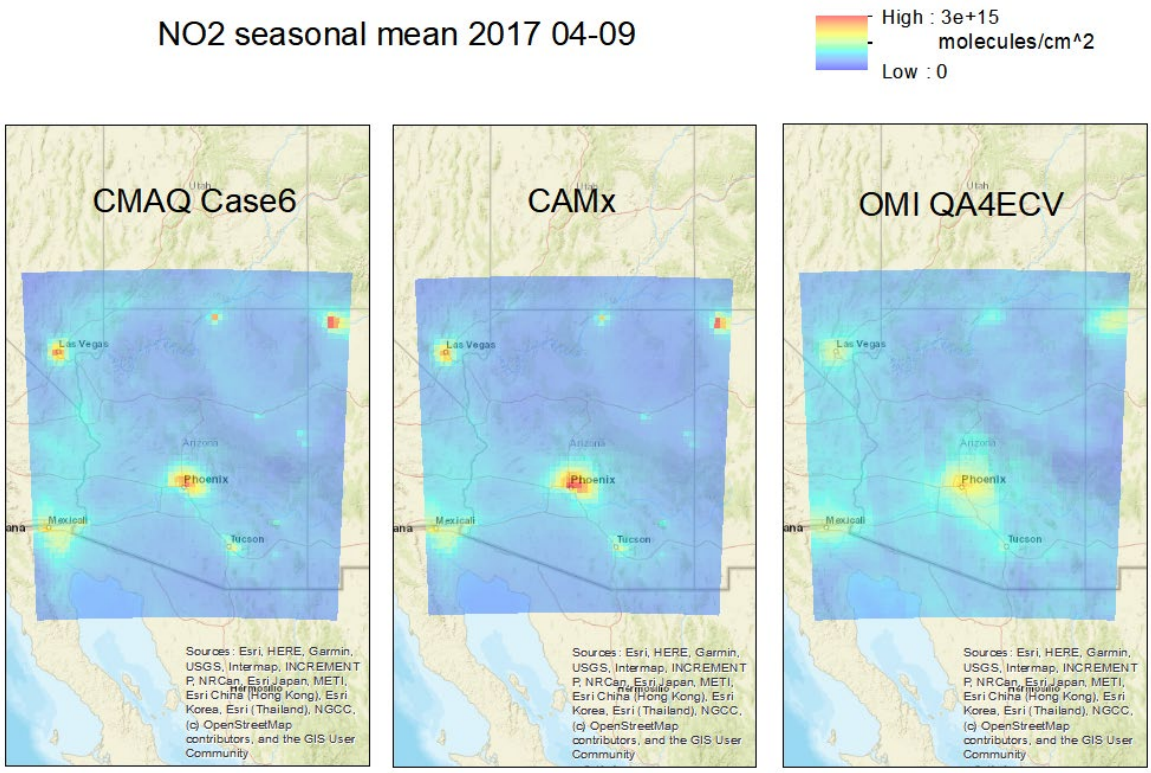

Figure 6-11 Evaluation of CMAQ and CAMx modeled seasonal mean (April-September 2017) tropospheric NO_2 columns against OMI satellite observations.

7 Conclusions

During the summer ozone season in the Maricopa 8-hour ozone nonattainment area, ozone levels are influenced by meteorological systems operating at multiple scales, including deep vertical mixing caused by stratospheric intrusion and blocking high-pressure systems, lower-level vertical mixing due to the development and dissipation of nocturnal inversion layers, long-range transport of upwind pollutants, and local mountain-valley breezes driven by terrain and topographic features. Additionally, strong solar radiation and drier air enhance ozone formation. Ozone exceedances are typically linked to the interaction of these large- and small-scale meteorological systems, in conjunction with local emissions. Note that urban heat flux has shown a strong upward trend since 2000, driven by the rapid growth of urbanization.

Characteristics of exceedances:

- Since 2000, extreme weather events in the Southwest, as indicated by the RCEI, have increased, and wildfire events, which are linked to these extreme conditions, have become more frequent. The variation in ozone exceedances has mirrored this trend. This suggests that changes in large-scale atmospheric systems are altering regional meteorological conditions, which in turn influence regional ozone levels. These extreme weather patterns,

including increased wildfires, may exacerbate ozone pollution, as smoke and other pollutants can contribute to higher concentrations of ozone in the atmosphere.
- The combination and interaction of favorable large- and local-scale systems contribute to extreme ozone concentrations and widespread exceedances, which result in the occurrence of the top 10 high ozone days for each year.
- Monitors with the highest frequency of exceedances are located downwind of the urban core.

Key formation factors:

- Local photochemical buildup due to intense solar radiation, high temperatures and stagnant conditions, combined with natural and anthropogenic emissions.
- Daytime temperatures are often above 100℉, with urban heat island effect causing overnight temperatures to remain elevated.
- Sustained circulation pattern of valley and mountain breezes traps ozone in basin.
- Westerly regional and long-range transport patterns bring pollution from California and wildfire smoke from the western states.
- Frequent long-range transport due to wind shifts during the summer monsoon season brings ozone and ozone precursors from Mexico into the region.
- Stratospheric intrusion contributes to downward transport of ozone-rich air mass from upper levels.
- The inversion layer traps ozone and ozone precursors from the previous day, enhancing ozone concentration due to strong vertical mixing after sunrise.
- Long-term OMI data confirm a significant regional NO_2 decrease, strongest 2005-2014 (likely reflecting emission controls), but the reduction rate has slowed considerably since.
- High-resolution TROPOMI/TEMPO link summer ozone exceedances to consistently higher NO_2 levels (esp. morning/early afternoon) and reveal profound, distinct impacts of wildfire smoke on NO_2/HCHO.

Areas for further study:

- Relationship between extreme weather conditions and increasing ozone concentration in recent years.
- The impacts of nocturnal inversions can be studied with vertical sounding observations to characterize the overnight vertical mixing processes and their effect on ozone levels on the following day.
- The impact of the upward trend in the urban heat island effect on the increase in surface ozone levels in recent years.
- Lightning occurs frequently with summer monsoon storms and is known to generate elevated NO_X in the atmosphere, but a quantitative analysis of the impacts of lightning NO_X is mainly dependent on the availability of observational data regarding lightning strikes.

8 References

ADEQ (2023). State of Arizona Air Monitoring Network Plan for the Year 2023, Arizona Department of Environmental Quality. May 2023.

Butler, A., A. Langford, and E. Ray (2021). Stratosphere-troposphere coupling and impacts on the surface, CSL uses observations and models to investigate the coupling between the stratosphere and troposphere. February 4, 2021

Caputi, D.J., I. Faloona, J. Trousdell, J. Smoot, N. Falk, and S. Conley (2019). Residual layer ozone, mixing, and the nocturnal jet in California's San Joaquin Valley. *Atmospheric Chemistry & Physics*, 19(7).

Conil, S., G. Bergametti, L. Langrene, M. Lopez, O. Masson, C. Pallares, and M. Ramonet (2025). Surface Ozone: Seasonal cycles, trends and events, a new perspective from the OPE station in France over the 2012–2023 period, EGUsphere [preprint], https://doi.org/10.5194/egusphere-2025-148, 2025.

Cooper, O. R., M. Trainer, A. M. Thompson, S. J. Oltmans, D. W. Tarasick, J. C. Witte, and B. J. Johnson (2007). Evidence for a recurring eastern North America upper tropospheric ozone maximum during summer. *Journal of Geophysical Research: Atmospheres*, 112(D23).

Danielsen, E. F. (1968). Stratospheric-tropospheric exchange based on radioactivity, ozone and potential vorticity. *Journal of Atmospheric Sciences*, *25*(3), 502-518.

Gaffney, J. S., N. A. Marley, P. J. Drayton, P. V. Doskey, V. R. Kotamarthi, M. M. Cunningham, J. C. Baird, J. Dintaman, H. L. Hart (2002). Field observations of regional and urban impacts on NO_2, ozone, UVB, and nitrate radical production rates in the Phoenix air basin. *Atmospheric Environment*, 36(5), 825−833.

Galani, E., D. Balis, P. Zanis, C. Zerefos, A. Papayannis, H. Wernli, and E. Gerasopoulos (2003). Observations of stratosphere-to-troposphere transport events over the eastern Mediterranean using a ground-based lidar system. *Journal of Geophysical Research: Atmospheres*, *108*(D12).

Gleason, K. L., J. H. Lawrimore, D. H. Levinson, T. R. Karl, and D. J. Karoly (2008). A revised US climate extremes index. *Journal of Climate*, 21(10), 2124-2137.

Hu, J., Y. Li, T. Zhao, J. Liu, X. M. Hu, D. Liu, Y. Jiang, J. Xu, and L. Chang (2018). An important mechanism of regional O3 transport for summer smog over the Yangtze River Delta in eastern China. *Atmospheric Chemistry and Physics*, 18(22), 16239-16251.

Hu, Y., M. T. Odman, A. G. Russell, N. Kumar, and E. Knipping (2022). Source Apportionment of Ozone and Fine Particulate Matter in the United States for 2016 and 2028. *Atmospheric Environment*, 285, 119226.

Huang, M., G. R. Carmichael, T. Chai, R. B. Pierce, S. J. Oltmans, D. A. Jaffe, K. W. Bowman, A. Kaduwela, C. Cai, S. N. Spak, A. J. Weinheimer, L. G. Huey, and G. S. Diskin (2013). Impacts of

transported background pollutants on summertime western US air quality: model evaluation, sensitivity analysis and data assimilation. *Atmospheric Chemistry and Physics*, 13(1), 359-391.

Jaeglé, L., R. Wood, and K. Wargan (2017). Multiyear composite view of ozone enhancements and stratosphere-to-troposphere transport in dry intrusions of northern hemisphere extratropical cyclones. *Journal of Geophysical Research: Atmospheres*, 122(24), 13,436–13,457. https://doi.org/10.1002/2017JD027656

Kaldunski, B., B. Pierce, and T. Holloway (2017). When Stratospheric Ozone Hits Ground-level Regulation: Exceptional Events in Wyoming. *Bulletin of the American Meteorological Society*, 98(5), 889-892.

Karl, T. R., R. W. Knight, D. R. Easterling, and R. G. Quayle (1996). Indices of climate change for the United States. *Bulletin of the American Meteorological Society*, 77(2), 279-292.

Langford, A. O., J. Brioude, O. R. Cooper, C. J. Senff, R. J. Alvarez, R. M. Hardesty, and S. J. Oltmans (2012). Stratospheric influence on surface ozone in the Los Angeles area during late spring and early summer of 2010. *Journal of Geophysical Research: Atmospheres*, 117(D21).

Langford, A. O. (2022). Measurements and modeling of the May 12, 2022 stratospheric intrusion, NOAA Chemical Sciences Laboratory Stratospheric Intrusion working Group meeting.

Lefohn, A. S., H. Wernli, D. Shadwick, S. Limbach, S. J. Oltmans, and M. Shapiro (2011). The importance of stratospheric–tropospheric transport in affecting surface ozone concentrations in the western and northern tier of the United States. *Atmospheric Environment*, 45(28), 4845-4857.

Lelieveld, J., P. Hoor, P. Jöckel, A. Pozzer, P. Hadjinicolaou, J. P. Cammas, and S. Beirle (2009). Severe ozone air pollution in the Persian Gulf region. *Atmospheric Chemistry and Physics*, 9(4), 1393-1406.

Li, J., M. Georgescu, P. Hyde, A. Mahalov, and M. Moustaoui (2015). Regional-scale transport of air pollutants: impacts of Southern California emissions on Phoenix ground-level ozone concentrations. *Atmospheric Chemistry and Physics*, 15 (16), 9345−9360.

Lin, M., A. M. Fiore, L. W. Horowitz, O. R. Cooper, V. Naik, J. Holloway, and T. B. Ryerson (2012). Transport of Asian ozone pollution into surface air over the western United States in spring. *Journal of Geophysical Research: Atmospheres*, 117(D21).

Lin, M., A. M. Fiore, L. W. Horowitz, A. O. Langford, S. J. Oltmans, D. Tarasick, and H. E. Rieder (2015). Climate variability modulates western US ozone air quality in spring via deep stratospheric intrusions. *Nature communications*, *6*.

MAG (2016). MAG 2017 Eight-Hour Ozone Moderate Area Plan for the Maricopa Nonattainment Area, Maricopa Association of Governments. December 2016.

MCAQD (2024), 2024 Air Monitoring Network Plan, Maricopa County Air Quality Department, May 2024.

Morris, G. A., B. Ford, B. Rappenglück, A. M. Thompson, A. Mefferd, F. Ngan, and B. Lefer (2010). An evaluation of the interaction of morning residual layer and afternoon mixed layer ozone in Houston using ozonesonde data, *Atmos. Environ*., 44, 4024–4034.

Neu, U., T. Künzle, and H. Wanner (1994). On the relation between ozone storage in the residual layer and daily variation in near-surface ozone concentration – A case study, *Bound.-Lay. Meteor*., 69, 221–247.

PCAQCD (2024). 2024 Ambient Monitoring Network Plan and 2023 Data Summary, Pinal County Air Quality Control District.

Prabhakar, G., C. Parworth, X. Zhang, H. Kim, D. Young, A. Beyersdorf, L. D. Ziemba, J. B. Nowak, T. Bertram, I. C. Faloona, and Q. Zhang (2017). Observational assessment of the role of nocturnal residual-layer chemistry in determining daytime surface particulate nitrate concentrations.

Pryor, S. C., and T. E. Hoffer (1992). A case study of pollutant transport from Los Angeles to the desert south-west. *Atmospheric Environment*. Part A. General Topics, 26(2), 243-250.

Pryor, S. C., I. G. McKendry, and D. G. Steyn (1995). Synoptic-scale meteorological variability and surface ozone concentrations in Vancouver, British Columbia. *Journal of Applied Meteorology*, 34(8), 1824-1833.

Ridley, B. A., J. G. Walega, J. E. Dye, and F. E. Grahek (1994). Distributions of NO, NOx, NOy, and O3 to 12 km altitude during the summer monsoon season over New Mexico. *Journal of Geophysical Research: Atmospheres*, 99(D12), 25519-25534.

Sheppard, P. R., A. C. Comrie, G. D. Packin, K. Angersbach, and M. K. Hughes (2002). The climate of the US Southwest. *Climate Research*, 21(3), 219-238.

SRPMIC (2024), 2023 Ambient Air Monitoring Network Plan Report, Salt River Pima-Maricopa Indian Community, June 2024.

Sillman, S. (1999). The relation between ozone, NOx and hydrocarbons in urban and polluted rural environments, *Atmos. Environ*., 33, 1821–1845.

Smith, A., N. Lott, and R. Vose (2011). The integrated surface database: Recent developments and partnerships. *Bulletin of the American Meteorological Society*, 92(6), pp.704-708.

Stevenson, D. S., F. J. Dentener, M. G. Schultz, K. Ellingsen, T. P. C. van Noije, O. Wild, and S. Szopa (2006). Multimodel ensemble simulations of present-day and near-future tropospheric ozone. *Journal of Geophysical Research*, 111, D08301. https://doi.org/10.1029/2005JD006338

Stohl, A., P. Bonasoni, P. Cristofanelli, W. Collins, J. Feichter, A. Frank, C. Forster, E. Gerasopoulos, H. Gäggeler, P. James, T. Kentarchos, H. Kromp-Kolb, B. Krüger, C. Land, J. Meloen, A. Papayannis, A. Priller, P. Seibert, M. Sprenger, G. J. Roelofs, H. E. Scheel, C. Schnabel, P. Siegmund, L. Tobler, T. Trickl, H. Wernli, V. Wirth, P. Zanis, and C. Zerefos (2003a). Stratosphere-troposphere exchange: A review, and what we have learned from STACCATO, *J. Geophys. Res.*, 108(D12), 8516,doi:10.1029/2002JD002490.

Stohl, A., H. Wernli, P. James, M. Bourqui, C. Forster, M. A. Liniger,P. Seibert, and M. Sprenger (2003b). A new perspective of stratosphere–troposphere exchange, *Bull. Am. Meteorol. Soc.*,84, 1565–1573,doi:10.1175/BAMS-84-11-1565.

Stull, R. B. (1988). An introduction to boundary layer meteorology, *Atmospheric Sciences Library*, 8, 499–543.

U.S. EPA (2008). Learn about Urban Heat Island. URL: https://www.epa.gov/heat-islands/learn-about-heat-islands

U.S. EPA (2016). Air Quality Modeling Technical Support Document for the Final Cross State Air Pollution Rule Update. *U.S. Environmental Protection Agency*. August 2016. URL: https://www.epa.gov/sites/default/files/2017-05/final_csapr_update_ozone_design_values_contributions_all_sites.xlsx.

U.S. EPA (2025). Air Quality System Data Mart (data server) available at http://www.epa.gov/aqsweb/documents/data_mart_welcome.html. Accessed 2025.

Venter, Z. S., K. Aunan, S. Chowdhury, and J. Lelieveld (2020). COVID-19 lockdowns cause global air pollution declines. *Proceedings of the National Academy of Sciences*, 117(32), 18984-18990.

Vingarzan, R. (2004). A review of surface ozone background levels and trends. *Atmospheric Environment,* 38(21), 3431-3442.

White, W. H., E. S. Macias, D. F. Miller, D. E. Schorran, T. E. Hoffer, and D. P. Rogers (1990). Regional transport of the urban workweek: Methylchloroform cycles in the Nevada-Arizona Desert. *Geophysical Research Letters*, 17(8), 1081-1084.

Wong, J. (2013). Upper Tropospheric Ozone Enhancement during the North American Monsoon evaluated using .the Weather Research and Forecasting Model with Chemistry (WRF-Chem) (Doctoral dissertation, University of Colorado at Boulder).

Xie, M., K. Zhu, T. Wang, P. Chen, Y. Han, S. Li, B. Zhuang, and L. Shu (2016). Temporal characterization and regional contribution to O3 and NOx at an urban and a suburban site in Nanjing, China, *Sci. Total Environ.*, 551, 533–545.

Zhang, J. and S. T. Rao (1999). The role of vertical mixing in the temporal evolution of ground-level ozone concentrations. *Journal of Applied Meteorology*, 38(12), 1674-1691.

Zhang, H., S. Wu, Y. Huang, and Y. Wang (2014). Effects of stratospheric ozone recovery on photochemistry and ozone air quality in the troposphere. *Atmospheric Chemistry and Physics*, 14(8), 4079-4086.

MAG 2025 CLEAN AIR ACT SECTION 179B(b) RETROSPECTIVE DEMONSTRATION OF THE IMPACT OF INTERNATIONAL EMISSIONS ON OZONE CONCENTRATIONS IN THE MARICOPA NONATTAINMENT AREA

APPENDIX C –
Evaluation of Atypical Exceedance Days of the 2015 Ozone Standard in the Maricopa Ozone Nonattainment Area for Wildfire Impacts (2021-2023)

SEPTEMBER 2025

MARICOPA ASSOCIATION of GOVERNMENTS

Evaluation of Atypical Exceedance Days of the 2015 Ozone Standard in the Maricopa Ozone Nonattainment Area for Wildfire Impacts (2021-2023)

Report Prepared for

Maricopa Association of Governments

September 2025

STi | Sonoma Technology

A SPHEROS ENVIRONMENTAL COMPANY

This document contains blank pages to accommodate two-sided printing.

Evaluation of Atypical Exceedance Days of the 2015 Ozone Standard in the Maricopa Ozone Nonattainment Area for Wildfire Impacts (2021-2023)

Prepared by

Charles R. Scarborough
Hilary R. Hafner
Steve T. Irwin
Jeff J. Beamish

Sonoma Technology
1450 N. McDowell Blvd., Suite 200
Petaluma, CA 94954
Ph 707.665.9900
sonomatech.com

Prepared for

Maricopa Association of Governments
302 North First Avenue, Suite 200
Phoenix, AZ 85003

Final Report
STI-8449

September 2025

Contents

1. OZONE TECHNICAL SUPPORTING DOCUMENTATION FOR ATYPICAL EVENTS 1
1.1 Purpose 1
1.1.1 Maricopa Nonattainment Area Description 1
1.1.2 Development of Atypical Event Dates 1
1.2 Methods and Data Sets 4
1.2.1 Identification of Wildfires and Surface Impacts 5
1.2.2 Meteorological Analyses 6
1.3 Prevailing Meteorological and Wildfire Conditions (2021-2023) 9
2. 2021 WILDFIRE EVENTS 15
2.1 Overview 15
2.2 June 15-16, 2021 15
2.2.1 Event Overview: June 15-16, 2021 15
2.2.2 Identification of Wildfire(s) 17
2.2.3 Meteorological Analysis 20
2.2.4 Surface Impacts 29
2.2.5 Event Statistics 37
2.2.6 Conclusion 39
2.3 June 28-29, 2021 40
2.3.1 Event Overview: June 28-29, 2021 40
2.3.2 Identification of Wildfire(s) 41
2.3.3 Meteorological Analysis 43
2.3.4 Surface Impacts 52
2.3.5 Event Statistics 60
2.3.6 Conclusion 61
2.4 July 1, 2021 62
2.4.1 Event Overview: July 1, 2021 62
2.4.2 Identification of Wildfire(s) 63
2.4.3 Meteorological Analysis 65
2.4.4 Surface Impacts 71
2.4.5 Event Statistics 78
2.4.6 Conclusion 79
2.5 July 20-22, 2021 80
2.5.1 Event Overview: July 20-22, 2021 80
2.5.2 Identification of Wildfire(s) 82
2.5.3 Meteorological Analysis 84
2.5.4 Surface Impacts 92
2.5.5 Event Statistics 100
2.5.6 Conclusion 102
2.6 August 3-4, 2021 103
2.6.1 Event Overview: August 3-4, 2021 103
2.6.2 Identification of Wildfire(s) 104
2.6.3 Meteorological Analysis 107

2.6.4 Surface Impacts 112
2.6.5 Event Statistics 119
2.6.6 Conclusion 121
3. ..... 2022 WILDFIRE EVENTS 123
3.1 ....Overview 123
3.2 ....June 15-16, 2022 123
3.2.1 Event Overview: June 15-16, 2022 123
3.2.2 Identification of Wildfire(s) 125
3.2.3 Meteorological Analysis 126
3.2.4 Surface Impacts 133
3.2.5 Event Statistics 141
3.2.6 Conclusion 143
3.3 ....July 15-17, 2022 144
3.3.1 Event Overview: July 15-17, 2022 144
3.3.2 Identification of Wildfire(s) 146
3.3.3 Meteorological Analysis 148
3.3.4 Surface Impacts 155
3.3.5 Event Statistics 161
3.3.6 Conclusion 163
4. ..... 2023 WILDFIRE EVENTS 165
4.1 ....Overview 165
June 22-26, 2023 165
4.1.1 Event Overview: June 22-26, 2023 165
4.1.2 Identification of Wildfire(s) 167
4.1.3 Meteorological Analysis 170
4.1.4 Surface Impacts 177
4.1.5 Event Statistics 186
4.1.6 Conclusion 189
4.2 ....June 30, 2023 189
4.2.1 Event Overview: June 30, 2023 189
4.2.2 Identification of Wildfire(s) 191
4.2.3 Meteorological Analysis 193
4.2.4 Surface Impacts 198
4.2.5 Event Statistics 202
4.2.6 Conclusion 203
4.3 ....July 24-29, 2023 204
4.3.1 Event Overview: July 24-29, 2023 204
4.3.2 Identification of Wildfire(s) 206
4.3.3 Meteorological Analysis 210
4.3.4 Surface Impacts 217
4.3.5 Event Statistics 223
4.3.6 Conclusion 226
4.4 ....July 31-August 1, 2023 227
4.4.1 Event Overview: July 31-August 1, 2023 227
4.4.2 Identification of Wildfire(s) 228
4.4.3 Meteorological Analysis 231

4.4.4 Surface Impacts 237
4.4.5 Event Statistics 243
4.4.6 Conclusion 245
4.5 August 17-18, 2023 245
4.5.1 Event Overview: August 17-18, 2023 245
4.5.2 Identification of Wildfire(s) 247
4.5.3 Meteorological Analysis 249
4.5.4 Surface Impacts 254
4.5.5 Event Statistics 259
4.5.6 Conclusion 260
5. REFERENCES 261

Figures

Figure 1-1. 2015 Eight-Hour Ozone Nonattainment Area Boundary (source: MAG 2025 Eight-Hour Ozone Plan – Submittal of Applicable Moderate Area Requirements for the Maricopa Nonattainment Area [April 2025]). 2

Figure 1-2. Ozone monitoring sites in the Maricopa Nonattainment Area (2025). 3

Figure 1-3. 2021 large fire occurrences across the United States. Numerous wildfires exceeding 100-300 acres occurred in Arizona, impacting local air quality. Source: NIFC 10

Figure 1-4. Mean 500 mb geopotential heights (meters) for June-September 2021. High pressure aloft over Arizona resulted in hot temperatures and enhanced PBL heights. Source: NOAA 11

Figure 1-5. 500 mb geopotential height anomalies for April-July 2022. Areas in yellow and orange indicate the persistence of an above-normal region of high pressure over the southwestern United States. Source: NOAA 12

Figure 1-6. Perimeters of 2023 wildfires across Canada. Smoke from these fires impacted air quality across a large portion of the United States during the summer months. Source: Canadian National Fire Database (CNFDB) 13

Figure 1-7. Mean 500 mb geopotential heights (meters) for May-August 2023. An upper-level high pressure ridge from Mexico to western Canada resulted in hot, dry conditions in Arizona. Source: NOAA 14

Figure 2-1. Hourly ozone concentrations (ppb) compared to all available data during the ozone season (April 1 – September 31) of the 6-year (2019-2024) period. Hourly means and 10th-90th percentiles are calculated using data on June 15-16. 17

Figure 2-2. Regional view of HMS smoke density and fire locations on June 14, 2021 18

Figure 2-3. Regional view of HMS smoke density and fire locations on June 15, 2021 19

Figure 2-4. Regional view of HMS smoke density on June 16, 2021 19

Figure 2-5. Continental view of HMS smoke density and fire locations on June 15, 2021. 20

Figure 2-6. Average geopotential height at 500 mb from June 15-16, 2021. 21

Figure 2-7. Surface analyses from 14:00 LST on June 15, 2021, (left) and 14:00 LST on June 16, 2021, (right) 22

Figure 2-8. HMS fire and smoke along with hourly concentrations of $PM_{2.5}$ at 8:00 LST June 15, 2021, (left) and 8:00 LST June 16, 2021, (right). 23

Figure 2-9. Visible satellite imagery from approximately 13:53 LST on June 15, 2021. Fire detections are indicated by orange dots. 23

Figure 2-10. Visible satellite imagery from approximately 12:57 LST on June 16, 2021. Fire detections are indicated by orange dots. 24

Figure 2-11. A zoomed-in view over the southwestern of MODIS Aqua AIRS CO retrieval during the atypical ozone date of June 15, 2021. The black box represents the approximate area of the NAA. 25

Figure 2-12. Observed atmospheric soundings from 5:00 LST (left) and 17:00 LST (right) June 15-16, 2021. 27

Figure 2-13. NOAA smoke and fire maps and NOAA HYSPLIT trajectory model runs with air parcels moving 48-hours before 00:00 – 20:00 LST between June 15-16, 2021, at 100 meters, 1,000 meters and 2,500 meters (AGL). Analysis performed by MAG. 28

Figure 2-14. Camera Images showing the southwest coordinal direction taken from the Estrella Mountain webcam on June 15 from 8:00 LST, 11:00 LST, 14:00 LST, and 17:00. 29

Figure 2-15. Camera Images showing the southwest coordinal direction taken from the Estrella Mountain webcam on June 16 from 8:00 LST, 11:00 LST, 14:00 LST, and 17:00. 30

Figure 2-16. Camera Images showing the south coordinal direction taken from the South Mountain webcam on June 15 from 8:00 LST, 11:00 LST, 14:00 LST, and 17:00. 30

Figure 2-17. Camera Images showing the south coordinal direction taken from the South Mountain webcam on June 16 from 8:00 LST, 11:00 LST, 14:00 LST, and 17:00. 31

Figure 2-18. Camera Images showing the east coordinal direction taken from the Superstition Mountain webcam on June 15 from 8:00 LST, 11:00 LST, 14:00 LST, and 17:00. 31

Figure 2-19. Camera Images showing the east coordinal direction taken from the Superstition Mountain webcam on June 16 from 8:00 LST, 11:00 LST, 14:00 LST, and 17:00. 32

Figure 2-20. Camera Images showing the west-northwest coordinal direction taken from the White Tank Mountain webcam on June 15 from 8:00 LST, 11:00 LST, 14:00 LST, and 17:00. 32

Figure 2-21. Camera Images showing the west-northwest coordinal direction taken from the White Tank Mountain webcam on June 16 from 8:00 LST, 11:00 LST, 14:00 LST, and 17:00. 33

Figure 2-22. Hourly concentrations of ozone, NO_2, and $PM_{2.5}$ at all sites in the nonattainment area. All ozone-exceeding sites are color-coded to highlight smoke impacts on concentrations, and all non-exceeding sites are black. The gray shaded areas represent June 15 and 16, 2021. 34

Figure 2-23. Hourly concentrations of $PM_{2.5}$ (top) and NO_2 (bottom) at the West Phoenix site. The 6-year (2019-2024) median is represented by the dashed line, and the 5th-95th percentile is represented by the shaded area. 35

Figure 2-24. Boxplot of OC to EC ratios at the JLG Supersite site using data collected during the ozone season (April-September) from 2019-2024. OC to EC ratios are calculated at POC 2 (x-axis). Available OC to EC ratios collected during the June 15-16 atypical ozone event are shown as a point. 36

Figure 2-25. Boxplots of speciated $PM_{2.5}$ collected at the JLG Supersite site collected during the ozone season (April-September) from 2019-2024. Available speciated $PM_{2.5}$

concentrations collected during the June 15-16 atypical ozone event are shown as a point. 37

Figure 2-26. Hourly ozone concentrations (ppb) compared to all available data during the ozone season (April 1 – September 31) of the 6-year (2019-2024) period. Hourly means and 10th-90th percentiles are calculated using data on June 28-29, 2021. 41

Figure 2-27. Regional view of HMS smoke density and fire locations on June 28, 2021. 42

Figure 2-28. Regional view of HMS smoke density and fire locations on June 29, 2021. 42

Figure 2-29. Average geopotential height at 500 mb from June 28 and 29, 2021. 43

Figure 2-30. Surface analyses from 2 p.m. MST June 28, 2021 (left) and 2 p.m. MST June 29, 2021 (right) 44

Figure 2-31. HMS fire and smoke along with hourly concentrations of $PM_{2.5}$ at 8:00 a.m. MST June 28, 2021 (left) and 8:00 a.m. MST June 29, 2021 (right). 45

Figure 2-32. Visible satellite imagery from approximately 1:22 p.m. MST on June 28, 2021. Fire detections are indicated by orange dots. 45

Figure 2-33. Visible satellite imagery from approximately 2:05 p.m. MST on June 29, 2021. Fire detections are indicated by orange dots. 46

Figure 2-34. A zoomed-in view over the southwestern U.S. of MODIS Aqua AIRS CO retrieval during the atypical ozone date of June 28, 2021. The black box represents the approximate area of the NAA. 47

Figure 2-35. A zoomed-in view over the southwestern U.S. of MODIS Aqua AIRS CO retrieval during the atypical ozone date of June 29, 2021. The black box represents the approximate area of the NAA. 48

Figure 2-36. Observed atmospheric soundings from 5 a.m. MST (left) and 5 p.m. MST (right) June 28-29, 2021 49

Figure 2-37. NOAA smoke and fire maps and NOAA HYSPLIT trajectory model runs (from Dysart –top, and the JLG Supersite – bottom) with air parcels moving 48-hours before 12:00 am - 8:00 pm MST between June 28 and June 29, 2021 at 100 meters, 1,000 meters, and 2,500 meters (AGL). Analyses performed by MAG. 51

Figure 2-38. Camera Images showing the southwest coordinal direction taken from the Estrella Mountain webcam on June 28 from 8:00 LST, 11:00 LST, 14:00 LST, and 17:00. 52

Figure 2-39. Camera Images showing the southwest coordinal direction taken from the Estrella Mountain webcam on June 29 from 8:00 LST, 11:00 LST, 14:00 LST, and 17:00. 53

Figure 2-40. Camera Images showing the south coordinal direction taken from the South Mountain webcam on June 29 from 8:00 LST, 11:00 LST, 14:00 LST, and 17:00. 53

Figure 2-41. Camera Images showing the south coordinal direction taken from the South Mountain webcam on June 29 from 8:00 LST, 11:00 LST, 14:00 LST, and 17:00. 54

Figure 2-42. Camera Images showing the east coordinal direction taken from the Superstition Mountain webcam on June 28 from 8:00 LST, 11:00 LST, 14:00 LST, and 17:00. 54

Figure 2-43. Camera Images showing the east coordinal direction taken from the Superstition Mountain webcam on June 29 from 8:00 LST, 11:00 LST, 14:00 LST, and 17:00. 55

Figure 2-44. Hourly concentrations of ozone, NO_2, and $PM_{2.5}$ at all sites in the nonattainment area. All ozone-exceeding sites are color-coded to highlight smoke impacts on concentrations, and all non-exceeding sites are black. The gray shaded areas represent June 28 and 29, 2021. 56

Figure 2-45. Hourly concentrations of $PM_{2.5}$ at the Mesa (top), North Phoenix (middle), and Glendale (bottom) sites. The 6-year (2019-2024) median is represented by the dashed line, and the 5th-95th percentile is represented by the shaded area. 57

Figure 2-46. Boxplot of OC to EC ratios at the JLG Supersite site using data collected during the ozone season (April-September) from 2019-2024. OC to EC ratios are calculated at POC 2 (x-axis). Available OC to EC ratios collected during the day before and after the June 28-29 atypical ozone event are shown as points. 59

Figure 2-47. Boxplots of speciated $PM_{2.5}$ collected at the JLG Supersite site collected during the ozone season (April-September) from 2019-2024. Available speciated $PM_{2.5}$ concentrations collected during the day before and after the June 28-29 atypical event are shown as points. 60

Figure 2-48. Hourly ozone concentrations (ppb) compared to all available data during the ozone season (April 1 – September 31) of the 6-year (2019-2024) period. Hourly means and 10th-90th percentiles are calculated using data on July 1, 2021. 63

Figure 2-49. Regional view of HMS smoke density and fire locations on June 30, 2021. 64

Figure 2-50. Regional view of HMS smoke density and fire locations on July 1, 2021. 65

Figure 2-51. Average geopotential height at 500 mb on July 1, 2021. 66

Figure 2-52. Surface analysis from 2 p.m. MST July 1, 2021. 67

Figure 2-53. HMS fire and smoke detections along with hourly $PM_{2.5}$ concentrations at 8:00 a.m. MST July 1, 2021. 68

Figure 2-54. Visible satellite imagery from approximately 1:53 p.m. MST on July 1, 2021. Fire detections are indicated by orange dots. 69

Figure 2-55. Observed atmospheric soundings from 5 a.m. MST (left) and 5 p.m. MST (right) July 1, 2021 70

Figure 2-56. NOAA smoke and fire maps and NOAA HYSPLIT trajectory model runs from the Tempe ozone monitor, with air parcels moving 48-hours before 12:00 am - 8:00 pm MST on July 1, 2021 at 100 meters, 1,000 meters, and 2,500 meters (AGL). Analysis performed by MAG. 71

Figure 2-57. Camera Images showing the southwest coordinal direction taken from the Estrella Mountain webcam on July 1 from 8:00 LST, 11:00 LST, 14:00 LST, and 17:00. 72

Figure 2-58. Camera Images showing the south coordinal direction taken from the South Mountain webcam on July 1 from 8:00 LST, 11:00 LST, 14:00 LST, and 17:00. 72

Figure 2-59. Camera Images showing the east coordinal direction taken from the Superstition Mountain webcam on July 1 from 8:00 LST, 11:00 LST, 14:00 LST, and 17:00. 73

Figure 2-60. Camera Images showing the west-northwest coordinal direction taken from the White Tank Mountain webcam on July 1 from 8:00 LST, 11:00 LST, 14:00 LST, and 17:00. 73

Figure 2-61. Social media post regarding smoke from the Tiger Fire moving over Phoenix on July 1, 2021 74

Figure 2-62. Social media post regarding smoke from the Tiger Fire moving over Phoenix on July 1, 2021 74

Figure 2-63. Hourly concentrations of ozone, NO_2, and $PM_{2.5}$ at all sites in the nonattainment area. All ozone-exceeding sites are color-coded to highlight smoke impacts on concentrations, and all non-exceeding sites are black. The gray shaded areas represent July 1, 2021 75

Figure 2-64. Hourly concentrations of $PM_{2.5}$ at the Mesa (top), North Phoenix (middle), and Tempe (bottom) sites. The 6-year (2019-2024) median is represented by the dashed line, and the 5th-95th percentile is represented by the shaded area. 76

Figure 2-65. Boxplot of OC to EC ratios at the JLG Supersite site using data collected during the ozone season (April-September) from 2019-2024. OC to EC ratios are calculated at POC 2 (x-axis). Available OC to EC ratios collected during the day before and two days after the July 1 atypical ozone event are shown as points. 77

Figure 2-66. Boxplots of speciated $PM_{2.5}$ collected at the JLG Supersite site collected during the ozone season (April-September) from 2019-2024. Available speciated $PM_{2.5}$ concentrations collected during the day before and two days after the July 1 atypical event are shown as points. 78

Figure 2-67. Hourly ozone concentrations (ppb) compared to all available data during the ozone season (April 1 – September 31) of the 6-year (2019-2024) period. Hourly means and 10th-90th percentiles are calculated using data on July 20-22, 2021. 81

Figure 2-68. Continental view of HMS smoke density and fire locations on July 20, 2021. 82

Figure 2-69. Continental view of HMS smoke density and fire locations on July 21, 2021. 83

Figure 2-70. Continental view of HMS smoke density and fire locations on July 22, 2021. 83

Figure 2-71. Average geopotential height at 500 mb from July 20 through 22, 2021 84

Figure 2-72. Surface analyses from 2 p.m. MST July 20, 2021 (A), 2 p.m. MST July 21, 2021 (B), and 2 p.m. MST July 22, 2021 (C). 85

Figure 2-73. HMS fire and smoke along with hourly concentrations of $PM_{2.5}$ at 8:00 a.m. MST each day from July 20 (A), July 21 (B) and July 22 (C), 2021. 86

Figure 2-74. Visible satellite imagery from approximately 2:23 p.m. MST on July 20, 2021. 86

Figure 2-75. Visible satellite imagery from approximately 1:28 p.m. MST on July 21, 2021. 87

Figure 2-76. Visible satellite imagery from approximately 1:11 p.m. MST on July 22, 2021. 87

Figure 2-77. A zoomed-in view over the southwestern U.S. of MODIS Aqua AIRS CO retrieval during the atypical ozone date of July 21, 2021. The black box represents the approximate area of the NAA. 88

Figure 2-78. A zoomed-in view over the southwestern U.S. of MODIS Aqua AIRS CO retrieval during the atypical ozone date of July 22, 2021. The black box represents the approximate area of the NAA. 89

Figure 2-79. Observed atmospheric soundings from 5 a.m. MST (left) and 5 p.m. MST (right) July 20 through July 22, 2021. 90

Figure 2-80. NOAA smoke and fire maps and NOAA HYSPLIT trajectory model runs from the Falcon Field ozone monitor, with air parcels moving 48-hours before 12:00 am - 8:00 pm MST on July 22 at 100 meters, 1,000 meters, and 2,500 meters (AGL). Analysis performed by MAG. 91

Figure 2-81. Camera Images showing the southwest coordinal direction taken from the Estrella Mountain webcam on July 20 from 8:00 LST, 11:00 LST, 14:00 LST, and 17:00. 92

Figure 2-82. Camera Images showing the southwest coordinal direction taken from the Estrella Mountain webcam on July 21 from 8:00 LST, 11:00 LST, 14:00 LST, and 17:00. 93

Figure 2-83. Camera Images showing the southwest coordinal direction taken from the Estrella Mountain webcam on July 22 from 8:00 LST, 11:00 LST, 14:00 LST, and 17:00. 93

Figure 2-84. Camera Images showing the south coordinal direction taken from the South Mountain webcam on July 20 from 8:00 LST, 11:00 LST, 14:00 LST, and 17:00. 94

Figure 2-85. Camera Images showing the south coordinal direction taken from the South Mountain webcam on July 21 from 8:00 LST, 11:00 LST, 14:00 LST, and 17:00. 94

Figure 2-86. Camera Images showing the south coordinal direction taken from the South Mountain webcam on July 22 from 8:00 LST, 11:00 LST, 14:00 LST, and 17:00. 95

Figure 2-87. Camera Images showing the east coordinal direction taken from the Superstition Mountain webcam on July 20 from 8:00 LST, 11:00 LST, 14:00 LST, and 17:00. 95

Figure 2-88. Camera Images showing the east coordinal direction taken from the Superstition Mountain webcam on July 21 from 8:00 LST, 11:00 LST, 14:00 LST, and 17:00. 96

Figure 2-89. Camera Images showing the east coordinal direction taken from the Superstition Mountain webcam on July 22 from 8:00 LST, 11:00 LST, 14:00 LST, and 17:00. 96

Figure 2-90. Camera Images showing the west-northwest coordinal direction taken from the White Tank Mountain webcam on July 20 from 8:00 LST, 11:00 LST, 14:00 LST, and 17:00. 97

Figure 2-91. Camera Images showing the west-northwest coordinal direction taken from the White Tank Mountain on July 21 from 8:00 LST, 11:00 LST, 14:00 LST, and 17:00. 97

Figure 2-92. Camera Images showing the west-northwest coordinal direction taken from the White Tank Mountain webcam on July 22 from 8:00 LST, 11:00 LST, 14:00 LST, and 17:00. 98

Figure 2-93. Hourly concentrations of ozone, NO_2, and $PM_{2.5}$ at all sites in the nonattainment area. All ozone-exceeding sites are color-coded to highlight smoke impacts on concentrations, and all non-exceeding sites are black. The gray shaded areas represent July 20-22, 2021. 99

Figure 2-94. Boxplot of OC to EC ratios at the JLG Supersite site using data collected during the ozone season (April-September) from 2019-2024. OC to EC ratios are calculated at POC 2 (x-axis). Available OC to EC ratios collected during the July 20-22 atypical ozone event is shown as a point. 100

Figure 2-95. Hourly ozone concentrations (ppb) compared to all available data during the ozone season (April 1 – September 31) of the 6-year (2019-2024) period. Hourly means and 10th-90th percentiles are calculated using data on August 3-4, 2021 104

Figure 2-96. Continental view of HMS smoke density and fire locations on August 2, 2021 105

Figure 2-97. Continental view of HMS smoke density and fire locations on August 3, 2021 106

Figure 2-98. Continental view of HMS smoke density and fire locations on August 4, 2021 106

Figure 2-99. Average geopotential height at 500 mb from August 3 through 4, 2021. 107

Figure 2-100. Surface analysis from 2 p.m. MST August 3, 2021 (A) and 2 p.m. MST 8/4/21 (B). 108

Figure 2-101. HMS fire and smoke along with hourly concentrations of $PM_{2.5}$ at 8:00 a.m. MST each day for August 3 and August 4, 2021. 109

Figure 2-102. Visible satellite imagery from approximately 12:58 p.m. MST on August 3, 2021. 109

Figure 2-103. Visible satellite imagery from approximately 1:40 p.m. MST on August 4, 2021 110

Figure 2-104. Observed atmospheric soundings from 5 a.m. MST (left) and 5 p.m. MST (right) August 3 through August 4, 2021. 111

Figure 2-105. NOAA smoke and fire maps and NOAA HYSPLIT trajectory model runs from the JLG Supersite ozone monitor, with air parcels moving 48-hours before 12:00 am - 8:00 pm MST on August 3 at 100 meters, 1,000 meters, and 2,500 meters (AGL). Analyses performed by MAG. 112

Figure 2-106. Camera Images showing the southwest coordinal direction taken from the Estrella Mountain webcam on August 3 from 8:00 LST, 11:00 LST, 14:00 LST, and 17:00 113

Figure 2-107. Camera Images showing the southwest coordinal direction taken from the Estrella Mountain webcam on August 4 from 8:00 LST, 11:00 LST, 14:00 LST, and 17:00 113

Figure 2-108. Camera Images showing the south coordinal direction taken from the South Mountain webcam on August 3 from 8:00 LST, 11:00 LST, 14:00 LST, and 17:00. 114

Figure 2-109. Camera Images showing the south coordinal direction taken from the South Mountain webcam on August 4 from 8:00 LST, 11:00 LST, 14:00 LST, and 17:00. 114

Figure 2-110. Camera Images showing the east coordinal direction taken from the Superstition Mountain webcam on August 3 from 8:00 LST, 11:00 LST, 14:00 LST, and 17:00. 115

Figure 2-111. Camera Images showing the east coordinal direction taken from the Superstition Mountain webcam on August 4 from 8:00 LST, 11:00 LST, 14:00 LST, and 17:00. 115

Figure 2-112. Social media post regarding smoke from the fires in the northwestern U.S. moving over Arizona on August 3, 2021. 116

Figure 2-113. Hourly concentrations of ozone, NO_2, and $PM_{2.5}$ at all sites in the nonattainment area. All ozone-exceeding sites are color-coded to highlight smoke impacts on concentrations, and all non-exceeding sites are black. The gray shaded areas represent August 3-4, 2021. 117

Figure 2-114. Hourly concentrations of $PM_{2.5}$ at the Mesa (top) and NO_2 at the North Phoenix (bottom) sites. The 6-year (2019-2024) median is represented by the dashed line, and the 5th-95th percentile is represented by the shaded area. 118

Figure 2-115. Boxplot of speciated $PM_{2.5}$ collected at the JLG Supersite site collected during the ozone season (April-September) from 2019-2024. Available speciated $PM_{2.5}$ concentrations collected during the day before and after the August 3-4 atypical event are shown as points. 119

Figure 3-1. Hourly ozone concentrations (ppb) compared to all available data during the ozone season (April 1 – September 31) of the 6-year (2019-2024) period. Hourly means and 10th-90th percentiles are calculated using data on June 15-16, 2022. 124

Figure 3-2. Regional view of HMS smoke density and fire locations on June 15, 2022. 125

Figure 3-3. Regional view of HMS smoke density and fire locations on June 16, 2022. 126

Figure 3-4. Average geopotential height at 500 mb from June 15 and 16, 2022. 127

Figure 3-5. Surface analyses from 2 p.m. MST June 15, 2022 (left) and 2 p.m. MST June 16, 2022 (right). 127

Figure 3-6. HMS fire and smoke along with hourly concentrations of $PM_{2.5}$ at 8:00 a.m. MST June 15, 2022 (left) and 8:00 a.m. MST June 16, 2022 (right). Fire detections are indicated by orange dots. 128

Figure 3-7. Visible satellite imagery from approximately 1:10 p.m. MST on June 15, 2022. Fire detections are indicated by orange dots. 129

Figure 3-8. Visible satellite imagery from approximately 1:53 p.m. MST on June 16, 2022. Fire detections are indicated by orange dots. 129

Figure 3-9. A zoomed-in view over the southwestern U.S. of MODIS Aqua AIRS CO retrieval during the atypical ozone date of June 16, 2022. The black box represents the approximate area of the NAA. 130

Figure 3-10. Observed atmospheric soundings from 5 a.m. MST (left) and 5 p.m. MST (right) June 15-16, 2022. 131

Figure 3-11. 48-hr back trajectories at 10 meters (green), 1250 meters (blue), and 2500 meters (red) above ground level (AGL) from 4:00 p.m. MST June 15, 2022. HMS satellite fire detections/smoke and hourly ozone (ppb) at 4:00 p.m. MST on June 13, 2022. 132

Figure 3-12. 24-hr back trajectories at 10 meters (green), 1400 meters (blue), and 2800 meters (red) above ground level (AGL) from 4:00 p.m. MST June 16, 2022. HMS satellite fire detections/smoke and hourly ozone (ppb) at 4:00 p.m. MST on June 15, 2022. 133

Figure 3-13. Camera Images showing the northeast coordinal direction taken from the Camelback Mountain webcam on June 15 from 8:00 LST, 11:00 LST, 14:00 LST, and 17:00. 134

Figure 3-14. Camera Images showing the northeast coordinal direction taken from the Camelback Mountain webcam on June 16 from 8:00 LST, 11:00 LST, 14:00 LST, and 17:00. 135

Figure 3-15. Camera Images showing the northeast coordinal direction taken from the Superstition Mountain webcam on June 15 from 8:00 LST, 11:00 LST, 14:00 LST, and 17:00. 135

Figure 3-16. Camera Images showing the northeast coordinal direction taken from the Superstition Mountain webcam on June 16 from 8:00 LST, 11:00 LST, 14:00 LST, and 17:00. 136

Figure 3-17. Camera Images showing the northeast coordinal direction taken from the White Tank Mountain webcam on June 15 from 8:00 LST, 11:00 LST, 14:00 LST, and 17:00 136

Figure 3-18. Camera Images showing the northeast coordinal direction taken from the White Tank Mountain webcam on June 16 from 8:00 LST, 11:00 LST, 14:00 LST, and 17:00 137

Figure 3-19. Hourly concentrations of ozone, NO_2, and $PM_{2.5}$ at all sites in the nonattainment area. All ozone-exceeding sites are color-coded to highlight smoke impacts on concentrations, and all non-exceeding sites are black. The gray shaded areas represent June 15-16, 2022. 138

Figure 3-20. Hourly concentrations of NO_2 at the West Phoenix (top) and Buckeye (bottom) sites. The 6-year (2019-2024) median is represented by the dashed line, and the 5th-95th percentile is represented by the shaded area. 139

Figure 3-21. Boxplot of OC to EC ratios at the JLG Supersite site using data collected during the ozone season (April-September) from 2019-2024. OC to EC ratios are calculated at POC 2 (x-axis). Available OC to EC ratios collected during the June 15-16 atypical ozone event are shown as a point. 140

Figure 3-22. Boxplots of speciated $PM_{2.5}$ collected at the JLG Supersite site collected during the ozone season (April-September) from 2019-2024. Available speciated $PM_{2.5}$ concentrations collected during the June 15-16 atypical ozone event are shown as a point. 141

Figure 3-23. Hourly ozone concentrations (ppb) compared to all available data during the ozone season (April 1 – September 31) of the 6-year (2019-2024) period. Hourly means and 10th-90th percentiles are calculated using data on July 15-17, 2022. 145

Figure 3-24. Continental view of HMS smoke density and fire locations on July 14, 2022. 146

Figure 3-25. Continental view of HMS smoke density and fire locations on July 15, 2022. 147

Figure 3-26. Continental view of HMS smoke density and fire locations on July 16, 2022. 147

Figure 3-27. Continental view of HMS smoke density and fire locations on July 17, 2022. 148

Figure 3-28. Mean 500 mb winds for July 15-17, 2022. High pressure aloft near the Four Corners region resulted in clockwise flow and easterly to southeasterly upper-level winds into central Arizona. Source: NOAA 149

Figure 3-29. NOAA HMS smoke analysis (grey contours) and satellite fire detections (red triangles) for the July 15-17, 2022 period showing the vast spread of smoke across Northern America. Source: NOAA 151

Figure 3-30. Upper-air skew-T diagrams from Tucson for the July 15-17, 2022 period at 5 p.m. PST. Deep mixing is allowing aloft air to be mixed down to the surface. Source: University of Wyoming 152

Figure 3-31. 48-hour HYSPLIT back trajectory (green – 50 m, blue – 2,200 m, red – 4,400 m AGL) ending 5 p.m. PST July 15, 2022, and NOAA HMS satellite fire detections (red triangles) and smoke analysis (grey contours) for July 13, 2022. Source: AirNow-Tech 153

Figure 3-32. 24-hour HYSPLIT back trajectory (green – 50 m, blue – 1,500 m, red – 3,500 m AGL) ending 5 p.m. PST July 16, 2022, and NOAA HMS satellite fire detections (red triangles) and smoke analysis (grey contours) for July 15, 2022. Source: AirNow-Tech 154

Figure 3-33. 24-hour HYSPLIT back trajectory (green – 50 m, blue – 2,000 m, red – 4,100 m AGL) ending 5 p.m. PST July 17, 2022, and NOAA HMS satellite fire detections (red triangles) and smoke analysis (grey contours) for July 16, 2022. Source: AirNow-Tech 154

Figure 3-34. Camera Images showing the northeast coordinal direction taken from the Camelback Mountain webcam on July 15 from 8:00 LST, 11:00 LST, 14:00 LST, and 17:00. 155

Figure 3-35. Camera Images showing the northeast coordinal direction taken from the Camelback Mountain webcam on July 16 from 8:00 LST, 11:00 LST, 14:00 LST, and 17:00. 156

Figure 3-36. Camera Images showing the northeast coordinal direction taken from the Camelback Mountain webcam on July 17 from 8:00 LST, 11:00 LST, 14:00 LST, and 17:00. 156

Figure 3-37. Camera Images showing the northeast coordinal direction taken from the Superstition Mountain webcam on July 15 from 8:00 LST, 11:00 LST, 14:00 LST, and 17:00. 157

Figure 3-38. Camera Images showing the northeast coordinal direction taken from the Superstition Mountain webcam on July 16 from 8:00 LST, 11:00 LST, 14:00 LST, and 17:00. 157

Figure 3-39. Camera Images showing the northeast coordinal direction taken from the Superstition Mountain webcam on July 17 from 8:00 LST, 11:00 LST, 14:00 LST, and 17:00. 158

Figure 3-40. Camera Images showing the northeast coordinal direction taken from the White Tank Mountain webcam on July 15 from 8:00 LST, 11:00 LST, 14:00 LST, and 17:00. 158

Figure 3-41. Camera Images showing the northeast coordinal direction taken from the White Tank Mountain webcam on July 17 from 8:00 LST, 11:00 LST, 14:00 LST, and 17:00. 159

Figure 3-42. Camera Images showing the northeast coordinal direction taken from the White Tank Mountain webcam on July 18 from 8:00 LST, 11:00 LST, 14:00 LST, and 17:00. 159

Figure 3-43. Hourly concentrations of ozone, NO_2, and $PM_{2.5}$ at all sites in the nonattainment area. All ozone-exceeding sites are color-coded to highlight smoke impacts on concentrations, and all non-exceeding sites are black. The gray shaded areas represent July 15-17, 2022. 160

Figure 3-44. Boxplot of OC to EC ratios at the JLG Supersite site using data collected during the ozone season (April-September) from 2019-2024. OC to EC ratios are calculated at POC 2 (x-axis). Available OC to EC ratios collected during the July 15-17 atypical ozone event are shown as a point. 161

Figure 4-1. Hourly ozone concentrations (ppb) compared to all available data during the ozone season (April 1 – September 31) of the 6-year (2019-2024) period. Hourly means and 10th-90th percentiles are calculated using data on June 22-26, 2023. 166

Figure 4-2. Continental view of HMS smoke density and fire locations on June 22, 2023. 167

Figure 4-3. Continental view of HMS smoke density and fire locations on June 23, 2023. 168

Figure 4-4. Continental view of HMS smoke density and fire locations on June 24, 2023. 168

Figure 4-5. Continental view of HMS smoke density and fire locations on June 25, 2023. 169

Figure 4-6. Continental view of HMS smoke density and fire locations on June 26, 2023. 169

Figure 4-7. Mean 500 mb wind speed and direction for June 22-26, 2023. Aloft high pressure in northern Mexico led to southwesterly flow into Phoenix at the upper levels of the atmosphere. Source: NOAA 170

Figure 4-8. NOAA HMS smoke plume analysis (grey contours) and satellite fire detections (red triangles) from June 22-26, 2023. Source: AirNow-Tech 172

Figure 4-9. Tucson skew-T upper-air diagrams valid 5 p.m. PST from June 22-26, 2023. Deep mixing was evident, indicating the transfer of aloft air down to the surface. Source: University of Wyoming 174

Figure 4-10. 24-hour back trajectory analysis for June 22 (left) and June 23 (right). Transport paths into the nonattainment area intersected with NOAA HMS smoke plumes (grey contours) and satellite fire detections (red triangles). Source: AirNow-Tech 175

Figure 4-11. NOAA HYSPLIT back trajectory analysis for June 24 (top), June 25 (middle), and June 26 (bottom). Transport paths into the nonattainment area intersected with NOAA HMS smoke plumes (grey contours) and satellite fire detections (red triangles). Source: AirNow-Tech 176

Figure 4-12. Camera Images showing the south coordinal direction taken from the South Mountain webcam on June 23 from 7:45 LST, 10:45 LST, and 12:00 LST. 177

Figure 4-13. Camera Images showing the south coordinal direction taken from the South Mountain webcam on June 25 from 6:30 LST, 7:30 LST, and 15:30 LST 178

Figure 4-14. Camera Images showing the south coordinal direction taken from the South Mountain webcam on June 23 from 8:00 LST, 10:30 LST, 12:30 LST, and 14:30 LST 178

Figure 4-15. Camera Images showing the east coordinal direction taken from the Superstition Mountain webcam on June 23 from 9:45 LST, 12:30 LST, 15:15 LST, and 18:00 LST. 179

Figure 4-16. Camera Images showing the east coordinal direction taken from the Superstition Mountain webcam on June 25 from 8:30 LST, 11:00 LST, 14:00 LST, and 17:00 LST. 179

Figure 4-17. Camera Images showing the east coordinal direction taken from the Superstition Mountain webcam on June 26 from 8:30 LST, 11:00 LST, 14:15 LST, and 17:00 LST. 180

Figure 4-18. Camera Images showing the west-northwest coordinal direction taken from the White Tank Mountain webcam on June 23 from 8:00 LST, 11:00 LST, 14:00 LST, and 17:00 LST. 180

Figure 4-19. Camera Images showing the west-northwest coordinal direction taken from the White Tank Mountain webcam on June 25 from 8:00 LST, 11:00 LST, 14:00 LST, and 17:00 LST. 181

Figure 4-20. Camera Images showing the west-northwest coordinal direction taken from the White Tank Mountain webcam on June 26 from 8:00 LST, 11:00 LST, 17:00 LST, and 18:00 LST. 181

Figure 4-21. Hourly concentrations of ozone, NO_2, and $PM_{2.5}$ at all sites in the nonattainment area. All ozone-exceeding sites are color-coded to highlight smoke impacts on concentrations, and all non-exceeding sites are black. The gray shaded areas represent June 22-26, 2023. 182

Figure 4-22. Hourly concentrations of $PM_{2.5}$ at the Mesa (top) and Tempe (bottom) sites. The 6-year (2019-2024) median is represented by the dashed line, and the 5th-95th percentile is represented by the shaded area. 184

Figure 4-23. Hourly concentrations of NO_2 at the West Phoenix (top) and JLG Supersite (bottom) sites. The 6-year (2019-2024) median is represented by the dashed line, and the 5th-95th percentile is represented by the shaded area. 185

Figure 4-24. Boxplot of OC to EC ratios at the JLG Supersite site using data collected during the ozone season (April-September) from 2019-2024. OC to EC ratios are calculated for data collected at POC 2 (x-axis). Available OC to EC ratios collected during the June 22-26 atypical ozone event are shown as points. 186

Figure 4-25. Hourly ozone concentrations (ppb) compared to all available data during the ozone season (April 1 – September 31) of the 6-year (2019-2024) period. Hourly means and 10th-90th percentiles are calculated using data on June 30, 2023. 191

Figure 4-26. Regional view of HMS smoke density and fire locations on June 30, 2023. 192

Figure 4-27. Social media post from the Arizona Department of Forestry and Fire Management from June 30 regarding the Diamond Fire burning on the outskirts of Phoenix. 192

Figure 4-28. 500 mb geopotential heights (blue lines) and winds (red barbs) for 5 p.m. PST on June 30. Based on wind barbs and the height pattern, northerly to northwesterly winds were present across central and northern Arizona, Source: University of Wyoming. 193

Figure 4-29. NOAA HMS smoke plume analysis (grey contours) and satellite fire detections (red triangles) from June 30, 2023. Source: AirNow-Tech. 194

Figure 4-30. Tucson skew-T upper-air diagrams valid 5 p.m. PST from June 30, 2023. Deep mixing was evident, indicating the transfer of aloft air down to the surface. Source: University of Wyoming 196

Figure 4-31. 12-hour back trajectory analysis for June 30 ending 5 p.m. PST. Transport paths into Phoenix intersected with NOAA HMS smoke plumes (grey contours) and were near satellite fire detections (red triangles). Source: AirNow-Tech 197

Figure 4-32. Camera Images showing the southwest coordinal direction taken from the Estrella Mountain webcam on June 30 from 6:30 LST, 8:45 LST, 10:15 LST, and 11:45 LST. 198

Figure 4-33. Camera Images showing the south coordinal direction taken from the South Mountain webcam on June 30 from 6:30 LST, 8:00 LST, 10:00 LST, and 12:45 LST. 199

Figure 4-34. Camera Images showing the east coordinal direction taken from the Superstition Mountain webcam on June 30 from 8:30 LST, 11:00 LST, 14:00 LST, and 17:15 LST. 199

Figure 4-35. Social media post regarding smoke from the Diamond Fire over Phoenix on July 1, 2023. 200

Figure 4-36. Hourly concentrations of ozone, NO_2, and $PM_{2.5}$ at all sites in the nonattainment area. All ozone-exceeding sites are color-coded to highlight smoke impacts on concentrations, and all non-exceeding sites are black. The gray shaded areas represent June 30, 2023. 201

Figure 4-37. Boxplot of OC to EC ratios at the JLG Supersite site using data collected during the ozone season (April-September) from 2019-2024. OC to EC ratios are calculated from data collected at POC 2 (x-axis). Available OC to EC ratios collected during the day before and two days after the June 30 atypical ozone event are shown as points. 202

Figure 4-38. Hourly ozone concentrations (ppb) compared to all available data during the ozone season (April 1 – September 31) of the 6-year (2019-2024) period. Hourly means and 10th-90th percentiles are calculated using data on July 24-29, 2023. 205

Figure 4-39. Local view of HMS smoke density and fire locations on July 26, 2023. 206

Figure 4-40. Local view of HMS smoke density and fire locations on July 27, 2023. 207

Figure 4-41. Continental view of HMS smoke density and fire locations on July 24, 2023. 207

Figure 4-42. Continental view of HMS smoke density and fire locations on July 25, 2023 208

Figure 4-43. Continental view of HMS smoke density and fire locations on July 26, 2023. 208

Figure 4-44. Continental view of HMS smoke density and fire locations on July 27, 2023 209

Figure 4-45. Continental view of HMS smoke density and fire locations on July 28, 2023 209

Figure 4-46. Continental view of HMS smoke density and fire locations on July 29, 2023. 210

Figure 4-47. Mean 500 mb (left) and 700 mb (right) winds for July 24-29, 2023. Upper-level high pressure resulted in southerly to southeasterly wind aloft in the Phoenix region. Source: NOAA 211

Figure 4-48. NOAA HMS smoke plume analysis (grey contours) and satellite fire detections (red triangles) from July 24-29, 2023. Source: AirNow-Tech 212

Figure 4-49. Tucson skew-T upper-air diagrams valid 5 p.m. PST from July 24-29, 2023. Deep mixing was evident each day, indicating vertical transfer of aloft air to the surface. Source: University of Wyoming....215

Figure 4-50. NOAA 24-hour back trajectory analysis ending 5 p.m. PST for the July 24-29, 2023 period. Each day's back trajectory analysis intersected a NOAA analyzed smoke plume from the previous day. Source: AirNow-Tech....216

Figure 4-51. Camera Images showing the southwest coordinal direction taken from the Estrella Mountain webcam on July 25 from 6:00 LST, 8:30 LST, and 10:45 LST. 218

Figure 4-52. Camera Images showing the south coordinal direction taken from the South Mountain webcam on July 25 from 6:00 LST, 8:30 LST, and 11:00 LST. 218

Figure 4-53. Camera Images showing the east coordinal direction taken from the Superstition Mountain webcam on July 26 from 8:00 LST, 11:00 LST, 14:00 LST, and 17:00 LST. 219

Figure 4-54. Camera Images showing the east coordinal direction taken from the Superstition Mountain webcam on July 27 from 8:00 LST, 11:00 LST, 14:00 LST, and 17:15 LST. 219

Figure 4-55. Social media post regarding smoke from the Diamond Fire over Phoenix on July 26, 2023. 220

Figure 4-56. Hourly concentrations of ozone, NO_2, and $PM_{2.5}$ at all sites in the nonattainment area. All ozone-exceeding sites are color-coded to highlight smoke impacts on concentrations, and all non-exceeding sites are black. The gray shaded areas represent July 24-29, 2023. 221

Figure 4-57. Hourly concentrations of NO_2 at the Buckeye (top) and JLG Supersite (bottom) sites. The 6-year (2019-2024) median is represented by the dashed line, and the 5th-95th percentile is represented by the shaded area....222

Figure 4-58. Boxplot of OC to EC ratios at the JLG Supersite site using data collected during the ozone season (April-September) from 2019-2024. OC to EC ratios are calculated at POC 2 (x-axis). Available OC to EC ratios collected during the July 24-29 atypical ozone event are shown as points. 223

Figure 4-59. Hourly ozone concentrations (ppb) compared to all available data during the ozone season (April 1 – September 31) of the 6-year (2019-2024) period. Hourly means and 10th-90th percentiles are calculated using data on July 31-August 1, 2023. 228

Figure 4-60. Local view of HMS smoke density and fire locations on July 31, 2023. 229

Figure 4-61. Regional view of HMS smoke density and fire locations on July 31, 2023 230

Figure 4-62. Continental view of HMS smoke density and fire locations on August 1, 2023 230

Figure 4-63. 500 mb geopotential heights (blue lines) and winds (red barbs) for 5 a.m. PST on July 31 (top) and August 1 (bottom). A broad ridge of high pressure over the southwestern United States and Rockies was the dominant pattern influencing central Arizona's weather. Source: University of Wyoming....232

Figure 4-64. NOAA HMS smoke plume analysis (grey contours) and satellite fire detections (red triangles) from July 31, 2023 (left) and August 1, 2023 (right). Source: AirNow-Tech 233

Figure 4-65. 5:00 p.m. PST skew-T diagrams from the Tucson upper-air weather station on July 31 (left) and August 1 (right). Upper-air data in Tucson indicates a deep PBL across southern and central Arizona on each day. Source: University of Wyoming 235

Figure 4-66. 6-hour back trajectory analysis ending 5 p.m. PST on July 31, 2023. Transport paths at 2,000 m AGL (blue) and 4,200 m AGL (red) intersect with NOAA analyzed smoke (grey contours) and were near satellite fire detections south of Phoenix (red triangles). Source: AirNow-Tech 236

Figure 4-67. 36-hour back trajectory analysis ending 5 p.m. PST on August 1, 2023. Transport paths intersect with NOAA analyzed smoke (grey contours) and satellite fire detections (red triangles) from the previous day. Source: AirNow-Tech 237

Figure 4-68. Camera Images showing the northeast coordinal direction taken from the Camelback Mountain webcam on July 31 from 16:00 LST, 17:15 LST, 18:15 LST, and 19:00 LST. 238

Figure 4-69. Camera Images showing the northeast coordinal direction taken from the Superstition Mountain webcam on July 31 from 17:00 LST, 17:45 LST, 18:15 LST, and 19:00 LST. 238

Figure 4-70. Social media post regarding smoke from the local fire to the south of Phoenix on July 31, 2023. 239

Figure 4-71. Social media post regarding smoke from the local fire to the south of Phoenix on July 31, 2023. 240

Figure 4-72. Hourly concentrations of ozone, NO_2, and $PM_{2.5}$ at all sites in the nonattainment area. All ozone-exceeding sites are color-coded to highlight smoke impacts on concentrations, and all non-exceeding sites are black. The gray shaded areas represent July 31-August 1, 2023. 241

Figure 4-73. Boxplot of OC to EC ratios at the JLG Supersite site using data collected during the ozone season (April-September) from 2019-2024. OC to EC ratios are calculated at POC 2 (x-axis). Available OC to EC ratios collected during the July 31-August 1 atypical ozone event are shown as a point. 242

Figure 4-74. Boxplots of speciated $PM_{2.5}$ collected at the JLG Supersite site collected during the ozone season (April-September) from 2019-2024. Available speciated $PM_{2.5}$ concentrations collected during the July 31-August 1 atypical ozone event are shown as a point. 243

Figure 4-75. Hourly ozone concentrations (ppb) compared to all available data during the ozone season (April 1 – September 31) of the 6-year (2019-2024) period. Hourly means and 10th-90th percentiles are calculated using data on August 17-18, 2023. 247

Figure 4-76. Continental view of HMS smoke density and fire locations on August 17, 2023. 248

Figure 4-77. Continental view of HMS smoke density and fire locations on August 18, 2023. 248

Figure 4-78. Mean 500 mb winds for August 17-18, 2023. High pressure aloft east of Arizona resulted in southerly to southeasterly upper-level winds in the nonattainment area. Source: NOAA 249

Figure 4-79. NOAA HMS smoke plume analysis (grey contours) and satellite fire detections (red triangles) from August 17, 2023 (left) and August 18, 2023 (right). Source: AirNow-Tech 250

Figure 4-80. 5 p.m. PST skew-T diagrams from the Tucson upper-air weather station on August 17, 2023 (left) and August 18, 2023 (right). Upper-air data in Tucson indicates an established PBL each day. Source: University of Wyoming 252

Figure 4-81. 72-hour back trajectory analysis ending 5 p.m. PST on August 17, 2023. The transport path at 1,900 m AGL (red) intersect with NOAA analyzed smoke (grey contours) from August 14. Source: AirNow-Tech 253

Figure 4-82. 48-hour back trajectory analysis ending 5 p.m. PST on August 18. The 1,100 m and 2,200 m AGL paths intersect with NOAA analyzed smoke (grey contours) from August 16 and were close to satellite fire detections from August 16. Source: AirNow-Tech 254

Figure 4-83. Camera Images showing the south coordinal direction taken from the South Mountain webcam on August 17 from 6:30 LST, 10:00 LST, 14:15 LST, and 16:45 LST 255

Figure 4-84. Camera Images showing the east coordinal direction taken from the Superstition Mountain webcam on August 17 from 8:30 LST, 11:30 LST, 14:30 LST, and 17:30 LST 255

Figure 4-85. Hourly concentrations of ozone, NO_2, and $PM_{2.5}$ at all sites in the nonattainment area. All ozone-exceeding sites are color-coded to highlight smoke impacts on concentrations, and all non-exceeding sites are black. The gray shaded areas represent August 17-18, 2023 256

Figure 4-86. Hourly concentrations of NO_2 at the Buckeye (top) and West Phoenix (bottom) sites. The 6-year (2019-2024) median is represented by the dashed line, and the 5th-95th percentile is represented by the shaded area 257

Figure 4-87. Boxplot of OC to EC ratios at the JLG Supersite site using data collected during the ozone season (April-September) from 2019-2024. OC to EC ratios are calculated at POC 2 (x-axis). Available OC to EC ratios collected during the day before and day after the August 17-18 atypical ozone event are shown as points. 258

Tables

Table 1-1. Dates determined to be most influential in determining design value impact from the larger set of wildfire influenced ozone exceedance days. 4

Table 2-1. Summary of identified atypical event June 15 and 16, 2021. 16

Table 2-2. Surface weather variables observed at Phoenix Sky Harbor Airport. 22

Table 2-3. Percentile of ozone measurements on the atypical dates compared with six years of ozone data (2019-2024). The percentile rank is calculated across the ozone production season in the nonattainment area (April 1-September 31) of 2019-2024. 38

Table 2-4. Summary of identified atypical event June 28 and 29, 2021. 40

Table 2-5. Surface weather variables observed at Phoenix Sky Harbor Airport. 44

Table 2-6. Percentile of ozone measurements on the atypical dates compared with six years of ozone data (2019-2024). The percentile rank is calculated across the ozone production season in the nonattainment area (April 1-September 31) of 2019-2024. 61

Table 2-7. Summary of identified atypical July 1, 2021. 63

Table 2-8. Surface weather variables observed at Phoenix Sky Harbor Airport. 67

Table 2-9. Percentile of ozone measurements on the atypical dates compared with six years of ozone data (2019-2024). The percentile rank is calculated across the ozone production season in the nonattainment area (April 1-September 31) of 2019-2024. 79

Table 2-10. Summary of identified atypical July 20-22, 2021. 81

Table 2-11. Surface weather variables observed at Phoenix Sky Harbor Airport. 85

Table 2-12. Percentile of ozone measurements on the atypical dates compared with six years of ozone data (2019-2024). The percentile rank is calculated across the ozone production season in the nonattainment area (April 1-September 31) of 2019-2024. 101

Table 2-13. Summary of identified atypical August 3-4, 2021. 104

Table 2-14. Surface weather variables observed at Phoenix Sky Harbor Airport. 108

Table 2-15. Percentile of ozone measurements on the atypical dates compared with six years of ozone data (2019-2024). The percentile rank is calculated across the ozone production season in the nonattainment area (April 1-September 31) of 2019-2024. 120

Table 3-1. Summary of identified atypical June 15-16, 2022. 124

Table 3-2. Surface weather variables observed at Phoenix Sky Harbor Airport. 128

Table 3-3. Percentile of ozone measurements on the atypical dates compared with six years of ozone data (2019-2024). The percentile rank is calculated across the ozone production season in the nonattainment area (April 1-September 31) of 2019-2024. 142

Table 3-4. Summary of identified atypical July 15-17, 2022. 145

Table 3-5. Daily maximum high temperatures and daily average surface wind speeds at KPHX..... 149

Table 3-6. Estimated PBL heights for Phoenix for the July 15-17, 2022 period..... 151

Table 3-7. Percentile of ozone measurements on the atypical dates compared with six years of ozone data (2019-2024). The percentile rank is calculated across the ozone production season in the nonattainment area (April 1-September 31) of 2019-2024. 162

Table 4-1. Summary of identified atypical June 22-26, 2023. 166

Table 4-2. Daily maximum temperatures and average daily wind speed at KPHX. 171

Table 4-3. Daily estimated PBL heights for Phoenix, sourced from the Tucson upper-air skew-T diagrams. 173

Table 4-4. Percentile of ozone measurements on the atypical dates compared with six years of ozone data (2019-2024). The percentile rank is calculated across the ozone production season in the nonattainment area (April 1-September 31) of 2019-2024. 187

Table 4-5. Summary of identified atypical June 30, 2023..... 190

Table 4-6. Daily maximum temperature and average daily wind speed at KPHX for June 30..... 194

Table 4-7. Percentile of ozone measurements on the atypical dates compared with six years of ozone data (2019-2024). The percentile rank is calculated across the ozone production season in the nonattainment area (April 1-September 31) of 2019-2024. 203

Table 4-8. Summary of identified atypical July 24-29, 2023. 204

Table 4-9. Daily maximum temperatures and average daily wind speeds at KPHX. 211

Table 4-10. Daily estimated PBL heights for Phoenix, sourced from the Tucson upper-air sounding data. 214

Table 4-11. Percentile of ozone measurements on the atypical dates compared with six years of ozone data (2019-2024). The percentile rank is calculated across the ozone production season in the nonattainment area (April 1-September 31) of 2019-2024. 224

Table 4-12. Summary of identified atypical July 31 – August 1, 2023. 227

Table 4-13. Daily maximum high temperatures and average daily wind speed from KPHX. 233

Table 4-14. Daily estimated PBL heights for Phoenix from the Tucson upper-air sounding data..... 234

Table 4-15. Percentile of ozone measurements on the atypical dates compared with six years of ozone data (2019-2024). The percentile rank is calculated across the ozone production season in the nonattainment area (April 1-September 31) of 2019-2024. 243

Table 4-16. Summary of identified atypical August 17-18, 2023..... 246

Table 4-17. Daily maximum high temperatures and average daily wind speeds from KPHX..... 250

Table 4-18. Daily estimated PBL heights for Phoenix from the Tucson upper-air sounding data..... 251

Table 4-19. Percentile of ozone measurements on the atypical dates compared with six years of ozone data (2019-2024). The percentile rank is calculated across the ozone production season in the nonattainment area (April 1-September 31) of 2019-2024. 259

1. Ozone Technical Supporting Documentation for Atypical Events

1.1 Purpose

This document includes technical analyses that show emissions from several large wildfires impacted air quality within the Maricopa Nonattainment Area for the 2015 ozone standard on 31 days during 2021, 2022, and 2023. This report supports the selection of wildfire-influenced atypical exceedance days during these three years. The process and rationale for selecting the atypical event days is explained in the main body of the MAG 2025 Clean Air Act Section 179B(b) Retrospective Demonstration of the Impact of International Emissions on Ozone Concentrations in the Maricopa Nonattainment Area. This report is noted as Appendix C to the MAG 2025 Clean Air Act Section 179B(b) Retrospective Demonstration. This analysis is comprised of a robust examination and documentation of compelling evidence for excluding the atypical event days from the modeling performed for the MAG 2025 Clean Air Act Section 179B(b) Retrospective Demonstration. Documentation for each atypical event includes but is not limited to:

- Summary narrative description of event.
- Identification, description, and duration of wildfires that contributed to the atypical event where available (events dominated by long-range transport of wildfire emissions may not point to specific wildfires, but rather several wildfires burning in the upwind region).
- Analyses and evidence that aloft wildfire-generated ozone or precursor emissions reached ground-level monitors.

Methods used to provide evidence are further explained in Section 1.2 of this report.

1.1.1 Maricopa Nonattainment Area Description

The eight-hour ozone Maricopa Nonattainment Area boundary for the 2015 ozone standard encompasses 5,287 square miles in and is included in **Figure 1-1**. Ozone monitoring site locations are shown in **Figure 1-2**.

1.1.2 Development of Atypical Event Dates

The dates identified as wildfire-impacted ozone exceedance days in 2021-2023 were determined in consultation with the Maricopa Association of Governments (MAG), Arizona Department of Environmental Quality, the Maricopa County Air Quality Department, and the Pinal County Air

Quality Control District. Each agency brought their own evaluation techniques and expertise to determine which ozone exceedance dates should be identified as being impacted by wildfires. The multi-agency collaboration identified 76 exceedance dates of the 2015 ozone standard impacted by wildfires within the nonattainment area. Further analysis reduced the number of ozone exceedance dates impacted by wildfires to 31 for purposes of analyzing design value iterative representations for purposes of a Clean Air Act 179B(b) retrospective demonstration. Further explanation of this process and rational is explained in the main body of the MAG 2025 Clean Air Act Section 179B(b) Retrospective Demonstration.

Table 1-1 lists agency-agreed dates impacted by wildfire smoke with ozone exceedances considered in this report.

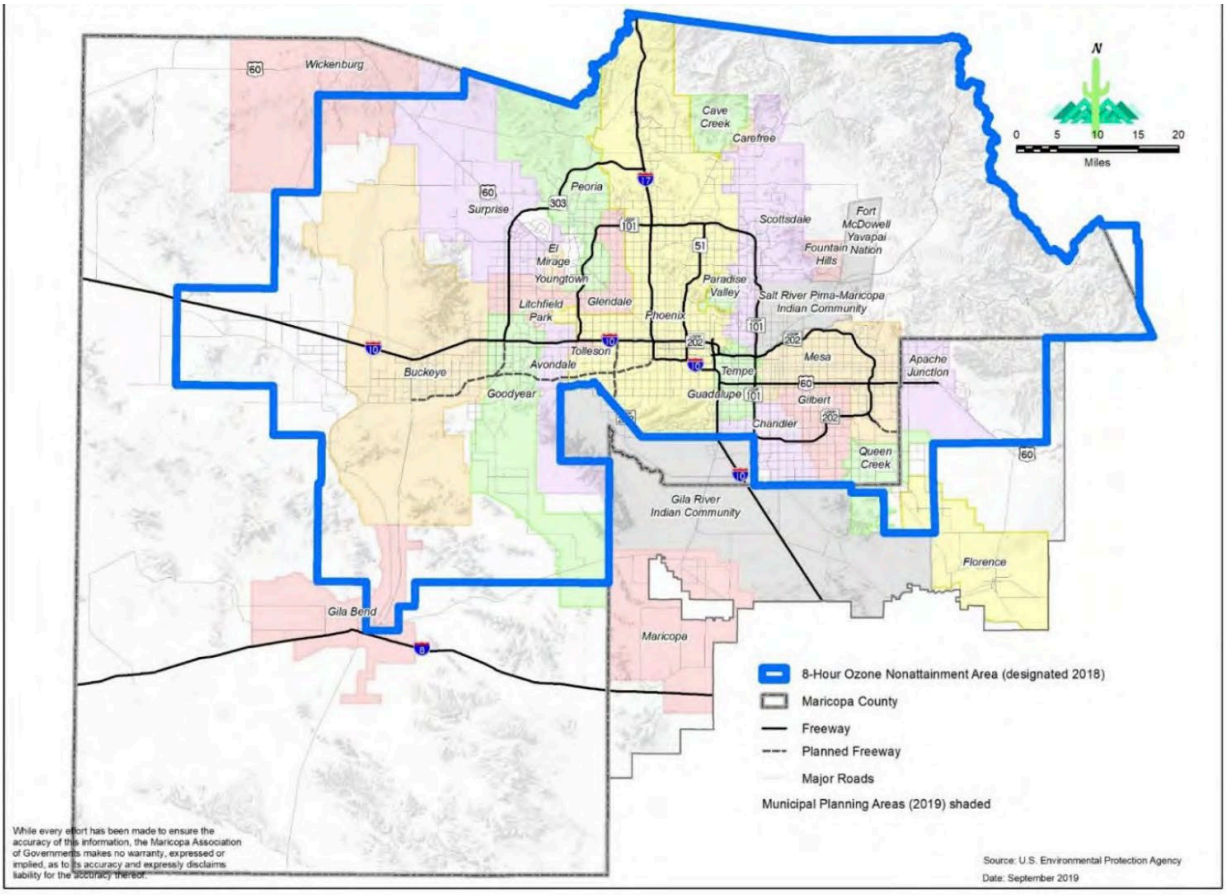

Figure 1-1. 2015 Eight-Hour Ozone Nonattainment Area Boundary (source: MAG 2025 Eight-Hour Ozone Plan – Submittal of Applicable Moderate Area Requirements for the Maricopa Nonattainment Area [April 2025]).

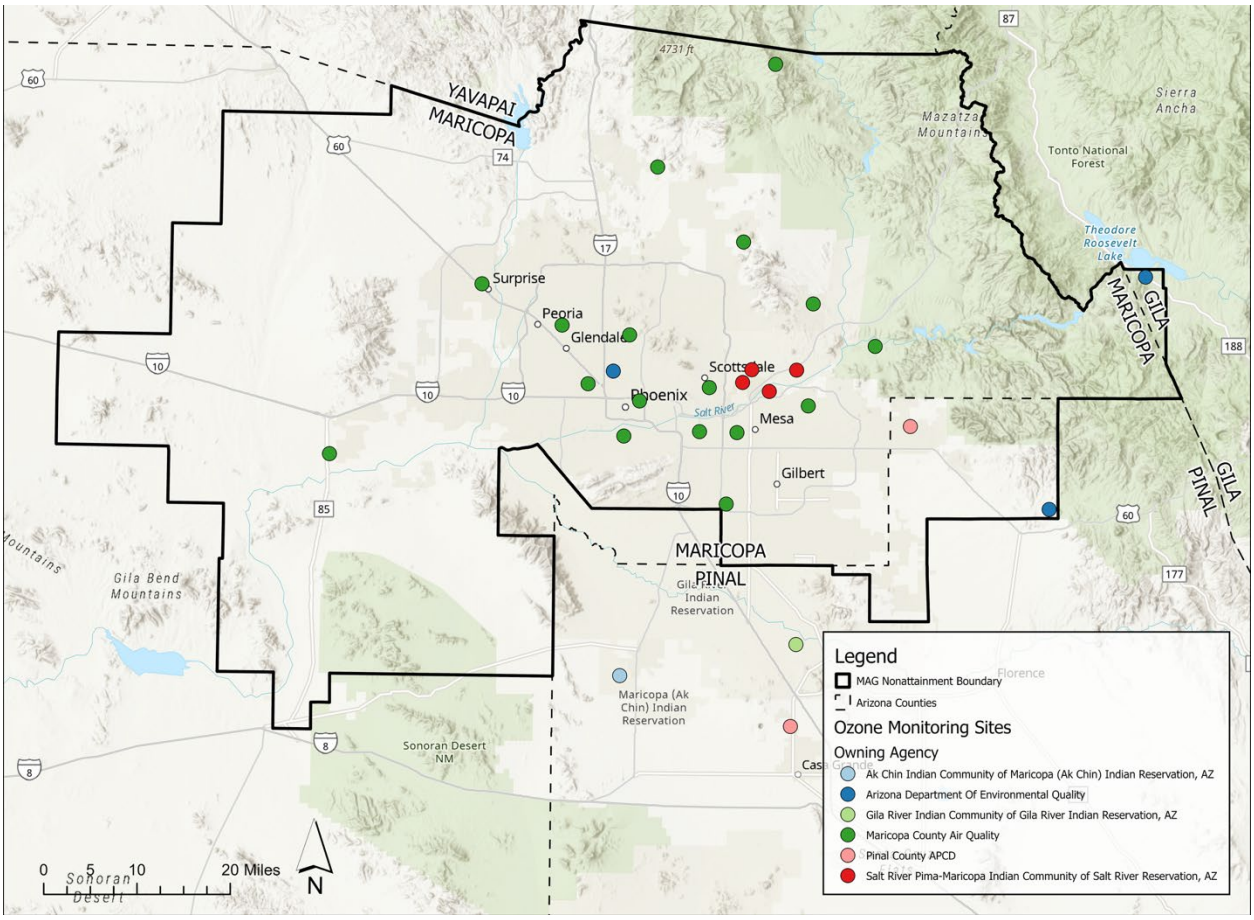

Figure 1-2. Ozone monitoring sites in the Maricopa Nonattainment Area (2025).

Table 1-1. Dates determined to be most influential in determining design value impact from the larger set of wildfire influenced ozone exceedance days.

2021	2022	2023
6/15/21	6/15/22	6/22/23
6/16/21	6/16/22	6/23/23
6/28/21	7/15/22	6/24/23
6/29/21	7/16/22	6/25/23
7/1/21	7/17/22	6/26/23
7/20/21		6/30/23
7/21/21		7/24/23
7/22/21		7/25/23
8/3/21		7/26/23
8/4/21		7/27/23
		7/28/23
		7/29/23
		7/31/23
		8/1/23
		8/17/23
		8/18/23

Note: Blue and tan shading indicate consecutive days in the same event

1.2 Methods and Data Sets

EPA modeling guidance allows for and recommends the exclusion of atypical or unrepresentative air monitoring data, such as wildfire-impacted ozone concentrations, in calculations for the base design period (Guideline on Air Quality Models, January 2017, Section 8.3.2 c.ii. and d.).

The focus of the analyses is to evaluate key indicators that wildfire-generated smoke, and ozone precursors from the smoke, have impacted ozone concentrations in the Maricopa Nonattainment Area. Analyses focused on the most relevant evidence that ozone concentrations in the nonattainment area were impacted by wildfires – and therefore are atypical in that they are elevating design value periodic concentrations. For example, satellite imagery can easily show when and where smoke from multiple large fires are burning as well as indicate how dense and widespread smoke production from those fires are during the period of an ozone exceedance.

The following subsections describe the methods and data sets used, and the multiple lines of evidence produced to show smoke impacts on ozone in the Maricopa Nonattainment Area for the 31 multi-agency identified atypical exceedance days.

1.2.1 Identification of Wildfires and Surface Impacts

HMS Fire Detection Maps

The National Oceanic and Atmospheric Administration (NOAA) Hazard Mapping System (HMS) Fire and Smoke Products were used to demonstrate the transport of fire emissions to the impacted monitors. The HMS Fire and Smoke Product consists of:

1. A daily fire detection product derived from three satellite data products to spatially and temporally map fire locations at 1-km grid resolution, and
2. A daily smoke product derived from visible satellite imagery that consists of polygons showing regions impacted by smoke.

The HMS smoke plume data are based on measurements from several environmental satellites and are reviewed by trained NOAA analysts to identify cases where smoke is dispersed by transport.

For long-range smoke transport, such as from Canadian fires, HMS maps at a continental scale are used to show the extent (and origin) of smoke. Regional or local scale maps are used to show smoke impacts from more locally or regionally based fires. The scale of the maps was specifically chosen to best match each event. Additionally, trajectories may indicate interaction with smoke in days prior to the atypical day and thus maps are shown for those days as well as the atypical days.

Surface Impacts

Cameras are deployed throughout the nonattainment area to record visible imagery useful in identifying smoke and dust impacts on the area. Imagery was obtained from **https://phoenixvis.net/**. While smoke may sometimes be visible, some ozone precursors such as nitrogen oxides (NOx) and volatile organic compounds (VOCs) may not be visible. Not all events have smoke visible by camera and in those cases, the webcam imagery was not included in the event discussion.

Speciated particulate matter (PM) data, including elemental and organic carbon (EC and OC), provide evidence of transported wildfire impacts to air quality monitoring locations. Particularly in cases of long-range transport, ozone precursor emissions from wildfires, elevated OC levels, and low EC/OC (or increased OC/EC) ratios indicate that volatile organic compound (VOC) emissions from the wildfire have impacted the air quality monitors. Note that the speciated PM data are only available every third day. For some events, the data from the day after or before an event was used to illustrate potential smoke impacts.

Hourly $PM_{2.5}$ concentration data can provide evidence that smoke from a wildfire has impacted an air quality monitor. Particularly when wildfires occur within or near the nonattainment area, elevated hourly $PM_{2.5}$ concentrations would be expected. For wildfires occurring further away from the nonattainment area, $PM_{2.5}$ impacts can be less evident and the EC/OC data become more important

in identifying the wildfire impacts on ozone concentrations. This analysis shows evidence that $PM_{2.5}$ concentrations can be at normal levels in long-range transport events, while elevated VOC emissions from wildfires still exist in the atmosphere and can dramatically impact ozone concentrations in urban areas like the Maricopa Nonattainment Area (Ozone Chemistry in Western U.S. Wildfire Plumes, Science Advances, 2021; Large Contribution of Biomass Burning Emissions to Ozone throughout the Global Remote Troposphere, Proceedings of the National Academy of Sciences [PNAS], 2021).

Unusual hourly spikes in ozone concentrations, particularly if they occur outside of the normal diurnal pattern, may be an indicator of ozone impacts from wildfires. Extremely high ozone spikes also may indicate additional ozone and ozone precursor emissions from wildfires.

1.2.2 Meteorological Analyses

Several analyses were conducted to describe the meteorological conditions that influenced each exceedance date. Understanding the atmospheric dynamics from the surface to the upper levels of the atmosphere can help determine the potential for ozone formation, smoke transport, subsidence of aloft smoke, and the potential for smoke to linger once it reaches the surface. Mixing heights and back trajectories provide further detail as to the origin of air masses affecting a region and whether those air masses contained active fires and smoke. Explanatory text regarding the analyses and graphics used was only included in the front matter here rather than repeating it through all the events in order to focus on the observations.

Upper-Level Analysis

The height of the 500 millibar (mb) pressure level above ground level as well as the curvature of the 500 mb height field is useful in discerning the potential for ozone production on the synoptic (large) scale. First, higher heights indicate the potential for warm air aloft. Warm air aloft can result in increased atmospheric stability which can lead to a decrease in atmospheric mixing. A decrease in vertical mixing can allow pollutants to accumulate near the surface and increase ozone production. Second, higher heights can also indicate warmer surface temperatures. Ozone production increases as temperature increases, so increased heights can also provide evidence for enhanced ozone production at the surface. And third, a ridge in the height fields and the associated anticyclonic curvature increases the potential for sinking air and sunny skies, conditions that are also conducive to ozone formation. In addition, sinking air can push aloft layers of smoke down to the surface, enhancing ozone development.

Surface Analysis

Surface pressure patterns is helpful in determining whether conditions at ground level are conducive to ozone formation. Surface high pressure generally indicates sinking air and increased stability

which can limit atmospheric mixing and increase ozone production. Conversely, surface low pressure can indicate rising air and increased atmospheric mixing, which can help reduce ozone formation. However, in the desert in the summer, surface low pressure can also be indicative of rising air due to warm surface temperatures. The increase in ozone production from warm surface temperatures can sometimes balance out the potential for air quality to improve due to enhanced atmospheric mixing in the vicinity of a weak surface low. Furthermore, surface pressure patterns can indicate the potential for wind. When lines of constant pressure (isobars) are packed closely together (strong pressure gradient), there is increased potential for wind and dispersion. Alternatively, when isobars are further apart (weak pressure gradient), periods of light winds and reduced dispersion are more likely, thus increasing ozone precursor concentrations.

Satellite Smoke and Fire Detections

Satellite imagery generated by the National Oceanic and Atmospheric Administration (NOAA) provides evidence that wildfire emissions are occurring through fire detections and smoke. If that smoke is present in or near the nonattainment area, there is a significant likelihood that ozone precursor emissions or ozone generated by the wildfire can impact air quality monitors within the nonattainment area. Satellite observations of smoke can be helpful in determining the potential for increased ozone precursors over a region. However, satellite detections of smoke can be hindered by clouds and can be difficult to see because ground colors in desert areas can be similar to smoke.

Satellite measurements of NOx, carbon monoxide (CO), and VOC (e.g., formaldehyde) levels can indicate the presence of elevated NOx from local wildfires, and elevated CO and VOC from long-range transport of wildfire smoke. In this report, the focus was on NOx and/or CO, with CO being most indicative of transported smoke. The addition of long-range transported VOC from wildfires is often significant enough to produce a change in the overall ratios of NOx and VOC at the surface within the nonattainment area which can increase ozone production.

Smoke Discussions

When available, NOAA smoke discussions are provided for the wildfire event days as additional documentation of smoke presence from known wildfires impacting the region. Meteorological Aerodrome Report (METAR) are coded hourly weather observations typically collected at airports and used by pilots and meteorologists. METAR reports contain useful information in describing atmospheric conditions, particularly when tracking smoke. METAR reports provide visibility observations, meteorological variables, and weather phenomena, including the presence of smoke. When available, METAR reports are included for the wildfire event days as additional evidence of smoke presence.

Soundings

Meteorologists use soundings to analyze vertical profiles of temperature, dewpoint, and wind speed above the surface. The main factors of interest when analyzing soundings for an event are stability and mixing heights from the air temperature traces. When the air temperature trace juts sharply to the right near the bottom of a sounding, that indicates an increase of temperature with height. That is a stable configuration known as a temperature inversion. Temperature inversions are common in the overnight and morning hours and can allow pollutants to accumulate near the surface due to inhibited vertical mixing with the upper troposphere. When the temperature trace is parallel to the lines called dry adiabats (upward and to the left), that is an unstable configuration, which allows pollutants to mix upward into the atmosphere. Unstable configurations are common during the daytime hours. While deep mixing generally hinders ozone development, when that mixing transports aloft smoke to the surface, ozone formation is enhanced.

The units of the x-axis on soundings are temperature in degrees Celsius, and the units of the primary y-axis are pressure in millibars, with height in meters or feet also annotated along that axis. The left vertical trace on each graph represents dewpoint temperature, and the right vertical trace represents air temperature. In addition, barbs along the secondary y-axis right of the images represent wind speed and direction. Each short barb indicates wind speeds of 5 knots, each longer barb indicates wind speeds of 10 knots, and flags represent wind speeds of 50 knots. By adding the value of the barbs and flags at a given height, the observed wind speed in knots is determined for each level. In addition, the orientation of the stick that the barbs are attached to indicates the direction that the wind is blowing from at each level.

Smoke Transport

NOAA HYSPLIT back trajectories were used to evaluate whether near-surface air originated from or passed through areas with active fires or satellite observed smoke. While there is some uncertainty regarding the height of observed smoke, it has been widely observed that the potential for local and long-range transport of wildfire-generated smoke, and the associated ozone precursor emissions increases as near-surface trajectories pass through upwind regions with fire and smoke.

In analyses performed by MAG for events in 2021, back trajectory heights were chosen based on the typical depth of the summer boundary layer in this region and heights used in previous analyses, with six trajectories per day generated at three heights: 100 meters, 1,000 meters, and 2,500 meters AGL. To expedite the analyses of 2021-2023, the MAG trajectories and colorized map versions for 2021 were used herein. For the analyses performed for events in 2022 and 2023, meteorologists at Sonoma Technology used observed boundary layer heights to select back trajectory altitudes, with heights near the surface, at the middle of the boundary layer, and at the top of the boundary layer evaluated for each day. These back trajectories originated during peak heating each afternoon to correlate with observed mixing heights and to best represent the transported air mass impacting maximum ozone production.

When available, social media or news reports are provided for the wildfire event days as additional documentation of smoke presence and air quality impacts from known wildfires impacting the region.

Event Statistics

Statistics are used to provide analysis of data, identify patterns, and make predictions as well as understand trends, evaluate outcomes, and make informed decisions based on evidence. Percentile ranking was used to quantify and interpret data to provide evidence that observed data (ozone exceedances) and the impacts of smoke, were outside the normal distribution, thus an atypical exceedance event. Event statistics summarize the percentile of ozone measurements on the atypical dates compared with six years of ozone data (2019-2024). The percentile rank is calculated across the ozone production season in the nonattainment area (April 1-September 31) of 2019-2024.

1.3 Prevailing Meteorological and Wildfire Conditions (2021-2023)

In 2021, wildfires burned over 520,000 acres in Arizona, part of the 7.1 million acres that burned nationally according to the National Interagency Fire Center (NIFC). Wildfire smoke impacts on the nonattainment area were primarily noted in the June-September period (**Figure 1-3**). During this time, the prevailing upper-level weather pattern at 500 mb (approximately 18,000 feet above ground level) consisted of high pressure over the southwestern United States and northern Mexico (**Figure 1-4**). This pattern is conducive for sinking air (known as subsidence), which compresses the lower atmosphere and leads to hot temperatures at the surface.

Hotter than normal temperatures were recorded at the Phoenix Sky Harbor Airport (KPHX) during this period, where the average temperature for June-September 2021 was tied for the 21st-warmest on-record. In addition, hot surface temperatures can generate deep planetary boundary layer (PBL) heights, which allows for the vertical transport of aloft air and any smoke from local and regional sources down to the surface. These conditions are favorable for the development and enhancement of ground-level ozone, particularly when mixed with ozone and ozone precursors emissions from wildfires.

Satellite products, such as HMS fire detections and smoke density contours, visible imagery, and upper-atmospheric CO concentrations, indicate that there were numerous fires burning throughout the mountainous terrain in western Mexico and western Canada. Smoke from these fires likely contributed to smoke plumes that blanketed the U.S. during 2021, 2022, and 2023.

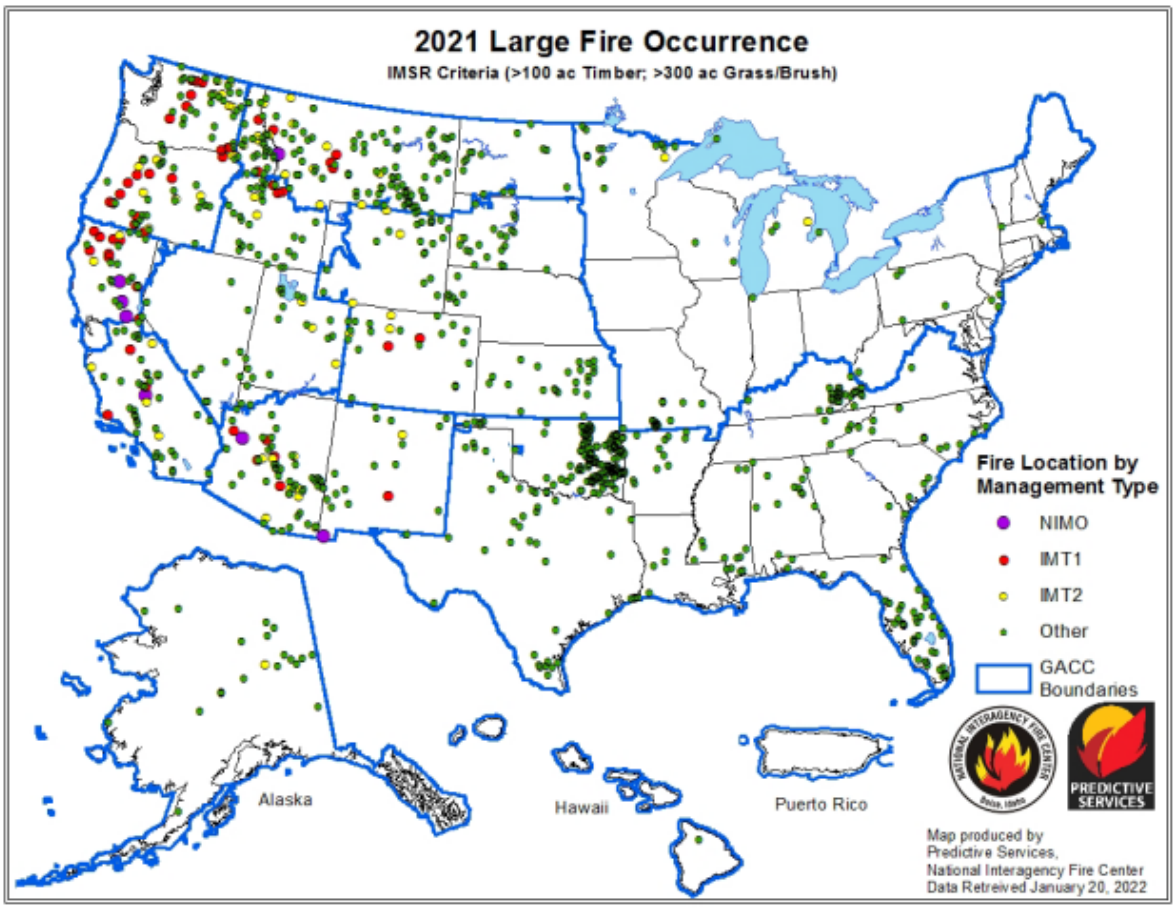

Figure 1-3. 2021 large fire occurrences across the United States. Numerous wildfires exceeding 100-300 acres occurred in Arizona, impacting local air quality. Source: NIFC

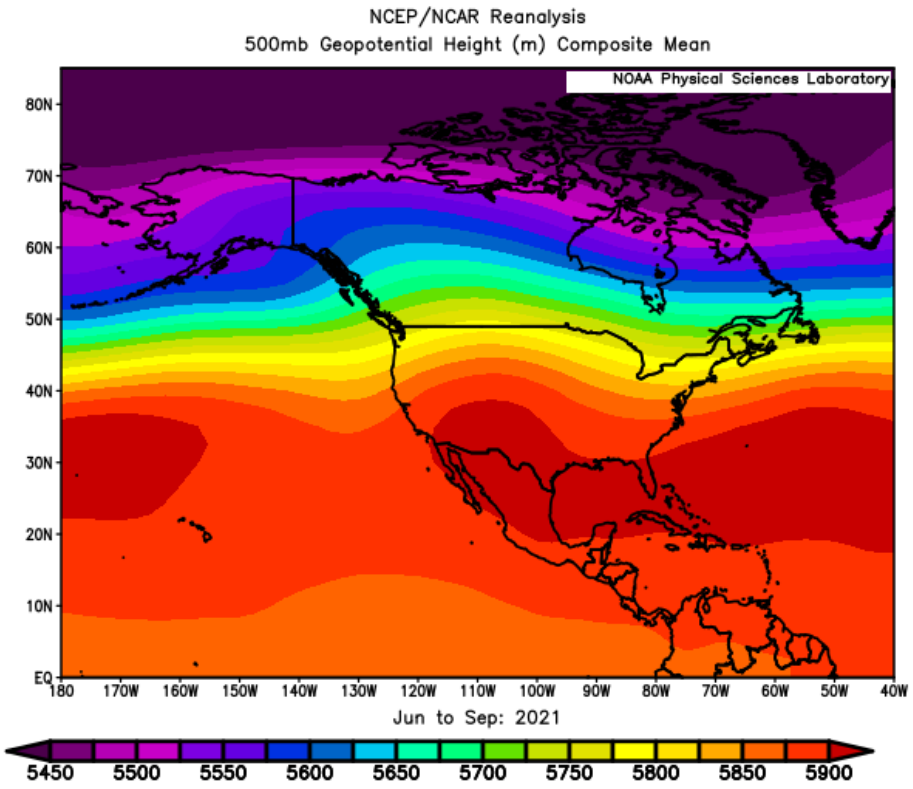

Figure 1-4. Mean 500 mb geopotential heights (meters) for June-September 2021. High pressure aloft over Arizona resulted in hot temperatures and enhanced PBL heights. Source: NOAA

For 2022, over 120,000 acres of Arizona land burned, while 7.6 million acres burned across the United States. Wildfire smoke impacts were generally in the April-July timeframe, which was tied for the 3rd warmest April-July for KPHX. Persistent high pressure aloft across the desert southwest led to subsidence and compressional heating, while days with sunny skies and hot temperatures enhanced vertical mixing (**Figure 1-5**). As a result, smoke transported into central Arizona during this timeframe would be carried down to the surface, helping increase ozone production in the nonattainment area.

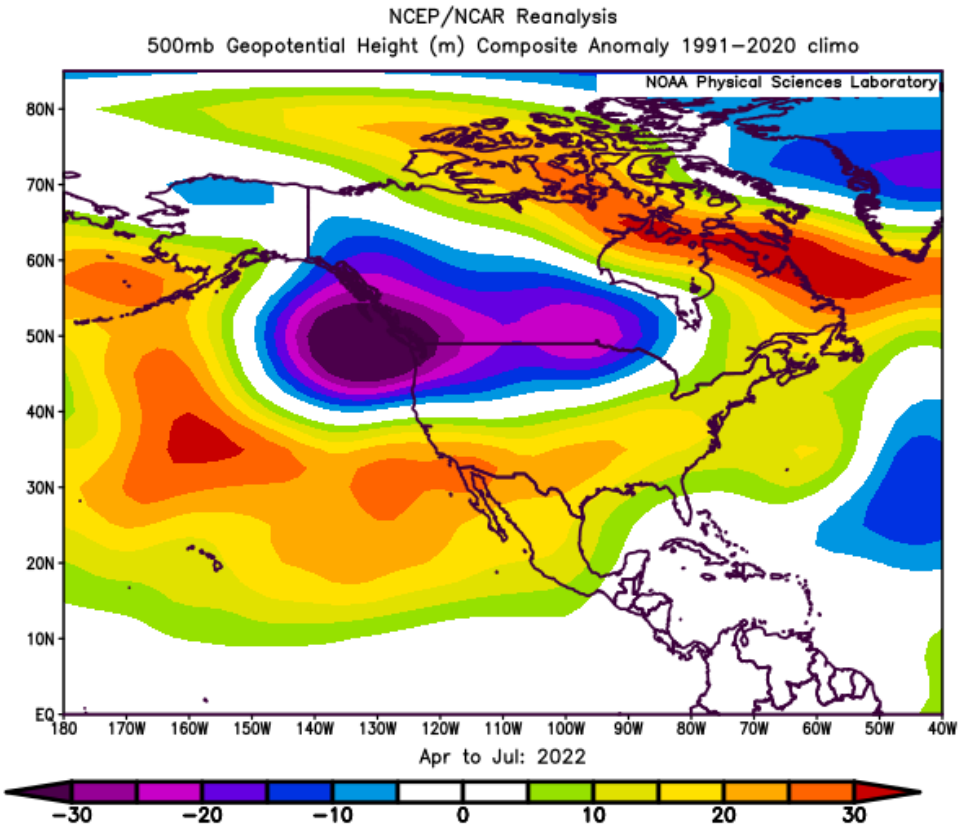

Figure 1-5. 500 mb geopotential height anomalies for April-July 2022. Areas in yellow and orange indicate the persistence of an above-normal region of high pressure over the southwestern United States. Source: NOAA

During 2023, over 185,000 acres of Arizona land burned, while nationally, acres burned decreased from 7.6 million the previous year to 2.7 million. However, the Canadian wildfire season was the most active on-record. According to the Canadian Interagency Forest Fire Center (CIFFC), 42.7 million acres burned in Canada in 2023, beating the old record of 17.5 million acres set in 1995. These fires produced copious amounts of smoke at the surface and aloft, which impacted much of the United States during the summer months (**Figure 1-6**). In Arizona, wildfire smoke impacts were noted in the May-August period. The prevailing weather pattern during May-August 2023 was high pressure at 500 mb centered over Mexico, with the associated ridge from Arizona to Louisiana, extending northward into western Canada (**Figure 1-7**). Due to subsidence and compressional heating, KPHX had the 3rd warmest and driest May-August period on record. On days with sunny skies and hot temperatures producing high PBL heights, aloft smoke from local and long-range sources would reach the surface, enhancing ozone development.

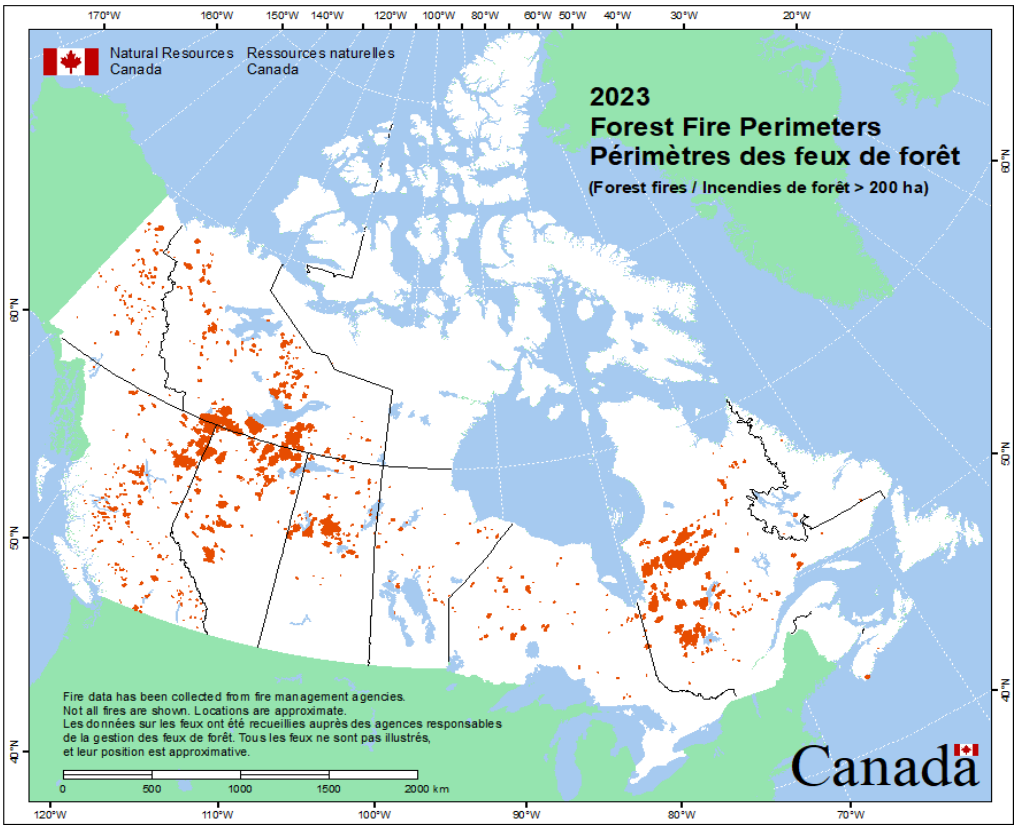

Figure 1-6. Perimeters of 2023 wildfires across Canada. Smoke from these fires impacted air quality across a large portion of the United States during the summer months. Source: Canadian National Fire Database (CNFDB)

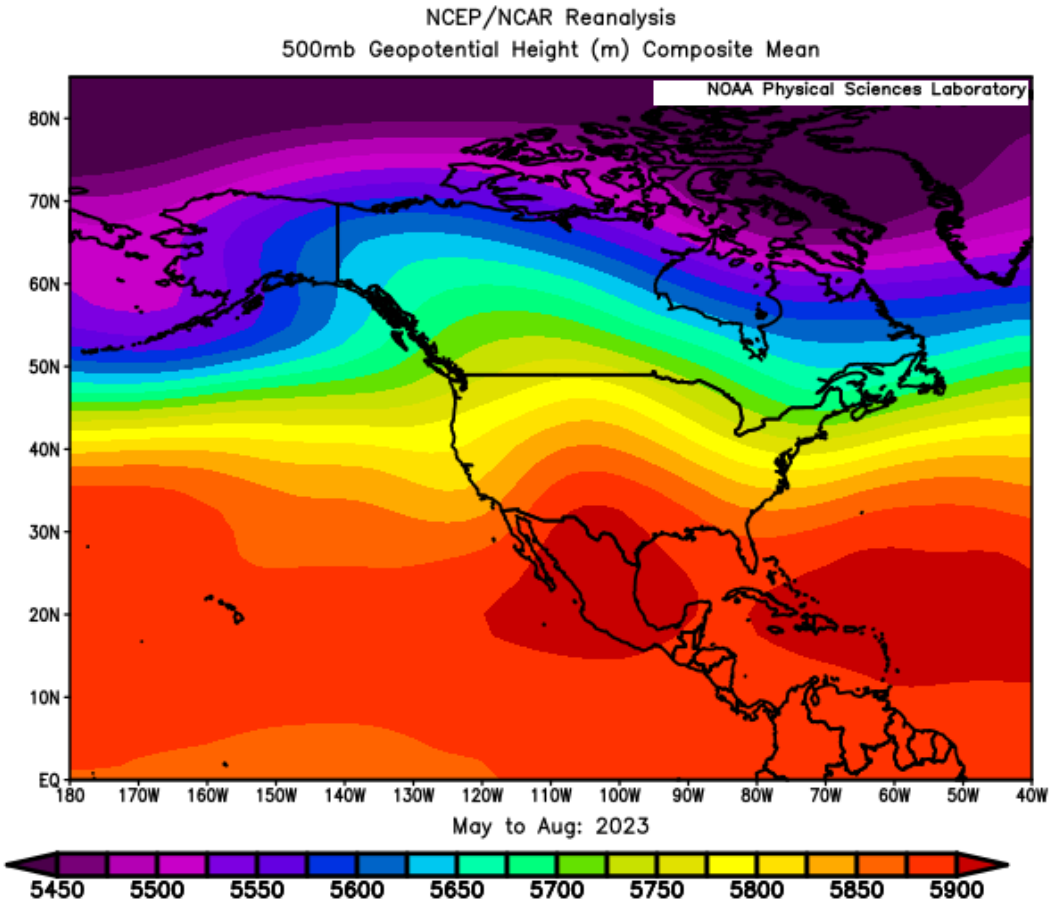

Figure 1-7. Mean 500 mb geopotential heights (meters) for May-August 2023. An upper-level high pressure ridge from Mexico to western Canada resulted in hot, dry conditions in Arizona. Source: NOAA

2. 2021 Wildfire Events

2.1 Overview

This section provides evidence that ozone concentrations were atypical exceedances on several days during 2021 and that those exceedances were impacted by wildfire smoke from local wildfires and smoke transported from regional wildfires.

2.2 June 15-16, 2021

2.2.1 Event Overview: June 15-16, 2021

This unrepresentative (atypical) ozone event took place on June 15-16, 2021, and affected twenty-one monitoring sites in the Maricopa Nonattainment Area: West Phoenix, Mesa, North Phoenix, Falcon Field, Glendale, Pinnacle Peak, Central Phoenix, South Scottsdale, South Phoenix, Tempe, Cave Creek, Dysart, Senior Center Air Monitoring Station, Red Mountain Air Monitoring Station, Lehi Air Monitoring Station, High School Air Monitoring Station, Fountain Hills, JLG Supersite, A J Maintenance Yard, Queen Valley, and Tonto NM (**Table 2-1**). The maximum daily 8-hr average (MDA8) ozone concentrations at the effected sites ranged from 72-108 ppb.

Time series graphs showing hourly ozone concentrations that exceeded the seasonal means (calculated using all available data from April 1 – September 31, 2019-2024) and 10th-90th percentiles at each site are shown in **Figure 2-1**. On June 15, hourly ozone measurements at many sites, such as Central Phoenix, North Phoenix, and Pinnacle Peak, were more than 10% above the mean seasonal values during the early afternoon hours. Measurements increased rapidly in the early afternoon and exceeded the 90th percentiles between 12:00 to 19:00 PST for most sites, indicating transport of ozone and ozone precursors from wildfires. In general, measurements returned to below the 90th percentile in the late evening on June 16.

Major wildfires burning in Arizona and neighboring states, notably the Telegraph fire in southeastern Arizona, and numerous fires burning in Mexico were identified as major contributors to this event. Evidence of wildfires includes (1) HMS smoke perimeters over the nonattainment area, (2) HYSPLIT trajectories and meteorological analysis showing accumulation of smoke in the nonattainment area, (3) visible smoke in camera images and video news coverage, (4) elevated $PM_{2.5}$ and NO_2 concentrations, OC to EC ratios, and $PM_{2.5}$ species, and (5) remote sensing imagery. This combination of evidence indicates that this is an atypical ozone event.

Table 2-1. Summary of identified atypical event June 15 and 16, 2021.

Event Date(s)	Event Ozone Concentration Percentile	Sites Exceeded During Event	Type of Event
June 15-16, 2021	94th - 100th	Twenty-One sites: West Phoenix, Mesa, North Phoenix, Falcon Field, Glendale, Pinnacle Peak, Central Phoenix, South Scottsdale, South Phoenix, Tempe, Cave Creek, Dysart, Senior Center Air Monitoring Station, Red Mountain Air Monitoring Station, Lehi Air Monitoring Station, High School Air Monitoring Station, Fountain Hills, JLG Supersite, A J Maintenance Yard, Queen Valley, Tonto NM	International/regional transport/local transport

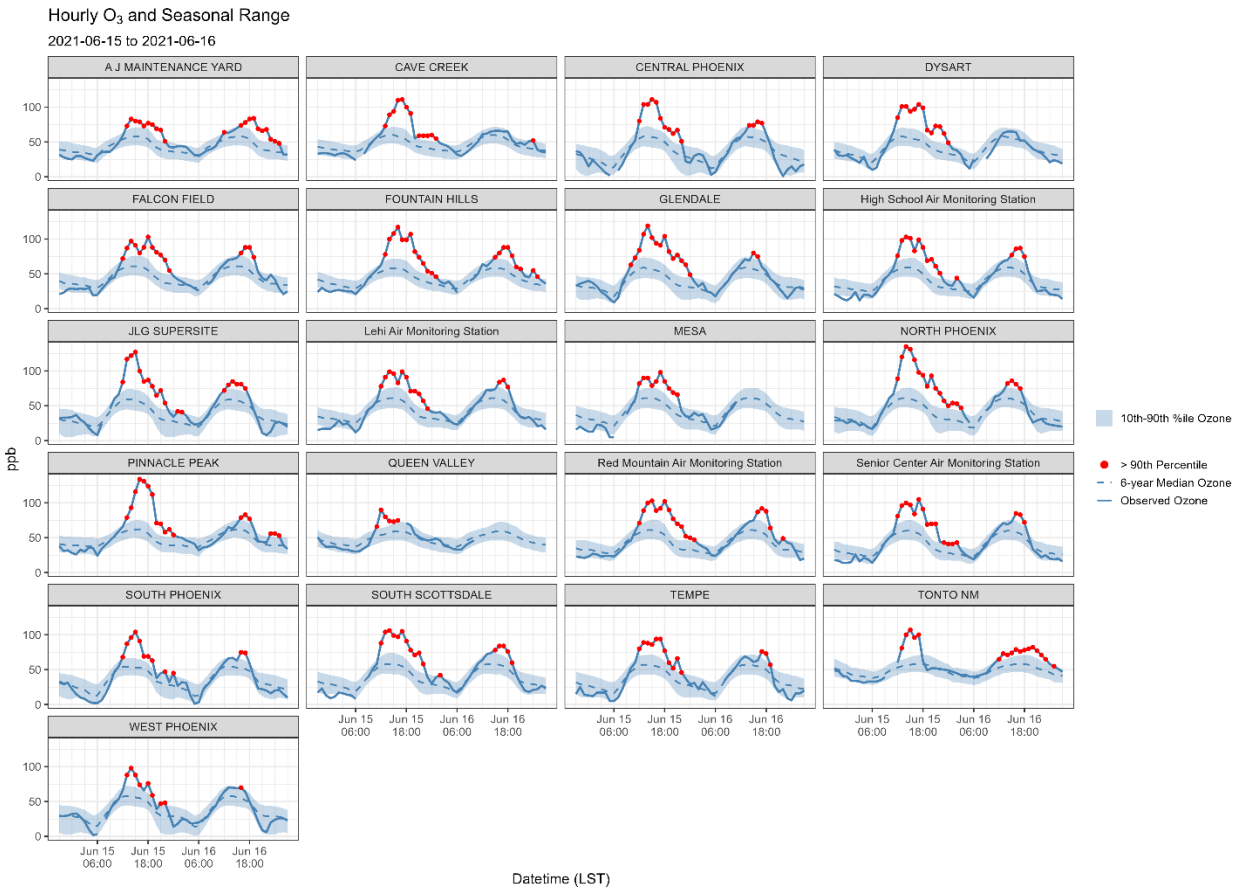

Figure 2-1. Hourly ozone concentrations (ppb) compared to all available data during the ozone season (April 1 – September 31) of the 6-year (2019-2024) period. Hourly means and 10th-90th percentiles are calculated using data on June 15-16.

2.2.2 Identification of Wildfire(s)

A large fire to the southeast of Phoenix was active in the days leading up to and during June 15-16, the exclusion days (**Figures 2-2 through 2-4**). As shown in Figure 2-2, smoke from June 14, the day before the June 15-16 exclusion days was actively spreading throughout the state of Arizona. On June 15, the entire NAA was blanketed by dense smoke plumes, and on June 16,[1]The Telegraph Fire, one of the largest fires in the state of Arizona's history, was first reported on June 4, expanded to 139,000 acres by June 16,and reached a maximum size of approximately 180,000 acres. Full containment of the fire was achieved on July 3, based on data from the Current Interagency Fire Perimeters.[2] The fire was in close proximity to the Phoenix metropolitan region, about 110 to 140 km to the east. Another fire – the Johnson Fire – in New Mexico near the Arizona/New Mexico border

[1] https://www.cnn.com/2021/06/15/weather/arizona-wildfires-telegraph-evacuations
[2] https://data-nifc.opendata.arcgis.com/datasets/nifc::wfigs-interagency-fire-perimeters/explore?location=-0.001339%2C95.978776%2C1.10

was also actively burning during the atypical ozone days. Numerous fires burning in western Mexico also likely contributed to the smoke plumes blanketing the southwestern U.S. during June 15-16 (Figures 2-5).

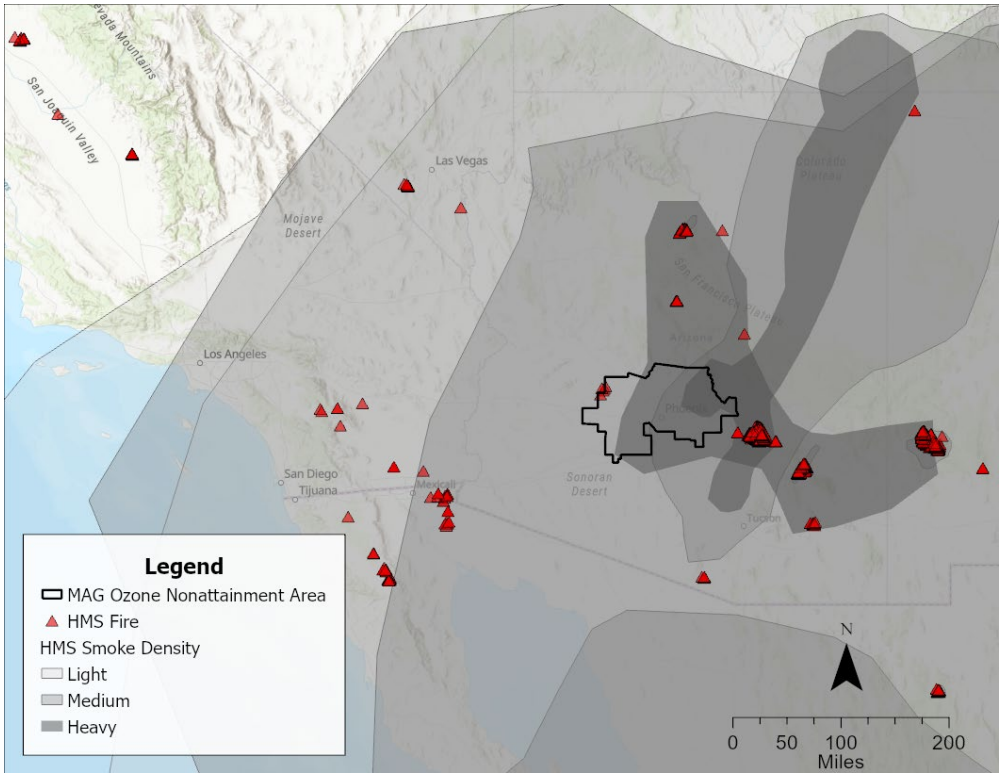

Figure 2-2. Regional view of HMS smoke density and fire locations on June 14, 2021.

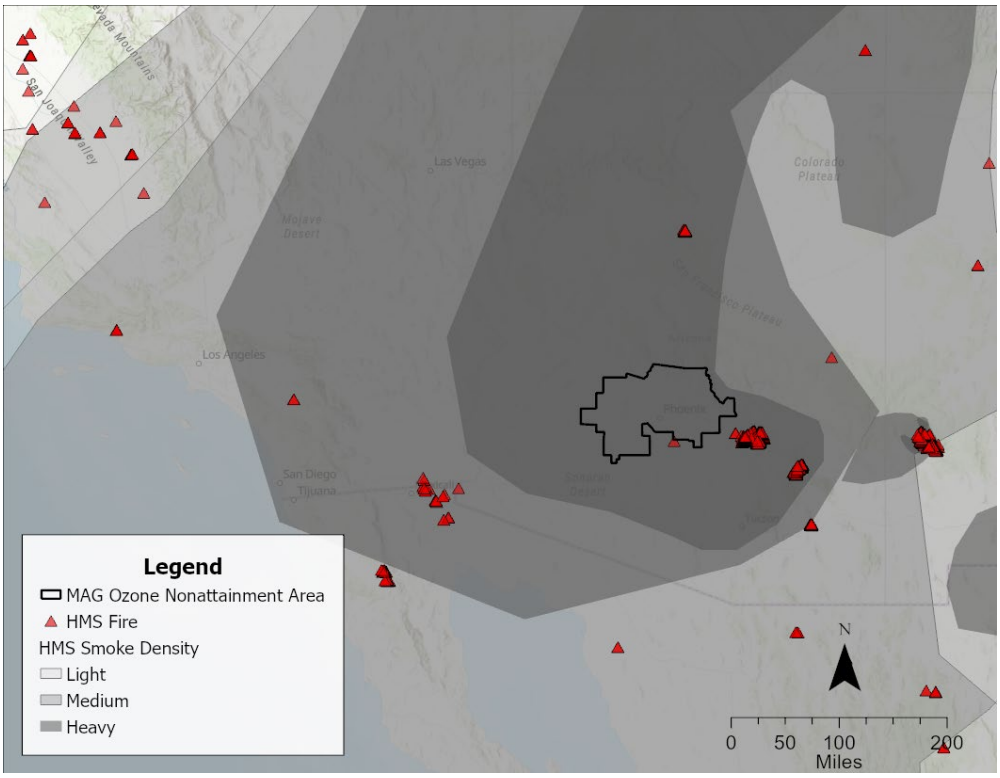

Figure 2-3. Regional view of HMS smoke density and fire locations on June 15, 2021.

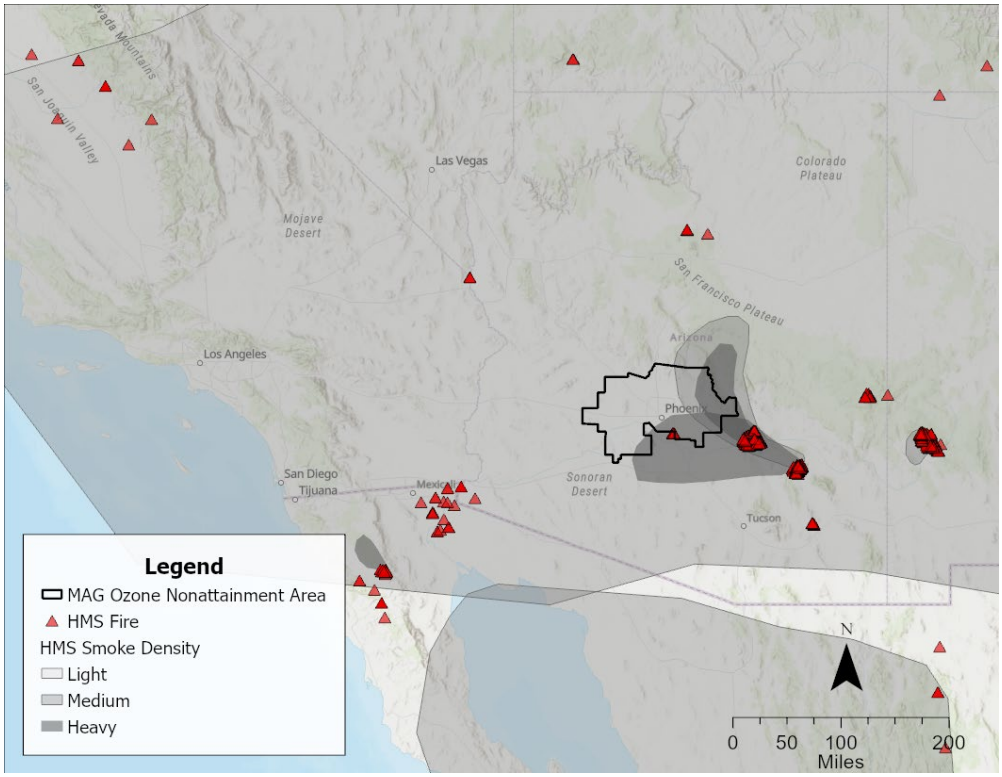

Figure 2-4. Regional view of HMS smoke density on June 16, 2021.

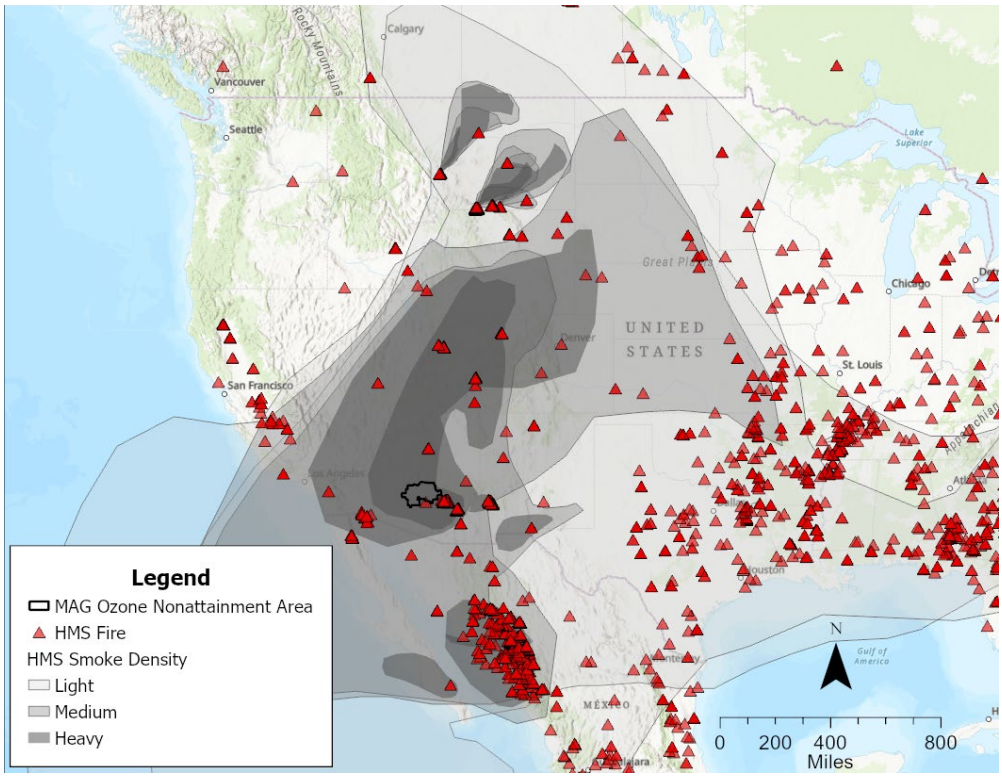

Figure 2-5. Continental view of HMS smoke density and fire locations on June 15, 2021.

2.2.3 Meteorological Analysis

Upper-Level Analysis

The contour plot of average geopotential height at 500 mb (approximately 18,000 feet) from June 15 and 16, 2021 in **Figure 2-6** shows a large ridge of high pressure centered over the Four Corners. The red colors over Arizona indicate 500 mb heights over 5950 meters, which is above normal for this time of year. These above normal heights indicate warm mid-level temperatures over the Desert Southwest, along with a potential reduction in atmospheric mixing. With the ridge directly over Arizona, mostly sunny skies and hot surface temperatures were also likely to aid ozone formation on these days.

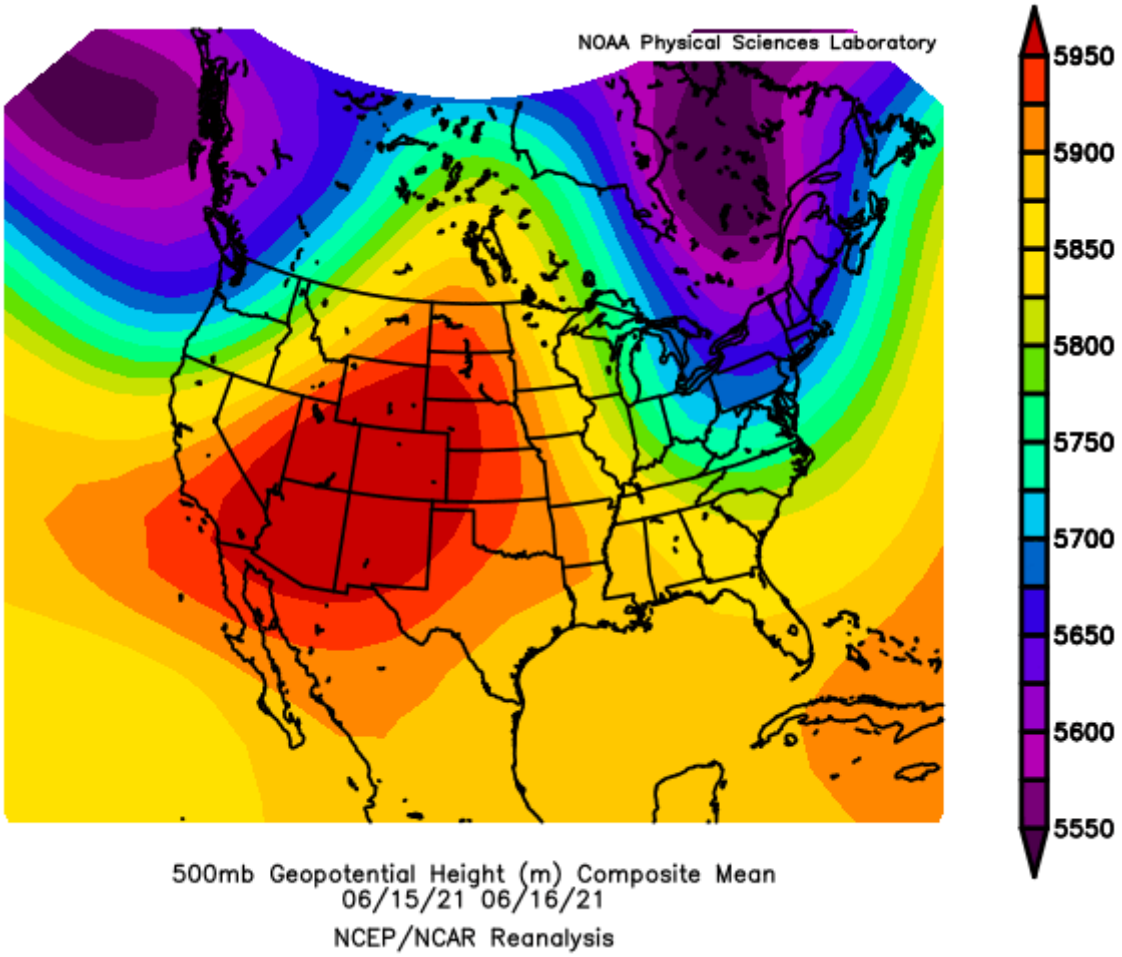

Figure 2-6. Average geopotential height at 500 mb from June 15-16, 2021.

Surface Analysis

Figure 2-7 shows a weak trough of surface low pressure near Phoenix each afternoon as hot temperatures generated rising thermals over the Desert Southwest. A weak pressure gradient over the region also indicates the potential for light winds. **Table 2-2** confirms that the above-normal heights aloft were associated with hot surface temperatures that aided ozone development. In addition, wind speeds averaged 6 mph or less each day, limiting pollutant dispersion over the nonattainment area.

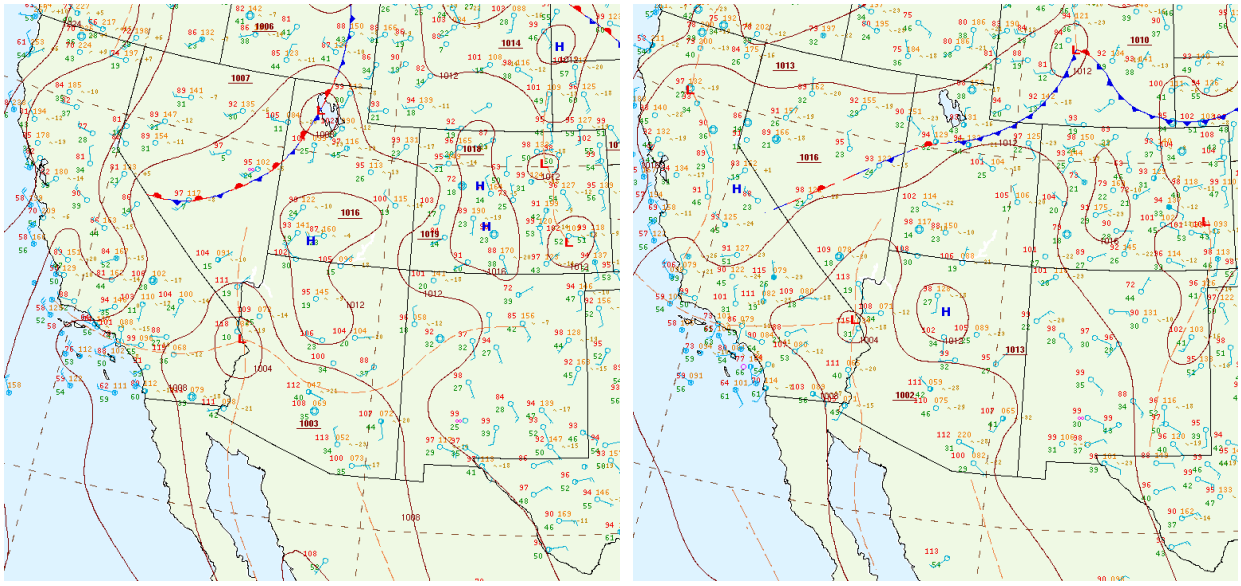

Figure 2-7. Surface analyses from 14:00 LST on June 15, 2021, (left) and 14:00 LST on June 16, 2021, (right).

Table 2-2. Surface weather variables observed at Phoenix Sky Harbor Airport.

Date	High Temp. (F)	Avg. WS (mph)	Avg. WD
6/15/2021	115	5	69
6/16/2021	115	6	272

Satellite Smoke and Fire Detections

Figure 2-8 shows satellites detected dense smoke over the nonattainment area on June 15 and 16 as multiple large fires burned across southeastern Arizona and western New Mexico. The dense smoke plumes over Phoenix are also apparent on visible satellite imagery each afternoon in Figures 2-9 and 2-10. Moderate Resolution Imaging Spectroradiometer (MODIS) Aqua Aerometric Information Retrieval System (AIRS) provides evidence of smoke transport over Arizona on June 15, with 500 mb CO concentrations of up to 185 ppbv over Phoenix (Figure 2-11).

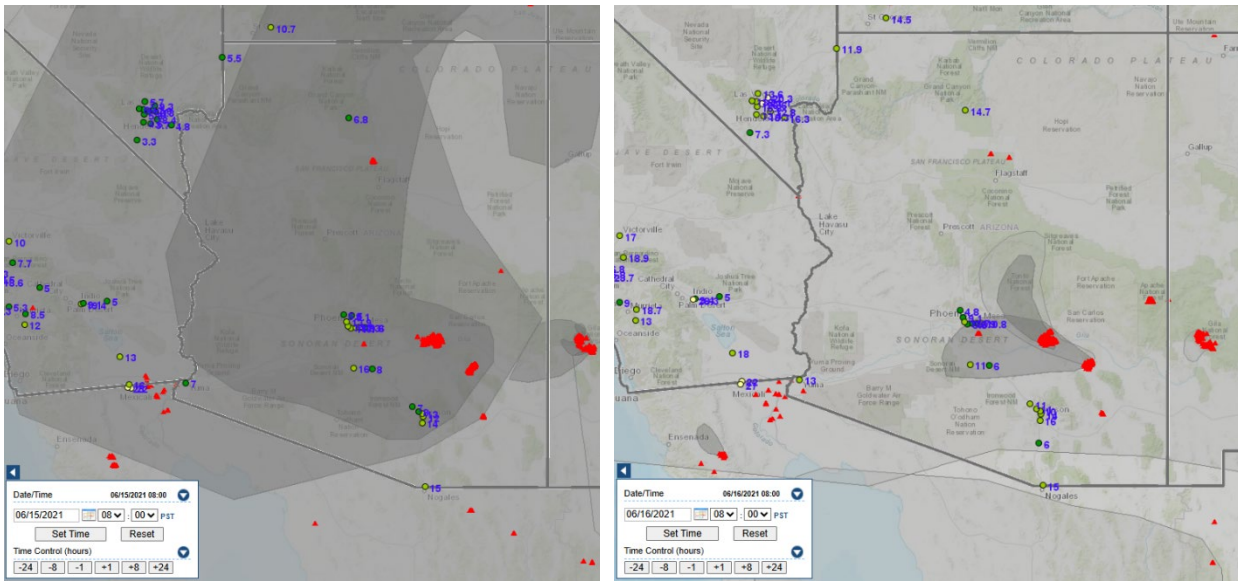

Figure 2-8. HMS fire and smoke along with hourly concentrations of $PM_{2.5}$ at 8:00 LST June 15, 2021, (left) and 8:00 LST June 16, 2021, (right).

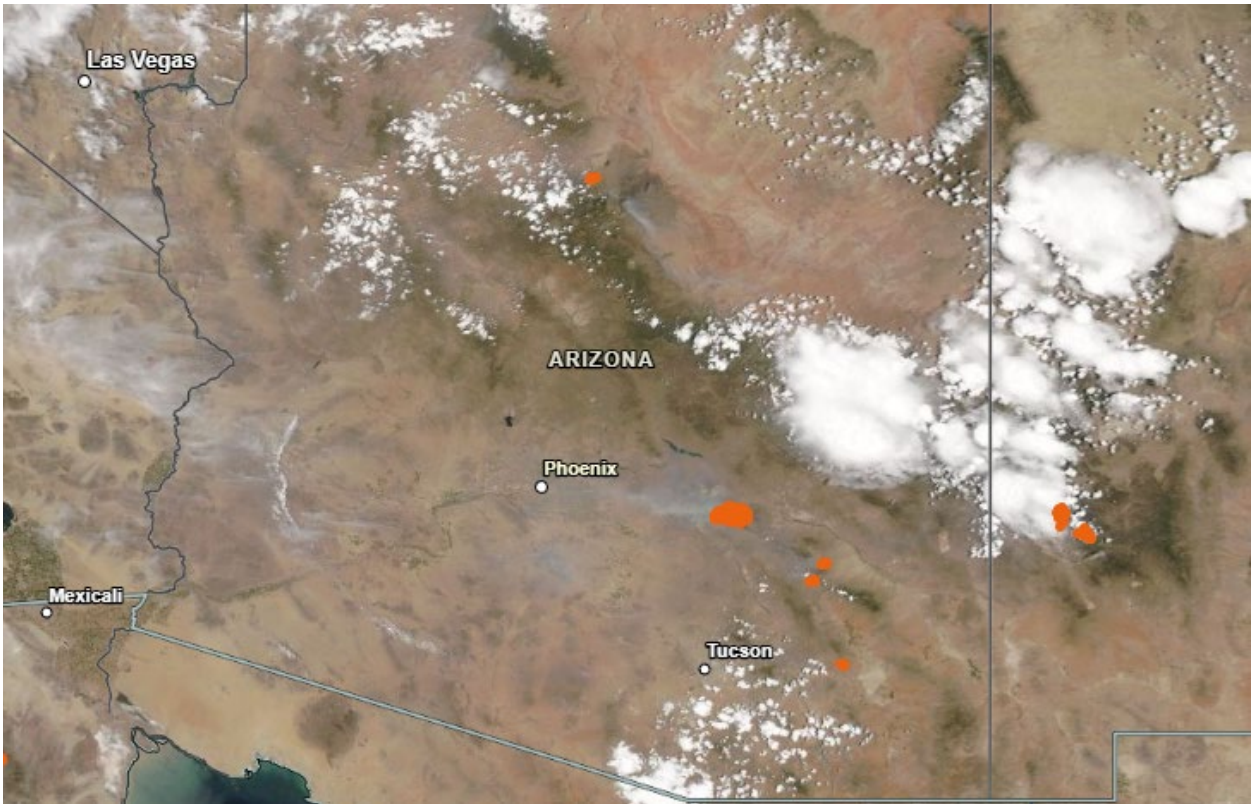

Figure 2-9. Visible satellite imagery from approximately 13:53 LST on June 15, 2021. Fire detections are indicated by orange dots.

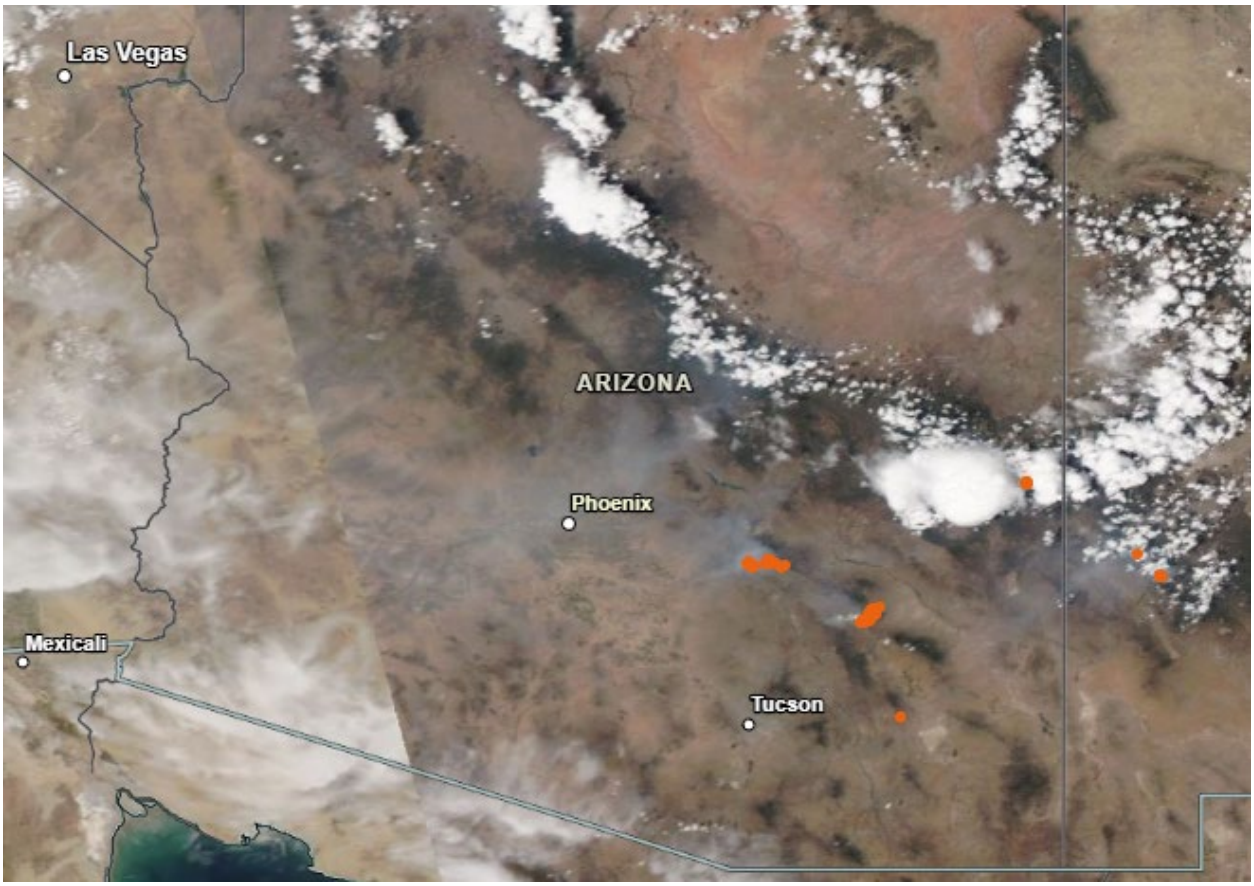

Figure 2-10. Visible satellite imagery from approximately 12:57 LST on June 16, 2021. Fire detections are indicated by orange dots.

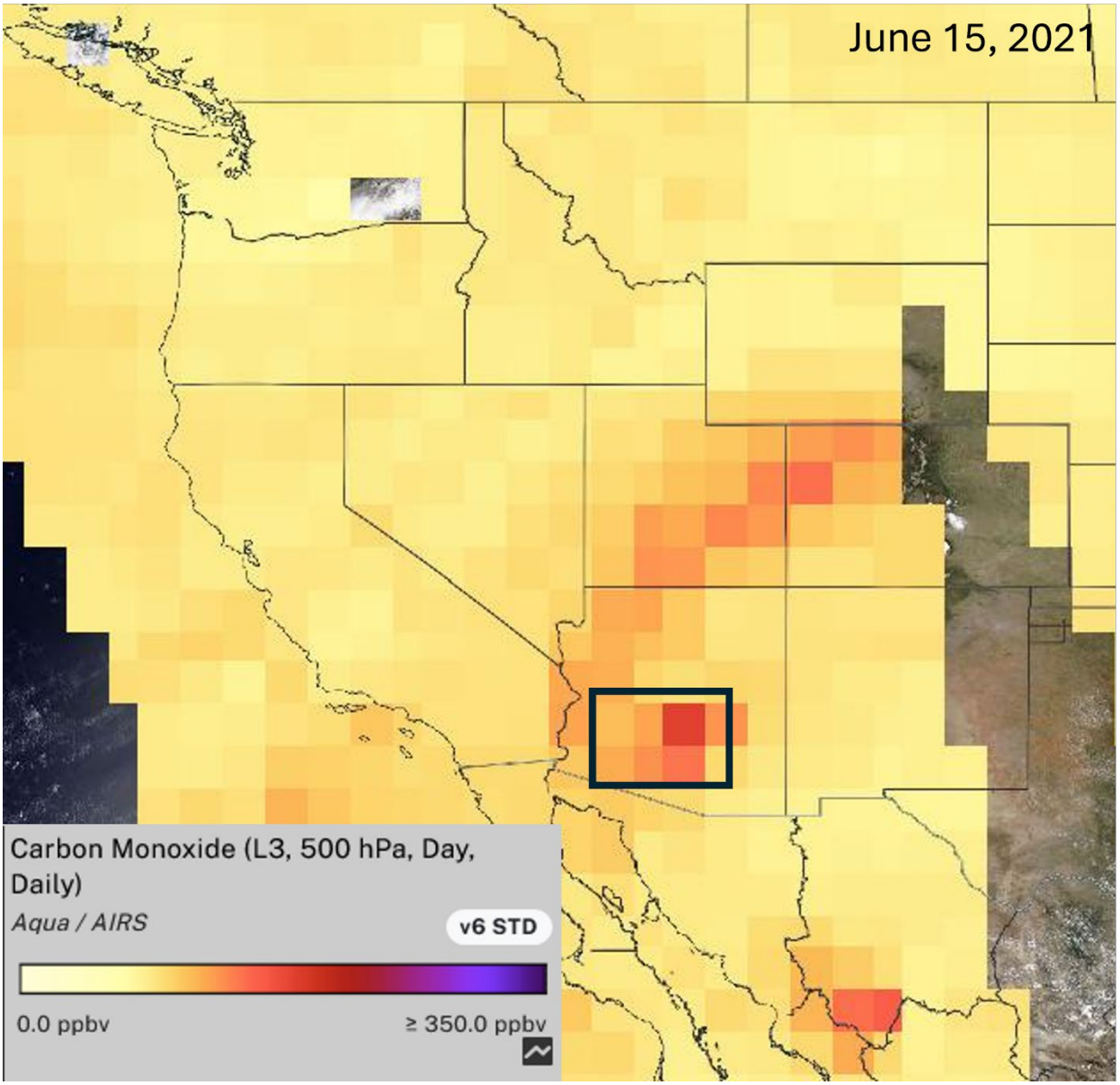

Figure 2-11. A zoomed-in view over the southwestern of MODIS Aqua AIRS CO retrieval during the atypical ozone date of June 15, 2021. The black box represents the approximate area of the NAA.

Smoke Discussions

NOAA's daily smoke discussions also note the moderate-to-heavy density smoke across Arizona on these days.

"**The enormous area of thin density smoke attributed primarily to ongoing wildfires burning mainly in western Mexico, Arizona**, Utah, New Mexico, and a new one in south central Montana was

seen this morning stretching from off the coast of western Mexico and southern California inland across the Southwestern U.S. and northward from there over the Rocky Mountain region all the way up into southern Alberta and southern Saskatchewan in southwestern Canada. **The smoke also covered much of the Central and Southeastern U.S.** and along and off the Mid-Atlantic coast and coastal areas of New York and southern New England, as well as the northern Gulf of Mexico. The band of aerosol across the South Central and Southeastern U.S. from Texas across the Gulf coast region to the eastern Carolinas was a bit more concentrated in density though some of this aerosol, in addition to thinner density smoke, was believed to be composed of other atmospheric pollutants pooled along a frontal boundary. Portions of the North Central and Northeast southward into the Ohio Valley region appeared to be relatively smoke free. Embedded within this large mass of thin density smoke were areas of thicker density smoke which were visible over northwestern Mexico including Baja and off the west coast of Baja. **Thicker smoke also extended across much of the Southwestern U.S.** and northward over Utah, western Colorado, and southern Wyoming." (NOAA NESDIS Text Narrative, June 15, 2021)

"A very large area of predominantly light smoke currently covers the majority of the Contiguous United States, with the exception of the northwestern, Great Lakes and New England regions. The smoke originates from **widespread fire activity across the southeastern, central and southwestern U.S.**, in addition to northwestern Mexico. Pockets of moderate-density smoke can be seen over the Dakotas traveling eastward, and over eastern Colorado, western Oklahoma and northern Texas where the smoke is moving toward the south. The Johnson Fire in Gila National Forest/western New Mexico, in addition to the **Pinnacle, Mescal and Telegraph fires in Gila and Graham Counties in southeastern Arizona were also actively burning this morning, releasing moderate-to-heavy density smoke toward the west-northwest.**" (NOAA NESDIS Text Narrative, June 16, 2021)

In addition, smoke was reported at Phoenix Sky Harbor Airport by METAR observations on June 15 and June 16.

Soundings

A morning sounding was available for Phoenix on June 15. However, Tucson was the closest sounding location available for the remainder of June 15 and June 16. **Figure 2-12** shows the observed atmospheric soundings from 5:00 LST (left) and 17:00 LST (right) June 15-16, 2021. The left panels in Figure 2-12 show temperature inversions and stable conditions on the mornings of June 15 and 16, confining pollutants near the surface.

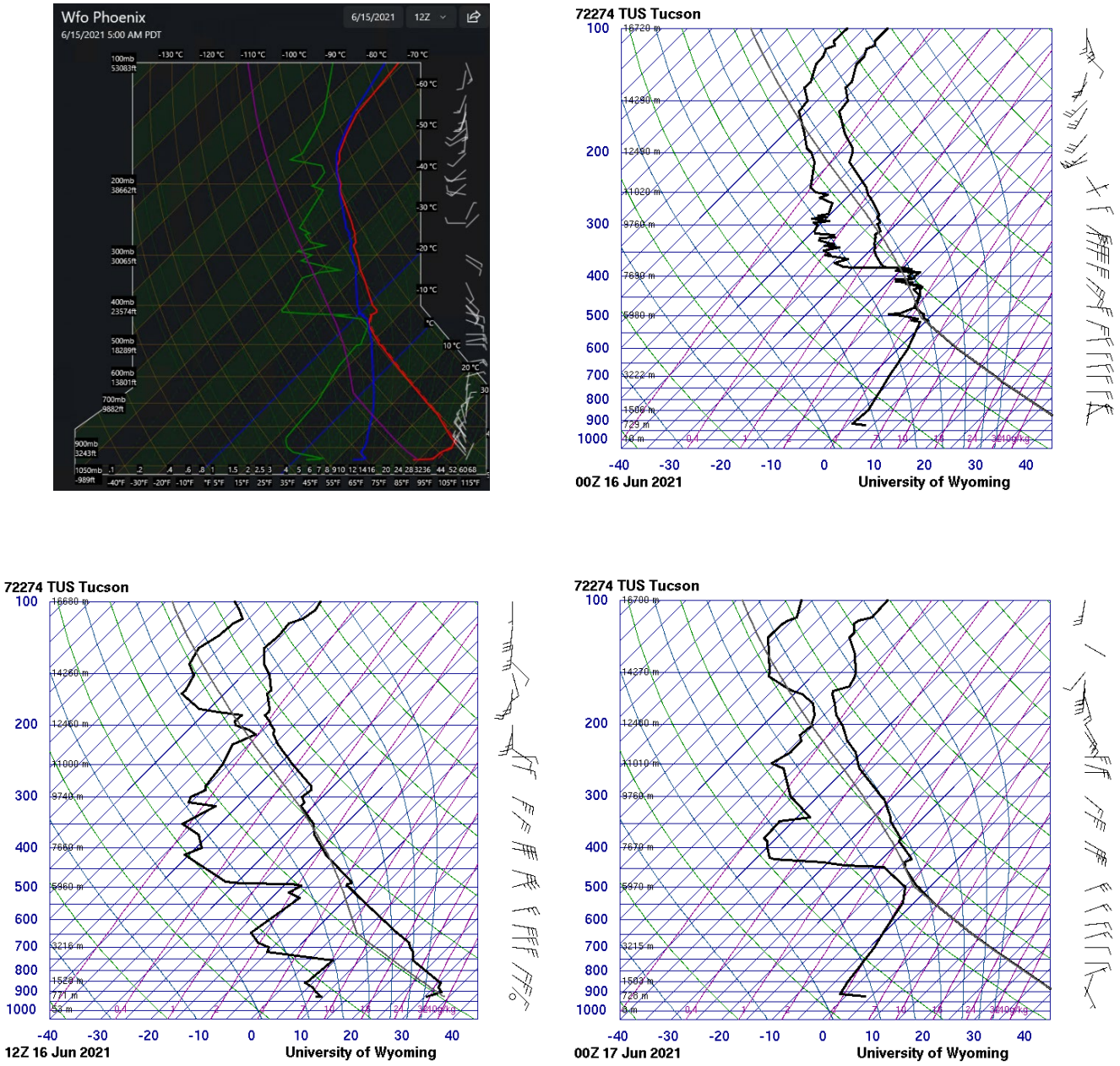

Figure 2-12. Observed atmospheric soundings from 5:00 LST (left) and 17:00 LST (right) June 15-16, 2021.

However, despite warm temperatures aloft, mixing improved greatly each afternoon due to hot surface temperatures (right panel) with mixing heights extending to 500 mb (5.5 km) on June 15 and 16. With smoke directly over Phoenix each afternoon, these deep mixing heights allowed the aloft smoke to mix to the surface and enhance ozone formation.

Smoke Transport

In addition to the smoke from nearby fires, smoke from distant fires also likely contributed to ozone development across Arizona on June 15 and 16. 48-hour back trajectories from 00:00 to 20:00 LST between June 11 and 12 at 100 meters, 1,000 meters, and 2,500 meters above ground level (AGL) calculated by NOAA's HYSPLIT model originated from areas impacted by medium to heavy smoke from fires in Mexico, Utah, New Mexico, and Montana (**Figure 2-13**).

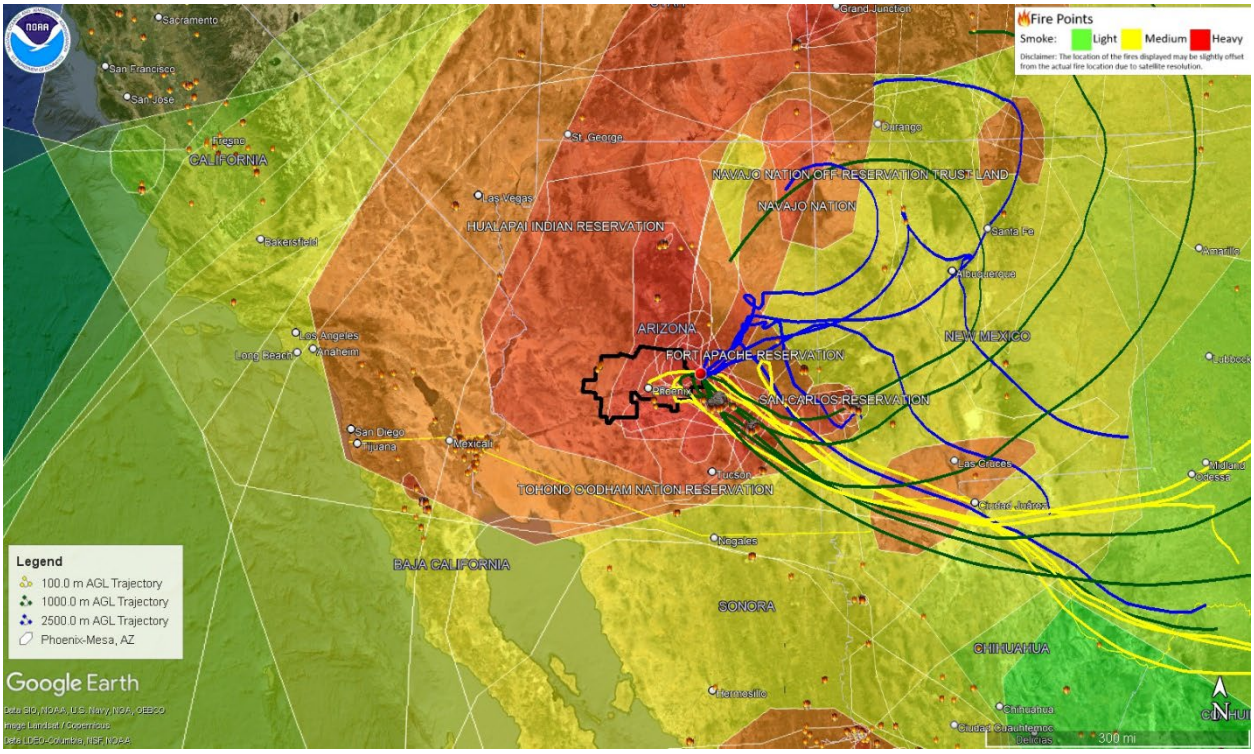

Figure 2-13. NOAA smoke and fire maps and NOAA HYSPLIT trajectory model runs with air parcels moving 48-hours before 00:00 – 20:00 LST between June 15-16, 2021, at 100 meters, 1,000 meters and 2,500 meters (AGL). Analysis performed by MAG.

Summary

For June 15-16, 2021, an upper-level ridge of high pressure over the Four Corners led to sunny skies and hot temperatures over southern Arizona, aiding ozone production in the nonattainment area. These hot and dry conditions also led to deep atmospheric mixing each afternoon, carrying dense aloft smoke from large fires across southeastern Arizona and western New Mexico to the surface. In addition, a weak pressure gradient at the surface produced light winds over the region each day, allowing smoke to accumulate in the nonattainment area as shown on visible satellite imagery each afternoon. These meteorological conditions and satellite images provide evidence that smoke contributed to enhanced ozone formation from June 15-16, 2021 in the nonattainment area.

2.2.4 Surface Impacts

Smoke plumes from the local and regional fires spread over Phoenix in the days leading up to June 15, 2021, and were visible in Phoenix during the morning of June 15. **Figures 2-14 through 2-21** show photos taken from the southwest-facing Estrella Mountain, south-facing South Mountain, east-facing Superstition Mountain, and west-northwest-facing White Tank Mountain webcams, where the smoke is visible throughout the day on both June 15 and 16. This prominent smoke plume was a news-worthy occurrence reported on by ABC; their report, "Wondering what's causing hazy skies? Smoke from Telegraph Fire blanketing the Valley", provided videos of the growing smoke plume (**https://www.abc15.com/news/local-news/smoke-from-telegraph-fire-blanketing-the-valley**).

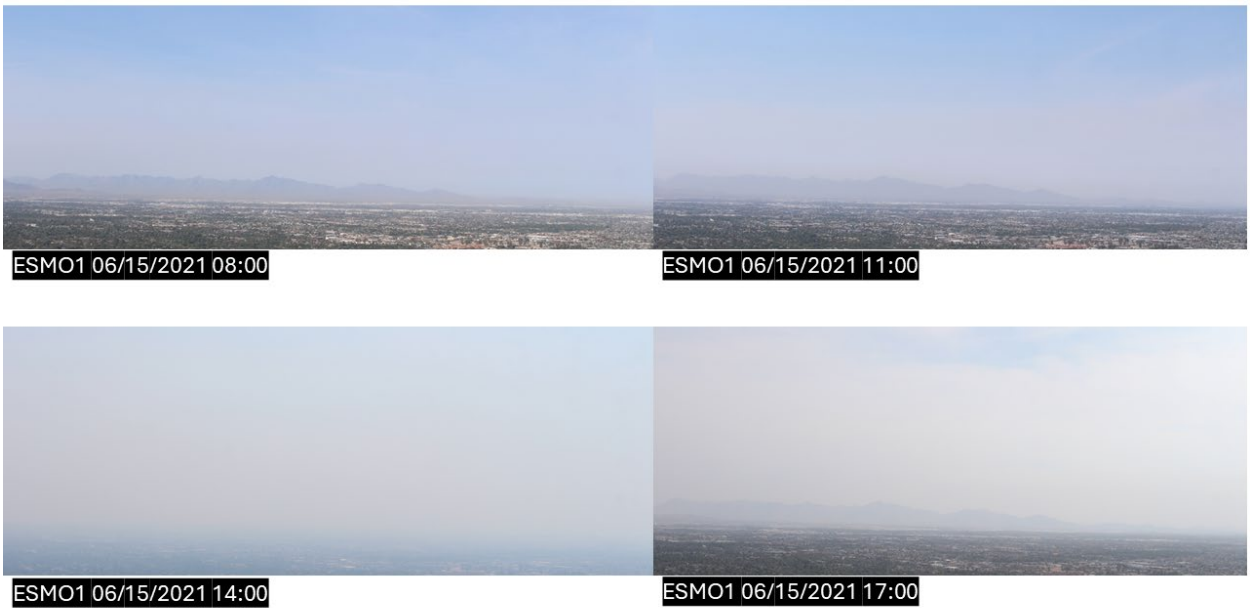

Figure 2-14. Camera Images showing the southwest coordinal direction taken from the Estrella Mountain webcam on June 15 from 8:00 LST, 11:00 LST, 14:00 LST, and 17:00.

Figure 2-15. Camera Images showing the southwest coordinal direction taken from the Estrella Mountain webcam on June 16 from 8:00 LST, 11:00 LST, 14:00 LST, and 17:00.

Figure 2-16. Camera Images showing the south coordinal direction taken from the South Mountain webcam on June 15 from 8:00 LST, 11:00 LST, 14:00 LST, and 17:00.

Figure 2-17. Camera Images showing the south coordinal direction taken from the South Mountain webcam on June 16 from 8:00 LST, 11:00 LST, 14:00 LST, and 17:00.

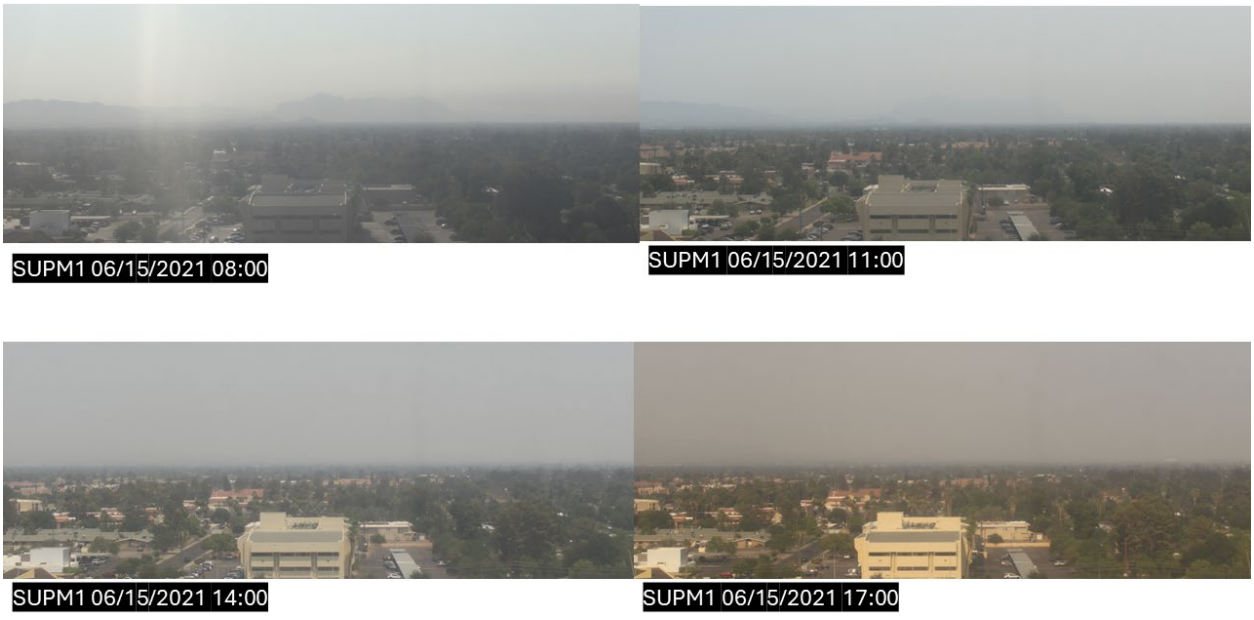

Figure 2-18. Camera Images showing the east coordinal direction taken from the Superstition Mountain webcam on June 15 from 8:00 LST, 11:00 LST, 14:00 LST, and 17:00.

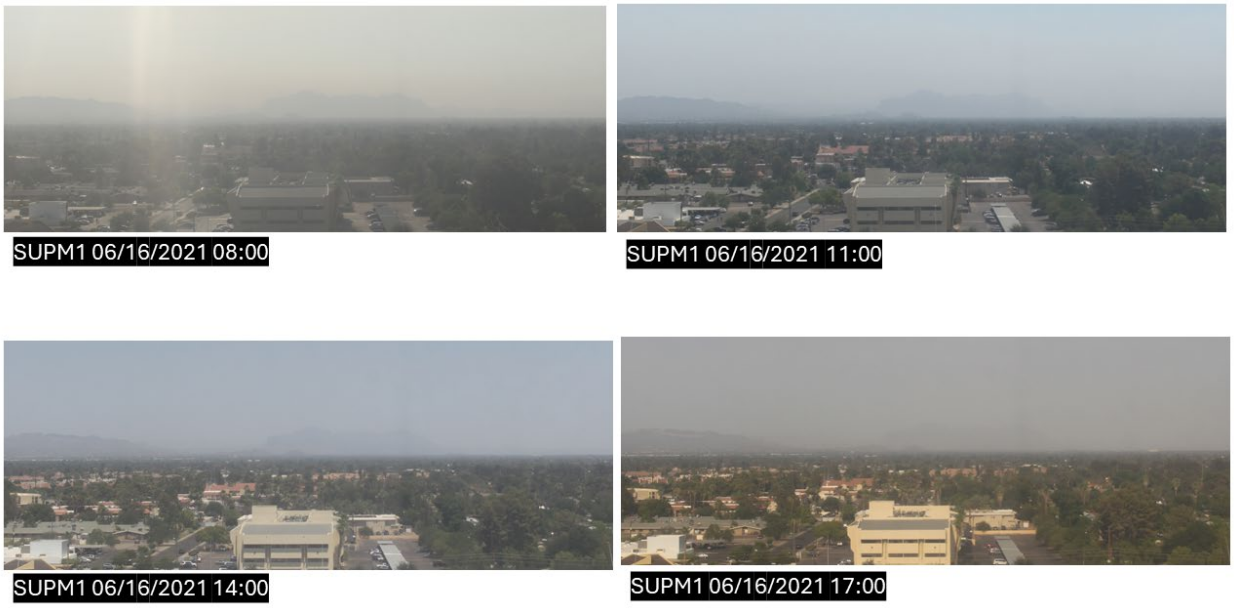

Figure 2-19. Camera Images showing the east coordinal direction taken from the Superstition Mountain webcam on June 16 from 8:00 LST, 11:00 LST, 14:00 LST, and 17:00.

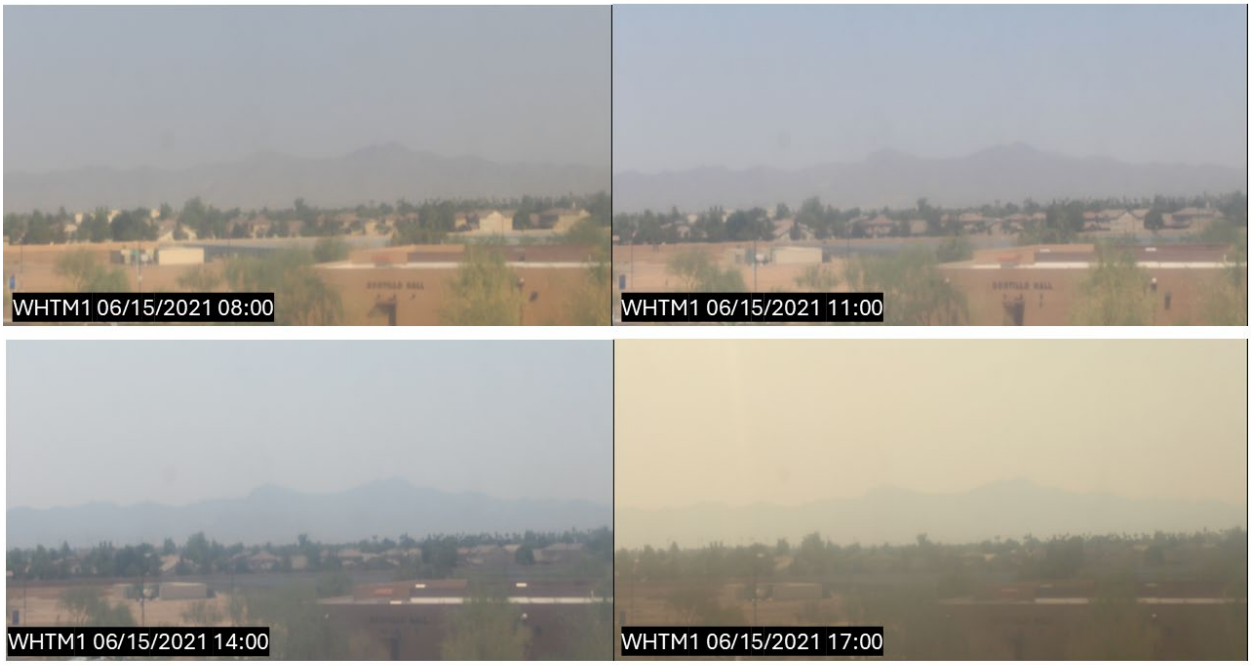

Figure 2-20. Camera Images showing the west-northwest coordinal direction taken from the White Tank Mountain webcam on June 15 from 8:00 LST, 11:00 LST, 14:00 LST, and 17:00.

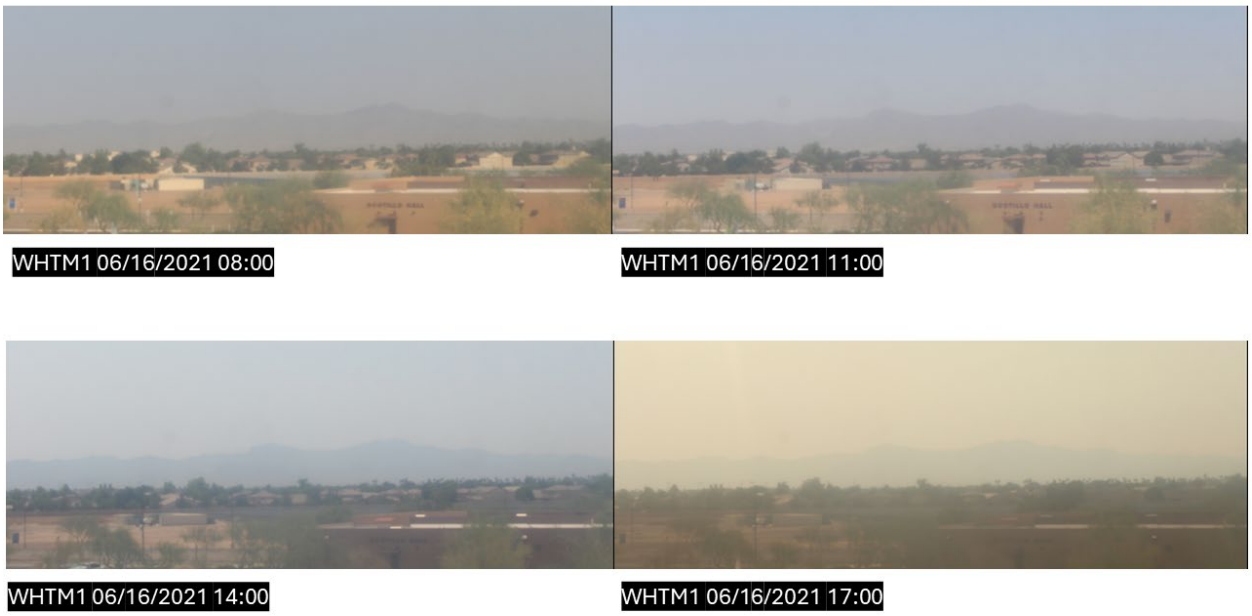

Figure 2-21. Camera Images showing the west-northwest coordinal direction taken from the White Tank Mountain webcam on June 16 from 8:00 LST, 11:00 LST, 14:00 LST, and 17:00.

Figure 2-22 shows an overall view of the magnitude of hourly pollutant concentrations measured in the nonattainment area in the two days before and after the June 15-16, 2021, atypical event. Hourly concentrations of ozone show a widespread and distinct peak on June 15 at all affected sites relative to the days surrounding the atypical event. Similarly, $PM_{2.5}$ concentrations at the exceedance-affected sites rise sharply at all $PM_{2.5}$-measuring sites during the afternoon of June 15, coinciding with the dramatic rise in ozone concentrations. $PM_{2.5}$ concentrations at all sites remain elevated into the early hours of June 16. Increased concentrations of $PM_{2.5}$ on June 15-16 are consistent with transport of more particulate matter during the flaming portion of a quickly spreading fire. Higher $PM_{2.5}$ concentrations were likely not from dust because conditions were not favorable (e.g., wind speeds were generally low) for wind-blown dust before and during the June 15-16 atypical event. Furthermore, there were no dust storm advisories or warnings before or during this atypical event.[3] Distinct and widespread enhancements in surface pollutant concentrations provide evidence that smoke from regional fires entered the region, mixed towards the surface, and had an atypical influence on ozone during the period. The rest of this section examines temporal abnormalities and site-specific trends for each supporting pollutant.

[3] **https://mesonet.agron.iastate.edu/vtec/search.php?mode=bypoint&lon=-112.1202&lat=33.4223&buffer=0.00&sdate1=2021-06-12&edate1=2021-08-04**

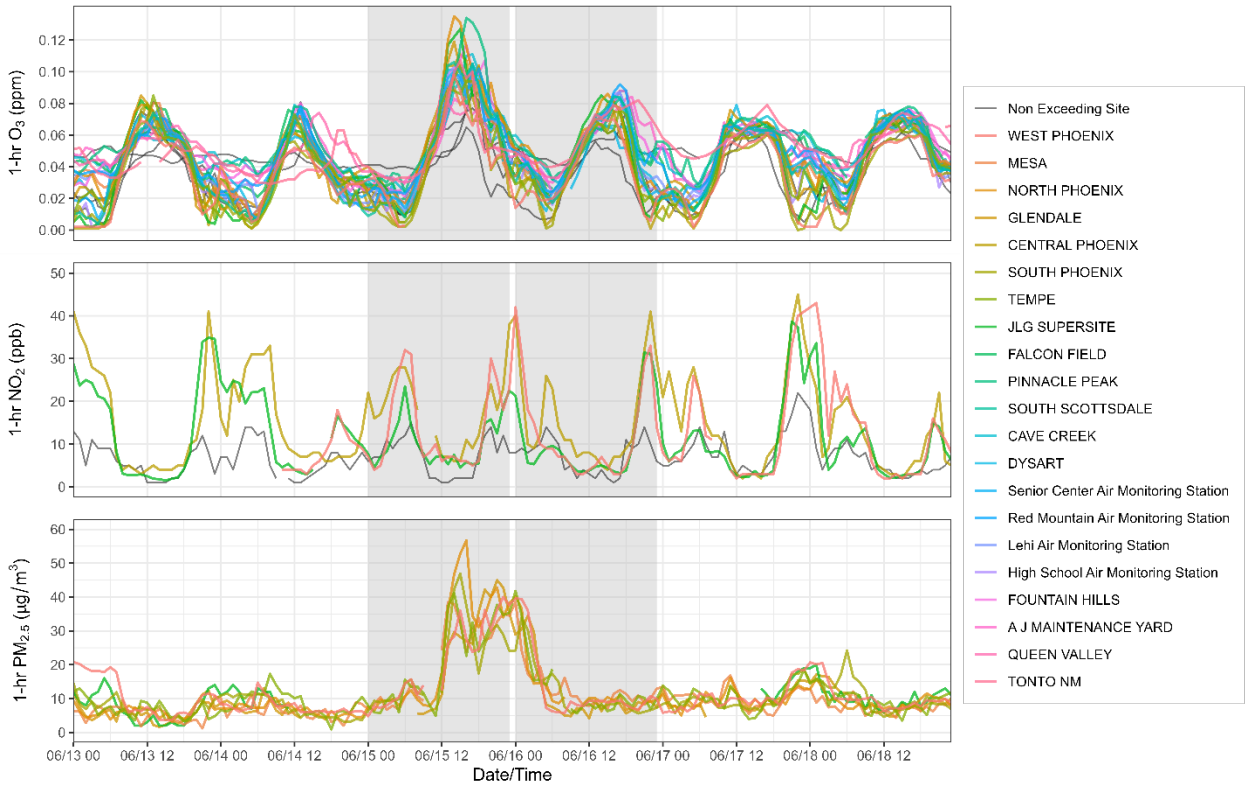

Figure 2-22. Hourly concentrations of ozone, NO_2, and $PM_{2.5}$ at all sites in the nonattainment area. All ozone-exceeding sites are color-coded to highlight smoke impacts on concentrations, and all non-exceeding sites are black. The gray shaded areas represent June 15 and 16, 2021.

$PM_{2.5}$ and NO_2 concentrations were enhanced in Phoenix on June 15 as emissions from the local and regional fires entered the region and mixed towards the surface, which provides further evidence that wildfire smoke was present as an atypical influence on ozone during the period. **Figure 2-23** shows hourly $PM_{2.5}$ concentrations at the West Phoenix site (one of the affected sites) overlaid on the 5th-95th percentile hourly concentrations during ozone season (April to September), calculated using all available data from 2019-2024. $PM_{2.5}$ concentrations rose sharply to a peak concentration of approximately 40 µg/m^3 at the West Phoenix site as smoke moved into the area, reaching concentrations that meet or exceed the 95th percentile average concentration between around 12:00 LST and midnight on June 15. Concentrations at the West Phoenix site fall to approximately normal levels on June 16. $PM_{2.5}$ concentrations at eight other affected sites exceeded the 95th percentile on June 15-16. Similarly, NO_2 concentrations at West Phoenix increased to nearly the 95th percentile around 6:00 LST on June 15, then exceeded the 95th percentile around midnight the same day.

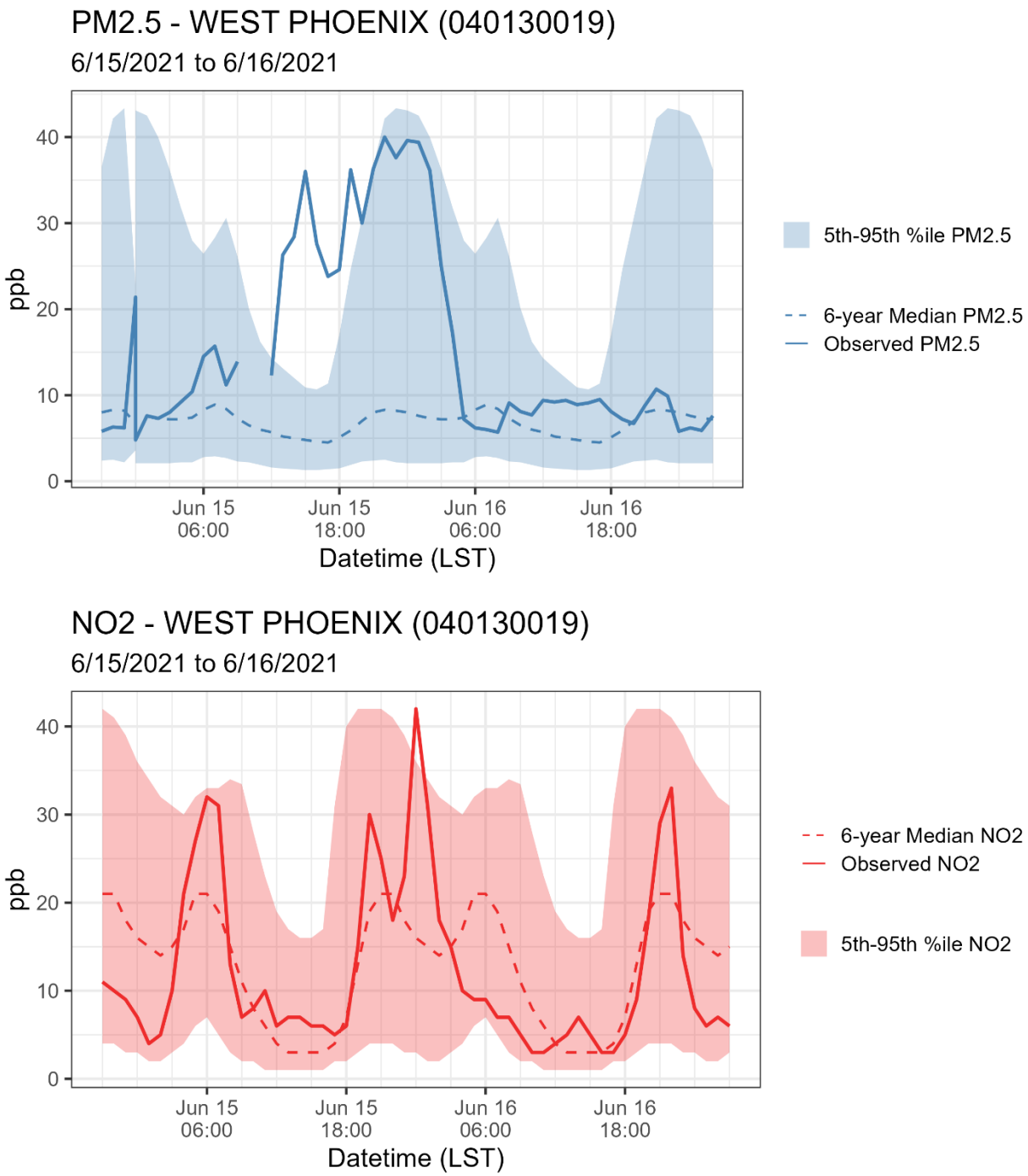

Figure 2-23. Hourly concentrations of $PM_{2.5}$ (top) and NO_2 (bottom) at the West Phoenix site. The 6-year (2019-2024) median is represented by the dashed line, and the 5th-95th percentile is represented by the shaded area.

The ratio of OC to EC taken at the JLG Supersite monitor was also examined for evidence that wildfire smoke entered the nonattainment area. Increases in this ratio are indicative of wildfire smoke.

Figure 2-24 shows boxplots of OC to EC ratios for available data collected during the ozone season between 2019-2024. The OC to EC ratio on June 15 was above the 75th percentile and nearly an upper outlier compared to all data. Elevated $PM_{2.5}$ species concentrations, particularly potassium, are also indicative of wildfire smoke. Figure 2-25 shows boxplots of speciated $PM_{2.5}$ collected at the JLG Supersite monitor during the ozone season between 2019-2024. Nearly all $PM_{2.5}$ observations collected on June 15 are elevated well above the 75th percentile. Elevated concentrations of aluminum, calcium, iron, and silicon are indicative of dust, but potassium on June 15 is also elevated and considered an outlier, which indicates the presence of smoke. These observations provide further evidence that ground-level wildfire smoke entered Phoenix on June 15 containing increased OC to EC ratios and potassium concentrations during the June 15-16 atypical ozone event.

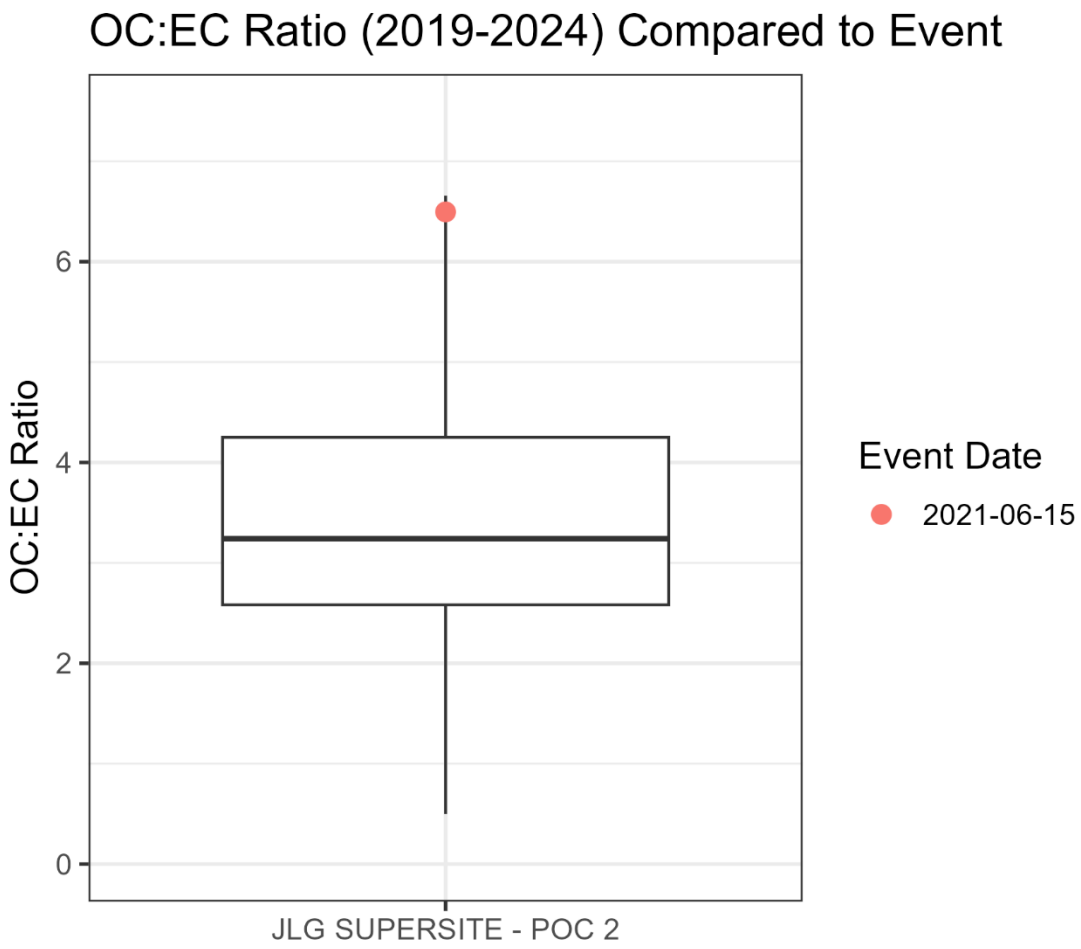

Figure 2-24. Boxplot of OC to EC ratios at the JLG Supersite site using data collected during the ozone season (April-September) from 2019-2024. OC to EC ratios are calculated at POC 2 (x-axis). Available OC to EC ratios collected during the June 15-16 atypical ozone event are shown as a point.

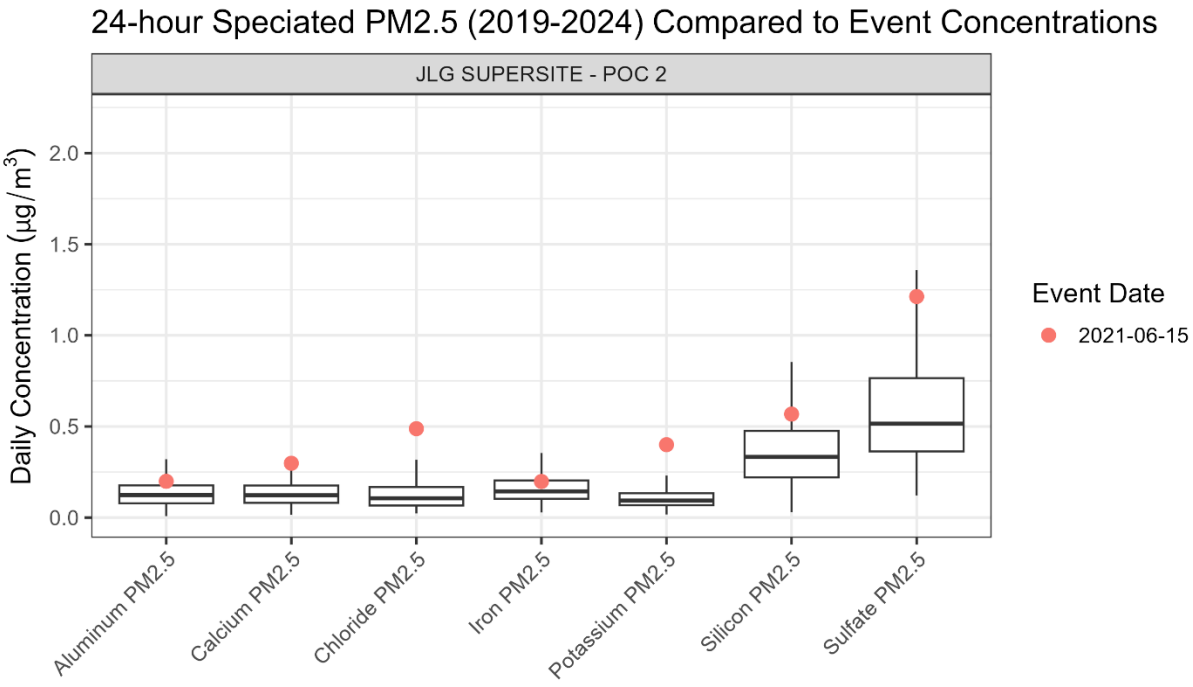

Figure 2-25. Boxplots of speciated $PM_{2.5}$ collected at the JLG Supersite site collected during the ozone season (April-September) from 2019-2024. Available speciated $PM_{2.5}$ concentrations collected during the June 15-16 atypical ozone event are shown as a point.

2.2.5 Event Statistics

Table 2-3 summarizes the measurements of ozone concentrations on June 15-16, 2021, as well as the percentile rank of the observation compared to six years of ozone season data (April 1-September 31, 2019-2024). Ozone MDA8 measurements ranged from the 94th-100th percentile on June 15-16, 2021.

Table 2-3. Percentile of ozone measurements on the atypical dates compared with six years of ozone data (2019-2024). The percentile rank is calculated across the ozone production season in the nonattainment area (April 1-September 31) of 2019-2024.

Date	Site Name	Site Code	Ozone MDA8 (ppb)	Percentile Rank
6/15/2021	Queen Valley	040218001	75	96
	West Phoenix	040130019	76	97
	A J Maintenance Yard	040213001	76	97
	South Phoenix	040134003	80	99
	Tempe	040134005	83	100
	Mesa	040131003	85	100
	Lehi Air Monitoring Station	040137022	88	100
	Falcon Field	040131010	89	100
	High School Air Monitoring Station	040137024	89	100
	Senior Center Air Monitoring Station	040137020	90	100
	Tonto NM	040070010	90	100
	Central Phoenix	040133002	91	100
	Cave Creek	040134008	91	100
	Red Mountain Air Monitoring Station	040137021	92	100
	Dysart	040134010	93	100
	South Scottsdale	040133003	96	100
	Glendale	040132001	97	100
	Fountain Hills	040139704	98	100
	JLG Supersite	040139997	100	100
	Pinnacle Peak	040132005	107	100
	North Phoenix	040131004	108	100

Date	Site Name	Site Code	Ozone MDA8 (ppb)	Percentile Rank
6/16/2021	North Phoenix	040131004	72	94
	Senior Center Air Monitoring Station	040137020	72	94
	High School Air Monitoring Station	040137024	72	94
	Lehi Air Monitoring Station	040137022	73	95
	South Scottsdale	040133003	74	96
	Fountain Hills	040139704	74	96
	A J Maintenance Yard	040213001	74	96
	JLG Supersite	040139997	75	96
	Falcon Field	040131010	76	97
	Red Mountain Air Monitoring Station	040137021	76	97
	Tonto NM	040070010	77	97

2.2.6 Conclusion

The concurrence of HMS smoke perimeters over the nonattainment area, HYSPLIT trajectories and meteorological analysis showing accumulation of smoke in the nonattainment area, visible smoke in camera images and video news coverage, elevated hourly $PM_{2.5}$ and NO_2 concentrations, elevated OC to EC ratios and potassium $PM_{2.5}$ concentrations, and remote sensing imagery, provide evidence that surface-level smoke was present during the period. Regional transport of smoke from large fires in Arizona and New Mexico, combined with smoke from numerous fires burning in Mexico on June 15-16, enhanced ozone concentrations outside of the typical diurnal profile, keeping ozone values high and affecting the MDA8 ozone concentrations at twenty-one sites. Multiple analyses showed that smoke fully encompassed the Maricopa Nonattainment Area on June 15-16, 2021, and statistics show ozone concentrations were atypical during this event.

This combined evidence indicates that the Telegraph Fire along with smoke plumes generated by numerous regional fires and fires in Mexico provided an atypical source of ozone and ozone precursors that caused enhanced ozone concentrations on June 15 and 16, 2021. Removal of these days as atypical events is supported by this analysis.

2.3 June 28-29, 2021

2.3.1 Event Overview: June 28-29, 2021

The unrepresentative (atypical) ozone event took place on June 28-29, 2021, and affected fourteen sites in the Maricopa Nonattainment Area: West Phoenix, Mesa, North Phoenix, Falcon Field, Glendale, Central Phoenix, South Scottsdale, South Phoenix, Tempe, Dysart, Buckeye, JLG Supersite, A J Maintenance Yard, and Queen Valley (**Table 2-4**). MDA8 ozone concentrations at the affected sites ranged from 71-82 ppb.

Time series graphs showing hourly ozone concentrations that exceeded the seasonal means (calculated using all available data from April 1 – September 31, 2019-2024) and 10th-90th percentiles at each site are shown in **Figure 2-26**. On June 28, hourly ozone measurements at many sites, such as A J Maintenance Yard, North Phoenix, and South Scottsdale, were above the 90th percentile during the early morning hours on June 28. Measurements increased throughout the day and continued to exceed the 90th percentile at most sites throughout the day on June 28 and into June 29, indicating transport of ozone and ozone precursors from wildfires. Some sites, including Buckeye, Central Phoenix, JLG Supersite, South Phoenix, and Tempe show distinct peaks in ozone concentrations near 100 ppb in the mid-afternoon on June 29, further indicating transport of ozone and ozone precursors from wildfires.

Major wildfires burning in Arizona and neighboring states, notably the Telegraph Fire in southeastern Arizona, were identified as major contributors to this event. Evidence includes (1) HMS smoke perimeters over the nonattainment area, (2) HYSPLIT trajectories and meteorological analysis showing accumulation of smoke in Phoenix, (3) visible smoke in camera images and video news coverage; (4) elevated $PM_{2.5}$ concentrations, OC to EC ratios, and $PM_{2.5}$ species, and (5) remote sensing imagery. This combination of evidence indicates that this is an atypical ozone event.

Table 2-4. Summary of identified atypical event June 28 and 29, 2021.

Event Date(s)	Event Ozone Concentration Percentile	Sites Exceeded During Event	Type of Event
June 28-29, 2021	95th - 99th	Fourteen sites: West Phoenix, Mesa, North Phoenix, Falcon Field, Glendale, Central Phoenix, South Scottsdale, South Phoenix, Tempe, Dysart, Buckeye, JLG Supersite, A J Maintenance Yard, Queen Valley	Regional/local transport

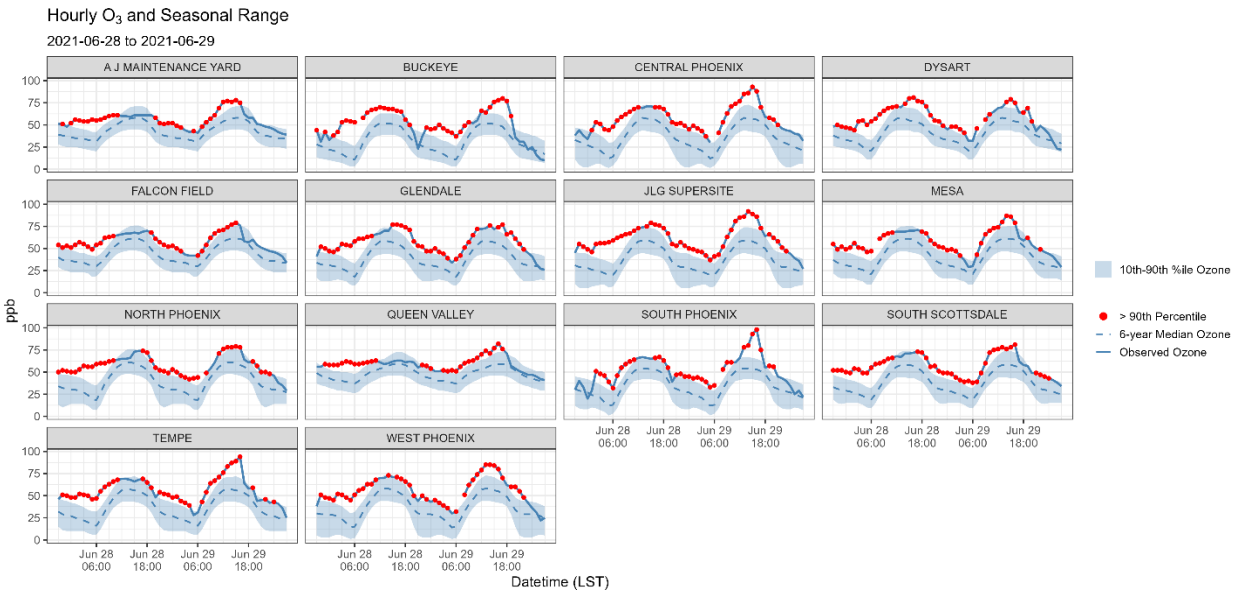

Figure 2-26. Hourly ozone concentrations (ppb) compared to all available data during the ozone season (April 1 – September 31) of the 6-year (2019-2024) period. Hourly means and 10th-90th percentiles are calculated using data on June 28-29, 2021.

2.3.2 Identification of Wildfire(s)

Several large local fires to the north and southeast of Phoenix were active in the days leading up to and during June 28-29, the exclusion days (**Figures 2-27 and 2-28**). The Telegraph Fire to the southeast of Phoenix was first reported on June 4 and expanded to a maximum size of approximately 180,000 acres until it was contained by July 3, four days after the June 28-29 atypical events. The Rafael Fire to the north of Phoenix was first discovered on June 18, 2021, and expanded to approximately 35,000 acres by June 23. The Rafael Fire expanded quickly, and by July 4, 2021, had grown to about 78,000 acres.[4] The Bear and Horton Fires to the east of Phoenix were first reported on June 16, 2021, and reached maximum sizes of approximately 24,000 and 12,000 acres, respectively, based on data from the WFIGS. Another fire – the Johnson Fire – in New Mexico near the Arizona/New Mexico border was also actively burning during the atypical ozone days. The combined smoke plumes from these active burning fires were widespread over the nonattainment area leading up to and during the June 28-29 atypical ozone event.

[4] https://www.weather.gov/fgz/DryLiFire2021

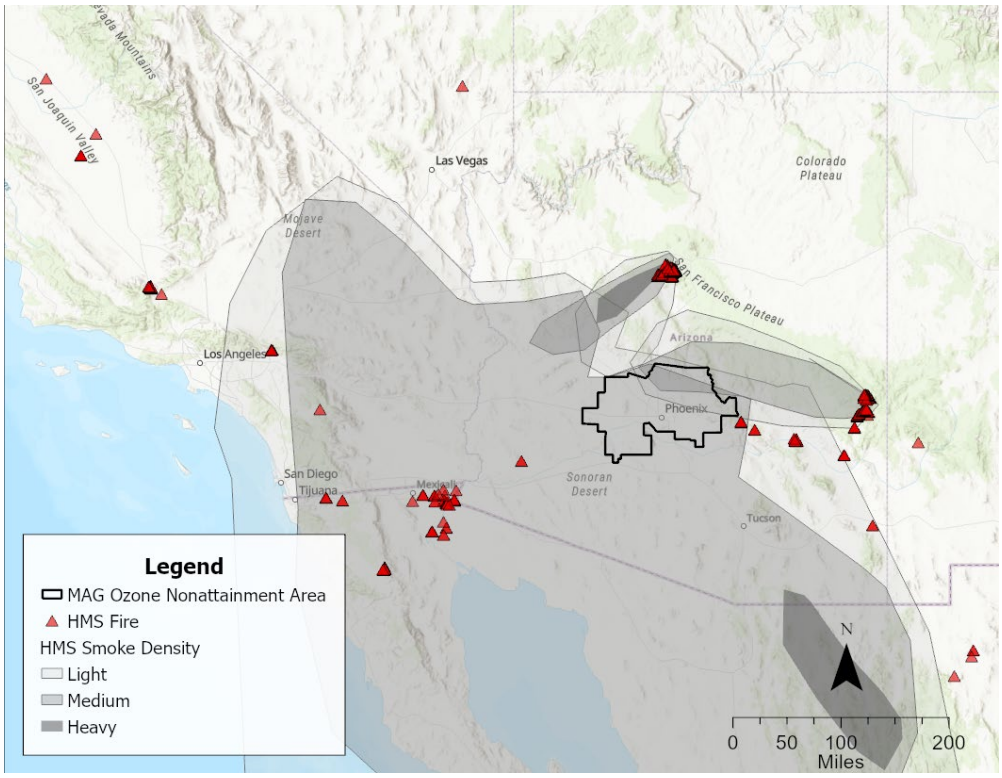

Figure 2-27. Regional view of HMS smoke density and fire locations on June 28, 2021.

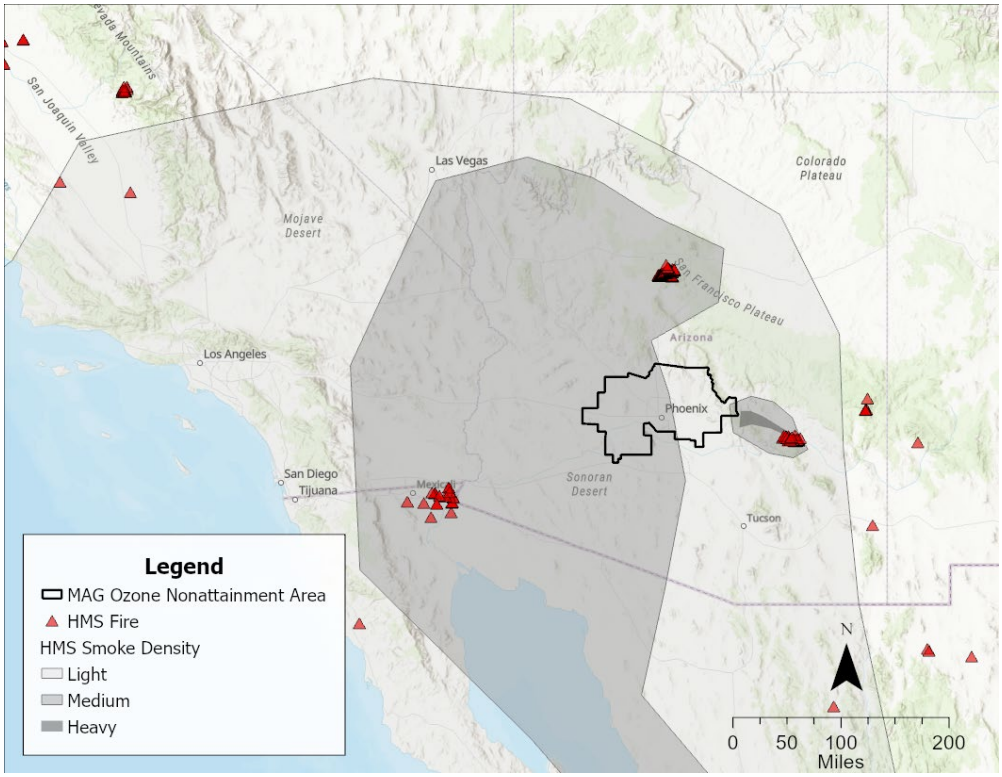

Figure 2-28. Regional view of HMS smoke density and fire locations on June 29, 2021.

2.3.3 Meteorological Analysis

Upper-Level Analysis

The contour plot of average geopotential height at 500 mb (approximately 18,000 feet) from June 28 and 29, 2021 in **Figure 2-29** shows a trough of low pressure (lower heights) east of Arizona, with heights over 5850 meters across Arizona. These heights are slightly below normal for this time of year, indicating slightly cooler-than-normal temperatures aloft aiding atmospheric mixing.

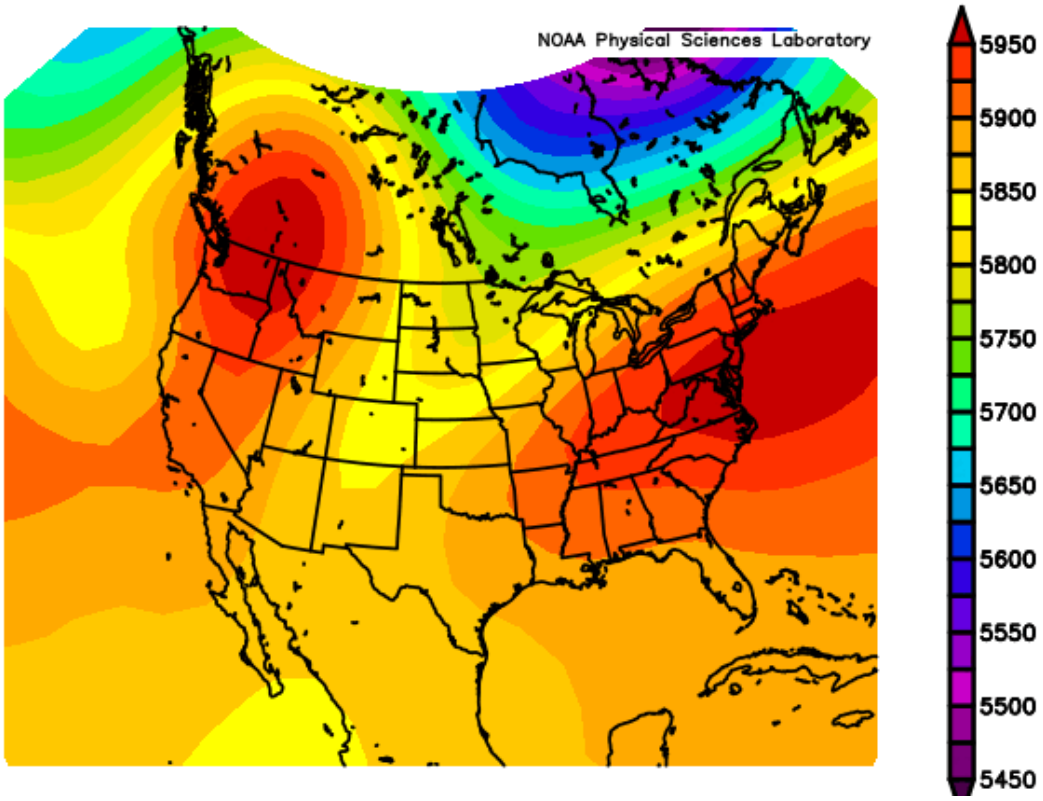

Figure 2-29. Average geopotential height at 500 mb from June 28 and 29, 2021.

Surface Analysis

Figure 2-30 shows a stationary front near Phoenix each afternoon. Converging winds along stationary fronts can lead to cloud and thunderstorm development, enhancing atmospheric mixing. However, that convergence can also lead to pollutant accumulation along the frontal boundary in the absence of rainfall. Meanwhile, with high pressure to the east and a surface low pressure system near Las Vegas, there is a moderate pressure gradient across the nonattainment area, generating easterly winds which aided dispersion.

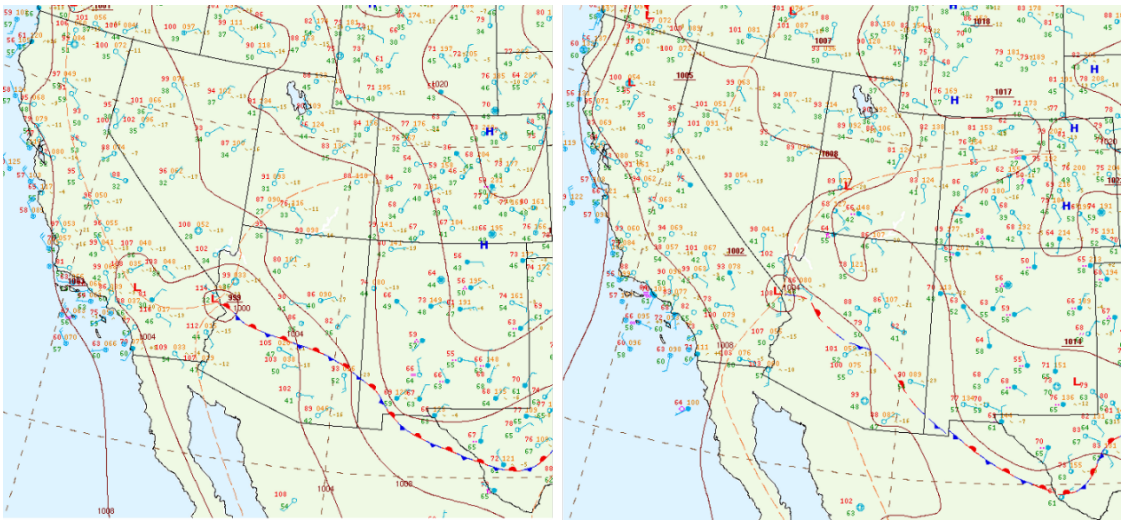

Figure 2-30. Surface analyses from 2 p.m. MST June 28, 2021 (left) and 2 p.m. MST June 29, 2021 (right).

Surface weather observations in **Table 2-5** show that despite the slightly below-normal temperatures aloft, very warm surface temperatures still developed, aiding ozone formation. Meanwhile, easterly winds averaged 10 mph each day, which is slightly stronger than would normally be observed on days with enhanced ozone production.

Table 2-5. Surface weather variables observed at Phoenix Sky Harbor Airport.

Date	High Temp. (F)	Avg. WS (mph)	Avg. WD
6/28/2021	109	10	111
6/29/2021	105	10	101

While moderate easterly winds would normally enhance dispersion and decrease ozone formation in the nonattainment area, with large ongoing fires to the easterly winds carried smoke into south-central Arizona. In the presence of partly sunny skies and warm surface temperatures, this smoke enhanced ozone formation over the region.

Satellite Smoke and Fire Detections

Despite regional cloud development associated with cool aloft temperatures, **Figure 2-31** shows satellites were still able to detect smoke across Arizona on June 28 and 29 as easterly winds carried smoke from large fires in eastern portions of the state into the nonattainment area. A thin haze is discernable on visible satellite imagery each afternoon in **Figures 2-32 and 2-33**. MODIS AIRS

provides evidence of smoke transport over Arizona on June 28 and 29, with 500 mb CO concentrations of up to 115 ppbv over Phoenix (**Figures 2-34 and 2-35**).

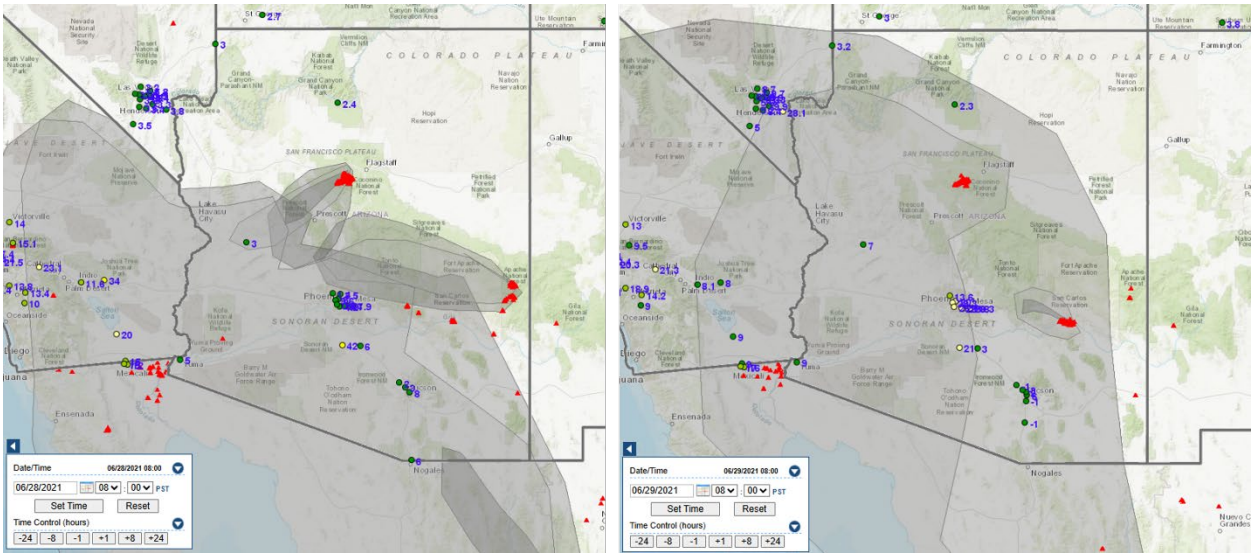

Figure 2-31. HMS fire and smoke along with hourly concentrations of $PM_{2.5}$ at 8:00 a.m. MST June 28, 2021 (left) and 8:00 a.m. MST June 29, 2021 (right).

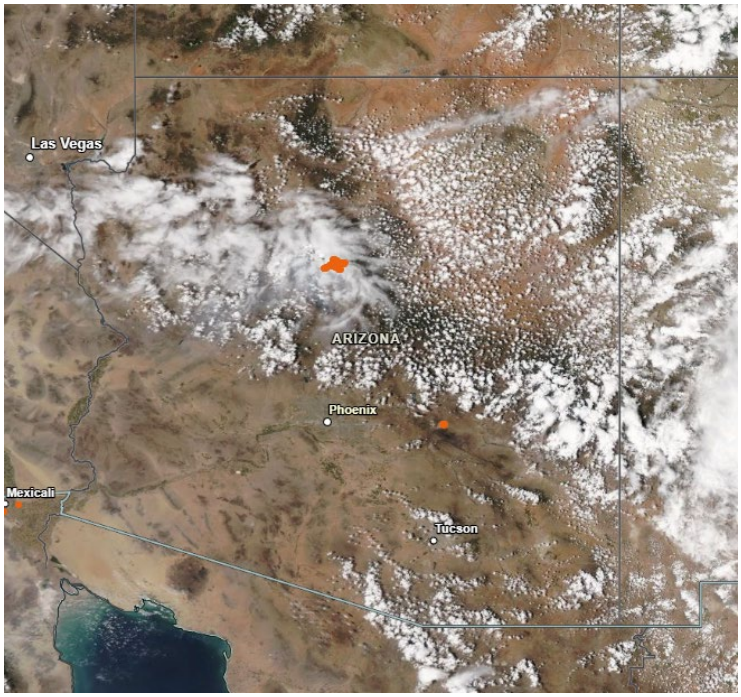

Figure 2-32. Visible satellite imagery from approximately 1:22 p.m. MST on June 28, 2021. Fire detections are indicated by orange dots.

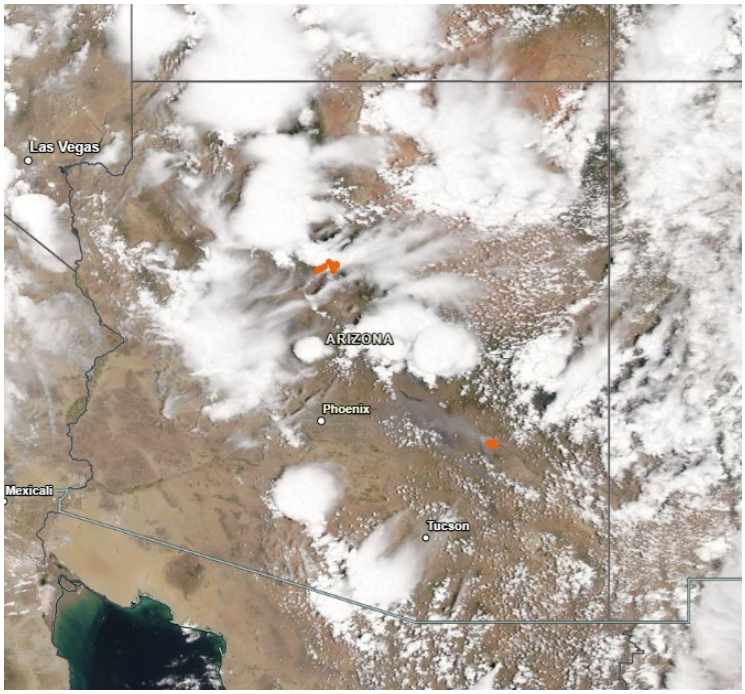

Figure 2-33. Visible satellite imagery from approximately 2:05 p.m. MST on June 29, 2021. Fire detections are indicated by orange dots.

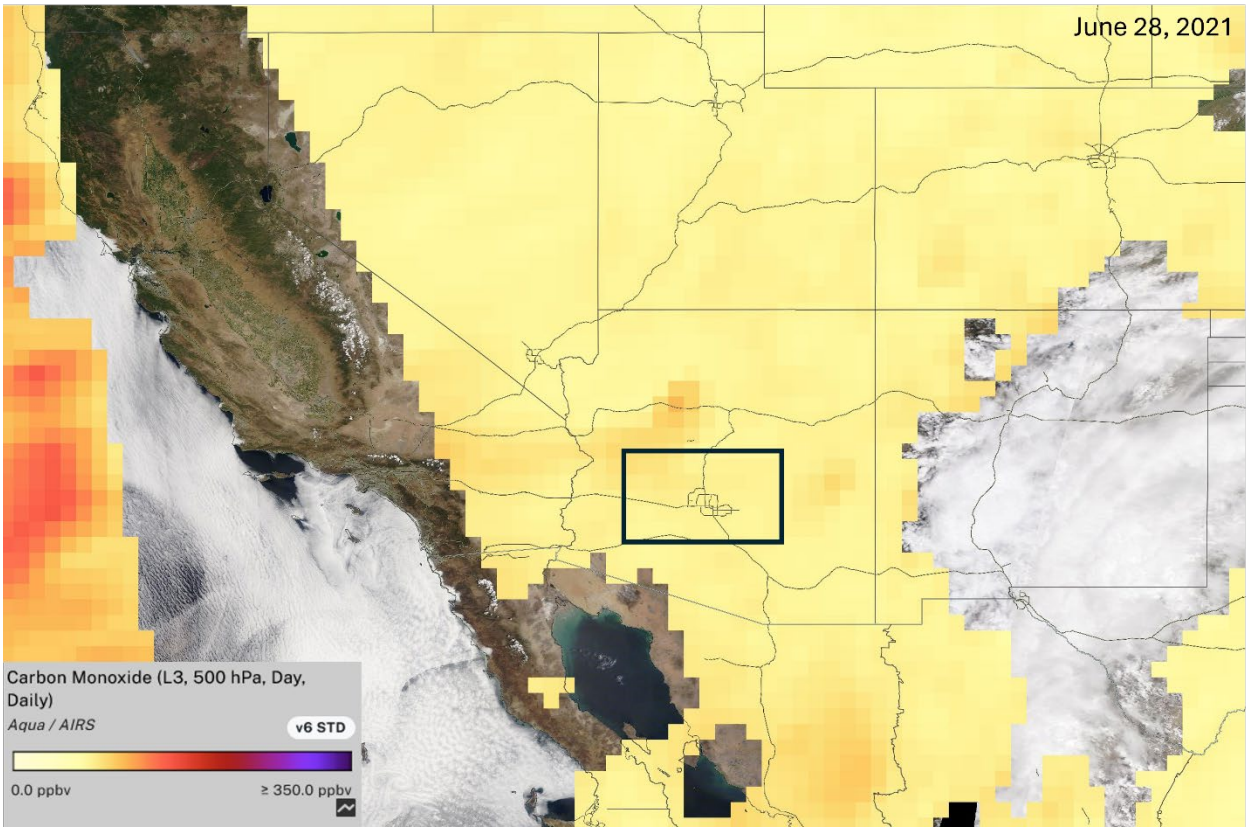

Figure 2-34. A zoomed-in view over the southwestern U.S. of MODIS Aqua AIRS CO retrieval during the atypical ozone date of June 28, 2021. The black box represents the approximate area of the NAA.

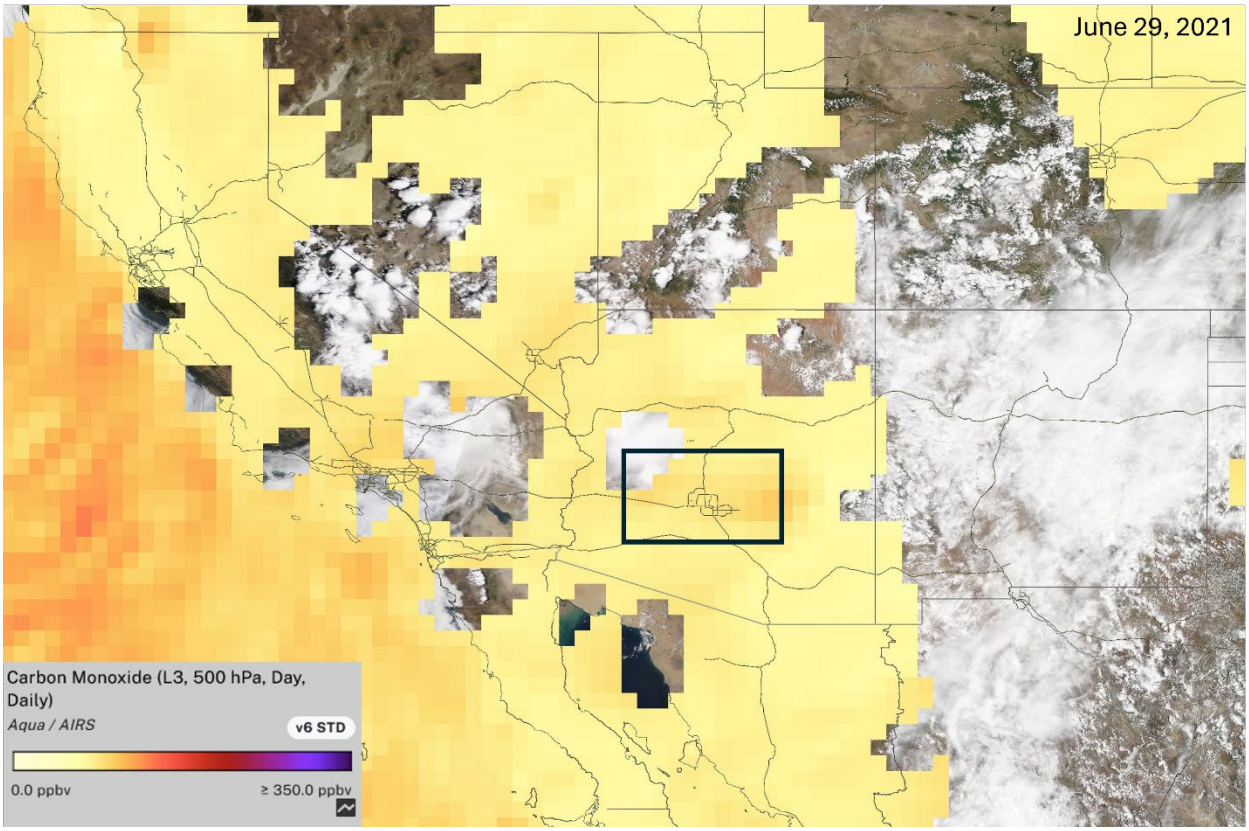

Figure 2-35. A zoomed-in view over the southwestern U.S. of MODIS Aqua AIRS CO retrieval during the atypical ozone date of June 29, 2021. The black box represents the approximate area of the NAA.

Smoke Discussions

NOAA's daily smoke discussions also note the light-to-moderate density smoke from several ongoing wildfire complexes in Arizona.

"**A large region of light to moderate density smoke emitted from the Rafael, Horton, and Bear wildfire complexes in Arizona was observed this evening. Thick density smoke was observed progressing southwest from both fire complexes. Smoke from the wildfires are progressing over most of Arizona**, northwestern Mexico, and southern California." (NOAA NESDIS Text Narrative, June 28, 2021)

"A large region of light to moderate density smoke emitted from the Rafael, Horton, and Bear wildfire complexes in Arizona was observed. Thick density smoke was observed near the fire complexes. Smoke from the wildfires are progressing over most of Arizona, Nevada, southern California, and out over the Pacific Ocean." (NOAA NESDIS Text Narrative, June 29, 2021)

In addition, smoke was reported at Phoenix Sky Harbor Airport by local METAR observations during the evening of June 27, and on the morning of June 29.

Soundings

There are no significant temperature inversions in the left panels in **Figure 2-36** which indicates conditions were not conducive to local pollutant accumulation during the morning hours. However, deep mixing heights each afternoon supported the transport of aloft smoke to the surface, with mixing heights extending up to 550 mb (4.1 km) on June 28 and 600 mb (3.9 km) on June 29.

Easterly winds in the lower portions of the soundings from June 28 and the morning of June 29 give additional evidence of smoke transport in the boundary layer from the east.

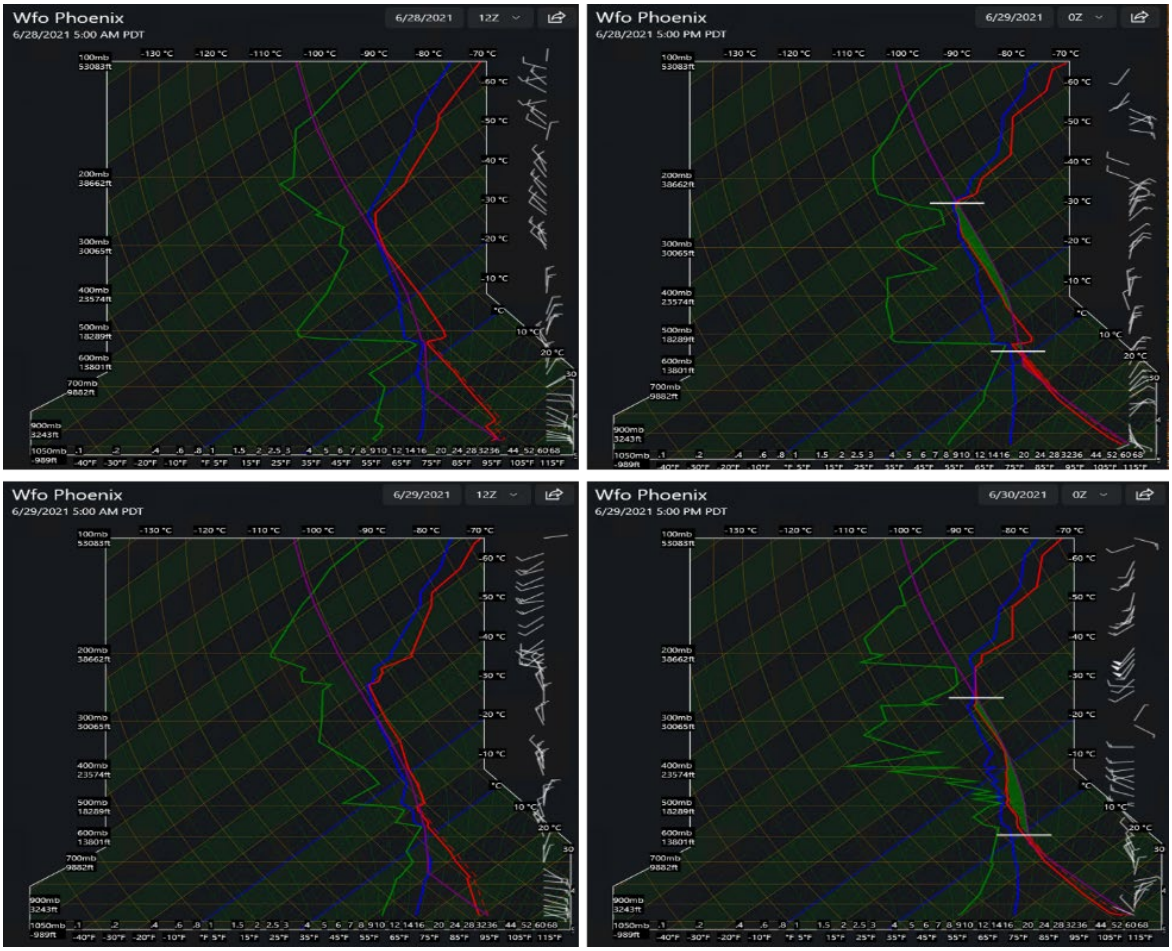

Figure 2-36. Observed atmospheric soundings from 5 a.m. MST (left) and 5 p.m. MST (right) June 28-29, 2021

Smoke Transport

Output from NOAA's HYSPLIT model also shows the potential for the transport of regional smoke into the nonattainment area. The images in **Figure 2-37** show 48-hour back trajectories from 12:00 a.m. to 8:00 p.m. MST between June 28 and June 29 at 100 meters, 1,000 meters, and 2,500 meters above ground level (AGL). These trajectories show that the air mass within the boundary layer originated from areas with medium to heavy smoke aloft being produced by the Rafael, Horton, and Bear wildfire complexes, which led to enhanced ozone production.

Summary

For June 28-29, 2021 a nearby trough of low pressure aloft aided cloud formation and atmospheric mixing over the region, conditions not typically associated with enhanced ozone production. However, the combination of a surface high pressure system to the east and a surface low pressure system near Las Vegas, generated easterly to northeasterly winds across south-central Arizona. These winds transported medium to heavy smoke from several wildfire complexes into the nonattainment area. HYSPLIT back trajectories confirm direct smoke transport from the ongoing fires each day, with smoke also visible over the area on daily satellite imagery. Therefore, in light of the overall meteorological pattern not being overly supportive of ozone development, there is strong evidence that the smoke from the large fires across Arizona combined with triple-digit heat each afternoon to enhance ozone formation.

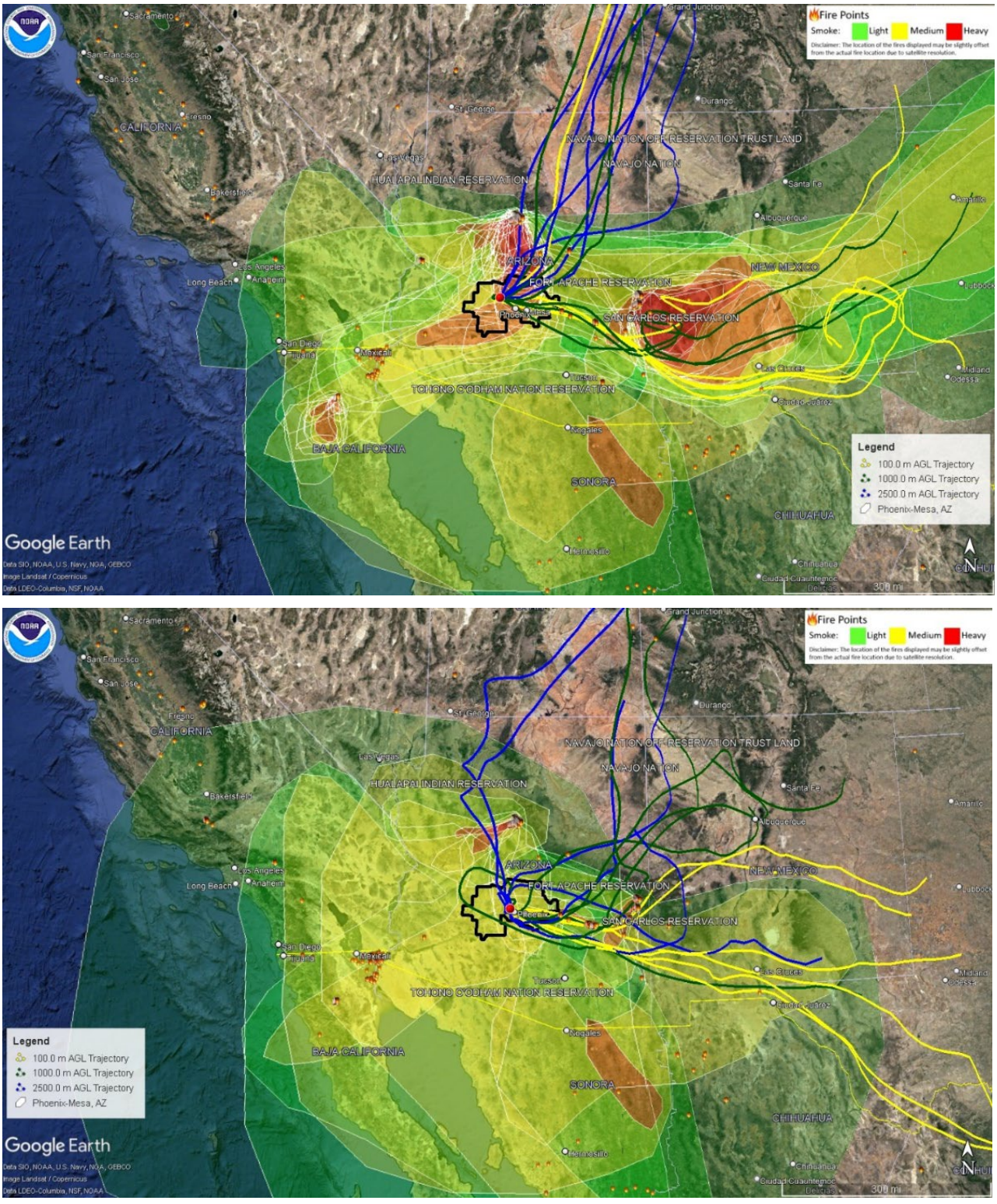

Figure 2-37. NOAA smoke and fire maps and NOAA HYSPLIT trajectory model runs (from Dysart –top, and the JLG Supersite – bottom) with air parcels moving 48-hours before 12:00 am - 8:00 pm MST between June 28 and June 29, 2021 at 100 meters, 1,000 meters, and 2,500 meters (AGL). Analyses performed by MAG.

2.3.4 Surface Impacts

Smoke plumes from the local and regional fires spread over Phoenix in the days leading up to June 28, 2021, and were visible in Phoenix during the morning on June 28. **Figures 2-38 through 2-43** show photos taken from the southwest-facing Estrella Mountain, south-facing South Mountain, and east-facing Superstition Mountain webcams, where the smoke is visible throughout the day on both June 28 and 29. This prominent smoke plume was a news-worthy occurrence reported on by AZ Central; their report, "Smoke from Arizona wildfires makes its way into metro Phoenix sky", provided photos of the growing smoke plume (**https://www.azcentral.com/story/news/local/arizona-wildfires/2021/06/28/phoenix-air-quality-not-severely-impacted-arizona-wildfire-smoke/7789050002/**).

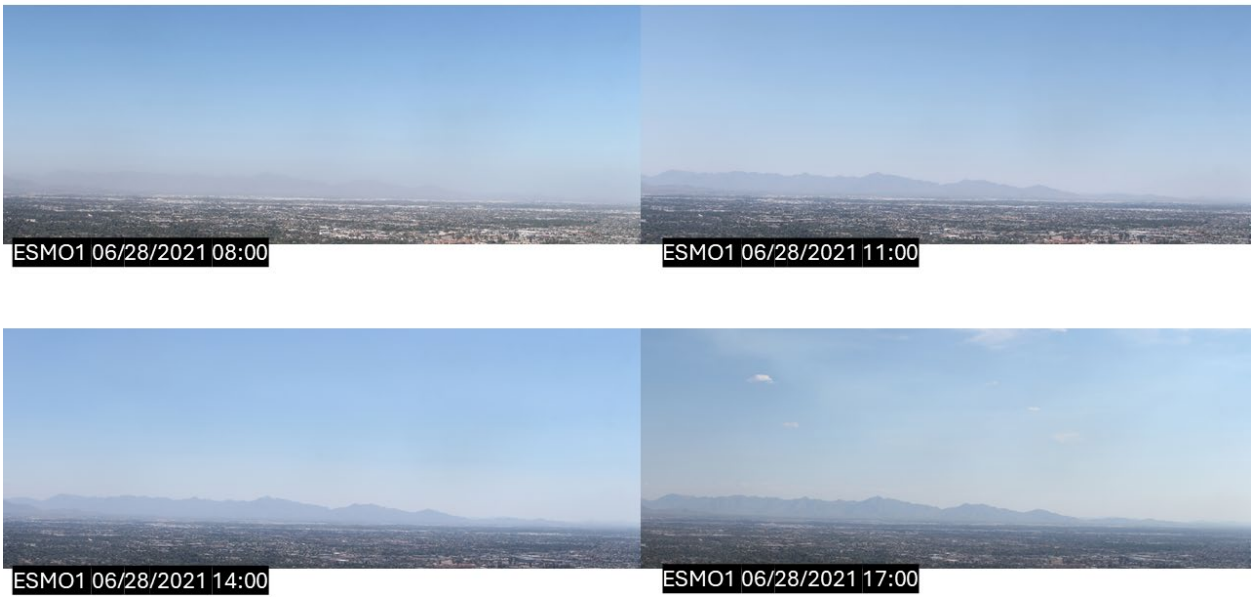

Figure 2-38. Camera Images showing the southwest coordinal direction taken from the Estrella Mountain webcam on June 28 from 8:00 LST, 11:00 LST, 14:00 LST, and 17:00.

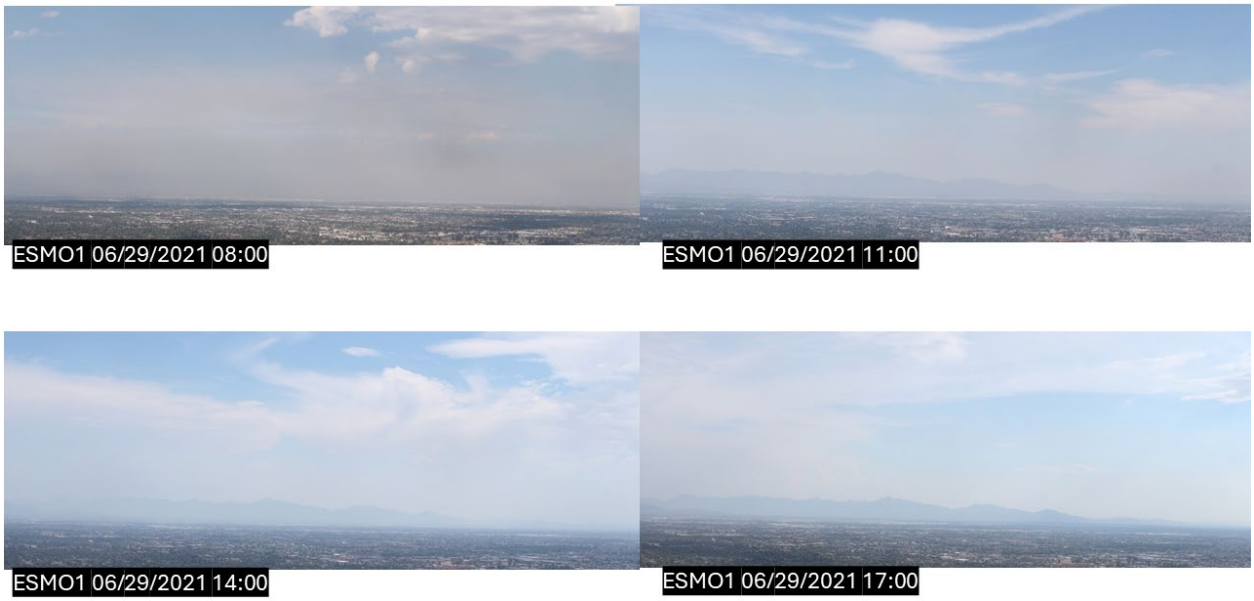

Figure 2-39. Camera Images showing the southwest coordinal direction taken from the Estrella Mountain webcam on June 29 from 8:00 LST, 11:00 LST, 14:00 LST, and 17:00.

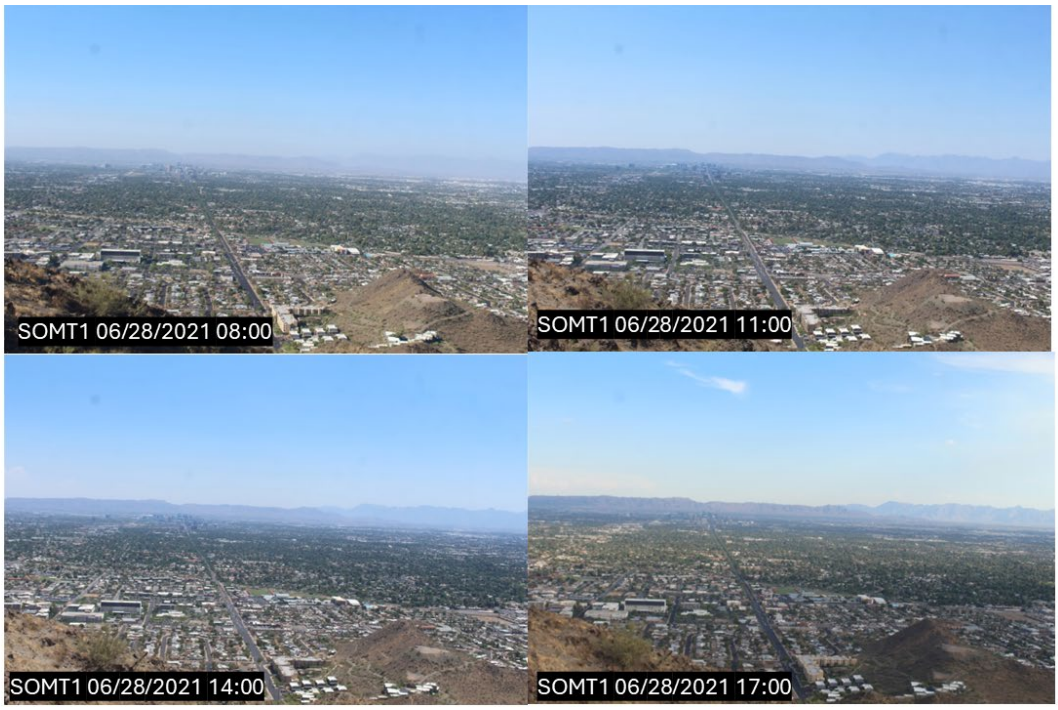

Figure 2-40. Camera Images showing the south coordinal direction taken from the South Mountain webcam on June 29 from 8:00 LST, 11:00 LST, 14:00 LST, and 17:00.

Figure 2-41. Camera Images showing the south coordinal direction taken from the South Mountain webcam on June 29 from 8:00 LST, 11:00 LST, 14:00 LST, and 17:00.

Figure 2-42. Camera Images showing the east coordinal direction taken from the Superstition Mountain webcam on June 28 from 8:00 LST, 11:00 LST, 14:00 LST, and 17:00.

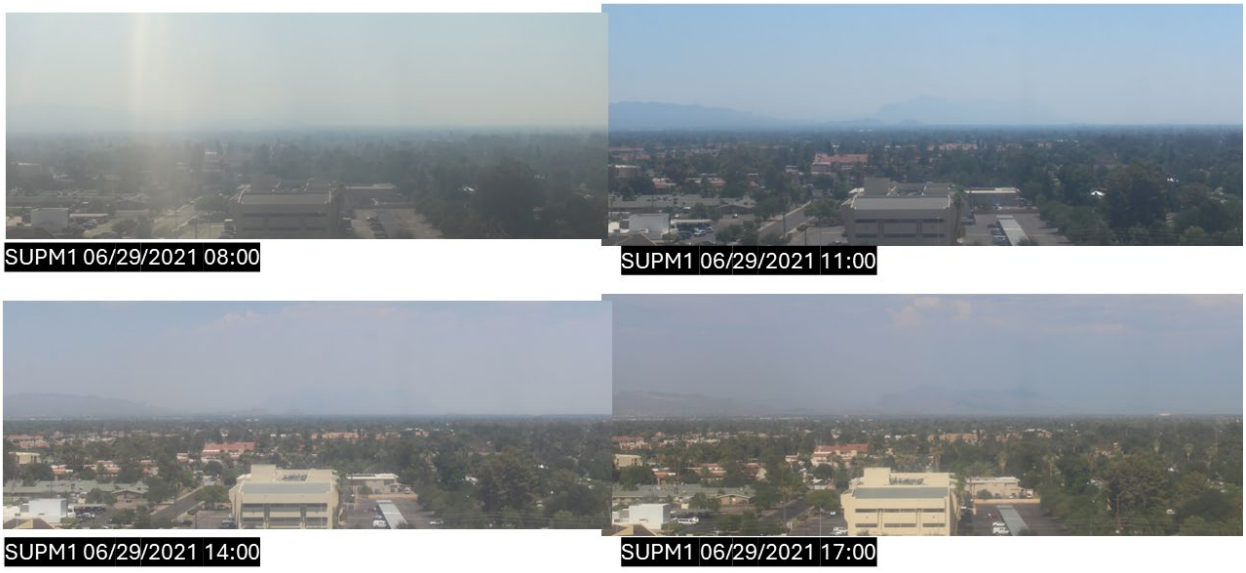

Figure 2-43. Camera Images showing the east coordinal direction taken from the Superstition Mountain webcam on June 29 from 8:00 LST, 11:00 LST, 14:00 LST, and 17:00.

Figure 2-44 shows an overall view of the magnitude of hourly pollutant concentrations measured in the nonattainment area in the two days before and after the June 28-29, 2021, atypical event. Hourly ozone concentrations do not exhibit a typical decrease to below approximately 40 ppb at night on June 28 and in the morning on June 29 that is characteristic of other nights in the time series, indicating overnight transport of ozone and ozone precursors. Furthermore, hourly concentrations of ozone show a widespread and distinct peak on June 29 at all affected sites relative to the days surrounding the atypical event. As noted in Section 2.3, concentrations on July 1, 2021, another atypical ozone event, are also elevated. Similarly, $PM_{2.5}$ concentrations at the exceedance-affected sites rise sharply at all $PM_{2.5}$-measuring sites during the late evening of June 28 into the morning of June 29, coinciding with the higher ozone concentrations during the time when ozone is typically depleted by NO titration. $PM_{2.5}$ concentrations at all sites remain slightly elevated throughout the remainder of the day on June 29. Increased concentrations of $PM_{2.5}$ on June 28-29 are consistent with transport of more particulate matter during the flaming portion of a quickly spreading fire. Higher concentrations of $PM_{2.5}$ was likely not from dust because conditions were not favorable (e.g., wind speeds were generally low) for wind-blown dust before and during the June 28-29 atypical event. Furthermore, there were no dust storm advisories or warnings before or during this atypical event. Distinct and widespread enhancements in surface pollutant concentrations provide evidence that smoke from regional fires entered the region, mixed towards the surface, and had an atypical influence on ozone during the period. The rest of this section examines temporal abnormalities and site-specific trends for each supporting pollutant.

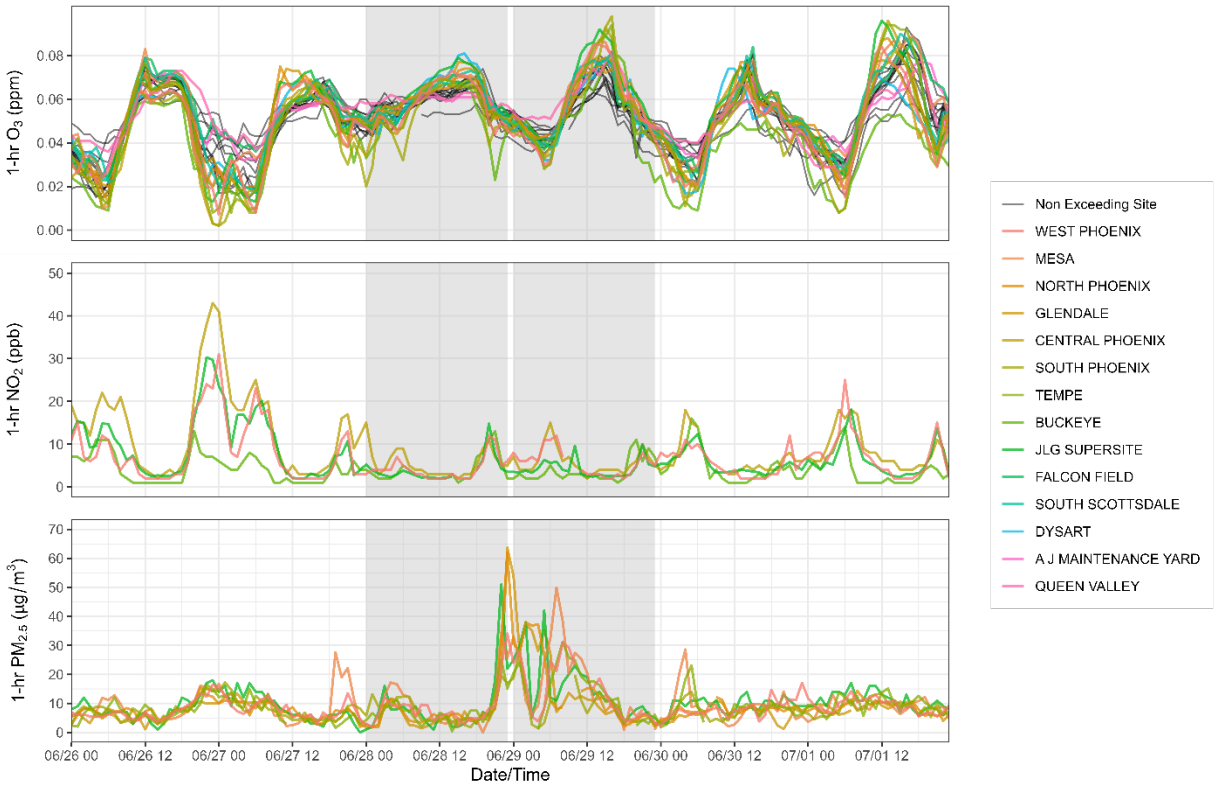

Figure 2-44. Hourly concentrations of ozone, NO_2, and $PM_{2.5}$ at all sites in the nonattainment area. All ozone-exceeding sites are color-coded to highlight smoke impacts on concentrations, and all non-exceeding sites are black. The gray shaded areas represent June 28 and 29, 2021.

$PM_{2.5}$ concentrations were enhanced in the nonattainment area on June 28-29 as emissions from local and regional fires entered the region and mixed towards the surface, which provides further evidence that wildfire smoke was present as an atypical influence on ozone concentrations during the period. **Figure 2-45** shows hourly $PM_{2.5}$ concentrations at the Mesa, North Phoenix, and Glendale sites (three of the affected sites) overlaid on the 5th-95th percentile hourly concentrations during ozone season (April to September), calculated using all available data from 2019-2024. $PM_{2.5}$ concentrations rose sharply to a peak concentration of between approximately 50 and 60 µg/m^3 at the sites as smoke moved into the area, reaching concentrations that exceed the 95th percentile average concentration between around 22:00 LST and midnight on June 28 and 6:00 LST on June 29. Concentrations at the North Phoenix and Glendale sites fall to approximately normal levels by the evening of June 29. $PM_{2.5}$ concentrations at five other affected sites exceeded the 95th percentile on June 28-29, 2021.

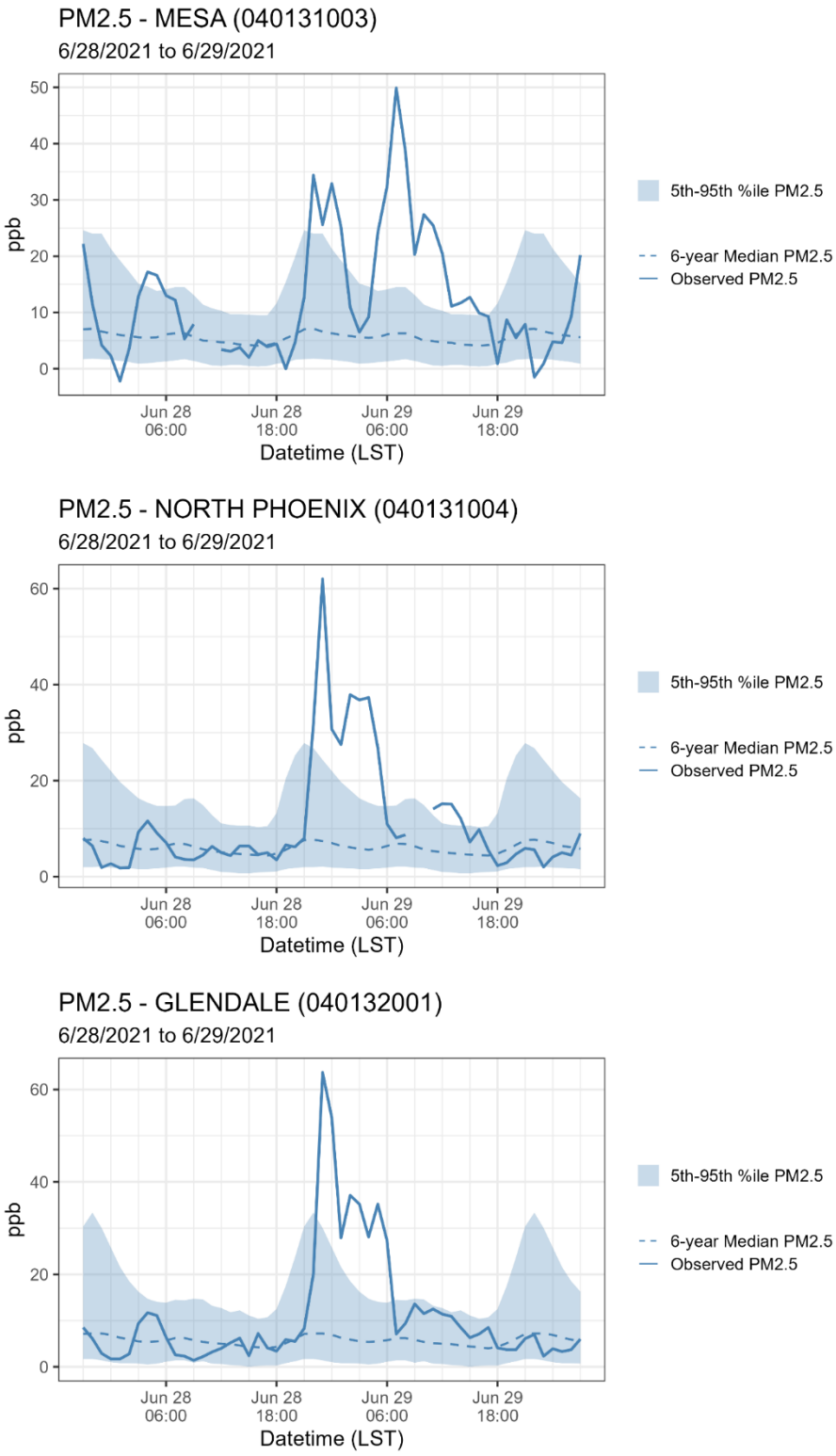

Figure 2-45. Hourly concentrations of $PM_{2.5}$ at the Mesa (top), North Phoenix (middle), and Glendale (bottom) sites. The 6-year (2019-2024) median is represented by the dashed line, and the 5th-95th percentile is represented by the shaded area.

OC, EC, and speciated data were not available on June 28-29, but samples collected before and after that date show evidence of smoke impacts. The ratio of OC to EC taken at the JLG Supersite monitor was also examined for evidence that wildfire smoke entered the nonattainment area. Increases in this ratio are indicative of wildfire smoke. **Figure 2-46** shows boxplots of OC to EC ratios for available data collected during the ozone season between 2019-2024. While speciated data were not available on June 28-29, the OC to EC ratio on June 27 and 30, one day before and after the atypical event, respectively, was above the 75th percentile compared to all data. Higher concentrations of $PM_{2.5}$ species, particularly potassium, are also indicative of wildfire smoke. **Figure 2-47** shows boxplots of speciated $PM_{2.5}$ concentrations collected at the JLG Supersite monitor during the ozone season between 2019-2024. Nearly all $PM_{2.5}$ observations collected on June 27 and 30 are elevated at least above the median, with some observations above the 75th percentile. Elevated concentrations of aluminum, calcium, iron, and silicon are indicative of dust, but potassium concentrations on June 27 and 30 are also elevated, which indicates the presence of smoke. These observations provide further evidence that ground-level wildfire smoke entered Phoenix in the days before and after – and very likely during - the June 28-29, 2021, atypical ozone event.

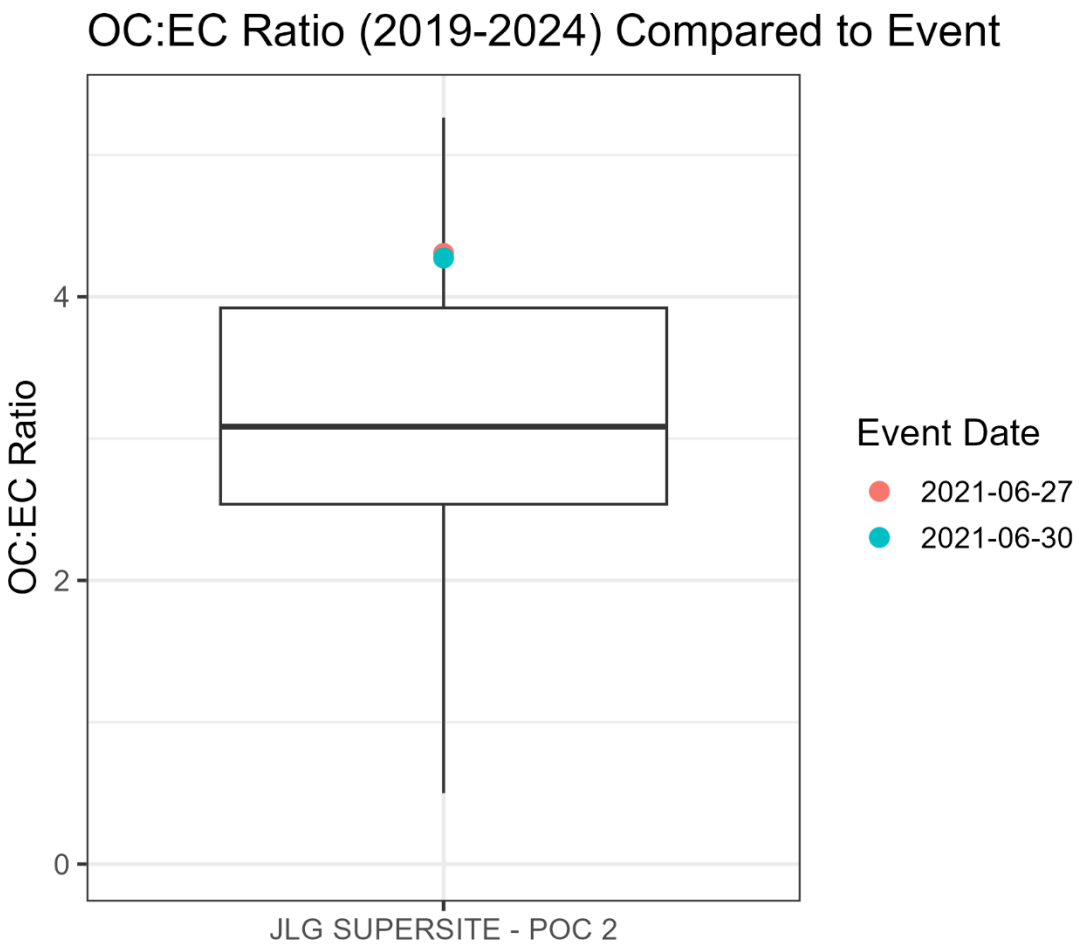

Figure 2-46. Boxplot of OC to EC ratios at the JLG Supersite site using data collected during the ozone season (April-September) from 2019-2024. OC to EC ratios are calculated at POC 2 (x-axis). Available OC to EC ratios collected during the day before and after the June 28-29 atypical ozone event are shown as points.

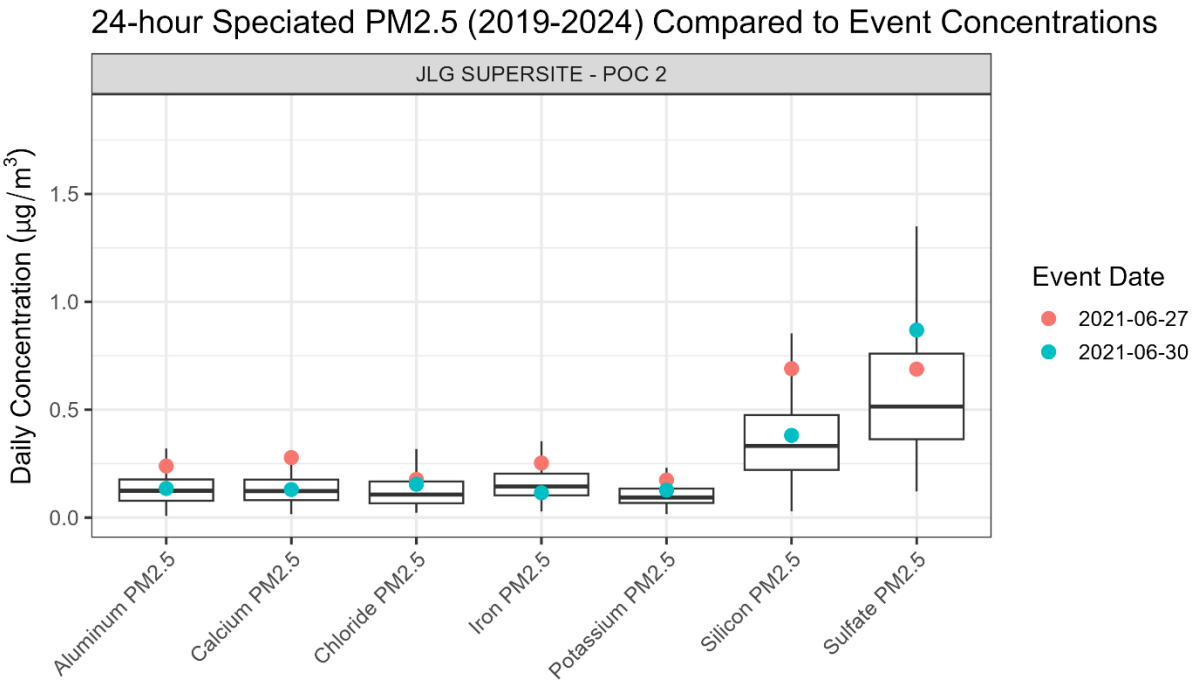

Figure 2-47. Boxplots of speciated $PM_{2.5}$ collected at the JLG Supersite site collected during the ozone season (April-September) from 2019-2024. Available speciated $PM_{2.5}$ concentrations collected during the day before and after the June 28-29 atypical event are shown as points.

2.3.5 Event Statistics

Table 2-6 summarizes the measurements of ozone concentrations on June 28-29, 2021, as well as the percentile rank of the observation compared to six years of ozone season data (April 1-September 31, 2019-2024). Ozone MDA8 measurements ranged from the 95th - 99th percentile on June 28-29, 2021.

Table 2-6. Percentile of ozone measurements on the atypical dates compared with six years of ozone data (2019-2024). The percentile rank is calculated across the ozone production season in the nonattainment area (April 1-September 31) of 2019-2024.

Date	Site Name	Site Code	Ozone MDA8 (ppb)	Percentile Rank
6/28/2021	Glendale	040132001	72	95
	JLG Supersite	040139997	74	97
	Dysart	040134010	75	97
6/29/2021	Buckeye	040134011	71	95
	A J Maintenance Yard	040213001	71	95
	Falcon Field	040131010	72	95
	Glendale	040132001	72	95
	North Phoenix	040131004	73	96
	Queen Valley	040218001	73	96
	South Scottsdale	040133003	74	97
	Mesa	040131003	76	98
	South Phoenix	040134003	76	98
	West Phoenix	040130019	78	99
	Tempe	040134005	78	99
	Central Phoenix	040133002	80	99
	JLG Supersite	040139997	82	99

2.3.6 Conclusion

The concurrence of HMS smoke perimeters over the nonattainment area, HYSPLIT trajectories and meteorological analysis showing accumulation of smoke in the nonattainment area, visible smoke in camera images and video news coverage, elevated hourly $PM_{2.5}$ concentrations, OC to EC ratios and potassium $PM_{2.5}$, and remote sensing imagery, provide evidence that surface-level smoke was present during the period. Regional transport of smoke from large fires in Arizona and New Mexico on June 28-29, enhanced ozone concentrations outside of the typical diurnal profile, keeping ozone values high and affecting the MDA8 ozone concentrations at fourteen sites. Multiple analyses showed that smoke fully encompassed the Maricopa Nonattainment Area on June 28-29, 2021, and statistics show ozone concentrations were atypical during this event.

This combined evidence indicates that the Telegraph Fire along with smoke plumes generated by numerous regional fires provided an atypical source of ozone and ozone precursors that caused

enhanced ozone concentrations on June 28 and 29, 2021. Removal of these days as atypical events is supported by this analysis.

2.4 July 1, 2021

2.4.1 Event Overview: July 1, 2021

The unrepresentative (atypical) ozone event took place on July 1, 2021, and affected eighteen sites in the Maricopa Nonattainment Area: West Phoenix, Mesa, North Phoenix, Falcon Field, Glendale, Pinnacle Peak, Central Phoenix, South Scottsdale, South Phoenix, West Chandler, Tempe, Senior Center Air Monitoring Station, Red Mountain Air Monitoring Station, Lehi Air Monitoring Station, High School Air Monitoring Station, Fountain Hills, JLG Supersite, and A J Maintenance Yard (**Table 2-7**). MDA8 ozone concentrations at the affected sites ranged from 71-86 ppb.

Time series graphs showing hourly ozone concentrations that exceeded the seasonal means (calculated using all available data from April 1 – September 31, 2019-2024) and 10th-90th percentiles at each site are shown in **Figure 2-48.** For example, on July 1, hourly ozone measurements North Phoenix was above the 90th percentile during the late morning hours. Measurements increased throughout the day and continued to exceed the 90th percentile at most sites, with some sites recording ozone concentrations of nearly 100 ppb, indicating transport of ozone and ozone precursors from wildfires.

Major wildfires burning in Arizona, notably the Telegraph Fire in southeastern Arizona, the Rafael Fire north of Phoenix, and the Bear and Horton Fires in eastern Arizona, were identified as major contributors to this event. Evidence includes (1) HMS smoke perimeters over the nonattainment area, (2) HYSPLIT trajectories and meteorological analysis showing accumulation of smoke in Phoenix, (3) visible smoke in camera images and news coverage, and (4) elevated $PM_{2.5}$ concentrations, OC to EC ratios, and $PM_{2.5}$ species. This combination of evidence indicates that this is an atypical ozone event.

Table 2-7. Summary of identified atypical July 1, 2021.

Event Date(s)	Event Ozone Concentration Percentile	Sites Exceeded During Event	Type of Event
July 1, 2021	93rd - 100th	Eighteen sites: West Phoenix, Mesa, North Phoenix, Falcon Field, Glendale, Pinnacle Peak, Central Phoenix, South Scottsdale, South Phoenix, West Chandler, Tempe, Senior Center Air Monitoring Station, Red Mountain Air Monitoring Station, Lehi Air Monitoring Station, High School Air Monitoring Station, Fountain Hills, JLG Supersite, A J Maintenance Yard	Regional/local transport

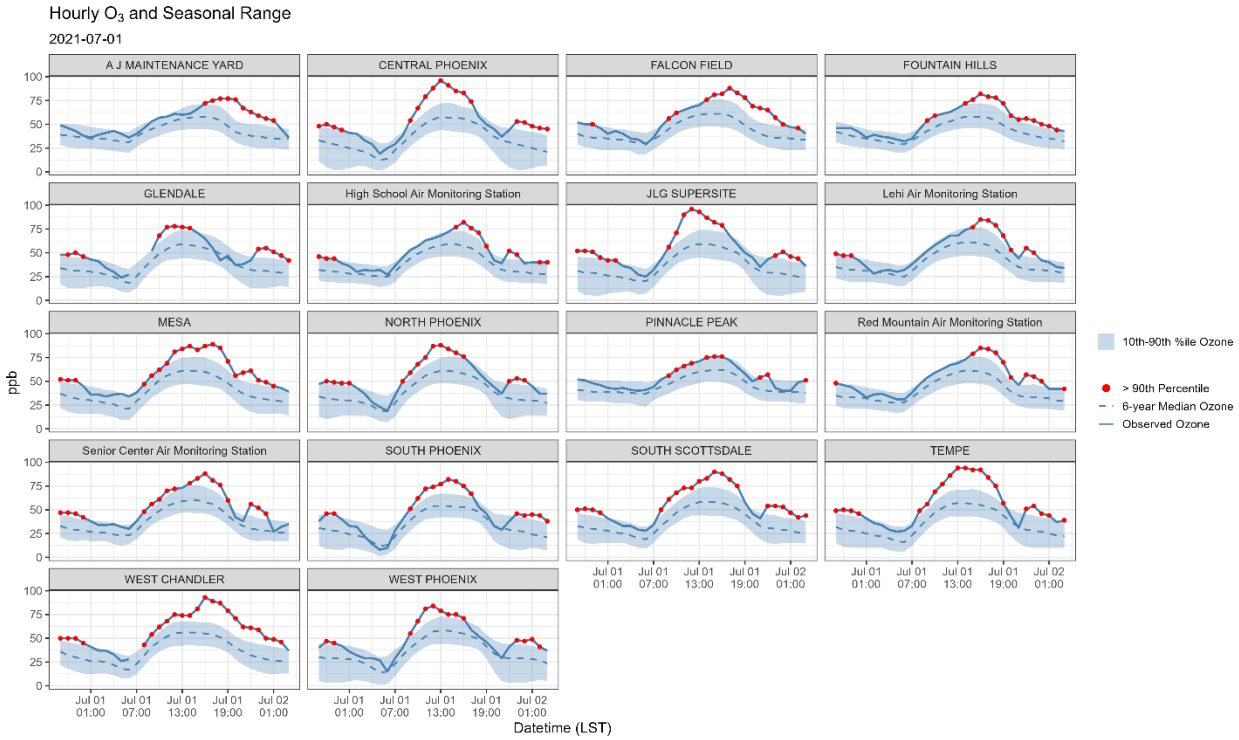

Figure 2-48. Hourly ozone concentrations (ppb) compared to all available data during the ozone season (April 1 – September 31) of the 6-year (2019-2024) period. Hourly means and 10th-90th percentiles are calculated using data on July 1, 2021.

2.4.2 Identification of Wildfire(s)

Several large local fires to the north and southeast of Phoenix were active in the days leading up to and during July 1, the exclusion day (**Figure 2-49 and 2-50**). The Telegraph Fire to the southeast of

Phoenix was first reported on June 4 and expanded to a maximum size of approximately 180,000 acres until it was contained by July 3, two days after the July 1 atypical event. The Rafael Fire to the north of Phoenix was first discovered on June 18, 2021, and expanded to approximately 35,000 acres by June 23. The Rafael Fire expanded quickly, and by July 4, 2021, had grown to about 78,000 acres.[5] The Bear and Horton Fires to the east of Phoenix were first reported on June 16, 2021, and reached maximum sizes of approximately 24,000 and 12,000 acres, respectively, based on data from the WFIGS. The Bear and Horton Fires were contained by September 8, 2021, and July 13, 2021, respectively. The combined smoke plumes from these active burning fires were widespread over the nonattainment area before and during the July 1 atypical ozone event. It should be noted that cloud cover obscured fire and smoke detections from many fires burning in the southwestern U.S. in the days leading up to and on July 1.

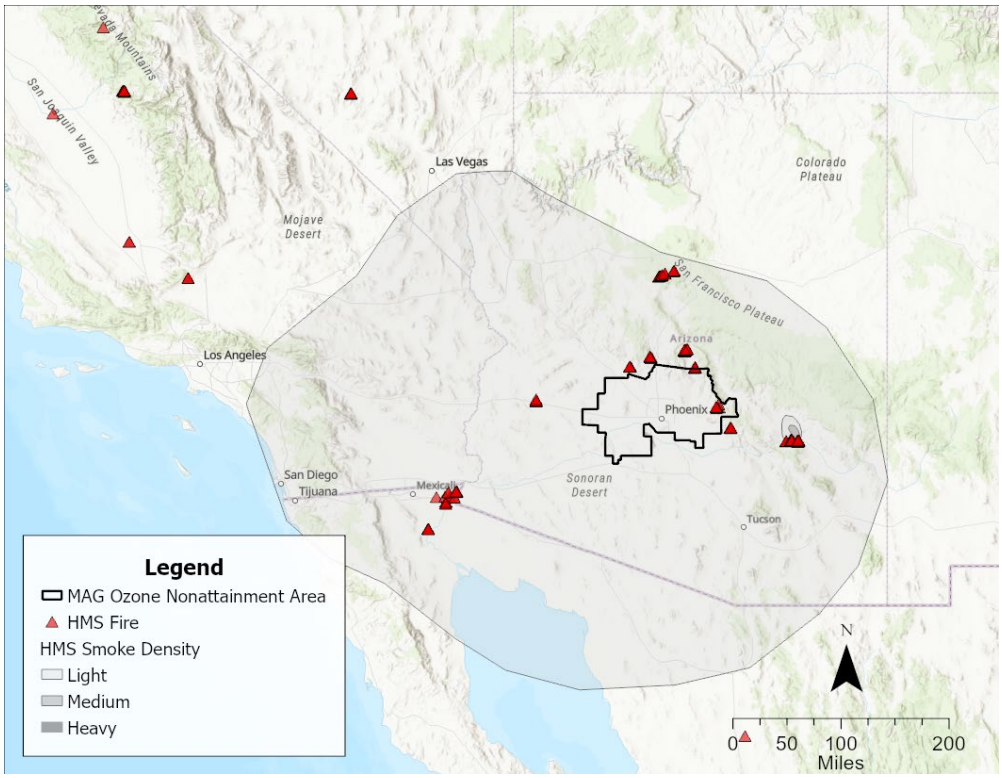

Figure 2-49. Regional view of HMS smoke density and fire locations on June 30, 2021.

[5] https://www.weather.gov/fgz/DryLiFire2021

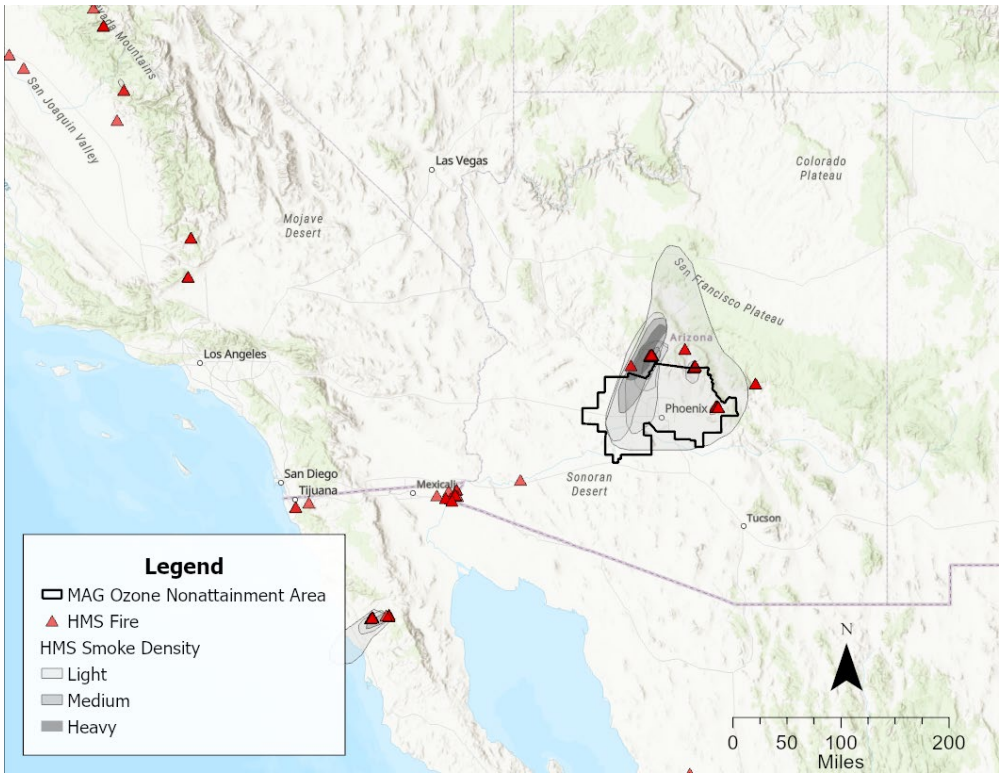

Figure 2-50. Regional view of HMS smoke density and fire locations on July 1, 2021.

2.4.3 Meteorological Analysis

Upper-level Analysis

The contour plot of average geopotential height at 500 mb (approximately 18,000 feet) from July 1, 2021, in **Figure 2-51** shows a broad ridge of high pressure across the western United States. The orange colors over Arizona indicate 500 mb heights over 5850 meters, which is normal for this time of year. However, the presence of the ridge aloft likely contributed to mostly sunny and hot conditions over Phoenix, aiding ozone formation on this day.

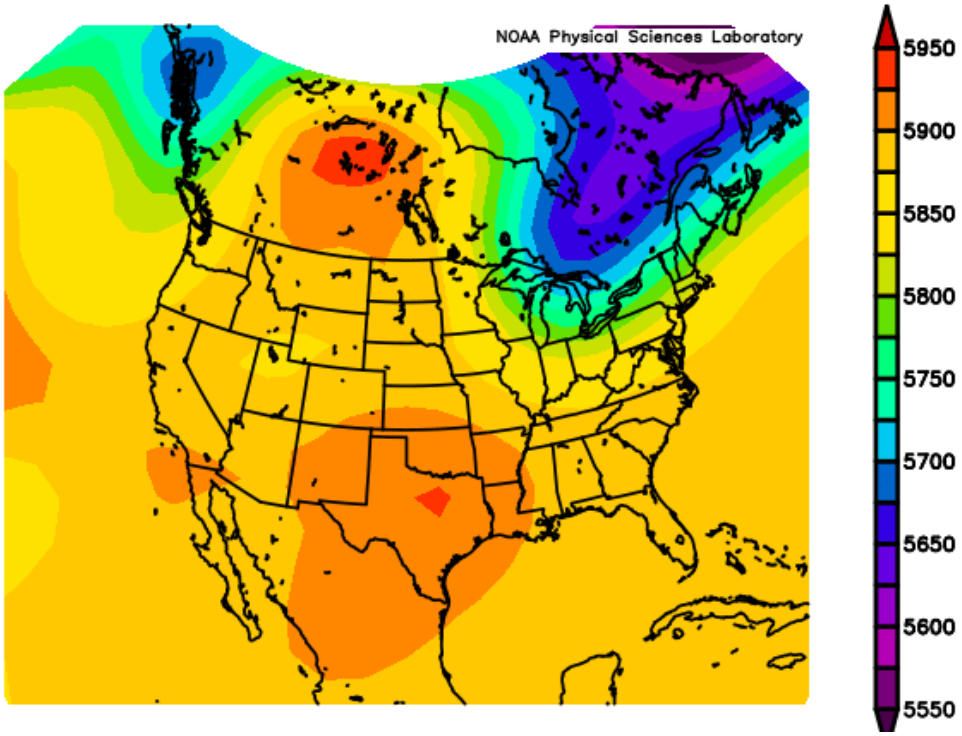

Figure 2-51. Average geopotential height at 500 mb on July 1, 2021.

Surface Analysis

Figure 2-52 shows a weak surface low-pressure system west of Phoenix on the afternoon of July 1 as hot temperatures generated rising thermals over the Desert Southwest. A weak pressure gradient over the region also indicates the potential for light winds.

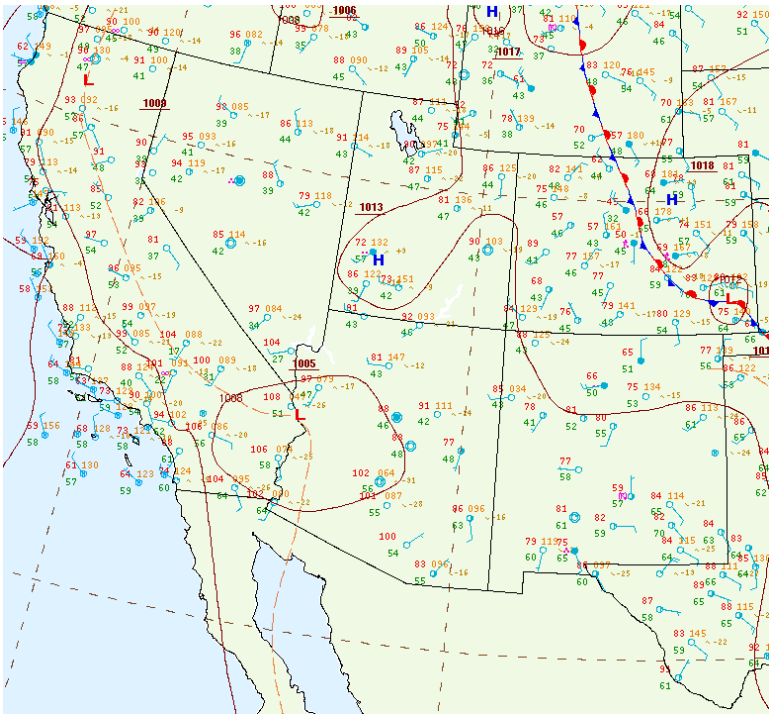

Figure 2-52. Surface analysis from 2 p.m. MST July 1, 2021.

Table 2-8 confirms that the ridging aloft was associated with hot surface temperatures that aided ozone development. In addition, the weak pressure gradient generated average wind speeds of only 6 mph, limiting dispersion in the nonattainment area.

Table 2-8. Surface weather variables observed at Phoenix Sky Harbor Airport.

Date	High Temp. (F)	Avg. WS (mph)	Avg. WD
7/1/2021	107	6	95

Satellite Smoke and Fire Detections

Figure 2-53 shows satellites detected medium to heavy smoke over the nonattainment area on July 1 as multiple large fires burned across central Arizona, contributing to increased levels of particles and ozone precursors.

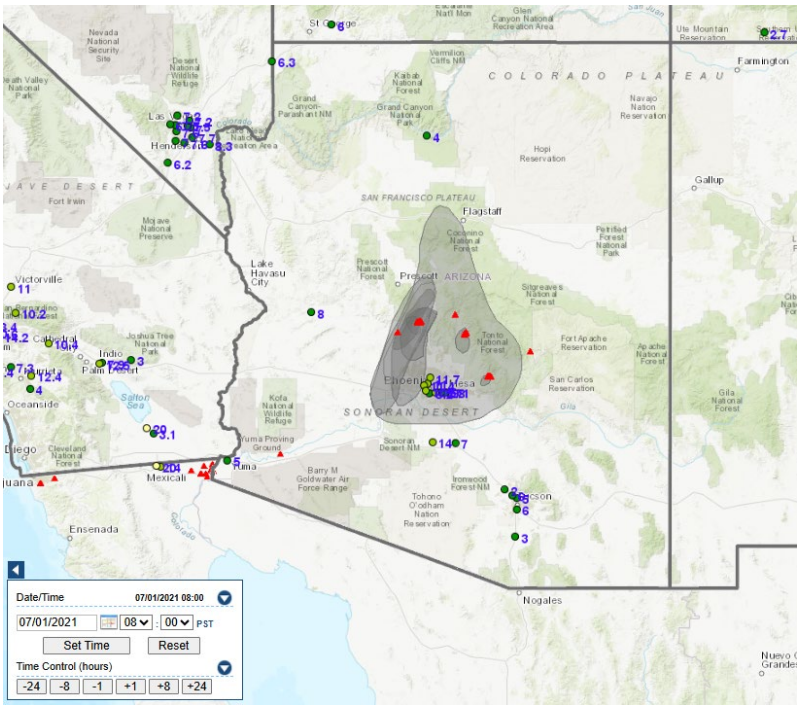

Figure 2-53. HMS fire and smoke detections along with hourly $PM_{2.5}$ concentrations at 8:00 a.m. MST July 1, 2021.

The smoke is hard to discern on visible satellite imagery in **Figure 2-54** from the afternoon of July 1 due to a high solar angle when the image was captured.

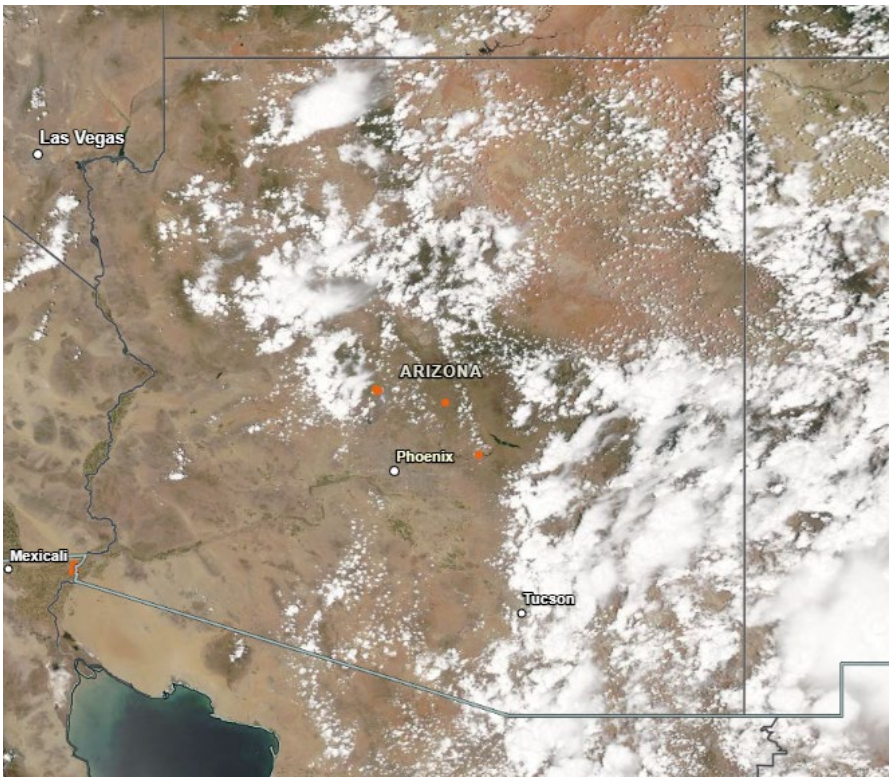

Figure 2-54. Visible satellite imagery from approximately 1:53 p.m. MST on July 1, 2021. Fire detections are indicated by orange dots.

Smoke Discussions

NOAA's daily smoke discussion noted the light-to-moderate density smoke across southern Arizona the prior evening.

"**Light to moderate density smoke was observed from recent wildfires over parts of southern Arizona**, however cloud cover from a weather system over the region has made smoke analysis difficult in the region this evening." (NOAA NESDIS Text Narrative, June 30, 2021)

Soundings

The left panel in **Figure 2-55** shows a weak temperature inversion confining local pollutants near the surface. However, mixing improved during the afternoon due to hot surface temperatures (right panel on Figure 2-55) with mixing heights extending to 700 mb (2.6 km) during the afternoon of July 1. With smoke directly over Phoenix, these mixing heights were sufficient to allow the aloft smoke to mix to the surface and enhance ozone formation.

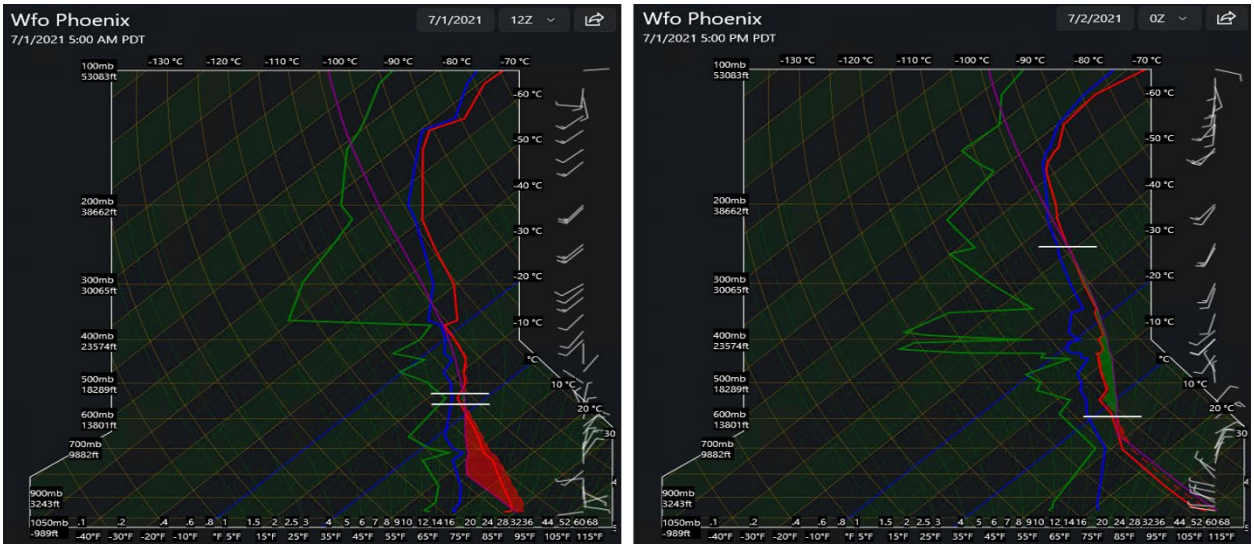

Figure 2-55. Observed atmospheric soundings from 5 a.m. MST (left) and 5 p.m. MST (right) July 1, 2021.

Smoke Transport

In addition to the smoke from nearby fires, smoke from more distant fires also potentially contributed to ozone development across Arizona on July 1. The 48-hour back trajectories from 12:00 a.m. to 8:00 p.m. MST on July 1 at 100 meters, 1,000 meters, and 2,500 meters above ground level (AGL) calculated by NOAA's HYSPLIT model originated from areas impacted by light-to-medium density regional smoke (**Figure 2-56**).

Summary

For July 1, 2021 a broad ridge of high pressure aloft produced partly sunny and hot conditions over the Phoenix area. As fires to the north and east of Phoenix produced smoke over the region, the hot and dry conditions promoted deep atmospheric mixing, allowing the aloft smoke to mix to the surface. HYSPLIT back trajectories confirm direct smoke transport from the nearby fires, while light winds at the surface allowed the smoke to linger. These conditions provide evidence that regional smoke combined with triple-digit heat to enhance ozone formation.

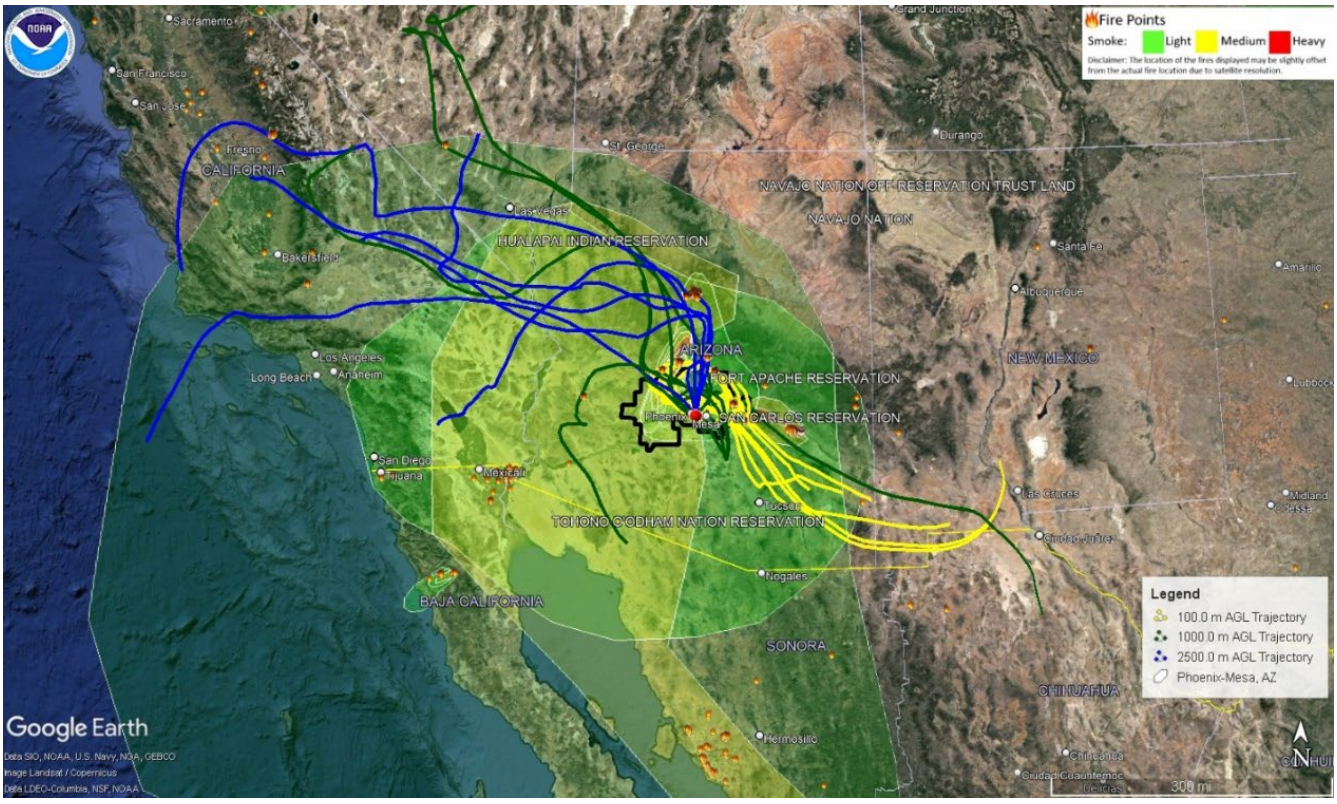

Figure 2-56. NOAA smoke and fire maps and NOAA HYSPLIT trajectory model runs from the Tempe ozone monitor, with air parcels moving 48-hours before 12:00 am - 8:00 pm MST on July 1, 2021 at 100 meters, 1,000 meters, and 2,500 meters (AGL). Analysis performed by MAG.

2.4.4 Surface Impacts

Smoke plumes from the local and regional fires spread over the nonattainment area in the days leading up to July 1, 2021, and were visible in Phoenix during the morning on July 1. **Figures 2-57 to 2-60** show photos taken from the southwest-facing Estrella Mountain, south-facing South Mountain, east-facing Superstition Mountain, and west-northwest-facing White Tank Mountain webcams, where the smoke is visible throughout the day on July 1. Smoke from the Tiger Fire on July 1, 2021, was noted by local meteorologists Matt Pace (**Figure 2-61**) and Sean McLaughlin (**Figure 2-62**).

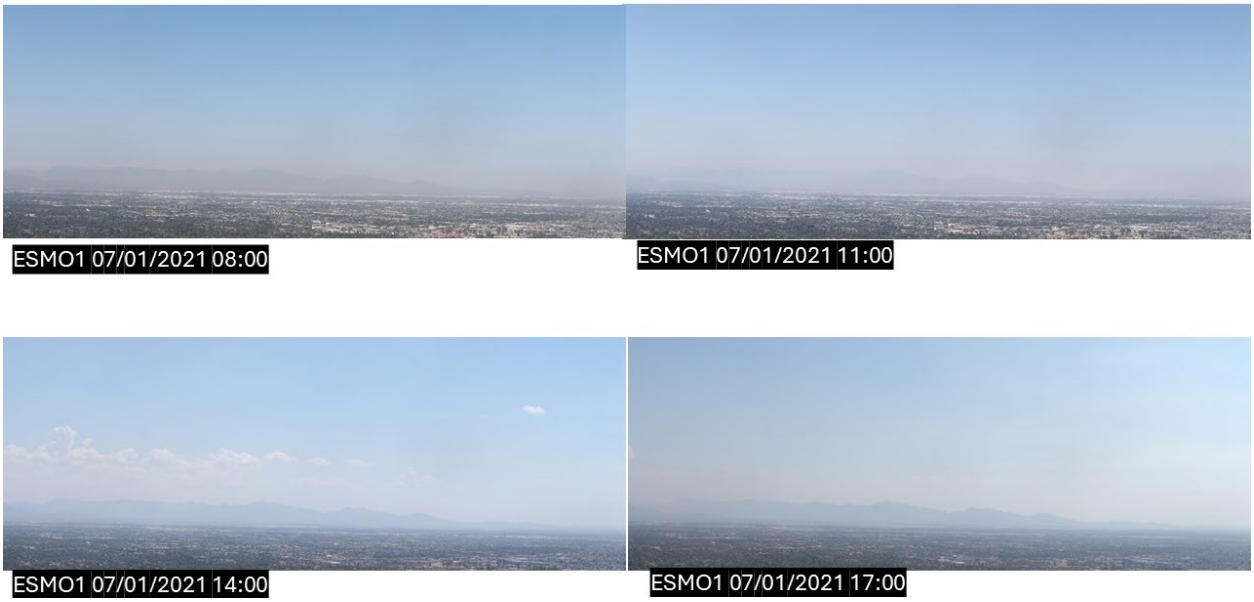

Figure 2-57. Camera Images showing the southwest coordinal direction taken from the Estrella Mountain webcam on July 1 from 8:00 LST, 11:00 LST, 14:00 LST, and 17:00.

Figure 2-58. Camera Images showing the south coordinal direction taken from the South Mountain webcam on July 1 from 8:00 LST, 11:00 LST, 14:00 LST, and 17:00.

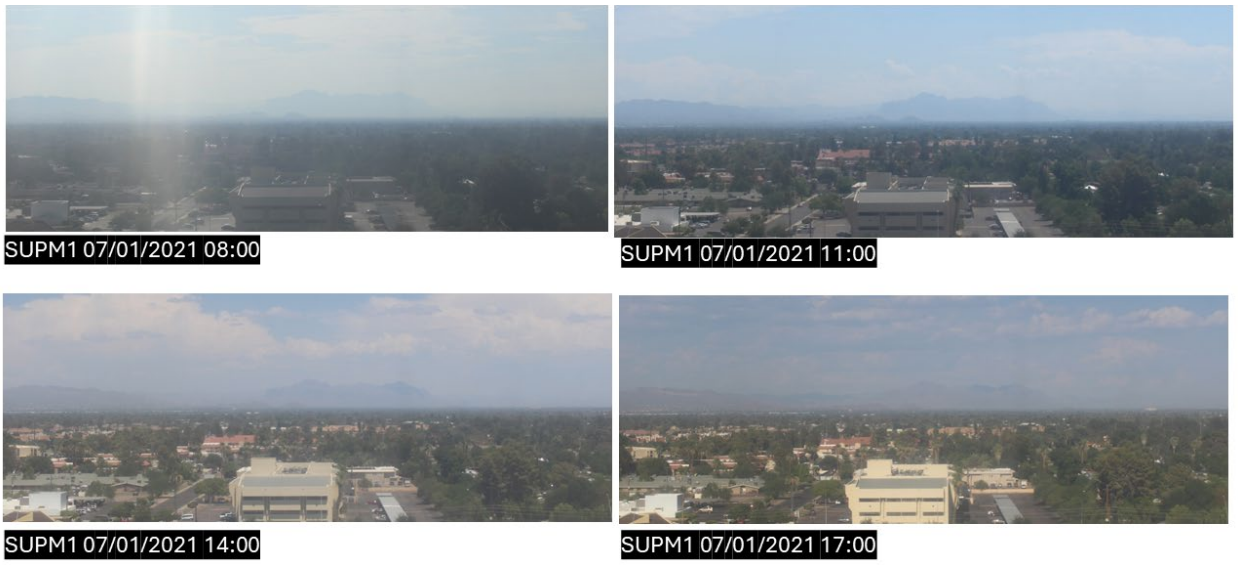

Figure 2-59. Camera Images showing the east coordinal direction taken from the Superstition Mountain webcam on July 1 from 8:00 LST, 11:00 LST, 14:00 LST, and 17:00.

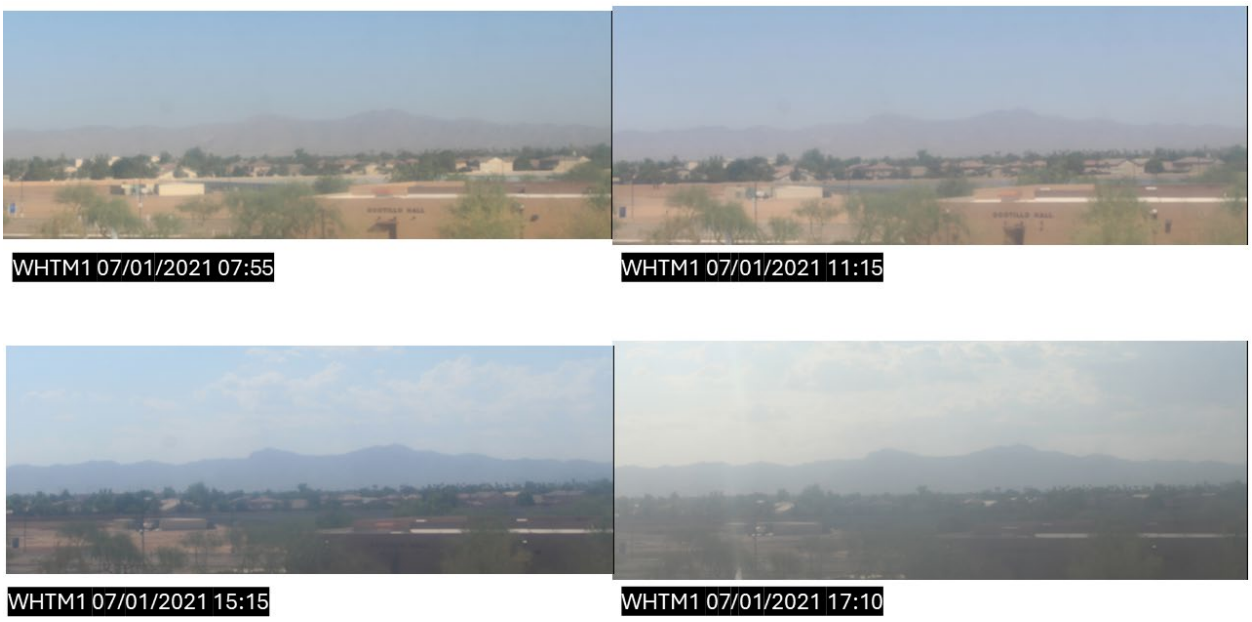

Figure 2-60. Camera Images showing the west-northwest coordinal direction taken from the White Tank Mountain webcam on July 1 from 8:00 LST, 11:00 LST, 14:00 LST, and 17:00.

Figure 2-61. Social media post regarding smoke from the Tiger Fire moving over Phoenix on July 1, 2021.

Figure 2-62. Social media post regarding smoke from the Tiger Fire moving over Phoenix on July 1, 2021.

Figure 2-63 shows an overall view of the magnitude of hourly pollutant concentrations measured in the nonattainment area in the two days before and after the July 1, 2021, atypical event. Hourly ozone concentrations show a widespread and distinct peak on July 1 at all affected sites relative to the days surrounding the atypical event. As noted in Section 2.3, June 29, 2021, another atypical ozone event, also exhibited elevated ozone concentrations. NO_2 concentrations at the exceeding sites are slightly elevated relative to concentrations on the days surrounding the July 1 event. Similarly, $PM_{2.5}$ concentrations at the exceedance-affected sites are slightly elevated relative to July 2 and 3. Higher concentrations of $PM_{2.5}$ were likely not from dust because conditions were not favorable (e.g., wind speeds were generally low) for wind-blown dust before and during the July 1 atypical event. Further, there were no dust storm advisories or warnings before or during this atypical

event.[6] Widespread enhancements in surface pollutant concentrations provide evidence that smoke from regional fires entered the region, mixed towards the surface, and had an atypical influence on ozone during the period. The rest of this section examines temporal abnormalities and site-specific trends for each supporting pollutant.

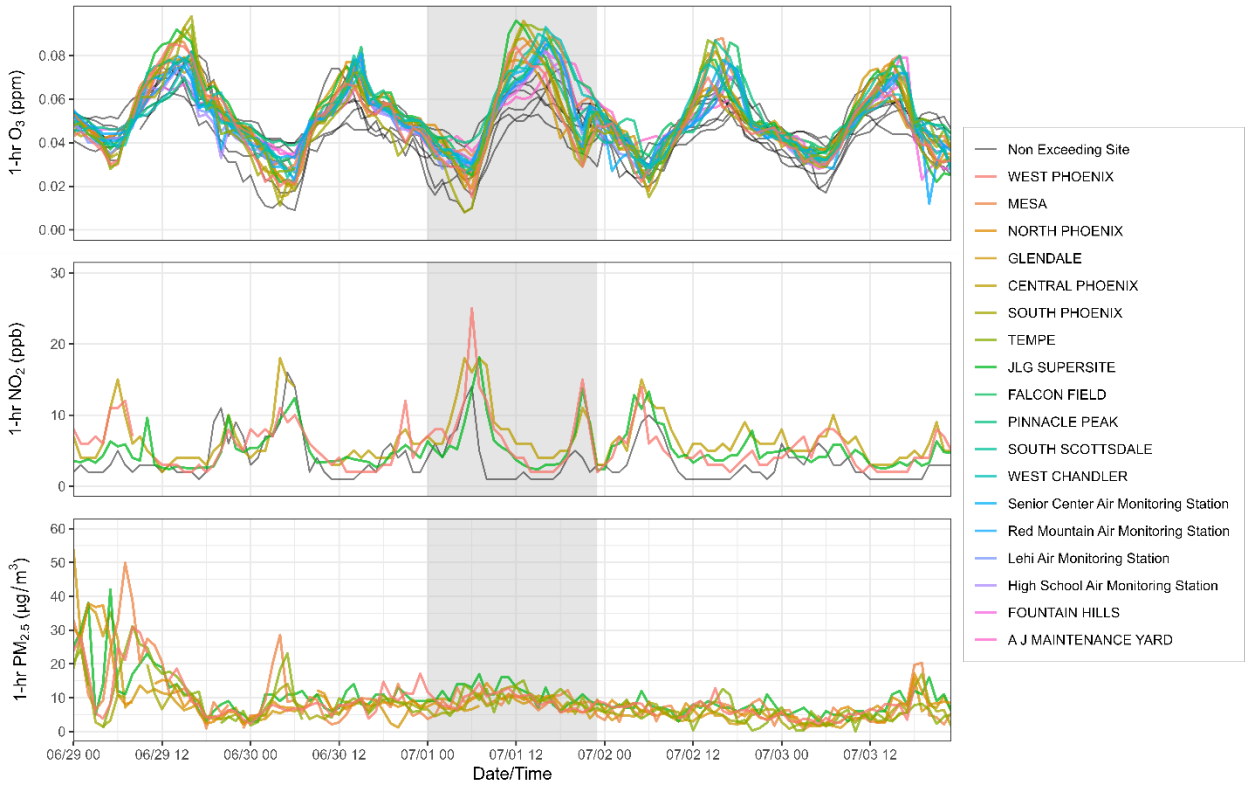

Figure 2-63. Hourly concentrations of ozone, NO_2, and $PM_{2.5}$ at all sites in the nonattainment area. All ozone-exceeding sites are color-coded to highlight smoke impacts on concentrations, and all non-exceeding sites are black. The gray shaded areas represent July 1, 2021.

$PM_{2.5}$ concentrations were enhanced in the nonattainment area on July 1 as emissions from local and regional fires entered the region and mixed towards the surface, which provides further evidence that wildfire smoke was present as an atypical influence on ozone during the period. **Figure 2-64** shows hourly $PM_{2.5}$ concentrations at the Mesa, North Phoenix, and Tempe sites (three of the affected sites) overlaid on the 5th-95th percentile hourly concentrations during ozone season (April to September), calculated using all available data from 2019-2024. $PM_{2.5}$ concentrations at the sites showed uncharacteristic diurnal profiles relative to the statistical medians. Typically, $PM_{2.5}$ concentrations decrease during the day as the boundary layer expands due to daytime heating and dilutes pollutants in the lower atmosphere. On July 1, $PM_{2.5}$ concentrations increased throughout the

[6] https://mesonet.agron.iastate.edu/vtec/search.php?mode=bypoint&lon=-112.1202&lat=33.4223&buffer=0.00&sdate1=2021-06-12&edate1=2021-08-04

morning and into the afternoon and reached or exceeded the 95th percentile during some hours, indicating influence from smoke.

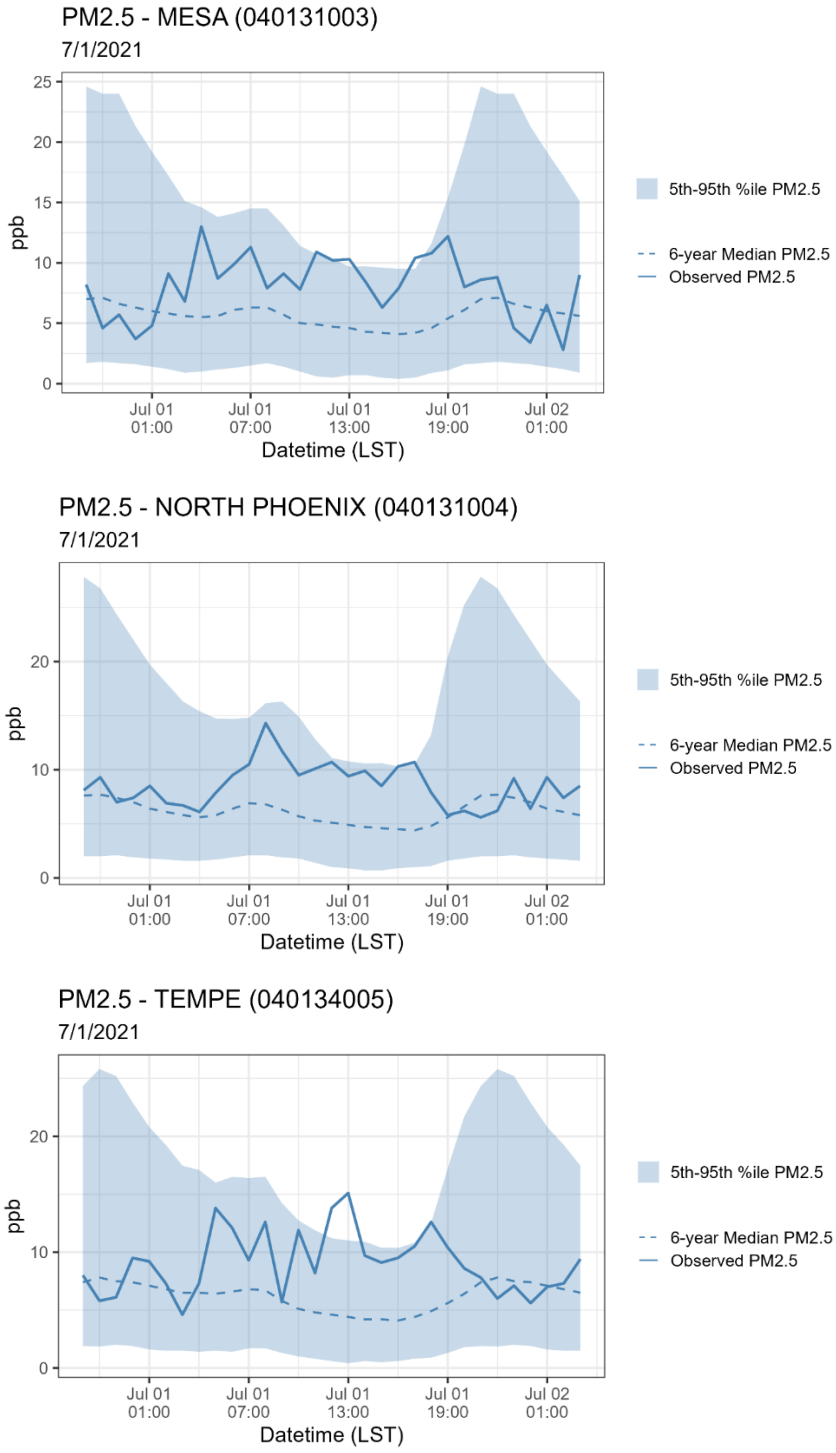

Figure 2-64. Hourly concentrations of $PM_{2.5}$ at the Mesa (top), North Phoenix (middle), and Tempe (bottom) sites. The 6-year (2019-2024) median is represented by the dashed line, and the 5th-95th percentile is represented by the shaded area.

OC, EC, and speciated data were not available on July 1, but samples collected before and after that date show evidence of smoke impacts. The ratio of OC to EC taken at the JLG Supersite monitor was also examined for evidence that wildfire smoke entered the nonattainment area. Increases in this ratio are indicative of wildfire smoke. **Figure 2-65** shows boxplots of OC to EC ratios for available data collected during the ozone season between 2019-2024. The OC to EC ratio on June 30, one day before the atypical event, was at the 75th percentile compared to all data; the ratio on July 3, two days after the atypical event, was well above the 75th percentile and considered an outlier relative to all data. Higher $PM_{2.5}$ species concentrations, particularly potassium, are also indicative of wildfire smoke. **Figure 2-66** shows boxplots of speciated $PM_{2.5}$ data collected at the JLG Supersite monitor during the ozone season between 2019-2024. Higher concentrations of aluminum, calcium, iron, and silicon are indicative of dust, but potassium on the days surrounding the July 1 atypical event are also elevated, which provides evidence that smoke was in the nonattainment area during this time. These observations provide further evidence that ground-level wildfire smoke entered Phoenix in the days leading up to, after, and most likely during the July 1, 2021, atypical ozone event.

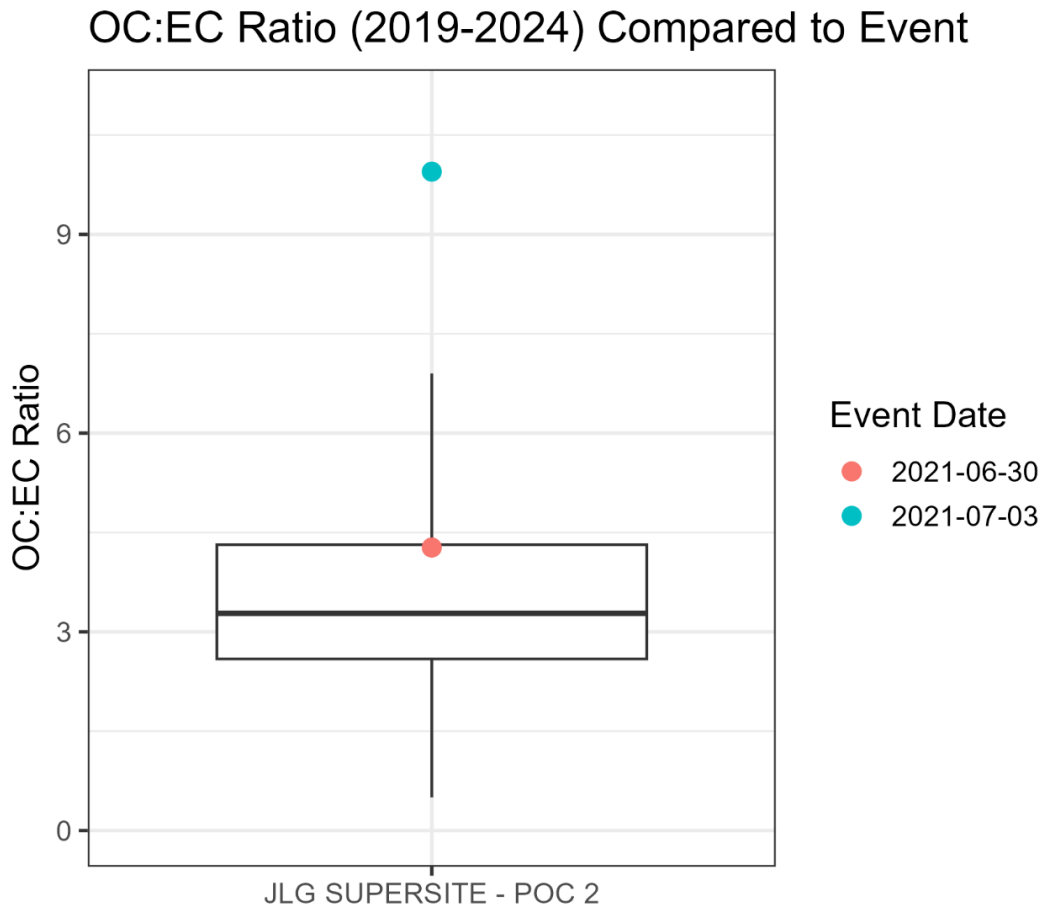

Figure 2-65. Boxplot of OC to EC ratios at the JLG Supersite site using data collected during the ozone season (April-September) from 2019-2024. OC to EC ratios are calculated at POC 2 (x-axis). Available OC to EC ratios collected during the day before and two days after the July 1 atypical ozone event are shown as points.

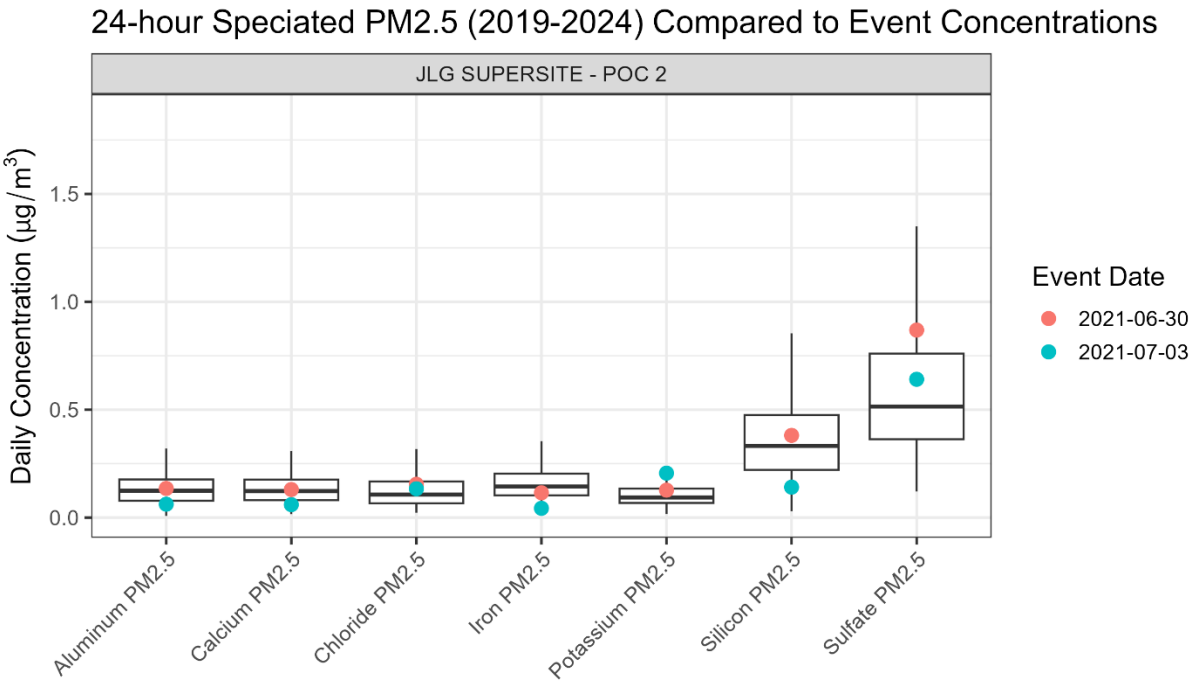

Figure 2-66. Boxplots of speciated $PM_{2.5}$ collected at the JLG Supersite site collected during the ozone season (April-September) from 2019-2024. Available speciated $PM_{2.5}$ concentrations collected during the day before and two days after the July 1 atypical event are shown as points.

2.4.5 Event Statistics

Table 2-9 summarizes the measurements of ozone concentrations on July 1, 2021, as well as the percentile rank of the observation compared to six years of ozone season data (April 1-September 31, 2019-2024). Ozone MDA8 measurements ranged from the 93rd - 100th percentile July 1, 2021.

Table 2-9. Percentile of ozone measurements on the atypical dates compared with six years of ozone data (2019-2024). The percentile rank is calculated across the ozone production season in the nonattainment area (April 1-September 31) of 2019-2024.

Date	Site Name	Site Code	Ozone MDA8 (ppb)	Percentile Rank
7/1/2021	West Phoenix	040130019	74	96
	Mesa	040131003	83	100
	North Phoenix	040131004	78	99
	Falcon Field	040131010	78	99
	Glendale	040132001	71	93
	Pinnacle Peak	040132005	71	93
	Central Phoenix	040133002	82	99
	South Scottsdale	040133003	80	99
	South Phoenix	040134003	73	95
	West Chandler	040134004	81	99
	Tempe	040134005	86	100
	Senior Center Air Monitoring Station	040137020	77	98
	Red Mountain Air Monitoring Station	040137021	75	97
	Lehi Air Monitoring Station	040137022	75	97
	High School Air Monitoring Station	040137024	71	93
	Fountain Hills	040139704	73	95
	JLG Supersite	040139997	83	100
	A J Maintenance Yard	040213001	71	93

2.4.6 Conclusion

The concurrence of HMS smoke perimeters over the nonattainment area, HYSPLIT trajectories and meteorological analysis showing accumulation of smoke in the nonattainment area, visible smoke in camera images and video news coverage, elevated hourly $PM_{2.5}$ concentrations, and OC to EC ratios and potassium $PM_{2.5}$ provide evidence that surface-level smoke was present during the period. Regional transport of smoke from large fires in Arizona on July 1, enhanced ozone concentrations outside of the typical diurnal profile, keeping ozone values high and affecting the MDA8 ozone concentrations at

eighteen sites. Multiple analyses showed that smoke fully encompassed the Maricopa Nonattainment Area on July 1, and statistics show ozone concentrations were atypical during this event.

This combined evidence indicates that the smoke plumes generated by numerous regional fires provided an atypical source of ozone and ozone precursors that caused enhanced ozone concentrations on July 1, 2021. Removal of these days as atypical events is supported by this analysis.

2.5 July 20-22, 2021

2.5.1 Event Overview: July 20-22, 2021

The unrepresentative (atypical) ozone event took place on July 20-22, 2021, and affected twenty sites in the Maricopa Nonattainment Area: West Phoenix, Mesa, North Phoenix, Falcon Field, Glendale, Pinnacle Peak, Central Phoenix, South Scottsdale, Tempe, Cave Creek, Dysart, Senior Center Air Monitoring Station, Lehi Air Monitoring Station, High School Air Monitoring Station, Blue Point-Sheriff Station-Tonto NF-Salt River Recreation Area, Fountain Hills, JLG Supersite, A J Maintenance Yard, Queen Valley, and Tonto NM (**Table 2-10**). MDA8 ozone concentrations at the affected sites ranged from 71-82 ppb.

Time series graphs showing hourly ozone concentrations that exceeded the seasonal means (calculated using all available data from April 1 – September 31, 2019-2024) and 10th-90th percentiles at each site are shown in **Figure 2-67**. During the afternoon on July 20, hourly ozone measurements at many sites, such as North Phoenix, JLG Supersite, and West Phoenix, exhibit distinct spikes in their diurnal profiles, indicating an outside influence on concentrations from wildfire smoke. Ozone concentrations generally fall to average levels in the evening of July 20 and early morning hours of July 21. Ozone concentrations then increase dramatically and again exceed the 90th percentile in the afternoon of July 21 and remain elevated throughout the rest of the atypical ozone event period.

Major wildfires burning throughout the northwestern U.S. and in western Canada were identified as major contributors to this event. Evidence includes (1) HMS smoke perimeters over the nonattainment area, (2) HYSPLIT trajectories and meteorological analysis showing accumulation of smoke in Phoenix, (3) visible smoke in camera images and news coverage, (4) elevated OC to EC ratios, and (5) remote sensing imagery. This combination of evidence indicates that this is an atypical ozone event.

Table 2-10. Summary of identified atypical July 20-22, 2021.

Event Date(s)	Event Ozone Concentration Percentile	Sites Exceeded During Event	Type of Event
July 20-22, 2021	93rd - 99th	Twenty sites: West Phoenix, Mesa, North Phoenix, Falcon Field, Glendale, Pinnacle Peak, Central Phoenix, South Scottsdale, Tempe, Cave Creek, Dysart, Senior Center Air Monitoring Station, Lehi Air Monitoring Station, High School Air Monitoring Station, Blue Point-Sheriff Station-Tonto NF-Salt River Recreation Area, Fountain Hills, JLG Supersite, A J Maintenance Yard, Queen Valley, and Tonto NM	International/long-range transport

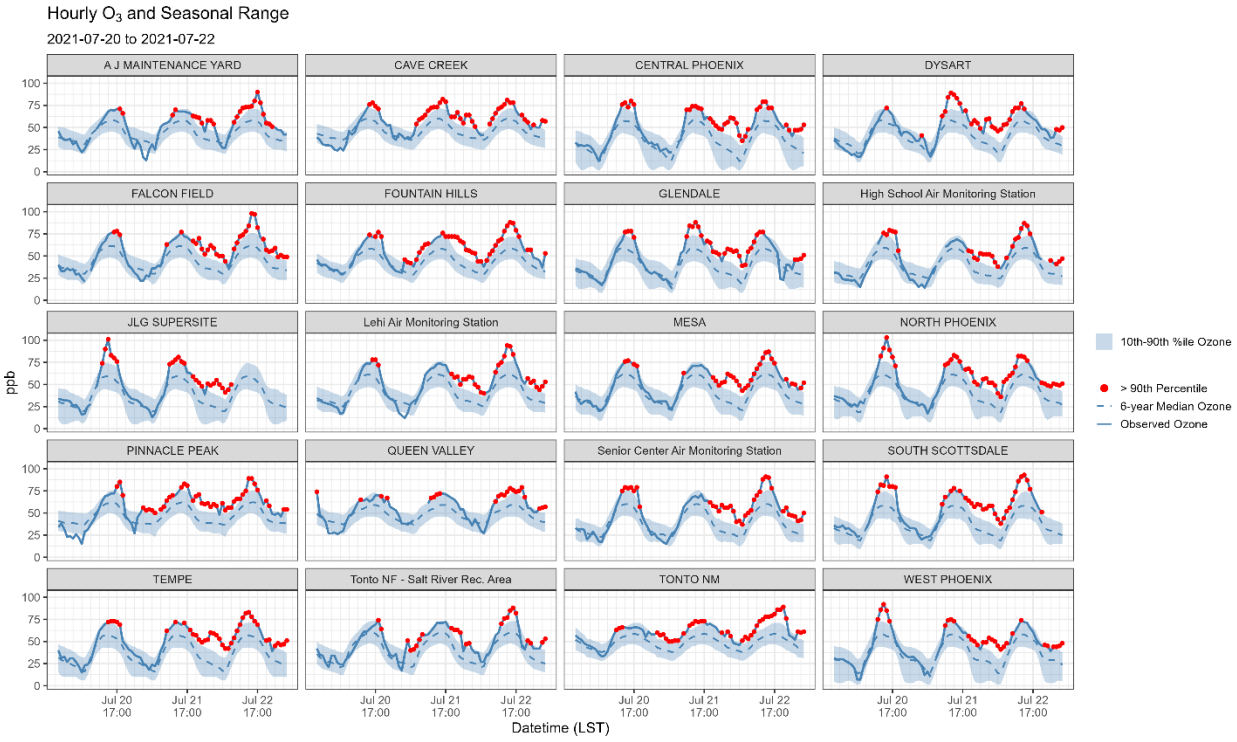

Figure 2-67. Hourly ozone concentrations (ppb) compared to all available data during the ozone season (April 1 – September 31) of the 6-year (2019-2024) period. Hourly means and 10th-90th percentiles are calculated using data on July 20-22, 2021.

2.5.2 Identification of Wildfire(s)

Multiple large fires in the northwestern U.S. and in Canada were active in the days leading up to and during July 20-22, the exclusion days (**Figures 2-68 to 2-70**). Smoke from these fires combined to blanket the continental U.S. during July 20-22.

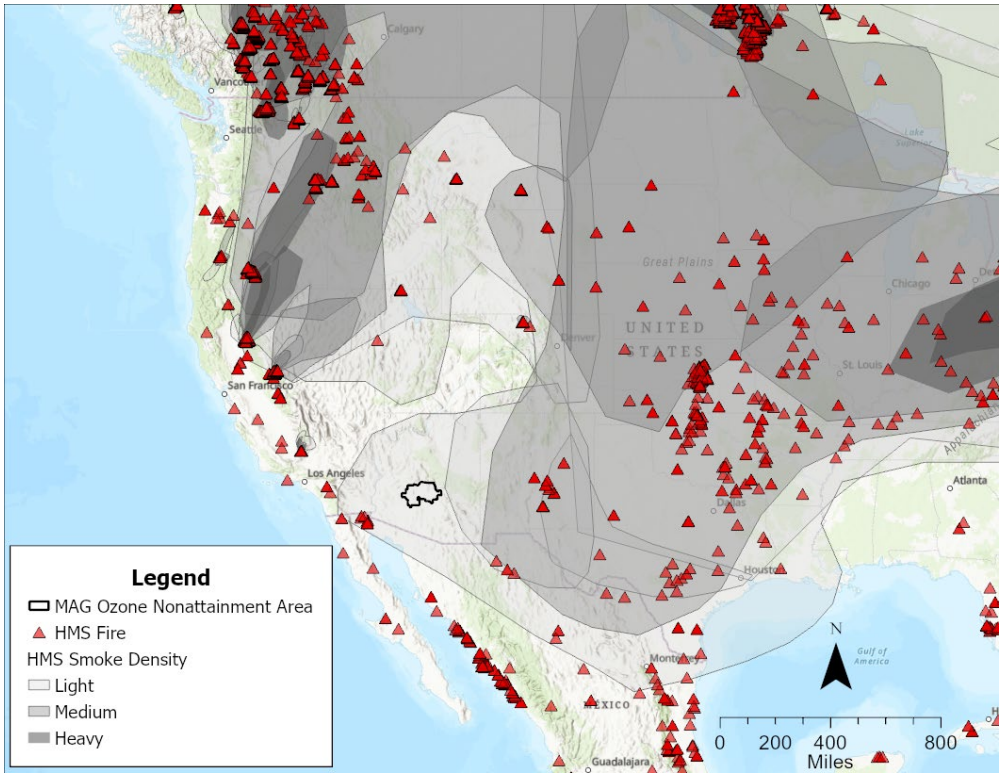

Figure 2-68. Continental view of HMS smoke density and fire locations on July 20, 2021.

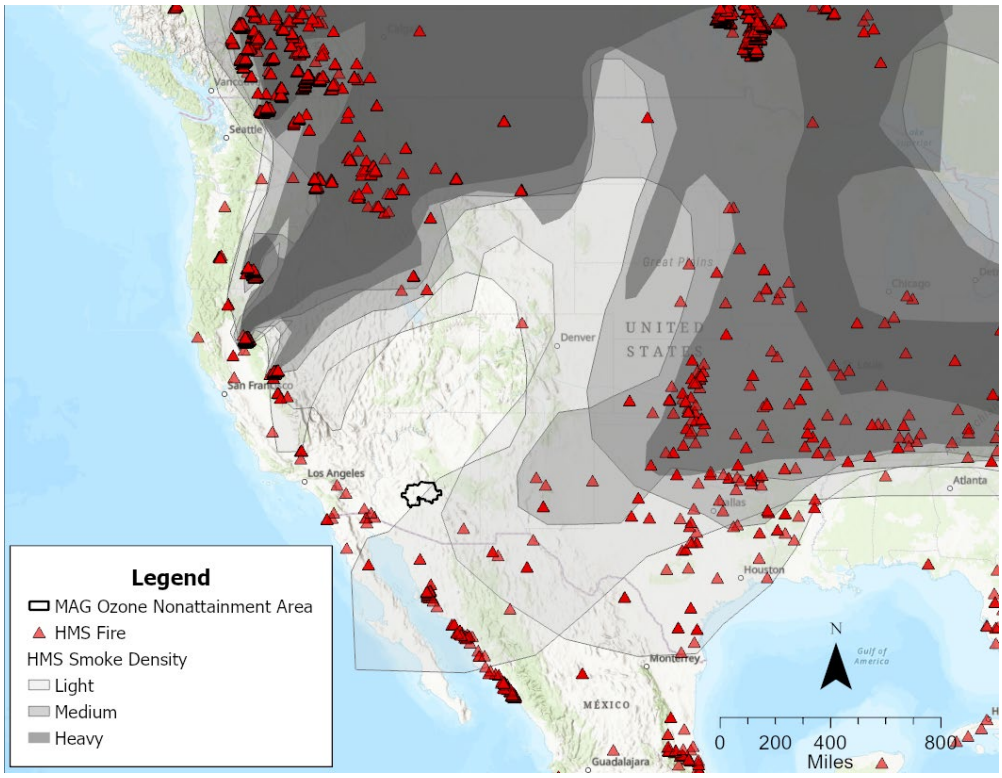

Figure 2-69. Continental view of HMS smoke density and fire locations on July 21, 2021.

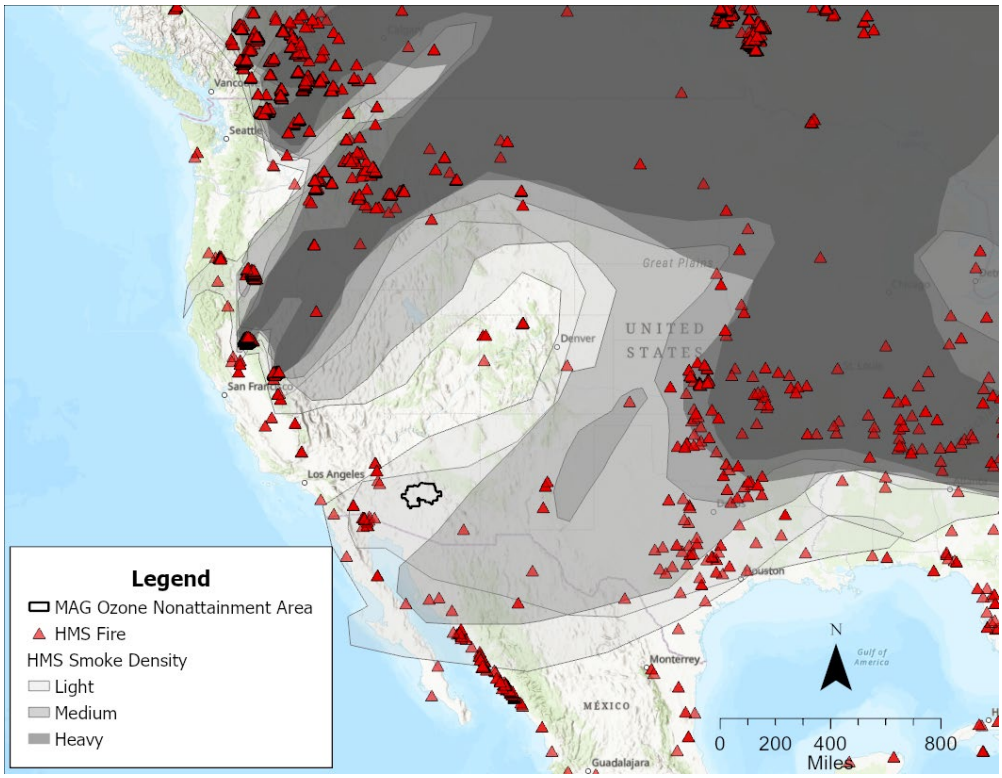

Figure 2-70. Continental view of HMS smoke density and fire locations on July 22, 2021.

2.5.3 Meteorological Analysis

Upper-Level Analysis

The contour plot of average geopotential height at 500 mb (approximately 18,000 feet) from July 20 through July 22, 2021, in **Figure 2-71** shows a ridge of high pressure aloft centered over the Four Corners. The red colors indicate 500 mb heights above 5925 meters across Arizona, which is above normal for this time of year. While scattered thunderstorms developed over the higher terrain due to moist and warm conditions, the upper-level ridge led to mostly sunny skies and warm temperatures in the nonattainment area, aiding ozone formation each day.

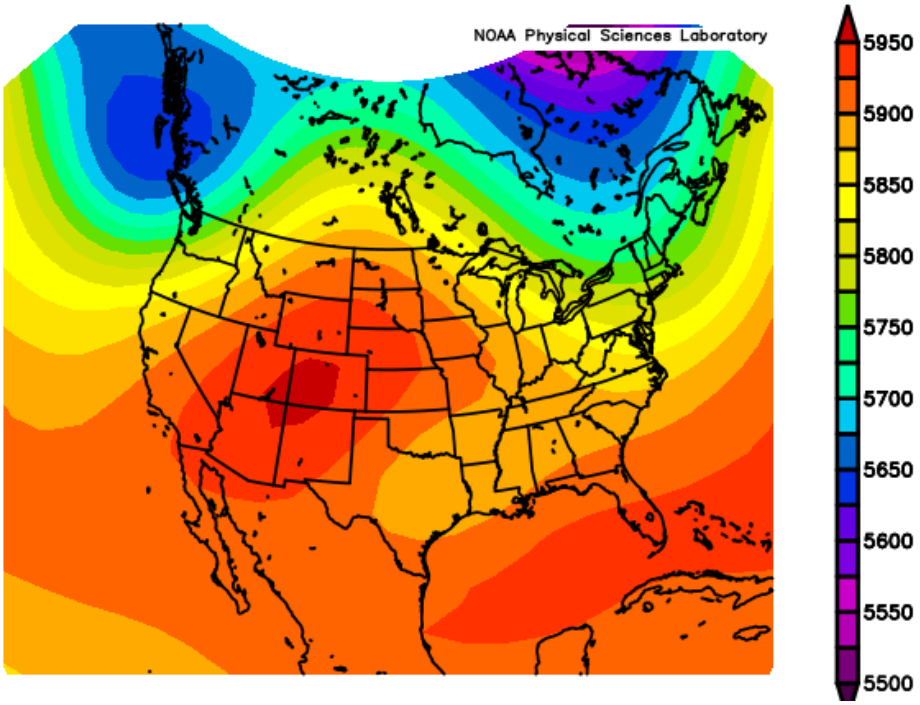

Figure 2-71. Average geopotential height at 500 mb from July 20 through 22, 2021.

Surface Analysis

Figure 2-72 shows a weak trough of surface low pressure across southern Arizona on these days, as hot temperatures led to rising thermals over the Desert Southwest.

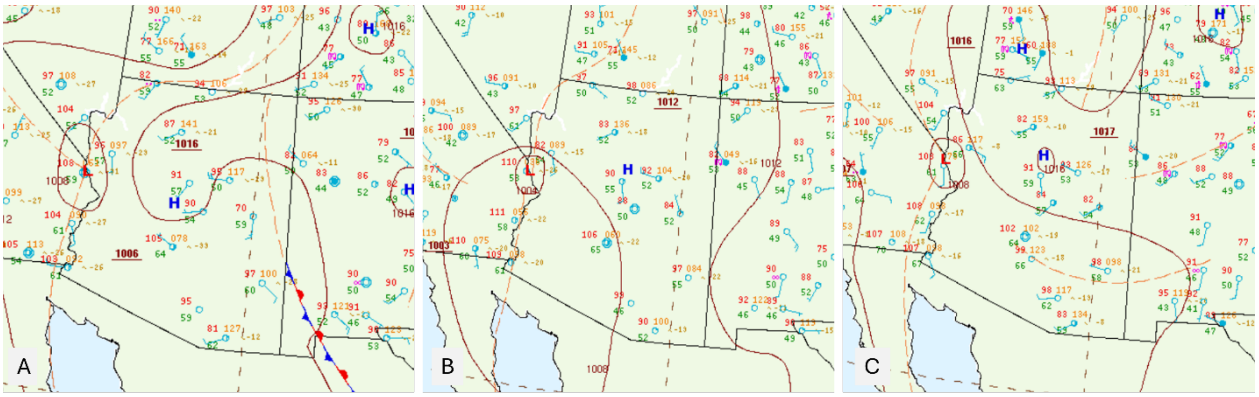

Figure 2-72. Surface analyses from 2 p.m. MST July 20, 2021 (A), 2 p.m. MST July 21, 2021 (B), and 2 p.m. MST July 22, 2021 (C).

In addition, a weak pressure gradient over Phoenix led to periods of light winds and limited dispersion. Surface weather observations in **Table 2-11** show that the above-normal heights at 500 mb coincided with hot surface temperatures, aiding ozone formation. And while average wind speeds were slightly higher than would normally be expected with enhanced ozone development toward the end of this event, wind speeds occasionally dipped below 5 mph each afternoon, hindering dispersion.

Table 2-11. Surface weather variables observed at Phoenix Sky Harbor Airport.

Date	High Temp. (F)	Avg. WS (mph)	Avg. WD
7/20/2021	109	7	264
7/21/2021	109	8	204
7/22/2021	106	10	107

Satellite Smoke and Fire Detections

Despite regional cloud development associated with thunderstorms over the higher terrain, **Figure 2-73** shows satellites were still able to detect light-to-medium density smoke over the nonattainment area July 20 through July 22. Regional haze can also be discerned on visible satellite imagery each afternoon in **Figures 2-74, 2-75, and 2-76**. MODIS AIRS provides evidence of smoke transport over Arizona on July 21 and 22, with 500 mb CO concentrations of up to 143 ppbv over Phoenix (**Figures 2-77 and 2-78**).

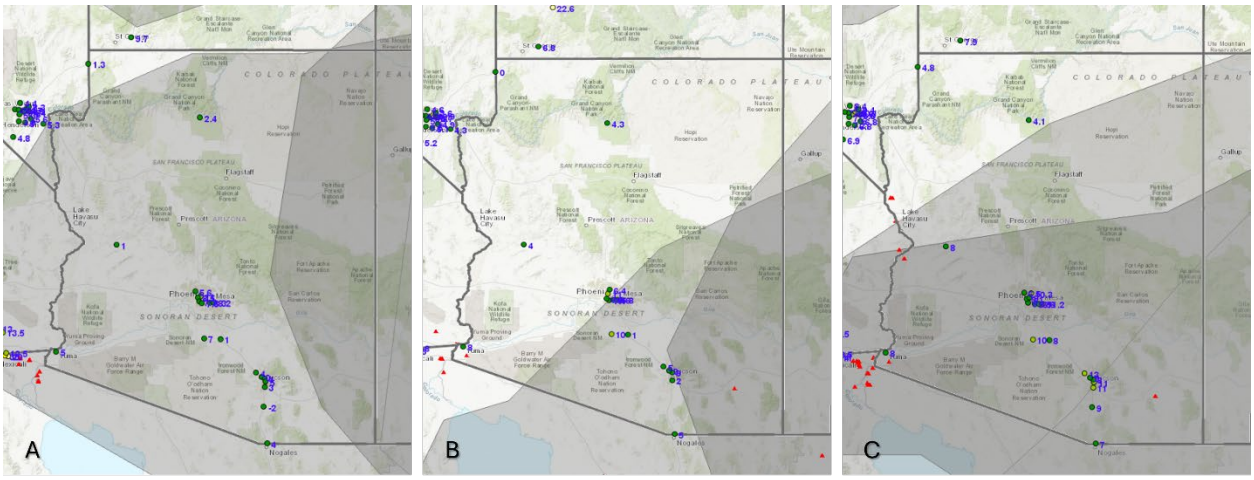

Figure 2-73. HMS fire and smoke along with hourly concentrations of $PM_{2.5}$ at 8:00 a.m. MST each day from July 20 (A), July 21 (B) and July 22 (C), 2021.

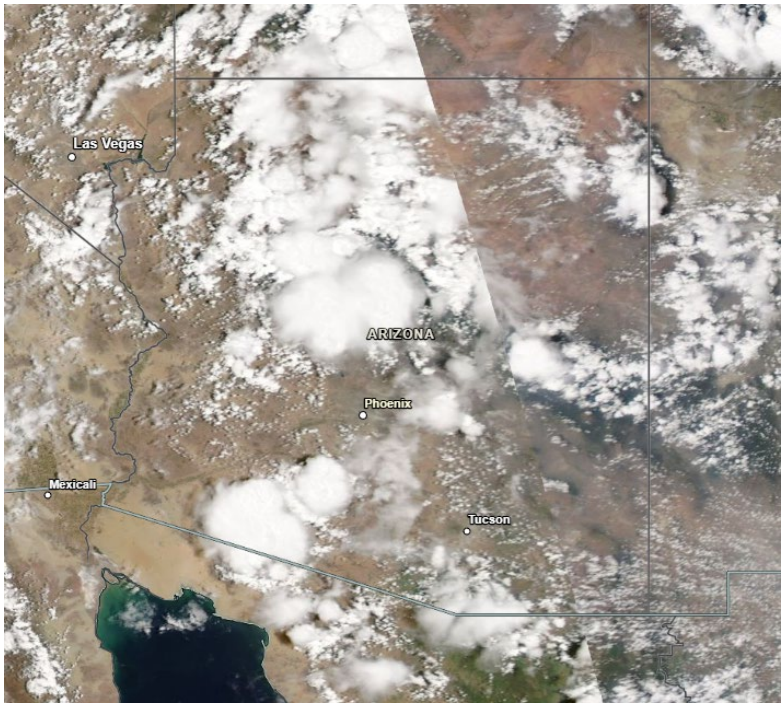

Figure 2-74. Visible satellite imagery from approximately 2:23 p.m. MST on July 20, 2021.

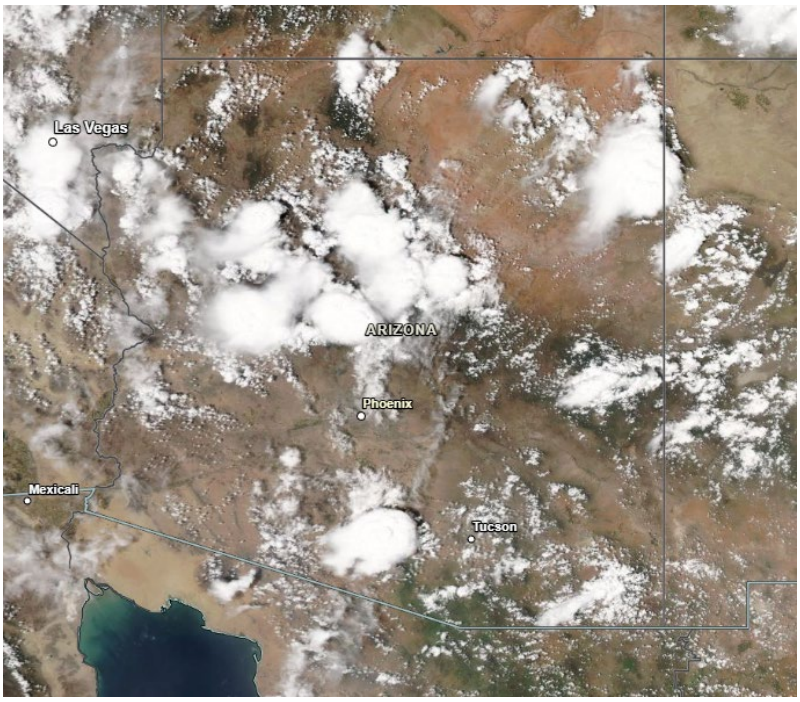

Figure 2-75. Visible satellite imagery from approximately 1:28 p.m. MST on July 21, 2021.

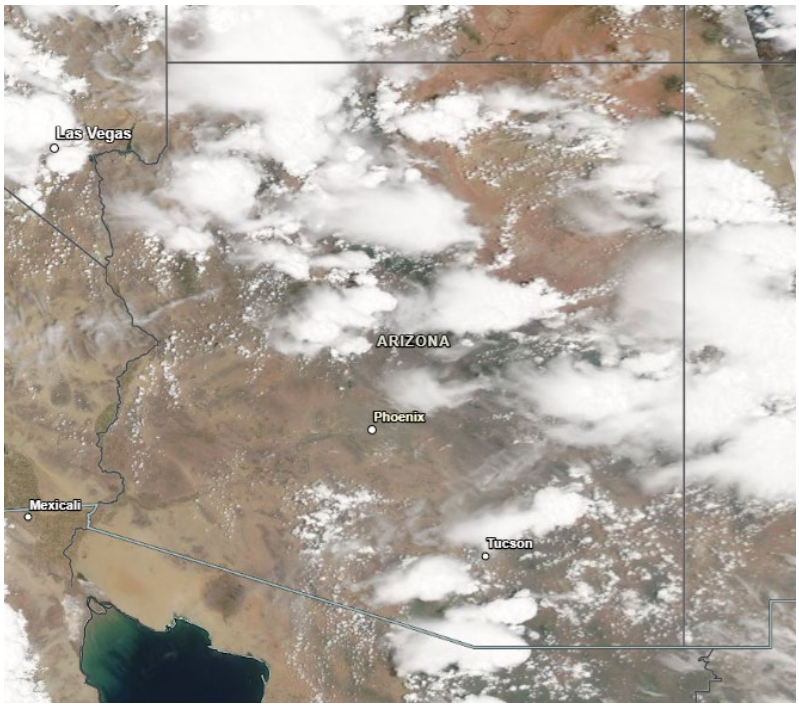

Figure 2-76. Visible satellite imagery from approximately 1:11 p.m. MST on July 22, 2021.

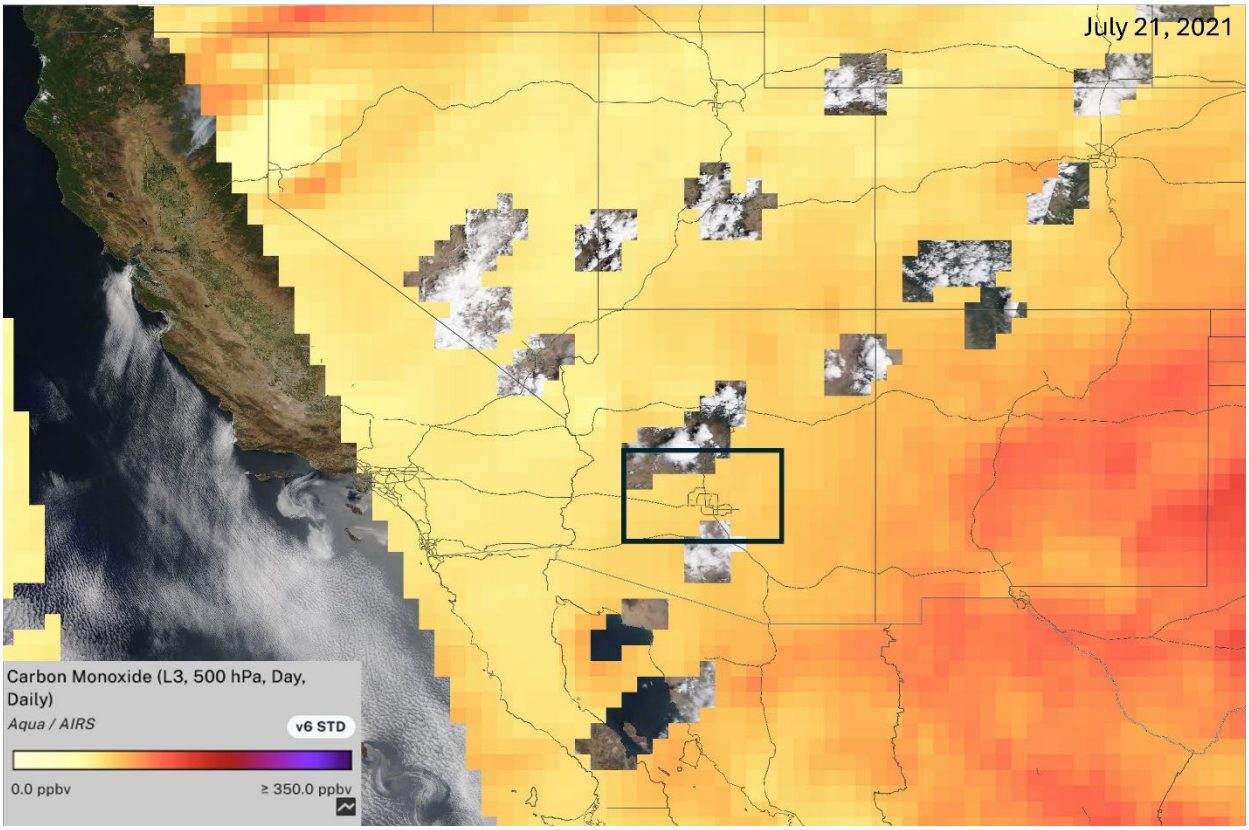

Figure 2-77. A zoomed-in view over the southwestern U.S. of MODIS Aqua AIRS CO retrieval during the atypical ozone date of July 21, 2021. The black box represents the approximate area of the NAA.

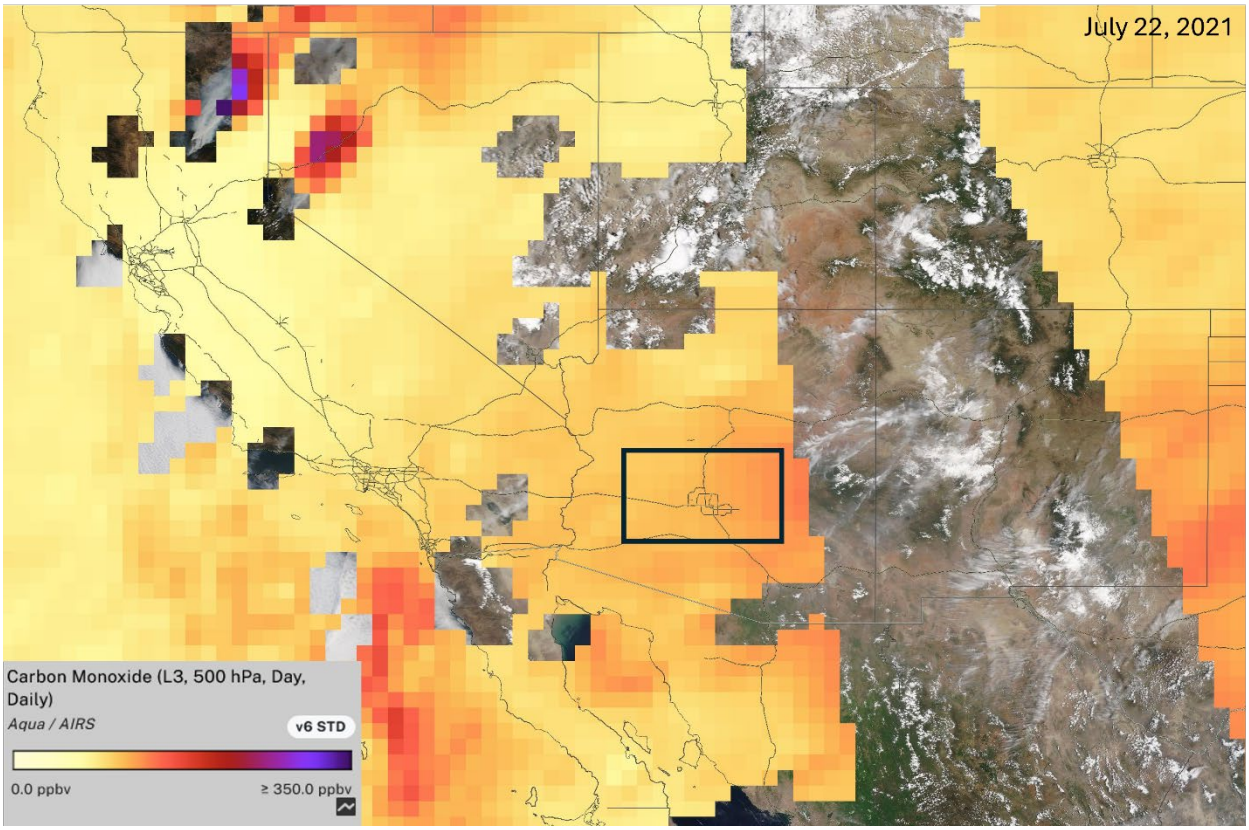

Figure 2-78. A zoomed-in view over the southwestern U.S. of MODIS Aqua AIRS CO retrieval during the atypical ozone date of July 22, 2021. The black box represents the approximate area of the NAA.

Smoke Discussions

NOAA's daily smoke discussion also notes a large area of smoke impacting much of the Continental United States.

"Ongoing wildfires with the largest and most intense areas over eastern Alaska/the Yukon, southeastern British Columbia/Pacific Northwest, and far southwestern Ontario/southeastern Manitoba continue to support **a huge light density plume** that covers eastern Alaska, most of central and southern Canada, and a **significant portion of the Continental U.S.**" (NOAA NESDIS Text Narrative, July 20, 2021)

In addition, smoke was reported by local METAR observations at Phoenix Sky Harbor Airport on July 22.

Soundings

There are no significant temperature inversions in the left panels in **Figure 2-79** which indicates conditions were not conducive to local pollutant accumulation during the morning hours due to limited mixing. However, deep mixing heights each afternoon supported the transport of any aloft smoke to the surface, with mixing heights extending near 700 mb (2.6 km) on all three days (right panels of Figure 2-79).

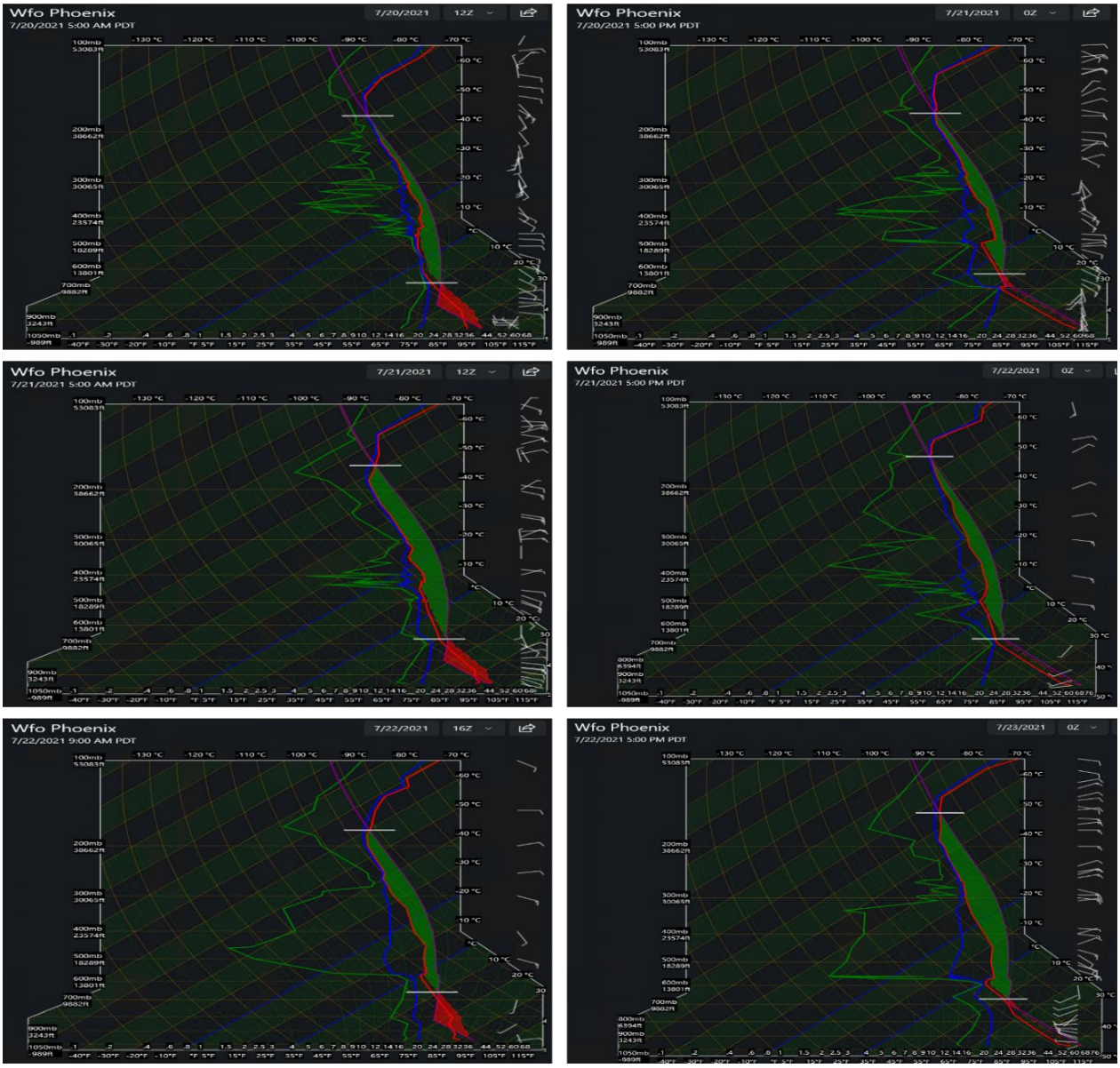

Figure 2-79. Observed atmospheric soundings from 5 a.m. MST (left) and 5 p.m. MST (right) July 20 through July 22, 2021.

Smoke Transport

Output from NOAA's HYSPLIT model also provides evidence for the transport of regional smoke into the nonattainment area. The images in **Figure 2-80** show 48-hour back trajectories from 12:00 a.m. to 8:00 p.m. MST between July 20 and July 22 at 100 meters, 1,000 meters, and 2,500 meters above ground level (AGL). These trajectories show that aloft winds within the boundary layer originated from areas impacted by light-to-medium density smoke from wildfires burning across the western and northwestern U.S. and Canada, potentially enhancing ozone formation.

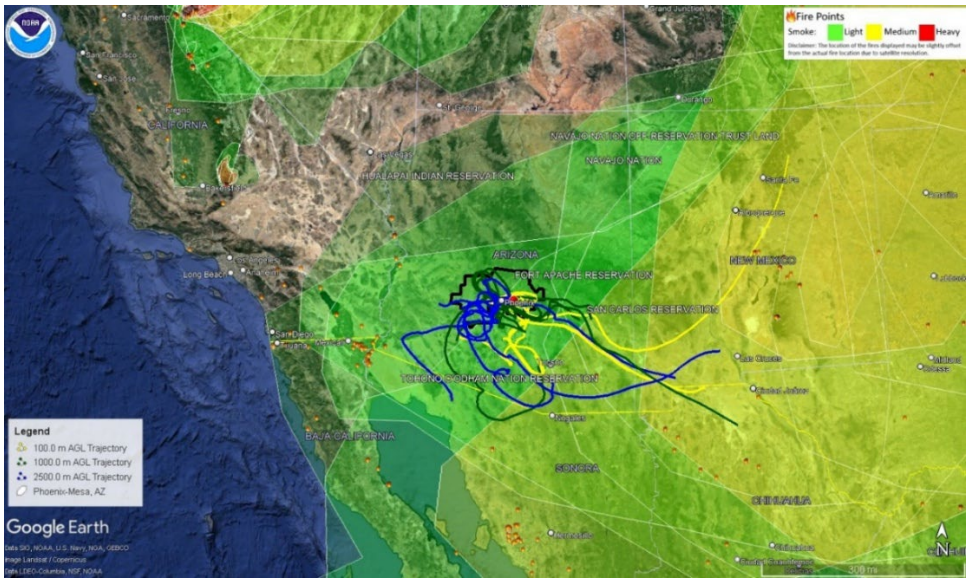

Figure 2-80. NOAA smoke and fire maps and NOAA HYSPLIT trajectory model runs from the Falcon Field ozone monitor, with air parcels moving 48-hours before 12:00 am - 8:00 pm MST on July 22 at 100 meters, 1,000 meters, and 2,500 meters (AGL). Analysis performed by MAG.

Summary

For July 20-22, 2021 a ridge of high pressure aloft centered near the Four Corners led to mostly sunny skies and hot temperatures in the Phoenix area. As evidenced by observed soundings from Phoenix, the hot temperatures led to deep mixing each afternoon. This deep mixing coincided with plumes of light to medium HMS smoke perimeters over south-central Arizona, showing the potential for aloft smoke to mix to the surface. In addition, HYSPLIT back trajectories for this period originated from an area of light to medium density smoke generated from fires in the western, and northwestern U.S. as well as Canada. Furthermore, MODIS AIRS displayed smoke transport during this event, with elevated CO concentrations observed over Phoenix. As a result, there is evidence that smoke enhanced ozone formation in the nonattainment area July 20-22, 2021.

2.5.4 Surface Impacts

Low visibility in Phoenix is apparent on July 20-22, 2021. While some of the haze is likely due to dust, smoke plumes from the fires burning in the northwestern U.S. and throughout Canada were present over the nonattainment area during the atypical ozone event and contributed to the haze. **Figure 2-81 through 2-92** show photos taken from the southwest-facing Estrella Mountain, south-facing South Mountain, east-facing Superstition Mountain, and west-northwest-facing White Tank Mountain webcams, where the visibility is low due to haze on July 20-22, 2021. The smoke plume that blanketed the continental U.S. received widespread news coverage, including a report by Reuters; their report, "Western wildfire smoke causes cross-country air pollution", provided photos and videos of the fires and smoke plumes (**https://www.reuters.com/world/us/smoke-us-west-wildfires-leaves-easterners-gasping-2021-07-20/**).

Figure 2-81. Camera Images showing the southwest coordinal direction taken from the Estrella Mountain webcam on July 20 from 8:00 LST, 11:00 LST, 14:00 LST, and 17:00.

Figure 2-82. Camera Images showing the southwest coordinal direction taken from the Estrella Mountain webcam on July 21 from 8:00 LST, 11:00 LST, 14:00 LST, and 17:00.

Figure 2-83. Camera Images showing the southwest coordinal direction taken from the Estrella Mountain webcam on July 22 from 8:00 LST, 11:00 LST, 14:00 LST, and 17:00.

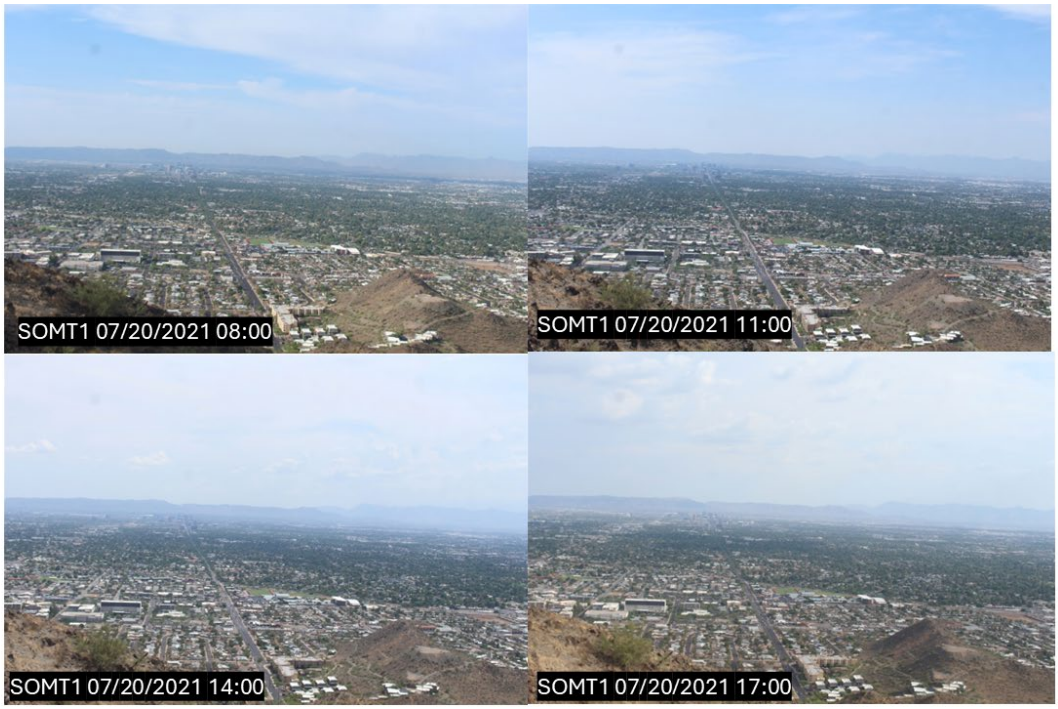

Figure 2-84. Camera Images showing the south coordinal direction taken from the South Mountain webcam on July 20 from 8:00 LST, 11:00 LST, 14:00 LST, and 17:00.

Figure 2-85. Camera Images showing the south coordinal direction taken from the South Mountain webcam on July 21 from 8:00 LST, 11:00 LST, 14:00 LST, and 17:00.

Figure 2-86. Camera Images showing the south coordinal direction taken from the South Mountain webcam on July 22 from 8:00 LST, 11:00 LST, 14:00 LST, and 17:00.

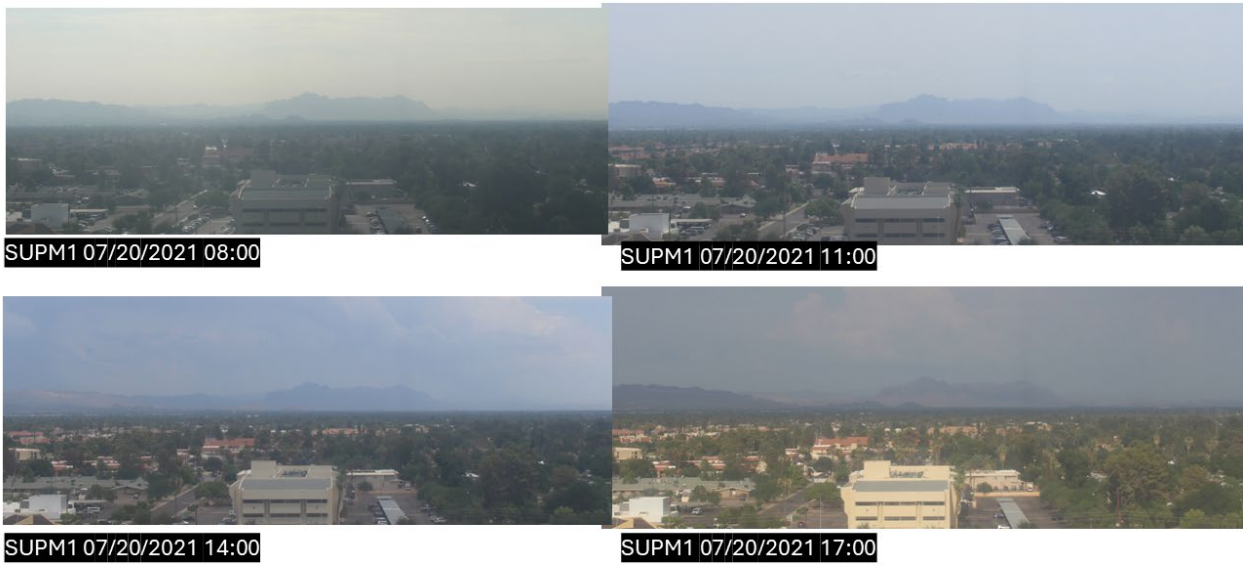

Figure 2-87. Camera Images showing the east coordinal direction taken from the Superstition Mountain webcam on July 20 from 8:00 LST, 11:00 LST, 14:00 LST, and 17:00.

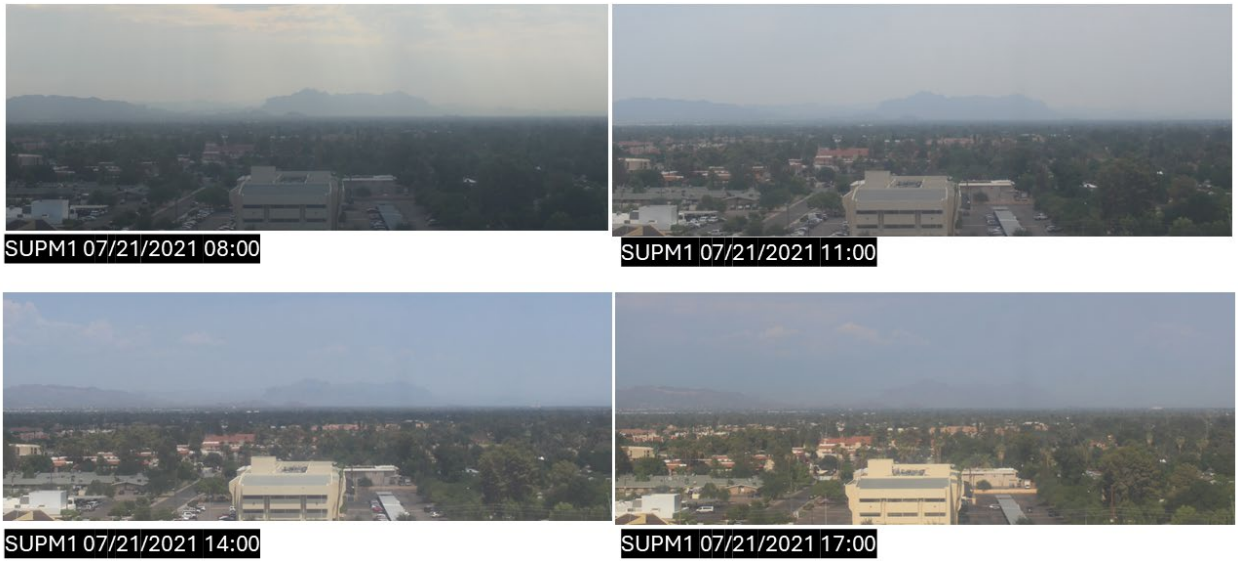

Figure 2-88. Camera Images showing the east coordinal direction taken from the Superstition Mountain webcam on July 21 from 8:00 LST, 11:00 LST, 14:00 LST, and 17:00.

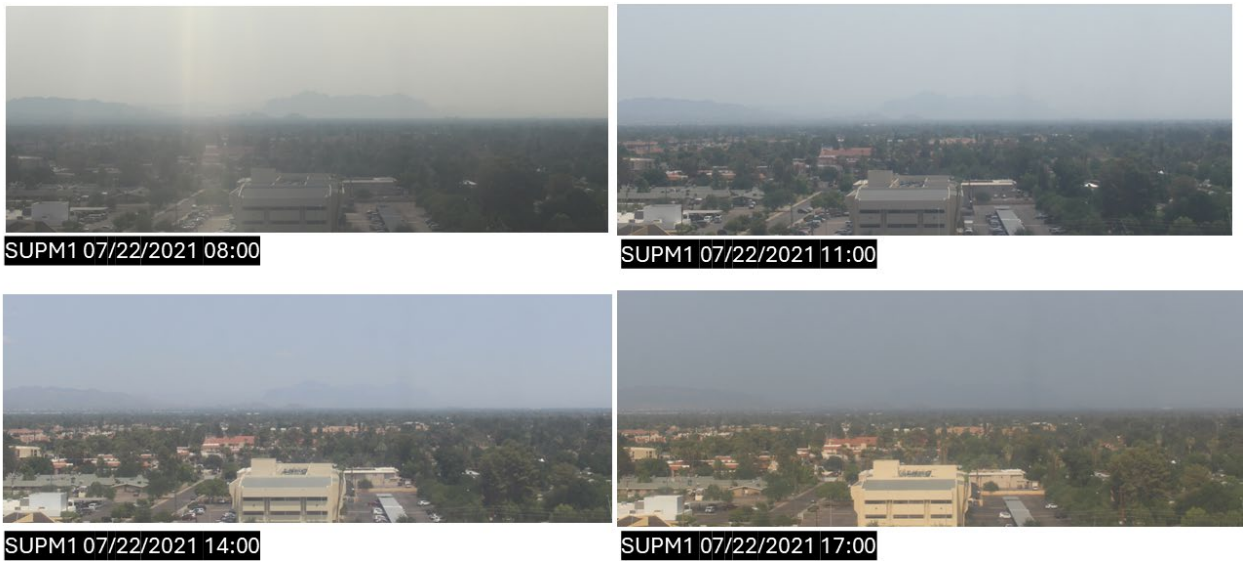

Figure 2-89. Camera Images showing the east coordinal direction taken from the Superstition Mountain webcam on July 22 from 8:00 LST, 11:00 LST, 14:00 LST, and 17:00

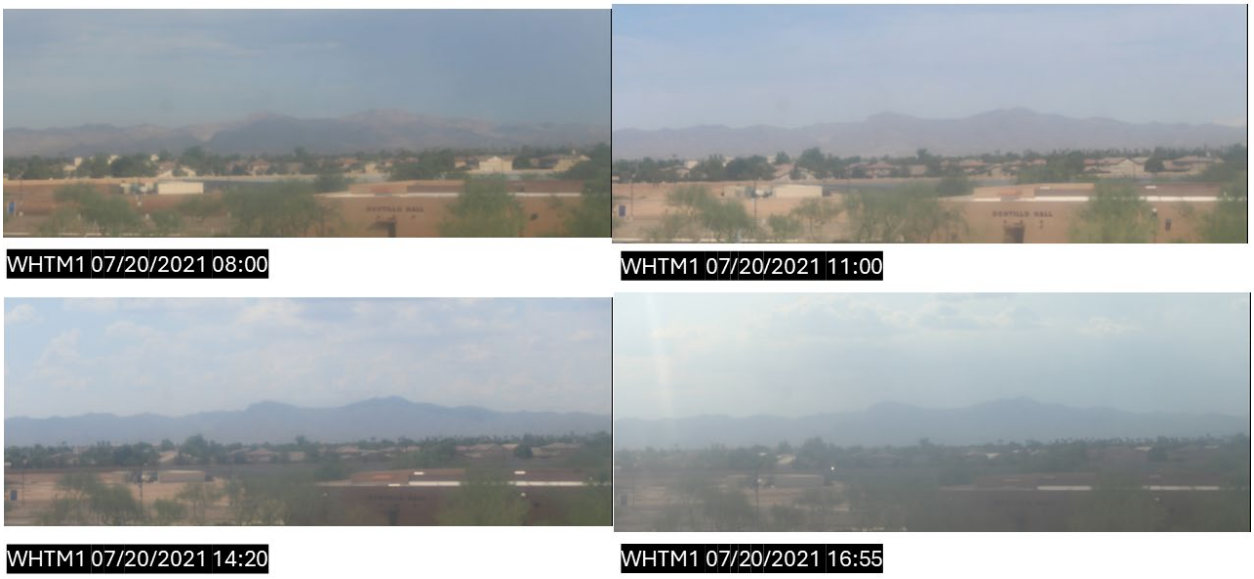

Figure 2-90. Camera Images showing the west-northwest coordinal direction taken from the White Tank Mountain webcam on July 20 from 8:00 LST, 11:00 LST, 14:00 LST, and 17:00.

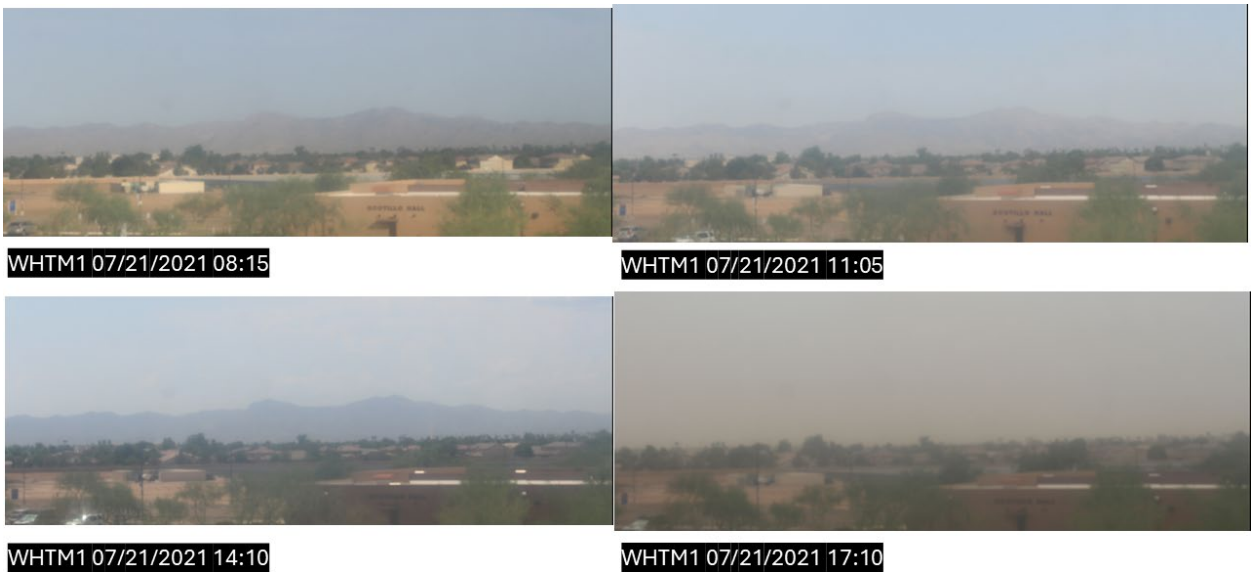

Figure 2-91. Camera Images showing the west-northwest coordinal direction taken from the White Tank Mountain on July 21 from 8:00 LST, 11:00 LST, 14:00 LST, and 17:00.

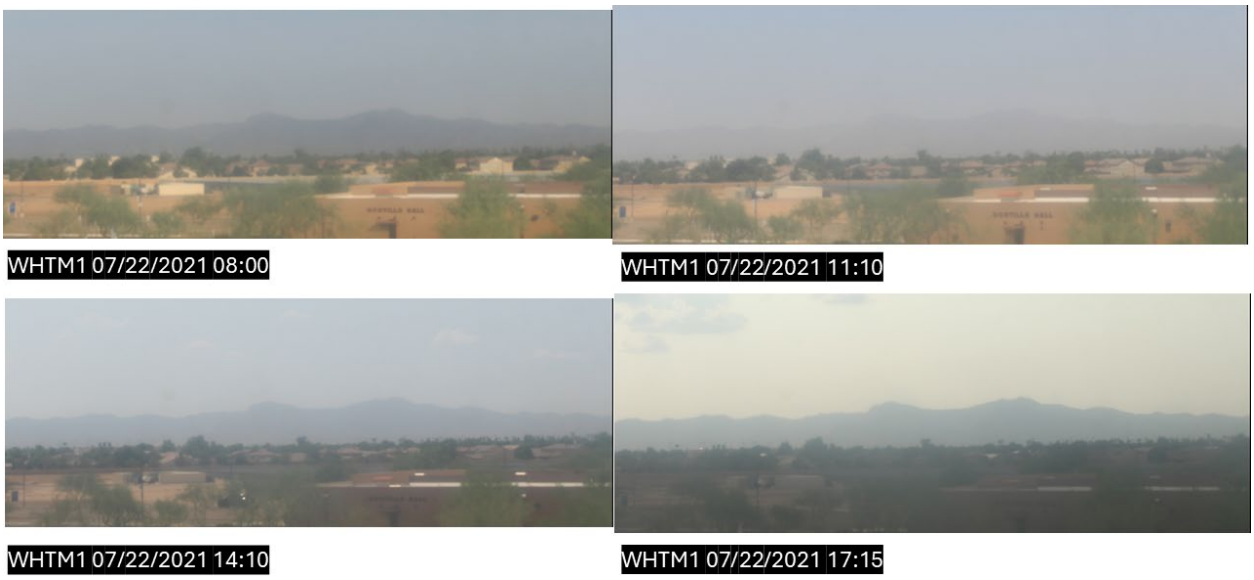

Figure 2-92. Camera Images showing the west-northwest coordinal direction taken from the White Tank Mountain webcam on July 22 from 8:00 LST, 11:00 LST, 14:00 LST, and 17:00.

Figure 2-93 shows an overall view of the magnitude of hourly pollutant concentrations measured in the nonattainment area during the two days before and after the July 20-22, 2021, atypical event. Hourly concentrations of ozone show widespread and distinct maximums on July 20-22 at all affected sites relative to the days after the event. $PM_{2.5}$ concentrations were elevated during some hours on July 22 and 23. However, speciated $PM_{2.5}$ data and storm reports[7] indicate that elevated $PM_{2.5}$ concentrations may have been due to wind-blown dust from monsoonal storms rather than smoke from wildfires.

[7] https://www.weather.gov/psr/StormReportfor2126July2021

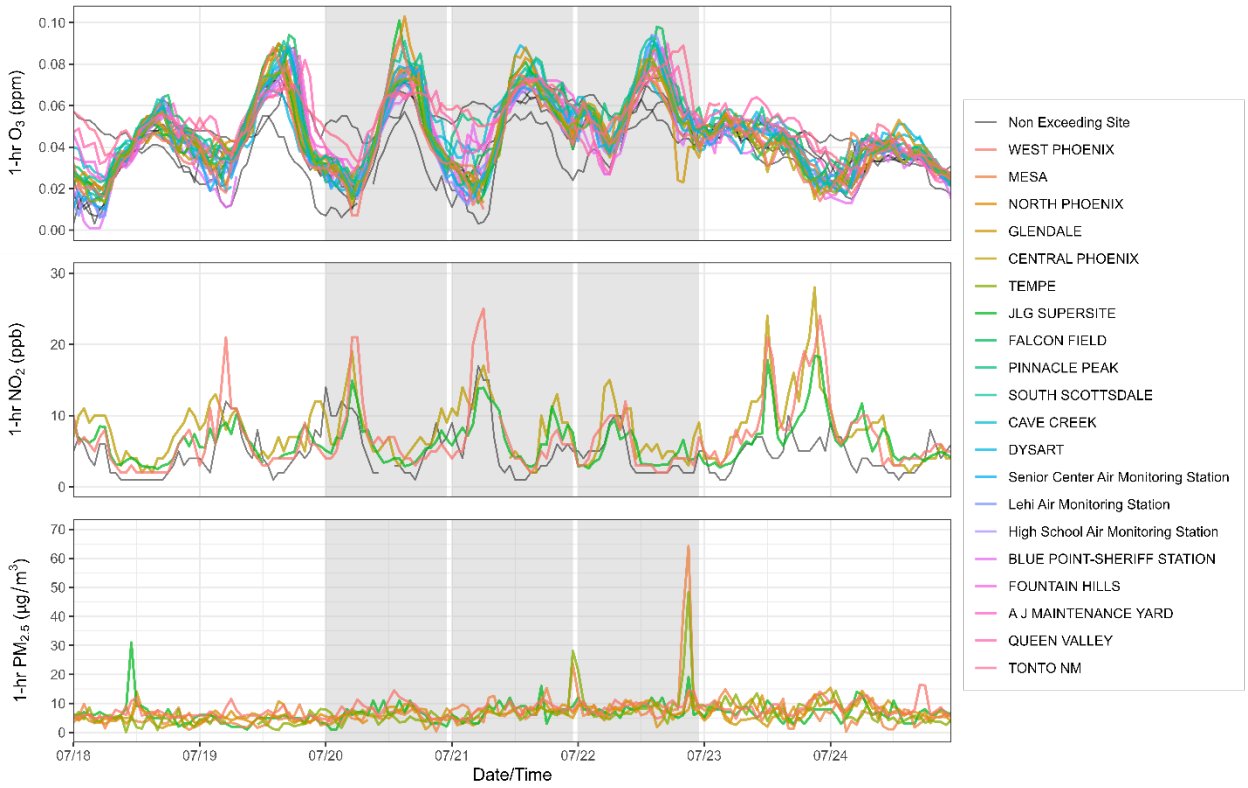

Figure 2-93. Hourly concentrations of ozone, NO_2, and $PM_{2.5}$ at all sites in the nonattainment area. All ozone-exceeding sites are color-coded to highlight smoke impacts on concentrations, and all non-exceeding sites are black. The gray shaded areas represent July 20-22, 2021.

The ratio of OC to EC taken at the JLG Supersite monitor was examined for evidence that wildfire smoke entered the nonattainment area. Increases in this ratio are indicative of wildfire smoke. **Figure 2-94** shows boxplots of OC to EC ratios for available data collected during the ozone season between 2019-2024. The OC to EC ratios on July 21 were elevated nearly to 75th percentile compared to all data. OC to EC ratios provide further evidence that ground-level wildfire smoke entered Phoenix during the July 20-22, 2021, atypical ozone event.

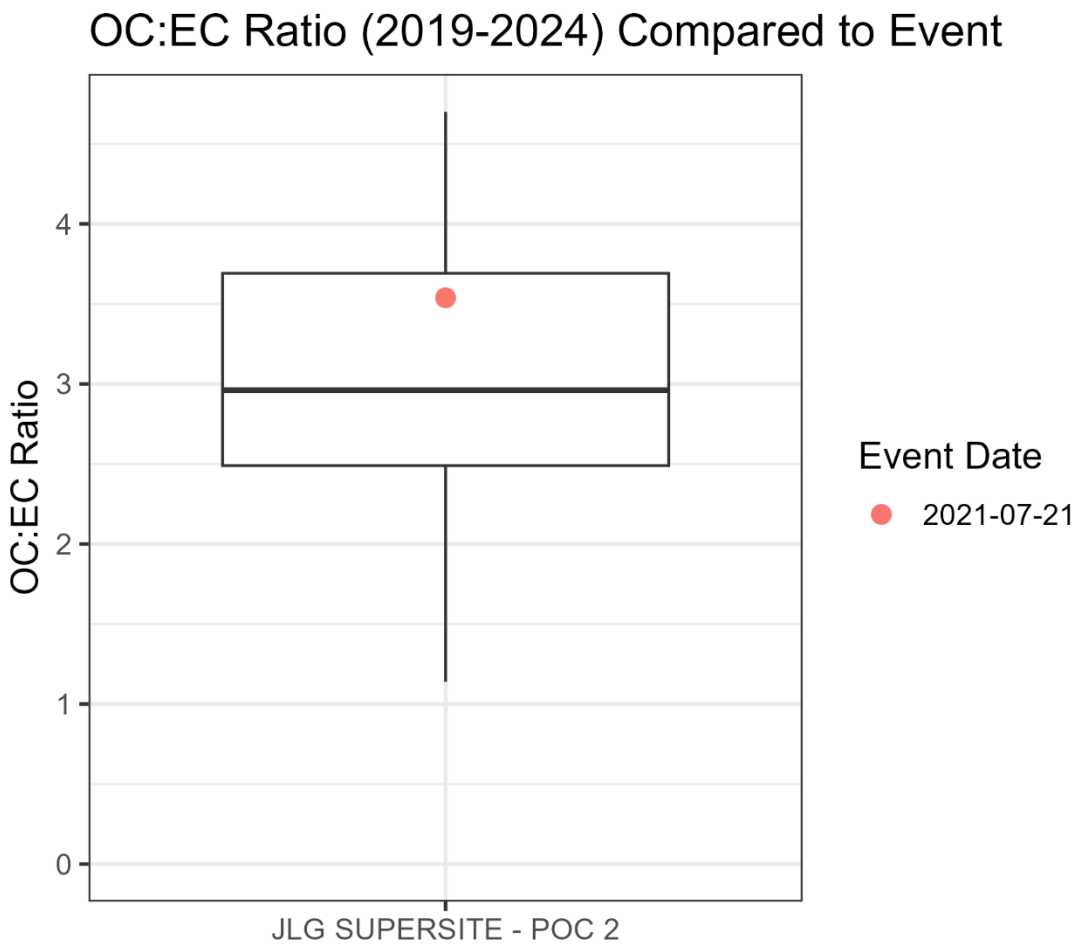

Figure 2-94. Boxplot of OC to EC ratios at the JLG Supersite site using data collected during the ozone season (April-September) from 2019-2024. OC to EC ratios are calculated at POC 2 (x-axis). Available OC to EC ratios collected during the July 20-22 atypical ozone event is shown as a point.

2.5.5 Event Statistics

Table 2-12 summarizes the measurements of ozone concentrations on July 20-22, 2021, as well as the percentile rank of the observation compared to six years of ozone season data (April 1-September 31, 2019-2024). Ozone MDA8 measurements ranged from the 93rd - 99th percentile on July 20-22, 2021.

Table 2-12. Percentile of ozone measurements on the atypical dates compared with six years of ozone data (2019-2024). The percentile rank is calculated across the ozone production season in the nonattainment area (April 1-September 31) of 2019-2024.

Date	Site Name	Site Code	Ozone MDA8 (ppb)	Percentile Rank
7/20/2021	Mesa	040131003	71	93
	Falcon Field	040131010	71	93
	Pinnacle Peak	040132005	72	94
	West Phoenix	040130019	73	95
	Senior Center Air Monitoring Station	040137020	73	95
	High School Air Monitoring Station	040137024	73	95
	South Scottsdale	040133003	78	98
	JLG Supersite	040139997	78	98
	North Phoenix	040131004	80	99
7/21/2021	Tonto NM	040070010	71	93
	South Scottsdale	040133003	72	94
	Fountain Hills	040139704	72	94
	JLG Supersite	040139997	72	94
	Cave Creek	040134008	73	95
	North Phoenix	040131004	74	96
	Pinnacle Peak	040132005	74	96
	Glendale	040132001	76	97
	Dysart	040134010	78	98

Date	Site Name	Site Code	Ozone MDA8 (ppb)	Percentile Rank
7/22/2021	Central Phoenix	040133002	71	93
	North Phoenix	040131004	74	96
	Tempe	040134005	74	96
	Cave Creek	040134008	74	96
	High School Air Monitoring Station	040137024	74	96
	Queen Valley	040218001	74	96
	Blue Point-Sheriff Station-Tonto NF-Salt River Recreation Area	040139702	75	96
	Mesa	040131003	76	97
	A J Maintenance Yard	040213001	76	97
	Pinnacle Peak	040132005	77	97
	Senior Center Air Monitoring Station	040137020	78	98
	Fountain Hills	040139704	78	98
	South Scottsdale	040133003	80	99
	Lehi Air Monitoring Station	040137022	80	99
	Tonto NM	040070010	81	99
	Falcon Field	040131010	82	99

2.5.6 Conclusion

The concurrence of HMS smoke perimeters over the nonattainment area, HYSPLIT trajectories and meteorological analysis showing accumulation of smoke in the nonattainment area, visible smoke in camera images and video news coverage, elevated OC to EC ratios, and remote sensing imagery, provide evidence that surface-level smoke was present during the period. Long-range transport of smoke from large fires in the northwestern U.S. and Canada, enhanced ozone concentrations outside of the typical diurnal profile, keeping ozone values high and affecting the MDA8 ozone concentrations at twenty sites. Multiple analyses showed that smoke fully encompassed the Maricopa Nonattainment Area on July 20-22, 2021, and statistics show ozone concentrations were atypical during this event.

This combined evidence indicates that smoke plumes generated by numerous fires in the northwestern U.S. and Canada provided an atypical source of ozone and ozone precursors that

caused enhanced ozone concentrations July 20-22, 2021. Removal of these days as atypical events is supported by this analysis.

2.6 August 3-4, 2021

2.6.1 Event Overview: August 3-4, 2021

The unrepresentative (atypical) ozone event took place on August 3-4, 2021, and affected eighteen sites in the Maricopa Nonattainment Area: West Phoenix, Mesa, North Phoenix, Falcon Field, Glendale, Pinnacle Peak, Central Phoenix, South Scottsdale, South Phoenix, West Chandler, Tempe, Cave Creek, Dysart, Buckeye, Senior Center Air Monitoring Station, Red Mountain Air Monitoring Station, Lehi Air Monitoring Station, and JLG Supersite (**Table 2-13**). MDA8 ozone concentrations at the affected sites ranged from 71-84 ppb.

Time series graphs showing hourly ozone concentrations that exceeded the seasonal means (calculated using all available data from April 1 – September 31, 2019-2024) and 10th-90th percentiles at each site are shown in **Figure 2-95.** On August 3, hourly ozone measurements at many sites, such as Mesa, Pinnacle Peak, South Phoenix, and South Scottsdale, were above the 90th percentile during the early morning hours on August 3. Measurements decreased to local minimums by 06:00 LST, then rapidly increased throughout the day and continued to exceed the 90th percentile at most sites throughout the day on August 3, indicating the influence of transported ozone and ozone precursors from wildfires. Ozone concentrations generally returned to normal during the evening and early morning hours of August 3 and 4, respectively, then increased again during the afternoon on August 4 to above the 90th percentile.

Major wildfires burning throughout the northwestern U.S. and in western Canada were identified as major contributors to this event. Evidence includes (1) HMS smoke perimeters over the nonattainment area, (2) HYSPLIT trajectories and meteorological analysis showing accumulation of smoke in Phoenix, (3) visible smoke in camera images and video news coverage, and (4) elevated NO_2 and $PM_{2.5}$ concentrations and OC to EC ratios. This combination of evidence indicates that this is an atypical ozone event.

Table 2-13. Summary of identified atypical August 3-4, 2021.

Event Date(s)	Event Ozone Concentration Percentile	Sites Exceeded During Event	Type of Event
August 3-4, 2021	95th - 99th	Eighteen sites: West Phoenix, Mesa, North Phoenix, Falcon Field, Glendale, Pinnacle Peak, Central Phoenix, South Scottsdale, South Phoenix, West Chandler, Tempe, Cave Creek, Dysart, Buckeye, Senior Center Air Monitoring Station, Red Mountain Air Monitoring Station, Lehi Air Monitoring Station, JLG Supersite	International/long-range transport

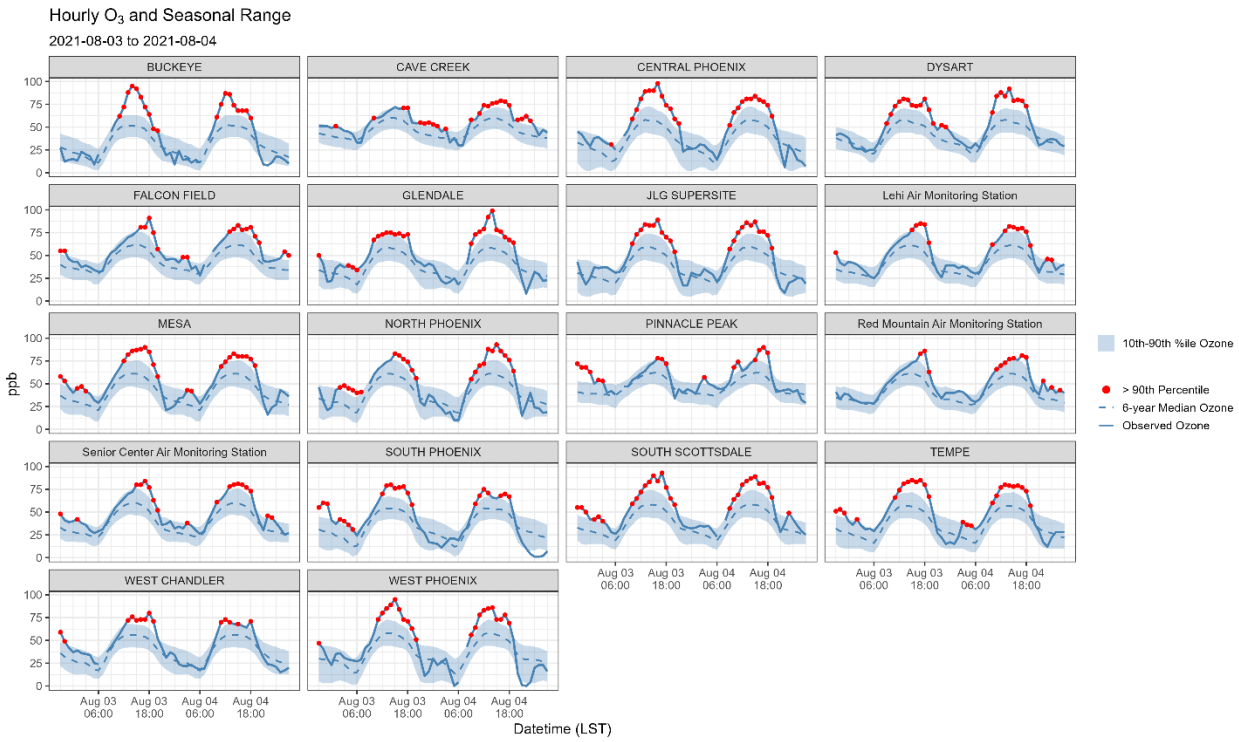

Figure 2-95. Hourly ozone concentrations (ppb) compared to all available data during the ozone season (April 1 – September 31) of the 6-year (2019-2024) period. Hourly means and 10th-90th percentiles are calculated using data on August 3-4, 2021.

2.6.2 Identification of Wildfire(s)

Multiple large fires in the northwestern U.S. and in Canada were active in the days leading up to and during August 3-4, the exclusion days (**Figures 2-96 to 2-98**). Smoke from these fires combined to blanket the continental U.S. during August 3-4 including the nonattainment area. The continental

view of HMS smoke density and fire locations is shown to illustrate the widespread nature of the smoke impacts across the country.

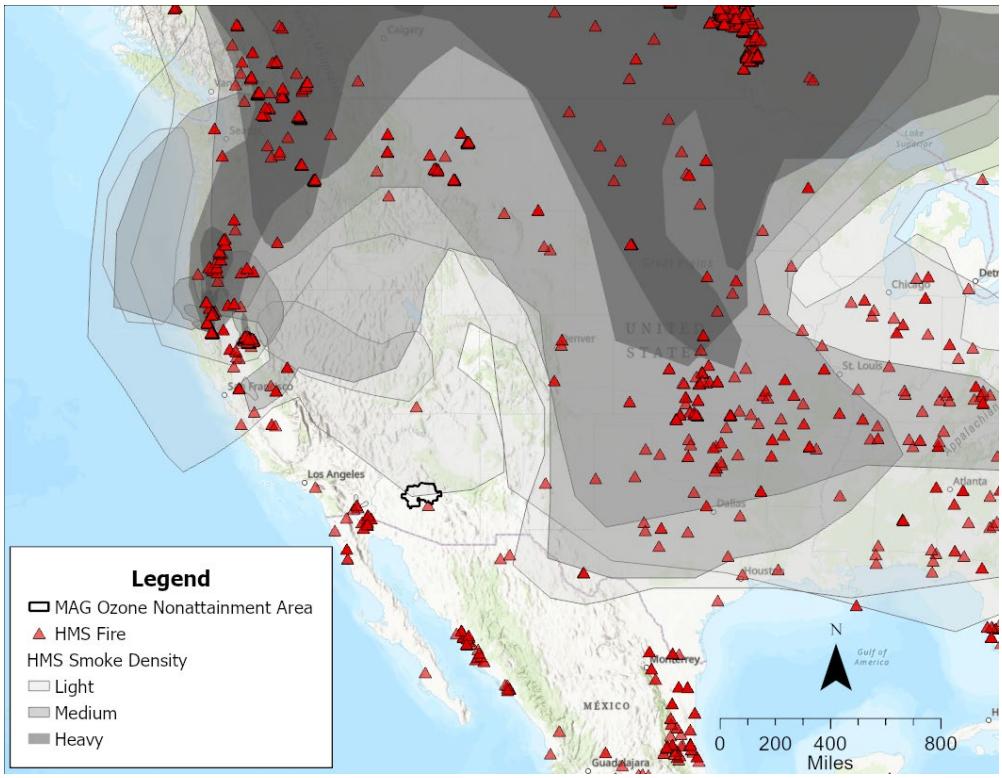

Figure 2-96. Continental view of HMS smoke density and fire locations on August 2, 2021.

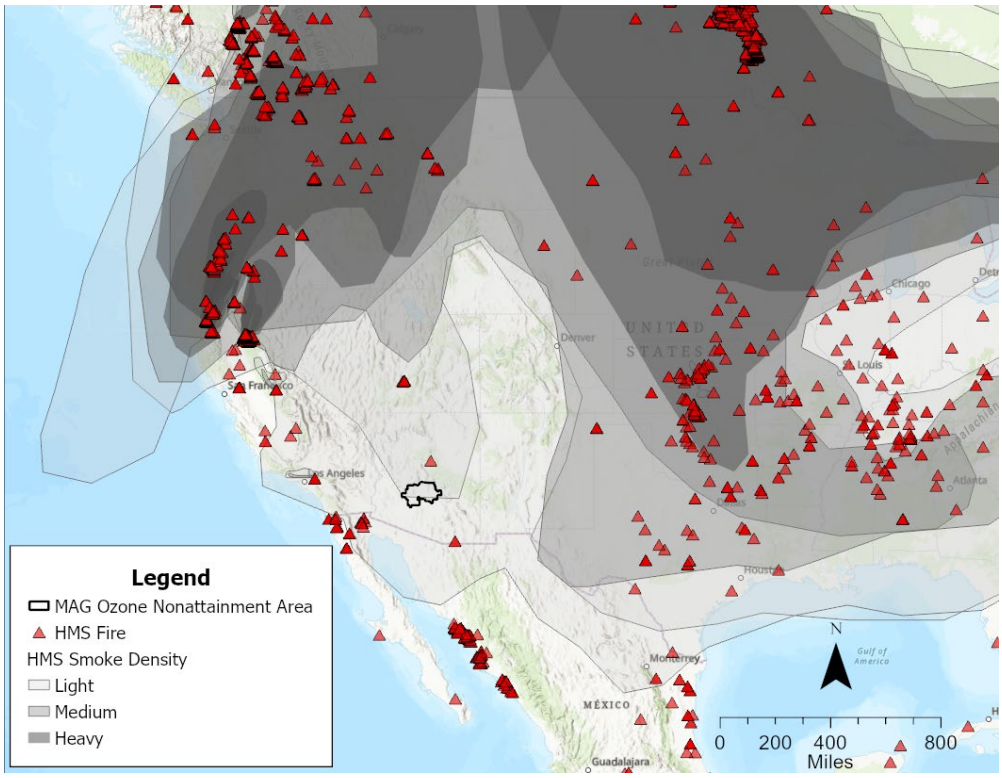

Figure 2-97. Continental view of HMS smoke density and fire locations on August 3, 2021.

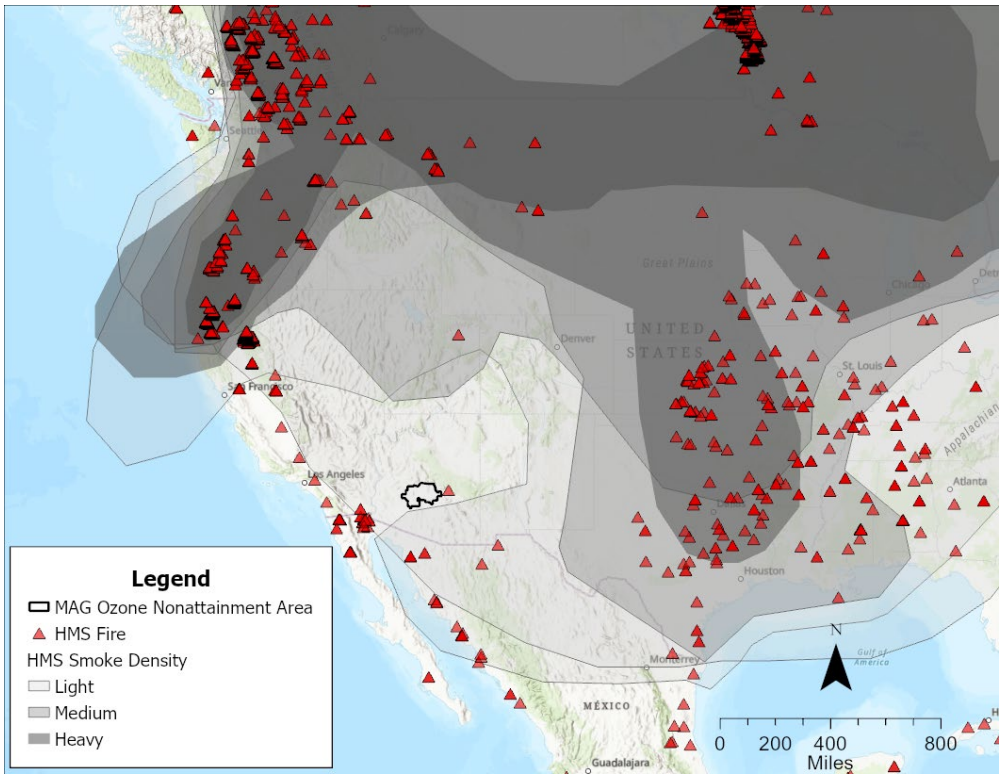

Figure 2-98. Continental view of HMS smoke density and fire locations on August 4, 2021.

2.6.3 Meteorological Analysis

Upper-level Analysis

The contour plot of average geopotential height at 500 mb (approximately 18,000 feet) from August 3 and August 4, 2021, in **Figure 2-99** shows a ridge of high pressure aloft centered over southern Nevada. The red colors near Phoenix indicate 500 mb heights above 5950 meters, which is above normal for this time of year. The ridge of high pressure aloft led to sunny skies and hot temperatures, aiding ozone formation each day.

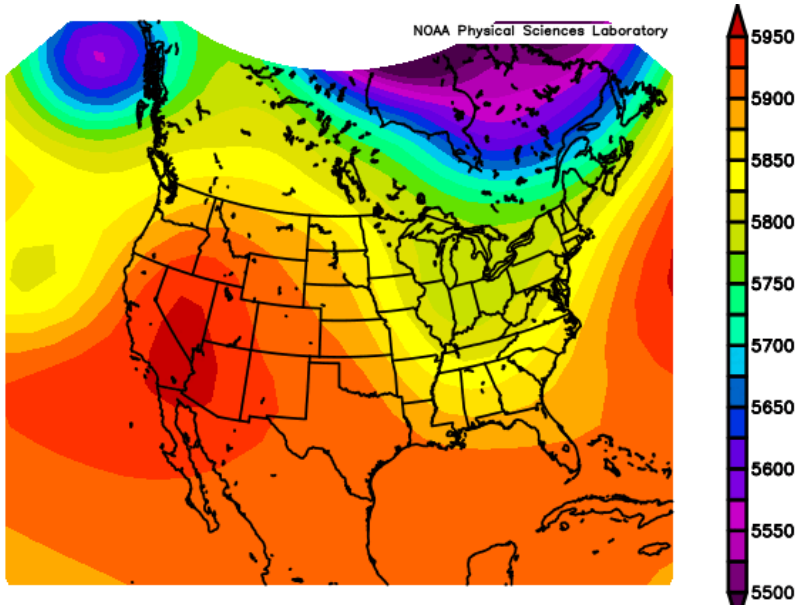

Figure 2-99. Average geopotential height at 500 mb from August 3 through 4, 2021.

Surface Analysis

Figure 2-100 shows a weak trough of surface low pressure across central Arizona on these days, as hot temperatures led to rising thermals over the Desert Southwest.

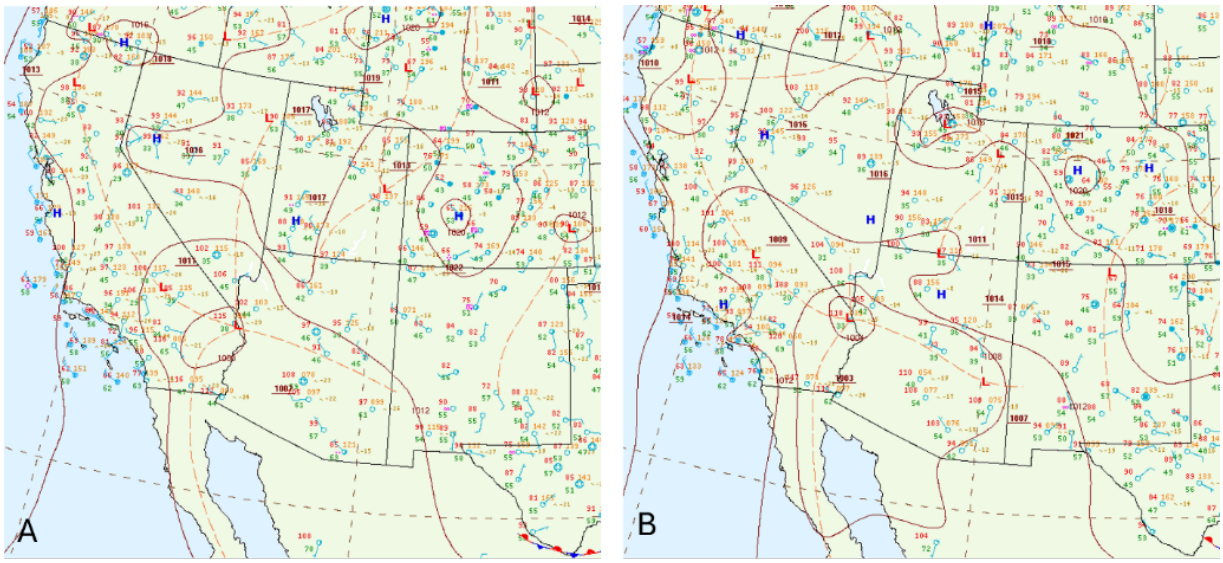

Figure 2-100. Surface analysis from 2 p.m. MST August 3, 2021 (A) and 2 p.m. MST 8/4/21 (B).

In addition, a weak pressure gradient over Phoenix led to periods of light winds and limited dispersion. Surface weather observations in Table 2-14 show that the above-normal heights at 500 mb coincided with hot surface temperatures, with highs of 112˚ F and 115˚ F aiding ozone formation. Furthermore, wind speeds averaged 6 mph both days, hindering dispersion.

Table 2-14. Surface weather variables observed at Phoenix Sky Harbor Airport.

Date	High Temp. (F)	Avg. WS (mph)	Avg. WD
8/3/2021	112	6	144
8/4/2021	115	6	109

Satellite Smoke and Fire Detections

Sunny skies allowed satellites to detect smoke over portions of Arizona each day of this event (Figure 2-101), with smoke detected directly over Phoenix on both August 3 and August 4. Thin regional haze is difficult to discern in Figures 2-102 through 2-103 due to the high sun angle when the images were taken.

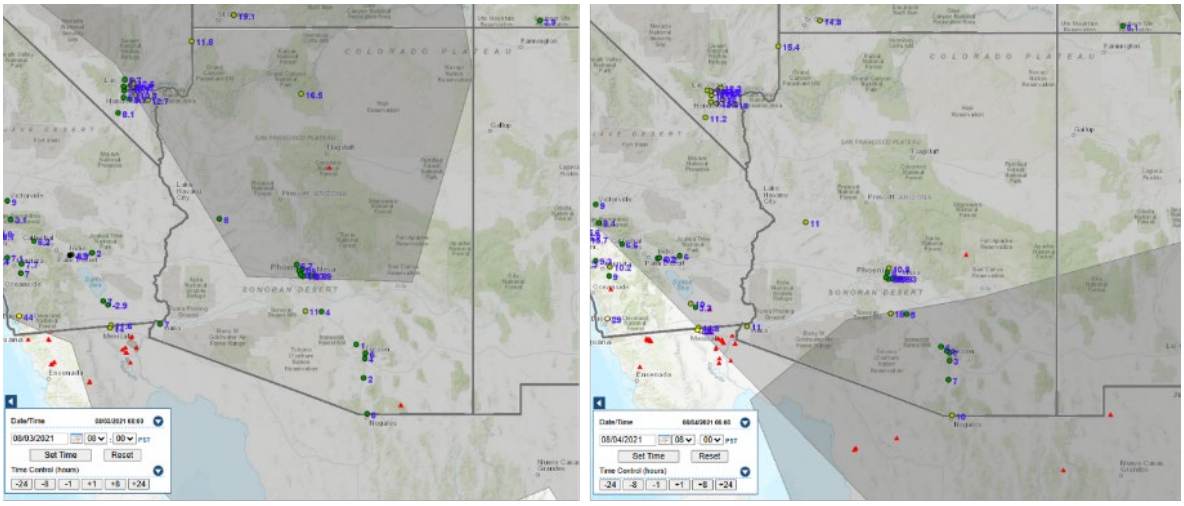

Figure 2-101. HMS fire and smoke along with hourly concentrations of $PM_{2.5}$ at 8:00 a.m. MST each day for August 3 and August 4, 2021.

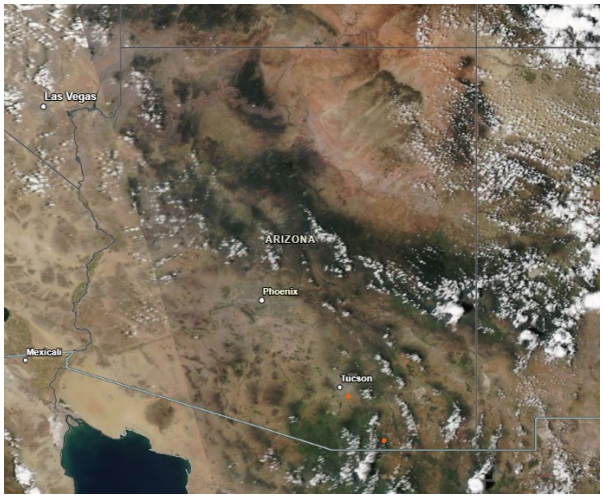

Figure 2-102. Visible satellite imagery from approximately 12:58 p.m. MST on August 3, 2021.

Figure 2-103. Visible satellite imagery from approximately 1:40 p.m. MST on August 4, 2021.

Smoke Discussions

NOAA's daily smoke discussion from August 3 notes a large area of smoke impacting much of the Continental United States.

"Continued wildfire activity across the western United States, western Canada and central Canada was producing a tremendous area **of smoke that was extending over most of the United States**, central and western Canada and into Alaska." (NOAA NESDIS Text Narrative, August 3, 2021)

Soundings

Weak to moderate strength temperature inversions were observed each morning during this event (left panels of **Figure 2-104**), limiting low-level mixing. Mixing improved each afternoon (right panels of Figure 2-104). Mixing heights on August 3 reached 700 mb (2.6 km) and on August 4 they reached 600 mb (3.8 km) as surface temperatures rose above 110 ˚F. With satellite observed smoke over Phoenix on each of these days, the deep mixing likely aided transport of aloft smoke to the surface.

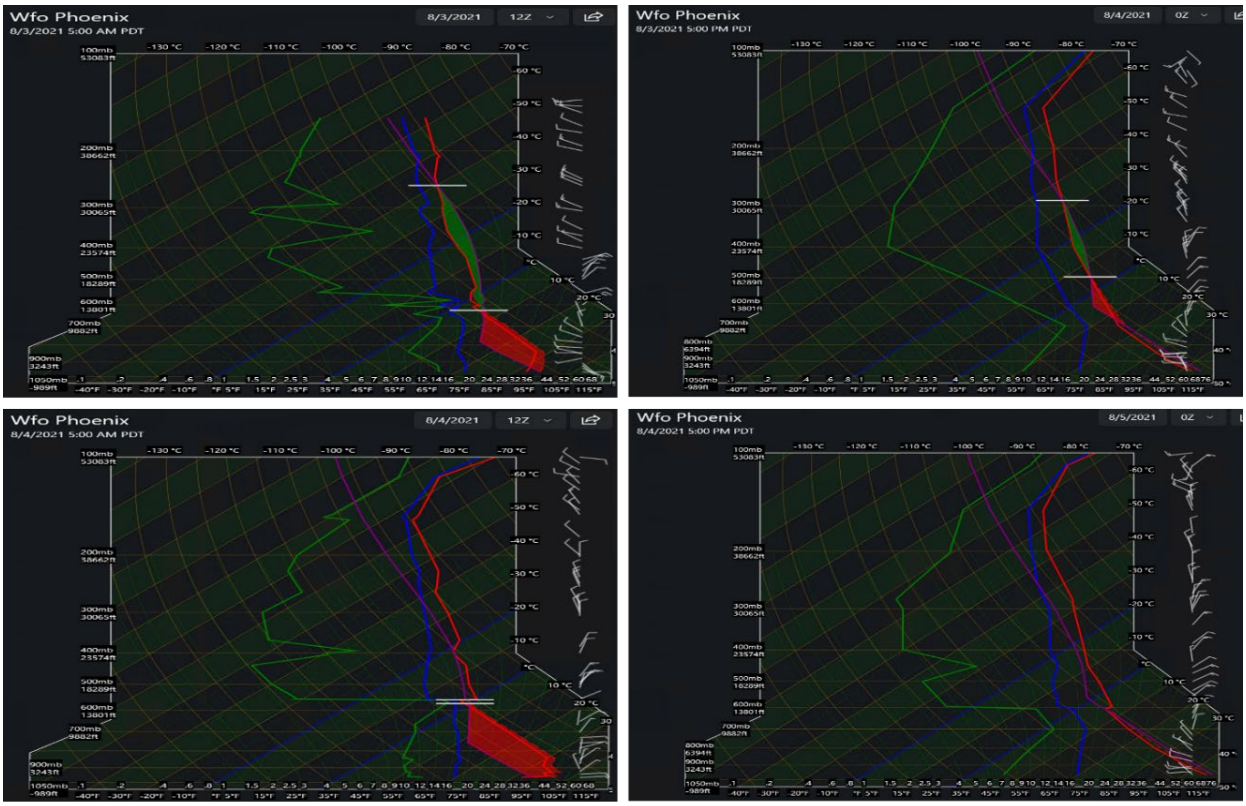

Figure 2-104. Observed atmospheric soundings from 5 a.m. MST (left) and 5 p.m. MST (right) August 3 through August 4, 2021.

Smoke Transport

Output from NOAA's HYSPLIT model also shows the potential for the transport of regional smoke into the nonattainment area. The images in **Figure 2-105** show 48-hour back trajectories from 12:00 a.m. to 8:00 p.m. MST on August 3 at 100 meters, 1,000 meters, and 2,500 meters above ground level (AGL). These trajectories show that aloft winds within the boundary layer originated from areas impacted by light-to-medium density smoke from fires in the western United States and Canada, likely enhancing ozone formation in the nonattainment area.

Summary

For August 3-4, 2021 a strong ridge of high pressure aloft centered over southern Nevada produced sunny skies and hot temperatures across Arizona. As evidenced by observed soundings from Phoenix, the hot temperatures led to deep atmospheric mixing each afternoon. This deep mixing coincided with plumes of light-to-medium HMS smoke perimeters over south-central Arizona, showing the potential for aloft smoke to mix to the surface. In addition, HYSPLIT back trajectories for this period originated from an area of light-to-medium density smoke generated from fires in the western U.S. and Canada. Furthermore, a weak pressure gradient led to light surface winds each day,

limiting dispersion of the smoke. As a result, there is evidence that smoke enhanced ozone formation in the nonattainment area August 3-4, 2021.

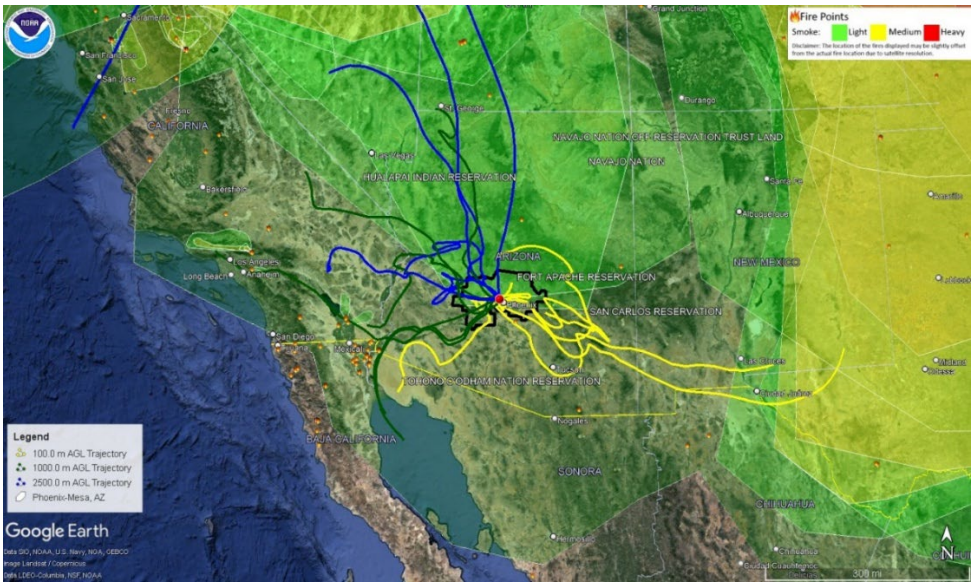

Figure 2-105. NOAA smoke and fire maps and NOAA HYSPLIT trajectory model runs from the JLG Supersite ozone monitor, with air parcels moving 48-hours before 12:00 am - 8:00 pm MST on August 3 at 100 meters, 1,000 meters, and 2,500 meters (AGL). Analyses performed by MAG.

2.6.4 Surface Impacts

Smoke plumes from fires burning in the northwestern U.S. and in Canada spread over Phoenix in the days leading up to August 3-4, 2021. **Figure 2-106 through 2-111** show photos taken from the southwest-facing Estrella Mountain, south-facing South Mountain, and east-facing Superstition Mountain webcams, where the smoke is visible throughout the day on August 3-4, 2021. Smoke from the fires burning in the northwestern U.S. and in Canada, was noted on August 3, 2021, by local meteorologist Matt Pace (**Figure 2-112**).

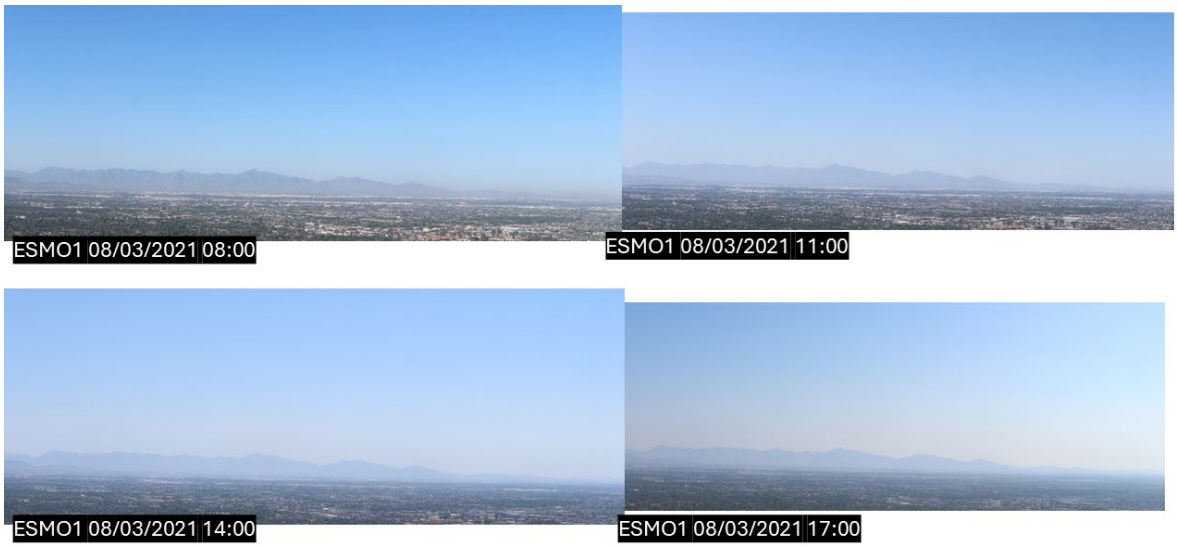

Figure 2-106. Camera Images showing the southwest coordinal direction taken from the Estrella Mountain webcam on August 3 from 8:00 LST, 11:00 LST, 14:00 LST, and 17:00.

Figure 2-107. Camera Images showing the southwest coordinal direction taken from the Estrella Mountain webcam on August 4 from 8:00 LST, 11:00 LST, 14:00 LST, and 17:00

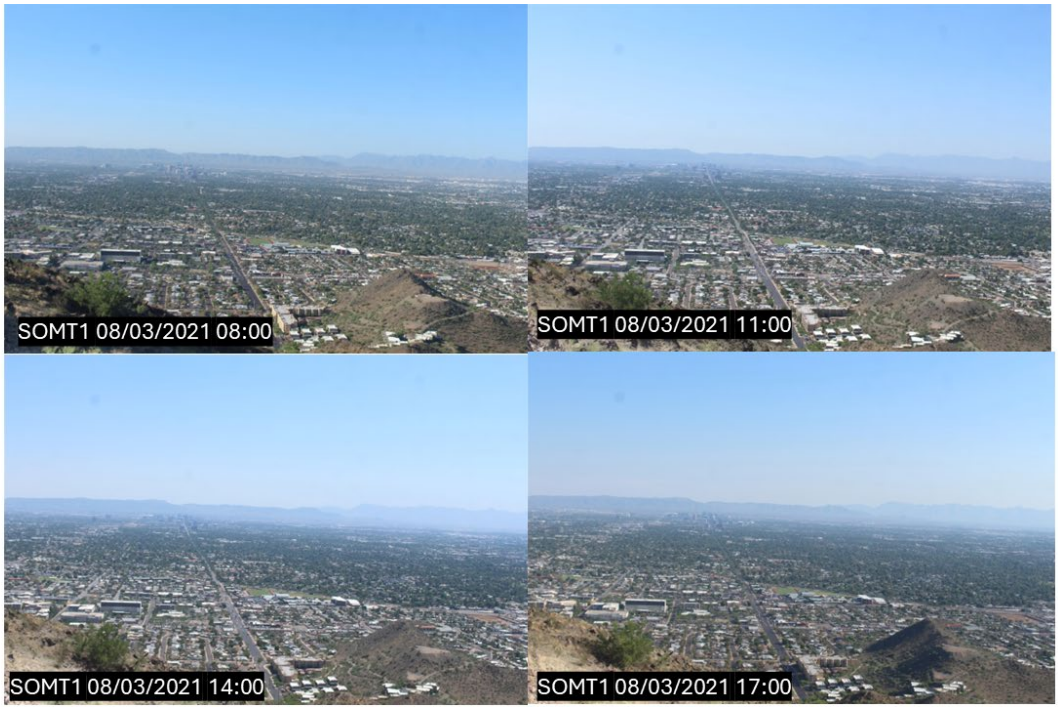

Figure 2-108. Camera Images showing the south coordinal direction taken from the South Mountain webcam on August 3 from 8:00 LST, 11:00 LST, 14:00 LST, and 17:00.

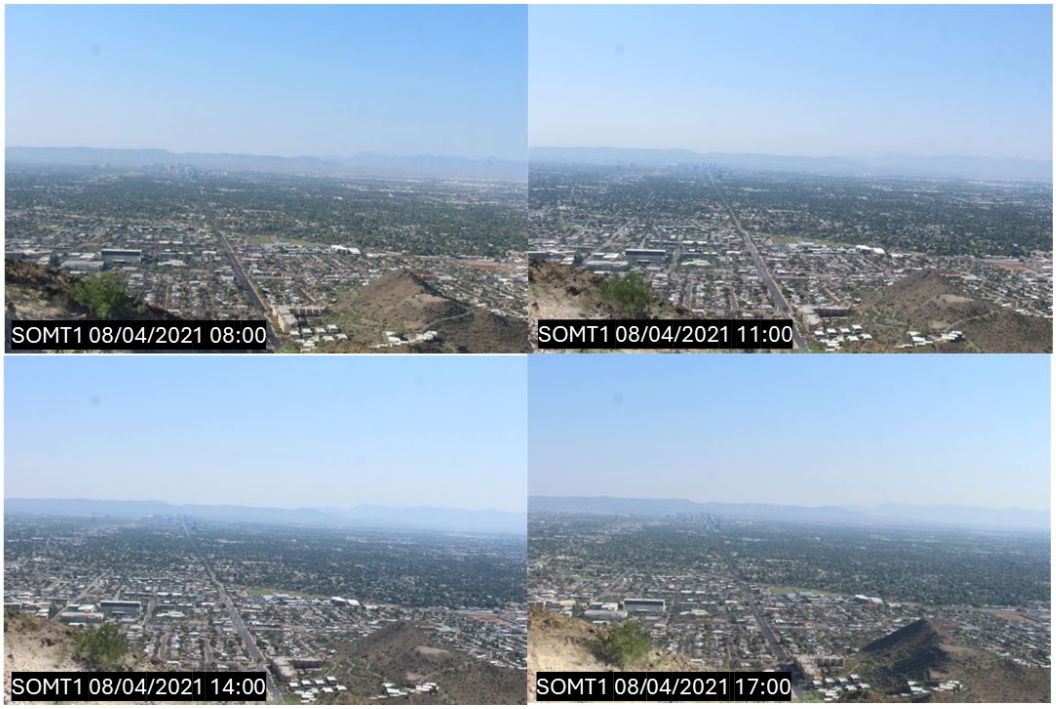

Figure 2-109. Camera Images showing the south coordinal direction taken from the South Mountain webcam on August 4 from 8:00 LST, 11:00 LST, 14:00 LST, and 17:00.

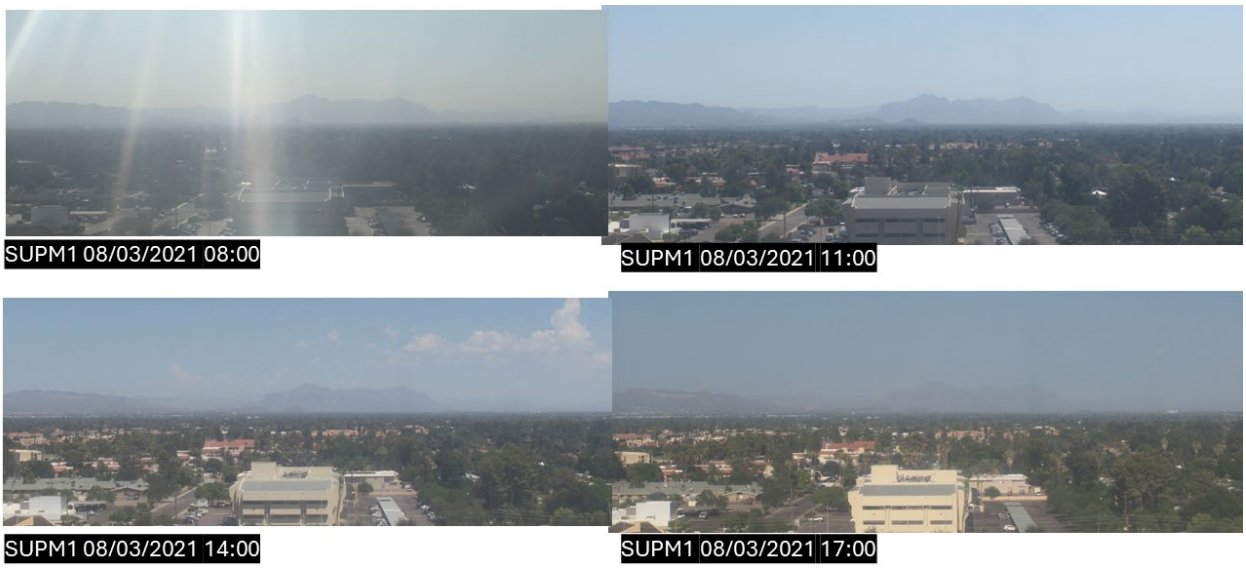

Figure 2-110. Camera Images showing the east coordinal direction taken from the Superstition Mountain webcam on August 3 from 8:00 LST, 11:00 LST, 14:00 LST, and 17:00.

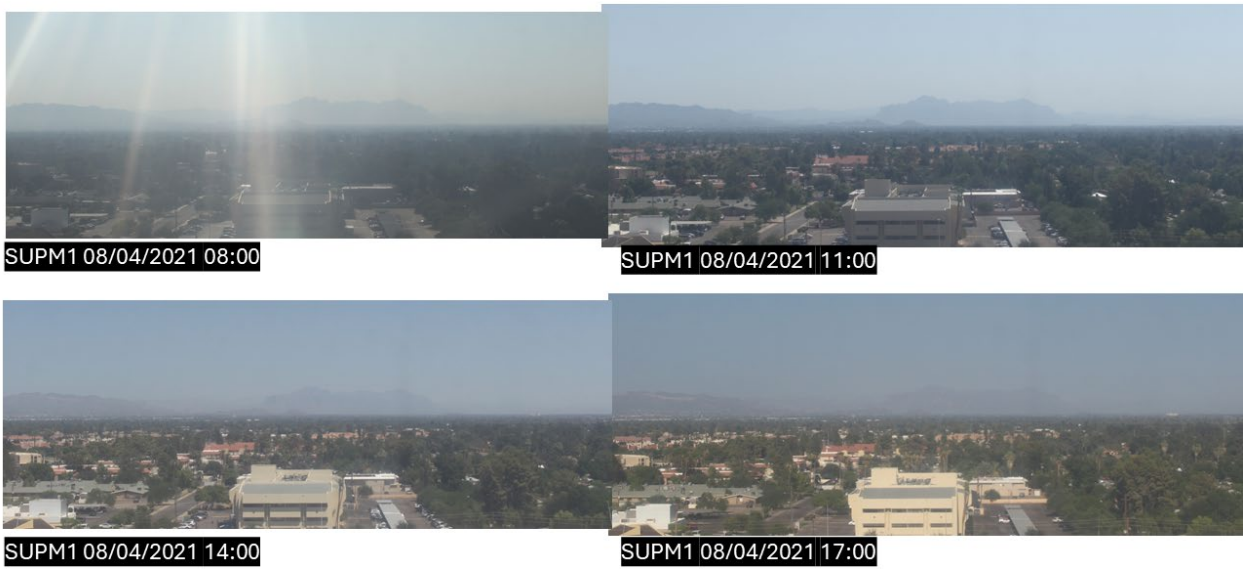

Figure 2-111. Camera Images showing the east coordinal direction taken from the Superstition Mountain webcam on August 4 from 8:00 LST, 11:00 LST, 14:00 LST, and 17:00.

Figure 2-112. Social media post regarding smoke from the fires in the northwestern U.S. moving over Arizona on August 3, 2021.

Figure 2-113 shows an overall view of the magnitude of hourly pollutant concentrations measured in the nonattainment area in the two days before and after the August 3-4, 2021, atypical events. Hourly concentrations of ozone show a widespread and distinct peak on August 3-4 at all affected sites relative to the days before the atypical event. Peak NO_2 concentrations were also elevated on August 3-4 relative to the surrounding two days, including a prominent secondary peak in the early morning hours on August 4. $PM_{2.5}$ concentrations at the exceedance-affected sites rise gradually at all $PM_{2.5}$-measuring sites throughout the day on August 3. $PM_{2.5}$ concentrations at all sites remain slightly elevated into the early hours of August 4. Elevated $PM_{2.5}$ concentrations were likely not from dust because conditions were not favorable (i.e., wind speeds were generally low) for wind-blown dust before and during the June 15-16 atypical event. Furthermore, there were no dust storm advisories or warnings before or during this atypical event.[8] Widespread enhancements in surface pollutant concentrations provide evidence that smoke from regional fires entered the region, mixed towards the surface, and had an atypical influence on ozone during the period. The rest of this section examines temporal abnormalities and site-specific trends for each supporting pollutant.

[8] https://mesonet.agron.iastate.edu/vtec/search.php?mode=bypoint&lon=-112.1202&lat=33.4223&buffer=0.00&sdate1=2021-06-12&edate1=2021-08-04

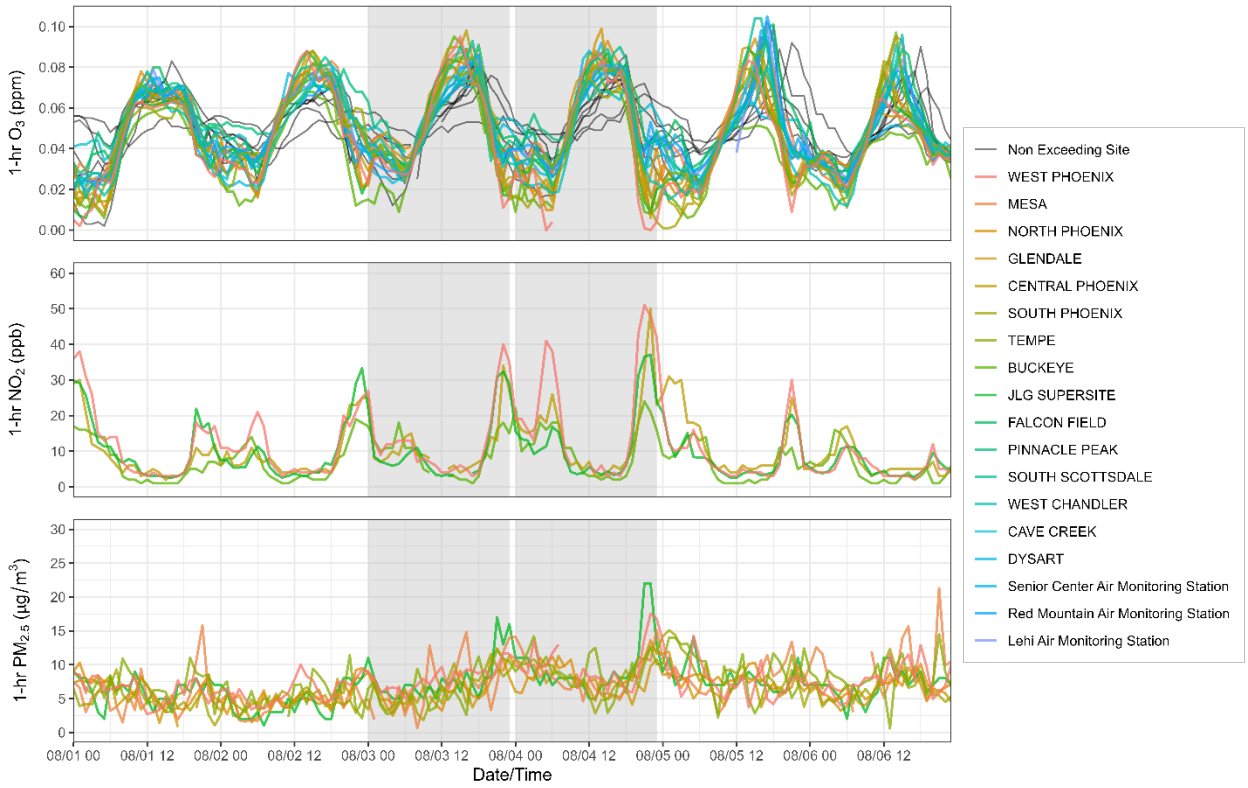

Figure 2-113. Hourly concentrations of ozone, NO_2, and $PM_{2.5}$ at all sites in the nonattainment area. All ozone-exceeding sites are color-coded to highlight smoke impacts on concentrations, and all non-exceeding sites are black. The gray shaded areas represent August 3-4, 2021.

$PM_{2.5}$ and NO_2 concentrations were enhanced in the nonattainment area on August 3-4 as emissions from the fires in the northwestern U.S. and Canada entered the region and mixed towards the surface, which provides further evidence that wildfire smoke was present as an atypical influence on ozone during the period. Figure 2-114 shows hourly $PM_{2.5}$ concentrations at the Mesa site (one of the affected sites) overlaid on the 5th-95th percentile hourly concentrations during ozone season (April to September), calculated using all available data from 2019-2024. $PM_{2.5}$ concentrations rose after 6:00 LST on August 3 into the afternoon and exceeded the 95th percentile during some hours. Typically, $PM_{2.5}$ concentrations decrease during the day as the boundary layer expands due to daytime heating and dilutes pollutants in the lower atmosphere. $PM_{2.5}$ concentrations at the Mesa site remain elevated above the statistical median over the remainder of the period. Similarly, NO_2 concentrations at the West Phoenix site increased to nearly the 95th percentile around 00:00 LST on August 4, then exceeded the 95th percentile around 5:00-6:00 LST and again after 18:00 LST the same day. A similar pattern in NO_2 concentrations is present at the Central Phoenix, Buckeye, and JLG Supersite sites, providing evidence that the smoke impacts were widespread and affected multiple air monitoring sites.

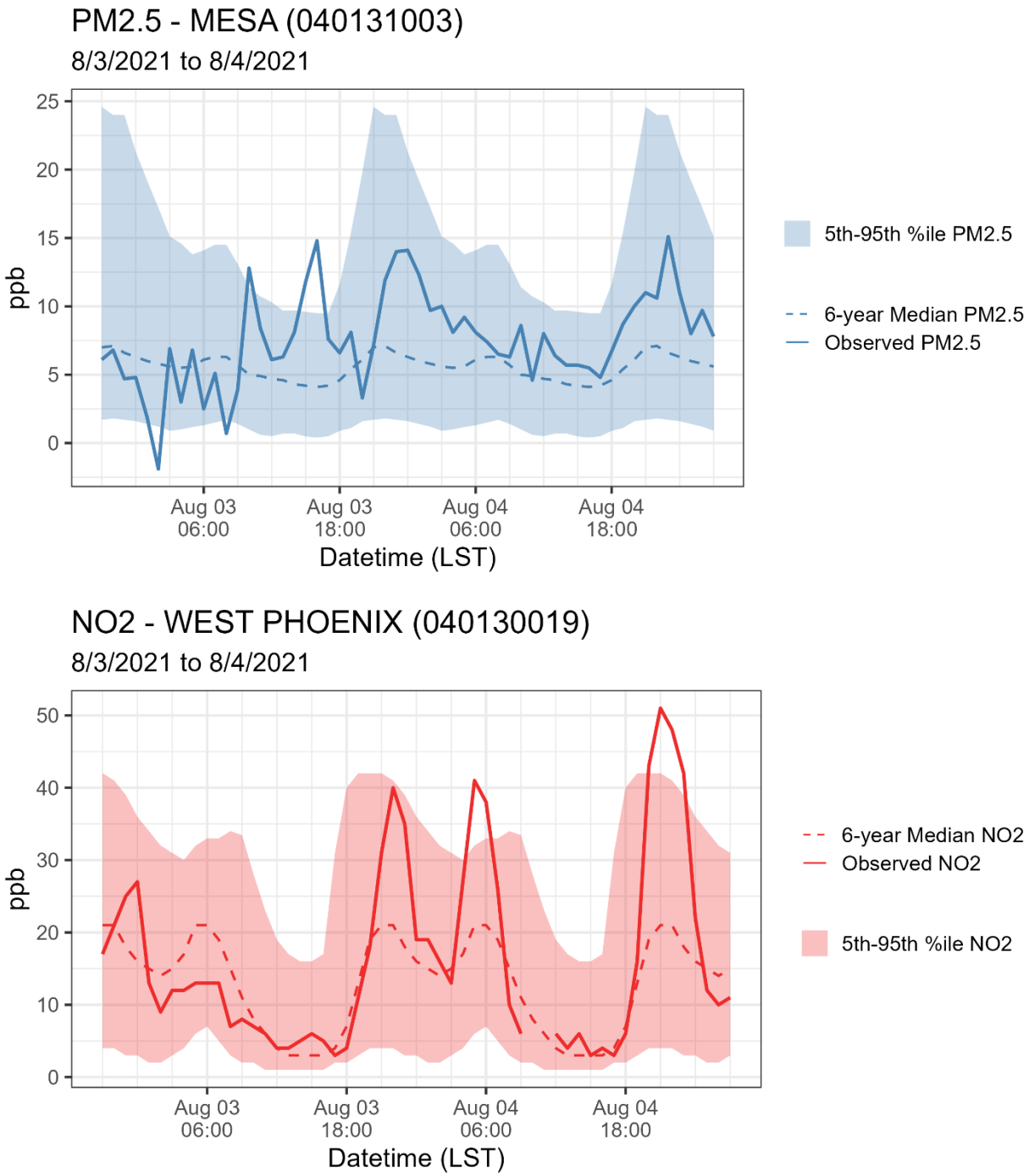

Figure 2-114. Hourly concentrations of $PM_{2.5}$ at the Mesa (top) and NO_2 at the North Phoenix (bottom) sites. The 6-year (2019-2024) median is represented by the dashed line, and the 5th-95th percentile is represented by the shaded area.

OC and EC data were not available on August 3-4, but samples collected before and after that date show evidence of smoke impacts. The ratio of OC to EC taken at the JLG Supersite monitor was also examined for evidence that wildfire smoke entered the nonattainment area. Increases in this ratio are

indicative of wildfire smoke. Figure 2-115 shows boxplots of OC to EC ratios for available data collected during the ozone season between 2019-2024. The OC to EC ratios on August 2 and 5, one day before and after the atypical event days, respectively, was above the 75th percentile compared to all data. OC to EC ratios provide further evidence that ground-level wildfire smoke entered Phoenix during the August 3-4, 2021, atypical ozone event.

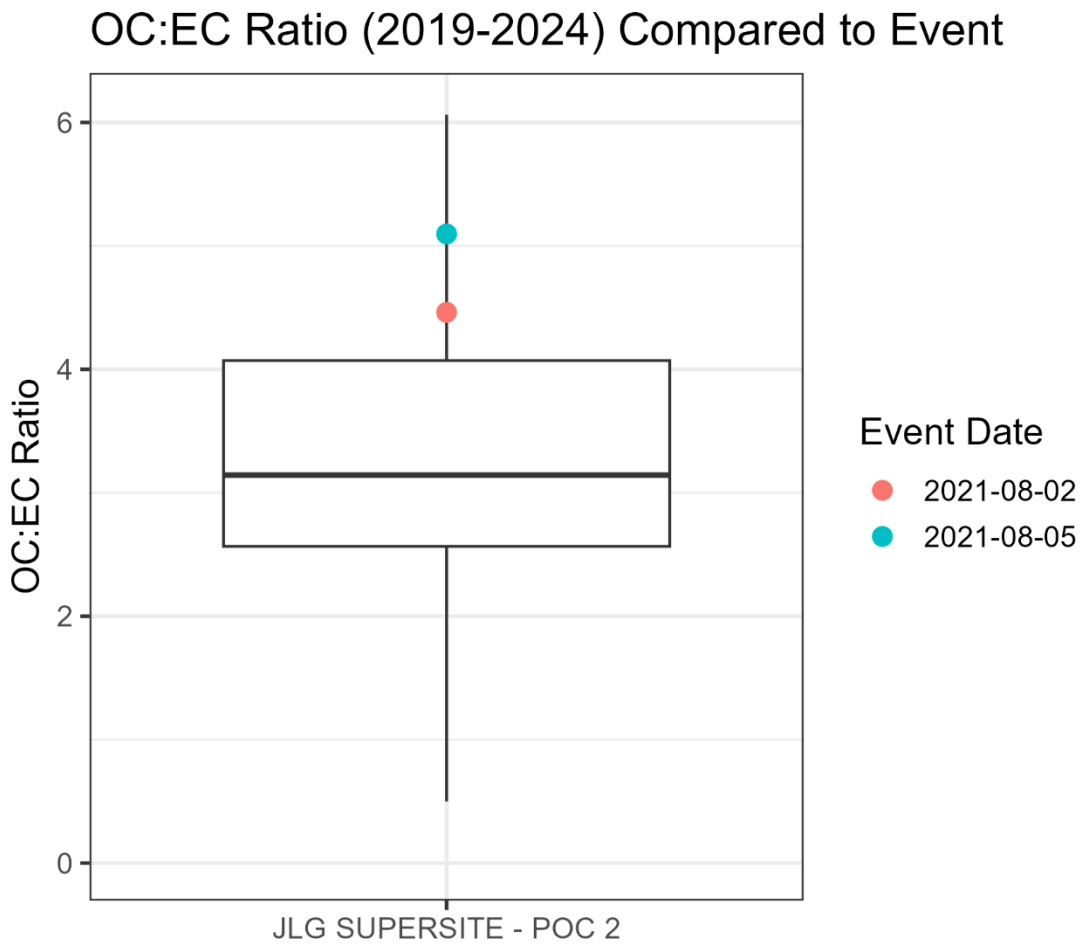

Figure 2-115. Boxplot of speciated $PM_{2.5}$ collected at the JLG Supersite site collected during the ozone season (April-September) from 2019-2024. Available speciated $PM_{2.5}$ concentrations collected during the day before and after the August 3-4 atypical event are shown as points.

2.6.5 Event Statistics

Table 2-15 summarizes the measurements of ozone concentrations on August 3-4, 2021, as well as the percentile rank of the observation compared to six years of ozone season data (April 1-September 31, 2019-2024). Ozone MDA8 measurements ranged from the 95th - 99th percentile on August 3-4, 2021.

Table 2-15. Percentile of ozone measurements on the atypical dates compared with six years of ozone data (2019-2024). The percentile rank is calculated across the ozone production season in the nonattainment area (April 1-September 31) of 2019-2024.

Date	Site Name	Site Code	Ozone MDA8 (ppb)	Percentile Rank
8/3/2021	West Phoenix	040130019	81	99
	Mesa	040131003	83	99
	North Phoenix	040131004	75	97
	Falcon Field	040131010	76	98
	Glendale	040132001	73	96
	Central Phoenix	040133002	84	99
	South Scottsdale	040133003	80	99
	South Phoenix	040134003	74	96
	West Chandler	040134004	72	95
	Tempe	040134005	79	99
	Dysart	040134010	76	98
	Buckeye	040134011	78	99
	Senior Center Air Monitoring Station	040137020	73	96
	Red Mountain Air Monitoring Station	040137021	72	95
	Lehi Air Monitoring Station	040137022	75	97
	JLG Supersite	040139997	79	99
8/4/2021	West Phoenix	040130019	78	99
	Mesa	040131003	77	98
	North Phoenix	040131004	81	99
	Falcon Field	040131010	77	98
	Glendale	040132001	80	99
	Pinnacle Peak	040132005	76	98
	Central Phoenix	040133002	78	99
	South Scottsdale	040133003	81	99
	Tempe	040134005	76	98
	Cave Creek	040134008	74	96

Date	Site Name	Site Code	Ozone MDA8 (ppb)	Percentile Rank
	Dysart	040134010	82	99
	Buckeye	040134011	73	96
	Senior Center Air Monitoring Station	040137020	75	97
	Red Mountain Air Monitoring Station	040137021	75	97
	Lehi Air Monitoring Station	040137022	76	98
	JLG Supersite	040139997	79	99

2.6.6 Conclusion

The concurrence of HMS smoke perimeters over the nonattainment area, HYSPLIT trajectories and meteorological analysis showing accumulation of smoke in the nonattainment area, visible smoke in camera images and video news coverage, and elevated hourly $PM_{2.5}$ concentrations and OC to EC ratios (before, after, and likely during the event days) provide evidence that surface-level smoke was present in the area during the period. Long-range transport of smoke from large fires in the northwestern U.S. and Canada, enhanced ozone concentrations outside of the typical diurnal profile, keeping ozone values high and affecting the MDA8 ozone concentrations at eighteen sites. Multiple analyses showed that smoke fully encompassed the Maricopa Nonattainment Area on August 3-4, 2021, and statistics show ozone concentrations were atypical during this event.

This combined evidence indicates that smoke plumes generated by numerous fires in the northwestern U.S. and Canada provided an atypical source of ozone and ozone precursors that caused enhanced ozone concentrations August 3-4, 2021. Removal of these days as atypical events is supported by this analysis.

3. 2022 Wildfire Events

3.1 Overview

This section provides evidence that ozone concentrations were atypical exceedances on several days during 2022 and that those exceedances were impacted by wildfire smoke from local wildfires and smoke transported from regional wildfires.

3.2 June 15-16, 2022

3.2.1 Event Overview: June 15-16, 2022

The unrepresentative (atypical) ozone event took place on June 15-16, 2022, and affected seventeen sites in the Maricopa Nonattainment Area: West Phoenix, Mesa, North Phoenix, Glendale, Pinnacle Peak, South Phoenix, Dysart, Senior Center Air Monitoring Station, Red Mountain Air Monitoring Station, Lehi Air Monitoring Station, High School Air Monitoring Station, Humboldt Mountain, Blue Point-Sheriff Station-Tonto NF-Salt River Recreation Area, Fountain Hills, JLG Supersite, Queen Valley, and Tonto NM (**Table 3-1**). MDA8 ozone concentrations at the affected sites ranged from 71-88 ppb.

Time series graphs showing hourly ozone concentrations that exceeded the seasonal means (calculated using all available data from April 1 – September 31, 2019-2024) and 10th-90th percentiles at each site are shown in **Figure 3-1.** On June 15, hourly ozone measurements at many sites, such as Fountain Hills, Glendale, Humboldt Mountain, and JLG Supersite, were above the 90th percentile during the late afternoon hours on June 15. The diurnal profiles of ozone concentrations at many sites exhibit a "lag" in maximum concentrations, peaking later in the afternoon compared to statistical averages. Ozone concentrations at some sites, including Fountain Hills, Humboldt Mountains, Pinnacle Peak, and others, remained elevated above the 90th percentile throughout the evening on June 15 and into June 16, indicating transport of ozone and ozone precursors from wildfires overnight. Ozone concentrations generally returned to normal during the evening hours of June 16.

Major wildfires burning in Arizona, namely the Contreras Fire to the south of Phoenix, the Fish Fire to the east of Phoenix, and multiple other large fires to the north of Phoenix, were identified as major contributors to this event. Evidence includes (1) HMS smoke perimeters over the nonattainment area, (2) HYSPLIT trajectories and meteorological analysis showing accumulation of smoke in Phoenix, (3) visible smoke in camera images and video news coverage, (4) elevated NO_2 concentrations, OC to EC ratios, and $PM_{2.5}$ species, and (5) remote sensing imagery. This combination of evidence indicates that this is an atypical ozone event.

Table 3-1. Summary of identified atypical June 15-16, 2022.

Event Date(s)	Event Ozone Concentration Percentile	Sites Exceeded During Event	Type of Event
June 15-16, 2022	92nd - 100th	Seventeen sites: West Phoenix, Mesa, North Phoenix, Glendale, Pinnacle Peak, South Phoenix, Dysart, Senior Center Air Monitoring Station, Red Mountain Air Monitoring Station, Lehi Air Monitoring Station, High School Air Monitoring Station, Humboldt Mountain, Blue Point-Sheriff Station-Tonto NF-Salt River Recreation Area, Fountain Hills, JLG Supersite, Queen Valley, Tonto NM	Regional/local transport

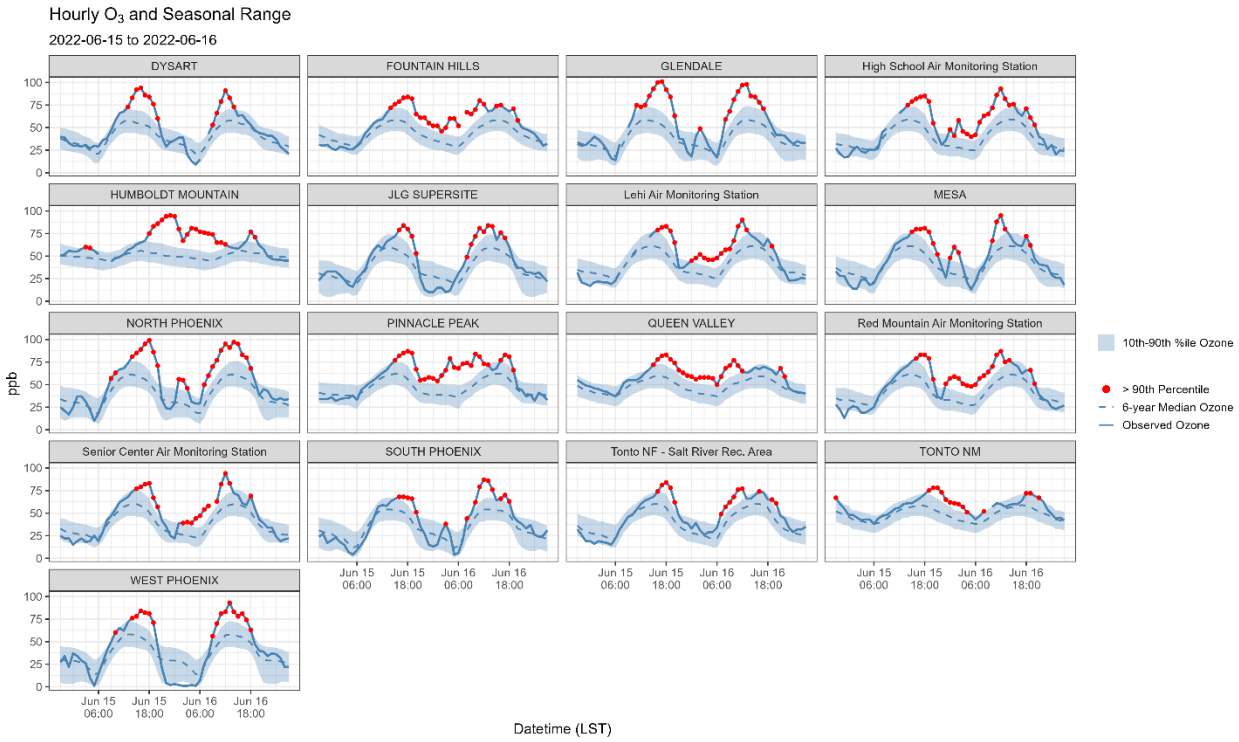

Figure 3-1. Hourly ozone concentrations (ppb) compared to all available data during the ozone season (April 1 – September 31) of the 6-year (2019-2024) period. Hourly means and 10th-90th percentiles are calculated using data on June 15-16, 2022.

3.2.2 Identification of Wildfire(s)

Several large local fires to the north, south, and east of the nonattainment area were active in the days leading up to and during June 15-16, 2022, the exclusion days. The Contreras Fire to the south of Phoenix was detected on June 11, 2022. By June 18, 2022, two to three days after the atypical event, the fire had grown to nearly 118,843 acres.[9] The Contreras Fire was contained by July 3, 2022, and had reached a size of approximately 29,500 acres, according to the WFIGS. The Fish Fire to the east of Phoenix was discovered on June 10, 2022, reached a maximum size of nearly 4,000 acres, and was contained by July 13, 2022. Multiple large fires to the north of Phoenix were in close proximity to one another, including the Haywire, Pipeline, and Slate Fires, and were active in early June. Actively burning fires in early June across Arizona caused smoke to blanket the state during the June 15-16 atypical ozone event (**Figures 3-2 and 3-3**).

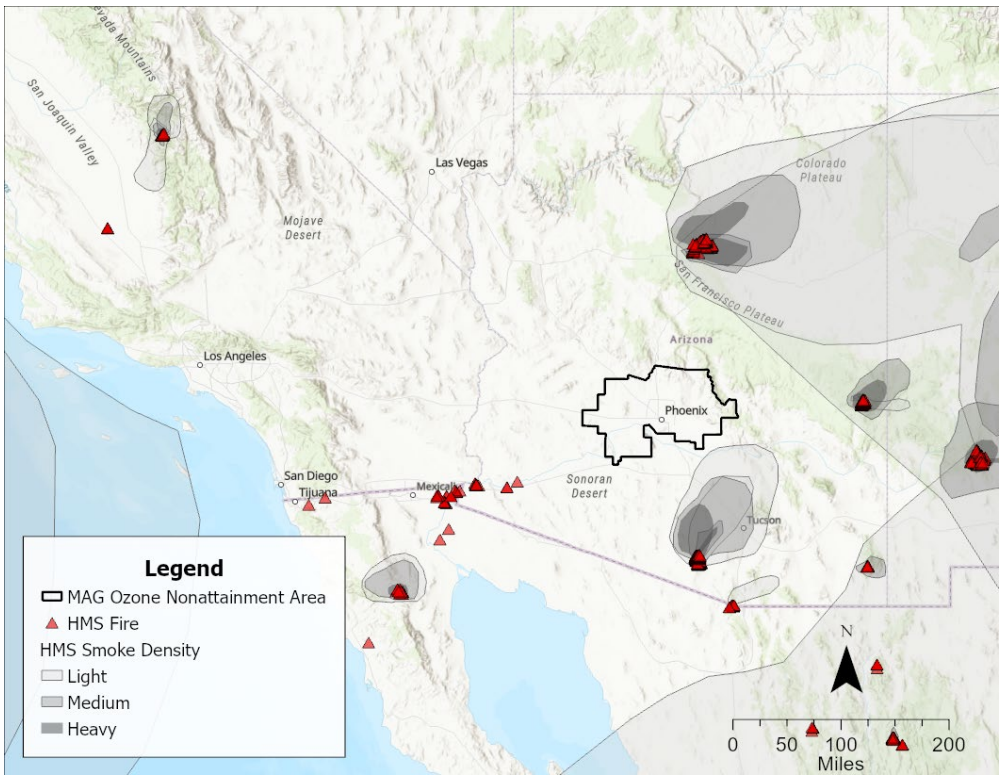

Figure 3-2. Regional view of HMS smoke density and fire locations on June 15, 2022.

[9] https://wildfiretoday.com/all-but-four-of-the-kitt-peak-observatory-structures-have-so-far-survived-the-contreras-fire/

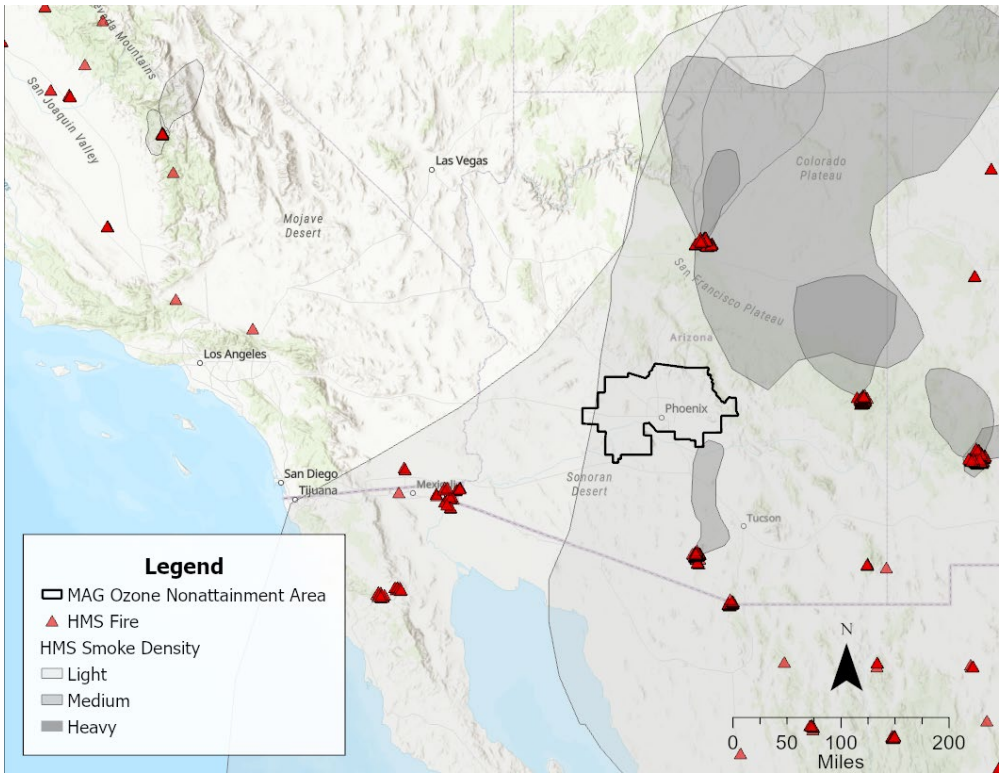

Figure 3-3. Regional view of HMS smoke density and fire locations on June 16, 2022.

3.2.3 Meteorological Analysis

Upper-level Analysis

The contour plot of average geopotential height at 500 mb (approximately 18,000 feet) from June 15 and 16, 2022 in **Figure 3-4** shows a broad ridge of high pressure stretching from the southeastern United States to northern Mexico. The orange colors over Arizona indicated 500 mb heights over 5850 meters, which is above normal for this time of year. These above-normal heights indicate warm mid-level temperatures over the Desert Southwest, along with a potential reduction in atmospheric mixing. With the ridge just south of Arizona, mostly sunny skies and hot surface temperatures were also likely enhancing ozone formation on these days.

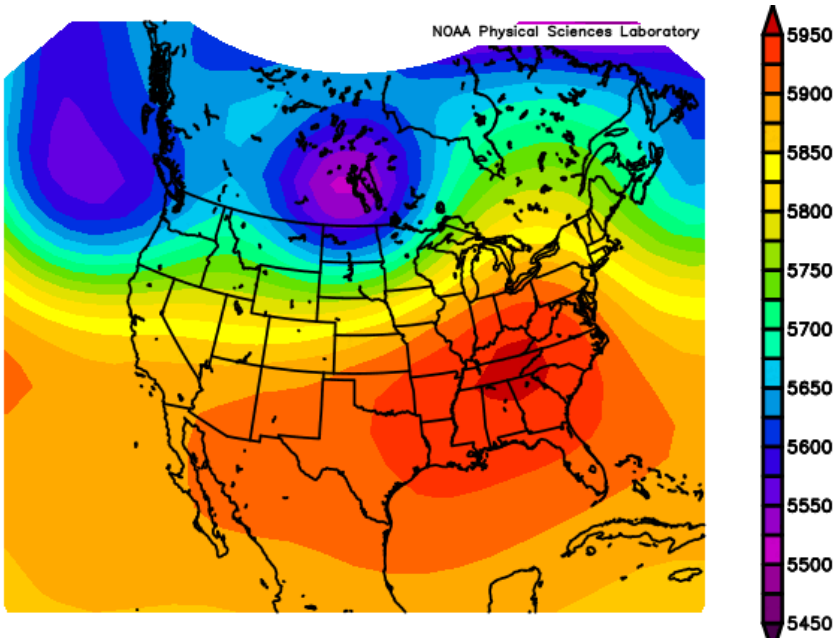

Figure 3-4. Average geopotential height at 500 mb from June 15 and 16, 2022.

Surface Analysis

Figure 3-5 shows a weak trough of surface low pressure just west of Phoenix on June 15, and near Phoenix on June 16 due to hot temperatures generating rising thermals over the Desert Southwest. A weak pressure gradient over the region also indicates the potential for light winds.

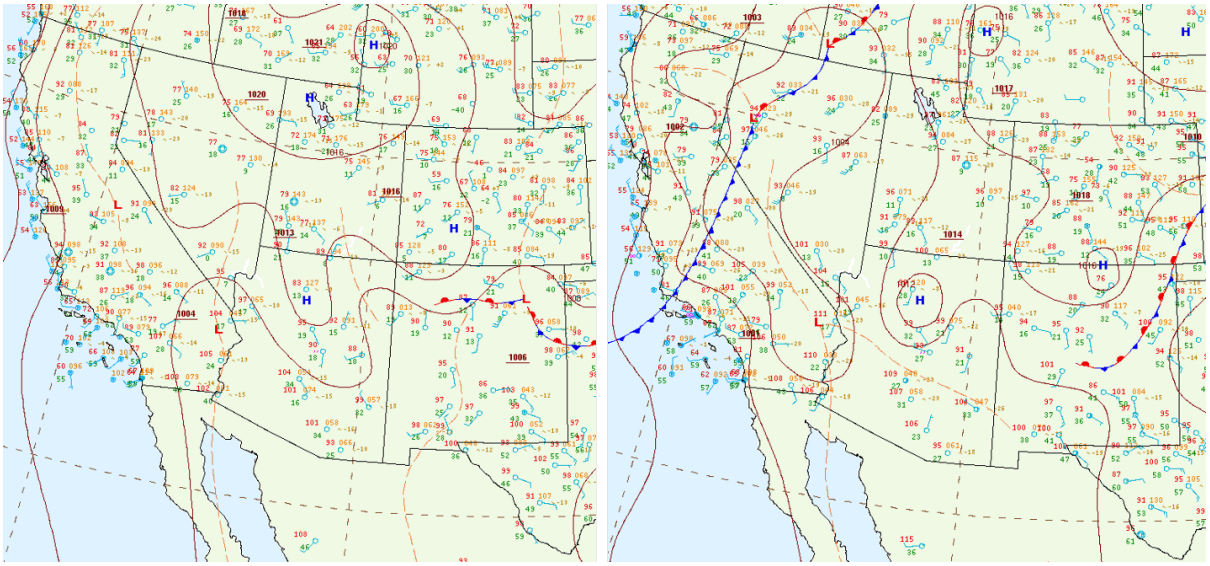

Figure 3-5. Surface analyses from 2 p.m. MST June 15, 2022 (left) and 2 p.m. MST June 16, 2022 (right).

Table 3-2 confirms that the above-normal heights aloft were associated with hot surface temperatures that aided ozone development. In addition, wind speeds averaged 4 to 7 mph, limiting pollutant dispersion over the nonattainment area.

Table 3-2. Surface weather variables observed at Phoenix Sky Harbor Airport.

Date	High Temp. (F)	Avg. WS (mph)	Avg. WD
6/15/2022	107	4	115
6/16/2022	113	7	261

Satellite Smoke and Fire Detections

Figure 3-6 shows satellites detected fires and medium-to-heavy density smoke just south of the nonattainment area on June 15, while medium density smoke covered almost the entire state of Arizona on June 16. While the broad plumes of regional smoke are difficult to discern on visible satellite imagery due to the high solar angle of the afternoon images, smoke is visible near the larger fire complexes in Figures 3-7 and 3-8. MODIS AIRS provides evidence of smoke transport over Arizona on June 16 with 500 mb CO concentrations of up to 136 ppbv near Phoenix (Figure 3-9).

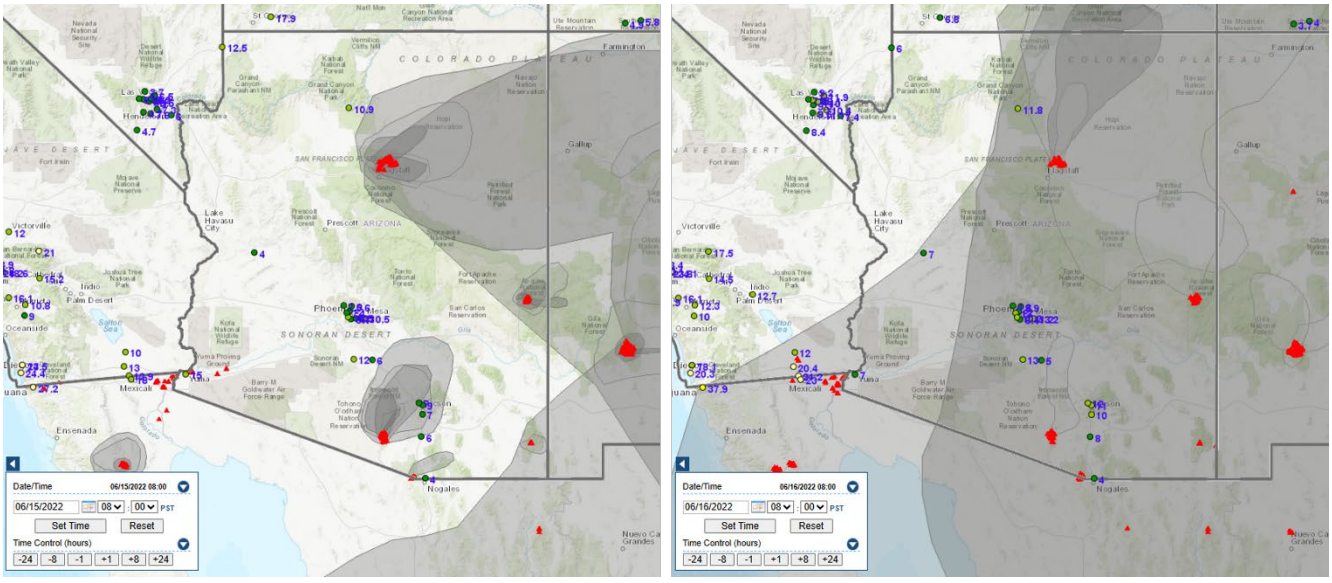

Figure 3-6. HMS fire and smoke along with hourly concentrations of $PM_{2.5}$ at 8:00 a.m. MST June 15, 2022 (left) and 8:00 a.m. MST June 16, 2022 (right). Fire detections are indicated by orange dots.

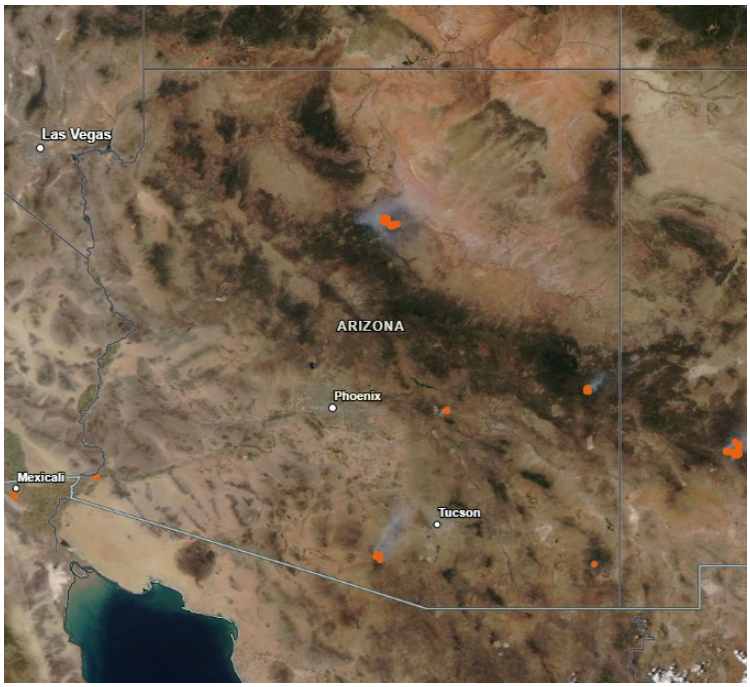

Figure 3-7. Visible satellite imagery from approximately 1:10 p.m. MST on June 15, 2022. Fire detections are indicated by orange dots.

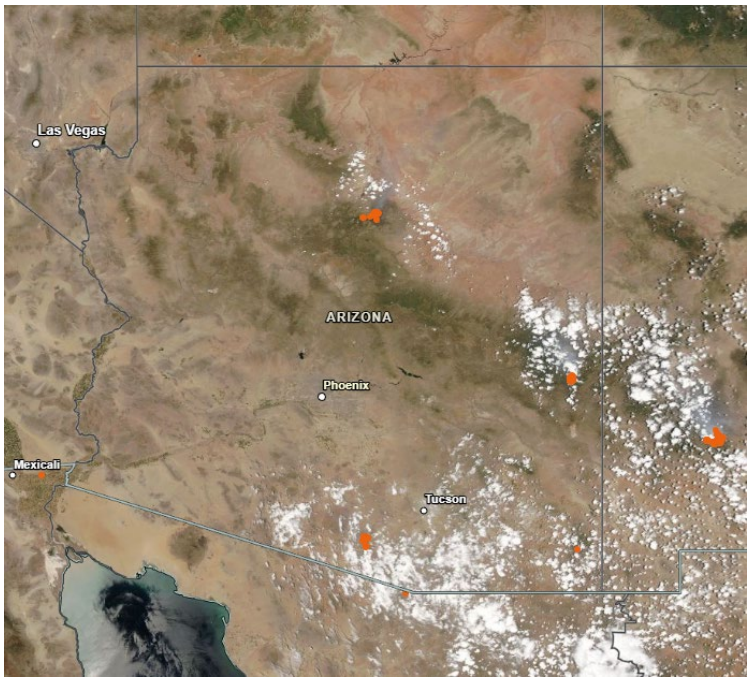

Figure 3-8. Visible satellite imagery from approximately 1:53 p.m. MST on June 16, 2022. Fire detections are indicated by orange dots.

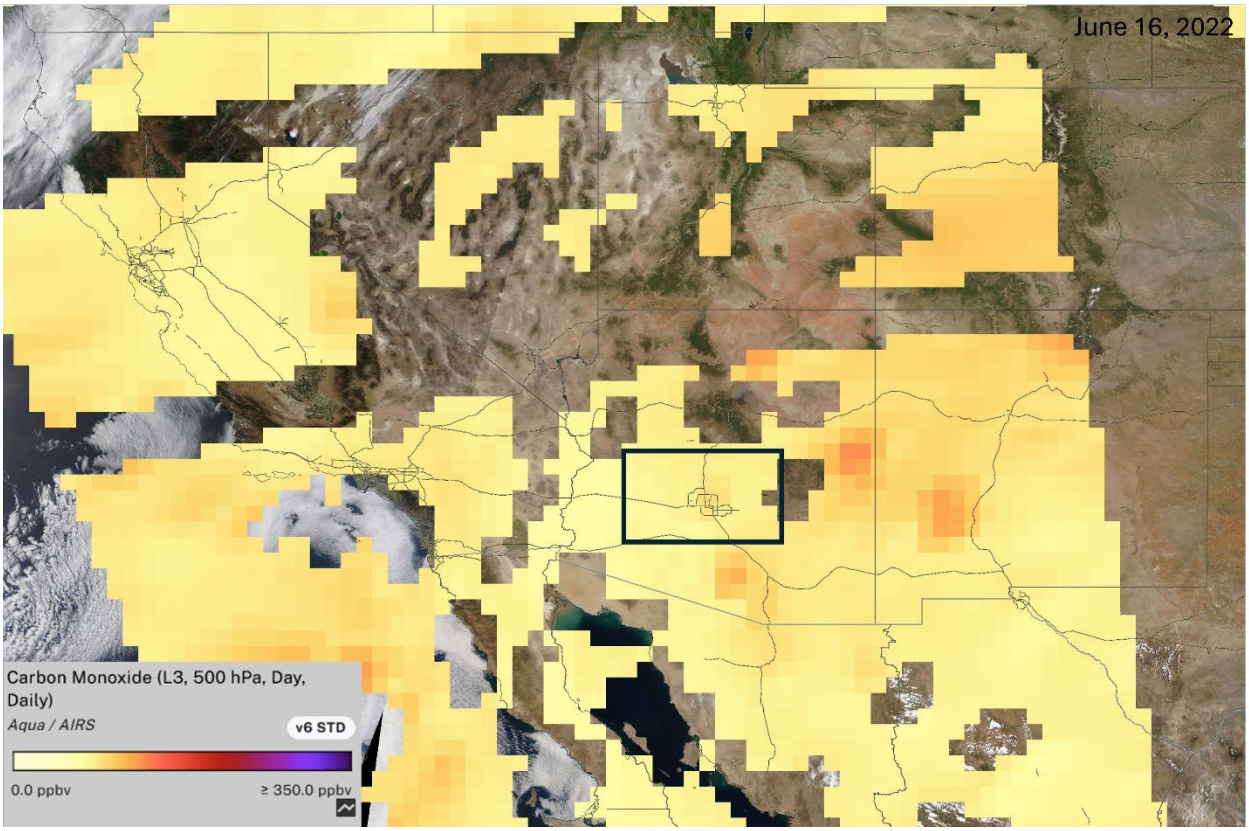

Figure 3-9. A zoomed-in view over the southwestern U.S. of MODIS Aqua AIRS CO retrieval during the atypical ozone date of June 16, 2022. The black box represents the approximate area of the NAA.

Smoke Discussions

NOAA's daily smoke discussions also note fires and varying density smoke across Arizona each day.

"A swath of varying density smoke from several larger wildfires burning in Arizona and New Mexico extended from portions of Arizona and New Mexico to the northeast across the central U.S. to as far as southern Wisconsin. Cloudiness farther to the north prevented additional information from satellite imagery on the extent of the smoke. The thickest smoke in this region was seen from the western Oklahoma panhandle to central Iowa." (NOAA NESDIS Text Narrative from June 15, 2022)

"A swath of varying density smoke from several larger wildfires burning in Arizona and New Mexico with contributions from seasonal burning extended from portions of Arizona and New Mexico to the northeast across the central and eastern U.S. to as far as the coastal Atlantic Ocean and southeastern Canada." (NOAA NESDIS Text Narrative from June 16, 2022)

In addition, smoke was reported at Phoenix Sky Harbor Airport by local METAR observations on June 15 and 16.

Soundings

While morning soundings were launched in Phoenix on June 15 and 16, soundings from Tucson were the nearest available each evening. The left panels in **Figure 3-10** show temperature inversions and stable conditions on the mornings of June 15 and 16, confining pollutants near the surface.

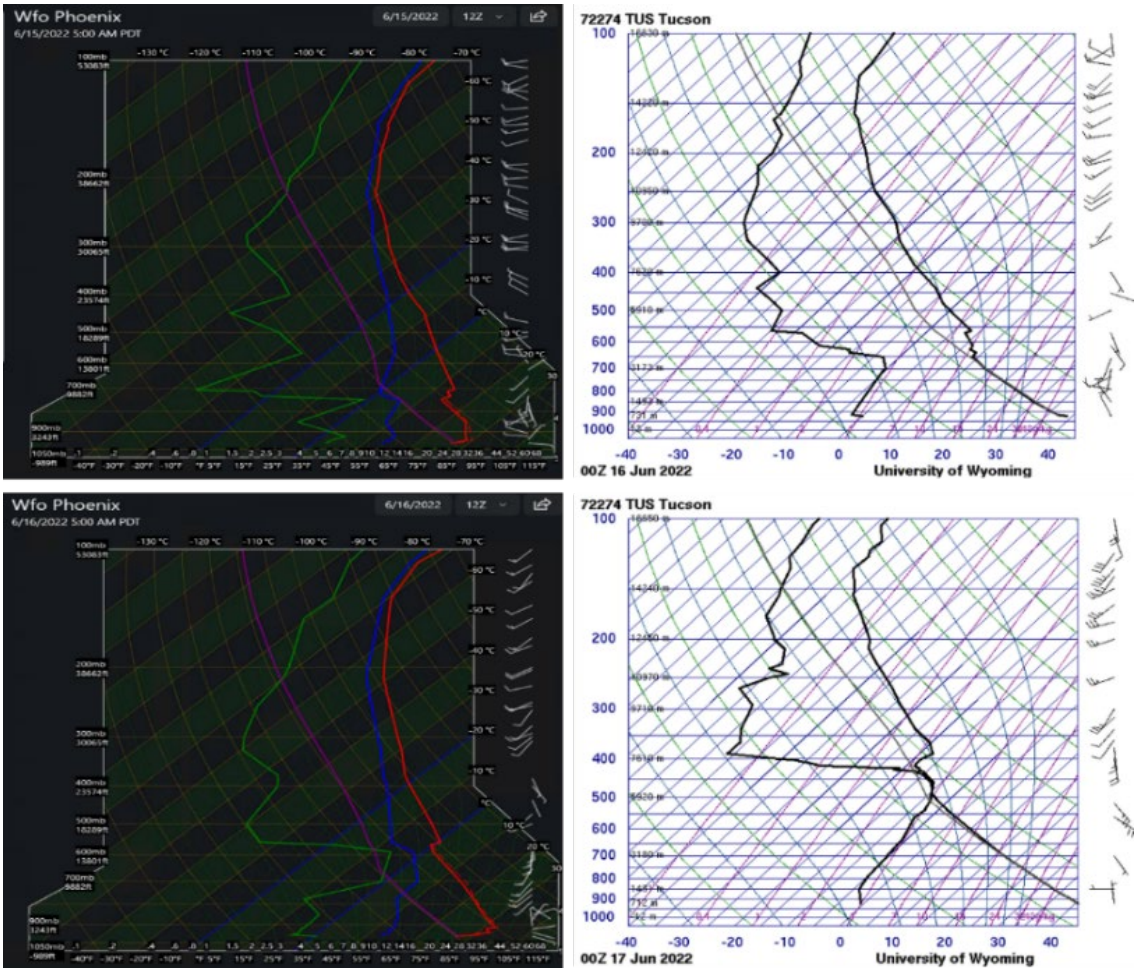

Figure 3-10. Observed atmospheric soundings from 5 a.m. MST (left) and 5 p.m. MST (right) June 15-16, 2022

However, despite warm temperatures aloft, mixing improved greatly each afternoon due to hot surface temperatures (right panels on Figure 3-10) with mixing heights extending to 650 mb (2.5 km) on June 15 and 500 mb (2.8 km) on June 16. This deep mixing allowed any aloft smoke to mix to the surface and enhance ozone formation.

Smoke Transport

Using the mixing heights of 2.5 km from the evening sounding on June 15, and 2.8 km from the evening sounding on June 16 HYSPLIT back trajectories were run throughout the depth of the boundary layer (layer of air available to mix to the surface) over the preceding 48 hours from June 15 and 24 hours from June 16 to determine the potential for smoke transport into the nonattainment area. Overlaying those trajectories with the HMS fire/smoke analysis from the previous days (**Figure 3-11 and Figure 3-12**) shows that smoke was available to be transported into the nonattainment area both afternoons. The primary source of smoke transport for June 15 was a broad plume of thin-density smoke over northern Mexico. For June 16, the broad plume of smoke over northern Mexico continued to be carried into the region, while the trajectory near the top of the boundary layer also crossed heavy smoke from fires in southern Arizona.

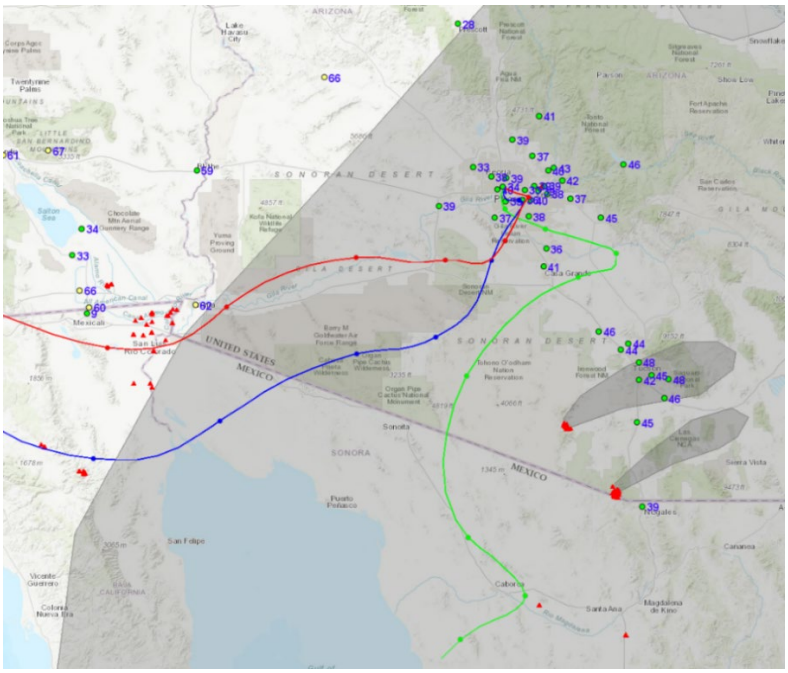

Figure 3-11. 48-hr back trajectories at 10 meters (green), 1250 meters (blue), and 2500 meters (red) above ground level (AGL) from 4:00 p.m. MST June 15, 2022. HMS satellite fire detections/smoke and hourly ozone (ppb) at 4:00 p.m. MST on June 13, 2022.

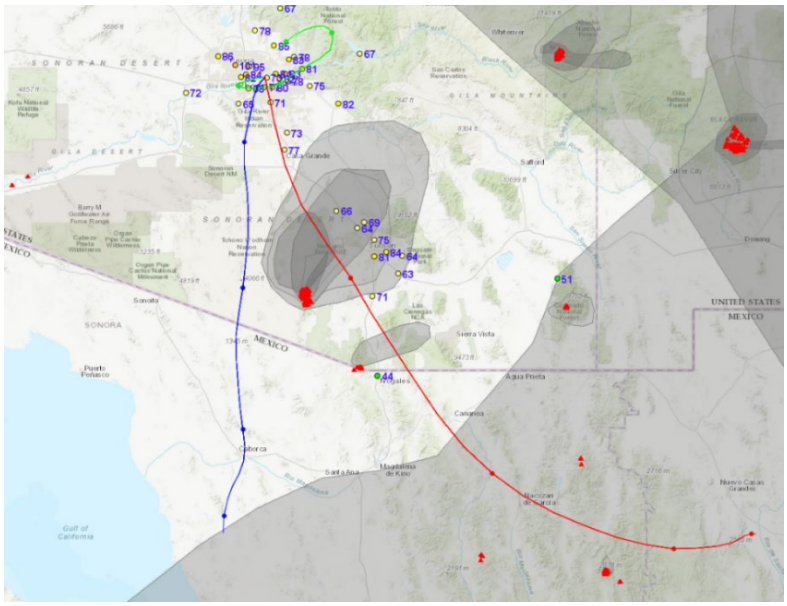

Figure 3-12. 24-hr back trajectories at 10 meters (green), 1400 meters (blue), and 2800 meters (red) above ground level (AGL) from 4:00 p.m. MST June 16, 2022. HMS satellite fire detections/smoke and hourly ozone (ppb) at 4:00 p.m. MST on June 15, 2022.

Summary

For June 15-16, 2022, an aloft ridge of high pressure just south of Arizona produced sunny skies and hot temperatures in the Phoenix area. In addition, light surface winds due to a weak pressure gradient hindered dispersion. While the hot temperatures, sunny skies, and light winds were conducive to ozone development, deep mixing each afternoon created the potential for aloft smoke to mix to the surface. HYSPLIT back trajectories show that boundary layer air originated from areas with light to heavy density smoke from northern Mexico to southern Arizona, increasing the probability that regional smoke contributed to ozone precursors each day. Smoke was also noted in local METAR observations at Phoenix Sky Harbor Airport on June 15 and 16. Furthermore, MODIS AIRS gave evidence of smoke transport over Arizona on June 16, with elevated concentrations of CO near Phoenix. These meteorological conditions, smoke observations and smoke transport patterns provide evidence for smoke-enhanced ozone production in the nonattainment area June 15-16, 2022.

3.2.4 Surface Impacts

Low visibility in Phoenix is apparent on June 15-16, 2022. While some of the haze is likely due to dust, smoke plumes from the local and regional fires were present over the nonattainment area during the atypical ozone event. **Figure 3-13 through 3-18** show photos taken from the northeast-facing Camelback Mountain, south-facing South Mountain, and west-northwest-facing White Tank Mountain webcams, where the visibility is low due to haze throughout the day on both June 15 and 16. The haze due to dust and smoke over Phoenix received news coverage from ABC15 in their

article, “Why do we have worsening air quality during summer months”, (https://www.abc15.com/weather/impact-earth/why-do-we-have-worsening-air-quality-during-summer-months). Smoke plumes from local and regional fires affecting air quality throughout Arizona were documented in mid-June 2022. News coverage from June 15 and 16, 2022 details smoke plumes affecting air quality in Flagstaff and Tucson, respectively. 3TV in their report, “Pipeline Fire near Flagstaff burns more than 22K acres; now 33% contained” (https://www.azfamily.com/2022/06/15/pipeline-fire-near-flagstaff-burns-more-than-22k-acres-now-33-contained/), and Tucson Sentinel in their report, “Air pollution in Tucson reaches harmful levels, made worse by smoke from Contreras Fire” (https://www.tucsonsentinel.com/local/report/061622_pima_ozone_advisory/air-pollution-tucson-reaches-harmful-levels-made-worse-by-smoke-from-contreras-fire/), provided photos and videos of smoke plumes in Flagstaff, AZ, and Tucson, AZ, respectively.

Figure 3-13. Camera Images showing the northeast coordinal direction taken from the Camelback Mountain webcam on June 15 from 8:00 LST, 11:00 LST, 14:00 LST, and 17:00.

Figure 3-14. Camera Images showing the northeast coordinal direction taken from the Camelback Mountain webcam on June 16 from 8:00 LST, 11:00 LST, 14:00 LST, and 17:00.

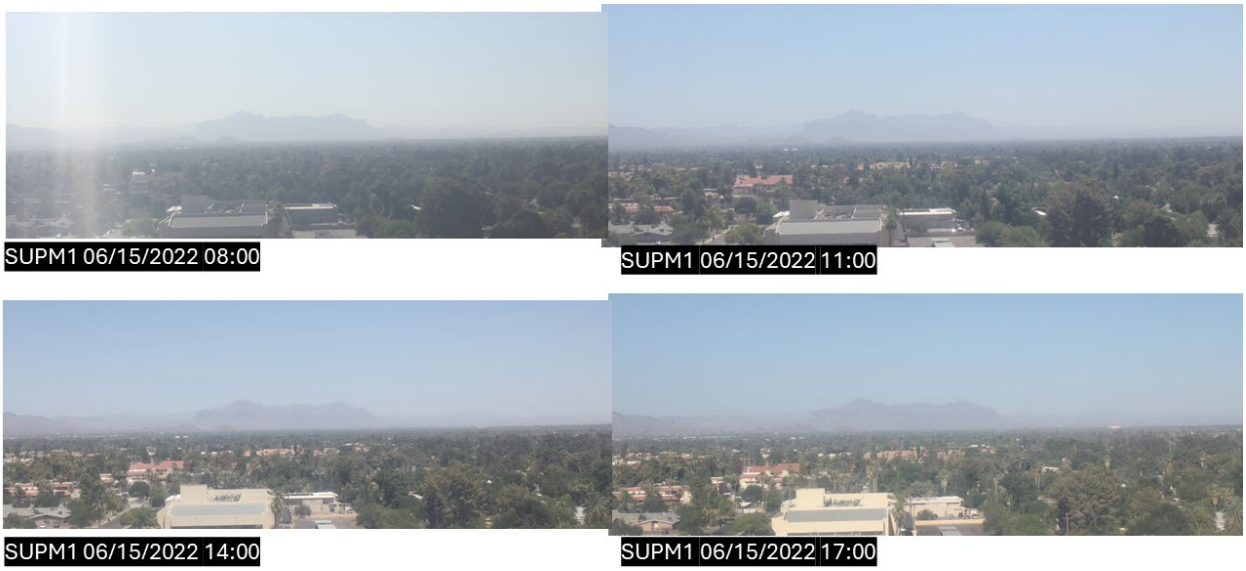

Figure 3-15. Camera Images showing the northeast coordinal direction taken from the Superstition Mountain webcam on June 15 from 8:00 LST, 11:00 LST, 14:00 LST, and 17:00.

Figure 3-16. Camera Images showing the northeast coordinal direction taken from the Superstition Mountain webcam on June 16 from 8:00 LST, 11:00 LST, 14:00 LST, and 17:00.

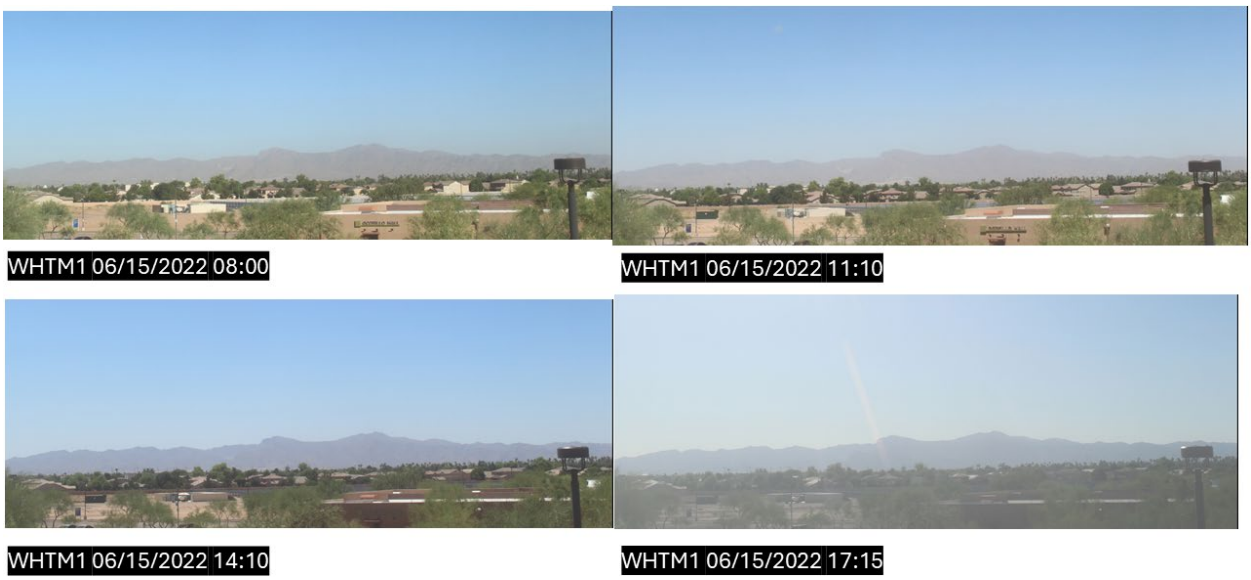

Figure 3-17. Camera Images showing the northeast coordinal direction taken from the White Tank Mountain webcam on June 15 from 8:00 LST, 11:00 LST, 14:00 LST, and 17:00.

Figure 3-18. Camera Images showing the northeast coordinal direction taken from the White Tank Mountain webcam on June 16 from 8:00 LST, 11:00 LST, 14:00 LST, and 17:00.

Figure 3-19 shows an overall view of the magnitude of hourly pollutant concentrations measured in the nonattainment area in the two days before and after the June 15-16, 2022, atypical event. Hourly concentrations of ozone show a widespread and distinct peak on June 15 and 16 at all affected sites relative to the days surrounding the atypical event. Hourly ozone concentrations at many affected sites do not exhibit a decrease to below approximately 40 ppb at night on June 15 and in the morning on June 16 that is characteristic of other nights in the time series, indicating overnight transport of ozone and ozone precursors. Furthermore, peak NO_2 concentrations were elevated on June 15-16 relative to the surrounding two days, including sustained elevated concentrations on the morning of June 16. Widespread enhancements in surface pollutant concentrations provide evidence that smoke from regional fires entered the region, mixed towards the surface, and had an atypical influence on ozone during the period. The rest of this section examines temporal abnormalities and site-specific trends for each supporting pollutant.

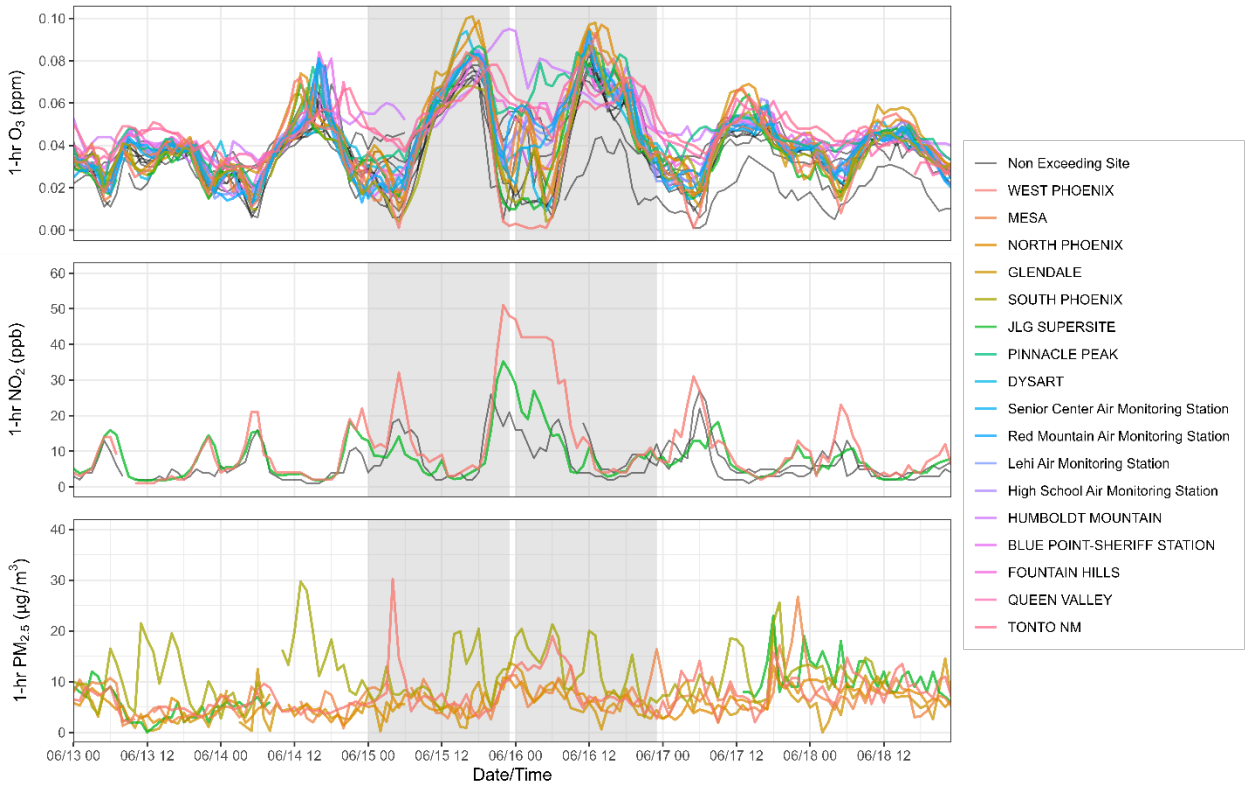

Figure 3-19. Hourly concentrations of ozone, NO_2, and $PM_{2.5}$ at all sites in the nonattainment area. All ozone-exceeding sites are color-coded to highlight smoke impacts on concentrations, and all non-exceeding sites are black. The gray shaded areas represent June 15-16, 2022.

Figure 3-20 shows hourly NO_2 concentrations at the West Phoenix (top) and Buckeye (bottom) sites. NO_2 concentrations at the West Phoenix site rapidly increased beginning around 18:00 LST on June 15 and increased to above the 95th percentile around 22:00-23:00 LST the same day. Concentrations remain elevated above the 95th percentile all night until around 7:00 LST on June 16. A similar pattern in NO_2 concentrations is present at the Buckeye and JLG Supersite sites, providing evidence that the smoke impacts were widespread and affected multiple air monitoring sites.

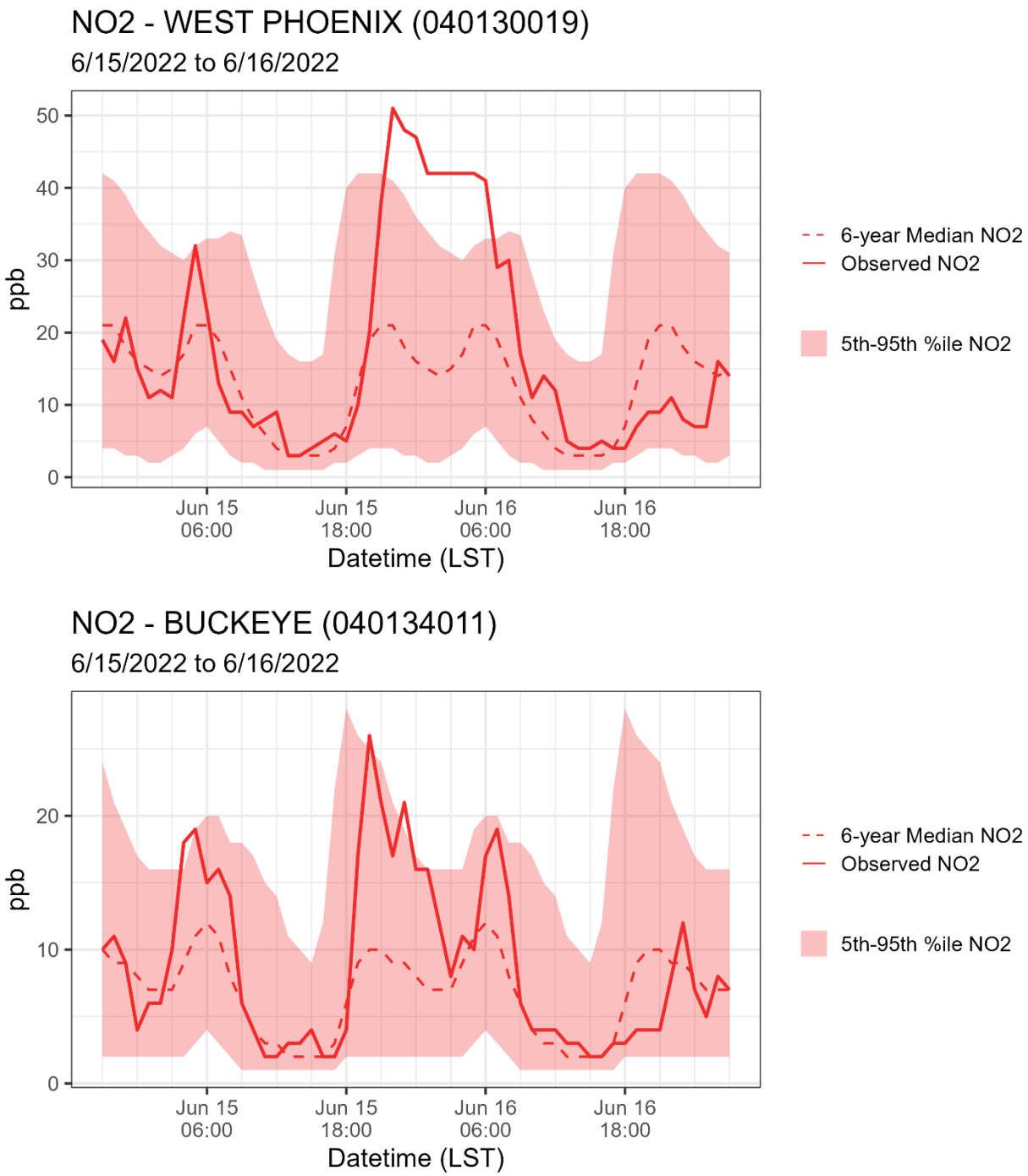

Figure 3-20. Hourly concentrations of NO_2 at the West Phoenix (top) and Buckeye (bottom) sites. The 6-year (2019-2024) median is represented by the dashed line, and the 5th-95th percentile is represented by the shaded area.

The ratio of OC to EC taken at the JLG Supersite monitor was also examined for evidence that wildfire smoke entered the nonattainment area. Increases in this ratio are indicative of wildfire smoke. **Figure 3-21** shows boxplots of OC to EC ratios for available data collected during the ozone season

between 2019-2024. The OC to EC ratios on June 16 were nearly at or above the 75th percentile compared to all data. Higher concentrations of $PM_{2.5}$ species, particularly potassium, are also indicative of wildfire smoke. Figure 3-22 shows boxplots of speciated $PM_{2.5}$ collected at the JLG Supersite monitor during the ozone season between 2019-2024. Most speciated $PM_{2.5}$ observations collected on June 16 are elevated above the 75th percentile. Elevated concentrations of aluminum, calcium, iron, and silicon are indicative of dust, but potassium is also elevated, which indicates the presence of smoke. These observations provide further evidence that ground-level wildfire smoke entered Phoenix on June 15-16 containing increased OC to EC ratios and potassium concentrations during the June 15-16, 2022, atypical ozone event.

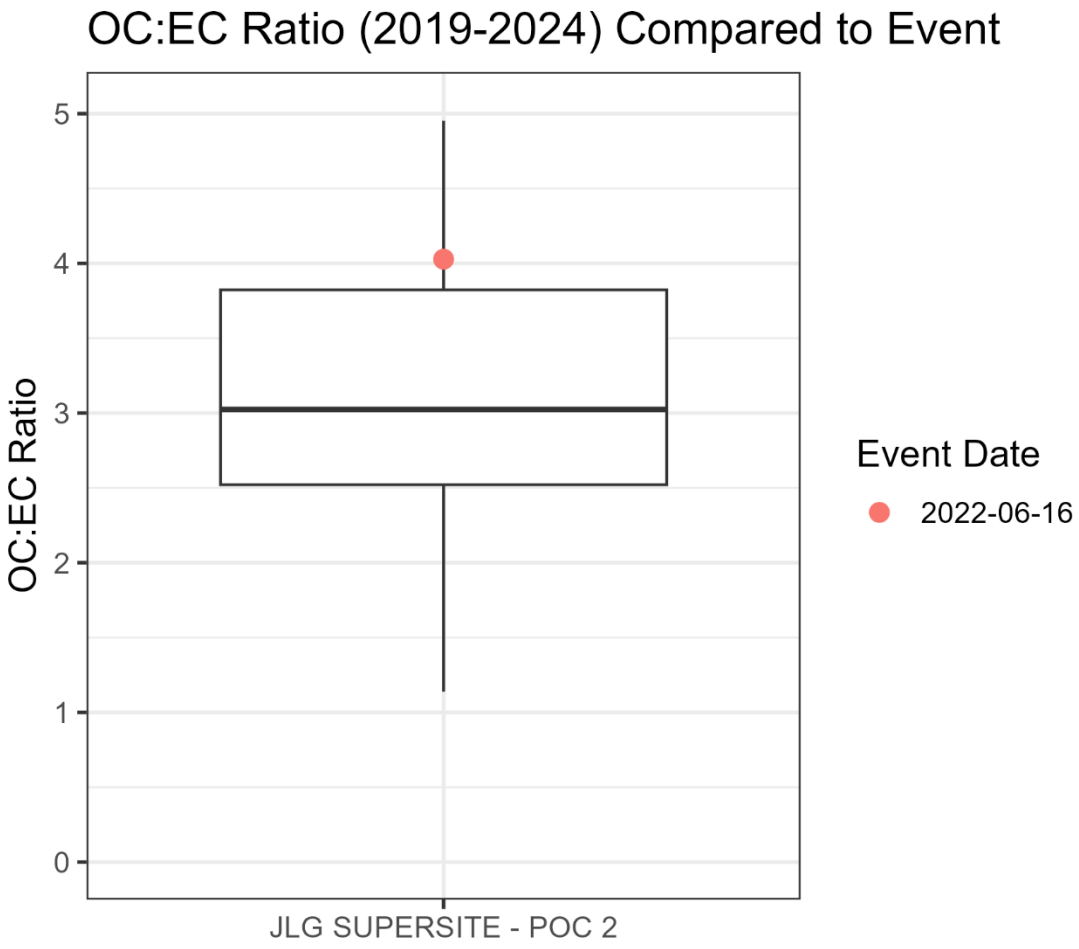

Figure 3-21. Boxplot of OC to EC ratios at the JLG Supersite site using data collected during the ozone season (April-September) from 2019-2024. OC to EC ratios are calculated at POC 2 (x-axis). Available OC to EC ratios collected during the June 15-16 atypical ozone event are shown as a point.

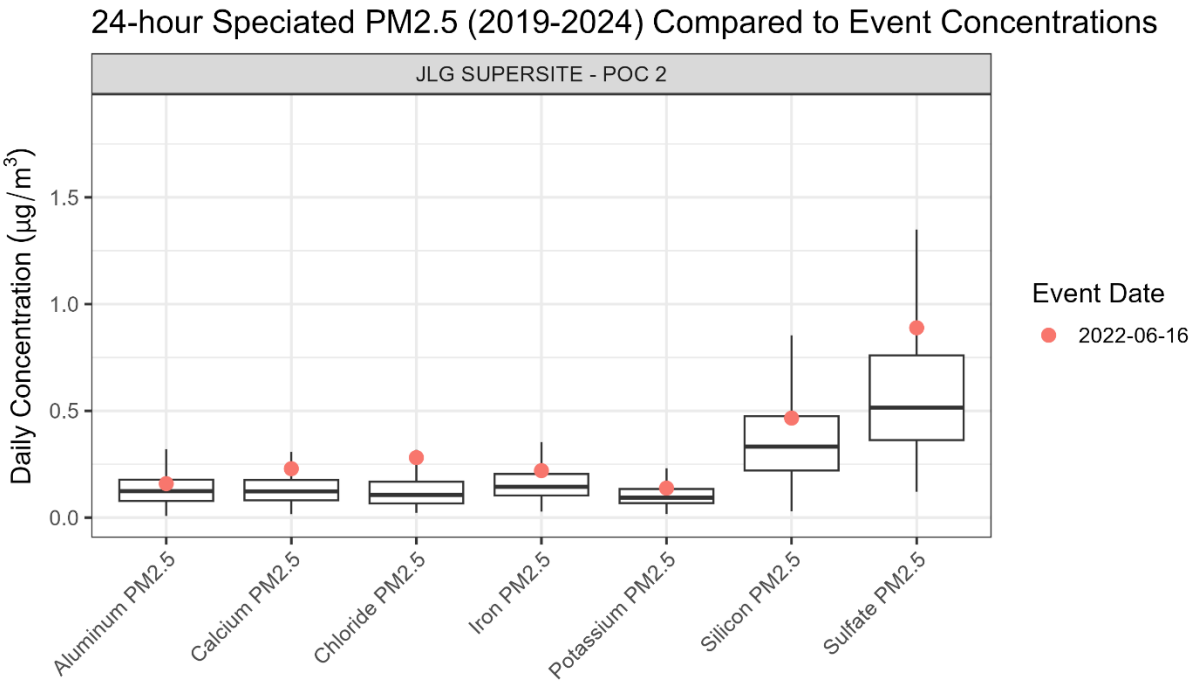

Figure 3-22. Boxplots of speciated $PM_{2.5}$ collected at the JLG Supersite site collected during the ozone season (April-September) from 2019-2024. Available speciated $PM_{2.5}$ concentrations collected during the June 15-16 atypical ozone event are shown as a point.

3.2.5 Event Statistics

Table 3-3 summarizes the measurements of ozone concentrations on June 15-16, 2022, as well as the percentile rank of the observation compared to six years of ozone season data (April 1-September 31, 2019-2024). Ozone MDA8 measurements ranged from the 93rd - 100th percentile on June 15-16, 2022.

Table 3-3. Percentile of ozone measurements on the atypical dates compared with six years of ozone data (2019-2024). The percentile rank is calculated across the ozone production season in the nonattainment area (April 1-September 31) of 2019-2024.

Date	Site Name	Site Code	Ozone MDA8 (ppb)	Percentile Rank
6/15/2022	Tonto NM	040070010	71	93
	Blue Point-Sheriff Station-Tonto NF-Salt River Recreation Area	040139702	72	94
	JLG Supersite	040139997	72	94
	Senior Center Air Monitoring Station	040137020	74	96
	West Phoenix	040130019	75	97
	Mesa	040131003	75	97
	Red Mountain Air Monitoring Station	040137021	75	97
	Fountain Hills	040139704	75	97
	Queen Valley	040218001	75	97
	Pinnacle Peak	040132005	77	98
	High School Air Monitoring Station	040137024	77	98
	Lehi Air Monitoring Station	040137022	78	98
	Dysart	040134010	82	99
	North Phoenix	040131004	85	99
	Glendale	040132001	87	100
	Humboldt Mountain	040139508	87	100

Date	Site Name	Site Code	Ozone MDA8 (ppb)	Percentile Rank
6/16/2022	Blue Point-Sheriff Station-Tonto NF-Salt River Recreation Area	040139702	71	93
	Dysart	040134010	72	94
	Fountain Hills	040139704	72	94
	South Phoenix	040134003	73	95
	Lehi Air Monitoring Station	040137022	73	95
	Mesa	040131003	74	96
	Red Mountain Air Monitoring Station	040137021	74	96
	Pinnacle Peak	040132005	75	97
	Senior Center Air Monitoring Station	040137020	75	97
	JLG Supersite	040139997	76	98
	High School Air Monitoring Station	040137024	77	98
	West Phoenix	040130019	80	99
	Glendale	040132001	85	99
	North Phoenix	040131004	88	100

3.2.6 Conclusion

The concurrence of HMS smoke perimeters over the nonattainment area, HYSPLIT trajectories and meteorological analysis showing accumulation of smoke in the nonattainment area, visible smoke in camera images and video news coverage, and elevated hourly NO_2 concentrations, OC to EC ratio, speciated $PM_{2.5}$, and satellite imagery provide evidence that surface-level smoke was present during the period. Regional transport of smoke from large fires in Arizona enhanced ozone concentrations outside of the typical diurnal profile, keeping ozone values high and affecting the MDA8 ozone concentrations at seventeen sites. Multiple analyses showed that smoke fully encompassed the Maricopa Nonattainment Area on June 15-16, 2022, and statistics show ozone concentrations were atypical during this event.

This combined evidence indicates that smoke plumes generated by large fires in Arizona provided an atypical source of ozone and ozone precursors that caused enhanced ozone concentrations June 15-16, 2022. Removal of these days as atypical events is supported by this analysis.

3.3 July 15-17, 2022

3.3.1 Event Overview: July 15-17, 2022

The unrepresentative (atypical) ozone event took place on July 15-17, 2022, and affected twenty-two sites in the Maricopa Nonattainment Area: West Phoenix, Mesa, North Phoenix, Falcon Field, Glendale, Pinnacle Peak, Central Phoenix, South Scottsdale, South Phoenix, West Chandler, Tempe, Cave Creek, Buckeye, Senior Center Air Monitoring Station, Red Mountain Air Monitoring Station, High School Air Monitoring Station, Blue Point-Sheriff Station-Tonto NF-Salt River Recreation Area, Fountain Hills, JLG Supersite, A J Maintenance Yard, Queen Valley, and Tonto NM (**Table 3-4**). MDA8 ozone concentrations at the affected sites ranged from 71-84 ppb.

Time series graphs showing hourly ozone concentrations that exceeded the seasonal means (calculated using all available data from April 1 – September 31, 2019-2024) and 10th-90th percentiles at each site are shown in **Figure 3-23.** On July 15, hourly ozone measurements at many sites, such as A J Maintenance Yard, Glendale, and Tempe, were above the 90th percentile during the early morning hours. Measurements decreased to local minimums by 06:00 LST, then rapidly increased throughout the day and continued to exceed the 90th percentile at most sites throughout the day on July 15, indicating transport of ozone and ozone precursors from wildfires. Ozone concentrations generally decreased during the evening and early morning hours of July 15 and 16, respectively, then increased again during the afternoon on July 16 to above the 90th percentile, with ozone concentrations at some sites exhibiting distinct peaks that do not temporally align with the statistical average maximum, indicating an outside influence on ozone concentrations. Similarly, hourly ozone concentrations rise sharply in the afternoon on July 17 to distinct peaks.

Major wildfires burning throughout the central and southern U.S. and in Canada were identified as major contributors to this event. Evidence includes (1) HMS smoke perimeters over the nonattainment area, (2) HYSPLIT trajectories and meteorological analysis showing accumulation of smoke in Phoenix, (3) visible smoke in camera images and video news coverage, and (4) elevated OC to EC ratios and speciated $PM_{2.5}$. This combination of evidence indicates that this is an atypical ozone event.

Table 3-4. Summary of identified atypical July 15-17, 2022.

Event Date(s)	Event Ozone Concentration Percentile	Sites Exceeded During Event	Type of Event
Jul 15-17, 2022	95th - 100th	Twenty-Two sites: West Phoenix, Mesa, North Phoenix, Falcon Field, Glendale, Pinnacle Peak, Central Phoenix, South Scottsdale, South Phoenix, West Chandler, Tempe, Cave Creek, Buckeye, Senior Center Air Monitoring Station, Red Mountain Air Monitoring Station, High School Air Monitoring Station, Blue Point-Sheriff Station-Tonto NF-Salt River Recreation Area, Fountain Hills, JLG Supersite, A J Maintenance Yard, Queen Valley, Tonto NM	International/long-range transport

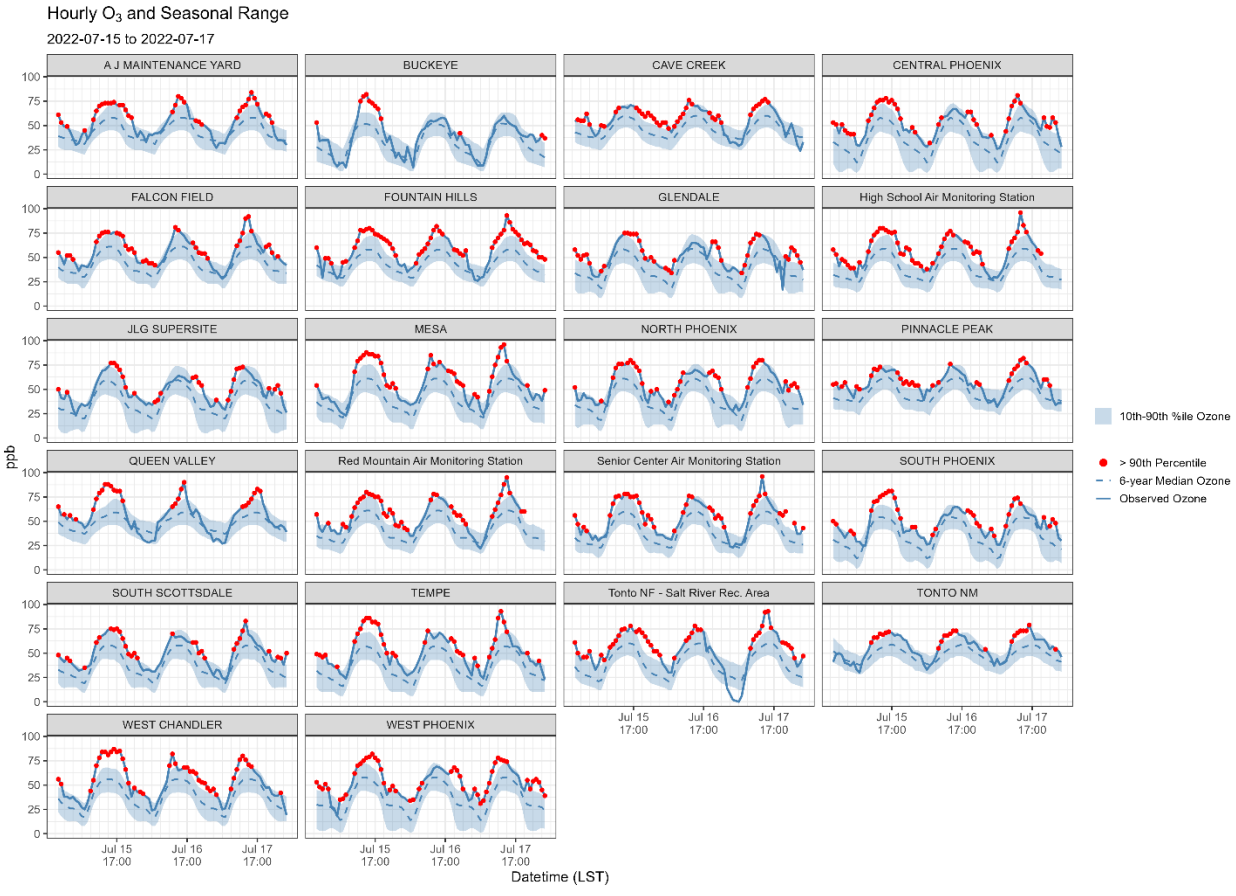

Figure 3-23. Hourly ozone concentrations (ppb) compared to all available data during the ozone season (April 1 – September 31) of the 6-year (2019-2024) period. Hourly means and 10th-90th percentiles are calculated using data on July 15-17, 2022.

3.3.2 Identification of Wildfire(s)

Multiple large fires in the central and southern U.S. and in Canada were active in the days leading up to and during July 15-17, the exclusion days (**Figures 3-24 through 3-27**). Smoke from these fires combined to blanket the continental U.S. during July 15-17.

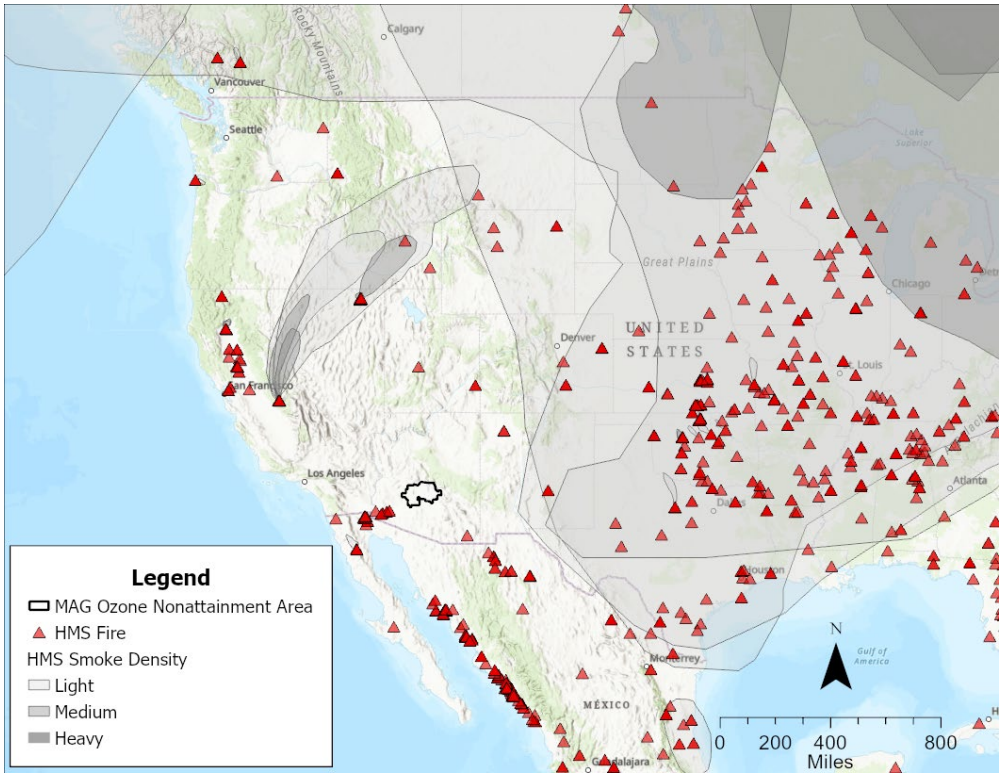

Figure 3-24. Continental view of HMS smoke density and fire locations on July 14, 2022.

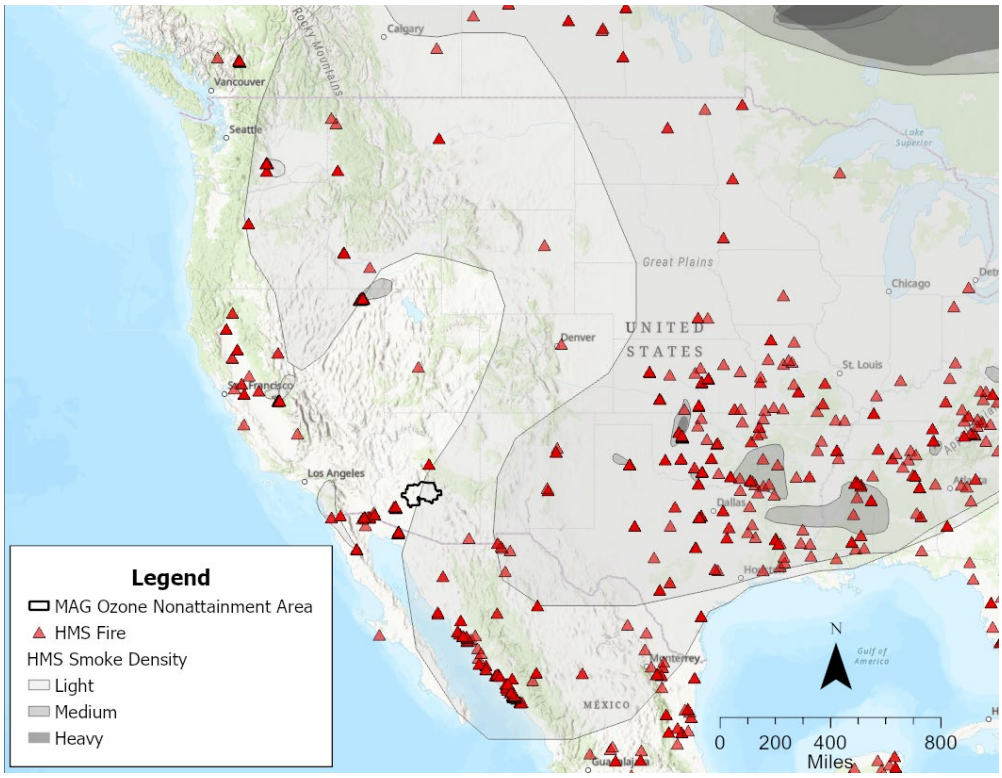

Figure 3-25. Continental view of HMS smoke density and fire locations on July 15, 2022.

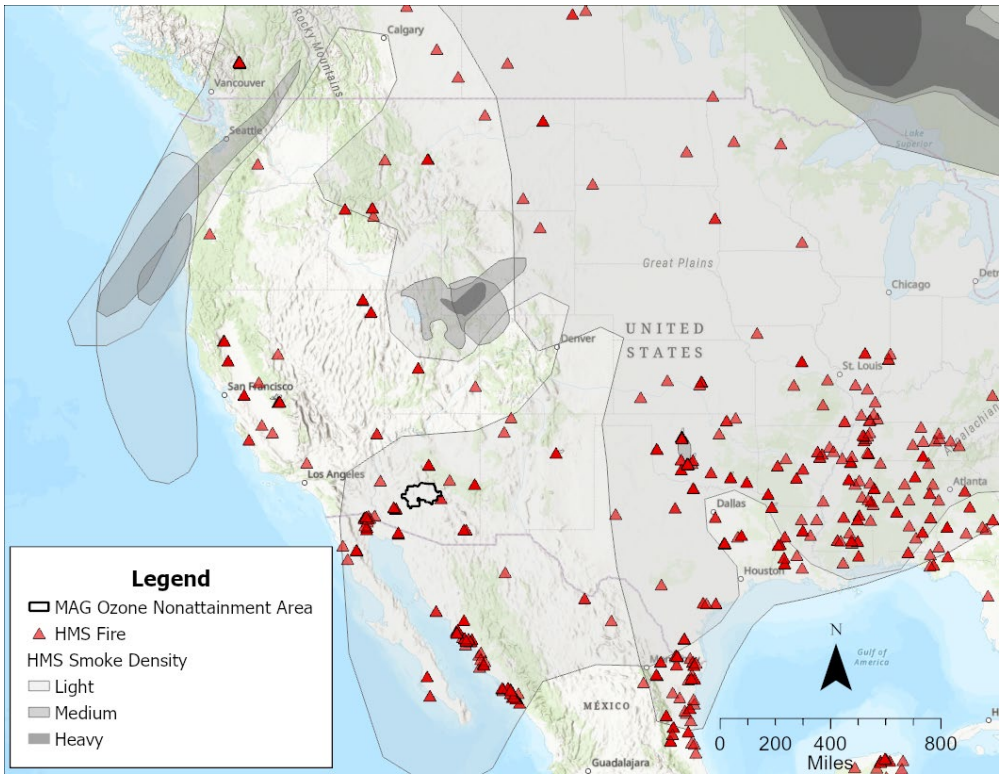

Figure 3-26. Continental view of HMS smoke density and fire locations on July 16, 2022.

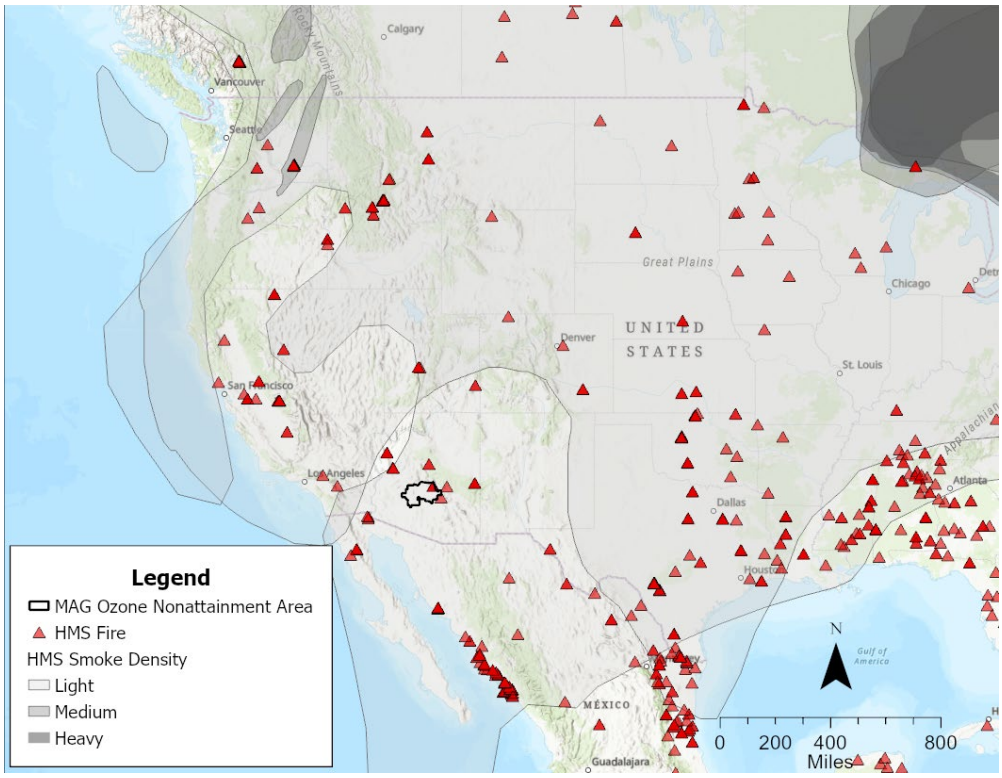

Figure 3-27. Continental view of HMS smoke density and fire locations on July 17, 2022.

3.3.3 Meteorological Analysis

Upper-Level Analysis

The upper-level weather pattern for the July 15-17, 2022 period is show in **Figure 3-28**. A broad area of high pressure at 500 mb moved from northeastern New Mexico to the Four Corners. Around the 500 mb high, the aloft wind flow was clockwise, with average 500 mb winds in the Phoenix metropolitan area prevailing from the east to southeast during the period.

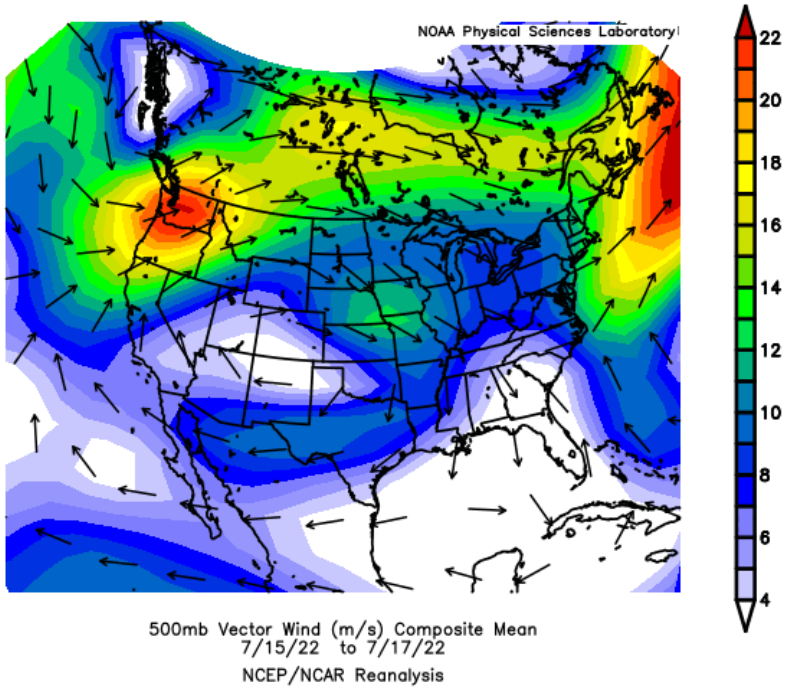

Figure 3-28. Mean 500 mb winds for July 15-17, 2022. High pressure aloft near the Four Corners region resulted in clockwise flow and easterly to southeasterly upper-level winds into central Arizona. Source: NOAA

Surface Analysis

Daily maximum high temperatures and the daily average wind speeds for the three-day period at the KPHX are shown in Table 3-5. Each day featured afternoon high temperatures exceeding 110°F, due to subsidence and associated compressional heating from the upper-level high pressure system shown in the figure above. Furthermore, partly sunny skies were recorded each day. These conditions supported the development of ground-level ozone. Average wind speeds during the three-day period were at or less than 10 mph, which likely limited dispersion and allowed pollutants to accumulate and carryover from day to day.

Table 3-5. Daily maximum high temperatures and daily average surface wind speeds at KPHX.

Date	Daily maximum high temperature (°F)	Average Wind Speed (mph)
July 15	112	7.0

July 16	114	8.5
July 17	112	9.9

Satellite Smoke and Fire Detections

The NOAA Hazard Mapping System (HMS) satellite fire detections and smoke plumes were examined to determine whether smoke was present over central Arizona on July 15-17. As shown in **Figure 3-29**, smoke was analyzed by NOAA over a broad portion of the United States, including central Arizona. In addition, numerous fires were detected by satellites over the central and southern United States, as well as portions of central and western Canada. With a persistent clockwise flow around the 500 mb high into the nonattainment area, conditions were conducive for smoke advection into central Arizona. This persistent clockwise air flow can be seen in the HMS smoke products on the continental spatial scale maps in Figure 3-29. Potential smoke transport paths into the nonattainment area can be found in the "Smoke Transport" section.

July 15

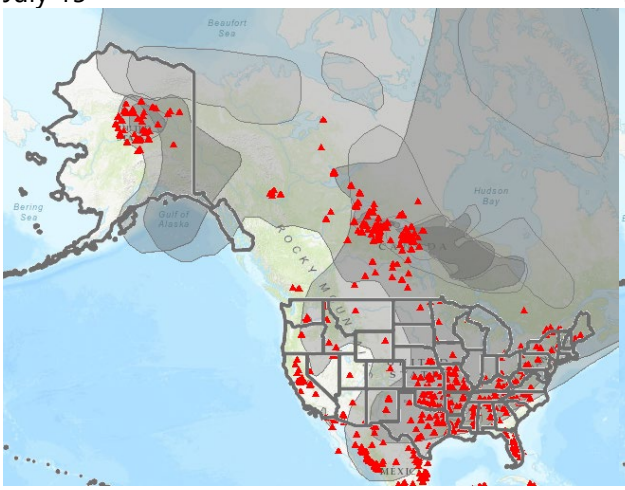

July 16

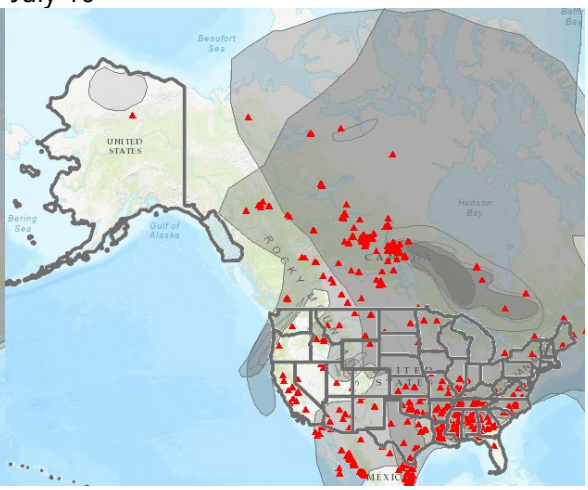

July 17

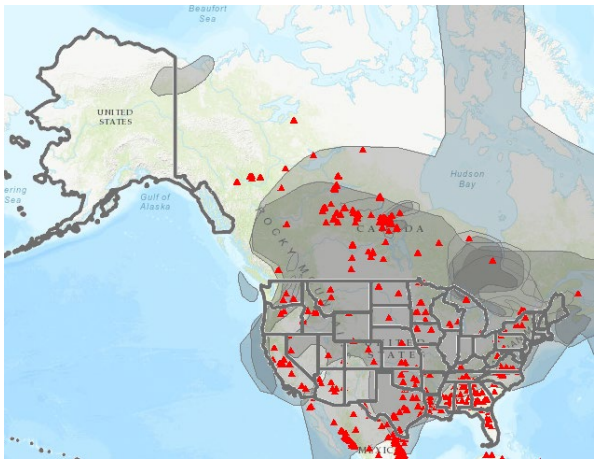

Figure 3-29. NOAA HMS smoke analysis (grey contours) and satellite fire detections (red triangles) for the July 15-17, 2022 period showing the vast spread of smoke across Northern America. Source: NOAA

Smoke Discussion

NOAA's daily smoke discussions noted the potential for smoke over the area but there was cloud cover obscuring the area. Smoke was widespread, but not mentioned specifically for the southeast U.S. on July 16 or 17.

"The Washburn Fire in east central California in the central Sierra-Nevada Mountains was responsible for an area of light density smoke extending from the fire to the north and into western Nevada. **Smoke may be more prevalent in the southwestern U.S. but cloud cover precluded further analysis**." (NOAA NESDIS Text Narrative from July 15, 2022)

Soundings

PBL heights for each day were estimated based on data from the Tucson upper-air soundings. **Table 3-6** shows each day's PBL height adjusted for the elevation of Phoenix. **Figure 3-30** contains the 5 p.m. PST upper air skew-T diagrams from Tucson. The skew-T diagrams, and estimated PBL heights, indicate deep mixing was occurring across central Arizona, allowing for the vertical transfer of air from aloft down to the surface.

Table 3-6. Estimated PBL heights for Phoenix for the July 15-17, 2022 period.

Date	Estimated PBL height (m)

July 15	4,400
July 16	3,500
July 17	4,100

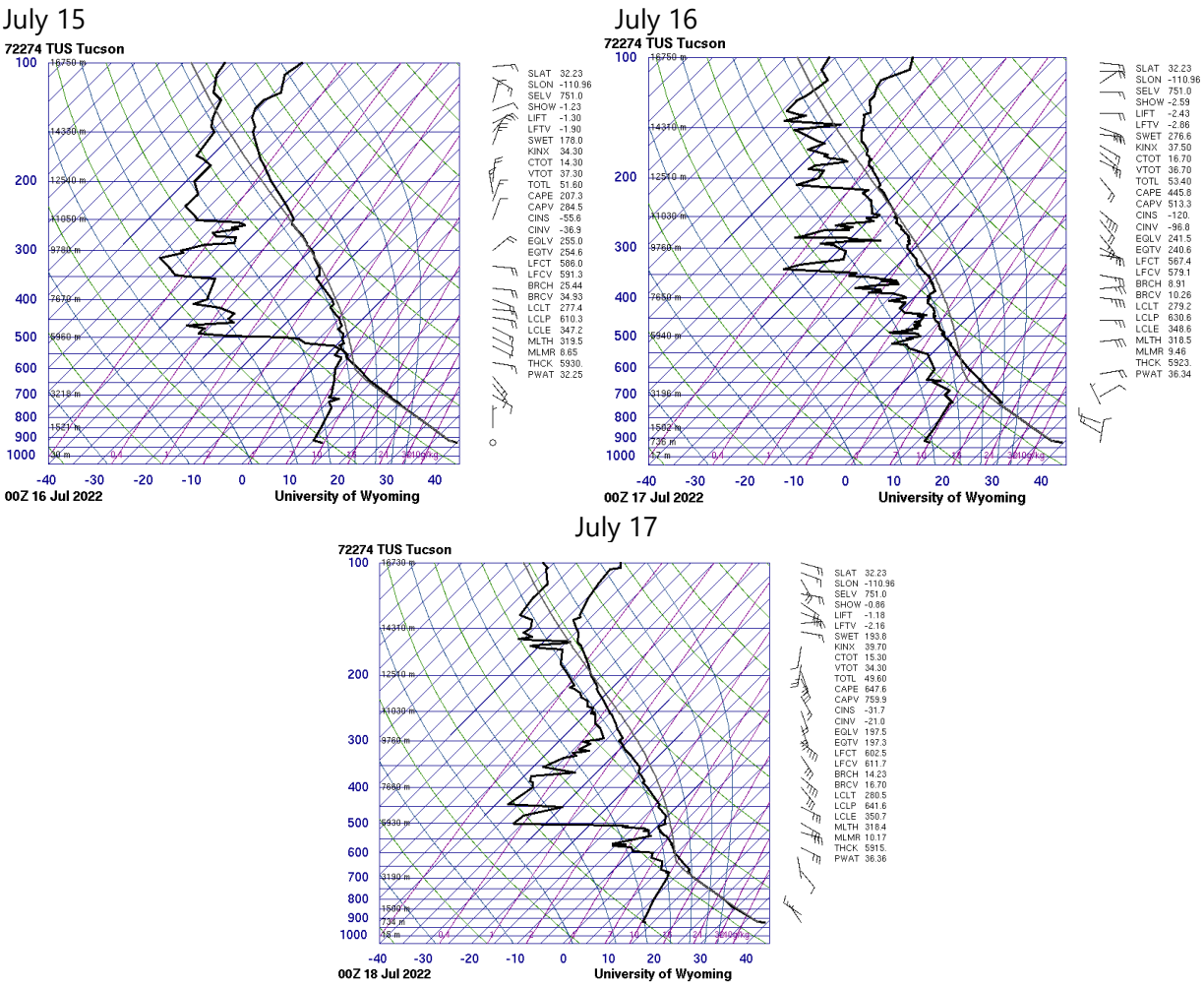

Figure 3-30. Upper-air skew-T diagrams from Tucson for the July 15-17, 2022 period at 5 p.m. PST. Deep mixing is allowing aloft air to be mixed down to the surface. Source: University of Wyoming

Smoke Transport

The PBL heights that were estimated were then used to determine potential smoke transport paths for each day, using the NOAA HYSPLIT trajectory tool. In addition, the NOAA HMS satellite fire

detections and smoke analysis were overlaid to better identify any transport paths. Figure 3-31 displayed the 48-hour back trajectory ending at 5 p.m. PST on July 15. The transport paths at 2,200 m and 4,400 m AGL intersect with the eastern edge of a large smoke plume over the central and eastern United States.

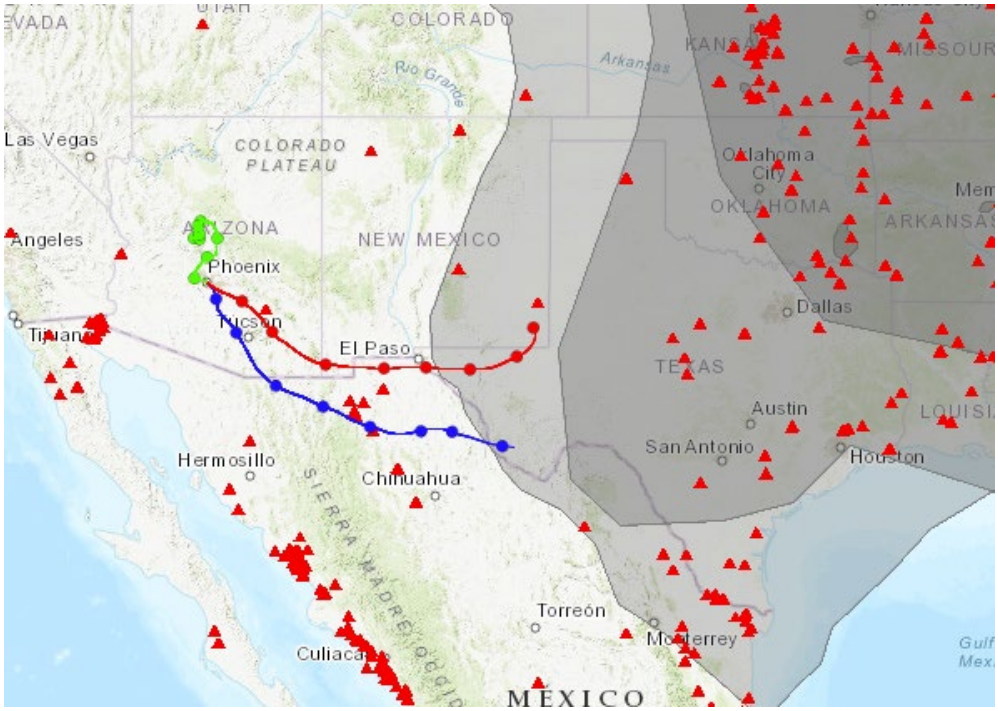

Figure 3-31. 48-hour HYSPLIT back trajectory (green – 50 m, blue – 2,200 m, red – 4,400 m AGL) ending 5 p.m. PST July 15, 2022, and NOAA HMS satellite fire detections (red triangles) and smoke analysis (grey contours) for July 13, 2022. Source: AirNow-Tech

For July 16 (Figure 3-32), a 24-hour back trajectory was calculated ending at 5 p.m. PST. The transport path at 3,500 m AGL intersected the smoke plume that was over Arizona and New Mexico from the previous day. HYSPLIT calculated a similar transport path for July 17. Figure 3-33 shows a 24-hour back trajectory ending at 5 p.m. PST, where the 2,000 m and 4,100 m paths intersect a broad smoke plume over Arizona and New Mexico from the prior day.

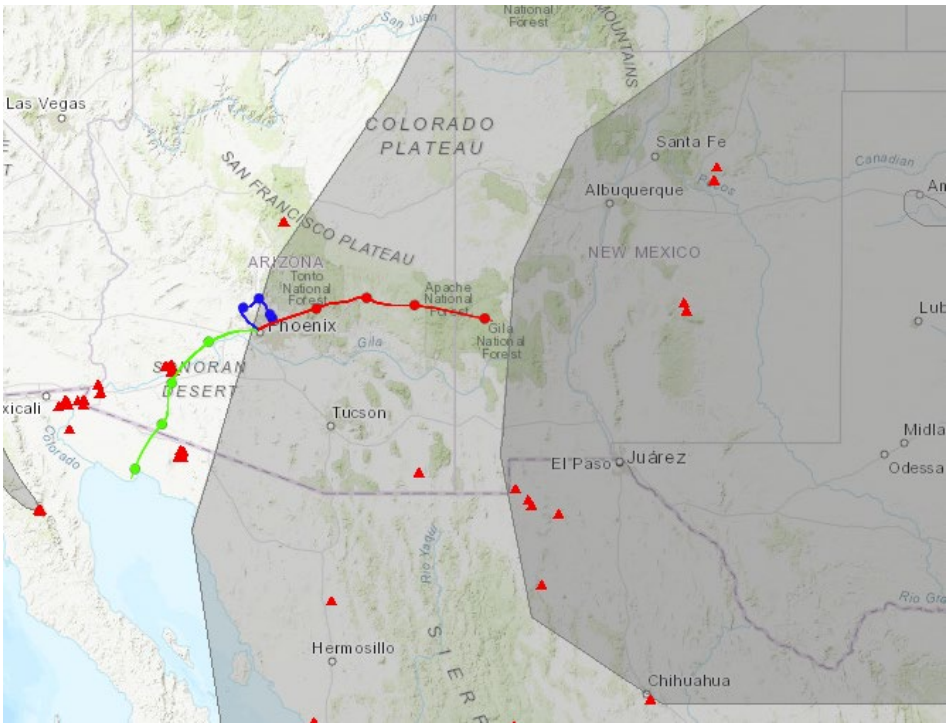

Figure 3-32. 24-hour HYSPLIT back trajectory (green – 50 m, blue – 1,500 m, red – 3,500 m AGL) ending 5 p.m. PST July 16, 2022, and NOAA HMS satellite fire detections (red triangles) and smoke analysis (grey contours) for July 15, 2022. Source: AirNow-Tech

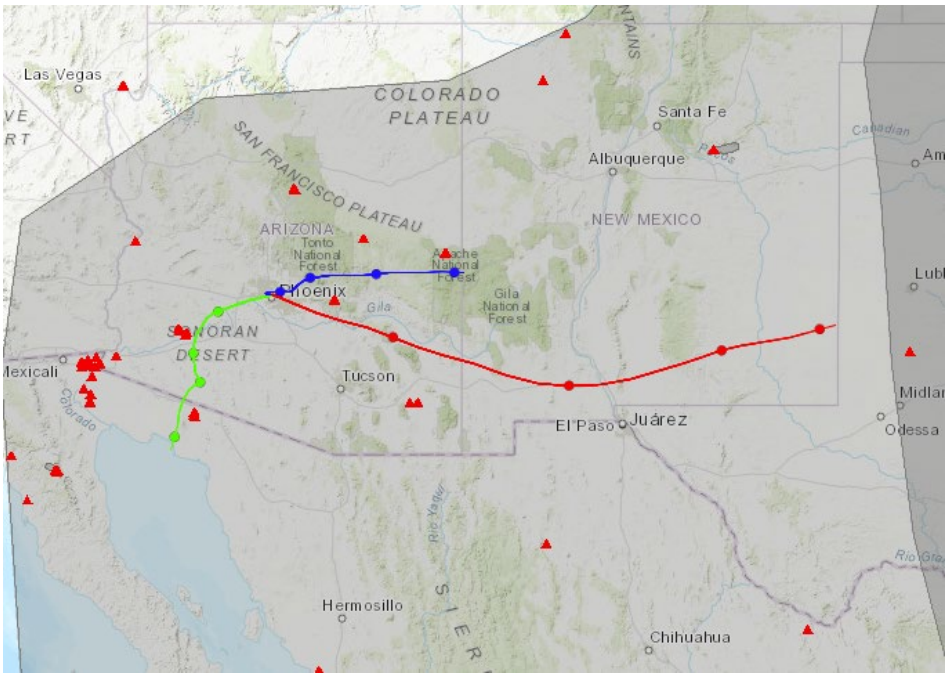

Figure 3-33. 24-hour HYSPLIT back trajectory (green – 50 m, blue – 2,000 m, red – 4,100 m AGL) ending 5 p.m. PST July 17, 2022, and NOAA HMS satellite fire detections (red triangles) and smoke analysis (grey contours) for July 16, 2022. Source: AirNow-Tech

Summary

For July 15-17, 2022, upper-level high pressure near the Four Corners region resulted in easterly to southeasterly flow aloft into central Arizona. These upper-level winds coincided with HYSPLIT trajectory paths within the PBL, which indicated the potential for long-range smoke transport into the nonattainment area during the three-day period. Furthermore, periods of sunshine and hot temperatures aided ozone formation, while light surface winds at KPHX throughout the period hindered dispersion and allowed any transported smoke and associated ozone precursors to accumulate. These conditions show evidence that smoke transport led to enhanced ozone production between July 15-17, 2022.

3.3.4 Surface Impacts

Low visibility in Phoenix is apparent on July 15-17, 2022. While some of the haze is likely due to dust, smoke plumes from the fires burning in the throughout the central and southern U.S. and in Canada were present over the nonattainment area during the atypical ozone event and contributed to the haze. **Figures 3-34 through 3-42** show photos taken from the northeast-facing Camelback Mountain, east-facing Superstition Mountain, and west-northwest-facing White Tank Mountain webcams, where the visibility is low due to haze on July 15-17, 2022, particularly when viewed from the Superstition Mountain webcam.

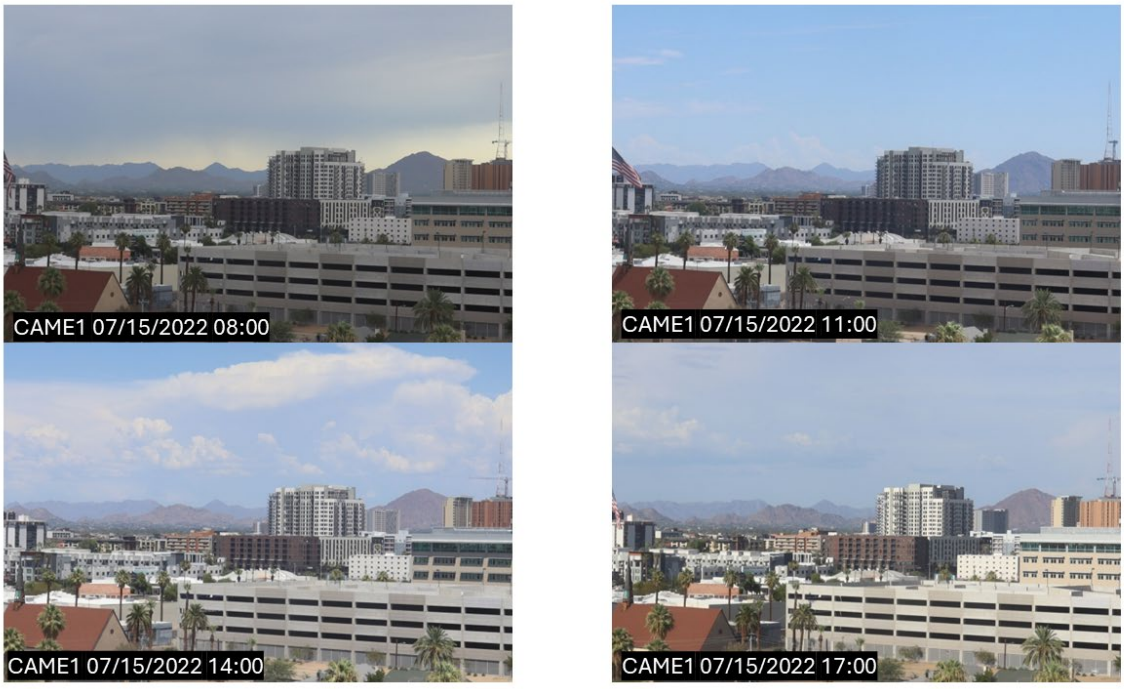

Figure 3-34. Camera Images showing the northeast coordinal direction taken from the Camelback Mountain webcam on July 15 from 8:00 LST, 11:00 LST, 14:00 LST, and 17:00.

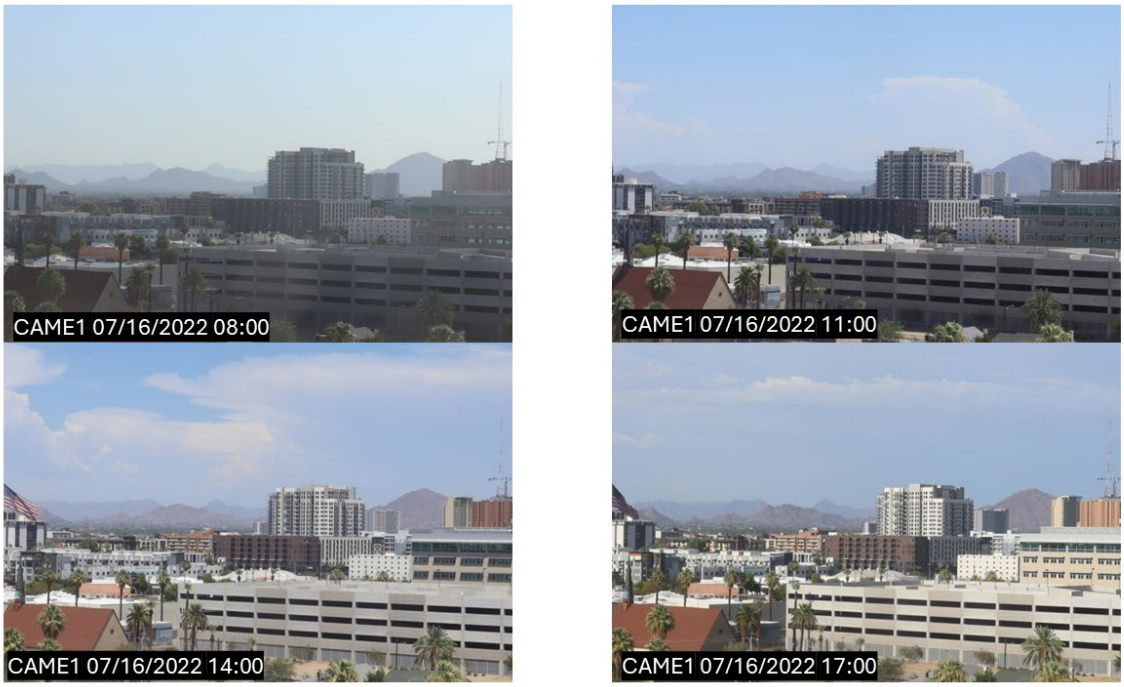

Figure 3-35. Camera Images showing the northeast coordinal direction taken from the Camelback Mountain webcam on July 16 from 8:00 LST, 11:00 LST, 14:00 LST, and 17:00.

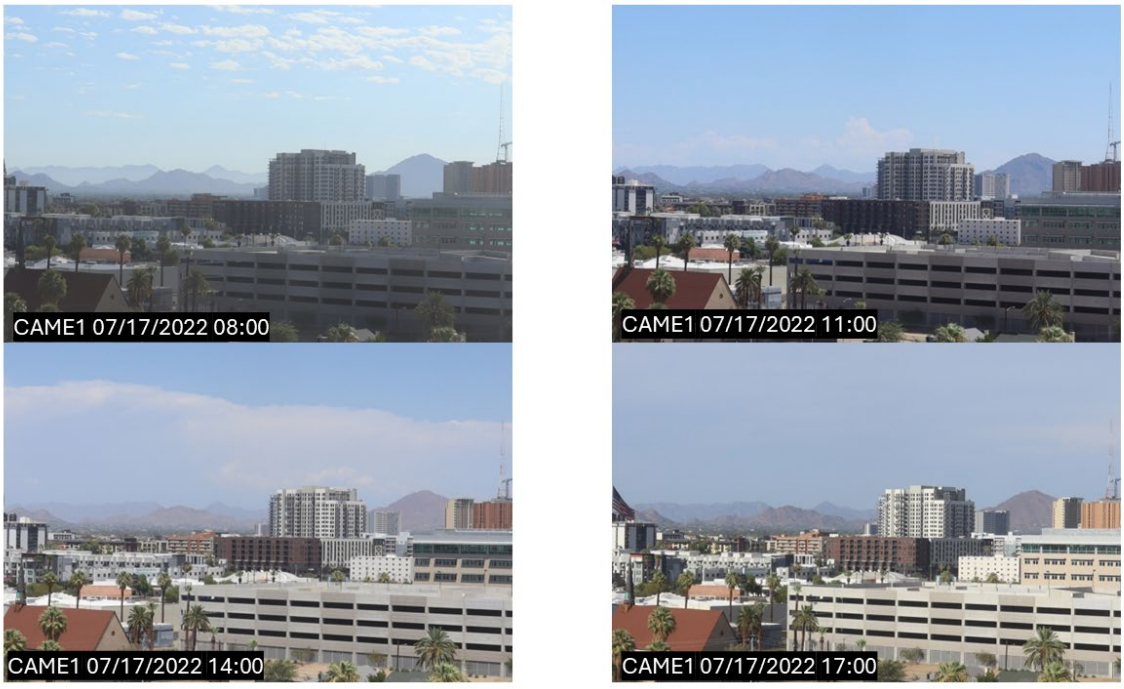

Figure 3-36. Camera Images showing the northeast coordinal direction taken from the Camelback Mountain webcam on July 17 from 8:00 LST, 11:00 LST, 14:00 LST, and 17:00.

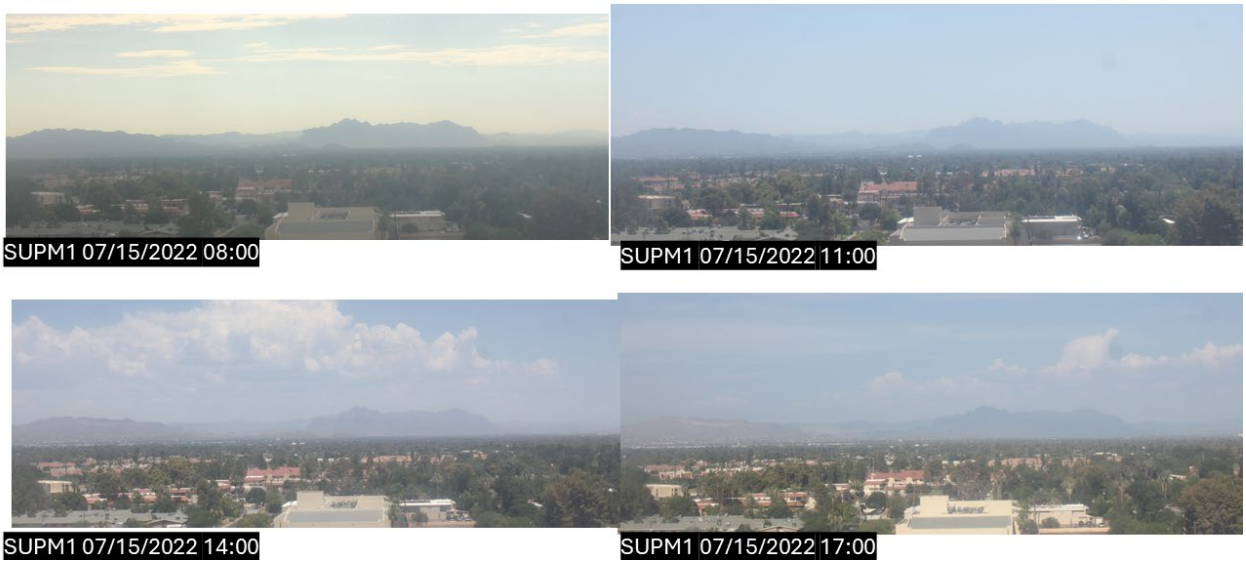

Figure 3-37. Camera Images showing the northeast coordinal direction taken from the Superstition Mountain webcam on July 15 from 8:00 LST, 11:00 LST, 14:00 LST, and 17:00.

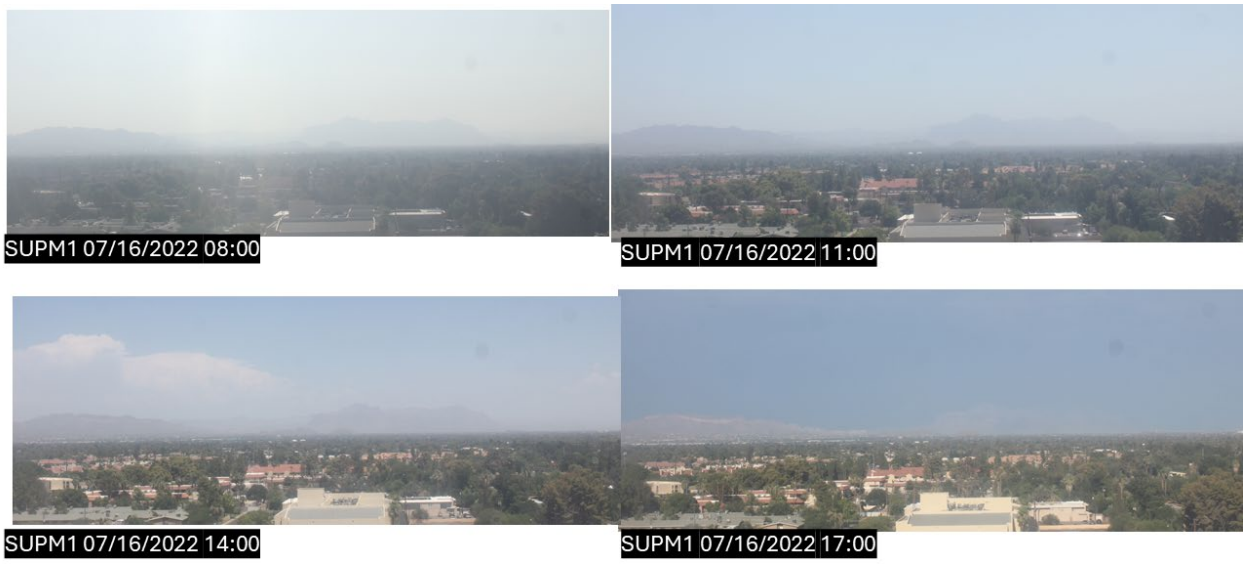

Figure 3-38. Camera Images showing the northeast coordinal direction taken from the Superstition Mountain webcam on July 16 from 8:00 LST, 11:00 LST, 14:00 LST, and 17:00.

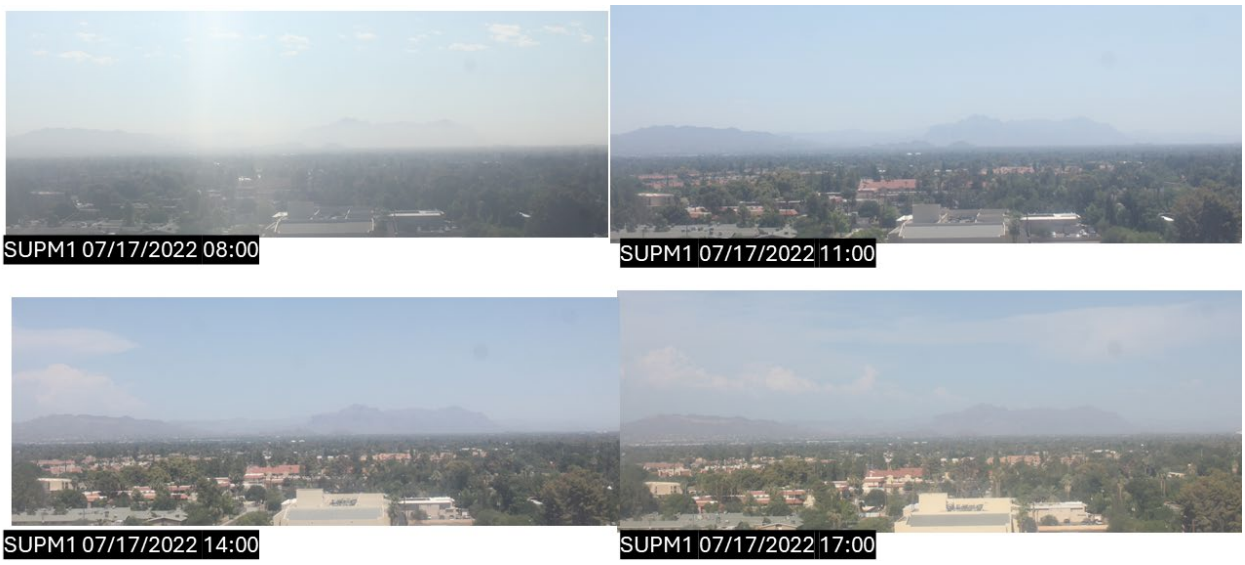

Figure 3-39. Camera Images showing the northeast coordinal direction taken from the Superstition Mountain webcam on July 17 from 8:00 LST, 11:00 LST, 14:00 LST, and 17:00.

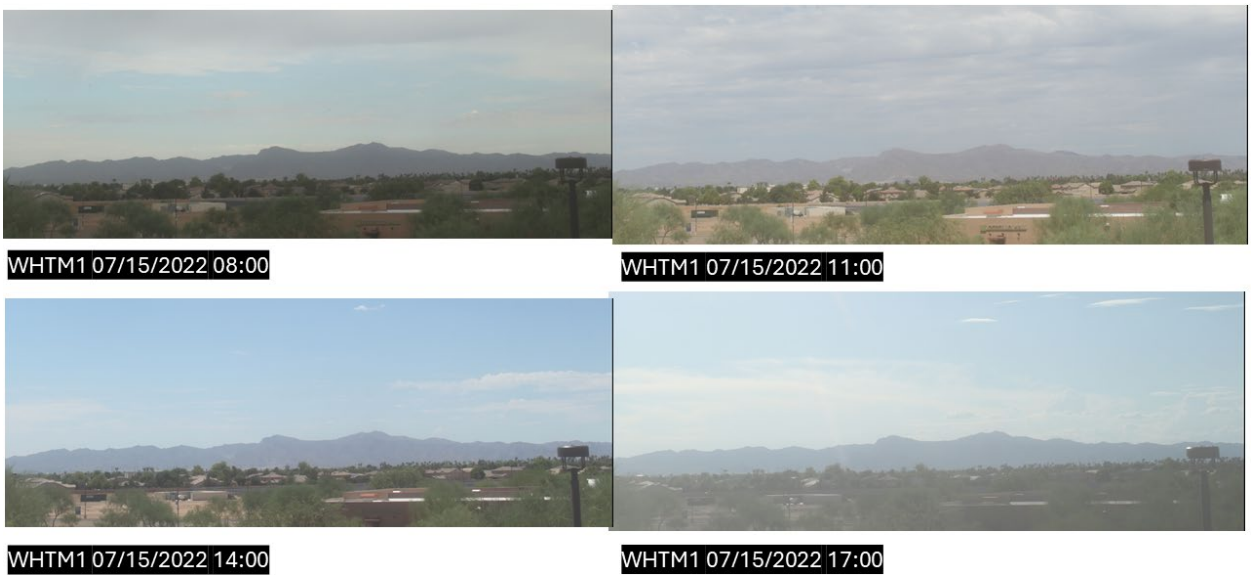

Figure 3-40. Camera Images showing the northeast coordinal direction taken from the White Tank Mountain webcam on July 15 from 8:00 LST, 11:00 LST, 14:00 LST, and 17:00.

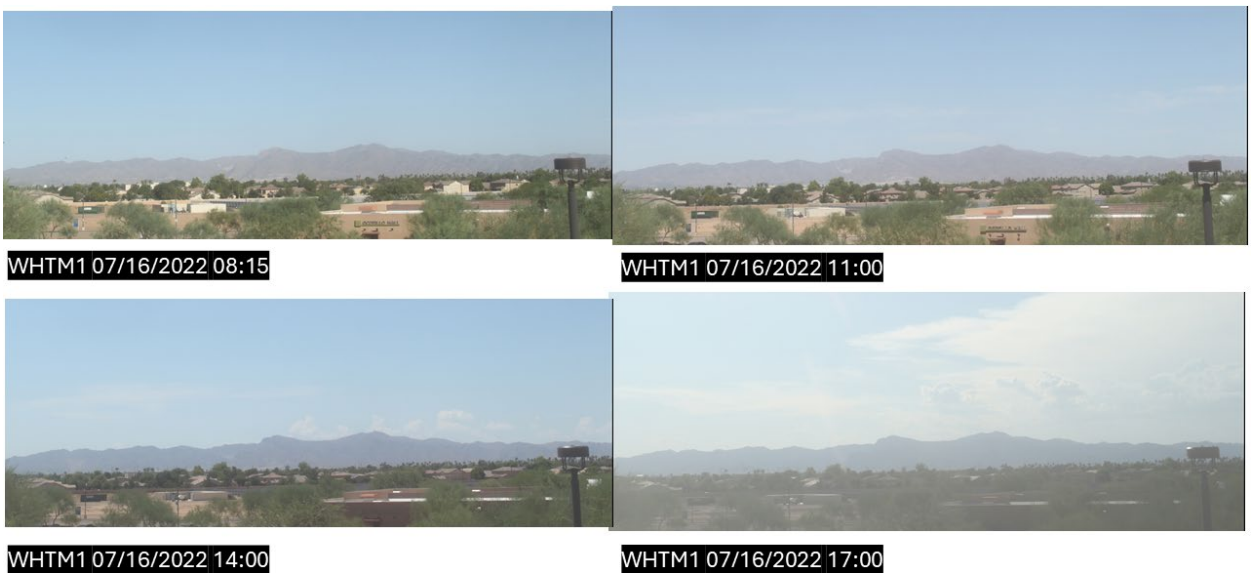

Figure 3-41. Camera Images showing the northeast coordinal direction taken from the White Tank Mountain webcam on July 17 from 8:00 LST, 11:00 LST, 14:00 LST, and 17:00.

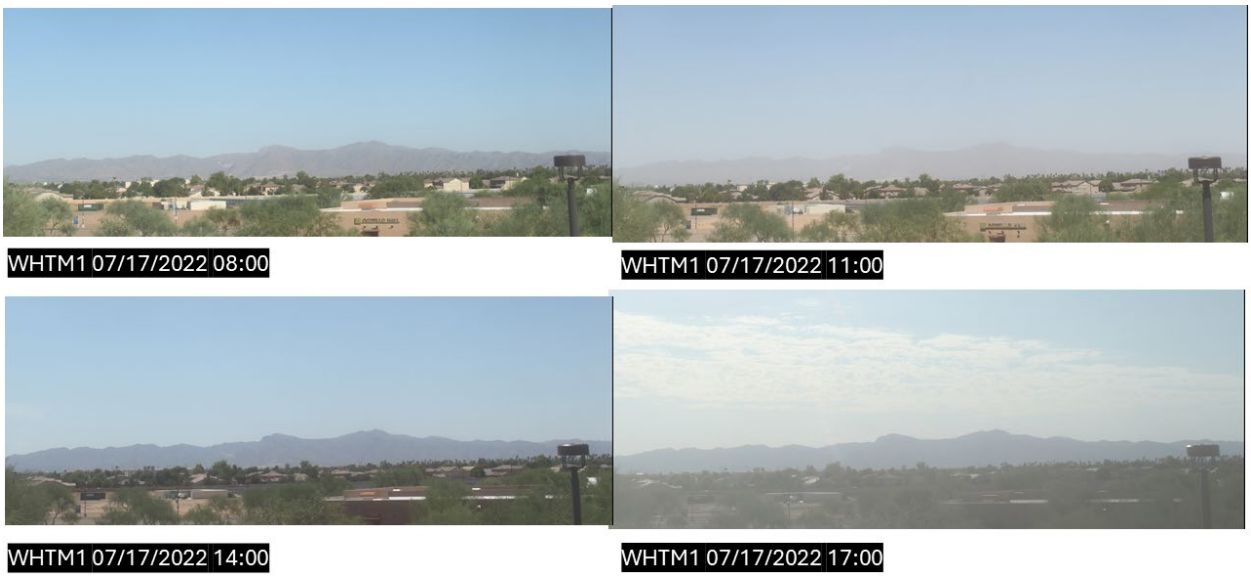

Figure 3-42. Camera Images showing the northeast coordinal direction taken from the White Tank Mountain webcam on July 18 from 8:00 LST, 11:00 LST, 14:00 LST, and 17:00.

Figure 3-43 shows an overall view of the magnitude of hourly pollutant concentrations measured in the nonattainment area in the two days before and after the July 15-17, 2022, atypical event. Hourly concentrations of ozone show widespread and distinct maximums on July 20-22 at all affected sites relative to July 15-17. $PM_{2.5}$ concentrations were elevated during some hours on July 16 and 17.

However, speciated $PM_{2.5}$ and storm reports[10] indicate that elevated $PM_{2.5}$ concentrations may have been due to wind-blown dust from monsoonal storms rather than smoke from wildfires.

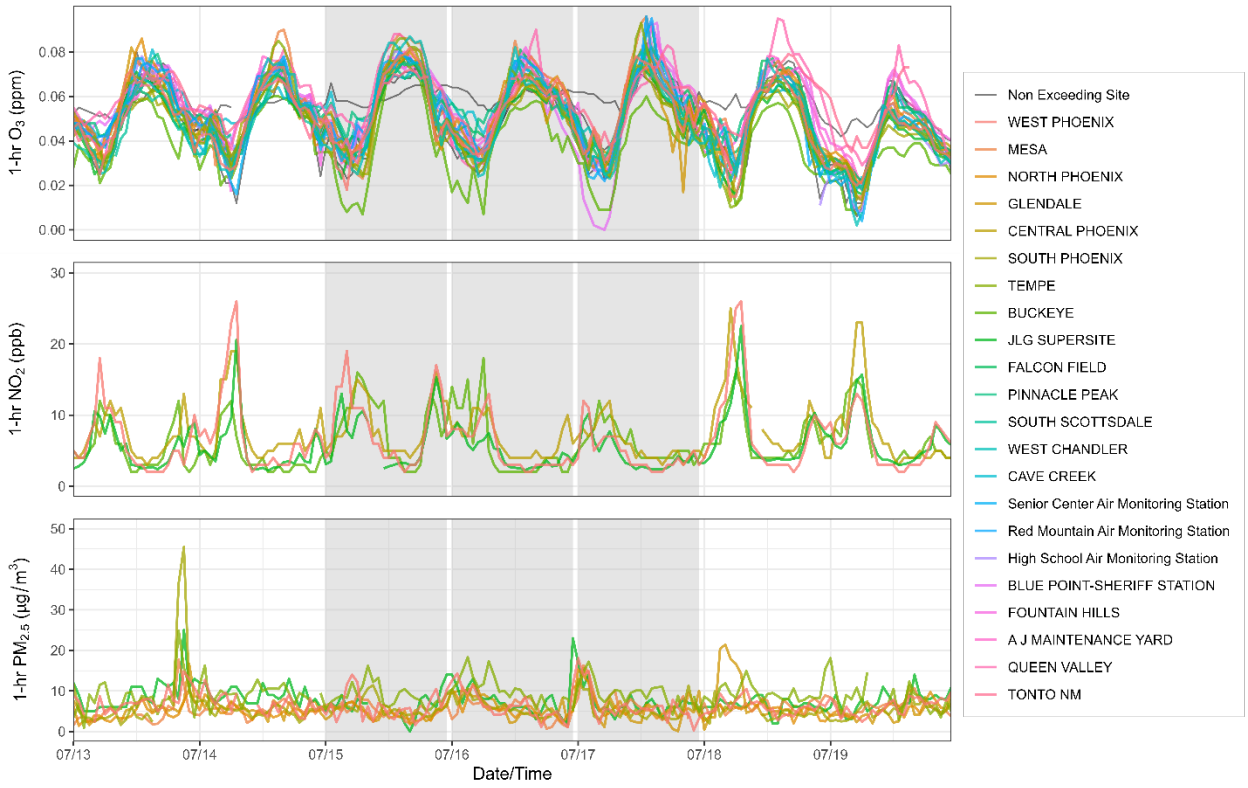

Figure 3-43. Hourly concentrations of ozone, NO_2, and $PM_{2.5}$ at all sites in the nonattainment area. All ozone-exceeding sites are color-coded to highlight smoke impacts on concentrations, and all non-exceeding sites are black. The gray shaded areas represent July 15-17, 2022.

The ratio of OC to EC taken at the JLG Supersite monitor was also examined for evidence that wildfire smoke entered the nonattainment area. Increases in this ratio are indicative of wildfire smoke. **Figure 3-49** shows boxplots of OC to EC ratios for available data collected during the ozone season between 2019-2024. The OC to EC ratio on July 16 was elevated well above the 75th percentile and considered an upper outlier compared to all data. These observations provide further evidence that ground-level wildfire smoke entered Phoenix on July 15-17 containing increased OC to EC ratios during the July 15-17, 2022, atypical ozone event.

[10] https://www.weather.gov/psr/July172022StormReport

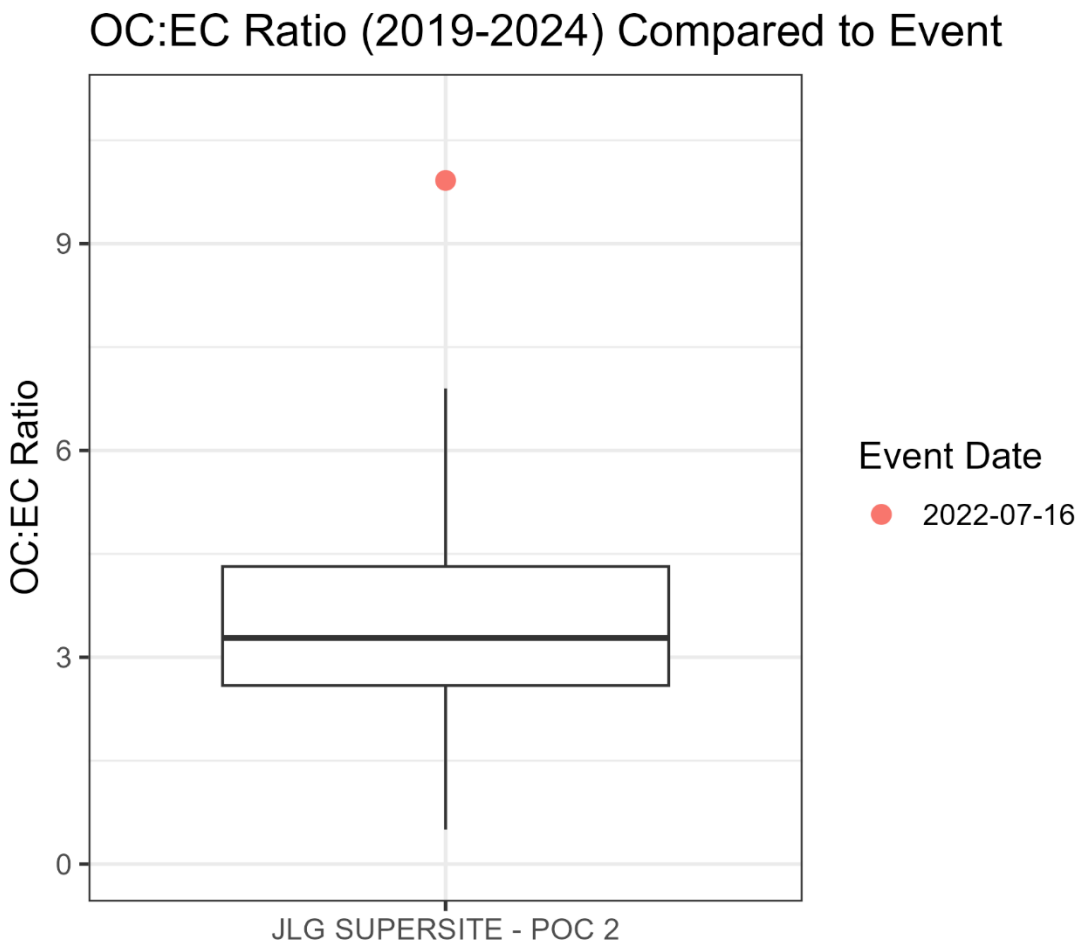

Figure 3-44. Boxplot of OC to EC ratios at the JLG Supersite site using data collected during the ozone season (April-September) from 2019-2024. OC to EC ratios are calculated at POC 2 (x-axis). Available OC to EC ratios collected during the July 15-17 atypical ozone event are shown as a point.

3.3.5 Event Statistics

Table 3-7 summarizes the measurements of ozone concentrations on July 15-17, 2022, as well as the percentile rank of the observation compared to six years of ozone season data (April 1-September 31, 2019-2024). Ozone MDA8 measurements ranged from the 95th - 100th percentile on July 15-17, 2022.

Table 3-7. Percentile of ozone measurements on the atypical dates compared with six years of ozone data (2019-2024). The percentile rank is calculated across the ozone production season in the nonattainment area (April 1-September 31) of 2019-2024.

Date	Site Name	Site Code	Ozone MDA8 (ppb)	Percentile Rank
7/15/2022	Mesa	040131003	84	100
	West Chandler	040134004	83	100
	Queen Valley	040218001	83	100
	Tempe	040134005	80	99
	West Phoenix	040130019	76	98
	South Phoenix	040134003	76	98
	High School Air Monitoring Station	040137024	76	98
	Fountain Hills	040139704	76	98
	North Phoenix	040131004	75	98
	Senior Center Air Monitoring Station	040137020	75	98
	Red Mountain Air Monitoring Station	040137021	75	98
	Falcon Field	040131010	74	97
	Central Phoenix	040133002	74	97
	Blue Point-Sheriff Station-Tonto NF-Salt River Recreation Area	040139702	73	97
	Glendale	040132001	72	96
	Buckeye	040134011	72	96
	A J Maintenance Yard	040213001	72	96
	South Scottsdale	040133003	71	95
	JLG Supersite	040139997	71	95
7/16/2022	Mesa	040131003	74	97
	Fountain Hills	040139704	73	97
	Falcon Field	040131010	71	95
	Red Mountain Air Monitoring Station	040137021	71	95

Date	Site Name	Site Code	Ozone MDA8 (ppb)	Percentile Rank
	High School Air Monitoring Station	040137024	71	95
	Queen Valley	040218001	71	95
7/17/2022	Mesa	040131003	78	99
	Fountain Hills	040139704	78	99
	Red Mountain Air Monitoring Station	040137021	77	99
	Blue Point-Sheriff Station-Tonto NF-Salt River Recreation Area	040139702	77	99
	High School Air Monitoring Station	040137024	75	98
	North Phoenix	040131004	74	97
	Falcon Field	040131010	74	97
	Pinnacle Peak	040132005	74	97
	Senior Center Air Monitoring Station	040137020	73	97
	Queen Valley	040218001	73	97
	Tempe	040134005	72	96
	A J Maintenance Yard	040213001	72	96
	West Phoenix	040130019	71	95
	Cave Creek	040134008	71	95
	Tonto NM	040070010	71	95

3.3.6 Conclusion

The concurrence of HMS smoke perimeters over the nonattainment area, HYSPLIT trajectories and meteorological analysis showing accumulation of smoke in the nonattainment area, visible smoke in camera images, and elevated OC to EC ratios provide evidence that surface-level smoke was present during the period. Long-range transport of smoke from large fires in central and southern U.S. and in Canada, enhanced ozone concentrations outside of the typical diurnal profile, keeping ozone values high and affecting the MDA8 ozone concentrations at twenty-two sites. Multiple analyses showed that smoke fully encompassed the Maricopa Nonattainment Area on July 15-17, 2022, and statistics show ozone concentrations were atypical during this event.

This combined evidence indicates that smoke plumes generated by numerous fires in the central and southern U.S. and in Canada provided an atypical source of ozone and ozone precursors that caused enhanced ozone concentrations on July 15-17, 2022. Removal of these days as atypical events is supported by this analysis.

4. 2023 Wildfire Events

4.1 Overview

This section provides evidence that ozone concentrations were atypical exceedances on several days during 2023 and that those exceedances were impacted by wildfire smoke from local wildfires and smoke transported from regional wildfires.

June 22-26, 2023

4.1.1 Event Overview: June 22-26, 2023

The unrepresentative (atypical) ozone event took place on June 22-26, 2023, and affected twenty monitoring sites in the Maricopa Nonattainment Area: West Phoenix, Mesa, North Phoenix, Falcon Field, Glendale, Pinnacle Peak, Central Phoenix, South Scottsdale, South Phoenix, Tempe, Cave Creek, Dysart, Red Mountain Air Monitoring Station, Lehi Air Monitoring Station, High School Air Monitoring Station, Humboldt Mountain, Blue Point-Sheriff Station-Tonto NF-Salt River Recreation Area, JLG Supersite, A J Maintenance Yard, and Tonto NM (**Table 4-1**). The maximum daily 8-hr average (MDA8) ozone concentrations at the effected sites ranged from 71-83 ppb.

Time series graphs showing hourly ozone concentrations that exceeded the seasonal means (calculated using all available data from April 1 – September 31, 2019-2024) and 10th-90th percentiles at each site are shown in **Figure 4-1**. On the afternoon of June 22, many sites such as Central Phoenix, JLG Supersite, and West Phoenix exhibited distinct and high peaks in ozone concentrations; these observations exceeded the 90th percentile relative to all data collected during the ozone season from 2019-2024. Ozone concentrations at some sites, such as Cave Creek, Humboldt Mountain, and Tonto NM, continuously exceeded the 90th percentile midway through the event period; these continuously elevated concentrations indicate an outside influence on air quality in Phoenix. Concentrations at many sites continued to exceed the 90th percentile and exhibit widespread and distinct maximums during the afternoons throughout the remainder of the atypical ozone event.

Numerous unidentified fires burning in Mexico were identified as major contributors to this event. Evidence includes (1) HMS smoke perimeters over the nonattainment area, (2) HYSPLIT trajectories and meteorological analysis showing accumulation of smoke in Phoenix, (3) visible smoke in camera images and video news coverage, and (4) elevated $PM_{2.5}$, NO_2, and OC to EC ratios. This combination of evidence indicates that this is an atypical ozone event.

Table 4-1. Summary of identified atypical June 22-26, 2023.

Event Date(s)	Event Ozone Concentration Percentile	Sites Exceeded During Event	Type of Event
June 22-26, 2023	93rd - 99th	Twenty sites: West Phoenix, Mesa, North Phoenix, Falcon Field, Glendale, Pinnacle Peak, Central Phoenix, South Scottsdale, South Phoenix, Tempe, Cave Creek, Dysart, Red Mountain Air Monitoring Station, Lehi Air Monitoring Station, High School Air Monitoring Station, Humboldt Mountain, Blue Point-Sheriff Station-Tonto NF-Salt River Recreation Area, JLG Supersite, A J Maintenance Yard, Tonto NM	International/regional transport

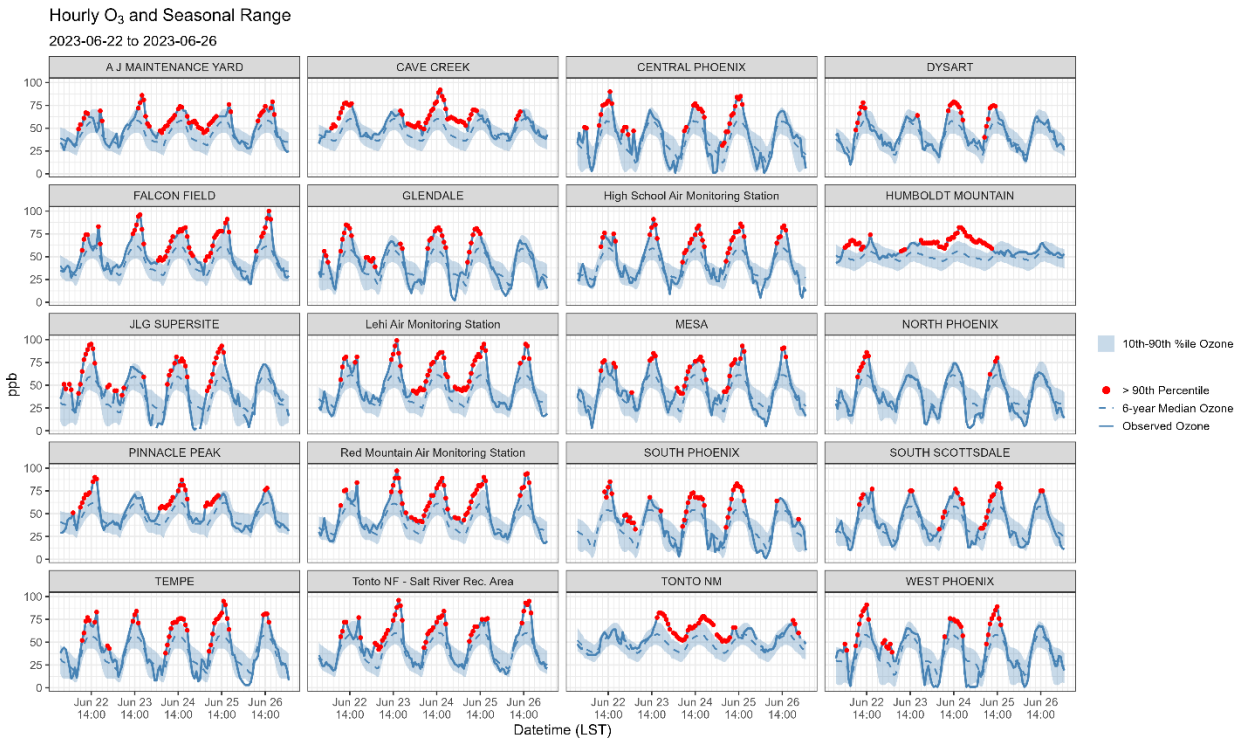

Figure 4-1. Hourly ozone concentrations (ppb) compared to all available data during the ozone season (April 1 – September 31) of the 6-year (2019-2024) period. Hourly means and 10th-90th percentiles are calculated using data on June 22-26, 2023.

4.1.2 Identification of Wildfire(s)

Multiple fires in Mexico were active in the days leading up to and during June 22-26, the exclusion days (**Figures 4-2 to 4-6**). Smoke from these fires along with numerous other fires across the U.S. and Canada combined to blanket the continental U.S. during June 22-26.

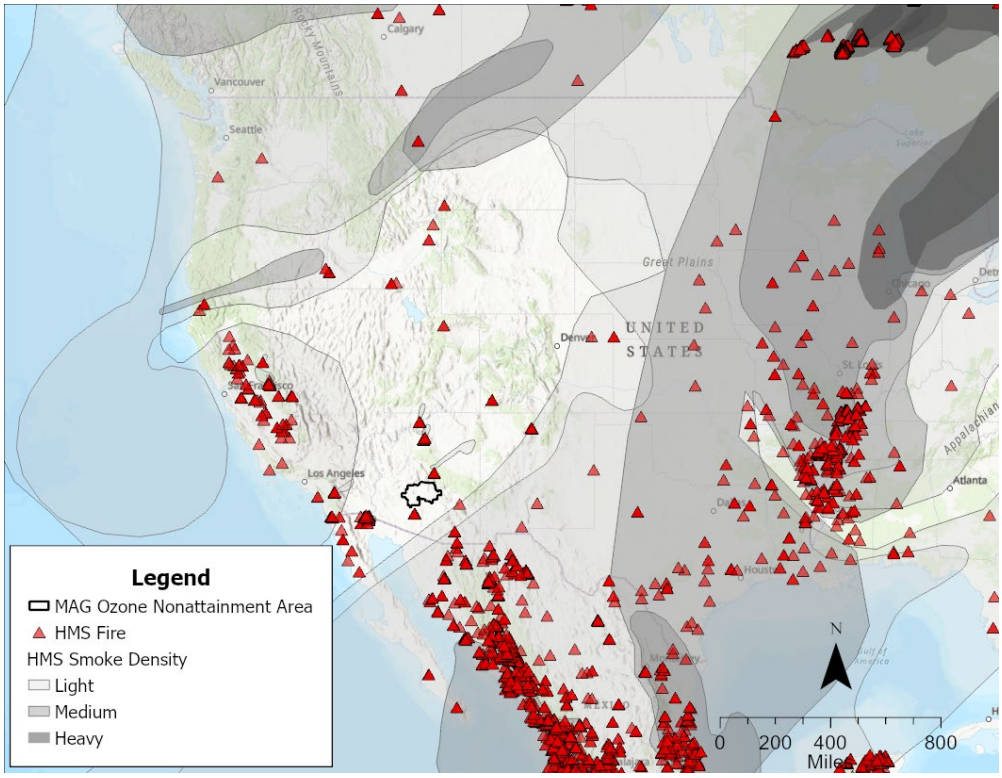

Figure 4-2. Continental view of HMS smoke density and fire locations on June 22, 2023.

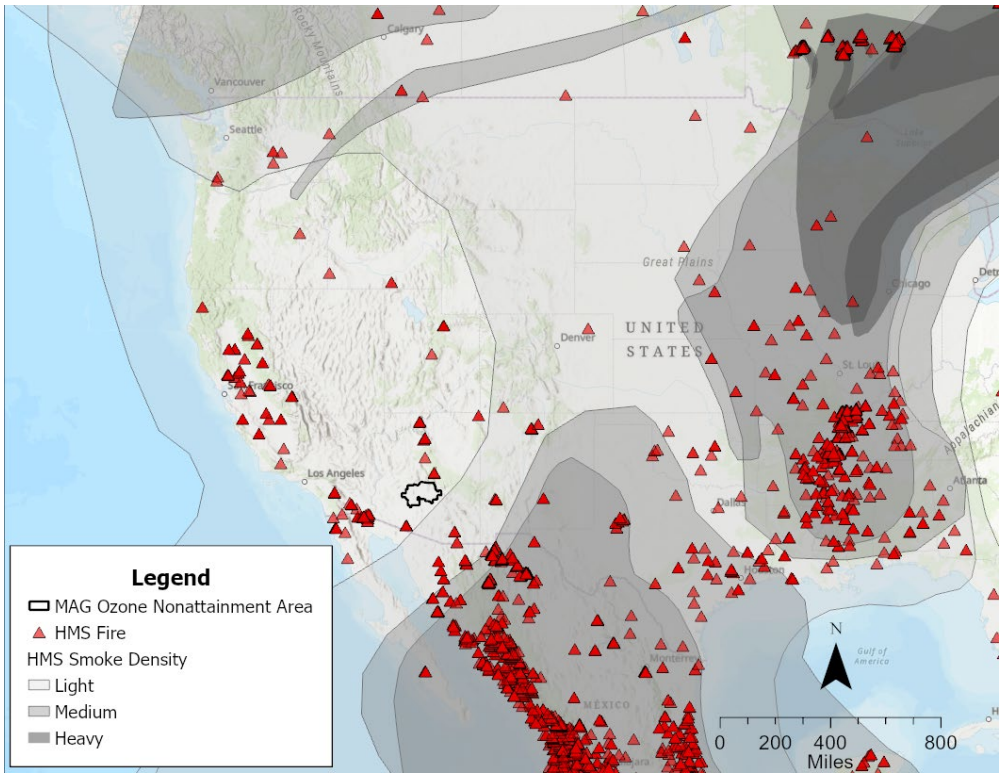

Figure 4-3. Continental view of HMS smoke density and fire locations on June 23, 2023.

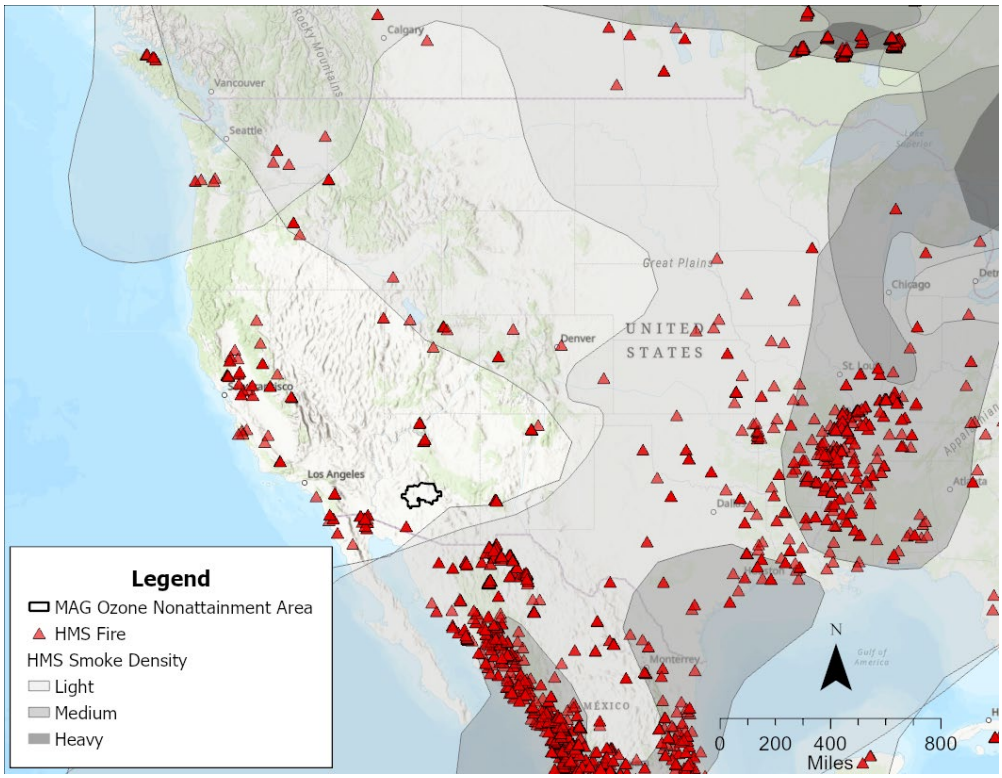

Figure 4-4. Continental view of HMS smoke density and fire locations on June 24, 2023.

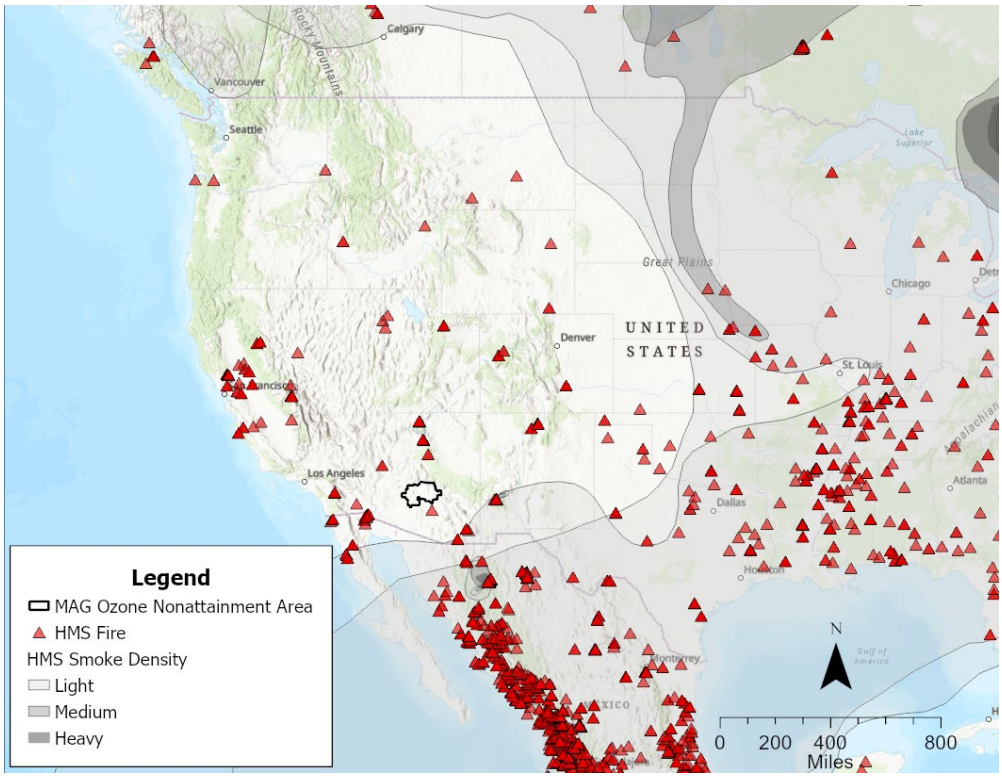

Figure 4-5. Continental view of HMS smoke density and fire locations on June 25, 2023.

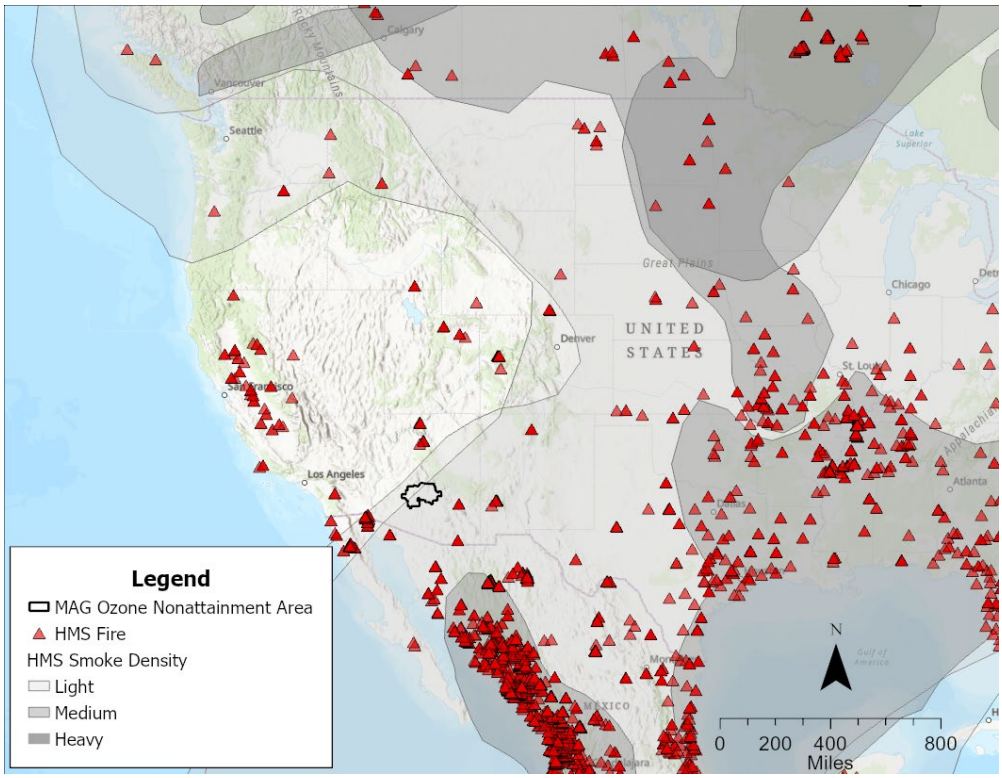

Figure 4-6. Continental view of HMS smoke density and fire locations on June 26, 2023.

4.1.3 Meteorological Analysis

Upper-level Analysis

For June 22-26, 2023, the overall upper-level weather pattern is shown in **Figure 4-7**, which was established using the mean 500 mb wind speed and direction. The prevailing pattern during this five-day period was a persistent trough of low pressure aloft off the Pacific Northwest and northern California coast. In addition, upper-level high pressure was present across northern Mexico. Between these two features, aloft winds in central Arizona were from the southwest.

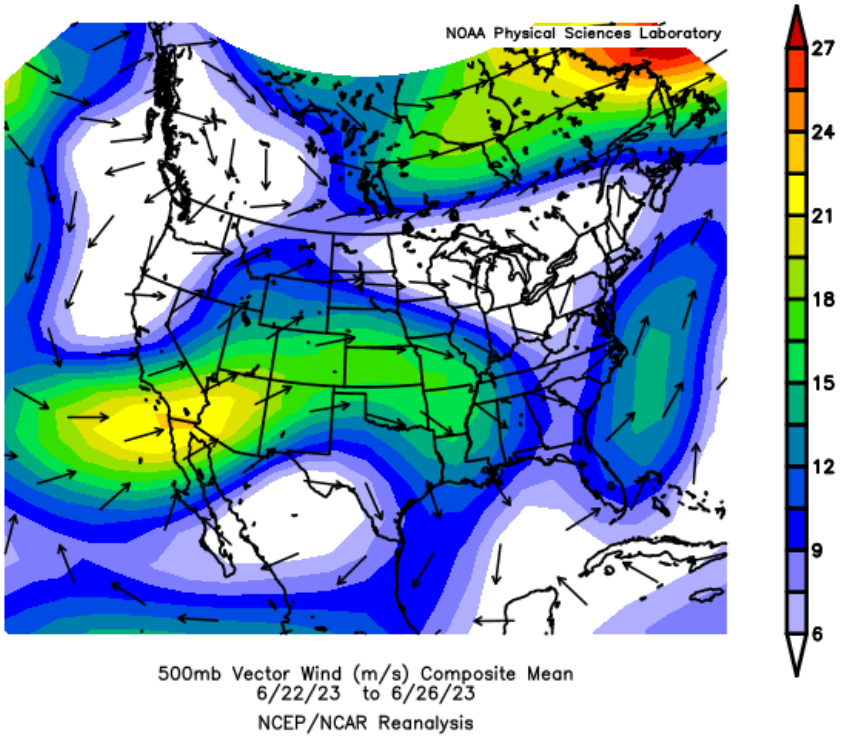

Figure 4-7. Mean 500 mb wind speed and direction for June 22-26, 2023. Aloft high pressure in northern Mexico led to southwesterly flow into Phoenix at the upper levels of the atmosphere. Source: NOAA

Surface Analysis

Within the PBL, sunny and hot conditions prevailed in the nonattainment area, due to the subsidence from the upper-level high over northern Mexico. **Table 4-2** contains the daily maximum temperatures and daily average wind speed at KPHX for the period. Afternoon high temperatures at KPHX exceeded 100°F between June 22-26 under abundant sunshine. Furthermore, daily average wind speeds at KPHX each day were around 4-7 mph, leading to pollutant and ozone precursor

accumulation, as well as day to day carryover. These conditions promoted the formation of ground-level ozone in central Arizona.

Table 4-2. Daily maximum temperatures and average daily wind speed at KPHX.

Date	Maximum temperature (°F)	Average daily wind speed (mph)
June 22	109	6.9
June 23	103	5.5
June 24	106	4.4
June 25	111	6.0
June 26	112	6.4

Satellite Smoke and Fire Detections

Figure 4-8 contains NOAA HMS smoke plume analysis and satellite fire detections across the southwestern United States. Smoke plumes were analyzed to the west, southeast, and east of the nonattainment area on June 22, with isolated fire detections across Arizona. By June 23, fire detections remained isolated across the state. However, NOAA analyzed smoke over Arizona. On June 24 and 25, NOAA analyzed smoke plumes south and east of Arizona, with few satellite fire detections within the state. Smoke was once again analyzed over Arizona on June 26. While some days did not have smoke analyzed over the state during the period, there is evidence of smoke transport into the nonattainment area, which is discussed in detail in the “Smoke Transport” section.

June 22

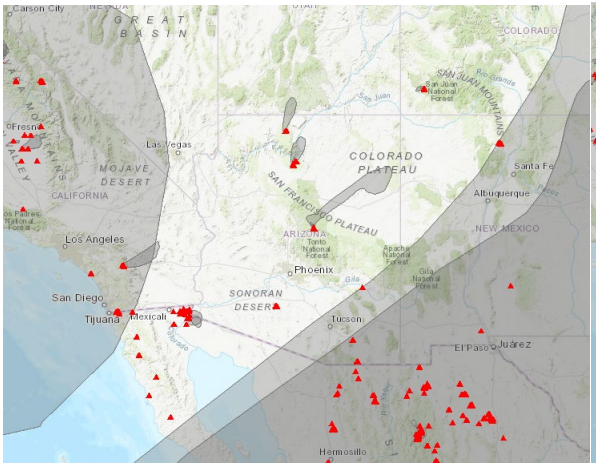

June 23

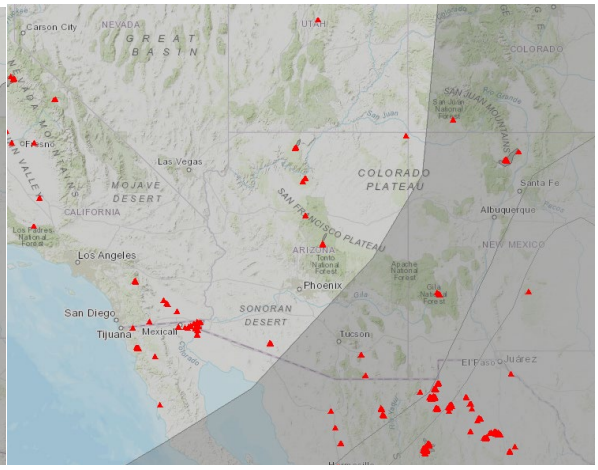

June 24

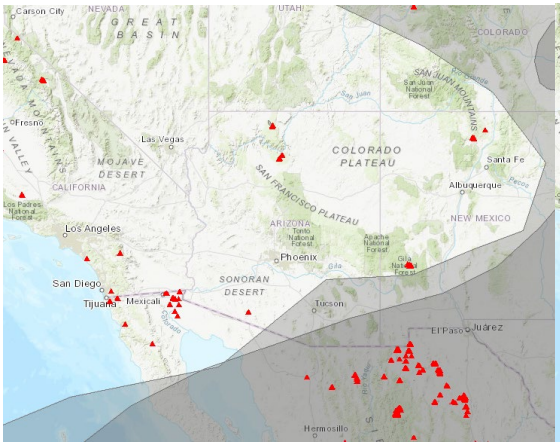

June 25

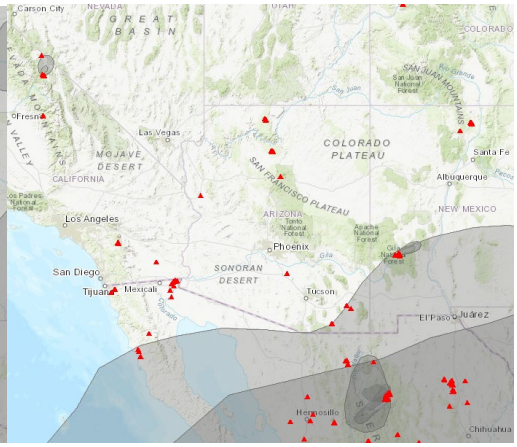

June 26

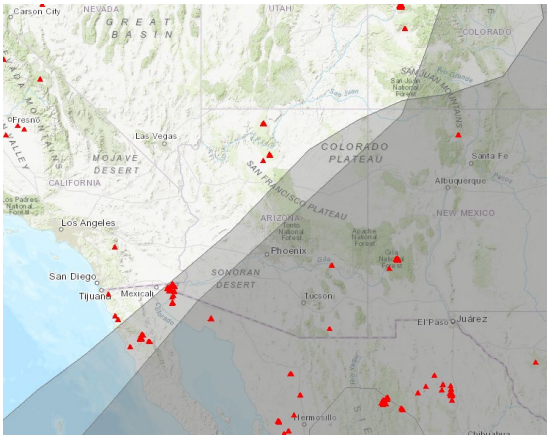

Figure 4-8. NOAA HMS smoke plume analysis (grey contours) and satellite fire detections (red triangles) from June 22-26, 2023. Source: AirNow-Tech

Smoke Discussions

NOAA's daily smoke discussions noted smoke from fires in Mexico impacting the southwest on June 22, 23, 24, and 26. The text for June 24 and 26 was nearly identical as the previous days and not shown here.

"**Seasonal fires and a few wildfires continue to burn mainly in Mexico**. As a result, a large area of light with patches of moderate density smoke covered Mexico, the western Gulf of Mexico, the Pacific well south and southwest of southern Mexico, **and portions of the southwestern and south-central U.S.** It is likely that some aerosols from industrial activities in Mexico and Central America may also be present with the smoke over this large region." (NOAA NESDIS Text Narrative from June 22, 2023)

"**Seasonal fires and a few wildfires continue to burn mainly in Mexico resulting in a large mass of thin to moderately dense smoke covering nearly all of Mexico, the southwestern and south central U.S.**, the western and northern Gulf of Mexico, northwestern Central America, and the Pacific Ocean extending well to the south and southwest of the southern coast of Mexico." (NOAA NESDIS Text Narrative from June 23, 2023)

Soundings

PBL heights in Phoenix for each day were estimated using the Tucson upper-air sounding data. Table 4-3 shows the estimated PBL heights for Phoenix between June 22-26, 2023, using the 5 p.m. PST Tucson data and adjusting for the elevation of Phoenix. The 5 p.m. PST skew-T diagrams from Tucson are in Figure 4-9, which indicate deep mixing within the PBL. This mixing was capable of transferring aloft air to the surface.

Table 4-3. Daily estimated PBL heights for Phoenix, sourced from the Tucson upper-air skew-T diagrams.

Date	Estimated PBL (meters)
June 22	3,100
June 23	3,100
June 24	3,500
June 25	5,500
June 26	4,800

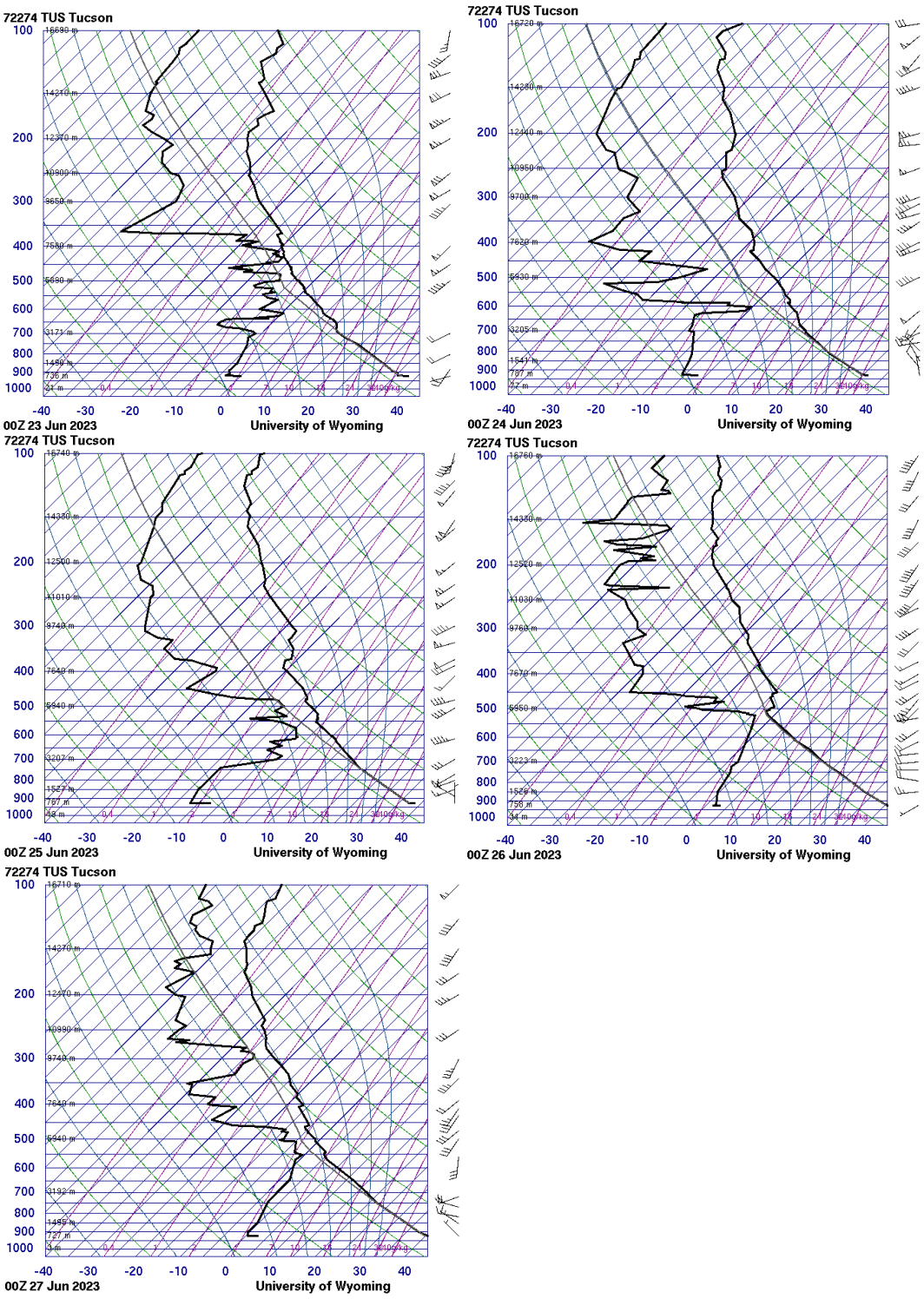

Figure 4-9. Tucson skew-T upper-air diagrams valid 5 p.m. PST from June 22-26, 2023. Deep mixing was evident, indicating the transfer of aloft air down to the surface. Source: University of Wyoming

Smoke Transport

With boundary layer conditions established, the NOAA HYSPLIT tool was used to identify transport paths into central Arizona during the 5-day period. Additionally, the potential for smoke transport into the nonattainment area was assessed by overlaying the HYSPLIT trajectory paths onto the NOAA HMS smoke analysis and satellite fire detections. The 24-hour back trajectory ending at 11 p.m. PST on June 22 (**Figure 4-10**) showed the 1,500 m AGL and 3,100 m AGL transport paths near a cluster of fire detections in the Sand Tank Mountains south of Phoenix. At the 500 m AGL level, the transport path entering the nonattainment area intersected analyzed smoke plumes and fire detections in the far northeastern portion of Baja California from the current and prior day. For the June 23 back trajectory analysis, the 500 m path entering nonattainment area again intersected the analyzed smoke plumes and satellite fire detections across northeastern Baja California.

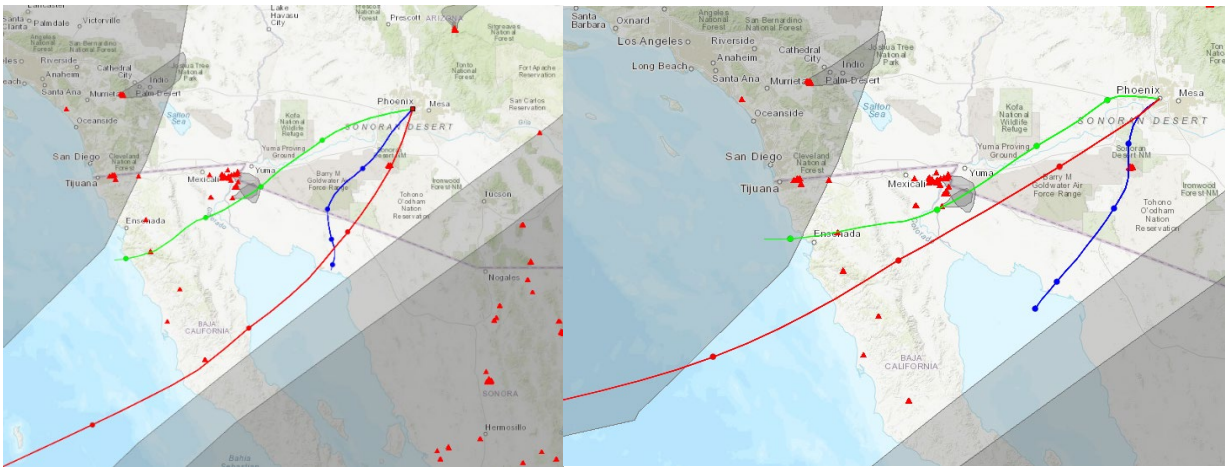

Figure 4-10. 24-hour back trajectory analysis for June 22 (left) and June 23 (right). Transport paths into the nonattainment area intersected with NOAA HMS smoke plumes (grey contours) and satellite fire detections (red triangles). Source: AirNow-Tech

Evidence of smoke transport into the nonattainment area continued for June 24-26, albeit from a different source. Back trajectory analysis ending at 11 p.m. PST on June 24 (**Figure 4-11**) showed the 3,500 m AGL transport path originating off the Mexico coast from June 21, where NOAA analyzed smoke from several fires on mainland Mexico. The transport of offshore smoke was also evident in the June 25 back trajectory analysis at the 2,500 m and 5,500 m levels, with these transport paths intersecting an analyzed smoke plume from June 23. On June 26, a 72-hour back trajectory analysis showed transport of offshore smoke from June 23 at the 2,400 m level. At the 4,800 m level, the transport path intersected analyzed smoke and several fire detections across western Mexico that were present on June 23.

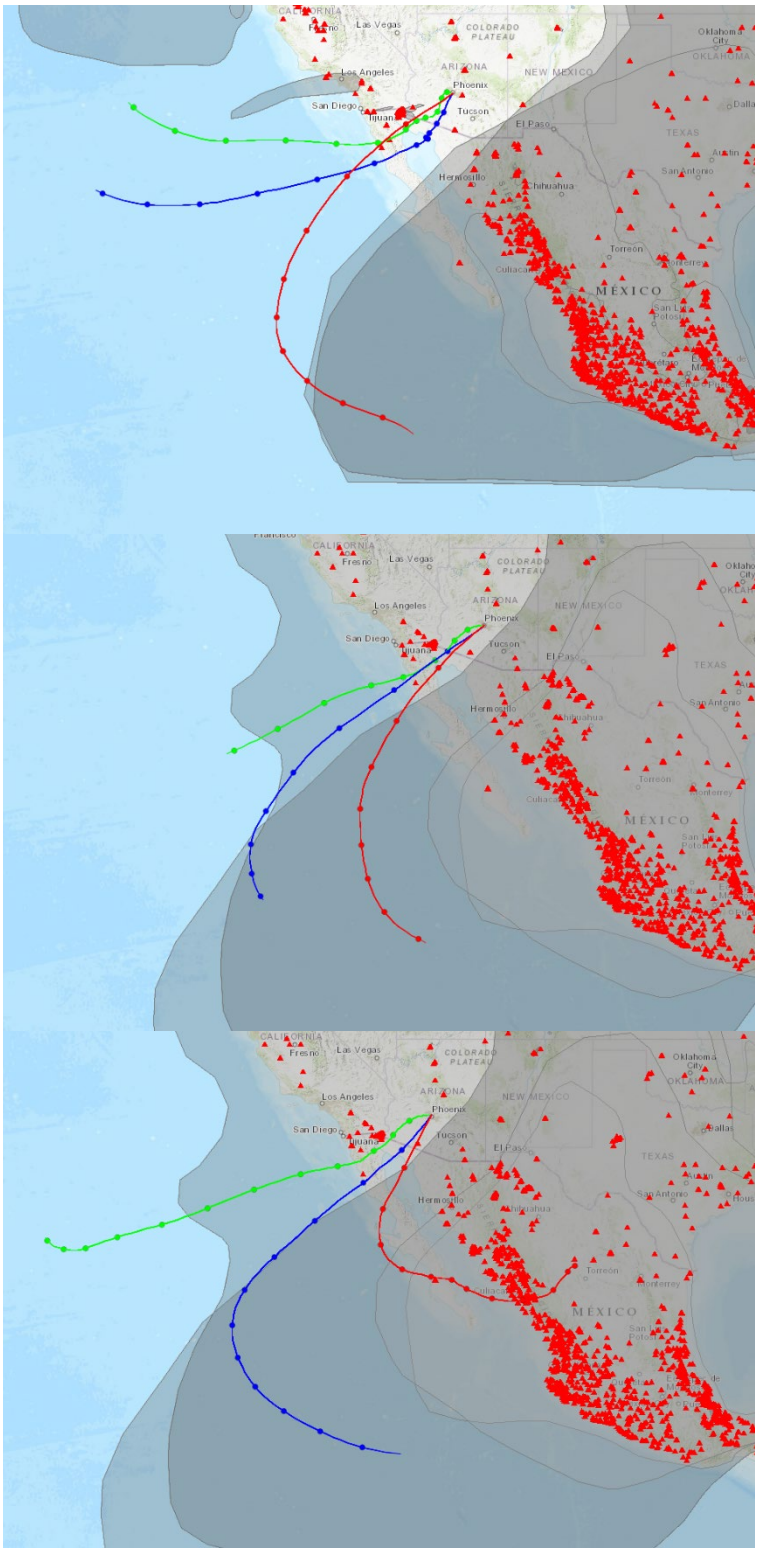

Figure 4-11. NOAA HYSPLIT back trajectory analysis for June 24 (top), June 25 (middle), and June 26 (bottom). Transport paths into the nonattainment area intersected with NOAA HMS smoke plumes (grey contours) and satellite fire detections (red triangles). Source: AirNow-Tech

Summary

During the June 22-26 period, upper-level high pressure over northern Mexico resulted in sunny and hot conditions, with southwesterly flow aloft into central Arizona. Per HYSPLIT trajectory analysis, southwesterly flow also existed within the PBL during the 5-day period, with HYSPLIT and NOAA HMS indicating smoke transport into the nonattainment area each day. In addition, surface winds each day were light, hindering dispersion and allowing pollutants and smoke to carryover from day to day. Due to these conditions, there is evidence of smoke transport and ozone enhancement impacting the nonattainment area from June 22-26.

4.1.4 Surface Impacts

Low visibility in the nonattainment area is apparent on June 22-26, 2023. While some of the haze is may be due to dust, smoke plumes from the fires burning throughout Mexico were present over the nonattainment area during the atypical ozone event and contributed to the haze. **Figures 4-12 through 4-20** show photos taken from the south-facing South Mountain, east-facing Superstition Mountain, and west-northwest-facing White Tank Mountain webcams, where the visibility is low due to haze on June 22-26, 2023. Select webcam images were chosen to coincide with days with noticeable increase in hourly $PM_{2.5}$ concentrations (see **Figure 4-21**).

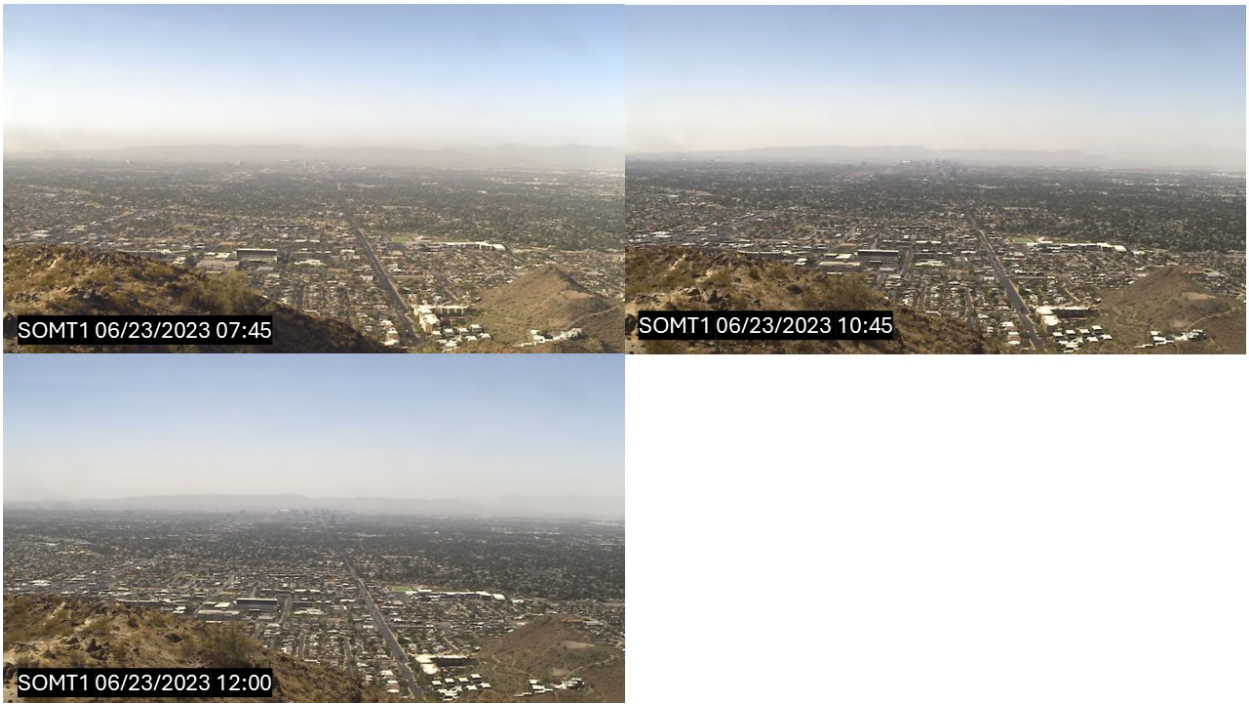

Figure 4-12. Camera Images showing the south coordinal direction taken from the South Mountain webcam on June 23 from 7:45 LST, 10:45 LST, and 12:00 LST.

Figure 4-13. Camera Images showing the south coordinal direction taken from the South Mountain webcam on June 25 from 6:30 LST, 7:30 LST, and 15:30 LST.

Figure 4-14. Camera Images showing the south coordinal direction taken from the South Mountain webcam on June 23 from 8:00 LST, 10:30 LST, 12:30 LST, and 14:30 LST.

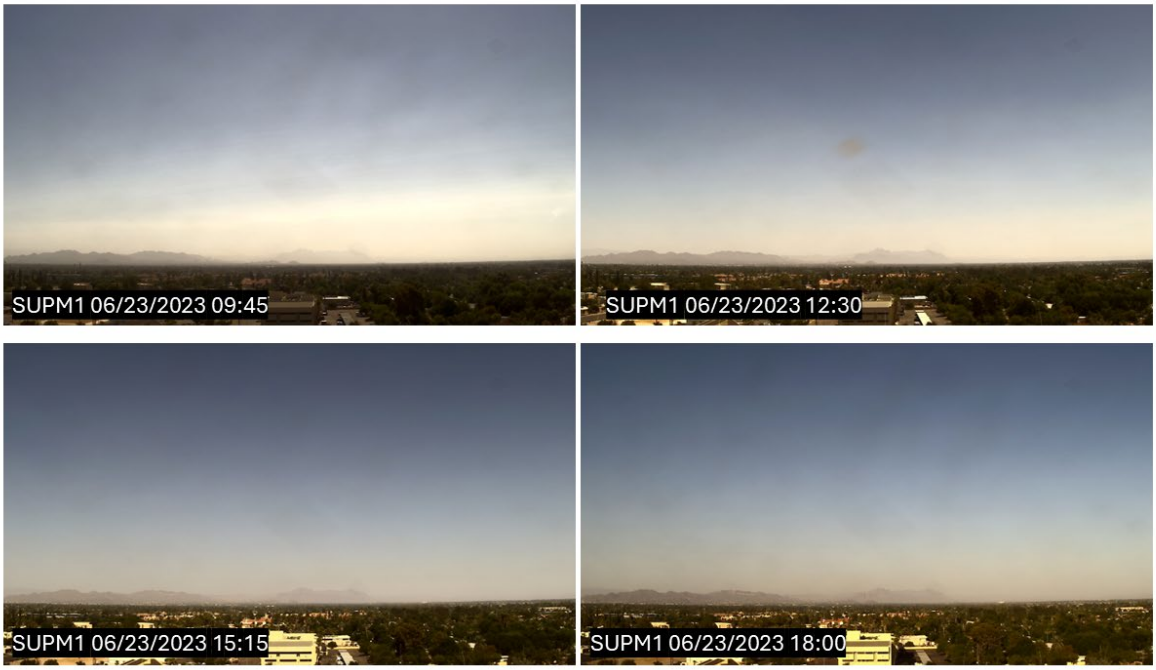

Figure 4-15. Camera Images showing the east coordinal direction taken from the Superstition Mountain webcam on June 23 from 9:45 LST, 12:30 LST, 15:15 LST, and 18:00 LST.

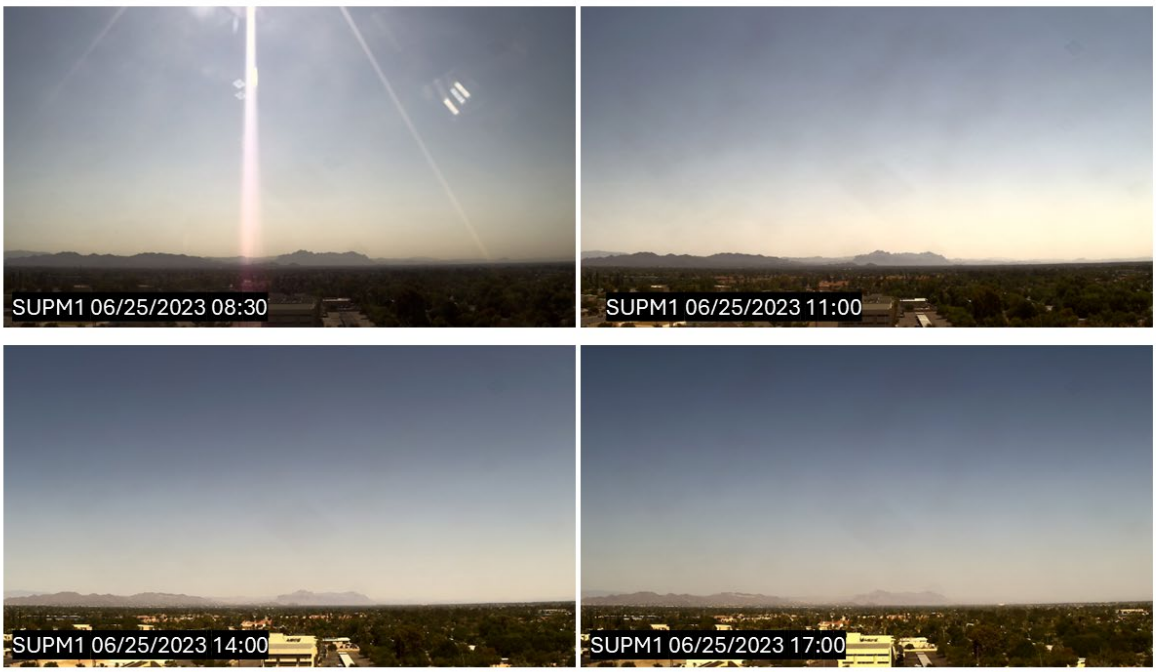

Figure 4-16. Camera Images showing the east coordinal direction taken from the Superstition Mountain webcam on June 25 from 8:30 LST, 11:00 LST, 14:00 LST, and 17:00 LST.

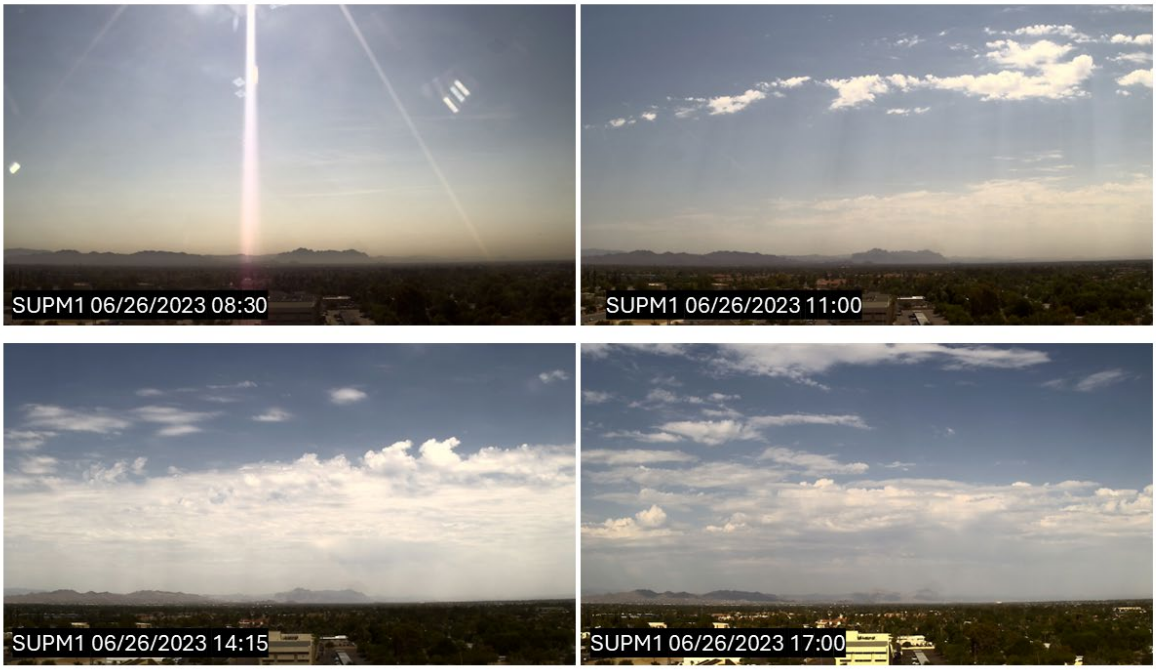

Figure 4-17. Camera Images showing the east coordinal direction taken from the Superstition Mountain webcam on June 26 from 8:30 LST, 11:00 LST, 14:15 LST, and 17:00 LST.

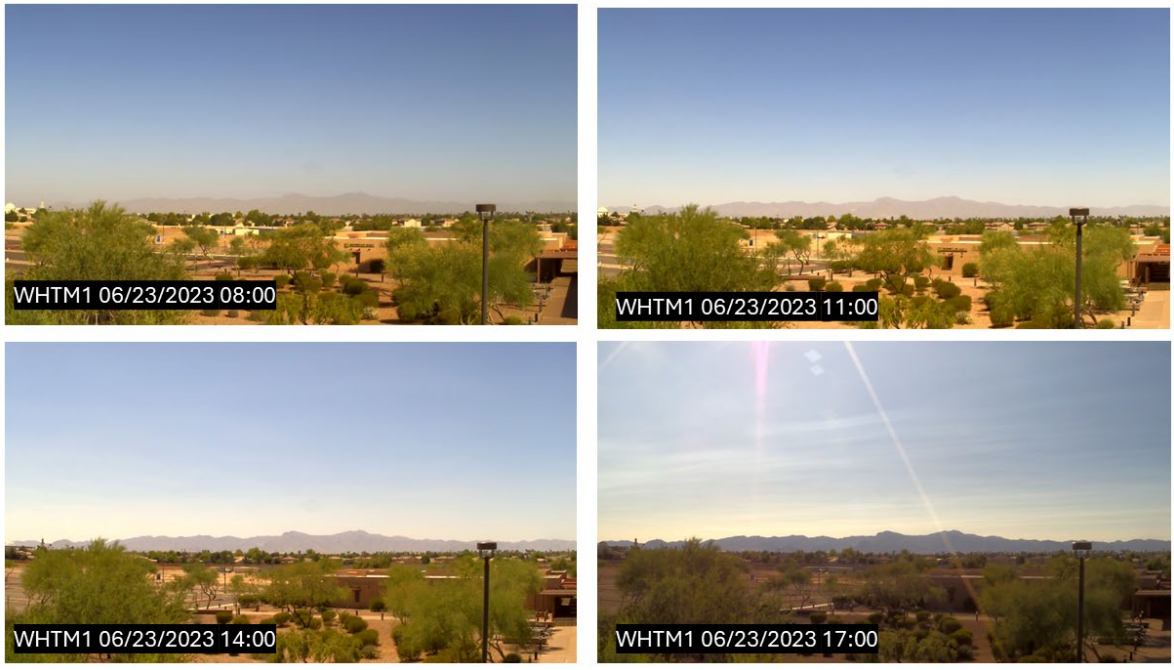

Figure 4-18. Camera Images showing the west-northwest coordinal direction taken from the White Tank Mountain webcam on June 23 from 8:00 LST, 11:00 LST, 14:00 LST, and 17:00 LST.

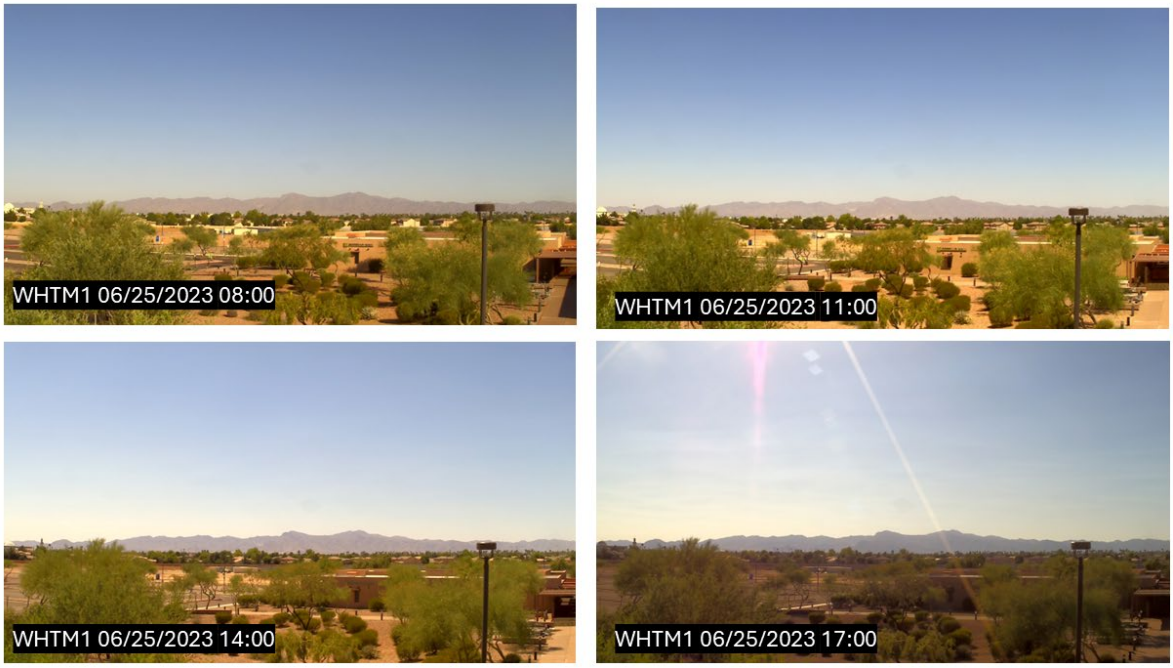

Figure 4-19. Camera Images showing the west-northwest coordinal direction taken from the White Tank Mountain webcam on June 25 from 8:00 LST, 11:00 LST, 14:00 LST, and 17:00 LST.

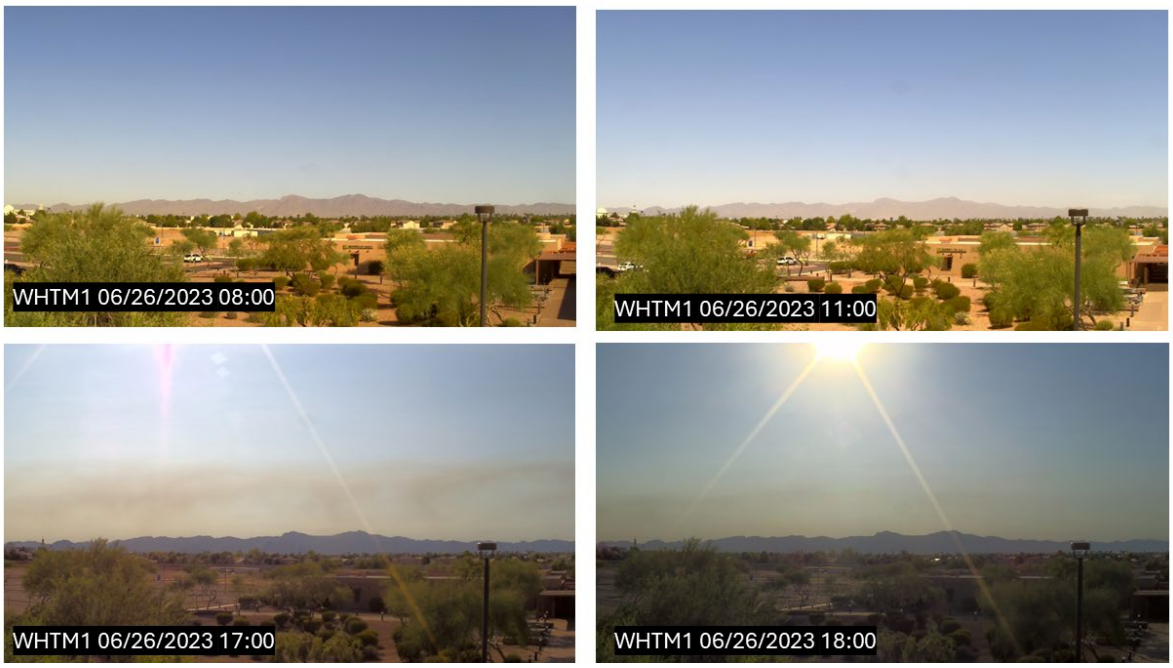

Figure 4-20. Camera Images showing the west-northwest coordinal direction taken from the White Tank Mountain webcam on June 26 from 8:00 LST, 11:00 LST, 17:00 LST, and 18:00 LST.

Figure 4-21 shows an overall view of the magnitude of hourly pollutant concentrations measured in the nonattainment area in the two days before and after the June 22-26, 2023, atypical event. Hourly

concentrations of ozone are elevated at all affected sites relative to the days surrounding the atypical event. Similarly, NO_2 concentrations at many sites, including West Phoenix and JLG Supersite, were elevated during most of the June 22-26 period. $PM_{2.5}$ concentrations at the exceedance-affected sites rise sharply at all $PM_{2.5}$-measuring sites during multiple instances throughout the June 22-26 period, particularly on the morning of June 23. $PM_{2.5}$ concentrations at all sites continue to exhibit widespread and distinct maximums from June 24 through the end of the event period. Higher $PM_{2.5}$ concentrations were likely not solely from dust because conditions were not favorable (e.g., wind speeds were generally low, no drought in the nonattainment area)[11] for wind-blown dust before and during the June 22-26 atypical event. Furthermore, there were no dust storm advisories or warnings before or during this atypical event.[12] Distinct and widespread enhancements in surface pollutant concentrations provide evidence that smoke from regional fires entered the region, mixed towards the surface, and had an atypical influence on ozone during the period. The rest of this section examines temporal abnormalities and site-specific trends for each supporting pollutant.

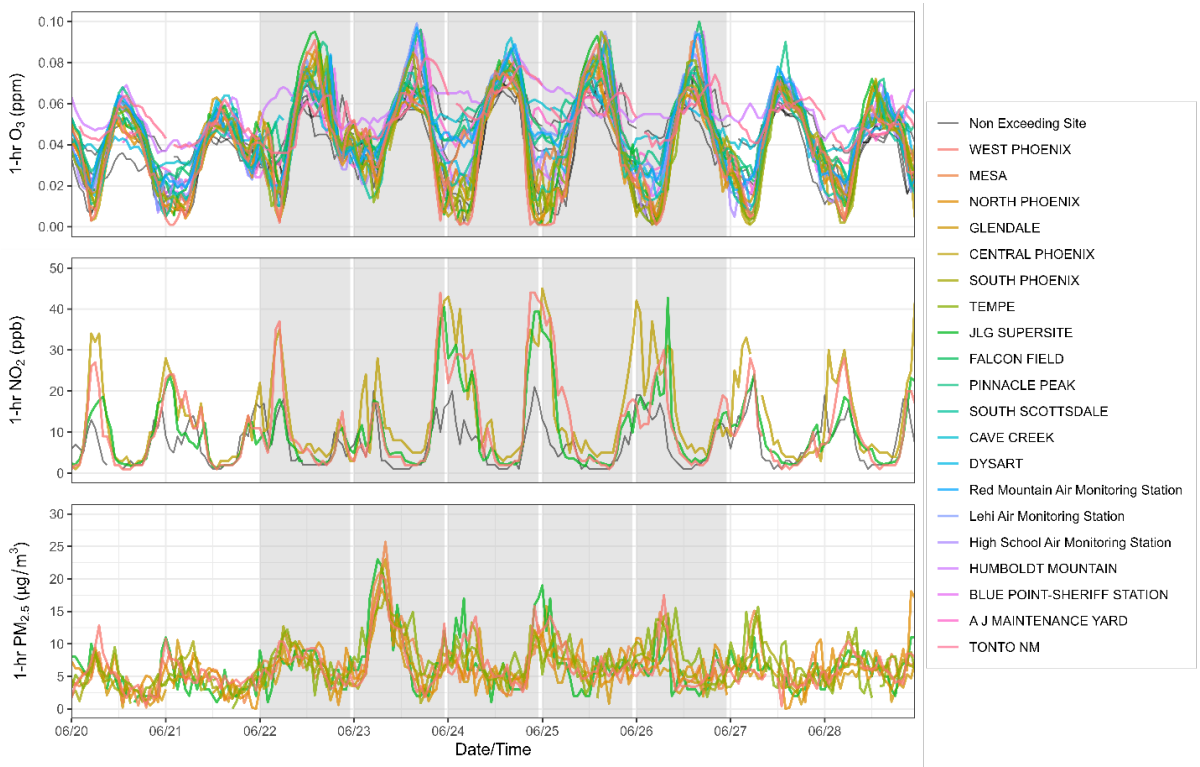

Figure 4-21. Hourly concentrations of ozone, NO_2, and $PM_{2.5}$ at all sites in the nonattainment area. All ozone-exceeding sites are color-coded to highlight smoke impacts on concentrations, and all non-exceeding sites are black. The gray shaded areas represent June 22-26, 2023.

[11] https://droughtmonitor.unl.edu/data/png/20230620/20230620_az_trd.png

[12] https://mesonet.agron.iastate.edu/vtec/search.php?mode=bypoint&lon=-112.1202&lat=33.4223&buffer=0.00&sdate1=2023-06-22&edate1=2023-08-18

Figure 4-22 shows hourly $PM_{2.5}$ concentrations at the Mesa (top) and Tempe (bottom) sites. $PM_{2.5}$ concentrations at both sites rapidly increased in the early morning hours on June 23 to above the 95th percentile and remained elevated until the afternoon the same day. Similar increases were present at other monitors, such as North Phoenix and Glendale. Similar but less dramatic increases were observed in subsequent days. $PM_{2.5}$ concentrations at Tempe exceeded the 95th percentile again during the morning of June 26. Elevated $PM_{2.5}$ concentrations outside of the typical diurnal profile indicate transport of smoke.

Figure 4-23 shows hourly NO_2 concentrations at the West Phoenix (top) and JLG Supersite (bottom) sites. NO_2 concentrations at both sites exhibit a distinct increase to above the 95th percentile during the evenings of June 23 and 24. Similar increases were observed at other monitors, such as Central Phoenix and Buckeye. NO_2 concentrations at JLG Supersite exceeded the 95th percentile again during the early morning of June 26. These observations provide evidence that smoke impacts were widespread and affected multiple air monitoring sites.

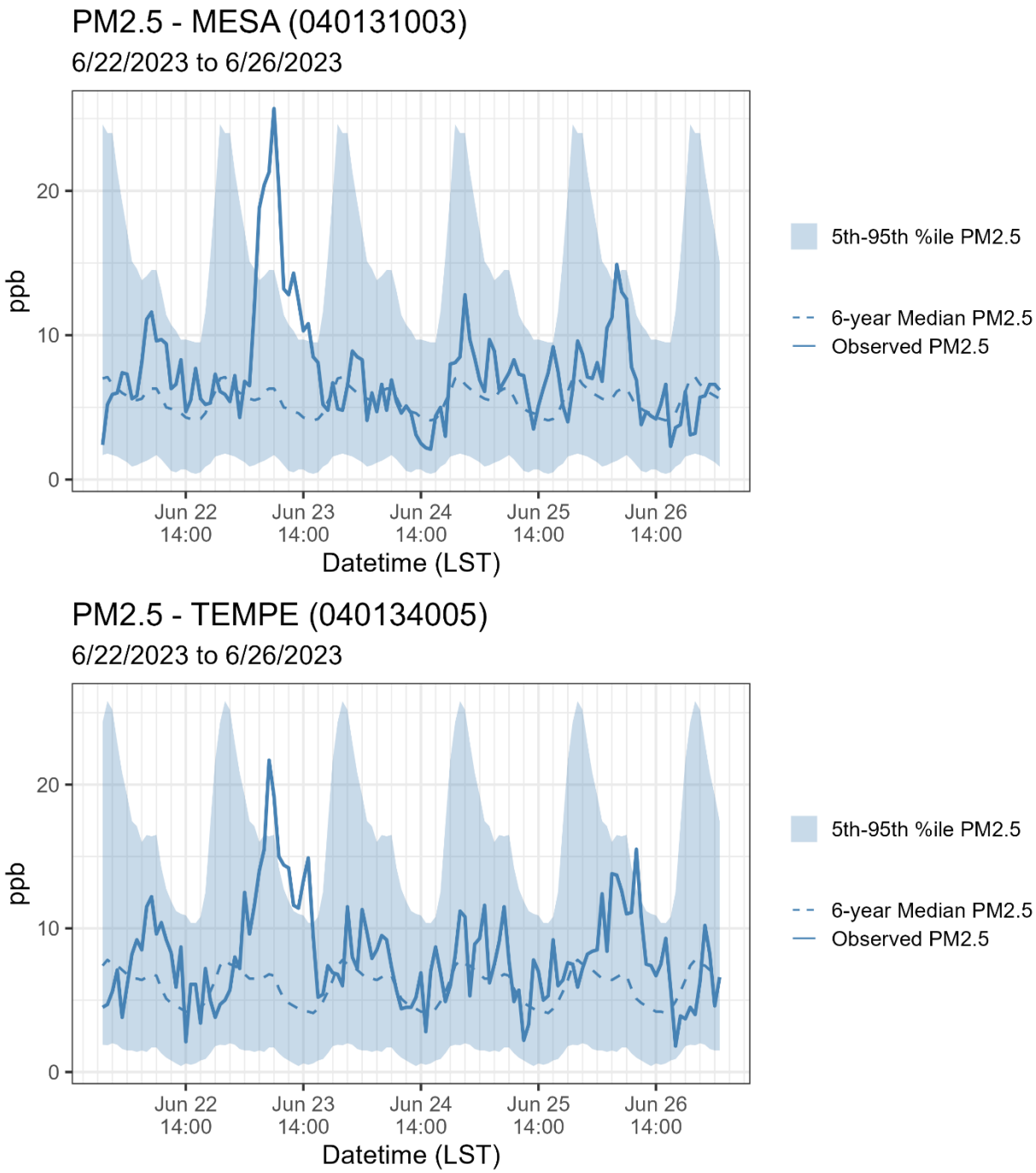

Figure 4-22. Hourly concentrations of $PM_{2.5}$ at the Mesa (top) and Tempe (bottom) sites. The 6-year (2019-2024) median is represented by the dashed line, and the 5th-95th percentile is represented by the shaded area.

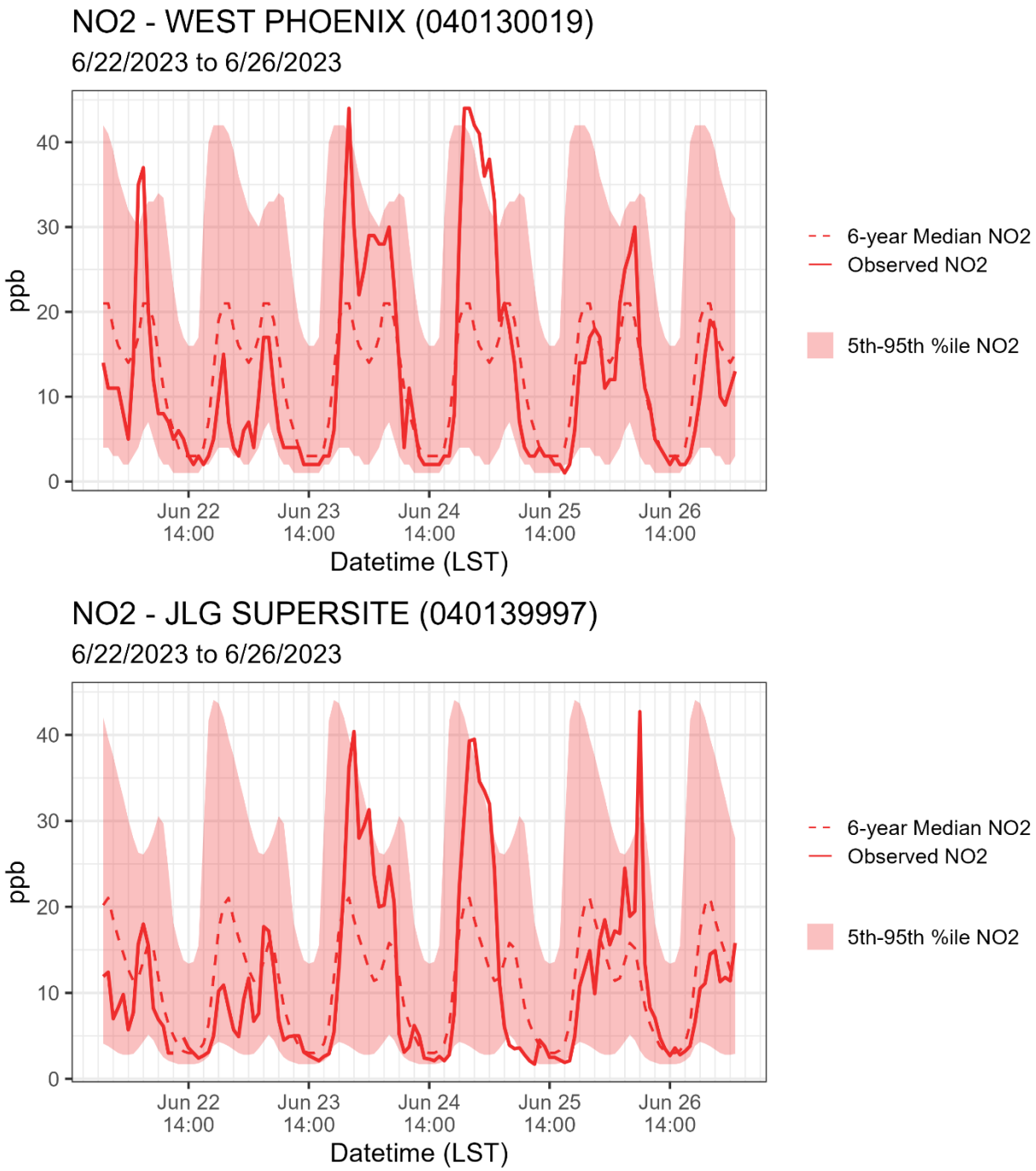

Figure 4-23. Hourly concentrations of NO_2 at the West Phoenix (top) and JLG Supersite (bottom) sites. The 6-year (2019-2024) median is represented by the dashed line, and the 5th-95th percentile is represented by the shaded area.

The ratio of OC to EC taken at the JLG Supersite monitor was also examined for evidence that wildfire smoke entered the nonattainment area. Increases in this ratio are indicative of wildfire smoke.

Figure 4-42 shows a boxplot of OC to EC ratios for available data collected during the ozone season between 2019-2024. The OC to EC ratio on June 23 was elevated well above the 75th percentile and considered an upper outlier compared to all data; the ratio on June 26 was above the median. These observations provide further evidence that ground-level wildfire smoke entered Phoenix on June 22-26 containing increased OC to EC ratios during the June 22-26, 2023, atypical ozone event.

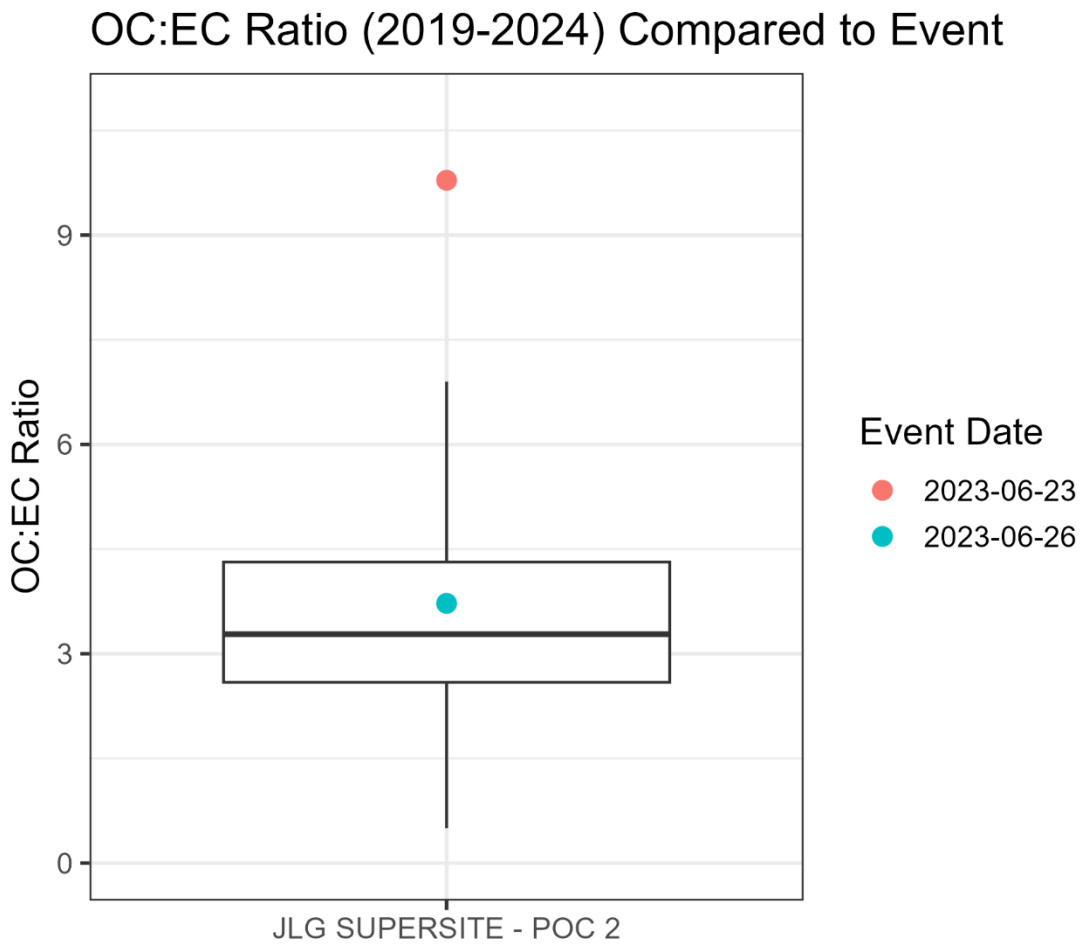

Figure 4-24. Boxplot of OC to EC ratios at the JLG Supersite site using data collected during the ozone season (April-September) from 2019-2024. OC to EC ratios are calculated for data collected at POC 2 (x-axis). Available OC to EC ratios collected during the June 22-26 atypical ozone event are shown as points.

4.1.5 Event Statistics

Table 4-4 summarizes the measurements of ozone concentrations on June 22-26, 2023, as well as the percentile rank of the observations compared to six years of ozone season data (April 1-September 31, 2019-2024). Ozone MDA8 measurements ranged from the 93rd - 99th percentile on June 22-26, 2023.

Table 4-4. Percentile of ozone measurements on the atypical dates compared with six years of ozone data (2019-2024). The percentile rank is calculated across the ozone production season in the nonattainment area (April 1-September 31) of 2019-2024.

Date	Site Name	Site Code	Ozone MDA8 (ppb)	Percentile Rank
6/22/2023	Tempe	040134005	71	93
	South Phoenix	040134003	72	94
	North Phoenix	040131004	73	95
	Glendale	040132001	73	95
	Cave Creek	040134008	73	95
	Lehi Air Monitoring Station	040137022	73	95
	Central Phoenix	040133002	75	97
	West Phoenix	040130019	76	97
	Pinnacle Peak	040132005	77	97
	JLG Supersite	040139997	83	99
6/23/2023	A J Maintenance Yard	040213001	71	93
	Mesa	040131003	73	95
	High School Air Monitoring Station	040137024	73	95
	Tonto NM	040070010	77	97
	Blue Point-Sheriff Station-Tonto NF-Salt River Recreation Area	040139702	78	98
	Red Mountain Air Monitoring Station	040137021	79	99
	Falcon Field	040131010	80	99
	Lehi Air Monitoring Station	040137022	80	99
6/24/2023	West Phoenix	040130019	71	93
	Tempe	040134005	73	95
	High School Air Monitoring Station	040137024	73	95
	Dysart	040134010	74	96
	Blue Point-Sheriff Station-Tonto NF-Salt River Recreation Area	040139702	74	96

Date	Site Name	Site Code	Ozone MDA8 (ppb)	Percentile Rank
	JLG Supersite	040139997	74	96
	Tonto NM	040070010	74	96
	Mesa	040131003	75	97
	Glendale	040132001	75	97
	Pinnacle Peak	040132005	75	97
	Falcon Field	040131010	76	97
	Humboldt Mountain	040139508	77	97
	Red Mountain Air Monitoring Station	040137021	78	98
	Lehi Air Monitoring Station	040137022	79	99
	Cave Creek	040134008	80	99
6/25/2023	Glendale	040132001	72	94
	South Scottsdale	040133003	72	94
	Central Phoenix	040133002	74	96
	West Phoenix	040130019	75	97
	South Phoenix	040134003	75	97
	High School Air Monitoring Station	040137024	76	97
	Mesa	040131003	78	98
	Falcon Field	040131010	79	99
	Red Mountain Air Monitoring Station	040137021	79	99
	Tempe	040134005	80	99
	JLG Supersite	040139997	80	99
	Lehi Air Monitoring Station	040137022	83	99
6/26/2023	Mesa	040131003	71	93
	High School Air Monitoring Station	040137024	72	94
	Red Mountain Air Monitoring Station	040137021	78	98
	Lehi Air Monitoring Station	040137022	78	98

Date	Site Name	Site Code	Ozone MDA8 (ppb)	Percentile Rank
	Falcon Field	040131010	80	99
	Blue Point-Sheriff Station-Tonto NF-Salt River Recreation Area	040139702	80	99

4.1.6 Conclusion

The concurrence of HMS smoke perimeters over the nonattainment area, HYSPLIT trajectories and meteorological analysis showing accumulation of smoke in the nonattainment area, visible smoke in camera images, and elevated $PM_{2.5}$, NO_2, and OC to EC ratios provide evidence that surface-level smoke was present during the period. Regional transport of smoke from numerous unidentified fires burning in Mexico, enhanced ozone concentrations outside of the typical diurnal profile, keeping ozone values high and affecting the MDA8 ozone concentrations at twenty sites. Multiple analyses showed that smoke fully encompassed the Maricopa Nonattainment Area on June 22-26, 2023, and statistics show ozone concentrations were atypical during this event.

This combined evidence indicates that smoke plumes generated by numerous fires in Mexico provided an atypical source of ozone and ozone precursors that caused enhanced ozone concentrations on June 22-26, 2023. Removal of these days as atypical events is supported by this analysis.

4.2 June 30, 2023

4.2.1 Event Overview: June 30, 2023

The unrepresentative (atypical) ozone event took place on June 30, 2023, and affected sixteen monitoring sites in in the Maricopa Nonattainment Area: Mesa, North Phoenix, Falcon Field, Glendale, Pinnacle Peak, Tempe, Cave Creek, Red Mountain Air Monitoring Station, Lehi Air Monitoring Station, High School Air Monitoring Station, Humboldt Mountain, Blue Point-Sheriff Station-Tonto NF-Salt River Recreation Area, JLG Supersite, A J Maintenance Yard, Queen Valley, and Tonto NM (**Table 4-5**). The maximum daily 8-hr average (MDA8) concentrations at the effected sites ranged from 71-79 ppb.

Time series graphs showing hourly ozone concentrations that exceeded the seasonal means (calculated using all available data from April 1 – September 31, 2019-2024) and 10th-90th percentiles at each site are shown in **Figure 4-25**. On the afternoon of June 30, many sites such as

Cave Creek, JLG Supersite, and Queen Valley exhibited distinct and high peaks in ozone concentrations; these observations exceeded the 90th percentile relative to all data collected during the ozone season from 2019-2024. Concentrations at many sites continued to exceed the 90th percentile throughout the remainder of the atypical ozone event on June 30.

Fires burning in northern Arizona, numerous unidentified fires burning in Mexico, and a local fire (Diamond Fire) were identified as contributors to this event. Evidence includes (1) HMS smoke perimeters over the nonattainment area, (2) HYSPLIT trajectories and meteorological analysis showing accumulation of smoke in Phoenix, (3) visible smoke in camera images and news coverage, and (4) elevated $PM_{2.5}$ and OC to EC ratios. This combination of evidence indicates that this is an atypical ozone event.

Table 4-5. Summary of identified atypical June 30, 2023.

Event Date(s)	Event Ozone Concentration Percentile	Sites Exceeded During Event	Type of Event
June 30, 2023	94th - 98th	Sixteen sites: Mesa, North Phoenix, Falcon Field, Glendale, Pinnacle Peak, Tempe, Cave Creek, Red Mountain Air Monitoring Station, Lehi Air Monitoring Station, High School Air Monitoring Station, Humboldt Mountain, Blue Point-Sheriff Station-Tonto NF-Salt River Recreation Area, JLG Supersite, A J Maintenance Yard, Queen Valley, Tonto NM	International/regional transport

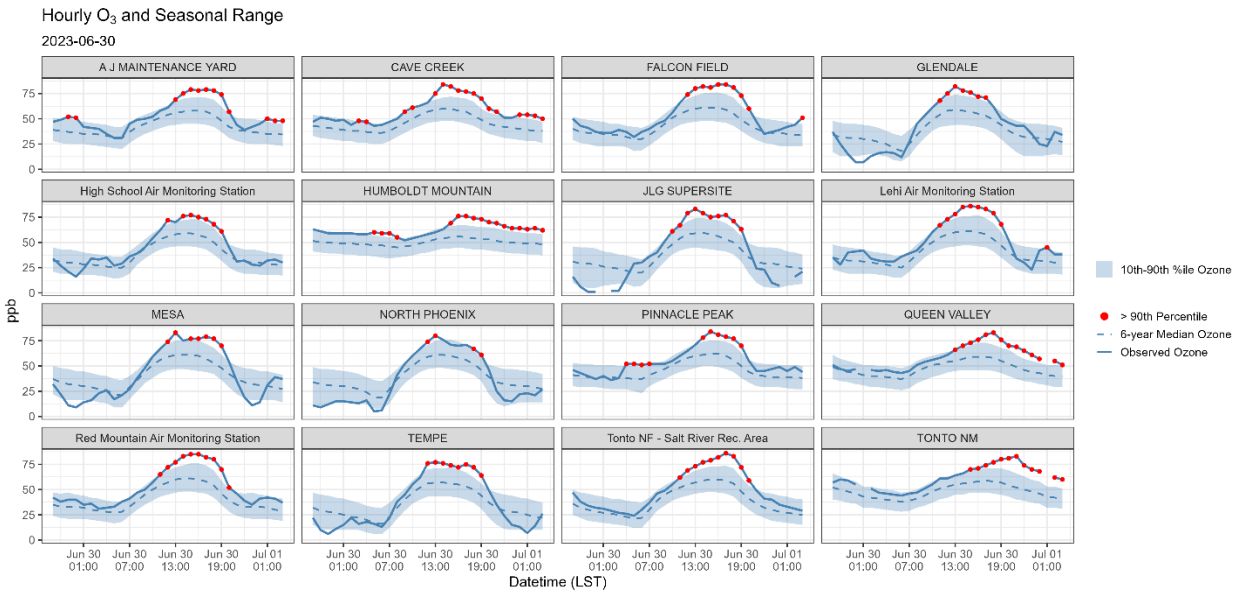

Figure 4-25. Hourly ozone concentrations (ppb) compared to all available data during the ozone season (April 1 – September 31) of the 6-year (2019-2024) period. Hourly means and 10th-90th percentiles are calculated using data on June 30, 2023.

4.2.2 Identification of Wildfire(s)

Multiple fires in northern Arizona and throughout Mexico were active in the days leading up to and during June 30, the exclusion day (**Figures 4-26**). Smoke from these fires combined to blanket Phoenix during June 30. The Diamond Fire, which started on June 27, 2023, at approximately 17:00 LST, located approximately 14 miles to the northeast of Scottsdale, Arizona, was also actively burning during the June 30 atypical event, and forced the evacuation of residents.[13] The fire was 93% contained on June 30, 2023, according to the Arizona Department of Forestry and Fire Management (**Figure 4-27**).

[13] https://www.azpm.org/p/azpmfeatures/2023/6/29/216585-over-1000-evacuees-return-to-arizona-homes-with-brush-fire-now-30-contained/

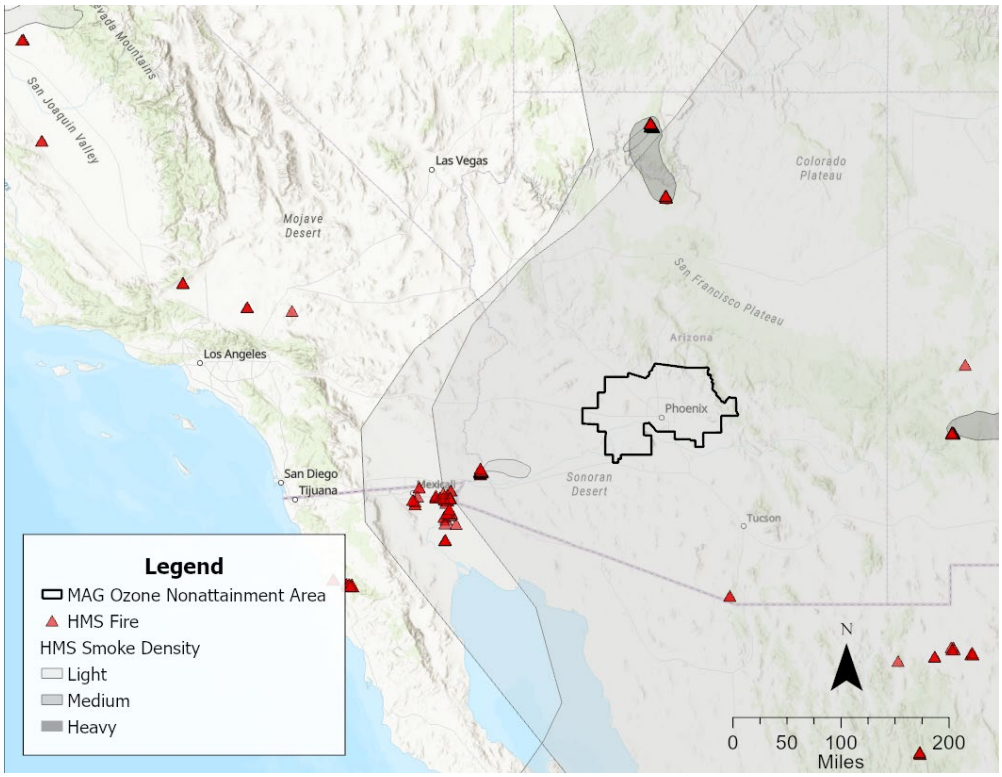

Figure 4-26. Regional view of HMS smoke density and fire locations on June 30, 2023.

Figure 4-27. Social media post from the Arizona Department of Forestry and Fire Management from June 30 regarding the Diamond Fire burning on the outskirts of Phoenix.

4.2.3 Meteorological Analysis

Upper-level Analysis

The 500 mb map at 5 a.m. PST on June 30 indicated a ridge of high pressure from western Montana to offshore of central California. A trough of low pressure aloft was present from eastern Wyoming to western Arizona. Aloft winds across Arizona at this time were westerly to west-northwesterly. At 5 p.m. PST on June 30, the aloft trough shown in **Figure 4-28** shifted eastward into Colorado and northern New Mexico. The upper-level ridge was established over California and Nevada, with northerly to northwesterly aloft winds in central and northern Arizona.

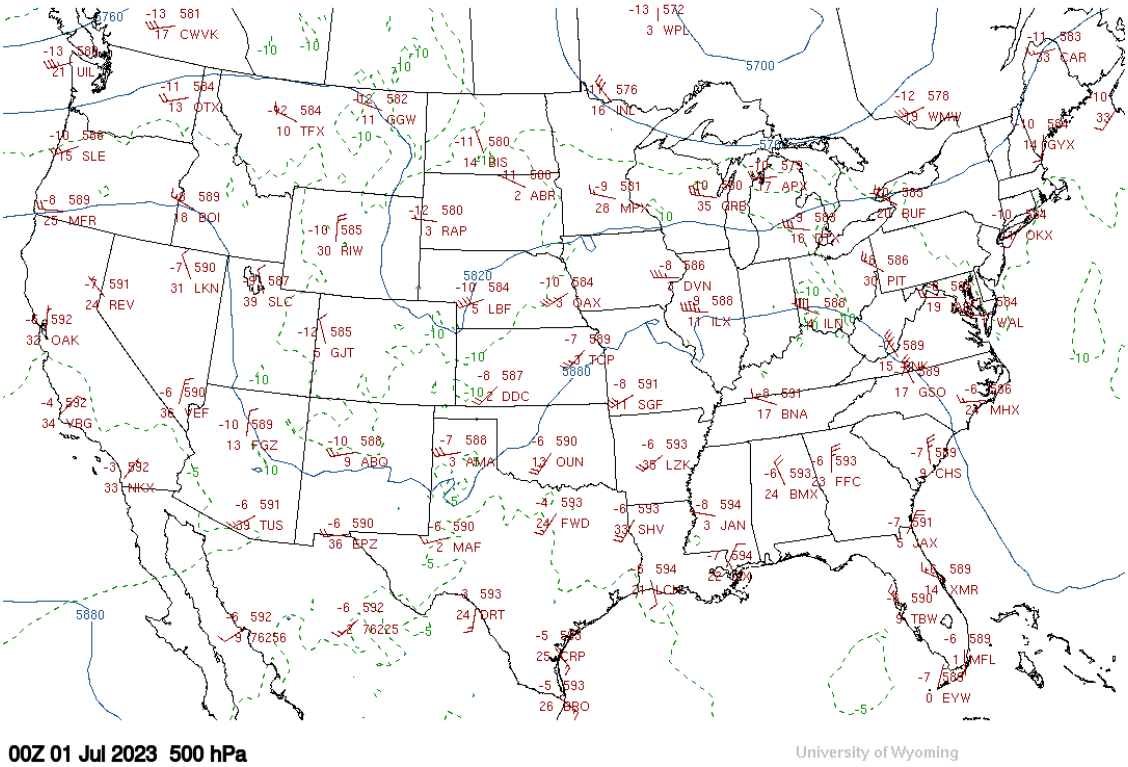

Figure 4-28. 500 mb geopotential heights (blue lines) and winds (red barbs) for 5 p.m. PST on June 30. Based on wind barbs and the height pattern, northerly to northwesterly winds were present across central and northern Arizona, Source: University of Wyoming

Surface Analysis

Within the PBL, the upper-level ridge of high pressure west of the state generated subsidence (sinking air), which led to sunny and hot conditions on June 30. Under sunny skies, high temperatures at KPHX reached 110°F, as show in **Table 4-6**. In addition, wind speeds for the day

averaged less than 6 mph, resulting in reduced dispersion and day-to-day pollutant carryover. These conditions were supportive for ground-level ozone production in the nonattainment area.

Table 4-6. Daily maximum temperature and average daily wind speed at KPHX for June 30.

Date	Maximum Temperature (F)	Average daily wind speed (mph)
June 30	110	5.1

Satellite Smoke and Fire Detections

Figure 4-29 contains NOAA HMS smoke plume analysis and satellite fire detections across the southwestern United States on June 30. On this day, smoke was analyzed over much of Arizona, including the nonattainment area. Furthermore, isolated fire detections were captured by satellite across the state. The most noteworthy fire detections were located near the Kaibab National Forest near the Grand Canyon. Potential smoke transport paths into Phoenix on June 30 can be found in the "Smoke Transport" section.

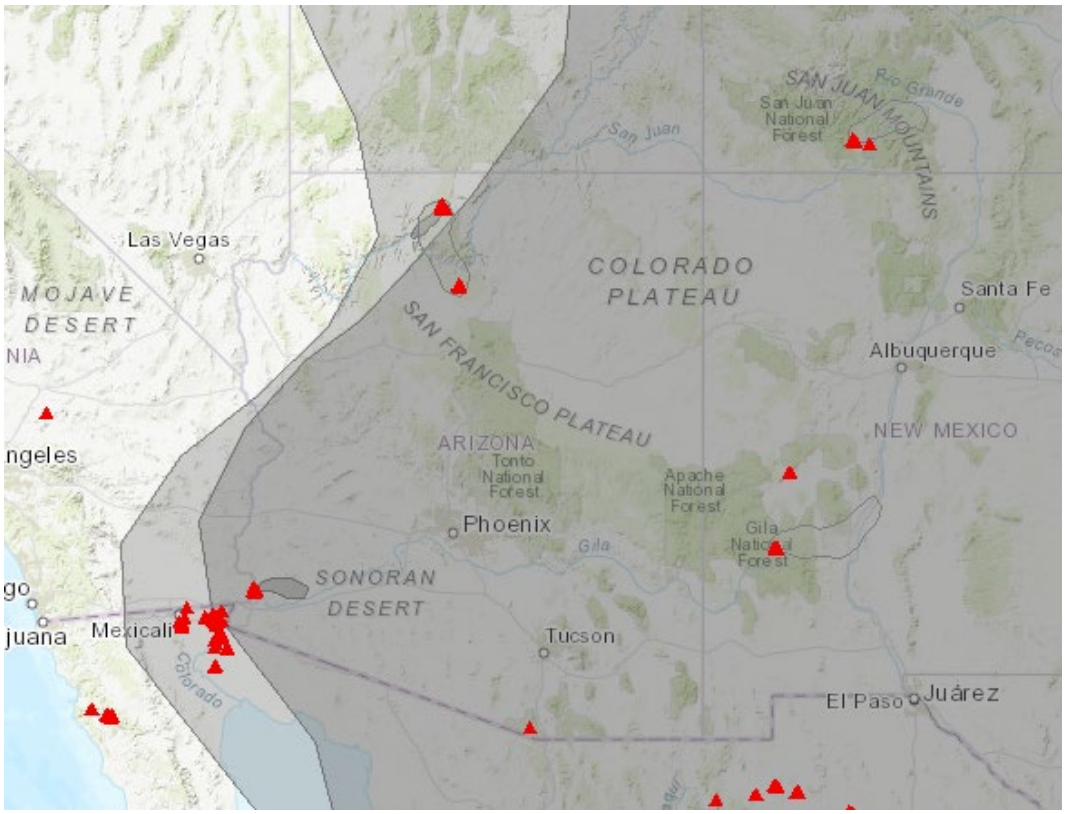

Figure 4-29. NOAA HMS smoke plume analysis (grey contours) and satellite fire detections (red triangles) from June 30, 2023. Source: AirNow-Tech

Smoke Discussions

The NOAA smoke discussion of 7 p.m. PST June 30, 2023 called out southerly smoke transport from fires in northern Arizona.

"The major wildfires across portions of Canada continue with a large are of smoke over much of Canada and extending to the south over the Central and Southeastern United States. The smoke also extends well off the east coasts of Canada and the United States as well as the Atlantic Ocean along the eastern U.S. coast and north-central region. To the west, some of the thinner density smoke had spread to the west and south over parts of the southwestern United States. Within this area, the thickest smoke was located mostly over Western Canada, northern Quebec, and parts of the Hudson Bay while moderate density smoke engulfed most of Canada, Northeastern U.S., and parts of norther U.S. within Montana and the Dakotas. Cloud cover over eastern Canada made it difficult to determine to the full extent of the thick density smoke from the Quebec fires throughout the day.

Scattered wildfire activity from northern Arizona and southwestern New Mexico were observed producing light to moderate density smoke plumes with smoke in Arizona was moving south as the fires in New Mexico were moving generally east." (NOAA NESDIS Text Narrative from June 30, 2023)

Soundings

PBL heights in Phoenix were estimated using the Tucson upper-air sounding data. **Figure 4-30** shows the 5 p.m. PST skew-T diagram for Tucson, which indicated a deep PBL from the surface up to approximately 675 mb, or 4,300 meters above ground level (AGL). When adjusting for the elevation of the nonattainment area, the estimated PBL height for Phoenix was 3,900 meters AGL. This PBL height is evidence of mixing of aloft air reaching the surface.

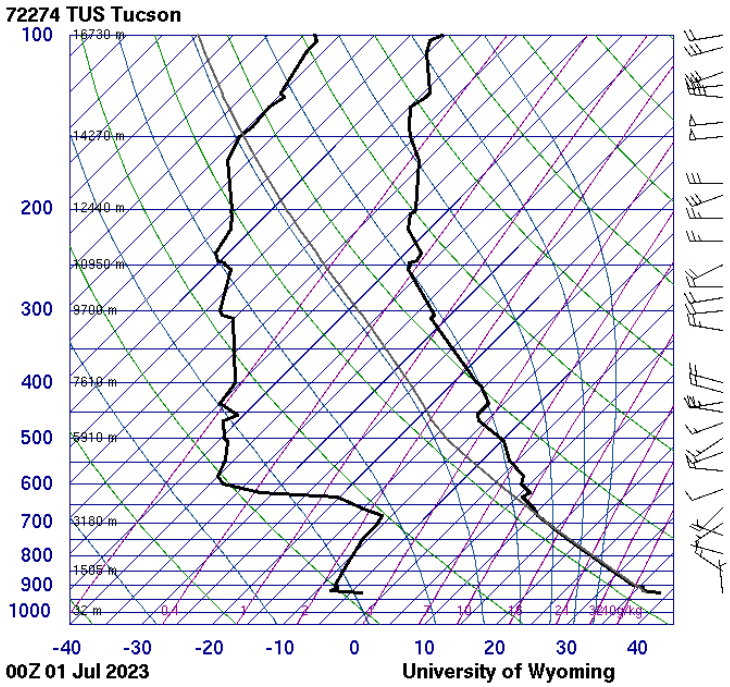

Figure 4-30. Tucson skew-T upper-air diagrams valid 5 p.m. PST from June 30, 2023. Deep mixing was evident, indicating the transfer of aloft air down to the surface. Source: University of Wyoming

Smoke Transport

With boundary layer conditions established, the NOAA HYSPLIT tool was used to identify transport paths into central Arizona. Additionally, the potential for smoke transport into Phoenix was assessed by overlaying the HYSPLIT trajectory paths onto the NOAA HMS smoke plume analysis and satellite fire detections. The 12-hour back trajectory ending on June 30 at 5 p.m. PST (**Figure 4-39**) showed northerly winds into Phoenix at 1,700 m AGL and 3,900 m AGL. Both paths intersected analyzed HMS smoke plumes and were near satellite fire detections over the Kaibab National Forest in far northern Arizona.

While the paths were west of the satellite fire detections, the NOAA smoke discussion for June 30 (**Figure 4-31**) mentioned southerly transport of smoke from northern Arizona fires.

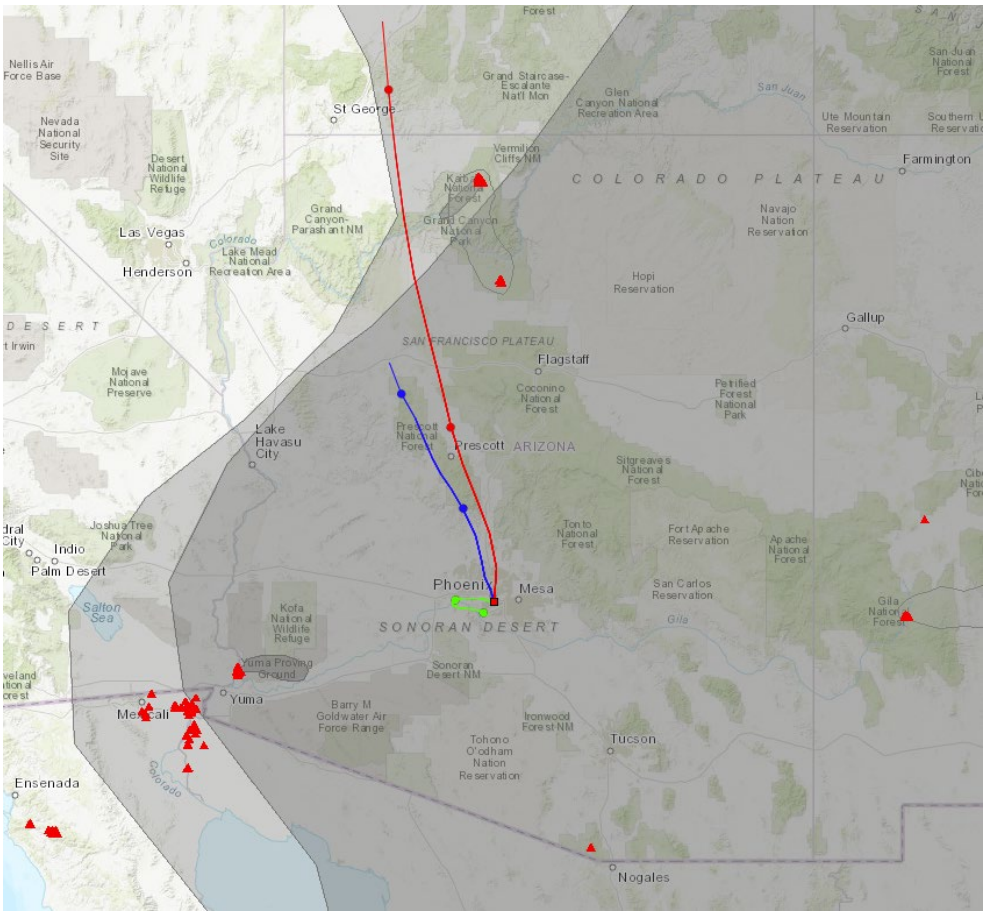

Figure 4-31. 12-hour back trajectory analysis for June 30 ending 5 p.m. PST. Transport paths into Phoenix intersected with NOAA HMS smoke plumes (grey contours) and were near satellite fire detections (red triangles). Source: AirNow-Tech

Summary

On June 30, 2023, an upper-level ridge of high pressure produced sunny and hot conditions conducive for ozone development. Surface winds during this period were light, inhibiting pollutant dispersion and allowing for pollutant accumulation. Additionally, the upper-level high generated northerly to northwesterly winds aloft across Arizona throughout much of the period, with HYSPLIT trajectories showing northerly flow into Phoenix within the PBL. Furthermore, HYSPLIT output and NOAA HMS indicated the potential for smoke transport into central Arizona from a fire burning in the Kaibab National Forest. Due to these conditions, there is evidence of smoke transport and ozone enhancement in the nonattainment area.

4.2.4 Surface Impacts

Smoke from fires burning in northern Arizona and Mexico spread over Phoenix in the days leading up to June 30, 2023. **Figure 4-32 through 4-34** show photos taken from the southwest-facing Estrella Mountain, south-facing South Mountain, and east-facing Superstition Mountain webcams, where the smoke is visible during some hours on June 30, 2023. Smoke from the Diamond Fire burning on the outskirts of Phoenix on June 30 also likely contributed to the smokey conditions in Phoenix, as noted by local residents (**Figure 4-35**).

Figure 4-32. Camera Images showing the southwest coordinal direction taken from the Estrella Mountain webcam on June 30 from 6:30 LST, 8:45 LST, 10:15 LST, and 11:45 LST.

Figure 4-33. Camera Images showing the south coordinal direction taken from the South Mountain webcam on June 30 from 6:30 LST, 8:00 LST, 10:00 LST, and 12:45 LST.

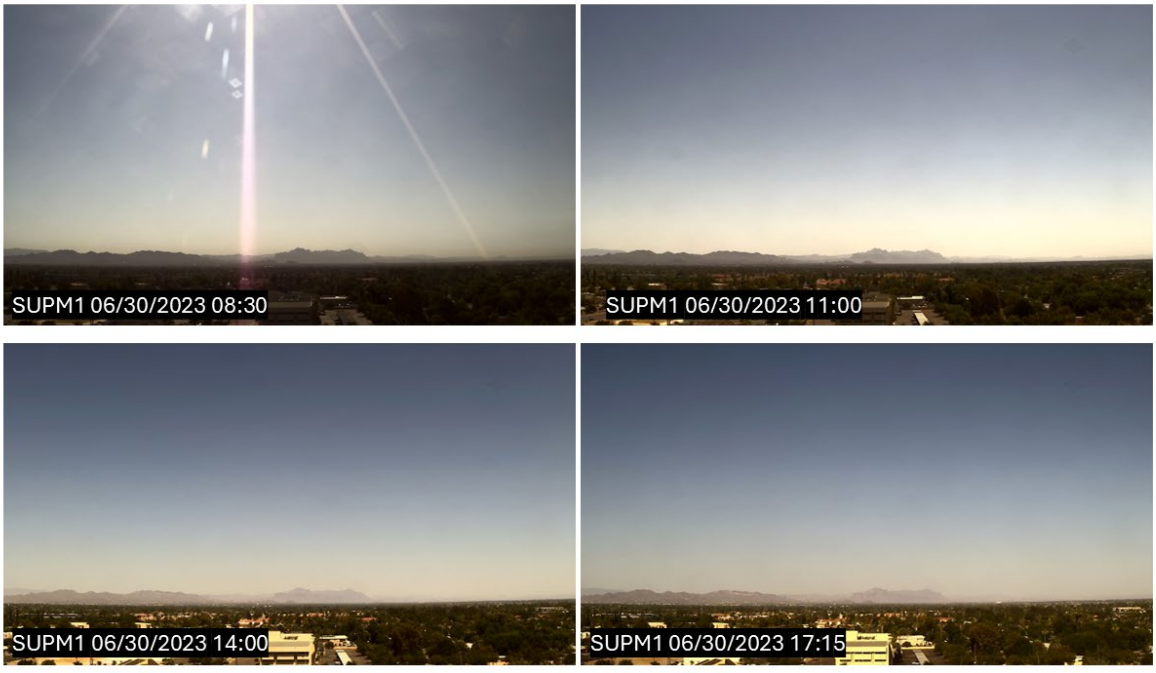

Figure 4-34. Camera Images showing the east coordinal direction taken from the Superstition Mountain webcam on June 30 from 8:30 LST, 11:00 LST, 14:00 LST, and 17:15 LST.

Figure 4-35. Social media post regarding smoke from the Diamond Fire over Phoenix on July 1, 2023.

Figure 4-36 shows an overall view of the magnitude of hourly pollutant concentrations measured in the nonattainment area in the two days before and after the June 30, 2023, atypical event. Hourly ozone concentrations are elevated at all affected sites relative to the days before the atypical event. NO_2 concentrations at JLG Supersite were elevated during the evening before and morning of June 30. $PM_{2.5}$ concentrations at the exceedance-affected sites rise sharply at all $PM_{2.5}$-measuring sites during the evening of June 30. Higher $PM_{2.5}$ concentrations were likely not solely from dust because conditions were not favorable (e.g., wind speeds were generally low, no drought in the nonattainment area)[14] for wind-blown dust before and during the June 30 atypical event. Furthermore, there were no dust storm advisories or warnings before or during this atypical event.[15] Distinct and widespread enhancements in surface pollutant concentrations provide evidence that smoke from regional fires entered the region, mixed towards the surface, and had an atypical influence on ozone concentrations during the period.

[14] https://droughtmonitor.unl.edu/data/png/20230627/20230627_az_trd.png
[15] https://mesonet.agron.iastate.edu/vtec/search.php?mode=bypoint&lon=-112.1202&lat=33.4223&buffer=0.00&sdate1=2023-06-22&edate1=2023-08-18

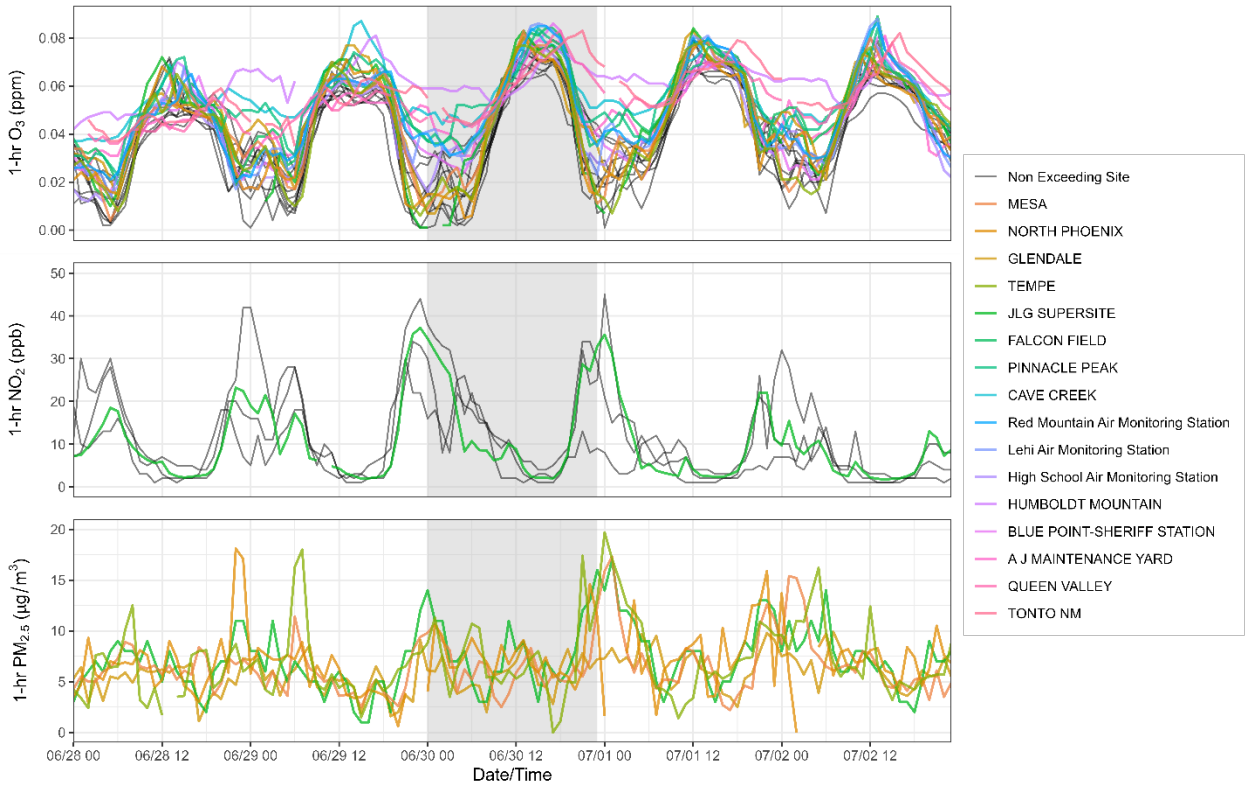

Figure 4-36. Hourly concentrations of ozone, NO_2, and $PM_{2.5}$ at all sites in the nonattainment area. All ozone-exceeding sites are color-coded to highlight smoke impacts on concentrations, and all non-exceeding sites are black. The gray shaded areas represent June 30, 2023.

OC and EC data were not available on June 30, but samples collected before and after that date show evidence of smoke impacts. The ratio of OC to EC taken at the JLG Supersite monitor was examined for evidence that wildfire smoke entered the nonattainment area. Increases in this ratio are indicative of wildfire smoke. **Figure 3-37** shows a boxplot of OC to EC ratios for available data collected during the ozone season between 2019-2024. The OC to EC ratio on June 29 and July 2 was elevated at and above the 75th percentile, respectively. These observations provide further evidence that ground-level wildfire smoke entered Phoenix around the June 30 atypical event containing increased OC to EC ratios.

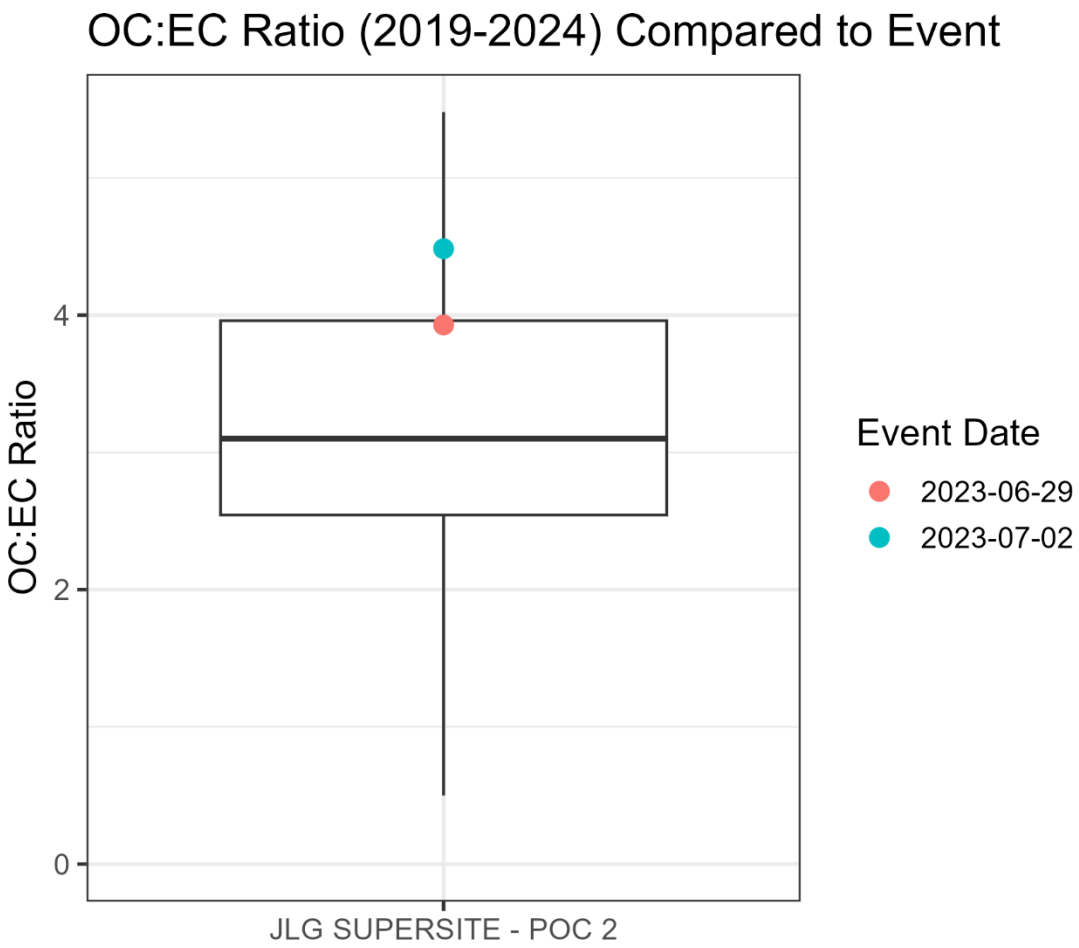

Figure 4-37. Boxplot of OC to EC ratios at the JLG Supersite site using data collected during the ozone season (April-September) from 2019-2024. OC to EC ratios are calculated from data collected at POC 2 (x-axis). Available OC to EC ratios collected during the day before and two days after the June 30 atypical ozone event are shown as points.

4.2.5 Event Statistics

Table 4-7 summarizes the measurements of ozone concentrations on June 30, 2023, as well as the percentile rank of the observation compared to six years of ozone season data (April 1 - September 31, 2019-2024). Ozone MDA8 measurements ranged from the 94th - 98th percentile on June 30, 2023.

Table 4-7. Percentile of ozone measurements on the atypical dates compared with six years of ozone data (2019-2024). The percentile rank is calculated across the ozone production season in the nonattainment area (April 1-September 31) of 2019-2024.

Date	Site Name	Site Code	Ozone MDA8 (ppb)	Percentile Rank
6/30/2023	Mesa	040131003	76	98
	North Phoenix	040131004	72	95
	Falcon Field	040131010	79	98
	Glendale	040132001	73	96
	Pinnacle Peak	040132005	75	98
	Tempe	040134005	73	96
	Cave Creek	040134008	75	98
	Red Mountain Air Monitoring Station	040137021	79	98
	Lehi Air Monitoring Station	040137022	79	98
	High School Air Monitoring Station	040137024	71	94
	Humboldt Mountain	040139508	71	94
	Blue Point-Sheriff Station-Tonto NF-Salt River Recreation Area	040139702	77	98
	JLG Supersite	040139997	75	98
	A J Maintenance Yard	040213001	74	97
	Queen Valley	040218001	74	97
	Tonto NM	040070010	76	98

4.2.6 Conclusion

The concurrence of HMS smoke perimeters over the nonattainment area, HYSPLIT trajectories and meteorological analysis showing accumulation of smoke in the nonattainment area, visible smoke in camera images, and elevated $PM_{2.5}$ and NO_2 concentrations, and OC to EC ratios provide evidence that surface-level smoke was present during the period. Long-range transport of smoke from numerous unidentified fires burning in Mexico, enhanced ozone concentrations outside of the typical diurnal profile, keeping ozone values high and affecting the MDA8 ozone concentrations at sixteen sites. Multiple analyses showed that smoke fully encompassed the Maricopa Nonattainment Area on June 30, 2023, and statistics show ozone concentrations were atypical during this event.

This combined evidence indicates that smoke plumes generated by numerous fires in Mexico provided an atypical source of ozone and ozone precursors that caused enhanced ozone concentrations on June 30, 2023. Removal of this day as an atypical events is supported by this analysis.

4.3 July 24-29, 2023

4.3.1 Event Overview: July 24-29, 2023

The unrepresentative (atypical) ozone event took place on July 24-29, 2023, and affected twenty-one monitoring sites in in the Maricopa Nonattainment Area: Twenty-One sites: West Phoenix, Mesa, North Phoenix, Falcon Field, Glendale, Pinnacle Peak, Central Phoenix, South Scottsdale, South Phoenix, Tempe, Cave Creek, Red Mountain Air Monitoring Station, Lehi Air Monitoring Station, High School Air Monitoring Station, Humboldt Mountain, Blue Point-Sheriff Station-Tonto NF-Salt River Recreation Area, Fountain Hills, JLG Supersite, A J Maintenance Yard, Queen Valley, and Tonto NM (**Table 4-8**). The maximum daily 8-hr average (MDA8) concentrations at the effected sites ranged from 71-90 ppb.

Time series graphs showing hourly ozone concentrations that exceeded the seasonal means (calculated using all available data from April 1 – September 31, 2019-2024) and 10th-90th percentiles at each site are shown in **Figure 4-38**. Throughout the atypical period, ozone concentrations exhibited widespread and distinct peaks, particularly on July 27 at sites such as Central Phoenix, JLG Supersite, Red Mountain Air Monitoring Site, and West Phoenix; these observations exceeded the 90th percentile relative to all data collected during the ozone season from 2019-2024.

Numerous fires burning in the western U.S. and Canada, as well as a local fire, were identified as major contributors to this event. Evidence includes (1) HMS smoke perimeters over the nonattainment area, (2) HYSPLIT trajectories and meteorological analysis showing accumulation of smoke in Phoenix, (3) visible smoke in camera images, and (4) elevated NO_2 and OC to EC ratios. This combination of evidence indicates that this is an atypical ozone event.

Table 4-8. Summary of identified atypical July 24-29, 2023.

Event Date(s)	Event Ozone Concentration Percentile	Sites Exceeded During Event	Type of Event
July 24-29, 2023	93rd - 100th	Twenty-One sites: West Phoenix, Mesa, North Phoenix, Falcon Field, Glendale, Pinnacle Peak, Central Phoenix, South Scottsdale, South Phoenix, Tempe,	International/long-range transport/regional transport

Event Date(s)	Event Ozone Concentration Percentile	Sites Exceeded During Event	Type of Event
		Cave Creek, Red Mountain Air Monitoring Station, Lehi Air Monitoring Station, High School Air Monitoring Station, Humboldt Mountain, Blue Point-Sheriff Station-Tonto NF-Salt River Recreation Area, Fountain Hills, JLG Supersite, A J Maintenance Yard, Queen Valley, Tonto NM	

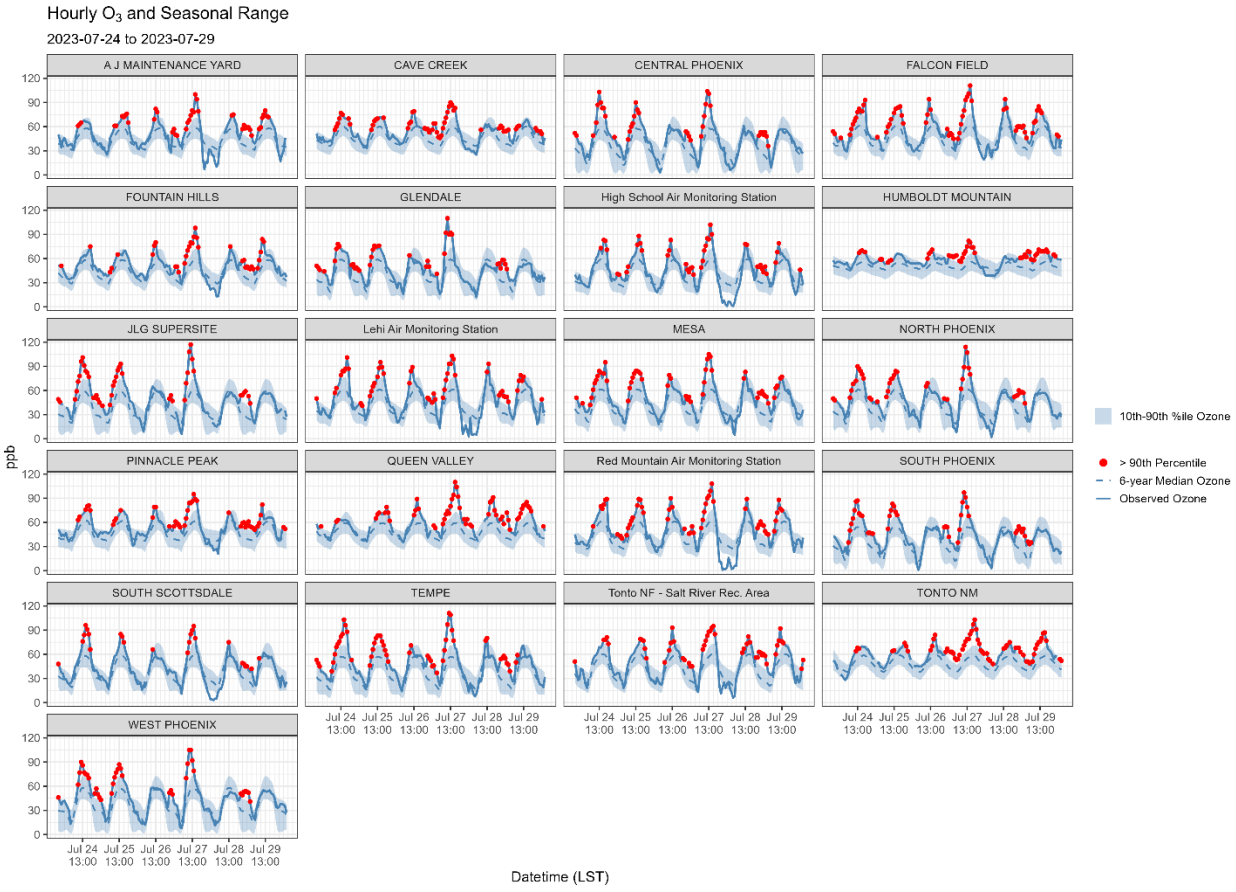

Figure 4-38. Hourly ozone concentrations (ppb) compared to all available data during the ozone season (April 1 – September 31) of the 6-year (2019-2024) period. Hourly means and 10th-90th percentiles are calculated using data on July 24-29, 2023.

4.3.2 Identification of Wildfire(s)

Multiple large fires in the western U.S. and in Canada were active in the days leading up to and during July 24-29, the exclusion days (**Figures 4-39 through 4-46**). Figures show local and continental views of the smoke to highlight nearby fires and long-range transport, respectively. Smoke from these fires combined to blanket the continental U.S. during July 24-29. The Diamond Fire, which started on July 22, 2023, at approximately 16:00 LST, located in Tonto National Forest approximately 30 miles to the northeast of the outskirts of Phoenix, was also actively burning during the July 24-29 atypical event. The fire grew to around 1,000 acres by July 26, 3,600 acres by July 27, and 4,700 acres by July 29. The fire continued to grow and was over 5,000 acres and 86% contained by August 7.[16]

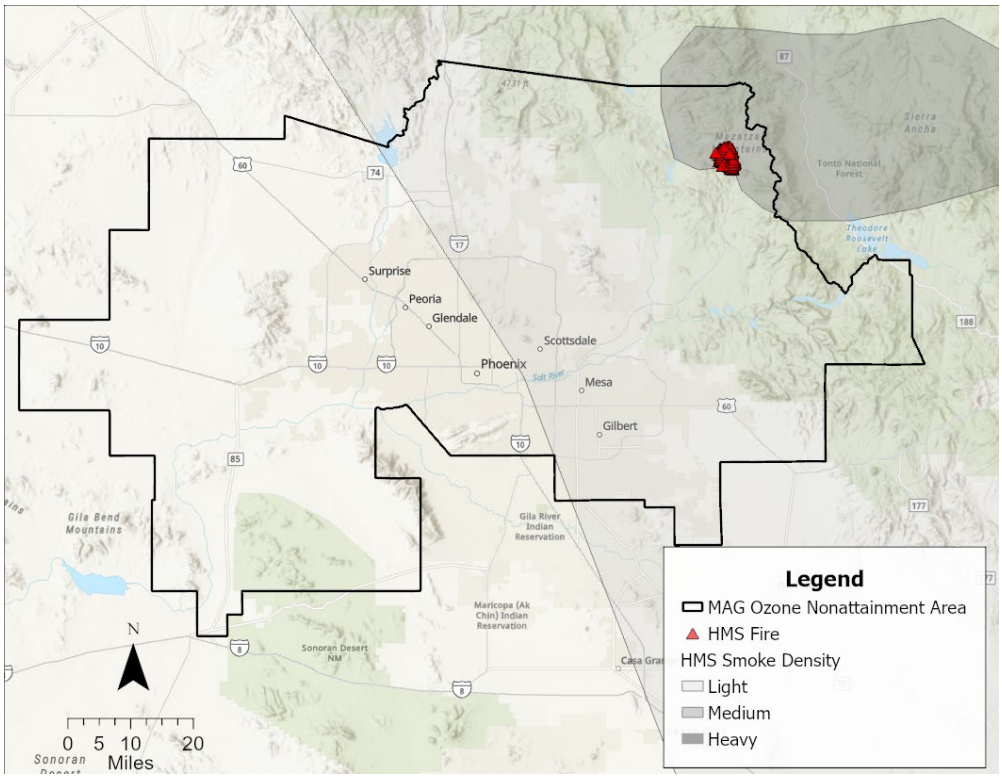

Figure 4-39. Local view of HMS smoke density and fire locations on July 26, 2023.

[16] https://www.kjzz.org/2023-07-29/content-1853142-diamond-fire-latest-wildfire-near-sunflower-arizona

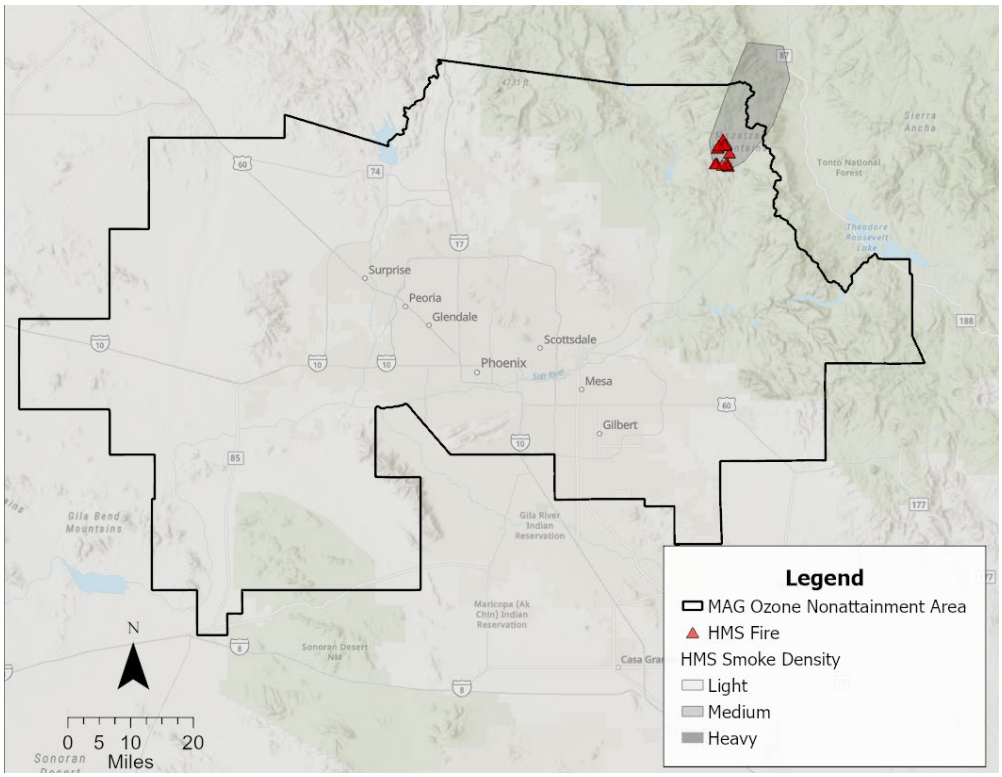

Figure 4-40. Local view of HMS smoke density and fire locations on July 27, 2023.

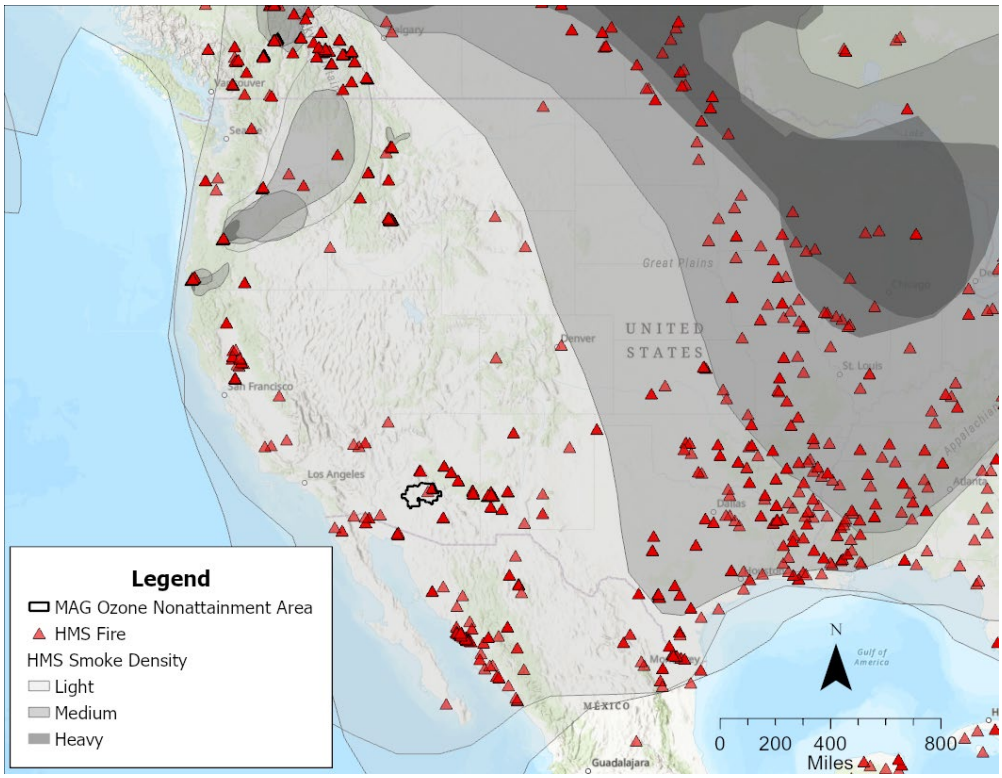

Figure 4-41. Continental view of HMS smoke density and fire locations on July 24, 2023.

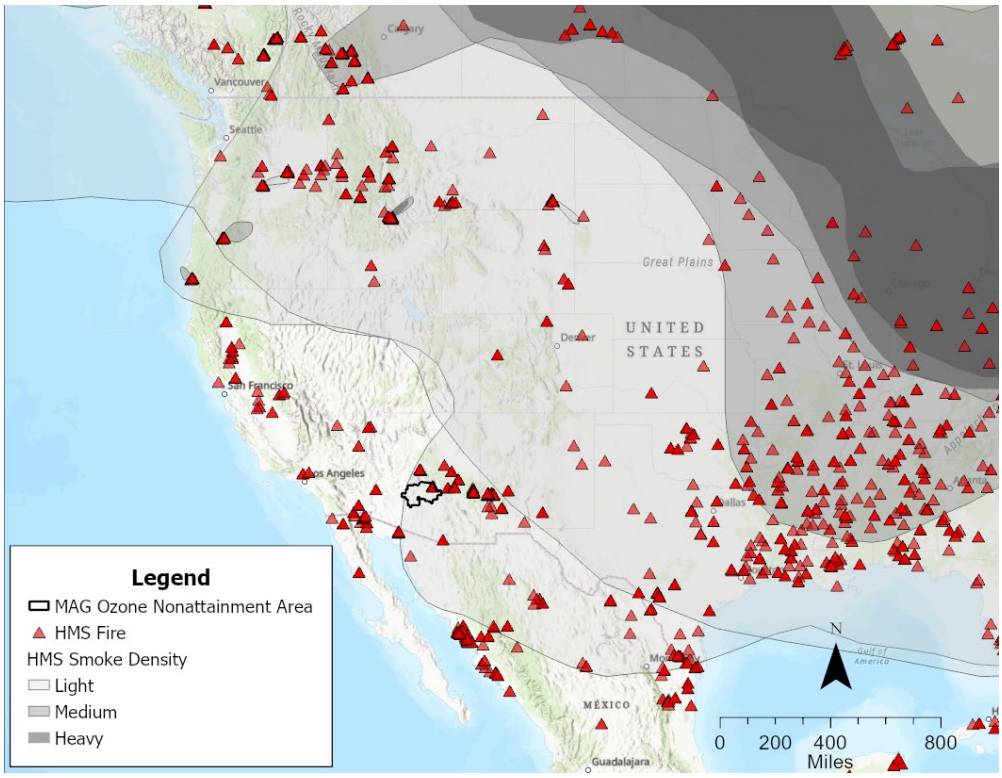

Figure 4-42. Continental view of HMS smoke density and fire locations on July 25, 2023

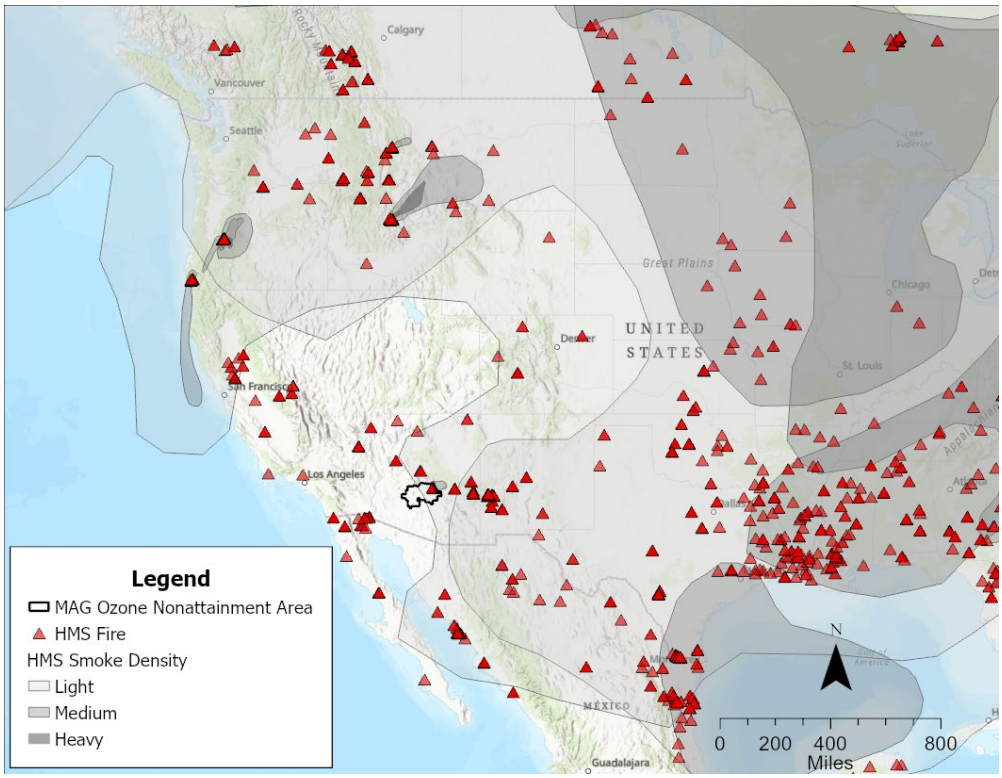

Figure 4-43. Continental view of HMS smoke density and fire locations on July 26, 2023.

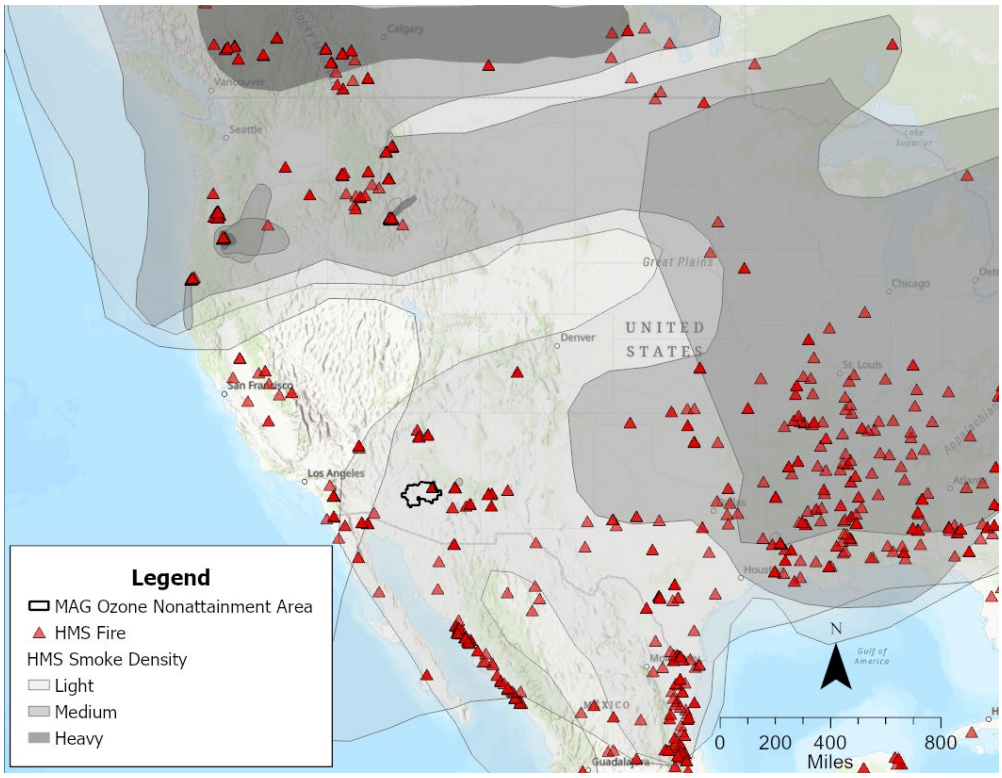

Figure 4-44. Continental view of HMS smoke density and fire locations on July 27, 2023

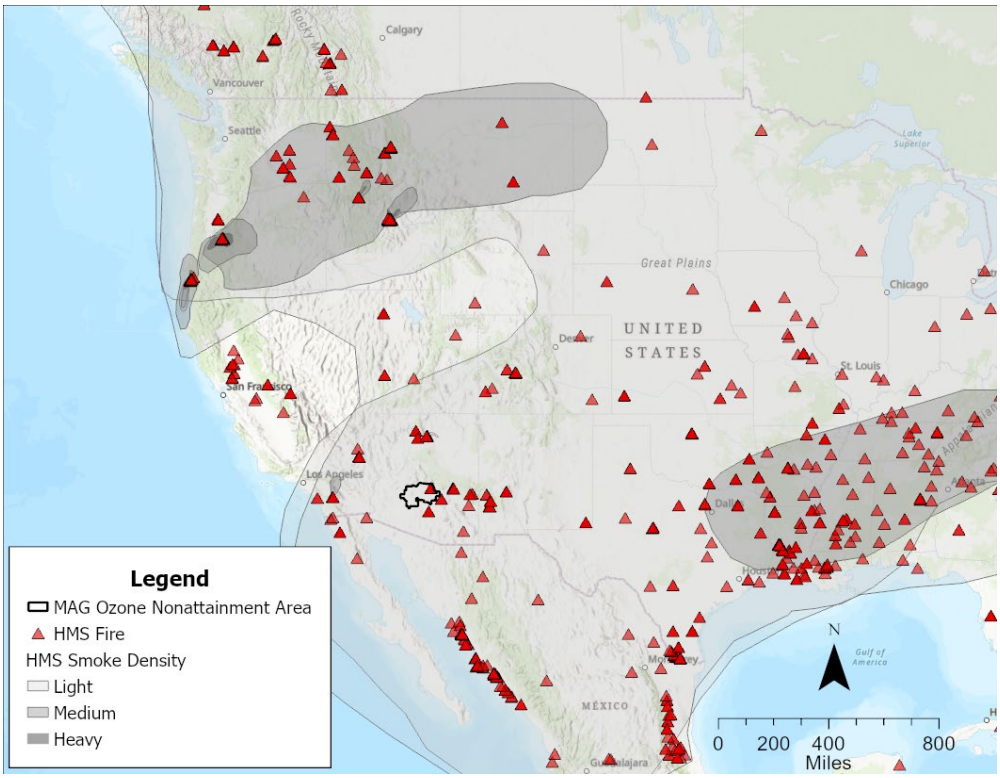

Figure 4-45. Continental view of HMS smoke density and fire locations on July 28, 2023

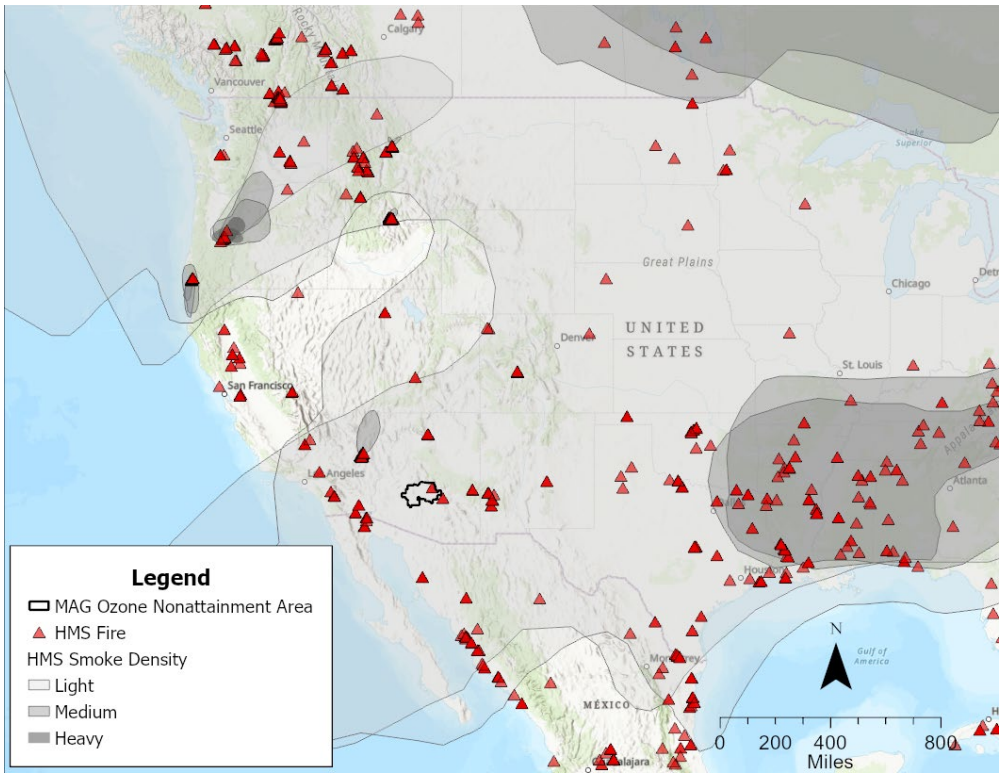

Figure 4-46. Continental view of HMS smoke density and fire locations on July 29, 2023.

4.3.3 Meteorological Analysis

Upper-level Analysis

At 500 mb during the ozone exceedance period of July 24-29, 2023, upper-level high pressure shown in **Figure 4-47** was positioned near the Four Corners region. In central Arizona, the clockwise wind flow around the upper-level high resulted in southerly to southeasterly winds at 500 mb. A similar wind pattern was also found at the 700 mb level, with high pressure over northern New Mexico yielding southerly to southeasterly winds.

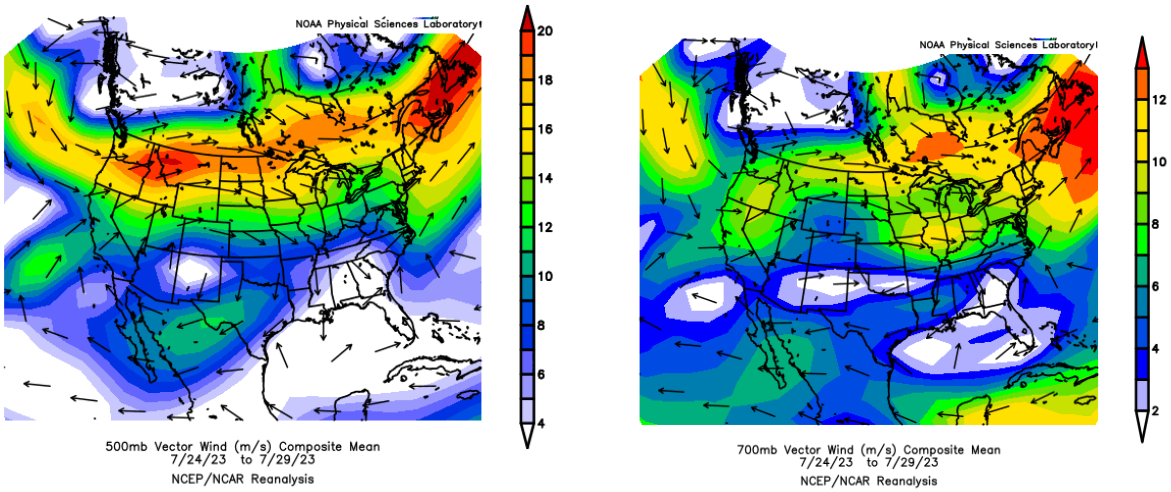

Figure 4-47. Mean 500 mb (left) and 700 mb (right) winds for July 24-29, 2023. Upper-level high pressure resulted in southerly to southeasterly wind aloft in the Phoenix region. Source: NOAA

Surface Analysis

The upper-level high led to subsidence (sinking air), with partly sunny and hot conditions prevailing across the nonattainment area. During the six-day period, afternoon high temperatures at KPHX ranged from 115-119°F. In addition, most days recorded light winds averaging less than 10 mph, which hindered dispersion and allowed pollutants to accumulate. These conditions were conducive for ground-level ozone formation each day across central Arizona. Table 4-9 displays each day's high temperature and daily average wind speed.

Table 4-9. Daily maximum temperatures and average daily wind speeds at KPHX.

Date	Maximum High Temperature (°F)	Daily average wind speed (mph)
July 24	116	6.0
July 25	119	7.4
July 26	118	10.7
July 27	115	8.0
July 28	116	8.5
July 29	115	6.8

Satellite Smoke and Fire Detections

Figure 4-48 contains NOAA HMS smoke plume analysis and satellite fire detections across the southwestern United States during the July 24-29, 2023 period. On each day, NOAA analyzed smoke over the nonattainment area, with satellites detecting scattered fires in central and east-central Arizona. Potential smoke transport paths into Phoenix for July 24-29, 2023 can be found in the "Smoke Transport" section.

July 24

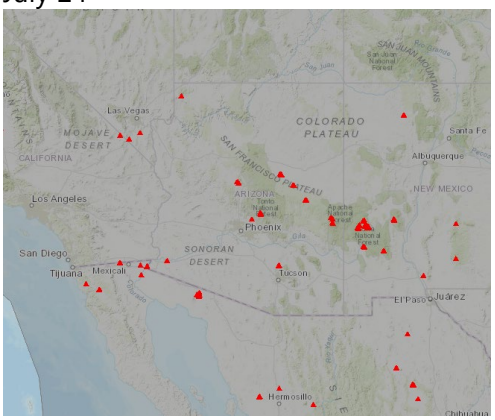

July 25

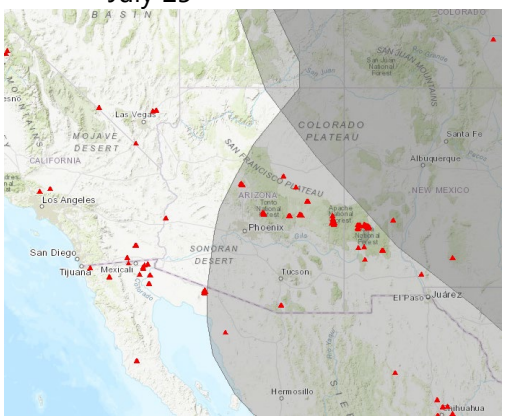

July 26

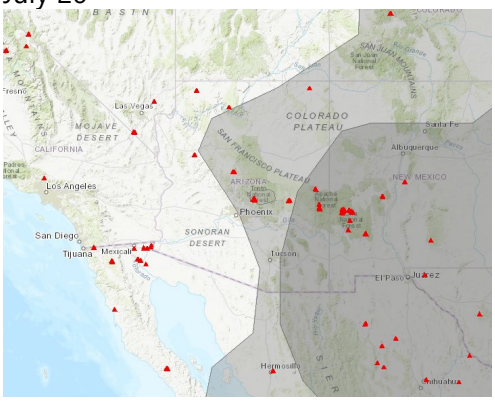

July 27

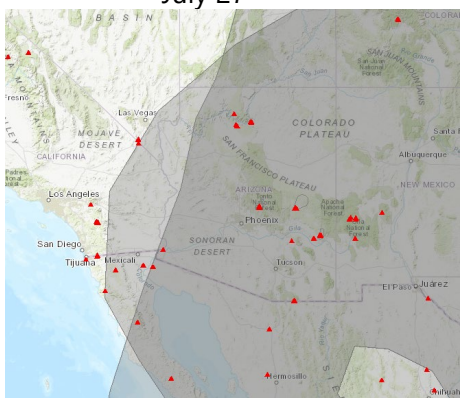

July 28

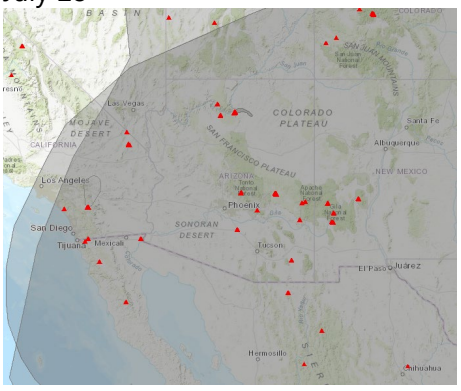

July 29

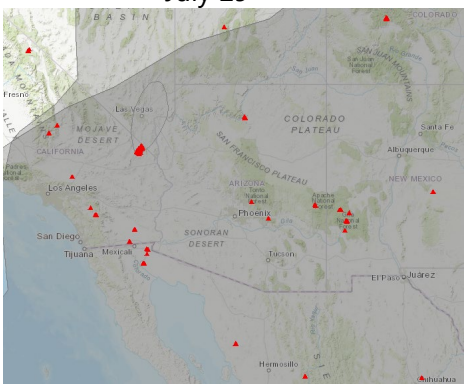

Figure 4-48. NOAA HMS smoke plume analysis (grey contours) and satellite fire detections (red triangles) from July 24-29, 2023. Source: AirNow-Tech

Smoke Discussions

NOAA's daily smoke discussion highlighted the potential sources for the analyzed smoke transported into the nonattainment area each day. For July 24 through July 26, NOAA analyzed a large area of Canadian wildfire smoke covering much of the CONUS. In the July 27 to July 29 discussions, light-density smoke from fires in Canada was discussed across much of CONUS. The daily discussions coincide with NOAA's HMS smoke analysis, which indicated smoke over central Arizona throughout the six-day period. Furthermore, the clockwise wind pattern at 500 mb and 700 mb suggest transport of the large Canadian smoke plume into Arizona.

"Heavy, dense smoke from fires in northwestern Canada was observed across northern Alberta and British Columbia, as well as much of Northwest Territory and the Yukon. Moderate smoke extended from eastern Alaska to northern Nunavut. Additional moderate smoke, presumed to be mostly from the same fires, also extended across the northwestern U.S. and border regions of Canada, extending eastward and southward across much of the eastern half of the U.S. except for Florida. **The area of light smoke extended from Eastern Alaska across the whole of Canada and much of the U.S. except California, Nevada, and smaller portions of the mountain west**. This area also extended down across the coastal regions of northern Mexico, where it mixed with smoke from various sources and probable remnant Saharan dust that were adding to the amount of total aerosol over the Gulf of Mexico." (NOAA NESDIS Text Narrative from July 27, 2023)

"Heavy, dense smoke from fires in northwestern Canada was observed across northern Alberta and British Columbia, as well as much of Northwest Territory and the Yukon. Moderate smoke extended from eastern Alaska to northern Nunavut. Additional moderate smoke, presumed to be mostly from the same fires, was observed across the northwestern U.S. and border regions of Canada, as well as over southeastern U.S. **The area of light smoke extended from Eastern Alaska across the whole of Canada and much of the U.S. except California, Nevada, and smaller portions of the mountain west**. This area also extended down across the coastal regions of northern Mexico, where it mixed with smoke from various sources and probable remnant Saharan dust that were adding to the amount of total aerosol over the Gulf of Mexico." (NOAA NESDIS Text Narrative from July 28, 2023)

Soundings

PBL heights in Phoenix for each day were estimated using the Tucson upper-air sounding data. **Table 4-10** shows the estimated PBLs for Phoenix between July 24-29, 2023, using the 5 p.m. PST Tucson data and adjusting for the elevation of Phoenix. The 5 p.m. skew-T diagrams from Tucson are in **Figure 4-49**, which indicate deep mixing within the PBL. This mixing was capable of transferring aloft air down to the surface.

Table 4-10. Daily estimated PBL heights for Phoenix, sourced from the Tucson upper-air sounding data.

Date	Estimated PBL (meters)
July 24	4,800
July 25	4,700
July 26	4,400
July 27	3,400
July 28	3,900
July 29	3,900

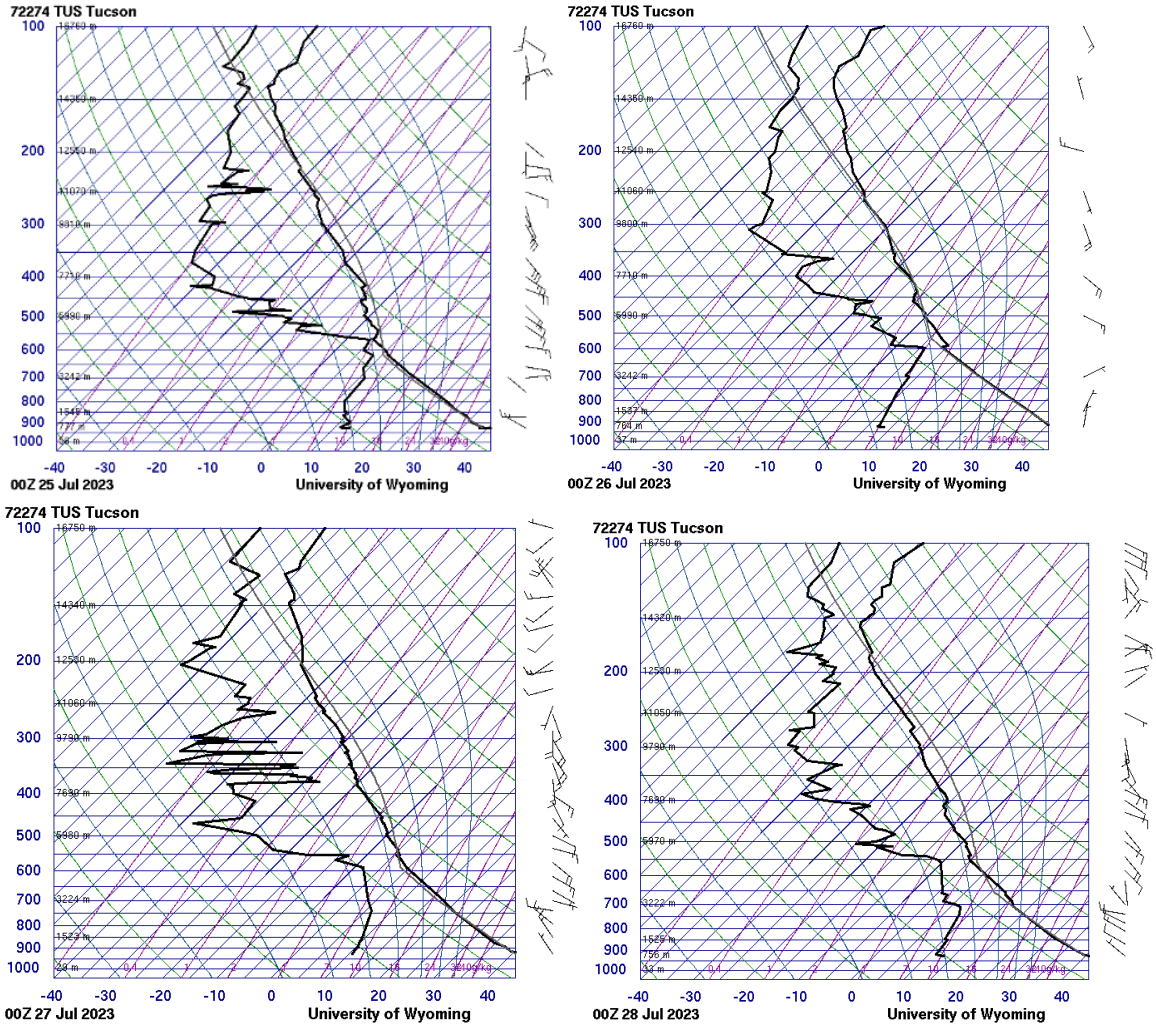

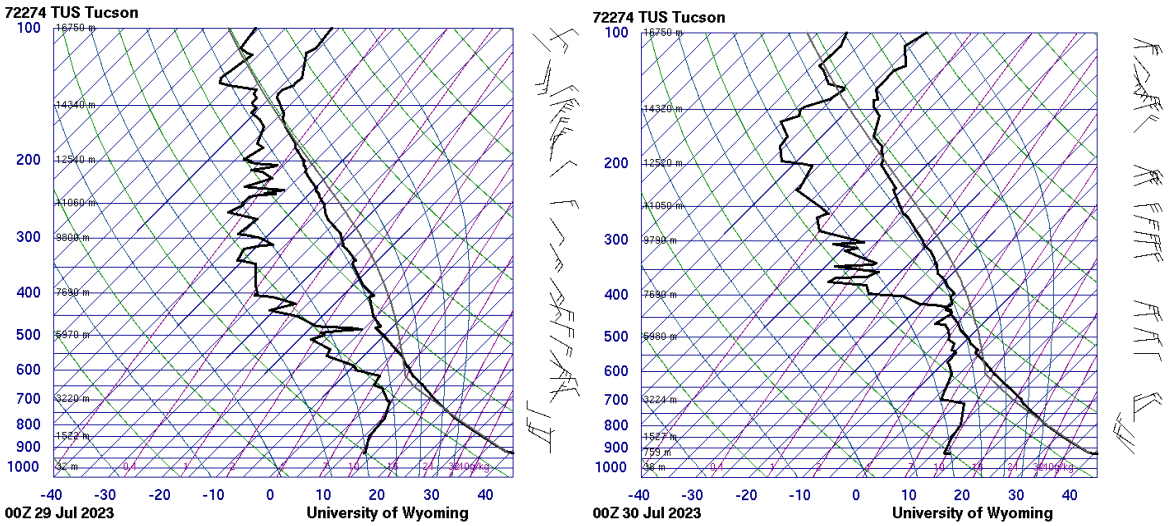

Figure 4-49. Tucson skew-T upper-air diagrams valid 5 p.m. PST from July 24-29, 2023. Deep mixing was evident each day, indicating vertical transfer of aloft air to the surface. Source: University of Wyoming

Smoke Transport

Using the estimated PBL heights, transport paths into central Arizona were examined using HYSPLIT 24-hour back trajectories plotted for each of the six days. In addition, the potential for smoke transport was assessed by overlaying the HYSPLIT trajectory paths onto the previous day's NOAA HMS smoke plume analysis and satellite fire detections. **Figure 4-50** shows each day contained at least one 24-hour back trajectory transport path that intersected analyzed smoke from the prior day. Additionally, transport paths on July 28 and 29 were near local fire detections.

July 24

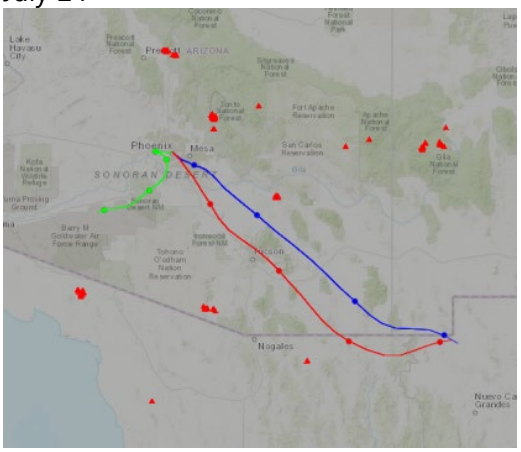

July 25

July 26

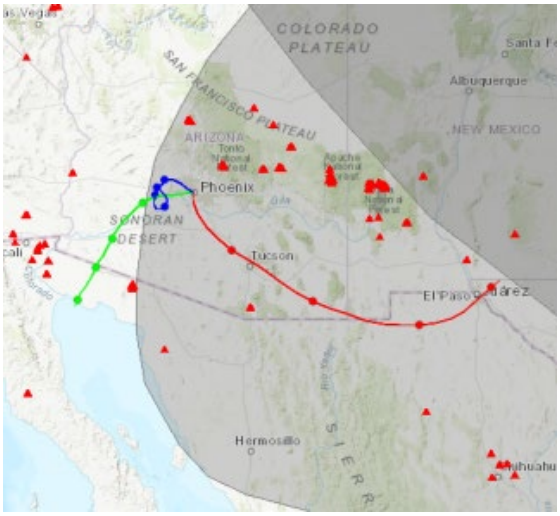

July 27

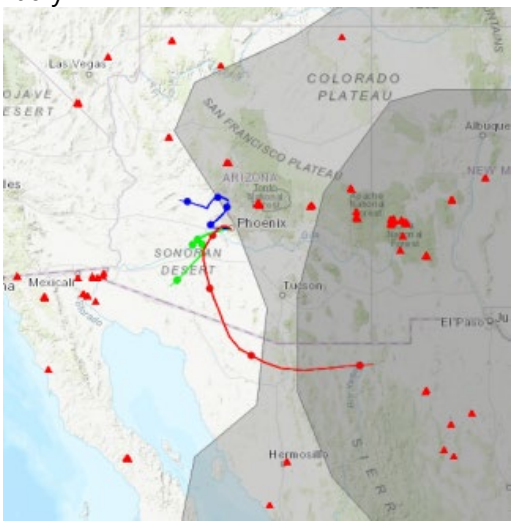

July 28

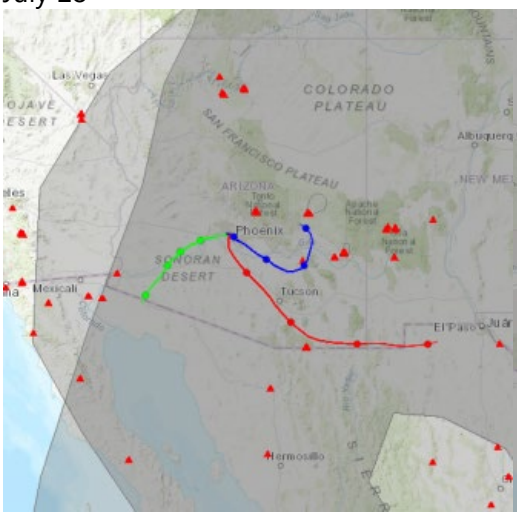

July 29

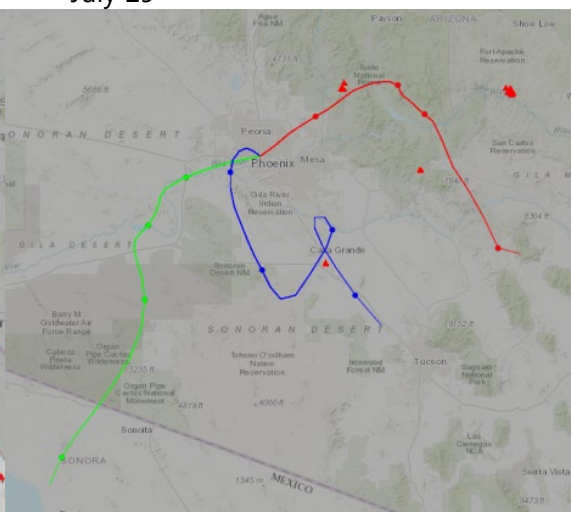

Figure 4-50. NOAA 24-hour back trajectory analysis ending 5 p.m. PST for the July 24-29, 2023 period. Each day's back trajectory analysis intersected a NOAA analyzed smoke plume from the previous day. Source: AirNow-Tech

Summary

From July 24 to July 29, a persistent area of high pressure aloft over the Four Corners region led to southerly to southeasterly upper-level winds in central Arizona. High pressure aloft also resulted in partly sunny skies and very hot temperatures supporting ozone development, with light surface winds throughout much of the six-day period hindering dispersion and allowing pollutants to accumulate. Furthermore, HYSPLIT back-trajectory transport paths within the PBL on each day intersected analyzed smoke by NOAA, with NOAA's smoke discussion highlighting fires in Canada as the source. HYPSPLIT trajectories for July 28 and 29 were also close to satellite fire detections in Arizona, indicating the potential for local transport. In addition, it is likely the upper-level wind pattern carried the broad Canadian smoke plume analyzed by NOAA into central Arizona. These conditions show evidence of smoke influencing ozone formation in the nonattainment area during the six-day period.

4.3.4 Surface Impacts

Low visibility in Phoenix is apparent on July 24-29, 2023. While some of the haze is may be due to dust, smoke plumes from the fires burning throughout the western U.S. and Canada, as well as the local Diamond Fire, were present over the nonattainment area during the atypical ozone event and contributed to the haze. **Figures 4-51 through 4-54** show photos taken from the southwest-facing Estrella Mountain, south-facing South Mountain, and east-facing Superstition Mountain webcams, where the visibility is low due to haze on July 24-29, 2023. Select webcam images were chosen based on the presence of smoke. Smoke from the Diamond Fire burning near the outskirts of Phoenix on July 26 also may have contributed to the smokey conditions in Phoenix, as noted by local residents (**Figure** 55).

Figure 4-51. Camera Images showing the southwest coordinal direction taken from the Estrella Mountain webcam on July 25 from 6:00 LST, 8:30 LST, and 10:45 LST.

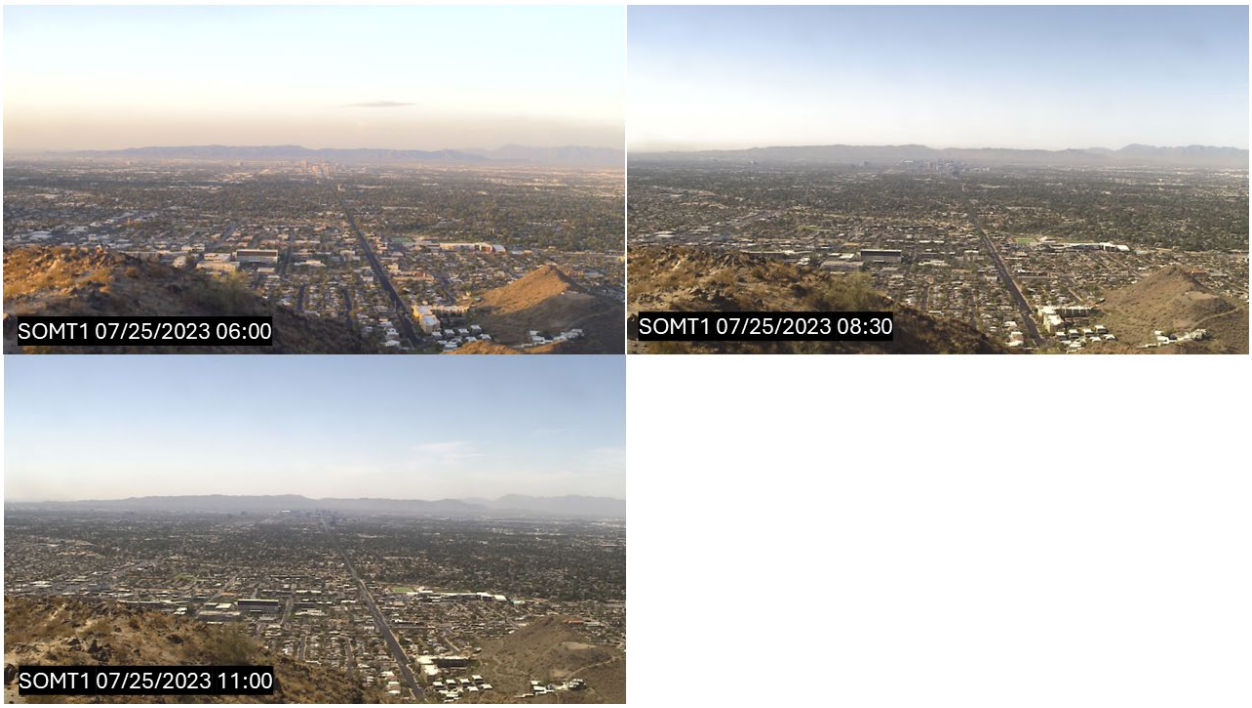

Figure 4-52. Camera Images showing the south coordinal direction taken from the South Mountain webcam on July 25 from 6:00 LST, 8:30 LST, and 11:00 LST.

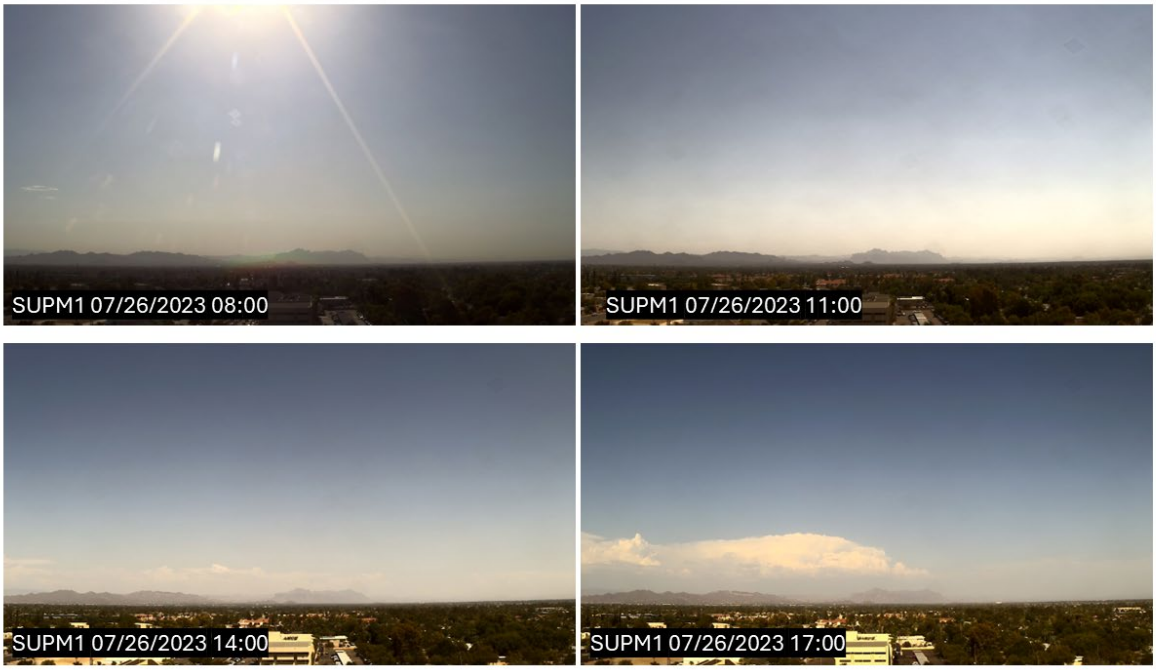

Figure 4-53. Camera Images showing the east coordinal direction taken from the Superstition Mountain webcam on July 26 from 8:00 LST, 11:00 LST, 14:00 LST, and 17:00 LST.

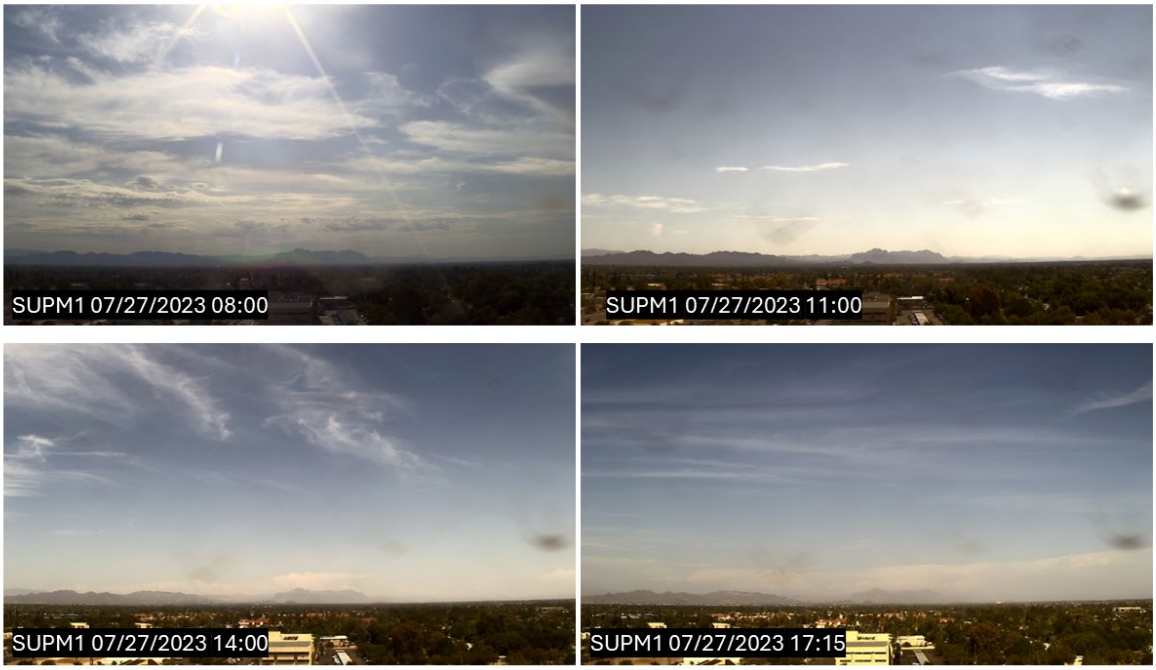

Figure 4-54. Camera Images showing the east coordinal direction taken from the Superstition Mountain webcam on July 27 from 8:00 LST, 11:00 LST, 14:00 LST, and 17:15 LST.

Figure 4-55. Social media post regarding smoke from the Diamond Fire over Phoenix on July 26, 2023.

Figure 4-56 shows an overall view of the magnitude of hourly pollutant concentrations measured in the nonattainment area in the two days before and after the July 24-29, 2023, atypical event. Hourly ozone concentrations are elevated at all affected sites relative to the days before the atypical event. As noted in Section 4.4, July 31, 2023, another atypical ozone event, also exhibited elevated ozone concentrations. Similarly, NO_2 concentrations at many sites, including non-exceeding sites, JLG Supersite, and Central Phoenix, were elevated during most of the July 24-29 period, indicating a buildup of ozone precursors in the nonattainment area. $PM_{2.5}$ concentrations were elevated during some hours, particularly at the end of July 26 into July 27. However, speciated $PM_{2.5}$ and dust storm warnings and advisories[17] indicate that elevated $PM_{2.5}$ concentrations may have been due to wind-blown dust rather than smoke from wildfires. Distinct and widespread enhancements in surface pollutant concentrations provide evidence that smoke from regional fires entered the region, mixed towards the surface, and had an atypical influence on ozone concentrations during the period.

[17] https://mesonet.agron.iastate.edu/vtec/search.php?mode=bypoint&lon=-112.1202&lat=33.4223&buffer=0.00&sdate1=2023-06-22&edate1=2023-08-18

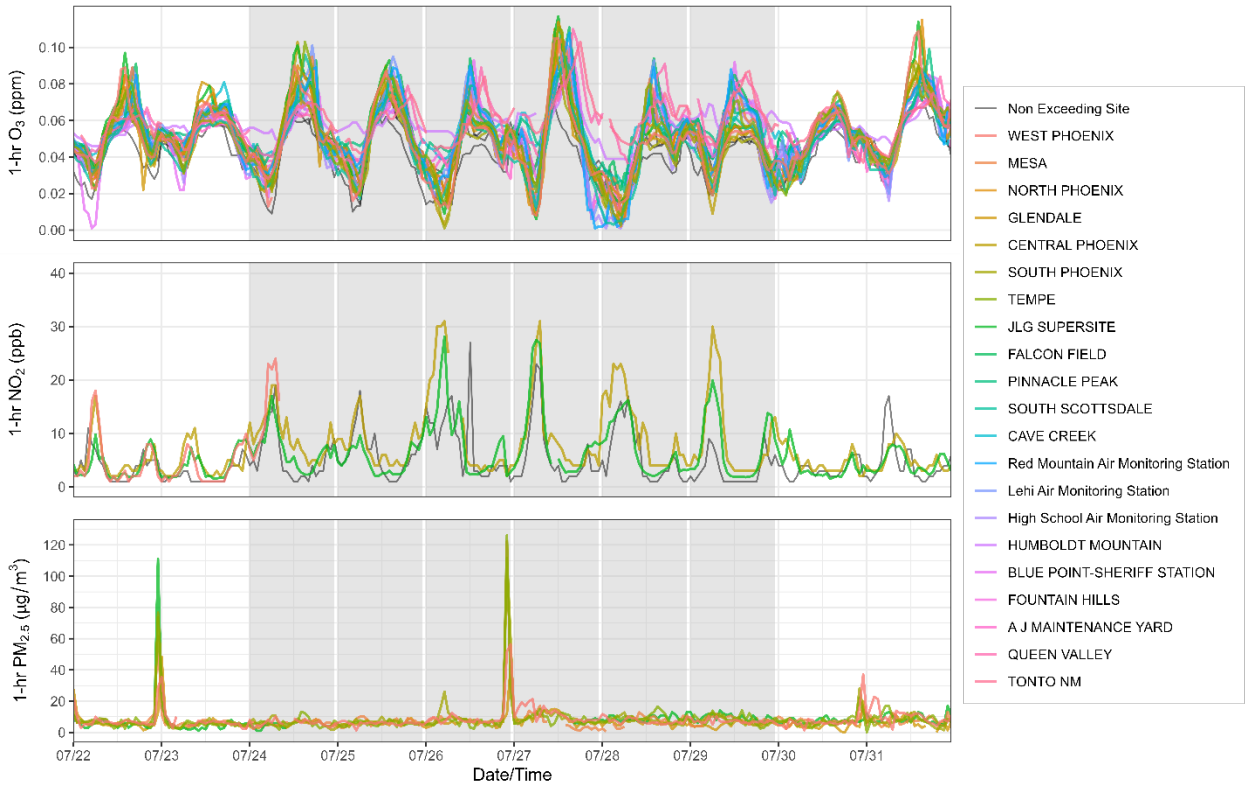

Figure 4-56. Hourly concentrations of ozone, NO_2, and $PM_{2.5}$ at all sites in the nonattainment area. All ozone-exceeding sites are color-coded to highlight smoke impacts on concentrations, and all non-exceeding sites are black. The gray shaded areas represent July 24-29, 2023.

Figure 4-57 shows hourly NO_2 concentrations at the Buckeye (top) and JLG Supersite (bottom) sites. Buckeye was a non-ozone-exceeding site. NO_2 concentrations at both sites exhibit a distinct increase to above the 95th percentile during the morning of July 26, followed by another distinct increase the following day. Similar increases were observed at other monitors, such as Central Phoenix and Buckeye. These observations provide evidence that smoke impacts were widespread and affected multiple air monitoring sites.

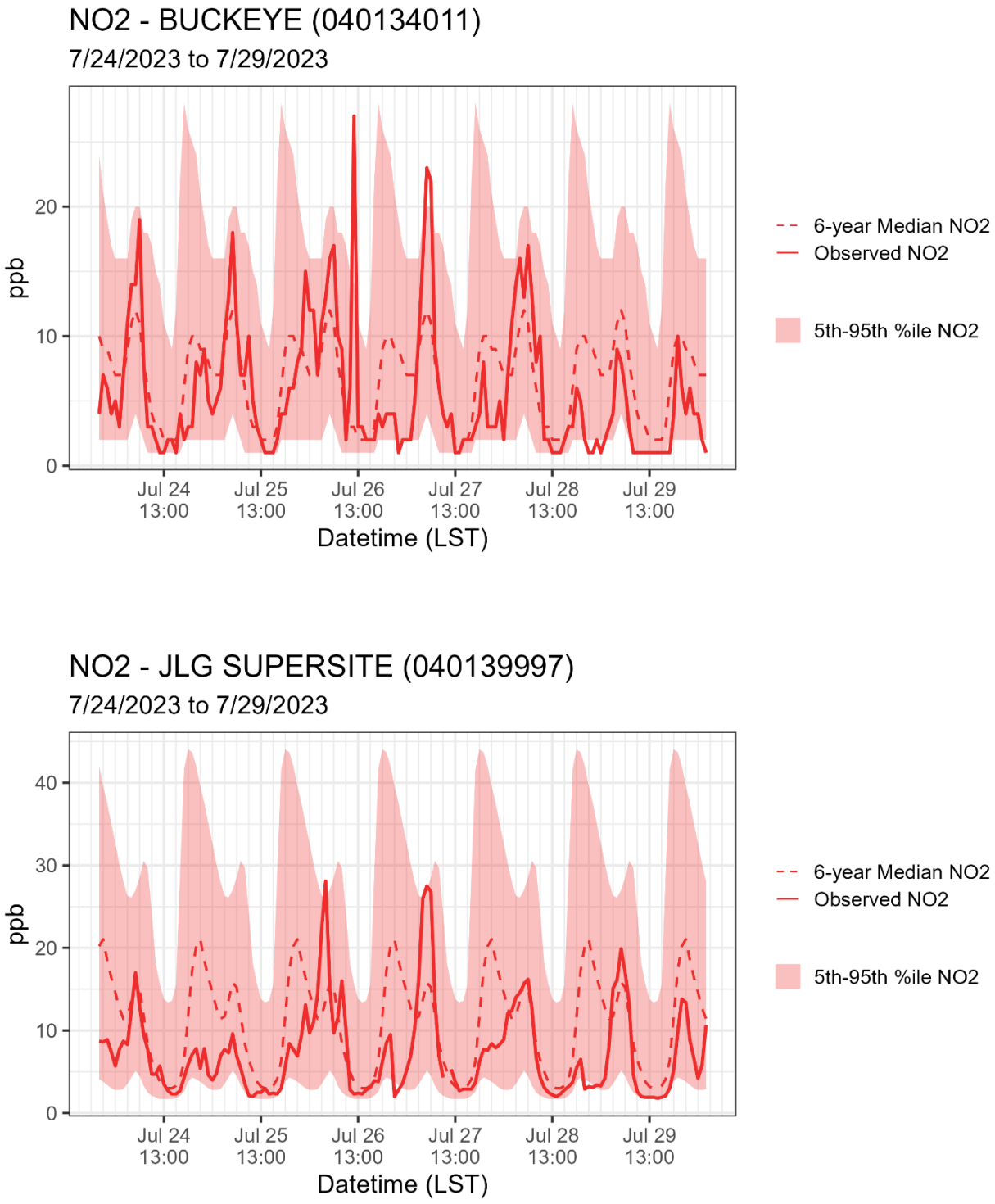

Figure 4-57. Hourly concentrations of NO_2 at the Buckeye (top) and JLG Supersite (bottom) sites. The 6-year (2019-2024) median is represented by the dashed line, and the 5th-95th percentile is represented by the shaded area.

OC and EC data were available on July 26 and 29. Figure 3-58 shows a boxplot of OC to EC ratios for available data collected during the ozone season between 2019-2024. The ratio of OC to EC taken at the JLG Supersite monitor showed increases in this ratio which are indicative of wildfire smoke. The OC to EC ratio in both samples was elevated above the 75th percentile. These observations provide further evidence that ground-level wildfire smoke entered Phoenix during the atypical event days containing increased OC to EC ratios.

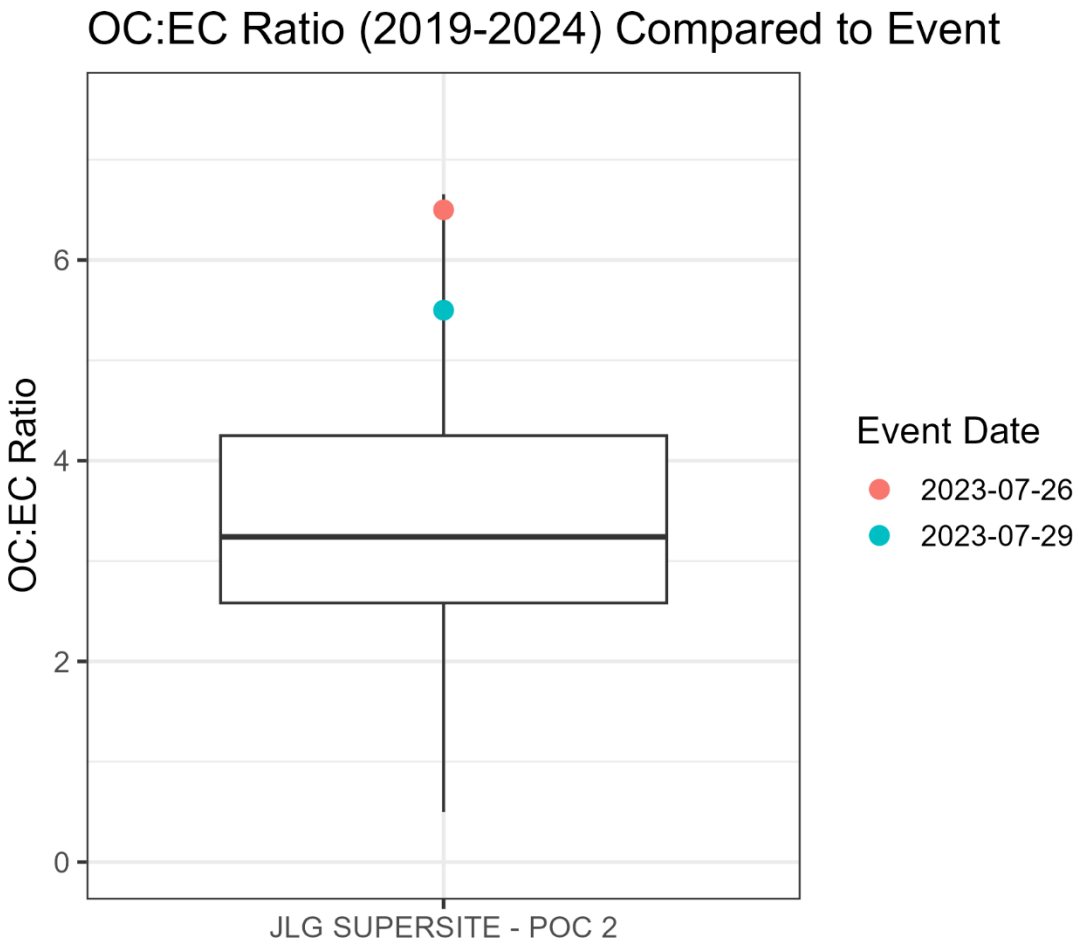

Figure 4-58. Boxplot of OC to EC ratios at the JLG Supersite site using data collected during the ozone season (April-September) from 2019-2024. OC to EC ratios are calculated at POC 2 (x-axis). Available OC to EC ratios collected during the July 24-29 atypical ozone event are shown as points.

4.3.5 Event Statistics

Table 4-11 summarizes the measurements of ozone concentrations on July 24-29, 2023, as well as the percentile rank of the observation compared to six years of ozone season data (April 1-September

31, 2019-2024). Ozone MDA8 measurements ranged from the 93rd - 100th percentile on July 24-29, 2023.

Table 4-11. Percentile of ozone measurements on the atypical dates compared with six years of ozone data (2019-2024). The percentile rank is calculated across the ozone production season in the nonattainment area (April 1-September 31) of 2019-2024.

Date	Site Name	Site Code	Ozone MDA8 (ppb)	Percentile Rank
7/24/2023	JLG Supersite	040139997	85	100
	Tempe	040134005	84	99
	Lehi Air Monitoring Station	040137022	82	99
	Mesa	040131003	80	99
	Central Phoenix	040133002	80	99
	Falcon Field	040131010	79	99
	North Phoenix	040131004	77	98
	South Scottsdale	040133003	77	98
	Red Mountain Air Monitoring Station	040137021	77	98
	West Phoenix	040130019	76	98
	Pinnacle Peak	040132005	73	96
	South Phoenix	040134003	72	94
	Blue Point-Sheriff Station-Tonto NF-Salt River Recreation Area	040139702	72	94
	Glendale	040132001	71	93
	High School Air Monitoring Station	040137024	71	93
7/25/2023	Mesa	040131003	79	99
	Lehi Air Monitoring Station	040137022	79	99
	JLG Supersite	040139997	79	99
	Falcon Field	040131010	78	99
	Tempe	040134005	77	98
	Red Mountain Air Monitoring Station	040137021	76	98

Date	Site Name	Site Code	Ozone MDA8 (ppb)	Percentile Rank
	West Phoenix	040130019	75	98
	North Phoenix	040131004	75	98
	Central Phoenix	040133002	72	94
	Queen Valley	040218001	72	94
	Glendale	040132001	71	93
	South Phoenix	040134003	71	93
	Blue Point-Sheriff Station-Tonto NF-Salt River Recreation Area	040139702	71	93
7/26/2023	Falcon Field	040131010	72	94
	Red Mountain Air Monitoring Station	040137021	71	93
	Lehi Air Monitoring Station	040137022	71	93
	Queen Valley	040218001	71	93
7/27/2023	Falcon Field	040131010	90	100
	Queen Valley	040218001	89	100
	Red Mountain Air Monitoring Station	040137021	88	100
	Tempe	040134005	87	100
	JLG Supersite	040139997	87	100
	Tonto NM	040070010	87	100
	Lehi Air Monitoring Station	040137022	86	100
	Mesa	040131003	85	100
	North Phoenix	040131004	85	100
	Blue Point-Sheriff Station-Tonto NF-Salt River Recreation Area	040139702	85	100
	West Phoenix	040130019	83	99
	Glendale	040132001	83	99
	Pinnacle Peak	040132005	83	99
	Fountain Hills	040139704	81	99
	Central Phoenix	040133002	80	99

Date	Site Name	Site Code	Ozone MDA8 (ppb)	Percentile Rank
	Cave Creek	040134008	80	99
	High School Air Monitoring Station	040137024	79	99
	A J Maintenance Yard	040213001	79	99
	South Scottsdale	040133003	76	98
	South Phoenix	040134003	76	98
	Humboldt Mountain	040139508	73	96
7/28/2023	Queen Valley	040218001	75	98
	Falcon Field	040131010	72	94
7/29/2023	Queen Valley	040218001	78	99
	Tonto NM	040070010	77	98
	Blue Point-Sheriff Station-Tonto NF-Salt River Recreation Area	040139702	75	98
	Falcon Field	040131010	74	97
	Red Mountain Air Monitoring Station	040137021	73	96
	Lehi Air Monitoring Station	040137022	71	93
	A J Maintenance Yard	040213001	71	93

4.3.6 Conclusion

The concurrence of HMS smoke perimeters over the nonattainment area, HYSPLIT trajectories and meteorological analysis showing accumulation of smoke in the nonattainment area, visible smoke in camera images, and elevated NO_2 concentrations, and OC to EC ratios provide evidence that surface-level smoke was present during the period. Long-range transport of smoke from numerous unidentified fires burning throughout the western U.S. and Canada, plus a local fire, enhanced ozone concentrations outside of the typical diurnal profile, keeping ozone values high and affecting the MDA8 ozone concentrations at twenty-one sites. Multiple analyses showed that smoke fully encompassed the Maricopa Nonattainment Area on July 24-29, 2023, and statistics show ozone concentrations were atypical during this event.

This combined evidence indicates that smoke plumes generated by numerous fires in the western U.S. and Canada, including a local fire, provided an atypical source of ozone and ozone precursors

that caused enhanced ozone concentrations on July 24-29, 2023. Removal of these days as atypical events is supported by this analysis.

4.4 July 31-August 1, 2023

4.4.1 Event Overview: July 31-August 1, 2023

The unrepresentative (atypical) ozone event took place on July 31-August 1, 2023, and affected twenty-two monitoring sites in in the Maricopa Nonattainment Area: West Phoenix, Mesa, North Phoenix, Falcon Field, Glendale, Pinnacle Peak, Central Phoenix, South Scottsdale, South Phoenix, Tempe, Cave Creek, Dysart, Red Mountain Air Monitoring Station, Lehi Air Monitoring Station, High School Air Monitoring Station, Humboldt Mountain, Blue Point-Sheriff Station-Tonto NF-Salt River Recreation Area, Fountain Hills, JLG Supersite, A J Maintenance Yard, Queen Valley, and Tonto NM (**Table 4-12**). The maximum daily 8-hr average (MDA8) ozone concentrations at the effected sites ranged from 71-89 ppb.

Time series graphs showing hourly ozone concentrations that exceeded the seasonal means (calculated using all available data from April 1 – September 31, 2019-2024) and 10th-90th percentiles at each site are shown in **Figure 4-59**. Throughout the atypical period, ozone concentrations exhibited widespread and distinct peaks, particularly on July 31 at sites such as Central Phoenix, JLG Supersite, North Phoenix, Pinnacle Peak, and West Phoenix; these observations exceeded the 90th percentile relative to all data collected during the ozone season from 2019-2024.

Numerous fires burning in the western U.S. and Canada, as well as a local fire, were identified as major contributors to this event. Evidence includes (1) HMS smoke perimeters over the nonattainment area, (2) HYSPLIT trajectories and meteorological analysis showing accumulation of smoke in Phoenix, (3) visible smoke in camera images, and (4) elevated NO_2 and OC to EC ratios. This combination of evidence indicates that this is an atypical ozone event.

Table 4-12. Summary of identified atypical July 31 – August 1, 2023.

Event Date(s)	Event Ozone Concentration Percentile	Sites Exceeded During Event	Type of Event
July 31-August 1, 2023	94th - 100th	Twenty-Two sites: West Phoenix, Mesa, North Phoenix, Falcon Field, Glendale, Pinnacle Peak, Central Phoenix, South Scottsdale, South Phoenix, Tempe, Cave Creek, Dysart, Red Mountain Air Monitoring Station, Lehi Air Monitoring Station, High School Air Monitoring	Local smoke (July 31), regional/long-range smoke (August 1)

Event Date(s)	Event Ozone Concentration Percentile	Sites Exceeded During Event	Type of Event
		Station, Humboldt Mountain, Blue Point-Sheriff Station-Tonto NF-Salt River Recreation Area, Fountain Hills, JLG Supersite, A J Maintenance Yard, Queen Valley, Tonto NM	

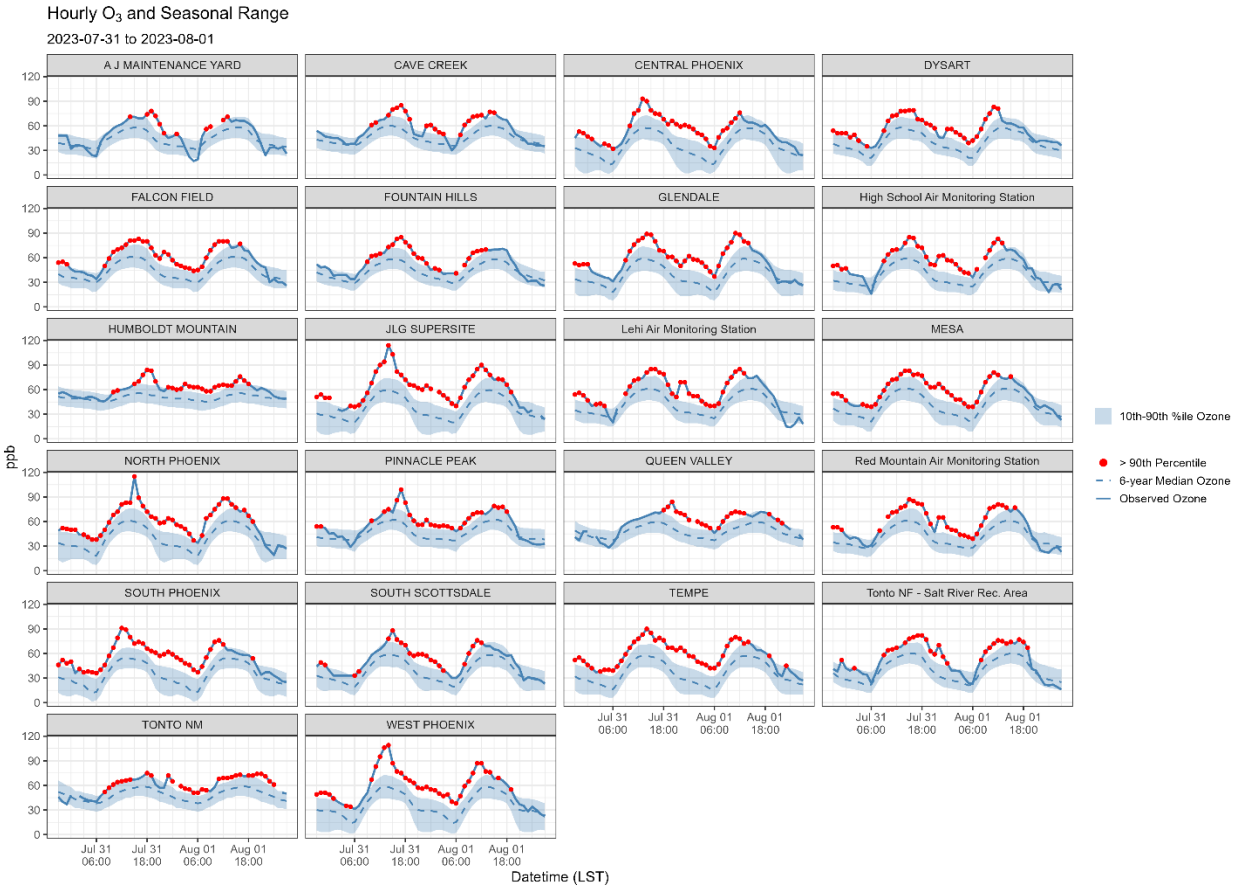

Figure 4-59. Hourly ozone concentrations (ppb) compared to all available data during the ozone season (April 1 – September 31) of the 6-year (2019-2024) period. Hourly means and 10th-90th percentiles are calculated using data on July 31-August 1, 2023.

4.4.2 Identification of Wildfire(s)

Numerous fires in Mexico, the western U.S., and in Canada were active in the days leading up to and during July 31-August 1, the exclusion days (**Figures 4-60 through 4-62**). Smoke from these fires combined to blanket the continental U.S. during July 31-August 1. A local fire to the south of Phoenix

began on July 30 at approximately 20:00 LST and continued to burn throughout July 31. The local fire was caused when lightning struck a tree farm near the city of Maricopa, Arizona.[18]

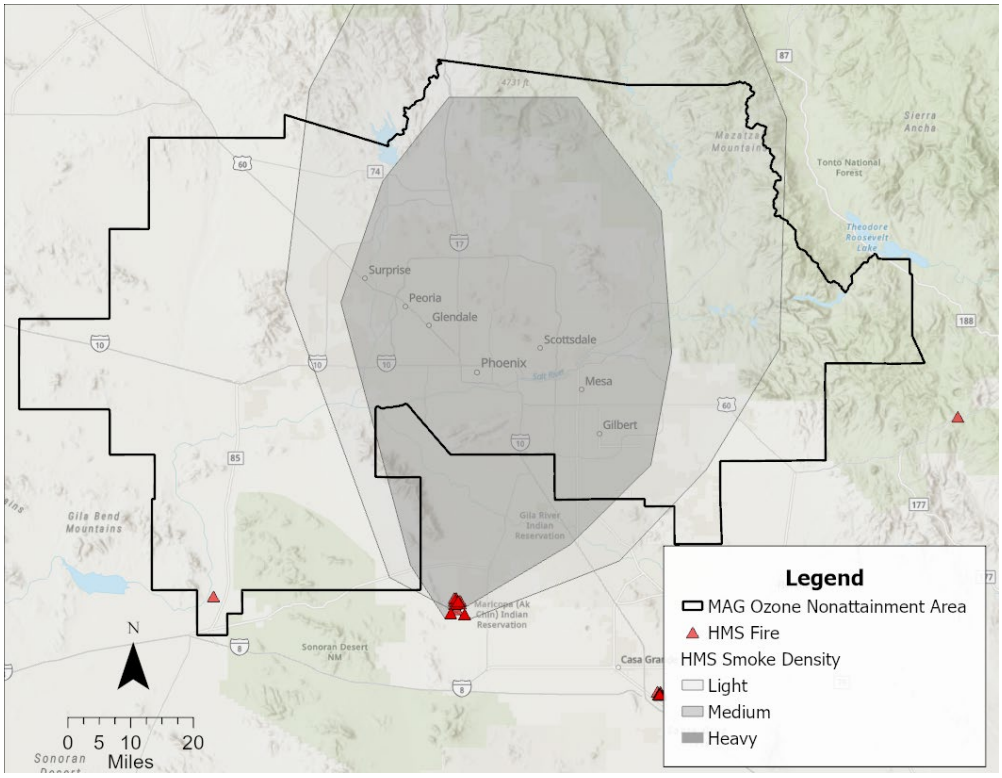

Figure 4-60. Local view of HMS smoke density and fire locations on July 31, 2023.

[18] https://www.12news.com/article/news/local/arizona/lightning-strike-causes-fire-tree-farm-maricopa/75-02f912e1-379c-4fd2-bdc2-87f92b7c474f

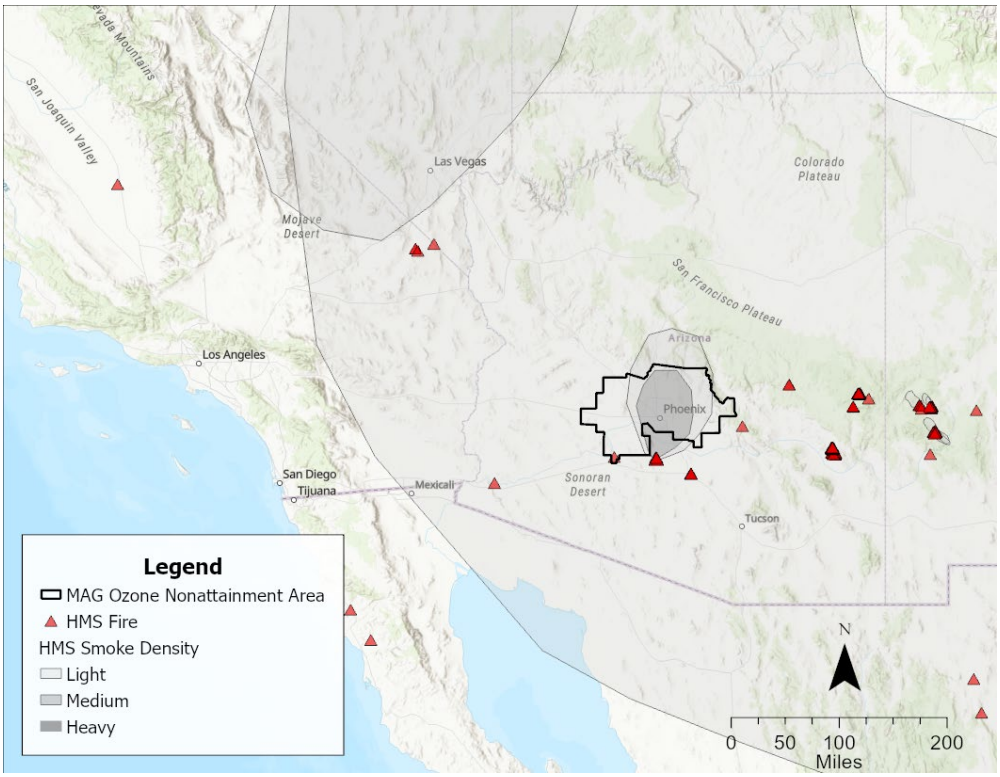

Figure 4-61. Regional view of HMS smoke density and fire locations on July 31, 2023

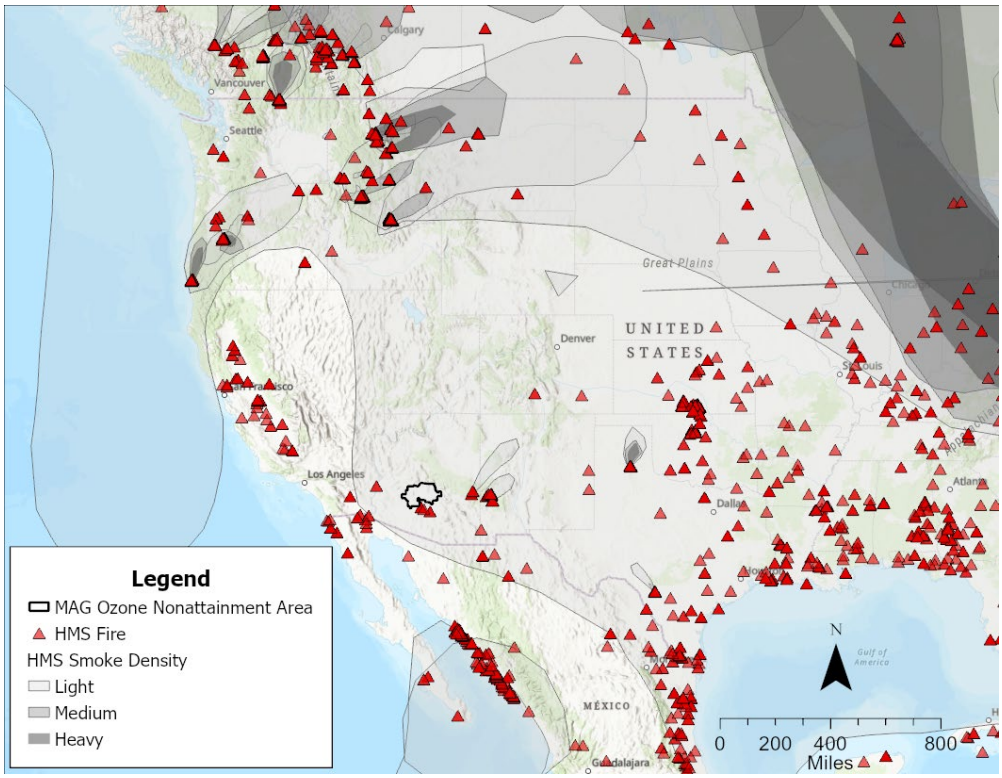

Figure 4-62. Continental view of HMS smoke density and fire locations on August 1, 2023

4.4.3 Meteorological Analysis

Upper-level Analysis

Figure 4-63 shows the upper-level weather pattern on the morning of July 31, which consisted of high pressure at 500 mb over Texas and Oklahoma, with an associated broad ridge across the Rockies and southwestern United States. The upper-level wind pattern at the Phoenix upper-air weather station was southeasterly. By the morning of August 1, the 500 mb pattern continued to show high pressure aloft over Texas and Oklahoma, with broad ridging aloft remaining over the Rockies and southwestern United States. An inverted trough was located over central Arizona, which led to an upper-level southwesterly wind pattern.

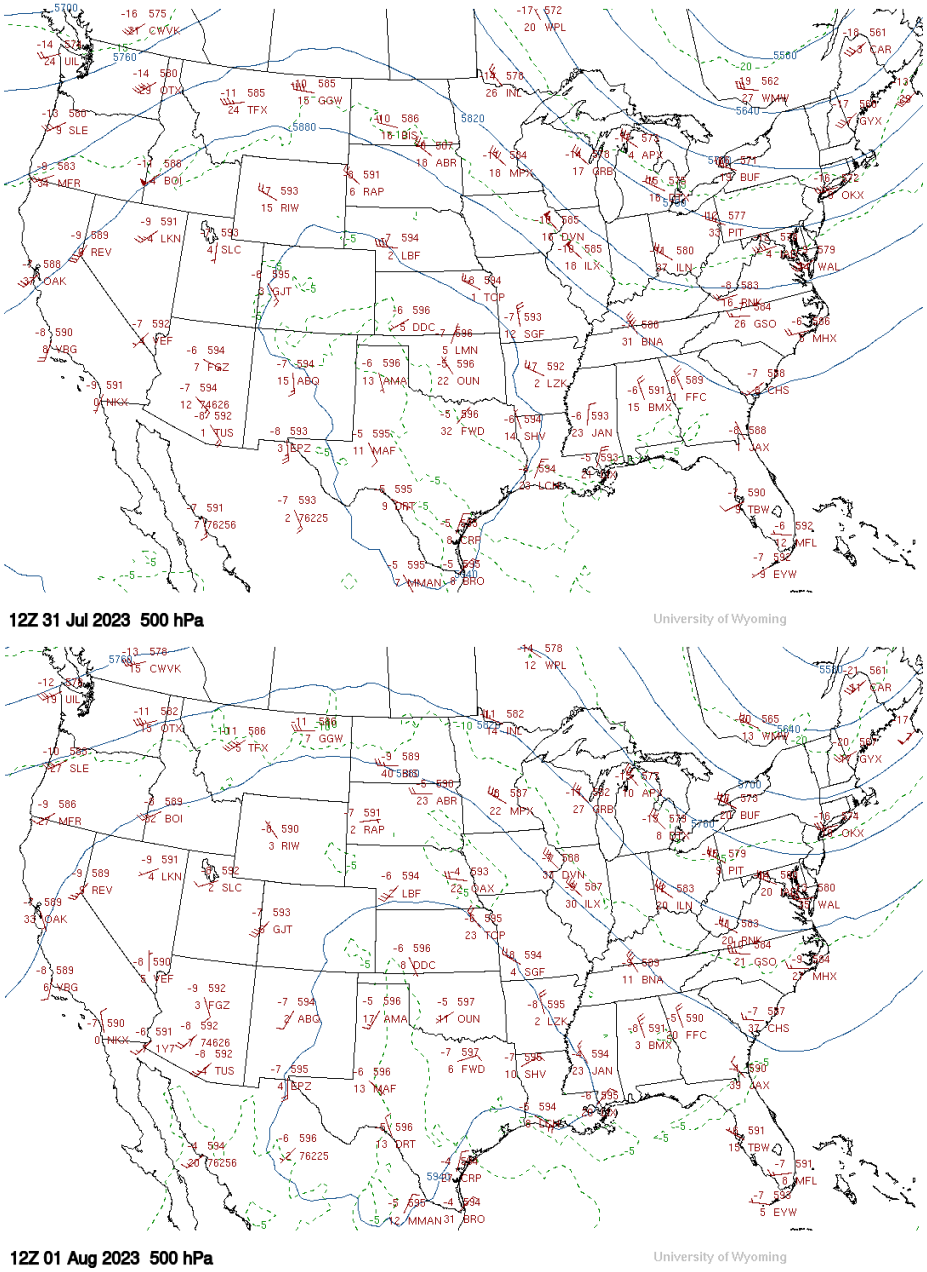

Figure 4-63. 500 mb geopotential heights (blue lines) and winds (red barbs) for 5 a.m. PST on July 31 (top) and August 1 (bottom). A broad ridge of high pressure over the southwestern United States and Rockies was the dominant pattern influencing central Arizona's weather. Source: University of Wyoming

Surface Analysis

Subsidence (sinking air) with the broad ridge aloft across the southwestern United States led to sunny and very hot associated conditions in the nonattainment area. As shown in **Table 4-13**, daytime highs at KPHX reached 108°F on July 31, followed by an afternoon high of 109°F on

August 1. Furthermore, surface winds at KPHX on both July 31 and August 1 were less than 10 mph throughout the morning and afternoon hours, hindering dispersion and allowing pollutants and ozone precursors to accumulate. These winds, combined with sunshine and very hot temperatures, promoted ozone formation each day.

Table 4-13. Daily maximum high temperatures and average daily wind speed from KPHX.

Date	Maximum temperature (°F)	Average daily wind speed (mph)
July 31	108	8.0
August 1	109	7.9

Satellite Smoke and Fire Detections

Figure 4-64 contains NOAA HMS smoke plume analysis and satellite fire detections across the southwestern United States during July 31 and August 1, 2023. On each day, NOAA analyzed smoke over the nonattainment area. In addition, satellites picked up fire activity south and east of Phoenix on both days. Potential smoke transport paths into Phoenix for July 31-August 1, 2023 can be found in the "Smoke Transport" section.

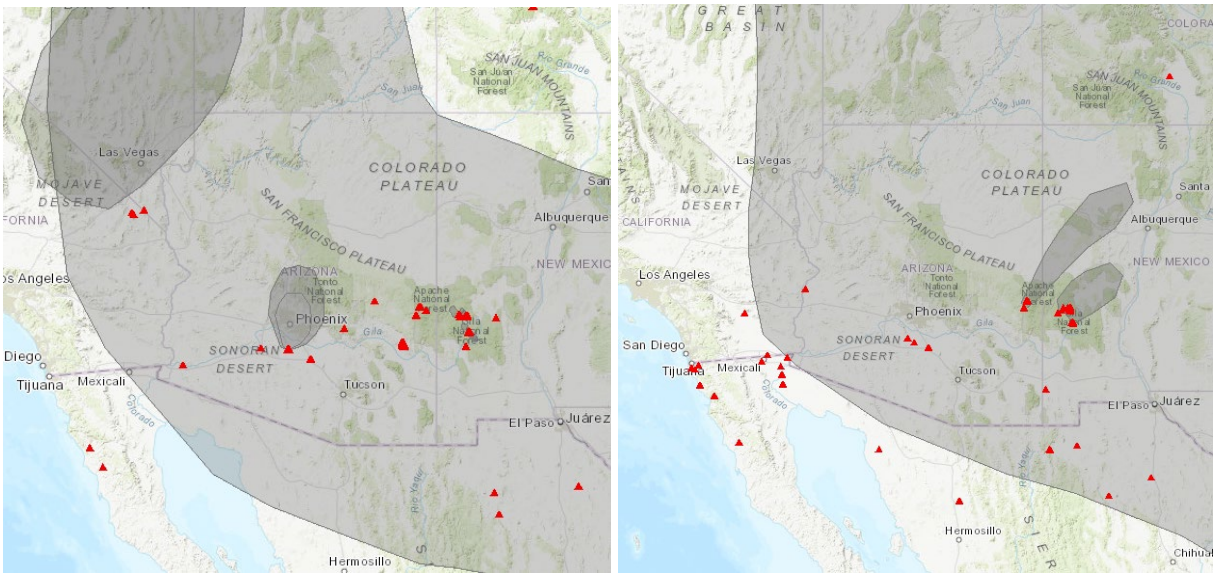

Figure 4-64. NOAA HMS smoke plume analysis (grey contours) and satellite fire detections (red triangles) from July 31, 2023 (left) and August 1, 2023 (right). Source: AirNow-Tech

Smoke Discussions

NOAA's daily smoke discussion highlighted the potential sources for the analyzed smoke transported into the nonattainment area.

"A very large area of light smoke continues to blanket much of Canada, the CONUS and the North Atlantic. In addition to those locations, the same layer covers portions of Alaska, the Arctic, and the far northeastern Pacific. The parent activity is mainly the ongoing wildfire activity across northwestern and central Canada, **with some contributions from a few other isolated wildfires across the western CONUS**. The thicker smoke from this activity was seen across the Northwest Territory, southern Nunavut, northern Alberta, northeastern Saskatchewan, much of Manitoba and western Ontario into the Upper Midwest and across the Great Lakes into the Northeastern CONUS and the St. Lawrence River Valley. A large cyclone over eastern Canada is continuing to draw the smoke counter-clockwise around the feature toward the Maritime Provinces. Smoke was also seen across the northern Gulf of Mexico and the Gulf Coast extending out over the Atlantic along a front that has acted to concentrate some remnant smoke." (NOAA NESDIS Text Narrative from July 31, 2023)

Soundings

PBL heights for the July 31-August 1 period were estimated for Phoenix using the Tucson upper-air sounding data and are shown in Table 4-14. According to the 5 p.m. PST data on July 31, the PBL height was approximately 4,200 m AGL after adjusting for the elevation of Phoenix. For August 1 at 5:00 p.m. PST, the estimated PBL was 3,300 m AGL. The deep PBL can be seen from the Tucson skew-T diagrams in Figure 4-65, which suggest vertical transfer of air from the upper-levels down to the surface.

Table 4-14. Daily estimated PBL heights for Phoenix from the Tucson upper-air sounding data.

Date	Estimated PBL (meters)
July 31	4,200
August 1	3,300

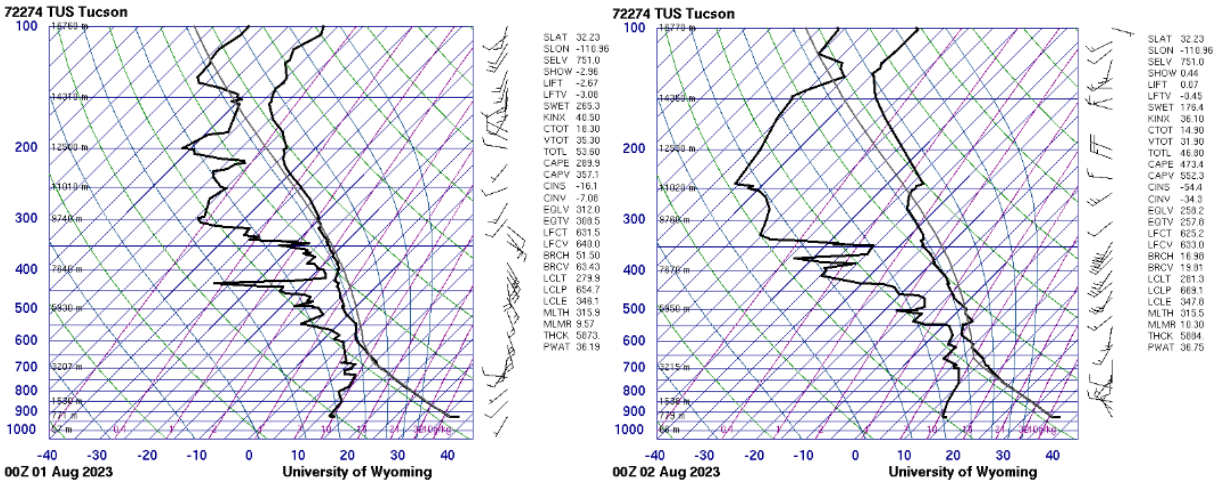

Figure 4-65. 5:00 p.m. PST skew-T diagrams from the Tucson upper-air weather station on July 31 (left) and August 1 (right). Upper-air data in Tucson indicates a deep PBL across southern and central Arizona on each day. Source: University of Wyoming

Smoke Transport

From the estimated PBL heights, transport paths were established using HYSPLIT. **Figure 4-66** contains the 6-hour HYSPLIT back trajectory ending at 5:00 p.m. PST July 31, which showed a southerly to south-southeasterly path into Phoenix at 2,000 and 4,200 m AGL. The 2,000 m path originated from near the Maricopa/Pinal County line, while the 4,200 m path started near Green Valley, Arizona. For August 1, a 36-hour HYSPLIT back trajectory was analyzed ending at 5 p.m. PST. The back trajectory for the 3,300 m path in **Figure 4-67** was southerly to south-southeasterly, with source air originating from the late evening of July 30 near Ciudad Obregon, Sonora and Los Mochis, Sinaloa.

To determine if pollutant transport into Phoenix occurred during the July 31-August 1 period, the established HYSPLIT trajectory paths were overlaid on the NOAA HMS smoke plume analysis and satellite fire detections. Using the July 31 HYSPLIT trajectory, the 2,000 m and 4,200 m paths were close to a cluster of fire detections southwest of the city of Maricopa, Arizona on the same day. These paths also intersected analyzed smoke across the region. For the August 1 HYSPLIT trajectory, the 3,300 m path intersected analyzed smoke plumes and was near fire detections from July 30 near the Sonora/Sinaloa, Mexico border, as well as the July 31 fire detections near the city of Maricopa, Arizona.

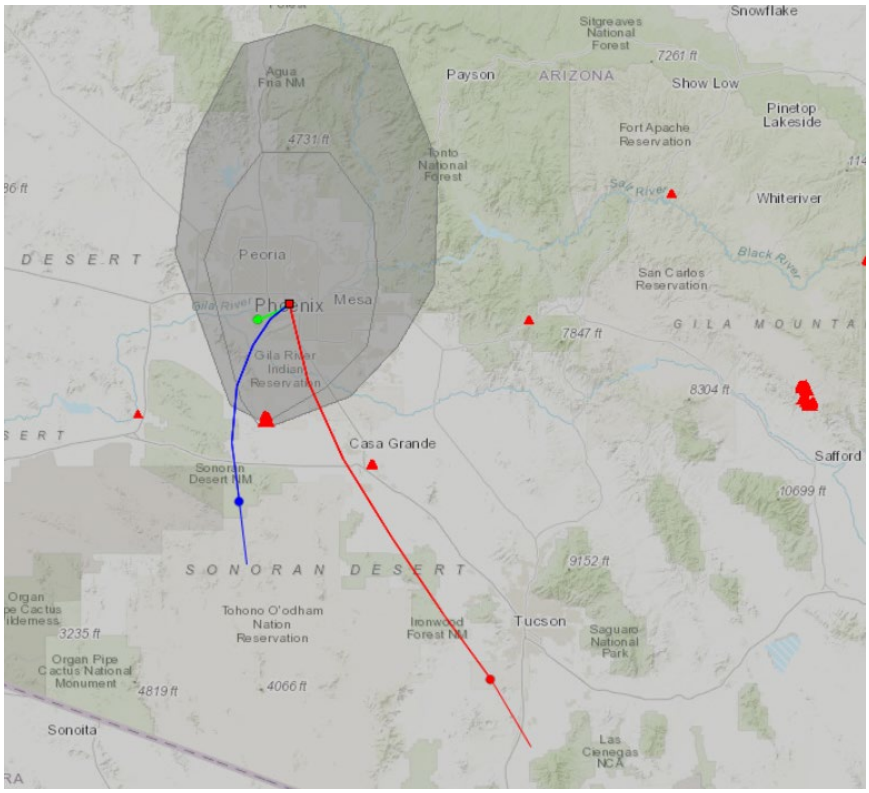

Figure 4-66. 6-hour back trajectory analysis ending 5 p.m. PST on July 31, 2023. Transport paths at 2,000 m AGL (blue) and 4,200 m AGL (red) intersect with NOAA analyzed smoke (grey contours) and were near satellite fire detections south of Phoenix (red triangles). Source: AirNow-Tech

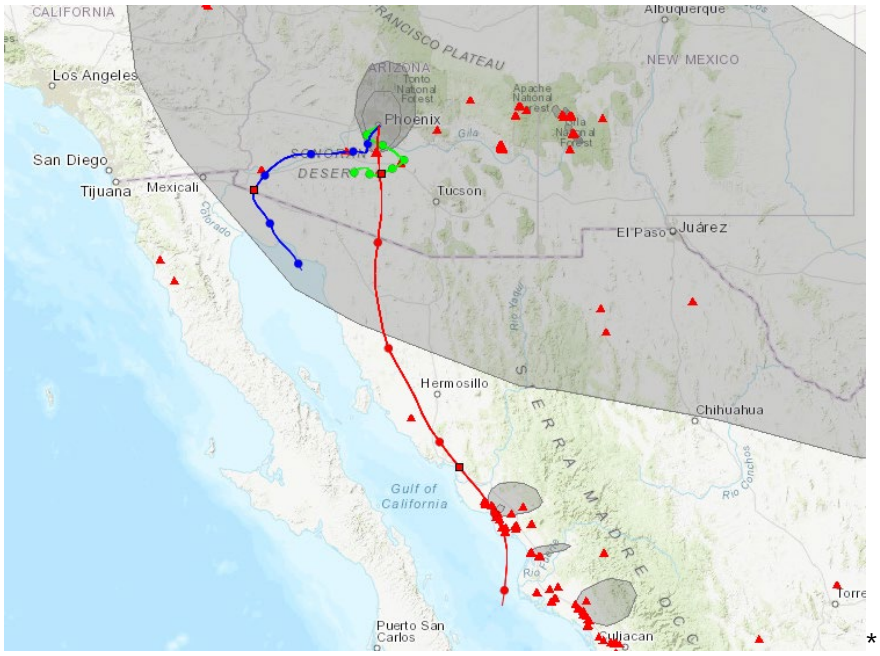

Figure 4-67. 36-hour back trajectory analysis ending 5 p.m. PST on August 1, 2023. Transport paths intersect with NOAA analyzed smoke (grey contours) and satellite fire detections (red triangles) from the previous day. Source: AirNow-Tech

Summary

For the July 31-August 1 period, a ridge of high pressure aloft promoted subsidence, which led to sunny and very hot conditions that supported ground-level ozone formation. Additionally, light surface winds each morning and afternoon in the nonattainment area allowed pollutants and ozone precursors to accumulate. Furthermore, transport paths within the estimated PBL intersected with analyzed smoke plumes and were close to satellite fire detections. Due to these conditions, there is evidence of smoke transport, which enhanced ozone development in central Arizona on these days.

4.4.4 Surface Impacts

Low visibility in Phoenix is apparent on July 31, 2023. Smoke plumes from the fires burning throughout Mexico, the western U.S., and Canada, as well as a local fire to the south of Phoenix, were present over the nonattainment area during the atypical ozone event and contributed to the haze. **Figures 4-68 through 4-69** show photos taken from the northeast-facing Camelback Mountain and the east-facing Superstition Mountain webcams. Select webcam images were chosen based on the presence of smoke. Smoke from the local fire was noted by local meteorologist Matt Pace (**Figure 4-70**) and another resident (**Figure 4-71**).

Figure 4-68. Camera Images showing the northeast coordinal direction taken from the Camelback Mountain webcam on July 31 from 16:00 LST, 17:15 LST, 18:15 LST, and 19:00 LST.

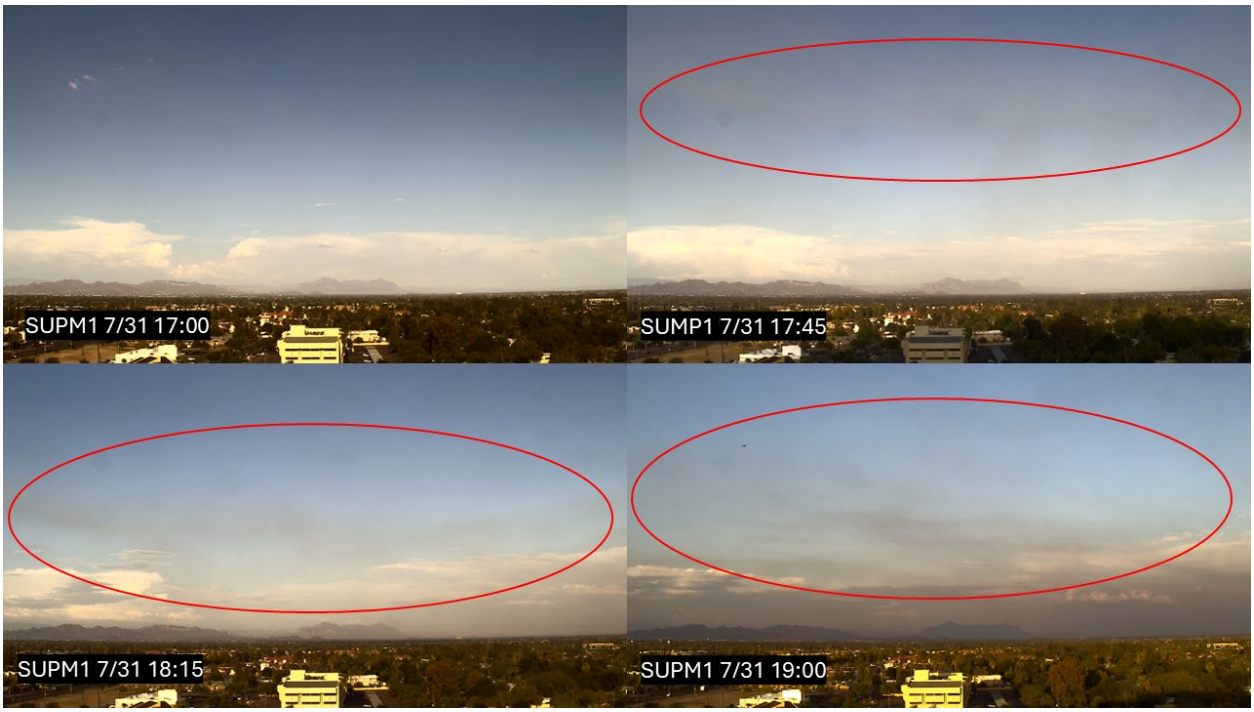

Figure 4-69. Camera Images showing the northeast coordinal direction taken from the Superstition Mountain webcam on July 31 from 17:00 LST, 17:45 LST, 18:15 LST, and 19:00 LST.

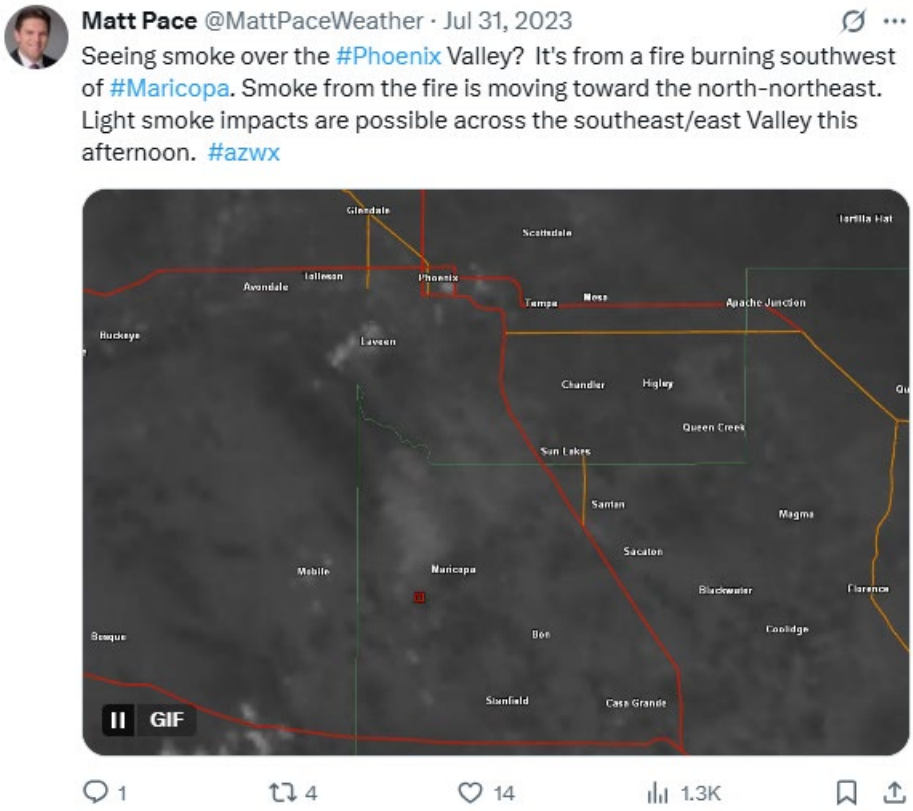

Figure 4-70. Social media post regarding smoke from the local fire to the south of Phoenix on July 31, 2023.

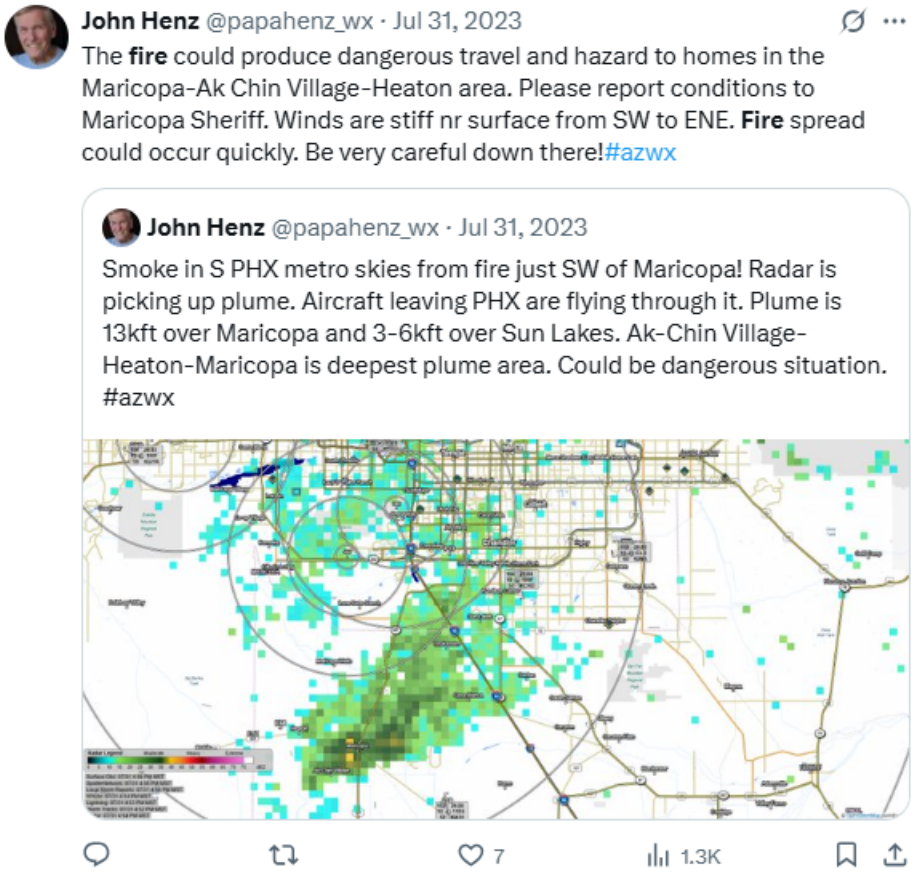

Figure 4-71. Social media post regarding smoke from the local fire to the south of Phoenix on July 31, 2023.

Figure 4-72 shows an overall view of the magnitude of hourly pollutant concentrations measured in the nonattainment area in the two days before and after the July 31-August 1, 2023, atypical event. Hourly ozone concentrations are elevated at all affected sites relative to the days before the atypical event. $PM_{2.5}$ concentrations at the exceedance-affected sites rise sharply at all $PM_{2.5}$-measuring sites during the evening of July 30. However, elevated $PM_{2.5}$ may have been due to monsoonal storms that occurred on July 30.[19] Elevated $PM_{2.5}$ concentrations were likely not solely from dust late in the evening on July 31 because the timing of elevated concentrations aligns with the transport of smoke from the fire burning to the south of Phoenix. Distinct and widespread enhancements in surface pollutant concentrations provide evidence that smoke from regional fires entered the region, mixed towards the surface, and had an atypical influence on ozone concentrations during the period.

[19] https://www.fox10phoenix.com/news/monsoon-storm-heads-toward-phoenix-july-30

Figure 4-72. Hourly concentrations of ozone, NO_2, and $PM_{2.5}$ at all sites in the nonattainment area. All ozone-exceeding sites are color-coded to highlight smoke impacts on concentrations, and all non-exceeding sites are black. The gray shaded areas represent July 31-August 1, 2023.

OC and EC data were available on August 1 and show evidence of smoke impacts. **Figure 4-73** shows a boxplot of OC to EC ratios for available data collected during the ozone season between 2019-2024. The ratio of OC to EC taken at the JLG Supersite monitor was above the 75th percentile and this increased ratio is indicative of wildfire smoke. **Figure 4-74** shows boxplots of speciated $PM_{2.5}$ collected at the JLG Supersite monitor during the ozone season between 2019-2024. Aluminum, potassium, silicon, and sulfate concentrations collected on August 1 are elevated above the 75th percentile. Elevated concentrations of aluminum and silicon are indicative of dust, but potassium is also elevated, which indicates the presence of smoke. These observations provide further evidence that ground-level wildfire smoke entered Phoenix on July 31-August 1 containing increased OC to EC ratios and potassium concentrations during the atypical ozone event.

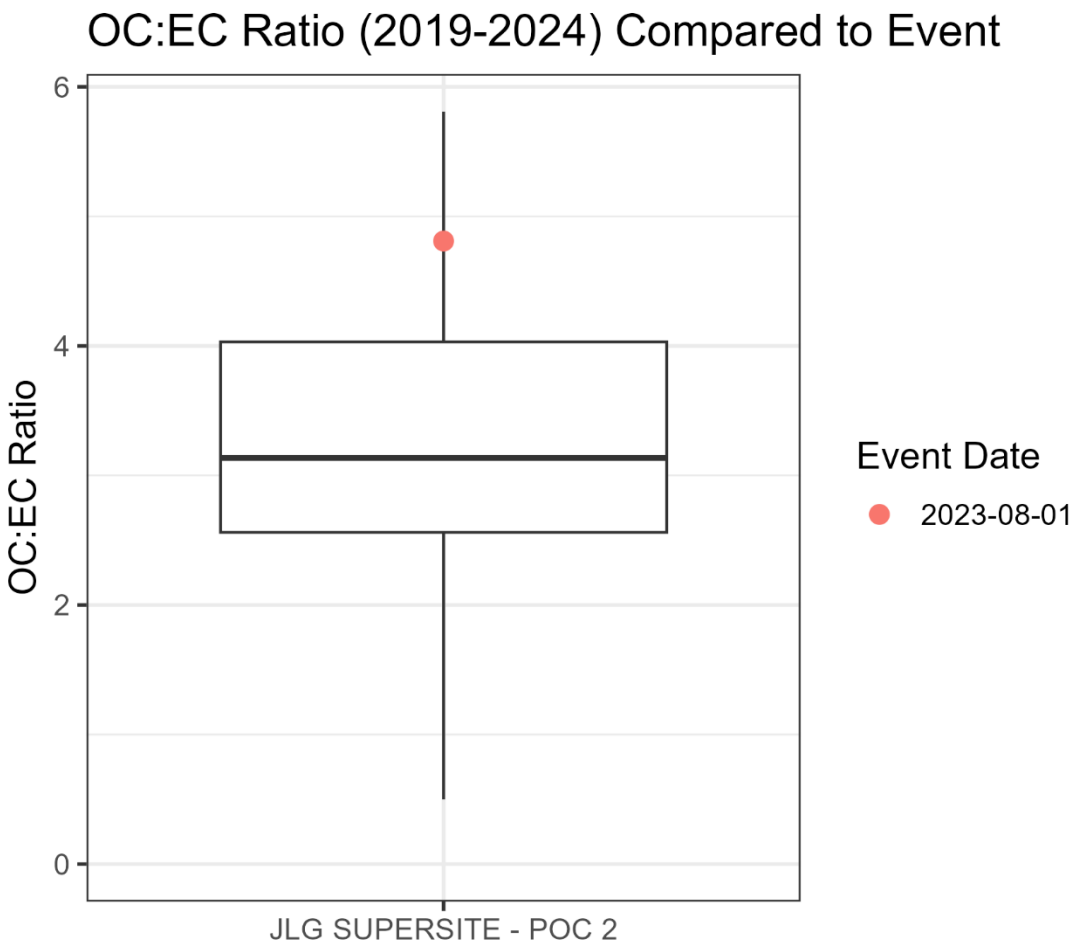

Figure 4-73. Boxplot of OC to EC ratios at the JLG Supersite site using data collected during the ozone season (April-September) from 2019-2024. OC to EC ratios are calculated at POC 2 (x-axis). Available OC to EC ratios collected during the July 31-August 1 atypical ozone event are shown as a point.

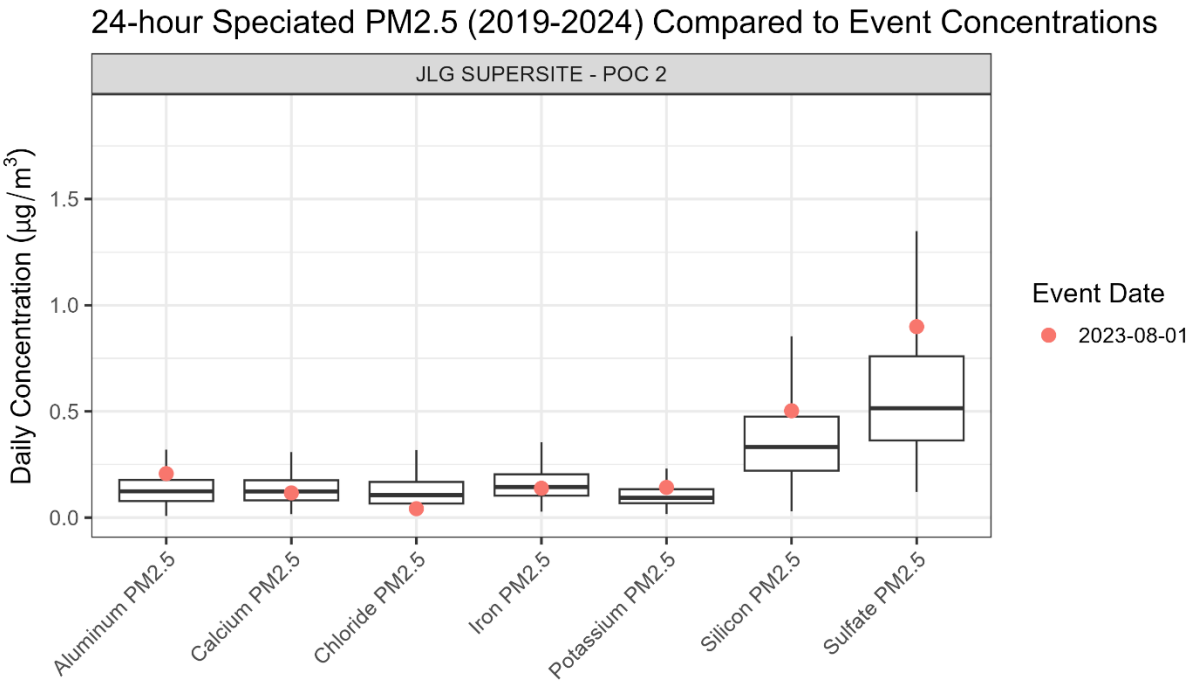

Figure 4-74. Boxplots of speciated $PM_{2.5}$ collected at the JLG Supersite site collected during the ozone season (April-September) from 2019-2024. Available speciated $PM_{2.5}$ concentrations collected during the July 31-August 1 atypical ozone event are shown as a point.

4.4.5 Event Statistics

Table 4-15 summarizes the measurements of ozone concentrations on July 31-August 1, 2023, as well as the percentile rank of the observation compared to six years of ozone season data (April 1-September 31, 2019-2024). Ozone MDA8 concentrations ranged from the 94th - 100th percentile on July 31-August 1, 2023.

Table 4-15. Percentile of ozone measurements on the atypical dates compared with six years of ozone data (2019-2024). The percentile rank is calculated across the ozone production season in the nonattainment area (April 1-September 31) of 2019-2024.

Date	Site Name	Site Code	Ozone MDA8 (ppb)	Percentile Rank
7/31/2023	A J Maintenance Yard	040213001	71	94
	South Scottsdale	040133003	72	94
	Humboldt Mountain	040139508	72	94
	Queen Valley	040218001	73	95

Date	Site Name	Site Code	Ozone MDA8 (ppb)	Percentile Rank
	Dysart	040134010	74	97
	Cave Creek	040134008	75	97
	High School Air Monitoring Station	040137024	75	97
	Blue Point-Sheriff Station-Tonto NF-Salt River Recreation Area	040139702	75	97
	Fountain Hills	040139704	75	97
	Pinnacle Peak	040132005	77	98
	Mesa	040131003	78	99
	Falcon Field	040131010	78	99
	South Phoenix	040134003	78	99
	Lehi Air Monitoring Station	040137022	78	99
	Glendale	040132001	79	99
	Central Phoenix	040133002	79	99
	Red Mountain Air Monitoring Station	040137021	79	99
	Tempe	040134005	80	99
	North Phoenix	040131004	84	100
	West Phoenix	040130019	87	100
	JLG Supersite	040139997	89	100
8/1/2023	Cave Creek	040134008	72	94
	High School Air Monitoring Station	040137024	72	94
	Tonto NM	040070010	72	94
	Pinnacle Peak	040132005	73	95
	Tempe	040134005	73	95
	Mesa	040131003	74	97
	Blue Point-Sheriff Station-Tonto NF-Salt River Recreation Area	040139702	74	97
	West Phoenix	040130019	75	97

Date	Site Name	Site Code	Ozone MDA8 (ppb)	Percentile Rank
	Falcon Field	040131010	75	97
	Red Mountain Air Monitoring Station	040137021	76	98
	Glendale	040132001	77	98
	Lehi Air Monitoring Station	040137022	77	98
	JLG Supersite	040139997	78	99
	North Phoenix	040131004	79	99

4.4.6 Conclusion

The concurrence of HMS smoke perimeters over the nonattainment area, HYSPLIT trajectories and meteorological analysis showing accumulation of smoke in the nonattainment area, visible smoke in camera images, and elevated $PM_{2.5}$ concentrations, OC to EC ratios, and speciated $PM_{2.5}$ (potassium) provide evidence that surface-level smoke was present during the period. Long-range transport of smoke from numerous fires burning in Mexico, the western U.S., and Canada, as well as a local fire to the south of Phoenix, enhanced ozone concentrations outside of the typical diurnal profile, keeping ozone values high and affecting the MDA8 ozone concentrations at twenty-two sites. Multiple analyses showed that smoke fully encompassed the Maricopa Nonattainment Area on July 31-August 1, 2023, and statistics show ozone concentrations were atypical during this event.

This combined evidence indicates that smoke plumes generated by numerous fires in Mexico, the western U.S., and Canada, as well as a local fire to the south of Phoenix, provided an atypical source of ozone and ozone precursors that caused enhanced ozone concentrations on July 31-August 1, 2023. Removal of these days as atypical events is supported by this analysis.

4.5 August 17-18, 2023

4.5.1 Event Overview: August 17-18, 2023

The unrepresentative (atypical) ozone event took place on August 17-18, 2023, and affected eighteen monitoring sites in the Maricopa Nonattainment Area: West Phoenix, Mesa, North Phoenix, Falcon Field, Glendale, Pinnacle Peak, Central Phoenix, South Scottsdale, South Phoenix, West Chandler, Tempe, Dysart, Red Mountain Air Monitoring Station, Lehi Air Monitoring Station, High School Air Monitoring Station, Blue Point-Sheriff Station-Tonto NF-Salt River Recreation Area, Fountain Hills,

and JLG Supersite (Table 4-16). The maximum daily 8-hr average (MDA8) concentrations at the effected sites ranged from 71-84 ppb.

Time series graphs showing hourly ozone concentrations that exceeded the seasonal means (calculated using all available data from April 1 – September 31, 2019-2024) and 10th-90th percentiles at each site are shown in Figure 4-75. Throughout the atypical period, ozone concentrations exhibited widespread and distinct peaks at sites such as Central Phoenix, JLG Supersite, South Phoenix, and Tempe on both days of the atypical event; these observations exceeded the 90th percentile relative to all data collected during the ozone season from 2019-2024.

Numerous fires burning Canada were identified as major contributors to this event. Evidence includes (1) HMS smoke perimeters over the nonattainment area, (2) HYSPLIT trajectories and meteorological analysis showing accumulation of smoke in Phoenix, (3) visible smoke in camera images, and (4) elevated NO_2 and OC to EC ratios. This combination of evidence indicates that this is an atypical ozone event.

Table 4-16. Summary of identified atypical August 17-18, 2023.

Event Date(s)	Event Ozone Concentration Percentile	Sites Exceeded During Event	Type of Event
August 17-18, 2023	92nd - 100th	Eighteen sites: West Phoenix, Mesa, North Phoenix, Falcon Field, Glendale, Pinnacle Peak, Central Phoenix, South Scottsdale, South Phoenix, West Chandler, Tempe, Dysart, Red Mountain Air Monitoring Station, Lehi Air Monitoring Station, High School Air Monitoring Station, Blue Point-Sheriff Station-Tonto NF-Salt River Recreation Area, Fountain Hills, JLG Supersite	International long-range transport

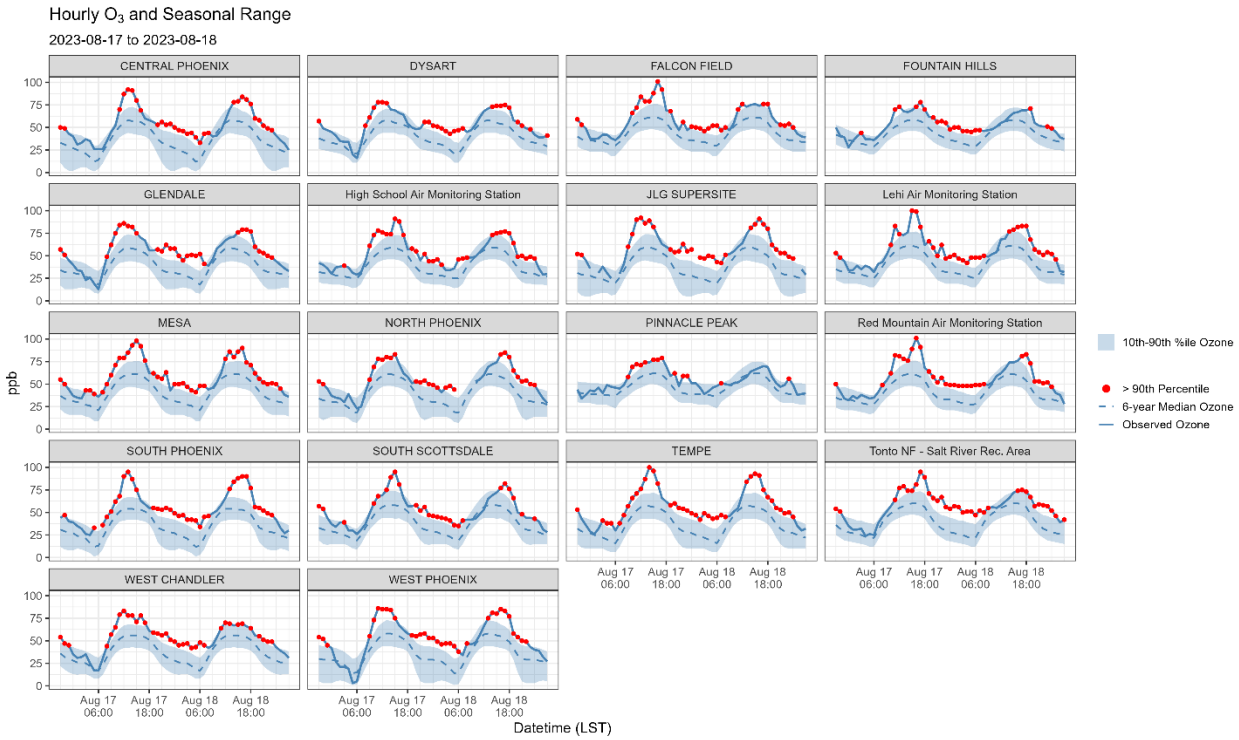

Figure 4-75. Hourly ozone concentrations (ppb) compared to all available data during the ozone season (April 1 – September 31) of the 6-year (2019-2024) period. Hourly means and 10th-90th percentiles are calculated using data on August 17-18, 2023.

4.5.2 Identification of Wildfire(s)

Multiple large fires in Canada were active in the days leading up to and during August 17-18, the exclusion days (**Figures 4-76 through 4-77**). Smoke from these fires combined to blanket the continental U.S. during August 17-18.

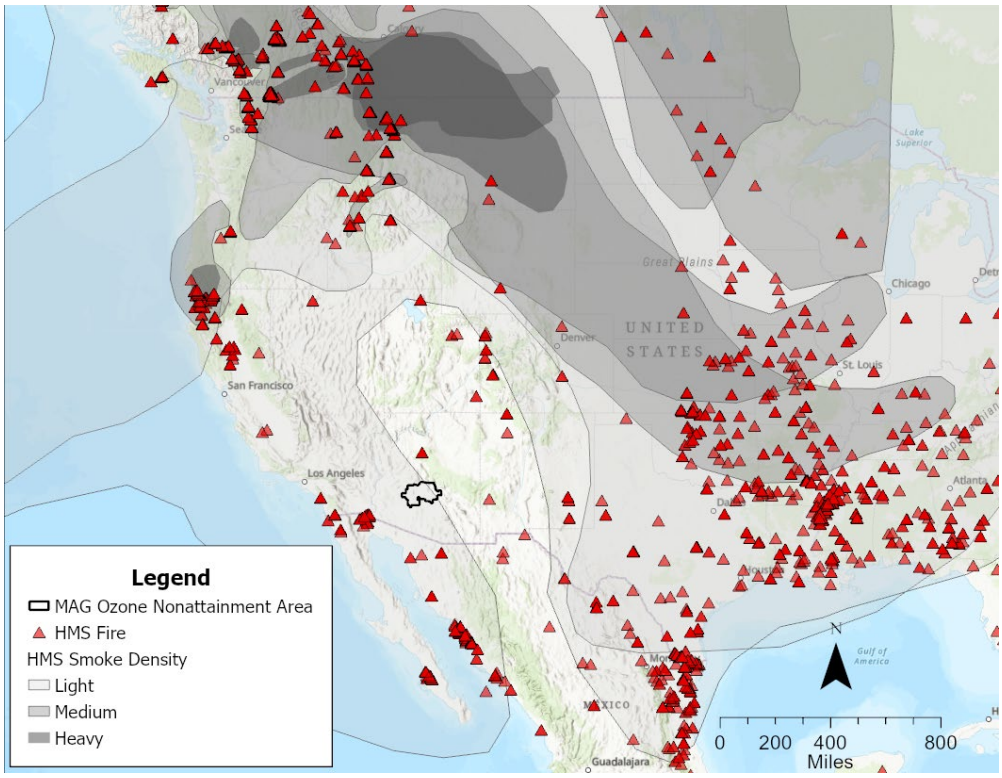

Figure 4-76. Continental view of HMS smoke density and fire locations on August 17, 2023.

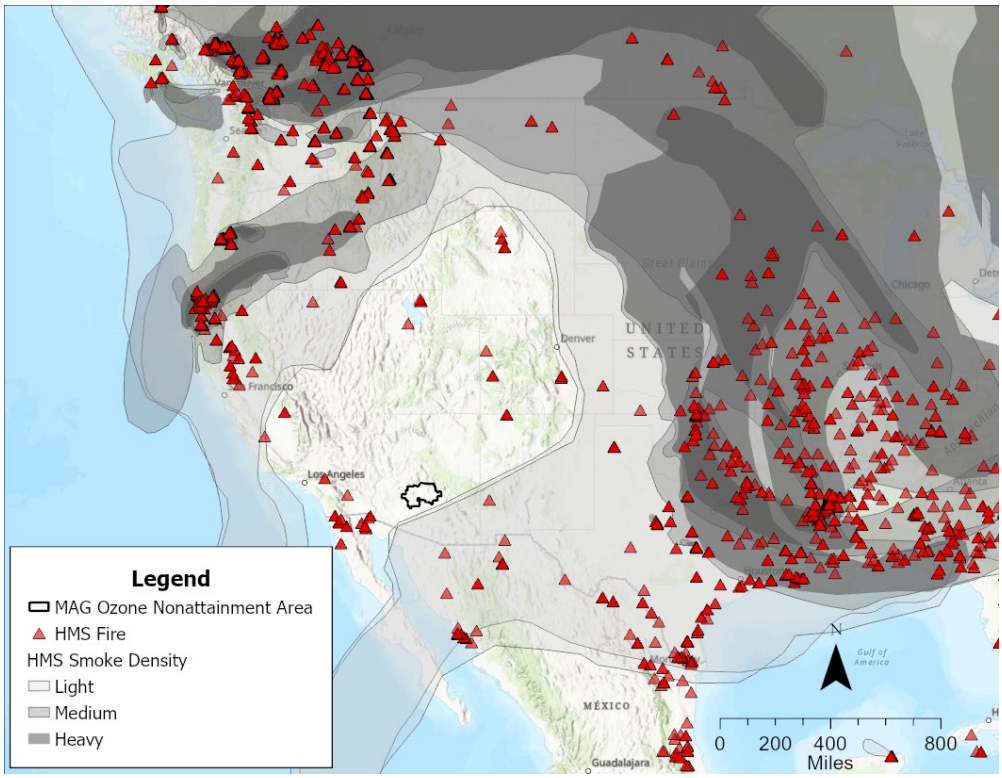

Figure 4-77. Continental view of HMS smoke density and fire locations on August 18, 2023.

4.5.3 Meteorological Analysis

Upper-level Analysis

At 500 mb on August 17, high pressure was positioned over Colorado and New Mexico, while a trough of low pressure aloft resided off the central California coast. The following day, August 18, the 500 mb high shifted eastward into the Texas and Oklahoma panhandles, while the upper-level trough remained off the California coast. On both days in central Arizona, the aloft wind pattern was southerly to southeasterly, as shown in the mean 500 mb winds in **Figure 4-78**.

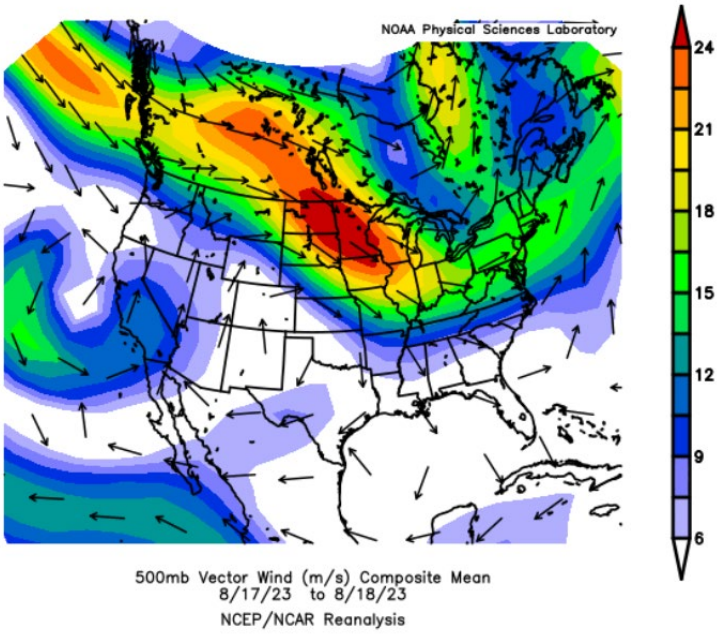

Figure 4-78. Mean 500 mb winds for August 17-18, 2023. High pressure aloft east of Arizona resulted in southerly to southeasterly upper-level winds in the nonattainment area. Source: NOAA

Surface Analysis

The upper-level high east of Arizona led to subsidence (sinking air) and compressional heating, which resulted in hot temperatures in Phoenix on both days. As **Table 4-17** indicates, the afternoon high temperature at KPHX for August 17 was 114°F with partly sunny skies. For August 18, the afternoon high at KPHX was 106°F. Both days also recorded average daily wind speeds less than 10 mph, which hindered dispersion and allowed pollutants to accumulate. These weather conditions favored ground-level ozone formation in central Arizona.

Table 4-17. Daily maximum high temperatures and average daily wind speeds from KPHX.

Date	Maximum temperature (°F)	Average daily wind speed (mph)
August 17	114	6.8
August 18	106	8.2

Satellite Smoke and Fire Detections

Figure 4-79 contains the NOAA HMS smoke plume analysis and satellite fire detections across the southwestern United States during the August 17-18, 2023 period. NOAA analyzed smoke over the nonattainment area on August 17, while an analyzed smoke plume was located south of Phoenix on August 18. Potential smoke transport paths into Phoenix for August 17-18, 2023 can be found in the "Smoke Transport" section.

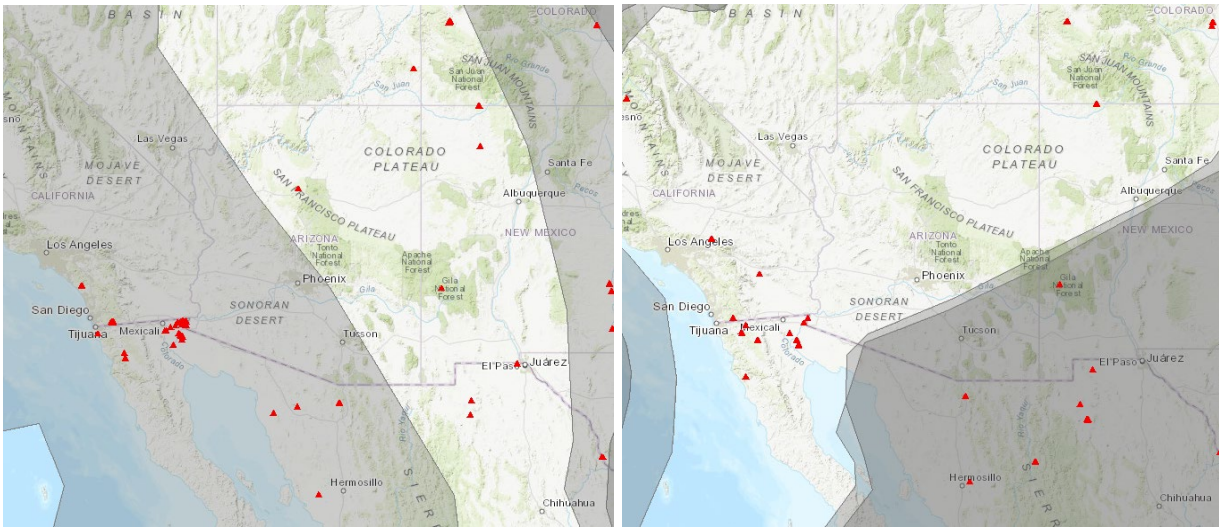

Figure 4-79. NOAA HMS smoke plume analysis (grey contours) and satellite fire detections (red triangles) from August 17, 2023 (left) and August 18, 2023 (right). Source: AirNow-Tech

Smoke Discussions

The smoke plume analyzed in Figure 4-79 was mentioned by NOAA in their August 14 discussion which highlighted smoke from Canadian wildfires across a large part of CONUS. The analyzed smoke plume in northern Mexico was also highlighted by NOAA in their August 16 smoke discussion, with smoke origins again from Canadian wildfires.

"**An exceptionally large area of smoke, emanating from the large wildfires occurring mainly in northeastern and west-central British Columbia, northern Alberta, south-central Northwest Territories, and west-central Quebec, continues to impact significant portions of Canada, the United States, and extending off the east coast of the United States and into the North Atlantic Ocean**. Moderate and thick density smoke blanketed a sizable part of western and south-central Canada. The fires in Quebec also produced moderate and thick density smoke moving northeast toward Newfoundland and Labrador." (NOAA NESDIS Text Narrative from August 15, 2023)

"**Very large wildfires burning in northwestern Canada were primarily responsible for an enormous batch of smoke which covered much of Canada as well as northeastern Alaska, the eastern two-thirds of the lower 48, northern Mexico, the northern Gulf of Mexico, and some of the western Atlantic off the east coast of the U.S. and Canada**. Embedded areas of thicker smoke were seen over far north central Canada, and in the region stretching from the southern part of the Northwest Territories and northern Alberta to the east and southeast extending as far east was western Quebec. Additional thicker smoke was seen over far eastern Canada, the Labrador Sea, and western Greenland." (NOAA NESDIS Text Narrative from August 16, 2023)

Soundings

PBL heights for the August 17-18, 2023 period in the nonattainment area were estimated by using the Tucson upper-air sounding data and are listed in **Table 4-18**. Using the 5 p.m. PST data on August 17, and adjusting for the elevation of Phoenix, the PBL height was estimated to be 1,900 m AGL. On August 18, the estimated PBL height for Phoenix was 2,200 m AGL. **Figure 4-80** displays the skew-T diagrams for 5 p.m. PST each day in Tucson. While the PBL heights during this period are not as deep as previous dates discussed, these diagrams show an established PBL capable of transferring aloft air down to ground level.

Table 4-18. Daily estimated PBL heights for Phoenix from the Tucson upper-air sounding data.

Date	Estimated PBL (meters)
August 17	1,900
August 18	2,200

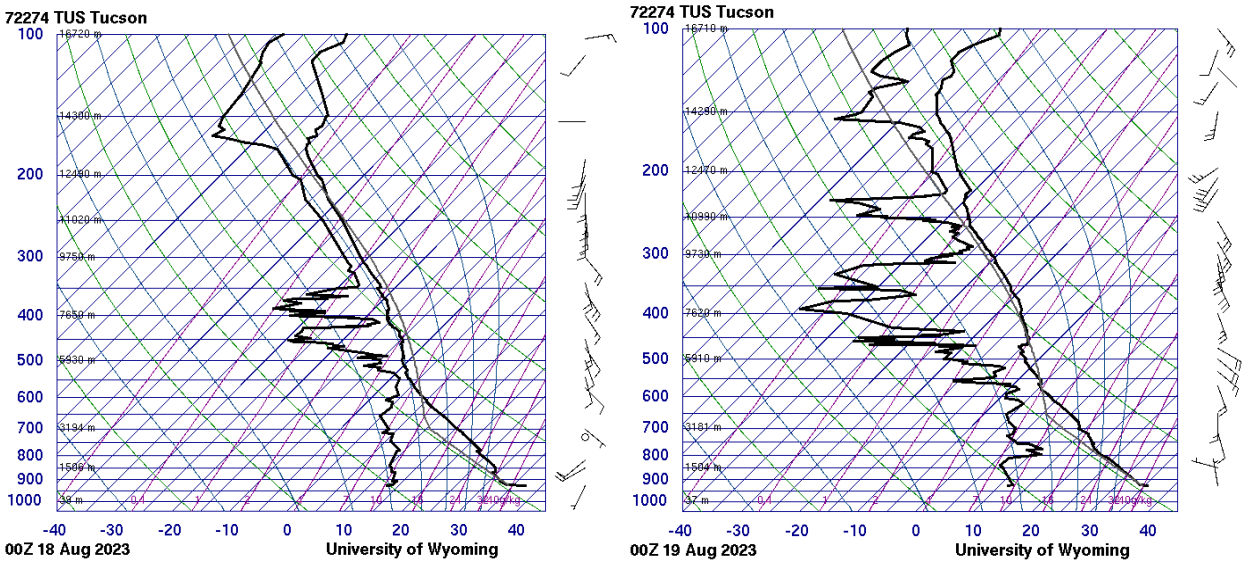

Figure 4-80. 5 p.m. PST skew-T diagrams from the Tucson upper-air weather station on August 17, 2023 (left) and August 18, 2023 (right). Upper-air data in Tucson indicates an established PBL each day. Source: University of Wyoming

Smoke Transport

From the estimated PBL heights, transport paths were established using the HYSPLIT model. In addition, to determine the potential for smoke transport into central Arizona, the HYSPLIT trajectories were overlaid on the NOAA HMS smoke plume analysis and satellite fire detections. Shown in **Figure 4-81** is the 72-hour back trajectory ending at 5 p.m. PST August 17, which indicated southeasterly flow into central Arizona, which was similar to the 500 mb wind pattern. Additionally, the source air in the 1,900 m AGL path originated from southern Texas on August 14, where a smoke plume was analyzed by NOAA.

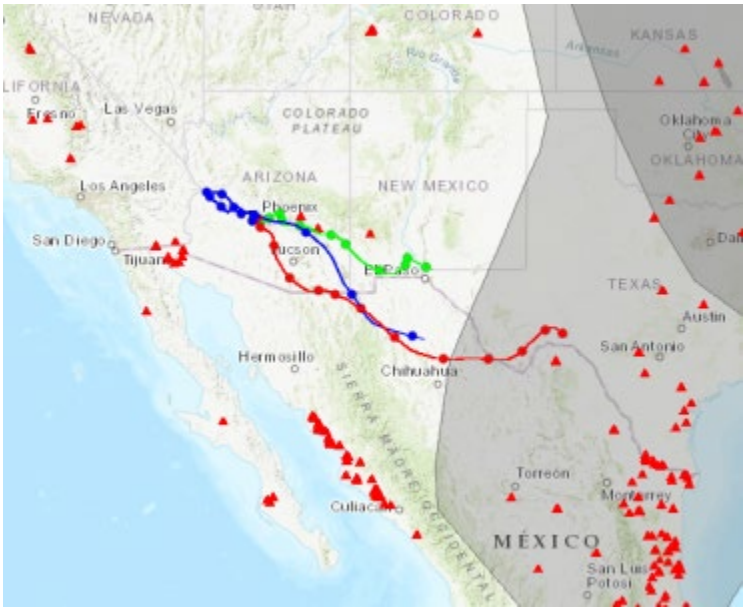

Figure 4-81. 72-hour back trajectory analysis ending 5 p.m. PST on August 17, 2023. The transport path at 1,900 m AGL (red) intersect with NOAA analyzed smoke (grey contours) from August 14. Source: AirNow-Tech

For August 18, a 48-hour back trajectory was used ending at 5 p.m. PST and is displayed in Figure 4-82. The resulting trajectory paths showed southerly flow entering central Arizona, which was similar to the 500 mb wind pattern, and the source air originated from Sonora, Mexico on August 16. Furthermore, the 1,100 m and 2,200 m AGL paths intersected analyzed smoke over northern Mexico from August 16, and were near fires detected by satellites across Sonora, Mexico on August 16.

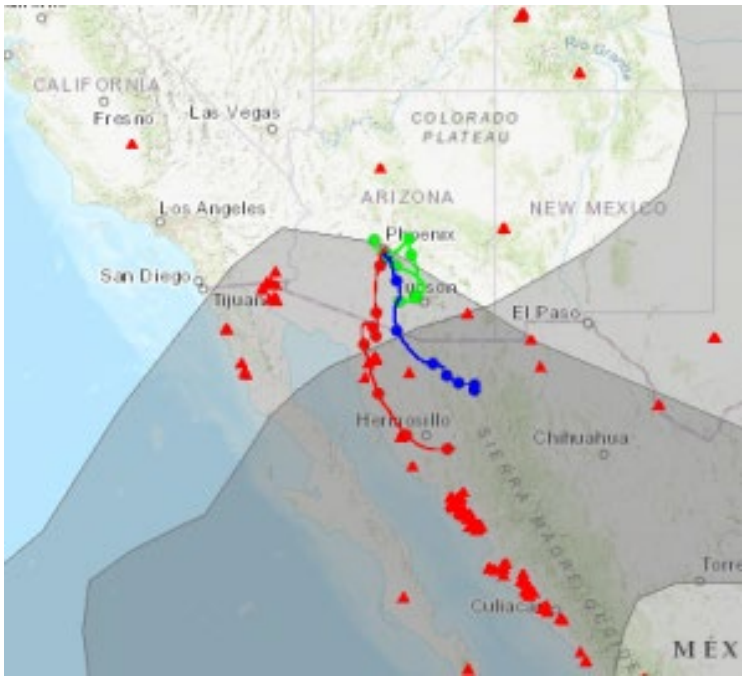

Figure 4-82. 48-hour back trajectory analysis ending 5 p.m. PST on August 18. The 1,100 m and 2,200 m AGL paths intersect with NOAA analyzed smoke (grey contours) from August 16 and were close to satellite fire detections from August 16. Source: AirNow-Tech

Summary

During the August 17-18, 2023 period, a ridge of high pressure aloft led to hot conditions and light surface winds within the PBL, which inhibited dispersion and supported ozone production in the Phoenix region. Additionally, each day's HYSPLIT trajectory within the PBL intersected analyzed smoke plumes and were near satellite fire detections on August 16. NOAA smoke discussions indicated the smoke source was from large Canadian wildfires. Due to these conditions, there is evidence that smoke was carried into central Arizona and enhanced ozone formation in the nonattainment area each day.

4.5.4 Surface Impacts

Smoke plumes from the fires burning throughout Canada were present over the nonattainment area during the atypical ozone event and contributed to hazy conditions. **Figures 4-83 through 4-84** show photos taken from the south-facing South Mountain and east-facing Superstition Mountain webcams. Select webcam images were chosen based on the presence of smoke.

Figure 4-83. Camera Images showing the south coordinal direction taken from the South Mountain webcam on August 17 from 6:30 LST, 10:00 LST, 14:15 LST, and 16:45 LST.

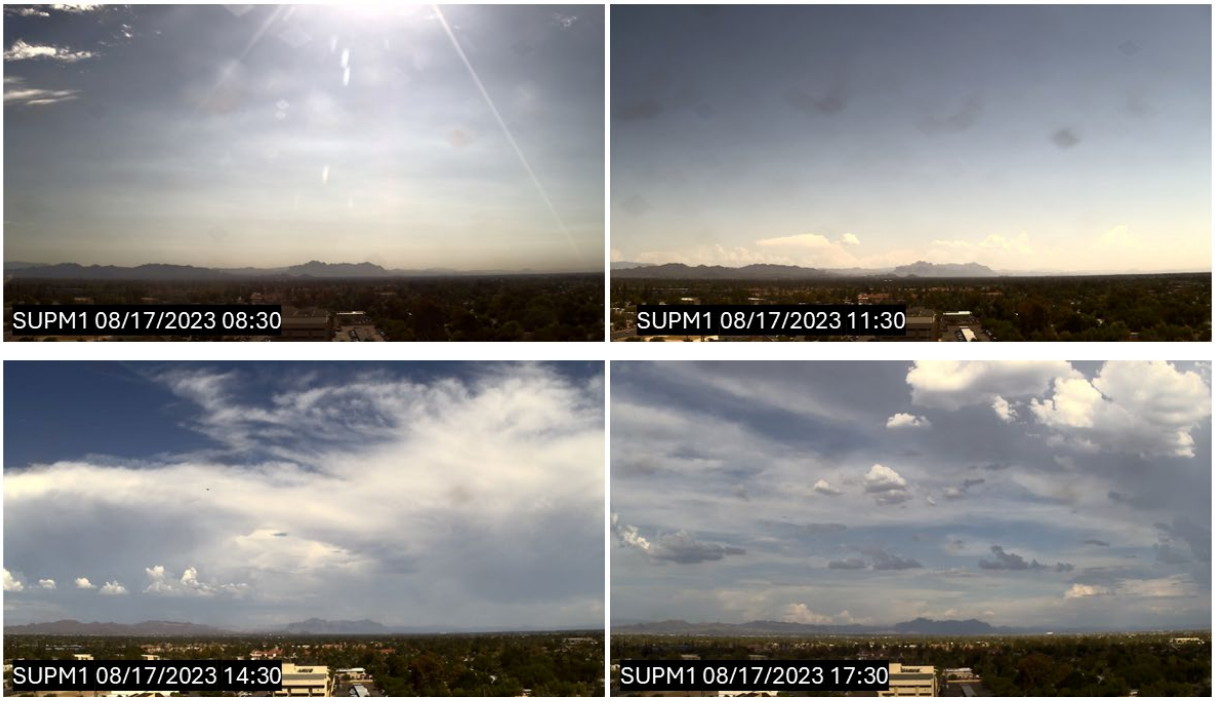

Figure 4-84. Camera Images showing the east coordinal direction taken from the Superstition Mountain webcam on August 17 from 8:30 LST, 11:30 LST, 14:30 LST, and 17:30 LST.

Figure 4-85 shows an overall view of the magnitude of hourly pollutant concentrations measured in the nonattainment area in the two days before and after the August 17-18, 2023, atypical event. Hourly ozone concentrations are elevated at all affected sites relative to the days before the atypical event. NO_2 concentrations were elevated on August 17, indicating buildup of ozone precursors. $PM_{2.5}$ concentrations were elevated during some hours August 17-18. However, a severe thunderstorm warning on August 16, and a dust storm advisory on August 18[20] indicate that elevated $PM_{2.5}$ concentrations may have been due to wind-blown dust from monsoonal storms rather than smoke from wildfires. The ozone and NO_2 enhancements in concentrations provide evidence that smoke from regional fires entered the region, mixed towards the surface, and had an atypical influence on ozone concentrations during the period.

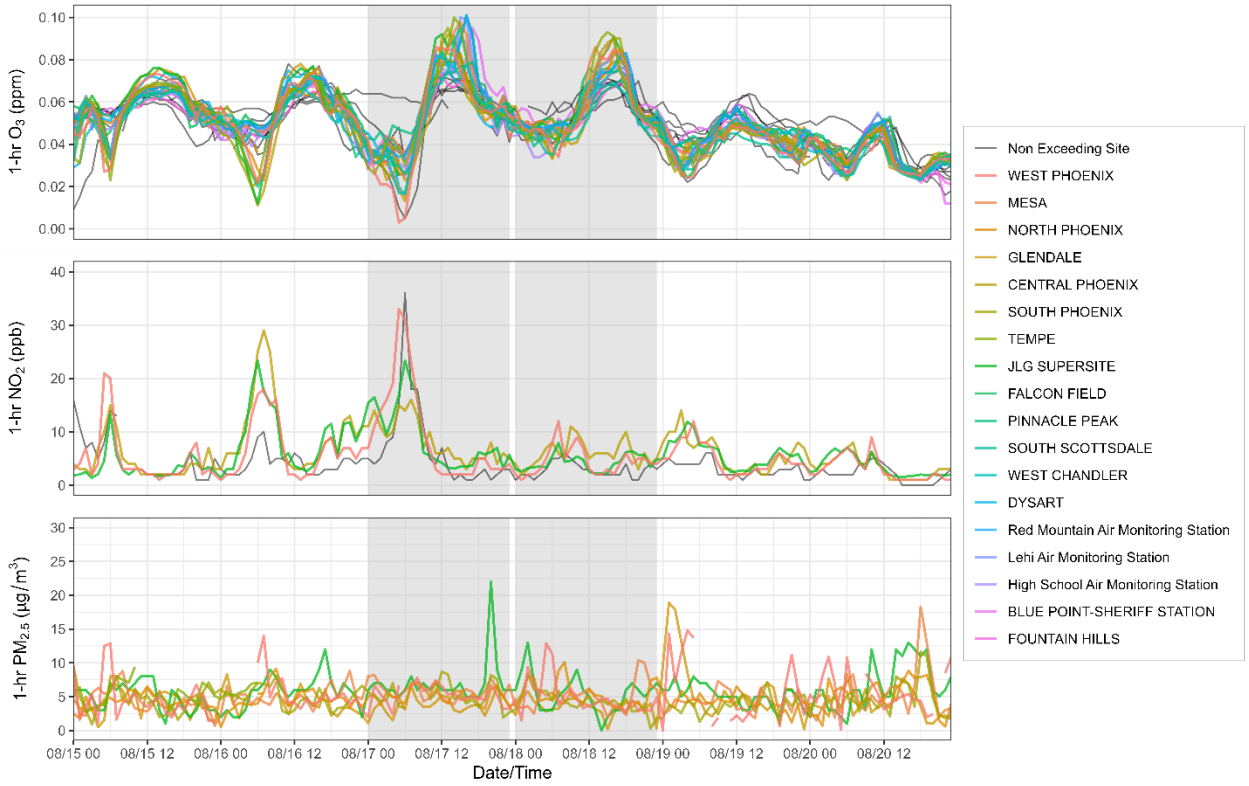

Figure 4-85. Hourly concentrations of ozone, NO_2, and $PM_{2.5}$ at all sites in the nonattainment area. All ozone-exceeding sites are color-coded to highlight smoke impacts on concentrations, and all non-exceeding sites are black. The gray shaded areas represent August 17-18, 2023.

Figure 4-86 shows a close up of hourly NO_2 concentrations at the Buckeye (top) and West Phoenix (bottom) sites. Buckeye was a non-ozone-exceeding site. NO_2 concentrations at both sites exhibit a

[20] https://mesonet.agron.iastate.edu/vtec/search.php?mode=bypoint&lon=-112.1202&lat=33.4223&buffer=0.00&sdate1=2023-06-22&edate1=2023-08-18

distinct increase to above the 95th percentile during the morning of August 17. These observations provide evidence that smoke impacts were widespread and affected multiple air monitoring sites.

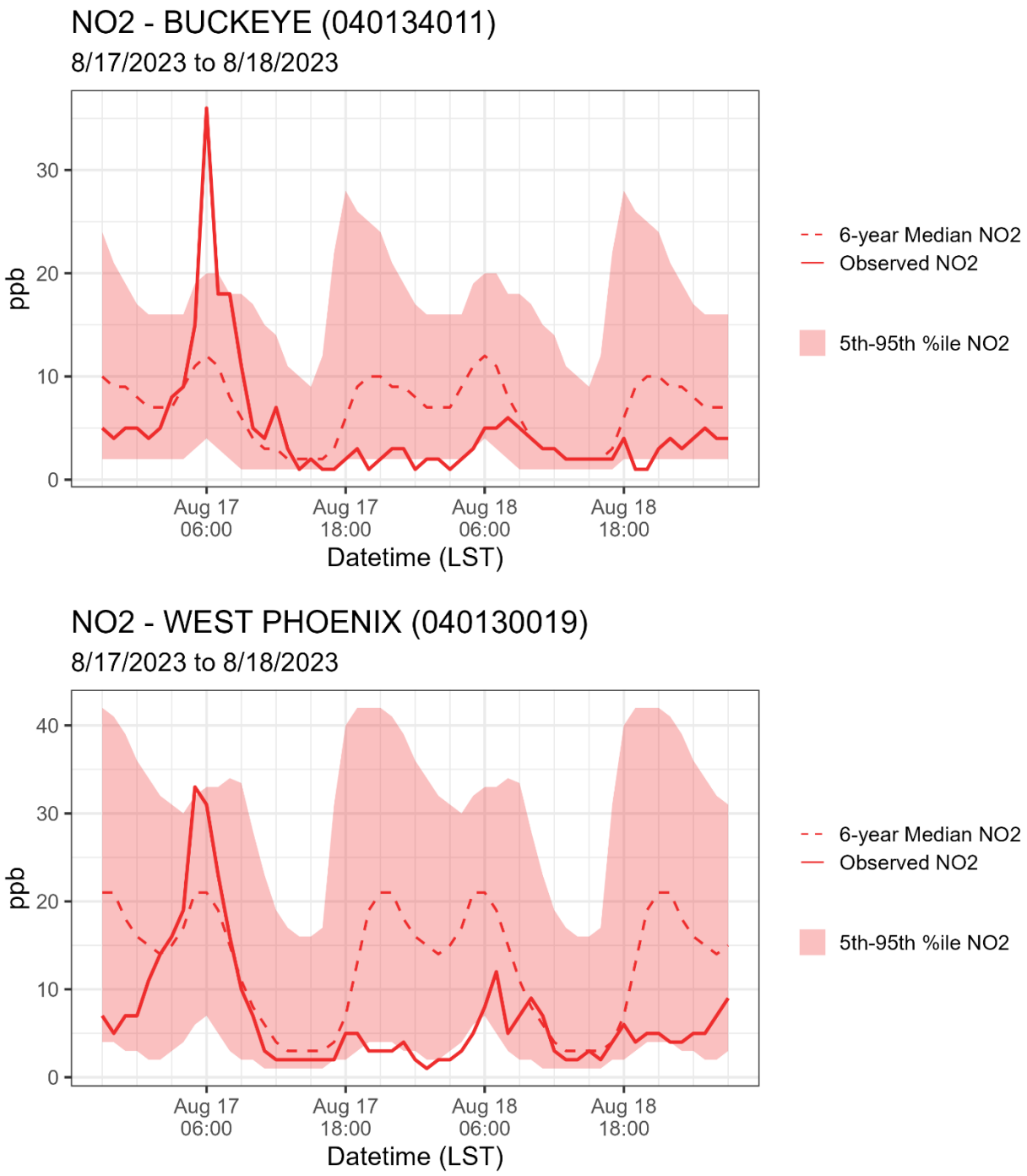

Figure 4-86. Hourly concentrations of NO_2 at the Buckeye (top) and West Phoenix (bottom) sites. The 6-year (2019-2024) median is represented by the dashed line, and the 5th-95th percentile is represented by the shaded area.

OC and EC data were not available on August 17-18, but samples collected before and after that date show evidence of smoke impacts. The ratio of OC to EC taken at the JLG Supersite monitor was also examined for evidence that wildfire smoke entered the nonattainment area. Increases in this ratio are indicative of wildfire smoke. Figure 4-87 shows a boxplot of OC to EC ratios for available data collected during the ozone season between 2019-2024. The OC to EC ratio on August 16 was elevated above the 75th percentile providing further evidence that ground-level wildfire smoke entered Phoenix around the August 17-18 atypical event.

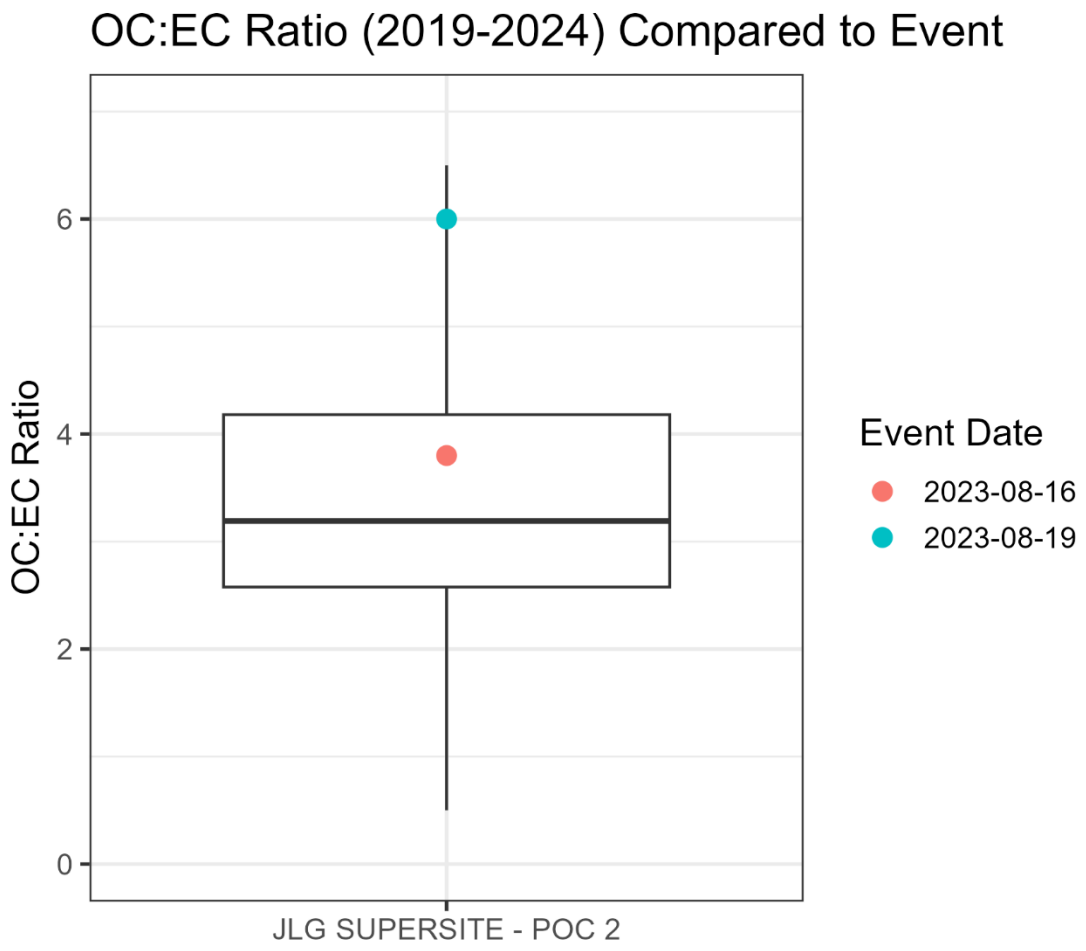

Figure 4-87. Boxplot of OC to EC ratios at the JLG Supersite site using data collected during the ozone season (April-September) from 2019-2024. OC to EC ratios are calculated at POC 2 (x-axis). Available OC to EC ratios collected during the day before and day after the August 17-18 atypical ozone event are shown as points.

4.5.5 Event Statistics

Table 4-19 summarizes the measurements of ozone concentrations on August 17-18, 2023, as well as the percentile rank of the observation compared to six years of ozone season data (April 1-September 31, 2019-2024). Ozone MDA8 measurements ranged from the 92nd - 100th percentile on August 17-18, 2023.

Table 4-19. Percentile of ozone measurements on the atypical dates compared with six years of ozone data (2019-2024). The percentile rank is calculated across the ozone production season in the nonattainment area (April 1-September 31) of 2019-2024.

Date	Site Name	Site Code	Ozone MDA8 (ppb)	Percentile Rank
8/17/2023	Dysart	040134010	71	92
	Fountain Hills	040139704	71	92
	Pinnacle Peak	040132005	74	95
	South Phoenix	040134003	74	95
	North Phoenix	040131004	75	96
	Central Phoenix	040133002	75	96
	South Scottsdale	040133003	75	96
	West Chandler	040134004	75	96
	West Phoenix	040130019	77	98
	Glendale	040132001	77	98
	High School Air Monitoring Station	040137024	78	98
	Tempe	040134005	80	99
	Blue Point-Sheriff Station-Tonto NF-Salt River Recreation Area	040139702	80	99
	Lehi Air Monitoring Station	040137022	81	99
	JLG Supersite	040139997	81	99
	Falcon Field	040131010	83	100
	Red Mountain Air Monitoring Station	040137021	83	100
	Mesa	040131003	84	100
8/18/2023	Dysart	040134010	71	92
	Glendale	040132001	72	93
	North Phoenix	040131004	73	94
	Central Phoenix	040133002	73	94

Date	Site Name	Site Code	Ozone MDA8 (ppb)	Percentile Rank
	Red Mountain Air Monitoring Station	040137021	73	94
	Falcon Field	040131010	74	95
	West Phoenix	040130019	75	96
	Lehi Air Monitoring Station	040137022	76	97
	JLG Supersite	040139997	77	98
	Mesa	040131003	78	98
	South Phoenix	040134003	78	98
	Tempe	040134005	79	99

4.5.6 Conclusion

The concurrence of HMS smoke perimeters over the nonattainment area, HYSPLIT trajectories and meteorological analysis showing accumulation of smoke in the nonattainment area, visible smoke in camera images, and elevated NO_2 concentrations and OC to EC ratios provide evidence that surface-level smoke was present during the period. Long-range transport of smoke from numerous unidentified fires burning in Canada enhanced ozone concentrations outside of the typical diurnal profile, keeping ozone values high and affecting the MDA8 ozone concentrations at eighteen sites. Multiple analyses showed that smoke fully encompassed the Maricopa Nonattainment Area on August 17-18, 2023, and statistics show ozone concentrations were atypical during this event.

This combined evidence indicates that smoke plumes generated by numerous fires in Canada provided an atypical source of ozone and ozone precursors that caused enhanced ozone concentrations on August 17-18, 2023. Removal of these days as atypical events is supported by this analysis.

5. References

Gelaro R., McCarty W., Suárez M.J., Todling R., Molod A., Takacs L., Randles C.A., and others (2017) The Modern-Era Retrospective Analysis for Research and Applications, Version 2 (MERRA-2). *Journal of Climate*, 30(14), 5419-5454, July 15. Available at https://journals.ametsoc.org/view/journals/clim/30/14/jcli-d-16-0758.1.xml.

Maricopa Association of Governments (2025) MAG 2025 Eight-Hour Ozone Plan – Submittal of Applicable Moderate Area Requirements for the Maricopa Nonattainment Area. April. Available at https://azmag.gov/portals/0/Environmental/Air-Quality/2025/Final-MAG-2025-Eight-Hour-Ozone-Plan-4-23-25.pdf.